CDW

Yury Holubeu *

November 21, 2025

This draft is not aimed for distribution.
Links below show the contents of problems.

Contents

Preface 7

I CDW in a Nutshell 8
0.1 Main Formulas and Ideas (?) . . . 8

II My Main Theory 9

III Examples and Solved Problems 10

IV Well-known and Important Articles 11

1 Density Waves in Solids by Gruiner 11
1.1 The One-Dimensional Electron Gas . . . 11
1.1.1 The Response Function of the One-Dimensional Electron Gas . . . 11
1.1.2 Instabilities in a One-Dimensional Electron Gas: g-ology . . . 15
1.1.3 Correlations and Fluctuations . . . 18
1.2 Materials . . . 20
1.2.1 Inorganic Linear Chain Compounds . . . 22
1.2.2 Organic Linear Chain Compounds . . . 28
1.3 The CDW Transition and Ground State: Mean Field Theory and Observations . . . 31
1.3.1 The Kohn Anomaiy and the Peierls Transition: Mean Field Theory . . . 32
1.3.2 Single Particle Transitions: Tunneling and Coherence Factors . . . 45
1.3.3 Experimental Evidences for the CDW Transition and Ground State . . . 47
1.4 The SDW Transition and Ground State: Mean Field Theory and Observations . . . 58
1.4.1 Mean Field Theory of the Spin Density Wave Transition . . . 59
1.4.2 Experimental Evidences for the SDW Transition and Ground State . . . 63
1.5 Fluctuation Effects . . . 68
1.5.1 Fluctuations in Quasi-One-Dimensional Metais . . . 69
1.5.2 Charge Density Wave Fluctuations in $K_{0.3}M$ o O_3 . . . 78
1.6 Collective Excitations . . . 80
1.6.1 Ginzburg-Landau Theory of Charge Density Wave Excitations . . . 82
1.6.2 Excitations of the Spin Density Wave Ground State . . . 93
1.6.3 Experiments on Charge Density Waves: Neutron and Raman Scattering . . . 95
1.6.4 Experiments on Spin Density Waves: AFMR and Magnetization . . . 99
1.7 Commensurability and Near Commensurability Effects . . . 101
1.7.1 Models of Commensurability Effects . . . 102
1.7.2 Experiments: Search for Commensurability Effects and Solitons . . . 109
1.8 The Interaction Between Density Waves and Impurities . . . 110
1.8.1 Theories of Density Wave-Impurity Interaction . . . 111
1.8.2 Experimental Evidence for Finite Correlation Lengths . . . 116
1.9 The Electrodynamics of Density Waves . . . 119

*https://yuriholubeu.github.io/, yuri.holubev@gmail.com

1.9.1 The Electrodynamics of Density Waves . . . 119
1.9.2 Frequency Dependent Conductivity of Charge Density Waves . . . 126
1.9.3 Frequency Dependent Conductivity of Spin Density Waves . . . 130
1.10 Nonlinear Transport . . . 131
1.10.1 Models of Density Wave Transport . . . 131
1.10.2 Experiments on the Nonlinear Dynamics of the Collective Modes . . . 136
1.11 Current Oscillations and Interference Effects in Driven CDW Condensates . . . 141
1.11.1 11.1 Introduction . . . 141
1.11.2 11.2 Current Oscillations . . . 142
1.11.3 Interference Phenomena . . . 151
1.11.4 Conclusions . . . 169

2 The dynamics of charge-density waves by Grüner 171
2.1 I. Introduction . . . 171
2.2 II. The Charge-density-wave Ground State . . . 173
2.2.1 A. The Peierls Transition: Theory . . . 173
2.2.2 B. The Peierls Transition: Materials and Experiment . . . 176
2.3 III. The Dynamics of the Collective Mode: Some Basic Results . . . 181
2.3.1 A. Fundamental Concepts . . . 181
2.3.2 B. Frequency- and Electric-field-dependent Conductivity . . . 187
2.3.3 C. Other Transport Coefficients . . . 194
2.3.4 D. Elastic Properties . . . 196
2.3.5 E. Nuclear Magnetic Resonance . . . 197
2.3.6 F. Current Oscillations . . . 198
2.4 IV. The Mechanisms of Pinning . . . 201
2.4.1 A. Impurity Pinning . . . 203
2.4.2 B. Experiments on Alloys and Irradiated Specimens . . . 205
2.4.3 C. Finite-size Effects: Pinning by Surfaces and by Extended Defects . . . 207
2.5 V. Models: a Short Overview . . . 209
2.6 VI. The Frequency- and Field-dependent Response . . . 215
2.6.1 A. Frequency-dependent Response . . . 215
2.6.2 B. Nonlinear Conductivity . . . 221
2.6.3 C. Experiments in the Presence of Joint Dc and Ac Electric Fields . . . 225
2.7 VII. Current Oscillations and Interference Effects . . . 230
2.7.1 A. Current Oscillations . . . 230
2.7.2 B. Interference Effects . . . 231
2.8 VIII. Disorder and Metastable States . . . 241
2.8.1 A. The Nonlinear Ac Response . . . 243
2.8.2 B. Time Domain Studies and Remanent Polarizations . . . 244
2.8.3 C. Transitions from Below to Above Threshold . . . 246
2.9 IX. Final Remarks . . . 248
2.10 References . . . 249

3 Electronic Properties of Inorganic Quasi-1D Compounds (part I) by Monceau 261
3.1 Preface To Part I . . . 261
3.2 Ground State Properties of Conducting Trichalcogenides . . . 261
3.2.1 1. Introduction . . . 261
3.2.2 2. Elementary Excitations . . . 263
3.2.3 3. Interactions . . . 267
3.2.4 4. Peierls Instability . . . 271
3.2.5 5. CDW Versus Bcs Instability . . . 285
3.2.6 6. Summary . . . 292
3.2.7 References . . . 293

3.3 Dynamical Properties of Quasi-one-dimensional Conductors: a Phase Hamiltonian Approach . . . 299
3.3.1 1. Introduction . . . 299
3.3.2 2. Phase Hamiltonian . . . 300
3.3.3 3. Phase Hamiltonian for the Peierls-fröhlich State . . . 317
3.3.4 4. Impurity Pinning and Anderson Localization . . . 331
3.3.5 5. CDW Conductivity in the Peierls-fröhlich State . . . 339
3.3.6 6. Transport Properties of nbse$_3$ and TaS_3 . . . 344
3.3.7 7. Summary . . . 348
3.3.8 Acknowledgements . . . 348
3.3.9 References . . . 348
3.4 Depinning Of Charge-density Waves by Quantum Tunneling . . . 355
3.4.1 1. Introduction . . . 355
3.4.2 2. Weak Impurity Pinning . . . 357
3.4.3 3. Equations of Motion for Phase . . . 357
3.4.4 4. Solutions of the Equations of Motion . . . 360
3.4.5 5. The Tunneling Model . . . 362
3.4.6 6. Response to Ac and Combined Ac and Dc Fields . . . 366
3.4.7 7. Conclusions and Acknowledgements . . . 369
3.4.8 References . . . 370
3.5 Solitons In One-dimensional Systems . . . 371
3.5.1 1. Introduction . . . 371
3.5.2 2. Sine-gordon Solitons . . . 373
3.5.3 3. Solitons in Magnetic Systems . . . 381
3.5.4 4. Solitons in Conducting Systems . . . 389
3.5.5 5. Solitons in Polyacetylene I . . . 396
3.5.6 5. Solitons in Polyacetylene II . . . 405
3.5.7 6. Sliding CDW Transport . . . 412
3.5.8 7. Summary . . . 423
3.5.9 References . . . 424
3.6 Theory Of the Superconducting Properties of Quasi-one-dimensional Materials . . . 434
3.6.1 1. Introduction . . . 434
3.6.2 2. Anisotropic Mass Model . . . 438
3.6.3 3. Josephson-coupled Chain Model . . . 450
3.6.4 4. Superconducting Networks . . . 459
3.6.5 5. Summary . . . 472

4 Charge Density Waves in Solids by L.P. Gor'kov, Gruner 473
4.0.1 Preface . . . 473
4.1 1. Introduction by L.P. Gofkov and G. Grüner . . . 474
4.1.1 1. Introduction . . . 474
4.1.2 2. The dynamics of the CDW mode: Fundamental concepts . . . 475
4.1.3 3. Interaction with defects . . . 476
4.1.4 4. Experiments . . . 477
4.1.5 5. Scope of the book and outstanding questions . . . 482
4.2 Structural, Electronic Properties and Design of Quasi-One-Dimensional Inorganic Conductors by Schlenker . . . 483
4.2.1 Introduction . . . 483
4.2.2 1. Transition metal trichalcogenides . . . 485
4.2.3 2. Pentachalcogenides: a bridged MX_3 structure . . . 501
4.2.4 3. One-dimensional chalcogenides from condensation of different chains . . . 502
4.2.5 4. One-dimensional chains stabilized by counter ions: halogenotetrachalcogenides 504
4.2.6 5. The particular case of $TaTe_4$ and $NbTe_4$ . . . 509
4.2.7 6. New trends: chain-chain stabilization, waved structures, clusters condensation 510

4.2.8 7. Quasi-one-dimensional oxides: the molybdenum blue bronze $A_{0.30}MoO_3$ . . . 513
4.2.9 8. Conclusions . . . 526
4.2.10 References . . . 530
4.3 The CDW Transition, Structural Studies by Pouget, Comes . . . 535
4.3.1 1. Introduction . . . 535
4.3.2 2. The charge density wave instability . . . 535
4.3.3 3. Electronic structure of some quasi-one-dimensional conductors . . . 544
4.3.4 4. Charge density wave fluctuations above the Peierls transition . . . 549
4.3.5 5. Disorder . . . 556
4.3.6 6. Interchain CDW coupling . . . 559
4.3.7 7. Phase diagrams . . . 562
4.3.8 8. Example of a complex phase diagram: $TTF-TCNQ$ . . . 562
4.3.9 9. Lattice distortion and electron-phonon coupling . . . 568
4.3.10 10. Excitations of the incommensurate CDW ordered state . . . 570
4.3.11 11. Concluding remarks . . . 572
4.3.12 References . . . 572
4.4 4 Dynamical Properties of Charge Density Waves . . . 575
4.4.1 1. Introduction . . . 576
4.4.2 2. Some basic notions on charge density waves . . . 576
4.4.3 3. Electrical transport: frequency and electric field dependent conductivity . . . 587
4.4.4 4. Electrical transport: spectral features . . . 601
4.4.5 5. Other transport coefficients and elastic properties . . . 604
4.4.6 6. Local probes . . . 607
4.4.7 7. Conclusions . . . 610
4.4.8 References . . . 611
4.5 5 Deformation and Phase-slip in Charge Density Waves in Quasi-One-Dimensional Conductors . . . 615
4.5.1 1. Introduction . . . 615
4.5.2 2. Phase coherence of the CDW . . . 616
4.5.3 3. Model of deformations and strains in the CDW . . . 623
4.5.4 4. Phase-slip in the CDW . . . 628
4.5.5 5. Conclusion . . . 633
4.5.6 References . . . 634
4.6 6 Charge Density Wave Current Oscillations and Interference Effects by Zettl . . . 636
4.6.1 Contents . . . 636
4.6.2 1. Introduction . . . 637
4.6.3 2. Models of CDW motion and oscillation phenomena . . . 640
4.6.4 3. Experimental issues pertaining to the narrow-band noise . . . 648
4.6.5 4. Electronic interference effects . . . 655
4.6.6 5. Driven CDWs and the theory of nonlinear dynamics . . . 669
4.6.7 6. Relevant length scales and domain structure . . . 678
4.6.8 7. Electro-elastic interference . . . 683
4.6.9 8. Conclusion . . . 686
4.6.10 References . . . 687
4.7 7 Theory of CDW Pinning by Weak Impurities by Vinokur . . . 689
4.7.1 1. Introduction . . . 689
4.7.2 2. Weak pinning in 1D CDW systems. Static properties . . . 692
4.7.3 3. Low-frequency conductivity of 1 D strongly disordered CDW . . . 703
4.7.4 4. Conclusions . . . 708
4.7.5 References . . . 708
4.8 8 Computer Simulations of CDW Dynamics by Littlewood . . . 709
4.8.1 1. Introduction . . . 709
4.8.2 2. Models for classical CDW dynamics . . . 711

4.8.3 3. Numerical simulations . . . 717
4.8.4 4. Conclusions . . . 737
4.8.5 References . . . 739
4.9 9 Transport Phenomena in CDW Conductors Microscopic Approach . . . 741
4.9.1 1. Introduction . . . 741
4.9.2 2. Kinetic equations . . . 743
4.9.3 3. Uniform sliding of the CDW . . . 747
4.9.4 4. Nonuniform distortions of the *CDW* . . . 750
4.9.5 5. Hall effect . . . 760
4.9.6 6. Conclusion . . . 763
4.9.7 Appendix . . . 764
4.9.8 References . . . 767
4.10 Phase Slipping, Generation of Narrow-Band Oscillations by CDW by Gorkov . . . 769
4.10.1 1. Introduction . . . 769
4.10.2 2. Phenomenological discussion . . . 770
4.10.3 3. Microscopic model . . . 772
4.10.4 4. Some features of phase slipping processes . . . 775
4.10.5 5. Some results of the numerical analysis . . . 779
4.10.6 6. Possible generalizations . . . 780
4.10.7 7. Concluding remarks . . . 781
4.10.8 References . . . 782
4.11 11 Solitons in Crystals of Charge Density Waves by Brazovskii . . . 783
4.11.1 1. Electrons and *CDW* . . . 783
4.11.2 1.1. The selftrapping in a 1D model . . . 783
4.11.3 1.2. Electrons and polarons in a quasi-1D CDW system . . . 785
4.11.4 2. Amplitude spin carrying solitons in a 1D model . . . 787
4.11.5 3. Spin carrying solitons in a system of coupled chains . . . 790
4.11.6 Note added in proof . . . 798
4.11.7 References . . . 798

V Old, Fundamental Theories 800

VI Special Effects, Properties: Main Articles 801

VII Experiments: Main Articles 802

VIII Other Theories in a Nutshell 803

5 title 803
5.0.1 title . . . 803

IX Other theories 804

X Other, Non-Typical Theory 805

6 CDW state high magnetic field quasi-1D mean field by Grigoriev, Lyubshin 805
0..1 Main idea of the article and what is important here? . . . 805
0..2 Introduction . . . 805
1. The Model and the mean-field theory of CDW in magnetic field. . . . 808

1..1 The model . . . 808
1..2 Mean field approach . . . 808
1..3 The Cosine Phase . . . 809
1..4 The Double Cosine Phase . . . 811
1..5 Free energy of cosine and double-cosine phases . . . 813
2. The phase diagram . . . 814
2..1 Transition line $T_c(H)$ and the normal-CDW_0-CDW_x tricritical point . . . 815
2..2 $T_c(H)$ transition line at perfect nesting . . . 816
2..3 Metal-CDW transition lines and tricritical points at finite t_b' . . . 817
2..4 Cosine and double-cosine phases at perfect nesting . . . 818
3. Discussion . . . 821

XI Typical Theory: Another Explanations 825

XII Articles about Potential Applications 826

XIII Other Experiments 827

XIV Appendix 828
.1 Appendix . . . 828
.1.1 Introductions from Books . . . 828
.1.2 Literature . . . 829

A Bibliography 830

Preface

Amazing facts

(I'll reveal it later)

Puzzles for motivation

(I'll reveal it later)

Part I
CDW in a Nutshell

0.1 Main Formulas and Ideas (?)

Part II
My Main Theory

Part III
Examples and Solved Problems

Part IV
Well-known and Important Articles

1 Density Waves in Solids by Gruiner

1.1 The One-Dimensional Electron Gas

The reduction of phase space from three dimensions (3D) to one dimension (1D) has several important consequences. Both interaction effects and random potentials have a more profound effect in one than in higher dimensions and fluctuations are also more important. Also, because of the simple Fermi surface in one dimension, the interaction between electrons can be expressed in terms of two coupling constants, one for $q = 0$ and one for $q = 2k_F$; leading to simple phase diagrams for the occurrence of the various broken symmetry ground states which arise as a consequence of these interactions.

1.1.1 The Response Function of the One-Dimensional Electron Gas

The Fermi surface of a one-dimensional electron gas is simple: it consists of two points, one at $+k_F$ and one at $-k_f$, for an extremely anisotropic metal, two sheets, a distance of $2k_F$ apart. The dispersion relation for a 1D free electron gas is given by $\epsilon(k) = \hbar^2 k^2/2m$, and the Fermi energy by

$$\epsilon_F = \frac{\hbar^2}{2m}\left(\frac{N_0\pi}{2L}\right)^2 = \frac{\hbar^2 k_F^2}{2m_l} \tag{1.1}$$

where N_0 is the total number of electrons, L is the length of the 1 D chain, and m_i, is the free electron mass.

The Fermi wavevector is

$$k_F = \frac{N_0\pi}{2L} = N_e\pi \tag{1.2}$$

where N_e, is the number of electrons per unit length and per spin direction. The density of states for one spin direction is

$$n(\epsilon) = \frac{L}{\pi\hbar}\left(\frac{m_e}{2\epsilon}\right)^{1/2} = \frac{L}{\pi\hbar v} \tag{1.3}$$

where the velocity v is given by the relation $m_e v = \hbar k$.

The particular topology of the Fermi surface leads to a response to an external perturbation which is dramatically different from that obtained in higher dimensions. The response of an electron gas to a time independent potential

$$\phi(\vec{r}) = \int_q \phi(\vec{q}) e^{\prime\prime\eta} \dot{r} d\vec{q} \tag{1.4}$$

is usually treated within the framework of linear response theory (see, for example, Kittel, 1963) (read it in Kittel!!!). The rearrangement of the charge density, expressed in terms of an induced charge

$$\rho^{\mathrm{md}}(\vec{r}) = \int_q \rho^{\mathrm{md}}(\vec{q}) e^{iq\cdot r} d\vec{q} \tag{1.5}$$

is related to $\phi(\vec{r})$ through

$$\rho^{\text{Ind}}(\vec{q}) = \chi(\vec{q})\phi(\vec{q}) \tag{1.6}$$

where $\chi(\vec{q})$, the so-called Lindhard response function, is given in d dimensions by

$$\chi(\vec{q}) = \int \frac{d\vec{k}}{(2\pi)^d} \frac{f_k - f_{k+q}}{\epsilon_k - \epsilon_{k+q}} \tag{1.7}$$

(derive this equation in the theory!!!)

where $f_k = f(\epsilon_k)$ is the Fermi function. For a three-dimensional spherical Fermi surface a straightforward calculation gives

$$\chi(\vec{q}) = -e^2 n(\epsilon_F) \left[1 + \frac{1-x^2}{2x} \ln\left|\frac{1+x}{1-x}\right|\right] \tag{1.8}$$

(derive this equation in the theory!!!)

where $n(\epsilon_F)$ is the density of states at the Fermi level per spin direction, and $x = q/2k_T \cdot \chi(\vec{q})$, as given by Eq. (1.8), decreases with increasing q and the derivative has a logarithmic singularity at $q = 2k_F$.

The situation is different for a one-dimensional electron gas. For wavevectors near $2k_F$, $\chi(q)$ can be evaluated by assuming a linear dispersion relation around the Fermi energy ϵ_p, as shown in Fig. 1.1,

$$\epsilon_k - \epsilon_F = \hbar v_F (k - k_F). \tag{1.9}$$

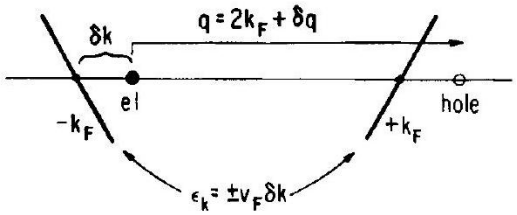


Figure 1.1. The dispersion relation for a free electron gas. The linear dispersion $\epsilon - \epsilon_F = \pm v_F(k - k_F)$ is used to evaluate the response function, Eq. (1.10).

The integral in $\chi(\vec{q}) = \int \frac{d\vec{k}}{(2\pi)^d} \frac{f_k - f_{k+q}}{\epsilon_k - \epsilon_{k+q}}$ can readily be evaluated near $2k_F$ leading to

$$\chi(q) = \frac{-e^2}{\pi\hbar v_F} \ln\left|\frac{q+2k_F}{q-2k_F}\right| = -e^2 n(\epsilon_f) \ln\left|\frac{q+2k_F}{q-2k_F}\right|. \tag{1.10}$$

In contrast to a 3D electron gas, the response function in one dimension diverges at $q = 2k_F$.

For small q values, $\chi(q)$ is given by the Thomas-Fermi approximation, $\chi(q) = -e^2 n(\epsilon_1)$. (why??)

The response function, evaluated for all q values, is displayed in Fig. 1.2, where for completeness $\chi(q)$ is also shown for a two- and a three-dimensional electron gas.

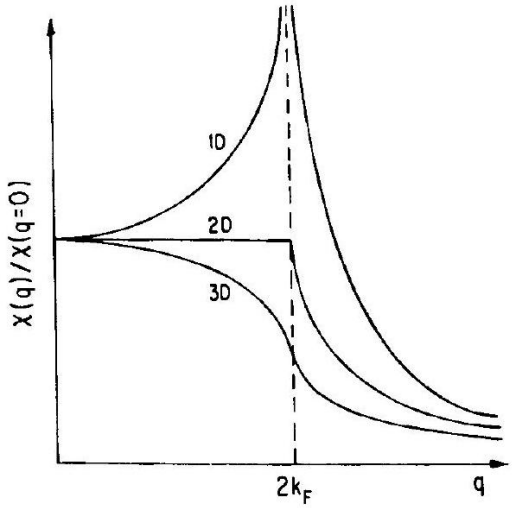


Figure 1.2. Wavevector dependent Lindhard response function for a one-, two-, and three-dimensional free electron gas at zero temperature.

(derive this plot in notes on cond matter!)

The fact that $\chi(q)$ diverges for $q = 2k_F$ in the one-dimensional case has several important consequences. Equation (1.6) implies that an external perturbation leads to a divergent charge redistribution; this suggests, through self-consistency, that at $T = 0$ the electron gas itself is unstable with respect to the formation of a periodically varying electron charge or electron spin density. (how are they connected? looks like different pehnomena) The period is related to k_F by

$$\lambda_0 = \frac{\pi}{k_r}. \tag{1.11}$$

The divergence of the response function at $q = 2k_F$ is due to the particular topology of the Fermi surface, sometimes called perfect nesting. Looking at $\chi(\vec{q}) = \int \frac{d\vec{k}}{(2\pi)^d} \frac{f_k - f_{k+q}}{\epsilon_k - \epsilon_{k+q}}$, the most significant contributions to the integral come from pairs of states - one full, one empty - which differ by $q = 2k_F$ and have the same energy, thus giving a divergent contribution to $\chi(q)$. However, in higher dimensions the number of such states is significantly reduced, as shown in Fig. 1.3 leading to the removal of the singularity at $q = 2k_F$.

(maybe I understood it, write why is it exactly, maybe with formulas)

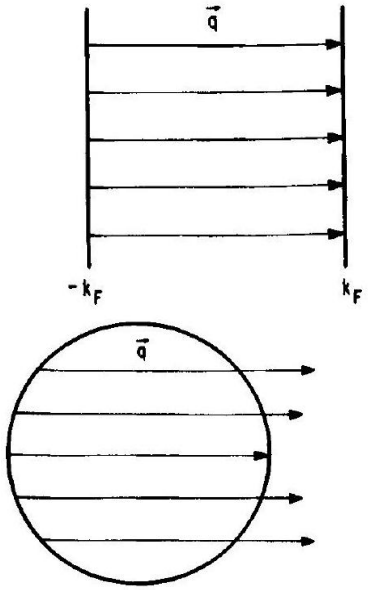


Figure 1.3. Fermi surface topology for a 1 D and 2 D free electron gas. The arrows indicate pairs of states, one full and one empty, differing by the wavevector $q = 2k_F$.
(discuss, what are the arrows, I was thinking about them before)

The quasi-one-dimensional character of the Fermi surface can be modeled by including a dispersion in the direction perpendicular to the direction along which the response function was evaluated. The dispersion relation

$$\epsilon(k) = \epsilon_0 + 2t_a \cos k_x a + 2t_b \cos k_y b \tag{1.12}$$

where a and b are the lattice constants in the x and y directions respectively, leads to a two-dimensional band structure. For $t_a \gg t_b$, and again using a linear dispersion in the x direction this dispersion relation reduces close to the Fermi energy to
(derive, maybe it is hot that hard?)

$$\epsilon(k) = \epsilon_0 + v_F \delta k - 2t_b \cos k_y b \tag{1.13}$$

with $\delta k = k - k_F$. The Fermi surface is determined by the condition

$$k_x = k_F + \frac{2t_b}{v_F} \cos k_y b + \mathcal{O}\left(t_b^2 \cos^2 k_y b\right) + \cdots \tag{1.14}$$

which leads to first the order in t_b (neglecting the third term in Eq. (1.14)), to a sinusoidal Fermi surface in the $k_x - k_y$ plane, as shown in Fig. 1.4.

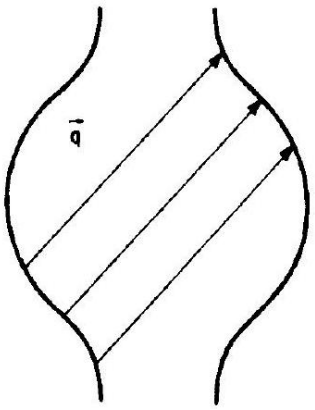


Figure 1.4. Fermi surface of a quasi-one-dimensional electron gas. The arrows indicate perfect nesting for small dispersion in one direction as discussed in the text. With increased dispersion, perfect nesting is no longer possible.

As for one dimension, we recover a large number of electron-like pairs with similar energies; and the condition for this now is given by the wavevector $\vec{Q} = (2k_F, \pi/b)$, as indicated in the figure. The response function $\chi(\vec{q})$ develops a singularity at $\vec{q} = \vec{Q}$, and in the two-dimensional phase space this corresponds to a periodic modulation, with a wavevector $q_{\|} = 2k_{\mathrm{f}}$ in the x direction. In the y direction $q_{\perp} = \pi/b$, and this corresponds to a situation where the modulation on the neighboring chains, separated by b, is out of phase.

Perfect nesting, as shown in Fig. 1.4, is obtained only in the limit when $t_b/t_a \to 0$, and is expected to be appropriate for materials with a substantial anisotropy of the single particle bandwidth. (??? think about it, I don't understand it yet)

With increasing t_b/t_a the last term in Eq. (1.14) becomes progressively more important and the nesting condition applies for a smaller number of electron-hole pairs. This leads to the gradual removal of the singularity of the response function at $q = 2k_k$.

At finite temperatures the numerator in $\chi(\vec{q}) = \int \frac{d\vec{k}}{(2\pi)^d} \frac{f_k - f_{k+q}}{\epsilon_k - \epsilon_{k+q}}$ is given by

$$\frac{1}{\exp(-\epsilon_k/k_BT)+1} - \frac{1}{\exp(\epsilon_k/k_BT)+1} = \tanh\frac{\epsilon_k}{2k_BT} \tag{1.15}$$

where ϵ_k is now measured from the Fermi energy ϵ_F. Then it becomes

$$\chi(q = 2k_F, T) = -e^2 n(\epsilon_F) \int_0^{\epsilon_0/2k_HT} \frac{\tanh x}{x} dx. \tag{1.16}$$

Here ϵ_0 is an arbitrarily chosen cutoff energy which is usually taken to be equal to the Fermi energy ϵ_F. The integral can be readily evaluated giving

$$\chi(2k_F, T) = -e^2 n(\epsilon_F) \ln\frac{1.14\epsilon_0}{k_BT}. \tag{1.17}$$

$\chi(2k_1)$ then has a logarithmic divergence as $T \to 0$. The response function can be evaluated for q values different from $2k_r$ and $\chi(q,T)$, obtained for various ϵ_0/k_BT values is displayed in Fig. 1.5.

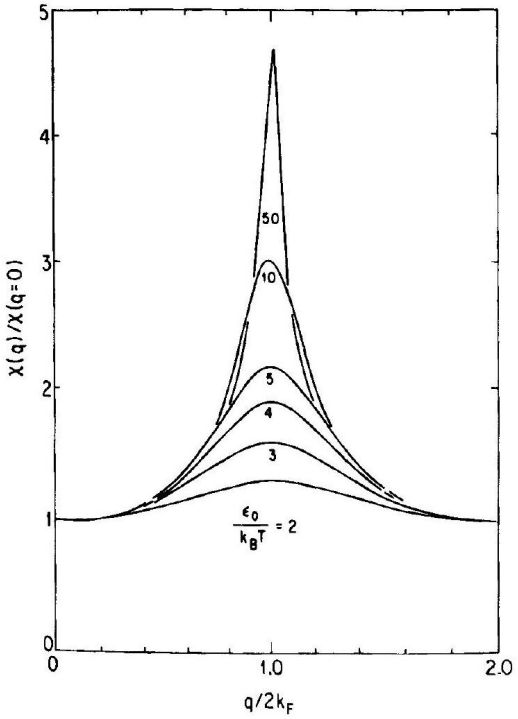


Figure 1.5. The response function of a one-dimensional free electron gas at various temperatures (after Heeger, 1979).

1.1.2 Instabilities in a One-Dimensional Electron Gas: g-ology

The divergent response function leads to various instabilities at low temperatures, and a simple mean field argument (which?) gives a finite transition temperature when this happens.

Without specifying the particular interaction let us assume that an external potential $\phi^{\text{ev}}(\dot{r})$ leads to a density fluctuation $\rho^{\text{nd}}(\vec{r})$, and therefore to a potential $\phi^{\text{ind}}(\vec{r})$ induced by $\rho^{\text{ind}}(\vec{r})$. This induced potential is assumed to have the form

$$\phi^{\text{ind}}(\vec{q}) = -g\rho^{\text{ind}}(\vec{q}), \tag{1.18}$$

where g is a coupling constant which is assumed to be independent of wavevector, and $\phi^{\text{ind}}(\vec{q})$ and $\rho^{\text{ind}}(\vec{q})$ are the Fourier components of the spatially dependent potential and density fluctuation. From Eq. (1.6)

$$\rho^{\text{ind}}(\vec{q}) = \chi(\vec{q})\phi(\vec{q}) = \chi(\vec{q})\left[\phi^{\text{ext}}(\vec{q}) + \phi^{\text{ind}}(\vec{q})\right] \tag{1.19}$$

and, together with Eq. (1.18), we obtain

$$\rho^{\text{ind}}(\vec{q}, T) = \frac{\chi(\vec{q}, T)\phi^{\text{ext}}(\vec{q})}{1 + g\chi(\vec{q}, T)}. \tag{1.20}$$

The above equation is suggestive of an instability for $g < 0$, which occurs when

$$1 + g\chi(\vec{q}, T) = 0 \tag{1.21}$$

Inserting the expression for $\chi(\vec{q}, T)$ from Eq. (1.17) into this expression, we obtain

$$1 + gn\left(\epsilon_F\right) \ln \frac{1.14\epsilon_0}{k_B T} = 0 \tag{1.22}$$

and the mean field transition temperature is given by

$$k_B T_{\text{MF}} = 1.14\epsilon_0 \exp\left(\frac{-1}{gn\left(\epsilon_F\right)}\right). \tag{1.23}$$

As will be discussed later, the density fluctuation $\rho^{\text{ind}}(\vec{q})$, reflects the formation of electron-electron or electron-hole pairs, with the ground state at $T = 0$ being a coherent superposition of the various pair states. The nature of the ground state depends on the electron-electron and electron-phonon interactions, which can be described by a q-dependent interaction potential $V(\vec{q})$.

The situation is particularly simple for a one-dimensional metal where the Fermi surface is two points at $\pm k_F$. (Solyom, 1979 and references cited therein; Emery, 1979). Electrons and holes on the right or left side are denoted by $e_+$and $e_-$and by $h_+$and h_-. With the spin degrees of freedom also included, four possibilities for pair formation may occur:

$e_+\sigma; e_-, -\sigma$	pairs with total momentum with total spin	$q = 0$
$e_+\sigma; e_-, \sigma$	pairs with	$S = 0$
		$q = 0$
$e_+\sigma; h_-\sigma$	pairs with	$q = 2k_F$
		$S = 0$
$e_+\sigma; h_-, -\sigma$	pairs with	$q = 2k_F$
		$S = 1$

The development of these states can be discussed using simple models with a mean field solution giving a finite transition temperature. However, as will be discussed later, the mean field solution is not appropriate in one dimension. Solutions of the models which go beyond the mean field treatment lie outside the scope of these notes (see, for example, Solyom, 1979). Consequently, only the main results will be stated here.

The first two of these states develop in response to interactions for which $q = 0$; this is called the particle-particle or Cooper channel. The resulting ground states are the well known (singlet or triplet) superconducting states of metals. The last two states, with a finite total momentum for the pairs, develop as a consequence of the divergence of the fluctuations at $q = 2k_F$; this is the particle-hole channel, usually called the Peierls channel. For these states we find a periodic variation of the charge density or spin density, and consequently, they are called the charge

density wave and spin density wave ground states. The period $\lambda_0 = \pi/k_F$ associated with the spatial variation of the charge or spin density

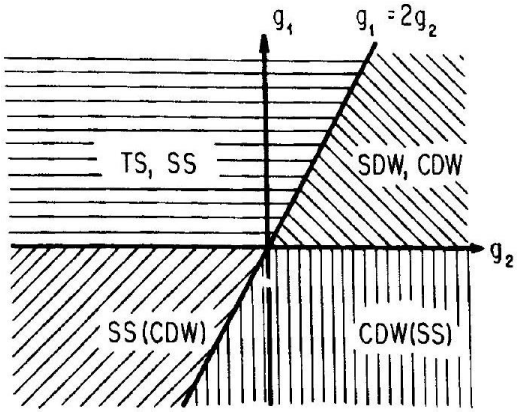


Figure 1.6. The phase diagram of the 1 D electron gas in the second order scaling approximation showing the most divergent type of fluctuations, for the coupling constants g_{1}, g_{2}. For the definition of the coupling constants and of the various ground states see the text and Solyom, 1979, and references cited therein.

also leads to a gap in the single particle excitation spectrum at the Fermi level. For an arbitrary band filling the period is incommensurate with the underlying lattice.

In 1 D the diagrammatic expansion of the Cooper channel contains contributions from the density fluctuations at $q = 2k_r$, and the density fluctuations also contain contributions from the $q = 0$ fluctuations (Solyom, 1979). Consequently, both the Cooper and Peierls response functions diverge at the same rate at low temperatures. Which of these states occurs depends on the detailed nature of electron-phonon and electron-electron interactions, and in one dimension the interaction can be represented as the combination of two coupling constants, g_1 and g_2; which represent the interactions with momentum transfer of $\pm 2k_F$ and zero, respectively. The occurrence of these states in the $g_1 - g_2$ phase space is shown in Fig. 1.6 and this so-called g-ology picture has been discussed in several reviews. Obviously a strictly onedimensional situation cannot occur in real materials even in compounds with rather highly anisotropic band structure, since
interchain interactions are also of importance. Systems which are composed of coupled chains have a phase diagram somewhat different from that shown in Fig. 1.6; but the four different ground states with features rather similar to those calculated for a purely one-dimensional band structure are still preserved for weak interchain coupling.

The various broken symmetry ground states have several common characteristics which are well known for the extensively studied superconducting state (see, for example, Schrieffer, 1963; Tinkham, 1975). For all condensates, the order parameter is complex, and can be written as

$$\Delta = |\Delta| e^{i\phi}. \tag{1.24}$$

For the superconducting ground states, gauge symmetry is broken; the phase is invariant under a gauge transformation. In contrast, for the density wave ground states, the translational symmetry is broken. While the time and spatial derivatives play an important role in the dynamics of the collective modes, the above difference between the superconducting and density wave ground states leads naturally to different collective excitations and also to differences in the coupling of the collective modes to applied electromagnetic fields. For the density wave ground states these collective excitations are called phasons and amplitudons, referring to fluctuations of the phase and amplitude of the condensate. For charge density waves, both occur below

the single particle gap, as will be discussed in Chapter 6 . In addition, in the spin density wave ground state (as in the triplet superconducting state), the spin rotational symmetry is also broken, leading to additional collective excitations, similar to those of conventional antiferromagnets. The features of the various broken symmetry states are summarized in Table 1.1.

The amplitude $|\Delta|$ is related to (or can be defined as) the single particle gap. In the case of electron-electron pairing this is the well known superconducting gap. In case of the density wave states, the gap occurs at $\pm k_F$. In the superconducting state, the collective mode leads to a supercurrent in response to *dc* fields. In the case of density waves, however, the collective mode does not contribute to the *dc* conduction (this is due to the interaction with impurities and lattice imperfections), and the appearance of a gap in the single particle excitation spectrum at the Fermi level

Table 1.1. Various broken symmetry ground states of one-dimensional metals. The Anderson-Higgs mechanism removes the low lying exitations in a singlet superconductor.

	Paring	Total Spin	Total Momentum	Broken Symmetry	Low Lying Collective Excitations
singlet superconductor	el-el	$S = 0$	$q = 0$	gauge	(AndersonHiggs)
triplet superconductor	el-el	$5 = 1$	$q = 0$	gauge	low lying magnetic excitations?
charge density wave	el-hole	$S = 0$	$q = 2k_r$	translational	phasons amplitudons
spin density wave	el-hole	$S = 1$	$q = 2k_1$	translational	phasons magnons

causes the material to become a semiconductor below the transition temperature.

The appearance of the single particle gap Δ also leads to a finite coherence length ξ_0, which corresponds to the spatial dimension of the electron-electron or electron-hole pairs. Crudely speaking, the pair wavefunctions are the superpositions of one electron state within the energy region around the Fermi level, and the corresponding spread of momenta is approximately

$$|\Delta| = \delta\left(\frac{p^2}{2m}\right) \simeq \hbar v_F \delta_p \tag{1.25}$$

where v_F is the Fermi velocity. This corresponds to a spatial range of $\xi_0 \simeq (\delta_p)^{-1} = \hbar v_F/\Delta$. The correct expression, the BCS coherence length, is given at zero temperature by (Schrieffer, 1964; Tinkham, 1975)

$$\xi_0 = \frac{\hbar v_F}{\pi|\Delta|}. \tag{1.26}$$

The temperature dependence of the order parameter and condensate density have the well known BCS form for all cases; and the gap is related to the mean field transition temperature, $T_{\rm MF}$, through the well known BCu relation $2|\Delta|(T = 0) = 3.52 k_{\rm B} T_{\rm MF}$ in the weak coupling limit. The condition when this limit applies is somewhat different for different ground states, as will be discussed later.

1.1.3 Correlations and Fluctuations

Because of the reduction of phase space, one-dimensional systems are unstable against fluctuations. These fluctuations lead to the absence of long range order at any finite temperature, and for $T \neq 0$ only short range correlations develop. The correlation length for models which involve the response of the electron gas to electron-phonon or electron-electron interactions, is related to the correlation length which characterizes the density fluctuations of the one-dimensional electron gas. These density fluctuations are described by the correlation function

$$\left\langle C^{\dagger}(\vec{r}), C(0)\right\rangle = \int \frac{d\vec{k}}{2\pi} f\left(\epsilon_k\right) e^{ik\cdot r} \tag{1.27}$$

where $C^{\dagger}$ and C are the creation and destruction operators of the electron density. The spatial dependence is approximately given by

$$\left\langle C^{\dagger}(\vec{r}), C(0)\right\rangle = \exp\left[\frac{|\vec{r}-\vec{r'}|}{\xi} + i\vec{q}\cdot\vec{r}\right] \tag{1.27a}$$

where ξ is the correlation length associated with the density fluctuations. For a one-dimensional metal, with a linear dispersion relation $\epsilon_k - \epsilon_F = \hbar v_F\left(k - k_F\right)$ as shown in Fig. 1.1,

$$\begin{aligned}\left\langle C^{\dagger}(\vec{r}), C(0)\right\rangle &= \int \frac{dk}{2\pi} \frac{e^{ikx}}{e^{\beta v_f|k-k_f|}+1} \\ &= \frac{ie^{ik_f x}}{-\beta v_F} \sum_{j=0}^{x} e^{-\pi(2)+1x/\beta v_f} \\ &= \frac{ie^{ik_F x}}{-\beta v_F} \frac{e^{-\pi x/\beta v_f}}{e^{-2\pi x/\beta v_f}+1}\end{aligned} \tag{1.28}$$

where $\beta = (k_B T)^{-1}$, and using Eq. (1.27a) the correlation length

$$\xi = \frac{\hbar v_F}{\pi k_{\mathrm{B}} T} \tag{1.29}$$

diverges as the temperature approaches $T = 0$. (think about why is it so??? I don't understand it now)

As will be discussed later, at low temperatures the collective excitations of the density wave states are described by the Hamil-
tonian

$$\mathscr{H} = A\int (\nabla\phi)^2 d\vec{r} = \int d^{\|}\vec{k}\,|\phi_k|^2\,k^2 \tag{1.30}$$

in dimension d where ϕ is the phase of the condensate and A is the elastic constant associated with the long wavelength deformations of the condensate. The thermal expectation value of the component $|\phi_k|^2$ is

$$\left\langle|\phi_k|^2\right\rangle = \frac{\left|d\phi_k \exp\left(-\frac{k^2|\phi_k|^2}{k_B T}\right)\right| \phi_k\Big|^2}{\int d\phi_k \exp\left(-\frac{k^2|\phi_k|^2}{k_B T}\right)} \tag{1.31}$$

which, after factorization becomes approximately

$$\left\langle|\phi_k|^2\right\rangle = \frac{k_R T}{k^2}. \tag{1.32}$$

Let us look at the correlation function which describes the spatial fluctuations of the phase variable. In the limit when the amplitude of the order parameter is close to its $T = 0$ value, the correlation function looks like

$$\left\langle\Delta^*(\vec{r})_1\Delta(0)\right\rangle = |\Delta_0|^2 \exp -\frac{1}{2}\left\langle[\phi(\vec{r}) - \phi(0)]^2\right\rangle \tag{1.33}$$

the term in the exponent,

$$\left\langle [\phi(\vec{r}) - \phi(0)]^2 \right\rangle = \int_k d^d\vec{k} \left\langle |\phi_k \right|^2 \Big\rangle \left(e^{\prime k} r - 1\right)^2 \tag{1.34}$$
$$= k_R T \int \frac{d^d\vec{k}}{k^2} \left(e^{\prime k} r' - 1\right)^2$$

The integral diverges for $d \leq 2$, and therefore there is no long range order at any finite temperature.

The argument advanced here is essentially the same as the argument for the absence of long range order for a Heisenberg antiferromagnet, and is due to the existence of low lying, gapless collective modes. If these excitations develop a gap (and this would occur for a commensurate density wave, as will be discussed in Chapter 7) long range order is restored. Arguments, aralogous to those applied for the Ising model (Ziman, 1964) apply for this latter situation and there is no long range order for $d \leq 1$ at finite temperatures.

1.2 Materials

(interesting section, but for experimenters, I'll look later)

A large number of organic and inorganic solids have crystal structures in which the fundamental structural units form linear chains. While most of these materials are insulators or semiconductors; several groups have partially filled electron bands, and consequently display metallic behavior at high temperatures.

The greatly different overlap of the electronic wave functions in the various crystallographic directions leads to strongly anisotropic, so-called quasi-one-dimensional electron bands discussed in the previous chapter. This is the prerequisite for the development of the instabilities at $q = 2k_k$. Among the different materials which display a variety of phase transitions, only the simplest examples of density wave formation will be discussed, where the charge or spin density wave fluctuations develop along identical chains and, subsequently, the interaction between the chains leads to a three-dimensional ordered ground state. The partially filled electron bands, where the number of electrons per site is not a simple fractional number (eg., $1/2, 1/3$, etc.), lead to density wave instabilities where the period $\lambda_0 = \pi/k_F$ of the density waves is incommensurate with the underlying lattice (for which the fundamental period is the lattice constant a). Materials with two-dimensional band structures (and consequently with 2D density wave ground states) will not be discussed. Materials which are composed of two or more different metallic chains (consequently displaying a variety of subtle instabilities) also lie outside the scope of this discussion.

While probably a coincidence, among the various compounds with a single conducting chain, inorganic linear chain compounds have been found to be examples of charge density wave condensates; while several groups of organic materials have been observed to develop a spin density wave ground state. In both cases a broad variety of experiments have been conducted to explore the normal state properties, with a focus on the parameters which characterize the single particle electron states, on the anisotropy, and on the strength of the electron-electron and electron-phonon interactions.

The crystal structures are in general complex. Several reviews listed in the Appendix discuss the structural properties of the various groups of linear chain materials in detail. Therefore only the basic features of the structural arrangements will be summarized here, with emphasis on the resulting electronic structure of these types of materials.

Because of the strong anisotropy, in many cases the bandwidths in the directions perpendicular to the chains are smaller than, or comparable to, the thermal energy $k_B T$ at room

temperature (or at temperatures above the density wave transition). Thus, expressions appropriate for a 1D electron gas can be used to evaluate parameters such as the Fermi energy ϵ_F, the Fermi velocity v_F, and the bandmass m_b, which can be extracted by using various experimentally accessible quantities. For a 1D band structure

$$k_F = \frac{\pi n}{a}; \quad v_F = \frac{\hbar k_F}{m_b} = \frac{\hbar n \pi}{a m_b} \tag{2.1}$$

where n is the number of electrons per unit cell and per spin direction. (The unit cell in one-dimension is given by the lattice constant a.) Deviations from the free electron behavior are usually included by assuming a bandmass m_b which is different from the free electron mass m_c. In the above equation n refers to the number of electrons for the 1D electron band, and is given by
$n = N_c a$, the total number of electrons per unit volume is given by $n_0 = N_c n_\perp$, with $n_\perp$ being the number of chains per unit area. Then, the density of states $n(\epsilon_F)$ for each spin direction is related to ϵ_F by

$$n(\epsilon_F) = \frac{N_c}{4\epsilon_F} = \frac{n}{4a\epsilon_F}. \tag{2.2}$$

In general, n (or N_e, the number of electrons per unit length) can be derived from electron counting arguments, as well as from the measured period $\lambda_0 = \pi/k_F$ of the density wave. If available from experiments, the plasma frequency

$$\omega_p = \left(\frac{4\pi n e^2}{m_b}\right)^{1/2} \tag{2.3}$$

can then be used to evaluate the bandmass. With n and m_b known, Eqs. (2.1) and (2.2) can be used to determine the Fermi energy ϵ_F.

The magnetic susceptibility

$$\chi_p = g^2 \mu_B^2 n(\epsilon_F) = g^2 \frac{\mu_B^2 N_F}{2\epsilon_F} = g^2 \frac{\mu_B^2 n}{2a\epsilon_F} \tag{2.4}$$

where g is the gyromagnetic factor and μ_B the Bohr magneton, can also be used; (where does this formula come from??)

together with k_F as obtained from the calculated band filling or from the period λ_0 of the measured lattice distortion, to derive the same parameters. Broadly speaking as electron-electron interactions lead to an enhancement of the magnetic susceptibility while ω_p does not reflect these interactions, the comparison of the two sets of parameters may also shed light on the importance of these interactions.

The above equations are based on a nearly free electron approach; a tight binding description is also often used to extract parameters such as the Fermi energy ϵ_F and Fermi velocity v_F from the measured quantities (how? a separate big question).

The two approaches lead to somewhat different values for the Fermi energy, Fermi velocity, and density of states. These differences, however, are not essential, particularly when one is interested only in the gross overall features of the phase transitions, and in the approximate values of the parameters which characterize the various broken symmetry ground states.

The expressions in Eqs. (2.1) and (2.2) which lead to the Fermi energy and Fermi velocity from measured quantities such as ω_p and χ are obviously appropriate only for a strictly 1D electron band, and should consequently be used only for a rather anisotropic bandwidth. This

anisotropy can be estimated by using the measured anisotropy of the *dc* electrical conductivity σ_{dc}, and crude arguments (Jerome and Schultz, 1982) lead to

$$\frac{\sigma_{\parallel}}{\sigma_{\perp}} = \left(\frac{v_{F\parallel}}{v_{F\perp}}\right)^2 \tag{2.5}$$

where $v_{F\parallel}$ and $v_{F\perp}$ are the Fermi velocities alon $_T$ and perpendicular to the chain direction.

The anisotropy of the optical reflectivity, in particular the anisotropic plasma frequency (if it exists in both directions), has also been used to assess the magnitude of the anisotropy of these materials.(how?? sounds like a special methods for experimenters)

1.2.1 Inorganic Linear Chain Compounds

A variety of inorganic materials have strongly anisotropic crystal, and consequently strongly anisotropic electronic structures; which often display various transitions from metallic to non-metallic states. Among the many groups of such materials, three have been explored in detail and these materials are by now well established examples of the charge density wave ground state.

2.1.1 Mixed Valence Platinum Chain Compounds

Platinum chain complexes are composed of a columnar array of units which incorporate a chain of Pt atoms with strongly overlapping *d* orbitals. Although a considerable number of compounds of such structure are known, most of the experiments have been performed on the material $K_2Pt(CN)_4Br_{0.3} \cdot 3.2H_2O$, usually called simply KCP or Krogmann's salt. The schematic crystal structure of this material is shown in Fig. 2.1. It consists of a columnar stacked array of $Pt(CN)_4$ units, with a rather short Pt-Pt separation of 2.894Å along the chain direction. The distance between the chains in 9.89Å leading to a strongly anisotropic separation between the Pt atoms in the different directions. The water molecules form a hydrogen-bonded material between the

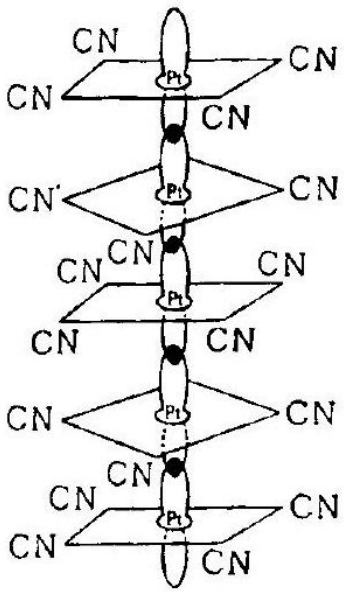


Figure 2.1. The crystal structure of the compound $\mathrm{K}{{2} \mathrm{Pt}(\mathrm{CN})}{4} \mathrm{Br}{{03} \cdot 3.2 \mathrm{H}}{2} \mathrm{O}$, called KCP, or Krogmann's salt.

CN^-ligands and the K^+ions provide a cross-link between the $Pt(CN)_4$ chains.

The $K_2^{2+}[Pt(CN)_4]^{2-}H_2O$ configuration has a full valency Pt^{2-} and consequently this material would be a semiconductor. The Br counterions remove electrons from the $Pt(CN)_4$ unit, and the resulting fractional charge $Pt^{17}(CN)_4$ leads to a partially filled electron band, the prerequisite for metallic behavior.

Indeed, the material is highly conducting at room temperature, with a conductivity along the chain direction of $\sigma_1 \sim 10^2\Omega^{-1}\text{cm}^{-1}$ (Carneiro, 1988). The conductivity is also highly anisotropic, and the ratio of the conductivities measured along and perpendicular to the chains is $\sigma_\parallel/\sigma_\perp \sim 10^5$. This anisotropy is also clearly evident in the optical properties (Bruesh et al., 1975; Geserich, 1988), and the reflectivity measured in the two different directions is displayed in Fig. 2.2. For $E\|c$, the optical conductivity is well described by the usual Drude form

$$\sigma(\omega) = \frac{\sigma_{dc}}{1 - i\omega\tau} = \frac{\omega_p^2\tau}{2\pi}\frac{1}{(1 - i\omega\tau)} \tag{2.6}$$

with a plasma frequency of $\omega_p = 2.9\text{eV}$ and a relaxation time of $\tau = 3 \times 10^{-15}\text{sec}$. The band filling of 1.7/2el = 0.85, obtained from charge transfer arguments as discussed before, gives a band-

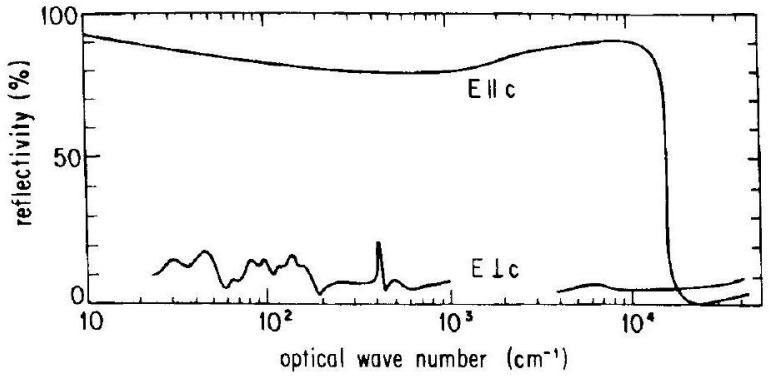


Figure 2.2. The optical conductivity of $\mathrm{K}_{2}\mathrm{Pt}(\mathrm{CN})_{4}\mathrm{Br}_{0.3}\cdot 3.2\mathrm{H}_{2}\mathrm{O}$ measured both parallel and perpendicular to the chain direction at room temperature (after Geserich, 1988); c refers to the chain direction.

mass of $m_p \simeq 1.0m_c$ as expected for strongly overlapping Pt orbitals forming wide conduction bands. This relatively wide electron band along the chain direction also follows from the small Pauli susceptibility measured at room temperature or above (Scott et al., 1979). These magnetic measurements also indicate that electron-electron interactions do not play an important role in these materials.

2.1.2 Transition Metalchalcogenides, MX_3 and $(MX_4)_n$ Y

Group IV or V transition metals, Nb or Ta , when combined with chalcogen atoms, S or Se , form a variety of linear chain compounds, several of which have partially filled electron bands and thus metallic behavior at high temperatures. (Rouxel and Schlenker, 1989; Meerschaut and Rouxel, 1976).

The basic constituent of the structure is a triangular prism of MX_6 units, with a cross-section close to an isosceles triangle as shown in Fig. 2.3. The transition metal atom (indicated by the solid circle in the figure) is located roughly at the center of the prism. The prisms are stacked on top of each other by sharing the triangular faces along the b-axis, and the chains are

staggered with respect to each other by half the height of the unit prism. Therefore, besides the six chalcogen atoms of an MX_6 prism, each transition metal is bonded to two more X atoms from neighbor-

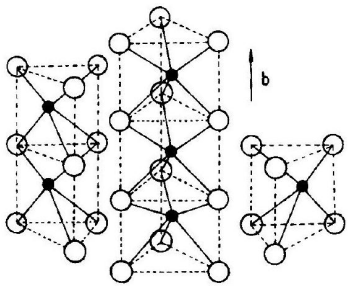


Figure 2.3. The schematic chain structure of the MX_{3} compounds. The M atoms are located roughly at the center of trigonal prisms built of atoms X.

ing chains, and its coordination number is eight. Various chains in the crystal structure have slightly different geometrical configurations, and the number of different chains varies from compound to compound. In $NbSe_3$ and TaS_3 three different chains are observed. The latter compound also occurs in two different crystallographic (monoclinic and orthorhombic) modifications.

In these compounds, the transition metal atoms have an electron configuration $4d^3 5s^1$ and some of the chalcogen atoms form covalently bonded pairs. The electron configuration can schematically be written as

$$3MX_3 = 2M^{5+}M^{4+}\left(X^{2-}\right)_5\left(X_2^{2-}\right)_2$$

which is suggestive of a quarter filled electron band involving the dorbitals of the transition metal atoms.

The schematic crystal structure of the tetrachalcogenides $(MX_4)_n Y$ with M = Ta or Nb, X = S or Se , and Y = I, Br or Cl is displayed in Fig. 2.4. (Gressier et al., 1984). Each transition metal (indicated by the solid circle on the figure) is coordinated to eight Se atoms (open circles) in a slightly distorted rectangular antiprismatic arrangement. Some of the materials undergo structural distortions (unrelated to CDW formation), but in the compounds $(TaSe_4)_2\,I$ and $(NbSe_4)_2\,I$ such distortions do not occur and these materials are relatively good metals at high temperatures. Al-

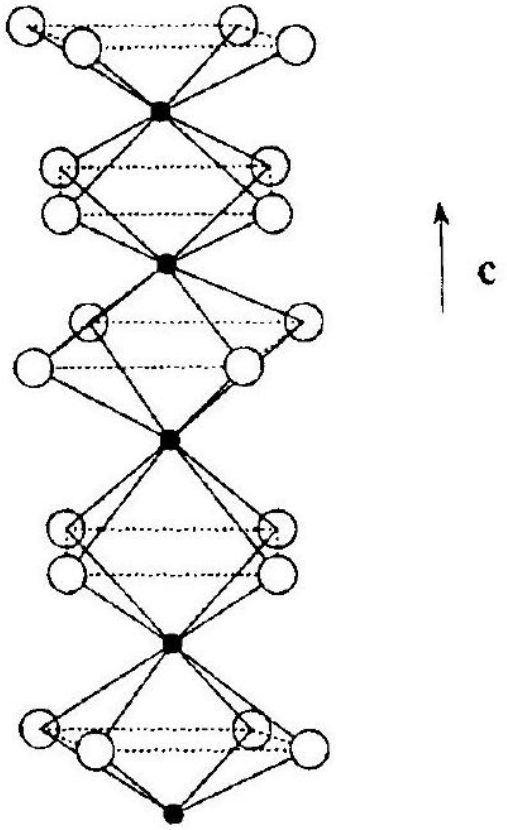


Figure 2.4. The schematic chain structure of the $\left(\mathrm{MX}{{4}\right)}{2} \mathrm{Y}$ compounds.

though the former compound may be formulated as $Ta^{4+}Ta^{5+}4\,[Se_2]^{2-}\,I$ from charge neutrality arguments, all $Ta-Ta$ distances are found to be identical (3.206Å) along the chain and the electron band is quarter filled; the same applies to the Nb compound. The Se atoms lie in planes approximately perpendicular to the c-axis (which is the chain direction in this case). These planes (separated by $c/4$) develop in a helicoidal way along the c-axis. The chains of $TaSe_4$ are parallel to the c direction and are well separated by the I atoms. The materials are relatively good metals along the chain direction with room temperature conductivities parallel to the chains, $\sigma_{\|}$, on the order of $10^3 - 10^4\Omega^{-1}\mathrm{cm}^{-1}$. The conductivity perpendicular to the chains is 10 to 10^3 times smaller, suggesting that the anisotropy of the bandwidth is substantial.

2.1.3 Transition Metal Bronzes

The term bronze is applied to a variety of crystalline phases of the transition metal oxides. Examples are the ternary molybdenum oxides of formula $A_{0.3}MoO_3$, where the alkali metal A can be K ,

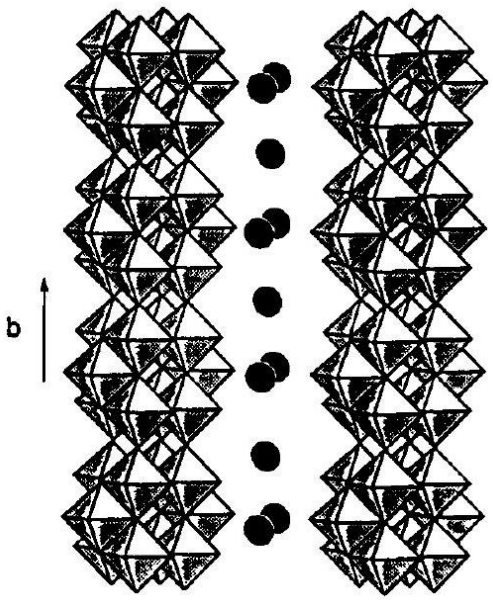


Figure 2.5. The schematic structure of $\mathrm{K}{\{0} \mathrm{MoO}}{3}$.

Ro cr Tl. They are often referred to as blue bronzes because of their deep blue color (Schlenker and Dumas, 1986).

The structure of $A_{0.3}MoO_3$ contains rigid units comprised of clusters of ten distorted MoO_6 octahedra, sharing corners along the monoclinic b-axis, as illustrated in Fig. 2.5. This corner sharing provides an easy path for the conduction electrons along the chain direction. The chains of distorted MoO_6 octahedra also share corners along the [102] direction and form infinite slabs separated by the alkaline cations.

The band structure, calculated for a slab of $Mo_{10}O_{30}$ clusters is fairly complicated (Whangboo and Schneemeyer, 1986), but such calculations give two overlapping bands at the Fermi level, both approximately 3/4 filled. This, as will be discussed in Chapter 3, is in agreement with the lattice distortion observed in the charge density wave state of the material. The Fermi surface has a pronounced two-dimensional character in this compound as evidenced by dc conductivity and optical studies. At room temperature, the conductivity measured along the chain direction is $\sigma_b = 3 \times 10^2 \Omega^{-1}$ cm^{-1}. In the two perpendicular directions the conductivity is $\sigma_{2a-c} = 10\Omega^{-1}$ cm^{-1} and $\sigma_{2a+\iota} = 0.5\Omega^{-1}$ cm^{-1}. The crude argument which gives Eq. (2.5) then leads to an

Table 2.1 Metallic state parameters of materials with a charge density wave ground state. The electron density n (not displayed) has been derived from the band filling and from crystal structure parameters. When two values are indicated, the upper is derived from the magnetic susceptibility and the lower from the plasma frequency.

	Band filling	$\chi\left(10^{-6}\frac{\text{emu}}{\text{cm}^3}\right)$	ω_p (eV)	m_b/m_c	ϵ_F (eV)	$v_F\,(10^7\text{cm/sec})$
$NbSe_3$	1/4	0.97		1.8	0.11	1.4
(ref. 1,5)			1.15	4.1	0.048	0.65
$K_{0.3}MoO_3$	3/4	0.55		1.54	0.24	2.3
(ref. 2, 6, 8)			2.7	0.94	0.39	3.8
$(TaSe_4)_2\,I$	0.85	0.12		0.24	0.68	9.9
(ref. 3, 6, 9)			1.2	2.8	0.059	0.87
KCP	0.85					
(ref. 4,5,7)			2.9	1.0	0.82	5.37
	$n\,(\epsilon_\text{F})$ (eV^{-1})	ω_{2k_1} (eV)				
$NbSe_3$ (ref. 1,5)	2.3					
	5.2					
$K_{0.3}MoO_3$	3.1					
(ref. 2,6)						
$(TaSe_4)_2\,I$	1.3					
(ref. 3,6)	14.4					
(ref. 4,5,7)	1.0	8×10^{-3} (ref. 9)				

1. H. P. Geserich, et al. Physica 143B, 174 (1986).
2. G. Travaglini and P. Wachter, Solid State Comm. 37, 599 (1981).
3. H. P. Geserich, et al. Physica 143B, 198 (1986).
4. P. Bruesh, et al. Phys. Rev. B12, 219 (1975).
5. J. C. Scott, et al. Phys. Rev. B10, 3131 (1979).
6. D. Johnston, et al. Solid State Comm. 53, 5 (1985).
7. K. Carneiro, et al. Phys. Rev. B13, 4758 (1976).
8. J. P. Pouget and P. Comes, In "Charge Density Waves in Solids" Eds. L. P. Gor'kov and G. Grüner, North Holland 1987.
9. S. Sugai, Physica 143B, 195 (1986). H. Fujishita, et al. Physica 143B, 201 (1986). anisotropy of the Fermi velocity of approximately 6 and approximately 25 for the two perpendicular directions. This has also been confirmed by optical studies (Travaglini et al., 1981).

The parameters of the single particle bands which occur along the chain directions are summarized in Table 2.1. In all cases the strong overlap of the wavefunctions leads to wide bands, with bandwidths significantly larger than the energy scale which, as will be discussed in Chapter 3, corresponds to the single particle gaps associated with the formation of the charge density wave ground state. The relatively low Pauli susceptibility also indicates that electron-electron interactions are small in these materials.

Because of the complicated crystal structures, the phonon spectrum of these materials is also fairly complicated. Which of the phonon modes couples to the electronic degrees of freedom is ultimately determined by neutron scattering experiments. The unrenormalized phonon frequency $\omega(2k_F)$ for the wavevector $q = 2k_F$ can be estimated from these experiments, and the various values are also displayed in Table 2.1.

1.2.2 Organic Linear Chain Compounds

Planar organic molecules often form linear chains with large overlap of the π orbitals along the chain direction. When combined with counterions or molecules, the resulting charge transfer salts may have partially filled bands leading to metallic properties. Some members of three groups of materials, based on the organic molecules M shown in Fig. 2.6 and having the composition MX_2, also develop a spin density wave ground state at low temperatures as established by a wide range of magnetic measurements.

The crystal structure of the material (tetramethyltetraselenafulvalene) PF_6, (TMTSF) PF_6, one member of the so-called Bechgaard salts (Bechgaard et al., 1980), is shown in Fig. 2.7. The material is built up of segregated stacks of TMTSF and PF_6 molecules. The structures of the compounds based on the MDTTTF and DMET molecules have the same basic features. All three molecules shown in Fig. 2.6 are good donors; and when combined with strong acceptors such as PF_6 and similar species, a charge transfer occurs from the M stacks to the X stacks. For a full charge transfer the M stacks become 3/4 filled. There is a

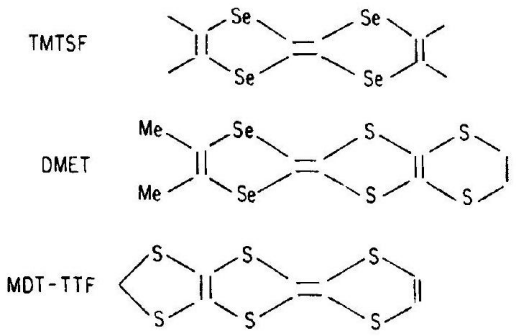


Figure 2.6. Planar organic acceptor molecules which form metallic charge transfer salts, and which undergo a transition to a spin density wave ground state at low temperatures. Me refers to methyl groups and the open ended lines to H .

significant overlap of electronic wavefunctions on the M stacks, with practically no overlap along the X stacks; consequently, band theory predicts metallic behavior along the chains. The materials which belong to the different groups do indeed show metallic conduction down to low temperatures, as shown in Fig. 2.8 (Bechgaard et al., 1980). The increase of resistivity at low temperatures is due to the removal of the Fermi surface upon the formation of the spin density wave ground state, as will be discussed in Chapter 4. The optical properties of (TMTSF) $_2PF_6$ are that of a Drude metal (Jacobsen et al., 1983), with high reflectivity R along the chain direction ($E \| a$), as shown in Fig. 2.8. In contrast, perpendicular to the chains ($E \| b$) nonmetallic reflectivity is observed at high temperatures. From the analysis of the optical properties the plasma frequencies can be extracted and these parameters, together with electron concentration, are displayed in Table 2.2. The magnetic susceptibility is of the Pauli type (Jerome and Schultz, 1982) and is weakly temperature dependent down to low temperatures where the phase transition occurs. The parameters ω_p and χ can then be used, together with the free electron expressions for these parameters, to extract the parameters which

characterize the single particle states, Fermi velocity v_F, Fermi energy ϵ_F, and the density of states $n(\epsilon_F)$.

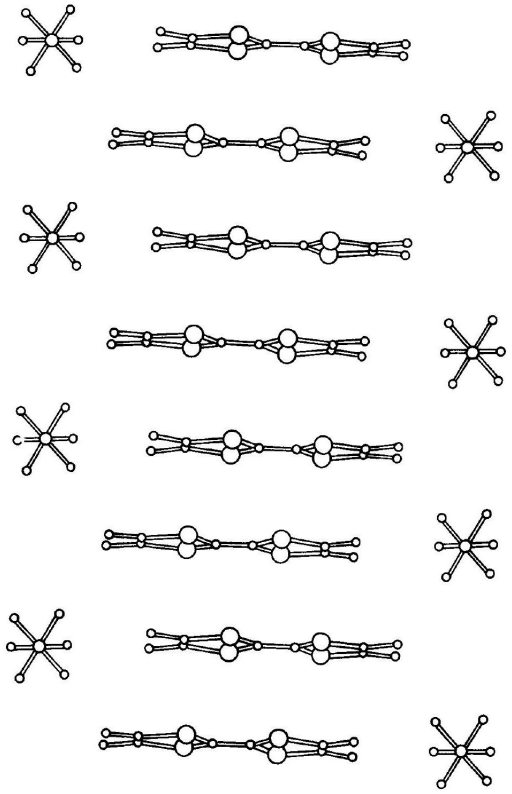


Figure 2.7. The schematic crystal structure of (tetramethyltetraselenafulvalene) $\mathrm{PF}{{6},\left(\mathrm{TMTSF}}{2} \mathrm{PF}_{6}\right.$.

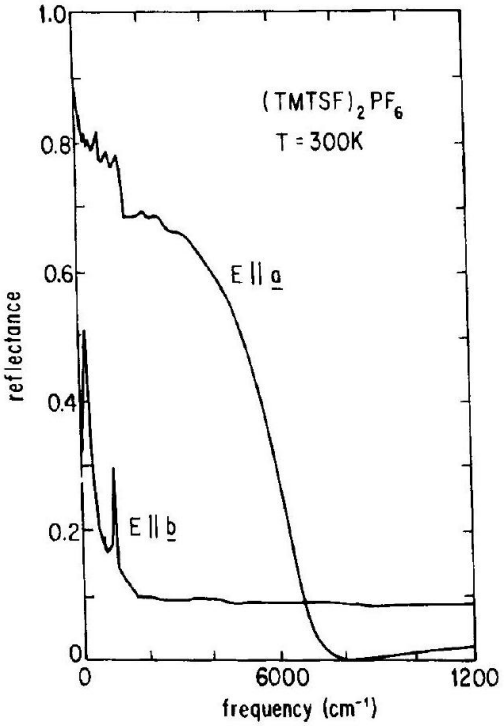


Figure 2.8. Optical reflectance of (TMTSF) PF_{6}, measured both parallel and perpendicular to the chain direction at room temperature; a refers to the chain direction and b is perpendicular to the chains. (Jacobsen et al., 1982).

The electrical conductivity is also highly anisotropic in these materials. The *dc* conductivity σ_{dc} measured perpendicular to the chain direction is usually small, indicating a transfer integral less than k_BT, the thermal energy. This then suggests a monmetallic, hopping type of electrical conduction along these directions. As discussed, this conclusion is supported by the optical reflectivity measured perpendicular to the chains. While the reflectivity for $E\|b$ does not show a well defined plasma edge, such a feature appears at low temperatures, indicating a crossover to an anisotropic but three-dimensional band structure, with the bandwidth larger than k_BT in both directions. From these studies,

Table 2.2 Parameters of the metallic state of two materials with a spin density wave ground state. The electron density has been evaluated from the band filling and crystal structure parameters.

	Band filling	$\chi\left(10^{-6}\frac{\text{emu}}{\text{cm}^3}\right)$	ω_p (eV)	m_b/m_c	ϵ_1 (eV)
(TMTSF) $_2$PF$_6$	1/4	0.58 (ref. 1)	2.9 (ref. 2)	1.3	6.1×10^{-2}
(DMET)$_2$Au(CN)$_2$	1/4	0.51 (ref. 3)		2.4	6.6×10^{-2}
	$v_F\left(10^7\frac{\text{cm}}{\text{sec}}\right)$	$n\left(\epsilon_r\right)$ (eV^1)			
	0.86	0.25			
(TMTSF) $_2$PF$_6$(DMET)$_2$Au(CN)$_2$	1.0	0.26			

1. K. Mortensen, et al., Phys. Rev. B25, 3319 (1982), D. Jerome and H. Schultz, Adv. Phys. 32, 299 (1982).

2. A Jacobsen, et al., Phys. Rev. B28, 7019 (1983).
[9] K. Kanoda, et al., Phys. Rev. B38, 39 (1988).
bandwidths of 2.5 meV and 1 meV are inferred for the two perpendicular directions, in contrast to the bandwidth along the TMTSF stacks which is on the order of 0.25 eV (Jerome and Schultz, 1982).

Members of other groups of organic linear chain compounds have also been found to develop a spin density wave ground state. The organic salts, (MDT-TTF) $_2$ X, where MDT-TTF stands for methilendithio-tetrathiafulvanele (shown in Fig. 2.6) have a metallic character for various counterions, and one member of the group, (MDT-TTF) $_2$Au(CN)$_2$, has a spin density wave transition at $T = 20$ K (Nakamura et al., 1990). This material, along with other members of the group, has a linear chain structure formed by MDT-TTF stacks with strongly overlapping orbitals in the stack direction. This then leads to a strongly anisotropic single particle band.

The molecule dimethylethylenedithio-diselenadithia-fulvalene, DMET also forms various charge transfer salts with different counterions and the composition is (DMET) $_2$X (Kikuchi et al., 1987; Kanoda et al., 1988). Some members of this family are
semiconductors while others remain metals to low temperatures where they undergo transitions to various broken symmetry states. In the compound (DMET) $_2$Au(CN)$_2$ the ground state is a spin density wave which develops at $T = 20$ K where a metal-toinsulator transition occurs with decreasing temperatures.

Optical studies have not been performed on these latter two groups of compounds, and magnetic susceptibility has only been measured in a few cases. Consequently, the parameters of the metallic band can be established only in a few cases and these are summarized in Table 2.2.

1.3 The Charge Density Wave Transition and Ground State: Mean Field Theory and Some Basic Observations

The charge density wave ground state develops in low-dimensional metals as a consequence of electron-phonon interactions. As the name suggests, the resulting ground state consists of a periodic charge density modulation accompanied by a periodic lattice distortion, both periods being determined by the Fermi wavevector k_F. Consequently both the electron and phonon spectra are strongly modified by the formation of the charge density waves. The phenomenon is usually described by discussing the behavior of a one-dimensional coupled electron-lattice system, with the electrons forming a one-dimensional electron gas, and the ions forming a linear chain. This description is adopted here.

The consequence of the electron-phonon interaction and of the divergent electronic response at $q = 2k_F$ in one dimension is a strongly renormalized phonon spectrum generally referred to as the Kohn anomaly (see Woll and Kohn, 1962 and references cited therein). By virtue of $\chi(q, T)$ this renormalization is strongly temperature-dependent, with $\omega_{\text{ren}\,,2k_i} \to 0$ at a finite temperature (within the framework of mean field theory). This identifies a phase transition to a state where a periodic static lattice distortion and a periodically varying charge modulation with a wavelength $\lambda_0 = \pi/k_F$ develops.

For a partially filled electron band, the period λ_0 is incommensurate with the underlying lattice. The periodically varying
lattice distortion leads in turn to a single particle gap at the Fermi level, turning the material into an insulator. The transition is generally referred to as the Peierls transition, since this was first suggested by Peierls (1955); the thermodynamics of the ground state have been worked out by Kuper (1955). Independently, Fröhlich (1954) suggested that the ground state can, under the influence of an applied electric field, carry an electric current. Hence the state is also often referred to as the Peierls-FröhlichKuper ground state.

In this chapter we first consider the effects of electron-phonon interactions for a one-dimensional electron gas and describe the Kohn anomaly for $T > T_{\mathrm{CIW}}^{\mathrm{MF}}$, the mean field transition temperature. This is followed by a discussion of the state of affairs at $T = 0$, described within the framework of a weak coupling theory. As will be discussed, in the weak coupling limit, where the single particle gap is much smaller than the Fermi energy ϵ_F, the thermodynamics of the phase transition and the temperature dependence of the order parameter are the same as those of a BCS superconductor, and extensive use of the expressions worked out for the superconducting state will be made when finite temperature effects are discussed.

The most important experimental evidence for these phenomena will be discussed next, including observations of the metal-to-insulator transition which occurs at T_{CDW} , the Kohn anomaly above T_{CDW}, the single particle gap, and the periodic lattice distortion below the phase transition.

It should be stressed at this point that serious deviations from the mean field treatment are expected because of the low-dimensional character of the materials in which the formation of charge density waves have been observed and also because of the relatively short coherence lengths which result from the high transition temperatures. These effects are related to fluctuations of the order parameter and will be discussed in Chapter 5.

1.3.1 The Kohn Anomaiy and the Peierls Transition: Mean Field Theory

In order to describe the transition to a charge density wave ground state let us consider a one-dimensional free electron gas coupled to the underlying chain of ions through electron-phonon coupling. The Hamiltonian for the electron gas is given in second quantized form as

$$\mathscr{H}_{\mathrm{el}} = \sum_k \epsilon_k a_k^\dagger a_k \tag{3.1}$$

where $a_k^\dagger$ and a_k are the creation and annihilation operators for the electron states with energy $\epsilon_k = \hbar^2 k^2/2m$. The formalism is similar if a tight binding approximation is used, however, this leads to numerical constants which are somewhat different from those which follow from the free electron approximation (Allender et al., 1974). Because spin dependent interactions are not important in the following discussion, the spin degrees of freedom are omitted and the density of states $n(\epsilon_F)$ refers to one spin direction.

The lattice vibrations are described by the Hamiltonian

$$\mathscr{H}_{ph} = \sum_q \left\{ \frac{P_q P_{-q}}{2M} + \frac{M\omega_q^2}{2} Q_q Q_{-q} \right\} \tag{3.2}$$

where Q_q and P_q are the normal coordinates and conjugate state momenta of the ionic motions respectively, ω_π are the normal mode frequencies, and M is the ionic mass. With the notation

$$\begin{aligned} Q_q &= \left(\frac{\hbar}{2M\omega_q}\right)^{1/2} \left(b_q + b_{-q}^\dagger\right) \\ P_q &= \left(\frac{\hbar M\omega_q}{2}\right)^{1/2} \left(b_q^\dagger - b_{-q}\right) \end{aligned} \tag{3.3}$$

the Hamiltonian is written as

$$\mathscr{H}_{\text{ph}} = \sum_q \hbar\omega_q \left(b_q^\dagger b_q + \frac{1}{2} \right) \tag{3.4}$$

where $b_q^\dagger$ and b_q are the creation and annihilation operators for phonons characterized by the wavevector q. In terms of these operators the lattice displacement is given by

$$u(x) = \sum_q \left(\frac{\hbar}{2NM\omega_q} \right)^{1/2} \left(b_q + b_{-q}^\dagger \right) e^{tqx} \tag{3.5}$$

where N is the number of lattice sites per unit length.

The description of the electron-phonon interaction is usually referred to as a rigid ion approximation: it is assumed that the ionic potential V at any point depends only on the distance from the center of the ion. In second quantized notation

$$\begin{aligned} \mathscr{H}_{el-ph} &= \sum_{h,k',1} \langle k|V(r-1-u)\,|k'\rangle\, a_k^\dagger a_{k'} \\ &= \sum_{h,k',1} e^{u(k'-k)(l+u)} V_{k-k'} a_k^\dagger a_{k'} \end{aligned} \tag{3.6}$$

where $V_h k'$ is the Fourier transform of the potential of a single atom $V(r), l$ gives the equilibrium lattice positions, and u is the displacement from the equilibrium position. For sufficiently small ionic displacement

$$c''^{k'} km = 1 + i\,(k'-k)\,u = 1 + iN'1/2\,(k'-k) \sum_i c''^q u_{iq} \tag{3.7}$$

The Hamiltonian, $\mathscr{H}_{\text{el - ph}}$, then has two parts. The first describes the interaction of the electrons with the underlying ions in their non-displaced positions. This term transforms the free electron spectrum into Bloch states, leading to gaps at the Brillouin zone edge. This term, will be neglected as we are interested in effects which occur at k_F, which is assumed to be away from the Brillouin zone boundaries. The second term is given by

$$\begin{aligned} \mathscr{H}_{el-ph} &= iN^{1/2} \sum_{k,k',l,q} e^{i(k'-k+q)}\,(k'-k)\,u_q V_{k-k'} a_k^\dagger a_{k'} \\ &= iN^{1/2} \sum_{k,k'} (k'-k)\,u_{k-k'} V_{k-k'} a_k^\dagger a_{k'} \end{aligned} \tag{3.8}$$

In terms of the phonon creation and annihilation operators, this interaction term becomes

$$\begin{aligned} \mathscr{H}_{\text{cl-ph}} &= i \sum_{k,k'} \left(\frac{\hbar}{2M\omega_{k-k'}} \right)^{1/2} (k'-k)\, V_{k-k'} \left(b_{k'-k}^\dagger + b_{k-k'} \right) a_{k'}^\dagger a_{k'} \\ &= \sum_{k,q} g_q \left(b_{-q}^\dagger + b_q \right) a_{k+q}^\dagger a_k \end{aligned} \tag{3.9}$$

where the electron-phonon coupling constant is

$$g_q = i \left(\frac{\hbar}{2M\omega_q} \right)^{1/2} |q| V_q. \tag{3.10}$$

With all the terms collected, the Hamiltonian, often called the Fröhlich Hamiltonian (Fröhlich, 1954), is written as

$$\mathscr{H} = \sum_k \epsilon_k a_k^\dagger a_k + \sum_q \hbar\omega_q b_q^\dagger b_q + \sum_{k,q} g_q a_{k+q}^\dagger a_k \left(b_{-q}^\dagger + b_q\right). \tag{3.11}$$

In the case of a 1 D electron gas, for which the dispersion relation is described by $\epsilon_k = \hbar v_F (k - k_T) = \pm v_F \delta k$ near $\pm k_I$ (see Fig. 2.1), (with the energy measured from the Fermi energy ϵ_F) the coupled electron-phonon system is unstable, and this instability has fundamental consequences for both the lattice and the electron gas.

The effect of the electron-phonon interaction on the lattice vibrations can be described by establishing the equation of motion of the normal coordinates. For small amplitude displacements

$$\hbar^2 \ddot{Q}_q = -\left[\left[Q_q, \mathscr{H}\right], \mathscr{H}\right] \tag{3.12}$$

(don't know such method yet..)

where $\ddot{Q}_q$ refers to the second time derivative of the coordinate. The above equation, utilizing the commutation relations

$$[Q_{q'}, P_{q'}] = i\hbar\delta_{q,q'} \tag{3.13}$$

becomes

$$\ddot{Q}_q = -\omega_q^2 Q_q - g\left(\frac{2\omega_q}{M\hbar}\right)^{1/2} \rho_q \tag{3.14}$$

where we have assumed that g is independent of q, and $\rho_q = \sum_k a_{k+q}^\dagger a_k$ is the q^{th} component of the electronic density. The second term on the right hand side is an effective force associated with the lattice dynamics and arises as a consequence of electron-phonon interactions. The ionic potential $g\left(2M\omega_q/\hbar\right)^{1/2} Q_q$ gives, through Eq. (1.6), a density fluctuation

$$\rho_q = \chi(q,T) g \left(\frac{2M\omega_q}{\hbar}\right)^{1/2} \mathrm{Q}_q \tag{3.15}$$

and with this mean field approximation Eq. (3.14) reads

$$Q_q = -\left[\omega_q^2 + \frac{2g^2\omega_{iq}}{M\hbar} x(q,T)\right] Q_q. \tag{316}$$

The above equation of motion gives a renormalized phonon frequency

$$\omega_{\text{ren. } q}^2 = \omega_q^2 + \frac{2g^2\omega_q}{\hbar}\chi(q,T). \tag{3.17}$$

As discussed in Chapter 1, for a one-dimensional electron gas $\chi(q,T)$ has its maximum value at $q = 2k_F$. Consequently, the reduction, or softening, of the phonon frequencies will be most significant at these wavevectors. The phonon frequency for $q = 2k$, becomes

$$\omega_{\text{ren},2k_1}^2 = \omega_{2k_1}^2 - \frac{2g^2 n\left(\epsilon_1\right)\omega_{2k_{\text{f}}}}{\hbar} \ln\left(\frac{1.14\epsilon_0}{k_B T}\right) \tag{3.18}$$

With decreasing temperature, the renormalized phonon frequency goes to zero and this defines a transition temperature, when a frozen-in distortion occurs. From Eq. (3.18)

$$k_B T_{\text{COW}}^{\text{MF}} = 1.14\epsilon_0 e^{-1/\lambda} \tag{3.19}$$

where λ is the dimensionless electron-phonon coupling constant

$$\lambda = \frac{g^2 n\left(\epsilon_\Gamma\right)}{\hbar\omega_{2k_1}} = g' n\left(\epsilon_F\right). \tag{3.20}$$

Close to the transition temperature a straightforward expansion gives the following temperature dependence

$$\omega_{\mathrm{ren},2k_1} = \omega_{2k_f}\left(\frac{T - T_{\mathrm{CDW}}^{\mathrm{MF}}}{T_{\mathrm{CDW}}^{\mathrm{MF}}}\right)^{1/2} \tag{3.21}$$

The phonon dispersion relation $\omega_{\mathrm{ren}\,,q}$, as determined by Eq. (3.17), is shown in Fig, 3.1 at various temperatures above the mean field transition temperature. This dispersion relation can be calculated by using the expression for $\chi\left(q = 2k_F, T\right)$ as given by Eq. (1.10). The detailed form, as expected, also depends on the phonon dispersion relation, and in Fig. 3.1 the situation appropriate for the renormalization of an acoustic phonon branch at various temperatures is displayed.

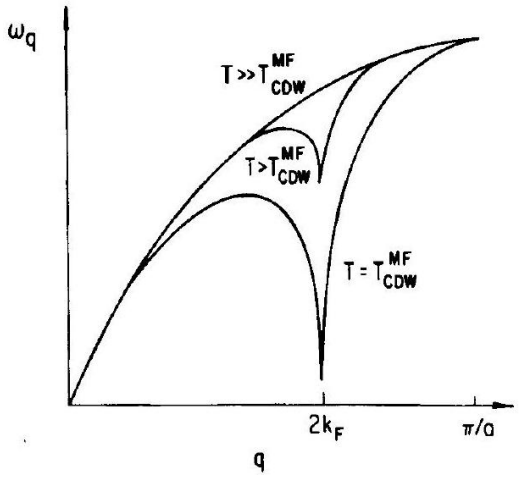


Figure 3.1. Acoustic phonon dispersion relation of a one-dimensional metal at various temperatures above the mean field transition temperature.

As discussed earlier, the phase transition is defined by the temperature where $\omega_{\mathrm{ren}\,,2k_F} \to 0$ and is due to the strongly divergent response function of the 1 D electron gas. The renormalization of the phonon frequencies also occurs in higher dimensions, however the reduction of the phonon frequencies is less significant. Expressions for $\chi(q,T)$ appropriate for a 2D and 3D electron gas can also be used to evaluate the renormalized phonon frequencies and these are shown, together with the 1D case, in Fig. 3.2. For the higher dimensions, the temperature dependence of $\chi(q,T)$ is weak, and for small electron-phonon coupling constants $\boldsymbol{\omega}_{\mathrm{ren}\,,q}$ remains finite at $T = 0$ and there is no phase transition.

Below the phase transition, the renormalized phonon frequency is zero, indicating a "frozen-in" lattice distortion, that is, a macroscopically occupied phonon mode with nonvanishing expectation values $\langle b_{2k_F}\rangle = \left\langle b^\dagger_{-2k_F}\right\rangle$. The order parameter is defined as

$$|\Delta| e^{i\phi} = g\left(\langle b_{2k_I}\rangle + \left\langle b^\dagger_{-2k_F}\right\rangle\right) \tag{3.22}$$

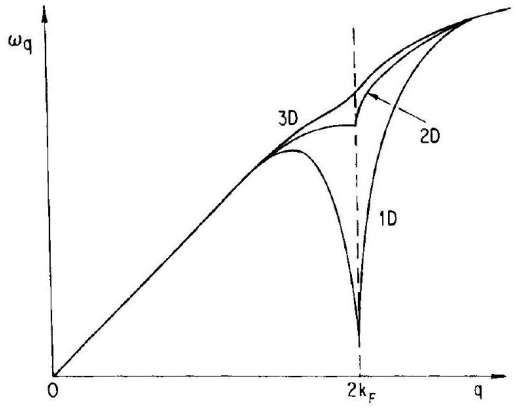


Figure 3.2. Acoustic phonon dispersion relations of one-, two-, and threedimensional metals.

and from Eq. (3.5) the lattice displacement is given by

$$\begin{aligned}\langle u(x)\rangle &= \left(\frac{\hbar}{2NM\omega_{2k_i}}\right)^{1/2}\left\{i\left(\langle b_{2k_i}\rangle + \left\langle b^{+}2k_i\right\rangle\right)e^{i2k_i} + c.c.\right\}\\ &= \left(\frac{\hbar}{2NM\omega_{2k_f}}\right)^{1/2}\frac{2|\Delta|}{g}\cos\left(2k_i x+\phi\right)\\ &= \Delta u\cos\left(2k_F x+\phi\right)\end{aligned} \tag{3.23}$$

with

$$\Delta u = \left(\frac{2\hbar}{NM\omega_{2k_r}}\right)^{1/2}\frac{|\Delta|}{g}.$$

With this mean field approximation Eq. (3.11) becomes

$$\mathscr{H} = \sum_k \epsilon_k a_k^\dagger a_k + \sum_q \hbar\omega_q\left\langle b_q^\dagger b_q\right\rangle + \sum_{k,q} g a_{k+q}^\dagger a_k\left\langle b_{-q}^\dagger + b_q\right\rangle \tag{3.24}$$

where $q = \pm 2k_F$. As $\langle b_{2k_t}\rangle = \left\langle b_{-2k_F}^\dagger\right\rangle$, the Hamiltonian becomes

$$\begin{aligned}\mathscr{H} = &\sum_k \epsilon_k a_k^\dagger a_k + 2g\sum_k\left[a_{k+2k_k}^\dagger a_k\left\langle b_{-2k_j}^\dagger\right\rangle\right.\\ &\left.+a_{k-2k_F}^\dagger a_k\left\langle b_{-2k_k}\right\rangle\right] + 2\hbar\omega_{2k_F}\left\langle b_{2k_F}\right\rangle^2\end{aligned} \tag{3.25}$$

With the order parameter defined in (3.22) the electronic part becomes

$$\mathscr{H}_{el} = \sum_k\left[\epsilon_k a_k^\dagger a_k + |\Delta|e^{i\phi}a_{k+2k}^\dagger, a_k + |\Delta|e^{-i\phi}a_{k-2k}^\dagger, a_k\right]. \tag{3.26}$$

In the spirit of the nearly free electron approximation we consider only states near the Fermi level, and states near $+k_F$ and near $-k_F$ are labelled by the subscripts 1 and 2 respectively. With this notation and using the dispersion relation $\varepsilon_k = \hbar v_\Gamma\left(k - k_F\right)$, Eq. (3.26) becomes

$$\begin{aligned}\mathscr{H} = &\sum_k\left[\epsilon_k\left(a_{1,k}^\dagger a_{1,k} - a_{2,k}^\dagger a_{2,k}\right)\right.\\ &\left.+|\Delta|e^{i\phi}a_{1,k}^\dagger a_{2,k} + |\Delta|e^{-i\phi}a_{2,k}^\dagger a_{1,k}\right].\end{aligned} \tag{3.27}$$

Here and in the following, k is measured relative to the Fermi wavevector k_F. The Hamiltonian can be diagonalized by a canonical transformation. We define a new set of operators by

$$\gamma_{1,k} = U_k a_{1,k} - V_k^* a_{2,k} = U_k e^{-i\phi/2} a_{1,k} - V_k e^{i\phi/2} a_{2,k} \tag{3.28a}$$

$$\gamma_{2,k} = V_k a_{1,k} + U_k^* a_{2,k} = V_k e^{-i\phi/2} a_{1,k} + U_k e^{i\phi/2} a_{2,k} \tag{3.28b}$$

with the constraint that $U_k^2 + V_k^2 = 1$. After some algebra, Eq. (3.27) in terms of $\gamma_{1,k}$ and $\gamma_{2,k}$, becomes

$$\begin{aligned}\mathscr{H} = \sum_k &\left[\epsilon_k \left(U_k^2 - V_k^2\right) - 2|\Delta| U_k V_k\right] \left(\gamma_{i,k}^\dagger \gamma_{i,k} - \gamma_{2,k}^\dagger \gamma_{2,k}\right) \\ &+ \left[2\epsilon_k U_k V_k + |\Delta| \left(U_k^2 - V_k^2\right)\right] \left(\gamma_{1,k}^\dagger \gamma_{2,k} + \gamma_{2,k}^\dagger \gamma_{1,k}\right)\end{aligned} \tag{3.29}$$

The Hamiltonian is diagonalized if the coefficients in front of the off-diagonal terms are zero; for example,

$$2\epsilon_k U_k V_k + |\Delta| \left(U_k^2 - V_k^2\right) = 0. \tag{3.30}$$

The condition $U_k^2 + V_k^2 = 1$ is satisfied if we choose

$$V_h = \cos\left(\frac{\theta_k}{2}\right) \tag{3.31a}$$

$$U_h = \sin\left(\frac{\theta_k}{2}\right) \tag{3.31b}$$

and then (3.30) becomes

$$\tan\theta_h = -\frac{|\Delta|}{\epsilon_h} \tag{3.32}$$

From (3.32) and (3.31) we obtain

$$V_k^2 = \frac{1}{2}\left(1 - \frac{\epsilon_k}{\left(\epsilon_k^2\right)^{1/2}}\right) = \frac{1}{2}\left(1 + \frac{\epsilon_k}{E_k}\right) \tag{3.33a}$$

$$V_k^2 = \frac{1}{2}\left(1 - \frac{\epsilon_k}{E_k}\right) \tag{3.3.3b}$$

with

$$E_h = \epsilon_l + \text{sign}\,(k - k_F)\left[\hbar^2 v_l^2 \left(k - k_F\right)^2 + \Delta^2\right]^{1/2} \tag{3.34}$$

Upon substitution of the expressions for U_k and V_k, Eq. (3.29) becomes

$$\mathscr{H} = \sum_k E_k \left(\gamma_{1,k}^+ \gamma_{1,k} + \gamma_{2,k}^+ \gamma_{2k}\right) + \frac{\hbar\omega_{2k}\Delta^2}{2g^2}. \tag{3.35}$$

Instead of the linear dispersion relation $\epsilon_k - \epsilon_\text{F} = \hbar v_f \left(k - k_F\right)$ appropriate for the metallic state the spectrum of excitations develops a gap in the charge density wave state, and the dispersion relation is shown in Fig. 3.3. The density of states is obtained from the condition

$$N_{\mathrm{CDW}}(E)dE = N_r(\epsilon)d\epsilon = N_r d\epsilon \tag{3.36}$$

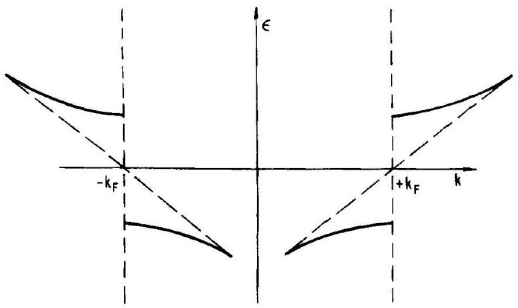


Figure 3.3. The dispersion relation for ϵ_{k} (dashed line) and E_k (full line) near the Fermi wavevectors $\pm k_1$.

assuming that the density of states in the metallic state, $N_c(\epsilon) = N_c$ is independent of the energy. With this assumption

$$\frac{N_{\mathrm{COW}}(E)}{N_e} = \frac{d\epsilon}{dE} = \begin{cases} 0 & |E| < \Delta \\ \frac{E}{(E^2-\Delta^2)^{1/2}} & |E| > \Delta \end{cases} \tag{3.37}$$

The density of states diverges as the gap is approached from below ($E < \epsilon_F$) or from above ($E > \epsilon_F$). The total number of states is the same in the normal and charge density wave states, and the increase of $N_{\mathrm{CDW}}\,(E)$ near Δ is due to the removal of the density of states within the region of the single particle gap. Both N_{CDW} and $N_e(\epsilon)$, which is assumed to be constant, are shown in Fig. 3.4.

The magnitude of the gap is obtained by minimizing the energy of Eq. (3.35). The opening of the gap leads to the lowering of the electronic energy, this is given by

$$E_{\mathrm{el}} = \sum_k \left(-E_k + v_F k\right) = n\left(\epsilon_F\right) \int_0^{\epsilon_F} \left(\epsilon - \left(\epsilon^2 + \Delta^2\right)^{1/2}\right) d\epsilon \tag{3.38}$$

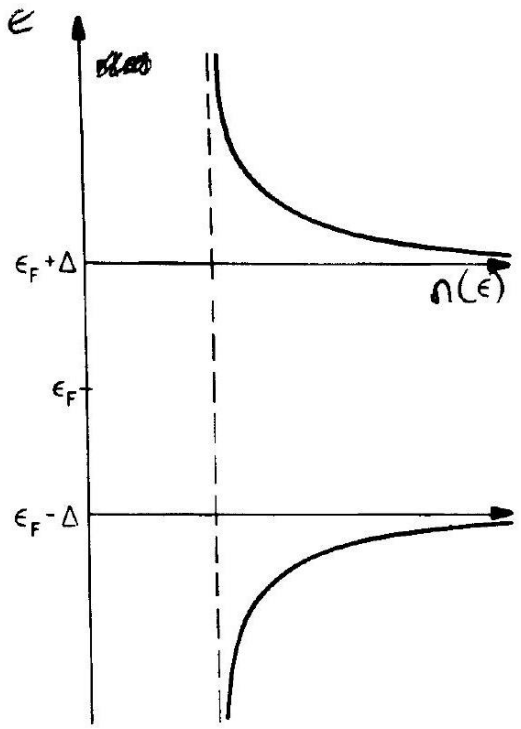


Figure 3.4. The energy dependence of the density of states near $\pm k_{1}$ in the metaliic (dashed line) and in the charge density wave (full line) states.

which after some algebra becomes

$$E_{\mathrm{cl1}} = \frac{n(\epsilon_F)}{2}\left\{\epsilon_F^2 - \left[\epsilon_r\left(\epsilon_F^2+\Delta^2\right)^{1/2} + \Delta^2 \log\frac{\epsilon_F + \left(\epsilon_F^2+\Delta^2\right)^{1/2}}{\Delta}\right]\right\}. \tag{3.39}$$

In the weak coupling limit ($\epsilon_F \gg \Delta$) the expansion of the log term gives

$$E_{\mathrm{cl}} = n(\epsilon_{\mathrm{F}})\left[-\frac{\Delta^2}{2} - \Delta^2 \log\left(\frac{2\epsilon_r}{\Delta}\right)\right] + \mathrm{O}\left(\frac{\Delta}{\epsilon_r}\right)\Bigg]. \tag{3.40}$$

The lattice distortion leads to an increase in the elastic energy, given by

$$E_{\mathrm{latt}} = \frac{N}{2} M\omega_{2k}^2 \langle u(x)\rangle^2 \tag{3.41}$$

which, with Eq. (3.23), becomes

$$E_{\mathrm{latt}} = \frac{\hbar\omega_{2k_i}\Delta^2}{2g^2} = \frac{\Delta^2 n(\epsilon_F)}{\lambda}, \tag{3.42}$$

where λ is the dimensionless coupling constant defined in Eq. (3.20). The total energy change is given by the two terms

$$E_{\mathrm{tot}} = E_{\mathrm{cl}} + E_{\mathrm{latf}} = n(\epsilon_i)\left[-\frac{\Delta^2}{2} - \Delta^2 \log\left(\frac{2\epsilon_I}{\Delta}\right) + \frac{\Delta^2}{2\lambda}\right]. \tag{3.4.3}$$

Straightforward minimization of the total energy leads, for $\lambda \ll 1$, to

$$\Delta = 2\epsilon_F e^{-1/\lambda} \tag{3.44}$$

and to the condensation energy

$$E_{\text{con}} = E_{\text{normal}} - E_{\text{CDW}} = \frac{n(\epsilon_F)}{2}\Delta^2. \tag{3.45}$$

The positive sign indicates that the CDW ground state has, in 1D, lower energy than the normal state. A comparison with Eq. (3.19) leads to

$$2\Delta = 3.52 k_B T_{\text{CDW}}^{\text{MF}}, \tag{3.46}$$

the well known BCS relation between the zero temperature gap and the transition temperature.

The ground state wave function

$$\begin{aligned} |\phi_0\rangle &= \left(\prod_{|k|<k_t} \gamma_{1,k}^\dagger \gamma_{2,k}^\dagger \right) |0\rangle \\ &= \prod_{|k|<k_t} \left(U_k e^{i\phi/2} a_{1,k}^\dagger - V_k e^{-i\phi/2} a_{2,k}^\dagger \right) \\ &\quad \times \left(V_k e^{i\phi/2} a_{1,k}^\dagger + U_k e^{-i\phi/2} a_{2,k}^\dagger \right) |0\rangle \end{aligned} \tag{3.47}$$

where $|0\rangle$ represents the vacuum. The electronic density is

$$\rho(x) = \langle \phi_0 | \, \Psi^*(x)\Psi(x) \, |\phi_0\rangle \tag{3.48}$$

where

$$\Psi(x) = \sum_k \left(a_{1,k} e^{i,k} + a_{2,k} e^{i,k,2} \right). \tag{3.49}$$

Substituting the operators $\gamma_{1,4}$ and $\gamma_{2,4}$ from Eq. (3.28) and using the relations

$$\langle \phi_0 | \, \gamma_{2,h}^\dagger \gamma_{2,h} \, |\phi_0\rangle = \langle \phi_0 | \, \gamma_{1,h}^\dagger \gamma_{1,h} \, |\phi_0\rangle = 1 \tag{3.50a}$$

$$\langle \phi_0 | \, \gamma_{1,h}^\dagger \gamma_{2,k} \, |\phi_0\rangle = \langle \phi_0 | \, \gamma_{2,h}^\dagger \gamma_{1,h} \, |\phi_0\rangle = 0 \tag{3.50b}$$

straightforward algebra gives

$$\rho(x) = \sum_k \left[U_k^2 + V_k^2 - U_k V_k e^{(2h_k)+(\$)} - V_k U_k e^{(2h_k)+(\$)} \right] \tag{3.51}$$

where U_k and V_k are given in Γq. (3.33). Integration over the occupied states leads, in the weak coupling limit, to a periodic charge density variation:

$$\rho(x) = \rho_0 \left[1 + \frac{\Delta}{\hbar v_l k_F \lambda} \cos(2k_F x + \phi) \right] \tag{3.52}$$

where ρ_0 is the (constant) electronic density in the metallic state. The dispersion relation, the electronic density, and the equilibrium lattice positions are shown, both above $T_{\text{CDW}}^{\text{MF}}$ and at $T = 0$ in Fig. 3.5. (For the purpose of demonstration of what happens, a half-filled band is shown on the figure. For this special case, $\lambda_0 = 2a$ and the density wave is not

incommensurate with the underlying lattice. These so-called commensurability effects will be discussed in Chapter 7.) The ground state exhibits a periodic modulation of the charge density and a lattice distortion (hence the name charge density wave state) and the single particle excitations have a gap Δ at the Fermi level. This turns the material into an insulator (if the condensate does not contribute to the electrical conduction) upon the formation of the charge density wave ground state. The period $\lambda_0 = \pi/k_F$ is incommensurate with the underlying lattice for an arbitrary band filling. In this case, the condensation entrgy, Eq. (3.45), is independent of the phase variable ϕ and this has important consequences both in terms of the collective excitations and of the response of the charge density wave to external *dc* and *ac* electromagnetic fields. Commensurability effects which lead to a position-dependent

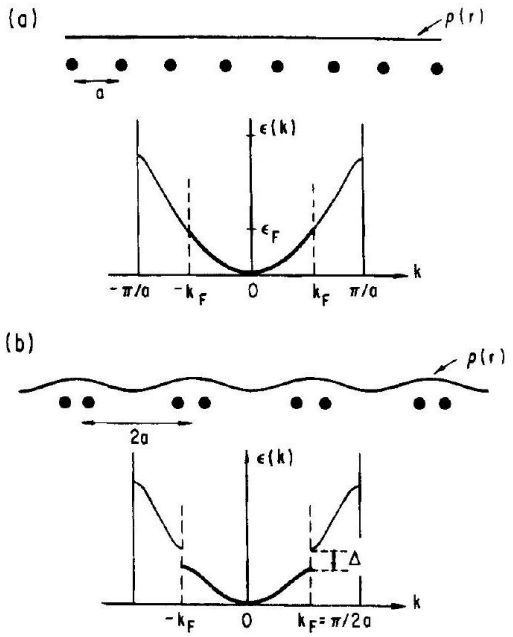


Figure 3.5. The single particle band, electron density, and lattice distortion in the metallic state above T_{CDW} and in the charge density wave state at $T = 0$. The figure is appropriate for a half-filled band.

condensation energy are neglected here; they will be discussed in Chapter 7. The above discussion of the charge density wave state has been at temperature $T = 0$. At finite temperature, thermally induced transitions across the gap lead to the screening of the electron-phonon interaction, to the reduction of the energy gain by the gap, and eventually to a phase transition. This can be discussed considering Eq. (3.17) which reads

$$\omega_{2k_f} = -\frac{2g^2}{\hbar}\chi\left(2k_F, T\right) \tag{3.53}$$

for $\omega_{\mathrm{ren},2k_f} = 0$. Because of the single particle gap, the response function $\chi(q,T)$ is different from that of a metallic one-dimensional band. Using arguments similar to those which lead to $\chi(q)$
as given by Eq. (1.17) we obtain

$$x\left(2k_F, T\right) = -n\left(\epsilon_l\right)\int_0^{\epsilon_{ll}} \tanh\left(\frac{\epsilon_k}{2k_BT}\right)\frac{d\epsilon_k}{\left(\epsilon_k^2\right)^{1/2}} \tag{3.54}$$

where ϵ_0 is a cutoff energy. With this response function, Eq. (3.18) reads (by setting $\omega_{\mathrm{ren},2k_1} = 0$ and using Eq. (3.20) for the coupling constant)

$$\frac{1}{\lambda} = \int_0^{\epsilon_0} \tanh\left(\frac{\epsilon_k}{2k_BT}\right) \frac{d\epsilon_k}{\left(\epsilon_k^2 + \Delta^2\right)^{1/2}}, \tag{3.55}$$

the same equation which describes the temperature dependence of the superconducting gap within the framework of the BCS theory (see for example, Schrieffer, 1964; Tinkham, 1975). Consequently, formulas worked out for superconductors can be used to describe the temperature dependences of various quantities in the charge density wave state. The temperature dependences of the order parameter $|\Delta(T)|$ and the condensate density $f(T)$ are the same as the temperature dependences which are given by the BCS theory. The former is determined by Eq. (3.55). At temperatures well below $T_{CDW}^{\rm MF}$ the temperature variation of $|\Delta|$ is weak, as only a small number of quasiparticles are excited across the single particle gap. Close to T_{CDW}^{MF}, where the gap approaches zero as $T \to T_{\rm CDW}^{\rm MF}$ from below, Eq. (3.19) reduces to

$$\frac{|\Delta(T)|}{|\Delta(0)|} = 1.74\left(1 - \frac{T}{T_{\rm CDW}^{\rm MF}}\right)^{1/2}. \tag{3.56}$$

The condensate density depends on the frequency and wavevector (Rice et al., 1979; Maki and Virosztek, 1990). In the static ($\omega \ll v_F q$) limit it is given by the relation

$$f(T) = |\Delta|^2 \pi T \sum_{\omega_n} \left(\omega_{in}^2 + \Delta^2\right)^{-3/2} \tag{3.57a}$$

and in the opposite, so-called dynamic limit ($\omega \gg v_\Gamma q$)

$$f_d(T) = |\Delta|^2 \int_\Delta^x dE \frac{\tanh\left(E/2k_BT\right)}{\left(E^2 - \Delta^2\right)^{1/2} E^2} \tag{3.57b}$$

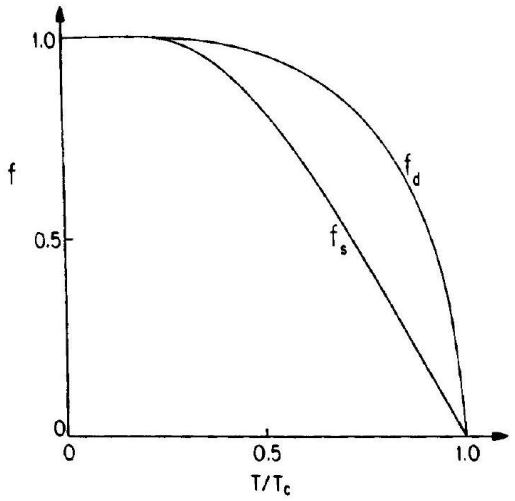


Figure 3.6. Temperature dependence of the static and dynamic condensate density as given by Eqs. (3.57a) and (3.57b).

As $T \to 0$, both f_s and $f_d \to 1$, and close to the transition temperature

$$\begin{aligned} f_s(T) &\simeq 2\left(1 - \frac{T}{T_{\rm CDW}^{\rm MF}}\right) \\ f_d(T) &= \frac{\pi}{4}\frac{|\Delta(T)|}{T_{\rm CDW}^{\rm MF}}. \end{aligned} \tag{3.58}$$

The temperature dependences of the two parameters are together with $\Delta(T)$ and $\omega_{\text{ren}}(T)$ displayed in Fig. 3.6 and Fig. 3.7.

The behaviors of the various thermodynamic quantities are the same as those of a superconductor. The specific heat is exponentially small at low temperatures, while at T_{CDW} there is a finite discontinuity, given by

$$\Delta C = n(\epsilon_F)\left(-\frac{d\Delta^2}{dT}\right) \tag{3.59}$$

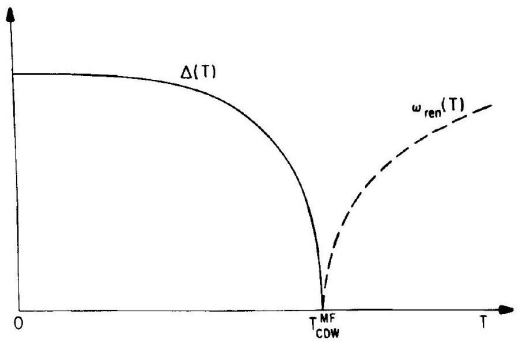


Figure 3.7. The temperature dependence of the renormalized phonon frequency ω_{ren}, 2 k$, for $T > T_{\text{COW}}^{\text{MF}}$ and the temperature dependence of the magnitude of the single particle gap $|\Delta|$ for $T < T_{\text{COW}}^{\text{MF}}$.

leading to

$$\Delta C = \frac{\pi^2 T_{\text{CDW}}^{\text{MF}} n(\epsilon_F) k_B^2}{7\zeta(3)} = 1.438\gamma_c T_{\text{CDW}}^{\text{MF}} k_B^2 n(\epsilon_F) \tag{3.60}$$

in the weak coupling limit. Here $\gamma_e = 2\pi^2/3n(\epsilon_F)k_B^2$ is the linear specific heat coefficient of the electron gas and $\zeta(3) = 1.202$ is the Riemann zeta function.

As usual, the behavior near the transition temperature can be discussed using the Landau theory of phase transitions. The functional form of the free energy is chosen to be

$$F = F(0) + n(\epsilon_F)\int dx\left\{a|\Delta|^2 + b|\Delta|^4 + \cdots\right\} \tag{3.61}$$

With $a = a_1(T - T_{\text{CDW}})$ and $b = \text{const}$, the temperature dependent order parameter is obtained from the equilibrium condition

$$\frac{\partial F}{\partial \Delta} = 0.$$

This, together with Eq. (3.61), leads to $|\Delta| = 0$ above the transition temperature, while for $T < T_{\text{CDW}}^{\text{MF}}$

$$|\Delta(T)| = \left(\frac{a_1}{2b}\right)^{1/2}\left(T_{\text{CDW}}^{\text{MF}} - T\right)^{1/2} \tag{3.62a}$$

which is identical to Eq. (3.56) if

$$\left(\frac{a_1}{8b}\right)^{1/2} = 1.74|\Delta(T=0)| \tag{3.62b}$$

The specific heat jump at the transition is

$$\Delta C = \frac{a_1^2 n\left(\epsilon_F\right)}{2bT_{\mathrm{CDW}}^{\mathrm{MF}}} \tag{3.63a}$$

which, by comparison to Eq. (3.60), leads to the following relation

$$\frac{a_1^2}{2bT_{\mathrm{CDW}}^{\mathrm{MF}}} = \frac{8\pi^2 T_{\mathrm{CDW}}^{\mathrm{MF}}}{7\zeta(3)} \tag{3.63b}$$

From Eqs. (3.62a) and (3.63a) the coefficients of the GinzburgLandau theory are given in terms of the microscopic parameters as

$$a = \frac{T}{T_{\mathrm{CDW}}^{\mathrm{MF}}}; \quad a_1 = \frac{1}{T_{\mathrm{CDW}}^{\mathrm{MF}}} \tag{3.64}$$

and

$$b = \frac{7\zeta(3)}{16\pi^2 \left(T_{\mathrm{CDW}}^{\mathrm{MF}}\right)^2} \tag{3.65}$$

near the mean field transition temperature.
Above $T_{\mathrm{CDW}}^{\mathrm{MF}}$, the minimum of the free energy is at $|\Delta| = 0$ and the slope, with respect to the fluctuating order parameter, is given by

$$\left.\frac{\partial^2 \mathrm{F}}{\partial \Delta^2}\right|_{|\Delta|=0} = a + 3b|\Delta|^2 = a_1\left(T - T_{\mathrm{CDW}}^{\mathrm{MF}}\right). \tag{3.66}$$

This slope corresponds to a restoring force for the oscillation of the order parameter, and the oscillation frequency is given, near T_{CDW} by

$$\omega_0 = \left(\frac{k}{M}\right)^{1/2} = \left(\frac{a_1}{M}\right)^{1/2} \left(T - T_{\mathrm{CDW}}\right)^{1/2} \tag{3.67}$$

in agreement with the temperature dependence of the frequency of the soft phonon mode at $q = 2k_F$, which was evaluated above in Eq. (3.21).

Some comments on the relevant cutoff frequency and the effects of higher dimensionality are in order here. For charge density waves, the energy gaps develop in response to a static distortion of the underlying lattice and relaxation effects do not play a role. Consequently, the entire electron spectrum is influenced by the electron-phonon interaction and the relevant cutoff energy is the Fermi energy ϵ_{F}. This is in contrast to the superconducting ground state, where retardation of the electron-phonon interaction is essential and leads in turn to a cutoff frequency on the order of ω_p, the Debye frequency. The difference between the two energy scales, with ϵ_F usually significantly larger than $\hbar\omega_D$, leads in general to values of $T_{\mathrm{CDW}}^{\mathrm{MF}}$ which exceed the typical superconducting transition temperatures.

The singularity of the density of states at the single particle gap, as given by Eq. (3.37), is due to the 1D character of the electronic spectrum. Higher dimensional effects, which can be described by a quasi-2D or quasi-3D band structure, lead to (along with a modification of the response function $\chi(\vec{q})$ the removal of these singularities at $q = 2k_F$, and thus to changes in the electronic energies upon the formation of the single particle gap (Huang and Maki, 1989). Consequently, the condition given by Eq. (3.46) is also affected, leading to a single particle gap and a transition temperature which is different from that which is appropriate for the strictly 1D case.

1.3.2 Single Particle Transitions: Tunneling and Coherence Factors

The single particle gap and density of states which develop below $T_{\mathrm{CDW}}^{\mathrm{MF}}$ as a consequence of charge density wave formation are, for the strictly one-dimensional case, identical to the spectrum of single particle excitations for the singlet superconductor. Although the ground states are different; because of this similarity, the formalism which has been developed for single particle tunneling in superconductors can be adopted to describe the occurrence of tunneling in the charge density wave ground state. To
date, tunneling has only been observed between a normal metal and materials with a charge density wave state, therefore expressions appropriate for this case will be reproduced here. In terms of the standard semiconductor model (also applied for superconductors; see for example Tinkham, 1975), the CDW ground state is viewed as a one-dimensional semiconductor and the density of states is given by Eq. (3.37). With the normal metal represented by an energy independent density of states N_c, the tunneling current is given by

$$I_{n,\mathrm{CDW}} = A\frac{G_{nn}}{e}\int_{-\infty}^{\infty}\frac{N_{\mathrm{CDW}}(E)}{N_c}[f(E)-f(E+cV)]dE \tag{3.68}$$

where G_{nn} is the tunneling conductance for normal metal to normal metal tunneling and $N_{\mathrm{CDW}}(E)$ is the density of states in the charge density wave state. As for a superconductor, at $T=0$ there is no tunneling current as long as $e|V|<|\Delta|$; for nonzero temperatures an (exponentially) small tunneling current is expected for voltages less than the single particle gap. The differential conductance dI/dV is given, in analogy to a superconductor by

$$G_{n,\mathrm{CDW}}|_{T=0} = \left.\frac{dI_{n,\mathrm{CDW}}}{dV}\right|_{T=0} = G_{nn}\frac{N_{\mathrm{CDW}}e|V|}{N_c} \tag{3.69}$$

and is, at temperatures $k_BT<|\Delta|$, directly proportional to the density of states.

In addition to normal metal-charge density wave tunneling, it is expected that other tunneling phenomena, such as charge density wave-charge density wave tunneling, and phonon structures may also be observed; and the formalism applied for superconductors may be adopted. This of course does not hold for tunneling involving coherent pairs, but it has also been suggested that effects similar to Josephson tunneling may occur as well (Artemenko and Volkov, 1983).

Single electron transitions, induced by external perturbations such as electromagnetic radiation, ultrasound, or nuclear relaxation are determined by coherence factors, in addition to density of state effects. Such coherence factors arise when the transition probabilities are calculated. Because the superconducting and
charge density wave ground states are invariant under different symmetry operations, the coherence factors will also be different in the two cases.

We write the external perturbation which acts on the single particle states as

$$\mathscr{H}_1' = \sum_{k,k'} B_{k',k}a_{k'}^{\dagger}a_k = \sum_{k,k'} B_{k',k}\left(a_{1,k'}^{\dagger}a_{1,k}+a_{2,k'}^{\dagger}a_{2,k}\right) \tag{3.70}$$

where the electron spin has been neglected. Here $B_{k',k}$ are the matrix elements which connect the usual one-electron states in normal metals. Each term is independent, and $|B_{k',k}|^2$ is proportional to the transition probability.

In the charge density wave state, the transition is written in terms of the quasiparticle states γ as

$$a^\dagger_{1,k'}a_{1,k} = \left(U^*_{k'}\gamma^\dagger_{1,k'} - V^*_{k'}\gamma_{2,k'}\right)\left(U_k\gamma_{1,k} - V_k\gamma^\dagger_{2,k}\right) \tag{3.71a}$$

$$\begin{aligned}=&U^*_{k'}U_k\gamma^\dagger_{1,k'}\gamma_{1,k} - V^*_{k'}V_k\gamma^\dagger_{2,k}\gamma_{2,k'}\\ &- U^*_{k'}V_k\gamma^\dagger_{1,k'}\gamma^\dagger_{2,k} - V^*_{k'}U_k\gamma_{2,k'}\gamma_{1,k}\end{aligned}$$

$$a^\dagger_{2,k'}a_{2,k} = \left(V_{k'}\gamma^\dagger_{1,k'} + U_{k'}\gamma_{2,k'}\right)\left(V^*_k\gamma_{1,k} + U^*_k\gamma^\dagger_{2,k}\right) \tag{3.71b}$$

$$\begin{aligned}=&V_{k'}V^*_k\gamma^\dagger_{1,k'}\gamma_{1,k} - U_{k'}U^*_k\gamma^\dagger_{2,k}\gamma_{2,k}\\ &+ V_{k'}U^*_k\gamma^\dagger_{1,k'}\gamma^\dagger_{2,k} + U_{k'}V^*_k\gamma_{2,k'}\gamma_{1,k}.\end{aligned}$$

Thus the transitions $a^\dagger_{1,k'}a_{1,k}$ and $a^\dagger_{2,k'}a_{2,k}$ connect the same quasiparticle states. Consequently, the transition probabilities of these transitions are not independent and the matrix elements must either be the same, or differ only in sign.

The first two terms on the right hand sides correspond to the scattering of quasiparticles by the external perturbation, these processes are important for energies significantly smaller than the single particle gap. The last two terms correspond to the creation or annihilation of two quasiparticles and such processes occur if the frequency of the external perturbation exceeds the gap frequency $\omega_g = 2\Delta/\hbar$. These processes are shown in Fig. 3.8.

The subscripts 1 and 2 refer to quasiparticles with $k > 0$ and $k < 0$ respectively, and the transition matrix element depends on whether the external perturbation is symmetric or antisymmetric when $k \to k - 2k_F$. The former is the case for ultrasonic attenuation (case I) as the interaction is between the one electron states and the scalar deformation potential of the ions. Then the transi-

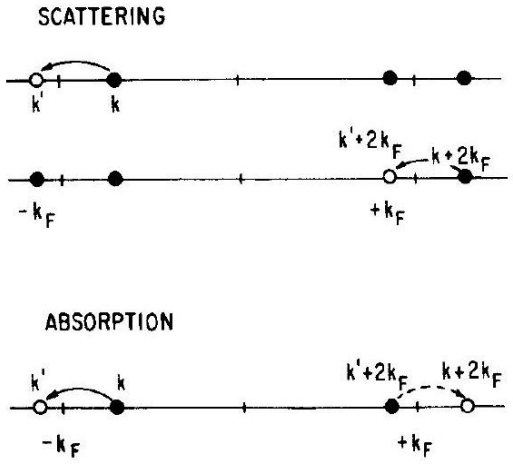


Figure 3.8. Scattering of single particles and creation of pairs of particles in the CDW state. In the upper part of the figure two scattering processes, both involving the same change of momentum $\Delta k=k\hat{}\{\}\{\prime\}-k$ are shown. The energy associated with these two simultaneous scatterings, $\hbar\omega \ll \Delta$. In the lower part creation of pairs of particles, both with momenta $|\Delta k| = k' - k$ are shown, these processes are important for $\hbar\omega \geq 2\Delta$.

tion matrix element is the same for the two transitions. In the case of electromagnetic absorption (case II) the interaction is through the term $\vec{p}\cdot\vec{A}$ where $\vec{A}$ is the vector potential, and the reversal of the momentum $\vec{p}$ leads to the change of the sign of the interaction.

In order to see the processes which are involved let us look at transitions in which the scattering of quasiparticles is involved. For these processes terms like

$$[U^*_{k'}U_k + V^*_k V_{k'}]\,\gamma^\dagger_{1,k'}\gamma_{1,k} \tag{3.72a}$$

and

$$[U^*_{k'}U_k - V^*_{k'}V_k]\,\gamma^+_{1,k'}\gamma_{1,k} \tag{3.72b}$$

arise. The first applies to ultrasonic attenuation, the second to electromagnetic absorption. From Eq. (3.71) the transition matrix element for the scattering of quasiparticles is then given by ($UU' \pm UV'$) and the creation or annihilation of pairs of quasiparticles by ($UU' \mp VU'$). The coherence factors are different from those appropriate for superconductors; the upper and lower signs
apply for interactions which are either invariant or change sign with changing the momentum related to the interaction with the external applied potential.

The calculation of the transition matrix elements proceeds along the lines worked out for the superconducting ground state, and we obtain (Tinkham, 1975)

$$(UU' \pm VV')^2 = \frac{1}{2}\left(1 \pm \frac{\Delta^2}{EE'}\right) \tag{3.73}$$

for scattering of quasiparticles, while for the creation or destruction of pairs of quasiparticles

$$(VU' \mp UV') = \frac{1}{2}\left(1 \mp \frac{\Delta^2}{EE'}\right). \tag{3.74}$$

The transition rates between energy levels which differ by $\hbar\omega$ are given by

$$\frac{\alpha_{\mathrm{CDW}}}{\alpha_{\mathrm{V}}} = \frac{1}{\hbar\omega}\int_{-x}^{x} \frac{(E(E+\hbar\omega) \pm \Delta^2)\,[f(E) - f(E+\hbar\omega)]}{(E^2-\Delta^2)^{1/2}\,[(E+\hbar\omega)^2 - \Delta^2]^{1/2}} \tag{3.75}$$

where the + and - signs apply for case I and II coherence factors respectively.

The evaluation of this integral continues along the lines which have been worked out for the superconducting case (Tinkham, 1975 and references cited therein). In the low frequency limit, the electromagnetic absorption has a temperature dependence of

$$\frac{\alpha_{\mathrm{CDW}}}{\alpha_N} = \frac{2}{1 + \exp\left(\Delta/k_B T\right)} \tag{3.76}$$

and sharply decreases with decreasing temperature. The expected behavior is the same as that of the ultrasonic attenuation in superconductors. Ultrasonic attenuation, like electromagnetic absorption for superconductors, is axpected to display a maximum somewhat below T^{MF}_{CDW}; the maximum depends on the excitation frequency and diverges at $T^{\mathrm{MF}}_{\mathrm{CDW}}$ as $\omega \to 0$.

In Eq. (3.70) the spin degrees of freedom are not included; for interactions, which involve spin flip processes, case II coherence
factors occur. Consequently, we expect a maximum in the nuclear spin lattice relaxation rate somewhat below $T^{\mathrm{MF}}_{\mathrm{CDW}}$, in a fashion which is similar to the Hebel-Slichter peak in conventional superconductors.

1.3.3 Experimental Evidences for the Charge Density Wave Transition and Ground State

A broad variety of experiments have been conducted on the various inorganic linear chain materials which were discussed in Chapter 2 and they have been summarized in various reviews listed in the Appendix. The second order phase transition which leads to the charge density wave ground state has been examined by measurements of various thermodynamic quantities

such as specific heat, thermal expansion, and elastic constants. The transition to a charge density wave ground state also leads to the development of a single particle gap at the Fermi level and is consequently accompanied by a metal-insulator transition. Therefore, the measurement of the various transport coefficients also gives clear evidence for the phase transition; the magnitude of the single particle gap can be extracted from these measurements. Finally, a variety of structural measurements, such as X-ray and neutron scattering and scanning tunneling microscope experiments, together with measurements of local properties (by nuclear magnetic resonance, for example), lead to the examination of the structural changes which accompany the phase transition. From these experiments the period and amplitude of the lattice distortion can also be extracted.

3.3.1 Transition Temperatures

Within the framework of mean field theory, the second order phase transition leads to a specific heat anomaly at $T_{\rm CDW}^{\rm MF}$, with a jump given by Eq. (3.60).

The specific heat measured in $K_{0.3}MoO_3$ over a broad temperature range is shown in Fig. 3.9 (Kwok et al., 1990). There is a well defined anomaly at $T = 183$ K and this identifies a phase transition to a three-dimensionally ordered ground state. This temperature, as will be discussed in Chapter 5, is different from the mean field transition temperature $T_{\rm CDW}^{\rm MF}$ as given by Eq . (3.19) because of

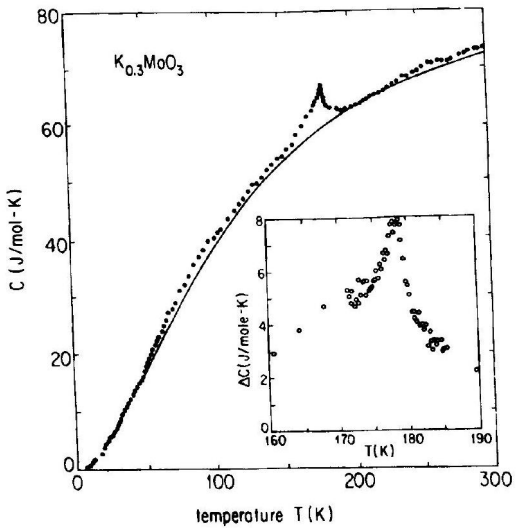


Figure 3.9. The temperature dependence of the specific heat of $\mathrm{K}_{0.3}\mathrm{MoO}_3$. (Kwok et al., 1990). The insert shows the specific heat near the transition, with a background subtracted.

fluctuation effects. Therefore, the transition temperature where a second order transition to the ground state with three-dimensional long range order occurs will be called $T_{\rm 3D}$. The peak which is observed at the transition is significantly larger than that predicted by Eq. (3.60); and instead of a sharp jump at $T_{\rm CDW}$ the transition is broad. Both features indicate the importance of fluctuation effects, as will be discussed in Chapter 5. Specific heat experiments have also been performed in other materials with a CDW ground state and in general the observations are similar to that shown in Fig. 3.9.

The metal-insulator transition can easily be detected by measurements of various transport coefficients. Figure 3.10 displays *dc* resistivity measurements conducted on various compounds (Grüner, 1988). In the metallic state, in the absence of a gap, the conductivity is expected to display a typical metallic behavior if

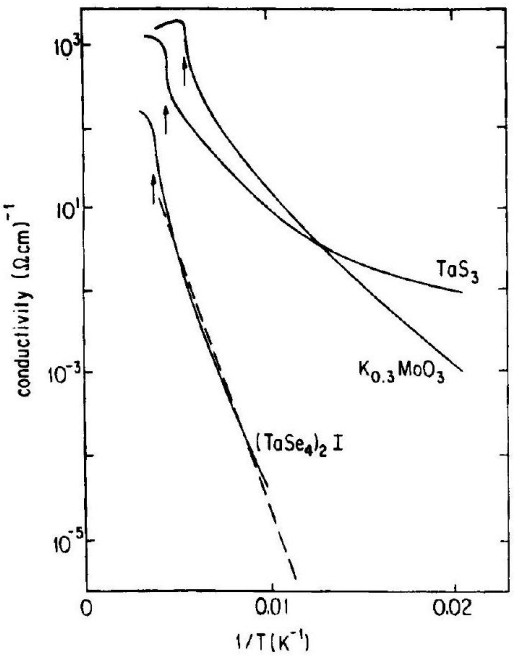


Figure 3.10. *dc* conductivity as a function of inverse temperature in some compounds with a charge density wave ground state (Grüner, 1988). The dotted line indicates the behavior given by Eq. (3.78).

no fluctuation effects are present. In the charge density wave state, the *dc* conductivity is described as

$$\sigma_{dc} = \mu n(T) \tag{3.77}$$

where μ is the mobility and $n(T) = n\,[1 - f_\varsigma(T)]$ with $f_\varsigma(T)$ given by Eq. (3.57). At low temperatures, where $|\Delta|$ is only weakly temperature dependent the dc conductivity has the following temperature dependence:

$$\sigma_{dc} = \mu(T) \exp\left(-\frac{\Delta}{k_B T}\right) \tag{3.78}$$

and with μ assumed to be temperature independent, the single
s Charge Density Wave Transition and Ground State: Mean Field Theory
particle gap can be extracted. The measurements of $\sigma_{dc}(T)$ displayed in Fig. 3.10 can be described by Eq. (3.69) from which values for the single particle gap can be extracted. Near the transition, from Eqs. (3.48) and (3.46),

$$\sigma_{t_1} = \mu N_r \left[1 - \frac{1.74\pi}{4\,(T_{3\mathrm{D}})^2}\,(T_{3\mathrm{D}} - T)^{1/2}\right] \tag{3.79}$$

and the temperature derivative of the resistivity, $\rho_{dc} = \sigma_{dc}^{-1}$, is approximately given by

$$\frac{d\rho_d}{dT} = \frac{d\rho_d}{d(1/T)} = \frac{1.74\pi}{2\mu N_c T_c^2}\frac{1}{(T_{31} - T)^{1/2}} \qquad \text{for } T \le T_{31} \tag{3.80}$$

with $dp_d/dT \simeq 0$ above the transition. Consequently, the derivative has a cusp singularity at $T_{3\mathrm{D}}$ within the framework of mean field theory. In general, the derivative $d\,[\log \rho_{dc}(T)]\,/d(1/T)$ is plotted, giving Δ directly for $T \to 0$, with a singularity at $T = T_{\mathrm{CDW}}$; a typical example is displayed in Fig. 3.11. Instead of a cusp one observes a broadened maximum, in agreement with the overall behavior of the specific heat. Both are the consequence of fluctuations; nevertheless,

the transition temperature can clearly be identified as the temperature when the peak in the derivative occurs.

The various transition temperatures and also the single particle gap values, as obtained from resistivity measurements for some compounds with a CDW ground state, are collected in Table 3.1. In all cases the value $2\Delta/k_BT_{3D}$ well exceeds the weak coupling BCS result of $2\Delta/k_BT_{3D} = 3.52$, suggesting that the transition temperatures are significantly lower than the mean field transition temperature, T_{CDW}^{MF}.
$NbSe_3$ is different from the materials which show metal-insulator transitions. Here the phase transition removes only part of the Fermi surface, and below T_{3D} the material remains a semimetal. Furthermore, the slightly different chains undergo phase transitions at different temperatures, called T_{3D}^1 and T_{3D}^2. The temperature dependence of the *dc* resistivity displayed in Fig. 3.12 (Monceau, 1987) clearly shows the two phase transitions.

Adaitional evidence for the development of a nonmagnetic, semiconducting ground state comes from magnetic susceptibility measurements. In the metallic state, $\chi(T)$ has the usual Pauli form

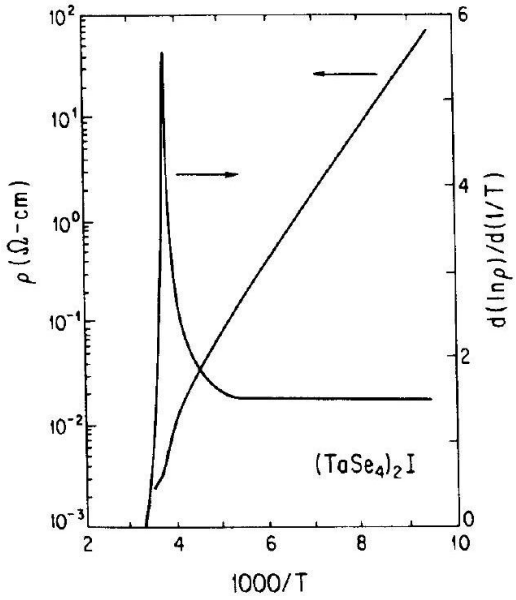


Figure 3.11. The temperature derivative of the de resistivity in $\left(\mathrm{TaSe}_{4}\right)_{2} \mathrm{I}$ along the chain direction. The peak identifies the phase transition at $T = 263$ K .

Table 3.1. Transition temperatures T_{i}, single particle gaps Δ_p (as obtained from the *dc* resistivity), Δ_{opt} (obtained from the optical conductivity, electron-phonon coupling constant λ (Eq. (3.44)), and coherence length ξ along the chain direction (Eq. 1.26)) for some linear chain compounds with a CDW ground state.

	T_c(K)	$2\Delta_\rho(K)$	$2\Delta_{opt}(K)$	λ	$\xi_{\|\|}(T=0)(\ddot{A})$
KCP	189	1400	1700	0.302	118
$K_{0.3}MoO_3$	183	920	1400	0.34	125
TaS_3	215	1600	1800	0.65	40
$NbSe_3$	$\begin{cases} 145 \\ 59 \end{cases}$	700[a]	n/a	0.53	61
$(TaSe_4)_2 I$	263	3000	2900	0.43	100

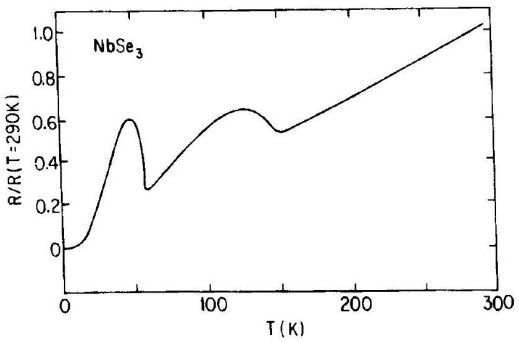


Figure 3.12. The temperature dependence of the *dc* resistivity of NbSe_{3}. Note the increase of ρ_{dc} at $T^1_{CDW} = 149$ K and $T^2_{CDW} = 59$ K.

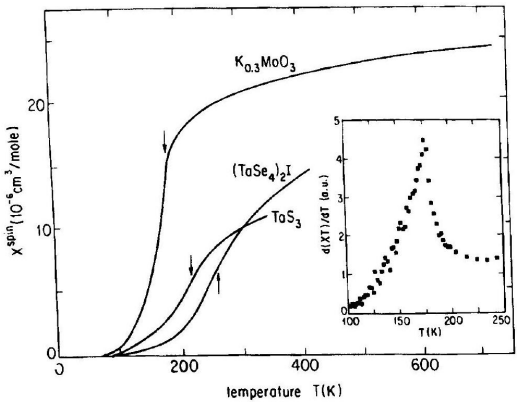


Figure 3.13. Temperature dependence of the magnetic susceptibility in several inorganic linear chain compounds with charge density wave ground states (Johnston et al., 1985). The arrows indicate the transition temperatures, and the insert shows the temperature derivative.

of Eq. (2.4), while below T_{3D} (which is proportional to the number of thermally excited carriers) the temperature dependence is given by Eq. (3.57). At low temperatures, $T \ll T_{350}$, this reduces to

$$\chi(T) \simeq \frac{\mu_B^2}{T} \exp\left(-\frac{\Delta}{k_B T}\right) \tag{3.81}$$

where the weak temperature dependence of the gap well below $T_{3\mathrm{D}}$ has been neglected.

The temperature dependences of the magnetic susceptibility of various materials are displayed in Fig. 3.13 (Johnston et al., 1985). The susceptibility is somewhat temperature dependent even above the transition, which is indicated by the arrows for the various compounds. This is again due to fluctuations, and as for the electrical resistivity, the transition temperatures are identified by evaluating the derivative $d_\chi(T)/d(1/T)$. Again, a rounded transition, such as that shown in the insert of Fig. 3.9, is observed.

3.3.2 The Kohn Anomaly

The phonon dispersion relation and its modification by electronphonon interactions has been studied in various compounds by

[0](a) tunneling experiments

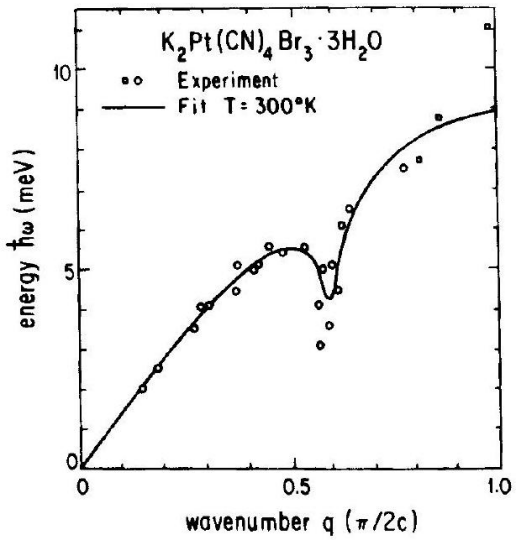


Figure 3.14. The phonon dispersion relation, measured above the charge density wave transition temperature in KCP (after Comes et al., 1975). For the details of the fit to the experimental results, see the original publication.

inelastic neutron scattering. The materials have a complicated crystal structure and consequently numerous phonon modes occur. Which of these interacts with the electron states depends on the electron-phonon coupling constants; the resulting distortions are difficult to calculate from first principles. In KCP the distortion involves a modulation of the repeat distances in the chain direction; in $K_{t)\ .3}MoO_3$ it is related to the transverse displacement of some Mo atoms; and in $NbSe_3$ it is a sociated with an out-of-phase modulation of the different chains. In Fig. 3.14, the phonon spectrum is displayed for KCP at a temperature somewhat above T_{31}. The sharp dip, at wavevector $q = 0.85\pi/a$ reflects the softening of the phonon branch and the full line is a fit to the renormalised phonon spectrum, including the renormalization of the phonon frequencies at wavevectors near $q = 2k_F$.

The temperature dependence of $\omega_{\text{ren}\ ,2k_t}$, as given by Eq . (3.18), can be examined in detail by approximating the renormal-

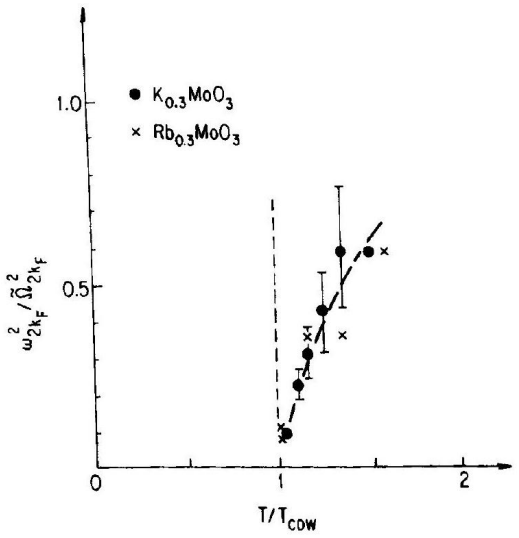


Figure 3.15. The renormalized phonon frequency as the function of temperature in $\mathrm{K}{{613} \mathrm{MoO}}{3}$. The dashed line is the prediction of the mean field theory, Eq. (3.21) (Pouget, 1987).

ized soft mode as a damped harmonic oscillator. Such an approach leads to a frequency dependent displacement-displacement correlation function, which for $q = 2k_F$ is given by (Pouget and Comes, 1989)

$$S\left(2k_r, \omega\right) = k_B T \frac{\mathrm{T}_{2k_f}}{\left(\omega - \omega_{\mathrm{ren}\ ,2k_f}\right)^2 + 4\Gamma_{2k_f}^2} \tag{3.82}$$

where Γ_{2k_1} is the damping constant associated with the oscillations of the renormalized phonon frequency. The temperature dependence of $\omega_{\mathrm{ren}\ ,2k_F}$ evaluated by fitting the measured scattering cross section to Eq. (3.82) is given in Fig. 3.15 for two compounds (Pouget, 1987). Close to $T_{\mathrm{CDW}}, \omega_{\mathrm{ren},2k_1}$ has a temperature dependence somewhat different from that predicted by mean field theory, Eq. (3.21). This suggests that fluctuations above the transition are important and will be discussed in Chapter 5.

3.3.3 The Energy Gap for $T < T_{\mathrm{CDW}}$

The *dc* conductivity measured below the phase transition was found to be a semiconductor like in most of the materials and $\sigma_{dc}(T)$ can be adequately fitted to Eq. (3.79). Such fits, at temperatures well below the transition temperatures lead to single particle gaps, as seen through thermal excitations. The gap values obtained in this manner are collected in Table 3.1. The single particle gaps have also been studied by optical methods, which all clearly identify the gap structure. An example is shown in Fig. 3.16 where the frequency dependent conductivity evaluated both above and below $T_{3\mathrm{D}} = 183$ K is shown. Above the transition the conductivity is Drude-like at low frequencies with an additional (most probably) interband transition. In contrast, at $T = 5$ K the conductivity is low below about 10^{-1}eV; indicating the appearance of the single particle gap. The gap, however, can only be evaluated by a detailed comparison of the measured frequency dependent conductivity and $\sigma(\omega)$ calculated for the Peierls state. Such a comparison will be made in Chapter 9. The gap values, quoted in Table 3.1, have been inferred from optical studies by performing such a comparison. In the material $NbSe_3$ optical studies cannot identify the gap structure because of the semimetallic character of the material for $T < T_{\mathrm{CDW}}$, and here single particle tunneling (Ekino and Akimitsu, 1987; Fournel et al., 1986) has been used to evaluate the gap.

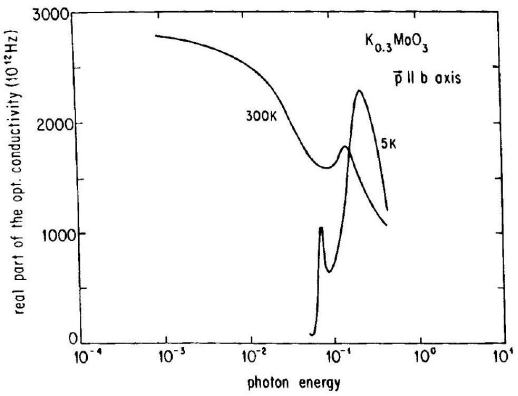


Figure 3.16. The optical conductivity of $\mathrm{K}_{0.3}\mathrm{MoO}_3$ measured along the chain direction both above and well below the charge density wave transition (Travaglini and Wachter, 1984; Degiorgi et al., 1991).

The measured single particle gaps, together with the Fermi energies evaluated in Chapter 2, lead by virtue of Eq. (3.44) to the electron-phonon coupling constant λ. In all cases λ is significantly smaller than one, indicating the weak coupling theory, for which $\Delta \ll \epsilon_F$, applies. Consequently, the likely explanation for the large single particle gaps (when compared with the transition temperature) is not strong coupling effects; but the fact that fluctuations due to the quasi-one-dimensional character of the materials strongly suppress the transition temperatures where the three-dimensional ordered ground state develops. Imperfect nesting, however, may also play a role (Huang and Maki, 1989).

The coherence lengths given by Eq. (1.26) can also be evaluated using the v_F values discussed in Chapter 2, together with the measured single particle gaps. The ξ_0 values obtained are also collected in Table 3.1. Because of the large gaps, the coherence length associated with the CDW state is short, extending only a
few lattice constants. The coherence lengths shown in Table 3.1 are the values along the highly conducting direction. Since $\xi = \hbar v_F/\pi\Delta$, for an isotropic gap and strongly anisotropic band structure, the coherence lengths are significantly shorter in the directions perpendicular to the chains. The band structure anisotropy. for $K_{0.3}MoO_3$, as discussed in Chapter 2, leads to coherence lengths $\xi_\perp(2a-c) = 7\text{Å}$ and $\xi_\perp(2a+c) = 1.5\text{Å}$ in the two perpendicular directions. This substantial anisotropy also leads to a rather small coherence volume

$$[\xi_{11} \cdot \xi_\perp(2a-c) \cdot \xi_\perp(2a+c)] \sim 420\text{Å}^3 \tag{3.83}$$

indicating that this volume contains only a few electron-hole pairs. Similar anisotropies have been found for other materials which develop a charge density wave ground state. Consequently the coherence lengths perpendicular to the highly conducting direction are small in these compounds as well.

3.3.4 The Lattice Distortion for $T < T_{\mathbf{CDW}}$

Below the transition a static modulation of the ionic positions occurs and, for a linear chain of atoms, the positions are given in the case of long range order by

$$X_n = na + \Delta u(T) \sin(n2k_F a + \phi) \tag{3.84}$$

where the amplitude of the distortion $\Delta u(T)$ is determined by Eq. (3.23); it has the same temperature dependence as the order parameter Δ. The new periodicity at $q = 2k_F$ leads to

new Bragg peaks, the positions of which give k_F directly. The intensities are related to the displacement Δu (Eagen et al., 1975).

In the absence of distortion, the scattering intensity is given by

$$I(k) = e^{-2W} \sum_H \delta\left(k - Ha^*\right) \tag{3,85}$$

where $a^* = 2\pi/a, e^{-2W}$ is the Debye-Waller factor, and H is the one-dimensional Miller index of reflection. Using Eq. (3.84) we can calculate the n^{th} order static structure factor $S_n\left(Ha^*\right)$, and the scattering intensity

$$I \simeq \sum_{n,H} S_n(H)\delta\left(k + n2k_F - Ha^*\right) \tag{3.86}$$

For a small amplitude lattice distortion the first term gives

$$l^{(1)}(k) = e^{-2W} \sum_H \delta\left(k - Ha^*\right)\left[1 - \frac{1}{2}Ak^2\right] \tag{3.87}$$

with A constant, describing the scattering intensity of the Bragg points. For small Δu the second term in the bracket is small, and the intensity of the Bragg reflections is only slightly modified by the formation of the periodic lattice distortion. The next term in Eq. (3.86) gives

$$l^{+}(k) = c^{-2W} \sum_H \delta\left(k - Ha^* \pm 2k_I\right) \frac{1}{2}\left(k\Delta u^2\right). \tag{3.88}$$

This describes a set of lattice points with a wavevector given by $k \pm 2k_i$ and with an intensity proportional to Δu^2, and thus proportional to the square of the order parameter. Therefore, the positions of the new peaks, which arise as a consequence of the new periodicity, lead to the period of the lattice modulation and, though the relation $\lambda_0 = \hbar/k_F$, to the Fermi wavevector. The measured intensity of these peaks allows for the evaluation of the temperature dependence of the order parameter (Pouget and Comes, 1989 and references cited therein).

For a three-dimensional order which develops in a system of (weakly) coupled chains the period of the lattice distortion is given by $\vec{Q}_{CDW} = (2k_F, Q_\perp)$; where $Q_\perp$ describes the ordering of the charge density wave modulation on the neighboring chains. For a system of coupled chains the expression analogous to Eq. (3.88) reads

$$l^t(k) = e^{-2W} \sum \delta\left(\vec{k} - \vec{R}^* \pm \vec{Q}_{\text{CDW}}\right) \frac{1}{2}\left(k\Delta u^2\right) \tag{3.89}$$

where $\vec{R}^*$ is a reciprocal lattice vector. Consequently, the new superlattice reflection points give $2k$, and $Q_\perp$ respectively.

Both X-ray and elastic neutron scattering have been used to evaluate the wavevector associated with the lattice distortion and the magnitude of the distortion as the function of temperature (these have been summarized by Pouget and Comes, 1989; and Pouget, 1987). The wavevectors associated with the ground state are collected in Table 3.2, where the first column always refers to the chain direction and the next two columns to directions perpendicular to the chains. In all cases the period λ_0 is incommensurate with the underlying lattice. Also, in the majority of cases

Table 3.2. Structural distortion parameters for the CDW state of various compounds. See P. Monceau (1985) and references cited therein.

	Superstructure				$\Delta u_{\max}$(Å) (exp)	$\mathcal{J}u_{\mathrm{mar}}$ ($\mathring{A}$) (Eq. 3.90)
	9		$q_\perp$			
KCP	0.3	0.5		0.5	0.027	0.049
$K_{0.3}MoO_3$	0.71	0.5		0.5	0.05	0.035
TaS_3	~ 0.25				n/a	-
$NbSe_3$	0.24	0		0	n/a	-
	0.26	0.5		0.5		
$(TaSe_4)_2\,I$	0.084	0.05		0.05	0.09	

the CDW modulations on the neighboring chains are antiphase. That is, the maxima of the CDW modulations on one chain are accompanied by minima on the neighboring chains. The more complicated structural arrangements such as those which occur in $(TaSe_4)_2\,I$ have not been accounted for to date. The temperature dependence of the lattice distortion is shown for some compounds in Fig. 3.17. In all cases a temperature dependence reminiscent of the temperature dependence of the order parameter as given by Eq. (3.19) is obtained. The full line on the figure is $|\Delta(T)|$ as given by the weak coupling BCS theory. The displacement amplitudes, also obtained from the scattering intensity, are summarized in Table 3.2. The amplitude is given in terms of the electron-phonon coupling constant, the unrenormalized phonon frequency, and the density of states as

$$\Delta u = \frac{2\Delta}{g}\left(\frac{\hbar}{2NM\omega_{2k_F}}\right)^{1/2}. \tag{3.90}$$

The parameters which appear on the right hand side have been evaluated before and are shown in Tables 2.1 and 3.1. The unrenormalized phonon frequency has been obtained from neutron scattering experiments and M has been chosen to be the mass of the basic structural unit (see Table 2.1). Consequently, Δu can be evaluated and the values calculated for the materials on which the amplitude of the lattice modulation was measured are also collected in Table 3.2.

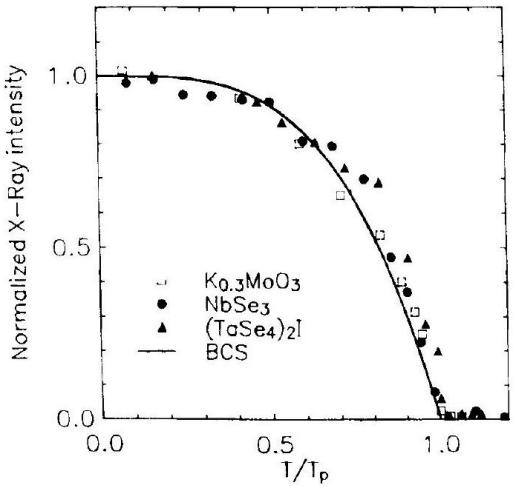


Figure 3.17. Temperature dependence of the lattice distortions in $\mathrm{K}_{0.3}\mathrm{MoO}_3$, $NbSe_3$, and $(TaSe_4)_2$ I. The full line is $\Delta(T)$ given by the weak coupling BCS limit (Grüner, 1988 and references given therein).

The periodic modulation of the charge density leads to a periodic modulation of electric field gradient at the nuclear sites; and consequently to changes in the nuclear magnetic resonance 'ine shape. For the charge density wave as given by Eq. (3.52), to first approximation, the resonance frequency at the nuclear site $\vec{R}$ is

$$\nu(\vec{R}) = \nu_0 + \delta\nu(R) = \nu_0 + \nu_1 \cos\left(\vec{Q}_{\mathrm{CDW}} \cdot \vec{R} + \phi\right) \tag{3.91}$$

where ν_0 is the resonance frequency in the absence of the charge density wave and ν_1 is proportional to the amplitude of the density wave. The resonance line shape which results from the distribution of the resonance frequencies can readily be calculated (Berthier and Segransan, 1987 and references cited therein) and gives

$$g(\nu) = \text{ const } \int_{\nu = \text{ const}} \frac{ds}{\vec{\nabla}(\delta\nu(\vec{R}))} \tag{3.92}$$

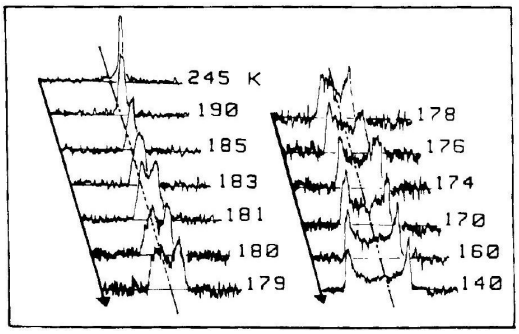


Figure 3.18. Nuclear magnetic resonance line shapes in $\mathrm{Rb}{{63}\mathrm{MoO}}{3}$ at several temperatures. The distance between the "wings" of the distribution is provortional to the amplitude of the density modulation (Berthier and Segransan, 1987).

For an incommensurate CDW we obtain (Ross et al., 1986; Janossy et al., 1987)

$$\begin{aligned} g(\nu) &= \text{ const } \cdot \nu_1 \left[1 - \left(\tfrac{\nu}{\nu_1}\right)^2\right]^{-1/2} && |\nu| < \nu_1 \\ g(\nu) &= 0 && |\nu| > \nu_1 \end{aligned} \tag{3.94}$$

Typical experiments on $Rb_{0.3}MoO_3$ are shown in Fig. 3.18. Above the transition the linewidth is determined by interactions different from the electric field gradient induced distribution, and below $T_{3D}, g(\nu)$ can be described by Eq. (3.93). The analysis leads to the temperature dependence of the amplitude of the density modulation; i.e., the temperature dependence of the order parameter (shown in Fig. 3.19) with the full line is the temperature dependence of the order parameter as given by the weak coupling BCS expression. The latter accounts for the experimental results except close to the transition temperature; where a critical exponent different from $\eta = \frac{1}{2}$ as expected for a mean field

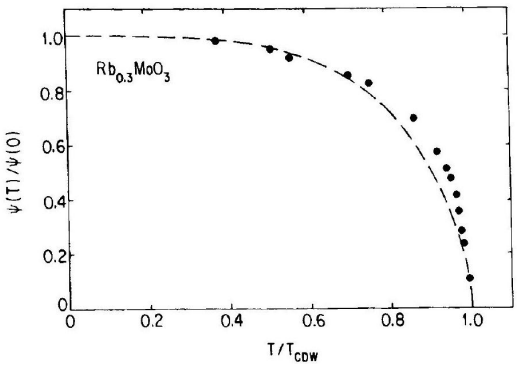


Figure 3.19. Temperature dependence of the amplitude of the density wave modulation in $\mathrm{Rb}_{0,3} \mathrm{MoO}_3$ (full circles). The dashed line is the temperature dependence of the order parameter as given by the weak coupling BCS theory (Berthier et al., 1992).

transition (see Eq. (3.62a)) is observed. This is most probably due to fluctuation effects.

Charge density waves have also been observed by scanning tunneling microscopy in various materials (Slough et al., 1989; Dai et al., 1991 and references cited therein). These measurements also give information about the period of the density wave modulation. The magnitude of the modulation, however, cannot be extracted from these measurements.

1.4 The Spin Density Wave Transition and Ground State: Mean Field Theory and Some Basic Observations

The spin density wave ground state of metals is thought to arise as a consequence of electron-electron interactions. Questions about the consequences of this interaction on the Fermi-liquid state have received considerable interest. There is also a great deal of literature on the various ground states which develop, and on the nature of low lying excitations, which occur in one-dimensional models (see for example, Anderson, 1990). The simplest possible description of this interaction is given by the following term in the Hamiltonian

$$\begin{aligned} \mathscr{H}_{\text{int}} &= \frac{U}{N} \sum_{q,\sigma} n_{q,\sigma} n_{-q,-\sigma} \\ &= \frac{U}{N} \sum_{k,k',q} a^{\dagger}_{k,\sigma} a_{k+q,\sigma} a^{\dagger}_{k',-\sigma} a_{k'-q,-\sigma} \end{aligned} \tag{4.1}$$

where U is the on-site Coulomb interaction. Together with the kinetic energy term, the so-called Hubbard Hamiltonian is given by

$$\mathscr{H} = \sum_{k,\sigma} \epsilon_k a^{\dagger}_{k,\sigma} a_{k,\sigma} + \frac{U}{N} \sum_{k,k',q} a^{\dagger}_{k,\sigma} a_{k+q,\sigma} a^{\dagger}_{k',-\sigma} a_{k'-q,-\sigma} \tag{4.2}$$

Many of the important aspects of the one-dimensional Hubbard model (see also Lieb and Wu, 1968), such as spin-charge separation, etc., will not be discussed here; we will simply assume that the 1D electron gas can be described in terms of a conventional Fermi liquid with the response functions as discussed in Chapter 1 , and confine ourselves to the mean field solution. As mentioned in the previous chapter this is done by arguing that while fluctuations are important, nevertheless for a system of coupled chains the ground state is similar to that given by the mean field solution. (Whether this argument is correct or not

remains to be seen; the experimental results discussed later are in fair agreement with those obtained from a mean field treatment.) As first discussed by Overhauser (1960, 1962) the ground state of Eq. (4.2) is a spin density wave state, and the transition together with the parameters of the state will be described within the framework of a mean field theory, with the assumption that $U \ll \epsilon_F$; which is equivalent to the weak coupling limit for superconductors. The ground state, as is the case for the CDW state, opens up a gap at the Fermi level in both spin subbands and, consequently, in the case of the complete removal of the Fermi surface (such as expected for a highly anisotropic band structure), a metal insulator transition results. The ground state also has a well defined magnetic response, similar to that of an antiferromagnet. Consequently, transport and magnetic measurements, together with local probes which sample the internal magnetic fields at the nuclear sites, have been used to evaluate the essential characteristics of the ground state.

1.4.1 Mean Field Theory of the Spin Density Wave Transition

The interaction between the electrons with opposite spin, as given by Eq. (4.1), leads to an enhanced response of the electron gas to an external magnetic field. This response can be simply described by using the mean field approximation. Assume that we apply an external magnetic field which varies along the chain direction as

$$H(x) = \sum_q H_q e^{\imath qx}. \tag{4.3}$$

The coupling to this field is described by an extra term in the Hamiltonian

$$\mathscr{H}'' = \sum_q M_q H_{-q} \tag{4.4}$$

where M_q is the q^{th} component of the magnetization. We also assume that the magnetic field is applied to the (arbitrary) z direction. The spin direction parallel (opposite) to H is denoted by $\uparrow$ ($\downarrow$). Then the expectation value of the magnetization is

$$\langle M_{iq} \rangle = \mu_B \left(\langle n_{iq,\uparrow} \rangle - \langle n_{iq,\downarrow} \rangle \right) = \chi_0(q) H_{iq}^{\text{eff}} \tag{4.5}$$

with

$$H_q^{\text{eff}} = H_q + \frac{U \left(\langle n_{q,\uparrow} \rangle - \langle n_{q,1} \rangle \right)}{2\mu_B} \tag{4.6}$$

where $\chi_0(q)$ is the wavevector dependent susceptibility in the absence of Coulomb interactions. The self-consistent equation for the difference $\Delta n_q = \langle n_{q,\uparrow} \rangle - \langle n_{q,\downarrow} \rangle$ is then

$$\mu_B \Delta n_q = \chi_0(q) \left(H_q + \frac{U \Delta n_q}{2\mu_B} \right) \tag{4.7}$$

The magnetization from Eqs. (4.5) and (4.7) is

$$\langle M_q \rangle = \frac{\chi_0(q)}{1 - \frac{U\chi_0(q)}{2\mu_B^2}} H_q = \chi_\parallel(q) H_q \tag{4.8}$$

and the response is described as that of an electron gas with an enhanced susceptibility

$$\chi_\parallel(q) = \frac{\chi_0(q)}{1 - \frac{U\chi_0(q)}{2\mu_B^2}} \tag{4.9}$$

For a uniform magnetization, $q = 0$ and with $\chi_0(0) = 2\mu_B^2 n(\epsilon_T)$, we obtain a static susceptibility

$$\chi(0) = \frac{2\mu_B^2 n(\epsilon_F)}{1 - Un(\epsilon_F)}, \tag{4.10}$$

which is enhanced by the well known Stoner factor. For a onedimensional electron gas $\chi_0(q)$ is strongly peaked at $q = 2k_f$, and the enhancement is most important for perturbations with this
wavevector. $\chi_1(2k_1, T)$ is strongly temperature-dependent (see Eq. (1.17)), which leads to a strongly temperature dependent response, and (with fluctuation effects neglected) to a phase transition at temperature $T_{\mathrm{SDW}}^{\mathrm{MF}}$ defined by

$$\frac{U_{\chi_0}(2k_F, T)}{2\mu_B^2} = Un(\epsilon_F) \ln \frac{1.14\epsilon_0}{k_B T} = 1. \tag{4.11a}$$

This gives

$$k_\beta T_{\mathrm{SDW}}^{\mathrm{MI}} = 1.14\epsilon_0 \exp(-1/\lambda_c), \tag{4.11b}$$

where the dimensionless electron-electron coupling constant is defined as

$$\lambda_i = Un(\epsilon_1). \tag{4.12}$$

Below $T_{\mathrm{SDW}}^{\mathrm{MI}}$ a static, spatially varying magnetization develops. By introducing the spatially dependent operators

$$\Psi_n(x) = \sum_k e^{\prime k} a_{k,\sigma} \tag{4.13}$$

the spin density is given as

$$S(x) = \frac{1}{2}\left[\Psi_\uparrow^\dagger(x)\Psi_\uparrow(x) - \Psi_\downarrow^\dagger(x)\Psi_\downarrow(x)\right] \tag{4.14}$$

$$= \frac{1}{2}\sum_{k,k'}\left\{a_{k,\uparrow}^\dagger a_{k',\uparrow} - a_{k,\downarrow}^\dagger a_{k',\downarrow}\right\} e^{-1(k-k')x} \tag{4.15}$$

Because of the divergent response function at $q = 2k_F$, we assume that only terms with $k' = k \pm 2k_f$ are important. Thus the above equation yields the expectation value

$$\langle S(x)\rangle = \frac{1}{2}\sum_k \left\{\left\langle a_{k,\uparrow}^\dagger, a_{k+2k_F\uparrow}\right\rangle - \left\langle a_{h,\downarrow}^\dagger a_{k+2k_{1,l}}\right\rangle\right\} e^{i2k_F\downarrow} + \text{ c.c.} \tag{4.16}$$

We write the expectation value as

$$S = |S|\mathcal{C}^{(t)} = \langle n_{2k_1\uparrow}\rangle = -\sum_k \left\langle a_{k,\uparrow}^\dagger a_{k+2k_1!}\right\rangle \tag{4.17}$$

$$= -\sum_k \left\langle a_{k,\downarrow}^\dagger a_{k+2k_1\downarrow}\right\rangle = -\langle n_{2k_1\downarrow}\rangle$$

assuming that the density modulations have the opposite sign

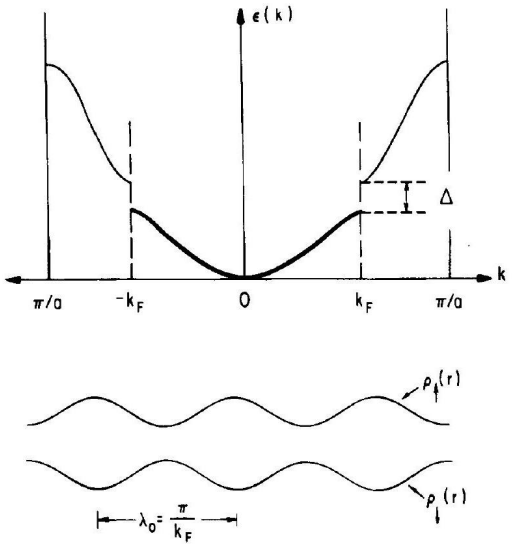


Figure 4.1. The dispersion relation and charge and spin density wave modulation for the two spin subbands in the spin density wave ground state.

(i.e., the same phase ϕ) in the two subbands. The situation, where the phases of the density modulations are different, leads to a complex spin density wave structure (such as spiral spin density waves); such states will not be discussed here. From Eq. (4.16) we obtain

$$\langle S(x)\rangle = 2|S|\cos\left(2k_F x + \phi\right). \tag{4.18}$$

Therefore, the spin density is spatially varying, with a period $\lambda_0 = \pi/k_F$ determined by the Fermi wavevector. There is no charge density modulation as $\langle n_{2k_i}\rangle + \langle n_{2k_j\downarrow}\rangle$ does not show any spatial variation; the situation is displayed in Fig. 4.1.

The magnetic moment μ is given as

$$\langle\mu\rangle = \mathrm{g}\mu_R\langle S\rangle = 2\mu_H\langle S\rangle \tag{4.19a}$$

and therefore the spatially dependent magnetic moment is

$$\langle\mu(x)\rangle = \mu_0\cos\left(2k_F x + \phi\right) \tag{4.19b}$$

where $\mu_0 = 4\mu_B|S|$. We define a complex order parameter

$$\Delta = |\Delta|e^{1(\phi)} = US \tag{4.20}$$

and use the following approximation for the interaction from Eq. (4.1).

$$\begin{aligned} AB &= [(A - \langle A\rangle) + \langle A\rangle][(B - \langle B\rangle) + \langle B\rangle] \\ &\approx \langle A\rangle B + \langle B\rangle A - \langle A\rangle\langle B\rangle \end{aligned} \tag{4.21}$$

where we neglect the higher order terms in $(A - \langle A\rangle)(B - \langle B\rangle)$. With this approximation the mean field Hamiltonian becomes (dropping a constant Hartree energy)

$$\begin{aligned} \mathscr{F}_{\mathrm{MI}} = &\sum_{k,\sigma t}\epsilon_k a^\dagger_{k,\sigma t}a_{k,\sigma t} + \frac{2N|\Delta|^2}{U} \\ &\times\left\{\sum_k \Delta e^{i\phi t}\left(a^\dagger_{k+2k_1}, a_{k,\uparrow} + a^\dagger_{k+2k_1\downarrow}a_{k,\downarrow}\right) + \text{ h.c. }\right\} \end{aligned} \tag{4.22}$$

The Hamiltonian is similar to Eq. (3.26) which describes the charge density wave ground state, and the procedure for obtaining the single particle gap, discussed in the previous chapter, can be adopted here. Straightforward diagonalization similar to that done for charge density waves leads to

$$\mathscr{H} = \sum_{k,\sigma} E_k \gamma^\dagger_{k,\sigma} \gamma_{k,\sigma} + \frac{2|\Delta|^2 N}{U} \tag{4.23}$$

with the dispersion relation for the operators $\gamma_{k,\sigma}$ given by

$$E_k = \epsilon_r + \text{sign}\,(k - k_F) \left[\hbar^2 v_F^2 \,(k - k_f)^2 + \Delta^2\right]^{1/2} \tag{4.24}$$

for both spin subbands.
The development of the single particle gap leads to a decrease of the kinetic energy, while the interaction term $E_M = 2|\Delta|^2/U$ (the second term in Eq. (4.22)) gives a positive energy for a finite magnetization. The equilibrium gap value is obtained from

$$\delta E_{\text{el}} + \delta E_M = 0 \tag{4.25}$$

and straightforward algebra similar to that which led to Eq. (3.44)
gives

$$\Delta(T = 0) = 2\epsilon_F \exp\left(-1/\gamma_c\right). \tag{4.26}$$

A comparison with Eq. (4.11b) leads to the weak coupling BCS relation $2\Delta = 3.52 k_B T_{\text{SDW}}^{\text{MF}}$ and as for charge density waves, the ground state energy is given by

$$E = -\frac{1}{2} n\left(\epsilon_F\right) |\Delta|^2. \tag{4.27}$$

The temperature dependence of the single particle gap, and also the amplitude of the spin density wave is given by the weak coupling BCS expression, and $\Delta(T)$ together with the temperature dependent condensate density are given by Eqs. (3.55) and (3.57).

Crudely speaking, the SDW ground state can be viewed as two charge density wave states- one for the "spin up" and one for the "spin down" subbands as shown in Fig. 4.1, with the charge density wave modulations given by

$$\rho_\uparrow(x) = \rho_0 \left[1 + \frac{\Delta}{v_F k_F \gamma_c} \cos\left(2k_F x + \phi\right)\right] \tag{4.28a}$$

$$\rho_\downarrow(x) = \rho_0 \left[1 + \frac{\Delta}{v_F k_F \lambda_c} \cos\left(2k_F x + \phi + \pi\right)\right]. \tag{4.28b}$$

The resulting spin density variation $\rho_\uparrow(x) - \rho_\downarrow(x)$, given by Eq. (4.18) with $|S| = |\Delta| N/U$ (see Eq. (4.21)), and the resulting charge density wave variation $\rho_\uparrow(x) - \rho_\downarrow(x) = \rho_0 = \text{const}$ are shown in Fig. 4.1. Both subbands however are tied to the Fermi surface; which will have important implications for the excitations and for the dynamics of the SDW ground state.

The above considerations are for an arbitrary spin orientation. In the case of a continuous spin symmetry the condensate density can be written as

$$\langle \vec{S}(x) \rangle = 2\vec{S} \cos\left(2k_F x + \phi\right) \tag{4.29}$$

where $\vec{S} = (S_x, S_y, S_z)$. Consequently, both the spin rotational and the translational symmetries are broken in the spin density wave state. This will have important consequences on the magnetic properties of the ground state and on the dynamics of the collective mode.

The description of the transition and ground state as given above is based on a strictly one-dimensional model. The materials which develop an SDW ground state, however, have significant transfer integrals perpendicular to the chain directions, and models for which this so called quasi-one-dimensional character is included are expected to be more appropriate. Taking into account the finite bandwidth in the perpendicular directions, the dispersion relation is given by (Yamaji, 1982, 1983; Huang and Maki, 199()).

$$\epsilon_k = -2t_n \cos ak_1 - 2t_n \cos bk_2 - 2t_1 \cos ck_3 - \mu \tag{4.30}$$

where μ is the chemical potential and t is the transfer integral in the various directions in the tight binding approximation. For $t_1 \gg t_1, t_1$ the condition for nesting

$$\dot{\epsilon_h} = -\dot{\epsilon_h} + j \tag{4.31}$$

with $\dot{Q} = (2k_1, \pi/b, \pi/c)$ is nearly, bu not completely satisfied, and this leads to deviations from the various expressions which have been obtained on the basis of strictly one-dimensional models. The transition temperature $T_{\mathrm{SDW}}^{\mathrm{MF}}$ decreases with increasing transfer integrals perpendicular to the chain direction, and the transition is completely removed for

$$\Delta(T=0) = \frac{t_b^2}{2} \cos\left(ak_F/t_a\right) \sin^2\left(ak_1\right) \tag{4.32}$$

with $\Delta(T=0)$ given by Eq. (4.26). Also, the spin density wave modulation is given by

$$\dot{S}(\dot{r}) = 2\vec{S} \cos(\vec{Q} \cdot \vec{r} + \phi) \tag{4.33}$$

with $\vec{Q} = (2k_r, \pi/b, \pi/c)$.

The behavior of the order parameter and of the various thermodynamic quantities can be described near $T_{\mathrm{SDW}}^{\mathrm{MF}}$ in terms of the Ginzburg-Landau theory; in a fashion which follows the description of the charge density wave transition near $T_{\mathrm{CDW}}^{\mathrm{MF}}$. Consequently, $\Delta(T)$, and ΔC are also given by Eqs. (3.62) and (3.63) in terms of the coefficients a and b of the Ginzburg-Landau free energy functional.

The evaluation of coherence factors proceeds along the same lines used for the charge density wave ground state, and the resulting transition probabilities, agree with those calculated for charge density waves. The ultrasonic attenuation reflects the case II coherence factors, and is expected to display a maximum below $T_{\mathrm{SDW}}^{\mathrm{MF}}$; while the conductivity is determined by case I coherence, and is expected to drop sharply below the transition.

1.4.2 Experimental Evidences for the Spin Density Wave Transition and Ground State

Evidence of transitions to a spin density wave state have been found in several of the organic linear chain compounds which were discussed in Chapter 2. Measurements of the various thermodynamic quantities have been performed only in a few cases and the principal observations on the transition have been in the transport and magnetic properties.

As for charge density waves, the development of the SDW ground state opens up a gap at the Fermi level, leading to a metal-insulator transition. The dc resistivity measured on three compounds which develop SDW ground states is displayed in Fig. 4.2. In all three cases there is a well defined transition from metallic to semiconducting behavior; and as for charge density waves, the transition temperatures, called T_{3D}, are identified through the measurement of the temperature derivative $d \ln \rho / d(1/T)$ (see Eq. (3.80)). Below T_{3D}, the conductivities are well described by Eq. (3.78), and the single particle gaps, together with the transition temperatures are collected in Table 4.1. These values, together with the parameters which characterize the

metallic state above T_{3D}, lead, using Eq. (1.26), to ξ_0 and by virtue of Eq. (4.12), to the coupling constant λ_e.

Values of the density of states above the transition, $n(\epsilon_F)$, have been evaluated from the magnetic susceptibilities measured above T_{3D}; and the values as given in Table 2.2 lead, using Eqs. (4.11) and (4.12), to the Coulomb energies (displayed in Table 4.1), which are significantly smaller the ϵ_F. In all of these compounds therefore, Coulomb effects lead to an SDW state, in the so-called weak coupling limit. The measured single particle gaps, together with the Fermi velocities, also lead to large coherence lengths, and the zero temperature values $\xi_{\|} = \hbar v_F/\pi\Delta$ are given in Table 4.1. As for charge density waves, because of the strongly

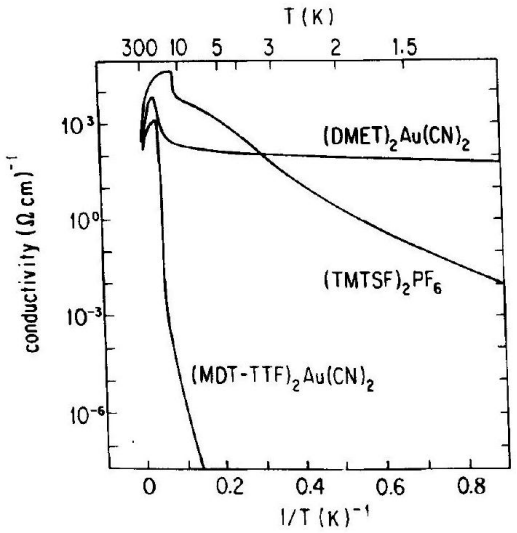


Figure 4.2. The temperature dependence of the *dc* conductivity in various materials which develop an SDW ground state at low temperatures. The TMTSF and MDT-TTF salts are semiconducting below \$T=11.5 \mathrm{˜K}\$ and 20 K respectively, the DMET salt remains semimetallic below the transition (Bechgaard, et al., 1980; Kikuchi et al., 1987; Nakamura et al., 1990).

anisotropic bandwidth in the various crystallographic directions, the coherence length is also anisotropic. This anisotropy has been measured only for the (TMTSF) $_2$X salts, and with the anisotropic Fermi velocities, as discussed in Chapter 2 we obtain $\xi_{1.y} \simeq 30\mathring{A}$, while in the z direction $\xi_{\perp} < c$ is the lattice constant.

The above values of the single particle gaps and Coulomb energies also suggest small magnetic moments associated with the spin density wave state. The amplitude of the SDW modulation may be written as

$$\frac{\mu}{\mu_B} = \frac{4|\Delta|}{U}. \tag{4.34}$$

The values of Δ and U as evaluated above lead to the reduced

Table 4.1. Parameters of the Spin Density Wave State in various compounds. Δ_{ρ} refers to the gap as evaluated from the temperature dependence of the *dc* resistivity.

	$T_{\mathrm{SDW}}\ (K)$	$2\Delta_{\rho}(K)$	λ Eq. (4.11)	$\xi_{\|}$(Å)	μ/μ_b (NMR)
(TMTSF) $_2PF_6$	$11.5^{(1)}$	30	0.26	320	$0.08^{(4,5)}$
(MDT-TTF) $_2Au(CN)_2$	$20^{(2)}$	NA			$0.1^{(6)}$
$(DMET)_2Au(CN)_2$	$20^{(3)}$	200	0.25	160	$0.1^{(7)}$
	μ/μ_B Eq. (4.34)	U(eV) Eq. (4.12)			
(TMTSF) $_2PF_6$	0.01	2.0			
$(DMET)_2Au(CN)_2$	0.008	2.0			

1. D. Jerome and H. Schultz, Adv. Phys. 31. 299 (1982).
2. T. Nakamura, et al. Solid State Comm. 75, 583 (1990).
3. K. Kikuchi, et al. Jap. J. Appl. Phys. Supp. 26-3, 1369 (1987).
4. T. Takahashi, et al. Physica 143B, 417 (1986).
5. J. M. Delrieux, et al. Physica 143B, 412 (1986).
6. K. Kanoda, et al. Phys. Rev. B42, 8678 (1990).
7. K. Kanoda, et al. Phys. Rev. B38, 39 (1988).

magnetic moments given in Table 4.1. The magnetic properties of the SDW state have not been calculated using the Hamiltonian Eq. (4.2). It is expected however, that the magnetic response and the collective excitations are close to those of an antiferromagnet; with localized spins which are a distance $\lambda_0/2$ apart and which correspond to a reduced moment μ and to an effective exchange constant I_{eff} . Therefore the Hamiltonian

$$\mathscr{H} = \left(\frac{\mu}{\mu_B}\right)^2 J_{\mathrm{eff}} \sum_i \vec{S}_i \cdot \vec{S}_{i+1} - \left(\frac{\mu}{\mu_B}\right)^2 D^* \sum_i S_i^r S'_{i+1} + \left(\frac{\mu}{\mu_B}\right)^2 E^* \sum_i \left(S_i^z S_{i+1}^z - S_i^y S_{i+1}^y\right) - \mathrm{g}\mu\vec{H} \sum_i \vec{S}_i \tag{4.35}$$

has been used to evaluate the parameters which characterize the SDW ground state. Here J_{eff} is the interaction along the chains, and D^* and E^* represent the hard- and intermediate-axis anisotropy energies respectively; the reduced moment is written as μ/μ_R. The above Hamiltonian leads to an anisotropic susceptibility, with

$$x_{i|} \to 0 \tag{4.36a}$$

$$x_{\cdot} = \frac{N_{\cdot} g^2 \mu_0^2}{2\left(\frac{\mu_0}{\mu_B}\right)^2 J_{\mathrm{eff}}} = \frac{N_{\cdot} g^2 \mu_B^2}{2J_{\mathrm{eff}}} \tag{4.ibb}$$

at zero temperature; the parallel direction refers to the magnetic field which is applied parallel to the easy axis along which the electron spins are aligned in the absence of an external magnetic field.

The effective exchange constant J_{eff} can be estimated using the following argument. In the spin density wave ground state a gap Δ develops for both spin subbands. However, there is no gap for spin-flip transitions, i.e., for transitions between the two spin subbands. In the presence of a magnetic field H, these subbands are shifted by $\pm\mu_B H$ and arguments applied for the Pauli susceptibility of the metallic state are appropriate. These lead to $\chi_\perp(T=0) = \chi_{\text{Pauli}}$ $(T > T_{\text{SDW}})$ and in the absence of anisotropy effects the susceptibility is unaffected by the SDW transition. Then

$$\frac{g^2\mu_R^2}{2J_{\text{vff}}} N_r = \mu_R^2 n(\epsilon_r) \tag{4.37}$$

gives

$$j_{\text{elf}} = \frac{N_r}{n(\epsilon_r)} = \epsilon_r = \hbar v_F k_1. \tag{4,38}$$

With ϵ_r as given in Table 2.2 we expect J_{eff} to be on the order of 1000 K for the various materials.

The anisotropy as implied by Eq. (4.36) has been observed in (TMTSF) $_2$X salts, and the susceptibility measured (Mortensen et al., 1981, 1982) in the AsF_6 salt is displayed in Fig. 4.3. The magnitude of $x_\perp$ leads, using Eq. (4.36a), to an effective coupling constant $J_{\text{eff}} = 740$ K. The Hamiltonian, Eq. (4.35), also leads to a spin-flop field given by

$$H_{,+} = \frac{\pi (2E^* J_{\text{eff}})^{1/2}}{\hbar\gamma} \tag{4.39}$$

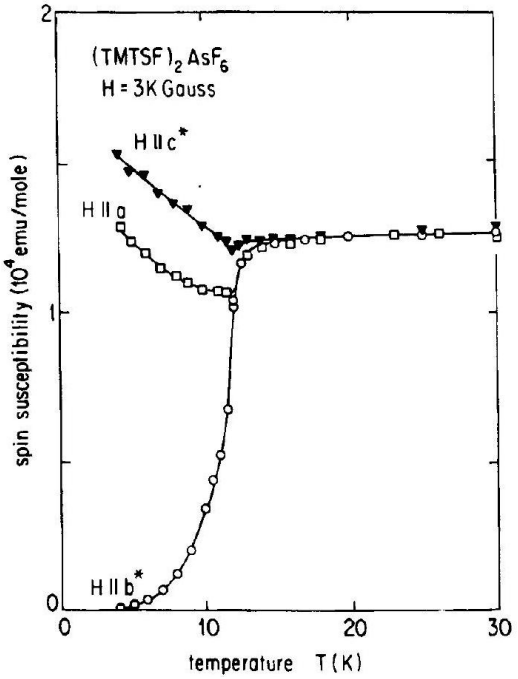


Figure 4.3. Temperature dependence of the single crystal spin susceptibility of (TMTSF) ${ }{2} \mathrm{AsF}}{6}$ in a magnetic field (H = 3kOe) lower than the spin-flop field. The axis b^*, a and c^* are respectively the easy, intermediate, and hard axis of the SDW state stable below 12 K (Mortensen et al., 1982).

where γ is the gyromagnetic ratio. Experiments at various magnetic fields, again in (TMTSF) $_2$X salts (Mortensen et al., 1982), clearly establish the existence of a spin-flop field,

which is on the order of $H_{sf} \simeq 6$kG, from which an anisotropy energy of $E = 3 \times 10^{-5}$ K has been estimated.

The spatial variation of the spin density as given by Eq. (4.18) leads to a spatial variation of the internal magnetic field at the nuclear sites given by

$$\delta H(\vec{r}) = \langle a_0 \rangle \, H_0 \frac{\mu}{\mu_B} \cos(2\vec{Q} \cdot \vec{r} + \phi) \tag{4,40}$$

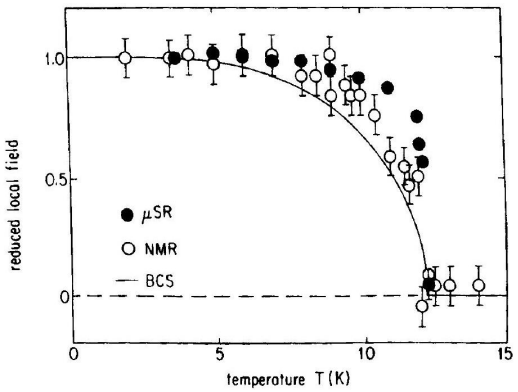


Figure 4.4. The temperature dependence of the normalized average internal field at the nuclear sites as measured by nuclear magnetic resonance and muon spin rotation (Le et al., 1991).

in the presence of an external *dc* magnetic field H_0 where $\langle a_0 \rangle$ is the hyperfine field interaction constant (a quantity which in general can be estimated). The internal field distribution, which is a sensitive function of the precise spatial dependence of the spin density, can be measured by local probes such as nuclear magnetic resonance (NMR) and muon spin rotation (μSR). Note that for a commensurate SDW, the distribution of the local fields at the nuclear sites is different from the distribution caused by an incommensurate SDW. Consequently, such studies can establish the incommensurate character of the density wave, and an elaborate analysis can also lead to the nesting wavevector, $\vec{Q} = (\, Q_1, 2k_F \,)$. This has been done for (TMTSF) PF_6, (Andrieux et al., 1981; Takahashi et al., 1986; Delrieux et al., 1981; Creuzet et al., 1982), leading to an SDW distortion wavevector ($0.5, 0.24, 0.06$) in units of a^*, b^*, and c^* (with b the chain direction); which is close to, but distinctively different from, a commensurate period $Q = (1/2, 1/4, 0)$. The period measured along the chain direction is also near the optimal nesting as arrived at by band structure
calculations (Yamaji, 1982, 1983). The incommensurate SDW has also been established by μ SR studies (Le et al., 1991). The magnitude of the magnetic field distribution, when measured at various temperatures, directly gives the temperature dependence of the order parameter and experimental results obtained both by NMR and μ SR studies displayed in Fig. 4.4. The full line of the figure is the order parameter $\Delta(T)$, obtained from the weak coupling BCS theory. The somewhat stronger temperature dependence observed near $T_{\rm SDW}$ may be due to the weakly first order nature of the transition to the spin density wave ground state. The magnitude of the spin density wave modulation can also be extracted from the experimental results, leading to μ/μ_B which is close to that evaluated from NMR studies. This value is somewhat larger than the magnetic moment evaluated from the measured single particle gap and Coulomb interaction energy by using Eqs. (4.12), and (4.34).

Magnetic susceptibility and NMR studies have also been conducted in (MDT-TTF) $_2$Au(CN)$_2$ (Kanoda et al., 1990) and in (DMET) $_2$Au(CN)$_2$ (Kanoda et al., 1988). In both cases, the magnetic properties are similar to those of an antiferromagnet with a small

magnetic moment; and the broadened NMR signal below T_{3D} clearly establishes that the spin density wave is incommensurate with the underlying lattice.

1.5 Fluctuation Effects

Asdiscussed in previous chapters, the mean field solution of one-dimensional models leads to finite transition temperatures T^{Mr} where long range order develops. This is an artifact of the mean field approximation which neglects the role played by fluctuations of the order parameter. In strongly anisotropic materials, because of the reduction of the phase space such fluctuation effects become important; and a strictly one-dimensional system with short range interactions does not develop long range order at finite temperatures. Instead, only short range correlations occur at low temperatures (Landau and Lifschitz, 1958).

Of course, the materials which have been discussed are not strictly one-dimensional; Coulomb interactions between electrons on neighboring chains and also one-electron interchain tunneling lead to coupling of the fluctuations on neighboring chains. Such coupling leads again to a finite transition temperature, T_{31}, below which three-dimensional long range order occurs. For weak interchain coupling, $T_{3\mathrm{D}}$ is significantly smaller than T^{MF}, the transition temperature given by the mean field approximation. The region below T^{MF} but above $T_{3\mathrm{D}}$ is characterized by onedimensional fluctuations which, sumewhat above $T_{3\mathrm{D}}$, cross over to fluctuations which (depending on the anisotropy) have a twoor three-dimensional character. In addition to such effects the short coherence lengths observed, especially for charge density waves, also lead to fluctuations near T_{3D}, in much the same way
that fluctuations arise in superconductors with short coherence lengths (Ginzburg, 1960).

Rigorous solutions for the behavior of the 1D chain with correlations which lead to a complex order parameter and also for the effects of interchain coupling are not available. The various approaches (Scalapino et al., 1975; Schultz, 1987), while leading to the same overall qualitative picture, give different expressions for the various characteristic temperatures and for the detailed temperature dependences of the experimentally accessible quantities. Here only a simplified description of the state of affairs is given, often referring to results which go well beyond the scope of these notes. The description which follows is appropriate for a set of weakly coupled chains where the mean field transition temperature is significantly higher than the temperature where threedimensional long range order develops. This approach is appropriate for highly anisotropic materials; while for compounds for which the anisotropy of the electronic band structure is not large a different approach based on fluctuation theories in conventional three-dimensional solids (extended to anisotropic systems) may be more appropriate. Such an approach is summarized by Schultz (1987).

Experimental evidence for fluctuation effects has been found in a variety of materials in which charge or spin density wave ground states occur at low temperatures. Our understanding of fluctuations which precede the charge density wave transition are more complete, due partly to the observable structural changes which accompany such transitions; but also due to the availability of large single crystals on which the experiments can be performed. The most detailed structural, optical, and thermodynamic experiments have been conducted on $K_{0.3}MoO_3$, a material which undergoes a CDW transition at $T = 183$ K. Consequently, experiments on this compound will mainly be discussed and contrasted with the various models of fluctuations.

1.5.1 Fluctuations in Quasi-One-Dimensional Metais

5.1.1 Fluctuations for a One-Dimensional Chain

For a one-dimensional chain which is described by the Fröhlich Hamiltonian Eq. (3.11) or by the Hubbard Hamiltonian, Eq. (4.1),
the order parameter is complex; and therefore when describing the temperature dependence of the correlation length, both the amplitude and phase fluctuations of the order parameter must be included. These fluctuations can be described by the GinzburgLandau functional, which for a one-dimensional chain is given as

$$F = F(0) + n\left(\epsilon_F\right) \int dx \left[a|\Delta|^2 + b|\Delta|^4 + c\left|\frac{d\Delta}{dx}\right|^2 \right] \tag{5.1}$$

where Δ is the complex order parameter.
The mean field description of the density wave transition was discussed in Chapters 3 and 4 in terms of the Landau theory; where the last term, representing the spatial fluctuations of the complex order parameter, is neglected. The shape of the free energy functional for a complex order parameter is shown in Fig. 5.1. At temperatures $T > T^{\mathrm{MF}}$, with the mean field transition temperature as given by Eqs. (3.19) and (4.11b) for charge and spin density waves respectively; the amplitude of the order parameter fluctuates near $|\Delta| = 0$. The amplitude fluctuations are progressively removed as the temperature decreases, and at temperatures well below T^{MF}, the amplitude of the order parameter

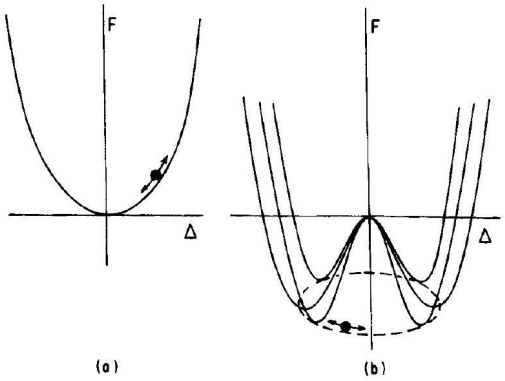


Figure 5.1. The free energy functional for a complex order parameter for $T>T_{\mathrm{MF}}(a)$ and for $T < T_{\mathrm{MF}}(b)$.

is close to its $T = 0$ value; and the phase of the order parameter rotates in the bottom of the potential well of $F(\Delta)$, as shown in Fig. 5.1. In this limit, the fluctuation of the order parameter is approximately given by

$$|\Delta|_0 \left\langle e^{i\phi(x)} \right\rangle \simeq |\Delta_0|\, e^{-\frac{1}{2}\left\langle \phi^2(x) \right\rangle} \tag{5.2}$$

where $|\Delta|_0$ is the magnitude of the gap at $T = 0$. For density waves the uniform phase $\phi =$ const corresponds to a frozen in lattice distortion with a wavevector $q = 2k_F$, and the spatial fluctuations of the phase are given in terms of the Fourier components as

$$\left\langle \phi^2(x) \right\rangle = \sum_{q-2k_j} \left\langle \phi^2_{q-2k_j} \right\rangle e^{i(q-2k_i),} = \sum_{q'} \left\langle \phi^2_{q'} \right\rangle e^{iq'x}. \tag{5.3}$$

The energy associated with each component $\phi_{q'}$ is approximately given by $n(\epsilon_F)\,\delta^2(\epsilon) = n(\epsilon_F)\,[\hbar v_F q']^2$ for a one-dimensional band. From the equipartition theorem

$$n(\epsilon_F)\,(\hbar v_F q')^2\,\langle\phi_{q'}^2\rangle = k_B T \tag{5.4}$$

which, together with (5.3), gives

$$\langle\phi^2(x)\rangle = \frac{\pi k_B T}{\hbar v_F}\int_0^{\pi/a}\frac{e^{tq'x}dq'}{(q')^2} \tag{5.5}$$

where we have replaced the summation with an integral over the Brillouin zone, and have used $n(\epsilon_F) = (\pi\hbar v_F)^{-1}$.

The integral on the right hand side diverges, and consequently, the order parameter as given by Eq. (5.2) has a vanishing expectation value at finite temperatures; hence there is no long range order.

The correlation function of the complex order parameter is given in this limit by

$$\langle\Delta^*(x),\Delta(0)\rangle = |\Delta|_0^2 e^{-\frac{1}{2}\langle[\phi(x)-\phi(0)]^2\rangle}. \tag{5.6}$$

The spatial dependence of the phase is given by the terms of the Fourier components

$$\langle[\phi^2(x)-\phi^2(0)]\rangle = \sum_{q'}\phi_{q'}^2\left(e^{tq'r}-1\right) \tag{5.7}$$

With the previous estimate of the energy associated with the fluctuating q component, we have

$$\langle[\phi^2(x)-\phi^2(0)]\rangle = \frac{\pi k_B T}{\hbar v_1}\int_0^{\pi/a}\frac{(1-\cos q'x)\,dq'}{(q')^2} = \frac{\pi k_B T}{\hbar v_1}x \tag{5.8}$$

and consequently,

$$\langle\Delta^*(x),\Delta(0)\rangle = |\Delta|_{ne^e}^2 - \frac{\pi k_B T}{h^2 u_1}\Big|\; x_1' = c\frac{|x|}{k_{10}} \tag{5.9}$$

with the phase-phase correlation length

$$\xi_{11} = \frac{\hbar w_1}{\pi k_B T} \tag{5.10a}$$

which is the same as that obtained in Chapter 1 for the density fluctuations of the 1D electron gas. All this is appropriate well below T^{MF} where amplitude fluctuations can be neglected, and only phase fluctuations are important. At high temperatures, where the fluctuations of the amplitude are important, the correlation length is somewhat different and is given by (Lee, Rice, and Anderson, 1973)

$$\xi_{1b} = \frac{[7\zeta(3)]^{1/2}v_I}{4\pi k_R T} \tag{5.10b}$$

where $\zeta(3)$ is the third order zeta function. Consequently, the correlation length displays an approximate $1/T$ dependence (see Scalapino et al., 1975) at all temperatures with a change of the prefactor near T^{Ml}.

The progressive development of density wave fluctuations is accompanied by corresponding changes in the phonon and electron densities of states. The susceptibility, which is related to the order parameter fluctuations, is defined as

$$\chi(q) = \frac{1}{k_B T} \int \langle \Delta^*(x), \Delta(0) \rangle \, e^{\prime\prime\eta} dx \tag{5.11}$$

and by virtue of the fluctuation dissipation theorem the static correlation function is given by

$$S(\eta) = k_B T \chi(q). \tag{5.12}$$

For charge density waves, the order parameter is related to
(or can be defined as) the periodic lattice distortion, and from Eq. (3.23)

$$S(q) = \frac{2\hbar g^2}{N M \omega_{2h_1}} \int \langle \Delta u(x), \Delta u(o) \rangle e^{i\prime\prime} dx \tag{5.13}$$

For spin density wave correlations, the order parameter is the staggered magnetization, and using Eq. (4.20)

$$S(q) = \frac{U^2}{N} \int \langle S(x), S(o) \rangle e^{|q|} dx \tag{5.14}$$

The fluctuations of the charge density wave order parameter can be examined by X-ray or neutron scattering. As there is no lattice distortion related to the development of spin density wave correlations, they can be studied only through magnetic neutron scattering. The scattering intensity is given by

$$l(k) = c^{-2W} \sum_H I \left(k - H_0 \cdot \vec{d} \pm 2k_\Gamma \right) S(q) \tag{5.15}$$

where $\vec{d} = d_\parallel, d_\perp$ represents the lattice points, and $d_\parallel$and $d_\perp$ are the lattice constants parallel and perpendicular to the chains, and H_0 is the Miller index of reflection. From Eq. (5.11)

$$\begin{aligned} \chi_{1D}(q_{11}) &= \frac{1}{k_B T} \int \left\langle |\Delta| \right\rangle^2 \exp\left[-\frac{x}{\xi_{1D}} \right] e^{u|r} dx \\ &= \frac{\langle |\Delta|^2 \rangle}{k_B T} \frac{\xi_{1D}/a}{1 + (q_1 \xi_{1D})^2} \end{aligned} \tag{5.16}$$

where a is the lattice constant along the chain direction. This then, through Eqs. (5.12) and (5.13) leads to a broadened scattering peak, with a width determined by $\xi_{1\mathrm{D}}$.

Long range order also leads to a well defined single particle gap, with a square root singularity at the gap which is characterized of a one-dimensional density of states as discussed in Chapter 3. Short range correlations lead instead to a pseudogap, with a suppressed density of states below the gap energy; the decrease of $D(\epsilon)$ for $\epsilon < |\Delta|$ becomes more pronounced for large correlation length. $D(\epsilon)$ has been calculated by Lee, Rice, and Anderson (1974) for a 1D Fröhlich Hamiltonian, and the results are shown

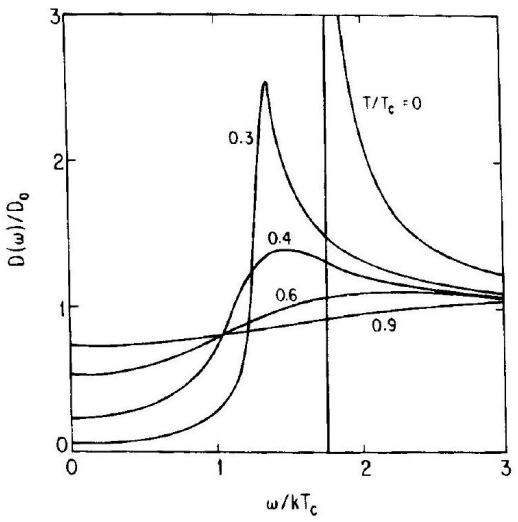


Figure 5.?. The density of states $D(\omega)$ for a one-dimensional chain undergoing a Peierls transition. $T_{\text {s }}$ refers to the mean field transition temperature (lee et al., 1973). D_0 is the (constant) density of states well above T_c.

in Fig. 5.2. In the Figure T_{r} refers to the mean field transition temperature, given in terms of the parameters of the model by Eq. (3.19).

5.1.2 Fluctuations for a System of Coupled Chains

The above picture is modified for a three-dimensional array of parallel chains. Due to interchain interactions density wave fluctuations on the neighboring chains become correlated and this leads to a transition to a ground state with three-dimensional, long range order. Let us assume a square lattice chains, with the lattice constant $d_{\perp}$. Then the interchain interaction can in general be written as

$$E_{\mathrm{int}} = n\left(\epsilon_F\right) \frac{2}{d_{\perp}^2} c_{\perp} \sum_{1,1} dx \,\mathrm{Re}\left[\Delta_1^*(x), \Delta_1(x)\right] \tag{5.17}$$

where i and j are the chain index and the summation is over nearest neighbors. In Eq. (5.17) we assume that the interchain

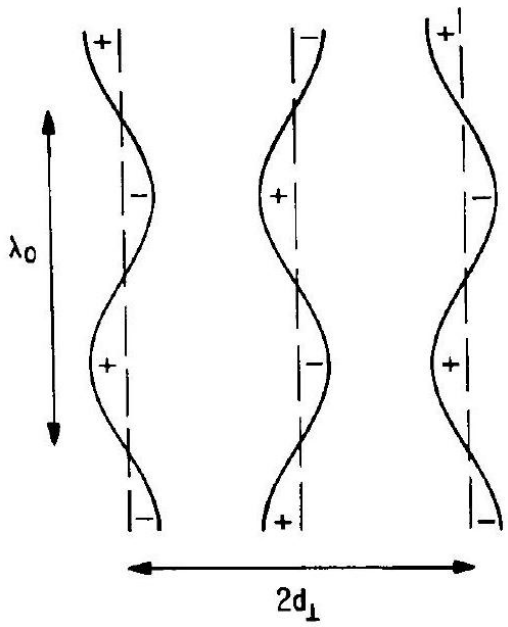


Figure 5.3. Charge density wave modulations on neighboring chains. Both Coulomb interactions and a quasi 2D Fermi surface lead to out of phase modulations of the density waves as shown in the figure.

interaction $c_\perp$ (and also the interchain distance) is the same in two directions perpendicular to the chain direction. In most cases $c_\perp > 0$, and E_{int} is minimum where the sign of the order parameter alternates between neighboring chains at distance $d$apart (shown in Fig. 5.3). This alternation can be taken into account by defining a new order parameter

$$\Delta(\vec{r}) = (-1)^{(1/y_i+z_i)/d_1}\Delta_i(x). \tag{5.18}$$

With this definition the order parameter $\Delta(\vec{r})$ is constant in case of long range order and its fluctuations can be described within the framework of the Ginzburg-Landau theory, as will be done later.

Two mechanisms were found to be important in establishing an interaction between the neighboring chains. Coulomb interactions between the charge density wave modulations $\Delta\rho(x)$ on neighboring chains of unit length are given by (Saub et al., 1976)

$$V_{t;} = \frac{1}{4\pi}\int_0^1 dx_j \frac{\Delta\rho\,(x_i)\,\Delta\rho\,(x_j)}{\left[d_\perp^2 + (x_1 - x_i)^2\right]^{1/2}}. \tag{5.19}$$

In terms of the phase difference $\boldsymbol{\phi} = \boldsymbol{\phi}_1 - \boldsymbol{\phi}_1$ of the density charge wave modulations on the neighboring chains,

$$V_u = \frac{(\Delta\rho)^2}{8\pi}\cos\phi \int_0^{1/2k_1} \frac{du\cos^2 u}{\left[u^2 + (2k_1 d_+)^2\right]^{1/2}} \tag{5.20}$$

where $u = 2k_1\,(x_i - x_j)$ and $\Delta\rho$ is the amplitude of the charge density modulations. The interaction, energy has a minimum when $\phi = \pi/2$. As $\Delta\rho$ is proportional to $\Delta n\,(\epsilon_F)$, the coefficient $c_\perp$ which appears in Eq. (5.17) is given by

$$c_1 = \frac{1}{8\pi}\int_0^{1/2k_1} \frac{du\cos^2 u}{\left[u^2 + (2k_F d_\perp)^2\right]^{1/2}}. \tag{5.21}$$

This type of coupling is probably dominant for charge density waves. However, there is no interaction arising from Coulomb effects for spin density waves; as there is no charge density wave modulation. Single particle tunneling between the chains also leads to ordering of density wave modulations on neighboring chains. This may be important both for charge and for spin density waves. The consequence of interchain tunneling is a two-dimensional (or quasi-three-dimensional) band structure, with a dispersion relation given by Eq. (1.12). The optimal nesting condition, discussed in Chapter 1, leads to alternating phase of the density modulations on the neighboring chains; which can be represented by an interchain coupling, the magnitude of which is given by (Horowitz et al., 1975).

$$c_{-} = 2\left(\frac{t_{\perp} d_L}{v_{F\|}}\right)^2 c. \tag{5.22}$$

where c is the Ginzburg-Landau coefficient defined in Eq. (5.1).
For c_1 as defined in Eq. (5.17) the wave vector dependent coupling constant is given by

$$c_{\perp}\left(q_{\perp}\right) = \frac{c_{\perp}}{2}\sum_{l} e^{iq_{\perp}d_{\perp}} = \frac{c_{\perp}}{2}\cos\left(q_{\perp}d_{\perp}\right). \tag{5.23}$$

This interchain coupling acts as an effective field, which tends to stabilize an ordered phase, with density wave modulation in opposite phase on neighboring chains. As usual the problem can be discussed within the framework of the mean field theory.

The susceptibility, $\chi\left(q_{\|}, q_{\perp}\right)$ can be written in the mean field approximation as

$$\chi\left(q_{\|}, q_{\perp}\right) = \frac{\chi_{1D}\left(q_{\|}\right)}{1 - Zc_{\perp}(0)\chi_{1D}\left(q_{\|}\right)} \tag{5.24}$$

where Z is the number of nearest neighbors. The divergence of $\chi\left(q_{\|}, q_{\perp}\right)$ defines a mean field transition temperature T_{31} of the system of coupled chains, which is then given by

$$1 - Zc_{\perp}(0)\chi_{1D}\left(q_{\|}\right)\left(T_{3D}\right) = 0 \tag{5.25}$$

As discussed earlier, the temperature dependence of $\xi_{1\mathrm{D}}$ and $\chi_{1\mathrm{D}}$ have not been evaluated for a complex order parameter and the behavior is known only well below and well above T^{MF}.$T_{3\mathrm{D}}$ can therefore be evaluated only for certain assumptions on the temperature dependence of the coherence length. For weak interchain coupling the behavior well below T^{MF} is important. Then the amplitude of the order parameter is close to its $T = 0$ value, and interchain coupling leads to an adjustment of the phase of the density wave modulations on the neighboring chains. The transition temperature can then be estimated using the following simple argument. Correlations over the coherence length $\xi_{10}(T)$ are coupled due to interchain interactions, and the energy gain due to such phase adjustment is on the order of

$$\Delta E_{\perp} = Zc_{\perp} n\left(\epsilon_F\right)|\Delta(T=0)|^2 \xi_{1D}(T). \tag{5.26}$$

This leads to a transition temperature $T_{3\mathrm{D}}$ which, in the spirit of the mean field approximation, is approximately given by

$$k_B T_{3D} \simeq \Delta E_{\perp}. \tag{5.27}$$

By virtue of Eq. (5.10a) we obtain

$$k_B T_{3D} = \left[\pi^{-1} Z C_{\perp} n\left(\epsilon_F\right)|\Delta(T=0)|^2 \hbar v_f\right]^{1/2} \tag{5.28}$$

in the limit where $T_{3\mathrm{D}} \ll T^{\mathrm{MF}}$ and only phase fluctuations play an important role. The same transition temperature is obtained using Eq. (5.25), with $\xi_{1\mathrm{D}}$ as given by Eq. (5.16).

In the case where the fluctuations of the amplitude are important and Eq. (5.10b) applies, the same relation, with a prefactor different from π^{-1}, is obtained. The transition temperature, T_{3D}, where three-dimensional order develops is, for a small interchain coupling c_1, significantly smaller than T_{MF} as given by Eq. (3.19); and the transition temperature approaches zero for vanishing interchain coupling, as expected.

Having evaluated the mean field transition temperature where 3D order develops; the behavior near T_{3D} can be discussed using the Ginzburg-Landau functional, and Eq. (5.4) together with the interchain coupling term, Eq. (5.17), becomes

$$\begin{aligned} F =& F(0) + \frac{1}{d_\perp^2} n\left(\epsilon_l\right) \int d^3\vec{r} \\ & \times \left\{ a|\Delta|^2 + b|\Delta|^4 + c\left|\frac{d\Delta}{dx}\right|^2 + c_\perp^* \left|\nabla_\perp \Delta(\vec{r})\right|^2 \right\} \end{aligned} \tag{5.29}$$

where $c_\mathrm{l}^* = c_\perp d_\perp^2$, and $\nabla_\perp$ is the gradient with respect to the transverse spatial variables. The spatially varying order parameter is written as

$$\Delta(x) = \sum_k \Delta_k e^{ikt} \tag{5.30}$$

and, in terms of Δ_k, F is given by

$$F = F(0) + \sum a_k \left|\Delta_k\right|^2 + \frac{b}{2} \sum_{k_1 k_2 k_3} \Delta_{k_1}^* \Delta_{k_2}^* \Delta_{k_3} \Delta_{k_1+k_2-k_3} \tag{5.31}$$

with

$$a_1 = a + ck_1^2 + c_\perp \left(k_4^2 + k_2^2\right). \tag{5.32}$$

If we neglect the last term in Eq. (5.31), the correlation function of the order parameter is given by

$$\left\langle \Delta^*(\vec{r}), \Delta(o) \right\rangle = \frac{1}{2\pi} \int d\vec{k} \left\langle \left|\Delta_k\right|^2 \right\rangle e^{ik\cdot r'} \tag{5.33}$$

From the fluctuation-dissipation theorem (note that here we assume that in 3D there is a phase transition, and a_k is finite)

$$\left\langle \left|\Delta_k\right|^2 \right\rangle = \frac{k_8 T}{a_k} \tag{5.34}$$

and with Eq. (5.32) the integral in Eq. (5.33) can be evaluated in three dimensions leading to

$$\left\langle \Delta^*(\vec{r}), \Delta(o) \right\rangle = \frac{1}{\left[\left(\frac{x}{\xi_\parallel}\right)^2 + \left(\frac{r_1}{\xi_1}\right)^2\right]^{1/2}} e^{-\left[\left(\frac{1}{\xi_1}\right)^2 + \left(\frac{r_2}{\xi_1}\right)^2\right]'\Big]'} \tag{5.35}$$

with the two correlation lengths

$$\xi_{11} = \left(\frac{c}{a}\right)^{1/2} \tag{5.36a}$$

$$\xi_\perp = \left(\frac{c_-}{a}\right)^{1/2} \tag{5.36b}$$

In the spirit of the Gaussian approximation we assume that near $T_{3D}, a = a'(T - T_{3D})$, and therefore

$$\xi_{\|} = \left(\frac{c}{a'}\right)^{1/2} (T - T_{3D})^{-1/2} . \tag{5.37a}$$

$$\xi_{\perp} = \left(\frac{c_{\perp}}{a'}\right)^{1/2} (T - T_{3D})^{-1/2} . \tag{5.37b}$$

Thus, both the on-chain and perpendicular correlation lengths diverge at T_{3D}, and the square root behavior of the coherence length is typical of the Ginzburg-Landau treatment in the Gaussian approximation of the fluctuations, where the last term in Eq. (5.31) is neglected. Near T_{3D} both $\xi_{|}$and $\xi_{\perp}$ are large, and $\xi_{\perp}$ exceeds $d_{\perp}$, the distance between the chains. In this region, the fluctuations have a three-dimensional character, with fluctuations on neighboring chains strongly coupled. With increasing temperature $\xi_{\perp}$ decreases, and at high temperatures it becomes smaller than d_1. In this temperature regime fluctuations on neighboring chains are decoupled and have a one-dimensional character. From (5.37b) this crossover from 3D to 1D fluctuations happens when

$$d_{\perp} = \left(\frac{c_{\perp}}{a'}\right) (T^* - T_{3D})^{-1/2} . \tag{5.38}$$

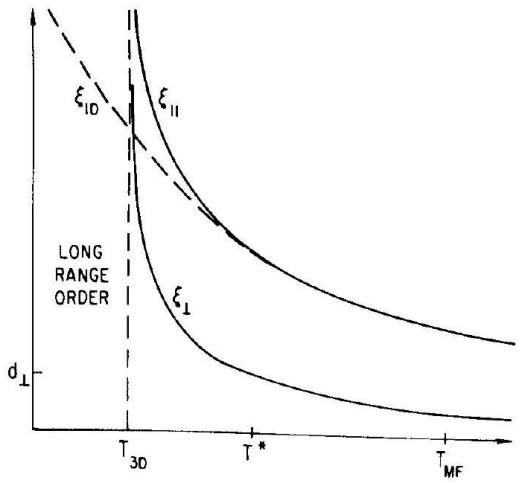


Figure 5.4. The temperature dependence of the correlation lengths parallel and perpendicular to the chains. The temperature dependence of the correlation length of a 1D chain (given by Eqs. (5.10a) and (5.10b) at low and at high temperatures) is also shown. The interchain lattice constant, d_{1}, is also indicated. T_{M1} is the mean field transition temperature, and there is a 1D to 3D crossover for fluctuations at T^*.

This then defines a crossover temperature

$$T^* = T_{31} + \frac{d_{\perp}^2 a'}{c_{\perp}} \tag{5.39}$$

The temperature dependences of $\xi_{|}$and ξ_2 are displayed in Fig. 5.4, together with ξ_{10} given by Eqs. (5.9) and (5.10) well below and well above T_{MF}.

The picture which emerges from the above analysis is as follows. At temperatures near T_{MF} , the system of coupled chains does not undergo a phase transition; instead correlations build up along the chains with the correlation length given by Eq. (5.10). Because the $2k_F$ fluctuations

on the neighboring chains are not correlated the scattering intensity $I(k)$ is essentially that of a 1D chain: the scattering cross section is that of parallel lines at a distance $2k_F$ from the Bragg diffraction spots. The situation, appropriate for a two-dimensional array of chains is shown in Fig. 5.5. Below approximately T^*, correlations among the fluctua-

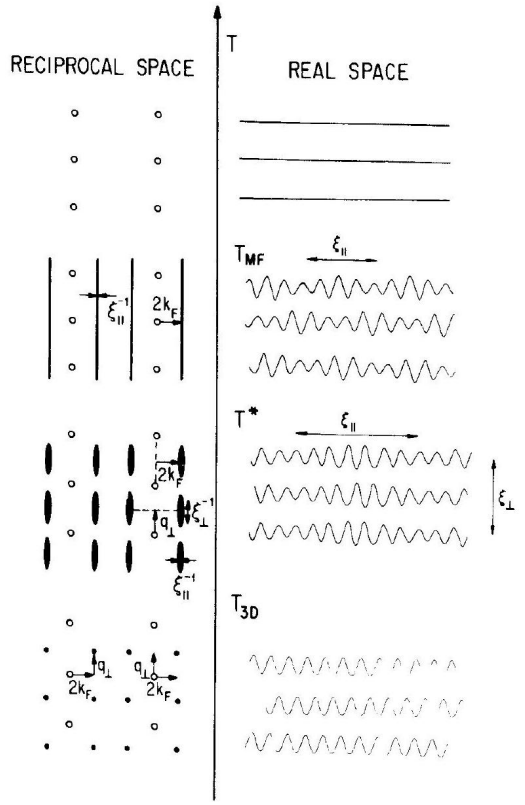


Figure 5.5. Fluctuations in a system of coupled chains in the 1D and 3D fluctuation regime and the corresponding long range correlations below T_{31}. The main features of the diffraction pattern are also displayed in the different temperature regions.

tions on neighboring chains develop, and the correlation function is given by Eq. (5.35). After some algebra the susceptibility

$$\chi(q) = \frac{1}{k_B T} \int \langle \Delta^*(\vec{r}), \Delta(0) \rangle \, e^{\prime q \cdot r} d\vec{r} = \frac{\chi(q=0)}{1 + \xi_{\parallel}^2 q_{\parallel}^2 + \xi_{\perp}^2 q_1^2}. \tag{5.40}$$

Because of the onset of 3D correlations (but absence of long range order) the scattering intensity $I(k)$ is that of a diffuse spot, with positions given by the $2k_F$ periodicity. The width of the spots is given by ξ_1 and $\xi_\perp$ in the directions parallel and perpendicular to the chains, as indicated in Fig. 5.5. With decreasing temperature the spot size progressively decreases due to the increasing correlation length. At $T = T_{30}$ long range order develops resulting in Bragg spots of (ideally) zero width and temperature dependent intensity as discussed in Chapter 3.

With additional fluctuation effects neglected, the behavior of the transition to the ordered ground state is mean-field-like. The short coherence lengths, in particular in the case of charge density wave transitions, however, suggest that critical fluctuations may be important. The temperature region ΔT where such fluctuations are of importance, is given by (Ginzburg, 1960)

$$\Delta T = \frac{k_B^2 T_{3B}}{\Delta C \left(\xi_{0\|} \xi_{0_\perp}\right)^2} \tag{5.41}$$

where ΔC is the measured specific heat anomaly at T_{3D} and $\xi_{0||}$ and $\xi_{0_\perp}$ are the zero temperature coherence lengths as defined by Eq. (1.26). Within this temperature region the temperature dependence of the various thermodynamic quantities is different from that which would follow from the mean field treatment. The temperature dependence of the correlation length is given by

$$\xi^{-1} \sim (T - T_{3D})^{\nu} \tag{5.42}$$

where the exponent depends on the dimensionality of the fluctuations. For three dimensions, and for a complex order parameter, the exponent $\nu = 0.67$ (Dietrich, 1976). The exponent ν is different from $\nu = 1/2$, which is appropriate for a mean field transition. This leads to a structure factor and to thermodynamic
quantities which have a temperature dependence distinctly different from those which are given by the mean field approximation.

1.5.2 Charge Density Wave Fluctuations in $K_{0.3}M\ o\ O_3$

The linear chain compound $K_{0.3}MoO_3$ undergoes a metal-insulator transition at $T_{3D} = 183$ K, and various experiments discussed in Chapter 3 give clear evidence for a charge density wave ground state below the temperature where long range order develops. Because of the availability of large single crystals, a wide range of transport, thermodynamic, and scattering experiments have been performed at temperatures above T_{3D}, and the important role of fluctuations has been established.

The single particle gap is $\Delta \simeq 700$ K at $T = 0$ (see Table 3.1), and this value, together with the weak coupling expression of the mean field transition temperature $2\Delta = 3.5 k_B T_{CDW}^{MF}$, leads to $T_{CDW}^{MF} = 330$ K; well above the temperature where long range order due to the coupling between the neighboring chains develops. There is therefore a large critical region where fluctuation effects are expected to be important.

These fluctuations have been examined in detail by neutron scattering measurements of the structure factor $S(q)$. Scans in different directions, when analyzed in terms of Eqs. (5.12) and (5.40), lead at room temperature (i.e., somewhat below T_{CDW}^{MF} but well above T_{3D}), to a behavior close to that shown in the upper half of Fig. 5.5. The correlation length along the chains is $\xi_{\|} = 20\mathring{A}$, exceeding the lattice constant, while in the directions perpendicular to the chains $\xi_\perp < d_\perp$; and consequently the fluctuations on the neighboring chains are decoupled. The correlation lengths increase with decreasing temperature and at $T^* = 200$ K, $\xi_\perp$ measured for both directions perpendicular to the chains exceeds $d_\perp$. Therefore at approximately this temperature a smooth transition to the region with 3D fluctuations occurs. The temperature dependence of the inverse coherence length, measured in the various crystallographic directions (parallel to the chains and in the two perpendicular directions), is shown in Fig. 5.6. The full line, which gives an appropriate representation of the experimental results of Eq. (5.42) with $\nu = 0.68$; is in excellent agreement with that expected for the $D = 3, n = 2$ universality class for a

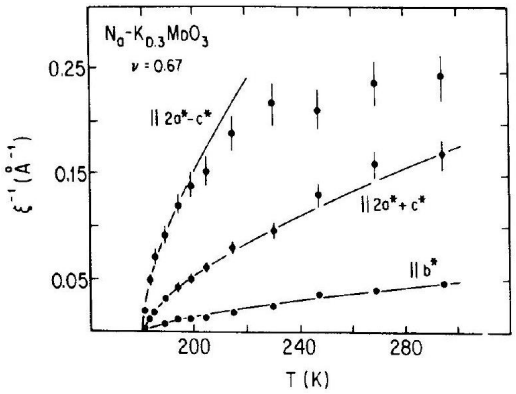


Figure 5.6. Temperature dependences of the inverse correlation lengths, measured in $\mathrm{K}{{03}, \mathrm{MoO}}{3}$ in three different directions. The full line is Eq. (5.42), near T_{31}, with $v = 2/3$. (Pouget, 1989; Pouget and Comes, 1989 and references cited therein). The mean field result is $\nu = 1/2$.

transition to an ordered state characterized by a complex order parameter. These experiments suggest that the Ginzburg critical region is large and ΔT is on the order of 20 K . This is not unreasonable, since the measured specific heat anomaly of $\Delta C = 3.6$ J(mole K)$^{-1}$ and the coherence volume $\xi_1\xi_1\xi_{12} = 420$ A^3 (Girault et al., 1989), indeed give $\Delta T = 20$ K. While the above discussion leads to well defined temperature ranges when one- or three-dimensional fluctuations occur, the actual state of affairs is certainly more complicated, as a description in terms of an isotropic interchain coupling $c_\perp$ is an oversimplification and the interchain coupling is different in the two crystallographic directions perpendicular to the chain direction. Consequently, a more detailed comparison between theory and experiment is not justified.

Fluctuation effects also lead to pronounced changes in the density of single particle electron states, and the gradual opening of the pseudogap has been inferred from the magnetic susceptibility and optical properties. The susceptibility $\chi(T)$ displayed in Fig. 5.7, first slowly decreases with decreasing temperature in

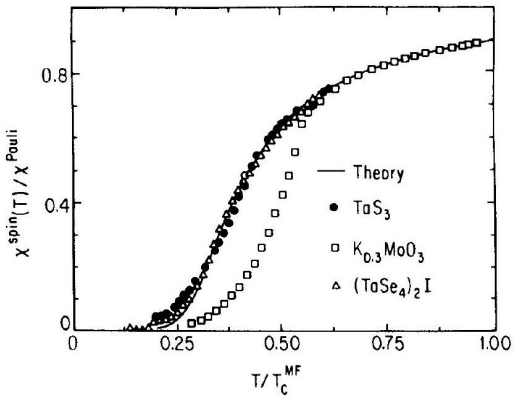


Figure 5.7. The temperature dependence of the magnetic susceptibility in $\mathrm{K}{{03}
\mathrm{MoO}}{3}$ and other compounds with CDW ground states. (Johuston et al., 1985). The full line is the result of a model calculation based on the theory of Lee et al. (1973).

the region near $T_{\mathrm{CDW}}^{\mathrm{MF}}$ where the fluctuations of the amplitude are important. The 3D transition temperatures are displayed in Table 3.1. Then using 2Δ (also given in Table 3.1) with Eq. (3.46) to evaluate T_{MF} gives the $T_{3\mathrm{D}}/T_{\mathrm{MF}}$ ratios 0,4; 0, 6; and 0,26 for TaS_3, $K_{0.3}MoO_3$, and $(TaSe_4)_2$ I. The rapid decrease somewhat above T_{3D} is due to the more pronounced development

of the pseudogap, with phase fluctuations of primary importance. The full line on the figure is the result of a model calculation, based on the theory of Lee, Rice, and Anderson (1973), which also leads to the density of states as shown in Fig. 5.2.

The gradual opening of the pseudogap has been directly confirmed by optical studies (Degiorgi and Grüner, 1992, Gorshunov et al., to be published), and the optical conductivity, measured at two different temperatures above T_{3D}, is shown in Fig. 5.8. The conductivity is depressed in the range between 100 and 10^3 cm^{-1}; indicating a pseudogap with decreasing temperatures, in full qualitative agreement with theory, worked out by

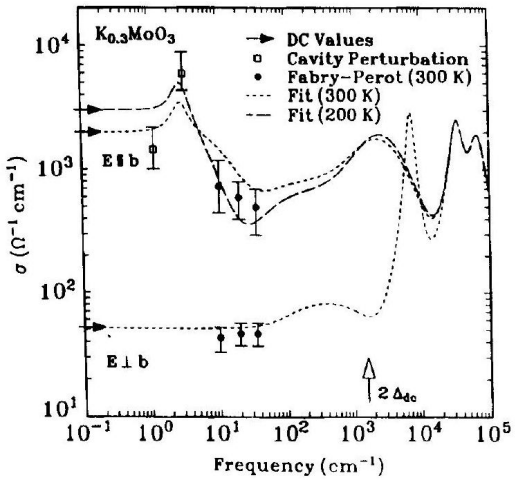


Figure 5.8. Optical conductivity measured at two different temperatures above $T_{31}=180$ K in $K_{11}MoO_3$ both parallel and perpendicular to the chain direction b. The notation "Fit" refers to the Kramers-Kronig type analysis of the reflectivity (Gorshunov et al., to be published).

Lee, Rice, and Anderson (1973). There is, however, a narrow peak near $\omega = 0$ along the chain direction, which becomes progressively more pronounced as T_{3D} is approached from above. This most likely is due to the fluctuating CDW segments which contribute to the conductivity. A detailed theory however, is not available to date.

The various thermodynamic quantities, such as specific heat, thermal expansion, and elastic properties are dominated, in the temperature range well above T_{3D}, by the (temperature dependent) contributions due to the underlying lattice. Consequently, such experiments do not give information on low-dimensional fluctuation effects. These quantities, however, have been explored at temperatures near T_{3D} and they give clear evidence for critical fluctuations and for deviations from the mean field approximation. The specific heat (Kwok and Brown, 1989; Kwok et al., 1990), thermal expansion (Hauser et al., 1991), and elastic properties (Aronowitz et al., 1990) all show significant deviations from the mean field behavior and are suggestive of a critical region of significant magnitude. The detailed behavior near T_{3D} depends on the available degrees of freedom and on dimensionality. As the charge density wave has two degrees of freedom, amplitude and phase, it belongs to the same universality class as the XY model. This analogy has also been widely used to analyze the various experimental results near the transition temperature, and some of the critical exponents have also been extracted (Aronowitz et al., 1990).

1.6 Collective Excitations

The excitations of the density wave states which are related to the spatially and time-dependent order parameter $\Delta(\vec{r}, t)$ are difficult to describe within the framework of a micro-

scopic description, and therefore are usually treated by using the timedependent Ginzburg-Landau theory in the long wavelength limit. As expected for a complex order parameter, both phase and amplitude excitations occur. To the first order the modes are decoupled and represent independent oscillations of the amplitude and phase of the order parameter.

In the $q = 0$ limit the phase excitation corresponds to the translational motion of the undistorted condensate. For an incommensurate density wave such translational motion does not change the condensation energy, and consequently the frequency of the phase mode is

$$\omega_\phi(q = 0) = 0 \tag{6.1}$$

Such translational motion, nevertheless, involves ionic motions in the case of charge density waves. This leads to an enhanced kinetic energy and hence to a large effective mass. Mass enhancement does not occur for spin density waves which do not couple to the underlying lattice.

In the $q = 0$ limit, the frequency of the oscillations of the amplitude mode is the same as the gap frequency for spin density
waves. For a charge density wave ground state fluctuations of the single particle gap $\delta\Delta$ with a frequency ω_A also lead to fluctuations of the ionic positions $\delta(\Delta u)$. This in turn leads to an oscillation frequency different from $\Delta/\hbar$. In the $q = 0$ limit, a $\delta\Delta$ change of the gap gives a change of the condensation energy $\frac{1}{2}n\left(\epsilon_F\right)(\delta\Delta)^2$; while the kinetic energy associated with the ionic displacements is given by $\frac{1}{2}MN_e\omega_A^2(q = 0)\left\{\delta(\Delta u)^2\right\}$ where Δu is the atomic displacement. Therefore

$$\frac{1}{2}MN_c\omega_A^2(q = 0)\left\{\delta(\Delta u)^2\right\} = \frac{1}{2}n\left(\epsilon_F\right)(\delta\Delta)^2 \tag{6.2}$$

and

$$\omega_A^2(q = 0) = \frac{n\left(\epsilon_F\right)(\delta\Delta)^2}{MN_c\{\delta(\Delta u)\}^2}. \tag{6.3}$$

Assuming that $\delta(\Delta u)/\Delta u = \delta\Delta/\Delta$, and using Eqs. (3.20) and (3.23), we obtain

$$\omega_A^2(q = 0) = \lambda^{1/2}\omega_{2k_1}. \tag{6.4}$$

Generally $\omega_{2k_i} < \Delta$ and $\lambda < 1$ for most materials with a charge density wave ground state; the amplitude mode frequency is well below the continuum of single particle excitations. Both modes are shown in the $q = 0$ limit in Fig. 6.1. The oscillations of the phase involve the displacement of electronic charge distributions with respect to the ionic positions; and consequently this mode is optically active. Such displacements do not occur for amplitude fluctuations and therefore the amplitude mode is expected to be Raman active.

In this chapter we first discuss these collective excitations for a one-dimensional chain with a charge density wave ground state and derive the dispersion relation of the excitations in terms of the parameters of the Ginzburg-Landau theory. These parameters can be related to the underlying microscopic theory in certain limiting cases. Consequently the dispersion relations can then be described in terms of the parameters of the microscopic theory.

The excitations of the spin density wave ground state are more complex, as both charge and spin degrees of freedom are important. The former are similar to excitations of the charge density wave state. The spin excitations are to some extent similar to excitations of an antiferromagnet; with the dispersion relation

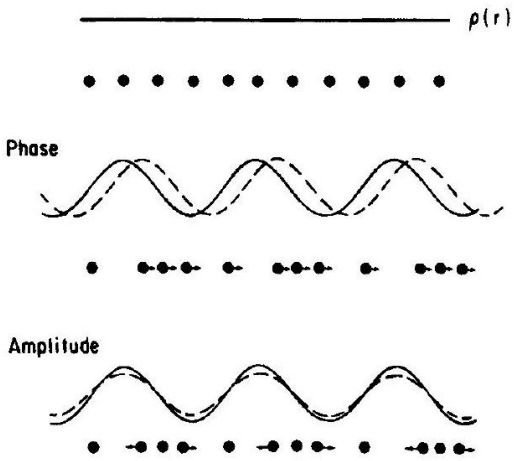


Figure 6. 1. Amplitude(A)and phase(ϕ)excitations of the charge density wave state in the $q = 0$ limit. Changes of both the charge density and ionic displacements are indicated. The upper part of the figure shows the charge density and the atomic positions in the metallic state.

determined by the parameters, such as the effective exchange constant J_{eff} , and effective magnetic moment μ .

1.6.1 Ginzburg-Landau Theory of Charge Density Wave Excitations

We write the free energy of a one-dimensional chain as
(????)
And then $-\mathcal{L} = \varepsilon - \beta_T$

$$F = F(0) + n\left(\epsilon_F\right) \int dx \left\{ a|\Delta|^2 + b|\Delta|^4 + c\left|\frac{d\Delta}{dx}\right|^2 + d\left|\frac{d\Delta}{dt}\right|^2 \right\} \tag{6.5}$$

The third term on the right hand side describes the energy associated with the spatial variation; the last term represents the kinetic energy, due the temporal fluctuations of the order parameter.

We assume that the time and spatially dependent order parameter can be written as

$$\Delta(x,t) = [|\Delta| + \delta(x,t)]e^{i\phi(x,t)}. \tag{6,6}$$

Here $|\Delta|$ is the magnitude of the spatial and temporal averaged gap, $\delta(x,t)$ describes the fluctuation of the amplitude of the order parameter, and $\phi(x,t)$ refers to phase fluctuations. Within the framework of this approximation, two modes, an amplitude mode and a phase mode, represent the long wavelength excitations of the condensate. Expanding the expression of the free energy for small δ and ϕ we obtain

$$\begin{aligned} F =& F(0) + n\left(\epsilon_F\right) \int dx \left\{ a|\Delta|^2 + a\delta^2 + c\left(\frac{\partial\delta}{\partial x}\right)^2 \right. \\ &\left. + d\left(\frac{\partial\delta}{\partial t}\right)^2 + \Delta^2 \left[c\left(\frac{\partial\phi}{\partial x}\right)^2 + d\left(\frac{\partial\phi}{\partial t}\right)^2 \right] \right\}. \end{aligned} \tag{6.7a}$$

The Lagrangian density which corresponds to the free energy is given by

$$\mathscr{L} = d\left(\frac{d\Delta}{dt}\right)^2 - c\left(\frac{d\Delta}{dx}\right)^2 - a\Delta^2 \tag{6.7b}$$

and the equations of motion for the amplitude and phase fluctuations are determined by the Lagrange equation

$$\frac{\partial\mathscr{L}}{\partial\phi} - \frac{\partial}{\partial t}\frac{\partial\mathscr{L}}{\partial\phi_1} - \frac{\partial\mathscr{L}}{\partial :}\frac{\partial\mathscr{L}}{\partial\phi_r} = 0 \tag{6.8a}$$

and

$$\frac{\partial\mathscr{L}'}{\partial\delta} - \frac{\partial}{\partial t}\frac{\partial\mathscr{H}}{\partial\delta_i} - \frac{\partial\mathscr{L}}{\partial x}\frac{\partial\delta}{\partial\delta_x} = 0, \tag{6.8b}$$

where the subscripts refer to the time and spatial derivatives of ϕ and δ. Then with Eq. (6.7) we obtain

$$d\frac{d^2\phi}{dt^2} - c\frac{d^2\phi}{dx^2} = 0 \tag{6.9a}$$

$$d\frac{d^2\delta}{dt^2} - c\frac{d^2\delta}{dx^2} + 2a\delta^8 = 0 \tag{6.9b}$$

We seek the wave-like solutions for the amplitude and phase mode

$$u_A = u_{A_1}e^{i(\omega t - qv)} \tag{6.10a}$$

$$u_\phi = u_{\phi_1}e^{i(\omega t - qv)} \tag{6.10b}$$

Where the displacement u can be parallel or perpendicular to the direction of the wave propagation. The former represents a longitudinal mode, the latter a transverse mode. The dispersion relations for the amplitude and phase oscillations are given by

$$\omega_\phi(q) = \left(\frac{c}{d}\right)^{1/2} q \tag{6.11a}$$

and

$$\omega_A = \left(\frac{-2a}{d} + \frac{c}{d}q^2\right)^{1/2} \tag{6.11b}$$

The excitations of the phase and amplitude modes are usually referred to as phasons and amplitudons, respectively. The parameters of the Ginzburg-Lanciau free energy can be derived in terms of the microscopic description of the charge density wave ground state, by calculating the spatial and temporal fluctuations using an appropriate decoupling procedure. Instead of such general treatment, only the long wavelength fluctuations which are associated with variations of the phase will be discussed; in the limit where the order parameter is close to its $T = 0$ value. Then the spatial and temporal fluctuations of the order parameter are given to the first order as

$$\left(\frac{d\Delta}{dx}\right)^2 \simeq |\Delta|^2\left(\frac{d\phi}{dx}\right)^2 \tag{6.12a}$$

$$\left(\frac{d\Delta}{dt}\right)^2 \simeq |\Delta|^2\left(\frac{d\phi}{dt}\right)^2. \tag{6.12b}$$

Such an approach is appropriate well below T_{MF} where the amplitude and phase of the order parameter can clearly be distinguished. Assume a smooth local variation of the phase, with $d\phi/dx$ constant over many CDW wavelengths. This, by virtue of $2\delta kx = \delta\phi$, leads to a change of the wavevector by $\delta k = \frac{1}{2}d\phi/dx\,\mathrm{sign}(k)$ at the two sides of the Fermi surface. Therefore, there is a shift of the single particle gap from $\pm k_F$ to $\pm\left(k_\Gamma + \frac{1}{2}d\phi/dx\right)$ as shown in Fig. 6.2a. If the gap follows the spatial fluctuations and is constrained to be at the Fermi level, the electronic density must be changed, and this is described by

$$\rho(x) = \rho_0 + \frac{1}{\pi}\frac{d\phi}{dx} \tag{6.13}$$

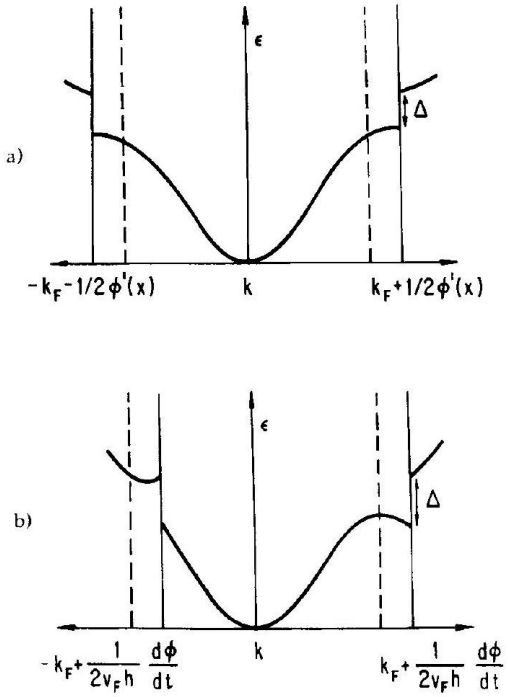


Figure 6.2. The displaced Fermi surface and the dispersion election in the case of a position- and a time-dependent phase. The states are filled up to the Fermi level, \$\pm\left[k_{1}+\frac{1}{2}(d \phi(x) / d x)\right]\$ in (a) and up to $\pm\,[k_1 \pm (1/2v, \hbar)(d\phi/dt)]$ in (b). The dotted lines refer to the Fermi surface with a position- and time-independent phase, and are at the positions $\pm k_1$ in both figures.

The energy associated with the spatially uniform phase is the energy difference between the state with and without the formation of the gap. At $T = 0$ this is simply the condensation energy $E = \frac{1}{2}n\,(\epsilon_F)\,\Delta^2$, and consequently,

$$a = -\frac{1}{2}. \tag{6.14}$$

The energy related to the fluctuations of the phase is the difference between the change of energy due to these fluctuations without the gap and with the single particle gap. As the condensation energy is independent of the position of the gap in k space, fluctuations do not change this energy. The change of the energy for the configuration without the gap is given at zero temperature, using the linear dispersion relation $d\epsilon = \pm\hbar v_{\mathrm{F}} dk$, by

$$E\left[\frac{d\phi}{dx}\right] = 4\int_0^{\phi'/2}\frac{\hbar v_F k dk}{2\pi} = \frac{\hbar v_I}{2\pi}\left(\frac{d\phi}{dx}\right)^2 \tag{6.15}$$

where the factor of 4 accounts for the two sides of the Fermi surface and for the two spin directions. By virtue of $n(\epsilon_F) = N_c/\hbar k_F v_F = (\pi\hbar v_F)^{-1}$, Eq. (6.15) reduces to

$$E\left[\frac{d\phi}{dx}\right] = \frac{n(\epsilon_F)\,\hbar^2 v_r^2}{4}\left(\frac{d\phi}{dx}\right)^2. \tag{6.16}$$

This, together with Eqs. (6.5) and (6.7), gives

$$r = \frac{\hbar^2 v_F^2}{4|\Delta|^2} \tag{6.17a}$$

In terms of the coherence length $\xi_0 = \hbar v_r/\pi|\Delta|$,

$$c = \frac{\pi^2}{16}\xi_0^2 \tag{6.17b}$$

The consequences of the temporal variations of the phase can be described similarly. Assuming a translational motion of the undistorted condensate, the drift velocity v_d is given in terms of the time varying phase by

$$v_d = \frac{1}{2k_F}\frac{d\phi}{dt}. \tag{6.18}$$

As a consequence, inversion symmetry in k space is broken, as shown in Fig. 6.2, and the gap, if tied to the moving condensate, appears at

$$\pm k_F + \delta k = \pm k_F + \frac{1}{2v_F}\frac{d\phi}{dt} \tag{6.19}$$

as $\hbar\delta k = mv_d$. In the presence of a condensate moving with a velocity v_d the dispersion relation is derived as follows (Boriak
and Overhauser, 1977; Schulz, 1977). We write the momentum in the moving reference frame as

$$\hbar\bar{k} = \hbar k + mv_d$$

and then the dispersion relation in the moving reference frame is related to the dispersion relation in the laboratory frame as

$$\epsilon(k) = \tilde{\epsilon}(\tilde{k}) + m\tilde{v}v_{ti} + \frac{1}{2}mv_d^2. \tag{6.20}$$

Following Eq. (3.34) the dispersion relation in the moving reference frame may be written as

$$\tilde{\epsilon}(\tilde{k}) = \pm\left(\hbar^2 v_F^2\left(\tilde{k} - \tilde{\epsilon}_F\right)^2 + \Delta^2\right)^{1/2} \tag{6.21}$$

and the dispersion relation in the laboratory frame is given (neglecting the last term in Eq. (6.20)) as

$$\epsilon(\bar{k}) = \pm\left(\hbar^2 v_F^2\left(\bar{k} - \bar{k}_F\right)^2 + \Delta^2\right)^{1/2} + \frac{mv_F v_d\left(\tilde{k} - \tilde{k}_F\right)}{\hbar^2 v_F^2\left(\tilde{k} - \tilde{k}_F\right)^2 + \Delta^2} \tag{6.22a}$$

where we have used the relation $\tilde{v} = \partial\tilde{\epsilon}/\partial\bar{k}$.
As $\tilde{k} - \tilde{k}_F = (k - k_F) + mv_d$, we obtain the following dispersion relation

$$\epsilon(k) = \pm \left(\hbar^2 v_F^2 \left(k - k_F - mv_d\right)^2 + \Delta^2\right)^{1/2} \pm \frac{mv_F v_d \left(k - k_F - mv_d\right)}{\left(\hbar^2 v_F^2 \left(k - k_F - mv_d\right)^2 + \Delta^2\right)^{1/2}} \tag{6.22b}$$

which is shown in Fig. 6.2b.
It is easy to see that $\epsilon\left(\pm k_F\right)$ and therefore the energy gap remains unchanged, and all the modifications occur away from the (displaced) Fermi surface. The electric current density which is related to the displaced Fermi see,

$$j = \int_{k_F - mv_d}^{k_f + mv_d} \frac{\partial\epsilon}{\partial k} dk = \epsilon\left(k_F + mv_d\right) - \epsilon\left(k_F - mv_d\right) = 0. \tag{6.23}$$

The moving condensate, however leads to an electric current

$$j_{\mathrm{DW}} = N_{\cdot} c v_d = -\frac{c}{\pi}\frac{d\phi}{dt} \tag{6.24}$$

as $N_t = 2k_F/\pi$.
The excess energy associated with the time dependent phase is evaluated using the same argument which has been used to evaluate the elastic energy. In the .bsence of the gap the change of the energy is given by

$$E\left[\frac{d\phi}{dt}\right] = 4\int_0^{k_i} \frac{\dot{\phi}}{2v_F} v_F k dk/2 = \frac{n\left(\epsilon_F\right)}{4}\left(\frac{d\phi}{dt}\right)^2 \tag{6.25}$$

The kinetic energy term as given by Eq. (6.21) represents the change of the total electronic energy and does not include the kinetic energy of the ions which exhibit an oscillating motion for a time-dependent phase. This energy leads to an enhancement of the dynamical mass, which can be estimated as follows: for a charge density wave moving with a uniform drift velocity v_d the total energy is given by

$$E_k = \frac{1}{2} m v_d^2 + \frac{1}{2} M(\omega/\Delta u)^2 \tag{6.26}$$

where M is the ionic mass, Δu is the atomic displacement, and ω is the angular frequency of the ionic oscillations. Here ω and v_d are related through $\omega = 2\pi v_d/\lambda_0$, and consequently

$$E\left[\frac{d\phi}{dt}\right] = \frac{1}{2} m v_d^2 \left(1 + \frac{4\pi^2/m^2}{\lambda_0^2}\frac{M}{m^2}\right) = \frac{1}{2} m^* v_d^2 \tag{6.27}$$

where m^* is called the effective mass. With $\lambda_0 = \pi/k_F$, and $\Delta u = \Delta/g\omega_{2k_1}$ we obtain

$$\frac{m^*}{m} = 1 + \frac{4k_F^2 n\left(\epsilon_F\right)\Delta^2}{N_c g \omega_{2k_1}^2 m} \tag{6.28}$$

which, with $k_F^2 = 2m\epsilon_F/\hbar^2$ and $N_c = 2n\left(\epsilon_F\right)\epsilon_F$ (both appropriate for a one-dimensional band) and with $\lambda = gn\left(\epsilon_F\right)$ leads to

$$\frac{m^*}{m} = 1 + \frac{4\Delta^2}{\lambda\hbar^2\omega_{2k_i}^2}. \tag{6.29}$$

The total kinetic energy is then given by

$$E\left[\frac{d\phi}{dt}\right] = \frac{n(\epsilon_F)}{4}\frac{m^*}{m}\left(\frac{d\phi}{dt}\right)^2 \tag{6.30}$$

and consequently, using Eq. (6.12),

$$d = \frac{1}{4}\frac{m^*}{m|\Delta|^2}. \tag{6.31}$$

The arguments which lead to Eq. (6.25) apply in the $\omega \to 0, q \to 0$ limit. At finite frequencies and wavevector (Virosztek and Maki, 1993)

$$\frac{m^*}{m} = \frac{m^*(\omega = 0, q = 0)}{m}\left[1 + \frac{2}{3}\left(\frac{\omega}{2\Delta}\right)^2 - \frac{2}{3}\left(\frac{v, q}{2\Delta}\right)^2\right] \tag{6.32}$$

at zero temperature, the expression is appropriate in the $\omega, v_1 q \ll \Delta$ limit. This frequency and wavevector dependence then modifies the dispersion relation of the amplitude and phase mode.

By inserting the appropriate expressions for the GinzburgLandau parameters into Eq. (6.11) the dispersion relation for the phase excitations is given at zero temperature by

$$\omega_\phi = \left(\frac{m}{m^*}\right)^{1/2} v_1 q = c_\phi q \tag{6.33}$$

where c_ϕ is called the phason velocity. The amplitude mode frequency, with $a = \frac{1}{2}$ and Eq. (6.11a), is

$$\omega_A = \lambda^{1/2}\omega_{2k}, \tag{6.34}$$

at $q = 0$. This is the same as Eq. (6.4). Eq. (6.11b) together with the wavevector-dependent effective mass, given by Eq. (6.32) gives (Lee, Rice, and Anderson, 1979)

$$\omega_A = \left(\lambda\omega_{2k_i}^2 + \frac{1}{3}\frac{m}{m^*}v_1^2 q^2\right)^{1/2} \tag{6.35}$$

for long wavelength fluctuations. The dispersion relations of the

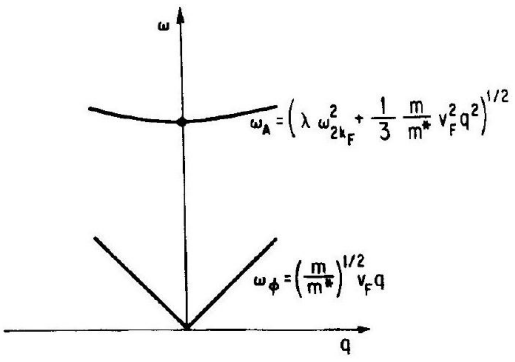


Figure 6.3. The dispersion relation of the phase and amplitude mode near $q = 0$ for a charge density wave ground state.

phase and amplitude modes are displayed in Fig. 6.3, and the two modes are sketched in Fig. 6.4 for a finite wavevector q.

The above arguments apply at zero temperature; the temperature dependence of the Ginzburg-Landau parameters a, c, and d are determined by the temperature dependence of

the gap $|\Delta(T)|$ and of the condensate density $f_0(T)$. With these included, the free energy reads (Fukuyama and Lee, 1978; Brazoskii and

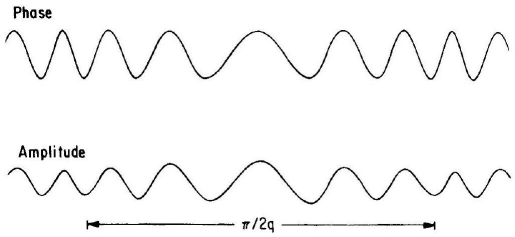


Figure 6.4. Phase and amplitude excitations with a finite wavevector q. Only the charge density is indicated on the figure, there are corresponding modifications in the atomic positions.

Dzyaloshimskii, 1976) Afain, stuald be $\varepsilon = 1-$ Ostor $= 2$

$$\left.\begin{array}{ll} F = & F(0) + \frac{1}{4} n\left(\epsilon_F\right) f(T) \int dx \\ & \left\{-2|\Delta|^2 + 2\delta^2 + |\Delta|^{-2}\left[\hbar^2 v_F^2 \left(\frac{\partial \delta}{dx}\right)^2 + \frac{m^*}{m}\left(\frac{\partial \delta}{\partial t}\right)^2\right]\right. \\ & \left. + \hbar^2 v_F^2 \left(\frac{\partial \phi}{\partial x}\right)^2 + \frac{m^*}{m}\left(\frac{\partial \phi}{\partial t}\right)^2\right\} \end{array}\right]$$

At finite temperatures both ω_A and c_ϕ are determined by the temperature dependence of $\Delta(T)$ and $f(T)$. The former is determined by Eq. (3.55) and the latter by Eq. (3.58). For the frequency of the phase excitations for small wavelengths ($\omega_A \gg v_l q$) the dynamic limit applies, and

$$\omega_A = \lambda^{1/2} \omega_{2k_F} \left[f_d(t)\right]^{1/2} \tag{0.37}$$

reduces to

$$\omega_A \sim \frac{1.55}{4} \lambda^{1/2} \omega_{2k_F} \left(1 - \frac{T}{T_{\mathrm{COW}}}\right)^{1/4} \tag{6.38}$$

close to the transition temperature T_{CDW}. The temperature dependence of the phase and amplitude mode are displayed in Fig. 6.5.

The temperature dependence of the effective mass, which determines the temperature dependence of the phase velocity,

$$\frac{m^*(T)}{m} = 1 + \frac{4\Delta^2(T)}{\hbar^2 \lambda \omega_{2k_1}^2} \frac{1}{f_s(T)} \tag{6.39}$$

is also determined both by the temperature dependent single particle gap and by the temperature dependent condensate density as $c_\phi < v_F$ the static limit is appropriate. By inserting the appropriate expressions for $\Delta(T)$ and $f_s(T)$, we obtain

$$\frac{m^*(T)}{m^*(T=0)} = 1.51 \tag{6.40}$$

close to the transition temperature. The frequency of the amplitude fluctuations approaches zero as $T \to T_{\mathrm{CDW}}^{\mathrm{MF}}$, while the velocity of the phase fluctuations remains finite as $T \to T_{\mathrm{CDW}}^{\mathrm{MF}}$.

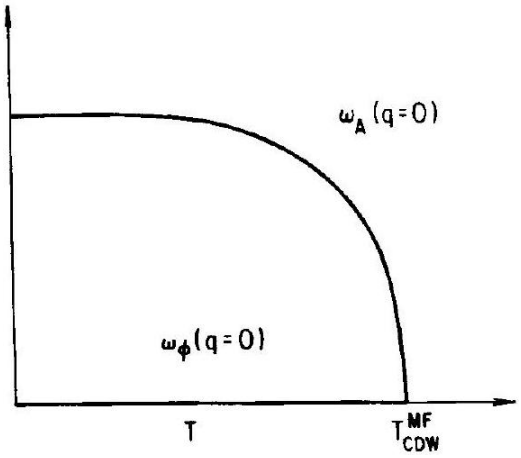


Figure 6.5. Temperature dependence of the frequency of the phase and amplitude modes, $\omega_{A}(q=0)$ and $\omega_\phi(q=0)$.

The above analysis applies in the absence of long-range Coulomb forces. Consequently the amplitude and phase mode dispersion relations are appropriate only for transverse modes, which do not involve the redistribution of electronic charges due to fluctuations, or for longitudinal modes where Coulomb interactions are screened by uncondensed electrons; i.e., at temperatures close to $T_{\rm CDW}^{\rm MF}$.

At zero temperature, with no screening by quasiparticles, the long range Coulomb interactions become important, and this leads to a gap in the phason spectrum for longitudinal excitations as first pointed out by Anderson and Higgs (Anderson, 1984). The argument which leads to the gap frequency is analogous to the argument which leads to the plasma frequency in metals. A density wave displacement Δu relative to the underlying ionic background leads to a polarization

$$\Delta P_0 = ne\Delta u \tag{6.41}$$

which gives rise to an electric field

$$E = -\frac{4\pi P}{\epsilon_0} \tag{6.42}$$

where ϵ_0 is the background dielectric constant due to single particle excitations across the semiconducting gap. The equation
of motion for the condensate is then

$$m^* \left(\frac{dx}{dt}\right)^2 = -4\pi ne^2 \epsilon_0^{-1} x \tag{6.43}$$

and this defines a characteristic frequency

$$\omega_p^* = \left(\frac{m}{m^*}\right)^{1/2} \omega_p \epsilon_0^{-1/2} \tag{6.44}$$

where

$$\boldsymbol{\omega}_H = \left(\frac{4\pi ne^2}{m_H}\right)^{1/2} \tag{6.45}$$

is the plasma frequency of the metallic state above $T_{\rm (T)W}$. The dielectric constant is given by

$$\epsilon_{11} = 1 + \frac{1}{6}\left(\frac{\omega_p}{\Delta}\right)^2 \tag{6.46}$$

for a one-dimensional semiconductor with a gap Δ, and consequently

$$\omega_b = 6^{-1/2}\left(\frac{m}{m^*}\right)^{1/2}|\Delta|^2 = \left(\frac{3\lambda}{2}\right)^{1/2}\omega_{2k_1} \tag{6.47}$$

by virtue of Eq. (6.30).

In the case of screening by the thermally excited quasiparticles the problem becomes somewhat complicated, and the frequency and damping constant associated with the phase excitations depend on factors like the Thomas-Fermi wavevector q_0, the diffusion content D_{qp} of the quasiparticles, and whether the static or dynamic limit ($\omega \gtrless v_1 q$) applies. Broadly speaking fluctuations with $q < q_0$ are screened, while no screening occurs for $q > q_0$. The Thomas-Fermi wavevector has been evaluated (Maki and Virosztek, 1992), and its temperature dependence is given by

$$q_{11} = \omega_p r_F^{-1}\left(1 - f_S\right)^{1/2} \tag{6.48}$$

where ω_p, is the plasma frequency and f_s is the static condensate density. With such screening included, the following dispersion relation is obtained for the longitudinal phase mode (Lee and

Fukayama, 1978; Kurihara, 1980; Barisic, 1985; Nakane and Takada, 1987)

$$\omega_\phi^2 = \left\{c_0^2 + \frac{m}{m^*}\frac{\Delta^2}{q^2 + q_0^2}\right\}q^2 \tag{6.49}$$

which for the two limits reduces (in the static limit) to

$$\omega_\phi^2 = \frac{c_{10}^2 q^2}{1 - f_s}, \quad q \ll q_0 \tag{6.50a}$$

$$\omega_\phi^2 = \frac{3}{2}\lambda\omega_{2k_1}^2 f_s + c_0^2 q^2 \quad q \gg q_0 \tag{6.50b}$$

with $c_0 = (m/m^*)^{1/2} v_F$. The dispersion relation given 'y the above equations is sketched in Fig. 6.6 at a temperature somewhat below T_{CDW}. Due to quasiparticle damping, the mode also becomes diffusive near $q = 0$ and strongly damped for finite q values in the region near q_0 and below.

The situation is analogous to that which occurs for superconductors, and to that known as the Carlson-Goldman mode (1973, 1975). At long wavelengths the condensate current is compensated by the quasiparticle current and the mode remains acoustic;

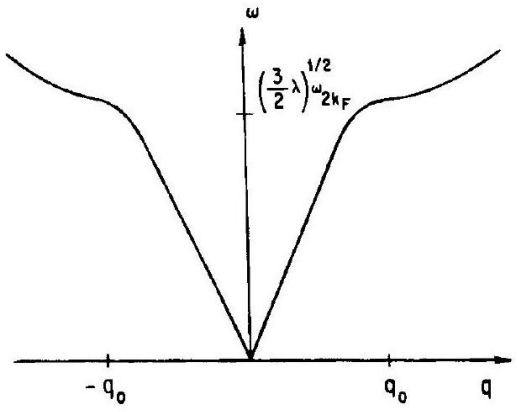


Figure 6.6. The dispersion relations of the phase mode at finite temperature in the presence of Coulomb effects and quasiparticle screening. The screening wavevector q_{0} is defined in the text. The mode becomes diffusive near $q = 0$, and is strongly damped for $q < q_0$.

for $q > q_0$ the condensate and quasiparticle currents oscillate in phase and are therefore subjected to Coulomb forces. As the quasiparticle density is strongly temperature dependent, ω_ϕ also has a strong temperature dependence (Nakane and Takada, 1985; Maki and Virosztek, 1990). Obviously, Coulomb effects do not play a role for the transverse modes; they remain acoustic in the entire temperature range. Similarly the amplitude mode remains unaffected by long range Coulomb effects.

In three dimensions, the fluctuations of all three spatial coordinates contribute to the free energy and the elastic term reads

$$F_{ct} = \frac{1}{4} n(\epsilon_F) \hbar^2 |\Delta|^{-2} \left[\int v_{F_1}^2 \left(\frac{d\Delta}{dx}\right)^2 dx + \int v_{F_1}^2 \left(\frac{d\Delta}{dy}\right)^2 dy + \int v_{F_2}^2 \left(\frac{d\Delta}{dz}\right)^2 dz \right] \tag{6.51}$$

with the on-chain Fermi velocity $v_{F_1} \gg v_{F_4}, v_{F_5}$. With the coherence length $\xi = \hbar v_I / \pi\Delta$ proportional to the Fermi velocity, Eq. (6.51) is usually written as

$$F = \frac{1}{4} \frac{n(\epsilon_r) \hbar^2 v_l}{a_y a_z |\Delta|^2} \int dr \left[\left(\frac{\partial\Delta}{\partial x}\right)^2 + \left(\frac{\xi_y}{\xi_\parallel}\right)^2 \left(\frac{\partial\Delta}{\partial y}\right)^2 + \left(\frac{\xi_z}{\xi_\parallel}\right)^2 \left(\frac{\partial\Delta}{\partial z}\right)^2 \right]. \tag{6.52}$$

Where v_F refers to the Fermi velocity along the chain direction. This leads to different dispersion relations for CDW fluctuations in the different directions, and

$$\begin{aligned} c_{\phi x} &= \left(\tfrac{m}{m^*}\right)^{1/2} v_{F_v} q && \text{parallel} \\ c_{\phi y}, c_{\phi z} &= \left(\tfrac{m}{m^*}\right)^{1/2} v_{F_{v,z}} q && \text{perpendicular.} \end{aligned} \tag{6.53}$$

The three amplitude modes have the same frequency at $q = 0$, but because of the different Fermi velocities, they display different q dependences for oscillations involving amplitude modes in the three different directions, as implied by Eq. (6.36).

The excitations of the amplitude and phase also contribute to the various thermodynamic quantities. At low temperatures, because of the gap in the excitation spectrum, the contribution from amplitude excitations is small. The excitations of the phase can be described using the formalism applied to acoustic phonons. We write the Hamiltonian density $\mathscr{H}$, corresponding to the free energy Eq. (6.5), as

$$\mathscr{H} = \frac{\pi^2}{2\rho} + c\left(\frac{d\phi}{dx}\right)^2 \tag{6.54}$$

where π is the momentum density. The mass density ρ is given by

$$\rho = \left[\frac{n\left(\epsilon_\Gamma\right)}{2}\frac{m^*}{m}\right]^{-1} \tag{6.55}$$

We express $\phi(x)$ and $\pi(x)$ in terms of the variables Q'_k and P'_k as

$$\phi(x) = L^{-1/2}\sum_q Q'_q e^{iq} \tag{6.56a}$$

$$\pi(x) = L^{-1}\sum_q P'_{qi} e^{iqx} \tag{6.56b}$$

by using periodic boundary conditions over the length L. Then the Hamiltonian becomes

$$\mathscr{H}' = \int \mathscr{H}\, dx = \sum_q \left(\frac{1}{2\rho}p'_{q_{p'_{-q}}} + cq^2 Q'_{q_{Q'_{-q}}}\right) \tag{6.57}$$

which, by using the transformation

$$a_q^\dagger = -i\left(2\rho\omega_\phi\right)^{-1/2} P'_{ij} + \left(\frac{c}{\omega_\phi}\right)^{1/2} qQ'_{-1j} \tag{6.58a}$$

$$a_q = i\left(2\rho\omega_\phi\right)^{-1/2} P'_{ij} + \left(\frac{c}{\omega_\phi}\right)^{1/2} qQ'_{q'} \tag{6.58b}$$

becomes

$$\mathscr{H} = \sum_\eta \omega_\phi a_{ql}^\dagger a_q \tag{6.59}$$

The dispersion relation, Eq. (6.34), is given in terms of c and the mass density as $\omega_\phi = (2c/\rho)^{1/2}q$, which, as has been shown earlier, is $\omega_\phi = c_\phi q$ where c_ϕ is the phase velocity.

The calculation of the low temperature specific heat follows the calculation of the specific heat due to phonons, and in the Debye approximation we obtain

$$C_V^\phi \simeq \left(2nk_B\right)^3\left(\frac{T}{\Theta_D}\right)^3 \tag{6.60}$$

where n is the total number of modes per unit length; for a CDW period of λ_0 this is given by $n = \lambda_0^{-1}$. The cutoff wavevector $q_{\max}$ is given by the relation

$$n = \frac{4\pi}{3}\left(\frac{1}{2\pi}\right)^3 q_{\max}^3 \frac{T_{\mathrm{CDW}}}{T_\Gamma} \tag{6.61}$$

where the factor $T_{\rm CDW}/T_F$ is due to the fact that a significant fraction of the lattice entropy has been removed at the phase transition. The Debye temperature then is

$$k_{1)}\theta_D^{\phi} = q_{\max}c_{\rm b} = 2\pi\left(\frac{3n}{4\pi}\right)^{1/3} v_F\left(\frac{m}{m^*}\right)^{1/2}\left(\frac{T_1}{T_{\rm CDW}}\right)^{1/3}. \tag{6.62}$$

Ir case of isotropic phason and phonon dispersion relations, the relative contributions of the two types of excitation to the specific heat is given by

$$\frac{C_V^{\phi}}{C_V^{\rm ph}} = \left(\frac{n_{\phi}}{n_{\rm ph}}\right)^3\left(\frac{\theta_D^{\rm ph}}{\theta_D^{\phi}}\right)^3. \tag{6.6.3}$$

The number of phonon modes per unit volume is proportional to a^3 with a the lattice constant, and therefore $n_{\phi}/n_{\rm ph} = (a/\lambda)^3$. With a typical sound velocity $c_0 \sim 5\times10^5$ cm/sec, and a typical phase velocity $c_{\phi} = v_F\,(m/m^*)^{1/2} = 10^5$ cm/sec, the two contributions are of the same order of magnitude.

The above arguments apply for an isotropic phase excitation spectrum. In the case of an anisotropic dispersion relation such as
that given by Eq. (6.52), the specific heat is modified and is given by

$$c_V^{\phi} = c_{V^{\phi}_{(10{\rm xtroppc})}}\cdot\left(\frac{\xi_{\|}^2}{\xi_y\xi_z}\right) \tag{6.64}$$

at low temperatures. As $\xi_y, \xi_z \ll \xi_{\|}$, a significant enhancement of the specific heat is expected due to anisotropy effects at low temperatures.

1.6.2 Excitations of the Spin Density Wave Ground State

Because of the magnetic character of the SDW ground state, the excitations are different from the excitations which occur for the CDW ground state. With both spin and charge degrees of freedom available, various types of amplitude and phase excitations may occur.

We write the time dependence of the phase fluctuations in the two subbands as $\delta\phi_{\uparrow} = e^{i\omega t}$ and $\delta\phi_{\downarrow} = e^{i\omega t+\phi}$. Similarly, the amplitude fluctuations are given by $\delta A_{\uparrow} = e^{i\omega t}$ and $\delta A_{\downarrow} = e^{i\omega t+\phi}$. An arbitrary phase ϕ leads, in both cases, to a periodic modulation of the charge density, such excitations however, are energetically not favored. To see what happens, consider the cases for which $\phi = 0$ or $\phi = \pi/2$; the various possibilities are shown in Fig. 6.7 in the $q = 0$ limit.

The top part of the figure indicates the displacement of both CDW modulations in the same direction ($\phi = 0$) and this leads in turn to the displacement of the spin density wave modulation without leading to an oscillating charge density wave component. The excitation is analogous to the phase excitations discussed for charge density waves. The next two parts of the figure describe two different excitations, both related to the change of the amplitudes of the density wave modulations in the two subbands. The first represents the amplitude fluctuations for which $\phi = \pi$. This however should lead to a charge density wave component of the order parameter and is consequently not allowed. The amplitude fluctuations may also occur in phase, and this leads to no charge redistribution but a change of the amplitude of the spin density wave modulation. This excitation corresponds to the amplitude mode as discussed earlier. The fourth possibility-charge density wave modulations, oscillating in opposite phase with $\phi =$

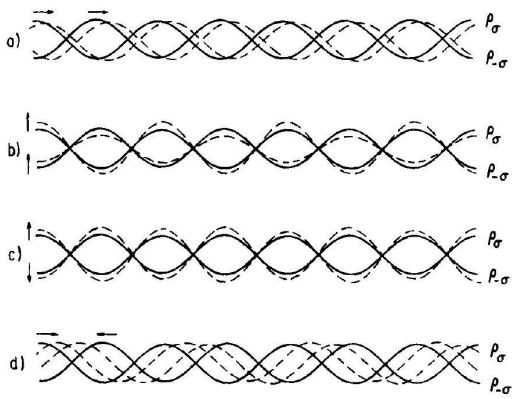


Figure 6.7. Tre amplitude and phase excitations of the spin density wave state in the $q = 0$ limit. The full lines represent the charge density wave modulation in the two subbands; the dashed lines represent the various amplitude and phase modes.

π-would also lead to an oscillating charge density wave component, and is thus forbidden.

This picture which follows from the above considerations for the charge excitations is similar to that described for charge density waves, with some modifications. The phase and amplitude excitations are analogous to those given by Eqs. (6.34) and (6.35) with two important differences. First, because the SDW modulation is not coupled to the lattice, the effective mass is the same as the bandmass, $m^* = m_b$, and consequently

$$\omega_\phi = v_F q. \tag{6.65}$$

Second, instead of Eq. (6.35), the frequency of the amplitude mode at $q = 0$ is given using $a = \frac{1}{2}$ and $d = 1/4\Delta^2$ (Psaltakis, 1984), by

$$\omega_A = \left((2\Delta/\hbar)^2 + (v_F q)^2\right)^{1/2} \tag{6.66}$$

The amplitude mode therefore is expected to occur above the gap
frequency, merging with the continuum of single particle excitations. This leads to the damping of the amplitude mode, similar to the damping of the amplitude mode of a superconductor (Littlewood and Varma, 1982).

Coulomb interactions modify the dispersion relations through the renormalized density of states due to these interactions. In the weak coupling limit this renormalization is given by the Stoner enhancement factor

$$n\left(\boldsymbol{\epsilon_r}\right) = n''\left(\boldsymbol{\epsilon_r}\right)\left(1 - Un''\left(\boldsymbol{\epsilon_l}\right)\right)^{-1} \tag{6.67}$$

which, through Eq. (6.21), translates into an enhanced kinetic energy. Consequently, the renormalized phason velocity is given by

$$v_l = v_l''\left(1 + Un''\left(\epsilon_F\right)\right). \tag{6.68}$$

The above expressions are appropriate in the weak coupling limit; a crossover from weak to strong coupling has been discussed by Shrieffer et al. (1989).

Next we turn to spin excitations. In the absence of spin-orbit and dipole-dipole interactions, the spin degrees of freedom have full rotational symmetry, this leads to excitations which are those of a 1D Heisenberg antiferromagnet. These excitations are described by the Hamiltonian in Eq. (4.35) which accounts for the static magnetic properties of the SDW ground state. Consequently, results which have been obtained for antiferromagnets can be adapted to describe the magnetic excitations of the spin density wave ground state.

In the absence of magnetic anisotropy fields, the equation of motion

$$h\frac{d}{dt}\langle\vec{S}\rangle = u\left[\langle\vec{S}\rangle \times \vec{H}_{\text{eff}}\right] \tag{6.69}$$

leads to the dispersion relation (Kittel, 1963) for the two magnon branches

$$\omega = 2J_{\text{eff}}aq = 2J_{\text{eff}}\frac{\lambda_0}{2}q \tag{6.70}$$

The effective coupling constant J_{eff} is given in terms of the parameter s of the metallic state by Eq. (4.38). This then leads to the dispersion relation

$$\omega = v_1 q. \tag{6.71}$$

Coulomb interactions and an enhanced density of states as given by Eq. (6.56) lead, through $n(\epsilon_F) = (\pi h v_l)^{-1}$, to a decrease of the Fermi velocity and therefore the dispersion relation reads as

$$\omega = v_r''\left(1 - U_{tt''}''(\epsilon_r)\right)q \tag{6.72}$$

in the case of Coulomb interactions.
Spin orbit and dipole-dipole interactions remove the rotational symmetry of the magnetic excitations and lead to an energy gap in the spin wave excitation spectrum. The gap and the dispersion relation depend sensitively on the orientation of the external magnetic field with respect to the preferred axis of magnetization. For anisotropy constants D^* and E^* the spin wave spectrum has two branches, and for zero magnetic field, in the $q = 0$ limit

$$\hbar^2\omega_+^2 = \frac{\mu}{\mu_R}\left(D^* + E^*\right)I_{\text{eff}} \tag{6.73}$$

$$\hbar^2\omega^2 = \frac{\mu}{\mu_R}2E^*I_{\text{eff}} \tag{6.74}$$

The magnetic field dependence of the resonant frequencies can also be calculated for various directions of the magnetic field (Torrance et al., 1982).

1.6.3 Experiments on Charge Density Waves: Neutron and Raman Scattering

Both the phase and amplitude mode dispersion relations can be examined using inelastic neutron scattering. Phase excitations lead to the displacement of the electronic charge density, and consequently the phase mode is optically active. The electrodynamics of the ground state will be discussed in Chapter 9. No charge fluctuation occurs for amplitude fluctuations, therefore the amplitude mode is Raman active. Both types of optical experiments have been extensively used to explore the excitations of the CDW ground state.

The phase mode has been measured in $K_{0.3}MoO_3$ by inelastic neutron scattering at temperatures somewhat below T_{CIW} (Pouget et al., 1991; Escribe-Filippini et al., 1987). The constant frequency scans together with the acoustic mode dispersion relation are displayed in Fig. 6.8. The linear dispersion observed is in full agreement with Eq. (6.7) and gives a phase velocity of $c_\phi =$

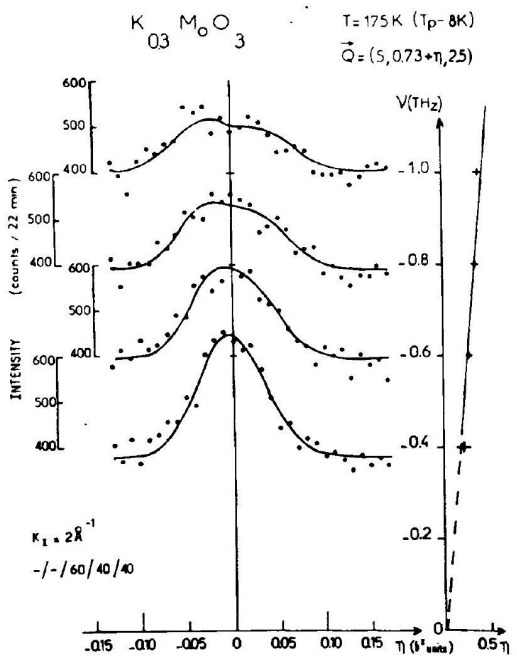


Figure 6.8. Constant frequency scans (left side) and dispersion (right side) of the phase mode branch of $\mathrm{K}_{0.3}\mathrm{MoO}_3$ and $T = 175$ K. The slope gives a phason velocity $v_\phi = 3.3 \pm 0.5 \times 10^5$ cm/sec in the chain direction (EscribeFilippini et al., 1987).

3.3×10^5 cm/sec. This, together with the Fermi velocity as given in Table 2.1 results in a mass enhancement $m^*/m \simeq 100$.

The mass enhancement can also be calculated using Eq. (6.25). The single particle gap $2\Delta = 1400$ K, together with λ and ω_{2k}, gives $m^*/m = 600$, in good agreement with the results obtained from the measurement of the phase velocity. The temperature dependence of c_ϕ has also been examined (Hennion et al., 1992) and was found to increase with decreasing temperature in accordance with what is expected from the increased role of Coulomb

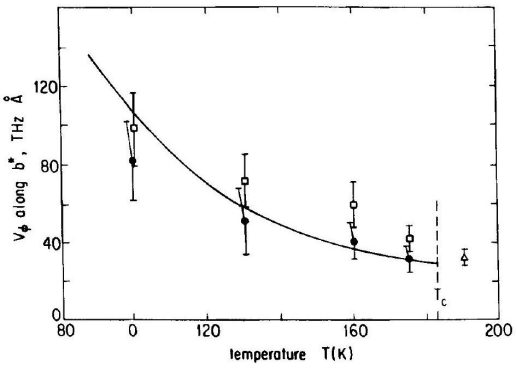


Figure 6.9. Temperature dependence of the phason velocity measured in $\mathrm{K}_{0.3}\mathrm{MoO}_3$ by neutron scattering (Hennion et al., 1992). The full line is the temperature dependence calculated by taking Coulomb effects into account (Maki and Virosztek, 1992; Maki and Grüner, 1991).

interactions as the thermally excited electrons are progressively removed. Fig. 6.9 shows c_ϕ, measured at different temperatures. The full line is calculated by evaluating the temperature

dependence of the phase velocity due to Coulomb effects at finite temperatures (Maki and Grüner, 1991; Maki and Virosztek, 1992).

The phason velocity was also found to be anisotropic, with the velocities measured perpendicular to the chain direction significantly smaller than the phason velocity along the chains. This anisotropy is in broad agreement with the anisotropic band structure of $K_{0.3}MoO_3$ and with the anisotropy of the coherence length. One also finds that the frequency of the mode remains finite as $q \to 0$, and this gap can be explained as the pinning of the phase mode by impurities; such pinning acts as a restoring force, shifting the phase oscillation frequency to a finite value as $q \to 0$.

The amplitude mode has been measured in several compounds both by neutron and by Raman scattering (Travaglini et al., 1983). The Raman spectrum, obtained at various temperatures on $K_{0.3}MoO_3$ is shown in Fig. 6.10 (Travaglini et al., 1983).
6. Collection Excitations

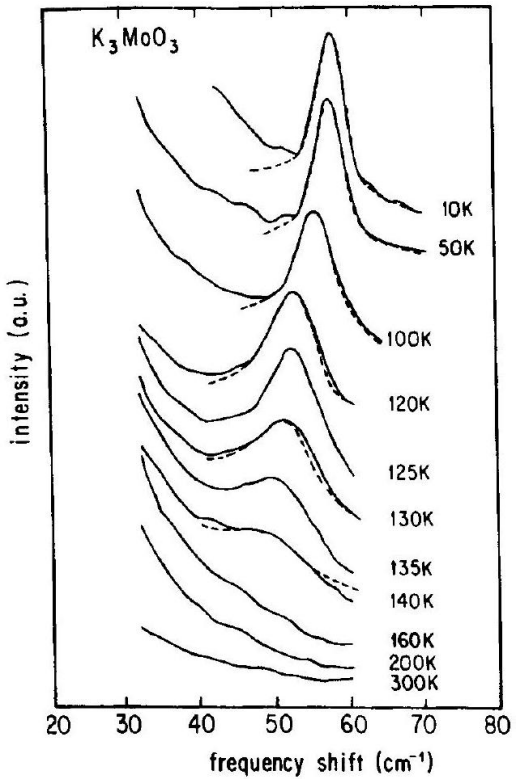


Figure 6.10. Raman spectrum of $\mathrm{K{{03} \mathrm{MoO}}{3}$ in the charge density wave state (Travaglini et al., 1983).

The mode, is analyzed in terms of a harmonic oscillator fit

$$I(\omega) = \frac{\beta(\omega) - 1}{\left(\omega_A^2 - \omega^2\right)^2 - (2\omega\Gamma)^2} \tag{6.75}$$

where ω_A is the oscillator frequency, Γ is the damping constant, and $\beta(\omega)$, is the Bose-Einstein factor. Fits to Eq. (6.75) are also displayed in the figure. As expected the intensity of the mode approaches zero at the phase transition, and Γ increases as the temperature increases.

The frequency of the amplitude mode, $\omega_A \simeq 1.7$THz at $T \to 0$, is comparable to the frequency of the unrenormalized phonon

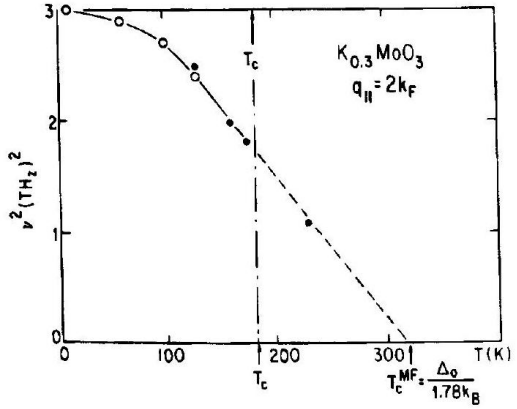


Figure 6.11. Temperature dependence of the amplitude mode frequency in $\mathrm{K}\{\{03\}\mathrm{MoO}\}\{3\}$. The dotted line is an extrapolation, assuming $\omega_a^2 \simeq \left(T_{\mathrm{COW}}^{\mathrm{MF}} - T\right)$ (Travaglini et al., 1983; Pouget and Comes, 1989).

mode $\omega_{2k_1} = 1.5$THz. This then, through $\omega = \lambda^{1/2}\omega_{2k_1}$ would imply that λ is close to number 1 in broad agreement with the d value arrived at in Chapter 3. The frequency decreases with increasing temperature, in qualitative agreement with what follows from the temperature dependent gap $\Delta(T)$ and condensate density $f(T)$. The temperature dependence $\omega_A(q = 0, T)$ is shown in Fig. 6.11 where measurements using both neutron (Pouget et al., 1991) and Raman scattering (Travaglini et al., 1983) are included. The full line is a fit to Eq. (6.38) with $T_{\mathrm{CDW}}^{\mathrm{MF}} = 320$ K, well above the transition temperature of $T_{\mathrm{3D}} = 180$ K. This, as discussed in the previous chapter, is due to fluctuation effects which reduce the transition where 3D order develops with respect to the mean field transition temperature.

The amplitude mode frequencies at $T = 0$ measured in various compounds with a charge density wave ground state are collected in Table 6.1; together with the values calculated using Eq. (6.35), the electron-phonon coupling constants λ, and the unrenormalized phonon frequencies ω_{2k}, as given in Tables 2.1 and 3.1. The effective mass values, measured by using neutron scattering or optical methods, together with the calculated values using Eq. (6.25), are also displayed.

Table 6.1. Amplitude mode frequencies and effective masses for various materials. The effective mass is calculated using the values of Δ and ω_{A} given in this Table and in Table 3.1

	ω_A (exp) (eV)	ω_A (Eq. 6.35) (eV)	m^*/m (exp)	m^*/m (Eq. 6.29)
KCP	$4.0 - 5.0 \times 10^{-3}$ (ref. 1)	4.4×10^{-3}	1000 (ref. 1)	660
$K_{0.3}MoO_3$	5.2×10^{-3} (ref. 2)	2.0×10^{-3}	300 (ref. 4)	260
$(TaSe_4)_2\,I$	9.4×10^{-3}		10^4 (ref. 5)	

1. K. Carneiro, in Electronic Properties of Inorganic Quasi-One-Dimensional Compounds, ed. by P. Monceau (Reidel, Dordrecht, 1985), Pt. 2 and references therein.

2. G. Travaglini, 1. Morke, and P. Wachter, Solid State Comm. 45, 289 (1983). J. P. Pouget et al. Phys. Ser. T25, 58 (1989).

3. S. Sugai, S. Kurihara and M. Sato, Physica 143B, 195 (1986), T. Sekine et al. Solid State Comm. 53, 767 (1985).

4. C. Escribe-Filippini, Synthet. Met. 19, 931 (1987).

5. T. W. Kim et al. Phys. Rev. B43, 6315 (1991).

It is expected that these excitations are accessible by thermal fluctuations and contribute to the various thermodynamic quantities. Because of the gap in the dispersion relation, contributions to the entropy from amplitude fluctuations are likely to be small. As discussed earlier, due to the linear dispersion relation, phase fluctuations lead to a specific heat which is proportional to T^3 at low temperatures where these fluctuations have a three-dimensional character. The strong anisotropy, however, may lead to a crossover to temperature regions where the character of these fluctuations is one- or two-dimensional. This in turn leads to temperature dependences different from the 3D case. A detailed analysis of the measured specific heat in various compounds has not been performed to date.

1.6.4 Experiments on Spin Density Waves: AFMR and Magnetization

The phase and amplitude modes which are related to charge excitations of the SDW state have not been measured, and neutron or Raman scattering studies of these materials have not been performed to date. Optical conductivity measurements, which couple to $q = 0$ phase excitations, are discussed in Chapter 9.

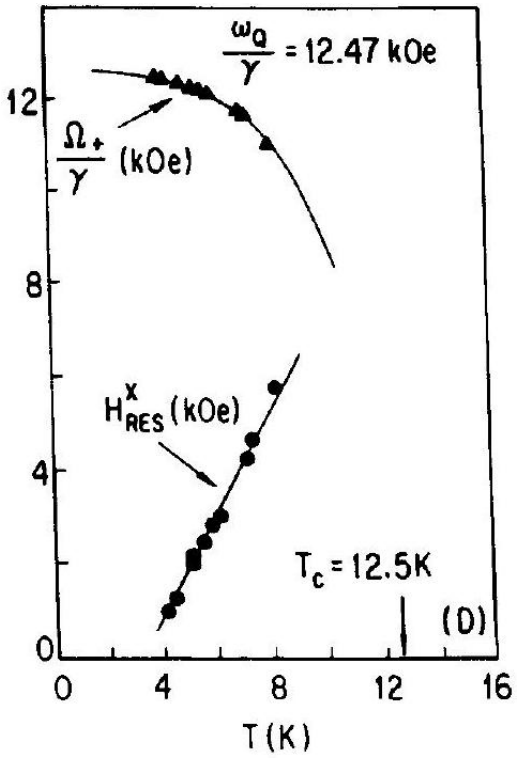


Figure 6.12. Observed resonance fields (circles) vs. temperature in (TMTSF) \${ }{{2} \mathrm{PF}}{6}\$ for H along the hard axis, which give the temperature dependence of ω_+, see Eq. (6.73) (Torrance et al., 1982).

The spin excitations have been examined in various materials through measurements of antiferromagnetic resonance. These experiments add little to our understanding of the SDW state, but give clear evidence that Eq. (4.35) is an appropriate starting point in describing the

magnetic properties of the ground state. The experiments, in general, are conducted at a fixed measurement frequency, while the magnetic field and/or temperature is varied. The resonance frequencies measured as a function of temperature are shown in Fig. 6.12. A comparison with calculated values gives a rough estimate of $\mu/\mu_B = 0.1$, in agreement with NMR and μSR studies (Torrance et al., 1982) discussed in Chapter 4.

As for the case of antiferromagnets, the thermally induced magnetic excitations also determine the temperature dependence of the magnetization. The magnetic susceptibility and antiferromagnetic resonance experiments can consistently be described in terms of an effective Heisenberg Hamiltonian, Eq. (4.35), which can also be used to evaluate the temperature dependence of the
magnetization, $M(T)$. As expected, the reduced dimensionality of the materials which develop an SDW ground state also has a pronounced influence on the number of thermally excited magnons. Because of the quasi-two-dimensional band structure, models which include a two-dimensional dispersion relation and phase space have been used to account for experiments (Uemura et al., 1992).

For weakly coupled Heisenberg chains, keeping only the gap Δ_0 associated with the larger antiferromagnetic resonance frequency ω_+, the dispersion relation in two dimensions is given by (Kittel, 1963)

$$\omega(k) = \omega_c \left\{\Delta_0^2 + k_1^2 x^2 + 2\alpha \left(1 - \cos k_y y\right)\right\}^{1/2} \tag{6.76}$$

where $\omega_c = 2J_{\text{eff}}\ (\mu/\mu_R)$ and we assume that the dispersion in the third direction can be neglected. Here $\alpha = J_{\text{eff}}\,/J_\perp$, where $J_\perp$ is an effective perpendicular coupling constant. 'he gap in the magnon excitation spectrum given by Eqs. (6.73) and (6.74) is $\omega_c\Delta_0$ and we have kept only one gap for the sake of simplicity. The dispersion in the third direction is also neglected because of the small bandwidth in that direction.

The above dispersion relation has a different character at high and low frequencies. For $\omega^2 - \omega_c^2\Delta_0^2 \gg \alpha\omega_{c'}^2, \omega(q)$ is nearly independent of q and the density of states is that of a 1D magnon spectrum given by

$$\rho(\omega) = \frac{1}{4\pi} \frac{\omega/\omega_{c'}^2}{\left[\left(\omega/\omega_{c'}\right)^2 - \Delta_0^2\right]^{1/2}} \tag{6.77}$$

For $\omega^2 - \omega_e^2\Delta_0^2 \ll \alpha\omega_e^2$ the dispersion relation can be expanded in terms of $k_y y$ and

$$\omega(k) = \omega_c \left\{\Delta_0^2 + k_x^2 x^2 + \alpha k_y^2 y^2\right\}^{1/2} \tag{6.78}$$

Consequently, the density of states in this limit is

$$\rho(\omega) = \frac{1}{4\pi} \frac{\omega}{\omega_t^2 \alpha^{1/2}} \tag{6.79}$$

An approximate form of the density of states, appropriate for both limits is given by

$$\rho(\omega) = \frac{1}{4\pi} \frac{\omega/\omega_i^2}{\left[\left(\omega^2/\omega_i^2\right) - \Delta_0^2 + \alpha\right]^{1/2}} \tag{6.80}$$

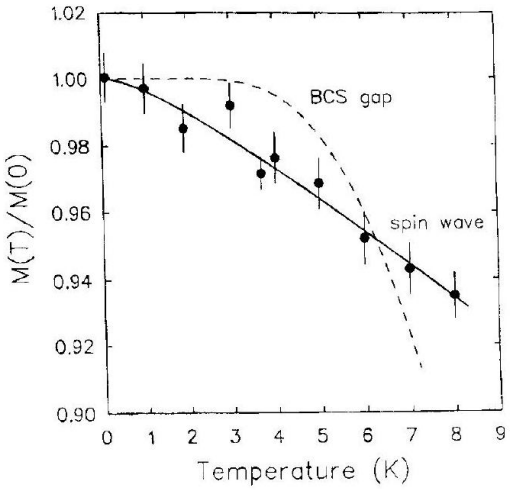


Figure 6.13. Temperature dependence of the magnetization $M(T)$ of $(\mathrm{TMTSF})_2\mathrm{PF}_6$ as measured by muon spin rotation. The full line is Eq. (6.81) with parameters given in the text (Le et al., 1993).

The magnetization is given at temperature T by (Kittel, 1963)

$$M(T) = M_0 \int_{\omega_1>}^{\omega_1 d} d\omega \frac{\rho(\omega)}{[(\omega^2/\omega_e^2) - \Delta_0^2]^{1/2} \left[\exp\left(\frac{\hbar\omega}{k_B T}\right) - 1\right]} \tag{6.81}$$

with the cutoff frequency defined as

$$\omega_d \int_{\omega_i,\Delta_j}^{\omega_d} d\omega \rho(\omega) = \frac{1}{2} \tag{6.82}$$

The magnetization calculated from Eq. (6.81) with the parameters established earlier is shown in Fig. 6.13, together with the magnetization as measured by muon spin rotation. At low temperatures, the temperature dependence is clearly determined by magnons and single particle excitations do not play an important role. Close to T_{SDW} both collective and single particle excitations may be important; but which of these determines the temperature dependence of the internal field remains to be seen.

1.7 Commensurability and Near Commensurability Effects

In the previous chapters we have discussed the phase transitions which lead to incommensurate charge and spin density wave ground states, and the various observations on these states. The periodic underlying lattice with period given by the lattice constant a has been neglected, and its coupling to the periodic charge and spin density wave modulation (with period $\lambda_0 = \pi/k_1$) has been ignored. As a result, the ground state is translationally invariant; the ground state energy and the single particle gap are independent of the phase variable ϕ. Also the collective excitations related to the phase remain gapless (in the absence of Coulomb interaction as discussed in Chapter 6). This is all valid for relatively weak lattice potentials, such as those expected here.

It is anticipated that the effect of the underlying lattice periodicity can be ignored as long as the period of the charge or spin density wave modulation is rather different from the wavelength λ_0. However, if the two periods are commensurate, i.e.,

$$\lambda_0 = \frac{N}{M} a \tag{7.1}$$

where N and M are integers, or are nearly commensurate (with Eq. (7.1) close to being obeyed) the interaction between the two periodicities becomes important. This then has several important consequences. The ground state energy becomes a periodic function of the phase variable ϕ, and the phase excitations develop a gap in the $q \to 0$ limit. Because of the quasiperiodic dependence of the ground state on the phase, various nonlinear excitations occur; the most common of these, soliton solutions, have been thoroughly explored. The situation is somewhat different near commensurability, where the density wave can distort itself in order to develop commensurate regions, separated by discommensurations.

These effects can be described by representing the lattice by the interaction term

$$\mathscr{H} = V_0\{1 - \cos(M\phi)\} \tag{7.2}$$

where, for simplicity, we assume that in Eq. (7.1) $N = 1$. The potential V_0 can be derived from a microscopic theory using weak coupling arguments and it decreases with an increasing degree of commensurability M. Having established the magnitude of V_0, the term given above can be added to the Lagrangian, which has been used before; and the excitations of the system can be described within the framework of the Ginzburg-Landau theory. This approach will be taken here.

Whether such commensurability effects can be seen in the materials which have been discussed before remains to be seen. Structural studies conducted in several materials, as well as electron counting arguments; suggest that at least some of the compounds are commensurate or close to commensurability. In these cases $\lambda_0 \simeq 4a$. As will be discussed, for such higher order commensurability the potential V_0 is small, and consequently the energy associated with the periodic variation of the phase is also small and can be easily overshadowed by other effects such as interactions with impurity potentials. Nonlinear excitations have also been searched for by a variety of optical experiments; clear evidence for such states, however, has not been found.

1.7.1 Models of Commensurability Effects

As discussed in Chapters 3 and 4, the condensation energy was found to be independent of the phase variable ϕ. The reason for this is that by approximating the dispersion of the electron gas by the expression $\epsilon_k - \epsilon_F = \hbar v_F\,(k - k_F)$ the underlying lattice periodicity is ignored. From Eq. (3.27) the equation of motion, is

$$\begin{aligned} E_k \cdot a_{1,k} &= \epsilon_k a_{1,k} + \Delta e^{-i\phi} a_{2,k} \\ E_k \cdot a_{2,k} &= -\epsilon_k a_{2,k} + \Delta e^{i\phi} a_{1,k} \end{aligned} \tag{7.3}$$

where only states on the left and right hand side of the Fermi surface are included. The new dispersion relation is obtained from

$$\begin{vmatrix} E_k - \epsilon_k & -\Delta e^{-i\phi} \\ \Delta e^{i\phi} & E_k + \epsilon_k \end{vmatrix} = 0 \tag{7.4}$$

giving $E_k = \pm\left(\epsilon_k^2 + \Delta^2\right)^{1/2}$ as in Eq. (3.34). Here we have assumed that states near $+k_F$ couple to states near $-k_I$ (and vice versa). As usual, the periodic lattice also leads to a mixture of states which differ by $\pm 2k_F, \pm 4k_F, \cdots$; however, it is assumed that only the first term is important as the other states (except those included in Eq. (7.3)) are far from the Fermi energy. In the case of commensurate density wave, however, this is not the case, and the situation is illustrated in Fig. 7.1 for a half filled and for a one-third filled band. The former corresponds to $\lambda_0 = 2a$ the latter to $\lambda_0 = 3a$. In the case of the half filled band $a_{2,k-2k_1}$ is

equivalent to $a_{1,k}$ and the equation of motion is (neglecting for the moment that a half filled band is a special case, and the order parameter is real)

$$\begin{aligned} E_k a_{1,k} &= \epsilon_k a_{1,k} + \Delta e^{-i\phi} a_{2,k} + \Delta e^{i\phi} a_{2,k} \\ E_k a_{2,k} &= -\epsilon_k a_{2,k} + \Delta e^{-i\phi} a_{1,k} + \Delta e^{i\phi} a_{1,k} \end{aligned} \tag{7.5}$$

giving

$$E_k = \pm \left(\epsilon_k^2 + 4\Delta^2 \cos^2 \phi\right)^{1/2} = \pm \left\{\epsilon_k^2 + 2\Delta^2(1 + \cos(2\phi))\right\}. \tag{7.6}$$

The dispersion relation now depends on the phase ϕ, and so does the single particle gap which has a maximum when $\phi = 0$, here

$$\Delta = 2\epsilon_F e^{-1/2\lambda} \tag{7.7}$$

For $\phi = \pi/2$, there is no single particle gap. For $\phi = 0$

$$E_k = \pm \left(\epsilon_k^2 + 4\Delta^2\right)^{1/2} \tag{7.8}$$

and the condensation energy (see Eq. (3.40)) is

$$E_{\text{el}} = n\left(\epsilon_F\right) \cdot 4\Delta^2 \ln\left(\frac{2\epsilon_F}{\Delta}\right) = \frac{n\left(\epsilon_F\right) \cdot 2\Delta^2}{\lambda} \tag{7.9}$$

using Eq. (7.7). In general, the phase dependent electronic energy can be written as

$$E_{\text{cl}} = \frac{n\left(\epsilon_{\text{f}}\right)\Delta^2}{\lambda} \cos 2\phi. \tag{7.10}$$

All this can be generalized to higher order commensurability. The potential as given by Eq. (7.1) connects electrons and holes with $\pm k_1$ in two different ways. There is a direct scattering from $-k_F$ to $+k_1$ as shown in Fig. 7.1. Alternatively, $M-1$ repeated scatterings each involving -$2k_F$ leads to the wavevector $2k_1(M-1)$. By symmetry however, this is equivalent to a scattering involving $+2k_F$ and therefore leads to the same final state. The process involves scattering into states which are far removed from ϵ_F, and this then leads to a reduction of the potential V_0. For a commensurability M one obtains

$$E_k = \pm \left(\epsilon_k^2 + 2\Delta^2 + \frac{2\Delta^M}{D^{M\cdot 2}} \cos M\phi\right)^{1/2} \tag{7.11}$$

where D is a cutoff energy, assumed to be on the order of the bandwidth or the Fermi energy (Lee, Rice, and Anderson, 1974). For $M = 2$ we recover Eq. (7.8). Integrating over the occupied states leads to the commensurability energy

$$E_{\text{commo}} = -\frac{n\left(\epsilon_i\right)\Delta^2}{\lambda} \left(\frac{\Delta}{D}\right)^{M-2} \cos M\phi \tag{7.12}$$

which reduces to Eq. (7.10) in the $M = 2$ case.

Having established the phase dependent condensation energy, this term can be added to the Lagrangian which describes the time and spatial dependence of the phase fluctuations, which were discussed in Chapter 6. The free energy, from Eq. (6.36), is given at $T = 0$ by (with amplitude fluctuations neglected here)

$$F(0) = \frac{1}{4} n(\epsilon_r) \int dx \left[\hbar^2 v_f^2 \left(\frac{d\phi}{dx} \right)^2 + \frac{m^*}{m} \left(\frac{d\phi}{dt} \right)^2 + \frac{1}{M^2} \omega_i^2 \frac{m_1^*}{m} \cos(M\phi) \right] \tag{7.13}$$

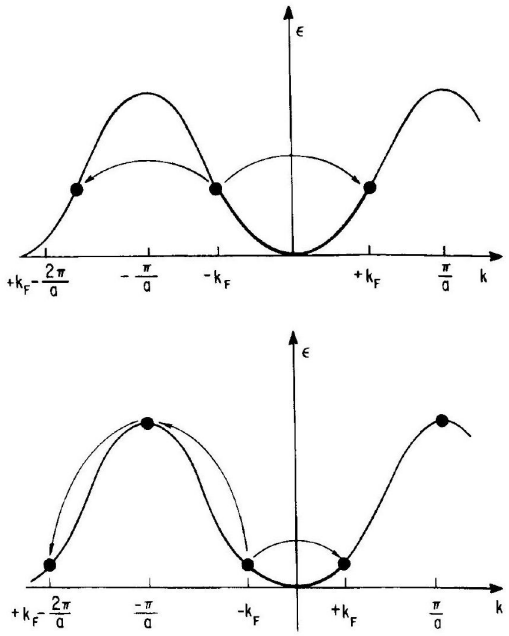


Figure 7.1. The dispersion relation for a half filled (top part) and one-third filled (bottom part) electron band. The scattering involving the wavevector $2 k_{1}$ and the scatterings (one in the half filled band and two in the one-third filled band case) which lead to $\pm k - 2\pi/a$ are indicated on the figure by the arrows.

with the notation

$$\omega_F^2 = \frac{4M^2}{\lambda} \frac{m\Delta^2}{m^*} \left(\frac{\Delta}{D} \right)^{M-2}. \tag{7.14}$$

The Lagrange equation, Eq. (6.8a), gives the following equation of motion

$$\frac{d^2\phi}{dt^2} - \hbar^2 v_r^2 \frac{m}{m^*} \frac{d^2\phi}{dx^2} + \frac{\omega_f^2}{M} \sin(M\phi) = 0 \tag{7.15}$$

the well-known Sine-Gordon equation.
First we look at the small amplitude displacements of the undistorted density wave around the equilibrium position. Then the potential is

$$V(\phi) = \frac{1}{2} \frac{d^2V}{dx^2} \phi^2 = \frac{\omega_F^2}{2M} \phi^2. \tag{7.16}$$

Assuming that the time and spatially dependent phase is given by $\phi = \phi \exp[i(\omega t - qx)]$ we obtain the following dispersion relation

$$\omega_\phi(q) = \left(\frac{\omega_f^2}{M} + v_f^2 \frac{m}{m^*} q^2\right)^{1/2} = \left(\frac{\omega_f^2}{M} + c_\phi^2 q^2\right)^{1/2} \tag{7.17}$$

where we have used the expression of the phase velocity given by Eq. (6.33). In contrast to Eq. (6.33) where the phase excitations are gapless the periodic potential leads to a gap in the excitation spectrum, and the dispersion relation is shown in Fig. 7.2.

For arbitrary distortions of the phase, the solution $M\phi(x,t) = s(\xi)$ is obtained by performing the Galilean transformation $t \rightarrow$

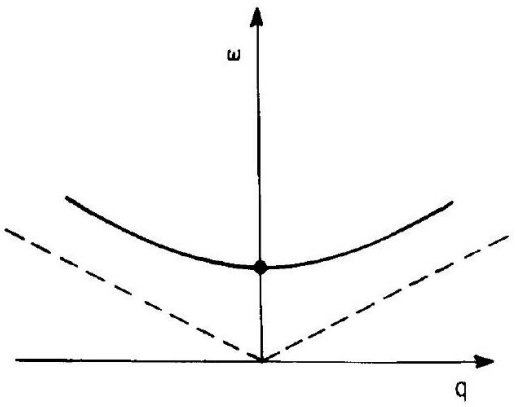


Figure 7.2. The phason dispersion relation for a commensurate (full line) and incommensurate (dashed line) density wave. The dispersion relations are given by Eqs. (7.17) and (6.33).

$t' = t$ and $x \rightarrow \xi = x - ut$. Then the integration with respect to ξ gives

$$\frac{1}{2}\left(c_\phi^2 - u^2\right)\left(\frac{ds}{d\xi}\right)^2 = -\frac{\omega_F^2}{M}\cos(s) + \text{const} \tag{7.18}$$

where we have the relations $\partial/\partial t = -u(\partial/\partial\xi)$ and $\partial/\partial x = d/d\xi$. Choosing the constant, $c = \omega_F^2/M$ we obtain

$$M\frac{ds}{d\xi} = \pm\frac{4\omega_F/M^{1/2}}{\left(c_\phi^2 - u^2\right)^{1/2}}\sin\left(\frac{s}{4}\right)\cos\left(\frac{s}{4}\right) \tag{7.19}$$

and the integration gives

$$\tan\left(\frac{Ms}{4}\right) = \exp\left\{\pm\frac{\omega_F/M^{1/2}}{\left(c_\phi^2 - u^2\right)^{1/2}}\right\} \tag{7.20}$$

Therefore,

$$\begin{aligned}\phi^\dagger(x,t) &= \frac{s(\xi)}{M} \\ &= \frac{4}{M}\tan^{-1}\left[\exp\left\{\pm\frac{\omega_F/M^{1/2}}{\left(c_\phi^2 - u^2\right)^{1/2}}(x-ut)\right\}\right]\end{aligned} \tag{7.21}$$

The above solution describes a phase charge of $2\pi/M$ over the region which has the size of approximately $d = v_r^2/\omega_F, m/m^*$, as shown in Fig. 7.3. This so-called soliton is invariant under the transformation $x - ut$, and consequently, propagating solutions with a constant velocity

u leave the shape of the solution unchanged. The energy associated with the soliton can be obtained by inserting the solution $\phi(x,t)$ as given by Eq. (7.21) into the free energy Eq. (7.13), and after some algebra we obtain

$$E_{\rm sol} = \frac{4}{\pi}\left(\frac{m^*}{m}\right)^{1/2} \frac{\hbar\omega_F}{\left(1-\frac{u^2}{c_\phi^2}\right)^{1/2}} = \frac{Mc_\phi^2}{\left(1-\frac{u^2}{c_\phi^2}\right)^{1/2}} \tag{7.22}$$

The creation of a soliton leads to a change of phase by $2\pi/M$ going (say) from the left hand to the right hand side of the soliton. As there is $2e$ charge associated with a density wave

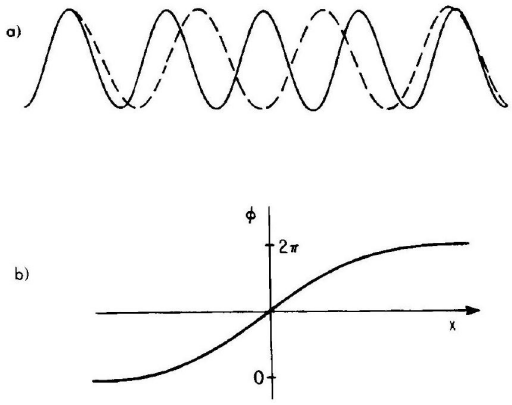


Figure 7.3. a) A density wave with a local distortion, as given by Eq. (7.21) (full line). The dashed line indicates the undistorted density wave. b) The spatial dependence of the phase ϕ.

period λ_0 (which corresponds to a phase $\pi/2$), a soliton excitation corresponds to a charge

$$c^* = \frac{2c}{M} \tag{7.23}$$

Obviously, solitons with a change of phase by $2\pi n/M$, where n is an integer, can also be created, and the excitations correspond to an effective charge $2en/M$. In general, we can show that the charge associated with any local configuration leading to the change of phase is given by

$$e^* = \frac{\phi(\infty)-\phi(-\infty)}{\pi}. \tag{7.24}$$

Until now we have considered only one electron band, neglecting the spin degrees of freedom. Consequently, only charged excitations can be created by creating a local distortion of the phase $\phi(x,t)$. Let us now assume that the charge density wave is formed by two bands, one with spin up and one with spin down.

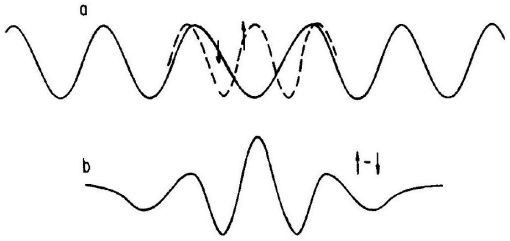


Figure 7.4. a) A charge density wave with different local distortions in the spin up (full line) and spin down (dashed line) subbands. b) The change of the phase in the different subbands is different, leading to a spin density modulation ($\uparrow - \downarrow$), as shown.

A soliton excitation $\phi(x,t)$ which is the same in both spin subbands returns our previous results and only charge excitations with charge $e^* = 2\pi/M$ occur. However, the form of the localized excitation can be different in the two subbands, generally leading to both charge and spin excitations. A simple example of such excitation (which may occur in response to an impurity potential) is shown in Fig. 7.4; where the curve shows the two soliton excitations of the two subbands, and the lower curve corresponds to the difference of the two charge excitations in the two subbands, i.e., a localized spin excitation.

The counting rule, Eq. (7.24), can be generalized by defining the following phases

$$\begin{aligned} \phi(x) &= \frac{\phi\downarrow(x) + \phi\uparrow(x)}{2} \\ \theta(x) &= \frac{\phi\uparrow(x) - \phi\downarrow(x)}{2} \end{aligned} \tag{7.25}$$

In terms of ϕ and θ,

$$\begin{aligned} e^* &= \frac{\phi(\infty) - \phi(-\infty)}{\pi} \\ S_z &= \frac{\theta(\infty) - \theta(-\infty)}{\pi} \end{aligned} \tag{7.26}$$

For the excitation, such as that shown in Fig. 7.4, $\phi(\infty) = \phi(-\infty)$ and therefore the change associated with the excitation is zero. However, the phase change is different in the two subbands, and $\theta(\infty) - \theta(-\infty) = 2\pi$. This leads to a spin $S = 1/2$ which is associated with the excitation. The above also suggests that for arbitrary phases fractional changes and fractional spins may be created, the notion of a fractional spin however is not universally accepted (see, for example, Horowitz (1989)).

The periodic lattice potential also leads to important, but somewhat different, effects when the density wave is not entirely, but only nearly, commensurate with the underlying lattice. For a commensurate and undistorted density wave the phase is constant. For a nearly commensurate density wave, in contrast, the local phase varies slowly with position and this variation is described as

$$\phi_1 = \phi_0 + qx \tag{7.27}$$

where q accounts for the deviation from commensurability and is written as

$$q = \frac{2\pi}{\lambda_0}\left(Ma - \lambda_0\right). \tag{7.28}$$

The free energy is then written as

$$F(0) = \frac{1}{2} n(\epsilon_f) \int dx \left[v_F^2 \left(\frac{d\phi}{dx} - q \right)^2 + \frac{m^*}{m} \left(\frac{d\phi}{dt} \right)^2 + \frac{\omega_F^2}{M} \frac{m^*}{m} \cos(M\phi) \right] \tag{729}$$

The solution is a periodic array of solitons, separated by regions where the density wave is commensurate with the underlying lattice. The situation is sketched in Fig. 7.5 where the linear variation of ϕ_l corresponds to an incommensurate density wave. The distance between the solitons, ℓ_5, follows from the simple consideration of the phase which must advance at the same rate for the soliton lattice as for the incommensurate density wave. As each soliton advances in phase by $2\pi/M$, the number of solitons over a distance x is $n = qx/(2\pi/M)$, and the distance

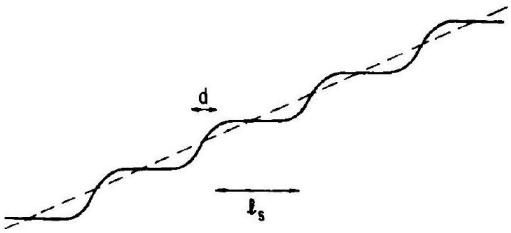


Figure 7.5. Variation of the local phase, ϕ_{ℓ}, for an incommensurate charge density wave (dotted line); and for a density wave which, due to interaction with the lattice, has commensurate regions, separated by discommensurations (full line). The distance between the solitons of with d is ℓ_4.

between them is

$$\ell = \frac{x}{n} = \frac{2\pi}{qM}. \tag{7.30}$$

Rather near to commensurability, $q \ll 1$, the distance between solitons is significantly larger than their width. In this limit $\phi(x,t)$ for each individual soliton is given by Eq. (7.22) and their interaction can be neglected.

Assuming the incommensurate density wave having zero energy (except of course the condensation energy), the energy of the soliton lattice is given by two terms. The first is the commensurability energy, which over the distance ℓ_s is $\ell_s E_{\rm comm}$. The second term, given by E_s, is the one associated with the solitons. Consequently, the total energy (per soliton) is

$$\begin{aligned} E_{\rm tot} &= \ell_s E + E_{\rm sol} \\ &= \frac{-2\pi}{Ma - \lambda_0} \frac{n(\epsilon_F)}{4M^2} \frac{m^*}{m} \hbar^2 \omega_F^2 + \frac{4}{\pi M^2} \left(\frac{m^*}{m} \right)^{1/2} \hbar \omega_F \end{aligned} \tag{7.31}$$

which after some algebra and using the expression for ω_F becomes

$$E_{\rm tot} = \frac{\hbar \omega_F}{M^2} \left(\frac{m}{m^*} \right)^{1/2} \left\{ -\frac{\pi M}{Ma - \lambda_0} \frac{n(\epsilon_F)\,\Delta}{\lambda^{1/2}} \left(\frac{\Delta}{D} \right)^{\frac{M-2}{2}} + \frac{4}{\pi} \right\}. \tag{7.32}$$

For a small deviation for commensurability $Ma - \lambda_0$ is small, the first term dominates, and the soliton lattice is stable. With increasing $Ma - \lambda_0$, a transition to an incommensurate density wave occurs. The approximate condition for this is given by $\ell E_{\text{comm}} = E_s$. For $M = 4$ this leads to

$$4a - \lambda_0 = \frac{2\pi^2}{\lambda^{1/2}} \frac{E_{\text{cond}}}{D} \tag{7.33}$$

where $E_{\text{cond}} = \frac{1}{2} n(\epsilon_F) \Delta^2$ is the condensation energy.
This crude argument neglects the (repulsive) interaction between solitons. This will become increasingly important as their separation becomes comparable to their spatial extension, which occurs near the soliton lattice-incommensurate DW transition. A sharp phase transition to an ordered state is not expected to occur in such a strictly one-dimensional system and arguments discussed in Chapter 5 also apply here. Interchain interactions, mediated either by Coulomb effects or by interchain tunneling alter this picture dramatically. Due to such interchain interactions we expect soliton arrays perpendicular to the chain direction, with the formation of such ordered structures leading to a phase transition from a 3D incommensurate density wave state to a 3D soliton lattice (or other discommensuration lattice) state.

In discussing the effects caused by the underlying periodic lattice potential we have assumed that the amplitude of the density wave is constant; consequently only variations of the phase variable have been considered. The nonlinear excitations are then called phase-solitons. Nonlinear excitations due to local changes of amplitude also occur, and such so-called amplitude solitons have also been widely discussed in the literature (see, for example, Bak and Pokrovsky, 1981 and references cited therein).

1.7.2 Experiments: Search for Commensurability Effects and Solitons

In several materials which have a charge or spin density wave ground state, the period of the density wave is commensurate or nearly commensurate with the underlying lattice. The wavevector is usually temperature dependent, and a typical dependence is shown for $K_{03}MoO_3$ in Fig 7.6. In this case the value $1 - q = a'$ refers to the wavevector which appears in the CDW modulation

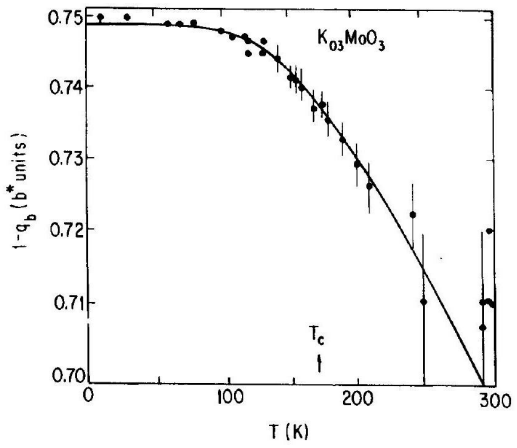


Figure 7.6. Temperature dependence of the charge density wavevector in $\mathrm{K}{{11}\mathrm{M}}{1}\mathrm{O}_{3}$. The notation used gives a CDW period $\lambda_1 = 4a$ (i.e., a f.uur times commensurability) for $1 - q_b = 0.75$. After J. P Pouget and R. Comes (1989).

which has the form of $\cos(q'x + \phi)$, and thus at low temperatures the period is close to four times the lattice constant. The situation is similar for TaS_3 and also in $NbSe_3$. In (TMTSF) PF_6 the spin density wave is commensurate along the conducting chains, with $\lambda_0 = 4a$, and most probably this is the case for the other members of this group of materials.

Because of this, commensurability and near commensurability effects have been searched for in these materials; clear evidence for these effects, such as a gap in the phason excitation spectrum or nonlinear excitations at energies below the single particle gap, have not been found.

The most likely reason for this is that at or near commensurability the pinning potential is small. For a typical material, such as $K_{0.3}MoO_3$, for which $\Delta = 700$ K, $m^*/m \simeq 400$ and $\lambda \simeq 0.5$ (see Chapter 3) the pinning energy from Eq. (7.14)

$$h\omega_1 \simeq 2 \times 10^{-2}\Delta \simeq 10^{-3}\text{eV},$$

is fairly small. As will be discussed in Chapter 8, the interaction of density waves with impurities also leads to a pinning of the collective mode, and the relevant energy is larger than that given above. Consequently, it is likely that impurity rather than commensurability effects are responsible for the finite frequencies observed for $q \to 0$ in various materials. This has been directly confirmed by experiments conducted on alloys of various materials. The soliton energy for the same set of parameters as used before is

$$E = \frac{4}{\pi}\left(\frac{m^*}{m}\right)^{1/2} \hbar\omega_F = 3 \times 10^{-2}\text{eV}$$

which is somewhat smaller than the single particle gap. The spatial extension of the soliton

$$d = \frac{(m/m^*)^{1/2}\, v_T}{\omega_F} \simeq 30\text{Å}$$

for $v_F \simeq 10^7$ cm/sec. These excitations, which involve the change of the phase of the collective mode, are expected to be optically active, and they have been searched for by a variety of optical probes without success. It has also been proposed that solitons contribute to the frequency and electric field dependent conductivity (Horowitz and Trullinger, 1984), however experimental evidence for such contributions has not yet been found.

1.8 The Interaction Between Density Waves and Impurities

Impurities which are distributed at random in the crystal have a profound influence on both the static and dynamic properties of density waves. Isoelectronic impurities (if they do not lead to a local lattice-distortion) do not couple to density waves while the electrostatic impurity potential $V\left(\vec{r} - \vec{R}_1\right)$ of the nonisoelectronic impurities leads to changes of both the amplitude and phase of the condensate near the impurity site $\vec{R}_1$. These changes have been discussed in terms of microscopic models, and the resulting spatial dependence of the charge and spin distribution has been evaluated. For small impurity potentials the amplitude of the density waves is only weakly modified, while for strong impurities (which can be represented by electrostatic potentials larger than the single particle gap) the amplitude collapses near $\vec{R}_t$ leading to bound states. The spatial extension of these states is on the order of the coherence length ξ, at zero temperature. For distances $\left|\vec{r} - \vec{R}_i\right| > \xi$ the influence of impurities can be described in terms of an interaction where the impurity potential couples directly to the phase ϕ of the condensate and the amplitude remains unaffected. The problem of many impurities distributed at random can be then treated within the framework of the Ginzburg-Landau description (Fukuyama and Lee, 1978; Lee and Rice, 1979).

Impurity potentials which couple directly to the phase ϕ of the condensate, destroy long-range order (Imry and Ma, 1975;

Sham and Patton, 1976; Efetov and Larkin, 1977) and lead to a finite phase-phase correlation length L_0. The length scale depends on the strength of the impurity potentials, on the impurity concentration, and on the properties of the density waves. The absence of long range order, and the appearance of many metastable states has been confirmed by a variety of structural, thermodynamic and electric measurements.

1.8.1 Theories of Density Wave-Impurity Interaction

The usual treatment of the problem deals with impurity effects at low temperatures where temperature induced fluctuations as well as quantum fluctuations of the collective mode are neglected. The Hamiltonian which describes the interaction is given withi' the framework of the Ginsburg-Landau theory by (see Eq. (6.36))

$$\mathscr{H} = \frac{\hbar^2 v_l^2 n\left(\epsilon_F\right)}{2} \int d\vec{r} (\vec{\nabla}\phi)^2 + \frac{\pi}{2} V_{\text{imp}}\left(\phi\right) \tag{8.1}$$

where anisotropy effects due to the anisotropic band structure are neglected. These can be included by renormalizing the length scales in the different orientations, as was done in Chapter 6. The first term is the normal elastic energy (see Eq. (6.51)) and the second describes the interaction between the collective mode and impurities. The approach is appropriate for long wavelength deformations; short wavelength modifications of the phase on the length scale $L < \xi_0 = \hbar v_r/\pi\Delta$ cannot be discussed with the framework of this description.

The mechanism which leads to an interaction between charge density waves and impurities is shown in Fig. 8.1. The impurity potential $V(\vec{x}) = V_0 \delta\left(\vec{r} - \vec{R}_1\right)$ at $\vec{R}$, induces a charge density oscillation with period $\lambda_0 = \pi/k_F$ (the well known Friedel oscillation) which is phase-matched to the density wave at position $\vec{R}_r$. For small impurity potentials this interaction can simply be written as

$$V_{\text{imp}}\left(\phi\right) = \int d\vec{r} V\left(\vec{r} - \vec{R}_1\right) \rho_1 \cos\left(\vec{Q}\vec{R} + \phi\left(\vec{R}_1\right)\right) \tag{8.2}$$

where ρ_1 is the amplitude of the charge density wave modulation. Obviously this is appropriate only if the impurity potential does not lead to modification of the amplitude of the collective

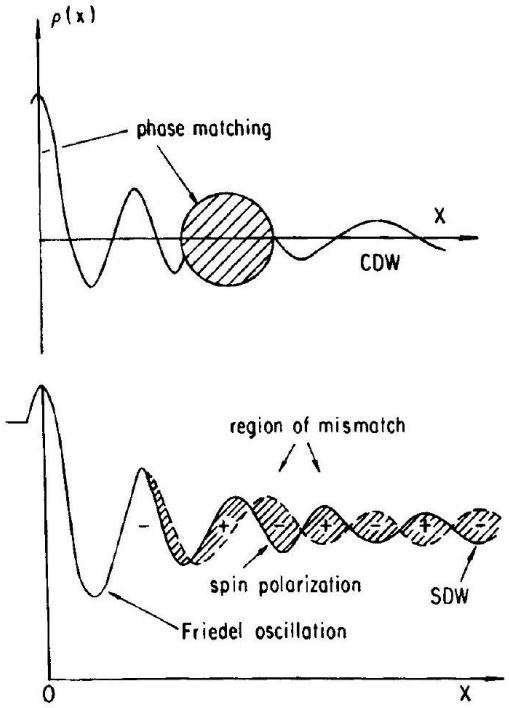


Figure 8.1. The local density distribution around a nonmagnetic impurity for a CDW and a SDW ground state (Tüttő and Zawadowski, 1985).

mode. This only occurs if V_0 is small. If V_0 is comparable to or larger than the single particle gap, bound impurity states may occur. These have been discussed in detail by Tüttő and Zawadowski (1985).

In the case of spin density waves, the situation is different. In the first order, charged impurities do not interact with the ground state. However, in second order the interaction between the impurity and the two subbands (both with a modulation of the charge density) is different (Fig. 8.1), leading to an interaction energy given by

$$V_{\mathrm{tmp}}(\phi) = \int d\vec{r} V\left(\vec{r} - \vec{R}_1\right) \rho_1 \cos\left(\vec{Q}_F \cdot \vec{R}_1 + 2\phi(R_1)\right). \tag{8.3}$$

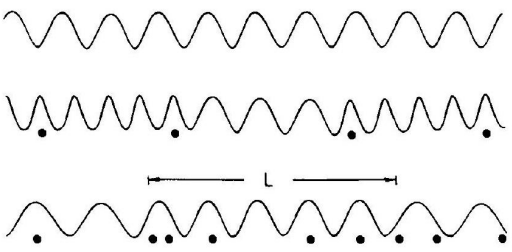


Figure 8.2. Strong and weak impurity pinning in one dimension. The phase is fully adjusted at each impurity for strong pinning; for weak pinning such phase adjustment occurs over a characteristic distance L_{10}.

Here ρ_1 represents the charge density wave modulations in the two spin subbands; as discussed in Chapter 4 these are displaced by $\phi = \pi$ with respect to each other.

In Eq. (8.1) the first term favors a uniform phase, $\phi = \mathrm{const}$, with distortions leading to an increase of the elastic energy due to the internal deformation of the collective mode. The

second term however, favors local distortions of the phase so that ϕ is adjusted to the impurity potential, thus decreasing the electrostatic interaction energy as given by Eqs. (8.2) and (8.3).

The various situations which may occur can easily be seen for a one-dimensional density wave interacting with randomly positioned impurities, such as that shown in Fig. 8.2. For an attractive potential at site $\vec{R}_1$, the phase $\phi\left(\vec{R}_i\right) = 0$ leads to the maximum charge density at the impurity site and if this happens, the potential energy gain with respect to the potential experienced by the undisturbed density wave with random phase $\phi\left(\vec{R}_1\right)$ at the impurity positions is approximately given by

$$V_{\text{pot}} = V_0 \rho_1 n_1. \tag{8.4}$$

This adjustment however, would lead to an increased elastic energy, and from Eq. (8.1) this is approximately given by

$$V_{\text{el}} \approx \hbar v_r \left(\frac{2\pi}{\langle \ell \rangle}\right)^2 = \hbar v_r n_1^2, \tag{8.5}$$

where $\langle \ell \rangle$ is the average distance between the impurities.

Consequently, the ratio

$$\epsilon = \frac{V_{\text{pot}}}{V_{\text{el}}} = \frac{V_0 \rho_1}{\hbar v_f n_i} \tag{8.6}$$

tells us whether the impurity-density wave interaction or the elastic term is more important. The situation where $V_{\text{pot}} \gg \mathrm{V_{el}}$ is called strong impurity pinning (the term pinning refers to the fact that the collective mode is "pinned" to the underlying lattice through the interaction with impurities); the case $V_{\text{pot}} \ll V_{\text{el}}$ represents weak impurity pinning.

For both cases long range phase coherence is lost. For large distances we can write

$$\langle \phi(\vec{r}), \phi(0) \rangle = e^{-\dot{r}/L_0} \tag{8.7}$$

with L_0 the so called phase-phase correlation length.

For $\epsilon \gg 1$, the potential energy term dominates and the total energy of the coupled collective mode and impurity is given by

$$E_{tot} = V_0 \rho_1 n_1. \tag{8.8}$$

As the phase is completely adjusted to the impurity positions at every impurity site, the average phase coherence length $L_0 \simeq \frac{1}{r}$ is the average distance between impurities.

The case for $\epsilon \leq \mathbf{1}$ is more interesting and in this limit scaling arguments can be used to evaluate the total energy and the phase-phase coherence length. In contrast to what happens for strong impurity potentials, expect the phase to adjust to many randomly positioned impurities with a length scale over which the phase varies by one wavelength significantly exceeding the average distance between impurities. The situation is shown in Fig. 8.3. Assuming that the length scale over which such adjustment occurs is L_0, in d dimensions the volume is L_0^d, and statistical arguments lead to an overall decrease of the potential energy

$$E_{\text{pot}} = -V_0 \rho_1 \left(L_0^d n_i\right)^{1/2} L_0^{-d} = -V_0 \rho_1 n_1^{1/2} L_0^{-d/2}. \tag{8.9}$$

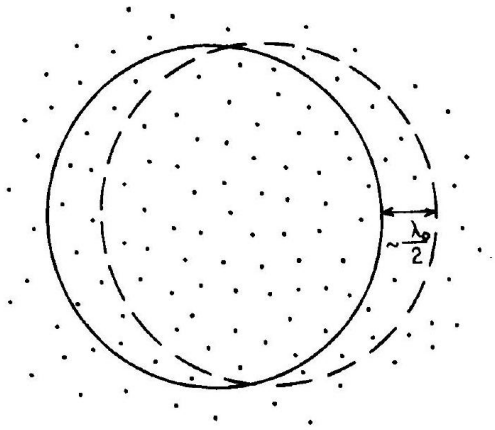


Figure 8.3. The weak impurity pinning in two dimensions. The full circle represents a region of undistorted density wave, the broken circle represents the density wave which is adjusted to optimize the interaction with the impurity potentials.

The change of the elastic energy, associated with such adjustment, comes from the gradient term in Eq. (8.1), and is given by

$$E_{\rm el} = \frac{\hbar v_F}{L_0^2}. \tag{8.10}$$

The total energy corresponding to the volume $L_0^{\rm d}$ is

$$E_{\rm tot} = E_{\rm pot} + E_{\rm el} = -V_0\rho_1 n_1^{1/2} L_0^{-d/2} + \frac{\hbar v_F}{L_0^2} \tag{8.11}$$

and by minimizing with respect to L_0 we obtain

$$-V_0\rho_1 n_1^{1/2}\left(\frac{d}{2}\right) L_0^{-(d/2)-1} + 2\hbar v_F L_0^{-3} = 0 \tag{8.12}$$

or

$$L_{01} = \left[\frac{dV_0\rho_1 n_1^{1/2}}{4\hbar v_F}\right]^{+\frac{2}{d-4}}. \tag{8.13}$$

Thus, the characteristic length L_0 is finite in any dimension $d < 4$, and there is no long-range order. In three dimensions, Eq. (8.13) gives

$$L_0 = \frac{(hv_F)^2}{(3/4)^2 V_0^2 \rho_1^2 n_\imath} \tag{8.14}$$

and the characteristic length is inversely proportional to the impurity concentration. From Eq. (8.7) thi total energy gain per unit volume

$$E_{\rm tot} = 2\left(\frac{3}{4}\right)^2 \frac{V_0^4\rho_1^4}{(\hbar v_F)^3} n_1^2, \tag{8.15}$$

is proportional to the square of the impurity concentration. The total energy per phase coherent volume is then given by $E_{\rm tot}$.

The above arguments can easily be generalized to an anisotropic band-structure, which we describe in terms of the anisotropic coherence length ξ, which is proportional to the Fermi velocity, see Eq. (6.17). Then the elastic term of the free energy reads

$$F_{\rm el} = \frac{n\left(\epsilon_F\right)\pi^2}{16}\int d\vec{r}\left\{\xi_x^2\left(\frac{\partial\phi}{\partial x}\right)^2 + \xi_y^2\left(\frac{\partial\phi}{\partial y}\right)^2 + \xi_z^2\left(\frac{\partial\phi}{\partial z}\right)^2\right\} \tag{8.16}$$

With $dy' = (\xi_y/\xi_x)\,dx$ and $dz' = (\xi_z/\xi_x)\,dz$ Eq. (8.16) becomes

$$F_{\rm cl1} = \frac{n\left(\epsilon_F\right)\pi^6}{16}\frac{\xi_y\xi_z}{\xi_x^2}\int d\vec{r}\xi_x^2\left(\vec{\nabla}'\phi\right)^2 \tag{8.17}$$

with $dr' = dx'dy'dz'$. The volume which is evaluated becomes $V = L^d\left(\xi_y\xi_z/\xi_x^2\right)$ instead of L_0^d. With this rescaling, Eq. (8.10) becomes

$$E_d = \hbar v_F L_0^{-2}\left(\frac{\xi_y\xi_z}{\xi_x}\right)^2 \tag{8.18}$$

and the potential energy, from (8.9) becomes

$$E_{\rm pot} = -V_0\rho_1\left(\frac{\xi_y\xi_z}{\xi_x^2}\right)^{1/2} n_i^{1/2}L_0^{-d/2} \tag{8.19}$$

Minimization of the total energy then gives a characteristic length

$$L_0 = \frac{\left(hv_F\right)^2}{(3/4)^2V_0^2\rho_1^2}\frac{1}{n_1}\frac{\xi_3^2}{\xi_y\xi_z} \tag{8.20}$$

and a total pinning energy

$$E_{\rm tot} = 2\left(\frac{3}{4}\right)\frac{V_0^4\rho_1^4}{\left(\hbar v_F\right)^3}n_t^2\left(\frac{\xi_i^2}{\xi_y\xi_z}\right) \tag{8.21}$$

The characteristic phase-phase correlation length along the chain direction is L_0, and in the perpendicular directions is given by

$$\begin{aligned} L_y &= \left(\frac{\xi_y}{\xi_x}\right)L_0 \\ L_z &= \left(\frac{\xi_z}{\xi_x}\right)L_0 \end{aligned} \tag{8.22}$$

Some numerical estimates of the characteristic lengths and total energies per domain are in order here. The impurity potential cannot greatly exceed the single particle gap, and therefore $V_0 \simeq 5\times10^{-2}$eV for a typical charge density wave gap. The amplitude of the CDW modulation $\rho_1 \simeq 10^{-2}$ for $v_F = 10^7$ cm/sec, leads to $\epsilon \sim 10^{-1}$ (see Eq. (8.6)) for $c = 1000$ppm. For this impurity concentration the weak impurity pinning limit applies. With the above parameters, the phase-phase correlation length is $L_0 = 3\times10^{-3}$ cm along the chain direction, and significantly smaller perpendicular to the chains. The total energy per phase coherent volume from Eq. (8.21) is, for an anisotropy $\xi_y/\xi_{\rm r} \sim 10^{-1}$ and $\xi_z/\xi_\lambda \sim 10^{-2}$, on the order of 0.1 eV , significantly exceeding the thermal energy k_BT well below the transition. Because of the smaller gap values, L_0 is larger and $E_{\rm tot}$ is smaller for materials with a spin density wave ground state.

The scaling arguments which lead to a finite correlation length for $d < 4$ are based on the assumption that phase excitations are gapless and can be described by the first term in Eq. (8.1). As discussed in Chapter 6, Coulomb interactions have a profound influence on the longitudinal fluctuations, while leaving the transverse modes unchanged. The consequence of this is that the collective mode can adjust to impurity potentials only through deformations which involve transverse distortions. Arguments

similar to those advanced above lead to a critical dimension $d = 3$. Consequently, in the presence of Coulomb interactions, impurities do not destroy the long range order in the 3D ordered density wave state. The situation is somewhat more complicated at finite temperatures where screening due to normal electrons is important. This leads to a characteristic Thomas-Fermi wavevector $q_0 = 4\pi e^2 n_{qp}/T$, with n_{qp} a thermally excited quasiparticle density. This then defines a length scale $L_{qp} = q_0^{-1}$, and phase fluctuations remain gapless for length scales which exceed L_{qp}. Consequently, the scaling arguments which lead to Eqs. (8.19) and (8.15) are valid as long as $L_0 > L_{qp}$, but are expected to be significantly modified where L_0 as given by these equations is smaller than the Thomas-Fermi screening length.

1.8.2 Experimental Evidence for Finite Correlation Lengths

Although the theory outlined earlier has often been used to describe various experimental findings, many complications may arise. These complications are most probably responsible for the diversity of observations. The collective mode can be descr.bed as an anisotropic elastic medium only in the limit where the coherence length ξ significantly exceeds the lattice constants both parallel and perpendicular to the chains. While this may occur for some materials, such as $NbSe_3$, in the majority of cases $\xi < d$ at least for one direction. If this happens, the problem will likely resemble a weakly coupled system of layers, with $E_{\rm lot}$ and L_0 given for each by the two-dimensional variant of the GinzburgLandau theory. This may lead to concentration dependences different from those given before.

The phase-phase correlation length L_0 is usually long, a crude estimate gives L_0 of a few microns to millimeters in relatively pure specimens. L_0 is somewhat smaller in directions perpendicular to the chains due to anisotropy effects. These length scales are comparable to the dimensions of the specimens, and in the limit of $L_0 > L_{\rm specimen}$ the low wavelength deformations of the collective mode are removed. This again modifies the concentration dependence of the characteristic energies and length scales and also suggests that some experimental findings may depend on the dimensions of the specimens investigated. Additional effects may be caused by surface effects, which may also contribute to $E_{\rm tot}$ in certain cases.

The absence of long-range order, as suggested by the theories discussed above, has several important effects on the static and dynamic properties of density waves. The finite phase-phase coherence length leads to the broadening of the X-ray diffraction lines which occur as a consequence of the charge density wave. Similar phenomena are implied for spin-density waves. In this case the structure factor for magnetic scattering would be modified. High resolution X-ray studies on materials in which impurities have been introduced by alloying or irradiation have been conducted in a few cases, and the absence of long range order is well established (Forro et al., 1983; Girault et al., 1988; Tamegai et al., 1987; DeLand et al., 1991; Sweetland et al., 1990).

The finite coherence length leads to broadening of the X-ray diffraction peaks, and the satellite peak profiles corresponding to the CDW wavevector $\vec{Q}$ can be written as

$$I^{\pm}(\vec{k}) \simeq \frac{\Gamma}{(\vec{k} - \vec{Q})^2 + \Gamma^2} \tag{8.23}$$

The half-width $\Gamma = 1/L_0$, and therefore gives the phase-phase correlation length L_0 directly. The X-ray intensity profile can be examined in different crystallographic directions, allowing for the measurement of the correlation lengths in different orientations. Such studies have been performed on alloys of $NbSe_3$ (Sweetland et al., 1990), and of $K_{0,3}MoO_3$ (DeLand et al., 1991). In both cases the coherence length was found to be anisotropic, with the anisotropy as expected for the anisotropic band structure. The concentration dependence of the width (referred to as full width at half maximum, FWHM) is displayed in Fig 8.4 for three orientations.

The measured width is strongly anisotropic due to the anisotropic correlation length. The concentration dependence is found to be

$$L_0 \sim \frac{1}{n_1^{1/2}} \tag{8.24}$$

in clear contrast to the consequences of weak impurity pinning which predicts that L_0 is inversely proportional to the impurity

8. The Interaction Between Density Waves and Impurities

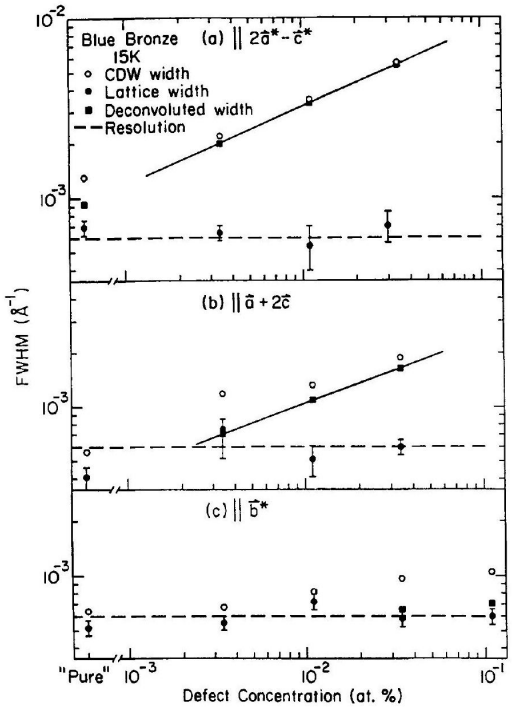


Figure 8.4. CDW satellite peak widths, widths of nearby lattice peaks, and deconvoluted widths versus defect concentration in $\mathrm{K}_{0.3}\mathrm{MoO}_3$. Widths are given as full widths at half maximum (FWHM). The CDW and lattice peaks are: (a) $(5, 0.75, -2.5)$ and $(4, 0, -2)$, (b) $(2, -0.25, 1.5)$ and $(2, 0, 1)$, and (c) $(1, 2.75, -0.5)$ and $(0, 2, 0)$. The resolution is shown as a dashed line (after DeLand, Mozurkewich, and Chapman, 1991).

concentration see (Eq. (8.20)). This disagreement between theory and experiment is not understood at present.

The disorder and the finite coherence length also lead to a distribution of energy levels for the various pinned density wave configurations, with thermally induced transitions between those configurations. This leads to a low temperature specific heat which is similar to that observed in various glasses and disordered systems (Biljakovich et al., 1986; Brown et al., 1988). For transitions between different configurations differing by an energy ϵ, the specific heat is given by the expression

$$C_V = k_B \left(\frac{\epsilon}{k_B T}\right) \mathrm{sech}^2 \left(\frac{\epsilon}{k_B T}\right) \tag{8.25}$$

which, for a broad distribution of energy levels up to a cutoff energy $\boldsymbol{\epsilon}_0$, gives, for $k_B T \ll \boldsymbol{\epsilon}_0$,

$$C_V = N_0 k_B T \tag{8.26}$$

where N_0 is the density of energy levels per unit energy. The low temperature specific heat, measured in various materials with a CDW ground state, is indeed large, and can approximately be described by Eq. (8.26). The experimental results are displayed in Fig. 8.5 together with a prototype glass, vitreous silicon. While these experiments clearly point to the disordered, glassy behavior of the condensate, which is pinned by randomly positioned impurities, no attempt has been made to relate the observed anomalies to the fundamental parameters of the problem, such as the phase-phase correlation length or the average pinning energy.

A more significant consequence of impurity-density wave interactions is the pinning of the collective modes to the underlying lattice. Due to this interaction charge and spin density waves cannot move freely in the lattice; but assume a well defined equilibrium position which is determined by the spatial distribution of impurities. A displacement out of this equilibrium position leads to a change in the collective mode-impurity interaction energy. For a rigid displacement of the collective mode, this is given by

$$E = -k\,(x - x_0)^2 \tag{8.27}$$

where x_0 refers to the equilibrium position and k is a reste ring
8. The Interaction Between Density Waves and Impurities

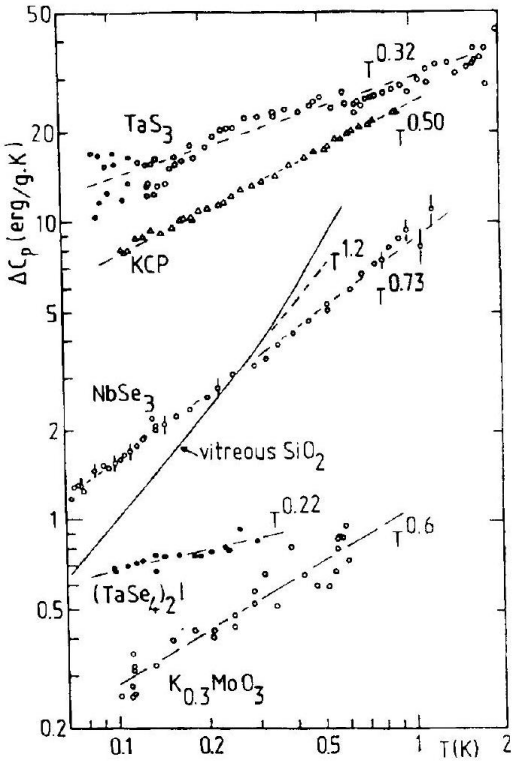


Figure 8.5. Residual specific heat of various materials in the CDW state. The phonon and nuclear hyperfine contributions to the specific heat have been subtracted from the data (after Biljakovich et al., 1989).

force. The latter can be estimated using the following crude argument. A rigid displacement of the (distorted) mode by roughly half the wavelength, $\lambda_0/2$, leads to a change in the impuritycollective mode interaction, and this change is on the order of the total pinning energy. Consequently,

$$k\left(\frac{\lambda_0}{2}\right)^2 \simeq E_{\rm tot} \tag{8.28}$$

with $E_{\rm tot}$ given by Eq. (8.8) or (8.15) for strong and weak impurity pinning. The restoring force therefore is given by

$$k \simeq \frac{4E_{\rm tot}}{\lambda_{10}} \tag{8.29}$$

Upon the influence of an applied ac field, the collective mode does not move freely. Due to the finite restoring force the oscillator frequency of the collective mode shifts from zero to a finite frequency. This frequency is well below the gap frequency $\omega_q = \Delta/\hbar$ for small impurity concentrations. Also, for small k a small dc electric field can induce a translational motion of the condensate, leading to sliding charge or spin density waves. These will be discussed in Chapters 10 and 11.

1.9 The Electrodynamics of Density Waves

Both charge and spin density wave condensates couple to electromagnetic fields and the fluctuations of the phase ϕ of the ground states lead to fluctuations of the electric current. In the absence of pinning due to impurities and lattice defects, the translational motion of the condensates will lead to a conductivity at zero frequency which, in the absence of damping, will also result in an infinite conductivity. This possibility was first raised by Fröhlich (1954). In addition to such effects related to the dynamics of the condensate, carrier excitations across the single particle gap lead to electromagnetic absorption, with an onset frequency of $\omega_X = 2\Delta/\hbar$ for the absorption process. These features are similar to those which are observed in superconductors; there are, however, several important differences which lead to electrodynamic properties fundamentally different from those of the superconducting ground state.

To the first order, the interaction of the collective modes and impurities can be represented as a restoring force k, leading to a collective mode contribution to the conductivity at finite frequency, which is approximately given by $\omega_0 \approx (k/m^*)^{1/2}$. The interaction of the collective modes with lattice vibrations and imperfections leads also to damping and therefore to a finite spectral width of the collective mode resonances. Furthermore,
the dynamics of the internal deformations of the collective modes will lead to long time or low frequency relaxational modes, with a frequency dependent response similar to those observed in glasses and strongly disordered solids.

These aspects are well understood for charge density waves where extensive optical experiments clearly identified the single particle excitations and the contribution of collective mode resonances. The state of affairs is less clear for spin density waves, where major disagreement between theory and experiment remains.

1.9.1 The Electrodynamics of Density Waves

As in a superconductor, the phase $\phi(x,t)$ plays an important role in the dynamics of the collective modes. The $q = 0$ phase mode corresponds to the translational motion of the condensed electrons, with the ions oscillating about their equilibrium positions. A rigid displacement of the density wave leads to an electric current, and the current density per chain $j_{\rm DW} = -n_{\rm DW} c v_d = -n_{\rm DW} e^{\rm e}(dx/dt)$. With $\phi = 2k_F x$ and two electrons per density wave period $\lambda_0 = \pi/k_F$,

$$j_{\rm DW} = -\frac{c}{\pi}\frac{d\phi}{dt}. \tag{9.1}$$

A compression of the wave leads to a change of the electronic density, and therefore

$$n_{\mathrm{UW}} = \frac{e}{\pi}\frac{d\phi}{dx} \tag{9.2}$$

at zero temperature. The cross derivatives of the above equations lead to the continuity equation

$$\frac{dj_{\mathrm{DW}}}{dx} + \frac{dn_{\mathrm{DW}}}{dt} = 0. \tag{9.3}$$

The relation that connects the electric current and condensate density to the time and spatial derivative of the phase $\phi(x,t)$ of the condensate is different from the relations that are appropriate
for a superconductor,

$$\mu = i\hbar\frac{d\phi}{dx} \text{ and } \mu = i\hbar\frac{d\phi}{dt} \tag{9.4}$$

where p_{s} and μ are the momentum and chemical potential, respectively.

The applied electric potential eE couples to the gradient of the phase, and the potential energy density is given by

$$H_L = \frac{cEx}{\pi}\frac{d\phi}{dx}. \tag{9.5}$$

Here (and also later in this chapter and in Chapter 10) the electric field E is applied along the chain direction.

The energy related to the spatial and temporal fluctuations of the phase has been derived in Chapter 6. From Eq. (6.7), the Lagrangian density (including the potential energy due to the applied electric field, and neglecting amplitude fluctuations), is given by

$$\mathscr{L} = T - (E_{cl} + H_E) = d\left(\frac{d\phi}{dt}\right)^2 - c\left(\frac{d\phi}{dx}\right)^2 - \frac{eEx}{\pi}\frac{d\phi}{dx}. \tag{9.6}$$

The Lagrangian equation

$$\frac{\partial\mathcal{L}}{\partial\phi} - \frac{\partial}{\partial t}\frac{\partial\mathcal{L}}{\partial\phi_1} - \frac{\partial}{\partial x}\frac{\partial\mathscr{L}}{\partial\phi_r} = 0 \tag{9.7}$$

with $\phi_1 = \partial\phi/\partial t$ and $\phi_1 = \partial\phi/\partial x$ then gives the equation of motion,

$$\frac{d^2\phi}{dt^2} - \hbar v_\Gamma^2\frac{m}{m^*}\frac{d^2\phi}{dx^2} = \frac{2k_F c}{m^*}E(\omega,k) \tag{9.8}$$

in the presence of an ac electric field $E(\omega,k) = E_0 e^{i(\omega t - kr)}$. The frequency and wavevector dependent conductivity $\sigma_{\mathrm{coll}}\,(k,\omega)$ then is given by

$$\sigma_{\mathrm{coll}}(k,\omega) = \frac{j(k,\omega)}{E(k,\omega)} = \frac{m}{m^*}\frac{i\omega\omega_p^2}{\omega^2 - \hbar v_F\frac{m}{m^*}k^2} \tag{9.9}$$

Because of the short coherence lengths, nonlocal effects are not important and the k dependence can be neglected. Then

$$\sigma_{\mathrm{coll}}\,(\omega) = \frac{j(\omega)}{E(\omega)} = \frac{m}{m^*}\frac{i\omega_p^2}{4\pi(\omega + i\delta)} \tag{9.10}$$

where $\omega_p^2 = 4\pi ne^2/m$ is the plasma frequency. The real part

$$\mathrm{Re}\,\{\sigma_{\mathrm{coll}}(\omega)\} = \frac{m}{8m^*}\omega_p^2\delta(\omega) \tag{9.11}$$

has a Dirac delta singularity at $\omega = 0$, with an oscillator strength

$$f = \int \mathrm{Re}\left\{\sigma_{\mathrm{coll}}(\omega)\right\} dw = \frac{\pi n e^2}{2m^*} \tag{9.12}$$

The imaginary part is obtained using the Kramer-Kronig relation

$$\mathrm{Im}\left\{\sigma_{\mathrm{coll}}(\omega)\right\} = -\frac{2\omega}{\pi}\int_{-\infty}^{\infty} \frac{\mathrm{Re}\left\{\sigma_{\mathrm{coli}}(\omega)\right\}}{\omega'^2 - \omega^2} dw' = \frac{m}{4\pi m^*}\frac{\omega_p^2}{\omega} \tag{9.13}$$

Because of the gap, the contribution from single particle excitations is expected to be similar to that of a semiconductor with a well defined absorption edge of energy $\hbar\omega = 2\Delta$. In the absence of the contribution from the collective mode, the optical conductivity coming from band-to-band transitions is given by

$$\sigma_{\mathrm{rp}}(\omega) = \frac{ne^2}{i\omega m_{\mathrm{b}}}(f(\omega) - 1) \tag{9.14}$$

where, for a one-dimensional semiconductor, (Wooten 1972)

$$f(\omega) = -\int dE_k \frac{2\Delta^2/E}{(\omega + i\eta)^2 - 4E^2} = \frac{2\Delta^2}{\omega y}\left(\pi i + \ln\frac{1-y}{1+y}\right) \tag{9.15}$$

where $E^2 = E_k^2 + \Delta^2, E_k = \epsilon_k - \epsilon_F$, and $y = \left(1 - 4\Delta^2/\hbar^2\omega^2\right)^{1/2}$. Because of the $E^{-1/2}$ singularity of the density of states in one dimension, $\sigma_{\mathrm{sp}}(\omega)$ has a singularity at the gap frequency ω_S. The low frequency dielectric constant is

$$\epsilon(\omega \to 0) = 1 - \frac{4\pi\,\mathrm{lm}\{\sigma\}}{\omega} = 1 + \frac{1}{6}\frac{\left(\hbar\omega_p\right)^2}{\Delta^2}. \tag{9.16}$$

The collective mode contribution to the conductivity modifies the oscillator strength in (9.14) and is given by (Lee, Rice, and Anderson, 1979)

$$f'(\omega) = \frac{f(\omega)}{1 + \left(\frac{m}{m^*} - 1\right) f(\omega)} = \frac{f(\omega)}{1 + \frac{\lambda\omega_{2k_1}}{4\Delta^2} f(\omega)} \tag{9.17}$$

and the conductivity reads

$$\sigma(\omega) = \frac{ne^2}{i\omega m}\left[\frac{f(\omega)}{1 + \frac{\lambda\omega_{2k_t}^2}{4\Delta^2} f(\omega)} - 1\right] \tag{9.18}$$

For $\omega = 0$, the Kramers-Kronig relation leads to Eq. (9.11) and the frequency dependent response is also modified at energies $\hbar\omega > \Delta$. In Fig. 9.1, $\mathrm{Re}\{\sigma(\omega)\}$ is shown for various values of the effective mass. The mass enhancement, $m^*/m \sim 100$, is a typical value for materials with a CDW ground state (this will lead to a curve similar to that shown in Fig. 9.1); for SDW's the effective mass is expected to be equal to the band mass. This difference leads also to different spectral weights associated with the single particle and collective mode contributions to the optical conductivity.

The relative weights of the collective mode and single particle contributions are determined by sum rule arguments. The total contribution to the sum rule

$$\int \left[\mathrm{Re}\left\{\sigma_{\mathrm{col1}}(\omega)\right\} + \mathrm{Re}\left\{\sigma_{\mathrm{sp}}(\omega)\right\}\right] d\omega = \frac{\pi n e^2}{2m_\eta} \tag{9.19}$$

is the same as the sum rule which is given in the metallic state

$$\int_0^x \mathrm{Re}\left\{\sigma_{\mathrm{m}}\right\}(\omega)d\omega = \int \frac{ne^2\tau}{m_b\left(1-\omega^2\tau^2\right)}d\omega = \frac{\pi ne^2}{2m_b} \tag{9.20}$$

Here the integrals include all contributions to σ which come from a band with bandmass m_b. In the density wave state collective mode contribution (see Eq. (9.12)) is

$$I_{\mathrm{coll}} = \int \mathrm{Re}\left\{\sigma_{\mathrm{coll}}(\omega)\right\} d\omega = \frac{\pi ne^2}{2m^*} \tag{9.21}$$

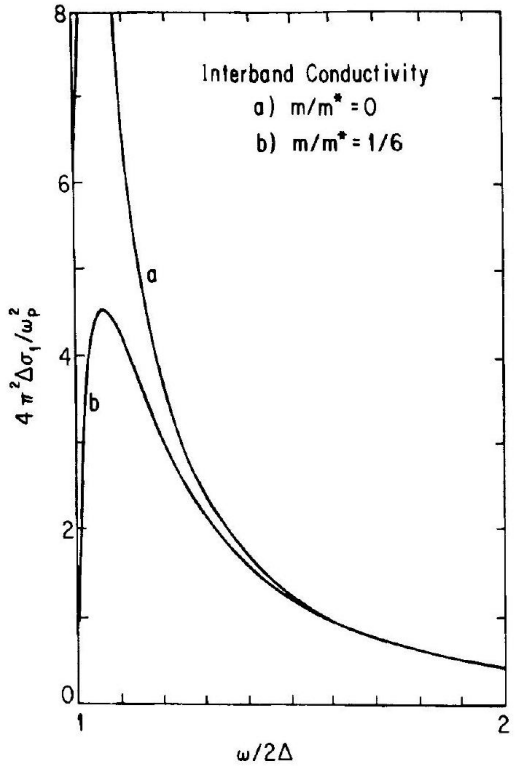


Figure 9.1. The frequency dependence of the conductivity $\operatorname{Re}\{\sigma(\omega)\}$ for $m^*/m = x$ and $m^*/m = 6$ (Lee et al., 1974).

while the single particle excitations give the contribution

$$I_{\mathrm{sp}} = \int \mathrm{Re}\left\{\sigma_{\mathrm{sp}}(\omega)\right\} d\omega = \frac{\pi ne^2}{2m_{\mathrm{b}}} - \frac{\pi ne^2}{2m^*} = \frac{\pi ne^2}{2m_b}\left[1 - \frac{m_b}{m^*}\right]. \tag{9.22}$$

For a large effective mass, $m^*/m_b \gg 1$, nearly all of the contribution to the total spectral weight come from single particle excitations, while for $m^*/m_b = 1$ all the spectral weight is associated with the collective mode, with no contribution to the optical conductivity from single particle excitations. The former is appropriate for charge density waves, while the latter is valid for spin density wave transport.

The above arguments are appropriate in the clean limit, $1/\tau \ll \Delta$, which is equivalent to the condition $\xi \ll l$ where l is the mean free path. The response for the opposite case, the so-called dirty limit $\xi \gg l$ has not been calculated. It is expected, however, that arguments advanced for superconductors (Tinkham, 1975) also apply for density wave ground states. As for superconductors, the collective mode contribution to the spectral weight is given by the difference

$$\delta \int \left[\mathrm{Re}\left\{\sigma_{\mathrm{m}}(\omega)\right\} - \mathrm{Re}\left\{\sigma_{\mathrm{sp}}(\omega)\right\}\right] d\omega \tag{9.23}$$

with $\sigma_{\mathrm{m}}(\omega)$ given by Eq. (9.19). This difference is approximately the area given by

$$\int_0^{\omega_{\mathrm{g}}} \mathrm{Re}\left\{\sigma_{\mathrm{m}}(\omega)\right\} d\omega \simeq \omega_g \tau \simeq \frac{\omega_p^2}{2\pi^2}\left(\frac{l}{\xi}\right) \tag{9.24}$$

in the dirty limit. Consequently, the spectral weight due to the collective mode contribution is reduced and an empirical form similar to Pippard's expression to the penetration depth (Pippard, 1953),

$$\frac{I^0_{\mathrm{coll}}}{I_{\mathrm{coll}}} = 1 + \frac{\xi}{\alpha I}, \tag{9.25}$$

can be anticipated, with α a numerical factor on the order of one. In the above equation I^0_{coil} is the spectral weight of the collective mode in the clean limit.

For a perfect crystal, and for an incommensurate density wave, the collective mode contribution occurs at $\omega = 0$ due to the translational invariance of the ground state. As has been discussed in Chapter 8, this translational invariance is broken and the collective modes are tied to the underlying lattice due to interactions with impurities. To the first order this can be described by a restoring force $k = \omega_0^2 m^*$. The interaction between the collective mode and the lattice imperfections, impurities, etc., may also lead to a finite relaxation time τ^*. With these effects the
equation of motion becomes

$$\frac{d^2\phi}{dt^2} + \frac{1}{\tau^*}\frac{d\phi}{dt} + \omega_0^2\phi = \frac{ne}{m^*}E(t) \tag{9.26}$$

leading in the presence of an *ac* electric field $E(t) = E_0(\omega)e^{l\omega t}$, to

$$\mathrm{Re}\{\sigma(\omega)\} = \frac{ne^2\tau^*}{m^*}\frac{\omega^2/\tau^*}{\left(\omega_0^2 - \omega^2\right)^2 + \left(\omega/\tau^*\right)^2} \tag{9.27a}$$

$$\mathrm{Im}\{\sigma(\omega)\} = \frac{ne^2}{m^*}\frac{\left(\omega_0^2 - \omega^2\right)\omega}{\left(\omega_0^2 - \omega^2\right)^2 + \left(\omega/\tau^*\right)^2} \tag{9.27b}$$

The collective mode contribution to $\sigma(\omega)$ now appears at finite frequencies, and both $\mathrm{Re}\{\sigma(\omega)\}$ and $\epsilon(\omega) = 4\pi\,\mathrm{Im}\,\sigma(\omega)/\omega$ are shown in Fig. 9.2. There are several characteristic frequencies which are given by the maxima of $\mathrm{Re}\{\sigma(\omega)\}$ and the zeros of the dielectric constant $\mathrm{Re}\{\epsilon(\omega)\}$. The collective mode contribution, Eq. (9.27), leads to a maximum and to a zero crossing for $\mathrm{Re}\,\sigma(\omega)$ and for $\mathrm{Im}\,\sigma(\omega)$ at ω_0. For $\omega \ll \omega_0$ the dielectric constant is given by

$$\epsilon_0 = 1 + \frac{4\pi\mu e}{m^*\omega_0^2} + \frac{4\pi n e^2\hbar^2}{m_b\Delta^2} = 1 + \epsilon_{\mathrm{coll}} + \epsilon_{\mathrm{ap}} \tag{9.28}$$

where the second and third terms on the right hand side represent the collective and single particle contributions to the dielectric constant. A second zero crossing occurs at

$$\omega_p^* = \left(\frac{4\pi n c^2}{m^*\epsilon_{\mathrm{rp}}}\right)^{1/2} \tag{9.29}$$

the plasma frequency of the collective mode, and in the region $\omega_p^* < \omega < \Delta/\hbar$ the dielectric constant is

$$\epsilon_{\rm vp} = 1 + \frac{4\pi n e^2 \hbar^2}{m_b \Delta^2} \tag{9.30}$$

The second maximum of $\mathrm{Re}\{\sigma(\omega)\}$ at 2Δ represents the single particle transitions, and $\mathrm{Re}\{\epsilon(\omega)\}$ has a crossover from negative to positive values at the plasma frequency $\omega_p = (4\pi n e^2/m_l)^{1/2}$.

For $m^* = m_b$, which is expected for a spin-density wave ground state, single particle excitations do not contribute to the

9. Electrodynamics of Density Waves

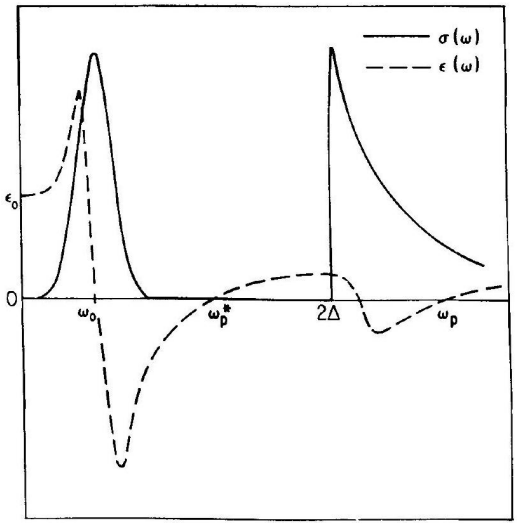


Figure 9.2. The frequency dependence of the optical conductivity \$\operatorname{Re}\{\sigma(\omega)\}\$ and dielectric constant $\mathrm{Re}\{\epsilon(\omega)\}$ for $m^*/m =\gg 1$. The pinning frequency $\omega_0 < \Delta$, and $1/\tau^* = \omega_0$. The various characteristic frequencies are discussed in the text.

optical conductivity, the collective mode contribution appears at $\omega = \omega_0$, and

$$\epsilon(\omega \to 0) = \frac{4\pi n e^2}{m_b \omega_0^2} \tag{9.31}$$

with a zero crossing at the plasma frequency ω_p.

The effect of impurities described by an average restoring force k is a gross oversimplification since it neglects the dynamics of the local deformations of the collective modes. The types of processes which have been neglected are shown in Fig. 9.3. The top displays an undistorted density wave, with a period $\lambda_0 = \pi/k_F$, and a constant phase ϕ. In the presence of impurities the collective mode is distorted and adjusted to maximize the energy gain due to interaction with the impurity potential; a distorted

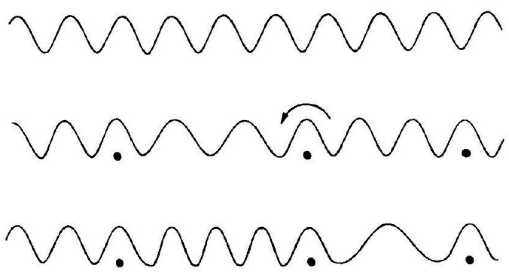


Figure 9.3. The dynamics of the internal deformations of density waves. The top part of the figure is the undistorted density wave; the middle part shows the mode distorted due to interaction with impurities (full circles); and the bottom part displays the rearrangement of the internal distortion by displacing the density wave by period over the impurity as indicated by the arrow. The process leads to an internal polarization.

density wave is shown in the middle section of the figure. A low-lying excitation, which involves the dynamics of the internal deformations, is shown at the bottom of Fig. 9.3; here a density wave segment has been displaced by λ_0, leading to a stretched density wave to the left and to a compressed density wave to the right of the impurity. The local deformation leads to an internal polarization by virtue of the displaced charge which accompanies the stretched or compressed density wave. This polarization is given by

$$P(\vec{r}) = 4\pi e \frac{\partial \phi(\vec{r})}{\partial \vec{r}}. \tag{9.32}$$

Such effects have been described as a broad superposition of Debye-type relaxation processes, and various phenomenological expressions have been proposed to account for the low frequency and long time behavior of the electrical response. Among these, the so-called Cole-Cole expression (see for example, Ngai, 1979 and references cited therein)

$$\epsilon(\omega) = \frac{\epsilon_0}{1 + (i\omega\tau_0)^{1-\alpha}} \tag{9.33}$$

with $\alpha < 1$, and with ϵ_0, and τ_0 an "average" dielectric constant
and relaxation time is frequently used to describe the so called "glassy" behavior of a variety of random systems. While these descriptions offer little insight into the microscopic details of the density wave dynamics, they are useful in establishing that the response is due to a broad distribution of relaxation times and/or frequencies. The local deformations, as shown in Fig. 9.3, lead to a spatially inhomogeneous local field $\delta E(k, \omega)$ and the relation between the two quantities is given by

$$\delta j(k, \omega) = \sum_{k'} \sigma\left(k, k', \omega\right) \delta E\left(k', \omega\right). \tag{9.34}$$

Because of the local fluctuations of the internal field, the experimentally measured conductivity $\sigma(\omega)$ which relates the spatial averages $\delta E(\omega)$ and $\delta j(\omega)$ through the expressions

$$\delta j(\omega) = \sigma(\omega)\delta E(\omega) \tag{9.35}$$

cannot be expressed as $\langle \sigma\left(k, k', \omega\right) \rangle = \sigma(k, \omega)\delta_{k,k'}$ and a more sophisticated treatment which includes the k dependence of the electric field fluctuations is required. This complicated issue has received considerable attention recently (Littlewood, 1987; Wonneberger, 1991).

Impurities also lead to changes in the single particle excitation spectrum, in much the same way that impurities lead to bound states in conventional semiconductors (Tutto and Zawadowski, 1985; Zawadowski, 1987.

1.9.2 Frequency Dependent Conductivity of Charge Density Waves

The electrical conductivity has been investigated over a broad spectral range in various materials and $\mathrm{Re}\,\sigma(\omega)$ is shown in Fig. 9.4 (Grüner, 1988) for some of the compounds in their charge density wave state. For clarity, phonon modes observed in the far infrared spatial range are omitted from the figure. The strong rise at frequencies approximately $10^{14}\mathrm{sec}^{-1}$ is due to single particle excitations across the gap. The arrows on the figures indicate the gap values which are obtained from the temperature dependence of the low field *dc* conductivity in the charge density wave state. The resonance which is observed in the microwave spectral range is due to the pinned collective mode with the resonance shifted to finite frequencies due to the interaction with impurities. This has

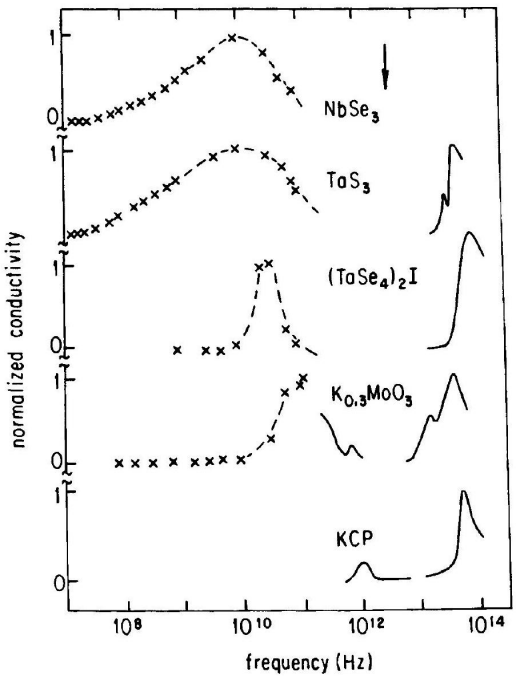


Figure 9.4. Frequency dependent conductivity measured in several compounds in their charge density wave state (Grüner, 1988). The arrow indicates the gap measured by tunneling for NbSe_3.

been directly confirmed by frequency dependent conductivity studies conducted in alloys (Kim et al., 1991) where increasing impurity concentrations lead to increasing pinning frequencies ω_0. The finite width of the collective mode resonances is due to damping effects, which to date have not been addressed by theory.

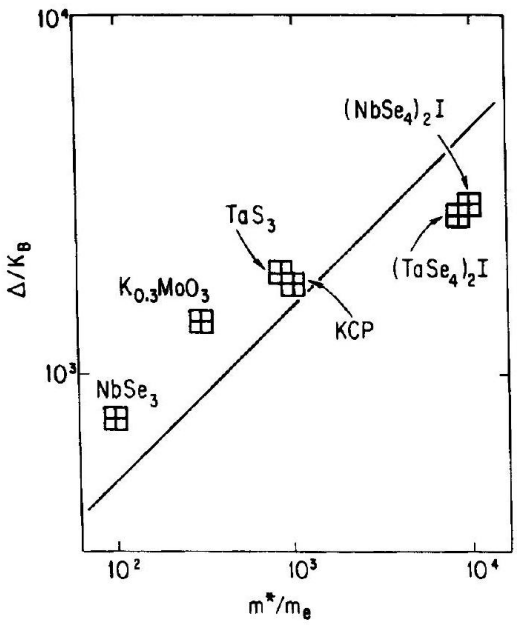


Figure 9.5. The measured effective mass values versus the measured single particle gaps for materials with a charge density wave ground state. The full line is Eq. (6.25) with $\lambda = 0.5$ and $\omega_{2 h_{f}}=50 \mathrm{˜K}$.

Spectral weight arguments discussed in Section 9.1 can be used to evaluate the effective mass of the condensates. We have evaluated m^*/m by describing the resonance with Eq. (9.27). The effective mass is given by Eq. (6.25) in terms of the single particle gap Δ, the dimensionless electron-phonon coupling constant λ, and the unrenormalized phonon frequency ω^0_{2k}. For the materials investigated, λ is somewhat less than one, while $\omega^{()}_{2k_i}$ is on the order of 5×10^{-2}eV and the variation of the mass enhancement from material to material is mainly due to differences in the magnitude of the single particle gaps. This is clearly shown in Fig 9.5 where the effective mass values are plotted as functions of the measured gap values. The full line on the figure is Eq. (6.25) with $\lambda = 0.5$ and ω_{2k_F} as given above.

The single particle contribution to the optical conductivity is described by Eq. (9.18); the expression leads to a square root

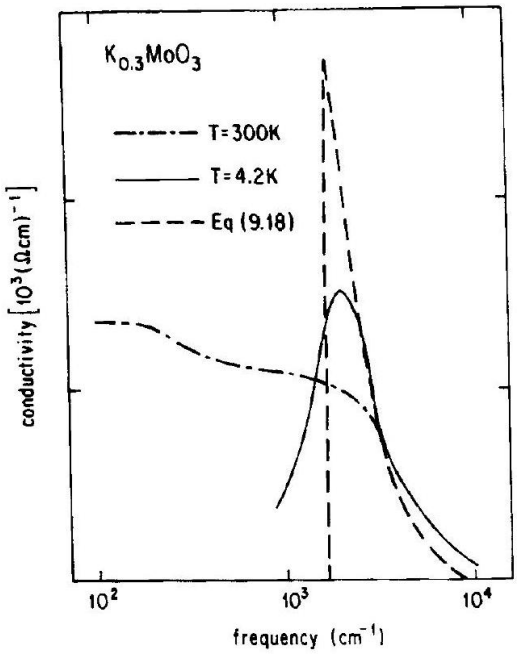


Figure 9.6. Measured and calculated optical conductivity for $\mathrm{K}{{03} \mathrm{MoO}}{3}$ in the charge density wave state. The conductivity measured above the charge density wave transition is also shown.

divergence of $\mathrm{Re}\,\sigma(\omega)$ for large effective mass at $\omega_{\mathrm{X}} = 2\Delta/\hbar$. This feature is clearly evident from the data shown in Fig. 9.4. The optical conductivity measured on $K_{0.3}MoO_3$ (Degiorgi et al., 1991) is compared with $\sigma(\omega)$ as given by Eq. (9.18) in Fig. 9.6, where the conductivity measured above the CDW transition is also shown. Several aspects of the single particle response are evident on the figure. The spectral weight of the single particle excitations at $T = 4.2$ K is (within the experimental error) the same as the spectral weight associated with the Drude response above the transition. As expected, due to the large effective mass the contribution of the collective mode to the total spectral weight is small (see Eqs. (9.21) and (9.22)). The measured conductivity $\sigma(\omega)$ also has a well defined peak reminiscent of the singularity which is given by Eq. (9.15). The broadened peak (in contrast to the sharp feature expected) may reflect the anisotropy of the single particle

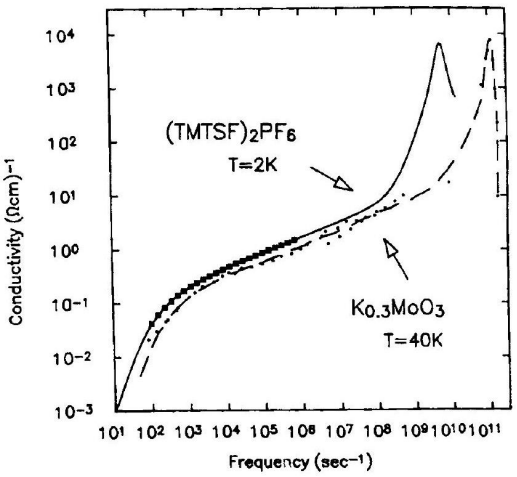


Figure 9.7. The conductivity of $\mathrm{K}_{0.3}\mathrm{MoO}_3$ and of (TMTSF) $\mathrm{PF_n}$ at low frequencies. The broad tail is due to the internal modes in both materials. The full and dotted lines are a guide to the eye.

gap but may also be due to impurities which are expected to remove the singularity and also introduce states in the gap.

The low frequency response has also been investigated in detail and the behavior is displayed in Fig. 9.7 in one of the compounds with a CDW ground state, $\mathrm{K_{03}MoO_3}$ (Degiorgi et al., 1991). The resonance which occurs at $\omega_0/2\pi = 100\mathrm{GHz}$ is due to the oscillations of the collective mode around the pinned equilibrium position, and to a first approximation, the resonance can be described by Eq. (9.27). The low frequency tail of the spectrum is due to the dynamics of the internal deformations of the collective mode, and the behavior has been described by the Cole-Cole expression, Eq. (9.33), or its modified variants. A theory which takes the local fluctuations of the condensate into account (Wonneberger, 1991 and references cited therein), can account for the collective mode dynamics in detail, with only a few free parameters.

The previous discussion of the single particle and collective mode contributions to the conductivity neglected the interaction between the ground state and optical phonons which occurs at frequencies ω_n. Such an interaction has several important consequences and leads to modifications of the phonon contributions to $\sigma(\omega)$ both as far as their spectral intensity and polarization are concerned. The reason for this is that the oscillation of the ionic positions at frequency ω_m leads, through a coupling to the charge density wave modulation, to oscillations of the condensate. Such oscillations can be described by the oscillations of the phase, with frequency ω_n. The polarization of the mode is then parallel to the wavevector of the charge density wave. For a spectrum of optical phonons at frequencies ω_n and coupled to the CDW with a dimensionless coupling constant λ_n, the optical conductivity is given by (Rice, 1976)

$$\sigma(\omega) = \frac{ne^2}{i\omega m_b}\left[f(\omega) - f(0) - \left(\frac{\hbar\omega}{2\Delta}\right)^2 f^2(\omega)\lambda' D_\phi(\omega)\right]. \tag{9.36}$$

The first two terms describe the optical conductivity of a onedimensional semiconductor. The last term is similar to the renormalization of $f(\omega)$, as discussed earlier for the zero frequency collective mode. Here however, $D_\phi(\omega)$ is due to coupling to the phonon modes. The propagator $D_\phi(\omega)$ describes the set of optical phason modes and this, by virtue of Eq. (9.36), leads to maxima in $\mathrm{Re}\{\sigma(\omega)\}$ at frequencies close to ω_n. The spectral weight of these modes is determined by the coupling constants λ_n, and due to the conservation of the total spectral weight, the spectral weight of the single particle excitations is reduced. The theory was first

applied (Rice, 1976) to the CDW state of the organic conductor TEA(TCNQ) $_2$, and recently to the charge density wave state of $K_{0.3}MoO_3$ (Degiorgi et al., 1991).

1.9.3 Frequency Dependent Conductivity of Spin Density Waves

The frequency dependent response of spin density waves is expected to be fundamentally different from the frequency dependent conductivity observed in the charge density wave state. Because the effective mass m^* is the same as the band mass, all

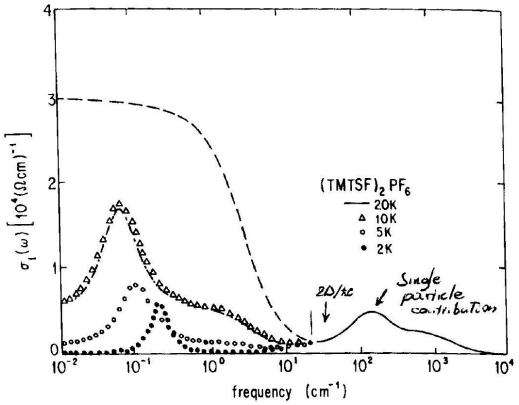


Figure 9.8. The frequency dependent conductivity in $\left(\mathrm{TMTSF}{{2}\mathrm{PF}}{6}\right.$ at several temperatures. Above $T_{\mathrm{SDW}} = 11.5$ K the low frequency conductivity is that of a Drude metal; below T_{SDW} the low frequency peak is due to the pinned mode.

the spectral weight is expected to be associated with the collective mode, with single particle excitations not contributing to $\sigma(\omega)$ in the clean limit; this limit is appropriate in (TMTSF) $_2$X salts which have been investigated in detail. The frequency dependent conductivity measured in (TMTSF) $_2PF_6$ (Quinlivan et al., 1991; Donovan et al., 1992), shown in Fig. 9.8; is in clear disagreement with the models of spin density wave dynamics discussed in Section 9.1. As for charge density waves, we recover a resonance in the microwave spectral range; the most likely explanation of which is that this resonance is the pinned spin density wave mode. The pinning frequency, $\omega_0 \simeq 3$GHz, is smaller than the single particle gap Δ. The increase of $\mathrm{Re}(\sigma(\omega))$ in the far infrared spectral range is not due to single particle excitations; the feature
has also been observed above the transition temperature at 11.5 K . The resonance which occurs at frequencies near $w_0/2\pi = 3$GHz has a small weakly temperature dependent spectral weight (Donovan et al., 1992) and is approximately two orders of magnitude smaller than the spectral weight which would correspond to an effective mass equal to the band mass m_b. This gross disagreement between theory and experiment is unaccounted for at present.

The dynamics of the internal deformations of the collective mode have also been examined and, as for charge density waves, a low frequency tail develops as a consequence of these deformations. This is shown in Fig. 9.7 where $\mathrm{Re}(\sigma(\omega))$ measured in the spin density wave state of (TMTSF) $_2PF_6$ is compared with $\mathrm{Re}\{\sigma(\omega)\}$ measured in the charge density wave state of $K_{0.3}MoO_3$. Theories derived for the low frequency dynamics of charge density wave states (Littlewood, 1987; Wonneberger, 1991) are also expected to give a good account of the experimental state for the spin density wave response.

1.10 Nonlinear Transport

In the charge and spin density state the *dc* electrical conductivity σ_{dc} is that of a semiconductor, with the temperature dependence determined by carriers excited across the (temperature dependent) single-particle gap. As discussed in the previous chapter, electrons which form the charge or spin density wave condensate do not participate in the conduction process for small *dc* electric fields. The reason for this is the interaction between the condensate and impurities and other lattice irregularities. This interaction shifts the oscillator strength associated with the collective modes to finite frequencies, with no contribution to the dc conductivity. The small characteristic frequencies which describe the oscillations of the collective mode about the pinned equilibrium positions are suggestive of weak restoring forces. It can be anticipated that small *dc* electric fields applied along the direction where the incommensurate density wave is developed can therefore induce a translational notion of the condensate; this phenomenon is called sliding density wave transport.

As was discussed previously, the dynamics of internal deformations play an important role in the frequency dependent response. It is therefore expected that such effects are also important for the dc nonlinear dynamics of the driven collective modes.

However, a highly oversimplified model-essentially an extension of the harmonic oscillator approach used to describe the ac response-reproduces many of the essential features of the experimental findings on the nonlinear transport process. As expected, the model is not capable of accounting for many observations which are related to the dynamics of the internal deformations. These have been treated by various approaches (see, for example, Littlewood, 1989 and references cited therein).

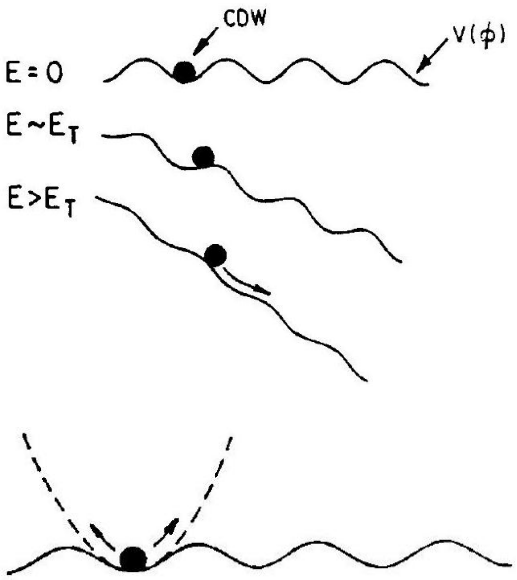
There is a vast amount of literature on the subject, which has been summarized in several reviews listed in the Appendix. We also find a broad variety of nonlinear effects, depending on the nature of the pinning boundaries (whether pinning is due to a dense set of weak impurity potentials or to a single grain boundary, for example), the size of the specimens (which can be larger or smaller than the phase-phase correlation length L_0 discussed in the previous chapter), or temperature-just to mention a few important variables. Therefore it is expected that no single model will account for the variety of observations.

1.10.1 Models of Density Wave Transport

A simple description of nonlinear transport due to moving density wave condensates neglects the internal dynamics of the mode and treats the dynamics of the rigid condensate, neglecting finite temperature fluctuation effects. It is assumed that the overall effect of the impurities can be described by an impurity potential V which pins the density wave to the underlying lattice; this then leads to an equilibrium density wave position at $x = 0$ where the density wave rests at the bottom of the potential well. Because of the intrinsic periodicity of the charge or spin density wave, the interaction energy which results from the interaction between impurities and the collective mode is written as

$$\mathscr{H} = V \cos(2k_f x + \phi) \tag{10.1}$$

where the interaction potential is a simple periodic function of the displacement x. Neglecting quantum and finite temperature effects, the problem is then that of a classical particle moving in a one-dimensional periodic potential, which is assumed to have the
dc conduction:



ac conduction:

Figure 10.1. The classical particle model of density wave transport. The upper part of the figure indicates the behavior in the presence of a *dc* electric field, the lower part refers to the response to small amplitude ac excitations.

form

$$V(x) = \frac{\omega_0}{2k_F} \sin 2k_F x. \tag{10.2}$$

The driving force due to the applied electric field is $F = cE$, and the equation of motion of the collective coordinate is given by

$$\frac{dx^2}{dt^2} + \frac{1}{\tau}\frac{dx}{dt} + \frac{\omega_0^2}{2k_F} \sin 2k_F x = \frac{eE}{m^*}. \tag{10.3}$$

The equation of motion for small amplitude displacements reduces to the equation (9.26). The consequences of this so-called classical particle model (Grüner et al., 1981) is shown for various *dc* electric fields in Fig. 10.1. For small *dc* fields the particle resides in the bottom of the slightly tilted well; there is no dc current

which would correspond to the translational motion. There is however a finite displacement which corresponds to a finite polarization P. With the increase of the *dc* field there is a well defined threshold field E_T, where the particle starts to roll down in the staircase potential. The condition for this is

$$eE_T\lambda_0 = \frac{2m^*\omega_0^2}{2k_F} \tag{10.4}$$

from which the threshold field is given by

$$E_T = \frac{m^*\omega_0^2}{2\pi ne}. \tag{10.5}$$

For small velocities the inertial term can be neglected and the equation of motion reads

$$\frac{1}{\tau}\frac{dx}{dt} = \frac{eE}{m^*} - \frac{\omega_0^2}{2k_F} \sin 2k_F x. \tag{10.6}$$

The time dependent displacement is given by the equation

$$\frac{1}{\tau}\int_0^{\lambda(t)} \frac{dx}{\frac{cE}{m^*} - \frac{\omega_0^2}{2k_F}\sin 2k_F x} = \int_0^t dt' = t \tag{10.7}$$

The integral can be evaluated and the time dependent displacement is determined by the equation

$$\frac{2}{\left[\left(\frac{eE}{m^*}\right)^2-\left(\frac{\omega_0^2}{2k_r}\right)^2\right]^{1/2}}\tan^{-1}\frac{\frac{eE}{m^*}-\left(\frac{\omega_0^2}{2k_1}\right)^2\tan\frac{x}{2}}{\frac{eE}{m^*}-\frac{\omega_0^2}{2k_F}}=tr. \tag{10.8}$$

In the limit of large electric fields $E \gg E_T, cE/m^* \gg \omega_0^2/2k_F$ and therefore

$$\frac{\frac{2}{cE}}{m^*}\tan^{-1}\left\{\tan\frac{x}{2}\right\}=t\tau \tag{10.9}$$

which gives

$$x(t)=\frac{\varepsilon E\tau}{m^*}t \tag{10.10}$$

and consequently a *dc* current

$$I=me\frac{dx(t)}{dt}=\frac{ne^2\tau}{m^*}E. \tag{10.11}$$

The dc conductivity

$$\sigma=\frac{mc^2\tau}{m^*} \tag{10.12}$$

is independent of electric field in this high field limit, it's value is determined by damping effects. At intermediate electric fields Eq. (10.8) represents a time dependent displacement, resulting in a time-dependent current. The time average is given by

$$\left\langle\tan^{-1}(y\tan y)\right\rangle_t=y \tag{10.1.3}$$

and consequently

$$\frac{2}{\left[\left(\frac{cE}{m^*}\right)^2-\left(\frac{\omega_0^2}{2k_F}\right)^2\right]^{1/2}}\left\langle\frac{x}{2}\right\rangle_1=\tau t \tag{10.14}$$

where $\langle x\rangle$ refers to the time averaged, *dc* displacement

$$\langle x\rangle=\frac{c\tau}{m^*}\left(E^2-E_T^2\right)^{1/2}. \tag{10.15}$$

The current

$$\langle j\rangle=nc\frac{d\langle x\rangle}{dt}=\frac{ne^2\tau}{m^*}\left(E^2-E_T^2\right)^{1/2} \tag{10.16}$$

is a strongly nonlinear function of the applied *dc* electric field. Because of this nonlinearity, two conductivities can be defined

$$\sigma_{\mathrm{t}}=\frac{\langle j\rangle}{E}=\frac{ne^2\tau}{m^*}\left[1-\left(\frac{E_\tau}{E}\right)^2\right]^{1/2} \tag{10.17}$$

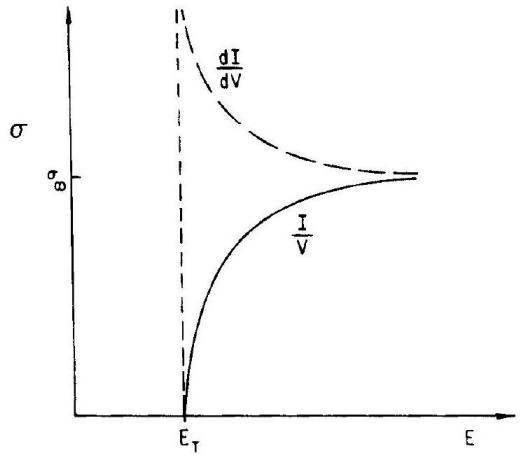


Figure 10.2. Cordial ($\sigma_{\tau}=\langle j\rangle / E$) and differential ($\sigma_d = d\langle j\rangle/dE$) conductivity which follows from the classical particle model.

the cordial, and

$$\sigma_d = \frac{d\langle j\rangle}{dE} = \frac{ne^2}{m^*}\left[1 - \left(\frac{E_r}{E}\right)^2\right]^{-1/2} \tag{10.18}$$

the differential conductivity. Both are shown in Fig. 10.2 as the function of applied *dc* electric field.

The equation of motion also leads to a time-dependent current, due to the acceleration and deceleration as the particle moves down in the staircase potential. The fundamental frequency corresponds to the displacement of the particle by one period $\lambda_0 = \pi/k_F = 2/n$ with n the number of electrons per unit length. The time average velocity is $\langle V\rangle = \lambda_0 f_0$, and the time averaged current density per chain is given by

$$\langle j\rangle = ne\langle V\rangle = ne\lambda_0 f_0, \tag{10.19}$$

and consequertly,

$$\langle j\rangle / f_0 = 2e \tag{10.20}$$

i.e., the frequency of the oscillations is proportional to the time
averaged current density. This also follows from the equation of motion which gives a fundamental frequency of the periodic component of the time dependent displacement $x(t)$,

$$f_0(E) = \frac{e^2\tau}{m^*}\left(E^2 - E_r\right)^2 \tag{10.21}$$

The time dependence of the velocity is non-sinusoidal and this leads to harmonics in the spectral density $I(\omega)$ of the Fourier transformed current. A straightforward calculation gives (see, for example, Grüner and Zettl, 1985 and references cited therein)

$$l_n \sim \left(\alpha^2 - 1\right)^{1/2}\left[\alpha - \left(\alpha^2 - 1\right)^{1/2}\right]^n \cos n\left[nt + \frac{\pi}{2} + \sin^1\alpha\right] \tag{10.22}$$

where $\boldsymbol{\alpha} = E/E_\Upsilon$, and $n = 1, 2, 3\ldots$.
The substitution $\theta = x$ leads to the dimensionless form

$$d^2\theta/dt^2 + \Gamma d\theta/dt + \sin\theta = E/E_t \tag{10.23}$$

where $1^{-} = (\omega_0\tau)^{-1}, E_T = (\lambda_0/2\pi)(m^*\omega_0^2/e^*)$, and time t is measured in units of ${\omega_0}^{-1}$. Equation (10.23) is formally identical to the equation which describes the behavior of resistive shunted Josephson junctions (see, for example, Barone and Paterno, 1982)

$$\frac{d^2\phi}{dt^2} + G\frac{d\phi}{dt} + \sin\phi = 1/l_j \tag{10.24}$$

where Φ is the phase difference across the junction, l is the current through the junction; and $G = (RC\omega_l)^{-1}$, where R and C are the resistance and capacitance of the junction, and $\omega_1 = 2cl_l/Cg.l_l$ is the *dc* critical Josephson current, and time is measured in units of ω_j^{-1}. This analogy suggests a close formal correspondence between phenomena observed in Josephson junctions and in materials displaying CDW transport. For example, the current oscillations described by Eq. (10.20) correspond to the ac Josephson effect while the threshold field E_T corresponds to the critical current I_I. This analogy has been extensively used to analyze a variety of interference experiments in the presence of combined *dc* and ac electric fields (Grüner, 1988 and references cited therein). Equation (10.23) is also analogous to the equation describing other systems; for example, a damped pendulum in a gravitational field or a phase-locked loop configuration of a volt-
age controlled oscillator. The equations of motion for these different systems are summarized in Table 10.1.

The model, which neglects the dynamics of the internal deformations of the collective mode, is expected to be appropriate only under circumstances where these deformations play a secondary role; this may happen in specimens with dimensions comparable to or smaller than the phase-phase correlation length discussed in Chapter 8. Since in the majority of specimens investigated this correlation length is of the order of microns for pure specimens, a full treatment of the dynamics of internal modes is required.

In the first approximation we assume that the amplitude of the density wave is constant, and only the phase is locally distorted around the impurities. Then interaction between the collective mode and impurities is given by Eq. (7.1); the full equation of motion, which takes this interaction into consideration reads

$$\begin{aligned} m^*\frac{d^2\phi(\vec{r})}{dt^2} + \Gamma\frac{d\phi(\vec{r})}{dt}\sum_t \rho_1 V_0\left(\vec{r} - \overrightarrow{R_1}\right)\sin\left(2k_1\vec{r} + \phi\left(r^*\right)\right) \\ = 2k_r eE \end{aligned} \tag{10.25}$$

where R_l (describing the impurity positions) is a random variable. The treatment of the nonlinear dynamics of this driven system is complex, and various approaches have been taken to discuss the nonlinear response in certain limits; they have been the subject of several reviews (Littlewood 1990, and references cited therein). Due to this complexity, computer simulations have been extensively employed and compared with the experimental results. An alternate approach (see, for example, Narayan and Fisher, 1992; Myers and Sethna, 1993) treats the problem of depinning as a critical phenomenon which leads to scaling forms for the response and correlation functions near the threshold field E_T. The exponents which determine the electric field dependence of the various parameters are somewhat different from those which follow from the single particle model.

This model of density wave transport applies to a situation where pinning by weak, randomly distributed impurities plays an important role. Under these circumstances the amplitude of the collective mode is not influenced by the impurity potentials. The dynamics are governed by the dynamics of the phase variable

Table 10.1. Correspondence between the motion of pendulum under gravitation, the Josephson equation and the classical model of CDW Transport.

CDW	Josephson Junctions
applied field E mass m^* damping coeff. $1/\tau$ threshold field E_T periodic potential Qx	dc current I_{dc} capacitance C conductan
$\frac{d^2x}{dt^2} = \frac{1}{\tau}\frac{dx}{dt} + \frac{\omega_0^2}{\theta}\sin\theta x = \frac{eE}{m}$	$I_{\mathrm{c,d}} = \frac{h}{2e}C\frac{d^2\phi}{dt^2} + \frac{h}{2e}\frac{1}{R}\frac{d\phi}{dt} + l\sin\phi$
$\frac{d^2\theta}{dt^2} + \Gamma\frac{d\theta}{dt} + \sin\theta = \frac{E}{E_T}$	$\frac{d^2\phi}{dt^2} + G\frac{d\phi}{dt} + \sin\phi = \frac{1}{I_1}$

$\phi(\vec{r})$. In the case of macroscopic defects, such as dislocations or grain boundaries (or even the boundaries associated with contacts), a different model should apply. At such presumably strong pinning centers the translational motion of the condensate under the influence of the dc electric field may lead to a transient, periodic collapse of the amplitude of the density wave. This in turn, leads to a 2π phase slip which relieves the elastic strain that accumulates due to the applied electric field. The GinzburgLandau expansion which also includes the amplitude fluctuations is given by (Gor'kov 1977)

$$\mathscr{H} = \mathscr{H}_{il} + \mathscr{H}_j + \mathscr{H}_E + V_{\mathrm{imp}}(\phi). \tag{10.26}$$

The energy due to the applied electric field, $\mathscr{H}_F$ is given by Eq. (9.5). The gradient energy is given by

$$\mathscr{K}_{cl} = \int dr \left\{ C_\Delta (\nabla|\Delta|)^2 + C_\phi (\nabla\phi)^2 \right\} \tag{10.27}$$

where $C_\perp$ and C_ϕ refer to the elastic constants, related to the change of the amplitude and phase of the order parameter. The energy associated with small amplitude fluctuations by

$$\mathscr{H}_\Delta = a \int dr (|\Delta| - |\vec{\Delta}|)^2 \tag{10.28}$$

where $|\bar{\Delta}|$ is the time average order parameter, and a is a constant. The impurity term is given by Eqs. (8.2) or (8.3).

The equation of motion, schematically written as

$$\frac{1}{\tau}\frac{d\Delta}{dt} = -\frac{\delta\mathscr{H}}{\delta\Delta} \tag{10.29}$$

is complicated, even for rather simple potentials, such as the plane boundary at a current or voltage contact. In this case, the strain accumulated at the boundary due to the applied electric field is periodically relieved due to phase slip processes; with every phase siip leading to an advancement of the density wave by the period λ_0. The role of phase slips, and consequently the current carried by the condensate, is determined by the elastic constants C_Δ and C_ϕ, by the relaxation time τ, and by the applied electric field E. The model also leads to a well defined threshold field where phase slips start to occur; current oscillations and nonlinear current-voltage characteristics are also a natural consequence of the equation of motion.

1.10.2 Experiments on the Nonlinear Dynamics of the Collective Modes

A broad variety of experiments have been conducted to establish the essential features of the nonlinear conduction caused by the driven collective modes. These include measurement

of the *dc* current-voltage characteristics, response to the system to combined *dc* and ac electric fields and evaluation of the spectral response, and fluctuations of the nonlinear current. Several review papers and Conference Proceedings listed at the end of the book in the Appendix deal with this subject, and therefore only a short summary will be given here.

Depending on factors like the size of the specimens, impurity concentration, and the presence (or absence) of extended defects such as grain boundaries; a variety of phenomena have been observed. The reason for this is that the dynamics of the collective mode depend sensitively on the nature of pinning provided by the various potentials $V(\vec{r})$ which break the translational invariance of the collective modes. In small specimens, with dimensions comparable to the phase-phase correlation length L_0, the dynamics of the internal deformations do not play a significant role; and the classical particle model is a good first approximation. For such sample dimensions, pinning by the surface of the specimens may also be important. In specimens where pinning is dominated by weak impurities, the dynamics are governed by Eq. (10.25) and the full treatment of internal deformations is required. In materials where pinning is principally due to one strong pinning center, the dynamics of both amplitude and phase fluctuations must be considered with phase slips and amplitude collapse at the pinning site dominating the dynamics of the collective mode. These different conditions lead to different current voltage characteristics, which are also influenced by the (temperature dependent) screening provided by the normal carriers which are excited across the single particle gap. Not surprisingly, therefore, a broad variety of observations have been studied under different conditions.

The *dc* conductivity, defined as j/E where j is the total current density and E is the applied electric field, is shown in orthorhombic TaS_3 in Fig. 10.3. The observation is typical of that found below T_{CDW} in relatively large specimens. Below a thresh-

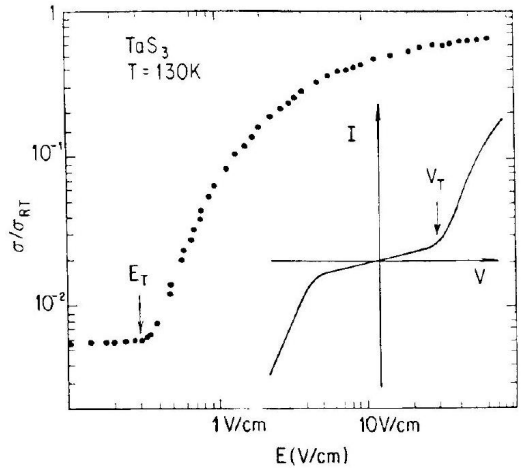


Figure 10.3. Electric-field-dependent cordial conductivity $\sigma_{1}(E)$ in $\sigma - TaS_3$ in the CDW state. The data are normalized to the room-temperature conductivity. The insert shows typical $dcI - V$ characteristics on the same material.

old field E_T, approximately 300mV/cm, the conductivity obeys Ohm's law, and the temperature dependence of this component reflects the exponential freezing out of the electrons excited across the single-particle gap. The onset of nonlinear conduction at E_T is smooth, as evidenced by the current-voltage characteristics displayed in the figure. A behavior similar to that displayed in Fig. 10.3 is found, in general, for the other compounds (first on $NbSe_3$, Monceau et al., 1976); the existence of the sharp threshold field E_T is well established.

The threshold field E_T increases with increasing impurity concentrations, and experiments on various materials either lead to $E_T \sim n_1$ or $E_T \sim n_1^2$. The former implies strong, the latter weak, impurity pinning (see Eqs. (8.8) and (8.15)). The issue is complicated; since factors

such as the size of the specimens, dimensionality effect, or other defects (grain boundaries, for example) are also important in determining the overall restoring force.

The behavior shown in the figure can be described in terms of a two-fluid model involving electrons excited across the gap and electrons in the collective mode. The former has an Ohmic contribution, the latter a nonlinear response. The total current can be written as

$$l_{\text{tot}} = l_n + l_{\text{cDW}} \tag{10.30}$$

where the subscripts n and CDW refer to current carried by the uncondensed and condensed electrons. The validity of such a two-fluid description has recently been demonstrated by generating nonlinear current-voltage characteristics in an open circuit configuration ($I_{\text{tot}} = 0$), where the voltage was generated through the thermoelectric effect (Beyermann et al., 1986).

Equation (10.30) implies a two-band model where the normal electrons and electrons in the CDW condensate provide separate and independent channels for the conduction process. While this description suggests a collective transport carried by the CDW when electric fields exceed threshold, other transport measurements performed in the nonlinear conductivity region provide direct evidence that the current at high fields is carried by a ground-state condensate (Grüner, 1988). The onset of nonlinear dc transport also leads to changes in other transport coefficients such as Hall effect and thermoelectric power. These have been analyzed in terms of the Onsager relations, which were extended for the nonlinear transport region. Although changes in various thermodynamic properties (such as the elastic contents) have been investigated, a microscopic theory of these effects is not available to date.

The fact that the charge-density wave contributes to the *dc* current for $E > E_T$ rather than being destroyed, has been established by performing X-ray experiments in the nonlinear conduction region (Fleming et al., 1978). The superlattice reflections were found to be independent of the applied electric field, even well into the nonlinear conduction region. The observation demonstrates that the charge-density wave amplitude remains unchanged, and the condensate executes a translational motion in the presence of an applied electric field. The most direct evidence for moving charge-density waves comes from NMR experiments. Transitions to the CDW state have profound influence on the NMR spectrum, mainly due to the inhomogeneous broadening caused by the charge-density wave modulation through quad-

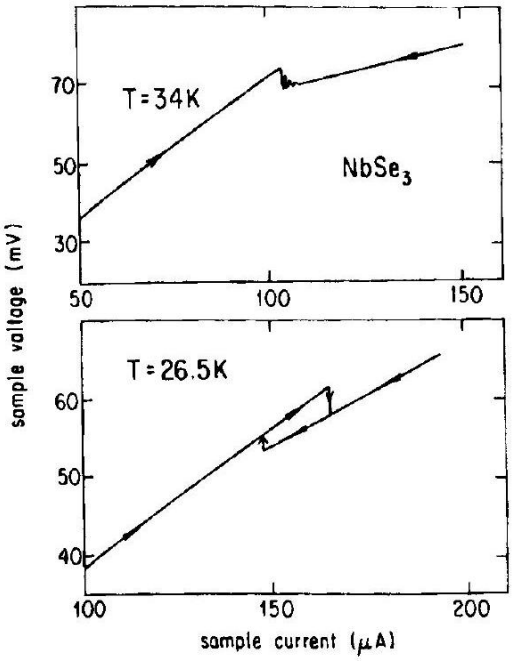


Figure 10.4. Current-voltage characteristics observed in NbSe_{3} at two different temperatures (Zettl and Grüner, 1982). The behavior is due to extended defects, such as gain boundaries in the specimen.

rupole effects. The NMR line shape in the presence of uniform CDW velocity has been worked out in detail as a function of the velocity u. The solution leads to a motional narrowing and the appearance of a central line at the unperturbed-perturbed Larmor frequency. Experiments on $NbSe_3$ (Ross et al., 1986) and $Rb_{03}MoO_3$ (Nomura et al., 1986; Ségranson et al., 1986) clearly established the motional narrowing associated with moving charge-density waves. A detailed analysis and the evaluation of CDW velocity require calculation of NMR line shapes. When this is done, the current is found to be caused by the translational motion of the condensate.

In several cases, the onset of nonlinear conduction is accompanied by switching from the pinned to the current carrying state, and the behavior observed first in $NbSe_3$ (Zettl and Grüner, 1982) is shown in Fig. 10.4. Experiments employing contacts which are moved to different positions along the conducting directions have established that this behavior is due to extended
defects, such as grain boundaries or dislocations; and the positions where the current-voltage characteristics, such as those shown in Fig. 10.4 are generated, have been located. The behavior is most likely due to the dynamics of the amplitude fluctuations, with the order parameter which executes a phase slip at the pinning center playing an important role. For a description of the phenomenon, both phase and amplitude degrees of freedom must be included. This has been done by applying Eq. (10.29) to a simple situation, such as one pinning center. Observations can be accounted for by such simple models.

At low temperatures, with the freeze-out of uncondensed electrons, long range Coulomb interactions become important. These remove the dynamics of internal deformations of the collective mode. This then leads to nonlinear transport due to the translational motion of the rigid condensate; a typical currentvoltage characteristic is shown in Fig. 10.5. The sharp threshold field E_T is again determined by impurities. The differential conductivity dI/dE is enormous, and whether it is limited by intrinsic effects or factors like contact effects has not yet been established.

With the electrical conduction both nonlinear and frequency dependent, a broad variety of

experiments can be performed in the presence of both *dc* and *ac* applied fields

$$E = E_{d_1} + E_{a_1} \cos \omega t. \tag{10.31}$$

Both the resulting *dc* and *ac* current can be observed. Experiments with small ac electric fields in general are straightforward to account for, in this limit the perturbative treatment of the nonlinear dynamics in terms of the ac drive is more appropriate. Such experiments, which include rectification and harmonic mixing can be described using the (experimentally established) frequency dependent and dc nonlinear characteristics (Grüner, 1988). The responses to large amplitude ac drives, such as depinning by ac fields are more complicated. Here qualitative arguments (Grüner et al., 1981) have been used to account for the experimental findings.

The observations on spin density waves are similar to those made on charge density waves (Grüner, 1993, and references cited therein). In materials like $(TMTSF)_2PF_6$, a sharp threshold field E_T is observed (Tomic et al., 1989), the magnitude of which is determined by the impurity concentration. Switching and hys-

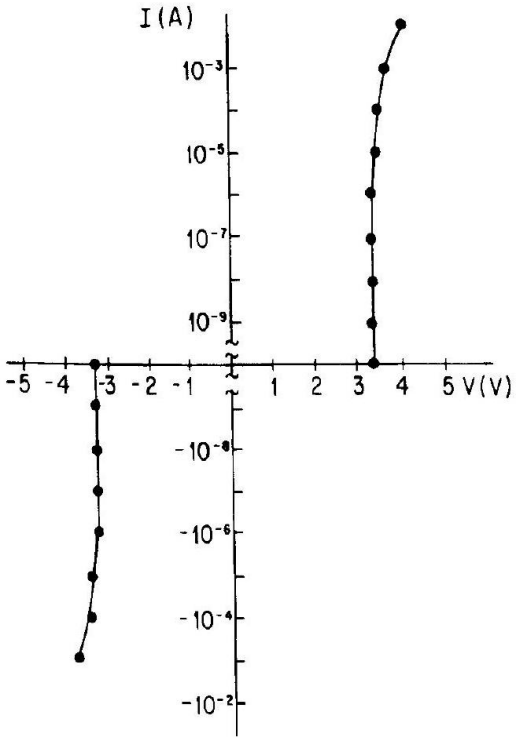


Figure 10.5. Current-voltage characteristics observed in $\mathrm{K}_{0,3}\mathrm{MoO}_3$ at low temperatures where screening by the uncondensed electrons is absent. The full line is a guide to the eye.

teresis effects, similar to those shown in Fig. 10.4, have also been found (Grüner, 1994 and references cited therein), presumably also due to pinning by extended defects such as grain boundaries. At low tempertures a different type of current-voltage characteristic has been observed (Mihály et al., 1992; Grüner, 1994). The results are suggestive of a tunneling process, which is different from single particle Zener tunneling; and which occurs at a significantly lower characteristic field than the fields which result from Zener tunneling across the gap.

1.11 Current Oscillations and Interference Effects in Driven Charge Density Wave Condensates

1.11.1 11.1 Introduction

With the response of the collective modes applied to both frequency and field dependent electric fields and also because of the periodic time dependent current in the nonlinear conductivity region, a broad variety of experiments, involving the application of *dc* and *ac* drives can be performed. These experiments can be classified as follows:

1. Frequency and electric field dependent conductivity where the time average current $\langle j(t)\rangle$ is measured in the presence of *dc* or small amplitude *ac* drives. The *dc* conductivity is defined as $\sigma_{dc} = \langle j(t)\rangle/E_{dc}$ where E_{dc} is the applied electric field; and the small amplitude *ac* response is characterized by $\sigma_{ac} = \mathrm{Re}(\sigma(\omega)) + i\,\mathrm{Im}\{\sigma(\omega)\}$, where $\mathrm{Re}\{\sigma(\omega)\}$ and $\mathrm{Im}\{\sigma(\omega)\}$ are the real and imaginary components of the conductivity. Here it is assumed that linear response theory is appropriate, and the response to a sinusoidal ac drive $E_{ac} = E_0 \sin\omega t$ is also sinusoidal, with no higher harmonics. Because the *dc* response is nonlinear, it is obvious that this is not valid for arbitrary ac fields, and nonlinear ac effects may occur for finite fields. These experiments serve as
tests of the various models leading to predictions concerning the *dc* and *ac* response of charge density waves. The ac response can also be used to evaluate the fundamental parameters of the problem, such as the effective mass m^*, the pinning frequency ω_1, and damping constant $1/\tau$. Frequency dependent conductivity studies have been performed over a rather broad frequency range, from audio to sub-millimeter wave frequencies. By now the ω dependent response of the pinned mode is fully explored in many materials. Similarly, the *dc* conductivity has been explored in detail and compared with various theories. Experiments performed at finite fields and frequencies have also been conducted. The nonlinear ac response has been examined in detail in various materials. Such studies are supplemented by the measurements of rectification and harmonic mixing performed over a broad range of frequencies and applied *dc* and *ac* fields. These studies will not be summarized here; it should be mentioned, however, that (perhaps not surprisingly) models which account for the *dc* and small amplitude ac response are successful in describing the response in finite fields and frequencies, as well as in the presence of simultaneous *ac* and *dc* excitations.

2. Spectral response in the current carrying state. In the nonlinear conductivity region, the spectral features of the current include large amplitude broad band noise and current oscillations (often called narrow band noise, NBN), with a fundamental given by Eq. (10.20) and several harmonics $f_n = nf_0$ with slowly decaying intensity. The current oscillations have a finite spectral width and also display temporal fluctuations which can be studied by examining the time dependence of the Fourier transformed current. The origin of the current oscillations has been studied by using imaginative lead configurations for current and voltage contacts and also by employing thermal gradients to break up the coherence which leads to current oscillations. The observation of current oscillations is suggestive of significant coherence throughout the specimens, and it is expected that the range of current-current correlations $\langle j(t, \overrightarrow{0}), j(t, \vec{r})\rangle$ is comparable to the dimensions of the samples. The finite widths associated with the current oscillations (when viewed by employing a spectrum analyzer which detects the Fourier transformed current) and broad band noise cannot be explained in terms of external noise repre-
senting the dynamics of the internal degrees of freedom within the condensate.

3. Interference experiments where both *dc* and *ac* fields are applied, and where either the *dc*

of the ac response is measured. Many of the observations are similar to those made on Josephson junctions, but the relevant frequencies for CDW dynamics are in the radiofrequency rather than the microwave spectral range.
Features of mode locking between the intrinsic current oscillations and the externally applied ac field are closely related to the features of the current oscillations; additional effects, such as synchronization and coherence enhancement by external drives, can also be investigated by the joint application of *dc* and *ac* drives. Also, in contrast to microwave signals, waveforms other than sinusoidal can be applied at radio frequencies; these can be used to examine phenomena such as transitions from the pinned to the current carrying state in detail.

This chapter focuses on current oscillations and interference phenomena in an attempt to give an overview of progress in the field, and to summarize the open experimental and theoretical questions.

1.11.2 11.2 Current Oscillations

11.2.1 General Features

The current-voltage characteristics, and cordial conductivity $\langle\sigma\rangle = \langle j\rangle/E$ of TaS_3 is displayed in Fig. 10.3. The term $\langle j\rangle$ refers to the time average *dc* current measured in the presence of an applied constant voltage, or to the applied dc current-depending on whether constant current or constant voltage configuration is used to measure the current voltage characteristics. (In principle, the current-voltage characteristics can be different depending on whether a constant current or constant voltage configuration is employed. This difference, however, has not been studied in detail.) In the nonlinear conductivity region, the current has, in addition to the dc, an oscillating component most conveniently studied by monitoring the Fourier transformed current. Whether an oscillating current or oscillating voltage is measured depends on the external conditions, both of which have

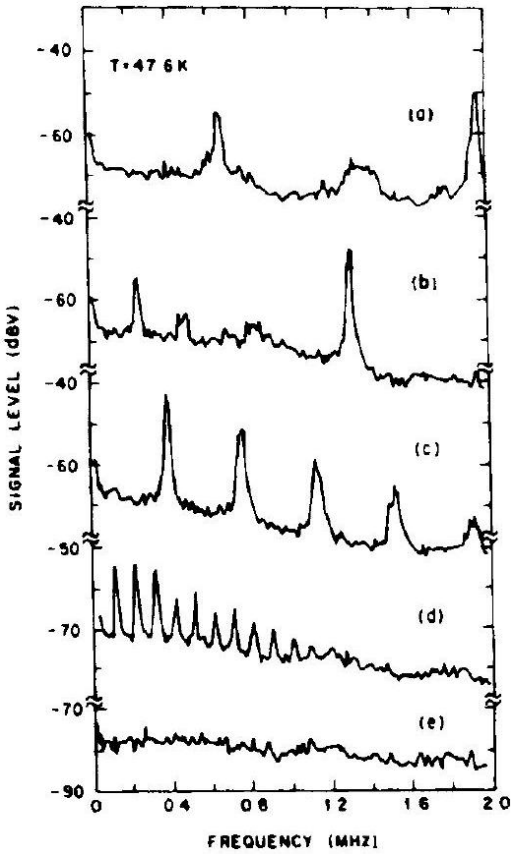


Figure 11.1. Fourier transform of the time dependent current in NbSe_{3} for various applied currents. Narrow band "noise" results if the current exceeds the threshold value for nonlinear conduction. Currents and de voltages are

(a) $I = 270\mu$ A, V = 5.81mV
(b) $I = 219\mu$ A, V = 5.05mV
(c) $I = 154\mu$ A, V = 4.07mV
(d) $l = 123\mu$ A, V = 3.40mV
(e) $I = V = .0$

The sample cross-sectional area $A \approx 136\mu$ m^2 (Fleming and Grimes, 1979).

been observed. In the following, however, I refer to the phenomenon as current oscillation or "narrow band noise" (NBN); the latter is the traditional notation used. The first observation by Fleming and Grimes (1979) in $NbSe_3$ is shown in Fig. 11.1. A substantial broad band noise (BBN) accompanies the nonlinear conduction, and a superimposed narrow band "noise", with a fundamental and several harmonics is also observed. The spectrum moves to higher frequencies with increasing applied

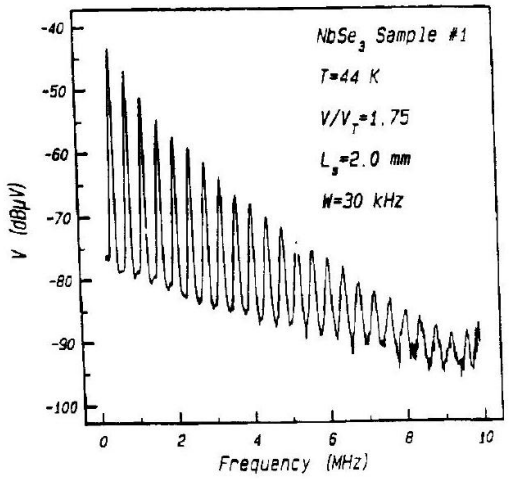


Figure 11.2. Spectrum of the voltage oscillations measured in response to an applied *dc* current of a 2.0 mm long NbSe_{3} sample at 44 K . A single fundamental and at least 23 harmonics are visible (Thorne et al., 1987).

voltage. Similar observations have subsequently been made on other materials where nonlinear conduction has been observed, namely in TaS_3 (both orthorhombic and monoclinic phase), $(TaSe_4)_2\,I$, $(NbSe_4)_{3.3}\,I$ and $K_{0.3}MoO_3$ or $Rb_{0.3}MoO_3$. By now the phenomenon can be regarded as one of the fundamental observations of charge density wave dynamics.

The overall features of the observed current oscillations depend on crystal quality and in general on the coherence associated with the current carried by the collective mode. It has been established (Ong et al., 1984a, 1984b; Ong and Maki, 1985), that current or voltage contacts can introduce excess peaks in the Fourier transformed spectrum; similarly mechanical damage to the specimens also leads to complicated "noise" patterns. In carefully manipulated specimens the current oscillations have a rather high quality factor and also display many harmonics (Weger et al., 1980). Figure 11.2 shows the experimental results for $NbSe_3$. The coherence associated with the current oscillations can be characterized by the quality factor Q of the peaks in the Fourier transformed current. The quality factor $Q = \Delta_f/f_0$, where Δ_f refers
to the width of the fundamental, was found to approach 10^5, in contrast to $Q \sim 4$ observed in Fig. 11.1.

As a general rule materials, where the electronic structure is more anisotropic, and consequently, the coherence perpendicular to the chain direction is less well defined, show broader current oscillation peaks; which are also less prominent for specimens with larger cross sections (Mozurkewich et al., 1983). These effects however, have not been investigated in detail. There is also a broadly defined correlation between the width of the narrow band noise and the amplitude of the broad band noise: in materials and in specimens of the same material with smaller broad band noise amplitude the Q of the Fourier transformed current peaks is larger. At one end of this spectrum, $NbSe_3$ has rather small broad band noise and high Q for the current oscillations in both CDW states; while $K_{0.3}MoO_3$ and $(TaSe_4)_2\,I$ both have large broad band noise at current oscillations with small quality factors. TaS_3 represents an intermediate case (Grüner, 1988). The quality of the crystals and of the voltage and current contacts can also be important (Beauchene et al., 1986) since macroscopic defects can lead to spurious velocity distributions in the specimens, while irregular contacts can lead to inhomogeneous current distributions.

Current oscillations have also been studied in the time domain by recording the time dependence of the current or voltage following a pulse excitation. Such experiments were performed

in $NbSe_3$ (Fleming, 1983; Bardeen et al., 1982), and current oscillations have been subsequently observed in TaS_3 and $K_{0.3}MoO_3$ (Fleming et al., 1986). The observation of oscillations in the time domain differs from studies employing Fourier transforms in several aspects. First, for a finite Q of the oscillations a dephasing is expected, with a time dependent amplitude $\Delta j(f)$ given by

$$\Delta j(f) \sim A\left[1 - \exp\left(-\frac{t}{\tau}\right)\right] \tag{11.1}$$

with $\tau \sim Q^{-1}$. Such a gradual decrease of the oscillation amplitude has been observed in all materials, with a more dramatic decrease for oscillation with smaller Q values (Parilla and Zettl, 1985 and references cited therein; Fleming et al., 1985; Thorne et al., 1987c). Because of the fluctuating oscillation frequency, the
time dependence of the oscillation amplitude most probably represents the dephasing of the various CDW domains, which are phase locked at the start of the applied pulse. Transient oscillations, induced by the sudden transition from the pinned to the current carrying state can also accompany the leading edge of the applied pulse. These transients have the fundamental oscillation frequency; the amplitude, however, is greatly enhanced over the steady state oscillation amplitude obsorved in the Fourier transform current under *dc* current or *dc* voltage drive conditions. Pulses of finite length of the order of few oscillation periods can also lead to mode locking, which will be discussed at length in Section 11.3. The observations can then be regarded as a form of interference and locking phenomena which are the consequences of competing periodicities; here the inverse frequency of the oscillations and the duration of the applied pulse.

11.2.2 Current-Frequency Relation

The frequency of the oscillations is approximately proportional to the current carried by the CDW (Monceau et al., 1980), and subsequently it has also been shown that the ratio of the current to the frequency varies with temperature, approximately as the number of condensed electron n_{CDW} (Bardeen et al., 1982). Fig. 11.3 shows the linear relation between I_{CDW} and f_0 in a wide frequency range for a pure $NbSe_3$ specimen (Bardeen et al., 1982); with the ratio I_{CDW}/f_0 as a function of T in the insert. Normalizing the CDW current for one chain, the above observations can be described as

$$\frac{j_{\mathrm{CDW}}}{f_0} = ce\frac{n_{\mathrm{CDW}}(T)}{n_{\mathrm{CDW}}(T=0)} \tag{11.2}$$

where j_{CDW} refers to the current per chain carried by the condensate. While the precise value of the constant c in Eq. (11.2) is still debated it is between 1 and 2 for a broad range of materials. For $NbSe_3$, TaS_3 (both orthorhombic and monoclinic form) and for $(TaSe_3)_2\,\mathrm{I}$, early experiments (Monceau et al., 1983) were suggestive of $I_{\mathrm{CDW}}/f_0 = e$; indicating that the fundamental periodicity is related to a displacement of the collective mode by a half wavelength $\lambda/2$. There are, however, several ambiguities in the analysis. In $NbSe_3$ only part of the conduction electrons are condensed

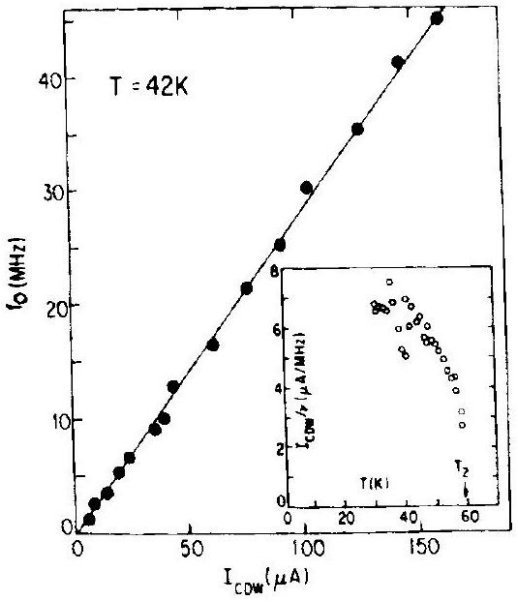


Figure 11.3. Relation between the CDW current and fundamental oscillation frequency in NbSe_3. The inset shows I_{CDW}/f_0 versus temperature (Bardeen et al., 1982).

into the collective mode, and the relation I_{CDW}/f_0 depends on the assumed number of condensed electrons. Similar problems arise in monoclinic TaS_3. The definition of the fundamental is complicated in $(TaSe_4)_2\,1$ where occasionally the second harmonic has a larger intensity than the fundamental. In orthorhombic TaS_3, the current-frequency relation in general is nonlinear due to the distribution of currents caused by the filamentary nature of the specimens. Using a mode locking technique to improve the coherence, the measured current-frequency relation in orthorhombic TaS_3 leads to (Brown and Grüner, 1985)

$$\frac{I_{\mathrm{CDW}}}{f_0} = (2 \pm 0.1)e \tag{11.3}$$

the above value was subsequently confirmed in an independent study which also employs mode locking (Latyshev et al., 1986). Careful NMR experiments on $K_{0.3}MoO_3$ specimens (Segransan et al., 1986) utilizing motional narrowing effects also lead to a relation $I_{\mathrm{CDW}}/f_0 = (1.9 \pm 0.1)e$ in close agreement with the findings on orthorhombic TaS_3.

The above relation between the current and oscillation frequency is related to the fundamental periodicity associated with the phase ϕ (Monceau et al., 1980). The CDW current, described in terms of drift velocity v_d of the (rigidly moving) condensate is given by $j_{\mathrm{CDW}} = n_c e v_d$. Associating the fundamental frequency with a CDW displacement by one period, $f_0 = v_d/\lambda_0$ this then leads to

$$\frac{j_{\mathrm{CDW}}}{f_0} = n_{\mathrm{r}}(T) e \lambda_0 \tag{11.4}$$

and with $\lambda_0 = \pi/k_F$ and $n_c = 2k_F/\pi$, Eq. (11.2) with a constant $c = 2$ is recovered. Alternatively, the fundamental frequency can be related to the energy difference ΔE between the two sides of the displaced Fermi. With

$$\Delta E \sim \frac{\delta E/\delta k}{\delta k/\delta v} v_d = 2 v_F v_d \tag{11.5}$$

$\Delta E = h f_0$ and $j_{\mathrm{CDW}} = n_c e v_d$ also leads to Eq. (11.2) with $c = 2$. The strictly linear relation between j_{CDW} and f_0 as shown in Fig. 11.3, also suggests that the CDW velocity is constant

throughout the specimen. Indeed j_{CDW} is proportional to f_0 over a broad range of currents and frequencies only in high quality materials. In materials where other, independent evidence suggests that disorder plays an important role, deviations from the linear relation between j_{CDW} and f_0 are observed (likely related to finite veloc-ity-velocity correlation lengths) (Brown and Grüner, 1985).

The amplitude of the oscillating current increases with increasing collective mode current and appears to saturate in the high electric field limit (Weger et al., 1982; Mozurkewich and Grüner, 1983). This has been studied in detail in $NbSe_3$, and the amplitude of the oscillating current is displayed in Fig. 11.4 as a function of oscillation frequency. In experiments where the oscillation amplitude was measured up to $f_0 = 700$MHz (Weger et al., 1982; Thorne et al., 1986a), the oscillation amplitude was found to saturate in the large velocity limit.

11.2.3 Size Effects and Fluctuation Phenomena

The current oscillations are suggestive of translational motion of the condensate in a periodic potential. Considerable effort has been made to gain information on the origin of the pinning by

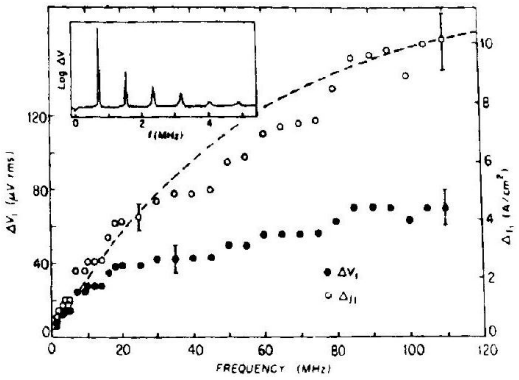


Figure 11.4. Amplitude of the fundamental oscillation in NbSe_{3} at 42.5 K , vs. oscillation frequency. The amplitude is plotted both as a voltage ΔV_1 (solid symbols, left-hand scale) and as an equivalent current density Δj_1 (open symbols, right-hand scale). The inset shows a typical spectrum. The dotted line follows from the equation of motion Eq. (10.3) (Mozurkewich and Grüner, 1983).

measuring the oscillation amplitude as a function of sample volume; as well as under nonequilibrium conditions such as those provided by temperature gradients applied to the specimens. Although all experiments indicate that the current oscillations disappear in the thermodynamic limit (Mozurkewich and Grüner, 1983) several questions remain, mainly centered around the detailed mechanisms of pinning and the mechanism of oscillating current generation.

Experiments performed both in $NbSe_3$ (Mozurkewich and Grüner, 1983) and in ($TaSe_4$) 2 I (Mozurkewich et al., 1984) specimens with different lengths and cross sectional areas are in agreement with a volume dependence of the relative oscillation amplitude

$$\frac{\Delta j_{\mathrm{CDW}}}{j_{\mathrm{CDW}}} = \text{ const. } \Omega^{-1/2} \tag{11.6}$$

where Ω is the volume of the specimen. The results can be understood by postulating that the specimens are composed of domains of size L^3 where the current is coherent, but the currents in different domains oscillate with random phase. In this case, the
oscilla.ion amplitude is given by

$$\frac{\Delta j_{\rm CDW}}{j_{\rm CDW}} = \Delta j_0 \left(\frac{L_3}{\Omega}\right)^{1/2} \tag{11.7}$$

where Δj_0 is the oscillation amplitude expected for a coherent (single domain) response. The latter can be estimated by assuming simple models (to be discussed later) and then $L^3 \sim 0.2\mu m^3$ as an appropriate lower limit of the domain volume is obtained in $NbSe_3$ and in $(TaSe_4)_2I$. The macroscopic domain size is most probably related to the Fukuyama-Lee-Rice (see Lee and Rice, 1979) coherence length discussed before. As discussed earlier Eq. (8.20) leads, with reasonable values for the impurity potential charge, density wave amplitude, impurity concentration, and Fermi velocity, to $L_0 = 100\mu$ along the chain direction. For an anisotropic band structure, the coherence length is also anisotropic (Lee and Rice 1979), and in the directions perpendicular to the chains the phase-phase correlation length $L_\perp$ is given by

$$L_\perp = \frac{v_{F\perp}}{v_{F\|}} L_\|. \tag{11.8}$$

A typical anisotropy of $v_{F\|}/v_{F\perp} \sim 30$ leads to $L_i \sim 0.3\mu$ m and to a domain size $V = L_0 L_\perp^2$ of about $1\mu m^3$, in broad agreement with the experimental results. A different set of experiments (Ong and Maki, 1985; Ong et al., 1984), performed on $NbSe_3$ however, indicates that for long specimens, the oscillation amplitude is independent of ℓ, the length of the specimens. This observation was used to argue that the oscillating current is generated at the contacts and not at the bulk (see also Jing and Ong, 1986). Subsequent experiments (Jing and Ong, 1986) where a length dependent oscillation amplitude was recovered, were also used to establish the range of phase coherence, and in $NbSe_3$ the experimental results are suggestive of $L_0 \sim 200\mu$. The difference between the two sets of experiments may reflect the difference in contact configurations, impurity concentration, etc. The issue was further investigated by Brown and Mihály (1985) who employed a sliding, nonperturbative contact configuration to measure the noise amplitude in different sections of the specimens investigated. The observations are consistent with independent domains oscillating with the same frequency, but with random phase, as suggested by Eq. (11.6). In several specimens evidence was also found for sudden jumps in the oscillation amplitude when the contacts were moved along the specimens, indicating oscillating current generation by macroscopic defects such as grain boundaries within the specimens.

Several studies have been made to determine whether the oscillating current is generated in the bulk or at the contacts by applying a temperature difference between the two ends of the specimens. The argument for conducting such experiments is simple: with the two contacts at different local temperatures T_1 and T_2, they are expected to generate oscillations at different frequencies; each of which corresponds to the local temperature. Narrow band noise generated in the bulk, however, may be smeared by a temperature gradient; or alternately split into several frequencies each corresponding to a velocity coherent domain. The first experiments (Zettl and Grüner, 1984, 1985) on small $NbSe_3$ specimens did not reveal any splitting of the fundamental oscillation, which was also determined by the average temperature $(T_1 + T_2)/2$ of the specimen. The result is indicative of velocity coherence, comparable to the length $\ell \sim 1$ mm of the specimen. In subsequent experiments (Ong et al., 1985; Verma and Ong, 1984), however, a splitting was found and this was taken as evidence for current generation at the contacts. Several groups (Brown et al., 1985a; Lyding et al., 1986) later showed that by increasing the temperature gradient, further splittings can be induced, demonstrating that the various oscillation frequencies cannot be associated with contacts alone. In Fig. 11.5, the observations made by Lyding et al. (1986) are shown. A fundamental observed at $f = 1.1$MHz for $\Delta T = 0$ is split into several peaks with increasing temperature gradient. The width of the peaks is approximately the same as that of the peak for $\Delta T = 0$, suggesting that the sample is broken up by the application of a temperature gradient into velocity coherent regions. The minimum

velocity coherence estimated from the number of peaks and the sample length is of the order of 100μ m, in qualitative agreement with the conclusions of earlier studies.

The current oscillations, such as displayed in Figs. 11.1 and 11.2, have large temporal fluctuations both in position and amplitude. The time scale of the fluctuations is significantly larger than the inverse fundamental frequency, and is typically on the scale

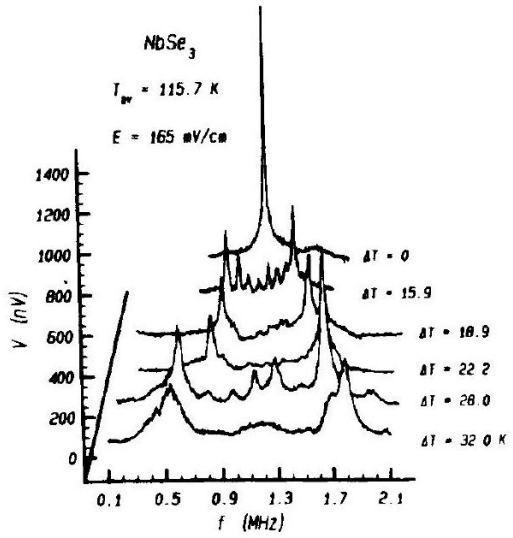


Figure 11.5. Splitting of the fundamental NBN peak for the upper Peierls transition of NbSe_{3} as a function of applied thermal gradient. The gradient is opened around an average temperature of 115.7 K and the sample length is 0.89 mm (Lyding et al., 1986).

of microseconds. The phenomenon was first studied by Brown et al. (1985b) and investigated in detail by Link and Mozurkewich (1988) and by Bhattacharya et al. (1987).

The probability densities of the noise voltages follow a Gaussian distribution, suggesting that the current oscillations have many of the characteristics of Gaussian noise; and cannot be regarded as a coherent signal over a substantial period of time (Link and Mozurkewich, 1988). This is demonstrated in Fig. 11.6 where the probability distribution of the NBN voltages obtained for repeated scales of approximately 1 m is displayed. The full line is a Gaussian distribution with a width $\sigma = 3.3\mu$ V. The distribution reflects the underlying probability density in the recorded oscillation amplitudes which are far enough removed from each other to be uncorrelated. This is appropriate for long sampling periods with strongly correlated oscillations expected for sampling with short time differences. A crossover from such coherent to Gaussian noise was also studied, and the typical time for the crossover is on the order of 10μsec for $NbSe_3$. Similar experiments have not been performed in other materials,

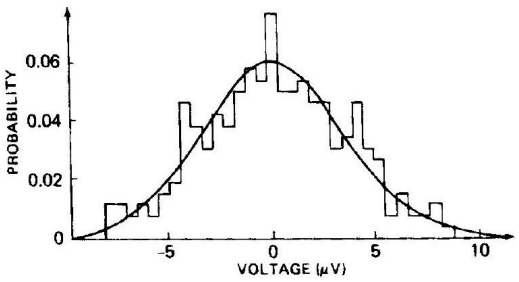


Figure 11.6. Histograms of voltages of narrow band noise in NbSe_{3}. The solid line represents the best fit Gaussian with $\sigma = 3.3\mu$ V (Link and Mozurkewich, 1988).

although temporal fluctuations of the oscillation amplitudes have been widely observed.

11.2.4 Broad Band Noise

The Fourier transformed spectra, such as displayed in Fig. 11.1, also have a significant broad band component, with an effective noise temperature corresponding to several thousand degrees of Kelvin (Richard et al., 1982; Zettl and Grüner, 1983). The amplitude of the noise is inversely proportional to the square root of the volume, $\Omega^{-1/2}$ (Richard et al., 1982), and the observation is suggestive of broad band noise generation in the bulk. In pure $NbSe_3$ specimens, however (Thorne et al., 1986b), the noise amplitude could clearly be related to the presence of macroscopic inhomogeneities (such as breaks in the specimens). This suggests that the broad band noise is generated at macroscopic boundaries such as grain boundary or breaks within the specimens. The issue here is similar to that raised in connection with the current oscillations; the most probable situation is that in general both macroscopic defects and impurities contribute to the broad noise since both lead to the disruption of the phase ϕ of the condensate. Clearly, detailed experiments on alloys with different impurity concentrations are required to clarify this point.

The spectral dependence can be described with a characteristic $\omega^{-\alpha}$ behavior with $\alpha < 1$ (Battacharya et al., 1985; Maeda et al., 1983, 1985) reminiscent of $1/f$ noise widely observed under
different circumstances in various current carrying conditions. The observed field, frequency, and temperature dependence of the broad band noise is inconsistent with a generalized form of the Nyquist noise (Maeda et al., 1983) and the following model has been proposed (Bhattacharya, 1985). For constant current, fluctuations of the threshold voltage V_T within the specimens (assuming that E_T depends on the position) lead to fluctuations of the cordial resistance $R = V/I$ and the noise voltage is given by

$$\left\langle \delta V^2(\omega) \right\rangle = I^2 \left\langle \delta R^2(\omega) \right\rangle = I^2 \left(\frac{\delta T}{\delta V_r} \right)^2 \left\langle \delta V_r^2(\omega) \right\rangle \tag{11.9}$$

It is also assumed that $\delta R/\delta V_T$ is proportional to $\delta V/\delta V_T$, i.e., R is a function of $V - V_T$ only, and that both quantities are independent of the frequency. (The latter is valid well below the pinning frequency ω_0.) Detailed measurements performed on TaS_3 indeed are in agreement with Eq. (11.9). The volume dependence of the noise indicates that it is an incoherent addition of fluctuations generated in coherent volumes, given by L^3. If the fluctuation of the effective pinning force δE_T is proportional to E_T, then

$$\left\langle \delta V_T^2(\omega) \right\rangle = \frac{E_T^2 L_0^3}{A} S(\omega) \tag{11.10}$$

where $S(\omega)$ is the spectral weight function, $\int S(\omega)d\omega = 1$, and A is the cross section of the specimens. Eq. (11.10) is a consequence of the assumption that the number of independent entities generating the broad band noise is given by Ω/L^3. An analysis of the experimental results leads to $L_0^3 \sim 1\mu m^3$ in TaS_3, in broad agreement with coherent volumes estimated from the volume dependence of the current oscillations in $NbSe_3$ and in $(TaSe_4)_2 \downarrow$ (Mozurkewich and Grüner, 1983; Mozurkewich et al., 1983).

1.11.3 Interference Phenomena

The nonlinear current-voltage characteristics and the observation of intrinsic current oscillations are suggestive of a variety of interference effects which may arise in the presence of combined *ac* and *dc* fields. In the case of Josephson junctions the phenomenon was used by Shapiro (1963) to demonstrate the existence of the ac Josephson effect and consequently many of the
(formally similar) observations in driven charge density wave systems are also called "Shapiro phenomena."

Harmonic mode locking was first observed by Monceau et al. (1980). The observation was used to explore the relation between the oscillation frequency and time averaged current. The experiments were extended to explore the formal analog between CDW dynamics and observations made on Josephson junctions, including the characteristic Bessel function dependence of the interference features on the drive amplitudes (Zettl and Grüner, 1984). Subharmonic mode locking (Brown et al., 1984) has also been explored in detail together with incoherent effects, coherence enhancement (Sherwin and Zettl, 1985) and spatio-temporal effects (Bhattacharya et al., 1987). In contrast to Josephson junctions where the characteristic frequency is in the microwave spectral range, here rf frequencies are important, and consequently, waveforms different from a sinusoidal drive can be employed (Brown et al., 1986a, b).

11.3.1 Harmonic Mode Locking

Interference effects were first detected by Monceau and coworkers (1980) in $NbSe_3$ subjected to *dc* and ac applied fields. The differential resistance dV/dI measured in the nonlinear conductivity region with an *ac* field of varying frequency is shown in Fig. 11.7, for various current levels. Steps in the direct I-V curves correspond to peaks in the derivative; they occur when the fundamental frequency of the current oscillations (or its harmonics) coincides with the applied frequency. Although the spectrum of the interference peaks is complicated because of spurious effects (introduced most probably by inhomogeneous carrier injection at electrical contacts) a fundamental and several harmonics, such as those labeled by $4\ F_2, 8\ F_2$, and $12\ F_2$ in the upper part of the figure, are evident. Spectra such as those shown in the figure were used to establish the linear current-frequency relations discussed earlier.

In carefully selected pure specimens, interference effects are also evident in direct I-V curves, such as that shown for $NbSe_3$ in Fig. 11.8 (Zettl and Grüner, 1984). The excitation applied to the sample had the form $V = V_{cd} + V_{ac}\cos(\omega t)$ with $\omega/2\pi = 100$MHz. For $V_{ac} = 0$, a smooth, nonlinear I-V curve is observed with a well-defined threshold voltage V_T where the conductivity starts to be nonlinear. At higher values of V_{ac}, well-defined steps, which

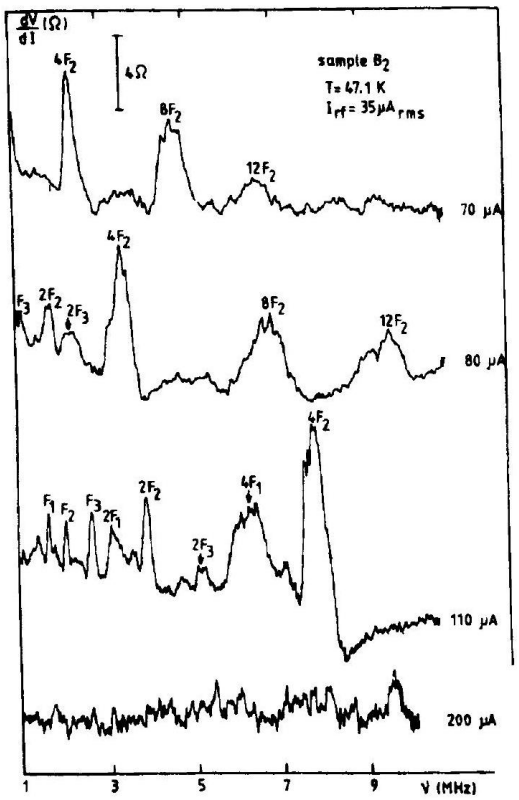


Figure 11.7. Differential resistance dV/dl in NbSe_{3} observed by sweeping the frequency of the rf current, for a constant dc current. The various sets of interference peaks are labelled by F_1, F_2, F_3, and $F_4 dc$ current (Monceau et al., 1980).

we shall index with an integer n, appear in the nonlinear region. The step height δV, as defined in the figure, in general first increases with increasing V_{ac} and then decreases. The position of the $n = 1$ step (identified in the figure) corresponds to a dc current I_{dc} which, in the absence of ac fields, yields an intrinsic oscillation of frequency $f_1 = 100\mathrm{MHz} = \omega/2\pi$. This has been
established by measuring the oscillation frequency directly. We should also note the presence of harmonic steps corresponding to $n = 2$ (where $f = 200\mathrm{MHz}$) and smaller subharmonic steps corresponding to $n = \frac{1}{2}$ (where $f_1 = 50\mathrm{MHz}$). The steps are thus clearly an interference effect between the intrinsic current oscillation and the externally applied rf excitation.

Similar experiments have been performed on TaS_3 (Brown and Grüner, 1985) and also on $K_{0.3}MoO_3$ (Fleming and Schneemeyer, 1986). For both materials the current oscillations are in general smaller and have a significantly larger spectral width. These features are also evident in the interference patterns, shown for TaS_3 in Fig. 11.9.

The definition of the step height is straightforward, and is indicated in Fig. 11.8; its dependence on the ac amplitide

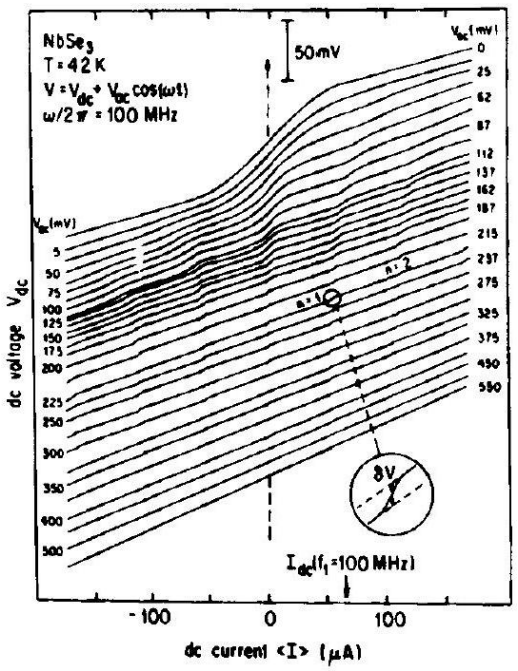


Figure 11.8. Shapiro steps in the $d c \mathrm{I}-\mathrm{V}$ traces for $NbSe_3$ when rf field is applied at frequency $\omega/2\pi = 100$MHz and amplitude V_{ac}. The step height δV is defined in the figure. No Shapiro steps are observed for $V_{ac} = 0$, while the maximum step height is at approximately $V_{ac} = 100$mV. The arrow indicates the *dc* current which yields a fundamental noise frequency $f_1 = 100$ MHz . The step index is n (Zettl and Grüner, 1984).

11. Current Oscillators and Interference Effects

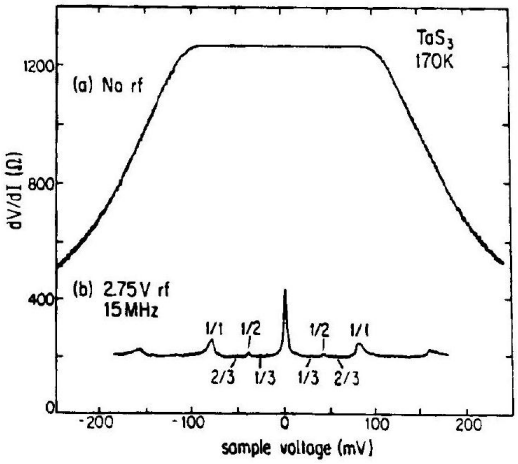


Figure 11.9. Differential resistance vs. *dc* sample voltage: (a) with no rf and, (b) in the presence of 2.75 Vrf at 15 MHz . The peaks in the derivative correspond to steps in the direct I-V curve (Brown and Grüner, 1985).

is shown in Fig. 11.10. These can be analyzed by employing the formal correspondence between the equation of motion of the classical particle model and that of the resistively shunted Josephson junction. For the latter the step height δI for the n^{th} step can be obtained by explicitly solving Eq. (10.3). In the high frequency limit ($\omega \gg 2eI_lR/1\hbar$), computer simulations (see, for example, Lindelof, 1981) and analytic approximations (Clark and Lindelof, 1976; Fack and Kose, 1971) show that the height of the n^{th} step is

$$\delta I(\omega) \approx 2I_j(\omega = 0) \left| \frac{I_n I_l(\omega)}{\omega G I_j(\omega = 0)} \right| . \tag{11.11}$$

where J_n is the Bessel function of order n. The critical current I_1 depends on the applied ac current as

$$I_j(\omega)/I_j(\omega = 0) \left| J_0 \left(I_1(\omega)/\omega G I_j(\omega) \right) \right| . \tag{11.12}$$

The corresponding equations for a CDW system are, by direct

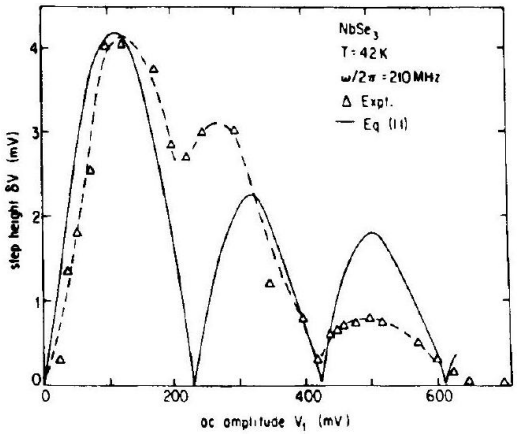


Figure 11.10. Step height δV versus ac amplitude V_{a} for Shapiro steps in $NbSe_3$. The rf frequency is 210 MHz and the step index is $n = 1$. The solid line is the prediction of the classical model, Eq. (10.3), with parameters $\omega_0^2\tau/2\pi = 80\text{MHz}.V_7 = 24\text{mV}, a = 0.17$ (Zettl and Grüner, 1984).

analogy to Eqs. (11.11) and (11.12)

$$\delta V = 2V_T(\omega = 0) \left| J_n \left(V_{\text{eff}} \right) \right| \tag{11.13}$$

and

$$V_r/V_r(\omega = 0) = \left| J_0 \left(V_{\text{eff}} \right) \right| , \tag{11.14}$$

with V_{eff} given by

$$V_{\text{eff}} = \frac{V_{ac}\omega_0^2\tau}{\omega V_T(\omega = 0)}. \tag{11.15}$$

The above equations are appropriate in the high frequency limit for a strongly damped system where the capacitive term (for the Josephson junction case) or the inertial terms (for the CDW case) can be neglected. Equation (11.13) predicts that the maximum step height $\delta V_{\max}$ depends only on the maximum value of I_n and is thus independent of frequency ω. In the low-frequency limit, still neglecting the junction capacitance or CDW inertia; computer calculations (Lindelof, 1981) lead to solutions for the step heights in the I-V characteristics which closely resemble

Bessel functions. In this low-frequency limit the maximum step height $\delta V_{\max}$ is a strong function of frequency ω.

Equations (11.13)-(11.15) are appropriate for a coherent response in the current-carrying state. If we assume that (due to either a distribution of the parameters which represent the

CDW response or inhomogeneities such as phase boundaries, etc.) only a fraction α of the sample responds collectively to the external field. Then phenomenologically Eq. (11.13) becomes

$$\delta V = 2\alpha V_T(\omega = 0)\,|J_n\,(V_{\text{eff}}\,)|\,, \tag{11.16}$$

while Eq. (11.14) remains unchanged. In general, α can be both frequency and voltage dependent, reflecting different amounts of coherence under different circumstances.

The parameters ω_0 and τ which determine V_{eff} can be derived from the low frequency ac response, or alternatively, a fit to the data (such as shown in Fig. 11.10), can be used to calculate these parameters. The full line in Fig. 11.10, is Eq. (11.15) with $\omega_0^2\tau = 503$ MHz and $\alpha = 0.17$. The former agrees well with $\omega_0\tau$ calculated directly from the frequency dependent response and the value of α indicates a highly coherent response (Zettl and Grüner, 1984).

The formalism also leads to a reduction of the threshold field which follows an oscillatory behavior (Lindelof, 1981), which was not observed in early experiments. Subsequent measurements on extremely well-defined specimens (Latyshev et al., 1987; Thorne et al., 1987b), however, clearly recovered the oscillatory behavior of V_T, as shown in Fig. 11.11.

Interference effects are also evident in the ac response measured in the nonlinear conductivity region. Fig. 11.12 shows the real and imaginary parts of the complex conductivity, $\text{Re}\,\{\sigma_{a_c}(\omega)\}$ and $\text{Im}\,\{\sigma_{ac}(\omega)\}$, as a function of applied *dc* bias, measured at $\omega/2\pi = 3.2$MHz. It is evident that neither the real nor the imaginary part of the frequency-dependent response is strongly affected by an applied *dc* voltage as long as $V_{dc} < V_T$. However, for $V_{dc} > V_T$, $\text{Re}\,\{\sigma_{ac}\}$ measured at 3.2 MHz , strongly increases and the ac dielectric constant ϵ, related to the ac conductivity by

$$\epsilon(\omega) = \frac{4\pi Im\,\{\sigma_{ac}(\omega)\}}{\omega} \tag{11.17}$$

strongly decreases for increasing V_{dc}. The dielectric constant ap-

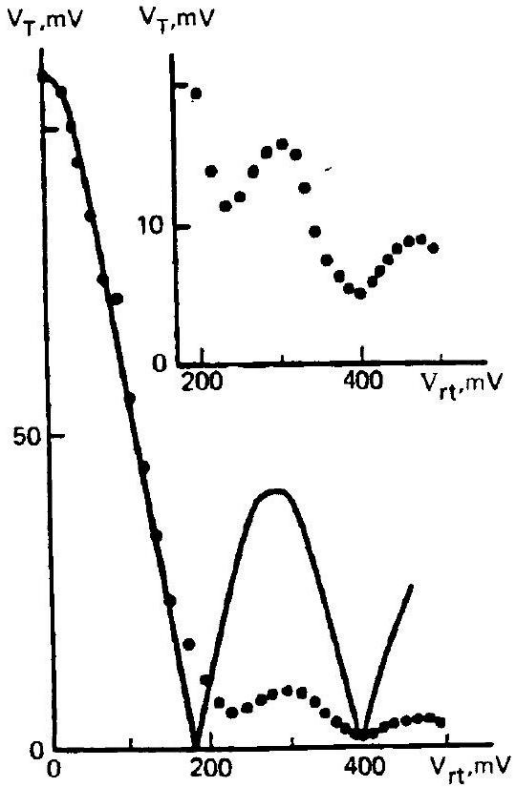


Figure 11.11. The *dc* threshold voltage versus ac amplitude for several applied ac frequencies. The period of the oscillations with ac amplitude is roughly proportional to the ac frequency. The solid lines are curves calculated by using Eq. (11.14) (Latyshev et al., 1987).

proaches zero for large *dc* drive showing that there is no appreciable out-of-phase component; $\mathrm{Re}\,\{\sigma_{ac}(\omega)\}$, on the other hand, approaches the high-frequency limit obtained from the frequency dependence of the small amplitude ac response (observed for the pinned charge density wave).

In addition to the overall behavior described above, Figs. 11.12a and 11.12b also show that for $NbSe_3$ both $\mathrm{Re}\,\{\sigma_{nc}(\omega)\}$ and $\epsilon(\omega)$ have sharp anomalies for well-defined values of V_{dc} in the nonlinear conductivity region. Specifically, $\mathrm{Re}\,\sigma_{ac}$ shows "steps" to higher conductivity values at $V_{dc} = 1.6, 2.3$, and 3.3 mV . At these same values of V_{dc}, ϵ shows well-defined inductive dips (Zettl and Grüner, 1984; Fleming et al., 1985). The ac response has not been calculated using the Josephson equation; but arguments

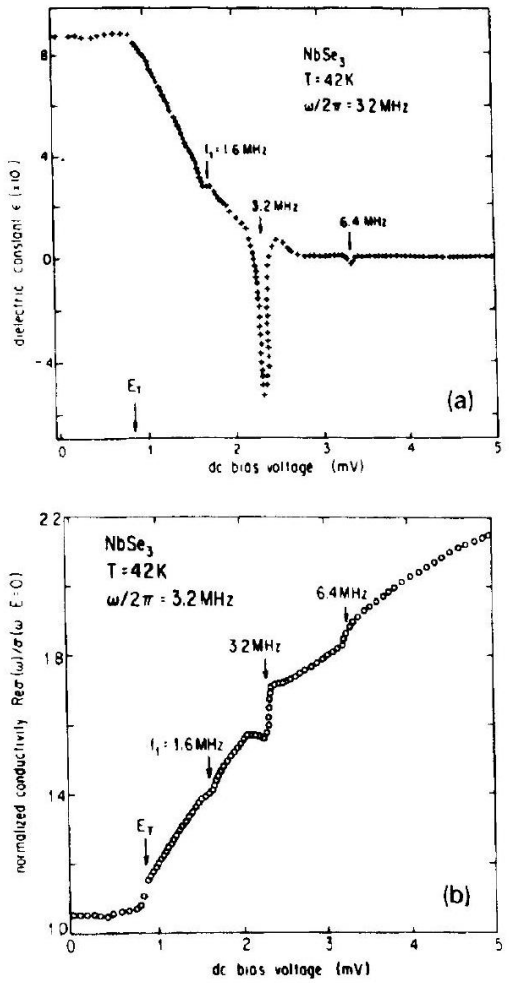


Figure 11.12. Real and imaginary part of the ac conductivity $\sigma(\omega)$ and dielectric constant $\epsilon(\omega)$ measured at $\omega / 2 \pi=3.2 \mathrm{MHz}$ as a function of applied *dc* bias voltage. The threshold field is indicated by an arrow (Zettl and Grüner, 1984).

similar to those used in nonlinear circuit theory can be applied to account for the observations (Zettl and Grüner, 1984).

11.3.2 Subharmonic Mode Locking

Interference phenomena have also been observed whenever $pf_{\text{ext}} = qf_0$ for q an integer, but not equal to one (Brown et al., 1985). These are called the subharmonic Shapiro steps, and a rich array of such steps is shown in Fig. 11.13, again observed in $NbSe_3$. A few of the p/q values are identified in the figure; these were made by plotting I_{CDW} versus ω_{ext} and checking that the steps were p/q times that for the fundamental. In general, features with small p and q are more conspicuous and are both taller and wider. A complete mode locking would correspond to a plateau in dV/dl at the same level as the differential resistance below threshold. This can be understood as follows. The steps are regions of locking between the internal and applied frequencies when $pf_{\text{ext}} - qf_{\text{int}}$ is sufficiently small. If locking within such

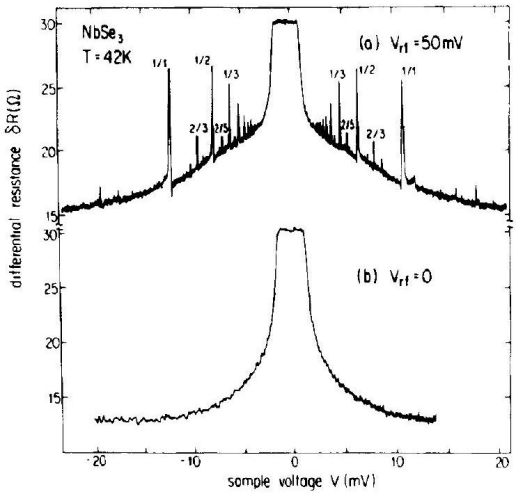


Figure 11.13. Differential resistance of NbSe_{3} with and without an applied rf voltage V_{rf}. The numbers indicate the various subharmonic steps (Brown et al., 1984).

regions is complete, the CDW velocity becomes fixed by f_{ext} and does not respond to changes in the applied dc voltage. Hence dV/dl rises to the linear resistance R_0, which is solely due to the uncondensed electrons. This situation holds if the CDW velocity is coherent throughout the specimen. In reality the velocity coherence length must be finite, and f_{int} may vary spatially. If the variation of f_{int} is larger than the width of the region over which locking can occur, locking will be incomplete, and dV/dl will rise to level less than R_0. Observations under such circumstances are called interference "features." Therefore, the height of dV/dl is expected to correlate to the degree of synchronization across the sample. The completeness of synchronization depends on various factors such as sample dimensions, ac amplitude, and frequency; and in Fig. 11.14, subharmonic peaks several of which display complete mode locking, are shown (Hall and Zettl, 1984). While complete mode locking is observed only for a few subharmonic interference peaks in Fig. 11.14; in subsequent experiments performed in carefully treated $NbSe_3$ specimens, up to 150 subharmonic steps between the threshold field and the $\frac{1}{i}$ harr onic step have been observed (Thorne et al., 1988).

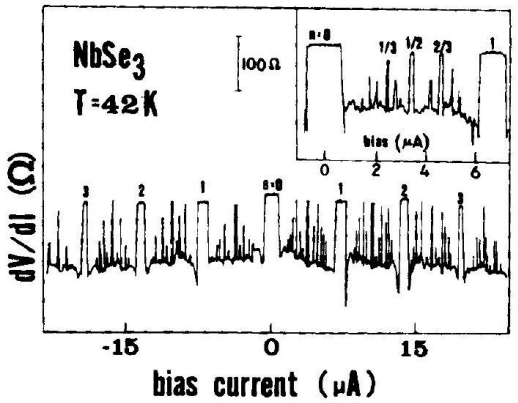


Figure 11.14. Mode locked Shapiro steps in $\mathrm{NbSe}_{\{z.\}}$ Over the mode locked region, dV/dl is independent of dc bias. The inset shows the subharmonic structure in detail, with corresponding p/s values (Hall and Zettl, 1984).

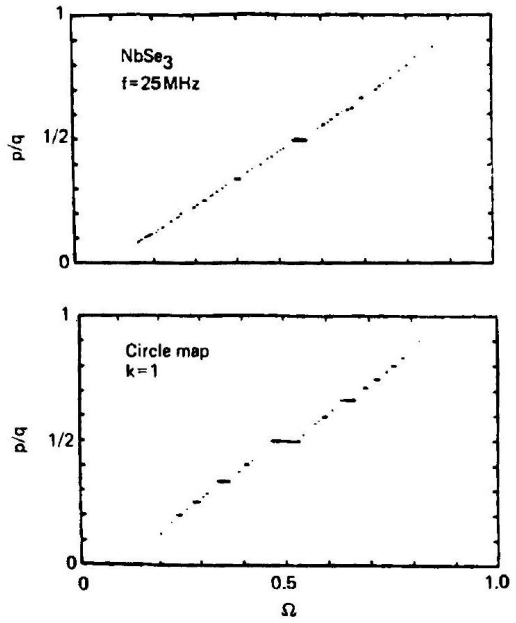


Figure 11.15. Widths of interference peaks for a NbSe_{3} sample and for the circle map, with p/q marked on the vertical axis (Brown et al., 1986).

The detailed dependence of the subharmonic steps on the ac amplitude and frequency was also investigated, and characteristic experimental results are displayed in Fig. 11.15. Similarly to the Shapiro step corresponding to the fundamental (see Fig. 11.10), subharmonic Shapiro steps also display a characteristic Bessel function behavior, and in general have an amplitude which is reduced when compared to the fundamental Shapiro step. Although it is anticipated that an analysis in terms of Eq. (10.3) will provide an adequate explanation of the experimental results displayed in Fig. 11.15, such analysis has not been performed to date.

The appearance of subharmonic mode locking has generated wide interest, mainly because within the framework of the classical particle model such as described by Eq. (10.3) no subharmonics are expected for an overdamped response (Waldram and $\mathrm{W_u}$, 1982; Renne and Poulder, 1974; Alstrom et al., 1984). Several rather different explanations have been advanced to account for the subharmonic mode locking, emphasizing the importance of internal degrees of freedom; assuming a nonsinusoidal potential or making the ad hoc assumption that inertia effects are important in the current carrying state.

In this latter case the time development of the phase δ is described by a return map (Bak et al., 1984; Alstrom et al., 1984)

$$\Theta_{n+1} = f\left(\Theta_n, \Omega\right) \tag{11.18}$$

where $1/\Omega$ is a "strobing rate" at which Θ is measured ($\Omega = f_1/f_{\mathrm{drive}}$ is a convenient choice for ac driven systems). The reduction of the relevant coordinates provides the motivation for the study of simple maps and their relation to complicated dynamical systems. This idea has often been applied successfully for Rayleigh-Bernard instabilities in fluids.

The widths of the subharmonic steps, shown in Fig. 11.13, can be analyzed analogously to that done for the circle map, where universal scaling properties have been conjectured for the quasiperiodic route to chaos (Bak, 1983; Bak et al., 1984; Azbel and Bak, 1984). The circle map is a one-dimensional map with the following rule for the phase

$$\Theta_{n+1} = f\left(\Theta_n\right) + \Omega - \left(K/2\pi\right)\sin\left(2\pi\Theta_n\right), \tag{11.19}$$

and is considered a classic problem of competing periodicities, one coming from the phase space variable (Θ_1 is defined module 1) and the other from Ω. For any value of $K \leq 1$ the interactions of the map may converge to a limit cycle such that $\Theta_{n+q} = p + \Theta_n$ for a nonzero interval Ω (indicating a p/q subharmonic). When $K = 1$ every rational Ω will result in this kind of trajectory, and the plateaus form a staircase structure such as shown in Fig. 11.16. The staircase is said to be complete if the number of steps in an interval I of width greater than a discrimination level r obeys

$$N(r) = \frac{1 - S(r)}{r} \sim r^{-D}, D < 1. \tag{11.20}$$

where $S(r)$ is the sum of the step widths that are greater than r.

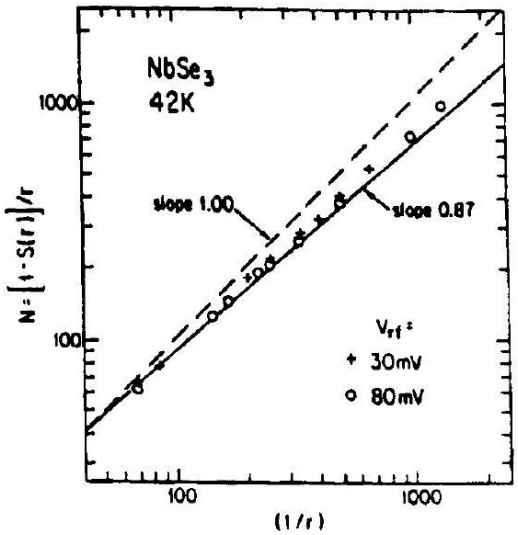


Figure 11.16. Experimental determination of the dimensionality D (see Eq. (11.20)).

The exponent D defines the (fractal) dimension of the staircase. For $K < 1$ the staircase is not complete and $D = 1$. At criticality ($K = 1$), $D = 0.87$ was calculated (Bak et al., 1984) and a similar value was found by analog simulations (Yeh et al., 1984), while for $K > 1$ the staircase structure breaks down and the motion is chaotic. A staircase, derived from differential resistance curves similar to that presented in Fig. 11.12, is also shown in Fig. 11.16. For both the circle map and $NbSe_3$ system, the smallest steps have been left out of the figure, but the two staircase structures are qualitatively similar, and in both cases the steps are in general larger for smaller q values.

The experimental results displayed in Fig. 11.12 have been used to evaluate the fractal dimension D (Brown et al., 1984). The construction $N(r)$ versus $1/r$ is shown in Fig. 11.17, leading to $D = 0.91 \pm 0.03$ in surprisingly good agreement with calculated values, and to those obtained from analog simulations. There are, however, several problems with such analysis. First, a complete staircase, $D < 1$ is expected only if the parameters of the system are measured at the phase boundary of the chaotic regime, i.e., for a well defined V_{ac} value. Experimental evaluations of D can also be limited by finite (instrumental or intrinsic) noise levels,

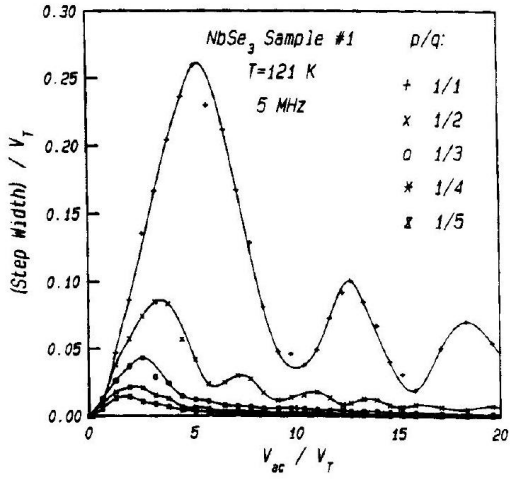


Figure 11.17. Widths of selected steps in the $dcI - V$ characteristic versus peak ac amplitude for the applied ac frequency of 5 MHz . The period of the oscillations with ac amplitude varies as $1/q$ for the p/q step. The solid lines are guides to the eye (Thorne et al., 1987b).

smearing out the smaller steps. Also, computer studies of the sine circle map (Yeh et al., 1984), indicate that $D \sim 0.9$ can be obtained over a finite range of the parameter $K \leq 1$ if the smaller steps are not considered in the evaluation. This may occur for the CDW system as well. The good agreement between the fractal dimension, observed experimentally, and calculated on the basis of simple equations of motion, is most probably fortuitous, and cannot be regarded as evidence for a transition to chaos in the driven nonlinear system.

An alternative, conceptually simple explanation for the subharmonic steps has been advanced by Bardeen (see Thorne et al., 1986). The argument is based on a sinusoidal potential and employes arguments used originally by Shapiro (1963) to account for the steps in the Josephson junctions irradiated by microwave fields. The theorem that no subharmonics are expected in the overdamped response holds only for a sinusoidal potential which does not have higher harmonic Fourier components. Any other
potential gives both harmonic and subharmonic locking, and consequently the observations are not surprising. The approach which is used to calculate the magnitude of the interference regions is the following (Thorne et al., 1986, 1987a). The current carried by the collective mode is given by equation

$$\phi(t) = \langle\phi\rangle_{L^3_{in}} \int_{L^3_{in}} \phi dr^3$$

and the time dependence of the average phase is, in the presence of applied ac and dc fields

$$\frac{d\Theta}{dt} = -\omega_{it} + A\cos(\omega_{\text{ext}}\, t)\,; \tag{11.21}$$

where ω_d is the drift frequency $\omega_d = v_d/\lambda_0$ and A is proportional to the amplitude of the applied ac current. The time dependence of the phase then is

$$\Theta(t) = \omega_d t + \left(\frac{A}{\omega}\right)\sin(\omega_{\text{ext}}\, t) + \Theta_0. \tag{11.22}$$

This pinning potential can be Fourier expanded

$$V(\Theta) = \frac{a_0}{2} + \sum_{q=1}^{\infty} a_q(q\alpha\theta) \tag{11.23}$$

where $\alpha = 1$ for a periodicity given by the wavelength λ_0. After some algebra

$$V(\theta) = \frac{q_0}{2} + \sum_{q=1}^{x} \sum_{p=\infty}^{\infty} a_q J_p \left(q\alpha \frac{A}{\omega} \right) x \cos\left[(p\omega - q\omega_0)\, t + q\alpha\theta_0 \right] \tag{11.24}$$

where J_p is the Bessel function of order p.
The conditions of phase locking depend on the equations of motion for the collective mode, but in general phase locking occurs if the time average pinning energy in the locked state is smaller than in the unlocked state. Without locking the time average pinning energy $\langle V(\theta) \rangle_t = a_0/2$, and for $p\omega_{\text{ext}} = q\omega_d$ an additional polarization energy

$$l \left\langle V\left(\theta_0\right) \right\rangle = \sum_q a_q I_q \left(q \frac{A}{\omega} \right) \cos\left(q\theta_0\right) \tag{11.25}$$

is obtained. The polarization energy is less than zero for a range
of $\theta_0 - \theta_m < \theta_0 < \theta_m$ and θ_m determines the width of the step. $V(\theta)$ as given by Eq. (11.24) has been used to evaluate θ_m for different p and q values. As expected, both the harmonics and the subharmonics display a characteristic Bessel function behavior in broad agreement with the experimental results. The period of the oscillations with ac amplitude A varies linearly with frequency and inversely with q also in agreement with the observations as indicated in Fig. 11.17. In general, the agreement between experiment and theory is satisfactory for a broad range of applied ac frequencies and amplitudes (Thorne et al., 1987b). A similar agreement would, however, be obtained by any potential which has the same periodicity as that of Eq. (5.14) and has smooth minima separated by cusps.

A rather difterent concept has been developed by Tua and Ruvalds (1985), by Littlewood (1986), and by Matsukawa (1987) by extending the models which incorporate the internal degrees of freedom (discussed in the previous section), to account for the interference phenomena observed. Both conclude that the internal degrees of freedom lead to subharmonic mode locking even under circumstances where single degree of freedom dynamics lead only to locking corresponding to harmonic frequencies. The classical dynamics of coupled domains has been used by Tua and Zawadowski (1984) to account for the current-voltage characteristics and for the finite size effects associated with the current oscillations. The extension of the model to combined *dc* and *ac* drives (Tua and Ruvalds, 1985) leads to subharmonic steps, and to an apparent complete Devil's staircase. The overall amplitudes of the subharmonics agree well with the experiments. The calculations also lead to a subharmonic structure which depends only slightly on the drive conditions, with no critical values dividing complete and incomplete staircase behavior; in striking agreement with the experimental observations. The amplitude of the steps was found to decrease with the increasing number of domains, and the steps disappear in the thermodynamic limit. This feature of the results is in clear contrast with the hydrodynamic treatment of Sneddon et al. (1982) which predicts that (while the current oscillations are a finite size effect) interference peaks are recovered in the thermodynamic limit. The origin of this disagreement is not fully understood.

The model where the internal degrees of freedom are incorporated following the Fukuyama-Lee-Rice model (Fukuyama and Lee, 1978; Lee and Rice, 1979) has also been used to study the response of charge density waves to a combination of *dc* and *ac* drives (Coppersmith and Littlewood, 1986). As discussed earlier, second order perturbation treatment in the hydrodynamic limit (Sneddon et al., 1982) leads to interfererice effects involving the fundamental and higher harmonics. Higher order perturbation theory leads to interference features (Coppersmith and Littlewood, 1985a, b), i.e., sharp peaks in the dI/dV curves; but not full mode locking with plateaus as displayed in Fig. 11.14. Complete mode locking is recovered by numerical simulations on finite size systems where the advance of the average phase $\langle \phi \rangle$ is monitored.

The results of the calculations, which display advances $\Delta\phi/2\pi$ corresponding to various mode lockings p/q, are shown in Fig. 11.18. The detailed waveform near mode locking has also been calculated by Coppersmith and Littlewood. The overall tendency of the experimental results, which are suggestive of so-called interference "features" (i.e., not complete mode locking) at high frequencies, and complete mode locking with well defined plateaus in dV/dI curves at low frequencies (Brown and Grüner, unpublished); is well reproduced by calculations which take the dynamics of internal degrees of freedom explicitly into account. Interference curves, calculated on the basis of single degree of freedom classical dynamics (called GZC) model (see Eq. (4.2)) and on the basis of the Fukuyama-Lee-Rice model are shown in Fig. 11.19, together with experimental curves, shown as the full line. The absence of well defined "wings" in experimental and numerical simulations based on the FLR model are taken as evidence of the dynamics of the internal mode. Both harmonic and subharmonic mode locking are also recovered by perturbational analysis of the Fukuyama-Lee-Rice model in the presence of combined *ac* and *dc* electric fields (Matsukawa, 1987). The model leads to clear anomalies in the current-voltage characteristics. Whenever $nq = mp$, complete mode locking such as shown in Fig. 11.14, for example, has not been recovered. Although the reason for this is not clear at present, it may be related to the deficiencies of the model itself (Bardeen, 1988), or to the breakdown of the perturbation theory. The conclusion has been sharply

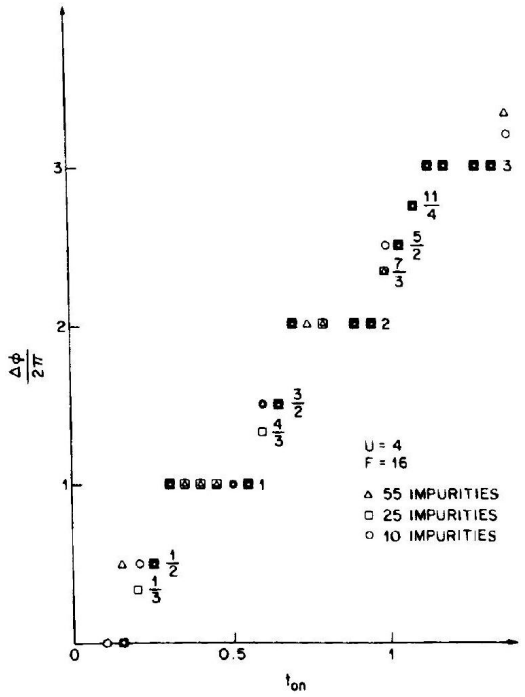


Figure 11.18. Number of wavelengths moved per pulse $\langle\Delta\phi\rangle 2\pi$ versus the pulse duration t_{on} with a fixed $E_{\mathrm{on}} = 16$ for two systems with $U = 4$; one with 55 degrees of freedom and the other with 10 . Locking is demonstrated because $\langle\Delta\phi\rangle 2\pi$ is always a rational fraction. The calculation is based on the Fukuyama-Lee-Rice model (Coppersmith and Littlewood 1986).

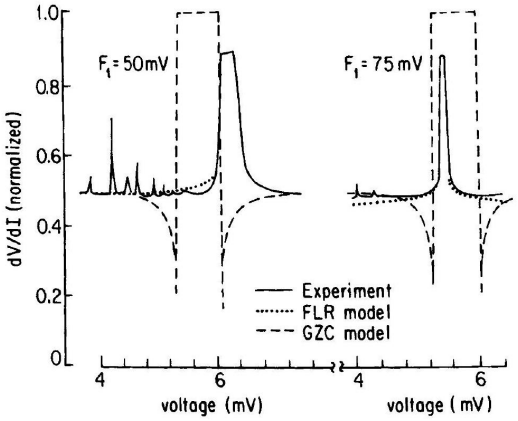


Figure 11.19. Differential resistance dV/dI plotted versus dc voltage V_{0} near the first harmonic feature Q.$v \sim \omega_{\rm AC}$ for $NbSe_3$ with ac frequency $\omega_{ac} = 25$MHz and ac voltage amplitude $V_1 \sim 50$ and 75 mV . The sample's threshold voltage $V_T \sim 2$mV. Also plotted are theoretical fits using the Fukuyama-Lee-Rice deformable model (dotted line) and the Grüner-Zawa-dowski-Chaikih one degree of freedom result (dashed line). The tops of the peaks are not calculated for FLR because the perturbation theory breaks down when the change in dV/dI is large (Coppersmith and Littlewood, 1986).

criticized recently by Thorne et al. (1987), who argued that complete mode locking can also be obtained at high frequencies, in apparent disagreement with the classical descriptions of charge density wave dynamics.

The disagreement between the various experimental results most probably reflects the difference in the degree of coherence in the materials investigated. As a rule, in small and pure specimens, where the phase-phase coherence length may exceed the dimensions of the samples; a highly coherent response, with
pronounced complete mode locking is observed even at high frequencies. In contrast, samples with less coherence display complete mode locking only at low frequencies. This difference, and the crossover between the two behaviors, has not yet been investigated in detail.

11.3.3 Nonsinusoidal and Pulse Drives

In the majority of cases, interference effects have been investigated by applying a sinusoidal ac field $E(\omega) = E_0 \sin(\omega_{\rm ext}\, t)$ of various amplitude and frequency. Most of the relevant theories have also been worked out for this particular case, mainly because all experiments on Josephson junctions involving microwave fields have been conducted under such circumstances (Lindelof, 1971). In the radiofrequency spectral range various periodic waveforms can be applied, and this has been used (Brown et al., 1986) to further investigate the various aspects of mode locking. For a periodic square wave drive which oscillates between two values, E_1 and E_2, the former for a time interval t_1, the latter for t_2, the fundamental period is $t = t_1 + t_2$. The terms t_1, t_2, E_1, and E_2 can independently be varied leading to a variety of conditions under which the dynamics of the collective mode can be investigated.

The difference between a sinusoidal drive and pulse drive, the latter with $t_1 = t_2$, is shown in Fig. 11.20. The sharp spikes in the upper part of the figure correspond to the fundamental interference peaks, with the $p/q = \frac{1}{2}$ subharmonics also evident on the figure. The amplitude of the interference peaks is approximately constant for the sinusoidal drive for small dc voltages, and starts to decrease when $|E_{dc} - E_{ac}| < |E_T|$; i.e., when the system is not driven back to the pinned configuration during the experiment. In contrast, the steps are suppressed near zero dc bias for the square wave drive, in the interval where the ac drive amplitude is large enough

that the applied field drives the system from above threshold to above threshold (with opposite polarity) without allowing it to relax to the pinned configuration. As with the sinusoidal drive, the interference peaks are again suppressed at large E_{dc}, for which $|E_{dc} - E_{ac}| < E_T$. The above difference between the results for a sinusoidal and a square wave drive is clearly due to the fact that a finite time in the pinned state is required to observe substantial interference effects. While the overall features of Fig. 11.20 can be reproduced by computer

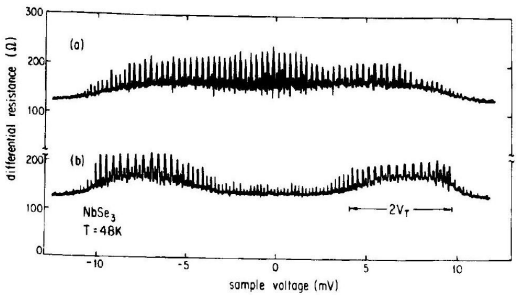


Figure 11.20. Differential resistance curves for (a) sinusoidal *ac* drive and (b) square wave drive for the same amplitude (Brown et al., 1986a, b).

simulations using only single degree of freedom dynamics (Brown et al., 1986a), experiments can also be conducted by varying t_q; the characteristic time spent below E_T, with $E_2 > E_T$ applied for time t_2 varied. Such experiments point to the importance of internal degrees of freedom in the dynamics of the collective mode. The measured step height is shown in Fig. 11.21 as a function of the time t_1 spent below threshold. As expected, the step height approaches zero as t_1 (called $t_$in the figure) gets shorter and saturates in the long time ($t_1 > \infty$) limit. For short times the step height δV can be described by the expression

$$\delta V \sim V_T \left(\frac{t_1}{\tau_0} \right) \tag{11.26}$$

where τ_0 is the characteristic relaxation time of the system. For an overdamped classical particle $\tau_0 = \omega_0^2 \tau$. In the long t_2 limit simple arguments (Brown et al., 1986a, b), based on the classical particle model lead to a step height

$$\delta V \sim V_T \left(\frac{t_1}{t_2} \right). \tag{11.27}$$

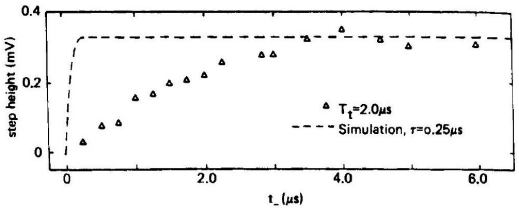


Figure 11.21. Step height amplitude vs. waiting time t. The dashed line is a fit to the simulation based on the classical particle model (Brown et al., 1986a, b).

Computer simulations, with $t_1 = 0.25\mu$ s, obtained by fitting the observed ω dependent response to Eq. (11.27), lead to the dotted line in Fig. 11.21. The difference between the observed step height and that which follows from the classical particle model is significant, and

is most probably a consequence of the dynamics of the internal degrees of freedom (Brown et al., 1986).

A different type of interference effect is called, in general, "pulse duration memory." The notion of pulse duration memory effect refers to the observation which is shown in Fig. 11.22 $K_{0.3}MoO_3$ (Fleming and Schneemeyer, 1986). Square wave voltage pulses which drive the system from the pinned to the current carrying state lead to transient current oscillations with frequencies given by Eq. (11.2). The amplitude of the oscillations gradually decreases with increasing time, and for $t \to \infty$ the magnitudes of the oscillations correspond to those which are measured under *dc* conditions by detecting the Fourier transformed current. This can be thought of as the consequence of gradual dephasing of the current oscillations which start with the same phase but which have slightly different frequencies depending on the local currents within the specimen. At the end of the pulse, there is a sharp upward cusp in the observed current, which occurs for a broad range of pulse durations t_0. The cusp suggests that the system adjusts itself to the pulse duration in such a way that its velocity is always rising as the pulse ends. Apparently, the system

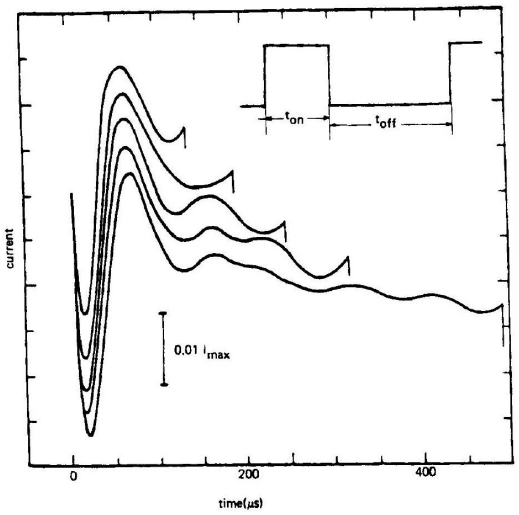


Figure 11.22. Current oscillations in response to a square-wave driving field of about $10 E_{T}$ (inset) in $K_{03}MoO_3$ at 45 K . The data was obtained in a current driven configuration and has been inverted; however the current oscillations are also clearly observed in a voltage-driven configuration. These oscillations have also been reproduced by numerical simulations for a onedimensional system with many degrees of freedom (Fleming and Schneemeyer, 1986).

"remembers" the length of preceding pulses, hence the name "pulse duration memory effect." The upward cusp, as shown in Fig. 11.22, is not observed for single pulses, although the current oscillations are evident.

Clearly a single particle description does not account for this finding as the current is determined by the derivative of the potential at the position of the particle at the end of each pulse.

This can be either negative or positive, depending on t_0. Consequently, the current at the end of each pulse is expected to be a sensitive function of the pulse duration. It has been proposed (Coppersmith and Littlewood, 1986) that the pulse duration memory effect is a consequence of the internal degrees of freedom, where a large number of metastable states and a negative feedback mechanism play a crucial role. A simplified one-dimensional version of the equation of motion, Eq. (10.25), has been examined numerically where a sequence of square wave pulses of length t_0 is applied; with the time $t_{\rm off}$ between pulses long enough for the system to relax to its appropriate metastable state between the applied pulses. The same model also

leads to the subharmonic mode locking discussed earlier. The calculated response waveforms closely resemble those observed by experiment and this is taken as evidence for the importance of internal degrees of freedom in the dynamics. A further elaboration of the model suggests that when the system with infinite degrees of freedom is subjected to identical repeated pulses, it attempts to reach a state for which further pulses do not induce further changes. The fixed point is the least stable, and the pulse duration memory effect is the system's signature of being on the verge of its region of stability.

11.3.4 Fluctuations and Coherence Enhancement

Fluctuation effects associated with the current oscillations, discussed in Section 11.2, are suggestive of coupled domains of size L_0^3 which oscillate at approximately the same frequency $f_0 = j/2e$ with random phase. The Gaussian distribution of the voltages of the narrow band noise shown in Fig. 11.6, is suggestive of independent phase dynamics for the various domains. The modelocking phenomena discussed earlier can be understood on the basis of the dynamics of a single degree of freedom system; however, the volume dependence of the current oscillation amplitudes suggest that the internal degrees of freedom, and the finite size effects are important (Mozurkewich and Grüner, 1983). Also, interference experiments performed for relatively small ac drives give mode locking smaller than that expected for a single degree of freedom dynamics, and this has been interpreted as partial mode locking (Zettl and Grüner, 1984). The reason for this is again most probably the absence of complete phase coherence
throughout the specimens. It is then expected that phase synchronization by the applied ac field leads also to the reduction of incoherent phenomena, such as the broad band noise, or the narrow band noise fluctuations observed in the current carrying state. These have been investigated recently in detail (Bhattacharya et al., 1987; Sherwin and Zettl, 1985). The broad band noise spectrum is significantly reduced during mode locking, with a total noise power reduced to that comparable to that observed in the pinned CDW state (Sherwin and Zettl, 1985). This most probably is related to the freeze-out of the internal degrees of freedom, and may signal the enhancement of the dynamic coherence length which characterized the current-current correlations. Such an effect has been recovered by a perturbational analysis of the Fukuyama-Lee-Rice model in the presence of combined dc and ac drives (Matsukawa, 1987). The reduction is most probably the consequence of phase synchronization between the various domains. This reduces the dynamics to that of a single domain with no fluctuations and consequently no broad band noise. The noise reduction depends on the applied ac amplitude, as shown in Fig. 11.23; where the total measured noise power is plotted as a function of ac current in this current-driven experimental arrangement. The gradual reduction of the noise power is suggestive of a gradual phase homogenization, and a

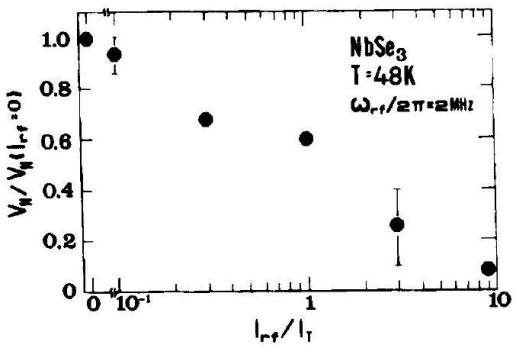


Figure 11.23. Total broad band noise amplitude vs. amplitude of an applied rf current in NbSe_{3}. Intense rf field suppresses the noise by homogenizing the CDW phase (Sherwin and Zettl, 1985).

complete phase homogenization is achieved for ac drive amplitudes which are typically about one order of magnitude larger than those which are required for complete mode-locking.

Fluctuations of the current oscillations are also influenced by the mode-locking, and both the amplitude and frequency fluctuations are reduced. The system synchronized at the $p/q = \frac{1}{2}$ subharmonic steps displays amplitude fluctuation reductions at short time scales, but may fluctuate between various mode locked states (characterized by different oscillation amplitudes) over a large time interval. No amplitude fluctuation reduction has been observed in a more detailed experiment (Bhattacharya et al., 1987) but the frequency distribution of the current oscillations was eliminated by mode-locking. The phenomenon is shown in Fig. 11.24. The upper part of the figure shows the fluctuations of the

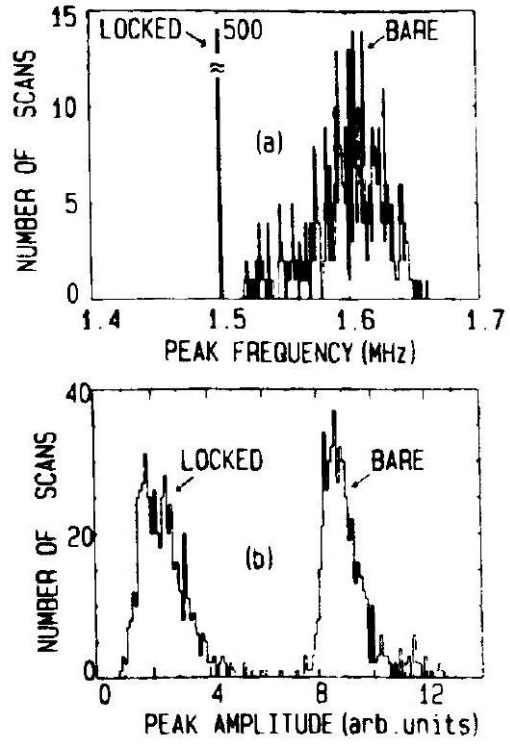


Figure 11.24. Histogram of the temporal fluctuation in frequency (a) and amplitude (b) of a "bare" NBN ($V_{a c}=0$) and a locked NBN ($p/q = 1/2$ at $\omega = 3$MHz). Results represent 500 scans of each case. In (b) the two histograms are shifted arbitrarily for clarity (Bhattacharya et al., 1987).

NBN in position and amplitude without the application of ac drive. When synchronization occurs, the NBN peak frequency does not fluctuate, but the amplitude fluctuation is unchanged. The absence of frequency distribution implies that at mode locking all temporal fluctuations of the oscillation frequency are quenched, i.e., the velocity degrees of freedom are eliminated.

Coherence enhancement and fluctuation suppression, such as observed in driven charge density wave systems, probably represent the most interesting consequences of nonlinear dynamics of many degree of freedom systems. Some aspects of this phenomenon, such as subharmonic mode-locking, under circumstances where a single degree of freedom system would not lead to subharmonic locking, have been explored. It remains to be seen whether or not the essential aspects of coherence can be accounted for.

1.11.4 Conclusions

The current oscillation phenomena which occur in driven charge density wave systems in the nonlinear conductivity region and associated interference effects in the presence of *dc* and *ac* drives are clear manifestations of a new type of collective transport phenomenon, carried by an electron-hole condensate. The linear relation between the time average current and oscillation frequency reflect the fundamental $2k_F$ periodicity associated with the electron hole condensate, and the mere existence of current oscillations in macroscopic specimens is suggestive of macroscopic length scales involved. The collective mode is characterized by an amplitude and phase; and the length scales are related to the phase-phase correlation length, determined by the impurity concentration and the parameters of the collective mode. The highly coherent response clearly demonstrates that they are comparable to the dimensions of the specimens investigated.

In spite of a broad variety of experiments performed in both the time and frequency domains and conducted by employing various combinations of *ac* and *dc* drive amplitudes, frequencies and waveforms, several unresolved questions remain. The linear relation between the time average currents and oscillation frequency is by now well confirmed in all materials which display

CDW transport phenomena; there is however, considerable uncertainty concerning the numerical factors involved. Experiments on TaS_3 suggest that simple arguments advanced in Section 11.2.2 are correct and the oscillation is related to the advancement of the phase by 2π, corresponding to the displacement of the collective mode by one wavelength. Careful experiments in other structurally simple model compounds, such as $(TaSe_4)_2\,I$ and $K_{0.3}MoO_3$ would be highly desirable. The relation, given by Eq. (11.2) holds also only at $T = 0$, and experiments on $NbSe_3$ indicate that the ratio j/f_0 is proportional to the number of condensed electrons. In contrast, in TaS_3 the ratio was found to be only weakly temperature dependent (Brown and Grüner, 1985). Further experiments, in particular the transition temperature near T_p, are needed to clarify whether the proposed relation

$$\frac{j}{f} = 2e\frac{n_{\mathrm{CDW}}(T)}{n_{\mathrm{CDW}}(T=\mathbf{0})} \tag{11.28}$$

is appropriate.

Considerable controversy exists concerning the spectral width of the current oscillations, and the related broad band noise. Broadly speaking, larger spectral widths are accompanied by larger broad band noise amplitudes suggesting that the two types of incoherent effects are strongly related; and that both are determined by the relative magnitudes of the phase-phase correlation length and dimensions of the specimens. One particular model (Bhattacharya et al., 1987) relates the broad band noise amplitude to the spatial and temporal fluctuations of the CDW current, through the relations $\langle \delta V^2 \rangle = \langle \delta I^2 \rangle R_N$; where R_N is the resistance due to

the normal electrons. Fluctuations in CDW velocity also lead to fluctuations in the oscillation frequency explaining the above overall correlation. Studies of the broad band noise amplitude performed on TaS_3 and $NbSe_3$ as a function of the dimensions of the specimens indicate that it is a bulk effect and that noise generation is due to randomly positioned impurities. In contrast, studies on rather pure $NbSe_3$ specimens indicate that macroscopic defects, such as grain boundaries, are the main source of broad band noise. Macroscopic defects, and also random impurities, have also been suggested as the source of the current oscillations. The most probable explanation for the variety of findings is that in general, both impurities and extended boundaries (such as grain boundaries, contacts, etc.) contribute to the noise generation (both broad band and narrow band); but more detailed studies in alloys, or in irradiated specimens where the concentration of pinning centers is systematically varied, are called for to settle this issue.

Fluctuation effects, and clear evidence that the current oscillations disappear in the thermodynamic, infinite volume limit, demonstrate that descriptions of CDW dynamics within the framework of single degree of freedom models is not appropriate. Various experiments however, suggest that the dynamics of the collective mode are characterized by macroscopic length scales. The static phase-phase correlation length (called the FukuyamaLee length) L_0 is, for typical impurity concentrations and CDW parameters, on the order of $10 - 100\mu$ m along the chain directions and one or two orders of magnitude smaller perpendicular to the chains. This leads to a typical "domain" size of $10^{-2}\mu m - 1\mu m$ in broad agreement with estimates of the phase-phase correlation length on the basis of the length dependent threshold field (Monceau et al., 1986; Gill, 1982; Zettl and Grüner, 1984; Borodin et al., 1986), current oscillation amplitudes (Mozurkewich and Grüner, 1983), and broad band noise (Bhattacharya et al., 1985; Richard et al., 1982) implying that the static and dynamic aspects of the problem are characterized by the same length scale (except perhaps near threshold, see Fisher, 1985). As L_0 is expected to be inversely proportional to the impurity concentration, similar experiments on alloys would be of great importance.

Interference effects confirm many of the conclusions which have been reached on the basis of the current oscillation studies alone, but also emphasize the formal similarity between the Josephson phenomena and nonlinear CDW transport. While for small amplitude ac drives fluctuation effects, volume dependences for interference effects, and current oscillations go hand in hand; large amplitude ac drives also lead to phase homogenization, and to interference effects which survive the passage to the thermodynamic limit. Whether or not this corresponds to the conclusions arrived at on the basis of the hydrodynamic treatment of the CDW dynamics (Sneddon et al., 1988) remains to be seen.

Considerable theoretical activity, generated by the observation of subharmonic interference peaks, led to several fundamentally different proposals on the origin of subharmonic locking. Early analysis indicated that the concept of Devil's staircase behavior tied to inertial effects may be appropriate. This possibility is now considered unlikely; two remaining suggestions, nonsinusoidal pinning potential and internal degrees of freedom, are able to explain a broad variety of interference features and mode locking. Most probably, both are important as there is no a priori reason why the pinning potential should be sinusoidal; and there is also a broad variety of independent experimental evidence for the importance of the dynamics of the internal modes of the condensate. The former effect may be more dominant for small specimens where pinning by boundaries such as the surface of the specimens and contacts are important; while the latter may dominate for larger and impure materials where pinning is due to randomly distributed impurities. While the experiments led to several interesting theoretical questions; such as why internal degrees of freedom dynamics mimics many effects which are also the consequence of inertial dynamics, or the concept of minimally stable states; the hope that driven charge density waves can be

appropriate model systems for general questions concerning nonlinear dynamics now appears to be remote. This is mainly because both randomly distributed pinning centers (which lead to a broadly defined localization problem) and extended pinning centers (leading to essentially a boundary problem) are, in general, equally important and cannot be easily separated.

Several issues related to the dynamics of charge density waves have not been discussed in this chapter. In particular, the charge density wave dynamics of specimens which display a so-called "switching" behavior (Zettl and Grüner, 1983; Hall et al., 1986) has not been mentioned. The phenomenon arises as the consequence of macroscopic defects which lead to dynamics similar to those observed in coupled Josephson junctions (Inoui and Doniach, 1987). Several observations concerning transitions to chaos have also not been discussed and I refer to a recent review (Zettl and Grüner, 1986), which covers this type of experiment. Mode-locking phenomena also occur in the elastic properties (Bourne et al., 1986), a not too surprising observation given the fact that the CDW can be regarded as a coupled electron-phonon system, and the earlier observations on nonlinear elastic properties.

Several models, with interesting dynamical properties have not been discussed. Among them, the dynamics of FrenkelKontorova type models have been studied in detail (Sneddon, 1984a; Coppersmith and Littlewood, 1985a,b), and have displayed many of the features which are the consequence of models where random impurity pinning is explicitly taken into account. Such models also lead to a broad variety of interference effects in the presence of combined *dc* and ac electric fields, as discussed earlier.

2 The dynamics of charge-density waves by Grüner

In many materials with a highly anisotropic band structure, electron-phonon interactions lead to a novel type of ground state called the charge-density wave. The condensate is pinned to the underlying lattice by impurities and by boundary effects, but can, even for small electric fields, carry current in a fashion originally envisioned by Fröhlich. This review discusses some of the underlying theories and the main experimental observations on this new collective transport phenomenon. The frequency- and electric-fielddependent conductivity, current oscillations, electric-field-dependent transport coefficients and elastic properties, together with nuclear-magnetic-resonance experiments, provide clear evidence for a translational motion of the condensate. Various theories, involving classical and quantum-mechanical concepts, are able to account for a broad variety of experimental findings, which were also made in the presence of combined dc and ac fields.

2.1 I. Introduction

More than 30 years have elapsed since the basic concepts of the phenomenon which is the subject of this review have surfaced. It was first pointed out by Peierls (1955) that a one-dimensional metal coupled to the underlying lattice is not stable at low temperatures. The ground state of the coupled electron-phonon system is characterized by a gap in the single-particle excitation spectrum and by a collective mode formed by electronhole pairs involving the wave vector $q = 2k_F$. The charge
density associated with the collective mode is given by

$$\rho(\mathbf{r}) = \rho_0 + \rho_1 \cos\left(2\mathbf{k}_F \cdot \mathbf{r} + \varphi\right) \tag{1.1}$$

where ρ_0 is the unperturbed electron density of the metal, and the condensate is called the charge-density wave (CDW). As in superconductors, the order parameter is complex and the phase φ of the condensate is of fundamental importance; its time and spatial derivatives are

related to the electric current and to the condensate density. As noted by Fröhlich (1954), in the absence of pinning and damping, the condensate can carry current leading to superconductivity.

These early ideas resurfaced when the first materials with highly anisotropic crystal and electronic structures became available. The formation of charge-density-wave ground states is by now well documented in a broad range of so-called low-dimensional solids. While some evidence for collective dynamical effects has been found by optical and dielectric measurements in certain organic materials, and also in the pseudo-organic compound potassium platinocyanide called KCP (see, for example, Devreese, Evrard, van Doren, 1979), transport phenomena clearly associated with the dynamics of the collective mode have been found to date mainly in various inorganic linear-chain compounds. Moving CDW's were perhaps first observed by Fogle and Perlstein (1972), who found nonlinear electrical conduction at low electric fields in the compound $K_{0.3}MoO_3$, called the blue bronze, at temperatures below a metal-insulator transition. While this observation received little attention, experiments on nonlinear conduction in the material $NbSe_3$, together with the strongly anomalous microwave conductivity (Monceau et al., 1976), clearly demonstrated the collective nature of the electrical conduction process simply because the energy scale associated with the applied dc field or ac frequency was orders of magnitude smaller than those which would lead to E - and ω-dependent single-particle conduction.

In contrast to superconductors, the phase excitations of the collective mode are gapless. Consequently, electrostatic potentials (due to impurities, grain boundaries, surface effects, etc.) break the translational symmetry and lead to the pinning of the collective mode. This results in a nonconducting but highly polarizable ground state and,
in the case of random impurity distributions, in the absence of long-range order. For weak pinning, the response of the system to dc and ac excitations is dominated by the dynamics of the collective mode with single-particle effects occurring only at optical frequencies. This leads to a strongly frequency-dependent response in the radio frequency to millimeter wave range and, in moderate dc electric fields, to a current-carrying state as originally envisioned by Fröhlich. The discovery of other inorganic linear-chain compounds with a CDW ground state and with an anomalous response to combinations of dc and ac excitations led to the rapid development of the field and to a dazzling variety of experimental observations, only partially accounted for by various theories at present.

This paper gives an overview of the experimental state of affairs, starting with a description of the charge-density-wave ground state, and a short overview of the materials and phase transitions. This is followed by a summary of the fundamental experimental observations on electrical conductivity, other transport coefficients, elastic properties, and experiments involving local probes. Pinning is a central concept that leads to the absence of a dc conduction and to the nonlinear and frequency-dependent phenomena; the broad variety of pinning centers is responsible for the large variation of observations concerning the details of the nonlinear $I-V$ characteristics, and, most probably, for differences in the observed ac response and interference phenomena. The various pinning mechanisms will be discussed in depth, and this is followed, after a short review of theories, by the detailed discussion of the frequency- and fielddependent response and various phenomena that occur in the presence of joint ac and dc excitations. Sections VII and VIII discuss two special topics where the dynamics of charge-density waves were also used to address broader questions concerning the dynamics of driven, many-degrees-of-freedom systems. The two sections, when contrasted, also point to the breadth of phenomena that are observed and that are related to the dynamics of charge-density waves.

Several reviews have appeared recently that discuss the early developments and various aspects of the field (Fleming, 1981; Grüner, 1983a, 1983b, 1983c; Ong, 1983; Grüner and Zettl, 1985; Gill, 1986a, 1986b; Monceau, 1986) which is also the subject of a recent monograph (Monceau, 1986) and proceedings (Charge Density Waves in Solids, edited by Gy. Hutiray

and J. Sólyom, 1985; Proceedings of the XV Yamada Conference on Physics and Chemistry of Quasi-One-Dimensional Conductors, edited by S. Tanaka and K. Uchinokura, 1986).

2.2 II. The Charge-density-wave Ground State

While charge-density waves also occur in materials with two- or three-dimensional band structures, they are predominantly a one-dimensional phenomenon. Consequently, most of the discussions concerning the ground state and the phase transition are based on idealized, one-dimensional models.

Due to the particular geometry of the Fermi surface, a one-dimensional (1D) electron gas is not stable at $T = 0$, and correlation effects lead to phase transitions and to different collective modes at low temperatures. Depending on the details of the electron-electron and electronphonon interactions, various ground states (such as singlet and triplet superconducting), spin-density wave (SDW), and CDW may occur. These (with the exception of triplet superconductivity) have been widely observed in various solids where the Fermi surface is strongly anisotropic. Several recent reviews (Berlinski, 1979; Heeger, 1979; Sólyom, 1979) discuss the nature of the CDW ground state and its thermodynamic and static properties in detail. Therefore only the main features of the phase transition and of the collective charge-densitywave mode will be discussed here, together with the evidence for CDW formation in various inorganic linearchain compounds.

2.2.1 A. The Peierls Transition: Theory

We consider a one-dimensional metal at $T = 0$. In the absence of electron-electron or electron-phonon interaction, the ground state corresponds to the situation shown in Fig. 1(a): The electron states are filled up to the Fermi level ε_F; the lattice is a periodic array of atoms with lattice constant a. In the presence of an electron-phonon

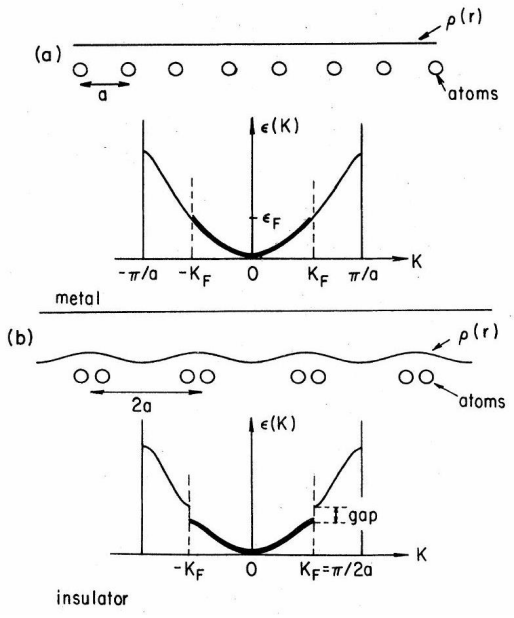


FIG. 1. Peierls distortion in a one-dimensional metal with a half-filled band: (a) undistorted metal; (b) Peierls insulator.

interaction, it is energetically favorable to introduce a periodic lattice distortion with period λ related to the Fermi wave vector k_F by

$$\lambda = \frac{\pi}{k_F}. \tag{2.1}$$

This distortion opens up a gap at the Fermi level as shown in Fig. 1(b), where the situation appropriate for a half-filled band is displayed. Since states only up to $\pm k_F$ are occupied, the development of a gap leads to a lowering of the electronic energy. In one dimension the single-particle gap Δ is proportional to the amplitude of the periodic lattice distortion u, and the decrease of the electronic energy is for small displacements proportional to $u^2 \ln u$. The distortion leads also to an increase of the elastic energy proportional to u^2 (Rice and Strässler, 1973). Consequently, for a small distortion, the total energy of the coupled electron-phonon system is smaller than that of the undistorted metal. The size of the gap and the magnitude of the distortion can be found from the condition for the maximum energy gain. The modification of the dispersion relation also leads to a position-dependent electron density much in the same way as in the nearly-free-electron theory of metals. The density will be a periodic function of the position x with the period also given by Eq. (2.1). (In the following, the direction along which the CDW develops shall in general be called the x direction, and the lattice constant in this direction shall be called a.) For an arbitrary band filling, the period of the charge-density wave (and also the accompanying periodic lattice distortion) is incommensurate with the underlying lattice, i.e., λ/a is irrational.

At finite temperatures normal electrons excited across the single-particle gap screen the electron-phonon interaction. This in turn leads to the reduction of the gap (Kuper, 1955) and of the magnitude of the lattice distortion, and eventually to a second-order transition at the so-called Peierls temperature T_p. The material is a metal above the transition while it is a semiconductor below T_p with a temperature-dependent gap $\Delta(T)$. The main features of this so-called Peierls transition and of the collective mode can be described by the mean-field treatment of the 1D electron-phonon Hamiltonian

$$\begin{aligned}\mathcal{H} = &\sum_{k,\sigma} \varepsilon_k c^+_{k\sigma} c_{k\sigma} + \sum_{k,\sigma} \hbar\omega^0_q b^+_q b_q \\ &+ \sum_{k,q,\sigma} g(k) c^+_{k+q,\sigma} c_{k,\sigma} \left(b_q + b^+_{-q}\right)\end{aligned} \tag{2.2}$$

where $c^+_k\,(c_k)\,, b^+_q\,(b_q)$ are the electron and phonon creation (annihilation) operators with momenta k and q, σ denotes the spin, ε_k and ω^0_q are the electron and phonon dispersions, and $g(k)$ is the electron-phonon coupling constant.

Defining a complex order parameter

$$\Delta e^{i\varphi} = g\,(2k_F) \left\langle b_{2k_F} + b^+_{-2k_F} \right\rangle \tag{2.3}$$

where Δ and φ are real, the displacement field of the ions is given by

$$\left\langle b^+_{2k_F} + b^+_{-2k_F} \right\rangle e^{2ik_F x} + \text{ c.c. } = \frac{2\Delta}{g\,(2k_F)} \cos\left(2k_F x + \varphi\right). \tag{2.4}$$

One can diagonalize the electronic part of the Hamiltonian by setting up a self-consistent equation in a meanfield approximation by replacing b_{2k_F} by $\langle b_{2k_F} \rangle$ and using a linear dispersion relation to describe the electron band near ε_F,

$$\varepsilon_k = v_F\,(|k| - k_F) \tag{2.5}$$

where v_F is the Fermi velocity. The thermodynamics of the CDW state closely resembles that of a superconducting ground state (Sólyom, 1979; Kuper, 1955). The gap Δ in terms of

the dimensionless electron-phonon coupling constant $\lambda' = g^2(2k_F)\left(\omega^0_{2k_F}\varepsilon_F\right)^{-1}$ is given by the BCS gap equation, and at $T = 0$,

$$\Delta = 2D\exp\left(-1/\lambda'\right) \tag{2.6}$$

where the cutoff energy D is the one-dimensional bandwidth. The temperature dependence of Δ also has the characteristic BCS form and vanishes at the transition temperature $T_P = \Delta(T=0)/1.76k_B$.

The temperature-dependent carrier concentration in the condensate $n_c(T)$ is also related to $\Delta(T)$, and close to T_p :

$$\frac{n_c(T)}{n_c(T=0)} = \frac{\pi\Delta(T)}{4k_BT_p} \tag{2.7}$$

while at $T = 0, n_c$ is equal to the number of electrons in the metallic state. The spatially dependent electron density can also be evaluated, and at $T = 0$,

$$\begin{aligned}\rho(x) &= \rho_0 + \frac{\Delta\rho_0}{\lambda' v_F k_F}\cos\left(2k_Fx+\varphi\right)\\ &= \rho_0 + \rho_1\cos\left(2k_Fx+\varphi\right)\end{aligned} \tag{2.8}$$

where ρ_0 is the electron density in the absence of electron-phonon interaction, and is given in one dimension by $\rho_0 = \pi/k_F$. The appearance of a gap in the single-particle excitation spectrum, together with the collective mode described by a complex order parameter [see Eq. (2.3)], is a feature reminiscent of superconductivity. The collective mode here, however, is formed by electron-hole pairs, involving the wave vector $2k_F$ as electrons and holes on the opposite side of the Fermi surface are combined to lead to the CDW and to the accompanying lattice distortion. Furthermore, due to the large cutoff frequency D, which appears in the gap equation (compared to the characteristic phonon frequency, which enters into the superconducting gap), the transition temperatures are considerably larger than superconducting transition temperatures. The fact that in 1D the CDW state is stable at $T = 0$ for whatever small electronphonon coupling constant λ', is the consequence of the logarithmically divergent response function

$$\begin{aligned}F(q,\omega) &= \sum_k \frac{f_{k+q}-f_k}{\varepsilon_k - \varepsilon_{k+q} + \hbar\omega}\\ &\sim \frac{1}{\pi v_F}\frac{2k_F}{q}\ln\left|\frac{1+q/2k_F}{1-q/2k_F}\right|\end{aligned} \tag{2.9}$$

where f is the Fermi distribution function. Consequently, there is an enhanced tendency for CDW formation in materials with highly anisotropic band structure; the latter is in general the consequence of a crystal structure where chains in the x direction are formed.

The mean-field (MF) description neglects the important role of one-dimensional fluctuations and, consequently, leads to a finite transition temperature T_{MF}, even for a strictly one-dimensional metal. Fluctuations strongly suppress the transition (Sólyom, 1979), and for a single 2D metallic chain a phase transition does not occur at finite temperatures. For a system of coupled chains, with coupling due either to the overlap of the electronic wave functions or to Coulomb interactions between the electrons on the neighboring chains, the phase transition is restored at $T \neq 0$ with most of the 1D correlations preserved in the ordered state below the phase transition temperature (Lee et al., 1973; Rice and Strässler, 1973). The general picture that emerges, then, is that materials that are composed of chains and are metals at high temperatures show strong 1D correlations along the chain direction even above a three-dimensional

(3D) transition T_{3D}, leading to a wide fluctuating region for the transition, $T_{3D} < T_p < T_{MF}$. Below T_{3D} the correlations on neighboring chains couple together, leading to three-dimensional long-range order (Sólyom, 1979). The CDW under such circumstances develops along the chain direction. Perpendicular to the chains, the periodic change and lattice modulation are either in-phase or out-of-phase on neighboring chains, depending on the relative magnitude of the perpendicular bandwidth and Coulomb correlations (Sólyom, 1979; Barisic, 1986).

2.2.2 B. The Peierls Transition: Materials and Experiment

Because of the enhanced tendency for nesting Fermi surfaces and, consequently, strongly singular response functions in lower dimensions, materials in which CDW transitions are readily observed have chain or layer structures. Organic conductors, of which tetrathiafulvalenetetracyanoquinodimethane (TTF-TCNQ) is the prototype of one group of solids, have been widely studied (see, for example, Heeger, 1979). Another group of compounds with a CDW ground state are inorganic layer compounds (Wilson et al., 1975) where two-dimensional (2D) charge-density waves develop. Materials discussed in this review are inorganic chain compounds, where the basic structural units form chains with strongly overlapping electronic wave functions along the chains and weak overlap in the perpendicular directions. This leads to a quasi-one-dimensional electronic band structure with relatively wide bands in the chain direction, the necessary
prerequisites for a Peierls transition.
The first inorganic linear-chain material in which CDW transitions were found is $NbSe_3$, the structure of which is shown in Fig. 2. The $NbSe_3$ units form infinite and relatively well-separated chains. They are linked together with $Nb-Se$ bonds in the perpendicular direction. The main features of this structural arrangement are also found in the other members of this tri-chalcogenide group, $TaSe_3, TaS_3$ (both orthorhombic and monoclinic forms, $o-TaS_3$ and $m-TaS_3$), and in the different modifications of NbS_3 (Meerschaut, 1983). While the bonding both within the chain and between the chains varies from compound to compound, this influences only the single-particle properties, such as the conductivity anisotropy, single-particle bandwidth, and the Peierls transition temperature. These differences, however, do not play an important role in the dynamics of the collective mode aside from that of setting an overall energy scale and correlation length. For a strictly onedimensional band, the electron configuration in $NbSe_3$ would correspond to a quarter-filled band (0.5e/at.), but the overlap of the wave functions between neighboring chains leads to a slight deviation from this value (Monceau et al., 1982; Monceau, 1986). Nearly-quarter-filled bands are also expected for other members of this family of compounds. Materials, called the halogen transitionmetal tetrachalcogens $(MX_y)_n$, where the transition metal $M =$ Nb or Ta, $X =$ S or Se , and $h =$ I, Br, or Cl , represent another group of materials where transitions to CDW ground states were observed. Here chains of (MX_y) units are separated by halogen chains. While $NbSe_3$

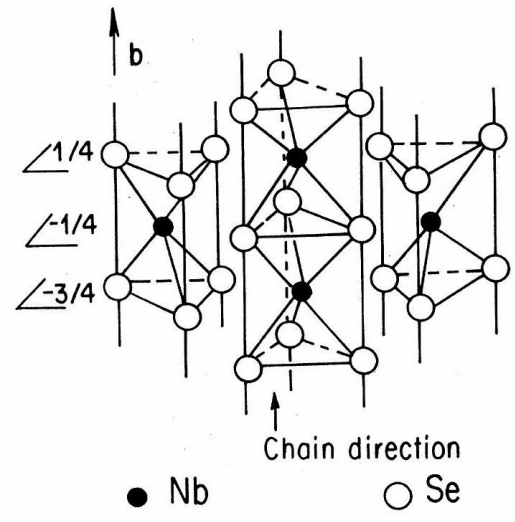


FIG. 2. Crystal structure of NbSe_{3}.

most of the members of this group are semiconductors (Rouxel, 1982), $(TaSe_4)_2\,I$ (Wang, Monceau, et al., 1983; Zettl and Grüner, 1983c), $(NbSe_4)_{3.33}\,I$ (Wang, Monceau et al., 1983), and $(NbSe_4)_2\,I$ (Fujishita et al., 1984) undergo Peierls transitions below room temperature.

Another group of linear-chain compounds, of which $K_{0.3}MoO_3$ and $Rb_{0.3}MoO_3$ are the prime examples, also develop charge-density-wave ground states below room temperature. The MoO_6 octohedra form chains, separated by chains of alkali-metal atoms (Fogle and Perlstein, 1972), leading to a quasi-two-dimensional crystal structure, but to nearly a one-dimensional band structure (Schlenker and Dumas, 1986).

In all of these compounds the highly anisotropic single-particle band is the consequence of not only the chain structure but also of the strong overlap of the d orbitals along the chain direction, with no direct $d-d$ overlap perpendicular to the chains. Consequently, the materials are relatively good metals along the chain directions with room-temperature conductivities parallel to the chains, $\sigma_{\|}$on the order of $\sim 10^3 - 10^4 \Omega^{-1}$ cm^{-1}. The conductivity perpendicular to the chains is between 10 and 10^3 times smaller (Fogle and Perlstein, 1972; Ong and Monceau, 1977; Ong and Brill, 1978). As σ is (in tight-binding approximation) proportional to the square of the transfer integral, this suggests a band with anisotropy between 3 and 30 . Both the magnetic susceptibility (Johnston, 1984; Johnston et al., 1985) and the thermoelectric power are small in these materials and are metallic at room temperature and above. Moreover, both can be analyzed using standard formulas appropriate for a narrow one-dimensional band. Such analysis leads to bandwidths of the order of $1 - 3$eV, typical to d-band metals, and Fermi velocities of the order of 3×10^7cm/sec. Detailed analysis of these features demonstrates that electron-electron interactions are not important in these compounds (Grüner and Zettl, 1985).

The above materials undergo a second-order metal-toinsulator (or metal-to-semimetal) transition at below room temperature, as evidenced by a wide range of transport, magnetic, and specific-heat studies. Furthermore, detailed structural studies demonstrate that these transitions are associated with the development of periodic lattice distortions that are incommensurate with the underlying lattice. The compound $NbSe_3$ shows sharp increases of the resistivity $\rho(T)$ (measured along the chain direction) at $T = 144$ K and $T = 59$ K (Haen et al., 1975), as shown in Fig. 3. This indicates a partial destruction of the Fermi surface at these temperatures, which is confirmed by Hall-effect (Ong and Monceau, 1977) and by magnetoresistance (Ong and Brill, 1978) studies. The two phase transitions, and the metalliclike character of $\rho(T)$ is believed to be the consequence of three structurally slightly different chains in the material (Wilson, 1979). One chain remains metallic down to low temperatures, while the two phase

transitions reflect the development of lattice distortions in the remaining two chains. Direct evidence for such distortions are obtained from electron

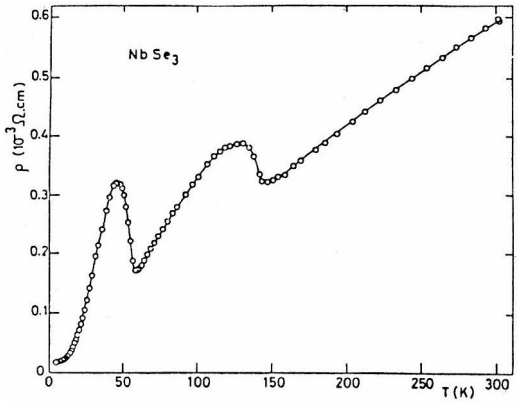


FIG. 3. Temperature dependence of the electrical resistance of NbSe_{3}. Sharp increases of $\rho(T)$ at 144 and 59 K signal the onset of two phase transitions involving different chains.

(Tsutsumi et al., 1978) and x-ray (Fleming et al., 1978, 1984) diffraction studies. Both phase transitions are associated with the development of incommensurate lattice distortions along the chain direction. For approximately 0.5e/ at. in $NbSe_3$, the band is approximately quarterfilled with k_F close to $\pi/4a$. In both CDW states the experimentally determined period is indeed close to $\lambda = 4b$ (the chain direction is denoted by b in this compound) but not exactly equal to 4 times the lattice period, i.e., the charge-density wave and periodic lattice distortion are incommensurate with the underlying lattice.

Another member of the group, TaS_3, occurs in two modifications, orthorhombic ($o-TaS_3$) and monoclinic ($m-TaS_3$). The former has one type of chain (this has not been determined by structural studies, but is suggested by the observation of a single phase transition) and one phase transition at $T_P = 220$ K, the latter two transitions at $T_1 = 240$ K and at $T_2 = 160$ K. In $o-TaS_3$, the whole Fermi surface is removed by the transition; consequently, the material is a semiconductor below T_P, as indicated by the temperature dependence of the dc conductivity measured along the chain direction. This is also the case for $(TaSe_4)_2 I$ and for $K_{0.3}MoO_3$, with the former having a Peierls transition at $T = 265$ K and the latter at $T = 180$ K . Besides the semiconducting behavior of the dc conductivities (all measured along the chain direction), other transport coefficients such as the thermoelectric power or Hall effect confirm that for low dc electric fields, the conductivity is due to carrier excitations across the singleparticle gap. They all can be described consistently in terms of standard formulas appropriate for band semiconductors. The materials, for which the conductivity is displayed in Fig. 4, are more anisotropic than $NbSe_3$. Consequently, 1D fluctuations play an important role above the three-dimensional ordering temperature, and

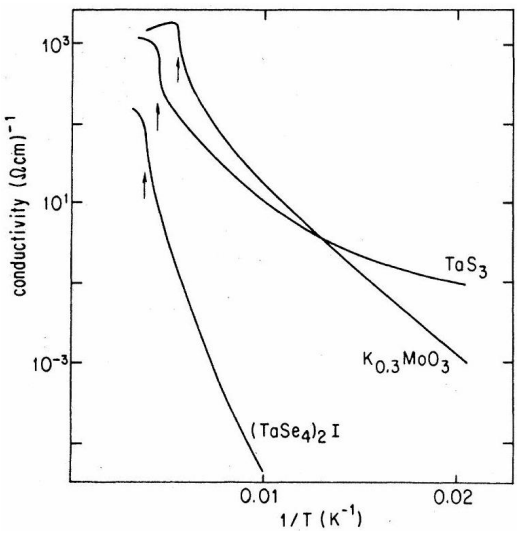


FIG. 4. Temperature dependence of the electrical conductivity in $o-\mathrm{TaS}_{3}$, in $(TaSe_4)_2\,I$, and in $K_{0.3}MoO_3$. The arrows represent the Peierls transition temperatures; they are evident by examining the temperature derivatives dR/dT.

the anomalies in the transport and magnetic properties can be well described (Johnston, 1984) in terms of theories that treat these fluctuation effects (Lee et al., 1973; Rice and Strässler, 1973).

The single-particle gaps have also been determined directly by optical measurements (Brill and Herr, 1983; Challener and Richards, 1984; Geserich et al., 1986). They agree in general with the gaps that are determined from the temperature dependence of the dc conductivity below T_P. In all cases the ratio $2\Delta/k_BT_p$ is significantly larger than the mean-field BCS value of $2\Delta/k_BT_p = 3.5$, most probably because of the large anisotropy that leads to a three-dimensional ordering temperature significantly smaller than the mean-field transition temperature. Large gap values have been observed also in $NbSe_3$ (Fournel, Sorbier, Konczykowski, and Monceau, 1986). Here strong-coupling effects have been suggested to be important. The gaps that have been obtained by tunneling are different from the single-particle gaps evaluated from optical studies (Challener and Richards, 1984); the reason for this difference is not clear.

The metal-to-semiconductor transition is also associated with the development of incommensurate CDW's in these compounds [TaS_3 : Tsutsumi et al., 1978, Roucau, 1983; $(TaSe_4)_2\,I$: Fujishita et al., 1984; $K_{0.3}MoO_3$: Pouget et al., 1983, Sato et al., 1983, Tamegai et al., 1985], with periods in qualitative agreement with those inferred from valence structure arguments. Below the phase transition, the phase-phase correlation length is extremely long, exceeding 1μ along the chain direction. This has been most thoroughly established by high-resolution synchrotron radiation studies in $NbSe_3$ (Fleming et al., 1984) and in $K_{0.3}MoO_3$ (Fleming et al., 1985c). Perpendicular to the chains, long correlation length was found in $K_{0.3}MoO_3$ (Fleming et al., 1985c); in other materials this could not be measured due to the mosaic structure of the crystals investigated. The temperature dependence of the amplitude of the superlattice reflections gives directly the order parameter Δ. The intensity of the reflections (proportional to Δ^2) as a function of temperature is shown in Fig. 5 for some of the

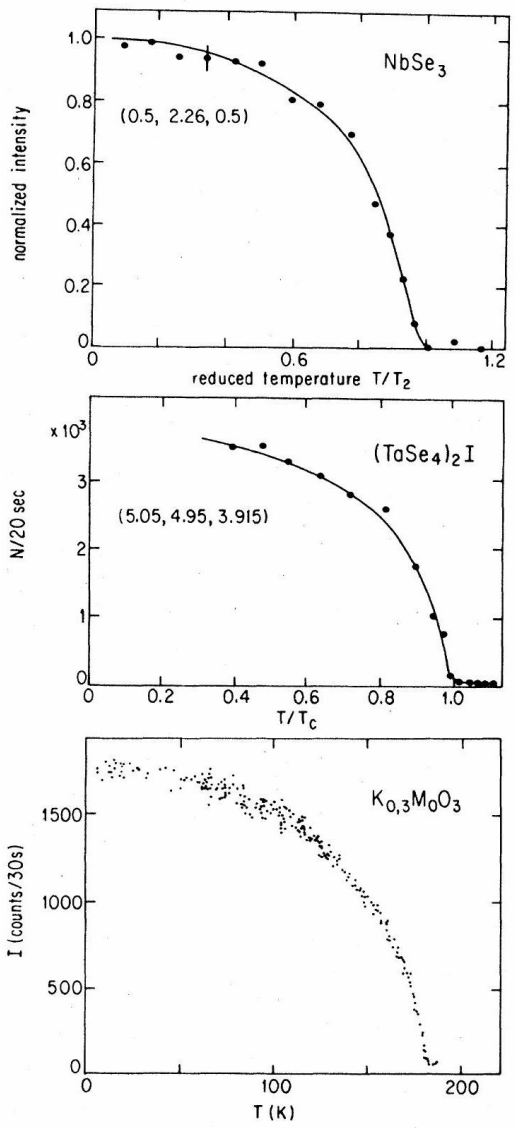


FIG. 5. Temperature dependence of the superlattice reflection intensities in NbSe_{3} (lower transition) (Fleming, 1980), in $(TaSe_4)_2\,I$ (Fujishita et al., 1984), and in $K_{0.3}MoO_3$ (Sato et al., 1983).

compounds. While a fit to a BCS-type temperature dependence for $\Delta(T)$ has not been attempted, it is evident that in all cases a description in terms of a temperaturedependent gap that goes to zero at the second-order phase transition is appropriate.

While in $NbSe_3$ and in $(TaSe_4)_2\,I$ the wave vector of the CDW is independent of the temperature and the lattice distortion remains incommensurate, in $o-TaS_3$ (Wang et al., 1983c) and in $K_{0.3}MoO_3$ (Sato et al., 1983; Fleming, Schneemeyer, and Moncton, 1985) the chargedensity wave becomes commensurate with $\lambda = 4a$ at low temperatures. This has been firmly established in $K_{0.3}MoO$, but in $o-TaS_3$ the evidence for lock-in at wave vector $\lambda = 4a$ is weaker. This is expected to have important consequences for the dynamics of the collective mode.

Unusual domain structures associated with the CDW superlattice have been found in $NbSe_3$ (Fung and Steeds, 1980) and in $o-TaS_3$ (Chen and Fleming, 1983). These were studied by examining the dark field electron microscope images associated with the superlattice reflections in the CDW state. Although many of the details are not entirely reproducible, a domain structure with a typical size of 1μ along the chain direction and approximately 300Å perpendicular to the chains has been observed in both compounds. Superimposed on this large-scale domain pattern

are smaller domains of the size of 20×20Å. The images are time dependent and the domains appear in constant motion, with a characteristic time scale on the order of seconds. The origin of this domain pattern has not been explained yet, although it is evident that it represents some kind of instability in the CDW superlattice. Slight changes in the direction of the wave vector $2k_F$, which characterizes the CDW distortion, may explain the observations (Fung and Steeds, 1980). It has also been suggested (Wilson, 1979; Bak, 1982a) that the small domains reflect discommensurations. As λ is close to $4a$ both in $NbSe_3$ and in TaS_3, the CDW's may become commensurate with the lattice over a macroscopic region by breaking into domains separated by phase slips between domains of commensurate CDW sections. The observed domain structure, however, has no clear relation to the dynamical behavior of charge-density waves. While the pattern is time dependent, an applied electric field that leads to a current-carrying CDW state does not induce any changes in the size or in the time dependence of the domain pattern. Although several observations concerning the response of CDW's to applied electric fields can be explained tentatively in terms of the dynamics of coupled domains, a direct correlation between these observations and those made by dark field electron microscope studies has not been attempted yet.

2.3 III. The Dynamics of the Collective Mode: Some Basic Results

In the Peierls state the material is expected to be a semiconductor, with the various properties determined
by carrier excitations across the single-particle gap. The dc resistivity due to these excitations displays an exponential temperature dependence, with deviations from Ohm's law only at rather high electric field. The optical properties are also determined by the gap, which, in general, corresponds to $\hbar\omega$ in the visible-to-infrared spectral range. In addition to these single-particle phenomena, the coupled electron-phonon system can contribute to charge transport by moving the CDW rigidly, while the ions that are involved in the periodic lattice distribution execute only oscillatory motion. The energy of an incommensurate CDW is independent of the phase φ; consequently, the translational motion could be induced by small dc electric fields. In the absence of damping, this would also lead to a supercurrent, as described by Fröhlich (1954).

No evidence for such anomalous conductivity is found when the experiments are performed in small dc fields; under such circumstances all transport coefficients can be described in terms of standard single-particle transport theories appropriate for a band semiconductor. It has been emphasized first by Lee, Rice, and Anderson (1974) that, in contrast to superconductors, the phase of the CDW condensate can be pinned to the lattice through the interaction with impurities, lattice imperfections, grain boundaries, etc. Consequently, the collective-mode contribution to the dc conductivity measured at low electric fields is zero. However, the pinning energy per electron can be much smaller than the single-particle energies Δ and ε_F, and, consequently, the response to finite amplitude dc and to ac excitations is dominated by the dynamics of the collective mode.

2.3.1 A. Fundamental Concepts

The dynamics of the collective mode is described in terms of a position- and time-dependent order parameter $\Delta(x,t)$. As $\Delta(x,t)$ is complex [see Eq. (2.3)], both amplitude and phase fluctuations occur. These can be described by assuming that the two types of fluctuations are decoupled and

$$\Delta(x,t) = (\Delta_0 + \delta)\, e^{i\varphi'} \tag{3.1}$$

where Δ_0 is the equilibrium order parameter, and δ and φ' are the fluctuations from the

equilibrium value. Then to lowest order in δ and φ' the amplitude mode corresponds to $\Delta_{2k_F} + \Delta_{-2k_F} = 2\Delta_0 + 2\delta$, and the phase mode corresponds to $\Delta_{2k_F} - \Delta_{-2k_F} = 2\Delta_0 \Delta\varphi'$. The dispersion relations of these modes were evaluated first by Lee, Rice, and Anderson (1974), using the electron-phonon Hamiltonian (2.2). The electron-phonon interaction transforms the acoustic phonons near the zone boundary into an optical and an acoustic branch with frequencies

$$\Omega_+^2 = \lambda' \left(\omega_{2k_F}\right)^2 + \frac{1}{3}\left(\frac{m}{m^*}\right)\left(v_F q\right)^2 \tag{3.2a}$$

$$\Omega_-^2 = \left(\frac{m}{m^*}\right)\left(v_F q\right)^2 = \left(c_0 q\right)^2, \tag{3.2b}$$

where the effective mass m^* is given in terms of fundamental parameters of the problem λ', ω_{2k_F} and Δ_s by

$$\frac{m^*}{m} = 1 + \frac{4\Delta_s^2}{\hbar^2 \lambda' \left(\omega_{2k_F}\right)^2} \tag{3.3}$$

at $T = 0$. Both modes soften with increasing temperature, while the temperature dependence of the effective mass is given by

$$\frac{m^*}{m} = 1 + \frac{4\Delta_s^2}{\hbar^2 \lambda' \left(\omega_{2k_F}\right)^2} \frac{n_c(T)}{n_c(T=0)} \tag{3.4}$$

with the temperature-dependent carrier density given by Eq. (2.7). While the amplitude mode has a gap, the phase mode is gapless; the $q = 0$ translational mode corresponds to zero excitation energy. The dispersion relation for Ω_+ and $\Omega_-$are shown in Fig. 6. The large effective mass m^* is the consequence of the coupled dynamics of the electrons and phonons: in the case of the $q = 0$ translational mode, the total kinetic energy includes both that of the electrons that execute translational motion and the ions that oscillate about their equilibrium positions. The amplitude mode $\Omega_+$is expected to be Raman active, while the phase mode carries a dipole moment as it involves the motion of condensed electrons across the background of the position changes of the ions. Consequently, the $q = 0$ phase mode carries a current. Equation (3.2) is appropriate in the long wavelength $q^{-1} \gg \lambda$ limit. For shortwavelength fluctuations, deviations from the above dispersion relation occur that are similar to those that arise for optical and acoustic phonons near a zone boundary. In addition, Coulomb interactions may shift the Ω_- branch up to optical frequencies. Uncondensed electrons, however, most likely screen the Coulomb interactions, and Eq. (3.2) is expected to be appropriate.

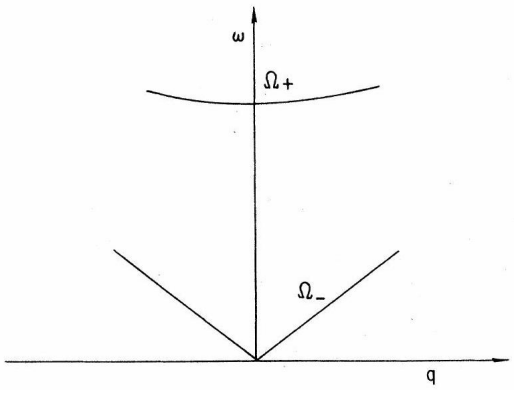


FIG. 6. Phase and amplitude mode dispersion relations.

With a characteristic Fermi energy $\varepsilon_F \sim 1$eV, singleparticle gap $\Delta_s \sim 0.1$eV, and phonon frequency $\omega_{2k_F} \sim 10^{-2}$eV, the electron-phonon coupling constant λ' is of the order of 0.5 [see Eq. (2.6)]. With these values, $\Omega_+(q=0) \sim 5 \times 10^{-3}$eV, which is smaller than Δ_s, and the effective mass is of the order of $m^*/m \sim 10^3$. Several attempts have been made to observe the amplitude mode by Raman scattering, but the mode has not yet been unambiguously determined (Tsang et al., 1978; Travaglini et al., 1983). Due to the gap in the dispersion relation for the amplitude mode, amplitude fluctuations do not play an important role at temperatures $kT \ll \Omega_+$. Therefore most of the descriptions of dynamical collective phenomena are in terms of the dynamics of the phase only. Such a description may be appropriate at low temperatures, but close to the Peierls transition important effects coming from the dynamics of the amplitude mode are expected to occur. By treating the phase as a classical field, the Lagrangian density in one dimension can be written (Brazovskii and Dzyaloshinskii, 1976; Fukuyama, 1976; Fukuyama and Lee, 1978)

$$\mathcal{L} = \frac{n_c}{4\pi}\left[\frac{m^*}{mv_F}\left(\frac{d\varphi}{dT}\right)^2 - \kappa^2\left(\frac{d\varphi}{dx}\right)^2\right] \tag{3.5}$$

to lowest order in the derivatives, and n_c is the carrier density along the chain direction. This form follows from the elimination of the electronic degrees of freedom from the Hamiltonian (2.2) (Brazovskii and Dzyaloshinskii, 1976). The first term on the right-hand side corresponds to the kinetic energy of a line mass m^*n_c per unit length. The second term represents the potential energy associated with the distortions of the collective mode, with a phenomenological elastic constant κ. The equation of motion corresponding to the above Lagrangian is

$$\frac{d^2\varphi}{dt^2} = \frac{m}{m^*}\kappa^2\frac{d^2\varphi}{dx^2} \tag{3.6}$$

The solutions for Eq. (3.6) are of the form $\exp[i(\omega t - qx)]$ with the dispersion relation

$$\Omega_-^2 = \frac{m^*}{m}\kappa^2(kq)^2 \tag{3.7}$$

comparison with Eq. (3.2b) gives the phenomenological elastic constant in terms of v_F as

$$\kappa = V_F \tag{3.8}$$

The plane-wave solutions represent the periodic compression and expansion of the CDW; these excitations are called phasons. The dispersion relations (3.2) and (3.7) also define a phason velocity

$$c_0 = \left(\frac{m}{m^*}\right)^{1/2} v_F \tag{3.9}$$

in which, for $v_F \sim 3 \times 10^7$ cm/sec and for $m^*/m \sim 10^3$, c_0 is approximately 10^6 cm/sec.

As in a superconductor, the phase $\varphi(x,t)$ plays an important role in the dynamics of the collective mode. The $q = 0$ phase mode corresponds to the translational motion of the condensed electrons, with the ions oscillating around their equilibrium positions. A rigid displacement of the CDW leads to an electric current, and the current density per chain $j_{\mathrm{CDW}} = -n_c e v_d = -n_{\mathrm{CDW}} e(d\varphi/dt)$. With $\varphi = 2k_F x$ and $\lambda = \pi/k_F$,

$$j_{\mathrm{CDW}} = \frac{e}{\pi}\frac{d\dot{\varphi}}{dt}. \tag{3.10}$$

A compression of the wave leads to a change of the electronic density, and therefore

$$n_c = \frac{e}{\pi}\frac{d\varphi}{dx} \tag{3.11}$$

at zero temperature. The cross derivatives of the above equations lead to the equation of continuity

$$\frac{dj_{\mathrm{CDW}}}{dx} + \frac{dn_c}{dt} = 0. \tag{3.12}$$

Equation (3.12) is more general than implied by its deviation above and is valid to all orders in the derivative expansion of the phase (Horovitz, 1986). Here and in the previous formulas, the subscript refers to the current carried by the CDW. Subsequently, the subscript will be used only if the effect of normal electrons leading to normal current is also important. Otherwise all quantities (current, current density, cordial and differential conductivity, etc.) refer to transport carried by the collective mode.

The above relations can also be derived by considering the modification of the dispersion relation of electrons in momentum space (Allender et al., 1974; see also Bjelis, 1987). As in a superconductor for a slowly varying $\varphi(x,t)$ (on the time scale much less than $\hbar/\Delta s$) the Fermi surface is tied to the position- and time-dependent condensate. We consider first a slowly varying $\varphi(x)$, for which $(1/k_F)\,(d\varphi/dx) \ll 1$. This can be described as a change in the wave vector $2k_F + d\varphi/dx$; consequently, the single-particle gap is shifted from $\pm k_F$ to $\pm\left[k_F + \frac{1}{2}(d\varphi/dx)\right]$, as shown in Fig. 7. If the electrons do not change their density, then the gap is removed from the Fermi surface. This leads to electrons in states above the gap and to a large increase of the total electronic energy. A change in the electron density, by tying the gap to the Fermi surface, involves less energy. As $\rho(x) = 2k_F(x)/2\pi$, the gap is at the Fermi level if

$$\rho(x) = \rho_0 + \frac{1}{\pi}\frac{d\varphi}{dx}, \tag{3.13}$$

the same relation as Eq. (3.11).

For a time-dependent phase $\varphi(t)$, with $d\varphi/dt = 2k_F v_{\mathrm{CDW}}$, the inversion symmetry is broken and the dispersion relation becomes asymmetric, as shown in Fig. 7(b). The electronic energies are given by (Allender et al., 1974)

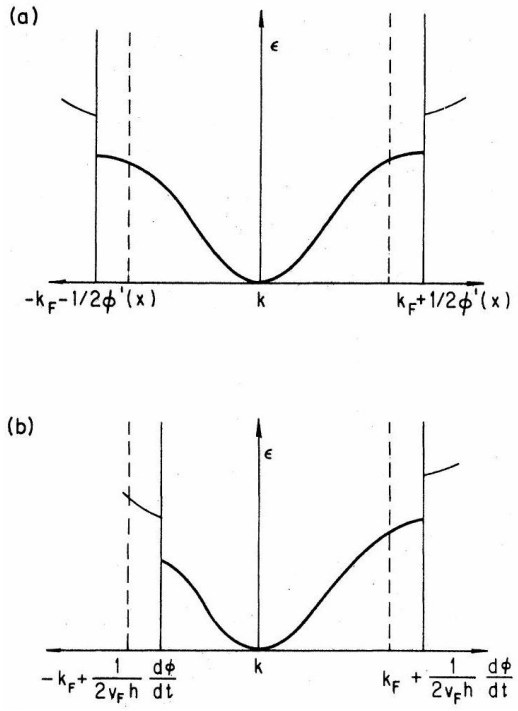


FIG. 7. Displaced Fermi surface for a position- (a) and for a time-dependent (b) phase. The states are filled up to the Fermi level, $\pm\left[k_F+\frac{1}{2}\left[d\,\phi(x)/d\,x\right]\right]$ in (a), and up to $\pm\left[k_F \pm (1/2v_f h)\,(d\phi/dt)\right]$ in (b) indicated in both cases by the solid lines. The dotted lines refer to the original Fermi surface at $\pm k_F$.

$$\varepsilon_{\pm k} = \left[\varepsilon(k) \pm \frac{1}{2}\left(\frac{d\varphi}{dT}\right)^2 + \Delta_s^2\right]^{1/2}. \tag{3.14}$$

The energies corresponding to the displacement Fermi surface are different for positive and negative momenta, leading to different occupation numbers for positive and negative k values. This then leads to a total current

$$j_{\mathrm{CDW}} = 2e\int \frac{d\varepsilon}{dk}\frac{dk}{2\pi} = \frac{e\,(\varepsilon_{+k}-\varepsilon_{-k})}{\pi} = -\frac{e}{\pi}\frac{d\varphi}{dt} \tag{3.15}$$

(where the integration is over all occupied states), the same as Eq. (3.10). This relation, and also Eq. (3.13), breaks down for strong local distortions of the condensate. In such cases both the amplitude and the phase perturbations have to be included. The relation that connects the electric current and condensate density to the time and spatial derivative of the phase $\varphi(x,t)$ of the condensate is different from the relations that are appropriate for a superconductor,

$$p_s = i\hbar\frac{d\varphi}{dx} \quad \text{and } \mu = i\hbar\frac{d\varphi}{dt},$$

where p_s and μ are the momentum and the chemical potential. This arises because, in contrast to the superconducting ground state, the charge-density-wave condensate is formed by electron-hole pairs, and pairing also involves the wave vector $2k_F$.

In the presence of an applied electric field $E(\omega) = E_0 e^{i\omega t}$, the equation of motion becomes

$$\frac{d^2\varphi}{dt^2} + \frac{m}{m^*}\hbar v_F^2\frac{d^2\varphi}{dx^2} = \frac{2k_F eE(\omega)}{m^*} \tag{3.16}$$

and the frequency-dependent conductivity

$$\sigma(\omega) = \frac{j(\omega)}{E(\omega)} = \frac{m}{m^*} \frac{i\omega_p^2}{4\pi(\omega + i\delta)} \tag{3.17}$$

where $\omega_p^2 = 8v_F e^2$ is the plasma frequency. The real part of the conductivity

$$\mathrm{Re}\,\sigma(\omega) = \frac{m}{4m^*}\omega_p^2 \delta(0) \tag{3.18}$$

has a Dirac δ singularity at $\omega = 0$, with an oscillator strength

$$f = \frac{\pi n e^2}{m^*} \tag{3.19}$$

Because of the gap Δ_s in the single-particle excitation spectrum, the ω-dependent response due to singleparticle processes also displays a gap resulting in $\sigma(\omega) = \sigma_{\mathrm{CDW}}(\omega) + \sigma_{\text{single particle}}(\omega)$ displayed in Fig. 8. The oscillator strength that appears at zero frequency is removed from the single-particle excitations that appear at $\omega > 2\Delta_s$. As a consequence, the one-dimensional singularity, which has the form of $(\omega - 2\Delta_s)^{-1/2}$, is removed, and $\sigma(\omega)$ becomes rounded, as shown in Fig. 8(a).

The appearance of a single-particle gap together with the zero-frequency collective mode is reminiscent of superconductivity. Here the $\omega = 0$ mode corresponds to the translationally invariant CDW which, in the absence of damping, would lead to a supercurrent. Various interactions between the CDW and the underlying lattice, however, remove the translational invariance and lead to pinning of the phase of the condensate. Such pinning is brought about by the local distortions of the condensate around pinning centers. When described in terms of a restoring force, pinning effects shift the collective-mode conductivity to finite frequencies (Rice and Strässler, 1973; Lee et al., 1974). With pinning represented by an average pinning frequency ω_0, and also including a phenomenological damping term $\Gamma(d\varphi/dt)$, the equation of motion becomes, for small amplitude displacements,

$$\frac{d^2\varphi}{dt^2} + \frac{1}{\tau}\frac{d\varphi}{dt} + \omega_0^2 \varphi = \frac{2k_F eE}{m^*} \tag{3.20}$$

The frequency-dependent conductivity that corresponds to Eq. (3.20) is given by

$$\sigma(\omega) = \frac{n_c e^2}{i\omega m^*} \frac{\omega^2}{\omega_0^2 - \omega^2 - i\omega/\tau} \tag{3.21}$$

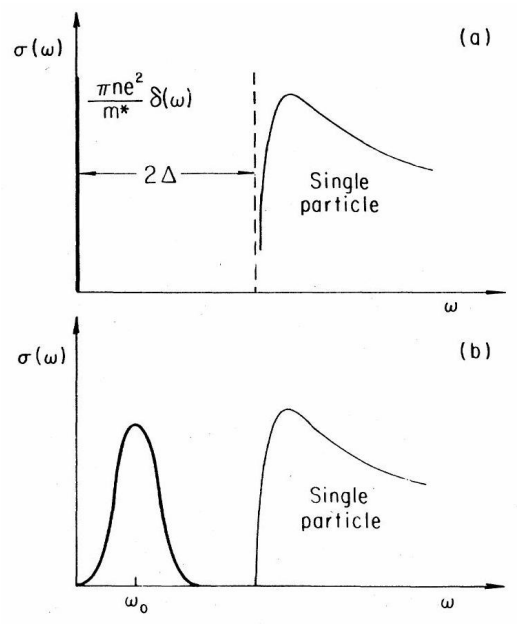


FIG. 8. Frequency-dependent response of the collective mode (a) without pinning, and (b) with pinning and damping. The response at frequencies $\omega > 2\Delta/h$ is due to single-particle excitations.

and is that of an optical mode centered around the frequency ω_0. The dc conductivity, $\mathrm{Re}\,\sigma_{\mathrm{CDW}}(\omega = 0) = 0$, and the zero-frequency dielectric constant is given (including the contribution from excitations across the gap Δ) as

$$\varepsilon(\omega = 0) = 1 + \frac{4\pi n_c e^2}{m^* \omega_0^2} + \frac{4\pi n e^2 \hbar^2}{m\Delta^2} \tag{3.22}$$

The second term on the right-hand side describes the contribution of the collective mode; the third term represents the contribution of single-particle excitations. For weak pinning, where $\hbar\omega_0 \ll \Delta$, Eq. (3.21) leads to the conductivity shown in Fig. 8(b), with the contribution of the pinned mode appearing well within the single-particle gap. This also leads to a giant dielectric constant at low frequencies and to a zero crossing at $\omega = \omega_0$.

Coulomb interactions have been completely neglected in the above analysis; consequently, the picture is expected to be appropriate near the Peierls transition, where the normal electrons are available to screen the Coulomb effects associated with the phason excitations.

2.3.2 B. Frequency- and Electric-field-dependent Conductivity

For band semiconductors the electrical conductivity is independent of frequencies for $\omega < \Delta/\hbar$ and is also independent of electric field for applied fields $eEl < \Delta$, where l is the mean free path. For a typical gap of the
order of 0.1 eV , nonlinear conduction occurs in the kV range, with frequency-dependent conduction observed at optical (infrared) frequencies. In contrast, in the materials discussed before, in the CDW ground state σ is both strongly nonlinear and frequency dependent. In Fig. 9, the frequency-dependent conductivity $\mathrm{Re}\,\sigma(\omega)$ measured along the chain direction is displayed in several compounds. Only experimental results in the region of the single-particle gaps (shown by solid lines) and in the dc to millimeter wave spectral range are displayed for clarity. The solid lines are the results of optical experiments, and the strong decrease of the conductivity with decreasing frequency demonstrates the existence of the singleparticle gaps. The gap values

evaluated from the optical experiments (Zeller, 1974; Geserich et al., 1986; Herr et al., 1986; Travaglini and Wachter, 1984) compare, in general, favorably with the gaps evaluated from the dc conductivity below T_p. The strong resonances observed in the millimeter wave spectral range (Ng et al., 1986; Reagor and Grüner, 1986; Reagor, Sridhar, and Grüner, 1986; Sridhar et al., 1986) indicate a collective response associated with the charge-density-wave ground state, as it is evident that the frequency-dependent response such as that displayed in the figure cannot arise from a singleparticle transport mechanism. The energy that corresponds to the frequency where $\mathrm{Re}\,\sigma(\omega)$ has a maximum is orders of magnitude smaller than the single-particle gap

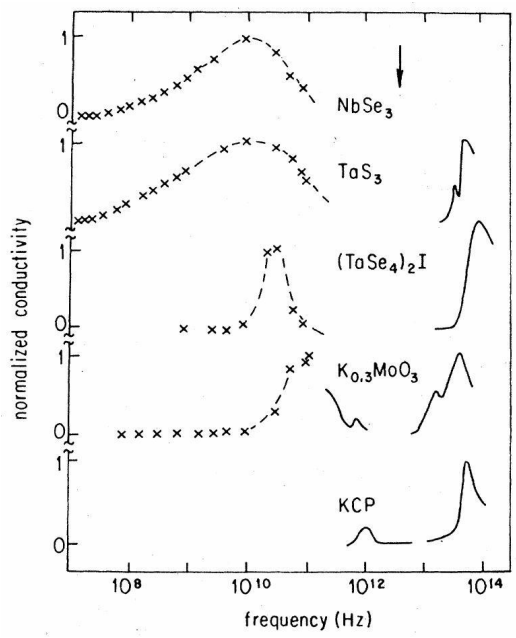


FIG. 9. The frequency-dependent conductivity of NbSe_{3}, $o-TaS_3$ and $(TaSe_4)_2\,I$, and $K_{0.3}MoO_3$. The solid lines represent the regions where the drop signals the single-particle gaps; the strong peaks in the millimeter wave spectral range are due to the response of the pinned collective mode.

and also the thermal energy kT. The oscillator strength that appears at finite frequency (in contrast to what is observed in a superconductor) suggests that the collective mode is pinned to the underlying lattice. This is borne out by detailed investigations on specimens where the impurity concentration is varied. The peak frequency ω_0 can be associated with the pinning frequency ω_0, as discussed in Sec. III. The finite width of the resonances observed may be due to damping effects associated with the dynamics of the collective mode, or, alternatively, can be the consequence of inhomogeneous broadening brought about by randomly positioned impurity pinning centers. Alternatively, a band of heavy carriers with a small gap would also lead to an overall behavior, which is displayed in Fig. 9.

The low-frequency dielectric constant is enormous, in general of the order of 10^7 or more, and this is the consequence of the large oscillator strength which occurs at low frequencies. The zero-frequency dielectric constant is given by

$$\varepsilon(\omega) = \frac{4\pi e^2}{m^*}\int_0^\infty \frac{\mathrm{Re}\,\sigma(\omega)}{\omega^2}d\omega$$

which for a narrow resonance reduces to $\varepsilon \sim 4\pi n e^2/m^*\omega_0^2$, in agreement with Eq. (3.22). Details of $\sigma(\omega)$ and also $\varepsilon(\omega)$ will be discussed later.

The small pinning energy associated with the collective mode suggests that for a small dc electric field, the collective mode can be driven into a current-carrying state with possibly nonlinear current-voltage characteristics. Indeed, nonlinear conductivity has been observed in all the materials discussed before, with a sharp onset field, called the threshold E_T, for the nonlinear conductivity. The detailed form of the nonlinear conduction varies depending on external factors such as temperature, impurity concentration, or macroscopic inhomogeneities (such as grain boundaries) in the specimen.

The dc conductivity, defined as j/E where j is the total current density and E is the applied electric field, is shown in orthorhombic TaS_3 in Fig. 10. Below, a threshold field E_T, approximately 300mV/cm, the conductivity obeys Ohm's law, and the temperature dependence of this component reflects the exponential freezing out of the electrons excited across the single-particle gap. The onset of nonlinear conduction is smooth, as evidenced by the current-voltage characteristics displayed in the figure. A behavior, similar to that displayed in Fig. 10, is found, in general, for the other compounds; the existence of the sharp threshold field E_T is well established. The behavior in the figure can be described in terms of a two-fluid model involving electrons excited across the gap and electrons concerned in the collective mode. The former has an Ohmic contribution; the other, a nonlinear response. The total current can be written as

$$I_{\rm tot} = I_n + I_{\rm CDW} \tag{3.23}$$

where the subscripts n and CDW refer to current carried by the uncondensed and condensed electrons. The validi-

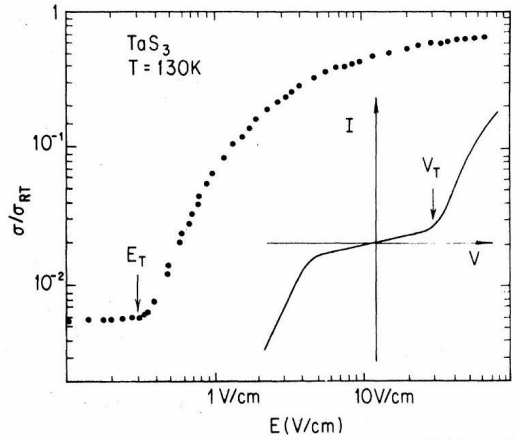


FIG. 10. Electric-field-dependent conductivity $\sigma(E)$ in $o-\mathrm{TaS}_{3}$. The data are normalized to the room-temperature conductivity. The inset shows typical dc I - V characteristics on the same material.

ty of such a two-fluid description has been clearly demonstrated recently by generating nonlinear current-voltage characteristics in an open circuit configuration ($I_{\rm tot} = 0$), where the voltage was generated through the thermoelectric effect (Beyermann et al., 1986).

The current-voltage characteristics are also often explored by measuring the differential resistance dI/dV, employing low-frequency lock-in techniques. While the method cannot be used at high fields because of heating effects, it is advantageous to study the behavior near threshold. The first such measurements where a welldefined E_T was evident is shown in Fig. 11.

The frequency- and field-dependent response is strongly related, and a smaller pinning frequency, and, consequently, a larger dielectric constant, leads to a smaller threshold field,

suggesting that both are related to an overall energy that characterizes the pinning of the collective mode.

The conductivities of various materials, when extrapolated to the infinite electric field limit or measured at frequencies $\omega_{\max}$ where $\mathrm{Re}\,\sigma(\omega)$ is maximum, are finite, and are close to the conductivities that would be observed in the absence of the phase transitions. In terms of a relaxation time τ, the conductivity at high fields or frequencies is written as

$$\sigma_{\mathrm{CDW}}\,(E \to \infty \text{ or } \omega_{\max}) = \frac{ne^2\tau}{m}, \tag{3.24}$$

suggesting that the ratio of the relaxation time to the mass is approximately the same for the uncondensed and condensed electrons, and

$$\frac{\tau_N}{m} \sim \frac{\tau}{m^*}, \tag{3.25}$$

where m is the band mass. This is approximately obeyed

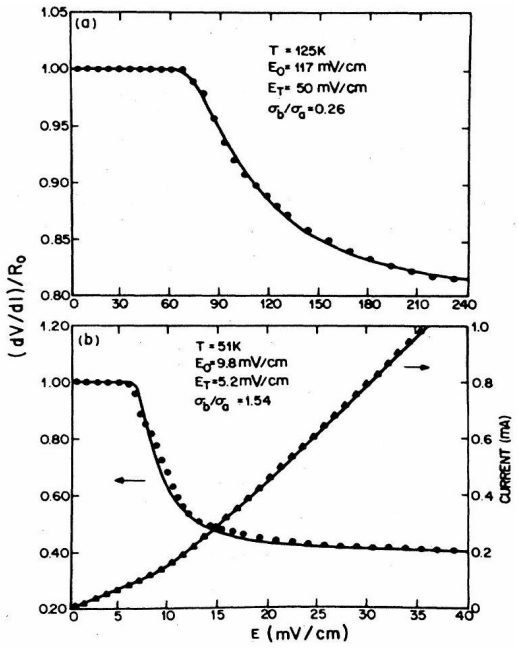


FIG. 11. Normalized differential resistance as a function of dc bias field for the upper (a) and lower (b) CDW states of NbSe_3. A threshold field for the onset of nonlinear conduction is clearly observed. The field dependence of the current is also shown for the low-temperature CDW state. The solid lines correspond to Eq. (5.1) using parameters indicated on the figure.

in $NbSe_3$ (Ong and Monceau, 1977), in $o-TaS_3$ (Sridhar et al., 1986), in $(TaSe_4)_2I$ (Reagor, Sridhar, and Grüner, 1985; Reagor, Sridhar, Maki, and Grüner, 1985), and in $K_{0.3}MoO_3$ (Reagor and Mozurkewich, 1985) at temperatures where the CDW's are incommensurate with the lattice. The high-field conductivity is weakly depressed by small amounts of impurities in $NbSe_3$ (Oda and Ido, 1982); in $o-TaS_3$ the high-frequency conductivity is also fairly insensitive to impurity effects (Reagor and Grüner, 1986). Both suggest that even for a "perfect" crystal, without impurities, sliding charge-density waves would lead to a finite conductivity.

The onset of nonlinear conduction is often rather dramatic and is accompanied by switching and hysteresis effects. These have been observed in $NbSe_3$ (Zettl and Grüner, 1982a), TaS_3 (Mihály and Grüner, 1984), and $K_{0.3}MoO_3$ (Maeda, Furuyama, and Tanaka, 1986; Maeda, Furuyama, Uchinokura and Tanaka, 1986); such effects usually become more pronounced with

decreasing temperature. An example is shown in Fig. 12, where $I - V$ curves recorded in $NbSe_3$ at two different temperatures are displayed. At higher temperatures the onset of nonlinear conduction is accompanied by an oscillatory instability, which, by lowering the temperature gradually, evolves into a hysteretic current-voltage characteristic. The behavior is due to extended pinning centers in the

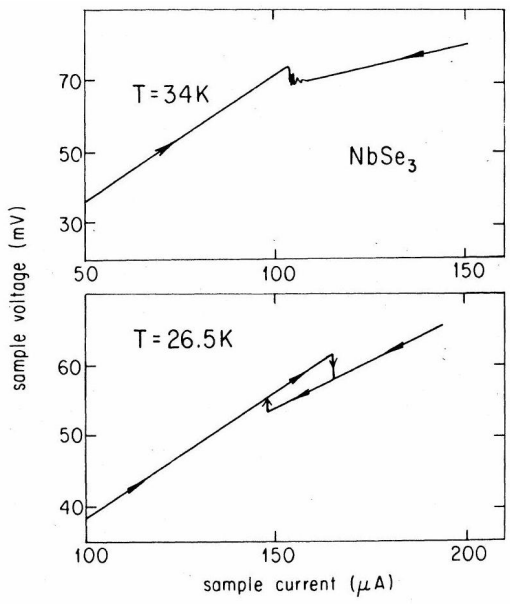


FIG. 12. Current-voltage characteristics observed in NbSe_{3} at two different temperatures (Zettl and Grüner, 1982a, 1982b, 1982c).

materials, and this has been demonstrated directly by locating (by using moving contacts) the exact positions where such behavior is generated (Brown and Mihály, 1985; Hall et al., 1986). At very low temperatures $T \ll T_p$ still a different type of nonlinearity, a rather steep current-voltage characteristic is observed (Mihály and Tessema, 1986), with a threshold field 1 or 2 orders of magnitude larger than E_T where the smooth nonlinear conduction such as that displayed in Fig. 11 occurs. The overall behavior of the current-voltage characteristics, shown in Fig. 13, and the threshold field are similar to those observed in ordinary semiconductors where the effect is due to hot electrons. Consequently, the behavior may be of single-particle origin and not related to the onset of charge-density-wave-transport. However, strong polarization effects, certainly due to deformations of the CDW, are observed below V_T. This would suggest that the nonlinear conduction and charge-density-wave dynamics are intimately related.

The fact that the charge-density wave is not destroyed, but contributes to the dc current for $E > E_T$, in experiments such as those displayed in Figs. 10-12 has been demonstrated by performing x-ray experiments in the nonlinear conduction region (Fleming et al., 1978, 1984). The superlattice reflections were found in the currentcarrying region with intensities equal to those measured without an applied field. The observation demonstrates that the charge-density wave executes a translational motion in the presence of an applied electric field. This

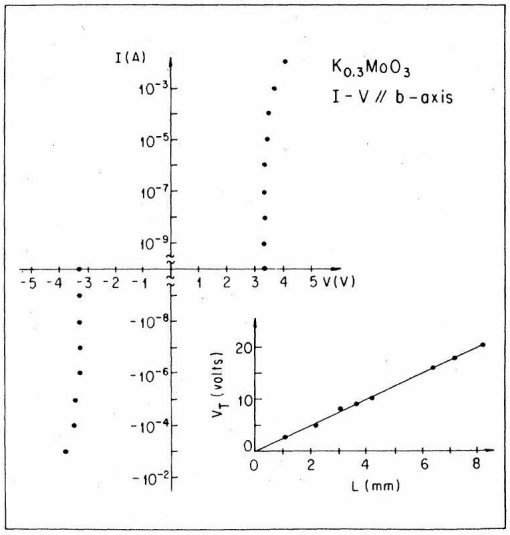


FIG. 13. Current-voltage characteristics measured in $\mathrm{K}_{0.3}\mathrm{MoO}_3$ at low temperatures. Beyond V_T a small change in the applied voltage leads to orders-of-magnitude increase of the current.

has been confirmed by a series of NMR experiments performed in various materials.

Other types of experiments also suggest that the CDW is, by the application of electric fields, driven out of the pinned configuration, and, furthermore, that the dynamics of the internal deformation of the mode is important. Here, the relaxation back to a pinned state is monitored through the measurement of the normal (Ohmic) resistance. Making the natural assumption that local changes of the CDW phase around pinning centers also lead to the changes in the resistance R_n of the normal electrons that are excited across the gap, the time evolution of this quantity can be used as a measure of the above relaxation process. Figure 14 shows R_n as a function of time after an applied electric field larger than E_T is removed (Mihály and Mihály, 1984). A slow, logarithmic time decay

$$R_n(t) - R_n(0) = A_0 \ln \frac{t}{t_0}$$

is observed over many decades in $o-\mathrm{TaS}_3$, with similar sluggish time response in other materials. Here R_{n0} is the normal electron resistance for an "equilibrium" configuration achieved as $t \to \infty$. The observation is qualitatively similar to those made on spin glasses after an applied magnetic field. This similarity is not accidental and suggests the absence of long-range order (and, consequently, a broadly defined "glassy" behavior) for a CDW that is pinned by randomly positioned impurities. More complicated phenomena, such as remanent dielectric polarization, are related to the above observation.

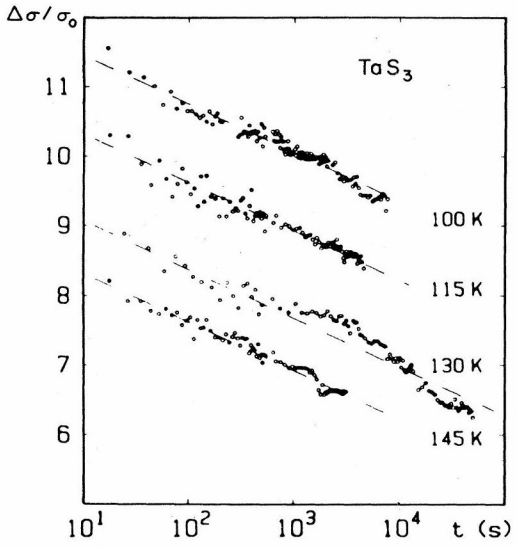


FIG. 14. Time dependence of the low-field dc conductivity after a thermal quench. The temperatures refer to the base temperature where the reaction is monitored (from Mihály and Mihály, 1984).

The long-time effects associated with these relaxation phenomena may also play a role in the details of the depinning process, and therefore also in determining current-voltage characteristics in the nonlinear conductivity region.

The parameters that characterize the frequency- and field-dependent conductivity vary from material to material, and they also display a characteristic temperature dependence. While in the majority of cases, pinning by impurities plays the most important role (except in rather pure specimens with small dimensions where boundary effects may be important), as a rule the threshold electric field E_T is smaller, and the low-frequency dielectric constant ε is larger in materials with smaller Peierls transition temperature. In Fig. 15 these two parameters are displayed for various materials as a function of temperature. The decrease of ε and increase of E_T near T_P is most probably related to the strongly temperaturedependent condensate density, but the low-temperature behavior of these parameters is unexplained. The decreasing ε and increasing E_T with decreasing temperature may be related to the local thermal oscillation of the impurities, but alternatively to temperature-induced local excitations of the collective mode. In $o - TaS_3$ and in $K_{0.3}MoO_3$, which become commensurate below about $T \sim 100$ K, pinning by the lattice may be important, but such effects presumably do not play an important role in the other compounds where the CDW remains incommensurate with the underlying lattice. It has also been suggested that temperature-driven fluctuations of the

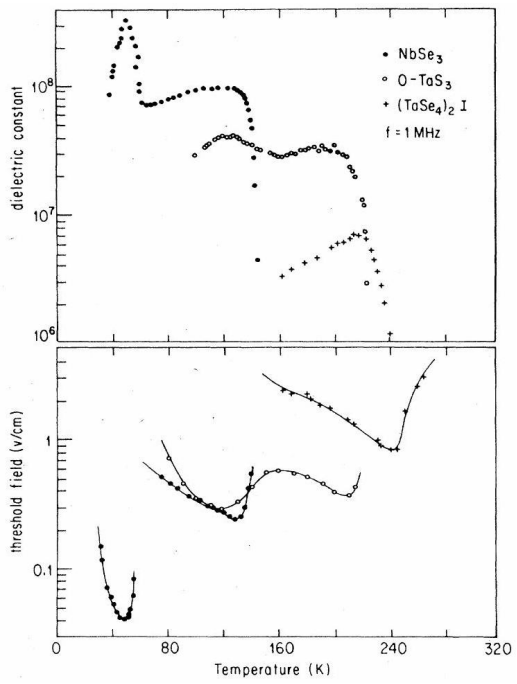


FIG. 15. Temperature dependence of the threshold electric field E_{T} and low-frequency dielectric constant (ε measured at $f = 4$MHz) in various materials. The solid lines are guides to the eye.

phase (a phenomenon similar to the Debye-Waller effect) lead to the temperature-dependent threshold field (Maki, 1986).

2.3.3 C. Other Transport Coefficients

While the low-field dc conductivity provides clear evidence for the metal-to-semiconductor transition associated with the development of the CDW ground state, other transport coefficients, such as thermoelectric power (TEP) and Hall effect, also reflect the removal of the Fermi surface by the transition. A small, metalliclike TEP above T_P is usually followed by a strong rise below the transition. This is accompanied by similar changes in the Hall constant. At temperatures below T_P these parameters can, in general, be accounted for by formulas developed for ordinary band semiconductors, with a temperature-dependent gap $\Delta_s(T)$ having the BCS form and disappearing at the transition. At low temperatures, where also the dc conductivity deviates from the exponential form, anomalies in the TEP (Allgeyer et al., 1982; Fisher, 1983; Johnston et al., 1983) and Hall effect (Ong, 1982) can also be found. It is likely these reflect the contribution of impurity states to the transport coefficients.

Equation (3.23) implies a two-band model where the normal electrons and electrons in the CDW condensate
provide separate and independent channels for the conduction process. While this description suggests a collective transport carried by the CDW when electric fields exceed threshold, other transport measurements performed in the nonlinear conductivity region provide direct evidence that the current at high fields is carried by a ground-state condensate.

Early measurements (Dee et al., 1979) of the thermoelectric power in $NbSe_3$ are in apparent conflict with the Fröhlich conduction mechanism. Detailed measurements on o-TaS $_3$ (Stokes et al., 1984) and subsequently on other materials indicate that no, or very little, entropy is associated with the nonlinear electrical conduction as expected for a current carried by a ground-state condensate. Both the measurement and the analysis of TEP experiments, when extended

to investigate nonlinear phenomena, require special care. First, conventional experiments use an open circuit, $J = 0$ configuration. In order to detect a contribution to the thermopower in the nonlinear regime, a finite current has to be applied. Second, conventional discussions of thermoelectric effects consider only small thermal and electric gradients in cases of systems initially in thermal equilibrium. For a system initially in a nonequilibrium steady state (driven by an electric field E) at a uniform temperature T, the electric and heat current densities δJ and δU are given by

$$\delta J(E) = \left.\frac{dJ}{dE}\right|_{E=E_0} \delta E + \frac{L_{12}\left(E_0\right)}{T^2}\nabla T \tag{3.26}$$
$$\delta U(E) = \left.\frac{dU}{dE}\right|_{E=E_0} \delta E + \frac{L_{22}\left(E_0\right)}{T^2}\nabla T$$

where ∇T is the applied (small) temperature gradient, and L_{12} and L_{22} are Onsager coefficients. The thermoelectric power, for constant current density is given by

$$S\left(E_0\right) = \frac{-L_{12}}{T^2 \left.\frac{dJ}{dE}\right|_{E=E_0}} \tag{3.27}$$

For a two-fluid model of the normal electrons and the CDW condensate as suggested by Eq. (3.23), the TEP is given by

$$S\left(E_0\right) = \frac{S_N \left.\frac{dJ}{dE}\right|_{\text{normal}} + S_{\text{CDW}} \left.\frac{dJ}{dE}\right|_{\text{CDW}}}{\left.\frac{dJ}{dE}\right|_{\text{normal}} + \left.\frac{dJ}{dE}\right|_{\text{CDW}}}, \tag{3.28}$$

where the subscripts refer to the differential conductivities for the normal and condensed electrons. For the case $S_{\text{CDW}} = 0$, the above equation reduces to

$$\frac{S\left(E_0\right)}{S_N} = \frac{\sigma'_N(E)}{\sigma'_N(E) + \sigma'_{\text{CDW}}(E)}. \tag{3.29}$$

Here $\sigma' = dJ/dE$ is the differential conductivity.

Therefore, for $S_{\text{CDW}} = 0$, the electric field dependence of the total measured thermopower S is expected to be the same as that of the inverse differential conductivity. In Fig. 16 these parameters measured in $o - TaS_3$ are displayed as a function of electric field. Within experimental error Eq. (3.29) is obeyed over a wide range of applied fields confirming that (to within the experimental error) $S_{\text{CDW}} = 0$.

The Peltier heat is related to the thermoelectric power by

$$\Pi(E) = TS\left(E_0\right)\left\{\sigma'\left(E_0\right) E_0 \left[J\left(E_0\right)\right]^{-1}\right\}, \tag{3.30}$$

and consequently $\Pi(E)$ associated with the nonlinear conduction is also close to zero. This analysis suggests that, in contrast to single-particle transport where the Wiedeman-Franz law applies, no or very little entropy transport is associated with the nonlinear electric conduction. The slight deviation from Eq. (3.28) observed at low temperatures can be accounted for by phonon-drag phenomena (Stokes et al., 1983). Similar conclusions are reached for $(TaSe_4)_2$ I and in the upper transition of $NbSe_3$, while at the lower phase transition in $NbSe_3$ the anomalous behavior (Dee et al., 1979) suggests that phonon-drag effects may be dominant. Such effects were studied subsequently by Kriza and Mihály (1987), who extended the early experiments on TaS_3 higher electric fields and found deviations from Eq. (3.29) that became more important at lower temperatures. The reason for this behavior is not clear at present, but it may signal the breakdown of a simple two-fluid model for large CDW velocities.

Within the framework of the two-fluid model, the Hall yoltage V_H, for a magnetic field H perpendicular to the chain direction, is given by

$$V_H = \frac{\sigma_N \mu_{N\perp} + \sigma_{\mathrm{CDW}} \mu_{\mathrm{CDW}\perp}}{(\sigma_N + \sigma_{\mathrm{CDW}})_\perp} HE, \tag{3.31}$$

where E is the electric field applied along the chain direc-

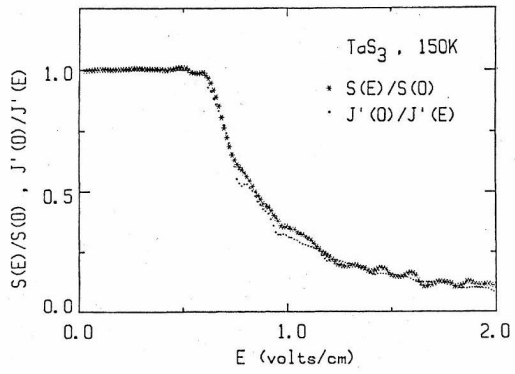


FIG. 16. Electric field dependence of the thermopower S and differential conductivity $I^{\prime}=d I / d V$ in o-TaS $_3$ (Stokes et al., 1984).

tion. $\mu_{N\perp}$ and $\mu_{\mathrm{CDW}\perp}$ are the contributions of the normal and CDW electrons, respectively, to the mobility perpendicular to the chain direction at electric field E, while $(\sigma_N + \sigma_{\mathrm{CDW}})_\perp$ refers to the total perpendicular conductivity that corresponds to the Hall voltage. Measurements performed in $NbSe_3$ (Kawabata et al., 1981; Tessema and Ong, 1981) lead to a Hall voltage that is proportional to the electric field up to fields of $E \sim 2E_T$; for such electric field values V_H is smaller than the threshold field E_T. Consequently, the current associated with the nonlinear conduction is extremely anisotropic and is not influenced by the Lorentz force. While this was subsequently confirmed in TaS_3 (Artemenko et al., 1984) for electric fields slightly exceeding E_T, for larger electric fields deviations from $V_H \sim E$ are found, the effect being more apparent at low temperatures. The most detailed experiments were performed recently on $K_{0.3}MoO_3$ (Forró et al., 1985) and in $NbSe_3$ (Everson et al., 1984); both point to the apparent breakdown of the two-fluid description at low temperatures and at high magnetic fields. In the former compound the CDW current is accompanied by normal electron backflow, while in $NbSe_3$ there is a conversion between the CDW and normal carriers by the magnetic field.

2.3.4 D. Elastic Properties

The metal-to-semiconductor transition is associated with pronounced anomalies of the elastic properties. The Young's modulus has a large dip, and the internal friction increases at T_P (Brill and Ong, 1978; Brill, 1982; Mozurkewich et al., 1985a, 1985b). These anomalies, not unexpected for a structural phase transition, are related to specific-heat anomalies within the framework of the Clausius-Clapeyron equation (see, for example, Testardi, 1975), which account for the changes in the elastic constant. Corresponding changes in the internal friction remain unexplained.

Both the Young's modulus and the internal friction show large anomalies in the nonlinear conductivity region. This was first investigated in o-TaS $_3$ (Brill and Roark, 1984; Brill et al., 1986), in $o-TaS_3$, $(TaSe_4)_2 I$, and $NbSe_3$ (Mozurkewich et al., 1985b; Xiang and Brill, 1988), and in $K_{0.3}MoO_3$ (Bourne et al., 1986). Experimental results for the electric field dependence of the elastic modulus $\Delta E'/E'$ and internal friction $\delta' \sim Q^{-1}$ (where Q is the quality factor

of the elastic resonance) measured in TaS_3 are displayed in Fig. 17. The onset of nonlinear conduction leads to a decrease of E' and an increase of δ'. Similar behavior was found in $NbSe_3$ and in $(TaSe_4)_2\,I$ (Mozurkewich et al., 1985b; Suzuki et al., 1986), but no effect was observed in $K_{0.3}MoO_3$ (Bourne et al., 1986). The shear modulus was also measured recently, showing significant anomalies as the function of applied electric field (Xiang and Brill, 1988).

While the detailed underlying mechanism for the observed effect is not clear, it is expected that a pinned CDW would contribute to the elastic constant while, for

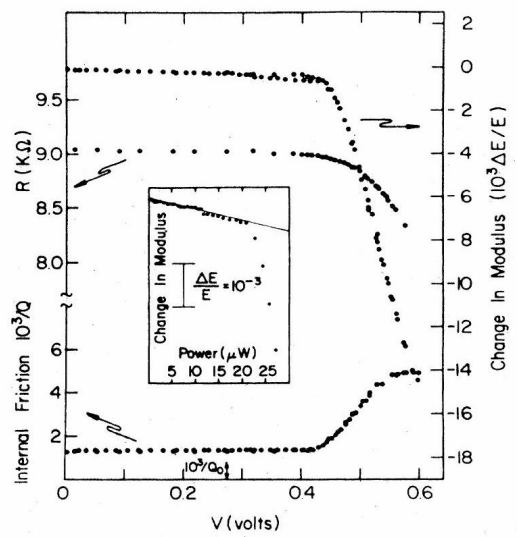


FIG. 17. Resistance, 1/ (quality factor), and relative change in modulus $\Delta E / E_{0}=2 \Delta f / f_{0}$ vs voltage at 149 K in TaS_3.O_0 is the quality factor in vacuum at zero voltage. Inset: $\Delta E/E_0$ vs power dissipated in sample at 149 K . The line shows the proportionality below threshold (Brill and Roark, 1984).

a completely unpinned mode, such contribution would be negligible. Moreover, damping effects associated with the dynamics of the internal modes can be responsible for the increased internal friction observed. The change of the elastic constant can be estimated by a mode coupling approach, where the phonon and phason branches are coupled through Coulomb forces (Mozurkewich et al., 1985b), or by calculating the longitudinal sound velocity (Coppersmith and Varma, 1984) and taking the internal degrees of freedom explicitly into account (Sneddon, 1986; Maki and Virosztek, 1988; Zeyher, 1988). Such calculations lead to the softening of the lattice in the sliding conductivity region. These models also give specific predictions concerning the electric field dependence of the bulk modulus and attenuation; these are in broad semiquantitative agreement with experiments performed mainly in TaS_3.

2.3.5 E. Nuclear Magnetic Resonance

The most direct evidence for moving charge-density waves comes from NMR experiments. Transitions to the CDW state have profound influence on the NMR spectrum, mainly because of the inhomogeneous broadening caused by the charge-density-wave modulation through quadrupole effects.

The development of the periodic modulation of the charge density leads to a periodic modulation of the electric-field-gradient tensor, and the frequency associated with the transitions between the nuclear levels is given by (Berthier and Ségranson, 1987)

$$\Delta v_{m\to m+1}(\mathbf{R}G) = \Delta v^0_{m\to m+1}(T\mathbf{C}) + \frac{\omega_1}{2\pi}\cos(2k_F\mathbf{r}+\varphi) + \frac{\omega_2}{2\pi}\cos^2(2k_F\mathbf{r}+\varphi) \tag{3.32a}$$

where the numerical factors ω_1 and ω_2 depend on the amplitude of the CDW and on the quadrupole moment. For an incommensurate CDW, Eq. (3.32a) leads to a line broadening, which can be calculated and contrasted with the experimentally found broadening. Such studies have clearly established the development of charge-density modulation below the Peierls transition. This has been studied in detail in $NbSe_3$ (Devreux, 1982; Wada et al., 1984) and in $Rb_{0.3}MoO_3$ (Butaud et al., 1985).

The NMR line shape in the presence of uniform CDW velocity has been worked out in detail (Kogoj et al., 1984) as the function of the velocity v. The solution leads to a motional narrowing and the appearance of a central line at the unperturbed Larmor frequency. While early studies (Douglass et al., 1985) did not reveal any motional narrowing, subsequent experiments in $NbSe_3$ (Ross et al., 1986) and in $Rb_{0.3}MoO_3$ (Nomura et al., 1986; Ségranson et al., 1986) clearly established the motional narrowing associated with moving charge-density waves. A detailed analysis and the reevaluation of CDW velocity require the calculation of NMR line shapes, with the added complication that often only part of the sample is involved in the nonlinear conduction process. Such analysis leads to CDW velocities in good agreement with those expected from studies summarized in the next section. The results suggest a distribution of CDW velocities in $Rb_{0.3}MoO_3$ (Berthier and Ségranson, 1987); such effects are much less evident in $NbSe_3$ (Ross et al., 1986).

2.3.6 F. Current Oscillations

Perhaps the most spectacular observation in the field is the detection of current oscillations in the nonlinear conductivity region. The phenomenon, which has been studied both in the time and in the frequency domain, is often referred to as "narrow-band noise." The term "noise," however, is misleading. Consequently, we refer to the phenomenon as current oscillations.

Depending on the experimental arrangement, either an oscillating current or an oscillating voltage is detected; the former for a constant voltage, the latter for a constant current drive. Due to the presence of normal electrons that lead to a normal component to the total current and thus contribute to the voltage drop across the specimen, the usual experimental configuration represents an intermediate situation. To first approximation, the current oscillation amplitude Δj_1 and the oscillating voltage ΔV_1 are related by $\Delta J_1 = \Delta V_1/R$, where R is the measured resistance of the specimen at a frequency that corresponds to the frequency of the oscillations.

Figure 18 shows the first observation by Fleming and Grimes (1979) made on $NbSe_3$, where the Fourier spectrum of the time-dependent voltage, recorded by a spec-

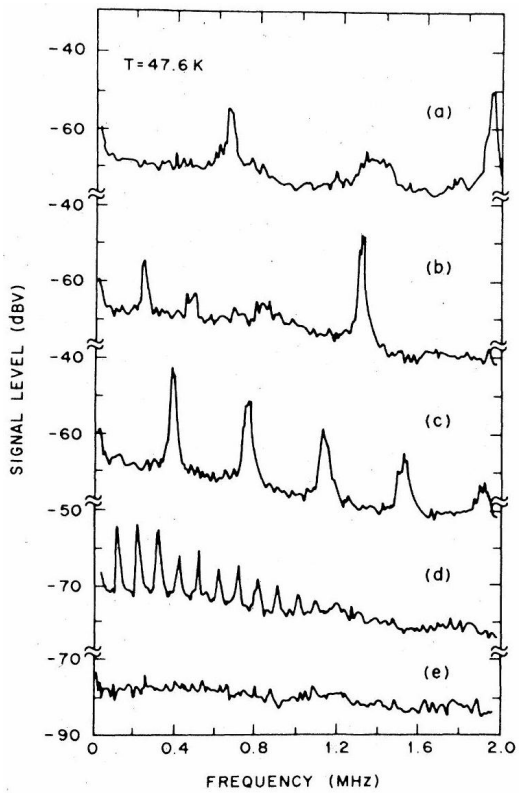


FIG. 18. Fourier transform of the time-dependent current in NbSe_{3} or various applied currents. Narrow-band "noise" results if the current exceeds the threshold value for nonlinear conduction. Currents and dc voltages are (a) $I = 270\mu$ A, $V = 5.81$mV; (b) $I = 219\mu$ A, $V = 5.05$mV; (c) $I = 154\mu$ A, $V = 4.07$mV; (d) $I = 123\mu$ A, $V = 3.40$mV; (e) $I = V = 0$. The sample cross-sectional area $A \approx 136\mu$ m^2 (Fleming and Grimes, 1979).

trum analyzer, is displayed. Only a structureless broadband noise is observed for electric fields below threshold, but for $E > E_T$ sharp peaks superimposed on a large amplitude broadband noise are evident. The spectrum consists of a fundamental frequency and of several harmonics with slowly decaying intensity. For increasing electric fields, the amplitude and the frequencies increase. The spectra shown in Fig. 18 indicate a time-dependent current with a periodic but nonsinusoidal time dependence. This was subsequently confirmed by studies in real time domain, following a pulse applied to the specimens (Bardeen et al., 1982; Fleming, 1982). Spectra, similar to those shown in Fig. 18, have been subsequently observed in all materials where nonlinear conduction occurs-in TaS_3 (Grüner, Zettl, Clark, and Thompson, 1981), in $(TaSe_4)_2$ **I** (Wang, Monceau et al., 1983), in $(NbSe_4)_{3.33}$ I (Wang, Saint-Lager et al., 1983), and in $K_{0.3}MoO_3$ (Dumas et al., 1983)-and consequently is a characteristic overall feature that accompanies the non-
linear conduction process.

The frequency of the oscillations is approximately proportional to the excess current carried by the CDW (Monceau et al., 1980); furthermore, the ratio of the excess current to the frequency varies with temperature, approximately as the number of condensed electrons n_c (Bardeen et al., 1982). Figure 19 displays the linear relation between I_{CDW} and f_0 in a wide frequency range for a pure $NbSe_3$ specimen (Bardeen et al., 1982), with the ratio I_{CDW}/f_0 as the function of T in the inset. Normalizing to CDW current for one chain, the above observations can be described as

$$\frac{j_{\mathrm{CDW}}}{f_0} = \mathrm{const} \times e \times \frac{n_c(T)}{n_c(T=0)}, \tag{3.32b}$$

where $j_{\rm CDW}$ refers to the current per chain. While the precise value of the constant in Eq. (3.32b) is still debated, it is between 1 and 2 for a broad range of materials.

The above relation between the current and oscillation frequency is associated with the fundamental periodicity associated with the phase φ. The CDW current, described in terms of drift velocity v_d of the (rigidly moving) condensate, is given by $j_{\rm CDW} = n_c e v_d$. Associating the fundamental frequency with a CDW displacement by one period, $f_0 = v_d/\lambda$, leads to

$$\frac{j_{\rm CDW}}{f_0} = n_c(T) e \lambda, \tag{3.33}$$

with $\lambda = \pi/k_F$ and $n_c = 2k_F/\pi$. Equation (3.32b) with a constant $c = 2$ is then recovered. Alternatively, the fundamental frequency can be related to the energy

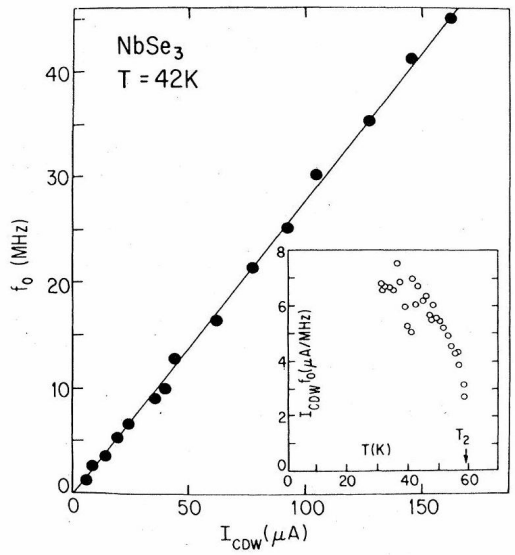


FIG. 19. Relation between the CDW current and fundamental oscillation frequency in NbSe_3. The inset shows $I_{\rm CDW}/f_0$ vs temperature (Bardeen et al., 1982).

difference ΔE between the two sides of the displaced Fermi surface shown in Fig. 7(b). With

$$\Delta E \sim \frac{\partial E}{\partial v} v_d = \frac{\partial E}{\partial k}\frac{\partial k}{\partial v} v_d = 2 v_F v_d \tag{3.34}$$

$\Delta E = h f_0$ and $j_{\rm CDW} = n_c e v_d$ also leads to Eq. (3.32) with $c = 2$. The strictly linear relation between $j_{\rm CDW}$ and f_0 as displayed in Fig. 19 suggests that the CDW velocity is constant throughout the specimen. Indeed $j_{\rm CDW}$ is proportional to f_0 over a broad range of currents and frequencies only in high-quality specimens. In materials where evidences suggest that disorder plays an important role, deviations from the linear relation between $j_{\rm CDW}$ and f_0 are observed (likely related to finite velocityvelocity correlation lengths).

The question of whether current oscillations are generated in the bulk or at boundaries, like current contact, has been hotly debated, and a variety of experiments have been designed to test the validity of both assumptions. While it is generally agreed that current oscillations are a finite-size effect and do not occur in the thermodynamic limit, the issue of current generation has not yet been resolved. Experiments where the noise amplitude was measured as the function dimensions of the specimens (Mozurkewich and Grüner, 1983a; Ong, Verma, and Maki, 1984) led to contradictory results. Experiments involving nonperturbative contacts that also can be moved along the length of the specimens favor bulk noise generation (Brown and Mihály,

1985). Various experiments have also been performed in the presence of a temperature gradient, which leads to different temperatures T_1 and T_2 at the site of the current contacts, placed, in general, at the ends of the specimens. In case of oscillating current generation at the contacts, under certain circumstances a splitting of the oscillation frequencies is expected. While the first experiments (Zettl et al., 1984) did not show such splitting in subsequent measurements (Ong, Verma and Maki, 1984; Ong and Maki, 1985), such splitting has indeed been detected. It has, however, been shown that a further increase of the temperature gradient leads to further splitting of the oscillation frequencies (Brown, Mozurkewich, and Grüner, 1985; Lyding et al., 1986). The multiple splittings suggest the formation of velocity coherent regions with a minimum length of the order of 100μ m. Similar conclusions have been reached by Monceau et al. (1986) by employing temperature gradients large enough to heat the contact regions above the transition temperature. The current oscillations were present under such circumstances, indicating that they are not generated exclusively by carrier injection at the contacts. While these experiments do not give a clear answer to the question of current generation, they do raise the important question of topological defects in charge-density waves and the possibility of phenomena associated with the dynamics of the amplitude of the order parameter (Gorkov, 1983; Batistic et al., 1984; Ong, 1984; Ong and Maki, 1985).

In addition to the current oscillations, the nonlinear
conduction is also accompanied by a substantial broad band noise with an effective noise temperature of several thousand degrees (Richard, Monceau, Popoular et al., 1982; Grüner and Zettl, 1983). The spectral dependence can be well described by an $f^{-\alpha}$ behavior (Bhattacharya et al., 1985; Maeda, Furuyama, and Tanaka, 1986), and the amplitude of the noise voltage is inversely proportional to the square-root volume, suggestive of fluctuations generated by independent pinning centers in the bulk (Richard, Monceau, and Renard, 1982; Bhattacharya et al., 1985). It has also been suggested, on the basis of experiments on intentionally damaged specimens (Thorne et al., 1987), that broad band noise is either generated by macroscopic defects or is mainly reflective of the distribution of various current oscillation components. The $1/f^{\alpha}$ spectrum may then represent the distribution of heat frequencies between various coherent regions separated by macroscopic defects. The phenomena have also been interpreted as due to a current noise, generated at various pinning centers (Wonneberger and Breymayer, 1984)

The amplitude, and also the phase of the current oscillation, displays characteristic time dependences (Brown et al., 1985b; Bhattacharya et al., 1987; Link and Mozurkewich, 1988). Fluctuations of both the position and the amplitude of the peaks in the Fouriertransformed spectrum are indicative of noise generation in various regions in the specimens, which then are weakly coupled through the nonlinear medium. Such weak coupling may lead to temporal locking of oscillations in the various regions of the specimens, with lockingunlocking effects leading to low-frequency fluctuations. The time-average width of the Fourier-transformed "narrow-band noise" scales with the observed broad band noise amplitude, indicating that the two are intimately related.

2.4 IV. The Mechanisms of Pinning

Both the frequency- and the electric-field-dependent conduction observed in materials with incommensurate charge-density-wave ground state are the consequence of the interaction between the collective mode and the lattice irregularities. The interaction leads to a finite pinning energy; this in turn shifts the oscillator strength to finite frequencies and also results in a finite dc threshold for nonlinear conduction. Pinning effects, together with the fundamental $2k_F$ periodicity of the problem, are also responsible for the current oscillation phenomena.

In contrast to superconductors, the relevant collective mode, the phason mode with the dispersion relation (3.2b), is gapless. The collective mode can distort around potentials repre-

sented by $V(\mathbf{r})$, thus lowering the total energy of the collective mode. The Ginzburg-Landau Hamiltonian for a potential that couples directly to the phase of the CDW is (Fukuyama and Lee, 1978)

$$\mathcal{H} = \frac{n_c \hbar v_F}{4\pi} \int (\nabla\varphi)^2 d\mathbf{r} + \int \rho_1 V(\mathbf{r}) \cos\left[2\mathbf{k}_F \cdot \mathbf{r} + \varphi(\mathbf{r})\right] d\mathbf{r} \tag{4.1}$$

The first term on the right-hand side represents the elastic energy associated with the long-wavelength phase deformations; the second represents the interaction of the collective mode with the pinning potential. It is assumed that the amplitude of the collective mode is not perturbed by the interaction between the collective mode and the potential $V(\mathbf{r})$. Consequently, Eq. (4.1) is expected to be appropriate for relatively weak potentials, which are substantially smaller than the band gap Δ_s. The combined effect of elastic and potential-energy terms in Eq. (4.1) is a decrease of the total energy. Because the potential depends on the position $V(\mathbf{r})$, the interaction also leads to pinning of the collective mode. For small amplitude displacements the pinning energy is given by $E_{\text{pin}} = K\left(x - x_0\right)^2/2$, where K is the restoring force constant and $(x - x_0)$ is the rigid displacement of the mode from the equilibrium position x_0, which is established as a result of the potential $V(\mathbf{r})$. In terms of a purely classical description of the small amplitude oscillations of the collective mode, the pinning frequency is $\omega_0^2 = K/m^*$, and the de dielectric constant is given by

$$\varepsilon = 1 + \frac{4\pi n_c e^2}{K} \tag{4.2}$$

which can be substantial for a small restoring force. A dc electric field leads to the translational motion of the condensate and, consequently, to a current-carrying state when the energy provided by the dc field over one period λ is larger than E_{pin}. The condition that follows from this argument leads to a threshold field

$$E_T = \frac{\lambda K}{2e} \tag{4.3}$$

The ω - and E-dependent responses of the pinned mode are strongly related. By taking $K = m^*\omega_0^2$, the relation between E_T and the characteristic pinning frequency ω_0 is

$$E_T = \frac{\lambda m^* \omega_0^2}{2e} \tag{4.4}$$

and the dielectric constant is related to E_T through the relation

$$E_T \varepsilon(\omega \to 0) = 4\pi e n_\perp \tag{4.5}$$

where $n_\perp$ is the number of chains per unit area. At $T = 0$, $n_{\text{CDW}} = 2n_1/\lambda$. These arguments completely neglect the role played by the internal modes of the condensate in the dynamics. It is assumed that after the long-wavelength deformations around the pinning potentials are established, the response to external dc and ac driving forces is accounted for by considering the time dependence of the average phase. The internal deformations, however, remain unchanged when going from the
pinned to the current-carrying state.
Since the restoring force drops out in Eqs. (4.4) and (4.5), they are expected to be appropriate for any pinning mechanism. Impurities, grain boundaries, lattice defects, and even the boundaries of the specimens may contribute to the overall restoring force. Because of early experimental evidences suggesting that impurities play an important role in pinning the collective mode, only impurity pinning has been considered in detail. Recently it has become increasingly more evident, however, that pinning by macroscopic defects and surfaces may also be important under certain circumstances.

2.4.1 A. Impurity Pinning

The interaction between impurities and the CDW has fundamental consequences on both the static and dynamic properties. As first argued by Sham and Patton (1976), Imry and Ma (1975), and Efetov and Larkin (1977), long-range order is destroyed by randomly positioned impurities, and, in less than four dimensions, the phasephase correlation function has the form

$$e^{i[\varphi(\mathbf{r})-\varphi(0)]} \approx e^{-r/L_0}, \tag{4.6}$$

where the characteristic length scale L_0 depends on the strength of the impurity potential and on the elastic properties of the condensate. L_0 can be evaluated using scaling arguments (Fukuyama and Lee, 1978). For a random impurity distribution, with impurity potentials $V(\mathbf{r}) = V_0\delta(\mathbf{r})$, Eq. (4.1) reads

$$\mathcal{H} = \frac{n_c\hbar v_F}{4\pi}\int(\nabla\varphi)^2 d\mathbf{r} + V_0\rho_1\sum_i \cos\left[2\mathbf{k}_F\cdot\mathbf{r}_i + \varphi\left(\mathbf{r}_i\right)\right] \tag{4.7}$$

with i referring to random impurity sites. In Eq. (4.7) it is assumed that spatial fluctuations of the phase $\varphi(\mathbf{r})$ occur for wavelengths large compared to the amplitude coherence length $\xi_a = hv_F/kT_p$, on the order of 100Å for typical materials. Also, amplitude fluctuations of the collective mode, together with quantum and finitetemperature effects, are neglected. The first term favors a spatially homogeneous phase, while the second term favors local distortions of the condensate where the phase is fully adjusted at every impurity site to obtain a maximum decrease of the potential energy. The ratio

$$\varepsilon' = \frac{V_0\rho_1}{\pi\hbar v_F} \tag{4.8}$$

tells whether the potential energy on elastic distortions is more important; $\varepsilon' > 1$ is called strong impurity pinning and $\varepsilon' < 1$ is called weak impurity pinning. For $\varepsilon' \gg 1$, where the elastic energy can be totally neglected, the pinning energy is simply due to total energy gain due to the electrostatic interaction with the impurities in $\varepsilon = V_0\rho_1 n_i$ and, consequently, the pinning energy (Fukuyama and Lee, 1978; Lee and Rice, 1979)

$$\varepsilon_{\text{pin}} = V_0\rho_1 n_i\frac{\lambda_2}{2} \tag{4.9}$$

and the restoring force constant $K = V_0\rho_1 n_i$. All the arguments advanced earlier apply, and Eq. (4.3) with Eq. (4.9) leads to a threshold field proportional to the impurity concentration. The phase-phase correlation length is expected to be of the order of the distance between impurities, as each impurity completely breaks the phase of the condensate.

The case of $\varepsilon \ll 1$ (weak impurity pinning) is more interesting, and scaling arguments can be used to evaluate the phase-phase correlation length. In d dimensions one can define a volume $(L_0)^d$ over which the phase is constant but is adjusted to impurity fluctuations to have a maximum decrease of the potential energy. This argument (Fukuyama, 1978; Fukuyama and Lee, 1978) leads to the potential-energy density

$$\varepsilon_{\text{pot}} = -V_0\rho_1\left(\frac{n_i}{L_0^d}\right)^{1/2}. \tag{4.10}$$

The elastic energy of the domain, using Eqs. (4.7) and (3.8), is given by

$$\varepsilon_{\text{elastic}} = \frac{n_\perp\hbar v_F}{4\pi}L_0^d\left(\frac{\pi}{L_0}\right)^2 d, \tag{4.11}$$

where $n_\perp$ is the number of chains per unit area. Minimizing the total energy density of the domain with respect to L_0 leads to a finite phase-phase correlation length for any dimension $d < 4$. In three dimensions

$$L_0^{-1} = \left(\frac{V_0\rho_1}{\pi\hbar v_F}\right) n_i \tag{4.12}$$

and the pinning energy

$$\varepsilon_{\text{pin}} = -\frac{1}{4}\varepsilon_{\text{pin}} = -\frac{1}{4}\frac{(V_0\rho_1)^4}{(\pi\hbar v_F n_\perp)^3} n_i^2. \tag{4.13}$$

An anisotropic band structure also leads to an anisotropic phase-phase correlation length. As L_0 is proportional to v_F, see Eq. (4.12), the correlation length in the various directions scales with the anisotropy of v_F. With typical band anisotropies of the order of 10, L_0 is expected to be approximately 10 times larger along the chain direction than it is perpendicular to the chains. The anisotropy of L can be included in equations of ε_{pin} and E_T by appropriate scaling. Such a procedure leads to additional numerical factors of the order of $(v_z v_y / v_x^2)$, where x refers to the chain direction. The concentration dependence of the parameter remains, however, unchanged. Arguments similar to those used before lead to ω_0, to ε ($\omega \to 0$), and to E_T with the following results:

$$\omega_0 = 2\pi \left(\frac{m}{m^*}\right)^{1/2} v_F L_0^{-1} \tag{4.14}$$

$$\varepsilon(\omega \to 0) = 1 + \frac{n_1^4 \hbar^4 \pi n^3 v_F^2 n_{\text{CDW}} e^2}{m^* V_0^4 \rho_1^4 n_i^2} \tag{4.15}$$

$$E_T = \frac{\pi\hbar v_F}{8e}\left[\frac{V_0\rho_1}{\pi\hbar v_F n_\perp}\right]^4 n_i^2 \tag{4.16}$$

In contrast to the strong pinning case, E_T is proportional to the square of the impurity concentration, while $\varepsilon(\omega \to 0) \sim n_i^{-2}$.

For a typical impurity potential of $V_0 = 10^{-2}$eV, with $v_F = 3 \times 10^7$ cm/sec, and a CDW amplitude $\rho_1 = 0.1$, an impurity concentration of 1000 ppm leads to $\varepsilon'' \sim 2$, suggesting that for relatively pure specimens, strong impurity pinning is appropriate, while for alloys, with a substantial amount of impurities, the weak impurity pinning limit occurs. From Eq. (4.12) the phase-phase correlation length $L_{0x} \sim 1$ mm in three dimensions, comparable with the length of the specimens investigated. With a typical bandwidth anisotropy of approximately 10 , the correlation length perpendicular to the chain direction is of the order of 0.1 mm , which is also comparable to the dimensions of typical specimens in this direction. This suggests that for pure specimens the phase is approximately constant over the volume, and that pinning by sources other than impurities (such as the surface or contacts) may also contribute. The pinning energy, for strong impurity pinning [see Eq. (4.14)], is on the order of 10^{-2} K with the above parameters. This is the same order of magnitude as the energy $\hbar\omega_0$, which corresponds to the peak in the frequency-dependent conductivity in various pure materials, shown in Fig. 9.

The discussion above, and the notion of weak and strong impurity pinning, is appropriate only for weak impurity potentials V_0 that do not perturb the amplitude of the collective mode considerably. The Ginzburg-Landau treatment, which leads, for example, to Eqs. (4.12) and (4.13), breaks down when $V_0 > \Delta$; in this case, bound states develop for weak impurities in the gap region, and for strong impurities outside the gap (Tüttō and Zawadowski, 1985). These, in principle, could be detected by optical experiments; however, no attempt has been made to search for the predicted features.

2.4.2 B. Experiments on Alloys and Irradiated Specimens

The importance of impurity pinning is confirmed by a broad range of studies where the electric field and frequency-dependent response is investigated in alloys or on specimens where impurities are created by irradiation. Early experiments (Ong et al., 1979; Brill et al., 1981) on $NbSe_3$ alloys suggested that E_T is proportional to n_i^2, in agreement with weak impurity pinning.

Experiments performed on alloys in a broad concentration range (Monceau, 1982; Underweiser et al., 1987), however, indicate that the situation is more complicated than that suggested by the scaling approach of Fukuyama and Lee (1978). In Fig. 20, E_T measured below the second phase transition is displayed as a function of the reciprocal residual resistivity ratio $(\mathbf{RRR})^{-1}$. The latter is proportional to the total strength of the impurity

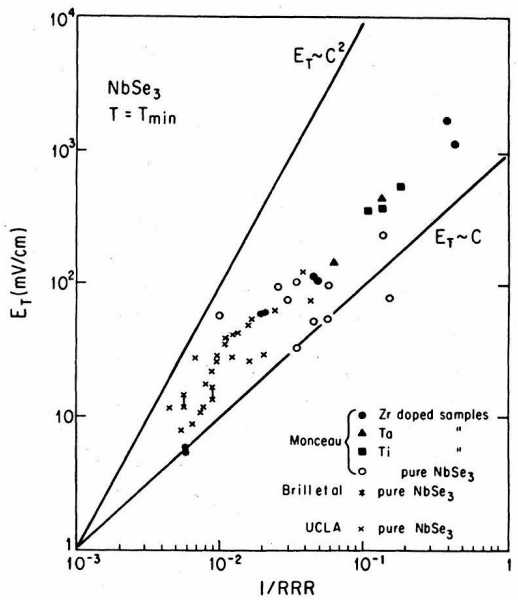


FIG. 20. Threshold electric field vs inverse residual resistivity ratio in pure NbSe_{3} and in alloys. The straight line represents the linear and the quadratic concentration dependence of E_T, $E_T \sim n_i^m$ (Monceau, 1982; Underweiser, 1987).

scattering and can consequently be regarded as a scaled impurity concentration n_i. While E_T strongly increases with increasing n_i, the functional dependence is somewhat stronger than linear, but weaker than n_i^2. The behavior is not understood at present. It may be the consequence of a crossover between strong impurity pinning for small concentration, and weak impurity pinning for large concentration of impurities. Alternatively, finitesize effects may play an important role for small impurity concentrations where the phase-phase correlation length becomes comparable to the dimension of the specimens. The large scatter of the data for relatively pure specimens also indicates that pinning centers other than impurities may become important. In contrast, in the upper CDW state of $NbSe_3$, E_T was found to be a linear function of n_i suggesting that the strong impurity limit is appropriate even for small impurity potentials such as those represented by the Ta atoms. In materials where defects are introduced by irradiation ($NbSe_3$: Fuller et al., 1981; TaS_3 : Mihály, Mihály, and Mutka, 1984; $K_{0.3}MoO_3$: Mutka et al., 1984), E_T is proportional to the defect concentration, suggesting strong impurity pinning. Such behavior, observed in electron-irradiated $Rb_{0.3}MoO_3$ and $K_{0.3}MoO_3$ (Mutka et al., 1984), is displayed in Fig. 21; the solid line corresponding to $E_T \sim n_i, E_T$ also increases with alloying for TaS_3, and this increase is proportional to the square of ΔT_P, the change of the Peierls transition temperature with alloying (Hsieh et al., 1983). As ΔT_P

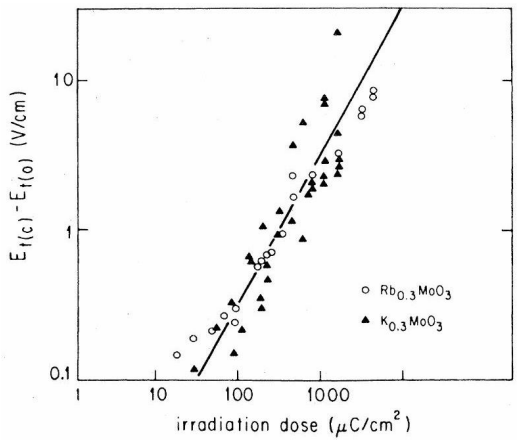


FIG. 21. Threshold electric field vs irradiation dose in $\mathrm{K}_{0.3}\mathrm{MoO}_3$ and $Rb_{0.2}MoO_3$ (from Mutka et al., 1984).

is proportional to $n_i^{1/2}$ (Mihály, Mihály, and Mutka, 1984), E_T increases linearly with the impurity concentration. In $Rb_{0.3}MoO_3$ doping increases E_T, roughly proportional to the square of the dopant concentration, suggesting that in this material doping the Rb chain may lead to weak-impurity-pinning effects (Schneemeyer et al., 1985). The strongly concentration-dependent threshold field is accompanied by corresponding changes in the frequency-dependent response. The pinning frequency has been measured directly by investigating the ω-dependent response both in TaS_3 (Reagor and Grüner, 1986) and in $(TaSe_4)_2I$ (Kim et al., 1987), but in the absence of the precise impurity concentrations, the functional dependence of ω_0 on n_i could not be evaluated. The relation between $\varepsilon(\omega \to 0)$ and E_T has, however, been

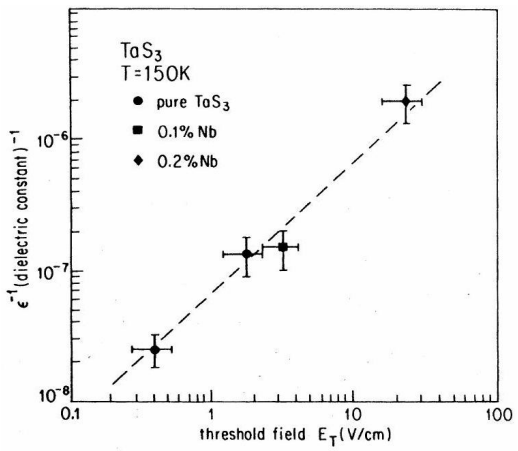


FIG. 22. Inverse low-frequency dielectric constant $\varepsilon(4\ \mathrm{MHz})$ vs threshold field E_T in o-TaS $_3$ alloys (Wu et al., 1985).

investigated by measuring both parameters on the same specimens of alloys $Ta_{1-x}Nb_xS_3$ (Wu, Mozurkewich, Mihály, and Grüner, 1984). The results are shown in Fig. 22. The solid line gives

$$\varepsilon(\omega \to 0)E_T = 0.75\mathrm{en}_\perp, \tag{4.17}$$

which is within an order-of-magnitude agreement with Eq. (4.5). Although the frequency-dependent response has not been investigated in detail, the relation $E_T \sim \omega_0^2$ was also confirmed

by frequency-dependent studies performed at microwave frequencies in irradiated $o - TaS_3$ (Mihály, Hutiray, and Mihály, 1983).

With the role of impurities clearly established by experiments performed on alloys and on irradiated specimens, it is expected that various correlation lengths (determined by the strength of impurity potentials, concentration, etc.) play a fundamental role in the dynamics of the collective mode.

The static phase-phase coherence length L_0 is related to the overall pinning energy, and Eq. (4.2), which is expected to be model independent, relates L_0 to the pinning frequency ω_0. With the parameters used before, $m^*/m \approx 10^3$ and $v_F = 3 \times 10^7$ cm/sec, a characteristic pinning frequency (derived from the frequency-dependent response, see Fig. 9) of approximately 10^{10}sec^{-1} leads to L_0 on the order of 10μ m. Equation (4.12) refers to the correlation length along the chain direction L_{0x}; because of the anisotropic Fermi surface, the correlation lengths in the perpendicular directions L_{0y} and L_{0z} are 1 to 2 orders of magnitude less than the above estimate.

The finite static correlation length leads to a broadening of the superlattice reflections and thus could, in principle, be determined by scattering experiments. Because of the limited resolution, such studies give only a lower bound on the range of phase correlations both parallel to the chains and in the perpendicular directions. Both in $NbSe_3$ and in $K_{0.3}MoO_3$, the diffraction peaks are resolution limited (Fleming et al., 1982, 1984). This sets a lower bound of $L_{0x} > 0.4\mu$ m in $NbSe_3$ and > 0.7 in $K_{0.3}MoO_3$; the phase coherence perpendicular to the chains extends over a distance of approximately 0.2μ m.

While the pinning frequencies are not available in different materials and for different impurity concentrations, the measured low-frequency dielectric constants can be used to estimate L_0 in the chain direction. Equation (4.15) when combined with Eq. (4.14) leads to

$$\varepsilon(\omega \to 0) = 1 + \frac{4\pi n_c e^2 L_{0x}^2}{\pi m v_F^2},$$

and $\varepsilon = 4 \times 10^7$ (appropriate for o- TaS_3) together with $v_F = 3 \times 10^7$ cm/sec leads to $L_{0x} = 50\mu$ m. Similar $\varepsilon(\omega \to 0)$ values are found in other pure materials, and consequently L_{0x} is expected to be the same order of magnitude. In alloys, the concentration-dependent dielectric constants (such as those displayed in Fig. 22) can be used to estimate the concentration dependence of the correlation length.

2.4.3 C. Finite-size Effects: Pinning by Surfaces and by Extended Defects

For relatively pure specimens where the overall impurity potential $\sum_i V_i$ is weak, other defects such as dislocations and grain boundaries may also play an important role; in small specimens, the surface of the specimens or the contacts may act as pinning centers. The latter has been investigated in several materials by measuring the threshold field as the function of the dimension of the specimens.

The total pinning energy in the case of boundary effects may come from pinning centers in the bulk, from the surface, and also from the pinning by the contacts placed (ideally) at the end of the specimens. These have a different dependence on the sample dimensions, and in general, in terms of restoring forces which act on the collective mode, can be written as

$$\begin{aligned} K &= K_{\text{bulk}} + K_{\text{surface}} + K_{\text{contact}} \\ &= t_1 AL + t_2 SL + t_3 A \end{aligned} \tag{4.18}$$

where A, L, and S refer to the cross section, length, and surface (per unit length) of the specimen. The constants t_1, t_2, and t_3 refer to the pinning strengths for unit dimensions. The threshold electric field is given in the presence of the various contributions to pinning by

$$E_T = \frac{V_T}{L} = \frac{\lambda}{2e}\frac{k}{AL} = \frac{\lambda}{2e}\left(t_1 + t_2\frac{S}{A} + \frac{t_3}{L}\right). \tag{4.19}$$

In the thermodynamic limit with boundary effects neglected, E_T is independent of the dimensions of the specimen. For surface pinning it increases with decreasing cross section (for a square cross section $E_T \sim A^{-1/2}$), and for contact pinning it increases with decreasing length, with E_T given by Eq. (4.19). The relative importance of these effects is determined by the constants t_1, t_2, and t_3.

Various experiments indicate that pinning by the contacts is important for short specimens. The threshold field E_T has been investigated as the function of length L of the specimens in $NbSe_3$ (Zettl and Grüner, 1984; Gill, 1985; Prester, 1985) and in TaS_3 (Mihály, 1983). The results displayed in Fig. 23, can be described well by

$$E_T = E_T\frac{(L + L_0)}{L} \tag{4.20}$$

with L_0 a characteristic length also given in the figure. While the experimental results can be accounted for by assuming a restoring force due to the contacts placed at the end of the specimens, or by assuming that a finite correlation length L_0 is important, recent experiments (Monceau et al., 1986) suggest that contact pinning is important. Indeed, for $L_0 \sim 100\mu$ the number of sites near or at the contacts is comparable to the number of

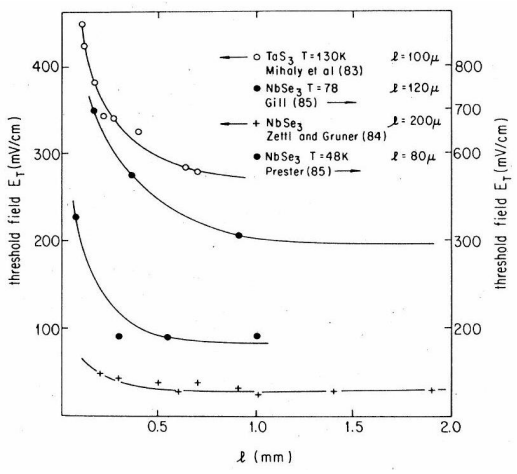


FIG. 23. Length dependence of the threshold field E_{T} in $NbSe_3$ and in TaS_3. The solid lines are fits to Eq. (4.19) with L_0 values given on the figure.

impurity sites. Thus impurity and contact pinning is comparable for comparable impurity and contact potentials.

Careful experiments have been reported recently on specimens with small cross section (Borodin et al., 1986; Gill, 1986c; see also Fig. 24). In both $o - TaS_3$ and in $NbSe_3$, the threshold field scales with the cross section of the specimens as $E_T \sim A^{-1/2}$, a clear indication for the importance of surface pinning in specimens where the cross section is smaller than approximately $100\mu^2$. A simple estimate suggests that the pinning potential due to surface

is approximately the same as an impurity potential. The above critical cross section is not unreasonable. For a specimen of square cross section with $A = 100\mu^2$,

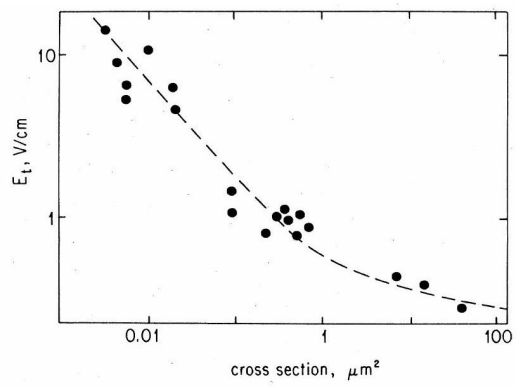


FIG. 24. Dependence of the threshold field E_{T} on the cross section of the specimens in the upper CDW state of $NbSe_3$.

the ratio of the surface-to-bulk atomic sites is approximately 10^2. If $t_1 \simeq t_2$, then an impurity concentration of 1% leads to an equal contribution to the pinning for impurities and for the surface. Careful experiments on specimens with different impurity concentrations are required to test the above experiments. It is clear, however, that for sample dimensions of $A \simeq 100\mu^2$ and $l \simeq 100\mu$, pinning by surfaces plays an important role.

2.5 V. Models: a Short Overview

A variety of models have been proposed to account for the main characteristics of the frequency- and electric-field-dependent conduction of the coherent current oscillations and low-frequency relaxation phenomena. They range from soliton models, which assume that commensurability effects are important (Horowitz and Krumhans, 1984; Horowitz et al., 1986) through Frenzel-Kontorova-type models (Bak, 1982b; Coppersmith, 1984) to models similar to those that describe plastic deformations of crystals (Feinberg and Dumas, 1986). While they are interesting as examples of nonlinear dynamical systems, it appears that commensurability effects-required to be essential in soliton or Frenzel-Kontorova models-are not important, while other models have not been developed to an extent where a comparison with theory is appropriate.

Two rather different approaches have been advanced to account for the variety of experimental findings. Both assume that the dynamics of the phase of the order parameter is important, and pinning is provided by inhomogeneities that couple directly to the phase. In both models, the frequency- and electric-field-dependent conduction is the consequence of the translational motion of the CDW condensate, as originally envisioned by Fröhlich (1954). Both models neglect a host of factors likely to be important, such as the dynamics of the amplitude mode and finite-temperature effects, among others. Consequently, the models are not expected to account for all the observations in all of the materials that have been investigated. Neglecting inertial effects, the equation of motion for the time dependence of the phase $\varphi(\mathbf{r})$ is given by

$$\frac{1}{\tau}\frac{d\varphi(\mathbf{r})}{dt} = -\frac{\delta H}{\delta \varphi} + \frac{k_F e E}{m^*} \tag{5.1}$$

treating the phase $\varphi(\mathbf{r})$ as a classical variable. For one dominant pinning center, or for specimens with small dimensions, the phase may be regarded as uniform throughout the specimen. The equation of motion then is

$$\frac{1}{\tau}\frac{d\varphi}{dt} + \omega_0^2 \sin\varphi = \frac{2k_F eE}{m^*} \tag{5.2}$$

the so-called "single-particle" model (Grüner, Zawadowski, and Chaikin, 1981; Monceau et al., 1986). The form of the potential has been chosen for its apparent simplicity, but other potentials have also been considered
(Grüner, Zawadowski, and Chaikin, 1981). They, too, follow from an electronic circuit analog (Weger et al., 1980, 1983), also proposed as a simple description of CDW transport. Equation (5.2) is that of a classical particle moving in a sinusoidal washboard potential, as shown in Fig. 25. The response to small amplitude ac fields is the same as that of a harmonic oscillator. For small applied dc fields, the particle is displaced from the bottom of the potential well; for electric fields exceeding a certain threshold field E_T, the particle starts to roll down in the washboard potential. This leads to a nonlinear time-average velocity $\langle v(t)\rangle$ and also to a timedependent component with a frequency proportional to $\langle v(t)\rangle$.

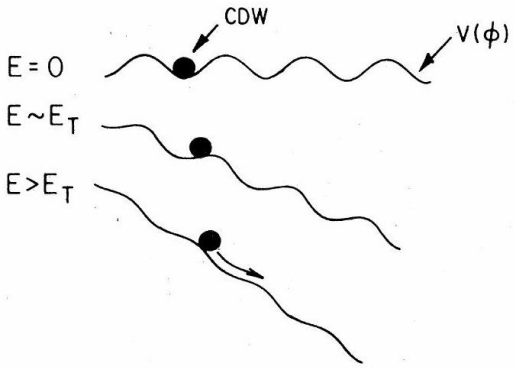
The current-voltage characteristics depend on whether the applied electric field E or the current is constant during the experiment. For E = const, the solution of Eq. (5.2) gives (Grüner, Zawadowski, and Chaikin, 1981)

$$\langle J(t)\rangle = \begin{cases} \sigma_N E + \frac{n_{\mathrm{CDW}} e^2 \tau}{m^*}\left(E^2 - E_T^2\right)^{1/2}, & E > E_T, \\ \sigma_N E, & E < E_T \end{cases} \tag{5.3}$$

where $\langle\ \rangle$ refers to time average, and the threshold field for the nonlinear conduction is given by

$$E_T = \frac{\lambda}{2\pi}\frac{m^*\omega_0^2}{e} \tag{5.4}$$

The current also has a time-dependent component in the nonlinear conductivity region, with fundamental frequency
dc conduction:



ac conduction:

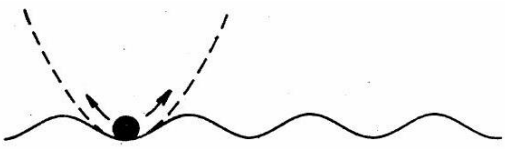


FIG 25. Classical particle model of charge-density-wave transport.

$$f_0 = \frac{2e\tau}{m^*\lambda}\left(E^2 - E_T^2\right)^{1/2} \tag{5.5}$$

Combining Eqs. (5.3) and (5.5), we see that the relation between the time-average current and oscillation frequency is given by Eq. (3.33). With $\lambda = \pi/k_F$ and $n_\parallel = k_F/\pi$, for one chain

$$\langle j(t)\rangle = 2ef_0 = \frac{4e^2\tau}{m^*\lambda}\left(E^2 - E_T^2\right)^{1/2} \tag{5.6}$$

When the applied current is constant, the equation of motion [eliminating E from Eqs. (5.2) and (5.3)]

$$\frac{1}{\tau}\left[1 + \left(n_{\mathrm{CDW}}e^2\tau/m^*\right)\right]\frac{d\varphi}{dt} + \omega_0^2 \sin\varphi = \frac{2k_F e}{m^*\sigma_N}J \tag{5.7}$$

has the same structure as Eq. (5.2) but with renormalized parameters and with a driving current replacing the applied electric field E. The measured electric field is time dependent, and the time-average electric field

$$\langle E(t)\rangle = \frac{1}{\sigma_N}\left| J - \frac{n_{\mathrm{CDW}}e}{2k_F}\frac{d\varphi}{dT}\right) \tag{5.8}$$

is given by

$$\langle E(t)\rangle = \frac{\dot{J}}{\sigma_N} - \frac{\left(n_{\mathrm{CDW}}e^2\tau/m^*\right)E_T}{\sigma_N + n_{\mathrm{CDW}}e^2\tau/m^*}\left[\left(J/J_T\right)^2 - 1\right]^{1/2}, \tag{5.9}$$

where J_T is the threshold current corresponding to the threshold field E_T. The time-dependent component leads also to a linear relation between j_{CDW} and f_0 as before. The current-voltage characteristics that follow from the two descriptions are fundamentally different. While both predict sharp threshold fields for the onset of nonlinear conduction and lead to the same high electric field limit given by

$$\sigma(E \to \infty) = \frac{n_{\mathrm{CDW}}e^2\tau}{m^*} + \sigma_N \tag{5.10}$$

A constant electric field leads to zero differential resistance, while for a constant current J an infinite negative differential resistance is obtained at threshold.

While this approach may be appropriate for rather small specimens, effects associated with the finite-phase correlation length L_0 may be important when L_0 approaches the dimensions of the specimens. Such a model was discussed by Klemm and Schrieffer (1983, 1984) and subsequently by Klemm and Robbins (1986). The equation of motion for $\delta\varphi(\mathbf{r}, t)$ is treated by perturbation in terms of the impurity fluctuations. The solution gives a large number of metastable states even within a single domain of size L_0^3. A finite threshold field, comparable to that given by Eq. (5.4), is obtained, with current-voltage characteristics different from those given by the classical particle model. In particular, the differential conductivity increases with increasing electric field (except close to threshold) in contrast to the equations that describe the
dynamics of a single degree of freedom. Current oscillations with features slightly different from those of the classical particle model are also recovered for a single domain. The model has also recently been extended to include finite-frequency effects (Robbins and Klemm, 1986). These become important at low frequencies and at fields close to the threshold field.

For sufficiently large specimens, close to the thermodynamic limit, a perturbation expansion in terms of impurity fluctuations breaks down, and Eqs. (4.1) and (5.1) represent a complicated nonlinear problem for which analytical solutions are not available for the full range of parameters. In the large velocity limit the effects of impurities can be treated perturbatively (Sneddon et al., 1982) by a hydrodynamic approach. The average velocity is determined by

dissipative processes associated with the dynamics of the local deformations, and in contrast to Eq. (5.3), the leading correction to the current is given by

$$\langle J(t)\rangle_t = \sigma_b E - A_1\sqrt{E} \tag{5.11}$$

in the infinite velocity limit. The frequency-dependent conductivity has a similar square-root behavior (Fisher, 1985; Robbins and Klemm, 1986), and in the high frequency, $\omega \gg \omega_0^2\tau$ limit

$$\sigma(\omega) = \sigma_b - \frac{A_2}{\sqrt{\omega}}. \tag{5.12}$$

Equations (5.11) and (5.12) imply a scaling between the ω - and E-dependent response in the high-velocity limit, i.e., the functional dependence on the frequency and field expected to be identical. Due to the local deformations of the charge-density wave around impurities, the velocity-velocity correlation function is finite and, consequently, the current oscillations disappear in the thermodynamic limit. The response to various joint ac and dc excitations has not been considered in detail in this limit. The dielectric constant, however, goes to zero for large velocities (Sneddon, 1984a, 1984b), and the amplitude of the Shapiro steps is independent of the volume (Sneddon et al., 1982).

The perturbation treatment of the local deformations breaks down for small velocities, and a nonperturbative treatment of the large number of nonlinearly interacting degrees of freedom is required. Computer simulations can be performed by going from the continuum equation to a discrete lattice version (Weisz et al., 1979; Sokoloff, 1981; Sokoloff and Horovitz, 1983; Matsukawa and Takayama, 1984) or by assuming that damping occurs only at the (discrete) lattice sites (Teranishi and Kubo, 1979; Pietronero and Strässler, 1983). In both cases the equilibrium configuration, and also the time-dependent phase at a particular site $i, \varphi(\mathbf{r}_i, t)$ is related to phases at other sites through a set of different equations. Due to the complexity of the problem, only one-dimensional models have been considered.

A different approach has been taken to treat the essential features of the dynamics in the nonperturbative re-
gime near threshold (Fisher, 1983, 1984, 1985). It is assumed that the phase-phase correlation length L_0 is much smaller than the dimensions of the specimens, and a discrete version of the Fukuyama-Lee-Rice model is proposed. The Hamiltonian on a discrete lattice is given by

$$\begin{aligned} H &= \sum_{i,j} \kappa'(\mathbf{r}_i - \mathbf{r}_j)(\varphi_i - \varphi_j)^2 - \sum_{i,j} V_j \cos(\varphi_i - \beta_j) \\ H_e &= \sum eE\varphi_i \end{aligned} \tag{5.13}$$

where the first term represents the elastic energy of the charge-density wave, with elastic constant κ', the second, the interaction of the CDW with impurities at sites j, with the phase β_j a random variable between 0 and π. H_e describes the coupling of the CDW to the applied electric field. An essentially similar model has been proposed by Tua and Zawadowski (1984), where the subscripts i and j refer to macroscopic domains rather than to impurity sites. The important features of the model are the infinite number of internal degrees of freedom and the randomness due to the preferred phases β_j. The development of the current-carrying state is treated as a dynamical critical phenomenon, with several critical exponents that characterize the dynamical properties of the system. The behavior in the presence of applied fields is described using relaxational dynamics, both in the meanfield approximation (Fisher, 1983) and for short-range interactions (Fisher, 1984, 1985). The model leads to various critical exponents

near E_T, among them the behavior of the average velocity. Above threshold is the most relevant to various observations. It is given by

$$\langle v(t)\rangle \sim (E - E_T)^{\xi}, \quad \xi = \frac{3}{2}. \tag{5.14}$$

The exponent is different from the one that follows from the single-particle model that leads to $\xi = \frac{1}{2}$. Several frequency scales are important both above and below E_T; they determine the detailed frequency dependence in the presence of a dc bias and the amplitude of the current oscillations close to threshold (Fisher, 1985).

A rather different situation may occur when a large pinning center, such as a grain boundary, situated in the bulk of the specimen is important. This can effectively decouple the sample into two coherent domains, with weak coupling between the domains. The dynamics of the coupled phases at the two sides of the barriers may display features different from that of a single degree of freedom, or infinite degree of freedom of dynamics. In particular, switching and hysteresis effects similar to those that occur in coupled Josephson junctions may follow from such models (Mihály, Chen, and Grüner, 1987). Similar features are recovered from models that assume that the amplitude mode goes to zero at the barriers (Inui and Doniach, 1987).

While all of the above models treat the phase of the condensate as a classical variable, a rather different approach has been taken by Bardeen (1979, 1980, 1984, 1986) by assuming that tunneling processes are responsi-
ble for the advancement of the average phase $\langle\varphi\rangle$ of the condensate. Advancement of the CDW phase by tunneling in a single chain was first treated by Maki (1977, 1978). Bardeen's model, which has been used extensively to analyze experimental results, relies heavily on phase coherence between the neighboring chains. The model, which applies in the weak impurity pinning limit, has evolved hand-in-hand with the experiments and at present it is able to account for a broad variety of observations made in the presence of dc and ac electric fields (see, for example, Thorne et al., 1987, and references cited therein). The model starts from the Fukuyama-LeeRice theory (Fukuyama and Lee, 1977; Lee and Rice, 1979) and replaces the phase-phase correlation length L_0, given by Eq. (4.12), with periodic pinning forces at distance L_0 apart. This leads to a position-dependent phase as shown in Fig. 26. Two degenerate solutions are possible for this particular pinning, and these are given by

$$\begin{aligned} \varphi_A &= \frac{\pi}{2}\sin\frac{\pi x}{L_0}, \\ \varphi_B &= -\pi - \frac{\pi}{2}\sin\frac{\pi x}{L_0} \end{aligned} \tag{5.15}$$

with both minimizing the pinning energy (Bardeen, 1986). The periodicity of the pinning fields to a pinning gap at the Fermi level and this has to be overcome by the dc field in order to induce nonlinear conduction. The pinning potential has the form of

$$V(\theta) \sim \begin{cases} -\cos\theta \text{ for } \frac{\pi}{2} < \theta < \frac{\pi}{2} \\ \cos\theta \text{ for } \frac{\pi}{2} < \theta < \frac{3\pi}{2} \end{cases}$$

which is distinctively different from the sinusoidal potential that appears in Eq. (5.2). The pinning gap is given by

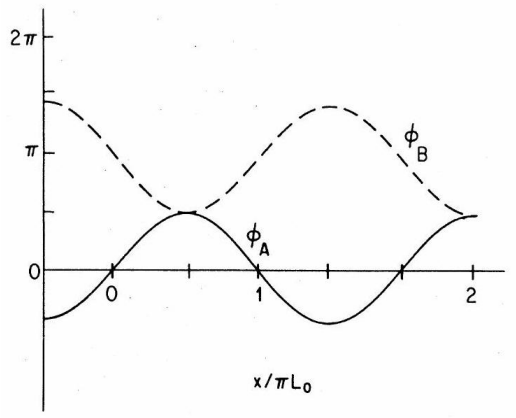


FIG 26. Phase variations that minimize the pinning energy in the tunneling model. $\phi_A(x)$ gives a minimum pinning energy when the average phase $\theta = 0$, while $\phi B(x)$ gives minimum when $\theta = -\pi$ (after Bardeen, 1986).

$$E_g = \frac{2}{\pi}\left(\frac{m^*}{m}\right)^{1/2} \pi\Omega_p \tag{5.16}$$

where $\Omega_p = \pi C_p/L_0$, with C_p the phason velocity given by Eq. (3.2b). The nonlinear conduction has the typical tunneling form

$$\sigma(E) = \sigma_\infty \left(1 - \frac{E_T}{E}\right) \exp\left(-\frac{E_0}{E}\right), \tag{5.17}$$

with

$$E_0 = \frac{m^*}{m}\frac{\pi^2\omega_p^2}{V_F e} \tag{5.18}$$

similar to the equation for single-particle (Zener) tunneling. The threshold field E_T is the consequence of the finite correlation length. The frequency-dependent conduction follows from Tucker's photon-assisted tunneling (PAT) theory (Tucker, 1979), giving (Bardeen, 1984, 1986) a scaling relation between the ω - and E-dependent response,

$$\sigma\left[\frac{\omega}{\omega_p}\right] = \sigma\left[\frac{E}{E_T}\right]. \tag{5.19}$$

According to Eq. (5.19) the small amplitude ac conductivity as the function of frequency has the same functional form as the dc conductivity on the function of electric field. Both saturate at the high-frequency and high-field limit, and Eq. (5.19) also implies a sharp threshold frequency ω_p.

A detailed discussion of the tunneling steps and of the microscopic wave functions that characterize the pinned and current-carrying state, as well as the possible effects of disorder, can be summarized by Bardeen (1986, 1987) in several reviews.

The model does not treat the low-frequency fluctuations that are assumed to be decoupled for the tunneling that occurs at high frequencies (Tucker, 1986), nor does it treat the polarization effects that are important for processes below threshold (Miller et al., 1985). Such processes are responsible for the absence of threshold frequency in contrast to Eq. (5.19).

2.6 VI. The Frequency- and Field-dependent Response

Based on the models discussed above, a variety of predictions have been made concerning the small amplitude ac response $\sigma(\omega)$ and the nonlinear dc response $\sigma(E)$. Detailed comparisons between theory and experiment are also available. The models also describe various experiments performed in the presence of both dc and ac applied excitations. The fact that many of the observations can be observed for rather different approaches concerning the dynamics of the collective mode is not too surprising, as theories that are in agreement with the experimentally observed $\sigma(\omega)$ or $\sigma(E)$ are expected to account also for most of the observations on $\sigma(\omega, E)$.

Many of the issues involved in analyzing the available experimental results are highly controversial at present; this is due partly to the fact that the experiments can be accounted for to a degree of accuracy using various starting points about the underlying theory, but also because the details of the nonlinear and frequency-dependent response are determined by the details of the pinning itself, and are dependent also on factors like temperature, size of the specimens, impurity concentration, etc.

2.6.1 A. Frequency-dependent Response

The frequency-dependent response of pinned CDW condensates has been explored in detail over an extremely broad spectral range, with experiments ranging from audio to the millimeter wave frequencies. The main features of the small amplitude response are displayed in Fig. 9; such representation emphasizes the highfrequency part of the response, with important features observed in the radio-frequency spectral range and below not visible in the figure.

The simplest approach to account for the frequencydependent conduction is to assume that the response is that of a harmonic oscillator with the equation of motion

$$\frac{dx^2}{dt} + \frac{1}{\tau}\frac{dx}{dt} + \omega_0^2 x = \frac{eE}{m^*} e^{i\omega t}, \tag{6.1}$$

where the pinning frequency ω_0 has been discussed before (see Sec. IV), the effective mass m^* is given in mean-field approximation by Eq. (3.4), and τ is a phenomenological damping constant. The real and imaginary part of the conductivity is given by

$$\mathrm{Re}\,\sigma(\omega) = \frac{ne^2\tau}{m^*} \frac{\omega^2/\tau^2}{\left(\omega_0^2 - \omega^2\right)^2 + \omega^2/\tau^2} \tag{6.2}$$

$$\mathrm{Im}\,\sigma(\omega) = \frac{ne^2\tau}{m^*} \frac{\left(\omega_0^2 - \omega^2\right)\omega/\tau}{\left(\omega_0^2 - \omega^2\right)^2 + \omega^2/\tau^2} \tag{6.3}$$

Frequency-dependent-conductivity measurements have been performed in all materials that show charge-density-wave transport phenomena, and, in general, Eq. (6.27) gives a good description of the experimental findings. In Fig. 27, $\mathrm{Re}\,\sigma(\omega)$ and $\mathrm{Im}\,\sigma(\omega)$ are displayed for TaS_3 with a solid line given by Eq. (5.2) with parameters given in the figure (Sridhar et al., 1986). The dotted line assumes a distribution of pinning frequencies, and the significance of this will be discussed later. The frequency-dependent response appears to be overdamped in TaS_3, and also in $NbSe_3$ (Reagor, Sridhar, and Grüner, 1986) in both CDW states, while in other materials a weakly damped response is observed - with τ, however, temperature and also impurity concentration dependent. The conductivity measured in $(TaSe_4)_2\,I$ and two different temperatures is shown in Fig. 28 (Kim et al., 1987). While ω_0 is slightly temperature dependent, the main effect is the strongly increased damping of the higher temperature. Similar behavior has been found in

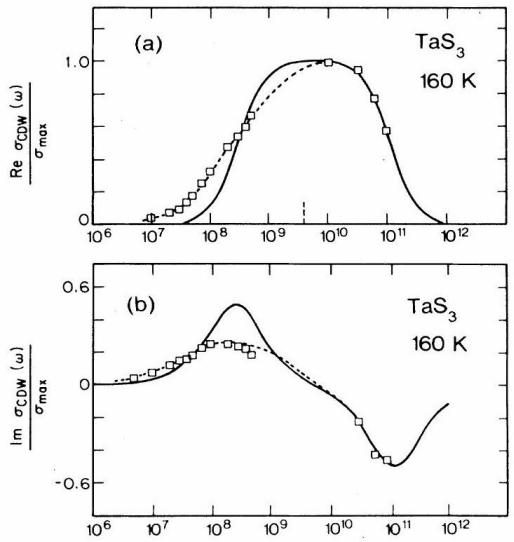


FIG. 27. Re $\sigma(\omega)$ and $\operatorname{Im} \sigma(\omega)$ measured in nominally pure TaS_3. The solid line is a fit to a harmonic oscillator response, Eq. (6.2), with parameters given in the figure.

$(NbSe_4)_2$ **I** (Phillip et al., 1987) and, although the data are far less complete, also in $K_{0.3}MoO_3$ (Ng et al., 1986). Fits such as those displayed in Figs. 27 and 28 can be used to evaluate the basic parameters-the pinning frequency ω_0, the effective mass m^*, and the damping constant τ-and these can be compared with theory.

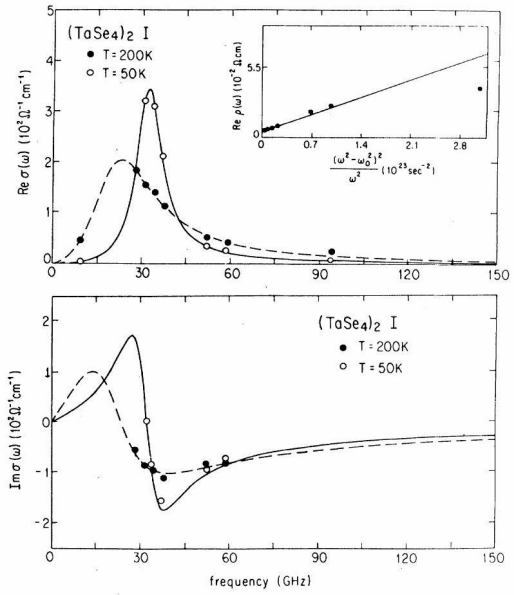


FIG. 28. $\operatorname{Re} \sigma(\omega)$ and $\operatorname{Im} \sigma(\omega)$ measured in nominally pure $(TaSe_4)_2$ I at two different temperatures. The solid line is a fit to a harmonic oscillator response, Eq. (6.2).

The pinning frequency ω_0 is in general of the order of 10^{11}sec^{-1} corresponding to a pinning energy $\hbar\omega_0 \sim 10^{-4}$ eV . It has also been shown, both in TaS_3 (Reagor and Grüner, 1986) and in ($TaSe_4)_2$ I (Kim et al., 1987), that impurities increase ω_0 dramatically, but, due to lack of knowledge about the precise impurity concentrations, in the alloys investigated the

concentration dependence could not be evaluated. In the strong pinning limit, the restoring force is given by $K = V_0\rho_1 n_i$ and, consequently, the pinning frequency

$$\omega_0 = \sqrt{\kappa/m^*} = \left(\frac{V_0\rho_1 n_i}{m^*}\right)^{1/2} \tag{6.4}$$

giving, with $V_0 = 10^{-2}\text{eV}, \rho_1 = 0.1, m^* = 10^3 m_c$ (the free-electron mass), and $n_i = 0.1\%$, a characteristic frequency of 10^{11}sec^{-1}, in good agreement with the experimental findings. It should be noted that ω_0 is higher for materials with high transition temperatures, and this is related to the higher threshold fields observed in materials with higher T_c (see, for example, Fig. 15). The significance of this is not clear, and the finding is surprising because ω_0 is expected to be determined by the residual impurity concentration, which certainly varies from material to material. Clearly detailed studies of ω_0 as a function of n_i in various materials would be highly desirable. The pinning frequency is also only weakly temperature dependent in the materials studied so far, in contrast to the strongly temperature-dependent threshold field E_T and dielectric constant $\varepsilon(\omega \to 0)$. This suggests that both E_T and $\varepsilon\,(\omega \ll \omega_0)$ are determined by processes that are not directly related to the harmonic oscillator response as given by Eq. (6.2).

The effective mass is found to be temperature independent (Reagor, Sridhar, and Grüner, 1986; Sridhar et al., 1986), except close to T_p where the ratio m^*/m is (approximately) independent of temperature, in agreement with theory (Lee and Rice, 1979). m^* varies from material to material and strongly increases with increasing transition temperatures. The mean-field theory predicts that

$$\frac{m^*}{m} = 1 + \frac{4\Delta_s^2}{\lambda'\omega_{2k_F}^2} \tag{6.5}$$

where Δ_s is the single-particle gap (not necessarily related to the transition temperature T_p, due to the anisotropic nature of these materials). The phonon frequency and the electron-phonon coupling constant are not expected to vary significantly from material to material, and, consequently, to a first approximation m^* should be proportional to Δ_s^2. Such a plot is shown in Fig. 29, where the single-particle gaps were evaluated from the optical data, from the temperature dependence of the dc resistivity below the transition, or from the analysis of the temperature-dependent magnetic susceptibility (Johnston et al., 1985), and from optical (Geserich et al., 1986; Herr et al., 1986) and tunneling (Latyshev and Savitskaya, 1986) studies. The error bars represent ambigui-

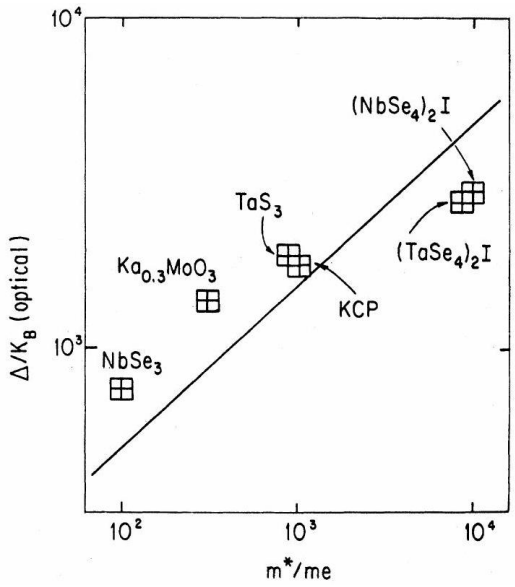


FIG. 29. Effective mass m^{*} / m_{e} vs the mean-field singleparticle gap Δ for various compounds. The solid line represents the relation $m^*/m_e \sim \Delta^2$.

ties associated with such determination of Δ (Reagor, 1987). In $NbSe_3$, it has been assumed that the BCS relation $\Delta = 35 k_B T_c$ is appropriate; this, however, appears to be in disagreement with recent tunneling measurements (Fournel, Sorbier, Konczykowski, and Monseau, 1986). The solid line in Fig. 29 is Eq. (6.5) with $\lambda' = 0.5$ and $\omega_{2k_F} = 50$ K, both reasonable values.

In all cases investigated so far, a Drude-type equation with a single relaxation time describes well the frequency-dependent response at frequencies $\omega > \omega_0$, and the relaxation time τ can be evaluated, both as the function of impurity concentration (where such studies are available). In TaS_3 (Reagor and Grüner, 1986; Sridhar et al., 1986), in $(TaSe_4)_2I$ (Reagor, Sridhar, and Grüner, et al., 1986; Kim et al., 1987), and in $(NbSe_4)_2I$ (Phillip et al., 1987), $1/\tau$ decreases with decreasing temperature and remains finite as $T \to 0$. Experimental results on two $(TaSe_4)_2I$ specimens and on alloys of $(Ta_{1-x}Nb_xSe_4)_2I$ with $x = 0.6\%$ are displayed in Fig. 30. The data can be well represented by the empirical equation

$$\frac{1}{2\pi\tau} = A + BT^2 \tag{6.6}$$

with A independent of the impurity concentration and B increasing with increasing number of impurities. This is in contrast to what is expected, as the temperaturedependent part should be the result of phonons or uncondensed electrons with the residual damping as $T \to 0$ of impurities. The observation is not explained at present.

The frequency-dependent response in the spectral range $\omega < \omega_0$ cannot be accounted for by a single harmonic oscillator response; the decrease of $\mathrm{Re}\,\sigma(\omega)$ with de-

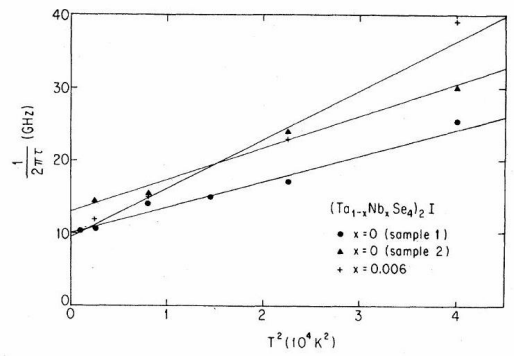


FIG. 30. Inverse relaxation time vs T^{2} in two $(TaSe_4)_2\,I$ specimens (A and B) and an alloy with 0.6%Nb. Samples A and B have a pinning frequency of $\omega_0 = 17$ and 35 GHz , respectively.

creasing ω is more gradual than what follows from Eq. (6.2). The behavior can be explained by assuming wide distribution pinning frequencies (Sridhar et al., 1986). Such an assumption gives, for a particular distribution, the dotted line of Fig. 31. While such an ad hoc assumption accounts for the main qualitative features of both $\mathrm{Re}\,\sigma(\omega)$ and $\mathrm{Im}\,\sigma(\omega)$, a different approach has been taken to describe the ω-dependent response in the radio frequency spectral range. At low frequencies both $\mathrm{Re}\,\sigma(\omega)$ and $\mathrm{Im}\,\sigma(\omega)$ can be described by a power-law frequency

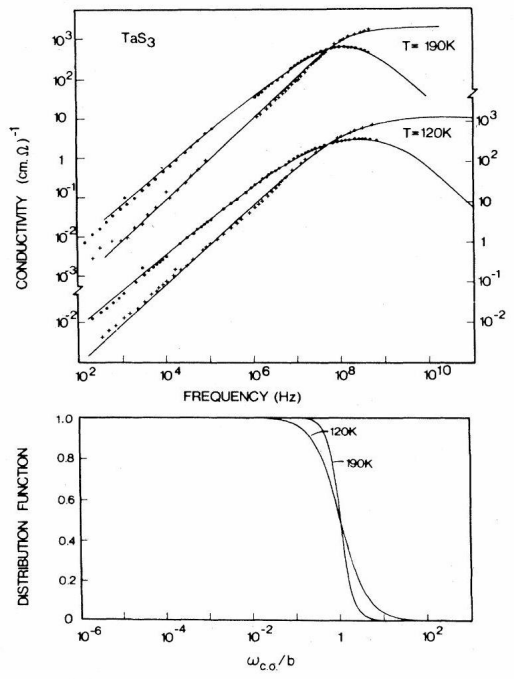


FIG. 31. Real and imaginary parts of the ac conductivity of TaS_3 vs frequency (Wu et al., 1985).

dependence (Wu, Mozurkewich, Mihály, and Grüner, 1986)

$$\sigma(\omega) = A\left(\frac{i\omega}{\omega_0}\right)^{\alpha} \quad \text{with } \alpha = 0.8 \tag{6.7}$$

Such behavior has been widely observed in various glasses and random systems (Ngai, 1979, 1980). The behavior also leads to a divergent dielectric constant $\varepsilon(\omega) = -4\pi\,\mathrm{Im}\,\sigma(\omega)/\omega$ as

$\omega \to 0$, and this is often referred to as zero-field cusp (Fisher, 1985; Littlewood, 1986). At low frequencies deviations from Eq. (6.7) are observed (Cava, Fleming, Littlewood, Rietman, Schneemeyer, and Dunn, 1984; Kalem et al., 1987), and the data are well represented in terms of an equation,

$$\varepsilon(\omega) = \varepsilon_{\mathrm{HF}} + (\varepsilon_0 - \varepsilon_{\mathrm{HF}}) \frac{1}{\left[1 + (i\omega\tau_0)^{1-\alpha}\right]^{\beta}} \tag{6.8}$$

where ε_0 and $\varepsilon_{\mathrm{HF}}$ are the zero- and high-frequency dielectric constants, τ_0 is an average relaxation time, and α, β (both less than one) are phenomenological parameters. Similarly to Eq. (6.7), Eq. (6.8) is also extensively used to describe the complex dielectric constant of various random and amorphous solids, and it has been found to account well for $\varepsilon(\omega)$ over a broad frequency range in pure (Cava, Fleming, Dunn, Rietman, and Schneemeyer, 1984) and in doped (Cava et al., 1985) $K_{0.3}MoO_3$, in TaS_3 (Cava et al., 1985; Kalem et al., 1987), in $NbSe_3$ (Cava, Fleming, Littlewood, Rietman, Schneemeyer, and Dunn, 1984), and in $(TaSe_4)_2I$ (Cava et al., 1986). A fit to data taken on $(TaSe_4)_2I$ is displayed in Fig. 32. The average relaxation time increases with decreasing temperature, and in all materials with a semiconducting CDW ground state the temperature dependence

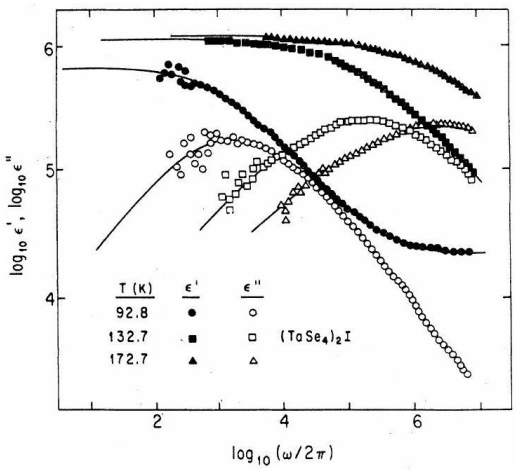


FIG. 32. Frequency dependence of the real (solid symbols) and imaginary (open symbols) parts of the dielectric constant for $\left(TaSe_4\right)_2I$ at three representative temperatures. Solid lines are from fits of Eq. (6.8) (from Cava et al., 1986).

$$\frac{1}{\tau_0} \exp\left(-\frac{\Delta_T}{k_B T}\right), \tag{6.9}$$

with Δ_T close to the single-particle gap, suggesting a close relation between the low-frequency CDW relaxation and the resistivity due to uncondensed electrons. The rather different behavior of the relaxation times evaluated from the high- and low-frequency transport data most probably reflects the different role of screening in different spectral regions. At high frequencies the small amplitude response is dominated by the oscillatory notion of the spatially averaged phase with the dynamics of local deformations not playing a significant role. Consequently, screening effects due to the normal electrons are not important. In contrast, at low frequencies Eqs. (6.7) and (6.8) suggest that the dynamics of local deformations are important. These involve the buildup of electric dipoles that have to be screened by the normal electrons. This screening time is often the order of the dc conductivity that rises exponentially with temperature, thus leading to Eq. (6.9) (Sneddon, 1984a, 1984b; Tucker et al., 1986; Littlewood, 1987).

Considerable effort has been made to account for the frequency-dependent response in terms of the tunneling model. The model predicts a scaling relation, given by Eq. (5.19), between $\sigma(E)$ and $\sigma(\omega)$. Early experimental results on $NbSe_2$ (Grüner, Clark, and Portis, 1981) and TaS_3 (Zettl and Grüner, 1982) could indeed be well represented by a scaling relation. No threshold frequency was, however, observed. Subsequently, it was suggested (Miller et al., 1985) that due to polarization effects, no threshold frequency occurs, and a revised scaling between ω and $E - E_T$ was postulated. This leads to an ω dependent conductivity having the form

$$\sigma(\omega) \sim \exp\left[-\frac{\omega}{\omega_p}\right].$$

Experiments that support this scaling theory have been summarized by Tucker (1986) and by Bardeen (1985a, 1985b). A behavior that can be represented as well as scaling has, however, been derived by Sneddon (1984a, 1984b, 1984c) and has also been shown to hold in the high-field and high-frequency limit (Robbins and Klemm, 1986), both of these on the basis of a classical description of the CDW dynamics.

2.6.2 B. Nonlinear Conductivity

Nonlinear conduction has been studied in more detail than the frequency-dependent response, and a variety of nonlinear phenomena have been observed, depending, even for the same material, on the temperature, impurity concentration, crystal perfection, and sample dimensions. In the majority of cases, the onset of nonlinear conduction at E_T is smooth, with a qualitative behavior similar to those displayed in Figs. 10 and 11. The phenomenological equation (5.17), first suggested by Fleming and

Grimes (1979) on the basis of experimental data displayed in Fig. 11, has subsequently been found to account for $\sigma(E)$ in other materials in a semiquantitative way over a broad range of electric fields. The behavior is in clear contrast to the prediction of the single-particle model, Eq. (5.6), which leads to a sharp rise of $\sigma(E)$ at fields close to E_T. The two functional dependences of σ and E are displayed in Fig. 33, together with numerical simulations by Tua and Zawadowski (1984) and by Matsukawa and Takayama (1986), both taking the dynamics of internal deformations into account. Both simulations depend on the parameters, such as the ratio between the elastic energy of the CDW and the interaction energy between the CDW and impurities. The majority of the experimental results reported to date on $NbSe_3$ follow the solid line closely, and this also is appropriate for TaS_3 (Zettl, Grüner, and Thompson, 1982). Due to heating effects, experiments have not been performed in $(TaSe_4)_2\,I$ in in $K_{0.3}MoO_3$, which would have allowed a close comparison between theory and experiment. Based on Fig. 33, it is clear, however, that both a classical description of the CDW dynamics, with internal degrees of freedom included, and the tunneling model can describe the main features of the nonlinear conduction in various materials over a broad range of electric fields.

Several groups have measured the details of nonlinear conduction, both in the high electric field (or in the high CDW velocity) limit, and at electric fields close to E_T. The perturbation equation of the deformable continuum model leads to a square-root field dependence of the current $\langle j(t)\rangle$ [see Eq. (5.6)], while in the high-velocity limit Eq. (5.17) leads to $\langle j(t)\rangle = \sigma_b E - A\sqrt{E}$. The experimental situation is highly controversial at present. While a $\sqrt{E}$ behavior was found in $NbSe_3$ by Maeda, Naito, and Tanaka (1985), a linear decrease of j with de-

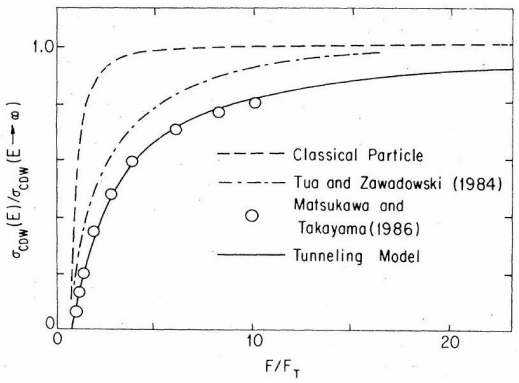


FIG. 33. Electric-field-dependent conductivity that follows from the classical particle model [Eq. (5.6)], from the tunneling model [Eq. (5.17)], and from calculations that take the dynamics of internal degrees of freedom into account. The experimental results follow the solid line closely.

creasing E was found by Zhang and Ong (1985), Oda and Ido (1982), and Tucker et al., (1981). In contrast, a stronger dependence, which could be described with an exponent of $n = \frac{3}{2}$, was found by Gill (1986c). The reason for these differences is not clear. Furthermore, crystal perfection, temperature, and other factors may also influence the experimental observations, and Joule heating may be difficult to avoid even by applying short electric field pulses.

Equally controversial is the experimental state of affairs near threshold, where the mean-field treatment of the dynamics of the many-degrees-of-freedom system leads to a power-law behavior, given by Eq. (5.14). Both the time-average current $\langle j(t)\rangle$ and the oscillation frequency f_0 were studied in various compounds; under ideal circumstances where the current density is uniform, $\langle j(t)\rangle$ is proportional to f_0, the ratio being independent of the applied field. While various groups have found that a power-law dependence can describe the experimental results well, in $NbSe_3$ the exponent is strongly temperature dependent, varying between 1.5 and 2.5 (Monceau et al., 1985). In TaS_3, $\xi = 1.5$ (Gill, 1985), and in $K_{0.3}MoO_3$, the current is a linear function of the applied field (Janossy et al., 1987). No attempt has been made to see whether these differences are due to different sample dimensions and/or whether the exponent varies from specimen to specimen.

In small samples the onset of nonlinear conduction tends to be sharp, and this often leads to well-defined peaks in the differential resistance dV/dI (Monceau et al., 1982; Borodin et al., 1986). An example of this behavior is displayed in Fig. 34, which also demonstrates the different behaviors that can be obtained depending on the temperature. The most likely explanation for the peaks in dV/dI is that they are a finite-size effect due to the phase-phase correlation length becoming comparable to the sample dimensions. This has been investigated in detail by Robbins and Klemm (1986) by using the model proposed originally by Klemm and Schrieffer (1983).

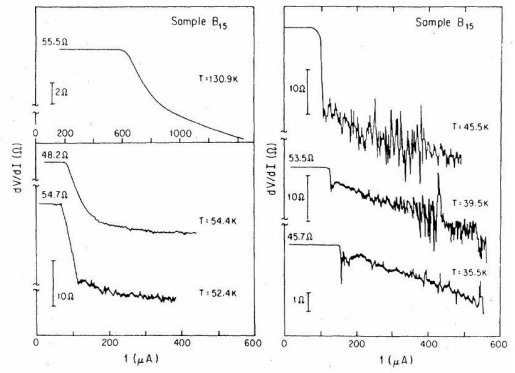


FIG. 34. Differential resistance dV/dI at various temperatures measured in NbS_{3}. The sudden onset of nonlinear conduction leads to a peak in the derivative (after Monceau et al., 1982a).

Finite-size effects play a particularly important role at low CDW velocities and at low frequencies, due to the divergence of the dynamical phase-phase coherence length in those limits. At high velocities and high frequencies, the dynamics of the internal modes become progressively more important. The effect leads to single-particle-like behavior near threshold, with a peak in dV/dI, with $\sigma(E)$ closely resembling the behavior obtained by Tua and Zawadowski (1984) and by Matsukawa and Takayama (1986). The resulting differential resistance curves, with different ratios $a = l/L_0$ of the sample length l to the phase-phase correlation length L_0, are shown in Fig. 35. The curve labeled by 0.0 corresponds to the classical particle model, and the crosses represent unpublished experimental results obtained on a sample of pure $NbSe_3$, with $l \simeq 1$ mm. As discussed in Sec. V, the behavior near threshold may depend on the experimental conductions: a constant electric-field drive leading to a positive differential resistance (DR) and E_T, with an infinite negative DR for constant applied current. The latter was investigated in detail (Hall et al., 1984b) in $NbSe_3$, and the relation to various dynamical instabilities such as $1/f$ noise and intermittent oscillations between various states has also been established.

Switching and hysteresis effects associated with the onset of nonlinear conduction were observed first in $NbSe_3$ (Zettl and Grüner, 1982b) and have also been found in TaS_3 (Mihály and Grüner, 1984; Kriza et al., 1985), in $(NbSe_4)_{3.33}\mathbf{I}$ (Wang, Saint-Lager, Monceau, Renaud, Gressier, Meerschaut, Guemas, and Rouxel, 1983) and in $K_{0.3}MoO_3$ (Dumas et al., 1983). The effect is related to extended pinning centers in the bulk of the specimens; this has been established by experiments where nonperturbative contacts were moved along the chain direction, and the current-voltage characteristics were investigated (Brown and Mihály, 1985; Hall et al., 1986). Models

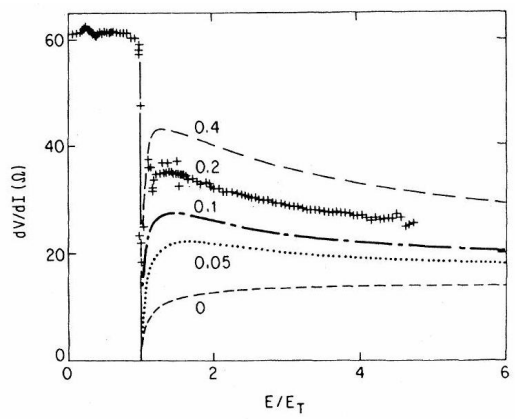


FIG. 35. Differential resistance calculated for finite sample sizes. The parameters shown in the figure are $a=l / L_{0}$ with l the length of the specimen and L_0 the phase-phase correlation length. Crosses represent experimental results on pure $NbSe_3$, of length $l \sim 1$ mm.

that attempt to account for switching assume that a large pinning center divides the specimen into two coherent regions each characterized by an average phase φ_L and φ_R, on the left- and right-hand side of the barrier. The coupling of the phases through the barrier may occur without the destruction of the CDW order parameter (Mihály, Chen, and Grüner, 1987) or through the development of an amplitude collapse of the pinning site (Hall et al., 1986). The coupled equations of motion, similar in structure to the equations of motion that were proposed to describe coupled Josephson junctions, lead, in certain parameter ranges, to switching and to time delay effects that are associated with the switching (Zettl and Grüner, 1982b; Janossy et al., 1985). The models, however, do not take into account the internal degrees of freedom in the two sides of the barrier; this may be important, in particular, to materials like TaS_3 where the phase coherence is less well established than in $NbSe_3$.

When switching occurs, intermittent chaotic behavior associated with the onset of the current-carrying state is also observed, although the phenomenon has not been investigated in detail. When the onset of the currentcarrying state is associated with switching and hysteresis phenomena, apparently random transitions between the two states are also detected (Grüner and Zettl, 1983; Mihály and Grüner, 1984). In this region a dramatic increase of the low-frequency noise is also observed (Hall et al., 1984a, 1984b). Although the random behavior may be due to temperature fluctuations, a more likely explanation is in terms of bistable states (Ben-Jacob et al., 1981). Such bistable configuration follows from the hysteretic nature of the transition, and any effect that leads to hysteretic behavior would also lead to the intermittent route to chaos.

The temperature dependence of the nonlinear conduction has been investigated recently in detail (Zhang and Ong, 1985; Fleming et al., 1986). The temperature dependence of the threshold field was discussed earlier. Close to the transition temperature, the magnitude of the nonlinear response in the large velocity limit was found to be close to the value that would be recovered in the absence of the Peierls transition (Monceau et al., 1976; Ong and Monceau, 1977; Zettl, Jackson, and Grüner, 1982); this has been discussed by Gorkov and Dolgov (1979) in terms of a two-fluid model. With decreasing temperature, the nonlinear current decreases and σ_{CDW} freezes out with a temperature dependence closely following the linear (Ohmic) current due to the electrons excited across the single-particle gap (Fleming et al., 1986). The behavior found for $(TaSe_4)_2\,I$ is displayed in Fig. 36. Writing the nonlinear current in terms of an electric-fielddependent damping,

$$\sigma_{\mathrm{CDW}}(E) = \frac{ne^2\tau(E)}{m^*} \tag{6.10}$$

suggests that (with n/m^* independent of the temperature) the CDW damping $\tau^{-1}(E)$ observed in moderate electric field diverges as the temperature is decreased.

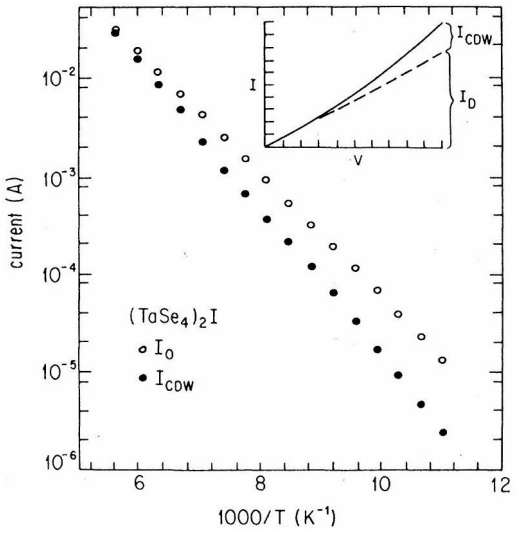


FIG. 36. Temperature dependence of linear and the nonlinear portion of the current in $\left(\mathrm{TaSe}\{4\}\right)\{2\}\ \mathrm{I}$ (Fleming et al., 1986).

This divergence is closely related to the divergent damping observed in the low-frequency dielectric relaxation. In both effects screening of the internal deformations by the normal electrons appears to be the rate limiting process in the field- and frequency-dependent response (Sneddon, 1984b; Littlewood, 1987).

2.6.3 C. Experiments in the Presence of Joint Dc and Ac Electric Fields

With the conductivity both strongly nonlinear and frequency dependent, a broad variety of experiments can be performed in the presence of both dc and ac applied fields,

$$E = E_{\mathrm{dc}} + E_{\mathrm{ac}} \cos \omega_{\mathrm{ext}} t \tag{6.11}$$

with either the dc or the ac response detected. The experiments lead to additional information on the response of the driven collective mode and, in principle, could also be used to distinguish between the various models proposed. Broadly speaking, the measurements can be divided in two groups: (1) those that test the overall nonlinear response $\sigma(E, \omega)$, and (2) those that focus on interference effects arising as a consequence of mode locking between the intrinsic current oscillation and the applied ac field. These will be discussed in depth in Sec. VII. Here only the nonlinear ac response will be summarized.

Both the ac and dc response have been studied in various materials in the presence of combined electric fields, and both classical approaches and the tunneling model have been extensively used to account for the experiments.

Many of the phenomena that occur in the presence of ac and dc electric fields have been calculated on the basis of the single degree of freedom, the so-called "classical particle," model (Wonneberger, 1979, 1983a, 1983b); Wonneberger and Breymayer, 1981; Breymayer et al.,

1982). The model leads to qualitative disagreement with experiments, in particular, near threshold. The reason for this is clear because the model also leads to divergent differential conductivity at E_T, also not observed. Models, which lead to ω - and E-dependent conduction in broad agreement with experiments, are in general also able to describe a variety of observations made in the presence of joint dc and ac fields. This most probably follows from nonlinear circuit theory and suggests that many of these experiments cannot be used to distinguish between the classical and quantum description of CDW dynamics. For other experiments, such as photonassisted tunneling, the predictions of the models are drastically different. However, other complications often make a direct comparison with the relevant theories difficult, if not impossible.

Experiments involving small applied ac electric fields are in general more straightforward to account for, since in this limit a perturbative treatment of the nonlinear dynamics in terms of the ac drive is appropriate. The first experiments of joint dc and ac fields, however, have been made in the large ac signal limit, where the ac-fieldinduced dc conduction was detected (Grüner, Zettl, Clark, and Bardeen, 1981). For a purely classical response, the dc conductivity is not modified by an applied ac signal for electric-field strengths $E_{\rm dc} + E_{\rm ac} < E_T$. However, a nonlinear dc response can be induced when $E_{\rm dc} + E_{\rm ac}$ exceeds the dc threshold electric field. The dc current $I_{\rm dc}$ detected for dc fields less than threshold E_T is a strong function of both $E_{\rm ac}$ and $\omega_{\rm ext}$ in $NbSe_3$ (Grüner, Clark, and Portis, 1981) and in $o - TaS_3$ (Zettl and Grüner, 1982b).

While detailed calculations on ac-field-induced ac conduction that are based on the classical particle model have not been performed to date, qualitative arguments can be advanced (Grüner et al., 1980; Grüner, Zettl, Clark, and Thompson, 1981) to account for the observations. For a pinned and strongly damped collective mode, the maximum displacement from the equilibrium position is given - for a parabolic potential - by

$$\delta x_0 = \frac{\left(eE_{\rm ac}/m^*\right)\omega_0^2}{\left[1 + \left(\omega/\omega_0^2\tau\right)^2\right]^{1/2}}. \tag{6.12}$$

If there is a critical displacement $x_{\rm crit}$ that leads to nonlinear dc conduction, then a critical ac field amplitude corresponding to the critical displacement is given by

$$E_{\rm crit}\left(\omega\right) = E_{\rm crit}\left(\omega = 0\right)\left[1 + \left(\omega/\omega_0^2\tau\right)^2\right]^{1/2}, \tag{6.13}$$

where $E_{\rm dc} + E_{\rm crit}\left(\omega = 0\right) = E_T$. The above equation describes well the nonlinear ac behavior of the system as
the function of applied field and of applied frequency, with parameters like E_T and $\omega_0^2\tau$ obtained from the measured dc nonlinear and small amplitudes ac response. The effect can also be described adequately in the framework of the tunneling model. The dc current density in the presence of an ac field is given by (Tucker, 1979; Tucker et al., 1981; Miller et al., 1983)

$$I_{\rm dc}\left(V_{\rm dc}, V_{\rm ac}\right) = \sum_{n=-\infty}^{\infty} J_n'^2\left(\frac{eV_{\rm ac}}{\hbar\omega}\right) I_{\rm dc}\left(V_{\rm dc} + \frac{n\hbar\omega}{e}\right), \tag{6.14}$$

where J_n' is the Bessel function of order n. With $I_{\rm dc}\left(V_{\rm dc}\right)$ and $\sigma(\omega)$ as input parameters, the $I_{\rm dc}\left(V_{\rm dc}, V_{\rm ac}\right)$ curves generated compare favorably with experiments both in $NbSe_3$ and in TaS_3. Various experiments have also been performed in the small ac signal limit, but in the nonlinear dc conductivity region. Both the ac and dc response can be detected in the presence of joint ac and dc excitation. Moreover, phenomena that arise in the presence of two applied ac fields can also be studied. The applied fields

$$E = E_{\mathrm{dc}} + E_{1\mathrm{ac}} \cos(\omega_1 t + \varphi) + E_{2\mathrm{ac}} \cos \omega_2 t \tag{6.15}$$

and the parameters that are measured are classified as follows.
(a) ac response: differential conductivity. Here I_{ac} is detected for $E_{2\mathrm{ac}} = 0$ with E_{dc} and ω_1 varied. In the low frequency, $\omega \to 0$ limit, the classical equation

$$I_{\mathrm{ac}} = \frac{dI_{\mathrm{dc}}}{dE_{\mathrm{dc}}} E_{1\mathrm{ac}} \tag{6.16}$$

leads to the differential conductivity; σ_{ac} gives directly the first derivative of the dc $I - V$ characteristics.
(b) Rectification. The dc response ΔI_r is detected, again with $E_{2\ \mathrm{ac}} = 0$. In the $\omega \to 0$ limit

$$\Delta I_r = \frac{1}{2} E_{1\mathrm{ac}}^2 \frac{d^2 I_{\mathrm{dc}}}{dE_{\mathrm{dc}}^2}, \tag{6.17}$$

and at low frequencies the rectified current is proportional to the second derivative of the $I - V$ curve.
(c) Harmonic mixing. The signal is detected at frequencies $\omega_1 - 2\omega_2$, and this, for $\omega_1 = 2\omega_2$, corresponds to a dc harmonic mixing current. In the low-frequency limit

$$\Delta I_{\mathrm{nm}} = \frac{1}{4} E_{1\mathrm{ac}}^2 E_{2\mathrm{ac}} \frac{d^3 I_{\mathrm{dc}}}{dE_{\mathrm{dc}}^3} \cos 2\varphi \tag{6.18}$$

i.e., the harmonic mixing signal is proportional to the third derivative of the current-voltage characteristics.

The ac conductivity in the presence of a dc field has been studied both in $NbSe_3$ (Longcor, 1981) and in TaS_3 (Miller et al., 1983, 1984; Zettl and Grüner, 1984). In Fig. 37, both the real and imaginary part of the ac conductivity for $o - TaS_3$ in a broad parameter range is

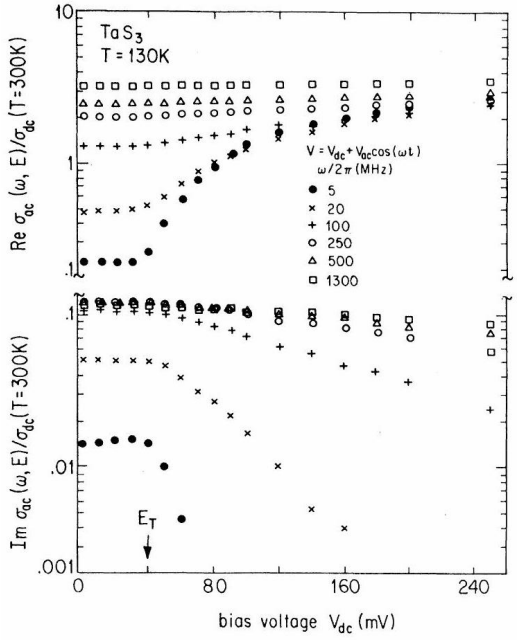


FIG. 37. Real and imaginary parts of the ac conductivity of orthorhombic TaS_{3} vs applied dc bias voltage V_{dc}. The threshold field for the onset of nonlinear dc conduction is indicated by an arrow (Zettl and Grüner, 1984).

displayed. The ac response is not affected by dc fields $E_{\rm dc} < E_T$, but both the in-phase and the out-of-phase components are enhanced with increasing dc bias in the nonlinear conductivity region. These experimental findings have not been accounted for in terms of the classical particle model, but an extension of the classical dynamics to a model for which coupled particles are considered accounts for the experiments in detail (Sneddon, 1984b, 1984c). In Fig. 38 the results of these calculations are displayed. Here σ' and σ'' refer to the in-phase and out-of-phase components of the ac conductivity; P and HP are parameters, which are related to the threshold field E_T and to a characteristic frequency determining the ω-dependent response in the absence of dc bias. Comparing this figure with Fig. 37, it is clear that all the important features of the experiments are recovered by calculations based on purely classical dynamics. In terms of photon-assisted tunneling theory, the ac current (Miller et al., 1983; Thorne et al., 1984) is

$$\begin{aligned} \mathrm{Re}\, I(\omega) &= \frac{1}{2\alpha\omega}\left[I_{\rm dc}\left(E_{\rm dc}+\alpha\omega\right) - I_{\rm dc}\left(E_{\rm dc}-\alpha\omega\right]\right. \\ \mathrm{Im}\, I(\omega) &= \frac{1}{2\alpha\omega}\left[I_{kk}\left(E_{\rm dc}+\alpha\omega\right) - 2I_{kk}\left(E_{\rm dc}\right)\right. \\ &\qquad \left.+I_{kk}\left(E_{\rm dc}-\alpha\omega\right)\right] \end{aligned} \tag{6.19}$$

where the imaginary part is written in terms of the Kramers-Kronig transform

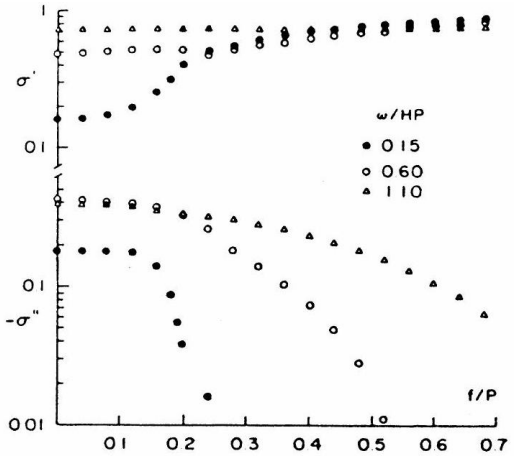


FIG. 38. ac response of an incommensurate chain with infinite-range interactions. HP is defined in the text; f/p refers to the dc field, σ' and σ'' to the real and imaginary ac conductivity (after Sneddon, 1984c).

$$I_{kk}\left(E_{\rm dc}\right) = P\frac{1}{\pi}\int_{-\infty}^{\infty}\frac{E_{\rm dc}}{\bar{E}_{\rm dc}-E_{\rm dc}}I_{\rm dc}\left(E_{\rm dc}\right) \tag{6.20}$$

and α is the voltage-frequency scaling parameter $\alpha = h/e$, as given by Eq. (5.44). With α evaluated from the measured $\sigma(\omega)$ and $\sigma(E)$, Eqs. (6.19) and (6.20) can be used to generate ac conductivity curves in the presence of a dc bias. These are shown in Fig. 39, together with experimental results on o-TaS $_3$ (Thorne et al., 1984).

The most straightforward experiment on rectification is photon-assisted tunneling (PAT). Here the classical and quantum theories lead to fundamentally different predictions. The name PAT refers to an experiment where the specimen is biased below threshold, and a small amplitude ac excitation is used to induce nonlinear conduction. For a purely classical system, no

rectified current is obtained for combined dc and ac fields $E_{\rm dc} + E_{\rm ac} < E_T$. In the quantum limit, Tucker's theory (1979) leads to a rectified current

$$\Delta I_r = \left(\frac{e^* E_{\rm ac}}{2\hbar\omega}\right)^2 [I_{\rm dc}\,(E_{\rm dc} + \alpha\omega) - 2I_{\rm dc}\,(E_{\rm dc}) - I_{\rm dc}\,(E_{\rm dc} - \alpha\omega)] \tag{6.21}$$

which for $V_{\rm dc} < V_T$ (and for $V_{\rm dc} - \alpha\omega_{\rm ext} < V_T$) reduces to

$$\Delta I_r = \left[\frac{e^* E_{\rm ac}}{2\hbar\omega}\right] I_{\rm dc}\,(E_{\rm dc} + \alpha\omega) \tag{6.22}$$

Thus the energy quantum $\alpha\omega$ can span the difference between $V_{\rm dc}$ and V_T even though a classical field amplitude $V_{\rm ac}$ is too small to do so. Early experiments on $NbSe_3$

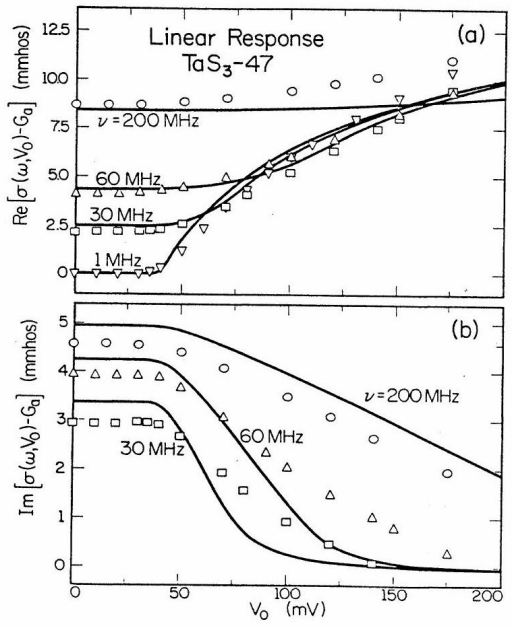


FIG. 39. Real and imaginary parts of the ac conductivity in o TaS_{3} vs applied dc voltage. The solid lines are calculated curves, using the tunneling model prediction Eq. (6.19) with parameters given in the text (Miller et al., 1985).

(Grüner, Zettl, Clark, and Bardeen, 1981) and on $o - TaS_3$ (Zettl and Grüner, 1982a, 1982b) failed to detect photonassisted tunneling for specimens biased below E_T and at frequencies where [on the basis of scaling relation between $\sigma(\omega)$ and $\sigma(E)$ the tunneling theory suggests significant ΔI_r. The reason for this is not entirely clear at present; if the tunneling model is appropriate, then a likely explanation lies in complicated low-frequency and long-time phenomena, which are associated with the development of the current-carrying CDW state (Lyons et al., 1985).

Detailed rectification experiments in the dc nonlinear conductivity region have been performed both in $NbSe_3$ (Richard et al., 1984) and in o-TaS (Miller et al., 1983; Thorne, 1984; Miller et al., 1985). Harmonic mixing has also been investigated in detail both in the radio frequency spectral region (Miller et al., 1983) and at microwave frequencies (Seeger et al., 1982, 1984a, 1985), and has been accounted for within the framework of the tunneling model. In particular, the experimental result that was observed is principal evidence for tunneling in the absence of phase shift in the small difference-frequency harmonic response (Miller et al., 1983,

1985; Thorne et al., 1986). Similar, small phase shifts were, however, obtained on the basis of the classical particle model by Wonneberger (1983a, 1983b), and detailed calculations by Liu and Sneddon (1987) on the basis of the Fukuyama-Lee-Rice model lead to a rather good agreement with all
of the essential features of the experiment conducted in a broad range of frequencies and electric field.

It appears therefore that both a classical description and the tunneling model can account for all the essential findings concerning the small amplitude ac response, the nonlinear dc response, and a wide class of experiments performed in the presence of the ac and dc fields. Detailed comparison between theory and experiments that often are claimed as clear evidence for one or another model are often not reproduced in other laboratories; consequently, the matter whether classical or quantum models are required to describe the dynamics of the collective mode remains controversial.

2.7 VII. Current Oscillations and Interference Effects

Since the discovery of Fleming and Grimes (1979) of the current oscillations in the nonlinear conductivity region a variety of experiments have been performed where interference effects between this intrinsic oscillation and the externally applied ac field have been studied. The experiments, similar in many respects to those performed in Josephson junctions, display a variety of phenomena that are of general interest (such as the possibility of various routes to chaos; see, for example, Zettl and Grüner, 1986). They also have been used to distinguish between the various models of charge-density-wave transport.

2.7.1 A. Current Oscillations

Questions as to whether the current oscillations are a bulk effect and whether they are generated at the contacts or also at other pinning centers have been addressed in Sec. III. While the question is not fully resolved, the existence of these oscillations, indicating a high degree of coherence, particularly in $NbSe_3$, is well established. In carefully prepared specimens the quality factor of the oscillations is high, and a fundamental with several harmonics with decreasing intensity is observed. An example is shown in Fig. 40 (Mozurkewich and Grüner, 1983b).

In recent experiments in $NbSe_3$ (Thorne et al., 1987) extremely coherent current oscillations were detected. In certain cases $Q \sim 30000$ was observed in the upper CDW state. The measured spectral width is a sensitive function of crystal perfection, and in samples of average quality the spectral width is significantly larger. The quality factors also depends strongly on temperature, and as a rule it decreases with decreasing T. In other materials, Q is significantly smaller; in good quality TaS_3 specimens $Q \sim 10$, while in $(TaSe_4)_2\,\mathbf{I}$ the value is of the order of 1 (Mozurkewich et al., 1983).

It also tends to be smaller in specimens with larger cross sections (Mozurkewich et al., 1983), as expected for loss of perpendicular dynamical coherence with an increased cross-sectional area. The above observations clearly establish the intimate relation between the quality

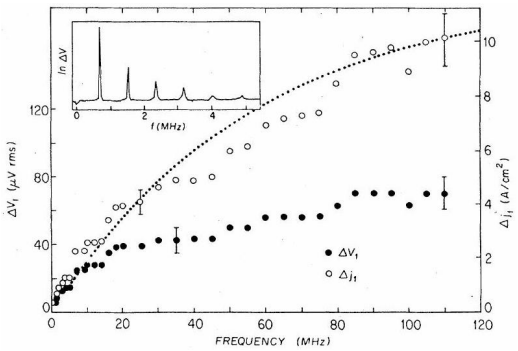


FIG. 40. Amplitude of the fundamental oscillation in NbSe_{3} at 42.5 K vs oscillation frequency. The amplitude is plotted both as a voltage ΔV_1 (solid symbols, left-hand scale) and as an equivalent current density Δj_1 (open symbols, right-hand scale). The inset shows a typical spectrum. The dotted line is Eq. (6.25). From Mozurkewich and Grüner (1983).

factor of current oscillations and dynamical coherence throughout the specimens. Whether normal electron screening is important in establishing such coherence in $NbSe_3$, and also in other materials near to T_p, remains to be seen.

Another fact that plays an important role in the generation of oscillating current is the existence of macroscopic defects. These have been studied by employing nonperturbative contacts (Brown and Mihály, 1985). For large extended defects, the amplitude fluctuations of the order parameter are also expected to be important, and several models have been suggested (see, for example, Maki, 1985, 1986). Because of the nonlinear response a mode locking is expected between the intrinsic current oscillation and an externally applied field. This was first detected by Monceau et al. (1980). The locking leads to a frequency pulling and, consequently, to a modification of the dc $I-V$ characteristic in the form of well-defined steps. The ac response is also influenced by mode locking, leading to inductive dips in the dielectric constant.

2.7.2 B. Interference Effects

While interference phenomena have been reported in various materials (Brown and Grüner, 1985; Brown et al., 1985a; Fleming, Dunn, and Schneemeyer, 1985; Wu et al., 1985; Latyshev et al., 1986), most of the experiments have been performed in $NbSe_3$. In this compound the phase-phase correlation length appears to be long, comparable to the dimensions of the specimens (Fleming et al., 1984), and, consequently, the response to external drives is highly coherent. This is responsible for the extremely coherent current oscillations observed in pure specimens in both CDW states, in contrast to the weak and broad Fourier components of the oscillating current in other material CDW states. The high degree
of dynamical coherence also suggests that internal degrees of freedom may be of less importance in this material than in others, and these can be included perturbatively when the observations are accounted for by any particular model.

In order to discuss these phenomena in detail, it is useful to recall the formal correspondence between the equation of motion, Eq. (5.2), and the Stewart-McCumber model of the resistively shunted Josephson junction (see, for example, Barone and Paterno, 1982), and to use the vast literature on the Josephson effects to account for observations associated with the dynamics of chargedensity waves. (The equation of motion is also equivalent to that of a damped, driven pendulum and of a phaselocked loop.) Including the inertial terms, Eq. (5.2) in dimensionless form reads

$$\frac{d^2\varphi}{dt^2} + \Gamma\frac{d\varphi}{dt} + \sin\varphi = \frac{E}{E_T}, \tag{7.1}$$

where $\theta = (\omega_0\tau)^{-1}$ and time is measured in units of ω_0^{-1}. The equation of motion of the resistively shunted Josephson junction is

$$\frac{d^2\theta}{dt^2} + G\frac{d\theta}{dt} + \sin\theta = \frac{I}{I_j} \tag{7.2}$$

where Γ is the phase difference across the junction, I is the current, $G = (RC\omega_j)^{-1}$, with R and C the junction resistance and capacitance and $\omega_j = 2eI_\tau/Ch$. Time is measured in units of ω_j^{-1}, and I_j is the critical current. The threshold electric field for CDW conduction corresponds to the critical Josephson current, and the pinned CDW state to the zero-resistance state in Josephson junctions. Current oscillations in the current-carrying CDW with $j_{\mathrm{CDW}}/f_0 = 2e$ per chain correspond to the ac Josephson effect with the voltage-frequency relation $V/f_0 = 2e/\hbar$. The latter was first demonstrated by detecting a change of the dc current-voltage characteristics in the presence of applied ac radiation. Steps in the I - V curve when $f_0 = f_{\mathrm{ext}}$ were first found by Shapiro (hence the name "Shapiro steps"), and, consequently, similar ac interference effects found in CDW systems will also be called Shapiro steps. Experiments of this kind were first performed in $NbSe_3$ by Monceau et al. (1982), who measured the differential resistance dV/dI in the presence of ac fields. Their results, obtained for keeping the dc current constant and varying the frequency of the applied ac field, are displayed in Fig. 41. Peaks in the derivative correspond to applied frequencies for which $\omega_{\mathrm{ext}} = n\omega_0$ with ω ranging from 1 to 4 , as indicated in the figure. Various sequences called F_1, F_2, and F_3 are detected, and this may be due either to the fibrous nature of the material or to the contact configuration used in the experiments. In small and highly uniform specimens, the interference is more dominant and shows up in direct $I - V$ curves (Zettl and Grüner, 1983b, 1984). Interference effects have also been observed recently in the elastic properties (Bourne et al., 1986). In Fig. 42, dc $I - V$ traces are shown in the presence of an applied field at constant

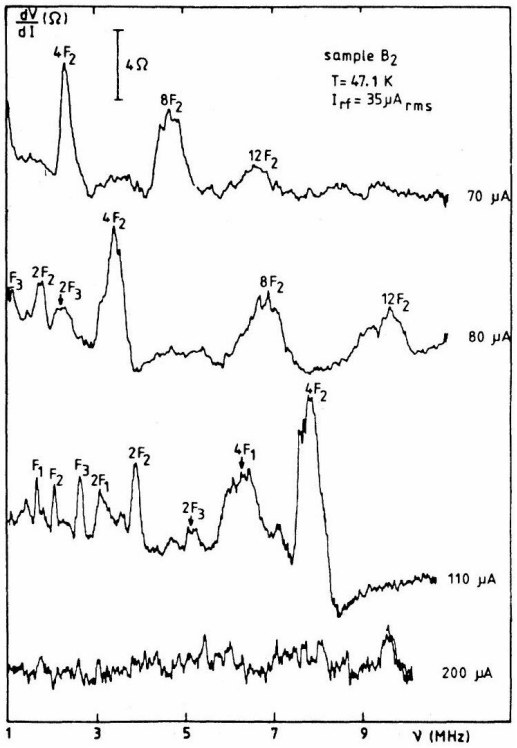


FIG. 41. Differential resistance dV/dI in NbSe_{3} observed by sweeping the frequency of the rf current, for a constant dc current. The various sets of interference peaks are labeled by F_1, F_2 and F_3 (Monceau et al., 1982).

frequency $f_{\rm ext} = 100$MHz. For $V_{\rm ac} = 0$, a smooth nonlinear I - V curve is obtained with a well-defined threshold voltage V_T for the onset of nonlinear conduction. Increasing $V_{\rm ac}$ results in the appearance of broad peaks at certain dc currents, and these become sharper with increasing ac amplitude. The position of the $n = 1$ step, indicated on the figure, corresponds to a dc current $I_{\rm dc}$ which, in the absence of ac fields, yields an intrinsic oscillation frequency $f_0 = 100$MHz, as established by direct measurements of the current oscillations. There are also harmonic steps corresponding to $n = 2$ (where the intrinsic oscillation frequency couples to the first harmonics of the external frequency), and a subharmonic step corresponding to $n = \frac{1}{2}$ is also visible in the figure. The step height δV first increases and then decreases with increasing $V_{\rm ac}$, while the threshold voltage V_T is strongly reduced by the applied ac fields. The step height and threshold field can be calculated by solving Eq. (7.1) directly [Fack and Kose (1971); Clark and Lindelof (1976); Lindelof (1981)]. In the high-frequency ($\omega \gg \omega_0^2\tau$) limit,

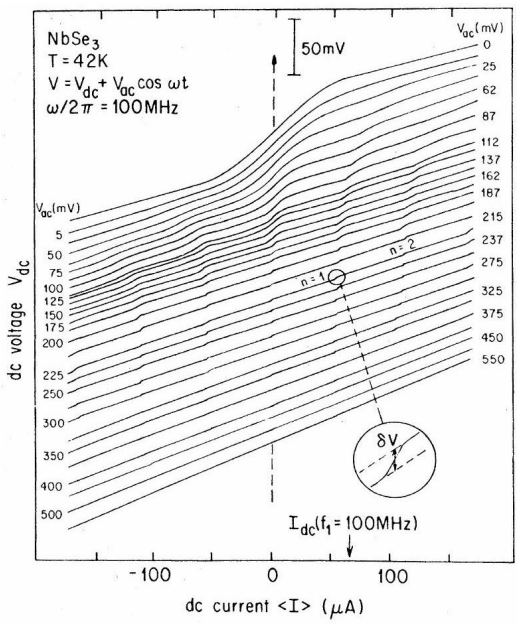


FIG. 42. Shapiro steps in the dc $I - V$ traces for NbSe_{3} when rf field is applied at frequency $\omega/2\pi = 100$MHz and of amplitude $V_{\rm ac}$. The step height δV is defined in the figure. No Shapiro steps are observed for $V_{\rm ac} = 0$, while the maximum step height is at approximately $V_{\rm ac} = 100$mV. The arrow indicates the dc current that yields a fundamental noise frequency $f_1 = 100$ MHz. The step index is n (Zettl and Grüner, 1984).

$$\begin{aligned} \delta V &= \beta 2 V_T(\omega = 0) J_n'\left(V_{\rm eff}\right) \\ V_T &= V_T(\omega \to 0) J_0'\left(V_{\rm eff}\right) \end{aligned} \tag{7.3}$$

where J_n' is the Bessel function of order n, and

$$V_{\rm eff} = \frac{V_{\rm ac}\omega_0^2\tau}{V_T(\omega \to 0)}. \tag{7.4}$$

The parameter β is phenomenological, representing the volume fraction of the specimen that responds coherently to the applied dc and ac fields. In Fig. 43 the $n = 1$ step height is shown as a function of the ac amplitude $V_{\rm ac}$. The solid line is Eq. (7.3) with parameters $\omega_0^2\tau/2\pi = 170$ MHz and $\beta = 0.17$. The characteristic Bessel function behavior is clearly recovered by experiment; furthermore, the crossover frequency $\omega_0^2\tau$ is in approximate agreement with that derived from the low-field ac conductivity measurements. The value $\beta = 0.17$ indicates that a large fraction of the specimen is responding coherently to the external perturbations. While analytical solutions are not available in the low-frequency $\omega < \omega_0^2\tau$ limit, computer simulations (Fack and Kose, 1971; Clark and Lindelof, 1976) also lead to Bessel function behavior with step heights strongly dependent on the frequency. The frequency dependence of the maximum step height (Zettl

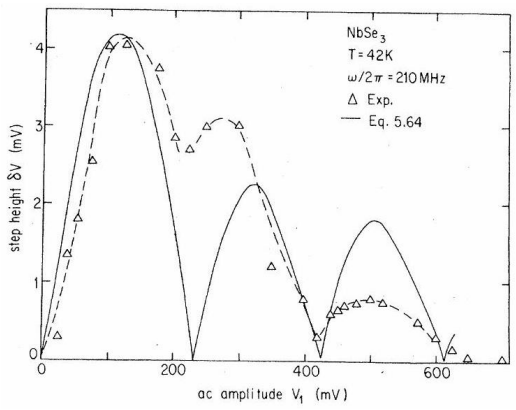


FIG. 43. Step height δV vs ac amplitude V_{ac} for Shapiro steps in $NbSe_3$. The rf frequency is 310 MHz and the step index is $n = 1$. The solid line is the prediction of the classical model, Eq. (7.3), with parameters $\omega_0^2\tau/2\pi = 80\text{MHz}.V_T = 24\text{mV}, \beta = 0.17$ (Zettl and Grüner, 1984).

and Grüner, 1984) can be analyzed in terms of the model leading to a crossover frequency, in agreement with the values quoted above. While the threshold voltage decreases with increasing V_{ac}, the Bessel function behavior predicted by Eq. (7.1) is not recovered by early experiments, and instead of displaying oscillations, V_T goes to zero smoothly with increasing V_{ac} . Subsequent experiments by Latyshev et al. (1987) and by Thorne et al. (1987) on carefully prepared specimens displayed oscillations in E_T, in full agreement with predictions based on Eq. (7.1).

Interference phenomena also influence the frequencydependent response, leading to steps in $\text{Re}\,\sigma(\omega)$ and inductive dips in $\varepsilon(\omega)$ at currents for which $f_0 \sim f_{\text{ext}}$. The dielectric constant ε and conductivity $\text{Re}\sigma$, both measured at fixed frequency $\omega_0/2\pi = 3.2\text{MHz}$, are shown in Fig. 44 as a function of dc bias voltage. The large step and strong inductive response at $V_{\text{dc}} \sim 2.3\text{mV}$ correspond to currents where $f_0 = f_{\text{ext}}$, and similar to the Shapiro-type steps, both a harmonic and subharmonic interference are evident. Although no calculations based on Eq. (7.1) are available, the interference effect can be accounted for by qualitative arguments that use mode locking between the intrinsic oscillation and the externally applied ac field (Zettl and Grüner, 1984). Not surprisingly, interference effects are observed also when $V_{\text{dc}} = \text{const}$ and the ac frequency is varied; these, however, have not been analyzed in detail. Frequency modulation effects related to interference phenomena have also been measured and analyzed (Stokes et al., 1987).

Interference effects have also been observed in TaS_3 (Brown and Grüner, 1985) and in $K_{0.3}MoO_3$ (Fleming, Dunn, and Schneemeyer, 1985), but, similar to the current oscillations, their magnitude is much weaker than those observed in $NbSe_3$. As discussed before, this may reflect a smaller degree of coherence in TaS_3, leading

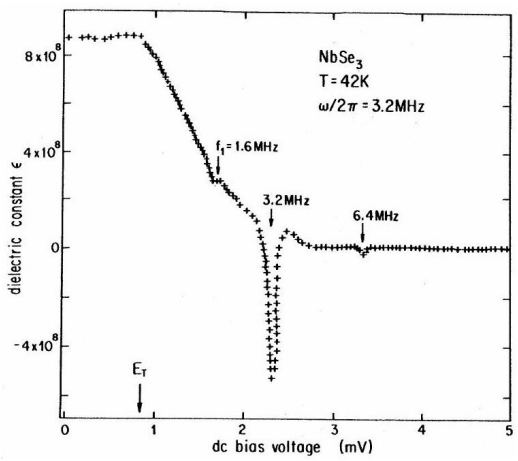


FIG 44. Real part of the ac conductivity $\operatorname{Re} \sigma(\omega)$ and dielectric constant $\varepsilon(\omega)$ measured at $\omega/2\pi = 3.2$MHz as a function of applied dc bias voltage. The threshold field is indicated by an arrow (Zettl and Grüner, 1984).

to smaller values of β in Eq. (7.3). In these cases, the interference peaks are also much broader than those observed in $NbSe_3$, suggesting a distribution of CDW velocities in the specimens. Such effects cannot be accounted for by models where the internal dynamics of the collective mode are neglected. Experiments where the derivative dV/dI is recorded instead of direct $I-V$ curves (Brown et al., 1984) show, aside from the harmonic locking structure, a rich subharmonic structure. In Fig. 45 the differential resistance, measured with and without an externally applied rf voltage at $\omega_{\rm ext} = 25$MHz, is displayed. For the low ac voltage used, the threshold for the onset of nonlinearity is not reduced significantly, but peaks (which correspond to steps in the direct I - V curves)

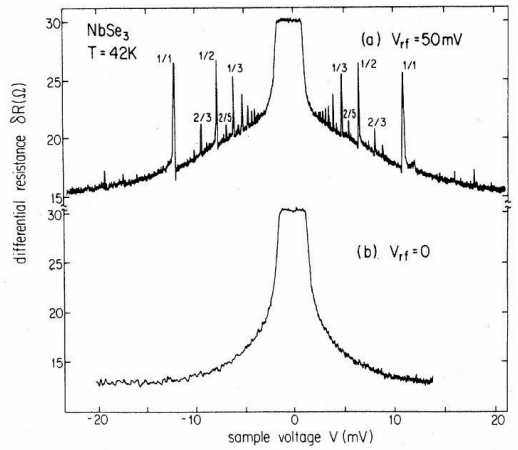


FIG. 45. Differential resistance of NbSe_3 with and without an applied rf voltage $V_{\rm rf}$. The numbers indicate the various subharmonic steps (Brown et al., 1984).

develop for a whole series of dc currents for which

$$p\omega_{\rm ext} = q\omega_0 \tag{7.5}$$

where p and q are integers. The ratio of p/q can be evaluated by plotting the frequency associated with a given peak versus the current $J_{\rm CDW}$ and comparing the slope $J_{\rm CDW}/\omega_{\rm ext}$ with that corresponding to the main Shapiro step, labeled by 1/1 in the figure. The steps $q = 1$

and $p \geq 1$ correspond to frequency locking between the internal frequency $f_0 = \omega_0/2\pi$ and all harmonics $p\omega_{\rm ext}$ of the applied rf field, as studied before (Zettl and Grüner, 1984), while steps that occur when $p/q < 1$ are called the subharmonic steps. Interference effects corresponding to subharmonic steps have been observed in the ac response (Zettl and Grüner, 1984; Fleming, Dunn, and Schneemeyer, 1985), and have also been detected in $o - TaS_3$ (Brown et al., 1985b). As the intrinsic oscillation contains many harmonics, and also the response of the nonlinear system to a sinusoidal ac field $E_{\rm ac} \cos \omega_{\rm ext}\, t$ is highly nonsinusoidal, it is natural to interpret the peaks as regions in which any harmonic of the internal frequency locks to any harmonic of the external field. Such behavior is in general referred to as a "devil's staircase" (Bak, 1982b). The interference peaks shown in Fig. 45 do not reflect complete mode locking, for which the differential resistance is the same as the ohmic resistance below E_T, and are usually referred to as "interference features." Complete mode locking and serveral subharmonics were first detected by Hall and Zettl (1984a, 1984b), and were subsequently observed by applying low frequencies and larger drive amplitude (Sherwin and Zettl, 1985; Thorne et al., 1987); an example for this behavior is displayed in Fig. 46. The condition under which complete mode locking is observed has not been completely settled, but most probably it is related to the extent of phase coherence throughout the specimens,

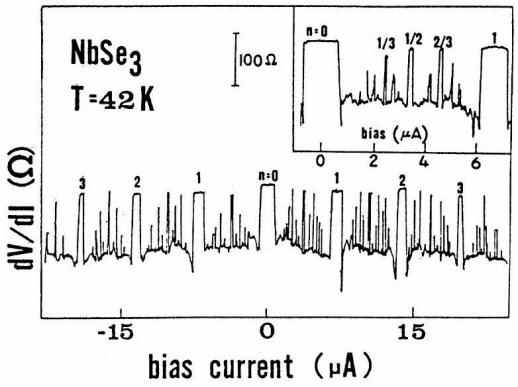


FIG. 46. Mode-locked Shapiro steps in NbSe_{3}. Over the mode-locked region, dV/dI is independent of dc bias. The inset shows the subharmonic structure in detail, with corresponding p/s values (Sherwin and Zettl, 1985).

since, as a rule, smaller samples with careful handling (and, consequently, less defects introduced during the contact preparation, etc.) display complete mode locking more readily. The effect of driven amplitude has been directly demonstrated by Sherwin and Zettl (1985) by performing broadband noise measurements in the presence of dc and ac drive. Broadband noise results from internal dynamics of the collective mode (Bhattacharya et al., 1985); consequently, its presence or absence clearly indicates the importance of internal dynamics of freedom. It was found that during mode locking the broadband noise is absence for complete mode locking, which is achieved for increasing ac drive; for small amplitude ac fields, only partial mode locking is observed.

Several dramatically different explanations have been advanced to account for the existence of the subharmonic steps. While an overdamped classical response, such as that given by Eq. (5.2), does not lead to subharmonic mode locking, inertial effects described by Eq. (7.1) restore subharmonic mode locking (Bak, 1982a, 1982b; Azbel and Bak, 1984). Furthermore, the main features of the mode-locking phenomenon can be studied by using a return map, which describes the time evolution of the CDW phase sampled at discrete times $t_m = 2\pi m/\omega_{\rm ex}$. Assuming that $\dot{\theta}_m$ is determined only by θ_m, due to dissipation, a "circle map"

$$\theta_{m+1} = \theta_m + \Omega + K \sin(2\pi\theta_m)/2\pi \tag{7.6}$$

results, where $\Omega = 2\pi f_0/\omega_{ex}$, and K describes the strength of the coupling between the system and the external perturbation-and is consequently assumed proportional to E_{ac}. The circle map is the return map appropriate to Eq. (7.1), as demonstrated by detailed numerical integrations (Bohr et al., 1984; Jensen et al., 1984). For finite-coupling K, mode locking occurs for certain values of ω_{ex} and f_0, i.e., f_0 remains fixed at $(p/s)\omega_{ex}$ over a finite range of E_{dc}. From Eq. (7.1) the time-averaged CDW current [and hence $(\partial\varphi/\partial t)$] is then dictated strictly by ω_{ex}. The mode-locked regions are separated by regions corresponding to free-running solutions of the phase.

The extent of the mode lock, i.e., the completeness of the devil's staircase, can in principle be determined directly from the subharmonic interference structure. Instrumental noise sets a lower limit to the size of the step that can be observed experimentally; consequently, the completeness of the staircase cannot be confirmed directly. The completeness of the staircase can, however, be examined by the following test: Choosing a discrimination level r, one adds up to the total width $S(r)$ of steps wider than r. If $N(r) = [I - S(r)]/r$ in an interval of unit length, then rN is the fraction of interval unoccupied by steps larger than r. For a complete staircase, $rN \to 0$ as $r \to 0$, and

$$N(r) = r^{-d} \tag{7.7}$$

with d defining the fractal dimension of the complementary Cantor set. As mentioned previously, the circle
map, Eq. (7.6), leads to $d = 0.87$, for $K = 1$. This univeral behavior has been confirmed by analog computer simulations and by studying a two-dimensional dissipative map (Alstrom et al., 1984). An analysis as described above, for experiments performed on $NbSe_3$ (Brown et al., 1984), gives a dimension $d = 0.91$, in striking agreement with theory.

There are, however, several serious problems with such an interpretation. First, one expects, on the basis of the circle map and corresponding simulations of Eq. (7.1), that the value of d depends critically on E_{ac} and on the selected range of p/s. Such behavior has not been observed in $NbSe_3$, and indeed a critical line cannot be clearly identified. Equally important, subharmonic steps are predicted by Eq. (7.4) only in the underdamped limit, and therefore should not exist in an overdamped system as determined from the frequency dependence of the low-field ac response. Furthermore, in the underdamped limit where Eq. (7.4) does predict subharmonic interference steps, chaos is also predicted on mode-locked steps. In contrast to this, for the samples displayed in Figs. 3 and 5, chaos is not observed for any combination of ac and dc drive parameters. In the language of the circle map, the fractal dimension $d \approx 0.91$ indicate that the system is at criticality ($K = 1$), yet the absence of chaos suggests $K = 1$ cannot be exceeded, irrespective of the magnitude of E_{ac}.

A conceptually simpler explanation has been advanced by Thorne et al. (1986, 1987) by assuming that the periodic potential is nonsinusoidal, but inertial effects and the effects of internal degrees of freedom are neglected. The magnitude of the subharmonic steps can be directly related to the components of the Fourier transform of the potential, and a good agreement has been obtained between experiment and theory for a potential

$$V(\theta) = \begin{cases} -\cos\theta \text{ for } -\frac{\pi}{2} < \theta < \frac{\pi}{2} \\ \cos\theta \text{ for } \frac{\pi}{2} < \theta < \frac{3\pi}{2} (\mathrm{mod}\, 2\pi) \end{cases} \tag{7.8}$$

Such potential is assumed for the tunneling model (Bardeen, 1986). The subharmonic step height, calculated and measured for the parameters given in the caption, are displayed in Fig. 47. The agreement is remarkable, suggesting that the above simple approach may be

appropriate. One should note, however, that the detailed form of the potential is probably not very important, as any potential with cusps [such as $\boldsymbol{V}(\theta)$ given by Eq. (7.8) as a triangle potential-potential, for example] leads to subharmonic mode locking with a smaller locking region for larger p and q values. More detailed experiments (Thorne et al., 1986) on $NbSe_3$ were also analyzed in detail, with a periodic potential such as that given by Eq. (7.8), which is completely adequate to account for all the features of the interference experiments.

A rather different approach has been taken by Tua and Ruvalds (1985) and by Coppersmith and Littlewood (1986), who assume that internal degrees of freedom are

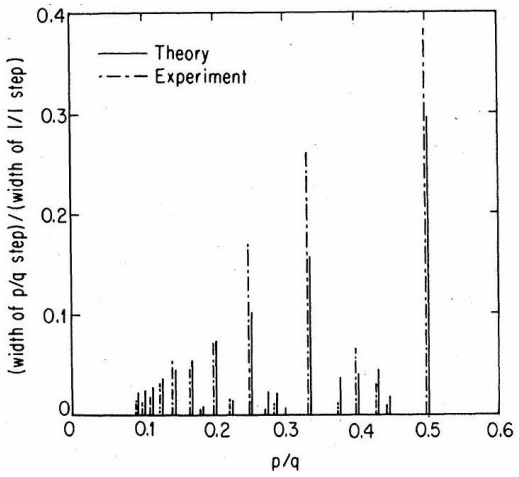


FIG. 47. Normalized step size $\delta V(p/q)\delta V(1/1)$ vs p/q. The solid lines are for a NbSe sample at \$T=42 \mathrm{˜K}\$ with $V_T\,(V_{\rm ac}=0)=2.0{\rm mV}, \omega_{\rm ac}/2\pi = 25{\rm MHz}$, and $V_{\rm ac}=30{\rm mV}$ peak to peak. The dotted lines are calculated by use of Eq. (10) and the pinning potential of Fig. 1(b), on assumption that $\omega_1/\omega = 1.6$. All 18 steps between $p/q = \frac{1}{11}$ and $\frac{1}{2}$ for which $q \leq 11$ are shown (Thorne et al., 1986).

essential in obtaining subharmonic steps. In a model of coupled domains (Tua and Ruvalds, 1985), a rich subharmonic structure is recovered in qualitative agreement with the experiments. The amplitude of the subharmonic disappears in the thermodynamic limit, in parallel with the disappearance of the current oscillations in this limit. Internal degrees of freedom, when treated perturbatively in the large CDW velocity limit, also lead to the emergence of subharmonics, with an increasing number of mode-locking regions having an increasing number of perturbative steps (Coppersmith and Littlewood, 1986). Such an approach leads to mode locking in the thermodynamic limit and allows a detailed calculation of the shape of the mode-locking curves. The results of such a calculation are displayed in Fig. 48, together with unpublished experimental results of Brown and Grüner (1988). The classical single-particle model (Grüner, Zawadowski, and Chaikin, 1981) leads to well-defined "wings" that accompany the mode-locked region. In contrast, the mode locking obtained by the model whose internal degrees of freedom are included (called the FLR, or Fukuyama-Lee-Rice, model on the figure) leads to no such wings, in agreement with experiment. In contrast to the experimental results displayed on the figure, substantial wings are also often observed (see, for example, Thorne et al., 1987), and the experimental state of affairs is far from being clear at present. The details of the mode locking appears to depend on several factors, such as sample quality, contact geometry, sample purity, and temperature, and a systematic investigation of these factors has not been performed as yet. Such experiments, however, ap-

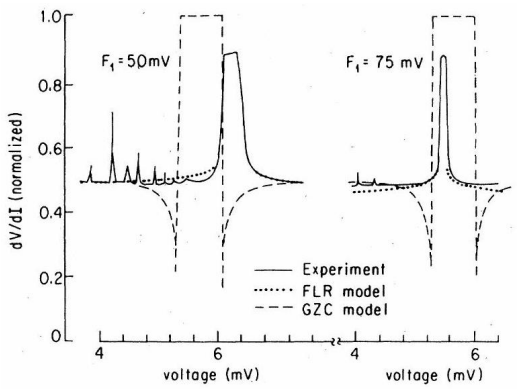


FIG. 48. Differential resistance dV/dI vs dc voltage V_{0} near the first harmonic feature $Q \cdot v \sim \omega_{\rm ac}$ for $NbSe_3$ with ac frequency $\omega_{\rm ac} = 25$MHz and ac voltage amplitudes $V_1 \sim 50$ and 75 mV (Brown and Grüner, 1988) for a sample with $V_T \sim 2$mV. Also shown are theoretical fits using the Fukuyama-Lee-Rice (FLR) deformable CDW model (dotted line) and the Grüner-Zawadowski-Chaikin (GZC) one-degree-of-freedom result (dashed line). For FLR, both curves are fitted by use of a single parameter of order unity, as discussed in the text. The tops of the peaks are not calculated because the perturbation theory breaks down when the change in dV/dI is large (Coppersmith and Littlewood, 1986).

pear to be essential in order to distinguish between the various proposed models. It is also conceivable that internal degrees of freedom are important under some circumstances and are negligible in different situations.

As discussed earlier, in certain specimens of $NbSe_3$ the onset of the current-carrying state is not smooth, and the current-voltage characteristics display well-defined switching and hysteresis behavior. When subjected to combined ac and dc electric drive fields, such specimens again display dramatic mode locking with hysteretic structure (Hall et al., 1984b). The dc response is like that predicted by the circle map and similar to that displayed in Fig. 46. However, the range of mode lock for the harmonic Shapiro steps, i.e., for $p = 1, 2, 3, \ldots$, $s = 1$, is substantially larger, and the harmonic steps virtually fill all of Ω space, as shown in Fig. 49(a). The simultaneously measured ac response is a complicated function of ac amplitude $E_{\rm ac}$ and frequency $\omega_{\rm ex}$, and dc bias $E_{\rm dc}$. With fixed $E_{\rm ac}$ and $\omega_{\rm ex}$, increasing $E_{\rm dc}$ leads, on each mode-locking step, to a period doubling route to chaos. This is displayed schematically in Fig. 49(a), which shows vertical windows, each corresponding to a partiuclar period (or chaos) for the response. The corresponding frequency response spectra are displayed in Fig. 49(b). Period-doubling bifurcations and a chaotic behavior, distinguished by large broadband noise, are clearly observed. A period doubling route to chaos can also be observed by keeping the dc bias constant and smoothly changing $E_{\rm ac}$ or $\omega_{\rm ex}$. By systematic variation of all three parameters, i.e., $E_{\rm dc}, E_{\rm ac}$, and $\omega_{\rm ex}$, the response boundary between period $1, 2, 4, \ldots$ and chaotic solutions may

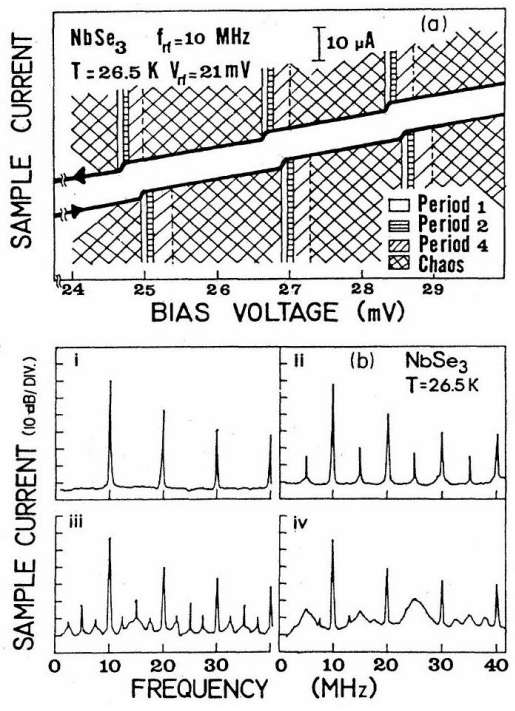


FIG. 49. (a) Schematic representation of the current response in the Shapiro step region of NbSe_{3}, for forward and reverse bias voltage sweeps. The heavy lines are the direct I - V traces, offset vertically for clarity; (b) frequency spectrum of the current response in the Shapiro step region. External rf drive frequency and amplitudes as in (a). (i) $V_{\rm dc} = 25.0$mV, period 1 ; (ii) $V_{\rm dc} = 25.1$mV, period 2; (iii) $V_{\rm dc} = 25.2$mV, period 4; (iv) $V_{\rm dc} = 25.5$mV, chaos (Hall et al., 1985).

be mapped out. In general, repetitive (hysteretic) period-doubling routes to chaos can be induced by varying all three parameters monotonically through a limited range of phase space.

A repetitive period-doubling route to chaos on each mode-locked Shapiro step suggests a modulo 1 variable for the CDW phase, such as θ_m in Eq. (7.6). This equation is identically recovered by changing Ω to $\Omega+n$, with n an integer. The periodicity of the bifurcation sequence in dc bias is thus consistent with the periodicity of the behavior predicted by the circle map. Similarly, perioddoubling routes to chaos on mode-locked Shapiro steps are predicted by Eq. (7.2) if the inertial term is retained (Kantz, 1981).

2.8 VIII. Disorder and Metastable States

The observation of current oscillations and the pronounced interference effects in the presence of ac and dc excitations are suggestive of a highly coherent response in the current-carrying state, with a phase-phase correlation length L_0 comparable to the dimensions of the specimens. Such a high degree of coherence can be achieved
only in relatively pure $NbSe_3$ specimens where the small threshold fields E_T for nonlinear conduction suggest through Eqs. (4.16) and (4.12) that L_0 is substantial, of the order of 1μ. This is confirmed directly by x-ray studies (Fleming et al., 1978, 1984). Consequently, the dynamics of internal modes may be largely neglected (for rather pure and small specimens), or can be included perturbatively by considering first the dynamics of the average phase $\langle\varphi\rangle$. The situation is somewhat different in TaS_3 where the small amplitude of the current oscillations and the relatively weak interference effects suggest that disorder and/or sample inhomogeneity play an important role. In the materials $(TaSe_4)_2\,\mathbf{I}$ and $K_{0.3}MoO_3$ the current oscillations, when Fourier

analyzed, give a substantial distribution of CDW velocities within the specimen, and interference effects are either not observed or are extremely weak. For these materials, the phasephase correlation length is presumably small. This, together with the relatively large sample dimensions both parallel and perpendicular to the chains, $L_{\|}$and $L_{\perp}$, leads to a situation where the number of degrees of freedom, or number of metastable states, is of the order $\left(L_{\text{sample}}/L_0\right)^3$, where $L_{\text{sample}} = \left(L_{\|}L_{\perp}^2\right)^{1/3}$, an "average" sample dimension, is large and can, for all practical purposes, be regarded as close to the thermodynamic limit. Under such circumstances, the dynamics of internal degrees of freedom are important. This may lead to observations similar to those made in spin-glass random-field magnets.

The close relation between the observations on lowfrequency and long-time relaxation phenomena in materials with a charge-density-wave ground-state and random-field systems is not surprising. Equation (5.13) is formally identical to the random-field $X-Y$ model,

$$H = \sum_{i,j} J_{ij}\mathbf{S}_i \cdot \mathbf{S}_j + \sum_i \left(h_i \mathbf{S}_i\right)^2,$$

in the limit where the angle θ between the neighboring spin direction is small. Arguments on the absence of long-range order and the behavior of the various correlation functions are appropriate for both systems, and it is expected that the dynamical behavior displays strong similarities for small amplitude driving fields. H_e in Eq. (5.13), however, corresponds to an applied torque in the random-field $X-Y$ model, and the electric polarization P_e corresponds to a rotational magnetization. The difference between the coupling to external fields leads to fundamentally different behavior in the large amplitude response: In the random $X-Y$ model the magnetization saturates in the infinite magnetic field limit, while for an applied torque there is a phase transition to a "phasewinding" state where all spins rotate under the influence of the applied torque. This transition corresponds to the transition from the pinned to the current-carrying CDW state. Furthermore, because of the large polarizability (related to the large length scale L_0) nonlinear response phenomena may become important even for moderate applied fields. Effects associated with metastable states
are also expected to be temperature dependent because of the possibility of temperature-driven transitions between the various metastable configurations.

The small amplitude ac response of various materials has been discussed in detail in Sec. VI. In the full frequency range, from dc to millimeter wave frequencies, the response can be described by a distribution of pinning frequencies (Wu et al., 1985). Alternatively, phenomenological equations, such as (6.7) and (6.8), have been used extensively to describe both $\mathrm{Re}\,\sigma(\omega)$ and $\mathrm{Im}\,\sigma(\omega)$; both are suggestive of "glassy dynamics", i.e., of the importance of internal degrees of freedom. Certain features, such as the anomalous low-frequency response of the dielectric constant, have been recovered by calculations (Fisher, 1985; Littlewood, 1986) based on the FLR model. The experimentally found behavior for various materials is displayed in Fig. 50. The strongly divergent response as $\omega \to 0$ is in clear conflict with single-degree-of-freedom dynamics, which would suggest a leading low-frequency behavior of

$$\varepsilon(\omega) \sim \varepsilon(\omega = 0) - B\omega^2. \tag{8.1}$$

Linked, as $\omega \to 0$, the behavior can be described as

$$\varepsilon(\omega) = \varepsilon(\omega = 0) - B'\omega^{\alpha'} \tag{8.2}$$

with $\alpha' < 1$. The behavior is usually referred to as the zero-frequency cusp. Whether $\varepsilon(\omega = 0)$ is finite and whether there is a crossover to a behavior given by Eq. (8.1) for very small frequencies and small excitation amplitudes is not clear. The behavior most probably depends on factors like sample dimensions or temperature.

2.8.1 A. The Nonlinear Ac Response

Dielectric constant measurements in the small amplitude $E_{ac} \to 0$ limit sample the relaxation effects around

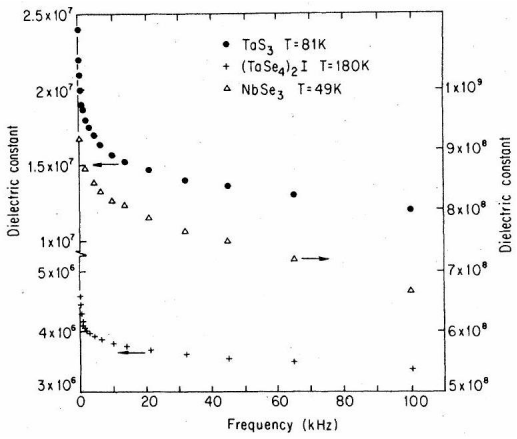


FIG. 50. Frequency-dependent dielectric constant in various materials (Wu et al., 1984).

the state, which has been reached prior to the excitation applied. This state is, in general, expected to be frozen in a metastable state (Fisher, 1983; Littlewood and Rice, 1982; Matsukawa and Takayama, 1984). Other metastable states close in energy to the "frozen-in" metastable state, but presumably far from its configuration space, can, however, be excited by the application of finiteamplitude dc or ac drives. The effect was first demonstrated by Cava, Fleming, Dunn et al. (1984) in $K_{0.3}MoO_3$, by measuring the dielectric response at various ac signal amplitudes. The data have been analyzed using

$$\varepsilon(\omega) = (\varepsilon_0 - \varepsilon_{HF}) \frac{1}{\left[1 + (i\omega\tau_0)^{1-\alpha}\right]^{\beta}} + \varepsilon_{HF} \tag{8.3}$$

where ε_0 and ε_{HF} are the static dielectric constant and τ_0 is a characteristic relaxation time. Both α and τ_0 were found to be dependent on the applied ac amplitude, suggesting a strong modification of the long-time response of the system by finite-amplitude ac fields. The effect was found to be less pronounced at higher frequencies, as expected for internal modes the dynamics of which is described by relaxational dynamics. Similar amplitudedependence ac response was found by Ong et al. (1985) in $o - TaS_3$.

The nonlinear ac response was further studied by monitoring the higher harmonic generation (Chen et al., 1988; Mihály and Grüner, 1987). For a linear system, the response to an excitation $V = V_0 \sin\omega_{ext}$ is purely sinusoidal, and no harmonics at frequencies $n\omega_{ext}$ are observed. In general, for a simple nonlinear system, the dielectric constant can be expressed in terms of powers of the excitation amplitude V_0 and $\varepsilon = \varepsilon^{(1)} + \varepsilon^{(3)}V_0^2 + \varepsilon^{(5)}V_0^4 + \cdots$ where $\varepsilon^{(2n+1)}$ represents the response of the system at frequency $(2n+1)\omega_{ext}$. Experimentally, the third harmonic response measured at frequencies $3\omega_{ext}$ was found to be both amplitude V_0 and frequency ω_{ext} dependent, and the observations can be described as (Chen et al., 1987)

$$\varepsilon(\omega) = A\frac{V_0^v}{\omega^\eta} \tag{8.4}$$

with both v and η less than one and $A = \text{const}$. This behavior, which is similar to the nonlinear susceptibilities observed in spin glasses both below and slightly above the glass transition

temperature, is unexplained at present. The behavior is most probably related to the apparent inductive response observed in low-frequency large-amplitude measurements in a Lissajous representation (Tessema and Ong, 1985).

2.8.2 B. Time Domain Studies and Remanent Polarizations

The highly anomalous frequency and electric-fielddependent response is strongly related to anomalous time-dependent effects and also to remanent polarization phenomena, the latter observed at low temperatures.

The response to steplike electric field excitations of the form of $V(t) = V_0\delta(t - t_0)$, where δ is a step function, is in general nonexponential and displays long-time tails. The functional form observed depends on various factors, such as temperature and drive amplitude. For small excitation amplitude the response appears to be exponential, but for large step excitations, the observed timedependent polarization was found to be well described by the so-called Kohlrausch equation (Kohlrausch, 1947; Jonscher, 1977),

$$P(t) = P_0\left\{1 - \exp\left[-\left(\frac{t}{\tau}\right)\alpha\right]\right\}, \tag{8.5}$$

with $\alpha < 1$ (Mihály and Tessema, 1986). Typical timedependent polarizations, obtained after various pulse excitations, are displayed in Fig. 51 (Mihály and Tessema, 1986). Here P_0 is the remanent polarization, τ and average relaxation time and the exponential $\alpha < 1$. Equation (8.4) has been used extensively to describe long-time relaxational phenomena in spin glasses and various random-field systems (Chamberlin, 1984; Chamberlin et al., 1984). Logarithmic time dependencies, in the form

$$P(t) = A\ln\frac{t}{\tau}, \tag{8.6}$$

have also been observed (Mihály and Mihály, 1984; Ong et al., 1985; Mihály et al., 1985). The above observations are clearly related to the frequency-dependent response, which is also described by fractional powers of frequency [see Eq. (8.4)]. In Eq. (8.5) P_0 refers to a remanent polarization. Because of the long-time response P_0 cannot be directly measured, and, in general, it is assumed that the polarization measured on substantial time after the pulse is applied is close to P_0. In addition, the remanent polarization can be detected only at low temperatures, where thermally induced transitions

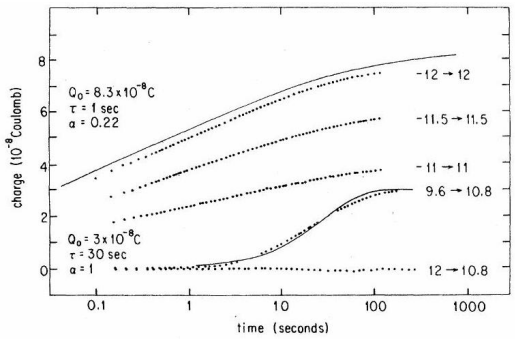


FIG. 51. Relaxation processes in response to a steplike external voltage drive measured on a blue bronze sample at $T=4.2 \mathrm{˜K}$. The numbers on the right-hand side indicate the voltage before and after the step. The continuous lines were obtained by using the stretched exponential formula (8.7) with parameters shown on the left-hand side.

between the various metastable states are not significant. P_0, i.e., a polarization close to P_0 has been measured in detail in $K_{0.3}MoO_3$ by applying a sequence of electric field excitations with successively larger amplitude. A typical hysteresis loop shown in Fig. 52 is recovered by such experiments.

At low temperatures, where the conductivity due to the normal electrons is small, the polarization can be measured directly. At higher temperatures this is not possible because of screening currents shown to the uncondensed electrons. The CDW polarization, however, is the result of frozen-in local distortions of the collective mode, and this leads to changes in the small-field (ohmic) resistance of the specimens. Although the detailed mechanism is not clear, the effect can be used to monitor the buildup of CDW polarizations at higher temperatures. This method was employed to establish the existence of remanent polarizations in $NbSe_3$ and in TaS_3 (Brown, Grüner, and Mihály, 1986). Furthermore, the polarization observed was shown to be a bulk effect and the result of long-range remanent deformations of the collective mode, which leads to the breakdown of translational invariance in the bulk (Tessema et al., 1985; Brown, Grüner, and Mihály, 1986). This has been directly demonstrated by measuring the polarization as the function of distance along the long axis of the specimens, which also corresponds to the chain direction. Furthermore, metastable states induced by the application of electric fields have been directly observed by x-rays (Fleming, Dunn, and Schneemeyer, 1985; Tamegai et al., 1985; Mihály, Lee, and Stephens, 1987). The remanent polarization increases dramatically with increasing applied voltage V_0, and the experimental results displayed on the figure are suggestive for a divergent polarization when the threshold field E_T is approached from below. This has been studied in detail (Wang and Ong, 1987; Mihály and Grüner, 1987), and the observations have been described in terms of a polarization catastrophe with critical exponents that describe the divergence of

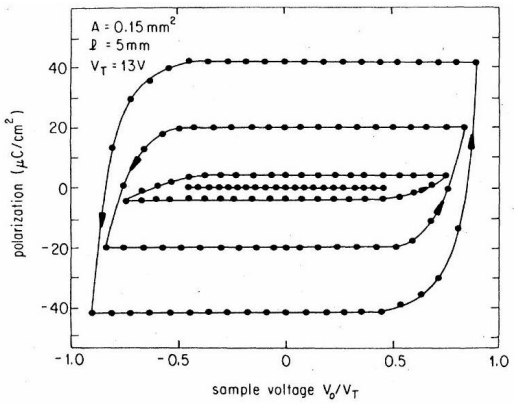


FIG. 52. Dielectric polarization loops observed in $\mathrm{K}_{0.3}\mathrm{MoO}_3$ at low temperatures. V_T refers to the threshold voltage for the onset of nonlinear conduction (Mihály and Tessema, 1986).

P_0. Because of the extremely long time scales involved, and because of the ambiguities as far as the detailed time dependences involved (whether logarithmic or stretched exponential), a clear-cut analysis of this novel type of critical phenomenon has not been possible to date. The behavior displayed in Fig. 52 is, however, well reproduced by numerical simulations (Matsukawa and Takayama, 1986) that are based on the Fukuyama-Lee-Rice model of impurity pinning. Numerical simulations have not yet been extended to treat the behavior near the threshold field. The problem has been treated by a simplified model (Mihály, Chen, and Grüner, 1987) that indeed leads to critical exponents for the divergent polarization and for the relaxation time τ, which appears in Eq. (8.5). The remanent polarization effects also suggest that special

procedures, similar to those that lead to demagnetization for ferromagnets, are required to arrive at an unpolarized CDW state. Such procedures, along with temperature-induced depolarization effects, have been discussed by Wang and Ong (1987).

At higher temperature, thermally induced transitions between the various metastable states destroy the remanent polarization and lead to the so-called thermally stimulated currents; the relaxation back to the unpolarized state is well described by a stretched exponential or by logarithmic (Mihály and Mihály, 1984) time dependence. These have been investigated by measuring the Ohmic resistance R of the specimens, assuming that changes in the CDW polarization lead to changes in the single-particle gap and thus to R.

Detailed studies performed on TaS_3 (Kriza and Mihály, 1986) over a broad time domain demonstrate that the time-dependent depolarization currents can be well described by the stretched exponential form. Moreover, the average relaxation time τ obeys the empirical form

$$\tau(T) = \tau_0 \exp\left(-\frac{\Delta}{kT}\right) \tag{8.7}$$

with 2Δ close to the single-particle gap in this material. The behavior is most probably related to the strongly temperature-dependent relaxation time obtained from the analysis of the low-frequency dielectric constant (Cava et al., 1985) and from the analysis of the temperature dependence of the nonlinear conduction (Fleming et al., 1986). Similar temperature- (and also field-) dependent relaxation time was observed in $K_{0.3}MoO_3$ for the fieldactivated relaxation (Wang and Ong, 1987) in $(TaSe_4)_2\,I$ (Tucker et al., 1986).

These studies, along with thermal and electric field cycling experiments (Wang and Ong, 1986; Duggan and Ong, 1986), raise interesting questions about the approach toward the ground state and about the dynamics near the ground state. Various distinct routes to equilibrium were found, and the extreme sensitivity of the ground state to small temperature changes was also established (Wang and Ong, 1986).

2.8.3 C. Transitions from Below to Above Threshold

A variety of interesting phenomena occur when the pinned CDW is driven through E_T to the currentcarrying state and back by the application of a sequence of various pulses. These are usually referred to as memory effects because the response to an applied pulse depends on the history polarization and deviation of the previous pulse. The observations are clearly metastable states in the pinned configuration, and their rearrangement under the influence of applied electric field.

The so-called pulse sign memory effect refers to the phenomenon where the response of the system to a pulse depends on the direction of the polarization of the previous pulse. When the electric field applied is the same direction as the preceding pulse, the response is fast, while a sluggish response is detected for a reverse polarization. The phenomenon was first observed in TaS_3 (Gill, 1981b; Gill and Higgs, 1983), and has subsequently been found in $K_{0.3}MoO_3$ and $NbSe_3$ (Fleming and Schneemeyer, 1983; Fleming, 1985b). The observations are shown in Fig. 53 for both $NbSe_3$ and $K_{0.3}MoO_3$.

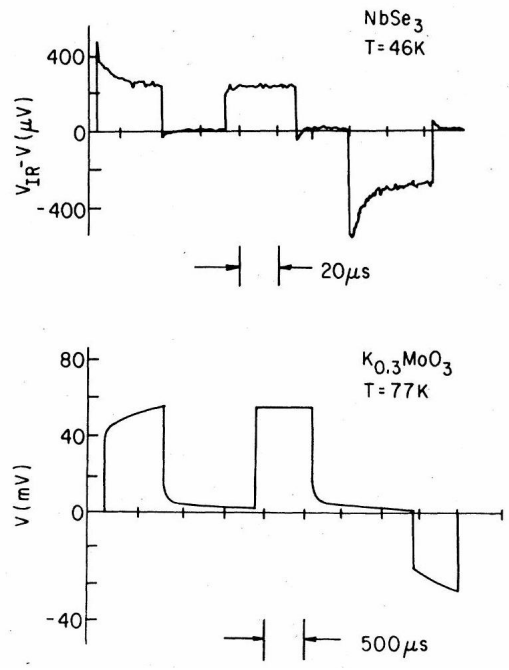


FIG. 53. Pulse sign memory effect. Response of NbSe_{3} and $K_{0.30}MoO_3$ to a repetitive series of constant-current pulses consisting of two positive pulses followed by one negative pulse. The amplitude of the pulses are in excess of threshold. When the current direction is reversed, the response becomes very slow. (a) for $NbSe_3$; the linear response is subtracted so that only $\mathrm{IR}_{\mathrm{linear}} - V(t)$ is plotted as a function of time; (b) the total signal $V(t)$ is plotted.

Both types of response phenomena-the so-called overshoot observed in $NbSe_3$ and the smooth gradual buildup of the response observed in $K_{0.3}MoO_3$, both for applied pulses in the reverse direction from the preceding pulse-are reproduced by numerical simulations based on the treatment of the Fukuyama-Lee-Rice model (Littlewood, 1986; Coppersmith and Littlewood, 1985a, 1985b). The explanation of the phenomenon is relatively straightforward. When the applied electric field is suddenly removed, the charge-density wave does not relax back to the equilibrium configuration, but remains in a polarized state (see, for example, Fig. 52). This polarized state is a metastable state with remanent local configurations of the CDW deformation, similar to those that characterize the current-carrying state in a particular current direction. Consequently, with these configurations already established before the next electric field pulse, the response to this pulse will be fast. This is the case when the pulse polarities are identical. Different local configurations represent the current-carrying state in the opposite current direction, and a sluggish response or overshoot results because the long-range correlations have to be "unwound" and then "rewound" in the opposite direction (Littlewood, 1986).

The notion of pulse deviation memory effect refers to features found in the transient voltage or current oscillations observed in the current-carrying state after the application of a sudden electric field pulse. The transient oscillations occur at the fundamental frequency of the current oscillations, but their amplitude decreases slowly with increasing time (Fleming, 1981; Zettl and Grüner, 1982a, 1982b) saturating at a constant value as $t \to \infty$. The initial phase of the oscillations is adjusted to the leading edge of the applied pulse, and, more important, at the end of the pulse the phase of the oscillations is also

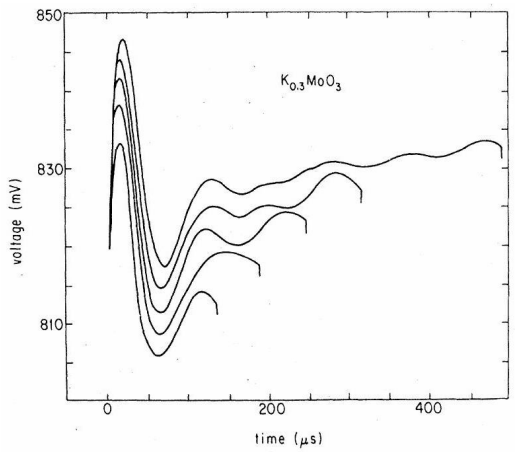


FIG. 54. Voltage response to repetitive pulse drive. For repetitive pulses of constant amplitude, the phase of the last transient oscillation is fixed relative to the end of the pulse for arbitrary pulse width (Fleming et al., 1986).

the same. The phenomenon is shown in Fig. 54. This so-called pulse duration memory effect (Brown, Mihály, and Grüner, 1986; Fleming and Schneemeyer, 1986) is clearly related to the mode-locking phenomena discussed in the previous section. However, it should not occur for a single-degree-of-freedom system (Coppersmith and Littlewood, 1986). Reasons why a many-degrees-of-freedom system should display pulse duration memory effects have been discussed recently (Tang et al., 1987), and concepts such as phase organization and dynamical selection of states have emerged from models that mimic the dynamics of charge-density waves. These effects are discussed in detail by Littlewood (1987).

2.9 IX. Final Remarks

During the past decade the field has advanced considerably, and the basic notions on the dynamics of chargedensity waves are well documented by a broad range of experimental studies. Most of the important features of this novel type of collective transport phenomenon are well established.

Several questions remain, however. Experiments on properties other than electrical conduction, such as Hall effect, thermoelectric power, and acoustic properties, clearly require an underlying microscopic theory, and the same is true for the high-frequency damping and for the temperature-dependent low-frequency damping processes. Little is known about the effects associated with the dynamics of the amplitude mode. While this may not be important at low temperatures, in most materials the gap associated with the amplitude excitations is less than kT_p, and also less than the temperatures where the experiments are conducted, and, consequently, should be important. In contrast, Coulomb effects are important at low temperatures because they can lead to long-range order, even in the presence of impurities, and lead to a gap in the phason spectrum (Fukuyama and Lee, 1978). Both effects (Wong and Takada, 1988) are expected to influence the dynamics of the collective mode. The question of whether quantum-mechanical concepts are required to describe the dynamics of charge-density waves is still hotly debated (Thorne et al., 1987, and references cited therein), and a broad variety of experiments involving joint ac and dc excitations have been interpreted in terms of quantum and classical models. Experiments on effects where the predictions of the two models are different, such as photon-assisted tunneling from the pinned to the current-carrying state, have not been successful to date.

Charge-density waves have also served in the past as models for the study of the dynamics of

driven nonlinear systems. Mode locking and interference phenomena (similar in many respects to those observed in Josephson junctions) were used to study the possibility of transitions to chaos, but because of the complexity of material problems (associated with pinning effects) most of the issues remain unresolved. Charge-density waves have also been used to study relaxation effects in random systems, with analogies to spin glasses and random field magnets. The effect of an applied electric field in CDW transport is analogous to an applied torque in random field magnets; this leads to a phase transition (in terms of the analogy to random-field systems), and then to a phase-winding state. Only initial attempts have been made to measure the various parameters near this novel type of driven phase transition, in particular, below E_T.

Practically nothing has been said in this review about the nonlinear and frequency-dependent transport, which is observed at low temperatures (Maeda, Furayama, and Tanaka, 1986; Mihály and Tessema, 1986; Mihály et al., 1988). The phenomenon, which is also accompanied by polarization divergences (Chen et al., 1988) and changes in the CDW deformations (Mihály, Crommie, and Grüner, 1987), appears to be rather different from the nonlinear and frequency-dependent response observed at high temperatures. The difference between the two regimes most probably is due to the effects associated with screening (Wong and Takada, 1987). At high temperatures, screening by the normal electrons leads to a gapless phason spectrum and, consequently, to the possibility of long-range deformations around impurities. In the absence of normal electrons, at low temperatures such screening is not possible. This results in a gap in the phason spectrum and, possibly, also long-range order even in the presence of random impurities. Charge transport where the dynamics of local deformations are important cannot occur with the nonlinearity determined by the translational motion of the rigid condensate (Littlewood, 1988). This low-temperature regime, with the possibility of true Fröhlich superconductivity, clearly deserves further investigation.

Relatively little is known about the various nonlinear excitations of the collective mode, which may occur at energies below the single-particle gap. Various solitonlike modes may occur, in particular, in systems that are close to commensurability, and higher harmonic phason modes (Sherwin et al., 1984; Travaglini and Wachter, 1984) have also been discussed.

Whether features in the observed optical spectra can be clearly identified with the fundamental features of the dynamics of the collective mode remains to be seen. Experiments on different materials and on alloys may clarify this aspect of CDW dynamics.

Nonlinear and frequency-dependent phenomena have also been reported recently in systems other than discussed in this review. In the organic linear-chain compound TTF-TCNO, the nonlinear response is clearly due to charge-density waves (Lacoe et al., 1986), with added complications that two charge-density waves are present where the nonlinear conduction was observed. Less clear is the situation in intercalated graphite (Iye and Dresselhaus, 1985) and on the material $Hg-Cd-Te$, which is assumed to undergo a phase transition to a Wignercrystal state. The electrical conductivity is a nonlinear (Osada et al., 1987) and a frequency- (Javadi et al., 1986) dependent organic linear-chain conductor with a spin-density-wave ground state. The question whether spin-density-wave dynamics is similar to the dynamics of charge-density waves deserves further investigation.

2.10 References

Allender, D., J. W. Bray, and John Bardeen, 1974, Phys. Rev. B 9, 119.
Allgeyer, R., B. H. Suits, and F. C. Brown, 1982, Solid State Commun. 43, 207.
Alstrom, P., M. H. Jensen, and M. T. Levinsen, 1984, Phys. Lett. A 103, 171.
Ambegaokar, V., and B. I. Halperin, 1969, Phys. Rev. Lett. 22, 1364.
Aronov, A. G., and V. L. Gurevich, 1974, Fiz. Tverd. Tela (Leningrad) 16, 2656 [Sov.

Phys.-Solid State 16, 1722 (1975)].
Artemenko, S. N., E. N. Dolgov, A. N. Krugov, Y. I. Latyshev, Y. S. Savitskaya, and V. V. Frolov, 1984, Pis'ma Zh. Eksp. Teor. Fiz. 39, 258 [JETP Lett. 39, 308].
Artemenko, S. N., and A. F. Volkov, 1981a, Pis'ma Zh. Eksp. Teor. Fiz. 33, 155 [JETP Lett. 33, 147].
Artemenko, S. N., and A. F. Volkov, 1981b, Zh. Eksp. Teor. Fiz. 81, 1872 [Sov. Phys.-JETP 54, 992].
Artemenko, S. N., A. F. Volkov, and A. N. Kruglov, 1986, Physica B 143, 146.
Azbel, M. Ya., and Per Bak, 1984, Phys. Rev. B 30, 3722.
Bak, Per, 1982a, Phys. Rev. Lett. 48, 692.
Bak, Per, 1982b, Rep. Prog. Phys. 45, 587.
Bak, Per, 1983, Proceedings of the International Symposium on Nonlinear Transport in Inorganic Quasi-One-Dimensional Conductors, Sapporo, Japan (unpublished).
Bardeen, John, 1979, Phys. Rev. Lett. 42, 1498.
Bardeen, John, 1980, Phys. Rev. Lett. 45, 1978.
Bardeen, John, 1982, Mol. Cryst. Liq. Cryst. 81, 719.
Bardeen, John, 1984, Physica B 126, 342.
Bardeen, John, 1985a, in Proceedings of the International School of Physics "Enrico Fermi," Vol. 89 (North-Holland, Amsterdam), p. 349.
Bardeen, John, 1985b, Phys. Rev. Lett. 55, 1010.
Bardeen, John, 1986, Physica B 143, 14.
Bardeen, John, 1987, Z. Phys. 67, 427.
Bardeen, John, E. Ben-Jacob, A. Zettl, and G. Grüner, 1982, Phys. Rev. Lett. 49, 493.
Bardeen, John, J. W. Lyding, W. G. Lyons, J. H. Miller, Jr., R. E. Thorne, and J. R. Tucker, 1987, Synth. Met. 19, 1.

Bardeen, John, and J. R. Tucker, 1985, in Charge Density Waves in Solids, Proceedings of the International Conference Held in Budepest, Hungary, 1984, Lecture Notes in Physics Vol. 217, edited by Gy. Hutiray and J. Sólyom (Springer, Berlin), p. 155.
Barisic, S., 1986, in Electronic Properties of Inorganic Materials with Quasi-One-Dimensional Structures, edited by P. Monceau (Reidel, Dordrecht/Boston/Lancaster), Part 1, p. 1.
Barnes, S. E., and A. Zawadowski, 1983, Phys. Rev. Lett. 51, 1003.

Barone, A., and G. Paterno, 1982, Physics and Applications of the Josephson Effect (Wiley, New York).
Batistic, I., A. Bjelis, and L. P. Gorkov, 1984, J. Phys. (Paris) 45, 1049.
Beasley, M. R., and B. A. Huberman, 1982, Comments Solid State Phys. 10, 155.
Ben-Jacob, E., 1983, Solid State Commun. 47, 603.
Ben-Jacob, E., Y. Braiman, R. Shainsky, and Y. Imry, 1981, Appl. Phys. Lett. 38, 822.
Berlinski, J., 1979, Rep. Prog. Phys. 42, 1243.
Berthier, C., and P. Ségranson, 1987, in Low Dimensional Conductors and Superconductors, NATO Advanced Study Institute, Series B, Vol. 155, edited by D. Jerome and L. G. Carol (Plenum, New York), p. 455.
Beyermann, W. P., L. Mihály, and G. Grüner, 1986, Phys. Rev. Lett. 56, 1489.
Bhattacharya, S., J. P. Stokes, M. J. Higgins, and R. A. Klemm, 1987, Phys. Rev. Lett. 59, 1849.
Bhattacharya, S., J. P. Stokes, M. O. Robbins, and R. A. Klemm, 1985, Phys. Rev. Lett. 54, 2453.
Birgenau, R. J., K. Yoshizava, R. A. Covely, G. Shirane, and K. Ikeda, 1983, Phys. Rev. B 28, 1438.

Bjelis, A., 1987, in Low Dimensional Conductors and Superconductors, NATO Advanced Study Institute, Series B, Vol. 155, edited by D. Jerome and L. G. Carol (Plenum, New

York/London), p. 409.
Bohr, T., P. Bak, and M. H. Jensen, 1984, Phys. Rev. A 30, 1970.
Borodin, D. V., F. Y. Nad, Y. S. Savitskaya, and S. V. ZaitsevZotov, 1986, Physica B 143, 73.
Bouffard, S., M. Sanguer, H. Mutka, J. Dumas, and C. Schlenker, 1985, unpublished.
Bourne, L. C., M. S. Sherwin, and A. Zettl, 1986, Phys. Rev. Lett. 56, 1952.
Brazovskii, S. A., and I. E. Dzyaloshinskii, 1976, Zh. Eksp. Teor. Fiz. 71, 2338 [Sov. Phys.-JETP 44, 1233].
Breymayer, H.-J., H. Risken, H. D. Vollmer, W. Wonneberger, 1982, Appl. Phys. B 28, 335.
Brill, J. W., 1982, Solid State Commun. 41, 925.
Brill, J. W., and S. L. Herr, 1983, Phys. Rev. B 27, 3916.
Brill, J. W., and N. P. Ong, 1978, Solid Commun. 25, 1075.
Brill, J. W., N. P. Ong, J. C. Eckert, J. W. Savage, S. K. Khanna, and R. B. Somoano, 1981, Phys. Rev. B 23, 1517.
Brill, J. W., and W. Roark, 1984, Phys. Rev. Lett. 53, 846.
Brill, J. W., W. Roark, and G. Minton, 1986, Phys. Rev. B 33, 6831.
Brown, S. E., and G. Grüner, 1985, Phys. Rev. B 31, 8302.
Brown, S. E., and G. Grüner, 1988, unpublished.
Brown, S. E., G. Grüner, and L. Mihály, 1986, Solid State Commun. 57, 165.
Brown, S. E., A. Janossy, and G. Grüner, 1985, Phys. Rev. B 31, 6869.
Brown, S. E., and L. Mihály, 1985, Phys. Rev. Lett. 55, 742.
Brown, S. E., L. Mihály, and G. Grüner, 1986, Solid State Commun. 58, 231.
Brown, S. E., G. Mozurkewich, and G. Grüner, 1984, Phys.
Rev. Lett. 52, 2277.
Brown, S. E., G. Mozurkewich, and G. Grüner, 1985a, Solid State Commun. 54, 23.
Brown, S. E., G. Mozurkewich, and G. Grüner, 1985b, in Charge Density Waves in Solids, Proceedings of the International Conference Held in Budapest, Hungary, 1984, Lecture Notes in Physics Vol. 217, edited by Gy. Hutiray and J. Sólyom (Springer, Berlin), p. 318.
Bruinsma, R., and L. Mihály, 1985, Bull. Am. Phys. Soc. 30, 364.
Burkov, S. E., and V. L. Pokrowsky, 1984, Solid State Commun. 46, 609.
Butaud, P., P. Ségranson, C. Berthies, J. Dumas, and C. Schlenker, 1985, Phys. Rev. Lett. 55, 253.
Cava, R. J., R. M. Fleming, R. G. Dunn, and E. A. Rietman, 1985, Phys. Rev. B 31, 8325.
Cava, R. J., R. M. Fleming, R. G. Dunn, E. A. Rietman, and L. F. Schneemeyer, 1984, Phys. Rev. B 30, 7290.
Cava, R. J., R. M. Fleming, P. Littlewood, E. A. Rietman, L. F. Schneemeyer, and R. G. Dunn, 1984, Phys. Rev. B 30, 3228.
Cava, R. J., P. Littlewood, R. M. Fleming, R. G. Dunn, and E. A. Rietman, 1986, Phys. Rev. B 33, 2439.
Challener, W. A., and P. L. Richards, 1984, Solid State Commun. 52, 117.
Chamberlin, R. V., 1984, Phys. Rev. B 30, 5393.
Chamberlin, R. V., G. Mozurkewich, and R. Orbach, 1984, Phys. Rev. Lett. 52, 867.
Chen, C. H., and R. M. Fleming, 1983, Solid State Commun. 48, 777.
Chen, C. H., L. F. Schneemeyer, and R. M. Fleming, 1984, Phys. Rev. B 29, 8765.
Chen, T., L. Mihály, and G. Grüner, 1987, Phys. Rev. B 36, 2931
Chen, T., L. Mihály, and G. Grüner, 1988, Phys. Rev. Lett. 60, 464.
Clark, T. D., and P. E. Lindelof, 1976, Phys. Rev. Lett. 37, 368.
Coppersmith, S. N., 1984, Phys. Rev. B 30, 410.
Coppersmith, S. N., and P. B. Littlewood, 1985a, Phys. Rev. B 31, 4049.
Coppersmith, S. N., and P. B. Littlewood, 1985b, in Charge Density Waves in Solids, Pro-

ceedings of the International Conference Held in Budapest, Hungary, 1984, Lecture Notes in Physics Vol. 217, edited by Gy. Hitiray and J. Sólyom (Springer, Berlin), p. 236.
Coppersmith, S. N., and P. B. Littlewood, 1986, Phys. Rev. Lett. 57, 1927.
Coppersmith, S. N., and C. M. Varma, 1984, Phys. Rev. B 30, 3566.
Dee, R. H., P. M. Chaikin, and N. P. Ong, 1979, Phys. Rev. Lett. 42, 1234.
Devreese, J. T., R. P. Evrard, and V. E. van Doren, 1979, in Highly Conducting One-Dimensional Solids, edited by J. T. Devreese (Plenum, New York/London).
Devreux, F., 1982, J. Phys. (Paris) 43, 1489.
Dolgov, E. N., 1984, Solid State Commun. 50, 405.
Douglass, D. C., L. M. Schneemeyer, and S. E. Spengler, 1985, Phys. Rev. B 32, 1813.
Duggan, D. D., T. W. Jing, N. P. Ong, and P. M. Lee, 1985, Phys. Rev. B 32, 1397.
Duggan, D. D., and N. P. Ong, 1986, Phys. Rev. B 34, 1375.
Dumas, J., C. Schlenker, J. Marcus, and R. Buder, 1983, Phys. Rev. Lett. 50, 757.
Efetov, K. B., and A. I. Larkin, 1977, Zh. Eksp. Teor. Fiz. 72, 2350 [Sov. Phys.-JETP 45, 1236].
Everson, M. P., and R. V. Coleman, 1983, Phys. Rev. B 28, 6659.
Everson, M. P., G. Eiserman, A. Johnson, and R. V. Coleman, 1984, Phys. Rev. B 30, 3582.
Fack, H., and V. Kose, 1971, J. Appl. Phys. 42, 320.
Feigelman, M. V., and V. M. Vinokur, 1983, Solid State Commun. 45, 603.
Feinberg, D., and J. Dumas, 1986, Physica B 143, 111.
Fisher, B., 1976, J. Phys. C 9, 1201.
Fisher, B., 1978, J. Appl. Phys. 49, 5339.
Fisher, B., 1983, Solid State Commun. 46, 227.
Fisher, B., 1984, Phys. Rev. B 30, 1073.
Fisher, D., 1983, Phys. Rev. Lett. 50, 1486.
Fisher, D., 1984, Physica B 126, 409.
Fişher, D., 1985, Phys. Rev. B 31, 1396.
Fleming, R. M., 1980, Phys. Rev. B 22, 5606.
Fleming, R. M., 1981, in Physics in One Dimension, Springer Series in Solid-State Sciences Vol. 23, edited by J. Bernasconi and T. Schneider (Springer, New York), p. 253.
Fleming, R. M., 1982, Solid State Commun. 43, 167.
Fleming, R. M., 1985, Physica B 143, 86.
Fleming, R. M., R. J. Cava, L. F. Schneemeyer, E. A. Rietman, and R. G. Dunn, 1986, Phys. Rev. B 33, 5450.
Fleming, R. M., R. G. Dunn, and L. F. Schneemeyer, 1985, Phys. Rev. B 31, 4099.
Fleming, R. M., and C. C. Grimes, 1979, Phys. Rev. Lett. 42, 1423.
Fleming, R. M., D. E. Moncton, J. D. Axe, and G. S. Brown, 1984, Phys. Rev. B 30, 1877.
Fleming, R. M., D. E. Moncton, and D. B. McWhan, 1978, Phys. Rev. B 18, 5560.
Fleming, R. M., and L. F. Schneemeyer, 1983, Phys. Rev. B 28, 6996.
Fleming, R. M., and L. F. Schneemeyer, 1984, Bull. Am. Phys.
Soc. 29, 470.
Fleming, R. M., and L. F. Schneemeyer, 1986, Phys. Rev. B 33, 2930.
Fleming, R. M., L. F. Schneemeyer, and R. J. Cava, 1985, Phys. Rev. B 31, 1181.
Fleming, R. M., L. F. Schneemeyer, and D. E. Moncton, 1985, Phys. Rev. B 31, 899.
Fogle, W., and H. Perlstein, 1972, Phys. Rev. B 6, 1402.
Forró, L., J. R. Cooper, A. Jánossy, and K. Kamaras, 1985, Phys. Rev. B 34, 9047.
Fournel, A., J. P. Sorbier, M. Konczykowski, and P. Monceau, 1986, Phys. Rev. Lett. 57, 2199.
Fournel, A., J. P. Sorbier, M. Konczykowski, P. Monceau, and F. Levy, 1986, Physica B 143,

177.

Frenkel, Y. I., and T. Kontorova, 1939, J. Phys. USSR 1, 139.

Fröhlich, H., 1954, Proc. R. Soc. London, Ser. A 223, 296.

Fujishita, H., M. Sato, and S. Hoshino, 1984, Solid State Commun. 49, 313.

Fukuyama, H., 1976, J. Phys. Soc. Jpn. 41, 513.

Fukuyama, H., 1978, J. Phys. Soc. Jpn. 45, 1474.

Fukuyama, H., and P. A. Lee, 1978, Phys. Rev. B 17, 535.

Fuller, W. W., G. Grüner, P. M. Chaikin, and N. P. Ong, 1981, Phys. Rev. B 23, 6259.

Fung, K. K., and J. W. Steeds, 1980, Phys. Rev. Lett. 45, 1696.

Geserich, H. P., G. Scheiber, M. Dürrler, F. Levy, and P. Monceau, 1986, Physica B 143, 198.

Gill, J. C., 1981a, Solid State Commun. 37, 459.

Gill, J.C., 1981b, Solid State Commun. 39, 1203.

Gill, J. C., 1982a, Solid State Commun. 44, 1041.

Gill, J. C., 1982b, Mol. Cryst. Liq. Cryst. 81, 73.

Gill, J. C., 1985, in Charge Density Waves in Solids, Proceedings of the International Conference Held in Budapest, Hungary, 1984, Lecture Notes in Physics Vol. 217, edited by Gy. Hutiray and J. Sólyom (Springer, Berlin), p. 377.

Gill, J. C., 1986a, Contemp. Phys. 27, 37.

Gill, J. C., 1986b, J. Phys. C 19, 6589.

Gill, J. C., 1986c, Physica 143B, 49.

Gill, J. C., and A. W. Higgs, 1983, Solid State Commun. 48, 709.

Gleisberg, F., and W. Wonneberger, in Charge Density Waves in Solids, Proceedings of the International Conference Held in Budapest, Hungary, 1984, Lecture Notes in Physics Vol. 217, edited by Gy. Hutiray and J. Sólyom (Springer, Berlin), p. 254.

Gorkov, L. P., 1977, Pis'ma Zh. Eksp. Teor. Fiz. 25, 384 [JETP Lett. 25, 358].

Gorkov, L. P., 1983, Pis'ma Zh. Eksp. Teor. Fiz. 38, 76 [JETP Lett. 38, 87].

Gorkov, L. P., and E. N. Dolgov, 1979, Zh. Eksp. Teor. Fiz. 77, 396 [Sov. Phys.-JETP 50, 203].

Grüner, G., 1982, Mol. Cryst. Liq. Cryst. 81, 17.

Grüner, G., 1983a, Proceedings of the International Symposium on Nonlinear Transport in Inorganic Quasi-One-Dimensional Conductors, Sapporo, Japan (unpublished).

Grüner, G., 1983b, Physica D 296, 1.

Grüner, G., 1983c, Comments Solid State Phys. 10, 183.

Grüner, G., 1983d, Physica D 8, 1.

Grüner, G., 1984, Physica B 126, 400.

Grüner, G., W. G. Clark, and A. M. Portis, 1981, Phys. Rev. B 24, 3641.

Grüner, G., L. C. Tippie, J. Sanny, W. G. Clark, and N. P. Ong, 1980, Phys. Rev. Lett. 45, 935.

Grüner, G., A. Zawadowski, and P. M. Chaikin, 1981, Phys. Rev. Lett. 46, 511.

Grüner, G., and A. Zettl, 1983, J. Phys. (Paris) Colloq. 44, C31745.

Grüner, G., and A. Zeṭtl, 1985, Phys. Rep. 119, 117.

Grüner, G., A. Zettl, W. G. Clark, and John Bardeen, 1981, Phys. Rev. B 24, 7247.

Grüner, G., A. Zettl, W. G. Clark, and A. H. Thompson, 1981, Phys. Rev. B 23, 6813.

Haen, P., P. Monceau, B. Tissier, G. Waysand, A. Meerschaut, P. Moline, J. Rouxel, 1975, in Low Temperature PhysicsLT14, edited by M. Krusius and V. Vuorio (North-Holland, Amsterdam), p. 445.

Hall, R. P., M. F. Hundley, and A. Zettl, 1986, Physica B 143, 152.

Hall, R. P., M. Sherwin, and A. Zettl, 1984a, Phys. Rev. B 29, 7076.

Hall, R. P., M. Sherwin, and A. Zettl, 1984b, Phys. Rev. Lett. 52, 2293.

Hall, R. P., M. Sherwin, and A. Zettl, 1985, in Charge Density Waves in Solids, Proceedings of

the International Conference Held in Budapest, Hungary, 1984, Lecture Notes in Physics Vol. 217, edited by Gy. Hutiray and J. Sólyom (Springer, Berlin), p. 314.
Hall, R. P., and A. Zettl, 1984a, Phys. Rev. B 30, 2279.
Hall, R. P., and A. Zettl, 1984b, Phys. Rev. B 30, 2279.
He, Da Ren, W. J. Yeh, and Y. H. Kao, 1982, Phys. Rev. B 30, 172.
Heeger, A. J., 1979, in Highly Conducting One-Dimensional Solids, edited by J. T. Devreese et al. (Plenum, New York/ London).
Herr, S. L., G. Minton, and J. W. Brill, 1986, Phys. Rev. 33, 8851.
Horovitz, B., 1986, in Solitons, Modern Problems in Condensed Matter Sciences, Vol. 17, edited by S. E. Trullinger, V. E. Zakharov, and V. L. Pokrovsky (North-Holland, Amsterdam), p. 691.
Horowitz B., A. Bishop, and P. S. Lombdale, 1986 Synth. Met. 13, 231.
Horowitz B., and J. Krumhansl, 1984, Phys. Rev. B 29, 2109.
Hsieh, P. L., F. de Czito, A. Janossy, and G. Grüner, 1983, J. Phys. (Paris), Colloq. 44, C3-1753.
Huberman, B. A., and J. P. Crutchfield, 1979, Phys. Rev. Lett. 43, 1743.
Huberman, B. A., J. P. Crutchfield, and N. Packard, 1980, Appl. Phys. Lett. 37, 750.
Humieres, D. D., M. R. Beasley, B. A. Huberman, and A. Liebchaber, 1982, Phys. Rev. A 26, 3483.
Hundley, M., R. P. Hall, and A. Zettl, 1985, Bull. Am. Phys. Soc. 30, 212.
Hutiray, Gy., G. Mihály, and L. Mihály, 1983, Solid State Commun. 48, 227.
Hutiray, Gy., and J. Sólyom, 1985, Eds., Charge Density Waves in Solids, Proceedings of the International Conference Held in Budapest, Hungary, 1984 (Lecture Notes in Physics, Vol. 217) (Springer, Berlin).
Imry, Y., and S. Ma, 1975, Phys. Rev. Lett. 35, 1399.
Inui, M., and S. Doniach, 1987, Phys. Rev. B 35, 6244.
Iye, Y., and G. Dresselhaus, 1985, Phys. Rev. Lett. 54, 1182.
Janossy, A., G. Mihály, and G. Kriza, 1984, Solid State Commun. 51, 63.
Janossy, A., G. Mihály, and L. Mihály, 1985, in Charge Density Waves in Solids, Proceedings of the International Conference Held in Budapest, Hungary, 1984, Lecture Notes in Physics Vol. 217, edited by Gy. Hutiray and J. Sólyom (Springer, Berlin), p. 412.
Janossy, A., G. Mihály, G. Pekker, and S. Roth, 1987, Solid State Commun. 61, 33.
Javadi, H. H., S. Sridhar, G. Grüner, L. Chiang, and F. Wudl, 1986, Phys. Rev. Lett. 55, 1216.
Jensen, M. H., P. Bak, and T. Bohr, 1984, Phys. Rev. A 30, 1960.
Johnston, D., 1984, Phys. Rev. Lett. 52, 2049.
Johnston, D., M. Maki, and G. Grüner, 1985, Solid State Commun. 53, 5.
Johnston, D. C., J. P. Stokes, P. L. Hsieh, and G. Grüner, 1983, J. Phys. (Paris), Colloq. 44, C3-1749.
Jonscher, A. K., 1977, Nature (London) 267, 673.
Joos, B., and D. Murray, 1984, Phys. Rev. B 29, 1094.
Kalem, C. B., N. P. Ong, and J. C. Eckert, 1987, unpublished.
Kantz, R. L., 1981, J. Appl. Phys. 52, 6241.
Kawabata, K., M. Ido, and T. Sambongi, 1981, J. Phys. Soc. Jpn. 50, 739.
Kim, T. W., W. P. Beyermann, and G. Grüner, 1987, unpublished.
Kinzel, W., 1983, Phys. Rev. Lett. 51, 1787.
Klemm, R. A., and M. O. Robbins, 1986, Physica B 143, 76.
Klemm, R. A., and J. R. Schrieffer, 1983, Phys. Rev. Lett. 51, 47.
Klemm, R. A., and J. R. Schrieffer, 1984, Phys. Rev. Lett. 52, 482.
Kogoj, M., S. Zumer, and R. Brinz, 1984, J. Phys. C 17, 2415.

Kohlrausch, R., 1947, Ann. Phys. (Leipzig) 12, 393.
Kriza, G., A. Janossy, and G. Mihály, 1985, in Charge Density Waves in Solids, Proceedings of the International Conference Held in Budapest, Hungary, 1984, Lécture Notes in Physics Vol. 217, edited by Gy. Hutiray and J. Sólyom (Springer, Berlin), p. 426.
Kriza, G., and G. Mihály, 1986, Phys. Rev. Lett. 56, 2529.
Kriza, G., S. Pekker, and K. Kamaras, 1987, Europhys. Lett. 3, 1027.
Kuper, C. G., 1955, Proc. R. Soc. London, Ser. A 227, 214.
Lacoe, R., H. J. Schulz, D. Jerome, K. Bechgaard, and J. Johannsen, 1986, Phys. Rev. Lett. 55, 2351.
Latyshev, Yu. T., V. E. Mihakova, Ya. S. Savitshaya, and V. V. Frolov, 1986, Physica B 143, 155.
Latyshev, Yu. T., V. E. Minakova, and Yu. A. Rzhakov, 1987, Pis'ma Zh. Eksp. Teor. Fiz. 46, 31 [JETP Lett. 46, 37].
Latyshev, Yu. T., and Ya. S. Savitskaya, 1986, Physica B 143, 180.
Latyshev, Yu. I., Ya. S. Savitskaya, and V. V. Frolov, 1984, Pis'ma Zh. Eksp. Teor. Fiz. 40, 72 [JETP Lett. 40, 807 (1984)].
Lee, P. A., and H. Fukuyama, 1972, Phys. Rev. B 17, 542.
Lee, P. A., and T. M. Rice, 1979, Phys. Rev. B 19, 3970.
Lee, P. A., T. M. Rice, and P. W. Anderson, 1973, Phys. Rev. Lett. 31, 462.
Lee, P. A., T. M. Rice, and P. W. Anderson, 1974, Solid State Commun. 14, 703.
Lindelof, P. E., 1981, Rep. Prog. Phys. 44, 949.
Link, B., and G. Mozurkewich, 1988, unpublished.
Littlewood, P. B., 1986, Phys. Rev. B 33, 6694.
Littlewood, P. B., 1987, Phys. Rev. B 36, 3108.
Littlewood, P. B., 1988, Solid State Commun. 65, 1347.
Littlewood, P. B., S. Coppersmith, and D. Fisher, 1988, unpublished.
Littlewood, P. B., and T. M. Rice, 1982, Phys. Rev. Lett. 48, 44.
Liu, S., and L. Sneddon, 1987, Phys. Rev. B 35, 7745.
Longcor, S., 1981, Ph.D. thesis (University of California, Berkeley).
Lyding, J. W., J. S. Hubacek, G. Gammie, and R. E. Thorne, 1986, Phys. Rev. B 33, 4341.
Lyons, W. G., R. E. Thorne, J. H. Miller, and J. R. Tucker, 1985, Phys. Rev. B 31, 6797.
MacDonald, A. H., and M. Plisbke, 1983, Phys. Rev. B 27, 201.
Maeda, A., T. Furuyama, and S. Tanaka, 1985, Solid State Commun. 55, 8156.
Maeda, A., T. Furuyama, and S. Tanaka, 1986, Solid State Commun. 55, 951.
Maeda, A., T. Furuyama, K. Uchinokura, and S. Tanaka, 1986, Physica B 143, 123.
Maeda, A., M. Naito, and S. Tanaka, 1983, Solid State Commun. 47, 1001.
Maeda, A., M. Naito, and S. Tanaka, 1985, J. Phys. Soc. Jpn. 54, 1912.
Maki, K., 1977, Phys. Rev. Lett. 39, 46.
Maki, K., 1978, Phys. Rev. B 18, 1641.
Maki, K., 1985, in Electronic Properties of Inorganic Quasi-One-Dimensional Compounds, Part I, edited by P. Monceau (Reidel, Dordrecht/Boston/Lancaster), p. 125.
Maki, K., 1986, Physica B 143, 59.
Maki, K., and A. Virosztek, 1987, Phys. Rev. B 36, 2910.
Matsukawa, H., and H. Takayama, 1984, Solid State Commun. 50, 283.
Matsukawa, H., and H. Takayama, 1986, Physica B 143, 80.
Meerschaut, A., 1983, J. Phys. (Paris), Colloq. 44, C3-1615.
Mihály, G., P. Beauchene, J. Marcus, J. Dumas, and C. Schlemkas, 1988, Phys. Rev. B 37, 1097.
Mihály, G., Gy. Hutiray, and L. Mihály, 1983, Phys. Rev. B 28, 4896.

Mihály, G., G. Kriza, and A. Janossy, 1984, Phys. Rev. B 30, 3578.
Mihály, G., and L. Mihály, 1984, Phys. Rev. Lett. 52, 149.
Mihály, G., L. Mihály, and H. Mutka, 1984, Solid State Commun. 49, 1009.
Mihály, L., Ting Chen, B. Alavi, and G. Grüner, 1985, Charge Density Waves in Solids, Proceedings of the International Conference Held in Budapest, Hungary, 1984, Lecture Notes in Physics Vol. 217, edited by Gy. Hutiray and J. Sólyom (Springer, Berlin), p. 455.
Mihály, L., T. Chen, and G. Grüner, 1987, Solid State Commun. 61, 751.
Mihály, L., M. Crommie, and G. Grüner, 1987, Europhys. Lett. 4, 103.
Mihály, L., and G. Grüner, 1984, Solid State Commun. 50, 807.
Mihály, L., and G. Grüner, 1987, in Nonlinearity in Condensed Matter, Springer Series in Solid-State Sciences Vol. 69, edited by A. R. Bishop, D. K. Campbell, P. Kumar, and S. E. Trullinger (Springer, Berlin), p. 308.
Mihály, L., Ki-Bong Lee, and P. W. Stephens, 1987, Phys. Rev. B 36, 1793.
Mihály, L., G. Mihály, and A. Janossy, 1985, in Charge Density Waves in Solids, Proceedings of the International Conference Held in Budapest, Hungary, 1984, Lecture Notes in Physics Vol. 217, edited by Gy. Hutiray and J. Sólyom (Springer, Berlin), p. 404.
Mihály, L., and G. Y. Tessema, 1986, Phys. Rev. B 33, 5858.
Miller, J. H., J. Richard, R. E. Thorne, W. G. Lyons, J. R. Tucker, and John Bardeen, 1984, Phys. Rev. B 29, 2328.
Miller, J. H., J. Richard, J. R. Tucker, and John Bardeen, 1983, Phys. Rev. 51, 1592.
Miller, J. H., R. E. Thorne, W. G. Lyons, J. R. Tucker, and John Bardeen, 1985, Phys. Rev. B 31, 5229.
Monceau, P., 1980, in Electronic Properties of Inorganic Quasi-One-Dimensional Materials, edited by P. Monceau (Reidel, Dordrecht/Boston/Lancaster).
Monceau, P., 1982, Physica B 109, 1890.
Monceau, P., 1985, in Electronic Properties of Inorganic Quasi-One-Dimensional Compounds, Part II, edited by P. Monceau (Reidel, Dordrecht/Boston/Lancaster), p. 139
Monceau, P., 1986, in Properties of Inorganic Quasi-OneDimensional Materials, Vol. II, edited by P. Monceau (Reidel, Holland).
Monceau, P., N. P. Ong, A. M. Portis, A. Meerschaut, and J. Rouxel, 1976, Phys. Rev. Lett. 37, 6902.
Monceau, P., M. Renard, J. Richard, and M. C. Saint-Lager, 1986, Physica B 143, 64.
Monceau, P., M. Renard, J. Richard, M. C. Saint-Lager, H. Salva, and Z. Z. Wang, 1983, Phys. Rev. B 28, 1646.
Monceau, P., M. Renard, J. Richard, M. C. Saint-Lager, and Z. Z. Wang, 1985, in Charge Density Waves in Solids, Proceedings of the International Conference Held in Budapest, Hungary, 1984, Lecture Notes in Physics Vol. 217, edited by Gy. Hutiray and J. Sólyom (Springer, Berlin), p. 279.
Monceau, P., J. Richard, and M. Renard, 1980, Phys. Rev. Lett. 45, 43.
Monceau, P., J. Richard, and M. Renard, 1982, Phys. Rev. B 25, 931.
Moses, D., and R. M. Boysel, 1985, Phys. Rev. B 31, 3202.
Mozurkewich, G., P. M. Chaikin, W. G. Clark, and G. Grüner, 1985a, Solid State Commun. 56, 421.
Mozurkewich, G., P. M. Chaikin, W. G. Clark, and G. Grüner, 1985b, in Charge Density Waves in Solids, Proceedings of the International Conference Held in Budapest, Hungary, 1984, Lecture Notes in Physics Vol. 217, edited Gy. Hutiray and J. Sólyom (Springer, Berlin), p. 353.
Mozurkewich, G., and G. Grüner, 1983a, Phys. Rev. Lett. 51, 2206.
Mozurkewich, G., and G. Grüner, 1983b, unpublished.
Mozurkewich, G., M. Maki, and G. Grüner, 1983, Solid State Commun. 48, 5.
Mutka, H., S. Bouffard, J. Dumas, and C. Schlenker, 1984, J. Phys. Lett. 45, L729.

Mutka, H., S. Bouffard, and L. Zuppiroli, 1985, in Charge Density Waves in Solids, Proceedings of the International Conference Held in Budapest, Hungary, 1984, Lecture Notes in Physics Vol. 217, edited by Gy. Hutiray and J. Sólyom (Springer, Berlin), p. 55.
Nad, F. Ya., 1985, in Charge Density Waves in Solids, Proceedings of the International Conference Held in Budapest, Hungary, 1984, Lecture Notes in Physics Vol. 217, edited by Gy. Hutiray and J. Sólyom (Springer, Berlin), p. 286.
Nerenberg, M. A., T. A. Blackburn, and S. Vik, 1984, Phys. Rev. B 30, 5084.
Ng, H. K., G. A. Thomas, and L. F. Schneemeyer, 1986, Phys. Rev. B 33, 8755.
Ngai, K. L., 1979, Comments Solid State Phys. 9, 127.
Ngai, K. L., 1980, Comments Solid State Phys. 9, 141.
Nomura, K., T. Sambongi, K. Kume, and M. Sato, 1986, Physica B 143, 117.
Oda, M., and M. Ido, 1982, Solid State Commun. 44, 1535.
Oda, M., and M. Ido, 1985, Solid State Commun. 50, 879.
Ong, N. P., 1982, Can. J. Phys. 60, 757.
Ong, N. P., 1983, J. Phys. (Paris), Colloq. 44, C3-1659.
Ong, N. P., and J. W. Brill, 1978, Phys. Rev. B 18, 5265.
Ong, N. P., J. W. Brill, J. C. Eckert, J. W. Savage, S. K. Khanna, and R. B. Somoano, 1979, Phys. Rev. Lett. 42, 811.
Ong, N. P., D. D. Duggan, C. B. Kalem, T. W. Jing, and P. A. Lee, 1985, in Charge Density Waves in Solids, Proceedings of the International Conference Held in Budapest, Hungary, 1984, Lecture Notes in Physics Vol. 217, edited by Gy. Hutiray and J. Sólyom (Springer, Berlin), p. 387.
Ong, N. P., and C. Gould, 1981, Solid State Commun. 37, 25.
Ong, N. P., C. B. Kalem, and J. C. Eckert, 1984, Phys. Rev. B 30, 2902.
Ong, N. P., and K. Maki, 1985, Phys. Rev. B 32, 6582.
Ong, N. P., and P. Monceau, 1977, Phys. Rev. B 16, 3443.
Ong, N. P., and P. Monceau, 1978, Solid State Commun. B 26, 487.
Ong, N. P., G. X. Tessema, G. Varma, J. C. Eckert, J. Savage, and S. K. Khanna, 1982, Mol. Cryst. Liq. Cryst. 81, 41.
Ong, N. P., and G. Verma, 1983, Phys. Rev. B 27, 4495.
Ong, N. P., G. Verma, and M. Maki, 1984, Phys. Rev. Lett. 52, 663.
Osada, T., N. Miura, and G. Saito, 1987, Solid State Commun. 60, 441.
Palmer, R. G., D. L. Stein, E. Abrahams, and P. W. Anderson, 1984, Phys. Rev. Lett. 53, 958.
Peierls, R. E., 1955, Quantum Theory of Solids (Oxford University, New York/London).
Phillip, A., A. Mayr, T. W. Kim, and G. Grüner, 1987, Solid State Commun. 62, 521.
Pietronero, L., and S. Strässler, 1983, Phys. Rev. B 28, 5863.
Portis, A. M., 1982, Mol. Cryst. Liq. Cryst. 81, 59.
Pouget, J. P., S. Kagoshima, C. Schlenker, and J. Marcus, 1983, J. Phys. (Paris) Lett. 44, L-113.
Pouget, J. P., A. H. Moudden, R. Moret, C. Escribe-Filippini, B. Mannion, J. Marcus, and C. Schlenker, 1985, in Charge Density Waves in Solids, Proceedings of the International Conference Held in Budapest, Hungary, 1984, Lecture Notes in
Physics, Vol. 217, edited by Gy. Hutiray and J. Sólyom (Springer, Berlin).
Prester, M., 1985, Phys. Rev. B 32, 2621.
Reagor, D., 1987, Ph.D. thesis (University of California, Los Angeles).
Reagor, D., and G. Grüner, 1986, Phys. Rev. Lett. 56, 659.
Reagor, D., and G. Mozurkewich, 1988, unpublished.
Reagor, D., S. Sridhar, and G. Grüner, 1985, in Charge Density Waves in Solids, Proceedings of the International Conference Held in Budapest, Hungary, 1984, Lecture Notes in Physics

Vol. 217, edited by Gy. Hutiray and J. Sólyom (Springer, Berlin), p. 308.
Reagor, D., S. Sridhar, and G. Grüner, 1986,Phys. Rev. B 34, 2212.
Reagor, D., S. Sridhar, M. Maki, and G. Grüner, 1985, Phys. Rev. B 32, 8445.
Rice, M. J., 1975, in Low Dimensional Cooperative Phenomena, edited by J. Keller (Plenum, New York).
Rice, M. J., and S. Strässler, 1973, Solid State Commun. 13, 1389.
Richard, J., P. Monceau, M. Popoular, and M. Renard, 1982, J. Phys. C 15, 7157.
Richard, J., P. Monceau, and M. Renard, 1982, Phys. Rev. B 25, 948.
Richard, J., R. E. Thorne, W. G. Lyons, J. H. Miller, and J. R. Tucker, 1984, Solid State Commun. 52, 183.
Robbins, M., and R. M. Klemm, 1986, Phys. Rev. B 34, 8496.
Ross, J. H., Z. Wang, and C. P. Slichter, 1986, Phys. Rev. Lett. 56, 663.
Roucau, C., 1983, J. Phys. (Paris), Colloq. 44, C3-1725.
Rouxel, J., 1982, Mol. Cryst. Liq. Cryst. 81, 31.
Salva, H., Z. Z. Wong, P. Monceau, J. Richard, and M. Renard, 1984, Philos. Mag. 49, 385.
Saso, T., Y. Suzumura, and H. Fukuyama, 1984, in Proceedings of the 17th International Conference on Low Temperature Physics, edited by V. Eckern, A. Schmid, W. Weber, and H. Wühl (North-Holland, Amsterdam), p. 1345.
Sato, M., H. Fujishita, and S. Hoshino, 1983, J. Phys. C 16, L877.
Schlenker, C., and J. Dumas, 1986, in Crystal Chemistry and Properties of Materials with Quasi-One-Dimensional Structures, edited by J. Rouxel (Reidel, Dordrecht/Boston/Lancaster).
Schlesinger, M. I., and E. W. Montroll, 1984, Proc. Nat. Acad. Sci. U.S:A. 81, 1280.
Schneemeyer, L. F., R. M. Fleming, and S. E. Spengler, 1984, Bull. Am. Phys. Soc. 29, 357.
Schneemeyer, L. F., R. M. Fleming, and S. E. Spengler, 1985, Solid State Commun. 53, 505.
Seeger, K., 1985, Solid State Commun. 53, 219.
Seeger, K., W. Mayr, and A. Phillip, 1982, Solid State Commun. 43, 113.
Seeger, K., A. Phillip, and W. Mayr, 1984, Solid State Commun. 50, 223.
Seeger, K., A. Phillip, and W. Mayr, 1985, Mol. Cryst. Liq. Cryst. 120, 55.
Ségranson, P., A. Jánossy, C. Berthier, J. Marcus, and P. Butaud, 1986, Phys. Rev. Lett. 56, 1854.
Sham, L. J., and B. R. Patton, 1976, Phys. Rev. B 13, 2151.
Shapiro, S., 1963, Phys. Rev. Lett. 11, 80.
Sherwin, M., R. Hall, and A. Zettl, 1984, Phys. Rev. Lett. 53, 1387.
Sherwin, M., and A. Zettl, 1985, Phys. Rev. B 32, 5536.
Sneddon, L., 1984a, Phys. Rev. B 30, 2979.
Sneddon, L., 1984b, Phys. Rev. B 29, 719.
Sneddon, L., 1984c, Phys. Rev. Lett. 52, 65.
Sneddon, L., 1986, Phys. Rev. Lett. 55, 1194.
Sneddon, L., M. Cross, and D. Fisher, 1982, Phys. Rev. Lett. 49, 292.
Sneddon, L., and K. Lox, 1987, Phys. Rev. Lett. 58, 1903.
Sokoloff, J.B., 1981, Phys. Rev. B 23, 1992.
Sokoloff, J. B., and B. Horovitz, 1983, J. Phys. (Paris), Colloq. 44, C3-1667.
Sólyom, J., 1979, Adv. Phys. 28, 201.
Sridhar, S., D. Reagor, and G. Grüner, 1986, Phys. Rev. B 34, 2223.
Stokes, J. P., S. Bhattacharya, and A. N. Bloch, 1987, Phys. Rev. B 34, 8944.
Stokes, J. P., A. N. Bloch, and G. Grüner, 1983, Bull. Am. Phys. Soc. 28, 426.
Stokes, J. P., A. N. Bloch, A. Janossy, and G. Grüner, 1984, Phys. Rev. Lett. 52, 372.
Stratonovich, R. L., 1958, Radiotekh. Elektron. 3, 497.
Suzuki, A., H. Mizubayashi, S. Okuda, and M. Doyama, 1986, Physica B 143, 161.
Takada, S., M. Wong, and T. Holstein, 1985, in Charge Density Waves in Solids, Proceedings of

the International Conference Held in Budapest, Hungary, 1984, Lecture Notes in Physics Vol. 217, edited by Gy. Hutiray and J. Sólyom (Springer, Berlin), p. 227.
Talopov, A. L., 1981, Zh. Eksp. Teor. Fiz. 81, 1890 [JETP Lett. 54, 1001 (1981)].
Tamegai, T., K. Tsutsumi, S. Kagoshima, Y. Kanai, M. Tani, H. Tomozawa, M. Sato, K. Tsuji, J. Harada, M. Sakata, and T. Nakajima, 1985, Solid State Commun. 56, 13.
Tami, M., Y. Nogami, and M. Sato, 1985, Solid State Commun. 56, 13.
Tanaka, S., and K. Uchinokura, 1986, Eds., Physics and Chemistry of Quasi-One-Dimensional Conductors, Proceedings of the Yamada Conference XV (Physica B 143).
Tang, C., K. Wisenfeld, Per Bak, S. Coppersmith, and P. Littlewood, 1987, Phys. Rev. Lett. 58, 1161.
Teranishi, N., and R. Kubo, 1979, J. Phys. Soc. Jpn. 47, 720.
Tessema, G. X., B. Alavi, and L. Mihály, 1985, Phys. Rev. B 31, 6878.
Tessema, G. X., and L. Mihály, 1987, Phys. Rev. B 35, 7680.
Tessema, G. X., and N. P. Ong, 1981, Phys. Rev. B 23, 5607.
Tessema, G. X., and N. P. Ong, 1983, Phys. Rev. B 27, 1427.
Tessema, G. X., and N. P. Ong, 1985, Phys. Rev. B 31, 1055.
Testardi, J., 1975, Phys. Rev. B 12, 3849.
Thompson, A. N., A. Zettl, and G. Grüner, 1981, Phys. Rev. Lett. 47, 64.
Thorne, R. E., W. G. Lyons, J. H. Miller, Jr., J. W. Lyding, and J. R. Tucker, 1986, Phys. Rev. B 34, 5988.
Thorne, R. E., W. G. Lyons, J. H. Miller, Jr., J. Richard, and J. R. Tucker, 1984, Solid State Commun. 50, 833.
Thorne, R. E., J. R. Tucker, and John Bardeen, 1987, Phys. Rev. Lett. 58, 828.
Travaglini, G., I. Mörkee, and P. Wachter, 1983, Solid State Commun. 45, 289.
Travaglini, G., and P. Wachter, 1984, Phys. Rev. B 30, 1971.
Tsang, J. C., C. Herman, and M. W. Shafer, 1978, Phys. Rev. Lett. 40, 1528.
Tsutsumi, K., T. Sambongi, S. Kagoshima, and T. Ishiguro, 1978, J. Phys. Soc. Jpn. 44, 1735.
Tua, P. F., and J. Ruvalds, 1984, Solid State Commun. 51, 293.
Tua, P. F., and J. Ruvalds, 1985, Solid State Commun. 54, 471.
Tua, P. F., and A. Zawadowski, 1984, Solid State Commun. 49,
19.
Tucker, J. R., 1979, IEEE J. Quantum Electron. 15, 1234.
Tucker, J. R., 1986, Phyisca B 143, 19.
Tucker, J. R., W. G. Lyons, J. M. Miller, R. E. Thorne, and J. W. Lyding, 1986, Phys. Rev. B 34, 9038.
Tucker, J. R., J. M. Miller, K. Seeger, and John Bardeen, 1981, Phys. Rev. B 25, 2979.
Tütto, I., and A. Zawadowski, 1985, Phys. Rev. B 32, 2449.
Underweiser, M., M. Maki, B. Alavi, and G. Grüner, 1987, Solid State Commun. 64, 181.
Verma, G., N. P. Ong, S. K. Khanna, J. C. Eckert, and J. W. Savage, 1983, Phys. Rev. B 28, 910.
Voss, R. F., and R. A. Webb, 1981, Phys. Rev. Lett. 47, 265.
Wada, S., R. Aoki, and O. Fujita, 1984, J. Phys. F 14, 1515.
Wang, Z. Z., P. Monceau, M. Renard, P. Gressier, L. Guemas, and A. Meerschaut, 1983, Solid State Commun. 47, 439.
Wang, Z. Z., and N. P. Ong, 1986, Physica B 143, 100.
Wang, Z. Z., and N. P. Ong, 1987, Phys. Rev. B 34, 5967.
Wang, Z. Z., M. C. Saint-Lager, P. Monceau, M. Renard, P. Gressier, A. Meerschaut, L. Guemas, and J. Rouxel, 1983, Solid State Commun. 46, 325.
Wang, Z. Z., K. Salva, P. Monceau, M. Renard, C. Roucau, R. Ayroles, F. Levy, L. Guemas, and A. Meerschaut, 1983, J. Phys. (Paris) Lett. 44, L311.

Weger, M., W. G. Clark, and G. Grüner, 1983, J. Phys. (Paris), Colloq. 44, C3-1673.
Weger, M., G. Grüner, and W. G. Clark, 1980, Solid State Commun. 35, 243.
Weger, M., G. Grüner, and W. G. Clark, 1982, Solid State Commun. 44, 1179.
Weisz, J. F., J. B. Sokoloff, and J. E. Sacco, 1979, Phys. Rev. B 20, 4713.
Williams, G., and D. C. Watts, 1970, Trans. Faraday Soc. 66, 80.
Wilson, J. A., 1979, Phys. Rev. B 19, 6456.
Wilson, J. A., F. J. DiSalvo, and S. Mahajan, 1975, Adv. Phys. 24, 117.
Wong, K. Y. M., and S. Takada, 1987, Phys. Rev. B 36, 5476.
Wonneberger, W., 1979, Solid State Commun. 30, 511.
Wonneberger, W., 1983a, Z. Phys. B 50, 23.
Wonneberger, W., 1983b, Z. Phys. B 53, 167.
Wonneberger, W., 1985, Solid State Commun. 54, 317.
Wonneberger, W., and H.-J. Breymayer, 1981, Z. Phys. B 43, 329.
Wonneberger, W., and H.-J. Breymayer, 1984, Z. Phys. B 56, 241.
Wu, Wei-yu, A. Janossy, and G. Grüner, 1984, Solid State Commun. 49, 1013.
Wu, Wei-yu, L. Mihály, and G. Grüner, 1985, Solid State Commun. 55, 663.
Wu, Wei-yu, L. Mihály, G. Mozurkewich, and G. Grüner, 1986, Phys. Rev. B 33, 2444.
Wu, Wei-yu, G. Mozurkewich, L. Mihály, and G. Grüner, 1984, Phys. Rev. Lett. 52, 2382.
Wu, Wei-yu, G. Mozurkewich, L. Mihály, and G. Grüner, 1986, Phys. Rev. B 33, 2444.
Xiang, X. D., and J. W. Brill, 1987, Phys. Rev. B 36, 2969.
Xiang, X. D., and J. W. Brill, 1988, unpublished.
Yeh, W. J., Da-Rem He, and Y. H. Kao, 1984, Phys. Rev. Lett. 52, 480.
Zawadowski, A., I. Tütto, S. E. Barnes, P. F. Tua, and J. Ruvalds, 1985, in Charge Density Waves in Solids, Proceedings of the International Conference Held in Budapest, Hungary, 1984, Lecture Notes in Physics Vol. 217, edited by Gy. Hutiray and J. Sólyom (Springer, Berlin), p. 240.
Zeller, H. R., 1974, in Low-Dimensional Cooperative Phenomena, NATO Advanced Study Institutes Series, Vol. 7, edited by H. J. Keller (Plenum, New York), p. 215.
Zettl, A., 1983a, Ph.D. thesis (University of California, Los Angeles).
Zettl, A., 1983b, Proceedings of the International Symposium on Nonlinear Transport in Inorganic Quasi-One-Dimensional Conductors, Sapporo, Japan (unpublished).
Zettl, A., and G. Grüner, 1982a, Phys. Rev. B 26, 2298.
Zettl, A., and G. Grüner, 1982b, Phys. Rev. B 25, 2081.
Zettl, A., and G. Grüner, 1983a, Phys. Rev. B 28, 2091.
Zettl, A., and G. Grüner, 1983b, Solid State Commun. 46, 501.
Zettl, A., and G. Grüner, 1983c, Solid State Commun. 46, 29.
Zettl, A., and G. Grüner, 1984, Phys. Rev. B 29, 755.
Zettl, A., and G. Grüner, 1986, Comments Condens. Matter Phys. 12, 265.
Zettl, A., G. Grüner, and A. H. Thompson, 1982, Phys. Rev. B 26, 5760.
Zettl, A., C. M. Jackson, and G. Grüner, 1982, Phys. Rev. B 26, 5773.
Zettl, A., M. B. Kaiser, and G. Grüner, 1984, Bull. Am. Phys. Soc.
Zettl, A., M. B. Kaiser, and G. Grüner, 1985, Solid State Commun. 53, 649.
Zeyher, R., 1988, unpublished.
Zhang, X. J., and N. P. Ong, 1985, Phys. Rev. Lett. 55, 2919.
Zhang, X. J., N. P. Ong, and J. C. Eckert, 1986, Phys. Rev. Lett. 56, 1206.

3 Electronic Properties of Inorganic Quasi-1D Compounds (part I) by Monceau

3.1 Preface To Part I

Intensive experimental and theoretical work has been undertaken these last few years in the understanding of the chemical and physical properties of quasi-one-dimensional compounds. This designation is ascribed to materials which exhibit large anisotropy ratios in some physical properties when measured along one direction with regard to orthogonal directions. The recently-acquired possibility for chemists to synthesize real, inorganic as well as organic, one-dimensional systems with fascinating physical properties has been one of the essential motivations which have attracted many new research workers. The first two volumes in the present series 'Physics and Chemistry of Materials with Quasi-One-Dimensional Structures' are intended to review the experimental and the theoretical progress made in this field in the last years. These volumes deal with electronic properties of inorganic compounds.

The physical properties of the platinum chain compounds, of the superconducting polymeric sulfur nitride and the transition metal tri- and tetrachalcogenides are reviewed in Part II. Some of the latter compounds have aroused much interest because they have been considered as prototypes for the electrical conduction mechanism proposed by Fröhlich in 1954 in his theory of superconductivity based on the motion of a charge density wave. Concepts and theoretical models developed to understand the properties of one-dimensional systems are described in the present volume. Two chapters are devoted to the description of the nature of the ground state resulting from the interplay between lattice instabilities and superconductivity and to the analysis of the superconducting properties of an assembly of weakly-coupled chains. Two different approaches, a classical one and the other involving macroscopic quantum effects, are used to account for the collective transport mechanism induced by a charge density wave motion. One chapter concerns the general properties of the non-linear excitations in the ground state of onedimensional systems, or solitons, and their contribution to transport properties. This book is intended to be of interest to solid state physicists - both students as well as advanced researchers - specialists in synthetic chemistry as well as scientists concerned with new materials.

I wish to express my sincere gratitude to the authors for their collaboration in this book and I warmly thank Prof. F. Lévy, the managing editor, for his suggestions and his constant encouragement.

3.2 Ground State Properties of Conducting Trichalcogenides

3.2.1 1. Introduction

In this review we shall discuss the equilibrium properties of the transition metal trichalcogenides MX_3(M = Ta, Nb, Hf, Zr, Ti; X = S, Se, Te) paying special attention to the conductors $NbSe_3$ and TaS_3, which exhibit incommensurate structural transitions. $NbSe_3$ not only undergoes structural instabilities [1,2] but under pressure it also shows [3] BCS-like superconductivity. The question of properties, the coexistence and the competition of structural instabilities and superconductivity in the $\mathbf{MX_3}$ compounds [4] will be the main concern of the present paper.

Transition metal trichalcogenides belong to a wider class of materials in which the existence of quasi-one-dimensional conducting electrons leads to interesting low-temperature phase transitions [5]. Historically, it was the search for high-temperature superconductivity [6] which provided the main motivation to the strong development of the quasi one-dimensional physics which has been so apparent in the two last decades. Even nowadays the superconductivity remains one of the most important goals of one-dimensional (1D) research [7], although many

other interesting effects, and in particular the non-linearities related to the structural instability have been found in the meantime [8]. The beginning of the one-dimensional history is thus usually associated with Little's proposal [9] for high-temperature superconductivity. The emphasis of this proposal was on a new mechanism for the effective electron-electron interaction. It was suggested that this can be mediated by the polarization fluctuations on the molecules surrounding the polymer backbone with conducting electrons. The one-dimensionality of the electron motion was merely a consequence of the geometrical requirements optimizing the interactions. However, it appeared soon on theoretical grounds [10] that the one-dimensionality of the electron motion may lead to novel physical effects. At the same time it was realized that the best known superconductors $M_3X(M = Nb, V, \ldots; X = Sn, Si, \ldots)$ have some one dimensional electronic properties [11, 12, 6]. This led to a branching in subsequent developments. One line of research was devoted to constructing models with approximate one-dimensional properties [6]. It turned out that the anisotropy of the electron propagation originates from the directional properties of the tightly-bound wave functions [12], rather than from the anisotropy of the underlying lattice. This was followed by investigation of electron-phonon coupling models in the tight-binding limit [13], including the intra- and interchain Coulomb forces between electrons. The analysis of these rather complicated model hamiltonians was carried out in the simple mean-field (ladder) approximations [6,12-14], as it was thought that the interchain couplings were large enough [15] to ensure their applicability at least in the $\mathbf{M_3X}$ compounds.

The other line of research started by examining the purely one-dimensional models, in spite of the lack of any well-established physical prototypes in these early times. The many-body complications associated with the one-dimensionality of the electron motion were carefully investigated in this approach. At first the weak-coupling, high temperature parquet summation was used [10, 16 − 18]. To a given order it takes correct account of the nontrivial coupling between the Cooper and density wave channels, characteristic for the one-dimensional electrons. This achievement was followed by an extremely rich development of the 1D theoretical models and methods, including Bethe's ansatz approach [19], renormalization group schemas [17, 20], bosonization [17, 20], mappings to equivalent models [17, 20] etc. The three-dimensional couplings [21, 22] were also progressively included in such considerations, with the general effect of stabilizing some particular types of the strong fluctuations found in the 1D theories [17, 23].

It turned out that the bridging between the tight binding models with their ladder approximations and the one-dimensional model results can be achieved in two ways. One way is to have the retarded (electron-acoustic phonon) interactions dominant close to the transition temperature. As we shall also see here, the strong retardation [14, 24] effects may reduce the parquet theory to the ladder one [18,25]. The second way is to have the interchain hopping energy large with respect to the transition temperature [17, 23]. The resulting ladder theories retain, however, some of the one-dimensional character, exploited in the early ladder treatments [12,13] of the tight-binding models [26]. The bridging was completed by noting that the tight-binding hamiltonian with long-range interchain Coulomb forces has similar properties, both in the parquet and ladder approximation, as the short-range hamiltonians, provided that the RPA screening is appropriately taken into account [27].

These theoretical developments went in parallel with the synthesis and characterisation of more and more new quasi-one-dimensional conductors [28,29,7]. The actual materials are believed to cover the whole theoretical spectrum, mentioned above. M_3X (Nb_3Sn etc) are certainly sufficiently three dimensional that the mean-field (ladder) approximations [6, 12, 13, 26] apply. TTF-TCNQ and $(TMTSF)_2PF_6$ families are likely to belong to the other extreme. They are nearly one-dimensional [7] and dominated by the unretarded Coulomb- and phonon-mediated interactions. The KCP family is also nearly one-dimensional but there the retardation effects in the dominant, phonon mediated interaction make [25] the simple single ladder approximation (i.e. the Peierls theory) qualitatively valid. As we shall argue here the situation

is similar in the $\mathbf{MX_3}$ ($NbSe_3$ etc) compounds at ambient pressure. However, high pressures bring the structural transition to low temperatures, where the retardation effects become unimportant. Nevertheless, the validity of the ladder approximations is maintained by the interchain hopping. In this regime the $\mathbf{MX}_3$ compounds present some similarities with the $\mathbf{M}_3\mathbf{X}$ materials.

This paper will not present the full spectrum of theories. Rather, we shall select those theoretical results and points of view which we believe to be relevant for the MX_3 compounds. In particular, we shall emphasize the role of the phonon-induced, retarded electron-electron interactions. Such an approach requires a discussion of the pertinent experimental results and represents, in consequence, an attempt at synthesising experiment and theory focussed on a given class of materials. The attempt is an early one, because the crucial experiment [30] showing definitively that $NbSe_3$ is a
quasi-one-dimensional conductor rather than the anisotropic three dimensional metal was performed only very recently, confirming some earlier indications in this direction [31, 32], which were not considered as being conclusive. In the same spirit of synthesis a related paper [33] will describe the physics of TTF-TCNQ like compounds as an example where the unretarded Coulomb forces between 1D electrons play an important role.

3.2.2 2. Elementary Excitations

2.1. Electronic Bands

The common feature of all transition metal trichalcogenides [34,4] is that each transition atom M lies in the centre of the trigonal prism of chalcogen atoms (Figure 1). The

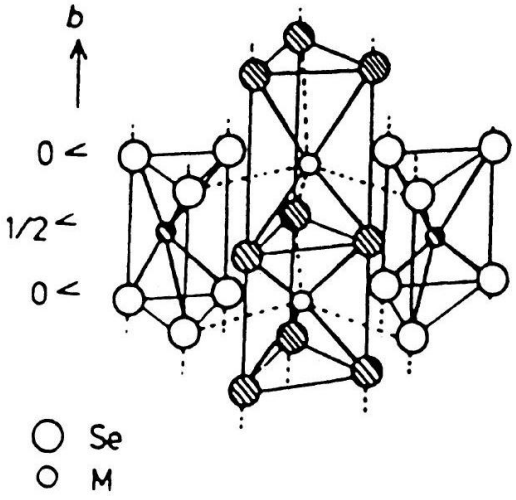


Fig. 1. Stacking of $\mathrm{MX
_{3}$ prisms along the b-axis. Open atoms are at O and shaded atoms at $1/2b$ (from reference [29]).}

prisms form infinite chains along the b-axis. However, the form of the prisms and the mutual position of the chains depend on the materials. This difference is accompanied by a large variation of the conducting properties. E.g. NbS_3 is an insulator with an appreciable dimerization along the chain, TaS_3 and $NbSe_3$ are metals exhibiting structural transitions, and $TaSe_3$ is a reasonably good anisotropic metal even at low temperatures.

These differences can be associated with the band structure at the Fermi level. Indeed, recent band calculations [35, 36], based on the tight-binding (TB) or closely related schemes, were able to explain the differences mentioned in the conductivity of all materials considered,

namely among $ZrSe_3, NbSe_3$ and $TaSe_3$. As the electron band structure is the basis for all later developments let us briefly review some of those results. We shall pay particular attention to $NbSe_3$, since it is the prototype material.
$NbSe_3$ (and one out of two modifications of TaS_3) is monoclinic, with space group $P2_1/m$. The unit cell contains six $NbSe_3$ units, which belong to six chains. From the crystallographic point of view, the chains are usually [4] subdivided in three groups
according to the degree of departure of the X-X-X prism basis from the equilateral triangle. The three groups in question are shown in Figure 2. Each equilateral triangle of the prism of the group II can receive six d-electrons. The pairing of Se atoms in isosceles triangles, moderate in group I and strong in group III, ejects one antibonding state per triangle above the Fermi level. Therefore only four electrons can go to the Se atoms in such triangles. Out of $6 \times 5d$-electrons in the unit cell, 4×4 thus go to

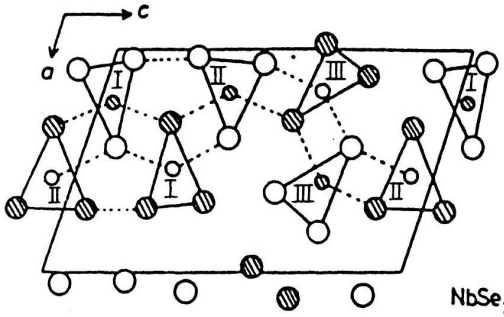


Fig. 2. Projection of the $\mathrm{NbSe
_{3}$ structure in the ac plane. Atoms as in Fig. 1 (from reference [29]).}

the isosceles triangles and 2×6 to the equilateral ones. The remaining two electrons stay in the conducting d-bands, presumably in those associated with the chains of the isosceles prisms belonging to the groups I and III. The deformation of the equilateral into the isosceles triangle thus results in a net charge transfer between the chains and the partial (quarter) filling of the bands [4, 35, 36]. The similar reasoning applied to $ZrSe_3$ and $TaSe_3$ explains their respective semiconducting and semimetallic behaviors [4, 35, 36].

The p, d separation [4] used here is quite useful for counting the electrons and the orbital degeneracy of the states (bands). However, there seem to be appreciable $p - d$ ($Se - Nb$) hybridisations along the chain, which dominate the longitudinal bandwidth. On the other hand, the question of the transverse (interchain) hopping was controversial for a long time. Especially puzzling in this respect were the small effective number of carriers [4] ($\sim 10^{19} e/cm^3$) deduced from high-temperature Hall effect measurements [37]. This led to the construction of the band model with small pockets [4] of electrons and holes for temperatures above the structural transitions, at 144 and 59 K . The corresponding supersturcture Bragg reflections occur [31, 34, 39] at (0 , 0.243, 0) and (0.5, 0.259, 0.5) positions in the Brillouin zone. The model with pockets was also able to account for such superstructure [4]. However, observation of the onedimensional sheets by X-ray diffuse scattering [30,31] rules it out, since it implies that the precursor effects be well-localized around the final superstructure positions (see Section 4.1.).

In the more recent alternative band models [35] the interchain overlaps are much weaker than in the model involving small pockets. The six chains are thus only slightly
inequivalent. They contribute six bands of the same nature to the neighbourhood of the Fermi level (Figure 3). As already mentioned, the longitudinal dispersion is due

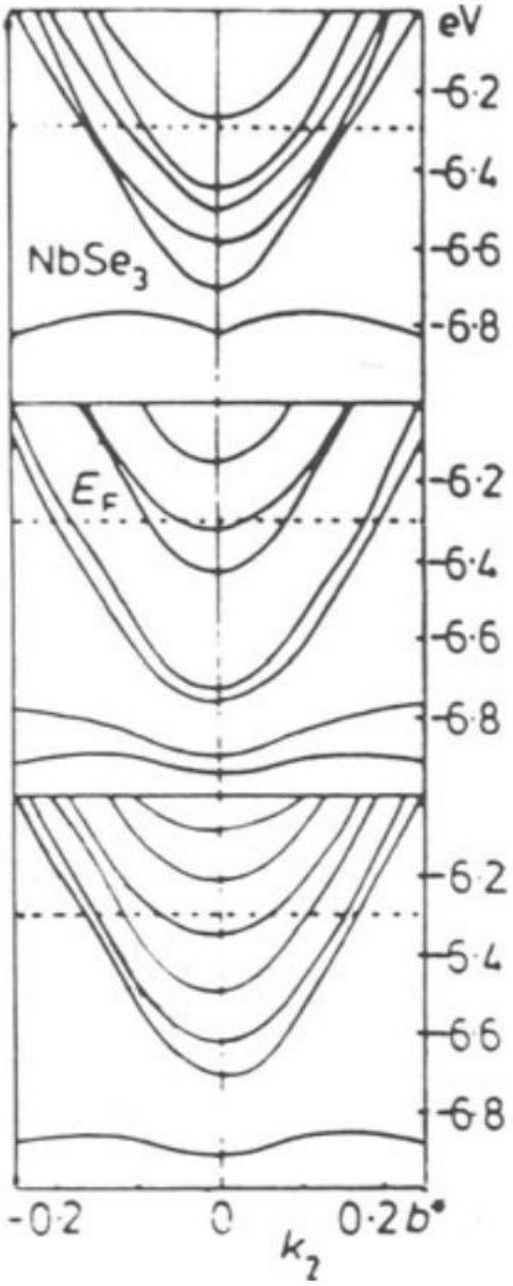


Fig. 3. Dispersion parallel to the chain direction for conducting bands in $\mathrm{NbSe _{3}$ along $(0, k, 0), (\pi/a, k, 0)$ and $(0, k, \pi/c)$ axes, starting from the top of the Figure (Ref. 35, copyright Institute of Physics, Bristol, England).}

to Nb − Se overlaps. The bands group two-by-two, as do the chains themselves. Four bands reach below the Fermi level. Therefore the four wave-vectors k_F fall in two groups, as actually observed through the $2k_F$ reflections. Consistently with small splittings among the bands, these $2k_F$'s are rather close, i.e. all four bands are nearly quarter-filled, in agreement with the preceding electron count.

Figure 3 suggests, further, that the transverse dispersion of $1d$ bands is comparable in both a and c transverse directions. This is somewhat surprising in view of the existence of the comparatively short contacts along the c-axis, but it should be noted that they involve the (group II) insulating chains. The most recent tight-binding band calculations [36] indicate however that the conducting bands have a nonvanishing group II character. This can lead to an effective transverse overlap larger in the c than in the a direction, and possibly explain the

observed anisotropy ratio [38] of conductivities $\sigma_c/\sigma_a \simeq 30$. Above all, the latest Hall effect measurements [37] at room temperature have shifted the estimation of the effective number of carriers from 10^{19} to 10^{21}e/cm^3, reaching qualitative agreement with the picture of quarter filled quasi-1D bands.

In what follows we shall thus use the band structure shown in Figure 3, or rather propose a simplified version of it. The simplification consists in ignoring the inequivalence of the four conducting chains. The longitudinal dispersion can be conveniently parametrized within the simple TB model

$$E(k) = -\frac{2t_{\rm SN}^2}{E_0} - \frac{2t_{\rm SN}^2}{E_0}\cos kb \tag{1}$$

where E_0 measures the difference between the atomic energies of the Nbd-state and the Se p-state. Their overlap $t_{\rm SN}$ is assumed small with respect to E_0. In addition we shall introduce the transverse hopping integral $t_\perp$, without specifying the kind of the transverse dispersion (nesting or not) it leads to. The existing band structure computations are not particularly specific on this account and in what follows we shall discuss different behaviors associated with different transverse dispersions.

Equation (1) also illustrates that the $E_0 \gg t_{\rm SN}$ band model can hardly by distinguished from the direct $t_{\rm NN}$ metal-metal bonding model. Sizeable differences between the two models arise in the corresponding electron - (acoustic, optic) phonon couplings, as will be indicated in Section 3.1. However, due to the lack of relevant information these differences will be mostly ignored there. Further band results (with electron-phonon coupling in mind) are therefore desirable.

2.2. Phonon Frequencies

The vibrational properties of the transition metal trichalcogenides were investigated rather extensively by Raman [40,41] and infrared techniques [42]. In order to understand the gross features of vibrations this investigation started with a simple ZrS_3-like structure [40,42], because the mode assignment is easier in this case. The characteristic vibrational frequences $\omega_{\rm ph}$ (measured in Kelvins) lie around 300 K . The exception is the mode at 500 K in which the two paired chalcogenide X atoms move in opposition of phase along the prism edge joining them (Fig. 1). The force constant corresponding to $\omega_{\rm ph} \sim 300$ K arises from the M − X bond and amounts to [40]

$$C \simeq 5 \times 10^4 \text{ K/Å}^2. \tag{2}$$

This force constant also determines the dispersion of the acoustic modes. Although the latter has not been measured, to our knowledge, Equation (2) sets the estimated Debye temperature $\omega_{\rm D}$ around 300 K .

In addition to that it was possible to measure directly the transverse dispersion of the Raman and infrared-active modes, i.e. the interchain elastic coupling [40-42]. The effective coupling constant $C_\perp$ turns out [40] to be about three times less than given in (2). Although elastically anisotropic, trichalcogenides are not quasi-one-dimensional from the vibrational point of view.

Due to its lower symmetry, $NbSe_3$ presents the splittings of the modes observed in the ZrS_3 structures [40]. Besides, there is an overall decrease $\Delta\omega_{\rm ph}$ of the phonon frequencies [40]. This decrease is usually imputed to the coupling of phonons to the conducting electrons of $NbSe_3$. Through the usual estimate [43] (see also Section 4.1)

$$\frac{\Delta\omega_{\rm ph}}{\omega_{\rm ph}} \simeq -\lambda_{\rm ph} \tag{3}$$

where $\lambda_{\rm ph}$ is the phonon mediated electron-electron coupling constant, this gives us an initial idea of the value of $\lambda_{\rm ph}$. We find $\lambda_{\rm ph} \simeq 0.1$, the value we wish to discuss in more detail in Section 3.1, which deals with interactions.

2.3. Plasma Frequency

In the present context it is also appropriate to mention the reflectivity measurements [44] which determine the plasma edge. The plasma frequency ω_0 is found to be equal to [44]

$$\omega_0 \simeq 1.15\text{eV}. \tag{4}$$

From this value it is possible to estimate the band-width W and long-range Coulomb interaction using the usual expression [45, 46, 27] for the plasma frequency ($n_{\rm F}-$ density of states per M atom, per spin)

$$n_{\rm F}\frac{e^2}{b} \simeq \frac{1}{4\pi}\left(\frac{\omega_0}{W}\frac{1}{k_{\rm F}b}\right)^2 \frac{ac}{4b^2}, \tag{5}$$

and knowing the lattice parameters [34] a, b, c. With [44]

$$W = \frac{4t_{\rm SN}^2}{E_0} \simeq 2.5\text{eV} \tag{6}$$

we have

$$n_{\rm F}\frac{e^2}{b} < 0.1. \tag{7}$$

As with Equation (3), this result leads us to the question of interactions discussed in the next Section.

3.2.3 3. Interactions

In the preceding section we have considered the non-critical renormalization of the elementary excitations (plasmons and phonons) by the interactions. However, the interactions also determine the subtle collective behavior of the system. For this reason we wish to proceed here with a more detailed discussion of the interactions. Sections IV and V will deal with the critical behavior induced by those interactions.

3.1. Electron-phonon Coupling

It is currently believed that the most important interaction in the conducting trichalcogenides is the coupling of the conducting electrons to the acoustic phonons. The main contribution to this coupling arises from the variation of the overlaps $t_{\rm SN}$ in Equation (1)
with acoustic deformation. The magnitude of this variation can be estimated by noting that [14]

$$\frac{{\rm d}t_{\rm SN}}{{\rm d}b} \simeq -q_{\rm SN}t_{\rm SN} \tag{8}$$

in the TB approximation. Here $q_{\rm SN}$ is the effective Slater coefficient of the Se and Nb wave-function [14]. The Nb $-$ Se splitting energy E_0 should not be much affected by the acoustic deformations, because it represents an intra-cell property, and the prisms move rigidly in acoustic modes. According to Equation (1) the variation (8) of $t_{\rm SN}$ gives rise to the variations of the effective overlap (the coefficient of $\cos kb$) and the mid-band energy. Equation (1) is thus an example of the band structure in which the electron-acoustic phonon couplings arising

from the variations of the effective overlaps and the mid-band energies are of the same order of magnitude. From this point of view the present situation contrasts with the usual metal-metal bonding TB models [14]. The wave-vector dependences of the two electron-phonon couplings are different [47]. However, we shall not be concerned with such details here, i.e. we shall take the couplings for the electrons at k_{F} through the phonons at $2k_{\mathrm{F}}$ (backward scattering) when both couplings act roughly additively. The corresponding coupling constant is

$$\lambda_{\mathrm{ac}} \simeq \frac{4W}{2\pi C q_{\mathrm{SN}}^{-2}} \tag{9}$$

with C and W given by Equations (2) and (6), respectively. Due to the large bandwidth W, λ_{ac} is around (below) 0.5 . The coupling of electrons via the optical phonons is expected to be somewhat weaker than (9). E.g. it is possible to construct the optical displacements which, to the first order, do not alter t_{SN}^2, in contrast to Equation (8). On the other hand the splitting energy E_0 in Equation (1) does contain some intersite contributions which could be sensitive to optic displacements. It is, however, hard to assess the order of magnitude of these variations. We shall thus proceed with the empirical estimate (3).

3.2. Coulomb Interactions

The basic picture which we are developing here is that of the TB electrons. The electron-phonon couplings discussed in the preceding subsection are short ranged (cf. Equation (8)). This is consistent with the phonon frequencies ω_{ac}, which vanish in the longwavelength limit. Despite this, the Coulomb interaction between electrons should be taken as being long-ranged at the outset [14] rather than as described by the Hubbard hamiltonian or its short-range extensions. The long range Coulomb forces lead to qualitatively important effects [48] in Nb_3Sn type of materials, where the structural instability occurs in the long wave-length limit. On the other hand the effects of the long (and short) range Coulomb forces are expected to be mainly quantitative in the present case, as we shall now proceed to argue.

The Coulomb interaction of two parallel strings of atoms carrying the charge density waves (CDW's) of the wave vector q and unit amplitude is [49]

$$\frac{e^2}{b} \sum_g e^{-igeb} K_0 \left(R_\perp |q+g|\right) e^{i\phi_\perp}. \tag{10}$$

Here K_0 is the modified zero-order Bessel function, g the longitudinal reciprocal wave vector, $R_\perp$ the distance between the strings, shifted relative to one another by ϵb, a fraction of b, Fig (4). $\phi_\perp$ is the relative phase of the CDW's on the strings. The total Coulomb

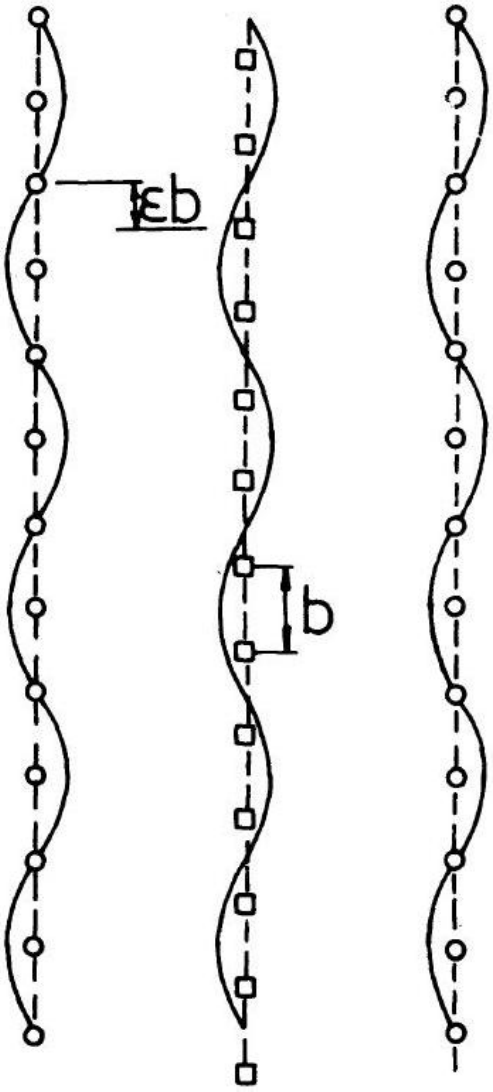


Fig. 4. $X(\circ)$ and $M(\circ)$ strings in $M_{3 $, carrying charge density waves.}

energy is obtained [49] by multiplying Equation (10) by the appropriate CDW amplitudes and by summing over all strings, after adding the intrastring terms. The latter are given by [49]

$$U_0 - \frac{e^2}{b} \log[2(1 - \cos qb)] \tag{11}$$

for the unit CDW amplitude. Here U_0 is the intra-atomic (Hubbard) matrix element for a given string of atoms.

In our case we can decompose each chain in four ($1\mathrm{Nb} + 3\mathrm{Se}$) strings, carrying the CDW's. The strong Nb-Se (M-X) hybridization [35, 36] forces all these CDW's to be in phase ($\phi_\perp = 0$ in Equation (10)). The appropriately weighted sum of the contributions (10) and (11) then gives the Coulomb intrachain energy for unit CDW amplitude per chain. The interchain Coulomb energy can be further evaluated as the sum of the interstring interactions between the chains. In this calculation it may be better to keep the relative phase $\phi_\perp$ of the CDW's on two chains as a free parameter. This is particularly indicated when the chains belong to different groups of Fig. 2 (for $NbSe_3$ we shall need only equivalent groups). Then all interstring interchain distances $R_\perp$ satisfy

$2k_F R_\perp > 1$, i.e. all K_0 's of Equation (10) are exponentially small. Such weak interchain interaction may lead to the thermally activated ordering of the thus-defined $\phi_\perp$, as is further discussed in Section 4.2. On the other hand, the Coulomb energy between the neighbouring chains which belong to the same group of Fig. 2, although considerably smaller than the intrachain one, is larger than the intergroup energy, because there are some short $2k_F R_\perp < 1$ distances within the group. Together with interchain hybridization and elastic coupling this interaction probably freezes the corresponding transverse phase to a definite value. In any case, we shall continue our analysis with only one phase $\phi_\perp$ per unit cell at a given structural transition and associate with it a small interchain coupling constant $g_1^\perp$. (The generalization to more phases, if necessary, is straightforward).

In contrast to that the intra- and interchain interactions between the long ($q < k_F$) waves is large, according to Equations (10) and (11). In the first instance this requires the introduction of the RPA screening [27]. In Section 4.2 it will be argued that the (logarithmic) theory with the RPA-screened forward ($q < k_F$) Coulomb interaction has much in common with the short-range (Hubbard-like) models, although some important differences persist. It turns out that to the leading order in the small parameter $n_F e^2/b$ (cf. Equation (7)), the effective on-chain forward coupling constant

$$n_F \frac{e^2}{b} \log \frac{1}{n_F \omega_0} < 1 \tag{12}$$

has the same effect as the complicated, screened, long-range Coulomb interaction. Whereas it is possible to start from the bare long range Coulomb interaction (10, 11), and express the effective coupling (12) in terms of this quantity using the RPA intraband screening, the same procedure does not work for the short range part of the interaction related to U_0 in Equation (11). The preliminary (pre-logarithmic) screening of U_0 is related to the 'interband' processes allowing the electrons to avoid each other on a given 'site' (prism). Although the principles of this screening are quite clear [50], its precise evaluation is lacking for conducting trichalcogenides. It is thus appropriate to take an effective U, which already includes the interband screening, and use it in the subsequent (logarithmic), conducting band theory. Its value can then be evaluated a posteriori, comparing the theoretical and the experimental results.

The property which is usually used to get an idea about U is the magnetic susceptibility. The magnetic susceptibility has been investigated by various methods [51,52], the most recent being the Knight shift measurements [53]. The paramagnetic susceptibility is rather large (of the order of 10^{-4}emu/ mole). In the high temperature range it is practically temperature independent. The structural transitions reduce the paramagnetic susceptibility roughly by 20%. Unfortunately, so far, there is no general agreement as to the source of the large low temperature paramagnetism [51-53]. One possibility is the large van Vleck component and the other is the spin susceptibility of those conducting electrons not involved in the transitions. In this situation it seems best to rely upon the high temperature one-dimensional regime. If $n_F U$ were large it would lead to appreciable temperature dependence of the 1D spin paramagnetic susceptibility.

Besides, such $n_F U$ would most likely produce the $4k_F$ phonon softening, which is not observed. All these results are well known from the theories of the strongly-correlated Coulomb gas [17, 20]. As already mentioned in the Introduction, the latter will not be reviewed here but rather in [33], in connection with TTF-TCNQ where this is more appropriate. Here we shall only conclude that

$$n_F U < 1. \tag{13}$$

Comparing Equations (9), (12) and (13) we can reasonably assume that

$$\lambda_{\rm ac} > g_{1,2} > g_1^{\perp}, \tag{14}$$

where $g_{1,2}$ represent the linear combinations of the coupling constants (12) and (13), which appear in backward and forward scattering of the two electrons, respectively;

$$g_1 \simeq n_{\rm F} U,$$
$$g_2 \simeq n_{\rm F} U + n_{\rm F} \frac{e^2}{b} \log \frac{\epsilon_{\rm F}}{\omega_0}.$$

Simplifying somewhat, we can say that the main reason for the inequality (14) is that $\lambda_{\rm ac}$ scales as W, in contrast to the $g_{1,2}$'s which go as W^{-1}, and because the trichalcogenides are large bandwidth materials.

3.2.4 4. Peierls Instability

In Sections 2 and 3 we have discussed the high temperature excitations and their interactions. This section is devoted to the description of a phase transition, which results from the interaction of these excitations. We shall start with the structural transition at ambient pressure.

In the preceding section we have discussed the respective strength of the phonon and Coulomb interactions. Beside its strength the interaction is also characterized by its cutoff frequency. The characteristic frequencies of the dominant, phonon mediated interaction are small, according to Section 2.2. This makes retardation effects important [14, 18, 24, 25, 26, 54]. Here we wish to emphasize that this is particularly true for temperatures comparable to or larger than the phonon frequencies. The extreme limit $T \gg \omega_{\rm ph}$ (or $\omega_{\rm D}$) will turn out to coincide with the Peierls theory [55].

4.1. Harmonic Theory - Kohn Anomaly

The bare electron-electron interaction mediated by a phonon with polarization γ and wavevector q is [43]

$$\lambda_\gamma \frac{\omega_\gamma^2(\mathbf{q})}{\omega^2 - \omega_\gamma^2(\mathbf{q})}. \tag{15}$$

The coupling constants λ_γ and the frequencies ω_γ(q) were thoroughly discussed in Sections (3.1) and (2.2), respectively.

The characteristic electron scattering processes involving phonons are shown in Figures 5 to 7 . In their evaluation at finite temperatures it is usual [43] to use the Matsubara formulation, where $\omega = i2\pi nT$ in Equation (15). If $2\pi T \ll \omega_\gamma$, there is a considerable range of integers n for which the interaction behaves as unretarded, and is given by $-\lambda_\gamma$. This is the familiar BCS limit [56] in which λ_γ is supplemented with the cut-off frequency ω_γ. If however

$$2\pi T > \omega_\gamma(\mathbf{q}) \tag{16}$$

there is only one [18, 25], $n = 0$, value for which the bare interaction (15) is λ_γ and for which it decreases rapidly, as n^{-2}. These small values of the interaction do not appear in the real (phonon momentum and energy conserving) processes such as that of Figure 5 or in the ladder generated by it in Figure 8, provided that $n = 0$ is chosen on the initial phonon line. In contrast to that, the virtual phonon exchanges such as those of Figure 6 and 7 involve summation over n. At high T they can thus be neglected [18, 25] with



Fig. 5. Electron-hole (bubble) correction to the backward scattering vertex. Full line, electron at $k_{F $; dashed line hole at $-k_F$; dot, electron-phonon coupling; wavy lines, phonons (here at $2k_F$).}

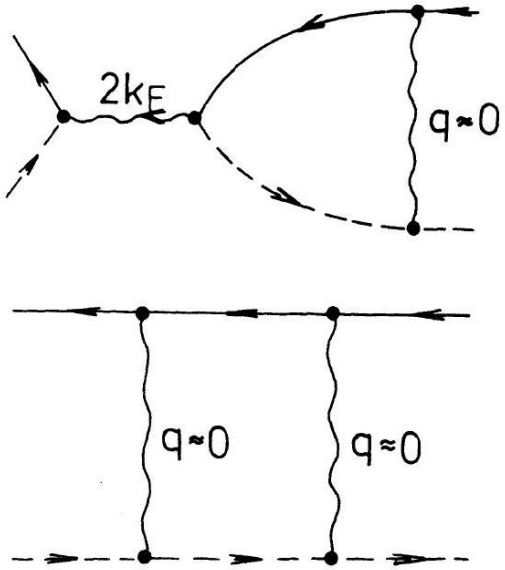


Fig. 6. Electron-hole corrections to (top) backward and (bottom) forward scattering vertices, which involve long wavelength ($q \simeq 0$) interactions (phonons).

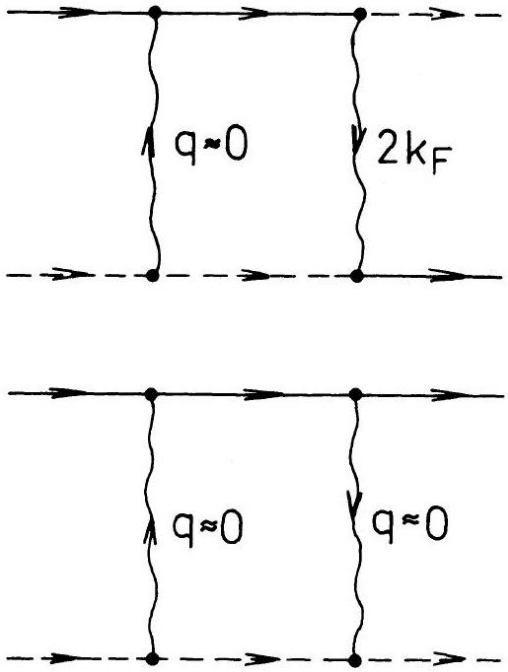


Fig. 7. Electron-electron corrections to (top) backward, and (bottom) forward scattering vertices, which involve long wave-length ($q \simeq 0$) interactions (phonons). Dashed line, electron at $-k_{F

$.}

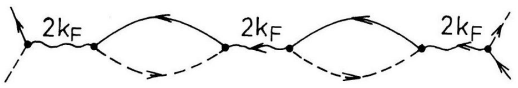


Fig. 8. Second-order ladder extension of Fig. 5.

respect to the real processes, due to the $(nT)^{-2}$ decrease of (15) for all finite n. In more physical terms, the motion of two electrons is not sufficiently correlated at high temperatures to make the virtual exchange of slow phonons efficient.

Implicit in the above argument is that the softening of the renormalized phonon frequencies $\tilde{\omega}_\gamma$ (as calculated, say, from the retained, real processes) is not too strong, so that the renormalized $n = 0$ vertex ($\sim \tilde{\omega}_\gamma{}^{-2}$) is not much larger than λ_γ. This is true for

$$T > T_{\mathrm{p}}^0 \tag{17}$$

where T_p^0 is the temperature at which the renormalization of $\tilde{\omega}_\gamma$ arising from real processes is of the order of ω_γ itself (i.e. $\tilde{\omega}_\gamma \simeq 0$). Whereas the condition (16) eliminates the quantum fluctuations of the phonon field, (17) can be alternatively understood as making the theory harmonic in displacements. This latter interpretation will become clear in Section 4.3.

Here we shall evaluate T_{p}^0 and discuss the real process contribution in some detail. The irreducible phonon self-energy Π corresponding to the ladder of Figure 8 is given by the simple electron-hole ($e - h$) bubble of Figure 9 and

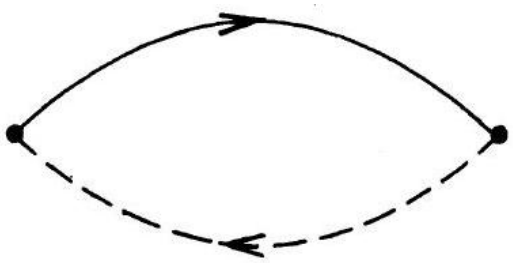


Fig. 9. Phonon self-energy corresponding to ladder extension of Figures 5 and 8.

$$\tilde{\omega}_\gamma^2 = \omega_\gamma^2 - \Pi. \tag{18}$$

The result of the evaluation of the $e-h$ bubble depends on the nesting properties [57-60, 54] of the electron Fermi surface. Good nesting means that there is a wave-vector $\mathbf{q_0}$ such that the Fermi surface translated by $\mathbf{q}_0$ coincides over an appreciable portion with the original Fermi surface. In this case the $e-h$ bubble is logarithmically singular for the phonons in the vicinity of q_0 ($q_{0\ \mathrm{b}} \simeq 2k_\mathrm{F}$)

$$\omega_\gamma^{-2}\Pi(\mathbf{q}_0) \simeq 2\lambda_\gamma \log\frac{\epsilon_\mathrm{F}}{T}. \tag{19}$$

The Kohn anomaly develops around $\mathbf{q}_0$.
T_p^0 of (17) is estimated by requiring that $\tilde{\omega}_\gamma \simeq 0$,

$$T_\mathrm{p}^0 \simeq \epsilon_\mathrm{F} e^{-1/2\lambda_\mathrm{ac}} \tag{20}$$

assuming that λ_ac is the largest among λ_γ 's, as was argued in Section 3.1.
Equations (19) and, consequently, (20) hold for [54]

$$T > t_\perp \frac{t_\perp}{\epsilon_\mathrm{F}}. \tag{21}$$

Expanding further $\Pi(\mathbf{q})$ in terms of the longitudinal and transverse component of $\mathbf{q}-\mathbf{q}_0$ gives longitudinal [61, 62] and transverse [54] characteristic lengths ξ_0 and $\xi_{0\perp}$ respectively, which characterize the slope of $\omega(\mathbf{q})$ around $\mathbf{q_0}$

$$\begin{aligned} \xi_0 &= \frac{b}{2\pi n_\mathrm{F} T}, \\ \xi_{0\perp} &\simeq \frac{t_\perp}{T} d_\perp \end{aligned} \tag{22}$$

where $d_\perp$ is of the order of a or c. According to (21) $\xi_{0\perp}$ can be larger or smaller than $d_\perp$, i.e. the softening can be localized around $\mathbf{q}_0$ or extended over the whole transverse Brillouin zone. Although related to it, $\xi_{0\perp}$ should not be confused with the transverse correlation length. The latter involves the critical dependence on temperature in the vicinity of the phase transition, whereas $\xi_{0\perp}$ only fixes the transverse length scale [25]. This will be further discussed in the next Section. The expressions (21) and (22) were derived for cosine transverse dispersion, which probably somewhat overestimates the
nesting ability of the actual Fermi surfaces. The other extreme is the complete absence of nesting, when the phonon self-energy behaves as [17]

$$\omega_\gamma^{-2}\Pi \simeq \lambda_\gamma \log\frac{\epsilon_\mathrm{F}^2}{T^2 + t_\perp^2} \tag{23}$$

irrespective of the transverse wave-vector. Inserting Equation (23) into Equation (18) determines T_{p}^0 as a fast function of $t_\perp$ when $T_{\mathrm{p}}^0 \simeq t_\perp$.
For

$$T > t_\perp \tag{24}$$

both cases (19) and (23) lead to practically the same behavior. $\omega_\gamma^{-2}\Pi$ is given by Equation (19), T_{p}^0 by Equation (20) and the transverse dispersion is either weak $\xi_{0\perp} < d_\perp$, as in Equation (22), or completely absent.

The observation [30, 31] of the nearly one-dimensional diffuse sheets at ambient pressure and temperature indicates therefore that the transverse overlaps $t_\perp$ are small with respect to the considered temperatures, i.e. Equation (24) holds. From this observation it is however impossible to infer anything about nesting. Admittedly, the diffuse sheets condense [30, 31, 38] into Bragg spots on decreasing the temperature, i.e. some transverse correlations do appear. However, as we shall see below, this is not necessarily due to nesting (22). We shall therefore withold our conclusion concerning this latter until Section 5.1., where it is argued on different grounds that nesting exists in $NbSe_3$.

Let us finally point out that the corrections to the extreme retarded limit (16) do not change the main conclusion reached above, namely that $t_\perp$ is small in $NbSe_3$. As will become clear in Sections 5.2. and 5.3, these corrections cannot diminish the transverse correlations without suppressing the $2k_{\mathrm{F}}$ structural instability altogether.

4.2. Coulomb Coupling of Peierls Deformations

Section 3.2. led us to the conclusion (14) that the Coulomb forces in transition metal trichalcogenides are presumably weaker than the phonon-induced couplings. This explains why we have started this section by completely omitting the Coulomb interactions between electrons. At present we wish to justify this approach by showing that nothing qualitatively new happens by introducing the on-chain Coulomb forces (12) and (13) in the limit (14). On the other hand the interchain Coulomb coupling of the $2k_{\mathrm{F}}$ waves $g_1^\perp$, although small, may be of qualitative importance.

Let us start by considering the Coulomb forces as perturbations [25]. The two loworder Coulomb corrections to the phonon self-energy II are shown in Figures 10 and 11.

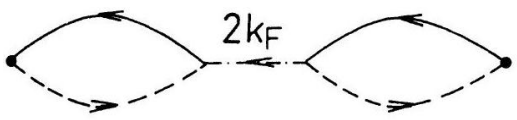


Fig. 10. Coulomb (dot-dashed line) correction to $2 k_{F $-phonon self-energy involving large momentum transfer.}

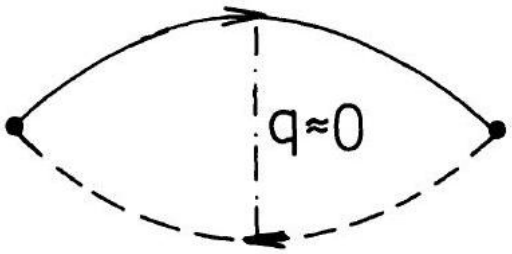


Fig. 11. Coulomb correction to $2 k_{F} $-phonon self-energy involving small momentum transfer.}

The two $e-h$ bubbles in Figure 10 may belong to the same chain, and the corresponding Coulomb energy (cf. Section 4.3) is that of the electron redistribution within the chain, induced by the $2k_{\mathrm{F}}$ deformation. The contribution of Figure 10 to $\omega_{\mathrm{ac}}^{-2}\Pi$ is

$$4\lambda_{\mathrm{ac}} g_1 \log^2 \frac{\epsilon_{\mathrm{F}}}{T}, \tag{25}$$

where $g_1 \simeq n_{\mathrm{F}} U$ of Equation (13), and either (21) or (24) is assumed. It should be noted that the contribution (25) is linear in λ_{ac}, just as (19) itself is. We remain thus within the harmonic approximation (cf. Section 4.3).

Similar conclusions hold for the process of Figure 11. Assuming $T > t_{\perp}$ the internal integration over the transverse momentum in Figure 11 concerns only the interaction, because the transverse hopping is negligible. The averaging of the interaction over the transverse momentum reduces it to the intrachain term. Integration over the longitudinal momentum transfer is dominated by the small (forward scattering) q values. Assuming Equation (11), the on-chain interaction is logarithmically singular in the longitudinal momentum q. The logarithmically singular interaction instead of the usual constant leads to the $\log^3 \epsilon_{\mathrm{F}}/T$ singularity of the process (11) instead of the usual $\log^2 \epsilon_{\mathrm{F}}/T$. However, when the three-dimensional RPA screening of the long-range Coulomb interaction is introduced, all interactions beyond the screening distance k_{TF}^{-1} or time ω_0^{-1} ($\omega_0 \simeq v_{\mathrm{F}}\, k_{\mathrm{TF}}$, Equation (4)) are screened out [27]. In consequence, the process (11) behaves as

$$-2\lambda_{\mathrm{ac}} g_2 \log^2 \frac{\epsilon_{\mathrm{F}}}{T} \tag{26}$$

which is similar to Equation (25), with g_1 replaced by [27]

$$g_2 \simeq n_{\mathrm{F}} U + \frac{n_{\mathrm{F}} e^2}{b} \log \frac{\epsilon_{\mathrm{F}}}{\omega_0} \tag{27}$$

of Section 3.2. Although the $\log^3 T$ singularity does not appear in (26), the trace of the logarithmic Coulomb singularity (11) remains present in the second term of Equation (27).

Now comparing Equations (19), (25) and (26) we see that for all $T > T_{\mathrm{p}}^0$ of Equation (17) the contributions (25) and (26) are smaller than (19), provided that $\lambda_{\mathrm{ac}} > g_{1,2}$ as is found in (14). This shows that, due to the inequality (14), the addition of the on-chain (screened) Coulomb forces does not alter the Peierls theory in an essential way for the conducting trichalcogenides. The conclusion is reached here on evaluting the low-order
corrections to the phonon self-energy Π, but it can be justified to any order of the leading logarithmic approximation. It turns out that the whole series for the phonon self-energy Π [18] (parquet or ladder, whichever is appropriate, according to Section 5.1.) can be expressed [27] in powers of $g_{1,2} \log \epsilon_{\mathrm{F}}/T$ and is rapidly convergent for $g_{1,2} \log \epsilon_{\mathrm{F}}/T < 1$ (i.e. at $T > T_{\mathrm{p}}^0$ for $\lambda_{\mathrm{ac}} > g_{1,2}$). For such temperatures the well-known (ladder or parquet) singularities [17,20] which occur in the phonon self-energy [18] for $g \log \epsilon_{\mathrm{F}}/T$ of the order or or much larger than

unity (in the ladder and parquet case, respectively), are simply irrelevant [25]. The formation of these singularities is arrested at (by) T_{p}^{0}.

Summarizing the conclusions reached in this section until now, $2\pi T_{\mathrm{p}}^{0} > \omega_{\mathrm{ac}}$ and $\lambda_{\mathrm{ac}} > g_{1,2}$ appear to be the conditions [25] for the applicability of the Peierls theory.

Let us now turn our attention to the interchain Coulomb coupling of the $2k_{\mathrm{F}}$ CDW's. As was explained in Section 3.2. this coupling is considerably smaller than the intrachain terms. Nevertheless it may be more important than the intrachain terms, provided that it dominates the interchain correlations. Then it plays a crucial role in establishing the long-range order of the $2k_{\mathrm{F}}$ superlattice.

In the perturbative limit under consideration, the leading interchain effect is given [21, 25] by the diagram of Figure 10. The two $e-h$ bubbles in this figure can be attributed to the neighbouring chains rather than to the same chain as in Equation 25. Then this figure represents the interaction of the two CDW's induced by the $2k_{\mathrm{F}}$ deformation on the neighbouring (groups of) chains. Ignoring (for simplicity) $t_{\perp}$, the corresponding contribution to $\omega_{\mathrm{ac}}^{-2}\Pi$ is [25]

$$4\lambda_{\mathrm{ac}} g_{1}^{\perp} \cos\phi_{\perp} \log^{2} \frac{\epsilon_{\mathrm{F}}}{T} \tag{28}$$

As in Section 3.2, $\phi_{\perp}$ here represents the relative phase of the two CDW's on the neighbouring (groups of) chains. On expanding (28) around the minimum of the Coulomb energy at $\phi_{\perp} = \pi$ we find the characteristic transverse distance [25]

$$\xi_{0\perp}^{2} \simeq d_{\perp}^{2} g_{1}^{\perp} \log^{2} \frac{\epsilon_{\mathrm{F}}}{T} \tag{29}$$

analogous to Equation (22), i.e. with λ_{ac} extraced from Equation (28).
For $T = T_{\mathrm{p}}^{0}$ Equations (20) and (29) give

$$\xi_{0\perp}\left(T_{\mathrm{p}}^{0}\right) \simeq d_{\perp} \frac{\sqrt{g_{1}^{\perp}}}{\lambda_{\mathrm{ac}}} \tag{30a}$$

This value can be compared with Equation (22) at T_{p}^{0}

$$\xi_{0\perp}\left(T_{\mathrm{p}}^{0}\right) \simeq d_{\perp} \frac{t_{\perp}}{\epsilon_{\mathrm{F}}} e^{1/2\lambda_{\mathrm{ae}}} \tag{30b}$$

or with the transverse correlation coming from the elastic coupling

$$\xi_{0\perp} \simeq d_{\perp} \sqrt{\frac{C_{\perp}}{\lambda_{\mathrm{ac}} C}} \tag{30c}$$

which involves the elastic constants $C \simeq 3C_{\perp}$ discussed in Section 2.2. The largest among the values (30) dominates the transverse correlations at T_{p}^{0}. In this respect we note that the elastic characteristic distance (30 c) is temperature-independent. The existence of the 1D regime at ambient temperature and pressure in $NbSe_3$ thus requires $\xi_{0\perp} < d_{\perp}$ in Equation (30c). Although $\xi_{0\perp}\left(T_{\mathrm{p}}^{0}\right) < d_{\perp}$ cannot be ruled out at the higher 144 K transition, the lower 59 K transition seems to be quite 3D. $\xi_{0\perp}\left(T_{\mathrm{p}}^{0}\right) > d_{\perp}$ at 59 K must therefore be sought between Equations (30a) and (30b). It can be noted in this respect that small λ_{ac} enhances the nesting correlations (30b) more than the Coulomb correlations (30a). However, λ_{ac} of Section 3.1 is not too small and the respective role of two interchain couplings is hard to assess. We shall thus postpone this discussion until Section 5.1, where different arguments in favor of the nesting model are given.

Here, we shall only realize that if $\xi_{0\perp}\left(T_{\mathrm{p}}^{0}\right) > d_{\perp}$ the 1D to 3D crossover occurs in the harmonic $T > T_{\mathrm{p}}^{0}$ regime. If, however, $\xi_{0\perp}\left(T_{\mathrm{p}}^{0}\right) < d_{\perp}$ this crossover occurs when anharmonic interactions of fluctuations are important and this is the problem we wish to adress now.

4.3. Anharmonic Interactions of Fluctuations

When the temperature is decreased towards T_p^0, i.e. when condition (17) is lifted, the simple bubble approximation of Figure (9) for the phonon self-energy Π ceases to hold. The leading correction [63-65] to the results (19) or (23) is shown in Figure (12).

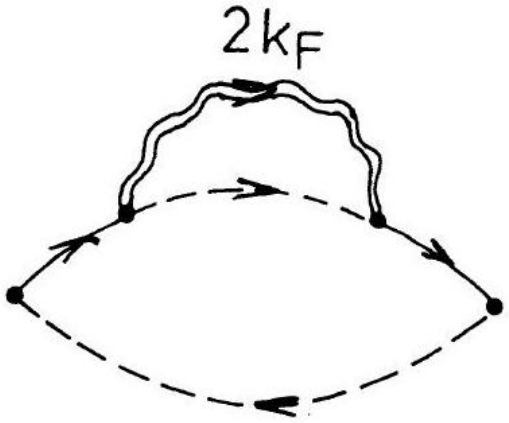


Fig. 12. Renormalization of the electron propagator in the phonon self-energy by $2 k_{F $ soft phonon, double wavy line, (pseudo-gap effect).}

It consists in the renormalization of the electron spectrum by the soft phonon at $2k_F$. The resulting electron pseudogap [64,65] is the precursor of the real Peierls [55] gap Δ_p.

Rather than going directly through the perturbation calculation of the phonon self energy we shall adopt here a somewhat different approach. Namely, we shall maintain the validity of the condition (16) for $T \simeq T_p^0$ and use $2\pi T_p^0 > \omega_{ac}$ to eliminate the quantum fluctuations of the phonon field. Treating this latter classically as the external field, we shall expand the electron deformation energy in powers of the field.

The lowest order term $E^{(2)}$ is shown in Figure (13). The wavy line with a cross represents the acoustic displacement $u_{2k}F_{+q}$ and the dot the corresponding deformation potential per unit length (cf. Equation (8)). Comparing Figure (9) and (13) it is clear that, apart from the normalization, $E^{(2)}$ and Π of the preceding Section are the same [14]. This can be illustrated in the one-dimensional regime, when



Fig. 13. Harmonic deformation energy due to coupling of $2 k_{F $ displacements to electrons. Wavy line with a cross, $2k_F$ displacement.}

$$E^{(2)} = \lambda_{ac}\left[\frac{T - T_p^0}{T_p^0} + \xi_0^2\left(q - 2k_F\right)^2\right] C\left|u_{q-2k_F}\right|^2. \tag{31}$$

For brevity we have included in $E^{(2)}$ the harmonic elastic energy $C|u|^2/2$ of Section 2.2. The only difference with Equations (18), (19) and (20) is that here we have expanded $\log T_p^0/T$ in terms of $\left(T - T_p^0\right)/T_p^0$. ξ_0 is of course the same as in Equation (22), with $T = T_p^0$.

The typical next-order term [66, 67](1/6)$E_N^{(4)}$ is shown in Figure (14) (there are

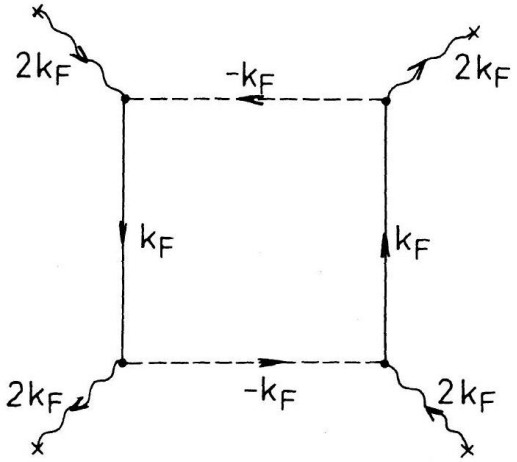


Fig. 14. Quartic deformation energy due to coupling of displacements to electrons.

six equivalent terms of this type). Its connection with the pseudo-gap is best understood by noting that by closing two displacement lines in Figure (14) to form the displacement correlator we get the result which is isomorphous to Figure (12). On the other hand, in the presént approach, we shall understand [66,67]

$$E_N^{(4)} \simeq \frac{0.1\lambda_{ac}^2}{2n_F\left(T_{\mathrm{p}}^0\right)^2} C^2 \left|u_{2k_F}\right|^4 \tag{32}$$

as the anharmonic interaction of the displacive fluctuations, the harmonic energy of which is $E^{(2)}$. As will become clear below, this will allow us to evaluate the correlations of the displacements more accurately than by the perturbation expansion (Figure 12), or by its self-consistent extensions.

Another advantage of the present approach is that the effects of the lattice discreteness can be straightforwardly included in such a calculation. These effects may be important when the wavelength of the deformation π/k_F is a multiple of the lattice constant [68]. This is precisely the case in conducting trichalcogenides, where $\pi/k_F \simeq 4b$. Under such circumstances there is an additional contribution to the quartic interaction. Its electronphonon part is shown in Figure (15). By using the Umklapp invariance [14] of the (tightbinding) electron propagator and electron-phonon coupling it follows

$$E_U^{(4)} = \frac{\delta}{6} \frac{0.1\lambda_{ac}^2}{n_F\left(T_p^0\right)^2} C^2 u_{\pi/2b}^4 \tag{33}$$

with

$$2\delta \simeq \frac{1}{\lambda_{ac}} \left(n_F T_p^0\right)^2 \simeq \frac{e^{-2/\lambda_{ac}}}{\lambda_{ac}}.$$

$E_U^{(4)}$ is δ times smaller than $E_N^{(4)}$ due to the appearance of excited states in Figure (15). Such $E_U^{(4)}$ can even be comparable to elastic Umklapp terms.

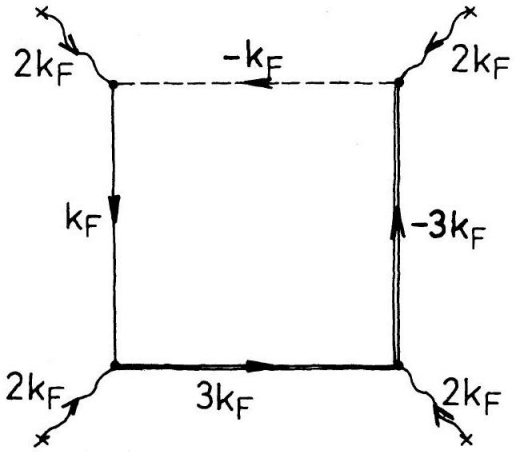


Fig. 15. Umklapp quartic deformation energy of the quarter filled tight-binding band. Double line, excited electron.

It is customary to express [68] the deformation energies (31), (32) and (33) in terms of the slowly-varying complex field $\psi = |\psi| e^{i\phi}$ defined by

$$u(y_j) = \psi \exp\left(i\frac{\pi}{2b} y_j\right) + \text{ c.c. }, \tag{34}$$

where $u(y_j)$ is the acoustic displacement of the j-th unit cell on the chain under consideration. The fast component of the displacement is taken out in Equation (34) and ψ can be thus considered as a slow field. Consequently Equations (31), (32) and (33) can be understood as the Landau expansion [68] in terms of this field.
$E^{(2)}$ is minimal at $2k_F$ rather than at $\pi/2b$, which, according to Equation (34), is the reference point of our expansion in terms of spatial variations of ψ. This mismatch generates [68] a term linear in $\partial\psi/\partial y$, i.e. the Lifshitz invariant. The latter appears in addition to the usual term [61,62], quadratic in gradient.
$E_N^{(4)}$ is a smooth function of the momentum and it is usual to retain only the part which is local in ψ.$E_U^{(4)}$, when expressed in terms of ψ, defined by Equation (34), is also local. Indeed $[\psi \exp(i(\pi/2b)y)]^4$ is the invariant of the translation group [68].

The resulting Landau energy density is [62,69]

$$\begin{aligned} f(y) =& A' \left[\frac{T - T_p^0}{T_p^0}|\psi|^2 + i\xi_0^2\kappa\left(\psi^*\frac{\partial\psi}{\partial y} - \psi\frac{\partial\psi^*}{\partial y}\right) + \right. \\ &\left. + \xi_0^2\left|\frac{\partial\psi}{\partial y}\right|^2\right] + B\left[|\psi|^4 + \frac{\delta}{3}\left(\psi^4 + \psi^{*4}\right)\right] \end{aligned} \tag{35}$$

A' and B are the shorthand notations for the coefficients of u 's in Equations (31) and (32), respectively, and

$$\kappa = \frac{\pi}{2b} - 2k_F \tag{36}$$

measures the distance between $2k_F$ and the commensurability point $\pi/2b$.
For $T < T_p^0$ and sufficiently large κ it is usual to omit [70, 71] the amplitude fluctuations, setting

$$|\psi|^2 \simeq |\psi_0|^2 \simeq \frac{n_F\left(T_p^0\right)^2}{0.1\lambda_{ac}C}\epsilon \tag{37}$$

where

$$\epsilon = \frac{T_p^0 - T}{T_p^0}$$

This value of $|\psi_0|^2$ is chosen to minimize the two first terms in the quadratic and quartic bracket of Equation (35), because, with κ large, the others are less important. At $T \simeq 0$ ($\epsilon \simeq 1$) Equation (37) is of the form of the familiar BCS law of corresponding states [36]

$$2\Delta_p \simeq 3.5 T_p^0 \tag{38}$$

if we set $\Delta_p^2 = \lambda_{ac} n_F^{-1} C |\psi_0|^2$. In fact the actual numerical coefficient in (37) is somewhat different from 3.5 because Equation (37) follows from the expansion. However the superconducting expansion has the same coefficient as (37). The complete analogy [61, 72] between the Peierls and BCS theories can be traced back to the neglect of the
elastic contribution to all but the quadratic term (31). Inserting now the value $|\psi_0|$ in Equation (35) reduces this equation to [68,73].

$$f = 10 n_F T_p^{0^2} \epsilon \left[\xi_0^2 \left(\frac{\partial \phi}{\partial y} - \kappa \right)^2 - \frac{\epsilon \delta}{3} \cos 4\phi \right]. \tag{39}$$

The functional minimization of this expression gives the well known sine-Gordon equation [68,73]

$$\xi_0^2 \frac{\partial^2 \phi}{\partial y^2} = \frac{2\epsilon\delta}{3} \sin 4\phi. \tag{40}$$

This equation is usually studied with a more general coefficient of the sine term. In our case such a coefficient would result from the introduction of the elastic anharmonic coupling, but here we shall avoid this inessential complication. The solutions of the sineGordon equation are either the constant values $\phi = \pi \cdot n/2$ or the soliton lattices [68,73] shown in Figure (16). A soliton is the region of the fast phase variation, which joins

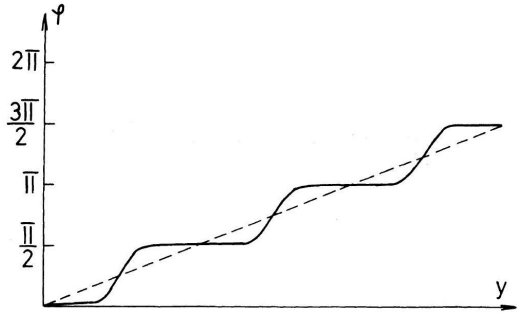


Fig. 16. Soliton lattice in the phase of the order parameter.

two regions where the phase is practically constant and equal respectively to $\pi n/2$ and $\pi(n+1)/2$. According to Equation (34) the constant values of ϕ correspond to the commensurate displacement, and the soliton corresponds to the discommensuration. The incommensurate phase is lower in energy (39) than the commensurate one for [73-76]

$$\kappa \xi_0 > \sqrt{8\epsilon\delta}/\pi\sqrt{3}. \tag{41}$$

For very large values of κ the soliton lattice reduces [73] to the line $\phi = \kappa y$, i.e. the Umklapp coupling, the right-hand side of Equation (40) is unimportant. The corresponding displacement

is the single harmonic. In the opposite limit $\kappa\xi_0 > \sqrt{8\epsilon\delta}/\pi\sqrt{3}$ the solitons become sparse and well-defined. However, in this limit, the coupling between the phase and amplitude fluctuations is relevant [69]. Unfortunately the resulting problem seems to be non-integrable, and has not been entirely elucidated so far. Usually, the periodic sine-Gordon solutions are followed through the commensurate-incommensurate transition, with the addition of some amplitude corrections. Finally the well-stabilized commensurate state is reached [77,78] for

$$\kappa\xi_0 \ll \sqrt{8\epsilon\delta}/\pi\sqrt{3}.$$

The functional minimization is usually considered sufficient when the fluctuation effects around the ground state are unimportant. This certainly is not the case of the $\xi_{0\perp}\left(T_p^0\right) < d_\perp$ limit which requires the inclusion of nonlinear excitations above the state of minimum energy determined above. (The nonlinearities are absent in this case only in the extreme incommensurate limit). Let us turn now to this problem.

The nonlinear excitations can be easily found [79,78] in the commensurate state. The species which dominates the spatial correlations is the (phase-amplitude) soliton. On the other hand, in the incommensurate case it is hard to go beyond the linearized [74-76] excitations of the solition lattice, and the problem of 1D fluctuations is therefore usually treated by a more powerful but physically less transparent transfer matrix method [70]. Without going into the details of these calculations let us quote the results [80-82] which are best expressed in terms of the structure factor. For $\kappa\xi_0 > \sqrt{8\epsilon\delta}/\pi\sqrt{3}$ and in the 1D regime the main superlattice reflection occurs at [82]

$$q_b^{(0)} \simeq 2k_F - \frac{\delta^2\epsilon^2}{72\xi_0^4\kappa^3} \tag{42}$$

with the inverse Lorentzian half-width [82]

$$\xi(T) \simeq \frac{20T_p^0}{\pi T} b\epsilon \left(1 - \frac{\delta^2\epsilon^2}{24\kappa^4\xi_0^4}\right) \tag{43}$$

This peak could correspond to the one-dimensional sheets observed [30, 31] by X-ray diffuse scattering. These sheets are narrow, i.e. $\xi(T)$ of Equation (43) is large. The incommensurate $\kappa\xi_0 > \sqrt{8\delta\epsilon}/\pi\sqrt{3}$ values of $q_b^{(0)}$ are observed. Independent evidence for large $\xi(T)$ is given by the recent dc current-voltage measurements [84].

In addition to the main reflection, the theory predicts [81,82] the occurrence of satellites related to the formation of the soliton lattice. The strongest satellite should occur at

$$q_b^{(1)} = q_b^{(0)} \pm \left(4\kappa - \frac{\epsilon^2\delta^2}{18\kappa^3\xi_0^4}\right) \tag{44}$$

$2\pi/\left(q_b^{(1)} - q_b^{(0)}\right)$ is the period of the soliton lattice in formation. The two satellite peaks differ [82] somewhat in width. The upper sign in Equation (44) goes with the width $5\xi^{-1}(T)$ and the lower with $3\xi^{-1}(T)$. The intensity of the satellite peaks is $\left(48\xi_0^2\kappa^2/\delta\epsilon\right)^2$ times lower than that of main reflection. Equations (42-44) describe the 1D anharmonic fluctuative regime. The concept of the soliton lattice remains meaningful even in the presence of 1D fluctuations, provided that the temperature is low enough ($\epsilon \simeq 1$). However the related effects are small due to the smallness of δ (cf. Equation (33)).

The similar analysis is required in the $\xi_{0\perp} > d_\perp$ case, when the soliton lattice competes with the 3D fluctuation effects for $\epsilon \ll 1.\epsilon \ll 1$ weakens the already weak ($\delta \ll 1$) commensurability pinning, as is clear from Equation (40) and (41), simultaneously increasing fluctuation effects (to be discussed in Section 5.2, Equation (57)). However, it can be speculated that the notion

of the soliton lattice remains meaningful because it corresponds to the effects local in the reciprocal space, whereas the fluctuations produce a comparatively broad diffuse background. This requires further investigations.

The expressions analogous to Equations (42) and (43) can also be derived in the opposite, commensurate limit. They may bear some relevance for the case of orthorhombic TaS_3, as will be discussed in the next subsection. Here we shall focus our attention on another aspect of the incommensurate problem. We know that the electron deformation energies in e.g. Equations (31)-(33) are related to the electron redistribution $\delta\rho$ produced by the deformation field. The electron coordinates are integrated out in these equations, but it is possible to find the explicit expansion of $\delta\rho$ in terms of ψ, analogous to Equation (35). Extending the previously known linear response results [14] to the next (second) order we find [85]

$$\delta\rho^{(2)} \simeq \frac{1}{2\pi i}\frac{\lambda_{ac}C}{2n_F\left(T_{\rm p}^0\right)^2}\left(\psi^*\frac{\partial\psi}{\partial y}-\psi\frac{\partial\psi^*}{\partial y}\right) \simeq \frac{\epsilon}{2\pi}\frac{\partial\phi}{\partial y}, \tag{45}$$

consistently with Equations (35) and (39). In contrast to the linear [14] response $\delta\rho^{(1)}$ which contains only the fast ($\simeq 2k_F$) components, the second-order response describes the accumulation of charge in the region of variation of ϕ, e.g. the soliton. Only the slow components of $\delta\rho$ appear in this term.

Equation (45) complements Equation (39). It shows that the change of phase by $\pi/2$ (phase soliton) accumulates the charge

$$e^* \simeq \epsilon\frac{e}{4} \tag{46}$$

It can be thus attempted to observe the soliton lattice through the charge accumulation [86] by analysing the dc/ac currents [87-92, 67, 8]. For $NbSe_3$ the experiments [9294, 8] have only been analysed [91] close to 59 K , resulting in a charge proportional to $\sqrt{\epsilon}$. These currents are thus due to the linear response of charge $\delta\rho^{(1)} \sim |\psi| \sim \sqrt{\epsilon}$. It might be that, close to $T_p \simeq T_p^0$, the linear response simply dominates the second order term $\delta\rho^{(2)}$ even if the latter corresponds to the well-formed soliton lattice. However, the soliton lattice may also be ill-defined for several reasons which we now wish to enumerate. The first is suggested by Equation (45) itself. The long-wave components of the charge density interact through the long-range Coulomb interactions. Although the Coulomb energy is (assumed to be) negligible in the main (logarithmic) approximation
of Equation (14), the Coulomb energy of the accumulated charge should be compared to the small ($\epsilon\delta$) commensurability term. It is adverse to the formation of the charged soliton lattice, but a detailed analysis is lacking so far. The other possible reasons for the absence of the soliton lattice are ϵ and/or δ in Equation (40). From this point of view the optimal situation for the formation of the well-defined soliton lattice is $\epsilon = 1$. According to the $T = 0$ extrapolation of the result (41), this requires $\sqrt{8\delta}/\pi\sqrt{3} < \kappa\xi_0 < 1$. Unfortunately the condition $\kappa\xi_0 < 1$ does not seem to be satisfied in $NbSe_3$, i.e. the anomaly seems to occur too far from the commensurability point [95]. This manner of reasoning, however, raises the question of the validity of the extrapolation procedure used here ($T = 0$ in $\epsilon, T = T_p^0$ in all other coefficients of Equation (39)), the problem to which we now turn.

In fact it is possible to include all powers of $|\psi|$ in the low-temperature analysis of the energy [96, 97] and charge density [98-101]. In the case of energy the results [96] do not differ qualitatively from the straightforward extrapolation of Equation (39) to low temperatures. The reason for this can be well understood in the incommensurate limit. The full solution [96] shows that the phase satisfies essentially the same equation as (39), obtained here from the expansion (35) on setting $T \simeq T_p^0$ in all coefficients except in $\epsilon = 1$. This is important, because the low T regime is dominated by the phase behavior. In other words, the full solution amounts to a more

precise determination of $\Delta_p(\epsilon)$ than is given by (37). From the energetic or correlation point of view the difference between Equation (37) and (38) for example, is inessential. Furthermore, there is no difference in the nature of structural fluctuations at $T \simeq 0$ and at T_p^0. At T_p^0 the latter are classical by virtue of condition (16) and at $T \simeq 0$ the temperature in this condition is replaced by Δ_p of Equation (38). Once the quantum fluctuations are eliminated at T_p^0 due to the large mass of ions (small ω_{ac}), they stay out at $T \simeq 0$.

The accurate $T \simeq 0$ solution of the Peierls problem led however to a qualitatively new result. The full [100] summation of the series initiated in (45) shows that the solitons and the antisolitons carry, at $T = 0$, the exact fractional charges $\pm e/4$, respectively, rather than similar but approximate values (46). In fact, results of this kind were first derived either by the numerical analysis of the corresponding discrete model, using a reasonable trial function for solitions [102, 103], or by analytically solving the space-dependent Bogoliubov equations [98].

In conclusion, the discrete Peierls model [14, 102], its appropriate Bogoliubov-like continuation [98, 99], or even the corresponding Landau expansion [62, 68, 92, 69], lead to essentially [104] the same results. However, it appeared recently that the fully discrete formulation is required for solving some special models, one of which is not too far from the model discussed here. In this model the elastic interaction and the electronphonon coupling are not expanded as in Equation (2) and (8), but rather a particular exponential dependence on displacement of the band-width and the elastic interaction is assumed [105]. This represents a generalization of the Toda chain, and, like the latter, does not show commensurability effects. The latter are introduced [106] through the departures from the original model. This could sometimes be a physically correct starting point of the investigation. Nevertheless we shall proceed here with our model, since the exponential behaviors are idealizations [6] even in the tight-binding limit.

4.4. Ordering by Interchain Coupling

In this subsection we shall consider the explicit effects of the interchain coupling. We shall start with the case $\xi_{0\perp}\left(T_p^0\right) < d_\perp$ when the ordering at $T_p < T_p^0$ is preceded by the 1D anharmonic regime of Equation (42-44). This might apply to the observed 1D regime in $NbSe_3$, although the latter could just as well be harmonic (Section 4.1 with $\xi_{0\perp}\left(T > T_p^0\right) < d_\perp, \xi_{0\perp}\left(T_p^0\right) > d_\perp$). Next we shall describe a mean-field ($\xi_{0\perp} > d_\perp$) theory of orthorhombic TaS_3. The small fluctuative corrections to the $\xi_{0\perp} > d_\perp$ results are described in Section 5.2.

In order to determine T_p for $\xi_{0\perp}\left(T_p^0\right) < d_\perp$ we shall use the interchain extension of the Landau theory, Section 4.3. We can afford to do that because the latter covers qualitatively correctly the one-dimensional regime, even for $T \ll T_p^0$. The first results for T_p were obtained along these lines in the extreme commensurate [107] or incommensurate [108, 71] limits. It turned out that the most important point is to take correct account of the one-dimensional fluctuations, whereas the interchain coupling could be treated in various approximations. The most popular was the mean-field approximation for the interchain coupling [109-112] when the given chain fluctuates in the average field of the others. However, this mean-field approximation proved inadequate [113] for the ordering of the soliton lattice. It led to different transition temperatures for the main and satellite peaks of the soliton lattice, Equation (42) and (44), respectively.

The solution of the interchain problem requires thereby the use of the transfer matrix method. The latter shows [114] that all the harmonics of the soliton lattice order at the same temperature as the main peak itself, namely at

$$T_p \simeq 40\sqrt{2} n_F \left(T_p^0\right)^2 \epsilon_p \frac{\xi_{0\perp}}{d_\perp}\left[1 - \frac{\delta^2 \epsilon_p^2}{3\xi_0^4 \kappa^4}\right] \tag{47}$$

where $\epsilon_p = \epsilon\left(T_p\right) \simeq 1$. The first term in Equation (47) represents the classical incommen-

surate result [71, 109-112], whereas the second arises from the commensurability pinning (33). As with the analogous corrections in Section 4.3, this latter seems to be negligible in $NbSe_3$. If furthermore (22) is assumed for $\xi_{0\perp}$ a particularly simple expression is obtained for T_p :

$$T_p \simeq t_\perp e^{-1/2\lambda_{ac}} \tag{47}$$

The above description of the ordering might be applicable to upper transition in $NbSe_3$ and its monoclinic analog TaS_3. The two transitions [31, 34, 39, 115] occur there at two entirely different wave-vectors $\mathbf{q}_0^{(a)}, \mathbf{q}_0^{(b)}$ and can be therefore treated independently, at least in the approximations corresponding to Equation (47). However, in orthorhombic TaS_3 the situation is somewhat different. Although this material too has to be described in terms of (at least) two types of chains [116], only one unstable wave-vector was observed [117]. In this respect it was recently pointed out that the harmonic (bilinear) interchain coupling can enforce the common wave-vector on both types of chains, if the two types of chains, taken separately, tend to develop the instabilities of similar wave-vector. The argument [116] goes as follows: the first transition occurs at $\mathbf{q}_{0b}^{(a)}$ on
one set of chains (transverse components are ignored for simplicity). Next the second type of chains sets in with the instability at $q_{0b}^{(b)} \simeq q_{0b}^{(a)}$. The harmonic interchain coupling of Section (4.1) and (4.2) connects only the same wave-vectors on the two type of chains. Therefore $q_{0b}^{(a)}$ drives the same $-q_{0b}^{(a)}$ component on the second set of chains. $q_{0b}^{(a)}$ is not a natural component for this set of chains. At low temperatures it is thus energetically more favorable to develop at

$$q_{0b} \simeq \left[q_0^{(a)} + q_{0b}^{(b)}\right]/2, \tag{48}$$

an instability which is common to both sets of chain. In some respects this is analogous to the case of a Peierls conductor in the magnetic field [98]. Incidentally, q_{0b} of Equation (48) turns out to be (nearly) commensurate, i.e. the 'commensurate' phase occurs here without any help from Umklapp coupling (33). This latter acts in the same direction as the harmonic interchain coupling.

The 'commensurate transition' in TaS_3 occurs at 140 K , well below the incommensurate transition at 215 K , and is accompanied by hysteresis [118]. It has been shown that such hysteresis can arise from nonlinear coupling among the continuous fields [119]. In the present case the fields in question can well be the relative phase of the two kinds of chains and the amplitude of the deformation on that family of chains which sets in around 140 K . In terms of those variables the bilinear interchain coupling is cosine-like in the relative phase and can lead to the soliton lattice in this variable.

The idea that interchain coupling or more precisely, interchain hopping $t_\perp$, can produce soliton lattices was first put forward [60] in the context of CH_x conductors. It has been argued there that in presence of appropriate transverse dispersion it is energetically preferable to associate some electrons with soliton (lattice) states then to put them in the conventional band states. The advantage of such theories is that they do not rely upon small δ (and ϵ) and can thus be relevant even for $NbSe_3$. A careful analysis of the transverse dispersion in conducting trichalcogenides is therefore desirable, for this reason and for reasons which will become clear in the next Section.

3.2.5 5. CDW Versus Bcs Instability

On applying pressure of a few kbar to $NbSe_3$ the structural transition is removed [3] as shown in Figure (17). The low-temperature ground state has all the properties of BCS superconductivity [$3, 120 - 122$].

Pressure is expected to increase the interchain couplings incorporated in ξ_{01}. The straightforward application of Equation (47) would suggest an increase, or at most a weak decrease of T_p, if T_p^0 is given by Equation (20), and the interchain parameters vary slowly 'with pressure. However, Equation (20) for T_p^0 is valid only if the conditions (21) and (24) are satisfied at T_p^0, i.e. if $T_p^0 > t_\perp^2/\epsilon_F$ or $T_p^0 > t_\perp$ for the nesting or non-nesting cases respectively. When $t_\perp^2/\epsilon_F$ or $t_\perp$ increases towards T_p^0 of Equation (20) the actual T_p^0 decreases steeply to zero. We are thus led to conclude that the decrease of T_p with pressure is due to vanishing of the mean field tendency T_p^0 to the structural instability.

This simple argument, although appealing, cannot be used straightforwardly in the low temperature range, because it is based on the condition (16)

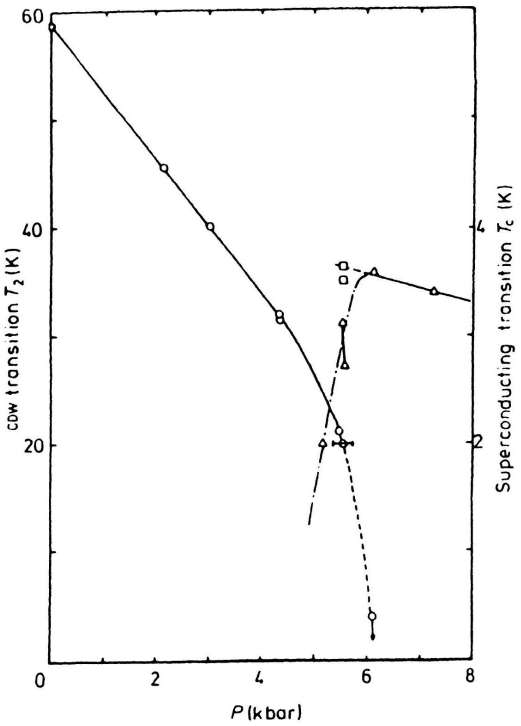


Fig. 17. Variation of $T_{\mathrm{CDW}}(\circ)$ and T_{BCS} (°) of $NbSe_3$ as a function of pressure (Ref. (3b), copyright Institute of Physics, Bristol, England).}

$$2\pi T_p^0 > \omega_{ac} \tag{16}$$

which ceases to hold. This means that the quantum fluctuations of the phonon field are becoming important. The structural transition continues to exist but it is driven by the electron system interacting in absence of the adiabatic parameter (16). Such transition is usually named the charge density wave (CDW) transition to distinguish it from the Peierls transition, which is driven adiabatically by the weakly interacting electron gas. Moreover, the virtual exchange of phonons by electrons can also produce BCS superconductivity beside the CDW transition. The competition of the CDW and BCS phases is discussed in the present chapter.

5.1. Mean-field Theory

In the temperature range

$$2\pi T < \omega_\gamma(\mathbf{q}) \tag{49}$$

the virtual exchange of phonons introduces the logarithmic singularity [14, 24, 18, 25] of the electron-electron ($e-e$) Cooper diagram, Figure (7), irrespective of the value of $t_\perp$. In the lowest order this singularity competes [10] with the logarithmic singularity of the $e-h$ channel, which exists provided that the above-mentioned conditions [22]

$$T > \frac{t_\perp^2}{\epsilon_F} \tag{21}$$

or

$$T > t_\perp \tag{24}$$

are fulfilled.

Consider next the coupling between the $e-e$ and the $e-h$ channels [23], e.g. the process shown in Figure (18). For simplicity let us neglect $t_\perp$ on the electron $e-e$ lines. Then the internal transverse integration means simply the averaging of the $e-h$ bubble over the transverse momenta. Assume now that there is nesting and that $T < t_\perp$. According to Equation (22) the $\log T$ singularity then only affects a small part ($\sim \xi_{01}^{-2}$) of the transverse Brillouin zone. Therefore the averaged $e-h$ bubble [123] is proportional to $\log t_\perp$ rather than to $\log T$. We conclude that this, the so-called parquet coupling between the $e-h$ and $e-e$ channels, is effective only if [23, 123]

$$T > t_\perp. \tag{24}$$

The same conclusion holds trivially in the non-nesting case.

Putting all this together, the parquet coupling between the channels has to be taken into account if the conditions

$$2\pi T < \omega_D \tag{49}$$

$$T > t_\perp \tag{50}$$

and

$$2\pi T_p^0 < \omega_D \tag{51}$$

are fulfilled simultaneously. The last of these conditions ensures the absence of the (pseudo)gap in the electron spectrum below ω_D, i.e. justifies the use of the bare electron lines in Figures 5, 6, 7, 18. Otherwise (i.e. if $2\pi T_p^0 > \omega_D$) the adiabatic Peierls theory is valid down to the lowest temperatures, as explained in the preceding sections.

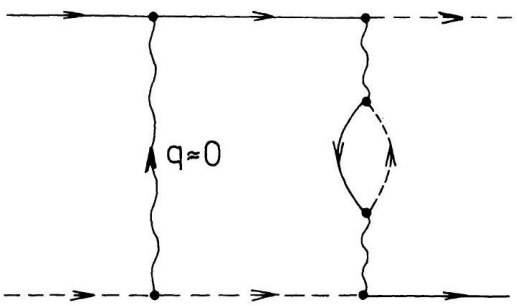


Fig. 18. Parquet coupling between electron-electron (Cooper) channel and electron-hole (density) channel. Low order vertex correction.

Next we wish to argue that these three conditions cannot be made consistent with assumption that $2\pi T_p^0 > \omega_D$ used in the preceding sections at ambient pressure. This is illustrated in Figure (19). In this figure it is shown schematically that when T_p^0 starts to decrease upon meeting (either the $t_\perp$ or) the $t_\perp^2/\epsilon_F$ line it cannot reach the parquet regime. The transition from the regime in which T_p^0 is almost independent of $t_\perp$ to the regime in which T_p^0 falls steeply [22] to zero is too fast for that.

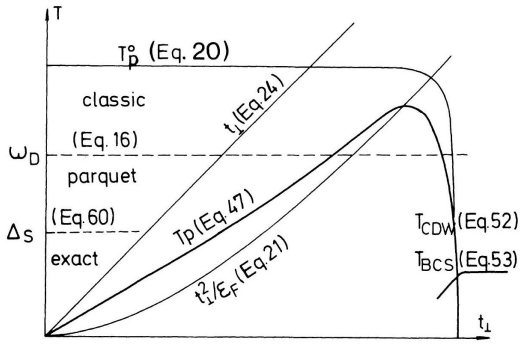


Fig. 19. Hierarchy (schematic) of various temperature and energy scales introduced in the equations of the text, variation with transverse overlap $t_{\perp}$ (i.e. with pressure).

The parquet corrections are therefore absent when T_p^0 falls below ω_D. However, other electron-hole ladder diagrams such as those shown in Figure (6), are activated in addition to the $e-h$ bubble of Figure (5). These processes involve the forward scattering mediated by phonons, which we shall denote by λ_2 in analogy to the Coulomb g_2 of subsection 3.2. The corresponding CDW transition temperature $T_{\rm CDW}$ is usually [26] written in the form

$$T_{\rm CDW} \simeq \omega_D \exp -(2\lambda_{ac} + \lambda_2)^{-1} > t_\perp, t_\perp^2/\epsilon_F, \tag{52}$$

where the inequality in (52) symbolizes the fast decrease of $T_{\rm CDW}$ with increasing $t_\perp$. Under pressure T_p^0 continuously transforms in $T_{\rm CDW}$. Note in this respect that the prefactor ϵ_F of Equation (20) is replaced in (52) by ω_D in order to emphasize that λ_2 contributes only at $T_{\rm CDW} < \omega_D$.

As already mentioned, the virtual exchange of phonons can produce BCS superconductivity beside the CDW instability. Indeed, the $e-e$ Cooper diagrams of Figure 7 are logarithmically singular for $2\pi T < \omega_D$, irrespective of the value of $t_\perp$. As the parquet corrections are absent, the transition temperature is given by the unmodified BCS expression [26]

$$T_{\rm BCS} \simeq \omega_D \exp -(\lambda_1 + \lambda_2)^{-1}. \tag{53}$$

Here λ_1 incudes the optical phonon contributions to the $e-e$ coupling additional to λ_{ac}.

In subsection 2.2 we have argued that the optic phonon coupling constants, which determined $\lambda_1 - \lambda_{ac}$ and λ_2 almost entirely (the forward interactions through longwavelength acoustic phonons are eliminated by retardation [10]) and are not expected to be particularly large. Indeed, Equation (52) is capable of explaining the corresponding observations in $NbSe_3$, without the optic phonon contributions. When $T_{\rm CDW}$ is suppressed by increasing $t_\perp$ it meets a finite $T_{\rm BCS}$, which depends only weakly on $t_\perp$.

At this stage it is appropriate to discuss the nesting versus the non-nesting (with Coulomb/elastic interchain coupling) picture. Both non-nesting and perfect nesting pictures lead, on the mean-field level, to the complete separation of the BCS and CDW phases. On the other hand, the experiments [3] show (Figure 17) that the sample which has undergone the CDW

transition becomes superconducting on further lowering the temperature. It is possible to explain this coexistence by allowing for an imperfect nesting between the Fermi surfaces [124, 125]. The imperfect nesting involves only a part of the Fermi surface. The corresponding dielectric gap opens over that part of the surface, leaving the rest available for the BCS instability. Assuming, for simplicity, that the corresponding density of states $n_F^{\rm BCS}$ is small with respect to n_F, we recover Equation (52) for $T_{\rm CDW}$, whereas λ 's in Equation (53) for $T_{\rm BCS}$ have to be scaled with $n_F^{\rm BCS}/n_F$. It should be further noted that the CDW and the BCS instability do not play symmetric roles in this argument. Indeed, if the BCS instability occurs at higher temperature, $T_{\rm BCS}$ of Equation (53) larger than $T_{\rm CDW}$ of Equation (52), it involves the whole Fermi surface, being independent of its nesting properties [124, 125]. The BCS
transition inhibits therefore the structural instability, in full agreement with experiments [3]. The type of observed coexistence between the structural and the BCS instabilities represents thus a good evidence in favor of the nesting model. In particular this led us to draw in Figure (19) the transition temperature $T_p, T_{\rm CDW}$ for this case. Figure (19) should not however be taken too seriously, because it is based on the cosine transverse dispersion, which has very good nesting properties (i.e. very small $n_F^{\rm BCS}$). The actual nesting is probably less perfect, i.e. the region between $t_\perp$ and the critical nesting line, $t_\perp^2/\epsilon_F$ in Figure (19), is much narrower.

5.2. Correlation Lengths and Landau Theories

The ladder approximations, being the leading approximations in the low temperature range, provide for the characteristic lengths $\xi_0, \xi_{0\perp}$. In the BCS case, these are given by formally the same expressions as the Equation (22). The CDW lengths might be somewhat different due to the vicinity of the saturation limit (21) or (24), imposed by $t_\perp$, but in the absence of a better estimate we shall continue to use Equations (22). Thus we have

$$\begin{aligned} \xi_0 &\simeq b\frac{\epsilon_F}{T_{\rm CDW,BCS}} \gg b \\ \xi_{0\perp} &\simeq d_\perp \frac{t_\perp}{T_{\rm CDW,BCS}} \gg d_\perp \end{aligned} \tag{54}$$

with $T_{\rm CDW}$ or $T_{\rm BCS}$ given by Equations (52) or (53), respectively. In this way the main difference with the Peierls case comes through the values of the transition temperatures at which we define ξ_0, ξ_{01}. The addition of the electron-electron Coulomb or elastic interchain coupling omitted here, can only further increase $\xi_{0\perp}^{\rm CDW}$.

The low temperature X-ray or neutron data under pressure, which in principle could give information about ξ_0 and $\xi_{0\perp}$ of the structural transition are missing so far. The measurement of the anisotropy of the second critical field for superconductivity H_{c_2}, also gives a direct access to these quantities for the superconducting case. The ladder approximation, i.e. Equations (53) and (54), defines the harmonic part of the Landau functional in terms of the usual BCS order parameter. The harmonic part alone can be used to determine H_{c_2}, provided that $\xi_{0\perp} > d_\perp$, as can be expected according to (54). It follows that [126, 127]

$$\frac{H_{c_2}^\perp}{H_{c_2}^\parallel} = \frac{\xi_{0\perp}}{\xi_0}. \tag{55}$$

The anisotropy of the critical field H_{c_2} was measured [120] on single crystals under pressure up to 7.7 kbar . The ratio (55) turned out to be of the order of 5.5. This can hardly be reconciled with Equations (54) and $\epsilon_F \gg t_\perp$ deduced previously from the high temperature behavior at ambient pressure. The comparatively small anisotropy ratio could be due to the effect of impurities [128]. The latter are expected to shorten

[43] the correlation lengths (54) and wash out [128, 129] some of the anisotropy. It can be also speculated following [130-133] that those few electrons which belong to the curved parts of the Fermi surface contribute more to $\xi_{0\perp}$ than the nearly 1D electrons. However, both possibilities require a more careful theoretical and experimental analysis.

It is interesting in this respect to mention the effect of doping [121, 122] on the superconducting properties. E.g. $NbSe_3$ was doped [121] with Ta and Ti . Ta is isoelectronic with Nb.5% of Ta in place of Nb suppresses the CDW transition. The BCS transition occurs instead at ambient pressure. The anisotropy of the characteristic lengths measured via the anisotropy of the critical fields is $\xi_0 \simeq 4\xi_{0\perp}$. Thus the (additional) impurities do not alter substantially the anisotropy ratio (55). The fact that in contrast to BCS superconductivity the impurities suppres the CDW instability agrees well with the simple mean-field arguments [134], which consider the effect of impurities on the processes shown in Figures 5, 6 and 7. However at present this fact does not help to uniquely distinguish the source of the low anisotropy ratio (55).

The experimentally determined value [120] of ξ_0 is 350Å, i.e. $\xi_{0\perp} \simeq 70\text{Å} > d_\perp$. This is consistent with the observed mean-field behavior [43] $H_{c_2} \simeq (T_{\rm BCS} - T)$ although the slight upward curvature [120] in $H_{c_2}(T)$ may be taken as an indication of the weak interchain coupling [120] (in this respect only the extreme $\xi_{0\perp} < d_\perp$ case has been considered [135, 7] so far).

Rather than going into the corrections to the linear dependence of H_{c_2} on temperature implied by $\xi_0 > \xi_{0\perp} > d_\perp$ we shall estimate now the corresponding effect on the width of the critical region. With $\xi_{0\perp} > d_\perp$ the interaction of fluctuations is less [25] important than in the case $\xi_{0\perp} < d_\perp$ studied in Section 4.3. The anisotropy (55), however, enhances [15,25] the corresponding effects with respect to those encountered in the 3D case. In order to estimate this enhancement we remember from Section 4.3. the formal analogy between the Peierls and the BCS Landau expansions. Using this analogy we have the BCS Landau functional

$$f = A' \left[\frac{T - T_{\rm BCS}}{T_{\rm BCS}} |\psi|^2 + \xi_0^2 \left| \frac{\partial \psi}{\partial y} \right|^2 + \xi_{0\perp}^2 \left| \frac{\partial \psi}{\partial z} \right|^2 + \xi_{0\perp}^2 \left| \frac{\partial \psi}{\partial x} \right|^2 \right] + B|\psi|^4 \tag{56}$$

with A' and B from Section 4.3, except that T_p^0 is replaced by $T_{\rm BCS}$, just as in going from Equation (22) to Equation (54). When $\xi_{0\perp} > d_\perp$ in Equation (56) it is meaningful to symmetrize this equation by rescaling the transverse variables through the transformation [15, 25] $(x', z')/\xi_0 = (x, z)/\xi_{01}$. The ensuing critical behaviors are 3D but enhanced by the scaling factors $\xi_0/\xi_{0\perp}$. E.g. the width ΔT of the critical region is enhanced by [15]

$$\frac{\Delta T}{T_{\rm BCS}} \sim \left(\frac{\xi_0}{\xi_{0\perp}} \right)^4 \tag{57}$$

over its isotropic value. Similar expressions hold for the specific heat, paraconductivity, depression of the transition temperature etc. Usually they are given [15, 25] for the general (rather then BCS) values of coefficients in Equation (56).

The similar type of reasoning applies of course to the CDW transition. The form (35) of the Landau expansion continues to hold for T below ω_D. The harmonic coefficients are the same as in Equation (35) except for the replacement of T_p^0 by $T_{\rm CDW}$ (λ_{ac} by $\lambda_{ac} + \lambda_2/2$), as was already mentioned for ξ 's of Equation (54). The effect of the virtual phonon excitations on the anharmonic coefficients has not been discussed in detail so far. However this question is of little importance in conducting trichalcogenides, where the optic phonons seem to be only relatively weakly coupled to the conducting electrons. We can thus safely think that the fluctuation effects are not more important than in the BCS estimation. Needless to say, the estimation (57) holds for the Peierls transition at T_p with $\xi_{0\perp} > d_\perp$.

5.3. Additional Remarks Concerning Many Body Corrections

The condition (16)

$$2\pi T_p^0 > \omega_D$$

have led us to the situation in which the one-dimensional many-body (parquet) effects are absent (remember $\lambda_{ac} > g_{1,2}$ too). This condition is certainly fulfilled for the higher transition in $NbSe_3$ at ambient pressure. The lower transition occurs at the temperature $T_p \simeq \omega_D/2\pi$ and $2\pi T_p^0 > \omega_D$ should be satisfied in this case too because $T_p^0 > T_p$. Nevertheless, from this point of view it is of some interest to present briefly a few results of the one-dimensional many-body approach.

As already mentioned in Section 5.1 the one-dimensional many-body effects are important if it turns out formally that

$$2\pi T_p^0 < \omega_D \tag{51}$$

In this case the parquet coupling between the $e-h$ and $e-e$ channels becomes important provided that [23, 122, 123]

$$\omega_D > T > t_\perp, \tag{49}$$

as discussed in this subsection. The parquet coupling results in the logarithmic renormalization [10, 16, 17, 18, 20] of the coupling constants λ_1 and λ_2

$$\tilde{\lambda}_1(T) = \frac{\lambda_1}{1 - \lambda_1 \log \frac{\omega_D}{T}}, \tag{58}$$

$$\tilde{\lambda}_2(T) = \lambda_2 - \frac{\lambda_1}{2} + \frac{\tilde{\lambda}_1(T)}{2}. \tag{59}$$

It can be used for temperatures above

$$\Delta_S \simeq \omega_D \exp - (\lambda_1)^{-1} \tag{60}$$

where the singularity in Equations (58) and (59) occurs. Thus the parquet renormalization can be used at all $T > t_\perp$ if

$$t_\perp > \Delta_S. \tag{61}$$

We can note that this requirement is not inconsistent with (49) and (50). For temperatures below $t_\perp$ the parquet coupling between the channels is absent, i.e. the ladder approximations are valid, as we already know from Figure (19). The effective couplings in these ladders are [23, 123] the values $\tilde{\lambda}_{1,2}(T \simeq t_\perp) = \bar{\lambda}_{1,2}$, which take into account the parquet renormalization in the range $\omega_D > T > t_\perp$. These values appear therefore in Equations (52) and (53) instead of the bare λ 's. Also the prefactor ω_D is replaced [23,123] by $t_\perp < \omega_D$. As is easily seen the parquet renormalization $\lambda \to \bar{\lambda}$ favors the CDW instability with respect to the BCS superconductivity. Furthermore the validity of ladder approximations implies the validity of the Landau expansions. This means that in the present case the fluctuations can be treated in a way analogous to that described in Section 5.2.

The situation is quite different if

$$\Delta_S > t_\perp. \tag{62}$$

In this case the parquet results cannot be used below Δ_S, where the transitions are expected to occur. Usually then the one dimensional problem is solved 'exactly' and $t_\perp$ introduced as a perturbation [109, 112, 7]. In this sense the approach is analogous to that [135] described in Section 4.4 except that it includes [109, 112, 7] quantum fluctuations [7]. (In Section 4.4 we had $T_p^0 > t_\perp$ instead of (62).)

For $T < \Delta_S$ the behavior in the one dimensional regime is determined by the properties of the (long wave) plasmons because Δ_S is in fact the gap in the SDW spectrum [20,17] so that these excitations are frozen out. The spectrum of plasmons is 1D acoustic [27] for $v_F|\mathbf{q}| > \omega_0$, where ω_0 is the plasma frequency (Coulomb gap) of Section 3.2. In the weak-coupling limit (7), (12) the Coulomb gap is thus important [27] only in the small $k_{TF} = \omega_0/v_F$ region of the Brillouin zone around the Γ point. In the remaining part the 1D acoustic plasmon spectrum is renormalized, first of all by phonons, due to the assumption (15). The zero point motion (quantum fluctuations) of those plasmons enters the behavior of the correlation functions. In particular the BCS and the CDW correlations compete again [112]. The long range order is introduced by the weak interchain coupling and particularly by $t_\perp < \Delta_S$. This latter coupling can be treated analogously to the Josephson coupling in the BCS case, i.e. via the $t_\perp/\Delta_S$ expression [112].

3.2.6 6. Summary

Our main purpose here was to situate the conducting trichalcogenides with respect to the existing theories and to describe briefly the relevant theoretical results. Using the experimental evidences we have thus established a required system of inequalities. The principal role is held by two of them

$$\lambda_{ac} > g \tag{14}$$

and

$$2\pi T_p^0 > \omega_D, \tag{16}$$

at ambient pressure. The first ensures that the (acoustic) phonon mediated electronelectron interaction dominates over the Coulomb interactions. The second says that the dominant interaction is strongly retarded at the characteristic temperature T_p^0. This simplifies considerably the theory, making the parquet coupling of $e-h$ and $e-e$ channels unimportant. The resulting mean-field theory is the familiar Peierls theory in which the weakly interacting electrons are coupled to the classic deformation field. The latter is the natural order parameter and its behavior depends crucially on the interchain coupling, which can be of elastic, nesting and/or Coulomb origin. The mean-field Peierls theory is reasonable provided that the interchain coupling is strong,

$$\xi_{0\perp}\left(T_p^0\right) > d_\perp,$$

but important fluctuative corrections occur in the opposite limit. Interesting commensurability effects appear provided that the $2k_F$ instability occurs close enough to the $2k_F$ commensurability point

$$\kappa\xi_0 < 1$$

as seems to be the case in the orthorhombic TaS_3.

When T_p^0 is decreased by applying pressure to $NbSe_3$ the condition (16) ceases to hold. The interchain coupling becomes then important on the mean-field (parquet) level, and not only

beyond the mean-field approximation, as was the case in the Peierls limit. At $2\pi T_p^0 \simeq \omega_D$ the continuity (Figure (19)) implies

$$T_p^0 < t_\perp$$

and therefore the parquet coupling between the $e-e$ and $e-h$ channels remains unactivated. Although somewhat more involved than the Peierls limit, this situation can still be described in terms of (the Landau expansions with) classic (CDW, BCS) order parameters. This contrasts with the parquet (or beyond it) situations.

The central inequality (16) and all what follows from it by continuity, has recently received a direct experimental confirmation [136]. The far infrared reflectivity measurements on $NbSe_3$ have demonstrated that the optic phonons fall in the low temperature dielectric gap $\Delta_p \simeq T_p^0 > \omega_D$. Even if the future experiments show that some inequalities used here are weakly or not at all satisfied, the present analysis may still represent a good starting point for the necessary corrections and modifications.

3.2.7 References

1. P. Haen, P. Monceau, B. Tissier, G. Waysand, A. Meerschaut, P. Molinié, J. Rouxel, Proceedings of the 14th Int. Conference on Low Temperature Physics, Otaniemi, Finland 1975, edited by M. Krusius and M. Vuorio (North Holland, Amsterdam 1975) Vol. 5, p. 445.

2. T. Sambongi, K. Tsutsumi, Y. Shiozaki, M. Yamamoto, K. Yamaya, Y. Abe, Sol. St. Commun. 22,729 (1977).

3. P. Monceau, J. Peyrard, J. Richard, P. Molinié, Phys. Rev. Lett., 39, 160 (1977); A. Briggs, P. Monceau, M. Nunez-Regueiro, J. Peyrard, M. Ribault, J. Richard, J. Phys. C 13, 2117 (1980).

4. For an excellent early review and approach see J. A. Wilson, Phys. Rev. 19, 6456 (1979), followed by J. Phys. F. 12, 2469 (1982).

5. For the latest results in this field see Proceedings of the International Conference on the Physics and Chemistry of Conducting Polymers and International CNRS Colloqium on the Physics and Chemistry of Synthetic and Organic Metals, Les Arcs, France 1982, ed. R. Comés and P. Bernier, J. Physique C 44, C3 (1983).

6. M. Weger, J. B. Goldberg, review in Sol. St. Phys. 28, 1 (1973).

7. D. Jérome, H. J. Schulz, Adv. in Physics 31, 299 (1982) and references therein.

8. P. Monceau, J. Richard, M. Renard, Phys. Rev. B 25, 931 and 948, 1982 and references therein.

9. W. A. Little, Phys. Rev. A 134, 1416 (1964).

10. Yu. A. Bychkov, L. P. Gor'kov, J. E. Dzyaloshinskii, Zh. Eksp. Teor. Fiz. 50, 738 (1966) [Sov. Phys. JETP 23, 489 (1966)].

11. M. Weger, Rev. Mod. Phys. 36, 175 (1964).

12. J. Labbé, S. Barišić, J. Friedel, Phys. Rev. Lett. 19, 1038 (1968).

13. J. Labbé, J. Friedel, J. Physique 27, 153 and 303 (1966).

14. S. Barišić, J. Labbé, J. Friedel, Phys. Rev. Lett. 25, 919 (1970); S. Barišić, Phys. Rev. B5, 932 and 941 (1972).

15. S. Barišić, S. Marčelja, Sol. St. Commun. 7, 1395 (1969).

16. I. E. Dzyaloshinskii, A. Y. Larkin, Zh. Eksp. Teor. Fiz. 61, 791 (1971) [Soviet Physics JETP 34, 422 (1972).

17. J. Solyom, Adv. in Physics 28, 201 (1979), and references therein.

18. L. P. Gor'kov, I. E. Dzyaloshinskii, Zh. Eksp. Teor. Fiz. 67, 397 (1974) [Sov. Phys. JETP 40, 1980 (1975)].

19. F. Woynarovich, J. Phys. C. 15, 85 and 97 (1982) and references therein, H. B. Thacker, Rev. Mod. Phys. 53, 253 (1981) and references therein.

20. V. J. Emery, Review, in Highly Conducting One-Dimensional Solids, edited by J. T. Devreese, R. P. Evrard and V. E. van Doren (Plenum, N.Y.) 1979.

21. S. Barišić, K. Šaub, J. Phys. C 6, L367 (1973).

22. B. Horovitz, H. Gutfreund, M. Weger, Phys. Rev. B 8, 3174 (1975).

23. V. N. Prigodin, Yu. A. Firsov, Zh. Eksp. Teor. Fiz. 76, 736 and 1602 (1979) [Sov. Phys. JETP 49, 369 and 813 (1979)].

24. G. Bergmann, D. Rainer, Z. Physik 263, 59 (1973).

25. S. BariSić, Lecture Notes in Physics (Springer) 65, 85 (1977).

26. For an updated presentation of the mean-field results see B. Horovitz, H. Gutfreund, M. Weger, Sol. St. Commun. 39, 541 (1981).

27. S. BariSić, J. Physique 44, 185 (1983).

28. G. A. Toombs, Phys. Reports C 40, 183 (1978) and references therein.

29. A. Meerschaut, J. Rouxel, J. Less Common Met. 39, 197 (1975).

30. J. P. Pouget, R. Moret, A. Meerschaut, L. Guemas, J. Rouxel, in Ref. [5], p. 1729.

31. K. Tsutsumi, T. Takagaki, M. Yamamoto, Y. Shiozaki, M. Ido, T. Sambongi, K. Yamada, Y. Abe, Phys. Rev. Lett. 39, 1675, (1977).

32. S. Tomić, K. Biljaković, D. Djurek, J. R. Cooper, Sol. St. Commun. 38, 109 (1981); S. Tomić, Sol. St. Commun. 40, 321 (1981).

33. S. Barišić, A. Bjeliis, in Theoretical Aspects of Bond Structures and Electronic Properties of Pseudo-One-Dimensional Solids, edited by H. Komimura, D. Riedel, Dordrecht (in press).

34. J. L. Hodeau, M. Marezio, C. Roucau, R. Ayroles, A. Meerchaut, J. Rouxel, P. Monceau, J. Phys. C 11, 4117 (1978).

35. D. W. Bullet, J. Phys. C 12, 277 (1979); Sol. St. Commum. 26, 563 (1978).

36. R. Hoffmann, S. Shaik, J. C. Scott, M-H Whangbo, M. J. Foshee, J. Sol. St. Chem. 34, 263 (1980); M.-H.Whangbo, P. Gressier, Inorgan.Chem. 23, 1305 (1984).

37. N. P. Ong, P. Monceau, Sol. St. Commun. 26, 487 (1978), revisited by G. X. Tassema, N. P. Ong, Phys. Rev. B 23, 5607 (1981).

38. N. P. Ong, Y. W. Brill, Phys. Rev. B 18, 5265 (1978); N. P. Ong, Phys. Rev. B 18, 5272 (1978).

39. R. M. Fleming, D. E. Moncton, D. B. McWhan, Phys. Rev. B 18, 5560 (1978).

40. T. J. Wieting, A. Grisel, F. Levy, Ph. Schmid, Lecture Notes in Physics, Vol. 95, Springer, New York, 1979, p. 354.

41. A. Zwick, M. A. Renucci, R. Carles, N. Saint-Cricq, J. B. Renucci, Physics B&C 105, 361 (1981).

42. S. Jandl, M. Banville, J. -Y. Harbec, Phys. Rev. B 22, 5697 (1980); S. Jandl, J. Deslandes, Can. J. Phys. 59, 936 (1981).

43. E. g. A. A. Abrikosov, L. P. Gor'kov, I. E. Dzyaloshinskii, Quantum Field Methods in Statistical Physics, Prentice-Hall, Englewood Cliffs, 1963.

44. H. P. Geserich, G. Scheiber, F. Lévy, P. Monceau, Sol. St. Commun. 49, 335 (1984).

45. I. E. Dzyaloshinskii, E. I. Kats, Zh. Eksp. Teor. Fiz. 55, 338 (1968) [Sov. Phys. JETP 28, 178 (1969)].

46. P. F. Williams, A. N. Bloch, Phys. Rev. B 10, 1097 (1974).

47. T. K. Mitra, J. Phys. C 2, 52 (1969).

48. S. Barišić, Sol. St. Commun. 9, 1507 (1971).

49. K. Šaub, S. Barišić, J. Friedel, Phys. Lett. 56A, 302 (1976).

50. J. Friedel, C. Noguera, Int. J. Quantum Chem. 23, 1209 (1983).

51. F. Y. di Salvo, J. V. Waszczak, K. Yamaya J. Phys. Chem. Solid 41, 1311 (1980).

52. J. D. Kulick, J. C. Scott, Sol. St. Commun. 32, 271 (1980).

53. F. Devreux, J. Physique 43, 489 (1982).

54. D. Horovitz, Phys. Rev. B 16, 3943 (1972).

55. R. E. Peierls, Quantum Theory of Solids, Oxford Univ. Press, London, 1955, p. 108.

56. J. Bardeen, L. N. Cooper, J. R. Schrieffer, Phys. Rev. 108, 1175 (1957).

57. H. Fröhlich, Proc. Roy. Soc. (London) 223A, 296 (1954).

58. W. Kohn, Phys. Rev. 115, 809 (1959); A. M. Afanas'ev, Yu. Kagan, Zh. Ekspe. Teor. Fiz. 43, 1456 (1962) [Soviet Physics JETP 161030 (1963)].

59. G. Beni, Sol. St. Commun. 15, 269 (1974).

60. S. A. Brazovskii, L. P. Gor'kov, J. R. Schrieffer, Phys. Scripta 25, 423 (1982).

61. B. R. Patton, L. J. Sham, Phys. Rev. Lett. 31, 631 (1973).

62. A. BjeliŠ, K. Šaub, S. BariSić, N. Cimento, 23B, 102 (1974).

63. P. A. Lee, T. M. Rice, P. W. Anderson, Phys. Rev. Lett. 31, 462 (1973).

64. M. J. Rice, S. Sträsler, Sol. St. Commun. 13, 1389 (1973).

65. A. Bjeliš, S. BariSíć, J. Physique Lettres 36, 169 (1975).

66. E. G. Brovman, Yu. Kagan, Zh. Eksp. Teor. Fiz. 52, 557 (1967) [Soviet Physics JETP 25, 365 (1967)] ; Zh. Eksp. Teor. Fiz. 57, 1329 (1969) [Soviet Physics JETP 30721 (1970)].

67. D. Allender, J. W. Bray, J. Bardeen, Phys. Rev. B 9, 119 (1974).

68. I. E. Dzyaloshinskii, Nobel Symposium 24, editors B. and S. Lundquist, Nobel Foundation, Stockholm, Academic Press, N.Y. and London, 1973, p. 143; S. A. Brazovskii, I. E. Dzyaloshinskii, Low Temperature Physics LT 14, Vol. 4, (1975) 337.

69. I. Batistić, S. BariSić, Sol. St. Commun. 33, 603 (1980).

70. D. J. Scalapino, M. Sears, R. A. Ferrell, Phys. Rev. B 6, 3409 (1972).

71. K. Uzelac, S. BariSić. J. Physique 36, 1267 (1975); and J. Physique - Lettres 38, 47 (1977).

72. M. J. Rice, S. Sträsler, Sol. St. Commun. 13, 125 (1973).

73. W. L. Mc Millan, Phys. Rev. B 14, 1496 (1976).

74. L. N. Bulaevskii, D. J. Khomski, Zh. Eksp. Teor. Fiz. 74, 1863 (1978) [Soviet Physics JETP 47, 971 (1978)].

75. V. L. Pokrovskii, A. L. Talapov, Zh. Eksp. Teor. Fiz. 75, 1151 (1978) [Soviet Physics JETP 48, 579 (1978)].

76. G. Theodorou, T. M. Rice, Phys. Rev. B 18, 2840 (1978).

77. P. Lederer, P. Pitanga, J. Physique 39, 993 (1978).

78. K. R. Subbaswamy, S. E. Trullinger, Phys. Rev. A 19, 1340 (1979).

79. J. A. Krumhansl, J. R. Schrieffer, Phys. Rev. B 11, 3535 (1975).

80. N. Gupta, B. Sutherland, Phys. Rev. A 14, 1790 (1976).

81. Y. Okwamoto, H. Takayama, H. Shiba, J. Phys. Soc. Japan 46, 1. '0 (1979).

82. J. Batistić, S. BariSić, J. Phys. Lettres 40, 613 (1979).

83. A. N. Filonov, G. M. Zaslavsky, Phys. Lett. 86A, 237 (1981).

84. G. Mihaly, Gy. Hutiray, L. Mihaly, Sol. St. Commun. 48, 203 (1983).

85. S. BariSić, I. Batistić, to be published.

86. P. Bak, Phys. Rev. Lett. 48, 692 (1982).

87. J. Bardeen, Sol. St. Commun. 13, 357 (1973).

88. P. A. Lee, T. M. Rice, P. W. Anderson, Sol. St. Commun. 14, 703 (1974). P. A. Lee, T. M. Rice, Phys. Rev. B 19, 3970 (1979).

89. J. Bardeen, Phys. Rev. Lett. 42, 1498 (1979); ibid 451978 (1980); Mol. Cryst. Liq. Cryst. 81, 719 (1981); G. Grüner, A. Zettl, W. G. Clark, J. Bardeen, Phys. Rev. B 24, 7247 (1981).

90. L. P. Gor'kov, Pisma Zh. Eksp. Teor. Fiz. 38, 76 (1983) [Soviet Physics JETP Lett. 38, 87 (1983)].

91. J. Bardeen, E. Ben-Jacob, A. Zettl, G. Grüner, Phys. Rev. Lett. 49, 493 (1982).

92. P. Monceau, J. Richard, M. Renard, Phys. Rev. Lett. 45, 43 (1980); Z. Z. Wang, M. C. SaintLager, P. Monceau, M. Renard, P. Gressier, A. Meerschaut, L. Guemas, J. Rouxel, Sol. St. Commun. 46, 325 (1983); Z. Z. Wang, P. Monceau, M. Renard, P. Gressier, L. Guemas, A. Meerschaut, Sol. St. Commun. 47, 439 (1983); P. Monceau, M. Renard, J. Richard, M. C. Saint-Lager, H. Salva, Z. Z. Wang, Phys. Rev. B 28, 1646 (1983).

93. M. Weger, G. Grüner, W. G. Clark, Sol. St. Commun. 35, 243 (1980).

94. G. Grüner, Mol. Cryst. Liq. Cryst. 81, 735 (1981).

95. M. J. Rice, Phys. Rev. Lett. 48, 1640 (1982).

96. S. A. Brazovskii, I. E. Dzyaloshinskii, Zh. Eksp. Teor. Fiz. 71, 2338 (1976) [Soviet Physics JETP 441233 (1976)].

97. A. Kotani, J. Phys. Soc. Japan 42, 408 and 416 (1977).

98. S. A. Brazovskii, Pisma Zh. Eksp. Teor. Fiz. 28, 656 (1978); [Soviet Physics JETP Lett. 28, 606 (1978)] and Zh. Eksp. Teor. Fiz. 78, 677 (1980) [Soviet Physics JETP 51, 342 (1980)]; S. A. Brazovskii, I. F. Dzyaloshinskii, N. N. Kirova Zh. Eksp. Teor. Fiz. 81, 2279 (1981) [Soviet Physics JETP 541209 (1981)].

99. H. Takayama, Y. R. Lin-Lin, K. Maki, Phys. Rev. Lett. 47, 986 (1981).

100. J. Goldstone, F. Wilczek, Phys. Rev. Lett. 47, 986 (1981).

101. I. Batistić, S. Barisić, in Ref. 5., p. 1543.

102. W. P. Su, J. R. Schrieffer, A. J. Heeger, Phys. Rev. Lett. 42, 1698 (1979); Phys. Rev. B 22, 2099 (1980); W. P. Su, Phys. Rev. B 27, 370 (1983).

103. M. J. Rice, Phys. Lett. 71A, 152 (1979).

104. Per Bak, V. L. Pokrovskii, Phys. Rev. Lett. 47, 958 (1981) suggest how to include the effects of discreteness beyond Equation (33).

105. S. A. Brazovskii, I. E. Dzyaloshinskii, I. M. Krichever, Zh. Eksp. Teor. Fiz. 83, 389 (1982) [Soviet Physics JETP 56, 212 (1982)].

106. I. E. Dzyaloshinskii, I. M. Krichever, Zh. Eksp. Teor. Fiz. 83, 1576 (1982) [Soviet Physics JETP 56, 908 (1982)].

107. W. Dieterich, Z. Physik 270, 239 (1974); Adv. in Phys. 25, 615 (1976).

108. G. Toulouse, N. Cimento 23B, 1974).

109. K. B. Efetov, A. J. Larkin, Zh. Eksp. Teor. Fiz. 66, 2290 (1974) [Soviet Physics JETP 39 1129 (1974)].

110. D. J. Scalapino, Y. Imry, P. Pincus, Phys. Rev. B 11, 2024 (1975).

111. P. Manneville, J. Physique 36, 701 (1975).

112. R. A. Klemm, H. Gutfreund, Phys. Rev. B 14, 1086 (1976).

113. G. Theodorou, I. Batistić, S. Barisić, Fizika (Yu) 12, 141 (1980).

114. I. Batistić, G. Theodorou, S. Barisić, Sol. St. Commun. 34, 499 (1980); J. Phys. C 14, 1905 (1980).

115. C. Rouceau, R. Ayroles, P. Monceau, L. Guemas, A. Meerschaut, J. Rouxel, Phys. St. Sol. (a) 62, 483 (1980).

116. Z. Z. Wang, H. Salva, P. Monceau, M. Renard, C. Rouceau, R. Ayroles F. Levy, L. Guemas, A. Meerschaut, J. Physique Lettres 44, 311 (1983); H. Salva, Z. Z. Wang, P. Monceau, J. Richard, M. Renard, Phil. Mag. 49, 385 (1984).

117. K. Tsutsumi, T. Sambongi, S. Kagoshima, T. Ishiguro, J. Phys. Soc. Japan 44, 1735 (1978).

118. A. W. Higgs, J. C. Gill, Socl. St. Commun. 47, 737 (1983).

119. A. Bjeliš, S. Barišić, Phys. Rev. Lett. 48, 684 (1982) and A. Bjeliš, personal communication.

120. A. Briggs, P. Monceau, M. Nunez-Regueiro, M. Ribault, J. Richard, J. Physique 42, 1453 (1981).

121. W. W. Fuller, Ph.D. Thesis, Univ. of California at los Angeles 1980; W. W. Fuller, G. Grüner, P. M. Chaikin, N. P. Ong, Chem. Scr. 17, 205 (1981); W. W. Fuller, P. M. Chaikin, N. P. Ong, Sol. St. Commun. 30, 689 (1979).

122. K. Nishida, T. Sambongi, M. Ido, Phys. Soc. Japan 48, 331 (1980).

123. V. J. Emery, R. Bruinsma, S. Barisić, Phys. Rev. Lett. 48, 1039 (1982); V. J. Emery in Ref. 5.

124. J. Friedel, J. Physique-Lettres 36, 279 (1975).

125. G. Bilboro, W. L. Mc Millan, Phys. Rev. B14, 1887 (1976).

126. D. R. Tilley, Proc. Phys. Soc. (London) 85, 1177 (1965); and 86, 678 (1965).

127. S. Barišić, P. G. de Gennes, Sol. St. Commun 6, 281 (1968).

128. P. W. Anderson, J. Phys. Chem. Sol. 11, 26 (1959).

129. M. D. Whitmore, J. P. Carbotte, J. Phys. F 11, 2585 (1981) and references therein.

130. H. Suhl, B. J. Matthias, L. R. Walker, Phys. Rev. Lett. 3, 552 (1959).

131. D. R. Tilley, Proc. Phys. Soc. (London) 84, 573 (1964).

132. V. K. Wong, C. C. Sung, Phys. Rev. Lett. 19, 1236 (1967).

133. B. T. Geilikman, R. O. Zaitsev, V. Z. Kresin, Sov. Phys. Sol. St. 9, 642 (1967).

134. A. A. Abrikosov, J. A. Ryzhkin, Lecture Notes in Phys. 65, 187 (1977).

135. L. A. Turkevich, R. A. Klemm, Phys. Rev. B 19, 2520 (1979).

136 W. A. Challender P. L. Richards, Sol. St. Commun. 52, 117 (1984).

3.3 Dynamical Properties of Quasi-one-dimensional Conductors: a Phase Hamiltonian Approach

3.3.1 1. Introduction

Since the realization of quasi-one-dimensional conductors, there have been extensive investigations into the electronic properties of other such low-dimensional systems, both experimentally and theoretically [1-4]. Above all, systems having a Peierls transition [5] have been investigated in detail. The novelty of this Peierls-Fröhlich (PF) [6] state lies in the novel possibility of the transport phenomenon being associated with the collective degree of freedom, i.e. the charge density wave (CDW) [7]. In a CDW, electrons follow the periodic lattice distortion adiabatically, resulting in a periodic spatial variation of the self-consistent charge density. Lee, Rice and Anderson [8] have shown that the low-lying excitation of CDW is due to the sliding motion associated with the lattice distortion, which is described by the phase of the complex order parameter, i.e. the periodic lattice distortion. This phase is related to the choice of the origin of coordinates and then to the translational symmetry of the system. Hence this sliding motion, or sliding conductivity, is sensitive to the impurity scattering and the Umklapp scattering [8]. These scattering mechanisms result in impurity and commensurability pinning, respectively, whose various interesting properties have been revealed since that time. In these investigations the phase Hamiltonian, which is the effective Hamiltonian to describe the motion of the phase and is derived from the full Hamiltonian with electronphonon interactions, has proved very useful [8-12]. Recently anomalous properties typically observed in $NbSe_3$ have also been discussed in a similar context [13,14] and by Monceau in Part II of this volume. In these cases the dynamics of phase motion has been treated classically. This is due to the fact that the effective mass of CDW is high since electrons are moving together with lattice distortions.

Beside these investigations on the PF state there has been great progress in the last ten years in the understanding of the many-body problem in one-dimension, since the problem can been treated with relatively high accuracy (sometimes exactly) due to the limited dimensionality. (See e.g. the review paper by Solyom [15].) One of the
main reasons for the development of such theoretical research is the success of the bosonization, which was first introduced by Tomonaga [16] in 1950. This bosonization of the interacting fermion fields has lately been refined and extended by Luther and Peschel [17], Luther and Emery [18], Mattis [19] and Haldane [20, 21] to treat more complicated interaction processes. Through these investigations quantum phase variables, which represent the charge and spin degrees of freedom of electrons (and are different from the phase variable in the PF state), have been naturally introduced, and the phase Hamiltonian has then been derived [22-25], which is equivalent to the original Hamiltonian given in terms of fermions. In this case the quantum mechanical description is inevitable.

In realistic systems electrons are mutually interacting and are coupled to the lattice distortions. Such systems will then be described by phase variables representing electrons on one hand and lattice distortions with amplitude and phase on the other. This is the phase Hamiltonian approach to the whole system, and has been imployed in the examination of excitation spectra and the classification of solitons in the PF state [26-28]. Such an approach also turns

out [29, 30] to be convenient in the discussion of the spin Peierls problem [31], which can be considered as a case of a strong repulsive interaction in the half-filled band.

The purpose of this review is to give a coherent description of the dynamical properties of electrons based on the phase Hamiltonian. In Section 2 the phase Hamiltonian is derived for interacting electrons, but without coupling to the lattice. In this section it is shown how conductivity and spin susceptibility are evaluated in terms of the phase variables. In Section 3 the PF state is discussed; especially the spin Peierls problem is examined in Section 3.7. In Section 4, the effects of impurities have been examined for the PF state on one hand and for the interacting electrons in the absence of PF state on the other. The latter is a new way to treat the Anderson localization [32-34] in the interacting systems. Based on the results obtained in the preceding sections the CDW conductivity in the PF state is examined in Section 5 and transport properties of MX_3 (M : transition metal, X : chalcogenide) will be discussed in Section 6 on a similar basis. A summary is given in Section 7.

We shall use units of $\hbar = k_B = 1$.

3.3.2 2. Phase Hamiltonian

2.1. Boson Representation and Phase Variables

We consider one-dimensional electrons represented by the following Hamiltonian, $\mathcal{H}$, [15]

$$\mathcal{H} = \mathcal{H}_0 + \mathcal{H}_{\rm int} \tag{2.1}$$

$$\mathcal{H}_0 = \sum_{k>0} v_F\,(k - k_F)\, a^+_{k\sigma} a_{k\sigma} + \sum_{k<0} v_F\,(-k - k_F)\, b^+_{k\sigma} b_{k\sigma}, \tag{2.2}$$

$$\begin{aligned}
\mathcal{H}_{\rm int} =& \frac{1}{L} \sum_{k_1,k_2,p} \sum_{\alpha,\beta} \big[\big(\gamma_{1//}\delta_{\alpha,\beta} + \gamma_{1\perp}\delta_{\alpha,-\beta}\big) \times \\
& \times a^+_{k_1\alpha} b^+_{k_2\beta} a_{k_2 + 2k_F + p\beta} b_{k_1 - 2k_F - p\alpha} + \\
& + \big(\gamma_{2//}\delta_{\alpha,\beta} + \gamma_{2\perp}\delta_{\alpha,-\beta}\big)\, a^+_{k_1\alpha} b^+_{k_2\beta} b_{k_2+p\beta} a_{k_1-p\alpha} + \\
& + \frac{\gamma_{3\perp}}{2}\delta_{\alpha,-\beta} \big(a^+_{k_1\alpha} a^+_{k_2\beta} b_{k_2 - 2k_F + p\beta} b_{k_1 + 2k_F - p - G\alpha} + \text{ h.c. } \big) + \\
& + \frac{\gamma_{4\perp}}{2}\delta_{\alpha,-\beta} \big(a^+_{k_1\alpha} a k_{2\beta} a_{k_2+p\beta} a_{k_1-p\alpha} + \\
& + b^+_{k_1\alpha} b^+_{k_2\beta} b_{k_2+p\beta} b_{k_1-p\alpha} \big) \big]
\end{aligned} \tag{2.3}$$

Here v_F and k_F are the Fermi velocity and the Fermi momentum, and $a_{k_\sigma}\left(a^+_{k_\sigma}\right)$and $b_{k\sigma}\left(b^+_{k_\sigma}\right)$are the annihilation (creation) operators of electrons with $k > 0$ and $k < 0$, respectively. Equation (2.2) defines the kinetic energy with the linear spectrum as shown in Figure 1. In this case the density of states per spin, $N(0)$, is given by $N(0) = (\pi v_F)^{-1}$.

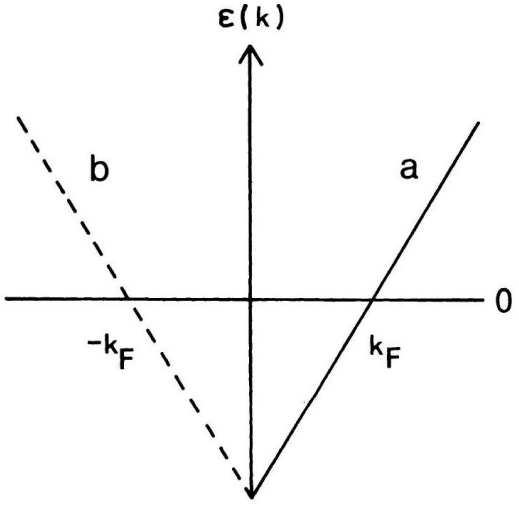


Fig. 1. Energy spectrum of one-dimensional electrons.

The interaction constants, $\gamma_{i//}$ and $\gamma_{i\perp}$, in Equation (2.3) are those between parallel and antiparallel spins. We will introduce dimensionless coupling constants, g_i, given by $g_i = \gamma_i N(0)/2 = \gamma_i/2\pi v_F$. Processes characterized by each $g_i (i = 1 \sim 4)$ are shown in Figure 2 , where solid and broken lines represent electrons with $k > 0$ and $k < 0$, respectively. In this figure the suffices, // and $\perp$, are not shown. It should be noted that the momentum transfer, q, through g_2 and g_4 processes is small, i.e. $|q| \ll 2k_F$, whereas that in g_1 is large, $|q| \simeq 2k_F$ and then this process is called backward scattering. The g_3 represents the Umklapp process, only present if $4k_F \simeq G, G$ being the reciprocal lattice vector. In Equation (2.3) all of the interactions are assumed to be instantaneous and local. This locality forbids processes corresponding to $g_{3//}$ and $g_{4//}$ due to the Pauli principle.

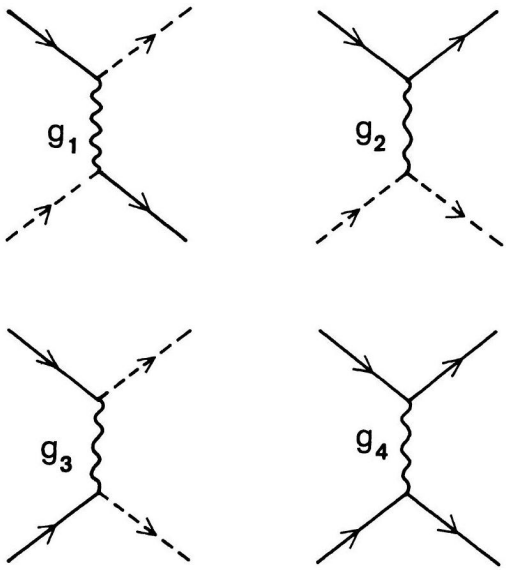


Fig. 2. Interaction processes, $g_{1 \sim g_{4}$.}

Some of the specific cases of $\mathcal{H}_{\text{int}}$ have been treated either rigorously or by the renormalization group. The example Tomonaga [16] first examined corresponds to taking $g_{2//} \neq 0$ and $g_i = 0$ otherwise. Investigations with more generality have been performed later by Luther and

Peschel [17], Luther and Emery [18] and Mattis [19], who found that the dynamical processes represented by electron field operators, $\psi_{is}(x)$ ($i = 1$ for $k > 0$ and $i = 2$ for $k < 0$), can be equivalently expressed by those of a boson field, $\phi_{is}(x)$, as follows;

$$\psi_{1s}(x) \to (2\pi\alpha)^{-1/2} \exp\left[-ik_F x - \phi_{1s}(x)\right] \equiv 0_{1s}(x) \tag{2.4}$$

$$\psi_{2s}(x) \to (2\pi\alpha)^{-1/2} \exp\left[+ik_F x + \phi_{2s}(x)\right] \equiv 0_{2s}(x) \tag{2.5}$$

where s is the spin index and α is the cut-off parameter to be set $\alpha \to 0$ whenever possible and ϕ_{is} 's are given by

$$\phi_{is}(x) = \sum_q A_q(x)\rho_{is}(q) \tag{2.6}$$

$$A_q(x) = \frac{2\pi}{Lq} \exp\left[-\frac{1}{2}\alpha|q| - iqx\right]. \tag{2.7}$$

Here L is the system size. In Equation (2.6) the density fluctuation operators, $\rho_{is}(q)(q > 0)$, are defined as follows,

$$\rho_{1s}(q) = \sum_{k>0} a^+_{k+qs} a_{ks} \tag{2.8a}$$

$$\rho_{1s}(-q) = \sum_{k>0} a^+_{ks} a_{k+qs} \tag{2.8b}$$

$$\rho_{2s}(q) = \sum_{k<-q} b^+_{k+qs} b_{ks} \tag{2.8c}$$

$$\rho_{2s}(-q) = \sum_{k<-q} b^+_{ks} b_{k+qs} \tag{2.8d}$$

As was found by Tomonaga [16], these operators, $\rho_{is}(q)$, satisfy following commutation relation,

$$\begin{aligned}[\rho_{1s}(-q), \rho_{1s'}(q')] &= [\rho_{2s}(q), \rho_{2s'}(-q')] \\ &= \frac{qL}{2\pi}\delta_{q,q'}\delta_{ss'}\end{aligned} \tag{2.9}$$

and commute otherwise.
The equivalence of ψ_{is} and 0_{is} is due to the fact that they yield same commutations with respect to $\rho_{is}(q)$; e.g. for $\rho_{1s}(q)$

$$[\psi_{1s}(x), \rho_{1s}(q)] = e^{-iqx}\psi_{1s}(x)$$
$$[0_{1s}(x), p_{1s}(q)] = e^{-iqx}0_{1s}(x)$$

and then for any operator, which is a functional of $\rho_{is}(q), \psi_{1s}(x)$ and $0_{1s}(x)$ act equivalently. (The equivalence of ψ_{is} and 0_{is} can also be shown directly [21, 35].)

In terms of $\rho_{is}(q), \mathscr{H}_0$ can be expressed as

$$\mathcal{H}_0 \text{ B} = \frac{2\pi v_F}{L} \sum_{q>0} \sum_s \left[\rho_{1s}(q)\rho_{1s}(-q) + \rho_{2s}(-q)\rho_{2s}(q)\right]. \tag{2.10}$$

This is due to the fact that the commutations of $\mathscr{H}_0$ and $\mathscr{H}_0$ B with respect to $\rho_{is}(q)$ are identical; e.g. for $\rho_{1s}(q)$

$$[\mathcal{H}_0, \rho_{1s}(q)] = v_F q \rho_{1s}(q) \tag{2.11a}$$

$$\left[\mathcal{H}_0{}^{\mathbf{B}}, \rho_{1s}(q)\right] = v_F q \rho_{1s}(q) \tag{2.11b}$$

Among various processes in $\mathscr{H}_{\text{int}}$, Equation (2.3), those with γ_2 and γ_4 can be written in terms of the quadratic forms of $\rho_{is}(q)$,

$$\begin{aligned}\mathcal{H}_{\text{int}}^{(1)} =& \frac{1}{L}\sum_{q>0}\left(\gamma_{2//}+\gamma_{2\perp}\right)\left[\rho_1(q)\rho_2(-q)+\rho_1(-q)\rho_2(q)\right]+\\ &+\frac{1}{L}\sum_{q>0}\left(\gamma_{2//}-\gamma_{2\perp}\right)\left[\sigma_1(q)\sigma_2(-q)+\sigma_1(-q)\sigma_2(q)\right]+\\ &+\frac{1}{L}\sum_{q>0}\gamma_{4\perp}\left[\rho_1(q)\rho_1(-q)+\rho_2(-q)\rho_2(q)\right]-\\ &-\frac{1}{L}\sum_{q>0}\gamma_{4\perp}\left[\sigma_1(q)\sigma_1(-q)+\sigma_2(-q)\sigma_2(q)\right]\end{aligned} \tag{2.12}$$

where $\rho_i(q)$ and $\sigma_i(q)$ are defined as follows,

$$\rho_i(q) = \frac{1}{\sqrt{2}}\left(\rho_{i\uparrow}(q)+\rho_{i\downarrow}(q)\right), \tag{2.13a}$$

$$\sigma_i(q) = \frac{1}{\sqrt{2}}\left(\rho_{i\uparrow}(q)-\rho_{i\downarrow}(q)\right). \tag{2.13b}$$

Thus $\mathcal{H}_0 B + \mathcal{H}_{\text{int}}^{(1)}$ is given by

$$\begin{aligned}\mathcal{H}_0^B + \mathcal{H}_{\text{int}}^{(1)} =& \frac{2\pi v_F}{L}\sum_{q>0}\Bigg[\left(1+\frac{g_{4\perp}}{2}\right)\left(\rho_1(q)\rho_1(-q)+\rho_2(-q)\rho_2(q)\right)+\\ &+\left(1-\frac{g_{4\perp}}{2}\right)\left(\sigma_1(q)\sigma_1(-q)+\sigma_2(-q)\sigma_2(q)\right)+\\ &+\left(\frac{g_{2//}+g_{2\perp}}{2}\right)\left(\rho_1(q)\rho_2(-q)+\rho_1(-q)\rho_2(q)\right)+\\ &+\left(\frac{g_{2//}-g_{2\perp}}{2}\right)\left(\sigma_1(q)\sigma_2(-q)+\sigma_1(-q)\sigma_2(q)\right)\Bigg]\end{aligned} \tag{2.14}$$

It is obvious that Equation (2.14) can be exactly solved, since it is quadratic in $\rho_{is}(q)$ with commutators, Equation (2.9). The fact that Equation (2.14) can be solved is more clearly seen by the introduction of the quantum-mechanical phase variables;

$$\begin{aligned}\theta_\pm(x) &= \frac{i}{\sqrt{2}}\sum A_q(x)\left[\rho_1(q)\pm\rho_2(q)\right]\\ &= \frac{i}{2}\left[(\phi_{1\uparrow}+\phi_{1\downarrow})\pm(\phi_{2\uparrow}+\phi_{2\downarrow})\right]\end{aligned} \tag{2.15}$$

$$\begin{aligned}\phi_\pm(x) &= \frac{i}{\sqrt{2}}\sum A_q(x)\left[\sigma_1(q)\pm\sigma_2(q)\right]\\ &= \frac{i}{2}\left[(\phi_{1\uparrow}-\phi_{1\downarrow})\pm(\phi_{2\uparrow}-\phi_{2\downarrow})\right]\end{aligned} \tag{2.16}$$

By use of Equation (2.9), $\theta_{\pm}(x)$ and $\phi_{\pm}(x)$ are seen to satisfy the following commutation relations

$$[\theta_{+}(x), P(x')] = i\delta(x - x') \tag{2.17}$$
$$[\phi_{+}(x), M(x')] = i\delta(x - x') \tag{2.18}$$

where $P(x)$ and $M(x)$ are

$$P(x) = -\nabla\theta_{-}/2\pi \tag{2.19}$$
$$M(x) = -\nabla\phi_{-}/2\pi \tag{2.20}$$

Commutations other than Equations (2.17) and (2.18) vanish. By use of $\theta_{\pm}(x)$ and $\phi_{\pm}(x)$, $\mathscr{H}_0 B + \mathscr{H}_{\rm int}^{(1)}$ can be written as

$$\mathcal{H}_0^B + \mathcal{H}_{\rm int}^{(1)} = \int \mathrm{d}x \left[A'_{\rho}(\nabla\theta_{+})^2 + C'_{\rho}P^2(x) + A'_{\sigma}(\nabla\phi_{+})^2 + C'_{\sigma}M^2(x)\right] \tag{2.21}$$

where

$$A'_{\rho} = \frac{v_F}{4\pi}\left(1 + \frac{g_{2//} + g_{2\perp} + g_{4\perp}}{2}\right), \tag{2.22a}$$
$$C'_{\rho} = \pi v_F\left(1 - \frac{g_{2/l} + g_{2\perp} - g_{4\perp}}{2}\right), \tag{2.22b}$$
$$A'_{\sigma} = \frac{v_F}{4\pi}\left(1 + \frac{g_{2/l} - g_{2\perp} - g_{4\perp}}{2}\right), \tag{2.22c}$$
$$C'_{\sigma} = \pi v_F\left(1 - \frac{g_{2/l} - g_{2\perp} + g_{4\perp}}{2}\right), \tag{2.22d}$$

Equation (2.21) is of a form of simple harmonic oscillators with excitation spectra linear in the momentum, $\omega_{\rho}(q)$ and $\omega_{\sigma}(q)$;

$$\omega_{\rho}(q) = 2\sqrt{A'_{\rho}C'_{\rho}}q \tag{2.23}$$
$$\omega_{\sigma}(q) = 2\sqrt{A'_{\sigma}C'_{\sigma}}q \tag{2.24}$$

The former (latter) represents the oscillation of θ_{+} (ϕ_{+}). The physical implication of phase variables can be extracted by noting the following facts. By Equations (2.6) and (2.7) we see ($\alpha \to 0$)

$$\begin{aligned}\nabla\theta_{+}/\pi &= \frac{\sqrt{2}}{L}\sum_{q} e^{-iqx}\left(\rho_1(q) + \rho_2(q)\right) \\ &\equiv n(x),\end{aligned} \tag{2.25}$$

$$\begin{aligned}\nabla\phi_{+}/2\pi &= \frac{1}{\sqrt{2}L}\sum e^{-iqx}\left(\sigma_1(q) + \sigma_2(q)\right) \\ &\equiv m(x),\end{aligned} \tag{2.26}$$

where $n(x)$ and $m(x)$ can be interpreted as local density fluctuations of charge and spin with long wavelength. Equations (2.17) and (2.18) together with Equation (2.25) and (2.26) also imply

$$[n(x)/2, \theta_-(x')] = -i\delta(x - x') \tag{2.27}$$
$$[m(x), \phi_-(x')] = -i\delta(x - x') \tag{2.28}$$

Consequently $\theta_-$and ϕ_-can be taken as quantum-mechanical representations of the local phase of superconductivity and of the azimuthal angle of the local spin density.

Other interaction processes in $\mathcal{H}_{\text{int}}$, i.e. γ_1 and γ_3 can be treated as follows. First the contribution with $\gamma_{1//}$ can be written as

$$-\frac{\gamma^L_{1//}}{L}\sum_{k_1k_2p}\sum_s a^+_{k_1s}a_{k_2+2k_F+ps}b_{k_2s}b_{k_1-2k_F-ps} \tag{2.29a}$$
$$= -\frac{\gamma_{1/}}{L}\sum_q\sum_s \rho_{1s}(q)\rho_{2s}(-q) \tag{2.29b}$$
$$= -\frac{\gamma_{1/}}{L}\sum_q [\rho_1(q)\rho_2(-q) + \sigma_1(q)\sigma_2(-q)] \tag{2.29c}$$

where we noted $k_1 \sim k_F$ and $k_2 \sim -k_F$ in Equation (2.29a). Equation (2.29c) is similar to Equation (2.14) and then this contribution is represented as Equation (2.21) with the slight modification of $A_\rho{}', A_\sigma{}', C_\rho{}'$ and $C_\sigma{}'$.

On the other hand the $\gamma_{1\perp}$-process has a different feature. By use of Equations (2.4) and (2.5) we obtain, as follows:

$$\frac{\gamma_{1\perp}}{2}\sum_s\int \mathrm{d}x\left[\psi^+_{1-s}(\dot{x})\psi^+_{2s}(x)\psi_{1s}(x)\psi_{2-s}(x) + \text{ h.c. }\right] \tag{2.30a}$$
$$= \frac{\gamma_{1\perp}}{2(2\pi\alpha)^2}\sum_s\int \mathrm{d}x\left[\exp\{\phi_{1-s} - \phi_{2s} - \phi_{1s} + \phi_{2-s}\} + \text{ h.c. }\right] \tag{2.30b}$$
$$= \frac{\gamma_{1\perp}}{2\pi^2\alpha^2}\int \mathrm{d}x\cos 2\phi_+(x) \tag{2.30c}$$

where $\phi_+(x)$ is defined by Equation (2.16).
Finally the γ_3-process will be transformed as follows.

$$\frac{\gamma_{3\perp}}{2}\sum_s\int \mathrm{d}x\left(\psi^+_{2s}\psi^+_{2-s}\psi_{1-s}\psi_{1s}e^{iGx} + \text{ h.c. }\right) \tag{2.31a}$$
$$= \frac{\gamma_{3\perp}}{2(2\pi\alpha)^2}\sum_s\int \mathrm{d}x\left[\exp\{i(G - 4k_F)x - \sigma_{1s} - \phi_{1-s} - \phi_{2s} - \phi_{2-s}\} + \right.$$
$$\left. + \text{ h.c. }\right] \tag{2.31b}$$
$$= \frac{\gamma_{3\perp}}{2\pi^2\alpha^2}\int \mathrm{d}x\cos[(G - 4k_F)x + 2\theta_+] \tag{2.31c}$$

Consequently the total Hamiltonian, $\mathcal{K}_0 + \mathcal{H}_{\text{int}}$ Equation (2.1), is transformed to the following phase Hamiltonian.

$$\mathcal{H} = \mathcal{H}_\rho + \mathcal{H}_\sigma, \tag{2.32}$$

$$\mathcal{H}_\rho = \int \mathrm{d}x \left[A_\rho (\nabla\theta)^2 + B_\rho \cos\left[(G - 4k_F)\, x + 2\theta\right)\right] + C_\rho P^2 \Big], \tag{2.33}$$

$$\mathcal{H}_\sigma = \int \mathrm{d}x \left[A_\sigma (\nabla\phi)^2 + B_\sigma \cos 2\phi + C_\sigma M^2 \right], \tag{2.34}$$

$$A_\rho = \frac{v_F}{4\pi}\left(1 - \frac{g_{1//} - g_{2//} - g_{2\perp} - g_{4\perp}}{2}\right), \tag{2.35}$$

$$B_\rho = v_F g_{3\perp}/2\pi\alpha^2, \tag{2.36}$$

$$C_\rho = \pi v_F \left(1 + \frac{g_{1/} - g_{2//} - g_{2\perp} + g_{4\perp}}{2}\right), \tag{2.37}$$

$$A_\sigma = \frac{v_F}{4\pi}\left(1 - \frac{g_{1//} - g_{2//} + g_{2\perp} + g_{4\perp}}{2}\right), \tag{2.38}$$

$$B_\sigma = v_F g_{1\perp}/2\pi\alpha^2, \tag{2.39}$$

$$C_\sigma = \pi v_F \left(1 + \frac{g_{1//} - g_{2//} + g_{2\perp} - g_{4\perp}}{2}\right). \tag{2.40}$$

Here $\theta(x) = \theta_+(x)$ and $\phi(x) = \phi_+(x)$.
It is to be noted that in the present interaction processes the charge and spin degrees of freedom are separated as $\mathcal{H}_\rho$ and $\mathcal{H}_\sigma$, respectively [18]. Unless $g_{3\perp}$ and $g_{1\perp}$ processes, which introduce non-linearity, are present, $\mathfrak{H}$, Equation (2.32), can be solved exactly, since the resulting Hamiltonian is simply harmonic. The excitation spectra in this case are linear in q as is schematically shown in Figure 3, where the velocities, v_ρ and v_σ, are given as follows

$$v_\rho = 2\sqrt{A_\rho C_\rho}, \tag{2.41}$$

$$v_\sigma = 2\sqrt{A_\sigma C_\sigma}. \tag{2.42}$$

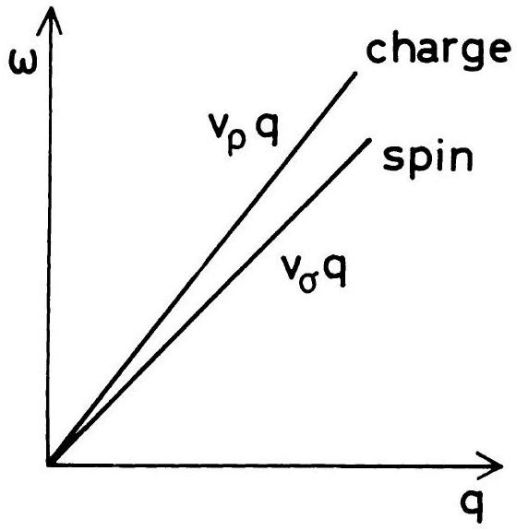


Fig. 3. Excitation spectra in the absence of the nonlinearity.

The present model for the interaction processes is very general and various limiting cases correspond to known models, which are as follows.

(i) Tomonaga-Luttinger (LT) model [16,36]

$$g_{2//} \neq 0, \quad g_i = 0 \text{ otherwise}$$

(ii) Spin-Dependent Tomonaga (SDT) model

$$g_{2//} \neq 0, \quad g_{2\perp} \neq 0, \quad g_i = 0 \quad \text{otherwise}$$

(iii) Bychkov-Gorkov-Dzyaloshinsky (BDG) model [37]

$$\begin{aligned} &g_{1//} = g_{1\perp} \equiv g_1 \neq 0, \\ &g_{2//} = g_{2\perp} \equiv g_2 \neq 0, \\ &g_i = 0 \text{ otherwise} \end{aligned}$$

(iv) Luther-Emery (LE) model [18]

$$\begin{aligned} &g_{1//} \neq 0, \quad g_{1\perp} \neq 0, \\ &g_{2//} \neq 0, \quad g_{2\perp} \neq 0, \\ &g_i = 0 \quad \text{otherwise.} \end{aligned}$$

The derivation of the phase Hamiltonian of the type of Equation (2.34) (for spin fluctuations) was first performed by Luther [24]. Efetov and Larkin [23] also noted the existence of the phase Hamiltonian for the charge fluctuations, and they used this in the calculation of the response functions. Suzumura [25] evaluated the various response functions based on $\mathscr{H}_\rho$ and $\mathscr{H}_\sigma$, Equations (2.33) and (2.34).

We have seen that the Hamiltonian of interacting fermions is given in terms of the phase variables. The physical quantities can also be expressed by these variables. In Equations (2.25) and (2.26) the local density fluctuations varying slowly in space are given in terms of $\nabla\theta$ and $\nabla\phi$. On the other hand the electron density operator with wave number around $\pm 2k_F$ is given by

$$\rho_{\pm 2k_F,S}(x) = \frac{1}{2\pi\alpha} \quad \exp\left[\pm i\left(2k_F x + \theta + s\phi\right)\right] \tag{2.43}$$

where $s = \pm 1$ is the spin index. Consequently, the total density operators of charge and spin, $N(x)$ and $M(x)$, are as follows

$$N(x) = \nabla\theta/\pi + \frac{2}{\pi\alpha}\cos\left(2k_F x + \theta\right)\cos\phi \tag{2.44}$$

$$M(x) = \nabla\phi/2\pi - \frac{1}{\pi\alpha}\sin\left(2k_F x + \theta\right)\sin\phi \tag{2.45}$$

2.2. The G-ology

There does not exist any phase transition at finite temperatures, T, in one-dimension [38]. However, various response functions have divergent singularities as $T \to 0$ which indicate the types of possible ordered states at $T = 0$ [15]. The phase diagram of the types of the ordered state in the plane of coupling constants is called the g-ology. For the g-ology we consider the following four operators [25];

$$O^+_{\mathrm{CDW}}(x) = \psi^+_{1\uparrow}\psi_{2\uparrow} = (2\pi\alpha)^{-1}\exp\left[-i\phi_+ + i\left(2k_Fx - \theta_+\right)\right] \tag{2.46a}$$

$$O^+_{\mathrm{SDW}}(x) = \psi^+_{1\uparrow}\psi_{2\downarrow} = (2\pi\alpha)^{-1}\exp\left[-i\phi_- + i\left(2k_Fx - \theta_+\right)\right] \tag{2.46b}$$

$$O^+_{\mathrm{SS}}(x) = \psi^+_{1\uparrow}\psi^+_{2\downarrow} = (2\pi\alpha)^{-1}\exp\left[-i\phi_+ - i\theta_-\right] \tag{2.46c}$$

$$O^+_{\mathrm{TS}}(x) = \psi^+_{1\uparrow}\psi^+_{2\uparrow} = (2\pi\alpha)^{-1}\exp\left[-i\phi_- - i\theta_-\right] \tag{2.46d}$$

These represent fluctuations of the charge density wave (CDW), the spin density wave (SDW), the singlet superconductivity (SS) and the triplet superconductivity (TS), respectively. The g-ology will be investigated by evaluating the response function

$$\chi_A\left(q, i\omega_\lambda\right) = \int_{-\infty}^{\infty}\mathrm{d}x\int_{-\beta}^{\beta}\mathrm{d}\tau\exp\left(-iqx - i\omega_\lambda\tau\right)\times \\ \times\left\langle T_\tau O_A(x,\tau)O^+_A(0,0)\right\rangle \tag{2.47}$$

where $\omega_\lambda = 2\pi\lambda T, \beta = T^{-1}$ and A stands for CDW, SDW, SS and TS and $O_A(x,\tau)$ is defined by

$$O_A(x,\tau) = e^{\mathscr{H}\tau}O_A(x)e^{-\mathscr{H}\tau} \tag{2.48}$$

In Equation (2.47), T_τ is the chronological operator and $\rangle$ is meant to take thermal average with respect to $\mathfrak{H}$, Equation (2.32). The separability of the Hamiltonian into the charge and the spin density fluctuations, $\mathscr{H}_\rho$ and $\mathscr{H}_\sigma$, allows the separate evaluations of $\langle T_\tau O_A(x,\tau)O_A{}^+(0,0),\rangle$ with respect to $\theta_\pm$and $\phi_\pm$.

As the temperature is lowered, $\chi_A(q,0)$ can have divergent singularities

$$\chi_A(q,0) \propto T^{-\gamma_A} \tag{2.49}$$

where $q = 2k_F$ for CDW and SDW and $q = 0$ for SS and TS.
We will explicitly examine $\chi_A\left(q, i\omega_\lambda\right)$ in the SDT model, which has exact solutions. In this case the Hamiltonian is harmonic and we then manipulate as follows, e.g., for the charge fluctuations and for large $|x|$,

$$\langle T_\tau\exp -i[\theta(x,\tau) - \theta(0,0)]\rangle \tag{2.50a}$$

$$= \exp\left[-\frac{1}{2}\left\langle T_\tau(\theta(x,\tau) - \theta(0,0))^2\right\rangle\right] \tag{2.50b}$$

$$= (2\pi T/\omega_F)^{\eta_1}\exp\left(|x|/\xi_1\right) - \exp\left(-|x|/\xi_1 - i2\pi T\tau\right)|^{-\eta_1} \tag{2.50c}$$

where $\omega_F = v_\rho\alpha^{-1}$ and

$$\eta_1 = \left[\left(1 - \frac{g_{2//} + g_{2\perp}}{2}\right)/\left(1 + \frac{g_{2//} + g_{2\perp}}{2}\right)\right]^{1/2}, \tag{2.51}$$

$$\xi_1 = v_F\left[1 - \left(\frac{g_{2//} + g_{2\perp}}{2}\right)^2\right]^{1/2}/\pi T \equiv v_\rho/\pi T \tag{2.52}$$

In deriving Equation (2.50c) from Equation (2.50b) we note the following as $|x| \to \infty$;
$\langle T_\tau(\theta(x,\tau) - \theta(0,0))^2\rangle$

$$= \frac{2C}{\pi}\rho T \sum_{\omega_l \int \ \mathrm{d}k \frac{1}{\omega_l^2+\omega_\rho(k)^2}}^{[1-\exp(ikx-i\omega_l\tau)]}$$

$$= \frac{2C}{\pi}\rho T \left[\int \mathrm{d}k \frac{1-\exp ikx}{\omega_\rho(k)^2} + \sum_{\omega_l\neq 0} \int \mathrm{d}k \frac{1}{\omega_l^2+\omega_\rho(k)^2} - \right.$$

$$\left. -T\sum_{\omega_l\neq 0} \int \mathrm{d}k \frac{\exp\left[i\left(kx-\omega_l\tau\right)\right]}{\omega_l^2+\omega_\rho(k)^2} \right]$$

$$= \frac{1}{\pi}\sqrt{\frac{C_\rho}{A_\rho}} \left[\frac{|x|}{\xi_1} + \ln \omega_F/2\pi T + \ln \left| 1-\exp\left(-\frac{2|x|}{\xi_1} - i2\pi T\tau\right)\right|\right]. \tag{2.53}$$

By use of Equation (2.50c) and the similar equation for the spin fluctuations, we obtain following γ_A defined in Equation (2.49).

$$\gamma_{\mathrm{CDW}} = 2-\gamma_\rho-\gamma_\sigma, \tag{2.54a}$$

$$\gamma_{\mathrm{SDW}} = 2-\gamma_\rho-\frac{1}{\gamma_\sigma}, \tag{2.54b}$$

$$\gamma_{\mathrm{SS}} = 2-\frac{1}{\gamma_\rho}-\gamma_\sigma, \tag{2.54c}$$

$$\gamma_{\mathrm{TS}} = 2-\frac{1}{\gamma_\rho}-\frac{1}{\gamma_\sigma}, \tag{2.54d}$$

where

$$\gamma_\rho = \left[\left(1-\frac{g_{2//}+g_{2\perp}}{2}\right) / \left(1+\frac{g_{2/l}+g_{2\perp}}{2}\right)\right]^{1/2}, \tag{2.55}$$

$$\gamma_\sigma = \left[\left(1-\frac{g_{2/l}-g_{2\perp}}{2}\right) / \left(1+\frac{g_{2/l}-g_{2\perp}}{2}\right)\right]^{1/2}. \tag{2.56}$$

In Figure 4 the types of response functions with the largest γ_A are shown in the plane of $g_{2\perp}$ and $g_{2//}$. This is the g-ology for the SDT model.

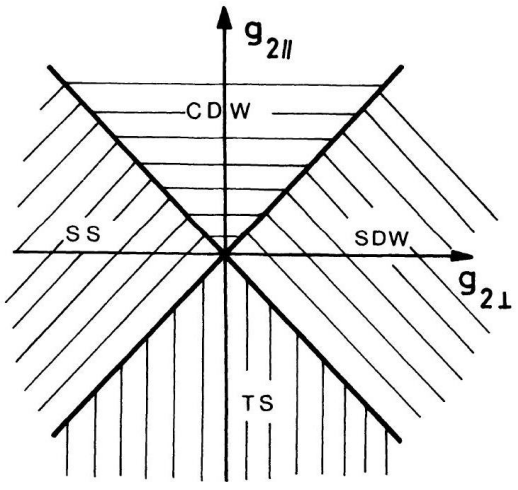


Fig. 4. The g-ology of the spin-dependent Tomonaga (SDT) model.

In the presence of B_ρ and/or B_σ, there do not exist exact solutions in general and some kind of approximations is inevitable. The self-consistent harmonic approximation (SCHA), which is proposed by Dashen et al. [39] and by Coleman [40] in the present context, is a simple one, and will be explained in the following. We consider the model quantum sine-Gordon Hamiltonian which typifies either $\mathscr{H}_\rho$ or $\mathscr{H}_\sigma$;

$$\mathcal{H} = \int \mathrm{d}x \left[A(\nabla\theta)^2 + CP^2 - B\cos 2\theta\right] \tag{2.57}$$

where B is assumed to be positive. In SCHA, $\cos 2\theta$ is approximated as

$$\cos 2\theta \to \exp\left[-2\left\langle\theta^2\right\rangle\right]\left[1 - 2\left(\theta^2 - \left\langle\theta^2\right\rangle\right)\right] \tag{2.58}$$

where $\langle\theta^2\rangle$ is the average to be taken with respect to the approximated Hamiltonian. By Equation (2.58) the excitation spectrum of Equation (2.57) is given by

$$\omega(q) = 2\left[C\left(Aq^2 + 2\bar{B}\right)\right]^{1/2} \tag{2.59}$$

where $\bar{B} = B\exp\left[-2\left\langle\theta^2\right\rangle\right]$, which will be evaluated as follows, at $T = 0$, by

$$\left\langle\theta^2\right\rangle = \frac{C}{L}\sum_q \frac{1}{\omega(q)} = \frac{1}{2\pi}\sqrt{\frac{C}{A}}\ln\frac{2\pi}{\alpha q_0}. \tag{2.60}$$

Here the integration over q in Equation (2.60) is cut off by α^{-1} and q_0 is defined by

$$q_0^2 = 2\bar{B}/A = (2B/A)\exp\left[-2\left\langle\theta^2\right\rangle\right] \tag{2.61}$$

Equations (2.60) and (2.61) constitute self-consistent equations for q_0, i.e.

$$q_0^2 = (2B/A)\left(\alpha q_0/2\pi\right)^{\frac{1}{\pi}\sqrt{\frac{C}{A}}}. \tag{2.62}$$

This equation always has a solution $q_0 = 0$, in which case the excitation spectrum does not have a gap. On the other hand it can have a physical non zero solution if the following inequality is satisfied;

$$(C/A)^{1/2} < 2\pi \tag{2.63}$$

In the presence of finite q_0 the excitation spectrum has a gap, $\omega_0 \equiv 2\sqrt{AC'}q_0$, as schematically shown in Figure 5. In this case there exists finite restoring force of the oscillations around $\theta = 0$ (i.e. the phase is pinned) but the force is reduced by $\bar{B}/B$ due to the smearing of the potential cause by the quantum oscillations. Unless Equation (2.63) is satisfied, $\omega_0 = 0$ even if $B \neq 0$ due to the overwhelming quantum fluctuations.

In the BGD model there exists such a type of nonlinearity in $\mathscr{H}_\sigma$, even though $\mathscr{H}_\rho$ is harmonic, i.e.

$$A_\sigma = \frac{v_F}{4\pi}\left(1 - \frac{g_1}{2}\right) \tag{2.64a}$$

$$C_\sigma = \pi v_F\left(1 + \frac{g_1}{2}\right) \tag{2.64b}$$

$$B_\sigma = v_F g_1/2\pi\alpha^2 \tag{2.64c}$$

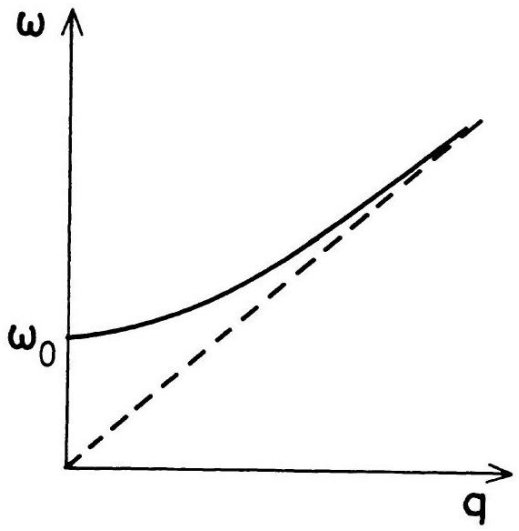


Fig. 5. Excitation spectrum for Equation (2.57).

From Equation (2.63) we see that the excitation spectrum is gapless if $g_1 > 0$ and that $\omega_0 \neq 0$ for $g_1 < 0$. The former (latter) corresponds to the weak (strong) coupling regime. The fact that $g_1 = 0$ separates these two regimes is in agreement with those obtained by the renormalization group treatment [15, 41, 42]. However it remains an unresolved difficulty to obtain, in terms of $\mathscr{H}_\rho$ and $\mathscr{H}_\sigma$, the correct exponents of the response functions even if $g_1 > 0$.

2.3. Conductivity and Spin-susceptibility

The Kubo formula for the conductivity, σ, is given by

$$\sigma(\omega) = i \int_0^\infty \mathrm{d}t e^{-i\omega t} \langle [J(t), P] \rangle, \tag{2.65}$$

where J and P are total electric current and dipole moment, $\dot{P} \equiv (\mathrm{d}/\mathrm{d}t)P = J$. The former is given by the phase variable as

$$J \equiv \int \mathrm{d}x j(x) = \frac{e}{\pi} \int \mathrm{d}x \dot{\theta} = \dot{P} \tag{2.66}$$

where $-e$ is the electronic charge. This is due to the continuity equation $j - e\partial n/\partial t = 0$, with the local number density, n, Equation (2.25). Thus $\sigma(\omega)$, Equation (2.65), is rewritten in terms of the Green function, $D(q, q'; i\omega_n)$, as follows

$$\sigma(\omega) = \frac{i\omega}{2} \left(\frac{e}{\pi}\right)^2 L D(0, 0; i\omega_n) \Big|_{i\omega_n \to \omega - i0^+}, \tag{2.67}$$

where

$$D(q, q'; i\omega_n) = \int_{-\beta}^{\beta} \mathrm{d}\tau e^{i\omega_n \tau} \langle T_\tau \theta_q(\tau) \theta_{-q'}(0) \rangle, \tag{2.68}$$

and

$$\theta(x) = \frac{1}{\sqrt{L}} \sum_q e^{iqx} \theta_q \tag{2.69}$$

In the case of quantum sine-Gordon Hamiltonian, Equation (2.57), treated in the selfconsistent harmonic approximation, $D(q, q', i\omega_n)$ is given as

$$D\left(q,q',i\omega_n\right)=\delta_{q,q'}\frac{4C}{\omega_n^2+\omega(q)^2} \tag{2.70}$$

where $\omega(q)$ is defined by Equation (2.59) and then the frequency dependence of $\sigma(\omega)$ is

$$\sigma(\omega)=\frac{2e^2}{\pi^2}CL\frac{i\omega}{\omega_0^2-\omega^2} \tag{2.71}$$

with $\omega_0\equiv\omega(q=0)$. If $\omega_0\neq 0$, i.e. in the presence of pinning of the phase, the static conductivity is vanishing, while if $\omega_0=0$,

$$\sigma(\omega)=\frac{2e^2}{\pi^2}CL\frac{1}{i\omega}=\frac{Ne^2}{m^*}\frac{1}{i\omega} \tag{2.72}$$

where $N=2k_FL/\pi$ is the total electron number and $m^*=\pi k_F/C$ is the effective mass. The divergence of $\sigma(\omega)$, in this case, Equation (2.72), is due to the sliding of the whole electronic system (sliding mode) [8].

The spin susceptibility, χ, per unit length is defined in terms of the magnetization, M, as

$$\chi=M/HL, \tag{2.73}$$

where H is the uniform magnetic field applied in the z-direction. By use of Equation (2.26), M is given by

$$M=-g\mu_B\sum_i\langle S_{iz}\rangle=-\frac{g\mu_B}{2\pi}\int \mathrm{d}x\langle\nabla\phi\rangle \tag{2.74}$$

where g and $\mu_B=e/2mc$ are the g-factor and the Bohr magneton, respectively, and S_i is the spin matrix. On the other hand, the Zeeman energy, $\mathcal{H}_z$, is written as follows

$$\mathcal{H}_z=h\int \mathrm{d}x\nabla\phi, \tag{2.75}$$

$$h=g\mu_BH/2\pi. \tag{2.76}$$

Thus the first term of the Hamiltonian for the spin part, $\mathfrak{H}_\sigma$, Equation (2.34) is modified by the magnetic field as follows (except some H-dependent constant),

$$A_\sigma(\nabla\phi)^2\to A_\sigma\left(\nabla\phi+q_0\right)^2 \tag{2.77}$$

$$q_0=h/2A_\sigma. \tag{2.78}$$

If $B=0$ in Equation (2.34), the spatial variation of ϕ in the ground state is given so as to minimize Equation (2.77) i.e. $\langle\nabla\phi\rangle=-q_0$ so that χ is given by

$$\chi=\left(g\mu_B\right)^2/8\pi^2A_\sigma \tag{2.79}$$

This is the Pauli paramagnetism modified by interactions.
In the presence of B_σ the classical part of $\mathscr{H}_\sigma$ has the following form (through redefinition of 2ϕ by ϕ and the renormalization and change of sign of numerical factors)

$$E=\int \mathrm{d}x\left[A\left(\nabla\phi-q_0\right)^2-B\cos\phi\right] \tag{2.80}$$

which has the typical energies to describe the commensurate-incommensurate (C − IC) transition [43, 44]. (In Equation (2.80) we assume $A>0, B>0, q_0>0$.)

The spatial variation of ϕ in the ground state is governed by the variational equation

$$2A\nabla^2\phi - B\sin\phi = 0 \tag{2.81a}$$

or

$$A(\nabla\phi)^2 + B\cos\phi = \text{ constant } \equiv C \tag{2.81b}$$

The constant, C, is to be determined so as to minimize E, Equation (2.80). If $C < |B|$, the variation of ϕ is bounded. On the other hand ϕ is steadily increasing as a function of x in the case of $C > |B|$ and the spatial extent, $2\pi/q$, for ϕ to vary 2π is given by

$$\frac{2\pi}{q} = \int_0^{2\pi} \mathrm{d}\phi \frac{\sqrt{A}}{\sqrt{C - B\cos\phi}} \tag{2.82}$$

The ground state energy per unit length, ϵ, is

$$\epsilon = \frac{q}{2\pi}\int_0^{2\pi/q} \mathrm{d}x \left[A\left(\nabla\phi - q_0\right)^2 - B\cos\phi\right] \tag{2.83a}$$

$$= Aq_0^2\left[1 - \sqrt{2}\pi\frac{\sqrt{s}}{kK(k)} + s\left\{4\frac{E(K)}{k^2K(k)} + 1 - \frac{2}{k^2}\right\}\right], \tag{2.83b}$$

$$\equiv Aq_0^2[1 - \sqrt{2}\pi\sqrt{s}f(k,s)] \tag{2.83c}$$

where use is made of Equation (2.82) to derive Equation (2.83b) from Equation (2.83a) and $s = B/Aq_0{}^2$. In Equation (2.83b) $E(k)$ and $K(k)$ are defined by

$$E(k) = \int_0^{\pi/2} \mathrm{d}\theta\sqrt{1 - k^2\sin^2\theta}$$

$$K(k) = \int_0^{\pi/2} \mathrm{d}\theta\frac{1}{\sqrt{1 - k^2\sin^2\theta}}$$

and $k^2 = 2B/(C + B)$. The constant, C, or equivalently, k, is determined by the condition $\partial\epsilon/\partial k = 0$ or $\partial f/\partial k = 0$, $f(k, y)$ being defined in Equation (2.83c). The C-IC transition occurs when $\partial f/\partial k = 0$ is satisfied at $k = 1$, i.e. at $q_0 = Q_c$ where

$$Q_c = \left(\frac{8B}{A\pi^2}\right)^{1/2} \tag{2.84}$$

The $y\,(\equiv Aq_0{}^2/B)$ dependence of q is schematically shown in Figure 6. The spatial variation of ϕ is given by [45, 46]

$$\sin\left\{\frac{1}{2}(2\phi - \pi)\right\} = \mathrm{sn}(x/dk; k) \tag{2.85}$$

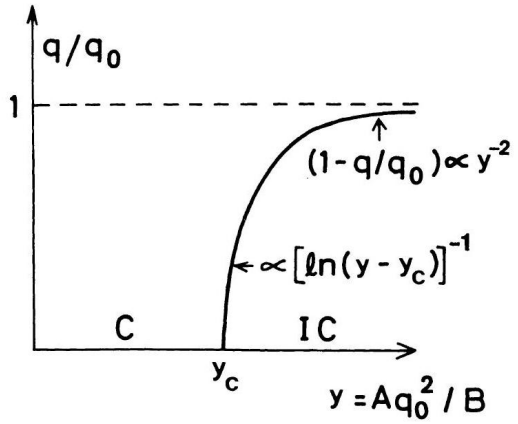


Fig. 6. The dependence of q defined by Equation (2.82) on $y=A q_{0 } ^{2} / B$.

where $d = (2A/|B|)^{1/2}$ and $\mathrm{sn}(z;k)$ is a Jacobian elliptic function with the parameter k. Its explicit spatial variation in the case $q_0 \gtrsim Q_c$ is shown in Figure 7. As seen the spatial variation is not a straight line but has structures known as discommensurations (DC) [47], or a soliton lattice (see Section 3.6).

Since the magnetization, M, is given by q as $M/L = g\mu_B q/4\pi^2$, the strong nonlinearity

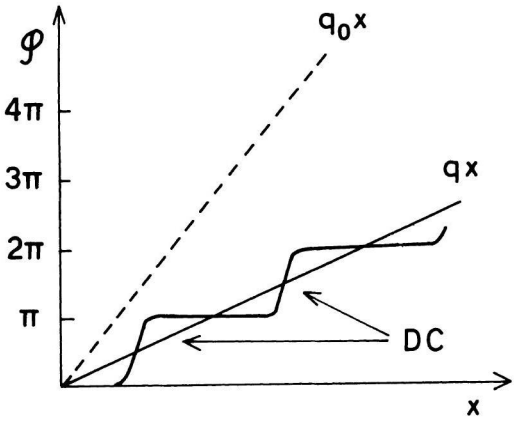


Fig. 7. Spatial variation of ϕ described by Equation (2.85).

of the spin susceptibility is expected. Detailed theoretical examinations on such nonlinearity have been given [48] in the context of the experimental finding in $(TMTSF)_2PF_6$ [49, 50].

2.4. Three-dimensionality and Phase Transition

So far we have discussed one-dimensional systems where there does not exist any phase transition at $T \neq 0$. In the presence of such three-dimensionality as interchain electron transfer or/and interchain interactions one can except a phase transition at finite temperature. In the present scheme the onset of true long range order can be viewed as the pinning of the phase variables to characterize each ordered state (see (2.46)). For the description of the onset of long range order the scheme originally proposed by Scalapino, Imry and Pincus [51] and by Efetov and Larkin [52] is most suited. In this scheme the large fluctuations intrinsic to one-dimensional systems are treated rigorously but the weak three-dimensionality is taken into account in the mean field approximation. This kind of approximation will be valid if the critical temperature,

T_c, of the onset of long range order is much lower than the mean field temperature, T_M, below which the short range order (SRO) is present along each chain. This situation is schematically shown in Figure 8.

In order to illustrate what this scheme implies in the phase Hamiltonian approach we consider the case where the three dimensionality is due to the Coulomb interactions between electrons on different chains forming a square lattice, R_i, (Figure 9). This interchain interaction can be written as

$$\mathcal{H}' = \frac{1}{2}\sum_{i\neq j}\int \mathrm{d}x \int \mathrm{d}x' \rho_i(x)\rho_j(x')\, v_{ij}(x-x')\,,$$

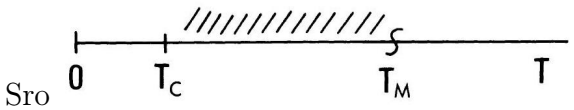


Fig. 8. Schematic representation of various regions in the phase transition of quasi-one-dimensional systems; T_{c}, the true three-dimensional transition temperature, and T_M, the mean field temperature.}

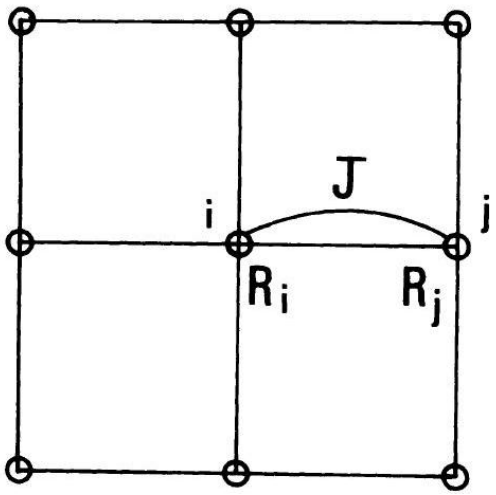


Fig. 9. Model lattice structure in the plane perpendicular to the chain axis.

where $\rho_i(x)$ is the electronic density on the i th chain and $v_{ij}(x-x')$ is given by

$$v_{ij} = \frac{e^2}{\epsilon_0}\frac{1}{\sqrt{(R_i-R_j)^2+(x-x')^2}},$$

where ϵ_0 is the dielectric constant. By use of Equation (2.44) for each chain we obtain

$$\mathcal{H}' = \frac{1}{2}\sum_{i\neq j} J_{ij}\int_{-\infty}^{\infty}\mathrm{d}x\cos\phi_i(x)\cos\phi_j(x)\cos\left(\theta_i(x)-\theta_j(x)\right), \tag{2.86}$$

where θ_i and ϕ_i are phase variables on the i-th chain and J_{ij} is given by

$$J_{ij} = \frac{2e^2}{\epsilon_0(\pi\alpha)^2}\int_{-\infty}^{\infty} \mathrm{d}x \cos 2k_F x \frac{1}{\sqrt{(R_i - R_j)^2 + x^2}}$$
$$= \frac{4e^2}{\epsilon_0(\pi\alpha)^2} K_0\left(2k_F \left|R_i - R_j\right|\right) \tag{2.87}$$

where $K_0(z)$ is the modified Bessel function. In the evaluation of Equation (2.86) we ignore the contribution from the first term in Equation (2.44), since this term does not lead to the pinning of the phase variables. In deriving Equation (2.87) we assumed that the spatial variation of $\theta_i(x)$ is relatively weak in the sense of $\left|\nabla\theta_i\right|/2k_F \ll 1$.

The interchain coupling of the type of Equation (2.86) but without the spin degree of freedom, ϕ_i, has been employed in the discussion of the phase transition in the Peierls systems [53-63], where the quantum fluctuations can also be ignored due to the large effective mass (see Section 3). In this case the effective Hamiltonian is reduced to

$$E = \int \mathrm{d}x \left[\sum_i A\left(\nabla\theta_i\right)^2 + J\sum_{(ij)} \cos\left(\theta_i - \theta_j\right)\right] \tag{2.88}$$

where J_{ij} only between the nearest neighbor chains, (i, j), is retained due to the strong z-dependence of $K_0(z)$ once $z \gtrsim 1$. In the case of a square lattice of our interest, we can change J to $-J$ in Equation (2.88) since the origin of phase variables on one kind of sublattice (Figure 9) can be shifted by π. (Such a transformation is not possible on a triangular lattice, which needs a different treatment.)

In the mean field approximation to the interchain coupling, Equation (2.88) is written as

$$E = \sum_i \int \mathrm{d}x \left[A\left(\nabla\theta_i\right)^2 - \Delta\cos\theta_i\right] \tag{2.89}$$

where the order parameter Δ is given by

$$\Delta = J\sum_j{}' \left\langle\cos\theta_j\right\rangle = zJ\left\langle\cos\theta_i\right\rangle \tag{2.90}$$

and z is the number of nearest neighbour chains ($z = 4$ for Figure 9). Equations (2.89) and (2.90) are self-consistent equations. The critical temperature, T_c, of the onset of long range order is obtained by linearizing the r.h.s. of Equation (2.90) in terms of Δ;

$$1 = (zJ/T_c)\int_{-\infty}^{\infty} \mathrm{d}x' K\left(x, x'\right) \tag{2.91}$$

$$K\left(x, x'\right) = \int \mathrm{d}\theta e^{-\beta_c E_0}\cos\theta(x)\cos\theta\left(x'\right) / \int \mathrm{d}\theta e^{-\beta_c E_0} \tag{2.92}$$

$$E_0 = A\int \mathrm{d}x(\nabla\theta)^2 \tag{2.93}$$

where $\beta_c = 1/T_c$. and the suffix i of the chain is omitted for brevity. The evaluation of $K\left(x, x'\right)$, Equation (2.92), can be made by the Fourier transformation of $\theta(x)$ as in Equation (2.69),

$$E_0 = \sum_k Ak^2\theta_k\theta_{-k}, \tag{2.94}$$

$$\cos\theta(x)\cos\theta(x') \to \frac{1}{2}\,\mathrm{Re}\exp i\left[\theta(x) - \theta(x')\right]$$
$$= \frac{1}{2}\,\mathrm{Re}\exp\left[i\frac{1}{L}\sum_k \theta_k\left(e^{ikx} - e^{ik}x'\right)\right]. \tag{2.95}$$

In Equation (2.95) we ignored the term $\mathrm{Re}\exp i\left[\theta(x) + \theta(x')\right]$ since it results in vanishing contribution. Now the integration over the functional space of θ is performed over those of each Fourier component of θ_k, which is a complex variable,

$$\int \mathrm{d}\theta \to \prod_{k>0}\int \mathrm{d}\theta'_k\mathrm{d}\theta''_k$$

where θ'_k and θ''_k are the real and imaginary parts of θ_k. The resulting Gaussian integration can be performed exactly and we obtain

$$K(x,x') = \frac{1}{2}\exp\left[-\frac{T}{L}\sum_{k>0}\frac{1-\cos k\,(x-x')}{Ak^2}\right]$$
$$= \frac{1}{2}\exp\left[-\left|x-x'\right|/\xi\right] \tag{2.96}$$

where ξ is the correlation length given by

$$\xi = 4A/T. \tag{2.97}$$

Consequently Equation (2.91) implies $1 = zJ\xi/T_c$ or [57, 59]

$$T_c = (4AZJ)^{1/2} \tag{2.98}$$

The physical reason for Equation (2.98) is simple: ξ is the characteristic length for the short range order in a chain and then the energy gain due to phase coherence between chain is of the order of $zJ\xi$, which should compete with the thermal fluctuation, T. The true long-range order will be established once $zJ\xi \sim T$.

Below T_c, Δ of Equation (2.90) is finite and is proportional to $(T_c - T)^{1/2}$ near T_c, which is the typical dependence in the mean field approximation. As the temperature is lowered the quantum fluctuations neglected in Equation (2.88) become important once T is comparable to the zone-boundary frequencies of phason; i.e. $T \lesssim v_\rho\alpha^{-1}$ or $v_\sigma\alpha^{-1}$. In this case the Hamiltonian is reduced to that of a quantum sine-Gordon equation of the type of Equation (2.57).

3.3.3 3. Phase Hamiltonian for the Peierls-fröhlich State

3.1. Peierls-fröhlich State

In the argument described in the preceding section we have implicitly replaced an underlying lattice by a rigid uniform background of positive charge. Here we examine explicitly its degrees of freedom and their coupling to electrons. Peierls [5] first pointed out that in one-dimensional conductors a metallic state is unstable in comparison to the insulating state, in which the lattice is distorted periodically with the wave number $2k_F$ associated with the CDW condensation with the same wave number, whereby a gap opens at the Fermi level in the electronic spectrum. This

is because the gain in the electronic energy due to the gap formation overcomes the expense of the elastic lattice
energy due to the distortion. Fröhlich [6] then argued that the CDW condensate can slide through a system without expenditure of energy, which was claimed at that time to be a possible origin of the superconductivity. It is now well-established that Fröhlich's superconducting mechanism does not work in actual conductors because the CDW condensate is pinned by impurity potential [8] and/or underlying lattice potential [8], and because its motion, even after depinning, suffers from frictions. Many interesting phenomena, however, associated with the Peierls-Fröhlich (PF) state have been observed in quasi-one-dimensional conductors, and they are extensively discussed in this volume.

Below, we first derive the phase Hamiltonian for the PF state in a clean one-dimensional conductor with k_F incommensurate to the reciprocal lattice vector. We then examine the effects of the underlying lattice (or commensurability) potential. Effects of the impurity potential will be explained in the next section in the context of Anderson localization. In this section we mostly ignore the mutual interactions, except in subsections 3.5 and 3.7.

3.2. Dynamics of Phonon Condensate

A model Hamiltonian describing electrons in a linear chain coupled to phonons is given by

$$\begin{aligned}\mathcal{H} =& \sum_{k,s} \epsilon_k c_{ks}^+ c_{ks} + \sum_q \omega_q \beta_q^+ \beta_q + \\ &+ \hat{g} \sum_{k,q,s} \frac{1}{\sqrt{2N\omega_q}} c_{k+qs}^+ c_{ks} \left(\beta_q + \beta_{-q}^+\right), \end{aligned} \tag{3.1}$$

where c_{k_s} and $\beta_q^+$are creation operators for the electron and longitudinal phonon, respectively, $\hat{g}$ is the electron-phonon coupling constant. Here we neglect both interactions between electrons and the coupling between different chains. Because of a perfect nesting of the Fermi surface in one dimension, static lattice distortion with wave number $2k_F \equiv Q$ exist in the ground state, associated with the CDW condensation with the same wave number. Therefore we shall be interested in electrons with momenta $k \simeq \pm k_F$ and in phonons with wave number $q \sim \pm Q$, and rewrite Equation (3.1) as

$$\begin{aligned}\mathcal{H} =& \mathcal{H}_0 + \omega_Q \sum_{|q| \ll Q} \left\{ \beta_{Q+q}^+ \beta_{Q+q} + \beta_{-(Q+q)}^+ \beta_{-(Q+q)} \right\} + \\ &+ \frac{\hat{g}}{\sqrt{2N\omega_Q}} \left[\sum_{\substack{k>0,s \\ |q| \ll Q}} a_{k-Q-q,s}^+ a_{k,s} \left(\beta_{-(Q+q)} + \beta_{Q+q}^+\right) + \text{h.c.} \right], \end{aligned} \tag{3.2}$$

where $\mathcal{H}_0$ is given by Equation (2.2) and we put $q \to Q + q$ and $\omega_{\pm(Q+q)} \simeq \omega_Q$. In the space-coordinate representation Equation (3.2) becomes

$$\mathcal{H} = \mathcal{H}_e\left(\phi_{ph}\right) + \mathcal{H}_{ph} \tag{3.3}$$

$$\begin{aligned}\mathcal{H}_e\left(\phi_{ph}\right) =& \sum_s \int \mathrm{d}x \psi_s^+(x) \left\{ -iv_F \sigma_3 \frac{\partial}{\partial x} + \right. \\ &\left. + \hat{g} \left[\sigma_- \phi_{ph}^*(x) e^{iQx} + \sigma_+ \phi_{ph}(x) e^{-iQx}\right] \right\} \psi_s(x) \end{aligned} \tag{3.4}$$

$$\mathcal{H}_{ph} = \int \mathrm{d}x \left\{ {\omega_Q}^2 \left|\phi_{ph}(x)\right|^2 + \left|\pi_{ph}(x)\right|^2 \right\} \tag{3.5}$$

Here we have introduced the spinor representation ${\psi_s}^+ = \left(\psi_{1s}^+, \psi_{2s}^+\right)$with Pauli matrices σ_i ($\sigma_\pm = \sigma_1 \pm i\sigma_2$). The phonon field $\phi_{ph}(x)$ and its conjugate momentum $\pi_{ph}(x)$ are defined by

$$\phi_{ph}(x) = \frac{1}{\sqrt{2\omega_Q N}} \sum_q e^{-iqx} \left(\beta_{Q+q}^+ + \beta_{-Q-q}\right), \tag{3.6}$$

$$\pi_{ph}(x) = i\sqrt{\frac{\omega_Q}{2N}} \sum_q e^{iqx} \left(\beta_{-Q-q}^+ - \beta_{Q+q}\right). \tag{3.7}$$

Note that the actual lattice distortion $d(x)$ is given by

$$d(x) = 2\,\mathrm{Re}\left\{\phi_{ph}(x)e^{-iQx}\right\} \tag{3.8}$$

i.e. the phonon field ϕ_{ph} here represents the slowly varying part of the lattice distortion. The PF state is characterized by a macroscopic condensation either of the $\pm Q$ phonon mode ($\langle\phi_{ph}\rangle \neq 0$, i.e. a periodic lattice distortion) or by that of the CDW ($\left\langle O_{\mathrm{CDW}}^+\right\rangle \neq 0$, O_{CDW}^+being defined in Equation (2.46a)). In equilibrium both are related by the condition

$$\left\langle \frac{\delta\mathcal{H}}{\delta\phi_{ph}^*} \right\rangle = {\omega_Q}^2 \langle\phi_{ph}\rangle + \hat{g}e^{iQx} \left\langle O_{\mathrm{CDW}}^+\right\rangle = 0 \tag{3.9}$$

Dynamical properties of the PF state are also characterized by dynamics either of the phonon condensate or of the CDW condensate. We will explain these two approaches separately and show that both approaches yield identical results in case where the coupling between lattice distortion and CDW is adiabatic.

Dynamics of the phonon condensate in the PF state was first discussed by Lee, Rice and Anderson [8]. Here we derive an effective Lagrangian $\mathscr{L}(\phi_{ph})$ following the mean field type analysis by Brazovskii and Dzyaloshinskii [64]. The method is to write the partition function, Z, of the system in the functional form of $\phi(x,\tau) \equiv e^{\mathscr{H}\tau}\phi_{ph}(x)e^{-\mathscr{H}\tau}$, thereby eliminating the electronic degrees of freedom. In other words, we derive the action for ϕ_{ph} in the Euclidian space. Neglecting a certain overall normalization constant we write

$$\begin{aligned} Z &= \int D\phi_{ph}(x,\tau) \exp\left[-\int_0^\beta \mathrm{d}\tau \mathscr{L}^{(0)}(\phi_{ph})\right] Z_e\left[\phi_{ph}(x,\tau)\right] \\ &\equiv \int D\phi_{ph}(x,\tau) \exp\left[-\int_0^\beta \mathrm{d}\tau \mathscr{L}(\phi_{ph})\right] \end{aligned} \tag{3.10}$$

where $\mathscr{L}^{(0)}(\phi_{ph})$ represents the free phonon part

$$\mathscr{L}^{(0)} = \int \mathrm{d}x \phi_{ph}^* \left\{-\frac{\partial^2}{\partial\tau^2} + \omega Q^2\right\} \phi_{ph} \tag{3.11}$$

and $Z_e\left[\phi_{ph}\right]$ is the electronic contribution to Z

$$Z_e\left[\phi_{ph}\right] = \mathrm{Tr}\left(T_\tau \exp\left[-\int_0^\beta \mathrm{d}\tau \mathcal{H}_e(\phi_{ph})\right]\right) \tag{3.12}$$

with $\mathcal{H}_e(\phi_{ph})$ being given by Equation (3.4). In Equation (3.12) Tr is over the electronic states in the presence of the potential $\phi_{ph}(x,\tau)$. This formulation is therefore based on the adiabatic approximation: electrons respond instantaneously to the phonon field.

Now we introduce the equilibrium value and the amplitude and phase fluctuations of the field ϕ_{ph}, i.e. Δ, δ and χ, respectively, by

$$\hat{g}\phi_{ph}(x,\tau) = \{\Delta + \delta(x,\tau)\}e^{i\chi}(x,\tau) \tag{3.13}$$

Then by a rotation of the spinor field defined by

$$\tilde{\Psi}_S = U^+ \Psi_S U$$
$$U = \exp\left(\frac{i}{2}\chi\sigma_3\right)$$

where $\tilde{\Psi}_s = \left(e^{ikF^x}\psi_{1s}, e^{-ikF^x}\psi_{2s}\right)$. Equation (3.4) becomes

$$\mathcal{H}_e = \mathcal{H}_e^0 + \mathcal{H}_e^{\text{fluc}} \tag{3.14}$$
$$\mathcal{H}_e^0 = \sum_s \int \mathrm{d}x \tilde{\Psi}_s^+(x) \left\{-iv_F\sigma_3\frac{\partial}{\partial x} + \Delta\sigma_1\right\}\tilde{\Psi}_s(x) \tag{3.15}$$

$\mathscr{H}_e^{\text{fluc}} = \sum_s \int \mathrm{d}x \tilde{\Psi}_s^+(x) \left\{\sigma(x,\tau)\sigma_1 + \frac{v_F}{2}\frac{\partial\chi}{\partial x}\sigma_0 + \frac{i}{2}\frac{\partial\chi}{\partial\tau}\sigma_3\right\}\tilde{\Psi}_s(x)$.

Without the fluctuation part, $\mathcal{H}_e$ fluc , Equation (3.12) is readily evaluated, and the self-consistent equation for Δ derived by the condition $\partial\mathscr{L}/\partial\Delta = 0$ becomes

$$\frac{\omega_{Q^2}}{\hat{g}^2} = 2T\sum_{\epsilon_n}\sum_{k>0}\frac{1}{\epsilon_n^2 + (v_F k)^2 + \Delta^2} \tag{3.17}$$

which is a BCS-type gap equation ($\epsilon_n = (2n+1)\pi T$). It results in a phase transition temperature T_{c0} and Δ at $T = 0$ given by

$$T_{c0} = 1.13\epsilon_F e^{-1/\lambda} \tag{3.18a}$$
$$\Delta = 2\epsilon_F e^{-1/\lambda} \tag{3.18b}$$

where

$$\lambda = \frac{\hat{g}^2}{\pi v_F {\omega_Q}^2} \tag{3.19}$$

is the dimensionless electron-phonon coupling constant.

If fluctuation effects are fully taken into account, the phase transition at a finite temperature disappears in one dimension. But the T_{c0} defined by Equation (3.18a) has the following physical significance: below around $0.25T_{c0}$ a short-range order of ϕ_{ph} is developed [65], so that we can practically regard the amplitude of ϕ_{ph} as being constant. The dynamics of the (quasi) phonon condensate are then analyzed by evaluating contributions of $\mathscr{H}_e$ fluc perturbationally, regarding $\delta, \partial\chi/\partial x$ and $\partial\chi/\partial\tau$ (but not necessarily χ itself) as small parameters. Their explicit evaluation is straightforward, by means of the thermal Green function technique [66], and the resulting Lagrangian becomes (after the analytical continuation $\tau \to it$)

$$\mathscr{L}(\delta,\chi) = \frac{1}{\pi v_F\lambda\omega_Q^2}\int \mathrm{d}x \left\{-\left(\frac{\partial\delta}{\partial t}\right)^2 + a_T\lambda\omega_Q^2\delta^2 + u_a^2\left(\frac{\partial\delta}{\partial x}\right)^2 + \right.$$
$$\left. + \Delta^2\left[-\left(\frac{\partial\chi}{\partial t}\right)^2 + u_p^2\left(\frac{\partial\chi}{\partial x}\right)^2\right]\right\} \tag{3.20}$$

where the velocities of the phase and amplitude modes, u_p and u_a, are given by

$$u_p^2 = \frac{\lambda\omega_Q^2}{4\Delta^2} a_T v_F^2 \tag{3.21}$$

$$u_a^2 = \frac{b_T}{3a_T} u_p^2 \tag{3.22}$$

with

$$a_T = \pi T \sum_{\epsilon_n} \frac{\Delta^2}{\left(\epsilon_n^2 + \Delta^2\right)^{3/2}} \tag{3.23a}$$

$$b_T = 3\pi T \Delta^2 \sum_{\epsilon_n} \frac{\epsilon_n^2}{\left(\epsilon_n^2 + \Delta^2\right)^{5/2}} \tag{3.23b}$$

The above coefficients, a_T and b_T, are unity at $T = 0$ and weakly dependent on T at low temperatures. Note that the time-derivative terms in $\mathscr{L}(0)$, Equation (3.11), appear directly in Equation (3.20), while the space-derivative terms are modified by the electron-phonon interaction (so that we have put $\omega_{Q+q} \simeq \omega_Q$ in Equation (3.2)). The electron-phonon interaction also reduces a gap in the amplitude mode ($\omega_Q \to \lambda^{1/2}\omega_Q$). The effective phase Hamiltonian $\mathcal{H}_{\text{eff}}^0$ is thus given by

$$\mathcal{H}_{\text{eff}}^0 = \pi v' \int \mathrm{d}x \left\{ p^2 + \frac{1}{4\pi^2} \left(\frac{u_p}{v'}\right)^2 \left(\frac{\partial\chi}{\partial x}\right)^2 \right\} \tag{3.24}$$

where $p = \partial\mathscr{L}/\partial\dot{\chi}$ and $v' = {u_p}^2/v_F$. The phase Hamiltonian Equation (3.24) has been derived by Pietronero et al. [9] and Fukuyama [10] by an intuitive argument.

The excitation spectra of the amplitude and phase modes derived from Equation (3.20) agree with those obtained by Lee, Rice and Anderson [8]. (We note that there is a difference of numerical factors between Equation (3.20) and the corresponding Lagrangian originally derived Brazovskii and Dzyaloshinskii [64], who do not consider spin.) Kurihara [67] and Takano [68] have also derived a similar Lagrangian to Equation (3.20), microscopically, but by separating $\hat{g}\phi_{ph}$ into its real and imaginary parts in the evaluation of the electronic contribution, instead of using the direct introduction of the amplitude and phase of $\hat{g}\phi_{ph}$ (Equation (3.13)). They have also calculated such higher-order terms in $\mathscr{L}(\delta, \chi)$ as $\delta^3, \delta\chi^2$ and $\delta^2\chi^2$.

3.3. Dynamics of CDW Condensate

We examine here dynamical properties of the PF state by a complementary approach, namely, the boson representation of the electronic state discussed in Section 2.1. By this approach, interactions between electrons are easily incorporated, as we will see, and $\mathcal{H}_e(\phi_{ph})$ of Equation (3.4) is written as

$$\mathcal{H}_e(\phi_{ph}) = \mathcal{H}_e + \mathcal{H}_{e-p} \tag{3.25}$$

$$\mathcal{H}_e = \int \mathrm{d}x \left\{ A_\rho (\nabla\theta)^2 + C_\rho p^2 + A_\sigma (\nabla\phi)^2 + C_\sigma M^2 \right\} \tag{3.26}$$

$$\mathcal{H}_{e-p} = \tilde{g} \int \mathrm{d}x \cos\phi \left\{ e^{-i\theta}\phi_{ph}(x) + e^{i\theta}\phi_{ph}^*(x) \right\} \tag{3.27a}$$

$$= -\frac{2}{\pi\alpha} \int \mathrm{d}x \Delta \cos\phi \cos(\theta - \chi) \tag{3.27b}$$

Hamiltonian (3.26) is just Equation (2.32), but without the B_ρ and B_σ terms (neglected for the moment). We made use of Equation (2.4) and (2.5) to derive Equation (3.27a) where $\tilde{g} = \hat{g}/\pi\alpha$ and then we put

$$\hat{g}\phi_{ph} = -\Delta e^{i\chi} \tag{3.28}$$

in Equation (3.27a) instead of Equation (3.13).

To discuss the physical significance of the term $\cos(\theta - \chi)$ in Equation (3.27b) it is very important to recognize whether the underlying lattice distortion is static (rigid) or moving with the CDW [26-28]. In case of the static distortion we fix Δ and χ. For simplicity let us consider the case with a uniform Δ and $\chi = 0$. Then Equation (3.25) describes a coupled sine-Gordon system of θ and ϕ, and both modes have an energy gap. At first glance, the gap may involve the cut-off paramater α, but we can show that in the SCHA scheme described in Section 2.2 the renormalized gap in the non-interacting limit coincides with the PF gap 2Δ. That is to say, the excitation spectrum, which corresponds to Equation (2.59), reduces to

$$\omega^2(q) = {v_F}^2 q^2 + 4\Delta^2. \tag{3.29}$$

for both θ and ϕ modes in the present problem. Thus in case of rigid lattice distortion θ and ϕ represent electron-hole pair excitations across the PF gap. It is worth pointing out here that the ground state energy evaluated by the SCHA scheme does not yield correct results. It appears to be due to failure of the SCHA scheme in evaluating shifts in individual energy levels of electrons caused by the lattice distortion, which are supposed to overcompensate the increase of the lattice elastic energy. We emphasize, however, that SCHA is in general a powerful scheme in discussing excitation spectra.

To investigate the case of moving lattice distortion we write down the equations of motion for θ, ϕ and χ deduced from the total Hamiltonian (3.3) as

$$\ddot{\theta} - 4C_\rho A_\rho \nabla^2\theta + \frac{4C_\rho}{\pi\alpha}\Delta\cos\phi\sin(\theta - \chi) = 0 \tag{3.30}$$

$$\ddot{\phi} - 4C_\sigma A_\sigma \nabla^2\phi + \frac{4C_\sigma}{\pi\alpha}\Delta\sin\phi\cos(\theta - \chi) = 0 \tag{3.31}$$

$$\Delta\ddot{\chi} - \frac{\hat{g}^2}{\pi\alpha}\cos\phi\sin(\theta - \chi) = 0 \tag{3.32}$$

Here we consider a situation where the amplitude Δ is static. The adiabatic motion of the CDW condensate coupled to the lattice distortion is represented by the condition

$$\theta = \chi + \chi_0 \tag{3.33}$$

where χ_0 is a certain constant. Then from Equations (3.30) and (3.32) we obtain the equation of motion for θ (or χ) as

$$\left(1 + \frac{4C_\rho\Delta^2}{\hat{g}^2}\right)\ddot{\theta} - 4C_\rho A_\rho\nabla^2\theta = 0 \tag{3.34}$$

In the weak coupling limit ($\lambda \ll 1$) of non-interacting electrons, Equation (3.34) becomes identical to the equation of motion derived from Equation (3.24). Thus we conclude that the phase Hamiltonian, Equation (3.24), with $\chi \sim \theta$ properly describes the dynamics of the CDW condensate adiabatically coupled to the lattice distortion [27, 69-72].

Note that in most of the phenomena of interest (low frequency response and not very close to the PF transition temperature), the dynamics of the CDW amplitude can be neglected.

3.4. Commensurability Energy

If the system is nearly commensurate with the periodicity of the lattice with degree M, (i.e. $G/2k_F \cong M$) there exists an extra energy called the commensurability energy, E_c, as has been noted by Lee, Rice and Anderson [8]. This energy is due to the $2k_F$ scattering of electrons by lattice distortion successively through the states whose momenta are near $(2l-1)k_F (1 \leq l \leq M)$ combined with the Umklapp scattering. In order to evaluate E_c explicitly we consider the tight-binding model (instead of the continuum model of Section 3.2) [70]

$$\mathcal{H}_0 = -\sum_{n,s} t_{n+1,n} \left(c^+_{n+1,s} c_{ns} + \text{ h.c. } \right) \tag{3.35}$$

with

$$t_{n+1,n} = t_0 - \hat{\gamma} \left(u_{n+1} - u_n \right) \tag{3.36}$$

where $c_{n,s}$ and u_n are related to the corresponding quantities in the continuum approximation as follows:

$$c_{n,s} a^{-1/2} = \psi_{1s}(x) + \psi_{2s}(x) \tag{3.37a}$$

$$u_n = \frac{1}{2i} u(x) \exp(i\chi - iQna) + \text{ c.c.} \tag{3.37b}$$

Here a is the lattice constant, $Q = 2k_F$ and $u(x)\exp(i\chi)\,(= \phi_{ph}(x)/2i)$ is the slowly varying part of lattice distortion. The coupling constant, $\hat{\gamma}$, in this tight-binding model is related to $\hat{g}$ in the continuum model by

$$\hat{g} = 2i\hat{\gamma} \left[\sin k_F a - \sin \left(k_F + Q \right) a \right].$$

Note that the factor i connecting the corresponding quantities in the two models is irrelevant, since it simply introduces a constant shift in the phase.

In the present model E_c is given as follows, [28],

$$E_c = -\frac{a}{2} g_M \sum_s \int \mathrm{d}x \left[u^{M-1} \exp[i(M-1)(\chi - Qx) + iGx] \psi^+_{2s} \psi_{1s} + \text{ h.c. } \right] \tag{3.38}$$

where g_M is

$$\begin{aligned} g_M =& \frac{2}{a} \left(-2\hat{\gamma} \sin k_F a \right)^{M-1} \cos 2k_F a \times \\ & \times \prod_{1<l<M} \cos 2lk_F a / \epsilon_{k_F} - \epsilon_{(2l-1)k_F} ! \end{aligned} \tag{3.39}$$

Here we noted that the energy band of electrons, $\epsilon(k)$, in this case is given by $\epsilon(k) = -2t_0 \cos ka$.

In terms of the phase variables, θ and ϕ, Equation (3.38) in the commensurate system ($MQ = G$) reduces to

$$E_c = -\tilde{g}_M \int \mathrm{d}x u^{M-1} \cos(\theta + (M-1)\chi) \cos\phi \tag{3.40}$$

where $\tilde{g}_M = g_M / \pi\alpha$.

3.5. Solitons

The total Hamiltonian describing a one-dimensional electron-lattice system with M commensurability (i.e. $G/2k_F = M$) consists of Equations (2.32), (3.5), (3.27a) and (3.40). In terms of our phase variables representing the electronic state, θ and ϕ, and the amplitude and phase of the slowly varying part of the lattice distortion, u and χ, this Hamiltonian is explicitly given by

$$\begin{aligned}\mathcal{H} = \int \mathrm{d}x \,\big[& A_\rho(\nabla\theta)^2 + C_\rho P^2 + \delta_{M,2} B_\rho \cos 2\theta + \\ & + A_\sigma(\nabla\phi)^2 + C_\sigma M^2 + B_\sigma \cos 2\phi + \\ & + \left\{\hat{g} u \cos(\theta - \chi) - \tilde{g} M u^{M-1} \cos(\theta + (M-1)\chi)\right\} \cos\phi + K' u^2 \big] \qquad (3.41a) \\ \equiv & E[\theta, \phi, u, \chi] + \int \mathrm{d}x \left[C_\rho P^2 + C_\sigma M^2\right] \qquad (3.41b)\end{aligned}$$

where $E[\theta, \phi, u, \chi] \equiv E_T$ is the classical potential energy and $K' \simeq (2\omega_Q)^2$.
Before a systematic analysis of the full Hamiltonian (3.41a), let us consider the simplest situation, namely $\phi(=0)$ and $u\,(=u_0)$ are fixed, $B_\rho = 0$, and with the adiabatic condition Equation (3.33) in the classical approximation. Then Equation (3.41a) reduces to

$$\mathcal{H}' = \frac{A}{2} \int \mathrm{d}x \left\{\dot{\theta}^2 + c_0^2 (\nabla\tilde{\theta})^2 + 2\omega_M^2 (1 - \cos\tilde{\theta})\right\} + \text{ const.} \qquad (3.42)$$

where $\tilde{\theta} = M\theta, A = (2M^2 C_\rho)^{-1}, {c_0}^2 = 4C_\rho A_\rho, {\omega_M}^2 = 2M^2 C_\rho \tilde{g}_M u^{M-1}$, and $\dot{\theta} = 2C_\rho P$ is used. (It should be noted that the non-linear term similar to that in Equation (3.42) results also from the interchain coupling in the IC system treated in the mean field approximation as shown in Equation (2.89). However this approximation to the threedimensionality is valid for low lying excitations only if the system consist of different kinds of chains.) Equation (3.42) is the well-known sine-Gordon Hamiltonian which bears nonlinear solitary waves, i.e., solitons [73]. Solitons are of current interest in various fields of condensed-matter physics [74]; in particular, in connection with the transport properties of the CDW condensate which is discussed elsewhere in this volume and below in Sections 5 and 6.

The Hamiltonian, Equation (3.42), has degenerate, uniform ground states $\tilde{\theta}(x) = 2\pi n$, n being an integer. The linear (small amplitude) excitation spectrum has a gap ω_0, in contrast to the phase mode (phason) in the incommensurate PF state as seen from Equation (3.24). Solitons are nonlinear (large amplitude) excitations connecting these discrete ground states. The soliton in the classical approximation is explicitly given by

$$\tilde{\theta}_S(x,t) = 4\tan^{-1}\left\{\pm \exp\left(\gamma_R \omega_0 (x - vt)/d\right)\right\}, \qquad (3.43)$$

where v is the velocity, $\gamma_R = (1 - v^2/c_0^2)^{-1/2}$, and $+(-)$ indicates soliton (antisoliton). The soliton is localized in space within a range of the order $2d$, where $d = c_0/\omega_0$. Its formation (excitation) energy E_S at $v = 0$ is given by

$$E_S = 8A\omega_0 c_0. \qquad (3.44)$$

Now let us return to the full Hamiltonian (3.41). In the classical approximation the ground states are given as configurations to minimize E_T with respect to all variables, θ, ϕ, u and χ. In the present model of Equation (3.41) the variational equations for u and χ result in equations relating u and χ with θ and ϕ (as we will see explicitly later), i.e., $E[\theta, \phi, u(\theta,\phi), \chi(\theta,\phi)] \equiv V[\theta, \phi]$. Thus the ground states can be specified in the plane of θ and ϕ. Due to the trigonometric dependence on θ and ϕ of the energy, E_T, there exists a discrete degeneracy in the ground state

as in the simpler case of Equation (3.42). The possible types of solitons, which are topological excitations connecting between these degenerate ground states, can be described as trajectories in the plane of these phase variables as x is varied from $-\infty$ to ∞. These trajectories can be given by the potential, $V[\theta, \phi]$, since solitons are variational solutions. Besides its formation energy, such as Equation (3.44), a soliton possesses its own charge and spin, Q and S, which are given by [26]

$$Q = -\frac{e}{\pi}[\theta(\infty) - \theta(-\infty)] \tag{3.45}$$

$$S = \frac{1}{2\pi}[\phi(\infty) - \phi(-\infty)] \tag{3.46}$$

These equations naturally result from Equations (2.25) and (2.26). In a quantummechanical treatment Equations (3.45) and (3.46) still hold if the phase, $\theta(x)$ and $\phi(x)$, are understood as those of the classical parts, $\theta_{cl}(x)$ and $\phi_{cl}(x)$ around which quantum fluctuations, $\hat{\theta}(x)$ and $\hat{\phi}(x)$ are present, i.e. $\theta(x) = \theta_{cl}(x) + \hat{\theta}(x)$ and $\phi(x) = \phi_{cl}(x) + \hat{\phi}(x)$. Ho [75] and Horovitz [76] derived equations similar to Equation (3.45) and (3.46) after the introduction of the order parameters of CDW and SDW. In their treatment θ and ϕ correspond to the phases of these order parameters.

In the following we will discuss the incommensurate, dimerized and trimerized cases separately. [26,28]

(i) Incommensureate Case

In this case we can ignore the Umklapp energy in E_T and take $u(x) > 0$. In the ground state θ always follows χ, which is arbitrary. Consequently θ can not be pinned. There exists, however, a discrete degeneracy in ϕ; i.e. $\phi = m\pi (m = 0, \pm 1, \pm 2, \ldots)$ for $B_\sigma < \tilde{g}^2/8K'$ and $\phi = \pi/2 + m\pi$ for $B_\sigma > \tilde{g}^2/8K'$. This is due to the fact that the variation of E_T with respect to u results in

$$2K'u + \tilde{g}\cos\phi = 0 \tag{3.47}$$

and the substitution of this relation into E_T yields

$$V[\theta, \phi] = \int \mathrm{d}x \left[A_\rho (\nabla\theta)^2 + A_\sigma (\nabla\phi)^2 + B\cos 2\phi - \frac{g^2 \cos^2\phi}{4K'} \right] \tag{3.48}$$

Thus possible solitons in this case are [77]

$$Q = 0, \quad S = \pm\frac{1}{2} \tag{3.49}$$

(ii) Dimerized Case ($M = 2$)

In the case of half-filled band, $E_T \equiv E_2$ is written as follows

$$\begin{aligned} E_2 = \int \mathrm{d}x \, \big[& A_\rho (\nabla\psi)^2 + A_\sigma (\nabla\phi)^2 - B_\sigma \cos 2\psi + B_\sigma \cos 2\phi + \\ & + K'u^2 - 2\tilde{g}u\cos\psi\cos\phi \big] \end{aligned} \tag{3.50}$$

where we put $\chi = \pi/2$ so that $u(x)$ represents an amplitude of the staggered displacement u_n, and $\psi = \theta + \pi/2$, and $\tilde{g}_2 \equiv \tilde{g}$. Varying with respect to $u(x)$, we obtain

$$u(x) = \frac{\tilde{g}}{K'}\cos\psi\cos\phi \tag{3.51}$$

Thus the effective Hamiltonian for ϕ and ψ is given as follows

$$V_2[\psi,\phi] = \int \mathrm{d}x \left[A_\rho(\nabla\psi)^2 + A_\sigma(\nabla\phi)^2 + U_2(\psi,\phi)\right] \tag{3.52}$$

$$U_2(\psi,\phi) = -\frac{\tilde{g}^2}{K'}\cos^2\psi\cos^2\phi - B_\rho\cos 2\psi + B_\sigma\cos 2\phi \tag{3.53}$$

It is clear that ψ and ϕ in the ground state are spatially constant. They are given by the minimum points of $U_2(\psi,\phi)$. It is seen that the ground state is dimerized under the following conditions,

$$\frac{2K'B_\sigma}{\tilde{g}^2} < 1, \quad \frac{2K'B_\rho}{\tilde{g}^2} > -1, \quad \text{and} \quad \frac{2K'}{\tilde{g}^2}(B_\sigma - B_\rho) < 1 \tag{3.54}$$

The magnitude of the bond alternation u_0 in the ground state and the energy E_0 per unit length are given by

$$u_0 = \tilde{g}/K', \tag{3.55}$$

$$E_0 = B_\sigma - B_\rho - \tilde{g}^2/K'. \tag{3.56}$$

Possible soliton excitations from this ground state are described as solutions of the following simultaneous equations.

$$A_\rho\nabla^2\psi - B_\rho\sin 2\psi - \frac{\tilde{g}^2}{K'}\sin\psi\cos\psi\cos^2\phi = 0, \tag{3.57}$$

$$A_\sigma\nabla^2\phi + B_\sigma\sin 2\phi - \frac{\tilde{g}^2}{K'}\sin\phi\cos\phi\cos^2\psi = 0. \tag{3.58}$$

Various types of solitons are characterized by the trajectories in the $\theta - \phi$ plane as x is varied from $-\infty$ to ∞, which is schematically shown in Figure 10. In this figure dots

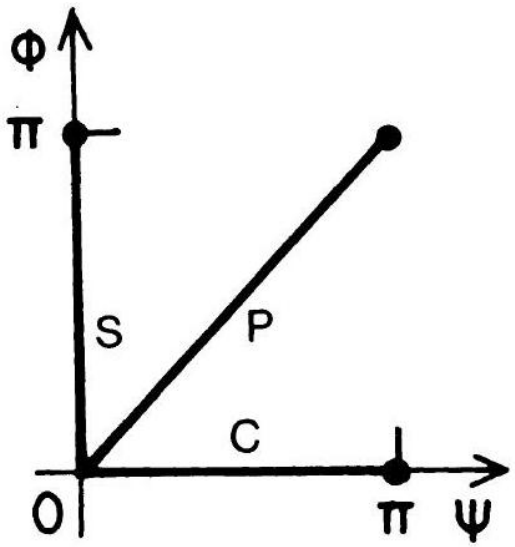


Fig. 10. Classifications of solitons in the dimerized system.

correspond to the configuration in the ground state. From this figure it is evident that the fundamental types of solitons are those denoted as C, S, and P;

$$\begin{array}{ll} C \text{ (Charge Soliton)} & : Q = \pm e, \quad S = 0, \\ S \text{ (Spin Soliton)} & : Q = 0, \quad S = \pm 1/2, \\ P \text{ (Polaron)} & : Q = \pm e, \quad S = \pm 1/2. \end{array}$$

These charge and spin solitons were discussed by Su, Schrieffer and Heeger [78. 79] and independently by Rice [80] based on the tight-binding model of Equations (3.35) and (3.36) to interpret various interesting properties of polyacetylene. Later Takayama, Lin-Liu and Maki [81] and Horovitz [82] found the exact solutions for these solitons in a continuum version of their model. Furthermore, the polaron has been observed in dynamical computations by Su and Schrieffer [83], and been analytically examined in a continuum limit by Campbell and Bishop [84] and by Brazovskii [85, 86]. In these investigations, however, the mutual Coulomb interaction between electrons is not explicitly considered. By the phase Hamiltonian approach described above [28], on
the other hand, we could easily take into account such interaction effects in the most general form, and can at the same time obtain a unified description for various solitons. In this respect it is to be noted that, though the net Q and/or S is not changed, the trajectories in $\theta - \phi$ plane are not necessarily straight in the presence of mutual interactions. For some choice of interaction paramaters the solitons of the type shown in Figure 11 can also be expected. These are termed charge (solid line) and spin (broken line) bisolitons.

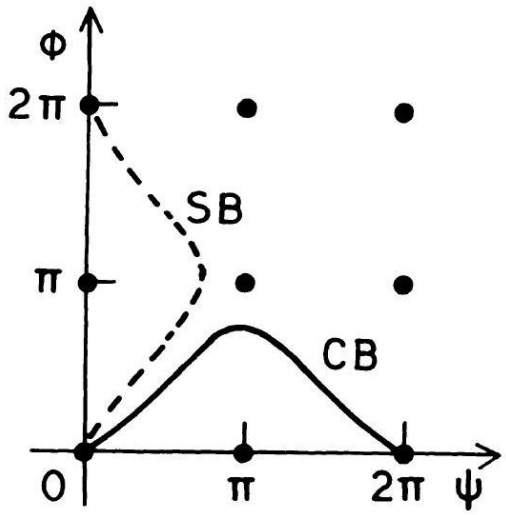


Fig. 11. Trajectories of charge and spin bisolitons.

(iii) Trimerized case ($M = 3$)
For a third-filled band, $E_T \equiv E_3$ is written as follows.

$$E_3 = \int \mathrm{d}x \left[A_\rho (\nabla\theta)^2 + A_\sigma (\nabla\phi)^2 + B_\sigma \cos 2\phi + K' u^2 + \right. \\ \left. + \left\{ \tilde{g} u \cos(\theta - \phi) - \tilde{g}_3 u^2 \cos(\theta + 2\chi) \right\} \cos\phi \right] \tag{3.59}$$

The local minimum condition for E_3 with respect to u and χ yields

$$v \equiv u \sin\chi = \frac{\tilde{g}}{2K'} \cos\phi \sin\theta [2\kappa \cos\theta \cos\phi - 1], \tag{3.60}$$

$$w \equiv u \cos\chi = -\frac{\tilde{g}}{2K'} \cos\phi [\cos\theta + \kappa \cos\phi \cos 2\theta], \tag{3.61}$$

where v and w are approximated by keeping terms up to first order of small parameter $\kappa = \tilde{g}_3/K'$. Substituting v and w into E_3, we obtain effective Hamiltonian for θ and ϕ as

$$V_3[\theta,\phi] = \int \mathrm{d}x \left[A_\rho(\nabla\theta)^2 + A_\sigma(\nabla\phi)^2 + U_3(\theta,\phi)\right] \tag{3.62}$$

$$U_3(\theta,\phi) = -\frac{\tilde{g}^2}{4K'}\cos^2\phi[1+\kappa\cos\phi\cos 3\theta] + B_\sigma\cos 2\phi \tag{3.63}$$

The ground states are trimerized in the following region

$$\frac{8K'B_\sigma}{\tilde{g}^2} < (1+\kappa) \tag{3.64}$$

As in the case of the dimerized system, various possible types of soliton excitations can be expected and they are schematically shown in Figure 12. The shapes of solitons are determined by the following equations.

$$A_\rho\nabla^2\theta - \frac{3}{8}\frac{\tilde{g}^2}{K'}\kappa\cos^3\phi\sin 3\theta = 0, \tag{3.65}$$

$$A_\sigma\nabla^2\phi + B_\sigma\sin 2\phi - \frac{\tilde{g}^2}{16K'}\sin 2\phi(2+3\kappa\cos\phi\cos 3\theta) = 0. \tag{3.66}$$

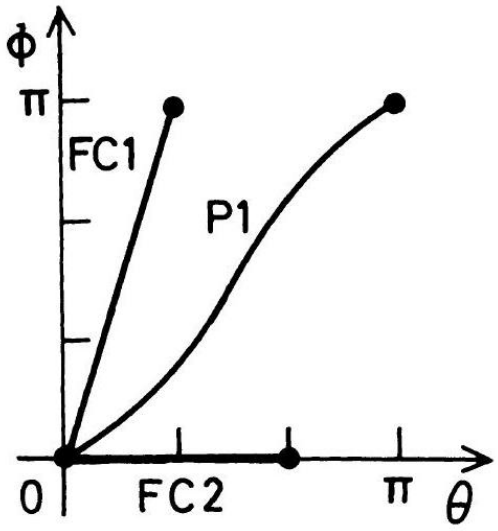


Fig. 12. Classification of solitons in the trimerized system.

The fundamental types of solitons classified typically as $FC1, FC2, P$ in Figure 12 have following features;

$FC1$ (Fractional Charge Soliton)	:	$Q = \pm e/3$,	$S = \pm\frac{1}{2}$,
$FC2$ (Fractional Charge Soliton)		: $Q = \pm 2e/3$,	$S = 0$,
P (Polaron)		: $Q = \pm e$,	$S = \pm\frac{1}{2}$.

These solitons with fractional charges in trimerized state without interactions between electrons have been discussed based on the tight-binding model by Su and Schrieffer [78, 87] and on its continuum version by Gammel and Krumhansl [88].

3.6. Soliton Lattice

Next we examine the incommensurate PF state which is nearly commensurate, i.e. $2k_F \cong G/M$. For simplicity we consider here only the charge degree of freedom in the presence of static lattice distortion. The effective phase Hamiltonian derived from Equations (3.5), (3.26), (3.38) becomes [89]

$$\mathcal{H}^{c}_{\text{eff}} = \pi v' \int \mathrm{d}x \left[p^2 + \frac{1}{4\pi^2 v'^2} \times \right. \\ \left. \times \left\{ {u_p}^2 \left(\nabla\theta - q_0 \right)^2 + \frac{2\omega_{M^2}}{M^2} (1 - \cos M\theta) \right\} \right] \tag{3.67}$$

instead of $\mathcal{H}^{0}_{\text{eff}}$ of Equation (3.24). Here $q_0 = 2k_F - G/M$ and ω_M, already appeared in Equation (3.42), is given in this case by ${\omega_M}^2 = {\omega_Q}^2 \left(\Delta/\epsilon_F\right)^{M-2}$. The ground state is determined by the classical part of Equation (3.67). The latter is essentially identical to Equation (2.80), which has already been discussed in Section 2.3. The stationary solution of Equation (3.67) is given by Equation (2.85) with $2\phi = M\theta$ and $d = u_p/\omega_M$ in this case. For a small q_0 this solution, as shown schematically in Figure 7, is regarded as a periodic array of solitons, i.e. a soliton lattice. Its period l is given by Equation (2.82), i.e. $l = 2\pi/q = 2dkK(k)$, where $K(k)$ is the complete elliptic integral with a parameter k.

It is worth noting here the difference between q_0 and q. In the susceptibility problem discussed in Section 2.3, q_0 is a given parameter proportional to an external magnetic field (Equation (2.78)), while q, or equivalently a parameter k (or a constant C in Equation (2.81b)), is determined so as to minimize the energy of Equation (2.80). In the present case the incommensurability of $2k_F$ to G, i.e., a nonvanishing q_0, is determined by the charge transfer between the band which undergoes the PF condensation and the remaining bands (which are often called as a charge reservoir). The degree of the charge transfer is in turn determined so as to minimize the total energy involving also the energy of the charge reservoir and then the problem is not determined within the band which undergoes the PF transition. What is observed directly in experiments on the incommensurate PF state is q. The nonvanishing parameter q_0 simply indicates that the charge transfer yields an incommensurate k_F. The situation is more clearly seen in the problem of a doped polyacetylene. Since there is no charge reservoir in this system, q is directly related to the excess charge introduced by doping through Equation (2.44) and (2.82) [69].

3.7 Spin-peierls State

In Section 3.5 we have emphasized that by the present phase Hamiltonian approach we can easily take into account the mutual Coulomb interaction. In the argument there, however, the mutual interaction is assumed to be weak and then the charge and spin degrees of freedom are treated on an equal footing. In the case of very strong repulsive interactions, however, the charge fluctuations are usually suppressed. Especially, if the band is half-filled, the low lying excitations are exclusively of spin origin. This is seen most easily in the Hubbard model

$$\mathcal{H} = \mathcal{H}_0 + U \sum_i n_{is} n_{i-s}, \tag{3.68}$$

where $\mathcal{H}_0$ is given by Equation (3.35) and $n_{is} = c^{+}_{is} c_{is}$. If $U \gg t_0$ in the half-filled band, the low lying excitations of Equation (3.68) are described by the following Hamiltonian of Anderson's kinetic exchange interactions;

$$\mathcal{H} = \sum_n J_{n+1,n} S_{n+1} S_n, \tag{3.69}$$

where $J_{n+1,n} = 4t_{n+1,n}^2/U$, and the problem is reduced to that of a spin-Peierls transition [31]. Below we explain an alternative phase Hamiltonian approach to this problem [29, 30].

(a) Undistorted lattice

If the lattice is undistorted, $J_{n+1,n}$ is uniform in space, $J_{n+1,n} = J$. The Hamiltonian is conveniently transformed into that of the spinless fermions by use of the JordanWigner transformation [31] ;

$$S_l^+ = \exp\left[-i\pi \sum_j^{l-1} a_j^+ a_j\right] a_l^+ = \left(S_l^-\right)^+ \tag{3.70a}$$

$$S_l^z = -\frac{1}{2} + a_l^+ a_l \tag{3.70b}$$

$$S_l^+ S_{l+1}^- = a_l^+ a_{l+1} \tag{3.70c}$$

The resulting Hamiltonian is

$$\mathcal{H} = \sum \epsilon(k) a_k^+ a_k + \frac{1}{N} \sum V(q) a_{k+q}^+ a_{k'-q}^+ a_{k'} a_k, \tag{3.71}$$

where

$$\epsilon(k) = J(\cos ka - 1) \tag{3.72a}$$

$$V(q) = J \cos qa \tag{3.72b}$$

Here a is the lattice spacing and the energy band of this spinless fermion is half-filled, i.e. $k_F a = \pi/2$. The second term of the r.h.s. of Equation (3.71) can be treated as in Section 2 by taking the scattering near or across the Fermi surface into account; i.e. $q \simeq 0$ or $|q| \simeq Q$ and $|q| \simeq 2Q$ (Umklapp scattering).

By repeating the argument of Section 2, we immediately see that Equation (3.71) can be transformed to the phase Hamiltonian, and the result is [29,30]

$$\mathcal{H} = \int \mathrm{d}x \left[A(\nabla\phi)^2 + CM^2 - D\cos 2\phi\right], \tag{3.73}$$

$$A = \frac{Ja}{8}, \tag{3.74}$$

$$C = \frac{\pi^2}{2} Ja \tag{3.75}$$

$$D = \frac{\pi^2 J}{8a} \tag{3.76}$$

Here the cut-off parameter, α, is chosen as a/π. The last term in r.h.s. of Equation (3.73) is due to the Umklapp scattering [91]. The results for A and C, Equation (3.74) and (3.75), already take into account of the corrections caused by the linearization of the energy spectrum, $\epsilon(k)$, Equation (3.72a), and have been adjusted along the procedures proposed by Cross and Fisher [92] so that Equation (3.73) yields the known exact results. The phase variable, $\phi(x)$, is related to the spin operator, $S_z(x)$, by

$$S_z(x) = \frac{1}{a}\cos\left(2k_F x + \phi(x)\right) + \frac{1}{2\pi}\nabla\phi(x) \tag{3.77}$$

The Umklapp term will be treated in SCHA, introduced in Section 2.2, and the result of this approximation is that for the values of A and C of Equation (3.74) and (3.75), $\bar{D} \equiv D \exp\left[-2\left\langle\phi^2\right\rangle\right] = 0$, i.e. the quantum fluctuations destroy the last term in Equation (3.73) and then there is no preference for any particular value of phase, ϕ, resulting in degeneracy with respect to its value, Reflecting this degeneracy, the spectrum of the excitation, which is the spin wave, does not have a gap.

It is to be noted that $\phi = 0$ corresponds to the Neel state, as may be seen from Equation (3.77). (On each lattice site, $R_n, 2k_F R_n$ is a multiple of π.) On the other hand, $\phi = \pi/2$ corresponds to the non-magnetic state. Then the degeneracy in ϕ implies that the ground state of a spin 1/2 Heisenberg antiferromagnet can have both aspects of the Néel state and the non-magnetic (singlet) state, as stressed by Anderson [93]. The present phase Hamiltonian approach reveals this fact very clearly [30].

(b) Distorted Lattice

In the presence of the coupling between spin and lattice distortion, we write $J_{n+1,n}$ in Equation (3.69) as

$$J_{n+1,n} = J\left[1 + \lambda \frac{u_{n+1} - u_n}{2a}\right] \tag{3.78a}$$

$$u_n = (-)^n u \tag{3.78b}$$

The modulation of the exchange constant introduces an extra energy to Equation (3.73), which is

$$\mathscr{H}' = \int \mathrm{d}x \left[-B \sin\phi + \frac{2Ku^2}{a}\right] \tag{3.79}$$

where

$$B = J\lambda u / a^2 \tag{3.80}$$

and K is the elastic constant. The B-term in Equation (3.79) prefers the state with $\phi = \pi/2$. The total Hamiltonian, $\mathcal{H}_0 + \mathcal{H}'$, can also be treated in SCHA, which leads to the conclusion that the energy gain of a spin system due to the coupling to the lattice distortion, i.e., the B-term, is proportional to $u^{4/3}$. This 4/3 power, which is in contrast to $u^2 l^2 u$ obtained in the mean field approximation, has been derived by Cross and Fisher [92] and is consistent with the result of numerical calculations [94, 95] and the renormalization group treatment [96-98]. The presence of such a large energy gain is due to the fact, mentioned previously, that the ground state contains wave functions of a singlet character, $\phi = \pi/2$.

It is to be noted that the present phase Hamiltonian is capable of describing such a subtle problem [30] as well as nonlinear excitations, i.e. solitons in this system [29], in a simple way.

3.3.4 4. Impurity Pinning and Anderson Localization

4.1. Impurity Pinning of CDW

So far only clean systems without imperfections have been considered. In actual systems there exist various kinds of randomness. In this section, the effects of impurities will be considered as a typical example of randomness.

The interaction energy between electrons and impurities is given by

$$\mathcal{H}_{\mathrm{imp}} = \sum_i \int \mathrm{d}x \rho(x) v\left(x - R_i\right), \tag{4.1}$$

where $\rho(x)$ is the local electron density and the summation is over impurity sites, R_i. The impurity potential, $v(x)$, is assumed to be of short range, $v(x) = \tilde{V}_0\delta(x)$. By use of Equation (2.44) we write Equation (4.1) as

$$\begin{aligned}\mathcal{H}_{\text{imp}} &= \tilde{V}_0 \sum_i \nabla\theta\left(R_i\right)/\pi + V_0 \sum \cos\phi\left(R_i\right)\cos\left(QR_i + \theta\left(R_i\right)\right) \\ &= \mathcal{H}_{\text{imp}}^{(1)} + \mathcal{H}_{\text{imp}}^{(2)} \end{aligned} \tag{4.2}$$

where $Q = 2k_F$ and $V_0 = 2\tilde{V}_0/\pi\alpha$. The first term on the r.h.s. of Equation (4.2) represents the coupling of long wave fluctuations to the impurities, whereas the second term corresponds to the backward scattering.

In the case of the PF state, which is considered in this sub-section, the spin degree of freedom is not essential, and needs not to be treated explicitly. Hence we ignore the factor $\cos\phi\left(R_i\right)$ by incorporating the possible effects into V_0. Bak and Brazovskii [59] indicated that $\mathcal{H}_{\text{imp}}^{(1)}$, through which only $\nabla\theta$ is coupled to the random potential, does not necessarily destroy the long range order. On the other hand it has been shown by a general argument [99-101] that the perturbation, which directly couples θ to impurities, destroys the long range order, and $\mathcal{H}_{\text{imp}}^{(2)}$ can be considered as an example of such a kind of perturbation [10, 11, 102, 103]. By this reason $\mathcal{H}_{\text{imp}}^{(2)}$ is more important
in the pinning problem and then we will mainly be concerned with this term. Consequently, by use of Equation (3.24), the ground state of the incommensurate CDW in the adiabatic approximation is described by the following Hamiltonian, with $A = v_F/4\pi$,

$$E = \int \mathrm{d}x \left[A(\nabla\theta)^2 + V_0 \sum_i \delta\left(x - R_i\right)\cos(Qx + \theta)\right]. \tag{4.3}$$

The problem characterized by Equation (4.3) is complicated because of the existence of two competing energies, the elastic energy (the first term) which prefers the spatially uniform phase, and the impurity energy (the second term) which introduces the distortion of the phase so that $\cos\left(QR_i + \theta\left(R_i\right)\right)$ can be as small ($V_0 > 0$ is assumed) as possible at each impurity. The former energy prefers the translationally invariant state, while the latter prefers the distorted phase fixed in space, reflecting the random configurations of impurities. This is the impurity pinning of the phase variable. As is easily understood, the problem is highly nonlinear and ordinary perturbation theory is not appropriate.

The characteristic parameter in the present problem is

$$\epsilon = V_0/n_i v_F, \tag{4.4}$$

where n_i is the average density of impurities. This is seen as follows; if the impurity potential dominates, then the phase will adjust itself so that $\Theta\left(R_i\right) = \pi$ with the modulus of 2π at each impurity site, where $\theta(x)$ is the total phase $\Theta(x) = Qx + \theta(x)$. The system will gain the impurity potential energy of $n_i V_0$, while paying the elastic energy of the order of $A\left(1/n_i\right)n_i^2 = O\left(n_i v_F\right)$ per impurity. Thus the ratio of these, which is given by Equation (4.4), is expected to characterize the impurity pinning mechanism in each system. In fact, in the strong pinning limit $\epsilon \gg 1$, the preferable configuration should satisfy the condition $\cos\theta = -1$ at each R_i as shown schematically in Figure. 13. In the

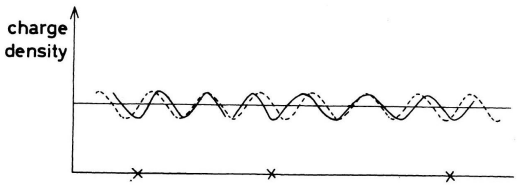


Fig. 13. Schematic representation of the case of the strong pinning, $\epsilon \gg 1$, where crosses represent impurities.

weak pinning limit $\epsilon \ll 1$, on the other hand, $\theta(x)$ is varying slowly from one impurity site to the next and $\Theta(R_i)$ are distributed almost randomly. But they are not completely random and the impurity pinning mechanism does exist, even in this limit. This is due to the following fact.

If $\epsilon \ll 1$, the characteristic length, L_0, can be considered, which is much longer than the average distance between impurities, ${n_i}^{-1}$, and over which θ varies of the order of π. This L_0 is to be determined variationally. For any point on a chain, $\mathbf{x}$, the phase is taken as common in the interval $(x - L_0/2, x + L_0/2)$, and we treat the impurity potential as [11, 104]

$$V_0 \sum_i{}' \cos\left(Qx_i + \theta\left(x_i\right)\right)$$

$$= V_0 \,\mathrm{Re}\, e^{i\theta(x)} \sum_i{}' e^{iQx_i} \tag{4.5a}$$

$$= V_0 \sqrt{n_i L_0}\cos(\alpha(x) + \theta(x)) \tag{4.5b}$$

where the summation is over impurities in the interval ($x - L_0/2, x + L_0/2$) and $\alpha(x)$ is as defined in Figure 14. In Equation (4.5a) it is assumed that Qx_i is completely random

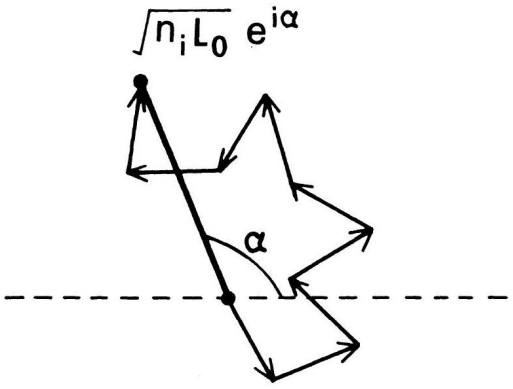


Fig.14. The determination of $\alpha(x)$ of Equation (4.5b) in the case of weak pinning, $\epsilon \ll 1$.

and $n_i L_0 \gg 1$. The fluctuation of a number of impurities in the interval L_0 is ignored. By definition $|\nabla\alpha| \simeq {L_0}^{-1}$. If $\theta(x)$ follows $\alpha(x)$, i.e. $\cos(\alpha(x) + \theta(x)) = -1$, there exists an energy gain from the impurity potential, $-\sqrt{n_i/L_0}V_0$, per unit length. Then E, Equation (4.3), is estimated as

$$\frac{E}{L} = A\frac{1}{bL_0^2} - \sqrt{\frac{n_i}{L_0}}V_0, \tag{4.6}$$

where b is a numerical factor of the order of unity; $b = 3/\pi^2$ if the phase difference from section to section is random between $-\pi$ and π and if the true solution smoothly interpolates between them.

The variation of Equation (4.6) with respect to L_0 results in

$$L_0{}^{-1} = \left[(b\pi V_0/v_F)^2\, n_i\right]^{1/3}, \tag{4.7a}$$

or in terms of ϵ, Equation (4.4),

$$(n_i L_0)^{-1} = (b\pi\epsilon)^{2/3} \tag{4.7b}$$

This is the result for the case of weak pinning. On the other hand, $L_0{}^{-1} \sim n_i$, in the case of strong pinning, i.e. $\epsilon \gg 1$.

The existence of finite L_0, in either case, results in a vanishing static conductivity at $T = 0$, since the pinning frequency ω_0 in Equation (2.71) will be typically of the order of $\omega(q)$ at $q = L_0{}^{-1}$. Analytical calculations of $\sigma(\omega)$ at $T = 0$ in the limits of weak and strong pinning have been done by Fukuyama and Lee [11], and the result is schematically shown in Figure 15. In contrast to the case with one definite ω_0, Re

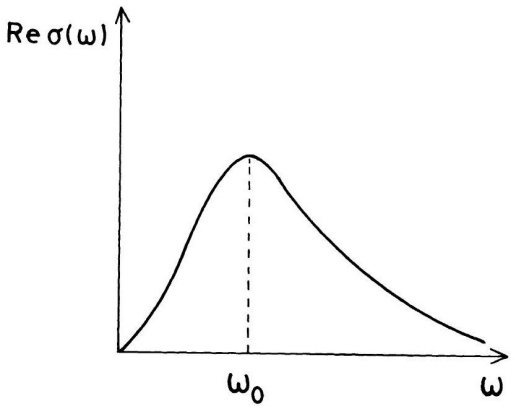


Fig.15. Schematic representation of $\operatorname{Re}\sigma(\omega)$.

$\sigma(\omega)$ has a broad spectrum reflecting the random configuration of impurities. More detailed analytical investigation of this problem has been performed by Feigelman [105] , who employed the transfer matrix and the distribution function for random systems and obtained results essentially similar to the previous discussions.

There exist also numerical calculations. Ternaishi and Kubo [106] solved the following equation for a fixed configuration of impurities derived by the variation of Equation (4.3) with respect to θ;

$$2A\nabla^2\theta + V_0 \sum_i \delta\left(x - R_i\right) \sin(Qx + \theta) = 0. \tag{4.8}$$

Their results for $\sigma(\omega)$ and the analytical results, are in close agreement, and the existence of two characteristic regime of weak and strong pinning has been confirmed. Similar results have also been obtained by molecular-dynamics studies by Koehler and Lee [107].

Weisz, Sokoloff and Sacco [108] extended the model to two and three dimensions on a discrete lattice and found that the low lying excitations are localized, i.e. pinned by impurities. Lee and Fukuyama [109] have shown the existence of finite L_0 even for the three dimensional systems with the long range Coulomb interactions which play an important role.

In the presence of finite electric field, E, one should take the following energy, E_e, into account;

$$E_e = PE = \frac{e}{\pi}\int \mathrm{d}x\theta(x)E \tag{4.9}$$

where P is the electric dipole moment defined in Equation (2.66). In the presence of E_e, Equation (4.9), one could expect a strong non-Ohmicity, which is actually demonstrated in the numerical calculations by Teranishi and Kubo [106]. Especially they found that at $T \neq 0$ the static conductivity is of activation type, the activation energy of which decreases linearly in proportion to the electric field. In this non-Ohmic conduction process, and also for the Ohmic conduction at $T \neq 0$, the large local changes of θ overcoming the potential barriers are essential (see also [144]).

As the field gets stronger the CDW is expected to be depinned [110,111]. Lee and Rice [112] estimated such depinning field, E_T, in quasi-one-dimensional systems by balancing the energy gain by impurity pinning with that by the electric field when the phase is advanced by 2π. They concluded that $E_T \propto n_i$ and ${n_i}^2$ for strong and weak pinning, respectively. (Quite recently Klemm and Schrieffer [113] obtained $E_T \propto {n_i}^2$ for weak pinning by different method.) Sokoloff [114] performed molecular-dynamical studies of the depinning by extending the calculations of Teranishi and Kubo [106] to longer chains and observed the existence of finite E_T (see also [215]).

In the commensurate or near-commensurate systems the energy to be considered is, instead of Equation (4.3), typically given by

$$E = \int \mathrm{d}x \left[A\left(\nabla\theta - q_0\right)^2 - B\cos M\theta + V_0 \sum_i \delta\left(x - R_i\right)\cos(Qx + \theta) \right] \tag{4.10}$$

In the case of $q_0 = 0$ and $M = 1$ [104] it is found that the long range order is found to be stable at absolute zero as far as the impurity potential is not too strong, while the glassy state (charge density glass (CDG)) where the phase is pinned by impurities is realized for strong impurity potentials. On the other hand, Nakanishi [115] examined the case of $q_0 = 0$ and $M = 3$, who found that the long range order is unstable for an arbitrary weak impurity potential in spite of the existence of the commensurability potential. Littlewood and Rice [116] examined the case where $q_0 \neq 0$ and $B = 0$ by Monte-Carlo calculations in the context of the pressure-induced hysteresis in Cr and found that the wave vector of CDW lags behind the equilibrium value, and that changes by addition or removal of phase solitons result in the characteristic feature of the glassy state: the metastability.

Similar problems but with $\mathcal{H}^{(1)}_{\mathrm{imp}}$ instead of $\mathcal{H}^{(2)}_{\mathrm{imp}}$ in Equation (4.2) have been considered. Baeriswyl and Bishop [117] examined the static correlation function and the dynamic structure factor in the case of $q_0 = 0$ and $M = 1$ and Rice et al. [118] considered the impurity pinning of the discommensurations for $q_0 = 0$ and arbitrary M. The dynamics of sine-Gordon solitons have also been examined by Fogel et al. [119] in the presence of an impurity.

The complete pinning at $T = 0$ so far explained is affected by thermal fluctuations and by possible thermal depinning, as the case may be [118, 120-122]. Above the critical temperature, T_P, of the Peierls transition the fluctuations affect the conductivity; in the temperature regime very close to T_P and then if L_0, Equation (4.7a), is shorter than the coherence length ξ, the impurity will reduce the conductivity [123] as ξ gets longer, while at higher temperatures where $\xi \ll L_0$ conductivity will increase as ξ gets longer since impurity scattering will be irrelevant [124, 125, 125a].

As has been discussed in detail so far, the important feature of the impurity pinning lies in the spatial distortions of the phase in the ground state, reflecting the random configurations of impurities. However, if the quantity of interest is not so sensitive to such spatial variations,

the pinning may conveniently be described by an averaged potential deduced from Equation (4.5b), i.e.

$$V_0 \sum_i \cos\left(Qx_i + \theta\left(x_i\right)\right) \rightarrow W \int \mathrm{d}x \cos\theta(x) \tag{4.11}$$

where $W \sim AL_0{}^{-2}$. In Section 5 we will see consequences of such simplifying approximation.

4.2 Anderson Localization

In the preceeding section we discussed the impurity pinning of the phase of the charge density wave in Peierls systems, and found that impurities play an essential role. Such impurity pinning in the Peierls system can be viewed as one aspect of Anderson localization, as we will see explicitly. In usual cases, without the Peierls distortion, however, the spin degree of freedom, ϕ, has to be taken into account. This will be examined in this section for one-dimensional systems.

Since the scaling theory by Abrahams et al. [32] there has been substantial progress nowadays in the microscopic understanding of Anderson localization [33, 34] and it is realized that the mutual interactions have profound effects on localization [34, 128130]. In 1D systems such combined effects of interactions and localization [131-133] will be more clearly seen than in other dimension since the randomness alone always results in localization irrespective of the location of the Fermi energy, ϵ_F [134], while the interactions alone lead to the divergences of the various response functions, as we saw in Section 2. The phase Hamiltonian gives a simple description to the examination of such a problem [135]. For the sake of clarity we confine ourselves to the SDT model for the mutual interactions.

Our model Hamiltonian is then

$$\mathcal{H} = \int \mathrm{d}x \left[A_\rho(\nabla\theta)^2 + C_\rho P^2 + A_\sigma(\nabla\phi)^2 + C_\sigma M^2 + \right. \\ \left. + \sum_i V_0 \cos\phi(x) \cos\left(2k_F x + \theta(x)\right) \delta\left(x - R_i\right)\right] \tag{4.12}$$

where the last term is due to the coupling to impurities distributed randomly over R_i. The impurity potential is assumed to be of short range and only the backward scattering is taken into account. The similarity of the Anderson localization and the impurity pinning problem of the Peierls phase is now clear when Equation (4.3) and (4.12) are compared. The presence of $\cos\phi$ in Equation (4.12) indicates the possible fluctuations of spin degree of freedom in the present interacting fermion system in contrast to the Peierls state. Another difference of the present problem from the Peierls phase is the importance of the quantum fluctuations represented by terms including P^2 and M^2 in Equation (4.12). This quantum effect is taken into account by writing $\theta = \theta_{\mathrm{cl}} + \hat{\theta}$ and $\phi = \phi_{\mathrm{cl}} + \hat{\phi}$ where θ_{cl} and ϕ_{cl} are slowly varying classical parts and $\hat{\theta}$ and $\hat{\phi}$ are quantum fluctuations around θ_{cl} and ϕ_{cl}. The latter, $\hat{\theta}$ and $\hat{\phi}$, are treated in the SCHA (see Section 2.3),

$$\begin{aligned}&\cos\phi(x)\cos\left(2k_Fx+\theta(x)\right)\\&\quad\to\gamma\left[1-\frac{1}{2}\left(\hat{\theta}(x)^2-\left\langle\hat{\theta}^2\right\rangle+\hat{\phi}(x)^2-\left\langle\hat{\phi}^2\right\rangle\right)\right]\times\\&\quad\times\cos\phi_{\rm cl}(x)\cos\left(2k_Fx+\theta_{\rm cl}(x)\right)\end{aligned}\tag{4.13}$$

$$\gamma=\exp\left[-\frac{1}{2}\left(\left\langle\hat{\theta}^2\right\rangle+\left\langle\hat{\phi}^2\right\rangle\right)\right]\tag{4.14}$$

In Equation (4.13) and (4.14), $\left\langle\hat{\theta}^2\right\rangle$ and $\left\langle\hat{\phi}^2\right\rangle$ are the averages to be determined selfconsistently. We ignore the spatial variations of these quantities. By this approximation the problem reduces essentially (but not exactly) to that of a classical system where the effective impurity potential contains the quantum effect through γ, Equation (4.14).

It is seen from Equation (4.13) that $\phi_{\rm cl}$ is not directly influenced by the random distribution of impurities and then that $\phi_{\rm cl}$ can be fixed so that $|\cos\phi_{\rm cl}|$ takes a maximum value. The characteristic length, L_0, of the distortion of $\theta_{\rm cl}$ to be determined can be treated by the same method as in Section 4.1. In the discussion of localizationdelocalization the weak pinning is relevant and $\theta_{\rm cl}$ is considered to be constant over distance, L_0, much longer than the average spacing of impurities and the energy gain due to such distortion of $\theta_{\rm cl}$ is given as in Equation (4.6)

$$\frac{1}{L_0}\sum_i{}'\cos\left(2k_FR_i+\theta_{\rm cl}\left(R_i\right)\right)=-\left(n_i/L_0\right)^{1/2}.\tag{4.15}$$

By Equations (4.13) and (4.15) the last term in the r.h.s. of Equation (4.12) is written as

$$-\left(\frac{n_i}{L_0}\right)^{1/2}V_0\gamma\int_0^L\mathrm{d}x\left[1-\frac{1}{2}\left(\hat{\theta}^2-\left\langle\theta^2\right\rangle+\hat{\phi}^2-\left\langle\phi^2\right\rangle\right)\right]\tag{4.16}$$

Then the self-consistency equation for γ, (4.14), is given by

$$\gamma=\exp\left[-\frac{1}{8\pi}\int_{-\alpha^{-1}}^{\alpha^{-1}}\mathrm{d}qT\sum_m\sum_{\nu=\rho,\sigma}\frac{1}{\omega_m^2/4C_\nu+A_\nu\left(q^2+q_{c\nu}^2\right)}\right]\tag{4.17}$$

where

$$A_\nu q_{c\nu}^2=\frac{\sqrt{n_iL_0}}{2L_0}V_0\gamma,\quad\nu=\rho,\sigma\tag{4.18}$$

and $\omega_m=2\pi mT, m$ being the integer. Equation (4.17) is evaluated as

$$\gamma=C\left(V_0/n_iv_F\right)^{\eta/(4-\eta)}\left(n_iL_0\right)^{(-\eta/2)/(4-\eta)}\tag{4.19}$$

where

$$C=\left[\left(\frac{\pi/2}{1+\tilde{\alpha}}\right)^{\eta_\rho/4}\left(\frac{\pi/2}{1+\left(g_{2//}-g_{2\perp}\right)/2}\right)^{\eta_\sigma/4}\left(n_i\alpha\right)^{\eta/2}\right]4/(4-\eta)\tag{4.20}$$

and $\tilde{\alpha}=\left(g_{2//}+g_{2\perp}\right)/2$. Quantities η_ρ,η_σ and η are defined by

$$\eta_\rho = \left[\frac{1-\left(g_{2//}+g_{2\perp}\right)/2}{1+\left(g_{2//}+g_{2\perp}\right)/2}\right]^{1/2} \tag{4.21}$$

$$\eta_\sigma = \left[\frac{1-\left(g_{2//}-g_{2\perp}\right)/2}{1+\left(g_{2//}-g_{2\perp}\right)/2}\right]^{1/2} \tag{4.22}$$

and $\eta = \eta_\rho + \eta_\sigma$. Thus the excess energy ΔE due to the distortion of $\theta_{\rm cl}$ is given by

$$\begin{aligned}\frac{\Delta E}{L} =& A_\rho/bL_0^2 - L_0^{-1}\sqrt{n_i L_0}V_0\gamma\left(1+\frac{\langle\theta^2\rangle}{2}+\frac{\langle\rho^2\rangle}{2}\right)+\\ &+\frac{1}{2L}\sum_{\nu=\rho,\sigma}\sum_q\left(\frac{b_\nu}{a_\nu}\right)^{1/2}\left[\left(q^2+q_{c\nu}^2\right)^{1/2}-|q|\right]\\ &=n_i^2 v_F\left[-\frac{(1-\eta/4)\gamma V_0/n_i v_F}{\sqrt{n_i L_0}}+\frac{1+\tilde{\alpha}}{4\pi b\left(n_i L_0\right)^2}\right]\end{aligned} \tag{4.23}$$

where b is same as in Equation (4.6). The minimization of Equation (4.23) with respect to L_0 results in the characteristic length given by

$$n_i L_0 = \left(\frac{\pi b C}{1+\tilde{\alpha}}\right)^{-(4-\eta)/2/(3-\eta)} \times \left(\frac{V_0}{n_i v_F}\right)^{-2/(3-\eta)} \tag{4.24}$$

Consequently $\eta = 3$ separates the region of localization and delocalization, i.e. $L_0 = \infty$. This is shown in Figure 16 in the plane of $g_{2//}$ and $g_{2\perp}$, where the broken lines are boundaries obtained in Figure 4.

Such a localization-delocalization transition induced by interactions has been indicated originally by Chui and Bray [131], Apel [132], Apel and Rice [133] by different methods.

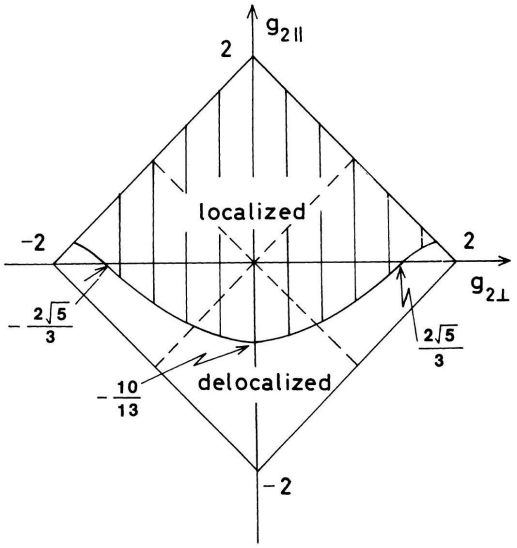


Fig. 16. Phase diagram of localized and delocalized regimes for SDT model (cf. Fig. 4).

In the impurity pinning problem treated in this and the preceeding subsections the dynamical properties (such as Ohmic conductivity) are determined by the fluctuations of phases $\hat{\theta}$ and $\hat{\phi}$ around those distorted ones $\theta_{\rm cl}$ and $\phi_{\rm cl}$ in the ground state. Such distortions of $\theta_{\rm cl}$ and $\phi_{\rm cl}$

are essential in the pinning and the simple perturbative treatment with respect to the impurity potential ignoring $\theta_{\rm cl}$ and $\phi_{\rm cl}$ is not generally justified though apparently acceptable results are obtained in some cases [10,126,127].

3.3.5 5. CDW Conductivity in the Peierls-fröhlich State

5.1 Langevin Equation Approach

Based on the phase Hamiltonian derived in the preceeding sections, we discuss here the dynamical nature of the CDW condensate and the resulting electrical conductivity in the PF state in the context of various interesting phenomena observed in quasi-onedimensional conductors $NbSe_3, TaS_3$ and so on (for the experimental details see the article by Monceau in Part II of this work). For this purpose we assume that the mutual Coulomb interaction between electrons can be neglected and the phase variable, ϕ, responsible for the spin density wave is discarded. Also we only consider the case that the CDW condensate coupled to the lattice distortion adiabatically, and the CDW phase θ is treated as classical variable. The effective Hamiltonian, which describes the dynamical properties of θ, is thus written as

$$\mathcal{H}_{\rm eff} = \pi v' \int {\rm d}x \left[p^2 + \frac{1}{4\pi^2 v'^2} \left\{ u_p^2 (\nabla\theta)^2 + 2\omega_F^2 V(\theta) \right\} - \frac{e}{\pi^2 v'} E\theta \right] \tag{5.1}$$

where $V(\theta)$ represents either the commensurability pinning potential in Equation (3.67), i.e., $\omega_F = \omega_M$ and $V(\theta) = (1 - \cos M\theta)/M^2$, or the averaged impurity pinning potential of Equation (4.11), i.e., $\omega_F = \omega_{imp} \equiv [2\pi v' W]^{1/2}$ and $V(\theta + 2\pi) = V(\theta)$ is assumed. The last term in Equation (5.1) is the coupling energy to an external electric field E, Equation (4.9).

For the proper description of transport properties associated with CDW dynamics we have to know its damping mechanism, which is not given by Equation (5.1). It arises partly from interactions between CDW and other modes, such as phonons not participating the CDW condensate and quasiparticles thermally excited (or those on other parts of the Fermi surface surviving even in the PF state). Besides the averaged pinning potential, Equation (4.11), impurities also cause damping of a CDW motion. Up to now, however, microscopic analysis of these damping mechanisms has been very limited [111, 136, 137, 137a]. We therefore introduce the following phenomenological argument: all the effects which give rise to the damping of a CDW motion are represented by random forces $F(x,t)$ on the CDW phase $\theta(x,t)$ and by the corresponding frictional force $-\eta p, \eta$ being the frictional constant. Consequently the equation of motion for θ is given by

$$\dot{p} = -\frac{\delta \mathcal{H}_{\rm eff}}{\delta\theta} - \eta p + F. \tag{5.2}$$

Substituting Equation (5.1) into Equation (5.2), we obtain the following Langevin equation

$$\frac{\partial^2\theta}{\partial t^2} - u_p^2 \frac{\partial^2\theta}{\partial x^2} + \eta \frac{\partial\theta}{\partial t} + \omega_F^2 \frac{\partial V}{\partial\theta} = 2v' eE + 2\pi v' F. \tag{5.3}$$

Usually the random force $F(x,t)$ is assumed to satisfy the conditions $\langle F(x,t) \rangle = 0$ and

$$\langle F(x,t) F(x',t) \rangle = \eta \frac{T}{\pi v'} \delta(x - x') \, \delta(t - t') \tag{5.4}$$

where T is the temperature. In the following subsections we discuss CDW conductivity derived from various limits of Equation (5.3).

At this point, we briefly mention three-dimensionality (3-D) effects on the CDW dynamics. Various interesting phenomena are in fact observed in the 3-D ordered PF state of

quasi-1-D conductors. Because of the coupling between CDW's on different chains, they move coherently. Since the resulting CDW motion is still predominantly in the chain direction [138-140], the 1-D description of Equation (5.3) will be appropriate as a simplest approximation, but the degree of the spatial extent of the coherence is an important problem when experimental results are to be analyzed quantitatively [112, 141, 142].

5.2. Classical Particle Model

The motion of a rigid CDW condensate (i.e. sliding motion of CDW) is described by Equation (5.3) without the spatial gradient term. In this case the effective momentum, charge and force are reinterpreted as those per unit length. In this case we obtain $p = M^*\dot{\theta}$ and the equation of motion

$$\frac{\partial^2\theta}{\partial t^2} + \eta\frac{\partial\theta}{\partial t} + \tilde{\omega}_F^2\frac{\partial V}{\partial\theta} = \left(\frac{n_s eE}{\pi} + \tilde{F}\right)/M^* \tag{5.5}$$

Here $\tilde{\omega}_F{}^2 = \omega_F{}^2/n_s$ and $M^* = n_s/2\pi v' \equiv n_s m^*$ plays a role of the effective mass of the CDW , where n_s is the density of electrons participating a sliding motion of CDW . The microscopic evaluation of n_s will be discussed later in Section 6. Similarly the current associated with the sliding CDW is given by

$$J_{\mathrm{CDW}} = \frac{n_s e}{\pi}\frac{\partial\theta}{\partial t} \tag{5.6}$$

Equation (5.5) describes a Brownian particle model in a periodic potential $V(\theta)$, and has been extensively studied in connection with the Josephson effect [143, 144] as well as the superionic conductivity [145, 146]. In the former case the potential $V(\theta)$ is undoubtedly a sinusoidal one, $1 - \cos\theta$, arising from the Josephson relation [147]. Usually the (Gaussian) random force $\tilde{F}$, which now satisfies $\left\langle \tilde{F}(t)\tilde{F}(t')\right\rangle = 2\eta M^* T\delta(t-t')$, is incorporated by a Fokker-Planck-type equation for the distribution function $P(p,\theta;t)$ derived from Equation (5.5). For a system with strong damping, or, more explicitly, if the condition

$$\left|\frac{\tilde{\omega}_F^2}{\eta^2}\left(\frac{\partial^2\bar{V}}{\partial\theta^2}\right)\right| \ll 1, \tag{5.7}$$

is satisfied, the Fokker-Planck-type equation can be reduced to the Smoluchowski equation for the distribution function of $\theta, S(\theta,t)$[143, 148]. If the effective mass M^* is large enough in addition to the condition of Equation (5.7), i.e.

$$\gamma \equiv \frac{2M^*\tilde{\omega}_F^2}{T} \gg 1 \tag{5.8}$$

a non-Ohmic conductivity with a sharp threshold field E_T is obtained. Explicitly we obtain the following expression for a dc current (we assume $V(\theta) \geq V(0) = V(2\pi) = 0$)

$$J(E) = \begin{cases} O\left(e^{-\gamma}\right), & E < E_T \\ J_c\left[\int_0^{2\pi}\frac{\mathrm{d}\theta}{(E/E_0)-(\partial V/\partial\theta)} + O\left(\gamma^{-1}\right)\right]^{-1}, & E > E_T \end{cases} \tag{5.9}$$

where $J_c = 2\pi E_0 J_\infty/E$ with $J_\infty = \left(n_s e/\pi\right)^2 E/\eta M^*$ and

$$E_0 = \frac{\pi M^*\tilde{\omega}_F^2}{n_s e} = \frac{\tilde{\omega}_F^2}{2v'e} \tag{5.10}$$

Notice that the electric force and the pinning force with $\mathrm{d}V/\mathrm{d}\theta = 1$ balance at $E = E_0$, and then E_T is given by $E_T = E_0\max(\mathrm{d}V/\mathrm{d}\theta)$. In the limit $\gamma \to \infty, J$ vanishes when $E < E_T$,

increases rather sharply at $E \gtrsim E_T$, and becomes proportional to E for $E \gg E_T$. The explicit dependences of J on E for $E > E_T$ are $J/J_\infty = (\epsilon^2 - 1)^{1/2}$ (A), $[\ln\{(\epsilon+1)/(\epsilon-1)\}]^{-1}$(B) and $\epsilon - 1/\epsilon$(C) with $V(\theta) = 1 - \cos\theta$(A), and $(1/2)\theta^2$(B) and $|\theta|$ (C) (in $|\theta| \leq \pi$), respectively, where $\epsilon = E/E_T$. These non-Ohmic conductivities $\sigma(E) = J/E$ are shown in Figure 17, where we have also shown for comparison the result of Bardeen's tunneling model [149]. Notice that the non-Ohmicity at $E \gg E_T$ derived from Equation (5.9) has a common behavior, $\sigma(\infty) - \sigma(E) \propto E^{-2}$, as long as $V(\theta)$ is continuous. On the other hand, J at $E \gtrsim E_T$ is proportional to $(E - E_T)^{1/2}$ if $\mathrm{d}V/\mathrm{d}\theta \simeq a - b\,(\theta - \theta_m)^2$ near its maximum ($\theta = \theta_m$), while $J \propto (E - E_T)$ for the potential (C).

The above results, in the limit of strong damping and large effective mass, are directly obtained from a simpler equation of motion

$$\eta \frac{\partial \theta}{\partial t} + \tilde{\omega}_F^2 \frac{\partial V}{\partial \theta} = e n_s E/\pi M^* \tag{5.11}$$

which was first introduced by Grüner et al. [150] and discussed further by Monceau et al. [141, 151]. In the case of superconducting Josephson effects Equation (5.11) with a sinusoidal potential $V(\theta)$ is called a resistively shunted junction model and has been extensively studied [144]. When $V(\theta) = 1 - \cos\theta$, Equation (5.11) is solved for a static field E larger than E_T, and $J_{\mathrm{CDW}}(t) = (n_s e/\pi)\,(\partial\theta/\partial t)$ is obtained as [144, 151]

$$J_{\mathrm{CDW}}(t) = J_\infty \sqrt{\epsilon^2 - 1} \left\{ 1 + 2 \sum_{n=1} K^n \cos n\,(\Omega t + \theta_0) \right\} \tag{5.12}$$

where $K = \epsilon - \sqrt{\epsilon^2 - 1}, \theta_0$ is an integration constant, and

$$\Omega = \frac{\tilde{\omega}_F^2}{\eta} \sqrt{\epsilon^2 - 1} = \frac{\pi}{e\eta} J\mathrm{CDW} \tag{5.13}$$

Here $J_{\mathrm{CDW}}^{\mathrm{DC}}$ is the first term of Equation (5.12), i.e. J given by Equation (5.9). The

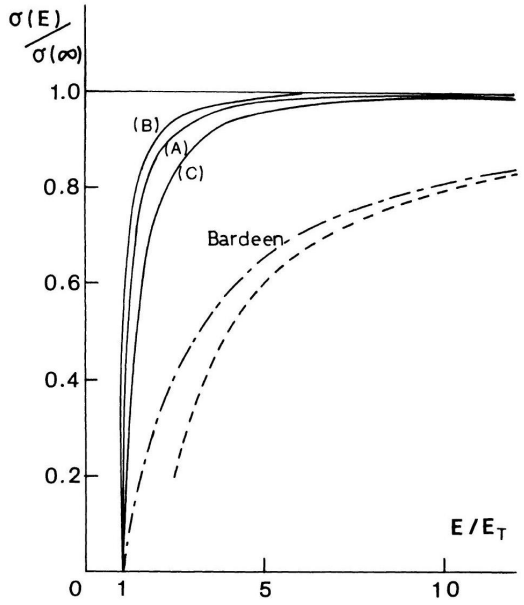


Fig. 17. The electric field dependences of the conductivity for various models. The broken line is explained in Section 6.1.

periodic variation of J_{CDW} reflects a sliding motion of CDW in the tilted (by E) periodic potential, suffering from a strong frictional force. The period is the time required for θ to change

by 2π, or in other words, the time required for CDW to traverse a wavelength $\lambda = 2\pi/Q$ in a real space. The fundamental frequency Ω of Equation (5.13), which is proportional to $J_{\rm CDW}^{\rm DC}$, can be interpreted as that of a narrow band noise, first observed by Fleming and Grimes [152]. Equation (5.12) also implies that the amplitudes of its higher harmonics are reduced by the factor K^n.

When only an ac external field with small amplitude is applied, overdamped oscillation around the bottom of the pinning potential ($\theta = 0$) takes place. The ac conductivity in this case is simply given by

$$\sigma(\omega) = \sigma_\infty \frac{i\omega\tau_{\rm eff}}{1 + i\omega\tau_{\rm eff}} \tag{5.14}$$

where $\sigma_\infty = n_S e^2/\pi^2\eta M^*$ and $\tau_{\rm eff} = \eta/\tilde{\omega}_F^2 V''(0)$.

More interesting is a case when both ac and dc fields are applied at the same time. One of the important problems in this case is to understand how the external ac field couples with the periodic variation of $J_{\rm CDW}$, Equation (5.12), when CDW is forced to slide by the dc field. Such synchronization phenomena are discussed within the present model by Richard et al. [151] to explain sharp peaks in their data on $\mathrm{d}V/\mathrm{d}I$ of $NbSe_3$ (see also [144]). Another important problem is an occurrence of non-Ohmicity under the combined ac and dc fields. When a dc field less than E_T is applied, the particle locates at the minimum of the potential. If the amplitude of an added ac field is so large that the particle sways out from the confining potential, dc current attributable to sliding CDW appears and the non-Ohmicity results. From this point of view Grüner et al. [153] have explained their data on ac-induced dc conductivity of $NbSe_3$.

5.3. Soliton and Soliton Lattice

Next we will take the possible spatial variations into account and consider dynamical properties associated with soliton lattices. The systematic part of Equation (5.3) is a nonlinear 'relativistic' wave equation:

$$\frac{\partial^2\theta}{\partial t^2} - u_p^2\frac{\partial^2\theta}{\partial x^2} + \omega_F^2\frac{\partial V}{\partial\theta} = 0 \tag{5.15}$$

There exists a class of exact nonlinear solutions, i.e. solitons, for a potential $V(\theta)$ which has degenerate minima and is only implicity dependent of x and t. The sine-Gordon soliton discussed in Section 3.5 is a typical example. The solution of Equation (5.15), $\theta_\pm(x-ut)$, and its excitation energy $E_\pm(u)$ are given by [154]

$$\pm\,\gamma_R(x-ut) = \frac{d}{\sqrt{2}}\int_{\theta_\pm(0)}^{\theta_\pm(x-ut)} \frac{\mathrm{d}\theta}{\sqrt{V(\theta)}} \tag{5.16}$$

$$E_\pm(u) = \frac{\gamma_R u_p^2}{\sqrt{2}\pi v' d}\int_0^{2\pi} \mathrm{d}\theta\sqrt{V(\theta)} \tag{5.17}$$

where $\gamma_R = \left(1 - u^2/u_p^2\right)^{1/2}$ and $d = u_p/\omega_F$. These are the generalization of Equation (3.43) and (3.44), respectively. The dynamical aspects of the soliton-bearing system described by Equation (5.15) has been extensively studied [154-156], although details of the dynamical processes, such as the creation or anihilation of solitons, have not yet fully been established.

Concerned with transport property of the PF state, Rice et al. [12] have first emphasized that such solitons are a new type of current-carrying excitations in a weakly pinned CDW condensate. An explicit evaluation of the static non-Ohmic conductivity, which is based on their idea, has been performed by Trullinger et al. [157]. They solved a discretized (in space) version of Equation (5.3) with $V(\theta) = 1 - \cos\theta$. This is a model of coupled pendulums subject

to random forces. Restricting to a strong damping case as in Section 5.2, they derived a Smoluchowski equation for $S(\{\theta_i\}, t)$, where the number of
variables θ_i is now macroscopic and coupled with each other. They introduce a factorization ansatz (the Hartree approximation) into the part of $S(\{\theta_i\}, t)$ which describes the response to an external force. When the external field is weak, the resulting conductivity at low temperature is Ohmic and proportional to E_S/T times the equilibrium density of excited solitons which is proportional to $(E_S/T)^{1/2}\exp(-E_S/T)$, where $E_S = E_{\pm}(0)$ of Equation (3.44). When the field exceeds a certain characteristic magnitude E_c, a non-Ohmicity develops rapidly, and then the conductivity saturates (again Ohmic) at high field limits. These qualitative features are in accordance with the experimental observations, though quantitative comparisons of E_c are difficult.

The Fokker-Planck-type equation for the same problem, but not restricted to the strong damping limit, has been examined by Imada [158] in the linear response regime involving an ac external field. He reproduces a central peak in the dynamical structure factor, which is attributable to solitons and is observed also in the computor simulations [159, 160]. The dynamical conductivity turns out to be not so sensitive to solitons, and the frequency dependence of $\sigma(\omega)$ is dominated by oscillations of the pinned CDW. Solitons give rise to significant, but relatively small contributions to $\sigma(\omega)$ only for $\omega \simeq 0$.

Büttiker and Landauer [161] have performed detailed analysis of the origin of the non-Ohmic conduction based on the same model discussed by Trullinger et al. [157] . They attributed it to combined processes of the nucleation of soliton and antisoliton pairs, their subsequent separation by the external force, and the eventual annihilation by collision with other solitons. Since only the overdamped case is of interest, the inertia term $\partial^2\theta/\partial t^2$ in Equation (5.3) has been neglected from the beginning, but the spatial correlation effect is fully taken into account, in contrast to the Hartree approximation by Trullinger et al. In particular the above-mentioned nucleation rate is evaluated by use of the classical energy of the saddle-point configuration $\theta_N(x)$ and the eigenvalues of the normal modes around $\theta_N(x)$. At $x = \pm\infty$, this configuration $\theta_N(x)$ approaches one of the local minima of the tilted sinusoidal potential θ_s, and moves into the next minimum in between. In case $(\Delta\Omega)^2 \equiv {\omega_F}^2 - 2ev'E \gtrsim 0$ they find a small-amplitude nucleus given by $\theta_N(x) = \theta_s + \Delta\theta_m \operatorname{sech}^2(x/2\xi)$, for which all the evaluations mentioned above can be carried out analytically, where $\Delta\theta_m = 3\sqrt{2}\Delta\Omega/\omega_F$ and $\xi = d/\sqrt{\cos\theta}$. They obtain a nonlinear conductivity proportional to $(\Delta E_N/T)^{1/2}\exp(-\Delta E_N/T)$ in the limit $\Delta\Omega \to 0$ and at low temperatures $\Delta E_N \gg T$, where $\Delta E_N = (3\sqrt{2}/5)E_S[\Delta\Omega/\omega_F]^{5/2}$. We also note here that Maki [162] has discussed a similar nucleation process of soliton and antisoliton pairs but through quantum mechanical tunneling. An extension of his theory to finite temperatures has been proposed [163], where a finite number of weakly bound soliton-antisoliton pairs already exist.

Solitons discussed so far are local excitations from a uniform commensurate ground state, as was explained in Section 3.5. When the wave number of CDW is nearly commensurate, the ground state configuration is a soliton lattice explained in Section 3.6. Now we briefly discuss a motion of the soliton lattice, in connection with the problem of the non-Ohmic conduction. A uniformly moving soliton lattice is described by Equation (2.85) with x replaced by $\gamma_R(x - ut)$. It is a solution of Equation (5.3) with vanishing E, F and η. With finite E and η, Equation (5.3) also describes a resistive Josephson line subject to a constant current density, and it has been investigated by Marcus and Imry [164]. The system exhibits non-Ohmic behavior very similar to that obtained by

Trullinger et al. [157]. When u reaches the critical velocity u_p, the soliton lattice cannot respond to the external field, instead a whole CDW starts to move. Weger and Horovitz [165] have argued that the non-Ohmicity appears through these two steps of different origins in an underdamped case, while in an overdamped case the Ohmic conduction due to a motion of the

soliton lattice is followed directly by the non-Ohmic conduction of a sliding CDW.

Based on a soliton lattice picture, Bak [166] has adopted a little different point of view. The soliton lattice is considered to be pinned by impurity potential as a whole CDW considered before. The non-Ohmicity appears, then, because of the depinning of the soliton lattice but not of a whole CDW. This idea leads to the following results. We see from Equation (3.46) that each soliton in this soliton lattice carries effective charge $2e/M$, M being the degree of the commensurability. The unit of charge is therefore fractional for $M \geq 3$ ($M = 4$ for $NbSe_3$) [78]. Also the fundamental noise frequency expected in the non-Ohmic regime has to be determined by the time required for CDW to traverse a period of the lattice. It is estimated in case of $NbSe_3$ to be ten times smaller than given by Equation (5.13).

3.3.6 6. Transport Properties of $nbse_3$ and TaS_3

Drastic non-Ohmic conductivity in the PF state of $NbSe_3$ was first observed by Monceau and co-workers [167, 168]. Extensive study since then [13, 14] has now established that, as described by Monceau in Part II, the various anomalous transport properties of $NbSe_3$ are attributable to dynamical nature of the CDW condensate, whose wave number is incommensurate but close to the $M = 4$ commensurability [169]. These anomalies include a very small characteristic field E_c (several mV/cm) which scales behavior of the non-Ohmicity [167], a sudden onset of the non-Ohmic conductivity at a well-defined threshold field E_T which is comparable to E_c [152,170] an ac linear conductivity very sensitive to the frequency [171], an occurrence of narrow band noises superimposed by a broad band noise in the non-Ohmic region [152,170] , certain hysteresis, such as 'overshooting' [172, 173] and 'switching' [174, 175], associated with a dynamical onset of the non-Ohmic conduction. Almost all of such peculiar transport properties are observed also in TaS_3 [176, 176a], where the properties of this material, even its crystal structure, depend sensitively on the sample preparation [177]. Quite recently similar transport properties have also been found in materials, which belong to a different class of quasi-1-D conductors from $NbSe_3$, namely in a blue bronze $K_{0.30}MoO_3$ [178] and a novel inorganic compound $(TaSe_4)_2\,I$ [179]. In this section we discuss these interesting transport properties based on the theories described in Section 5, i.e. theories derived from phase Hamiltonian approach to the CDW dynamics.

6.1. Dc Non-ohmic Conductivity

The experimental fact that the non-Ohmic behavior is scaled by a small characteristic field E_c excludes an idea that the phenomenon is due to quasi-particles excited above the PF gap. Further the existence of a well-defined threshold field E_T denies a possibility that nonlinear excitations, such as solitons described in Section 5.3, could be responsible
for the non-Ohmic conductivity. Actually the large excitation energy of solitons, though reduced by an applied field, is already incompatible with the very small characteristic field E_c. (This does not necessarily mean that conduction of excited solitons does not exist in any circumstances [140, 180].) The existence of a well-defined, but small, E_T implies that some large entities carrying electric charge start to move as a whole at this field. Based on this fact two models have been proposed up to now: the sliding of a whole CDW and that of a soliton lattice on the CDW mentioned in Section 5.3. The latter proposal, i.e. the sliding soliton lattice, due to Bak [166] is based on the fact that $NbSe_3$ [169] (and monoclinic TaS_3 [177]) has an incommensurate CDW close to the $M = 4$ commensurability. This model, though not yet examined in detail [181], yields essentially the same results as the former models and the differences are in the unit of elementary charge and in the narrow-band noise frequency, which are not yet conclusive experimentally [166, 175].

As regards the model of the sliding CDW there exist two points of view. The one is a classical particle model, first proposed by Grüner, Zawadowski and Chaikin [150], and explained in Section 5.2, and the other is Bardeen's model, in which the depinning of CDW is interpreted as a (macroscopic) quantum tunneling process [149,182]. The latter model is explained by Bardeen himself in this volume. Both of these models can explain some, but not all, of the transport phenomena mentioned above, as we will see in the following. Here we discuss some details of the stationary non-Ohmic conductivity based on the classical particle model.

The experimental data of the (excess) non-Ohmic conductivity above the threshold field E_T in $NbSe_3$ are well fitted with the following empirical formula

$$\frac{\sigma(E)}{\sigma(\infty)} = (1 - 1/y)\exp(-1/y) \tag{6.1}$$

where $y = E/E_T$[183, 184]. The classical particle model with the periodic model potentials discussed in Section 5.2 does not reproduce Equation (6.1), in particular, its asymptotic behavior at large y as mentioned below Equation (5.10).

One of the possible modifications of the model is to introduce distribution of CDW domains [141, 151, 185]. Actually by assuming an exponential distribution of the spatial extent of coherent regions Portis [185] has derived almost the same expression as Equation (6.1) for the excess current

$$J(E) = \sigma_b\,(E - E_T)\exp\left(-E_c/\left(E - E_T\right)\right), \quad (E > E_T) \tag{6.2}$$

which was proposed empirically by Fleming [170]. In this treatment the depinned and then mobile region increases as the field is increased. Consequently the non-Ohmicity in this model results from the field dependence of the effective carrier number, which appears not to be the case experimentally [13]; i.e. the mobility, not the carrier number, varies once the sliding commences. We believe this is a very important point to be seriously checked by experiments. If the non-Ohmicity is entirely due to the change in the mobility, then Bardeen's tunneling theory, which reproduces Equation (6.1), has also to be reconsidered. By his theory [149], the prefactor ($1 - 1/y$) in Equation (6.1),
which predominantly governs the increase of J_{CDW} just above E_T, is due to the increase of the number of carriers. Another difficulty of this domain-distribution model is in the distribution of E_T, which results in the existence of sliding domains among those still pinned [141].

In order to incorporate, within the classical particle model, further possible change in the mobility than that due to a simple tilting of the potential by the field E, i.e. $V(\theta) - E\theta/E_c$, we have to introduce a certain field dependence of the effective potential $V(\theta)$ itself. An underlying assumption of this idea is that the pinning mechanism is predominantly due to impurities (or defects) which are randomly distributed. Stationary configurations of the CDW phase, which are determined by the two competing energies as explained in Section 4.1, are expected to depend sensitively on the field E, so that the effective potential $V(\theta)$ is, too. This picture, which is similar to that of spin glasses in the presence of the magnetic field [186-188], may be compatible also with the hysteretic phenomena mentioned above. In connection with this variable potential model we note [189] that the empirical formula Equation (6.1) might be interpreted as an interpolation of a function which is proportional to $(1 - 1/y)$ near $y = 1$ and (1-2/y) at large y. The triangular potential is shown in Section 5.2 to reproduce the same feature near $y = 1$. On the other hand, the sawtooth potential, which is defined by $V(\theta) = a(\theta - 2n\pi)$ in $2n\pi \leq \theta < 2(n + 1)\pi$ and then has discontinuities, yields $\sigma(E)/\sigma(\infty) = 1 - a/y$, where y = E/E_0, with E_0 being given by Equation (5.10). Thus a variable potential $V(\theta)$, from the triangular, (C) of Section 5.2 with $E_T = E_0$, to a sawtooth-type with $a \simeq 2$ is expected to reproduce $\sigma(E)$ qualitatively similar to that given by Equation (6.1) (see Figure 17 where the broken line represents $\sigma(E)$ of the sawtooth potential with a fixed $a = 2$).

Although this example of the variable potential is purely phenomenological, it indicates the important roles played by internal degrees of freedom of the CDW condensate in the presence of an external field. A theory, in which the coupling of the internal modes with a sliding CDW itself is taken into account, has been proposed by Sneddon et al. [190]. They predicted $E^{-1/2}$ dependence of the non-Ohmic conductivity at large E, which seems not to be observed in the experiments by Oda and Ido [191] with E as large as $50E_T$. If their data are replotted as in [190], a distinct deviation from the $E^{-1/2}$ dependence is seen at $E \geq 15E_T$ [191]. On the other hand $J(E)$ convex downwards at $E \gtrsim E_T$ has been recently derived by Fisher [190a] for a model impurity potential whose amplitude is also random. (See also note added in proof.)

6.2. Ac Linear Conductivity

The remarkable ω-dependence of the ac conductivity even at low frequencies ω is another feature associated with the CDW condensate [171, 192]. In the case of a strong damping in the classical particle model, the dynamics is an overdamped oscillation yielding the ac conductivity of Equation (5.14). This picture is, of course, oversimplified. As mentioned above, internal degrees of freedom of the CDW condensate, which are expected to have their own dynamics, certainly have to be taken into account. Cooperative modes involving many degrees of freedom cannot follow the external field if it changes too rapidly. Even for low frequency we may rather expect that some portions of the CDW, not necessarily
as a whole, follow the field. This means that the potential $V(\theta)$, which determines τ_{eff} ($\propto V''(O)^{-1}$) in Equation (5.14), is not necessarily identical to $V(\theta)$, which governs motions of a whole CDW [174]. The above considerations have to be taken into account also in analysis of the ac-induced dc conductivity, which is briefly mentioned at the end of Section 5.2. The effect is reduced at higher frequencies [153]. This property is expected from the above argument, but is opposite to that expected from the tunneling theory. On the other hand it is not clear for the moment that the scaling relation between the dc non-Ohmic conductivity $\sigma(E)$ and the ac linear conductivity $\sigma(\omega)$, which has been predicted by the tunneling theory [149, 193] and has been observed in $NbSe_3$ [194], can be accounted for by the impurity pinning [216].

Recently Horovitz and Trullinger [195] have analyzed the ac conductivity $\sigma(\omega)$ of a nearly commensurate case. Their discussions are based on Equation (5.3) but with $F = 0$ in contrast to those by Imada [158] for the commensurate case with $F \neq 0$. They emphasize the role of solitons, or more explicitly, the modification of the continuum modes (phasons) by the presence of solitons, and claim that the ω-dependence becomes sharper as a CDW is closer to the commensurability.

\{}paragraph6.3. Noise Associated with the Non-ohmic Conductivity Another dramatic phenomenon associated with the CDW dynamics is the occurence of narrow band noises superimposed by a broad band noise, which are observed only in the non-Ohmic region [152]. The narrow band noise spectrum consists of a few or a single [196] fundamental harmonics and their subharmonics [151, 152]. There have been some proposals that the phenomena may be attributed to a chaotic motion of the CDW condensate [197-200]. Since, however, the fundamental frequency Ω_0 of narrow band noise obeys Equation (5.13) well, as already mentioned [151], it is now thought that the narrow band noise is tightly connected to a uniform motion of a whole CDW (or a soliton lattice). A problem remains concerning the relationship between Ω_0 and $J_{\text{CDW}} = en_s v$ with the velocity v; in other words, concerning a characteristic period l_0 in space defined by $\Omega_0 = 2\pi v/l_0$. As pointed out in Section 5.3, $l_0 = l$, the period of the lattice, in the sliding soliton-lattice model. In the sliding CDW (as a whole) model, l_0 depends on the pinning potential: $l_0 = \lambda\,(\simeq 4a$ for $NbSe_3)$, the wave-length of CDW , for the impurity pinning, while $l_0 = a$, the period of the underlying lattice, for the commensurability pinning. This will be answered once an accurate value of n_s is determined experimentally [201-203]. Other mechanisms of the narrow band noise have also been proposed by Portis [185] and Barnes and

Zawadowski [204]. We also note that Ong et al. [205, 206] have recently claimed that the noise phenomena are not a bulk effect, but they are observed only in the inhomogeneous region in a sample near the contact to leads.

The power spectrum of the large broad band noise, which appears also in the nonOhmic regime, follows a $f^{-\alpha}$ dependence with $\alpha = 0.8$ in $NbSe_3$ [207] and $\alpha = 0.4$ in TaS_3 [208]. The mechanism of this broad band noise has not yet been well established [207-209].

M6.4. Hysteresis Recently observations on dynamical process of the CDW depinning reveal further interesting aspects of the sliding CDW. When the pulsed electric field applied to $NbSe_3$ were alternative in sign, the voltage developed across the specimen rises beyond its dc value, towards which it subsequently decays with a time constant of the order of several 10μ s. This is an 'overshooting' phenomenon first observed by Gill [172]. Grüner and Zettl [175] reported a 'switching' phenomenon; i.e. a jump or 'switch' observed in the intermediate region of Ohmic and non-Ohmic conductivity in dc I-V traces for $NbSe_3$ (see also [141, 174]). These hysteresis, which become more distinct at lower temperatures, indicate that some large entities carrying electrical charge are by no means rigid. They are hardly explained by the commensurability potential in Equation (3.67) alone or by the simplified impurity potential of Equation (4.11). We certainly need to consider a number of metastable configurations under the original random potential of Equation (4.5a), and dynamical transfer of the system between such metastable states [210,211]. Such hysteresis phenomenon of CDW in the presence of randomness has been noted before by Littlewood and Rice [116] in another context. As mentioned before, these hysteresis also remind us of remanent phenomena in spin glasses [186-188], although their characteristic time scales differ greatly in two systems. We think the idea of charge-density-glass (CDG) [104] has to be further investigated.

M6.5. Theoretical Problems Compared with the huge accumulation of experimental data, theoretical development is yet far from satisfactory. Various experimental observations described above certainly require theories involving dynamics of the internal degrees of freedom of the CDW condensate. Even if only the simple commensurability potential is taken into account, or if the impurity effect is represented by the simplified potential of Equation (4.11), full analysis of the Langevin type equation (5.3), derived from our phase Hamiltonian approach, is not easy because of the nonlinear aspect of the equation. In a theory of the charge-density-glass mentioned just above, one has to incorporate also the randomness, which makes the problem quite complicated. Numerical experiments, such as those done by Teranishi and Kubo [106], Sokoloff [144] and Littlewood and Rice [116], will be helpful in this context. Recently Pietronero and Strässler [212] have extended such numerical analysis and examined the characteristic behavior of the excess current at $E \gtrsim E_T$ as well as that of the narrow band noise.

It is a formidable task to explain all the phenomena associated with CDW dynamics by a microscopic theory, i.e. directly from the fundamental Hamiltonians such as Equation (3.1) and (4.1). It is only possible at the moment to evaluate the various parameters, which appear in the phenomenological theorias or in analysis of experiments. Some of them, such as u_p, v' and ω_F ($= \omega_M$, or $\omega_{\rm imp}$), are already explained in the previous sections. For example the phason velocity u_p is weakly dependent on temperature in the PF state, since a_T/Δ^2 in Equation (3.21) is so (within the mean field approximation). Concerned with n_s in Equation (5.5), the density of electrons which participate a sliding motion of CDW, one needs some cautions as discussed in detail by Lee and Rice [112].

The microscopic derivation of the effective phase Hamiltonian described in Section 3.1 is quite analogous to that of the Ginzburg-Landau equation in superconductivity [188, 213]. From this analogy one may simply expect that n_s is proportional to the square of the order parameter, or $n_s \propto \Delta^2$, just below the transition temperature, T_c [7]. However this is not the case experimentally [142, 184]. In the ground state ($T = 0$) all electrons except those in other parts of the Fermi surface are in the CDW condensate so that n_s equals to the total electron

density in the above sense. The gap Δ is simply related with the amplitude of the charge density modulation. As the temperature is raised the number of quasiparticles excited across the PF gap increases. Thus an external electric field is fed to accelerate partly such quasiparticles and partly electrons still in the CDW condensate. The microscopic evaluation of the former process leads to the result $n_s \propto \Delta$ near T_c [112], which is also obtained by the argument on the proper Galilean transformation properties of an energy [136]. From this result combined with the expectation that the amplitude of impurity pinning potential, ${\omega_F}^2$, is proportional to $\Delta^\alpha (0 < \alpha < 1)$ [112], the threshold field E_T for the non-Ohmic conductivity is expected to diverge at T_c from below (see Equation (5.10) and note $\tilde{\omega}_F{}^2 = {\omega_F}^2/n_s$), which is actually observed in $NbSe_3$ [171] and TaS_3 [214] but not in $K_{0.30}MoO_3$ [178]. The increase of E_T at lower temperatures can be understood qualitatively by the increase of effective pinning potential due to less thermal fluctuations as was discussed by Okabe and Fukuyama [120] in different context. Up to now microscopic arguments on the relaxation mechanism of a CDW motion are very limited as pointed out in Section 5.1.

3.3.7 7. Summary

One of the interesting characteristics of quasi-one-dimensional conductors is the transport phenomenon due to such collective modes as CDW. These collective modes are considered essentially as bosons as far as the low lying excitations are concerned. In CDW the phase of the lattice distortions can describe these excitations and the phase Hamiltonian has been a convenient theoretical tool. Moreover even the electronic excitations can also be described by boson operators in the case of purely one-dimensional systems, since the possible linearization of the Bloch energy band for the description of excitations near the Fermi energy results in the excitation spectrum similar to familiar phonons. This bosonization has naturally introduced the quantum phase variables to represent electrons. Thus the phase Hamiltonian, different from the previous one, has been employed in various discussions. These two phase Hamiltonians can be combined to describe the whole dynamical processes of the complex systems of mutually interacting electrons coupled to the lattice distortions. We have tried to give a comprehensive theoretical review from this particular point of view, and to discuss the results in the context of very fascinating experimental findings observed in the Peierls-Fröhlich state.

3.3.8 Acknowledgements

One of authors (HF) thanks Y. Suzumura, S. Inagaki, J. Hara, T. Nakano and K. Takano for useful discussions, while the other (HT) thanks T. Sambongi and M. Ido for informative discussions about experiments on MX_3.

3.3.9 References

1. H. J. Keller (Ed.) Chemistry and Physics of One-Dimensional Metals (1976), Plenum Press, New York.

2. J. T. Devreese. R. P. Evrard and V. E. van Doren (Eds.) Highly Conducting One-Dimensional Solids (1979), Plenum Press, New York.

3. J. Bernasconi and T. Schneider (Eds.) Physics in One Dimension (1981), Springer Verlag, Berlin, Heidelberg, New York.

4. J. de Physique, Proceedings of the International CNRS Colloquim on the Physics and Chemistry of Synthetic and Organic Metals (Les-Arcs, Dec. 1982). 44, C3 (1983).

5. R. E. Peierls, Quantum Theory of Solids (1955), Oxford University Press, Oxford.
6. H. Frölich, Proc. Roy. Soc. A223, 296 (1954).
7. D. Allender, J. W. Bray and J. Bardeen, Phys. Rev. B9, 119 (1974).
8. P. A. Lee, T. M. Rice and P. W. Anderson, Solid State Commun. 14, 703 (1974).
9. L. Pietronero, S. Strässler and G. A. Toombs, Phys. Rev. B12, 5213 (1975).
10. H. Fukuyama, J. Phys. Soc. Japan 41, 513 (1976).
11. H. Fukuyama and P. A. Lee, Phys. Rev. B17, 535 (1978).
12. M. J. Rice, A. R. Bishop, J. A. Krumhansl and S. E. Trullinger, Phys. Rev. Lett. 36, 432 (1976).
13. N. P. Ong, Can. J. Phys. 60, 59 (1982).
14. G. Grüner, Comments on Solid State Physics 10, 183 (1983).
15. J. Solyom, Adv. in Phys. 28, 201 (1979).
16. S. Tomonaga, Prog. Theor. Phys. 5, 349 (1950).
17. A. Luther and I. Peschel, Phys. Rev. B9, 2911 (1974).
18. A. Luther and V. J. Emery, Phys. Rev. Lett. 33, 589 (1974).
19. D. C. Mattis, J. Math. Phys. 15, 609 (1974).
20. F. D. M. Haldane, J. Phys. C. 12, 4791 (1979).
21. F. D. M. Haldane, Phys. Rev. Lett. 45, 1358 (1980).
22. R. Heidenreich, B. Schroer, R. Seiler and D. Uhlenbrock, Phys. Lett. 54A, 119 (1975).
23. K. B. Efetov and A. I. Larkin, Soviet Physics-JETP 42, 390 (1976).
24. A. Luther, Phys. Rev. B15, 403 (1977).
25. Y. Suzumura, Prog. Theor. Phys. 61, 1 (1979).
26. J. Hara, T. Nakano and H. Fukuyama, J. Phys. Soc. Japan 51, 341 (1982).
27. K. Takano, T. Nakano and H. Fukuyama, J. Phys. Soc. Japan 51, 366 (1982).
28. J. Hara and H. Fukuyama, in ref. 4; J. Phys. Soc. Japan 52, 2128 (1983).
29. T. Nakano and H. Fukuyama, J. Phys. Soc. Japan 49, 1679 (1980); 50, 2489 (1981).
30. S. Inagaki and H. Fukuyama, J. Phys. Soc. Japan 52, 2504 (1983); 52, 3620 (1983).
31. J. W. Bray, L. V. Interrante, I. S. Jacobs and J. C. Bonner in Extended Linear Chain Compounds (1982) vol. 3, Plenum Press, New York.
32. E. Abrahams, P. W. Anderson, D. C. Licciardello and T. V. Ramakrishnan, Phys. Rev. Lett. 42, 673 (1979).

33. P. W. Anderson, Physica 117 and 118 B + C, 30 (1983).

34. Y. Nagaoka and H. Fukuyama (Eds.) Anderson Localization (1982) Springer Verlag, Berlin, Heidelberg, New York.

35. S. Takada and S. Misawa, Prog. Theor. Phys. 66, 101 (1981).

36. J. M. Luttinger, J. Math. Phys. 4, 1154 (1963).

37. Yu. A. Bychkov, L. P. Gorkov and I. E. Dzyaloshinskii, Soviet Physics-JETP 23, 489 (1966).

38. T. M. Rice, Phys. Rev. 104A, 1889 (1965).

39. R. Dashen, B. Hasslacher and A. Neveu, Phys. Rev. D11, 3424 (1975).

40. S. Coleman, Phys. Rev. D11, 2088 (1975).

41. N. Menyhard and J. Solyom, J. Low Temp. Phys. 12, 529 (1973).

42. J. Solyom, J. Low Temp. Phys. 12, 547 (1973).

43. P. Bak, Rept. on Prog. in Phys. 45, 587 (1982).

44. L. A. Turkevich and S. Doniach, Ann. of Phys. 139, 343 (1982).

45. A. L. Fetter and M. J. Stephen, Phys. Rev. 168, 475 (1968).

46. B. Sutherland, Phys. Rev. A8, 2514 (1973).

47. W. L. McMillan, Phys. Rev. 14, 1496 (1976).

48. S. Iwabuchi and H. Fukuyama, in ref. 4, p. 1001.

49. J. C. Scott, H. J. Pedersen and K. Bechgaard, Phys. Rev. Lett. 45, 2125. (1980).

50. K. Mortensen, Y. Tomkiewicz, T. D. Schultz and E. M. Engler, Phys. Rev. Lett. 46. 1234 (1981).

51. D. J. Scalapino, Y. Imry and P. Pincus, Phys. Rev. B11, 2042 (1975).

52. K. B. Efetov and A. I. Larkin, Soviet Physics-JETP 39, 1129 (1974).

53. P. Bak and V. J. Emery, Phys. Rev. Lett. 36, 978 (1976).

54. K. Saub, S. Barisic and J. Friedel, Phys. Lett. 56A, 302 (1976).

55. T. D. Schultż and S. Etemad, Phys. Rev. B13, 4928 (1976).

56. S. Nakajima and Y. Okabe, J. Phys. Soc. Japan 42, 1115 (1977).

57. J. Yamauchi, K. Sato, S. Iwabuchi and Y. Nagaoka, J. Phys. Soc. Japan 44, 460 (1978).

58. K. Sato, S. Iwabuchi, J. Yamauchi and Y. Nagaoka, J. Phys. Soc. Japan 45, 515 (1978).

59. P. Bak and S. A. Brazovskii, Phys. Rev. B17 3154 (1978).

60. H. Fukuyama, J. Phys. Soc. Japan 45, 1266 (1978).

61. I. Batistic, G. Theodorou and S. Barisic, Solid State Commun. 34, 499 (1980).

62. L. N. Bulaevskii, A. I. Buzdin and D. I. Khomskii, Solid State Commun. 35, 101 (1980).

63. Y. Suzumura and H. Fukuyama, J. Phys. Soc. Japan 49, 915 (1980); 49, 2081 (1980).

64. S. A. Brazovskii and I. E. Dzyaloshinskii, Soviet Physics-JETP 44, 1233 (1976).

65. P. A. Lee, T. M. Rice and P. W. Anderson, Phys. Rev. Lett. 31, 462 (1973).

66. A. A. Abrikosov, L. P. Gorkov and I. E. Dzyaloshinskii, Method of Quantum Field Theory in Statistical Physics (1963), Prentice-Hall, Englewood Cliffs.

67. S. Kurihara, J. Phys. Soc. Japan 44, 2011 (1978), and ibid. 48, 1821 (1980).

68. K. Takano, Prog. Theor. Phys. 68, 1 (1982).

69. E. J. Mele and M. J. Rice, Phys. Rev. B23, 5397 (1981).

70. H. J. Schulz, Phys. Rev. B18, 5756 (1978).

71. M. Nakahara and K. Maki, Phys. Rev. B25, 7789 (1982).

72. J. T. Gammel and J. A. Krumhansl, Phys. Rev. Lett. 49, 899 (1982).

73. A. C. Scott, F. Y. F. Chu and D. W. McLaughlin, Proc. IEEE 61, 1443 (1973).

74. A. R. Bishop and T. Schneider (Ed.) Solitons and Condensed Matter Physics (1978), SpringerVerlag, Berlin.

75. T. L. Ho, Phys. Rev. Lett. 48, 946 (1982).

76. B. Horovitz, Phys. Rev. Lett. 48, 1416 (1982); and in ref. 4, p. 1519.

77. J. A. Krumhansl, B. Horovitz and A. J. Heeger, Solid State Commun. 34, 945 (1980).

78. W. P. Su and J. R. Schrieffer, Phys. Rev. Lett. 46, 738 (1981).

79. W. P. Su, J. R. Schrieffer and A. J. Heeger, Phys. Rev. Lett 42, 1698 (1979), and Phys. Rev. B22, 2099 (1980).

80. M. J. Rice, Phys. Lett. 71A, 152 (1979).

81. H. Takayama, Y. R. Lin-Liu and K. Maki, Phys. Rev. B21, 2388 (1980).

82. B. Horovitz, Phys. Rev. B22, 1101 (1980).

83. W. P. Su and J. R. Schrieffer, Proc. Natl. Acad. Sci. USA 77, 5626 (1980).

84. D. K. Campbell and A. R. Bishop, Phys. Rev. B24, 4859 (1981).

85. S. A. Brazovskii, Soviet Physics-JETP Lett. 28, 606 (1978).

86. S. A. Brazovskii and N. N. Kirova, Soviet PhysicsJETP Lett. 334 (1981).

87. W. P. Su, Phys. Rev. B27, 370 (1983).

88. J. T. Gammel and J. A. Krumhansl, Phys. Rev. B27, 7659 (1983).

89. S. A. Brazovskii, I. E. Dzyaloshinskii and S. P. Obukhov, Soviet Physics-JETP 45, 814 (1977).

90. E. Pytte, Phys. Rev. B10, 4637 (1974).

91. F. D. M. Haldane, Phys. Rev. Lett. 45, 1358 (1980).

92. M. C. Cross and D. S. Fisher, Phys. Rev. B19, 402 (1979).

93. P. W. Anderson, Mater. Res. Bull. 8, 153 (1973).

94. W. Duffy, Jr., and K. P. Barr, Phys. Rev. 165, 647 (1968).

95. J. C. Bonner and H. W. J. Blöte, Phys. Rev. B25, 6959 (1982).

96. H. P. van de Braak, W. J. Caspers, P. W. Wiegel and M. W. M. Willeme, J. Stat. Phys. 18, 579 (1978).

97. J. N. Fields, H. W. J. Blöte and J. C. Bonner, J. Appl. Phys. 50, 1807 (1979).

98. J. L. Black and V. J. Emery, Phys. Rev. B23, 429 (1981).

99. Y. Imry and S. K. Ma, Phvs. Rev. Lett. 35, 1399 (1975).

100. L. J. Sham and B. R. Patton, Phys. Rev. B13, 3151 (1976).

101. D. J. Bergmann, T. M. Rice and P. A. Lee. Phys. Rev. B15, 1706 (1977).

102. K. B. Efetov and A. I. Larkin, Soviet Physics-JETP 45, 1236 (1977).

103. L. P. Gorkov, Soviet Physics-JETP Lett. 25, 358 (1977).

104. H. Fukuyama, J. Phys. Soc. Japan 45, 1474 (1978).

105. M. V. Feigelman, Soviet Physics-JETP 52, 555 (1980).

106. N. Teranishi and R. Kubo, J. Phys. Soc. Japan 47, 720 (1979).

107. T. R. Koehler and P. A. Lee, Phys. Rev. B16, 5263 (1977).

108. J. F. Weisz. J. B. Sokoloff and J. E. Sacco, Phys. Rev. B20, 4713 (1979).

109. P. A. Lee and H. Fukuyama, Phys. Rev. B17, 542 (1978).

110. J. B. Sokoloff, Phys. Rev. B16, 3367 (1977).

111. M. L. Boriack and A. W. Overhauser, Phys. Rev. B16, 5206 (1977).

112. P. A. Lee and T. M. Rice,Phys. Rev. B19, 3970 (1979).

113. R. A. Klemm and J. R. Schrieffer, Phys. Rev. Lett. 51, 47 (1983).

114. J. B. Sokoloff, Phys. Rev. B23, 1992 (1981) and in ref. [4] , p. 1667.

115. K. Nakanishi, J. Phys Soc. Japan 46, 1434 (1979).

116. P. B. Littlewood and T. M. Rice, Phys. Rev. Lett. 48, 44 (1982).

117. D. Baeriswyl and A. R. Bishop, J. Phys. C. 13, 1403 (1980).

118. T. M. Rice, S. Whitehouse and P. Littlewood, Phys. Rev. B24, 2751 (1981).

119. M. B. Fogel, S. E. Trullinger, A. R. Bishop and J. A. Krumhansl, Phys. Rev. B15, 1578 (1977).

120. Y. Okabe and H. Fukuyama, Solid State Commun. 20, 345 (1976).

121. S. T. Chui, Phys. Rev. B19, 4333 (1979).

122. A. Houghton, R. D. Kenway and S. C. Ying, Phys. Rev. B23, 298 (1981).

123. H. Fukuyama, T. M. Rice and C. M. Varma, Phys. Rev. Lett. 33, 305 (1974).

124. B. P. Patton and L. J. Sham, Phys. Rev. Lett. 31, 631 (1973), ibid. 33, 638 (1974).

125. S. Kurihara, J. Phys. Soc. Japan 44, 2011 (1978).

125a.. S. Takada and E. Sakai, Prog. Theor. Phys. 59, 1802 (1978).
126. S. Kurihara, J. Phys. Soc. Japan 4.1, 1488 (1976).
127. K. Okamoto, Prog. Theor. Phys. 68, 1443 (1982).
128. B. L. Altshuler and A. G. Aronov, Solid State Commun. 30, 115 (1979).
129. B. L. Altshuler, A. G. Aronov and P. A. Lee, Phys Rev. Lett. 44, 1288 (1980).
130. H. Fukuyama, J. Phys. Soc. Japan 48, 2169 (1980).
131. S. T. Chui and J. W. Bray, Phys. Rev. B16, 1329 (1977); B19, 4020 (1982).
132. W. Apel, J. Phys. C 15, 1973 (1982).
133. W. Apel and T. M. Rice,Phys. Rev. B26, 7063 (1982).
134. V. L. Berezinsky, Soviet Physics-JEFT 38, 620 (1974).
135. Y. Suzumura and H. Fukuyama, J. Phys. Soc. Japan 52, 2870 (1983).
136. M. L. Boriack and A. W. Overhauser, Phys. Rev. B17, 2395 (1978).
137. T. M. Rice, P. A. Lee and M. C. Cross, Phys. Rev. B20, 1345 (1979).
137a. J. E. Sacco, J. B. Sokoloff and A. Widom, Phys. Rev. B20, 5071 (1979).
138. G. X. Tessema and N. P. Ong, Phys. Rev. B23, 5607 (1981).
139. K. Kawabata, M. Ido and T. Sambongi, J. Phys. Soc. Japan 50, 739, 1992 (1981).
140. T. Takoshima, M. Ido, K. Tsutsumi, T. Sambongi, S. Homma, K. Yamaya and Y. Abe, Solid State Commun. 35, 911 (1980).
141. P. Monceau, J. Richard and M. Renard, Phys. Rev. B25, 931 (1982).
142. J. Bardeen, E. Ben-Jacob, A. Zettl and G. Grüner, Phys. Rev. Lett. 49, 493 (1982).
143. V. Ambegaokar and B. I. Halperin, Phys. Rev. Lett. 22, 1364 (1969).
144. P. E. Lindelof, Rep. Prog. Phys. 44, 949 (1981).
145. P. Fulde, L. Pietronero, W. R. Schneider and S. Strässler, Phys. Rev. Lett. 35, 1776 (1975).
146. W. Dieterich, I. Peschel and W. R. Schneider, Z. Phys. B27, 177 (1977).
147. B. D. Josephson, Adv. Phys. 14, 419 (1965).
148. G. Wilemski, J. Statis. Phys. 14, 153 (1976).
149. J. Bardeen, Phys. Rev. Lett. 45, 1978 (1980).
150. G. Grüner, A. Zawadowski and P. M. Chaikin, Phys. Rev. Lett. 46, 511 (1981).
151. J. Richard, P. Monceau and M. Renard, Phys. Rev. B25, 948 (1982).
152. R. M. Fleming and C. C. Grimes, Phys. Rev. Lett. 42, 1923 (1979).
153. G. Grüner, W. G. Clark and A. M. Portis, Phys. Rev. B24, 3641 (1981).
154. J. F. Currie, J. A. Krumhansl, A. R. Bishop and S. E. Trullinger, Phys. Rev. B22, 477 (1980).
155. J. A. Krumhansl and J. R. Schrieffer, Phys. Rev. B11, 3535 (1975).
156. H. Takayama and K. Maki, Phys. Rev. B21, 4558 (1980).

157. S. E. Trullinger, M. D. Miller, R. A. Guyer, A. R. Bishop, F. Palmer and J. A. Krumhansl, Phys. Rev. Lett. 40, 206 (1978).
158. M. Imada, J. Phys. Soc. Japan 50, 401 (1981).
159. T. Schneider and E. Stoll, Phys. Rev. B23, 4631 (1981).
160. W. C. Kerr, D. Baeriswyl and A. R. Bishop, Phys. Rev. B24, 6566 (1981).
161. B. Büttiker and R. Landauer, Phys. Rev. Lett. 43, 1453 (1979).
162. K. Maki, Phys. Rev. Lett. 39, 46 (1977), Phys. Rev. B18, 1641 (1978).
163. G. Mihaly and L. Mihaly, Solid State Commun. 29, 645 (1979).
164. P. M. Marcus and Y. Imry, Solid State Commun. 33, 345 (1980).
165. M. Weger and B. Horovitz, Solid State Commun. 43, 583 (1982).
166. P. Bak, Phys. Rev. Lett. 48, 692 (1982).
167. P. Monceau, N. P. Ong, A. M. Portis, A. Meerschaut and J. Rouxel, Phys. Rev. Lett. 37, 602 (1976).
168. N. P. Ong and P. Monceau, Phys. Rev. B16, 3443 (1977).
169. K. Tsutsumi, T. Takagaki, M. Yamamoto, Y. Shiozaki, K. Ido, T. Sambongi, K. Yamaya and Y. Abe,Phys. Rev. Lett. 39, 1675 (1977).
170. R. M. Fleming, Phys. Rev. B22, 5606 (1980).
171. N. P. Ong and P. Monceau, Phys. Rev. B16, 3443 (1977).
172. J. C. Gill, Solid State Commun. 39, 1203 (1981).
173. R. M. Fleming, Solid State Commun. 43, 167 (1982).
174. G. X. Tessema and N. P. Ong, Phys. Rev. B27, 1417 (1983).
175. G. Grüner and A. Zettl, Phys. Rev. B26, 2298 (1982).
176. G. Grüner, Mol. Cryst. Liq. Cryst. 8117 (1982).
176a. K. Hasegawa, A. Maeda, S. Uchida and S. Tanaka, Physica 117B & 118B, 599 (1983).
177. C. Roucau, R. Ayroles, P. Monceau, L. Guemas, A. Meerschaut and J. Rouxel, Phys. Stat. Sol. 62a, 483 (1980).
178. J. Dumas, C. Schlenker, J. Marcus and R. Buder, Phys. Rev. Lett. 50, 757 (1983).
179. M. Maki, M. Kaiser, A. Zettl and G. Grüner, Solid State Commun. 46, 497 (1983).
180. R. Allegyer, B. H. Suits and F. C. Brown, Solid State Commun. 43, 207 (1982).
181. G. Grüner and A. Zettl, in ref. [4] , p. 1631.
182. J. Bardeen, Phys. Rev. Lett. 42, 1498 (1979).
183. J. Richard and P. Monceau, Solid State Commun. 33, 635 (1980).
184. M. Oda and M. Ido, Solid State Commun. 44, 1535 (1982).
185. A. P. Portis, Mol. Cryst. Liq. Cryst. 81, 59 (1982).
186. J. L. Tholence and R. Tournier, J. de Phys. 35, C4-229 (1974).
187. P. Monod, J. J. Prejean and B. Tissier, J. Appl. Phys. 50, 1324 (1979).
188. J. Ferre, J. Rajchenbach and H. Maletta, J. Appl. Phys. 52, 1697 (1981).
189. H. Takayama and H. Matsukawa, unpublished.
190. L. Sneddon, M. C. Cross and D. S. Fisher, Phys. Rev. Lett. 49, 292 (1982).
190a. D. S. Fisher, Phys. Rev. Lett. 50, 1486 (1983).
191. M. Oda and M. Ido, personal communications.
192. G. Grüner, L. C. Tippie, J. Sanny, W. G. Clark and N. P. Ong, Phys. Rev. Lett. 45,935 (1980).
193. R. J. Tucker, IEEE J. Quant. Electron. 15, 1234 (1979).
194. G. Grüner, A. Zettl, W. G. Clark and J. Bardeen, Phys. Rev. B24, 7247 (1981).
195. B. Horovitz and S. E. Trullinger, Solid State Commun. 49, 195 (1984).
196. M. Weger, G. Grüner and W. G. Clark, Solid State Commun. 44, 1179 (1982).
197. B. A. Huberman and J. P. Crutchfield, Phys. Rev. Lett. 43, 1743 (1979).
198. J. P. Crutchfield, J. D. Farmer and B. A. Huberman, Phys. Rep. (Phys. Lett. Sec. C) 92, 47 (1982).

199. S. Chatterjee and S. V. Subramanyam, Solid State Commun. 41, 541 (1982).
200. D. Bennett, A. R. Bishop, S. E. Trullinger, Z. Phys. B47, 265 (1982).
201. N. P. Ong and P. Monceau, Solid State Commun. 26, 487 (1978).
202. N. P. Ong and J. W. Brill, Phys. Rev. B18, 5265 (1978).
203. R. J. Wagner and N. P. Ong, Solid State Commun. 46, 491 (1983).
204. S. E. Barnes and A. Zawadowski, Phys. Rev. Lett. 51, 1003 (1983).
205. N. P. Ong and G. Verma, Phys. Rev. B27, 4495 (1983).
206. N. P. Ong, G. Verma and K. Maki, Phys. Rev. Lett. 52, 663 (1984).
207. J. Richard, P. Monceau, M. Papoular and M. Renard, J. Phys. C 15, 7157 (1982).
208. A. Zettl and G. Grüner, Solid State Commun. 46, 29 (1983).
209. M. Papoular, Phys. Rev. B25, 7856 (1982).
210 D. W. Ruesink, J. M. Perz and I. M. Templeton, Phys. Rev. Lett. 45, 734 (1980).
211. E. W. Fenton, Phys. Rev. Lett. 45, 736 (1980).
212. L. Pietronero and S. Strässler, Phys. Rev. B28, 5863 (1983).
213. H. Takayama, Prog. Theor. Phys. 48, 382 (1972).
214. A. H. Thompson, A. Zettl and G. Grüner, Phys. Rev. Lett. 47, 64 (1981).
215. H. Matsukawa and H. Takayama, Solid State Commun. 50, 283 (1984).
216. L. Sneddon, Phys. Rev. Lett. 52, 65 (1984).

[Note added in proof]. In a recent computer work [215] based on the Hamiltonian of Equations (4.3) and (4.9), the total impurity force acting on the CDW phase in the non-Ohmic regime is shown to have a constant part, i.e. the effective potential $V(\theta)$ involves partly a saw-tooth type, although its magnitude is not large enough to reproduce experimental results of $NbSe_3$ (Equation (6.1)). In this context it is worth pointing out that if $\partial\theta/\partial t = \pi J/n_s e = \pi\sigma(E)E/n_s e$ with $\sigma(E)$ of Equation (6.1) substituted into Equation (5.11), then it turns out that the pinning force $-\tilde{\omega}_F^2 \partial V/\partial\theta$ at $E \gg E_T$ is twice as large as that just at $E = E_T$. Such increase of the pinning force after the CDW is depinned has not yet explored in the classical medium model for the CDW condensate.

3.4 Depinning Of Charge-density Waves by Quantum Tunneling

3.4.1 1. Introduction

A review of the basic theories that have been given for charge transport by the Fröhlich mechanism of moving charge-density waves is given in this book in the chapter by Fukuyama and Takayama. This chapter will review the theory of and evidence for depinning of incommensurate CDW's that are pinned by weak impurities by quantum tunneling. By weak is meant that a single impurity cannot pin the phase of the wave but pinning results from fluctuations in impurity concentration as suggested by the theories of Fukuyama and Lee [1] and Lee and Rice [2].

Quantum tunneling was suggested in the initial papers on conduction in $NbSe_3$ by Monceau et al. [3] who found that the nonlinear dc current, $I(E)$, as a function of the electric field, E, could be expressed approximately in the form:

$$I(E) = \sigma_a E + \sigma_b E \exp\left[-E_0/E\right] \tag{1.1}$$

The exponential suggests Zener tunneling across a small pinning gap. However the model was rejected because the gap required for the small values of the depinning fields E_0 ($\sim 1-2$ V/cm below the upper transition, T_1, and $\sim 0.1-0.2$ V/cm below T_2) was found to be much smaller than thermal energy, $k_B T$, and so would be wiped out by thermal effects. In 1979, the author [4a] pointed out that the model could be revived if applied only to the coherent motion of electrons in the condensate of the CDW. In the absence of pinning, an

incommensurate CDW should be accelerated freely by an electric field. The Peierls gaps move with the Fermi sea and do not affect the motion of the condensate, but they do inhibit excitation of individual particles. If the number of electrons involved in the coherent motion is sufficiently large ($\sim 10^9$ or 10^{10}), the total energy involved is much larger than k_BT.

The discovery that there is a threshold field for nonlinear conduction by Fleming and Grimes, [5] since confirmed by many others, suggested [4b] that electrons can be accelerated and pick up energy from the field only over a distance, L, which is interpreted as the distance over which there is phase coherence of the CDW. This model also suggested that the voltage across L could be treated in analogy with the voltage across a super-conductor-insulator-normal (SIN) tunnel junction or an SIS junction. In an important paper, J. R. Tucker [6] extended the Tien-Gordon theory of photon-assisted tunneling in tunnel junctions to discuss the quantum limits of detection and mixing in such
junctions. A complete quantum theory was given for response to combined ac and dc fields, treating $\hbar\omega$ as a quantum of energy.

When taken over bodily and applied to the CDW problem, Tucker's theory made a number of predictions that could be tested experimentally. One of these was a scaling relation between the frequency and field dependence of the conductivity. This relation has been confirmed in a number of experiments on $NbSe_3$ and TaS_3, mainly by Grüner and Zettl [7, 8]. However, other predictions of the theory in its original form failed. In particular photon-assisted tunneling in the sense of observing a rectified signal by biasing below threshold with the energy quantum $\hbar\omega$ to go above threshold was not observed.

In 1982, J. R. Tucker instigated an experimental program at Illinois to study detection and mixing in CDW systems to try to better understand effects of ac and combined ac and dc voltages on CDW systems. Experiments with Miller, Richard and others showed that dc biases below threshold had little or no effect on any ac response. This suggested a revised form of scaling in which scaling is between the frequency and the voltage above threshold rather than to the total applied voltage. This revised form of scaling has been remarkably successful in accounting for a wide range of detection and mixing experiments and gives strong evidence in favor of the tunneling model.

This short history shows that the tunneling model has developed from a close interaction between theory and experiments. It has come in large part intuitively from experiment rather than derived from basic microscopic theory. If the theory is correct, quantum effects of frequencies in the range of $10^6 - 10^{10}$ Hz have been observed in transport phenomena at temperatures as high as 200 K . The CDW system should be a fertile field for the study of macroscopic quantum phenomena.

In Section 2 is described the Fukuyama-Lee-Rice theory of impurity pinning. The classical equations of motion for the phase of the CDW are given in Section 3. Solutions of these equations near threshold and for currents well above threshold are given in Section 4. The tunneling model for depinning is introduced in Section 5. All of the energy and momentum transferred to the electron-phonon system that makes up the CDW must go through the electrons, and it is here that the quantum step is required. Section 6 gives a brief discussion of the application of Tucker's theory and its application to detection and mixing phenomena.

No attempt is made to discuss hysteresis and memory effects or alternative theories that have been derived to account for various CDW phenomena with different models. Other theories of impurity pinning, such as that of Barnes and Zawadowski [9] may be consistent with the tunneling model.

This chapter is based in large part on an invited talk given in March 1983, at a meeting of the American Physical Society and on lectures [10] given at the International School of Physics 'Enrico Fermi', Varenna, Italy, in July 1983 and at an International Symposium at Hokkaido University, Sapporo, Japan, in October 1983.

3.4.2 2. Weak Impurity Pinning

According to the theory of Fukuyama and Lee [1] and Lee and Rice, [2] when the pinning is weak so that a single impurity cannot pin the phase of the CDW, pinning is determined by fluctuations in numbers of impurities in regions whose volume is
determined by a balance between the increase in kinetic energy from changes in electron density required to change the phase of the wave and the energy gain from the phasedependent impurity pinning energy. The Lee-Rice phase-coherent regions are of length L and volume $\Omega = \left(\xi_\perp/\xi_\parallel\right)^2 L^3$, where $\xi_\perp$ and $\xi_\parallel$are coherence distances transverse and parallel to the chain direction. The increase in kinetic energy (K.E.) per electron is of order $\hbar^2/\left(2mL^2\right)$, the energy required to confine an electron to the length L, and the negative pinning energy, proportional to the fluctuation, $N_i^{1/2}$, in number impurities is the region, varies as $L^{3/2}$. Here, N_i is the total number of impurities in Ω.

It is found that L varies inversely with the impurity concentration, c_i. In reasonably pure crystals ($c_i \sim 10^{-6}$), L is quite large, of the order of 3×10^{-3} cm for $NbSe_3$, and the phase coherent volume, Ω, is of order 10^{-12} cm^3. The pinning energy is of order $0.1\hbar^2/\mathrm{mL}^2$ or $\sim 10^{-23}$ergs/ elec. With an electron density of $1.5 \times 10^{21}/\mathrm{cm}^3$ there are of the order of 10^{10} electrons in a coherent volume. The pinning energy in Ω is of the order of 10^{-13}ergs, larger than the thermal energy at 100 K . Note that the total pinning energy in Ω is proportional to L so that it is the larger Lee-Rice regions that are stable against thermal fluctuations.

The phase can be adjusted to any value between 0 and $2\pi(\mathrm{mod}\,2\pi)$ at a point in the center of Ω (say $x = 0$) by adding to the phase of the uniform CDW slowly varying functions of the form

$$\phi_A = \frac{\pi}{2}\sin\left(\frac{\pi x}{L} + \phi_0\right) \tag{2.1a}$$

$$\phi_B = \pi + \frac{\pi}{2}\sin\left(\frac{\pi x}{L} + \phi_0\right) \tag{2.1b}$$

where ϕ_0 in the range $-\pi/2 < \phi_0 < \pi/2$. The change δn in the electron density in Ω is positive for this choice of ϕ_0. Equally well, one can adjust the phase to any value at $x = 0$ by taking ϕ_0 in the range $\pi/2 < \phi_0 < 3\pi/2$, in which case the δn is negative.

The phase can be adjusted with either sign of charge, so that there are many metastable configurations. This may be related to the observed hysteresis and memory effects. It should be noted that the one electron per chain in a distance L is sufficient to adjust the phase.

3.4.3 3. Equations of Motion for Phase

The possibility that CDW's formed below a critical temperature may become depinned and move through the lattice was suggested by Fröhlich [11] in 1954 as a model for a one-dimensional superconductor. The moving CDW's transport electrons with the drift velocity v_d and if there were no dissipation the current would persist in time. It is now known that a moving CDW does dissipate energy, so it is not a superconductor. Nevertheless, Fröhlich's model, based on pairing of electrons and holes with wave vectors differing by $2k_F$, does have features in common with the BCS theory of superconductivity in which there is pairing of electrons with a common total momentum. Both give an energy gap at the Fermi surface and may be described by a complex order parameter
with amplitude and phase. Both yield a Ginzburg-Landau type theory for the order parameter near T_c.

Fröhlich used an elastic continuum model in which below T_c a phonon with wave vector $Q = 2k_F$ is macroscopically occupied. If the CDW moves with a velocity v_d, the charge density becomes

$$\rho = \rho_0 + \rho_1 \cos 2k_F\,(x - v_d t) \tag{3.1}$$

Peierls gaps appear at the boundaries of the moving 1D Fermi surface (FS) defined by the wave vectors $-k_F + q, k_F + q$, where $\hbar q = m v_d$. In a more general band model, [12] m is the band mass at the FS. At low temperatures, in the absence of quasiparticle excitations, the current is the same as it would be in the absence of the Peierls gaps:

$$j = n e v_d, \tag{3.2}$$

a feature in common with a superconductor with a gap.
The moving CDW may be regarded as a macroscopic occupation of a phonon of wave vector $2k_F$ and frequency $\omega_d = 2k_F v_d$. The energy difference between the two sides of the Fermi surface is $2\hbar k_F v_d$, just equal to the energy quantum $\hbar\omega_d$ of the phonon. The CDW is the equilibrium resulting from emission and absorption of $2k_F$ phonons by the electrons. For a uniform v_d the only degree of freedom is a coherent motion of all of the electrons in the volume so as to change v_d. Excitation of individual electrons is inhibited by the Peierls gap.

In a moving CDW the ions oscillate about their equilibrium positions so that the total kinetic energy is much larger than that of the electrons alone. The total K.E. per electron associated with the motion may be written [11]

$$\text{K.E./elec } = \frac{1}{2}\,(m + M_F)\,v_d^2, \tag{3.3}$$

where $M_F \sim 10^3$ m is the Fröhlich mass representing the K.E. of the ion motion.
A density and drift velocity varying slowly in space and time may be described by the phase, $\phi(x,t)$, of the CDW relative to the lattice. The charge density is defined by

$$\rho = \rho_0 + \rho_1 \cos \phi(x,t) \tag{3.4}$$

The electron density, $n(x,t)$, per chain is given by the local value of $2k_F/\pi$, or [12]

$$n(x,t) = (1/\pi)\partial\phi/\partial x \tag{3.5}$$

The particle current per chain, nev_d, is given by [12]

$$j(x,t) = -(1/\pi)\partial\phi/\partial t \tag{3.6}$$

Equality of cross-derivatives gives the equation of continuity

$$\frac{\partial j}{\partial x} + \frac{\partial n}{\partial t} = 0. \tag{3.7}$$

Equations (3.5) and (3.6) imply that each node of the CDW carries two electrons. These equations can be generalized to the three-dimensional case.

To describe slow variations in space and time, one may write

$$\phi(x,t) = 2k_F x + \theta_0(x) + \theta(x,t) \tag{3.8}$$

where θ is a slowly varying function of space and time. The phase $\theta_0(x)$ is that required to minimize the energy from fluctuations in impurity concentration with weak impurity pinning. The pinning energy is then proportional to a periodic function, $V(\theta)$, of the change, θ, in phase from that which gives the energy minimum, $\theta_0(x)$. The equation of motion for θ is generally written in the form (see Chapter 2, Equation (5.1))

$$\frac{\partial^2\theta}{\partial t^2} - u_P^2\frac{\partial^2\theta}{\partial x^2} + \omega_P^2\frac{\mathrm{d}V}{\mathrm{d}\theta} = \frac{2k_F eE}{M_F} = \frac{2k_F e^* E}{m} \tag{3.9}$$

where $u_P = (m/M_F)^{1/2} v_F$ is the phason velocity, ω_P is the pinning frequency, $e^* = (m/M_F)\, e$ and $V(\theta) \to \theta$ when θ is small. In the semi-classical approach a phenomenological damping term is added to (3.9).

Phase is also an important variable to describe current flow in a superconductor, but the relations are different. The space derivative gives the canonical momentum of the superfluid, $p_s = mv_s = -i\hbar\nabla\theta$ (in the absence of a magnetic field) and the time derivative gives the chemical potential, $\mu = i\hbar\partial\theta/\partial t$. Equality of the cross-derivatives give the equation of motion:

$$\frac{\partial p_s}{\partial t} = -\nabla\mu. \tag{3.10}$$

Zero current flow implies that the phase is constant everywhere so that there is longrange coherence in phase.

In a CDW system there is long-range coherence in phase only if the current-density is the same everywhere, a requirement much more difficult to achieve. Important correlation functions are the phase-phase correlation function, $\langle\theta(x)\theta(x')\rangle$, the density-density correlation function,

$$\left\langle n(x)n(x') = \pi^{-2} \left\langle \frac{\partial\theta}{\partial x}\frac{\partial'\theta}{\partial x'} \right\rangle \right. \tag{3.11}$$

and the current-current correlation function:

$$\langle j(x,t)j(x',t)\rangle = \pi^{-2} \left\langle \frac{\partial\theta(x,t)}{\partial t}\frac{\partial\theta(x',t)}{\partial t} \right\rangle. \tag{3.12}$$

The length L defined by (3.11) for the phase or density correlation function, determined by minimizing the impurity pinning energy, is typically of the order of 10^{-3} cm. The length, L_j, determined by the current-current correlation function may be much
larger. In a few exceptionally pure and uniform specimens of $NbSe_3$, L_j is of the order of the sample size, [13] 10^{-1} cm.

In the latter, $\theta(x,t)$ is a function only of the time coordinate required to give a uniform current density:

$$\theta(x,t) = \theta(t) \tag{3.13}$$

The equation for the time variation is then

$$\frac{\mathrm{d}^2\theta}{\mathrm{d}t^2} + \omega_P^2 \frac{\mathrm{d}V(\theta)}{\mathrm{d}\theta} = \frac{2k_F eE(t)}{M_F} \tag{3.14}$$

Even when L_j is less than sample size, Equation (3.14) may be used to calculate the acceleration of the current by the field over regions of size L_j. To take dissipation into account in steady state one may balance the acceleration by the field with the loss due to dissipation. In a simple relaxation time approximation,

$$\left(\frac{\partial^2\theta}{\partial t}\right)_{\text{field}} + \frac{1}{\tau^*}\frac{\partial\theta}{\partial t} = 0 \tag{3.15}$$

As we shall see in Section 5, quantum tunneling effects are required to determine the acceleration of the electrons by the field from a quantum version of the semiclassical equation (3.14).

It should be recognized that although in this section the equations are written for a single chain, many parallel chains are involved in the coherent motion of a CDW. When applied to the coupled system of electrons and macroscopically occupied phonons, they are essentially classical. It is believed that quantum tunneling is required only to discuss the acceleration

through forces applied to the electrons. In the following section which shall give solutions of these classical equations and in Section 5 discuss the basis for the tunneling model.

3.4.4 4. Solutions of the Equations of Motion

We shall first give the solutions of the equation of motion (3.14) in the absence of applied fields and dissipation. There is an energy integral of

$$\frac{\mathrm{d}^2\theta}{\mathrm{d}t^2} + \omega_P \frac{\mathrm{d}V(\theta)}{\mathrm{d}\theta} = 0 \tag{4.1}$$

which is

$$\frac{1}{2}(\ \mathrm{d}\theta/\mathrm{d}t)^2 + \omega_P^2 V(\theta) = W = \ \text{const.} \tag{4.2}$$

The first term represents the kinetic energy and the second the potential energy of the phase-dependent pinning energy.

The threshold solution is that corresponding to $W = 0$. Consider the solutions

$$\theta_A = -\frac{1}{2}\pi \sin \omega_P t, \quad \theta_B = -\pi + \frac{1}{2}\pi \sin \omega_P t. \tag{4.3}$$

For both, we have from (4.2) with $W = 0$:

$$\omega_P^2 V(\theta) = -\frac{1}{2}(\ \mathrm{d}\theta/\mathrm{d}t)^2 = -\left(\pi^2\omega_P^2/8\right)\cos^2 \omega_P t \tag{4.4}$$

which gives, with use of (4.3),

$$V(\theta) = -\frac{1}{2}\left(\left(\frac{1}{2}\pi\right)^2 - \theta^2\right) \quad \left(-\frac{1}{2}\pi < \theta < \frac{1}{2}\pi\right) \tag{4.5}$$

The current is proportional to

$$-\frac{\mathrm{d}\theta_{A,B}}{\mathrm{d}t} = \pm\frac{1}{2}\pi\omega_P \cos \omega_P t \tag{4.6}$$

where the $+$ sign corresponds to A and the $-$ sign to B. To get a unidirectional current one must alternate the solutions θ_A and θ_B :

$$\begin{array}{llll} \theta_A & \text{for} & -\frac{1}{2}\pi < \omega_P t < \frac{1}{2}\pi & \mathrm{mod}\, 2\pi \\ \theta_B & \text{for} & \frac{1}{2}\pi < \omega_P t < \frac{3}{2}\pi & \mathrm{mod}\, 2\pi. \end{array} \tag{4.7b}$$

Note that at the cross-over, $\theta_A = \theta_B$ and the current is zero. The current is proportional to:

$$-(\mathrm{d}\theta/\mathrm{d}t) = \frac{1}{2}\pi\omega_P \left|\cos \omega_P t\right| \tag{4.8}$$

The pinning energy for this solution is always negative

$$V(\theta) = -\left(\pi^2/8\right)\cos^2 \omega_P t = -\frac{1}{2}\left(\pi^2/4 - \theta^2\right), \quad -\pi/2 < \theta < \pi/2. \tag{4.9}$$

This function, plotted in Figure 1, may be expanded into a series of harmonics:

$$V(\theta) = -\frac{1}{2}\left(\pi^2/6 + \cos 2\theta - \frac{1}{4}\cos 4\theta + \frac{1}{9}\cos 6\theta - \ \text{etc.}\ \right) \tag{4.10}$$

The amplitudes of the harmonics vary inversely with the square of the order, n.
The zero energy solution ($W = 0$) is that for which the system just has sufficient energy to surmount the potential barriers and represents the dividing line between oscillatory solutions (θ_A or θ_B) for $W < 0$ and progressive motion in either the positive or negative direction for $W > 0$, with the system oscillating between A and B type solutions to keep the pinning energy always negative. The period for unidirectional motion is π in θ or 2π in the argument 2θ.

The solution for large current flow, $\omega_d \gg \omega_p$ is

$$\theta = -\omega_d t - \frac{\omega_P^2}{4\omega_d^2} \sin 2\omega_d t + \text{ harmonics} \tag{4.11}$$

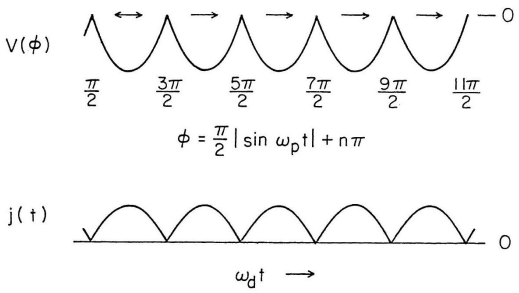


Fig. 1. Pinning potential $V(\phi)$ and current at threshold corresponding to energy just sufficient to surmount peaks at energy $W = 0$. (See Equation (4.9)).)

The current is then proportional to

$$-\frac{\partial\theta}{\partial t} = \omega_d + \frac{\omega_P^2}{2\omega_d} \cos 2\omega_d t + \text{ harmonics} \tag{4.12}$$

and the potential proportional to

$$V(\omega_d t) = -\frac{1}{2}\omega_P^2 \left(\frac{\pi^2}{6} + \cos 2\omega_d t + \text{ harmonics} \right) \tag{4.13}$$

as in (4.10) with $\omega_d t = \theta$. Solutions may be given that bridge between (4.8) and (4.12).
It is believed that the oscillating component of (4.12) is a source of 'narrow-band noise', although there may be other contributions. In samples in which the current is coherent in phase throughout the volume, the oscillating component varies inversely with the dc current as predicted by (4.12). The harmonics are found to decrease approximately with the square of the order n, also in accordance with (4.12).

The harmonics are neglected in the sine-Gordon approximation, giving

$$V(\theta) = -\frac{1}{4}(1 + \cos 2\theta). \tag{4.14}$$

If ω_P^2 is redefined by a factor of two, in the limit $\omega_d \gg \omega_P$,

$$\frac{\partial^2\theta}{\partial t^2} + \frac{1}{2}\omega_P^2 \sin 2\theta = \frac{2k_F eE}{M_F}. \tag{4.15}$$

This equation, with the addition of damping terms, is analogous to that for a resistively shunted Josephson junction. It has been used with success [14] to account for resistivity peaks observed when the dc characteristic is measured in the presence of an applied ac voltage when the ac frequency coincides with the frequency of the oscillatory current or one of its harmonics.

As we shall see in Section 5, Equations (4.1) and (4.15) for the acceleration of the CDW velocity require modification for the quantum-tunneling model. For example, the equations do not give the observed gradual increase in dc conductivity when the voltage increases beyond threshold, but predict an abrupt increase with a current varying as $(E^2 - E_{th}^2)^{1/2}$. The threshold field, E_{th} is that for which the right-hand side of (4.15) is equal to the maximum of the force from the potential $\omega_P^2 V(\theta)$ on the left, or

$$E_{th} = \frac{M_F \omega_P^2}{2k_F e} = \frac{m\omega_P^2}{2k_F e^*} \tag{4.16}$$

Although the electrons contain only a tiny fraction of the momentum and energy of the CDW system, all supplied to the system from applied electric fields must be transferred through the electrons.

3.4.5 5. The Tunneling Model

As discussed in Section 1, the tunneling model was first suggested by the observation of a nonlinear current increasing with field as $E \exp[-E_0/E]$. It was proposed that in order to displace the Fermi sea of electrons so as to give a current flow, a small pinning gap must be overcome. Zener tunneling of electrons through a small gap would give an expression of this form, but the model was rejected because the required gap is orders of magnitude less than $k_B T$. In 1979, the author [4] pointed out that such a model could be used if applied only to the coherent motion of electrons in the condensate, not to excitations of individual electrons. The latter are inhibited by the much larger Peierls gap. If the Peierls gaps move with the Fermi sea, as in the Fröhlich model, they do not affect the motion of the condensate as a whole.

By equating the wave vectors involved in zero-point motion of the electrons at the pinning frequency, ω_p, and those involved in creating a gap at the Fermi surface, the pinning gap was taken to be equal to $\hbar\omega_p$. The number of electrons involved in the coherent motion, N_e, must be large enough so that $N_e \hbar\omega_p > k_B T$. The phase-coherent region is that of Lee-Rice and involves many parallel chains.

The expression for E_0 in the Zener tunneling probability, $P(E) = \exp[-E_0/E]$, is, for a gap $\hbar\omega_P$,

$$E_0 = \frac{\pi\hbar\omega_P^2}{4v_F e^*} = \frac{\hbar\omega_P}{2\xi_0 e^*}, \tag{5.1}$$

where $2\xi_0$ is twice the Pippard coherence distance

$$2\xi_0 = \frac{4v_F}{\pi\omega_P}. \tag{5.2}$$

In this formalism, the only way the CDW is taken into account is the replacement of e by e^*. Nearly all of the crystal momentum picked up by the electrons from the electric field is transferred to the macroscopically occupied phonons. The effective charge $e^* = (m/M_F)\, e$ reflects that the equation of motion for the displacement of the Fermi sea is

$$h\frac{\mathrm{d}q}{\mathrm{d}t} = e^* E \tag{5.3}$$

It should be noted that the depinning field, E_0, in (5.1) is close to the classical threshold field. E_{th}, from (4.6) which may be written

$$E_{th} = \frac{\hbar\omega_P^2}{2v_F e^*} = \frac{2}{\pi} E_0 \tag{5.4}$$

indicating that the semiconductor model with a pinning gap equal to $\hbar\omega_p$ includes essentially the same physics as the equations of motion for the phase described in Section 4.

In 1979, Fleming and Grimes [5] showed that there is a threshold field for the onset of nonlinear conduction, and this has subsequently been verified in many other studies. The tunneling theory was modified [4] (1980) to give a threshold field by including what corresponds in ordinary semiconductors to a free path effect. Electrons can gain energy and momentum from the field at most over a free path. In our case, this corresponds to the distance L for phase coherence in the Lee-Rice theory. The threshold field is then expected to be given approximately by

$$e * E_{th} L = \hbar\omega_p \tag{5.5}$$

The value of E_0 also modified by replacing $2\xi_0$ by L. While the L 's that appear in E_{th} and E_0 should be of the same order of magnitude, they need not be exactly the same. In $NbSe_3$, $E_0 \cong E_{th}$ below T_2 and $E_0 \cong 2E_{th}$ below T_1. In TaS_3, E_0 is $\sim 2-3$ times E_{th}.

In the 1980 paper, it was shown that data of Richard and Monceau [15] on the dc current as a function of E in $NbSe_3$ at several different temperatures below T_2 could be fitted well for $E > E_0$ by the expression:

$$I = \sigma_a E + \sigma_b (E - E_{th}) \exp(-E_0/E) \quad (E > E_0) \tag{5.6}$$

The fit to the data with $E_{th} = E_0$ is shown in Figure 2.
Except for sharing of crystal momentum with the phonons, included by the replacement of e by e^*, electrons are freely accelerated over phase-coherent distances represented by the Lee-Rice distance, L. This is illustrated in the Zener diagram of Figure 2 which shows the energy bands tilted by the electric field as a function of a space coordinate in the chain-direction. In order to have tunnering, one must go from an occupied state in the lower band to an unoccupied state in the next higher band. The reduction in states available for tunneling accounts for the factor $E - E_{\text{th}}$ preceding the exponential tunneling probability in (5.6).

The effective height of the tunneling barrier in real space may be estimated from the

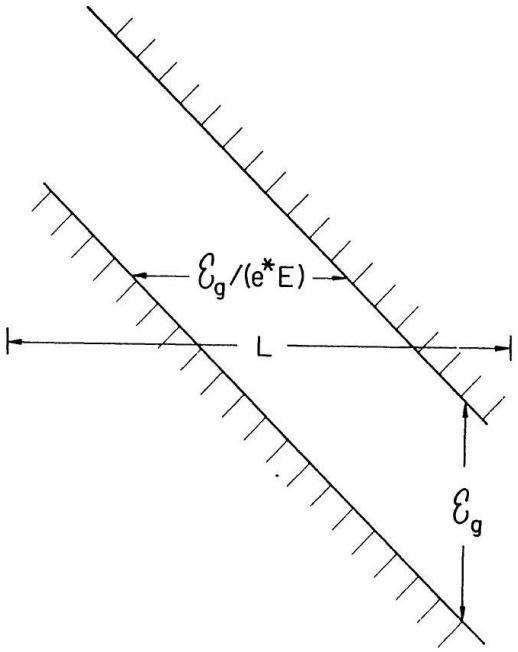


Fig. 2. Zener diagram showing energy bands tilted in space by an electric field, E. The field must be applied within a correlation length L to be effective in accelerating the electrons. (From ref. [4b].)

exponential decay of the wave function in the tunneling region. [7a] The decay is given by the imaginary part, κ of the wave vector, $k_F + i\kappa$

$$\kappa^2 = \frac{m\left(\Delta^2 - \epsilon^2\right)}{2\hbar^2 E_F}, \tag{5.7}$$

where the energy gap is $\epsilon_q = \hbar\omega_p = 2\Delta$ and ϵ is measured from midgap. The barrier corresponding to an energy ϵ is:

$$V_B = \frac{\left(h\omega_P\right)^2}{16E_F}\left(1 - \frac{\epsilon^2}{\Delta^2}\right)^{1/2} \tag{5.8}$$

where E_F is the Fermi energy. Tunneling occurs across a distance ξ_T determined by

$$e^* E\xi_T = \hbar\omega_P. \tag{5.9}$$

Essentially the same barrier may be obtained from the potential $V(\theta)$ of (4.10) illustrated in Figure 1. The argument is that there is no current flow in the lowest state corresponding to an energy $\frac{1}{2}\hbar\omega_p$. To obtain current flow, one must mix in the wave function from the next quantum state, which is higher by $\hbar\omega_p$. In a field E, this requires that tunneling occurs across the same distance, ξ_T, as in the semiconductor model.

The equation of motion of an electron in the condensate of the CDW may be obtained from (3.14) by replacing $\partial^2\theta/\partial t^2$ by $2k_F\partial v_d/\partial t$ and $\mathrm{d}V/\mathrm{d}\theta$ by $(2k_F)^{-1}\ \mathrm{d}V/\mathrm{d}x$. The pinning energy is then $m\omega_P^2(V(\theta) - V(0))/\left(4k_F^2\right)$ and the average over x or θ is

$$\langle V_B\rangle = \frac{\left(\hbar\omega_P\right)^2}{16E_F}\left\langle\theta^2\right\rangle = \frac{\left(\hbar\omega_P\right)^2}{16E_F}\cdot\frac{\pi^2}{12}, \tag{5.10}$$

which is not far from (5.8). The average of (5.8) over ϵ introduces a factor $\pi/4$ in place of $\pi^2/12$. Presumably the threshold field enters in the same way as in the semiconductor model.

The elementary tunneling step is to add a wave vector $2k_F$ to the combined electronphonon system. A pair of electrons transferred a distance L corresponds to displacing a segment of length L of the CDW by one wavelength. If an electron were transferred from one side the Fermi surface to the opposite, with an increase in wave vector by $2k_F$, it would have to share its momentum with the phonons, giving a net increase of $(e*/e)2k_F$. Thus the contribution to the current is if the charge were e^* rather than e.

However, this is not the only effect of dissipation of wave vector from the electrons to the macroscopically occupied phonons. It was pointed out in a footnote to the 1980 paper [4] that Maki's theory [16] for the creation of a pair of solitons by tunneling also has an exponential factor $\exp(-E_0/E)$, but that the expression for E_0 differed from that in the depinning problem in that the Fermi velocity, v_F, is replaced by the phason velocity, $u_P = (m/M_F)^{1/2} v_F$. It was suggested that there might be a difficulty in Maki's derivation, but it was shown to be exact at least for one value of a parameter involved. Further, the experimental data indicated that in the Zener theory the Pippard distance $2\xi_0$, roughly v_F/ω_P, should be replaced by the much smaller Lee-Rice distance, L, of order u_P/ω_P. These difficulties were resolved by Wonneberger [17] who extended the theory of Caldeira and Leggett [18] to take into account the effect of dissipation of wave vector by the electrons on the tunneling probability. In a corrected version of the theory, E_0 is similar to the Zener expression, (5.1), but with v_F replaced by u_P.

Only a simplified version of Wonneberger's theory will be given here. Caldeira and Leggett [18] showed that for tunneling through a barrier extending over a distance ξ, the correction to the tunneling probability $\exp(-B_0)$ introduced by damping is to replace B_0 by $B = B_0 + \Delta B$, where

$$\Delta B = \frac{\pi}{4}\eta^*\xi^2 \tag{5.11}$$

Here η^* is a viscosity coefficient such that the viscous force is $\eta^* v$ where v is the velocity of the particle.

We are here concerned with the damping introduced by electrons giving up most of the energy and momentum gained from the electric field to the macroscopically occupied phonons. The energy gained by the electron-phonon system when an electron tunnels across the pinning gap in $(\alpha+1)\hbar\omega_P$, where $\alpha = M_F/m$ is the Fröhlich mass ratio. If the tunneling distance is $\xi(E)$, the average froce is

$$\langle \eta^* v_F \rangle = eE = \frac{(\alpha+1)\hbar\omega_P}{\xi(E)} \tag{5.12}$$

giving $\xi(E) = \hbar\omega_P/e^*E$. The average viscosity coefficient is

$$\eta^* = \frac{(\alpha+1)\hbar\omega_P}{v_F\xi(E)} \tag{5.13}$$

so that

$$\Delta B_{\text{eff}} = \frac{\pi(\alpha+1)\hbar\omega_P\xi(E)}{4v_F} = (\alpha+1)B_0 \tag{5.14}$$

where B_0 is the Zener tunneling probability

$$B_0 = \frac{\pi\hbar\omega_P^2}{4v_F e^* E} \tag{5.15}$$

Thus ΔB_{eff} is not a small correction but is much larger than B_0. Caldeira and Leggett used a formalism in which $t \to it$ and τ_B is the 'bounce' time in the inverted potential well.

Wonneberger used τ_b as a variational parameter to obtain the tunneling probability. The optimum value is that which makes $B_0 + \Delta B$ a minimum, or to choose τ_b to minimize

$$\frac{\tau_b}{2} + \frac{\tau_{b0}^2}{2\tau_b}(1 + 2(1 + \alpha)) \tag{5.16}$$

This gives:

$$\tau_b = \tau_{b0}(3 + 2\alpha)^{1/2} \tag{5.17}$$

and, neglecting 3 compared with 2α,

$$B = B_0(2\alpha)^{1/2} = B_0\,(2M_F/m)^{1/2} \tag{5.18}$$

This correction gives the Zener expression with v_F replaced by $u_P/\sqrt{2}$ and an expression for E_0 similar to that derived by Maki.

Tunneling of an electron adds $2k_F$ to the wave vector of the electron-phonon system in a Lee-Rice region of volume Ω. This is divided between the parallel chains in the region and between the electrons and macroscopically occupied phonons. The various states corresponding to the one degree of freedom in the region may be defined by the total wave vector which is an integral multiple of $2k_F$.

3.4.6 6. Response to Ac and Combined Ac and Dc Fields

The expression (5.6) for the dc current as a function of field has been found to give a good fit to a large amount of data on $NbSe_3$ and TaS_3. Other expressions have been suggested on empirical grounds but (5.6) appears to fit the data as well as any. The threshold field, E_{th}, is determined by a phase coherent length such that $e^*E_{th}L = \hbar\omega_P$.

It is assumed that electrons in the CDW condensate are not scattered except by sharing their momentum by the phonons, indicated by the replacement of e by e^*. This suggests an analogy with Tucker's [6] theory of photon-assisted tunneling in superconductor-insulator-superconductor (SIS) tunnel junctions, with the voltage $V = EL$ corresponding to the voltage across the SIS junction. The threshold voltage $V_T = E_{th}L$. Tucker showed that the response to ac and combined ac and dc voltages may be derived from the nonlinear dc response.

For small signal ac, with $V = V_0 + V_1 \cos\omega t$, Tucker finds for the ac response, $I_{ac}\cos\omega t$,

$$I_{ac} = \frac{eV_1}{2\hbar\omega}\left[I_{dc}\left(V_0 + \frac{\hbar\omega}{e}\right) - I_{dc}\left(V_0 - \frac{\hbar\omega}{e}\right)\right] \tag{6.1}$$

where $I_{dc}(V)$ is the dc current for an applied voltage V. In the classical limit ($\hbar \to 0$) this gives just the usual classical result

$$I_{ac} = V_1\left[\frac{\mathrm{d}I_{dc}(V)}{\mathrm{d}V}\right]_{V=V_0} \tag{6.2}$$

Thus quantum theory replaces a derivative by a finite difference.
It was suggested initially that to apply to the CDW problem, one replace V_0 by EL and e by e^*. For $V_0 = 0$, this gives for the response to $V_1\cos\omega t$,

$$I_{ac}(\omega) = \frac{e^*V_1}{\hbar\omega}I_{dc}\left(\frac{\hbar\omega}{e^*}\right) \tag{6.3}$$

or expressed in terms of conductivities

$$\sigma(\omega) = \sigma_{dc}\,(\hbar\omega/e^*L) \tag{6.4}$$

with $\sigma_{dc}(E)$ defined to be I/E rather than $\mathrm{d}I/\mathrm{d}E$. This gives a scaling relation between ac and dc response.

The only data available at the time this suggestion was made were a few measurements of Grüner et al. [19] at different frequencies at one temperature on $NbSe_3$ below T_2. These are shown in the plot of Figure 3. There is good agreement except near threshold. There is no threshold frequency for changes in $\sigma(\omega)$, but $\sigma(\omega)$ increases gradually as the frequency is increased from zero. Many subsequent measurements by Grüner, Zettl and others [7, 8] have shown that the scaling relation holds accurately for $\omega > 2\omega_T$, where ω_T is the frequency corresponding to E_{th} for both $NbSe_3$ and TaS_3 at many different temperatures. The excess in $\sigma(\omega)$ for $\omega \sim \omega_T$ was attributed to absorption by the pinned mode with a peak for $\omega = \omega_T = \omega_P$.

Other predictions of Tucker's photon-assisted tunneling theory failed when applied to the CDW problem. Great success has been achieved in using SIN and SIS junctions as detectors in the submillimeter wave length range by biasing below threshold, $V < V_T$, (in this case from the superconductor gaps) but with a frequency large enough so that

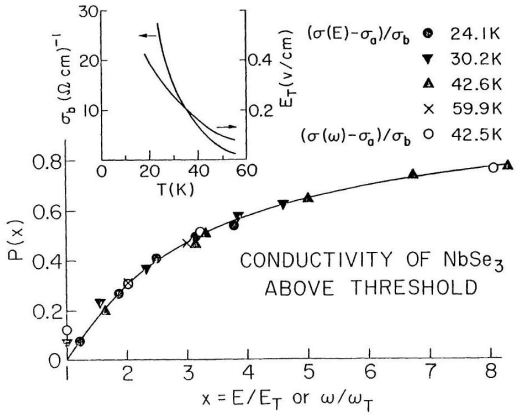


Fig. 3. Field, $\sigma(E)$, and frequency, $\sigma(\omega)$ dependent conductivities of NbSe_3 plotted on reduced scales. The solid line is a plot of $P(x) = (1 - 1/x)\exp[-1/x]$ based on tunneling theory with $E_{th} = E_0$. The data points for field dependent conductivity are from J. Richard and P. Monceau, ref. 15, and on ac conductivity from Grüner et al. (from ref. 4b).}

$V + (\hbar\omega/e)$ is above threshold. It was initially hoped to use the nonlinear characteristics of CDW conductors as detectors in a similar way, to bias below threshold, $V < V_{th}$, and to use the effective voltage from the frequency, $\hbar\omega/e^*$, to bring the total above threshold. Experiments by Grüner and Zettl [7] showed that there is no detected signal unless the total voltage, $V_0 + V_1 \cos\omega t$, is above threshold, V_T.

In 1982, Tucker initiated a program at Illinois to study detection and mixing in $NbSe_3$ and TaS_3. In a series of experiments by Miller, Richard and Tucker, it was found that dc biases below threshold had little or no effect on any ac response. Miller proposed a revised form of the theory in which scaling is to the voltage beyond threshold, $V' = V - V_T$ rather than to V. Negative values of V' correspond to $V + V_T$, with $V < -V_T$. Values of V in the range $-V_T < V < V_T$ correspond to $V' = 0$. This revised form of the theory has been remarkably successful in accounting for a wide range of detection and mixing experiments.

When applied to small-signal ac conductivity, the result is

$$I_{ac} = \frac{eV_1}{2\hbar\omega}\left[I'\left(V' + \frac{\hbar\omega}{e^*}\right) - I'\left(V' - \frac{\hbar\omega}{e^*}\right)\right] \tag{6.5}$$

where

$$I'(V') = I_{\mathrm{CDW}}(V) = \sigma_b V' \exp\left[-E_0/\left(E_{th}+E'\right)\right] \tag{6.6}$$

and E' is the field corresponding to V'. In the limit $V'=0$, this gives for the ac response

$$\sigma(\omega) = \sigma_b \exp\left[-\omega_0/\left(\omega_{th}+\omega\right)\right] \tag{6.7}$$

where ω_0 is the frequency corresponding to E_0 and ω_{th} that corresponding to E_{th}.
The revised-scaling gives a correction to the conductivity from CDW motion at $\omega = 0$, which is physically unrealistic, so that one expects that there is a lower frequency limit for which scaling applies. Below this limit, the ac should be considered a slowly varying dc and merge at very low frequencies to the dc response. The lower limit is probably the order of a few MHz for $NbSe_3$ and TaS_3.

A qualitative justification for the revised scaling may be given in terms of the threshold solution illustrated in Figure 1. At threshold, the system may go equally well to right or the left. If biased with a V' giving a small current to the right and an ac is superimposed such that $V' - (\hbar\omega/e^*)$ is negative, the latter would give a contribution corresponding to a current to the left. Near threshold, very little is required to swing the current from moving right to moving left.

The revised scaling gives not only improved agreement with ac conductivity near threshold, but also removes previous discrepancies with rectification and mixing experiments. In the small signal limit, the rectified current for an applied voltage $V \equiv V_0 + V_1 \cos\omega t$ is:

$$\Delta I = \frac{V_1^2}{2}\left\{\frac{I'\left(V_0'+\alpha\omega\right) - 2I'\left(V_0\right) + I'\left(V_0'-\alpha\omega\right)}{(\alpha\omega)^2}\right\} \tag{6.8}$$

The classical second derivative is replaced by a quantum finite difference, with $\alpha = \hbar/e^*$ if V is the voltage across L. If biased below threshold, $V_0' = 0$ and so rectified signal is to be expected.

From (6.8), one can calculate ΔI from the dc characteristic, $I'(V')$ and the scaling parameter, α, with no other adjustable parameters. Good quantitative agreement has been found for measurements over a range of bias voltages, frequencies and temperatures for both TaS_3 [20] and $NbSe_3$ [21]. Frequencies are in the range $10^6 - 10^9$ Hz. What discrepancies were found are largely accounted for by the fact that ac voltages (of the order of $10-20\%V_T$) were not quite in the small signal limit. A finite amplitude ac depresses the threshold voltage, V_T, and also introduces some broadening of the curves.

Further evidence comes from experiments on harmonic mixing, which classically depends on the third derivative, $\mathrm{d}^3 I_{dc}/\mathrm{d}V^3$ of the dc current. An applied voltage, V_2, at a frequency of the second harmonic beats against the second harmonic of an ac applied voltage, V_1, arising from the nonlinear characteristic. If the applied voltage is

$$V(t) = V_0 + V_1\cos\left(\omega_1 t + \phi\right) + V_2\cos\omega_2 t \tag{6.9}$$

there will be a rectified signal proportional to $V_1^2 V^2$ and varying with the phase as $\cos(2\phi + \psi)$. The signal expected is the finite difference third derivative

$$\Delta I = \frac{V_1^2 V^2}{16}\left\{\frac{I'\left(V_0'+2\alpha\omega\right) - 2I'\left(V_0'+\alpha\omega\right) + 2I'\left(V_0'-\alpha\omega\right) - I'\left(V_0'-2\alpha\omega\right)}{(\alpha\omega)^3}\right\} \tag{6.10}$$

with the phase shift $\psi = 0$. This differs from the classical overdamped oscillator model where ψ is expected to increase from zero at frequencies small compared with the cross-over frequency $\omega_c = \omega_P^2\tau$ to $\pi/2$ when $\omega \gg \omega_c$. In experiments of Miller et al. [20] on TaS_3, no phase shifts were found for frequencies as high as $\nu_1 = 500$MHz, $\nu_2 = 1$GHz, much

larger than the cross-over frequency of $\sim$ 80MHz. When effects of finite amplitude ac are taken into account, there is good quantitative agreement with measurements taken at several different frequencies as a function of the dc bias.

An observed discrepancy is that the theory predicts a zero bias signal while none was observed. However, it was found that the expected signal is recovered if there is a finite frequency difference $\omega_0 = \omega_2 - 2\omega_1$ between the applied frequency, ω_2, and that generated from the fundamental at a frequency ω_1. A more detailed understanding of the response of the CDW when biased below threshold will be required to account for this frequency dependence. Frequencies of the order of $5 - 10$MHz are required for the harmonic mixing signal to reach saturation in TaS_3 and $NbSe_3$, and these are approximately those expected from theory.

Harmonic mixing was suggested and first studied in $NbSe_3$ in the microwave range by Seeger, Mayr and Phillip [22]. They found signals of the magnitude expected by the tunneling model and in a recent study found that the singal varies as $V_1^2 V_2$ down to values such that $V_1 + V_2 < V_T$ and that there is no phase shift as a function of amplitude of the applied microwave voltages. However, they were unable to measure the absolute value of the phase shift and thus verify that it is zero rather than $\pi/2$ (the latter expected from the overdamped oscillator model).

While Tucker's theory for superconducting junctions applies to ac fields of arbitrary amplitude, there are additional problems when applied to the CDW problem. It is known that large amplitude, high frequency ac fields decrease the threshold voltage for dc currents from motion of CDW's. The threshold becomes even sharper with increasing amplitude of the ac, with the second derivative, $\mathrm{d}^2I/\mathrm{d}V^2$ having a narrower and higher peak. Further, Shapiro-like steps or resistivity peaks occur when the frequency of the applied ac coincides with that of the oscillatory current associated with CDW motion or one of the harmonics. These effects have been studied by Zettl and Gruner [14] in experiments on $NbSe_3$ below T_2. They have been interpreted in terms of a sine-Gordon equation similar to (4.15) with a damping term added. To include quantum tunneling with these other effects requires that appropriate corrections be made to the semiclassical (3.14).

It is suggested in (3.15) that one calculate, using quantum tunneling, the acceleration of the current by the field, $\partial^2\theta/\partial t^2$, and to balance this against the decay of the current by damping terms. To get the response to dc, one could simply replace the electric field on the right hand side of (3.14) by

$$EP(E) = (E - E_{th}) \exp\left[-E_0/E\right] \tag{6.11}$$

This would give the correct dc current and 'narrow band' noise associated with it. To derive effects of dc combined with large amplitude ac would require some way of calculating the effect of the ac on the dc response as well as interaction with the oscillatory currents of the 'narrow band' noise.

Such a theory may require a more basic derivation of the equations of motion of the CDW from the microscopic theory of the system of interacting electrons, phonons and impurities. Hopefully, this would allow one to treat the coupling of ac and dc fields of arbitrary amplitude.

3.4.7 7. Conclusions and Acknowledgements

There is strong evidence that quasi-one-dimensional metals in which charge-density waves are formed are macroscopic quantum systems that exhibit quantum effects of frequencies in the megaHertz range at temperatures as high as 200 K . The only reason that the evidence is not completely conclusive is that no direct evidence for quantum effects such as the photon steps observed in SIS junctions has been found.

As the materials and experiments become more refined and the theory is further developed, the study of CDW systems should be an excellent field for the study of macroscopic quantum phenomena in a new range of variables.

The author is indebted to many people who have aided in the initiation and development of the quantum tunneling model of CDW depinning. The work started at the University of Karlsruhe in the fall of 2978 where the author was visiting under an award from the Alexander Humboldt Foundation. During this time, he benefited from discussions with A. Schmid. He is particularly grateful to G. Grüner, J. H. Miller, Jr. and J. R. Tucker for helping to provide the close interaction between theory and experiment during which the theory has developed to the present stage. Many others have been very helpful and provided important ideas or experimental information, including R. M. Fleming, A. J. Leggett, W. G. Lyons, K. Maki, P. Monceau, N. P. Ong, J. Richard, R. E. Thorne, W. Wonneberger and A. Zettl.

This chapter was written in part while the author was a visitor at the Institute for Theoretical Physics, University of California, Santa Barbara and he is grateful for the support received.

3.4.8 References

1. H. Fukuyama and P. A. Lee, Phys. Rev. B17, 535 (1978).
2. P. A. Lee and M. Rice, Phys. Rev. B19, 3970 (1979).
3. P. Monceau, N. P. Ong, A. M. Portis, A. Meerschaut and J. Rouxel, Phys. Rev. Lett. 37, 602 (1976); N. P. Ong and P. Monceau, Phys. Rev. B16, 3443 (1977).
4. John Bardeen, (a) Phys. Rev. Lett. 42, 1498 (1979); (b) ibid 45, 1978 (1980); (c) Mol. Cryst. Liq. Cryst. 81, 1 (1981).
5. R. M. Fleming and C. C. Grimes, Phys. Rev. Lett. 42, 1423 (1979).
6. J. R. Tucker, J. Quantum Electron. 15, 1234 (1979).
7. (a) G. Grüner, A. Zettl, W. G. Clark and J. Bardeen, Phys. Rev. B24, 7247 (1981); (b) A. Zettl, G. Grüner and A. H. Thompson, Solid State Comm. 39, 899 (1981).
8. For a review, see G. Grüner, Physica 8D, 1 (1983).
9. S. E. Barnes and A. Zawadowski, Phys. Rev. Lett. 51, 1003 (1983).
10. Proceedings of the International School of Physics, 'Enrico Fermi', Varenna, Italy, 1983 (to be published). Proceedings of the International Symposium on Nonlinear Transport and Related Phenomena in Inorganic Quasi-One-Dimensional Metals, Hokkaido Univ., Sapporo, Japan, October 20-22,1983.
11. H. Fröhlich, Proc. Roy. Soc. London, Ser. A 223, 296 (1954).
12. D. Allender, J. W. Bray and John Bardeen, Phys. Rev. B9, 119 (1974).
13. John Bardeen, E. Ben-Jacob, A. Zettl and G. Grüner, Phys. Rev. Lett. 49, 493 (1982).
14. A. Zettl and G. Grüner, Phys. Rev. B29, 755 (1984).
15. J. Richard and P. Monceau, Solid State Comm. 33, 635 (1980).
16. K. Maki, Phys. Rev. Lett. 39, 46 (1977), Phys. Rev. B18, 1641 (1978).

17. W. Wonneberger, Z. Phys. B50, 23 (1983).

18. A. O. Caldeira and A. J. Leggett, Phys. Rev. Lett. 46, 211 (1981).

19. G. Grüner, L. C. Tippie, J. Sanny, W. G. Clark and N. P. Ong, Phys. Rev. Lett. 45, 935 (1980).

20. J. H. Miller, Jr., J. Richard, J. R. Tucker and John Bardeen, Phys. Rev. Lett. 51, 1592 (1983).

21. J. H. Miller, Jr., J. Richard, R. E. Thorne, W. G. Lyons, J. R. Tucker and John Bardeen, Phys. Rev. B29, 2328 (1984).

22. K. Seeger, W. Mayr and A. Phillip, Solid State Commun. 43, 113 (1982).

3.5 Solitons In One-dimensional Systems

3.5.1 1. Introduction

Although a soliton related phenomenon has been discovered by Scott-Russel [1] in 1834, it took a long time for solitons to acquire their present popularity. The object of the present chapter is two-fold: First we would like to familiarize the readers with the notion of solitons. This will be done through a brief historical introduction and with the help of some examples. Then some salient features of the sine-Gordon soliton are summarized in Section 2. Second we shall describe applications of the soliton notion to real systems. Section 3 is devoted to the magnetic systems, while Sections 4, 5 and 6 are devoted to the conducting systems. The general background for the present review may be found in [2-7]. In the following we shall sketch how the notion of soliton is developed and finds application in many branches of physics.

How Scott-Russel [1] discovered the marvellous phenomenon of solitary wave in a water channel belongs already to a folklore. Indeed the stability of a water bump gliding smoothly over the water channel should be quite impressive. However, it took some time until this wonderful phenomenon was formulated as a special solution of the nonlinear equation discovered by Korteweg and de Vries [8]. In their work the importance of the nonlinearity in the solitary wave is delineated for the first time. Since then the subject appeared to be almost forgotten by the physics community, although meantime the sine-Gordon equation (another canonical equation) was discovered by Kochendörfer and Seeger [9] as the continuum version of a model of dislocation introduced by Frenkel and Kontorova [10].

The real renaissance of solitons is due largely in the development of computer technology after World War II. In a well-known computer experiment Fermi et al. [11] discovered to their surprise that most of one-dimensional anharmonic lattices are nonergodic; the systems appeared to return to their initial configuration after a finite lapse of time. Later Toda [12] demonstrated that this recurrence phenomenon is due to solitary waves in anharmonic lattices. In 1965, while studying the collision between two solitary waves of the Korteweg-de Vries (KdV) equation numerically, Zabusky and Kruskal [13] discovered the intriguing stability of these solitary waves; the solitary waves reappear after colliding without change in their shapes and velocities. The only effect of the collision is a finite displacement from their original trajectories. This feature prompted Zabusky and Kruskal to call these stable solitary waves as 'solitons' in analogy to elementary particles. Then in 1967 Gardner et al. [14] succeeded in showing that the initial value problem of the KdV equation is solved completely by a few steps of linear operations (inverse scattering method). Therefore the remarkable stability of solitons is partially due to the special character of the KdV equation; the KdV equation is completely integrable. Then in rapid succession it was discovered that there is a large class of nonlinear

equations in $1+1$ dimensions (one space and one time dimension), which are integrable [15-17]. Interested readers can consult an excellent review on this subject by Scott et al. [18]. So far we have described the soliton physics as a branch of mathematical physics. However, there is another strand of development on solitons, which focus on their topological aspect.

It was first realized by Finkelstein [19] that some of the nonlinear solutions of field equations can be classified in terms of homotopy classes; the solitons are classified according to the mapping between the real n-dimensional physical space surrounding the soliton and the manifold formed by the ground state field configuration. Although Finkelstein called these solitons 'kinks', it is now common practice among field theorists to call these solitons 'topological' solitons or simply solitons. This approach has been recently generalized to quantum field theory [20], liquid crystal and superfluid ^{3}He [21, 22].

The topological solitons are of particular importance in condensed matter physics. A condensed phase is characterized by an order parameter [23]. Furthermore, the ground states of a condensed phase are in general highly degenerate; there is a finite subspace in the order parameter space corresponding to the ground states. In this circumstance the topological solitons play a crucial role in the physics of the condensed states. Typical condensed states are: the superconducting state in metals, superfluid ^{4}He, superfluid ^{3}He, ferromagnet, antiferromagnet, charge density wave (CDW) state and spin density wave (SDW) state; although, in some of the condensates, two order parameters can coexist. The first three condensates are superfluid. Among other solitons the superfluid state allows linear solitons; the Onsager-Feynman vortices in superfluid ^{4}He and the Abrikosov vortices in superconductors [24] are the most well-known examples. In quasi-two-dimensional systems, the linear solitons become point-like objects and play a crucial role in the destruction of the two-dimensional order [25,26]; the two-dimensional crystal melts by unbinding of dislocation pairs, while the two-dimensional superfluid is destroyed by unbinding of vortex pairs.

Far more common topological solitons are the domain walls, which exist whenever the ground states of the condensate allow only discrete symmetry. Domain walls in ferromagnets [27], composite solitons in superfluid $^3\mathrm{He}-\mathrm{A}$ [28], n-solitons in superfluid $^3\mathrm{He}-\mathrm{B}$ [29, 30], discommensurations [31, 32] and ϕ-solitons in CDW states [33], and solitons in trans-polyacetylene [34, 35] are well-known examples. In the quasi-onedimensional systems the domain wall is a point-like object with microscopic energy. Then, as first realized by Krumhansl and Schrieffer [36], solitons play a fundamental role in the thermodynamics of the quasi-one-dimensional systems; the crossover between the topologically disordered high temperature phase to the quasi-ordered low temperature phase is controlled by thermally activated solitons. Indeed, recent excitement in soliton physics is, in part, due to the experimental observation of magnetic solitons in quasi-onedimensional magnetic systems [37-39].

In the case of quasi-one-dimensional conductors, on the other hand, evidence for solitons appears rather scarce, except in trans-polyacetylene. In spite of lively controversy about the existence of solitons both in pristine-polyacetylene and doped polyacetylene,
the present author believes that the soliton is the central notion which can correlate a large amount of experimental data on polyacetylene.

Furthermore the phase vortices in the CDW states in quasi-one-dimensional conductors like $NbSe_3$[40, 41] may be of importance in the interpretation of anomalous transport properties of these systems. We shall describe later in detail these solitons in CDW states.

Soliton physics is further enriched, recently, by field theorists, who consider solitons as models of particles in quantum field theory [19,20]. An impressive advance has been achieved recently in the quantum field theory of solitons in $1+1$ dimensions [42-44]. There is now an exciting possibility that some of the predictions in quantum field theory in $1+1$ dimensions may be confronted with experiment in quasi-one-dimensional condensed matter.

3.5.2 2. Sine-gordon Solitons

2.1. Some Examples

A sine-Gordon (SG) equation is one of the canonical nonlinear equations, which not only have soliton solutions but also is completely integrable [3]. This implies that the initial value problem of the classical sine-Gordon equation is completely solvable [17]. More recently the quantum sine-Gordon system in $1+1$ dimensions has been shown to be solvable by the Bethe Ansatz [45]. Therefore the sine-Gordon equation in soliton physics plays a role similar to the hydrogen atom in quantum mechanics. Furthermore, as we shall see shortly, the sine-Gordon equation is ubiquitous in condensed matter physics [2, 6]. A number of equations describing magnetic systems [46-49] and charge density wave (CDW) condensates [31, 32] reduce to the sine-Gordon equation in certain limits.

A. Mechanical Model [2]

First let us consider a series of pendula connected by elastic strings as shown in Figure 1, which is readily made by attaching pins to a rubber band. The angle ϕ_i, the i th pendulum, from the vertical direction, obeys the following equation of motion

$$I\frac{\mathrm{d}^2\phi_i}{\mathrm{d}t^2} = -mg\sin\phi_i + K\left(\phi_{i+1} - 2\phi_i + \phi_{i+1}\right) \tag{2.1}$$

where I, m and K are the moment of inertia, the mass of the pendulum, and the elastic constant, respectively. When the angle ϕ_i depends slowly on i, we can take the continuum limit of Equation (2.1) and we obtain;

$$\phi_{tt} = C_0^2\phi_{xx} - \omega_0^2\sin\phi \tag{2.2}$$

where

$$C_0 = (K/I)^{1/2}a, \quad \omega_0 = (mg/I)^{1/2} \tag{2.3}$$

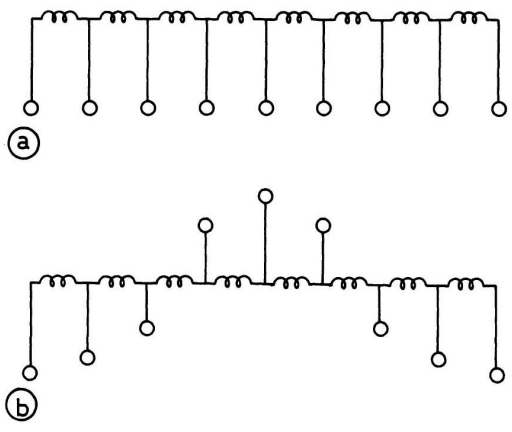


Fig. 1. A series of pendula connected by springs are shown. (a) the equilibrium configuration and (b) a configuration with one soliton.

and a is the distance between two adjacent pendula. Here suffices t and x on ϕ mean partial derivative in t and $x(=ia)$ respectively. A soliton in the present model is a 2π-twist in a series of pendula, as shown in Figure 1b.

B. One Dimensional Model of Dislocation

Frenkel and Kontrova [10] studied a one dimensional model, shown in Figure 2, to describe the motion of a slip in a crystal. It consists of two chains of atoms; the lower chain is assumed to be fixed to the regular lattice position while the atoms in the upper chain can move. The lower chain of atoms create a periodic potential of the form

$$V(\phi_i) = A\left[1 - \cos\left(2\pi\phi_i/a\right)\right] \tag{2.4}$$

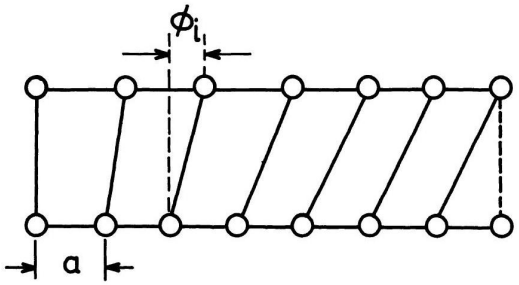


Fig. 2. The upper chain of atoms contains one slip (dislocation), while the lower chain of atoms are fixed at the regular positions.

for the i th atom in the upper chain with displacement ϕ_i from the equilibrium position. The equation of motion for ϕ_i is then given by

$$m\phi_{i,tt} = -\frac{2\pi A}{a}\sin\left(2\pi\phi_i/a\right) + K\left(\phi_{i+1} - 2\phi_i + \phi_{i-1}\right) \tag{2.5}$$

where m is the mass of the i th atom and K is the elastic constant between two atoms in the upper chain. Again the continumm limit [3] of Equation (2.5) reduces to Equation (2.2) where now C_0 and ω_0 are given by

$$C_0 = (K/m)^{1/2}a, \quad \omega_0 = \frac{2\pi}{a}(A/m)^{1/2}$$

and

$$\phi = 2\pi\phi_i/a \tag{2.6}$$

Here the soliton corresponds to a propagating slip (or dislocation) with rest energy:

$$E_s = \frac{4a}{\pi}(KA)^{1/2} \tag{2.7}$$

The present model describes lossless motion of dislocation; the slip moves uniformaly without change in its velocity. This continuum version has been extensively studied by Seeger and his collaborators [9,50] .

C. Magnetic Flux in a Josephson Junction

Let us first consider two superconductors separated by a thin insulating barrier (say an oxide film of thickness $10 - 20$Å). As shown by Josephson [51] the pair of electrons can tunnel from one superconductor to another leading to weak coupling between the wave functions Ψ_1 and Ψ_2 describing the condensates of the two superconductors across the junction. When $\phi\,(=\phi_1 - \phi_2) \neq 0$, where ϕ_1 and ϕ_2 are the phases of Ψ_1 and Ψ_2, there is a flow of supercurrent J per unit area across the junction

$$J = J_0 \sin\phi \tag{2.8}$$

where J_0 is a constant depending on the characteristic of the junction and temperature. Furthermore if a voltage V is applied across the junction the phase difference ϕ increases with time as

$$\phi_t = \frac{2e}{\hbar} V \tag{2.9}$$

These are the celebrated dc and ac Josephson effect, respectively. Now let us consider a Josephson junction with a large area, which extends in the $x - y$ plane. A large area

Josephson junction is characterized in terms of a transverse (scalar) voltage V and a transverse current $\mathbf{J}$ (the surface current on the junction) which obey [52, 53]

$$\begin{aligned} &\nabla V = L\mathbf{J}_t \\ &\nabla \cdot \mathbf{J} = -CV_t - J_0 \sin\phi \\ &\nabla\phi = -\frac{2e}{\hbar} L\mathbf{J} \\ &\phi_t = \frac{2e}{\hbar} V \end{aligned} \tag{2.10}$$

where $\mathbf{J}$ and $\boldsymbol{\nabla}$ are two dimensional vectors lying in the surface. The capacitance C and the reactance L of the junction are given by:

$$C = \epsilon/d, \quad L = (2\lambda_L + d) \tag{2.11}$$

where ϵ is the dielectric constant, d the gap between the two superconductors and λ_L is the London penetration depth. Eliminating V and $\mathbf{J}$ from Equation (2.9), we obtain

$$LC\phi_{tt} - \nabla^2\phi = -\frac{2e}{h} LJ_0 \sin\phi \tag{2.12}$$

the two-dimensional SG equation. The state of the junction is completely determined by ϕ. Of technical importance is the Josephons transmission line, which consists of two thin tapes of superconductors separated by thin oxide layer. In this limit Equation (2.11) reduces to the (one-dimensional) sine-Gordon equation. The soliton here describes a moving magnetic flux line along the junction. The flux or the fluxon carries a single flux quantum

$$\Phi = \int_{-\infty}^{\infty} V \, \mathrm{d}t = \frac{h}{2e}[\phi(\infty) - \phi(-\infty)] = \frac{h}{2e} \equiv \Phi_0 \tag{2.13}$$

with $\Phi_0 = h/2e \cong 2 \times 10^{-7}$ gauss cm^2

These propagating fluxons may be used as a signal unit in a future high speed computer. So far, in deriving Equation (2.11), the voltage loss across the junction has been completely neglected. If the loss mechanism is included, the moving fluxon will decelerate or sometimes a fluxon and an antifluxon will annihilate each other upon collision.

Besides these semi-macroscopic examples we have described, it is known that some of quasi-one-dimensional planar ferromagnets and planar antiferromagnets in a magnetic fields are described to a good approximation by the sine-Gordon equation, as we shall see in Section 2. Furthermore, a sine-Gordon equation will provide the simplest model to describe a commensurate-incommensurate CDW transition, which will be analysed in Section 4.

2.2. Classical Solutions

We shall consider again Equation (2.2), which can be derived from the Lagrangian;

$$\mathscr{L} = \frac{A}{2}\int \mathrm{d}x \left\{\phi_t^2 - C_0^2\phi_x^2 - 2\omega_0^2(1-\cos\phi)\right\} \tag{2.14}$$

where coefficient A is an arbitrary scaling factor in the classical theory. In the quantum field theory A is of prime importance, since the quantum action is measured by $\hbar$ and A provides the scale of the soliton mass. One of the fundamental features of the sine-Gordon system is that its equilibrium configuration (the vacuum in the quantum field theory) is infinitely degenerate;

$$\phi = 0, \pm 2\pi, \pm 4\pi, \ldots \tag{2.15}$$

Corresponding to this degeneracy the SG system has solutions;

$$\phi_s(x,t) = 4\tan^{-1}\left(e^{ms}\right) \tag{2.16}$$

$$\phi_s^-(x,t) = 4\tan^{-1}\left(e^{-ms}\right) \tag{2.17}$$

where $m = \omega_0/C_0, s = \gamma(x-vt)$ and

$$\gamma = \left(1 - v^2/c_0^2\right)^{-1/2} \tag{2.18}$$

They are mobile domain walls separating two equilibrium configurations; ϕ_s and $\phi_s^-$are called soliton and antisoliton. Besides isolated solitons, the soliton-soliton scattering and the soliton-antisoliton scattering solutions are given by [50,54]

$$\tan(\phi/4) = v\frac{\sinh(m\gamma x)}{\cosh(m\gamma t)} \tag{2.19}$$

and

$$\tan(\phi/4) = v^{-1}\frac{\sinh(m\gamma vt)}{\cosh(m\gamma x)} \tag{2.20}$$

respectively where $\gamma = (1 - v^2/c_0^2)^{-1/2}$. Equation (2.19), for example, describes two solitons with velocity v and $-v$ in the limit $|t| \to \infty$;

$$\tan(\phi/4) \cong \begin{cases} v[\exp(m\gamma(x+vt)) - \exp(-m\gamma(x-vt))] & \text{for } t \to -\infty \\ v[\exp(m\gamma(x-vt)) - \exp(-m\gamma(x+vt))] & \text{for } t \to +\infty \end{cases} \tag{2.21}$$

Therefore Equation (2.19) implies that solitons with velocity v and $-v$ are displaced in their position by

$$\Delta = -2(m\gamma)^{-1}\ln v \tag{2.22}$$

after the collision. More generally it is shown that the only effect of collision between two solitons or between a soliton and an antisoliton is a spatial displacement (i.e. a phase shift) compared to their unperturbed trajectories in the absence of collision.

Moreover the bound states of soliton and antisoliton are given by

$$\tan(\phi/4) = u^{-1}\frac{\sin(m\tilde{\gamma}ut)}{\cosh(m\tilde{\gamma}x)} \tag{2.23}$$

where $\tilde{\gamma} = (1 + u^2/{c_0}^2)^{-1/2}$ and u is a parameter. It is easy to see that the solution (2.23) can be obtained from Equation (2.20) by continuing analytically v to iu. The quantum mechanical

analog of the solution corresponding to a purely imaginary velocity (or momentum) is the bound state. Since Equation (2.23) describes a localized oscillation of ϕ_t or ϕ_x, these solutions are called breathers or bions. Furthermore making use of the inverse scattering method [17] any localized initial perturbation results in solitons, antisolitons and breathers after a lapse of time. In this sense we may think of solitons, antisolitons and breathers as basic constituents of the sine-Gordon system.

In the case of the sine-Gordon system an exact N-soliton, M-antisoliton solution can be constructed [18].

2.3. Statistical Mechanics

In the one-dimensional system, the soliton given by Equation (2.16) has energy

$$E_S(v) = E_S\gamma, \quad E_S = 8A\omega_0 C_0 \tag{2.24}$$

When the sine-Gordon system is in thermal equilibrium, solitons can be treated as particles [36], and indeed the classical statistical mechanics of the sine-Gordon system can be formulated in terms of solitons [55, 56]. However, we shall describe here an alternative method, the transfer integral method (TIM) developed by Scalapino et al. [57]. This method reduces calculation of the free energy and the correlation lengths to solving an eigenvalue equation as long as we are interested in the classical limit. Of course the results thus derived can be interpreted in terms of solitons. First we shall introduce the Hamiltonian corresponding to Equation (2.14)

$$\mathcal{H} = \frac{A}{2}\int \mathrm{d}x \left\{\phi_t^2 + c_0^2\phi_x^2 + 2\omega_0^2(1-\cos\phi)\right\} \tag{2.25}$$

where π the conjugate operator to ϕ is given by

$$\pi = A\phi_t \tag{2.26}$$

The thermodynamics of the sine-Gordon system is determined from the partition function defined by

$$Z\left(=e^{-\beta F}\right) = \int \mathrm{D}\pi(x) \int \mathrm{D}\phi(x) e^{-\beta H} \tag{2.27}$$

where $\mathrm{D}\pi(x)$ and $\mathrm{D}\phi(x)$ are functional integrals over the static configuration of $\pi(x)$ and $\phi(x)$, respectively. In the classical limit the $\mathrm{D}\pi(x)$ and $\mathrm{D}\phi(x)$ integrations are performed separately, and the free energy F is given as [57,58]

$$F = \frac{T}{l}\ln\left(\frac{C_0}{lT}\right) + A{\omega_0}^2\epsilon_0 \tag{2.28}$$

where l is the lattice constant (the $\mathrm{D}\pi(x)$ integral is carried out after discretizing $\pi(x)$ as π_i, and l^{-1} refers to the degrees of freedom associated with the system) and ϵ_0 is the lowest eigenvalue of the eigenequation;

$$\left(-\frac{1}{2m^*}\frac{\mathrm{d}^2}{\mathrm{d}\phi^2} + (1-\cos\phi)\right)\psi_n(\phi) = \epsilon_n\psi_n(\phi) \tag{2.29}$$

and

$$m^* = (A\omega_0 C_0\beta)^2 = (\beta E_S/8)^2\,. \tag{2.31}$$

Of particular interest is ξ_1, which is the correlation length associated with the correlation function sensitive to the topological order [59]. Indeed ξ_1 is expressed in terms of the soliton density as [59]

$$\xi_1 = 4n_s \tag{2.32}$$

where n_s is the total soliton density, to be defined later.
Recently Equation (2.29) has been studied both numerically [60] and perturbationally [61-63]. In the classical limit F_ϕ can be expanded in a double series as [61-63]

$$\begin{aligned} F_\phi = A{\omega_0}^2\epsilon_0 =& E_s m \left\{ \frac{1}{2}t - \frac{1}{4}t^2 - \frac{1}{8}t^3 - 3t^4/16 - 53t^5/2^7 - \right. \\ & - \frac{297t^6}{2^8} - \frac{3971t^7}{2^{10}} - (t/2\pi)^{1/2}e^{-1/t}\left(1 - \frac{7t}{8} - \frac{59t^2}{2^7} - \frac{897t^3}{2^{10}} - \right. \\ & \left. - \frac{75005t^4}{2^{15}} - \frac{1916273t^5}{2^{18}} - \frac{113580575t^6}{2^{22}}\right) + \\ & + \pi^{-1}e^{-2/t}\left(\ln\frac{4\gamma}{t} - \frac{5t}{4}\left(1 + \ln\frac{4\gamma}{t}\right) - \right. \\ & \left. \left. - \frac{t^2}{4}\left(23 + 2\ln\frac{4\gamma}{t}\right) + \cdots\right)\right\} \end{aligned} \tag{2.33}$$

where $m = \omega_0/C_0, t = (\beta E_S)^{-1}$ and $\gamma = 1.781$, the Euler constant. The first term in the bracket of Equation (2.33) is interpreted as being due to anharmonic phonons, while the second term is due to thermal solitons [note that $n_s \propto e^{-1/t}$]. The last term is due to the soliton-soliton interaction [63]. Indeed the total soliton density is given within the same approximation by [61,62]

$$n_s = m(2/\pi t)^{1/2}e^{-t^{-1}}\left(1 - \frac{7t}{8} - \frac{59t^2}{2^7} - \frac{897t^3}{2^{10}}\cdots\right) \tag{2.34}$$

The earlier version of the ideal soliton gas phenomenology [55, 56] was able to account for only the lowest order term in t in the coefficient of Equation (2.34). However, it is recently shown that the higher order corrections in t can be found [64], by making use of the method of collective coordinates developed by Gervais and Sakita [65].

Equation (2.32) together with Equation (2.34) indicates that the inverse of the correlation length ${\xi_1}^{-1}$ increases exponentially as the temperature decreases below E_s. Furthermore, the specific heat of the sine-Gordon system is obtained from Equation (2.33) as [63]

$$\begin{aligned} C_s =& -T\frac{\partial^2 F}{\partial T^2} \\ =& l^{-1} + m\left\{\frac{t}{2} + \frac{3t^2}{4} + \frac{9t^3}{4} + \frac{265t^4}{2^5} + \frac{4455t^5}{2^7} + \cdots + \right. \\ & + 4(2\pi)^{-1/2}t^{-5/2}e^{-1/t}\left(1 - \frac{15t}{8} - \frac{203t^2}{2^7} - \frac{2985t^3}{2^{10}} - \right. \\ & \left. - \frac{275165t^4}{2^{15}}\cdots\right) - 32\pi^{-1}t^{-3}e^{-2/t}\left(\ln\frac{4\gamma}{t} - \frac{9t}{4}\left(1\ln\frac{4\gamma}{t}\right) + \right. \\ & \left. \left. + t^2\left(\frac{11}{8} - \frac{13}{32}\ln\frac{4\gamma}{t}\right)\right)\right\} \end{aligned} \tag{2.35}$$

The specific heat is shown as function of t in Figure 3, which is taken from [63].
The specific heat has a broad peak around $T = 0.22E_s$ indicating the crossover from the topologically disordered high temperature phase to the topologically ordered low temperature

phase. It is clear from the Figure that the two-soliton term is essential to obtain the specific heat consistent with the numerical result. In particular, the peak in the specific heat at $t = 0.22$ will be shifted to a much higher value if the two-soliton term is neglected. The topological order is destroyed by the presence of thermally excited solitons. Therefore the existence of the sine-Gordon solitons in the one-dimensional system is most clearly seen in the anomaly in the specific heat and in the temperature dependence of the coherence length ξ_1.

2.4. Topological Conservation

We shall now describe a remarkable conservation law associated with the sine-Gordon system [20]. Without loss of generality we can assume that $\phi(\infty, t)$ and $\phi(-\infty, t)$ are at one of the ground states. Then we have

$$Q = \frac{1}{2\pi} \int_{-\infty}^{\infty} \mathrm{d}x \phi_x(x, t) = n - m = N \tag{2.36}$$

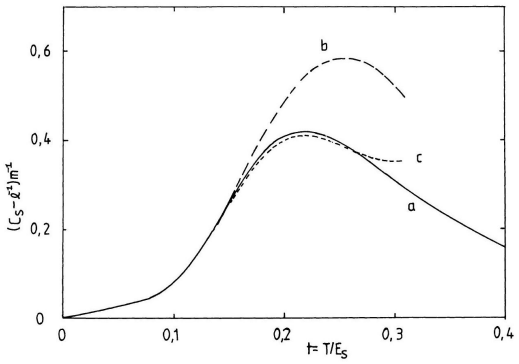


Fig. 3. The specific heat of the sine-Gordon system is shown as function of reduced temperature $t= T / E_{S} : (a) the classical numerical result [60], (b) the one soliton approximation, (c) the expression containing the two soliton contribution as well.}

with N integer, where we have assumed that

$$\phi(\infty, t) = 2\pi n, \quad \phi(-\infty, t) = 2\pi m \tag{2.37}$$

The quantity Q is the topological charge of the system and the integer N is the difference between the soliton number n_s in the system

$$N = n_s - n_s^- \tag{2.38}$$

The topological charge Q is conserved in the presence of any local perturbation on the SG system and therefore plays a very similar role to the electric charge in quantum electrodynamics for example. In terms of homotopy the topological charge indexes the mapping between two physical points $x = \infty$ and $x = -\infty$ to a discrete set of ground states of the sine-Gordon system.

2.5. Quantum Field Theory

The sine-Gordon Lagrangian (2.14) may be considered to describe a quantum system in $1 + 1$ dimensions. Then it is more convenient to rewrite Equation (2.14) as

$$\mathscr{L} = \frac{1}{2}\int \mathrm{d}x \left\{ \phi_t^2 - \phi_x^2 - \frac{2m^2}{g^2}(1 - \cos g\phi) \right\} \tag{2.39}$$

where

$$m = \omega_0, g = A^{-1/2} \tag{2.40}$$

and the present ϕ corresponds to $\sqrt{A}\phi$ in Equation (2.14). Furthermore we take $C_0 = 1$ for simplicity. If we assume that Equation (2.39) describes a quantum system, we have to eliminate divergences associated with the quantum fluctuation. In the case of the sine-Gordon system, this is done [43] simply by renormalizing mass m; we can rewrite Equation (2.39) as

$$\mathscr{L} = \frac{1}{2}\int \mathrm{d}x \left\{ {\phi_t}^2 - {\phi_x}^2 - \frac{2m_0^2}{g^2}(1 - N(\cos g\phi)) \right\} \tag{2.41}$$

where

$$m_0^2 = m^2 e^{-g^2 D/2}, D = \left\langle \phi^2 \right\rangle \tag{2.42}$$

and the normal product is defined by

$$V(\phi) = N\left\{ \exp \frac{1}{2}\frac{\partial^2}{\partial \phi^2} V(\phi) \right\} \tag{2.43}$$

Diagrammatically the normal product eliminates all the single loop contractions associated with $V(\phi)$. In general, D diverges logarithmically with the cut-off momentum Λ

$$D = \frac{1}{2\pi} \ln \left(\frac{2\Lambda}{m_0} \right)$$

and therefore in the quantum field theory only m_0 has physical meaning. On the other hand in applying a field theoretic model to the quasi-one-dimensional condensed systems, the systems in general has a natural cut off associated with the underlying crystalline lattice. Furthermore, in this circumstance both m and m_0 are observable [66]. We shall discuss the related examples in Section 3.

Making use of the semi-classical approximation Dashen et al. [42] have shown that the soliton energy is now given by

$$E_s = \frac{8m_0}{g^2} - \frac{m_0}{\pi} \tag{2.44}$$

where the second term is the mass correction due to the quantum fluctuation. Furthermore, the breathers are quantized; they are bosons with masses given by

$$E_n = 2E_s \sin\left(n g'^2/16 \right) \tag{2.45}$$

with $n = 1, 2, \ldots < 8\pi g'^{-2}$ and

$$g'^2 = g^2 \left(1 - g^2/8\pi \right)^{-1} \tag{2.46}$$

A simplified derivation of Equation (2.45) is following; making use of the BohrSommerfeld quantization condition, we obtain;

$$\int_{-\infty}^{\infty} \mathrm{d}x \int \pi(x) \mathrm{d}\phi(x) = \int_{-\infty}^{\infty} \mathrm{d}x \int_0^T \mathrm{d}t \pi(x) \phi_t(x) = 2\pi n \tag{2.47}$$

with n integer and T is the period of the breather solution. Now inserting the breather solution (2.23) slightly modified to be consistent with the Lagrangian (2.39)

$$\pi(x,t) = \phi_t(x,t) = \frac{4m\tilde{\gamma}}{g}\cos(m\tilde{\gamma}ut)\left(1 + u^{-2}\frac{\sin^2(m\tilde{\gamma}ut)}{\cosh^2(m\tilde{\gamma}x)}\right)^{-1} \tag{2.48}$$

with

$$\tilde{\gamma} = \left(1+u^2\right)^{-1/2}$$

into Equation (47) and integrating over x and t (note that $T = 2\pi(m\bar{\gamma}u)^{-1}$), we obtain

$$u^{-1} = \tan\left(\frac{ng^2}{16}\right) \tag{2.49}$$

which yields

$$E_n = 2E_s\tilde{\gamma} = 2E_s\sin\left(\frac{ng^2}{16}\right) \tag{2.50}$$

Finally the fluctuation of the quantum field around the classical solution, Equation (2.48), gives rise to additional corrections, which lead to Equation (2.45). Further, Dashen et al. [42] established that Equation (2.45) gives the correct bound state spectrum of the soliton and antisoliton up to the order of g^6 by perturbation analysis. Finally Dashen et al. [42] established that there is no other bosonic excitation at low temperatures; the breathers exhaust the bosonic excitations of the system. Later the above mass spectrum was confirmed by Luther [67] who exploited the relation between the bound state spectrum of the XYZ chain [68] and that of the sine-Gordon system. Therefore as far as the low temperature behavior is concerned the sine-Gordon system is described completely in terms of breathers, solitons and antisolitons; there is no room for the phonon modes which plays an important role in the thermodynamics of the sine-Gordon system in the classical limit (see Subsection 2.3).

Indeed, following the pioneering work of Bergknoff and Thacker [45], who solved the energy spectrum of the sine-Gordon system alias Massive Thirring model by Bethe Ansatz, it is possible to formulate the thermodynamics of the sine-Gordon system in terms only of solitons and breathers [69-73].

How the breathers are transformed into phonons in the classical limit is an intriguing question, which is discussed in [72]. In the weak-coupling limit the thermodynamics of the sine-Gordon system can be constructed by the functional integral technique [55]. in particular, it is shown that the classical statistical mechanics breaks down when $T \simeq m$ the mass of the phonon (or the mass of the lowest breather mode). Therefore in analysing the observed specific heat of quasi-one-dimensional systems, it is rather important to know the phonon mass to see if the classical theory is applicable or not. Such comparison of the present theory with observed specific heat in the quasi-one dimensional magnetic system will be discussed in Section 3.

3.5.3 3. Solitons in Magnetic Systems

3.1. Introduction

There are many magnetic insulators in which the interspin interaction in one direction (we call this direction the chain direction) is much stronger than the interactions in other directions. Most of these insulators undergo a phase transition into a three-dimensional magnetically-ordered state at low enough temperature T_N. However, in many cases we can describe these magnetic systems as one-dimensional systems when the temperature is somewhat above the Néel temperature T_N. For a general review on such magnetic systems the reader may consult Steiner

et al. [74]. We shall describe here three typical magnetic systems where, in our opinion, the existence of magnetic solitons is clearly established, namely $CsCoCl_3$, $(CH_3)_4 NMnCl_3$(TMMC) and $CsNiF_3$.

3.2. Ising-like Antiferromagnetic Chain

Perhaps the simplest magnetic system, which has soliton like excitations is the Ising-like antiferromagnetic chain described by the following Hamiltonian;

$$\mathcal{H} = 2J \sum_n S_n^z S_{n+1}^z + 2\epsilon J \sum_n \left(S_n^x S_{n+1}^x + S_n^y S_{n+1}^y \right) \tag{3.1}$$

where S_n is the spin operator with $S = \frac{1}{2}$ at site n, and $|\epsilon| \ll 1$ and $J > 0$ (antiferromagnetic coupling). The magnetic properties of quasi-one-dimensional systems like $CsCoCl_3$ and $CsCoBr_3$ [74] are well described by Equation (3.1). The Néel ground state of this system is doubly degenerate. In the limit of small ϵ the ground state configurations are shown Figures 4 (a) and (b). Further, as was first shown by Villain [75], there are low energy excitations which are shown in Figure 4(c) and (d). These excitations are magnetic solitons (or domain walls, which separate two distinct Néel ground states). The second term in Equation (3.1) transfers the soliton from one site to another and within the tight binding approximation the soliton energy is given by

$$E_s(k) = J[1 + 2\epsilon \cos(2ak)] \tag{3.2}$$

where k is the wave vector associated with the moving soliton and a is the lattice constant. The velocity of soliton with momentum k is given by

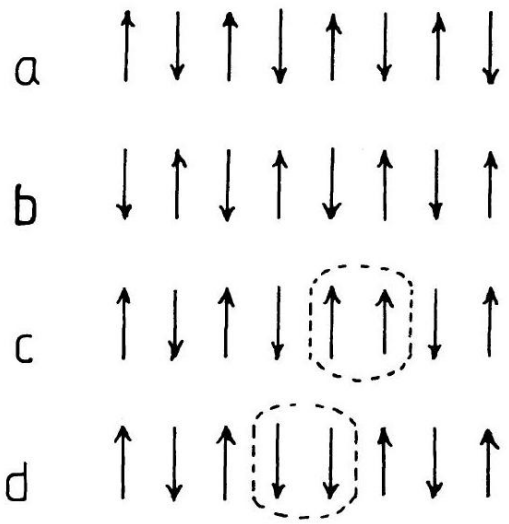


Fig. 4. The ground state spin configurations (a) and (b) of Ising-like antiferromagnetic chain. (c) and (d) are the soliton configurations, where the arrows indicate the spin direction.

$$v = \frac{\mathrm{d}E_S(k)}{\mathrm{d}k} = -4\epsilon a J \sin(2ak) \tag{3.3}$$

and the density of soliton with momentum k is given by the usual Boltzmann distribution when $\beta J \gg 1$

$$n_s(k) = \exp\left(-\beta E_s(k)\right) \tag{3.4}$$

The system described by Equation (3.1) has spin wave excitations in addition to solitons. However, the spin waves have larger excitation energies [76].

Villain [75] has predicted that the longitudinal spin correlation function is dominated by the soliton. In particular, for $|q - \pi/a| \gg K$, where q is the transferred momentum and K^{-1} is the longitudinal correlation length in the Ising limit (a more accurate expression including the correction due to ϵ will be given later)

$$e^{-Ka} = \tanh\left(\frac{1}{2}\beta J\right) \tag{3.5}$$

Villain obtained the dynamical structure factor associated with the single soliton excitation;

$$\begin{aligned} S_{zz}(q,\omega) =& (2\pi Z)^{-1}\frac{2aK}{(Ka)^2 + 4\cos^2\left(\frac{1}{2}aq\right)}\times \\ & \times \frac{e^{\beta\omega/2}}{\left(\Omega_q^2 - \omega^2\right)^{1/2}}\cosh\left[\frac{1}{2}\left(\Omega_q^2 - \omega^2\right)^{1/2}\cot(aq)\right], \quad \text{for } |\omega| < \Omega_q \\ =& 0, \quad \text{for } |\omega| > \Omega_q \end{aligned} \tag{3.6}$$

where $\Omega_q = 4|\epsilon J \sin(aq)|$

$$Z = N^{-1}\sum_k \exp[-2\beta J\epsilon\cos(2ak)] \tag{3.7}$$

This structure factor has a sharp cut-off at $\omega = \pm\Omega_q$ and has been observed in recent neutron scattering experiments on $CsCoCl_3$ and $CsCoBr_3$ by Yoshizawa et al. [77] and by Nagler et al. [78], respectively. When $|q - \pi/a| \leq K$ on the other hand, Equation (3.6) is no longer applicable, since the structure factor is dominated by the multi-soliton term in this limit [79]. Within the ideal soliton gas approximation for solitons [36], the asymptotic expression for large m limit of the spin correlation function is given by [79];

$$\left\langle \left[S^z_{n+m}(t), S^z_n(t)\right]\right\rangle = \exp\left\{i\pi m - 4\int_{-\pi/2a}^{\pi/2a}\frac{\mathrm{d}k}{2\pi}n_s(k)\,|x - v_k t|\right\} \tag{3.8}$$

where $x = ma$, and $n_s(k)$ and v_k have been defined in Equations (3.4) and (3.3), respectively. A factor of 4 in the second term in the exponential of Equation (3.8) arises from the fact that there are two types of solitons as shown in Figures 4(c) and (d), and that a soliton between the n and the $n+m$ site changes the sign of the correlation function. Unfortunately this additional factor 2 was neglected in the expression given in [79]. Equation (3.8) is well approximated as

$$\left\langle \left[S^z_{n+m}(t) S^z_n(t)\right]\right\rangle = \exp\left\{i\pi x/a - K\left(x^2 + v_0^2 t^2\right)^{1/2}\right\} \tag{3.9}$$

where

$$K = 4\bar{n}_s = 2a^{-1}e^{-\beta J} I_0(2\epsilon\beta J) \tag{3.10}$$

and

$$v_0 = 4a\left(\pi\beta I_0(2\epsilon\beta J)\right)^{-1}\sinh(2\epsilon\beta J) \tag{3.11}$$

where $I_0(z)$ is the modified Bessel function. Here $\bar{n}_s$ is the soliton density, K^{-1} is the correlation length, which includes the correction due to the ϵ-dependent term in Equation (3.1), and v_0 is the thermal velocity of solitons. In the low temperature limit ($\beta J \gg 1$) and

$\epsilon \to 0, K$ in Equation (3.10) reduces to that in Equation (3.5). The corresponding dynamical structure factor is then given by

$$S_{zz}(q,\omega) = \frac{K}{2\pi v_0}\left[(q-\pi/a)^2 + (\omega/v_0)^2 + K^2\right]^{-3/2} \tag{3.12}$$

We note that this dynamical structure factor with $K = 4\bar{n}_s$ is quite general and finds application in a number of quasi-one-dimensional antiferromagnetic systems.

3.3. Planar Antiferromagnetic Chain in a Magnetic Field

Another magnetic system of great current interest is an antiferromagnetic chain of spins described by

$$\mathcal{H} = -2J\sum_n \mathrm{S}_n \cdot \mathrm{S}_{n+1} - 2D\sum_n S_n^z S_{n+1}^z - H\sum_n S_n^x \tag{3.13}$$

where $J < 0$ and the chain direction is taken as the z direction. This Hamiltonian with $S = 5/2, J = -15K$ and $D = 2.5K$ quite well describes a quasi-one-dimensional compound $(CH)_3NMnCl_3$(TMMC)[80, 81]. The last term in Equation (3.13) describes the magnetic energy in a magnetic field H in the x direction (we took $\mu_B = 1$ for simplicity, so H has the dimension of energy). Furthermore, according to Walker et al. [80], TMMC can be considered as a planar model below $T = 20$ K. We are interested here in this low temperature regime. Then we can parameterize $\mathbf{S}_n$ as [47-49];

$$S_n = \left(\left(S^2 - \Pi_n^2\right)^{1/2}\cos\phi_n, \quad \left(S^2 - \Pi_n^2\right)^{1/2}\sin\phi_n, \quad \Pi_n\right) \tag{3.14}$$

with $\left[\ \Pi_n, \quad \phi_n{}'\ \right] = -i\delta_{nn}{}'$
Substituting Equation (3.14) in Equation (3.13) and neglecting the higher-order terms in $\Pi_n S^{-1}$, we obtain in the continuum limit;

$$\mathcal{H} = (2a)^{-1}\int \mathrm{d}z\left\{\frac{1}{4}(2|J| - D)^{-1}\phi_t^2 + 2a^2|J|S^2\phi_z^2 + \frac{1}{8}|J|^{-1}H^2\cos^2\phi\right\} \tag{3.15}$$

where a is the lattice constant.
The ground state of Equation (3.15) is given by $\phi = \pm\pi/2$. (The spin in the ground state is perpendicular to the external field $\mathbf{H}$.) As is immediately apparent, ϕ obeys a sineGordon equation. A soliton is given by

$$\phi(z,t) = \pi/2 + 2\tan^{-1}\{\exp[m\gamma(z - vt)]\} \tag{3.16}$$

with the soliton energy

$$E_S(v) = SH\gamma \tag{3.17}$$

where

$$\begin{aligned} &m = H(4a|J|S)^{-1}, \quad C = 2aS[2(2|J| - D)|J|]^{1/2} \quad \text{and} \\ &\gamma = \left(1 - v^2/c^2\right)^{-1/2} \end{aligned} \tag{3.18}$$

In the antiferromagnetic chain the soliton describes a π-twist in the spin as shown in Figure 5. As in the example of the preceding subsection, the spin correlation function $\langle[S^y(z,t)S^y(0,0)]\rangle$ reflects directly the topological order of the system; the sign of this correlation function changes whenever a soliton crosses a line connecting two points (z, t) and (0,0). This situation is

analoguous to the $\phi - \phi$ correlation function in the ϕ^4 theory discussed by Krumhansl and Schrieffer [36]. The soliton gives rise to a large central peak in this correlation function [47-49]. Such a central peak has been observed through the inelastic neutron scattering experiment on TMMC in magnetic fields by Boucher et al. [38]. The correlation function is given [47, 48] as $\langle [S^y(z,t)S^y(0,0)] \rangle = \exp(i\pi z/a) S^2 \left\langle \sin^2 \phi \right\rangle \exp\{-2N(z,t)\}$ where

$$N(z,t) = \frac{1}{\pi} \int_{-\infty}^{\infty} \mathrm{d}p |z - vt| n_s(v) \tag{3.19}$$

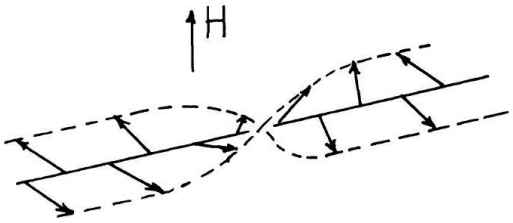


Fig. 5. The spin configuration of a soliton in planar antiferromagnetic chain in a magnetic field.

and $n_s(v)$ is the density of soliton with velocity v given by [55, 56, 64]

$$n_s(v) = 2\beta m \exp\left(-\beta E_s(v)\right) \tag{3.20}$$

where $E_S(v)$ and m have been defined in Equations (3.17) and (3.18), respectively. Here Equation (3.20) is the expression appropriate only in the classical limit (see Section 2). Note a similarity between Equation (3.19) and Equation (3.8). $N(z,t)$ may be approximated as [48]

$$N(z,t) = 2\bar{n}_s \left(z^2 + v_0^2 t^2\right)^{1/2} \tag{3.21}$$

with

$$\bar{n}_s = \frac{1}{2\pi} \int_{-\infty}^{\infty} \mathrm{d}p n_s(v) \cong \frac{2m}{c} \left(\frac{\beta E_S}{2\pi}\right)^{1/2} \left(1 - \frac{7\left(\beta E_S\right)^{-1}}{8} - \frac{59\left(\beta E_S\right)^{-2}}{2^7}\right) \exp\left(-\beta E_S\right) \tag{3.22}$$

and

$$v_0 \cong \left(\frac{1}{2}\pi\beta E_S\right)^{-1/2} \tag{3.23}$$

where $\bar{n}_s$ is the total soliton density (we include a few higher-order terms in $(\beta E_S)^{-1}$ following Equation (2.34)) and v_0 is the thermal velocity of solitons. As in the case of the preceding example, there are two kinds of solitons (right-handed and left-handed twist). Finally the Fourier transform of Equation (3.19) yields

$$S_{yy}(q,\omega) = S^2 \left\langle \sin^2 \phi \right\rangle 2\pi K v_0^{-1} \left[(q - \pi/a)^2 + (\omega/v_0)^2 + K^2\right]^{-3/2} \tag{3.24}$$

where

$$K = 4\bar{n}_s \tag{3.25}$$

which is formally the same as Equation (3.12).
Both the ω and q dependence of the central peak of TMMC in magnetic fields have been

studied in great detail by Regnault et al. [82], which confirms the theoretical expression (3.24). In particular, both the width and the shape of the central peak is well described by Equation (3.24) with $\bar{n}_s$ and v_0 given by Equations (3.22) and (3.23),
respectively, except that the classical soliton energy given by Equation (3.17) has to be replaced by the renormalized soliton energy $E_S^{\rm ren} \cong 0.77 E_S^{\rm cl}\left(E_S^{\rm cl} = SH\right)$. The latter discrepancy may be interpreted by the quantum correction [66], although the estimated quantum correction appears to be somewhat too large ($E_s^{\rm ren} = 0.60 E_s^{\rm cl}$). Another possible source of discrepancy is that, in a high magnetic field, the off-plane spin fluctuation may no longer be neglected and this fluctuation will give rise to an additional renormalization in $\bar{n}_S$ for example [83]. Experiments in a higher magnetic field can, in principle, clarify these different contributions.

The above neutron scattering experiment not only demonstrates the existence of solitons, which are thermally activated in TMMC in a magnetic field for $2\ {\rm K} < T < 5\ {\rm K}$ and $H/T \gtrsim$ 10k0e/k, but also establishes that the magnetic solitons behave like free particles. Therefore the ideal soliton gas model provides an excellent description of magnetic properties of TMMC. More recently Boucher and Renard [39] have measured the nuclear spin relaxation rate T_1^{-1} of ^{15} N atoms in TMMC in a magnetic field. Since T_1^{-1} is proportional to the local spin correlation function, we have

$$T_1^{-1} \propto \int {\rm d}q S_{yy}(q,\omega) \propto v_0^{-2} K\left[(\omega/v_0)^2 + K^2\right] \sim \left(v_0^2 K\right)^{-1} \tag{3.26}$$

which is actually observed experimentally.
The above free-particle-like behavior of solitons may be destroyed by introducing impurities in TMMC, since the impurities will scatter solitons. Then when the soliton mean free path l becomes $l\bar{n}_s \ll 1$, soliton behaves diffusively [79]. Such diffusive regimes have been studied in [84-86]. In particular, $S_{yy}(q,\omega)$ and T_1^{-1} in this regime are given by [79, 86] ;

$$S_{yy}\left(q_1,\omega\right) \propto 8KD^{-1}\left[\left(K^2 + (q-\pi/a)^2\right)^2 + 24(\omega/D)^2\right]^{-1} \tag{3.27}$$

$$T_1^{-1} \propto 2K\left[K^4 + 20(\omega/D)^2\right]^{-3/4} \tag{3.28}$$

where $D = lv_0$ and v_0 have been defined in Equation (3.23). Recently both neutron scattering and nuclear spin relaxation experiments on TMMC doped by 0.3% to 1%Cu atoms in a magnetic field have been performed by Boucher et al. [87]. They observed T_1^{-1} given in Equation (3.28), when the soliton mean free path l is about $100\times$ the atomic constant, which indicates clearly that, in this system, the soliton behavior is diffusive.

Recently Borsa [88] reported the specific heat of TMMC in the presence of magnetic fields. However, we shall defer the discussion of the specific heat to Subsection 3.5.

3.4. Planar Ferromagnetic Chain in a Magnetic Field

The magnetic properties of quasi-one-dimensional magnets like $CsNiF_3$ are well described by the Hamiltonian;

$$\mathcal{H} = -2J\sum_n \mathbf{S}_n \cdot \mathbf{S}_{n+1} + A\sum_n \left(S_n^z\right)^2 - H\sum_n S_n^x \tag{3.29}$$

where $\mathbf{S}_n$ is the spin operator at site n and the chain direction is taken along the z direction. Here a magnetic field $H/g\mu_B$ is applied perpendicular to the chain direction. For $CsNiF_3$ we have $S = 1, J = 11.8K, A = 9.5K$ and $g = 2.4$ [37]. This is the first magnetic system in which observation of magnetic solitons was reported [37]. At low temperatures where the spin fluctuation is mainly restricted to the $x-y$ plane (i.e. $T \lesssim (AJ)^{1/2}$), Equation (3.29) is recast as [46] ;

$$\mathcal{H} = -2JS^2 \sum_n \cos\left(\phi_{n+1} - \phi_n\right) + A \sum_n \Pi_n^2 - HS \sum_n \cos\phi_n \tag{3.30}$$

where we have parametrized

$$S_n = \left[\left(S^2 - \Pi_n^2\right)^{1/2} \cos\phi_n, \quad \left(S^2 - \Pi_n^2\right)^{1/2} \sin\phi_n, \quad \Pi_n\right]$$

with

$$\left[\ \Pi_n, \quad \phi'_n\ \right] = -i\delta'_{nn} \tag{3.31}$$

and higher-order terms in Π_n/S are neglected. Finally in the continuum limit Equation (3.30) reduces to the sine-Gordon Hamiltonian;

$$\mathcal{H} = a^{-1} \int \mathrm{d}z \left[(4A)^{-1}\phi_t^2 + (\mathrm{a}SJ)^2\phi_z^2 - SH\cos\phi\right] \tag{3.32}$$

where a is the lattice constant. Here the planar symmetry of the ground state is broken by an external field H. The sine-Gordon soliton of Equation (3.32) is given by

$$\phi(z,t) = 4\tan^{-1}[\exp(m\gamma(z - vt))] \tag{3.33}$$

with

$$m = a^{-1}(H/2JS)^{1/2} \tag{3.34}$$

The soliton energy is given by

$$E(v) = 8S^{3/2}(2JH)^{1/2}\gamma \tag{3.35}$$

The soliton describes a moving 2π-twist in magnetization as shown in Figure 6 and carries local magnetization given by

$$\delta\mathbf{M}(z,t) = S\left[-\operatorname{sech}^2 s, 2\operatorname{sech} s \tanh s, (2aSA)^{-1}m\gamma v \operatorname{sech} s\right] \tag{3.36}$$

As shown by Mikeska [46], the magnetic soliton gives rise to an additional contribution to the spin correlation functions;

$$S_{xx}(q,\omega) \propto 2n_s(v)[(2\pi cq/m)\operatorname{cosech}(\pi cq/2m)]^2 \tag{3.37}$$

$$S_{yy}(q,\omega) \propto 2n_s(v)[(2\pi cq/m)\operatorname{sech}(\pi cq/2m)]^2 \tag{3.38}$$

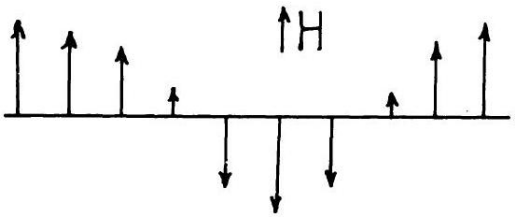


Fig. 6. The soliton in a planar ferromagnetic chain in a magnetic field.

where $n_s(v)$ is the density of solitons with velocity v,

$$N_S(v) \cong 2\beta m \exp\left(-\beta E_S(v)\right) \tag{3.39}$$

in the classical limit and v in Equations (3.37) and (3.38) should be taken to be $v = \omega/q$. The central peak given by Equation (3.37) has been observed in $CsNiF_3$ in a magnetic field by inelastic neutron scattering by Kjems and Steiner [37]. Except the fact that the soliton energy required to describe the experimental data is somewhat smaller (by about $20 - 30\%$) than that expected from Equation (3.35), Equation (3.37) quite well describes the observed neutron scattering cross-section. The discrepancy in the soliton energy can be understood as the effect of the mass renormalization due to the quantum fluctuation [66]. Although there is still controversy as to whether the observed central peak is due to the thermal magnons or the thermal solitons [89], the author believes that the thermal magnon contribution is too small to account for the observed central peak.

More recently the specific heat measurement of $CsNiF_3$ has been reported by Ramirez and Wolf [90]. We shall discuss the specific heat of the quasi-one-dimensional planar magnets in the following subsection.

3.5. Specific Heat of the Planar Magnets in a Magnetic Field

As already mentioned the specific heats of TMMC and $CsNiF_3$ in magnetic fields were reported [88,90]. Initial attempts to describe the observed peaks in the specific heat in terms of the single soliton term (the second term in Equation (2.35)) lead to confusion. The observed peaks appeared to imply too small a soliton energy. However, the inclusion of the two soliton term (see Equation (2.35)) improved the agreement greatly. On the other hand, the classical expression (2.35) cannot describe the observed rapid decreases in the specific heat for $t \leqslant 0.2$, which are actually due to the quantum freezing of the magnons in these systems. A more satisfactory comparison is made with the specific heat of the sine-Gordon system within the Bethe Ansatz [91]. Some of these fits are shown in Figure 7, which is taken from [91]. As may easily be seen the theory appears to describe quite well, not only the peak positions, but also the general temperature-dependence of the specific heat. In drawing the figure the following renormalized soliton energies $E_s^r = 0.7E_S$ is used for $CsNiF_3$. For TMMC the classical theory with $E_s^r = 0.84E_s$ appears to describe the observed specific heat, although the predicted peak in the specific heat appears to be somewhat lower than that observed. These renormalized soliton energies are not inconsistent with the ones due to the quantum fluctuation [66].

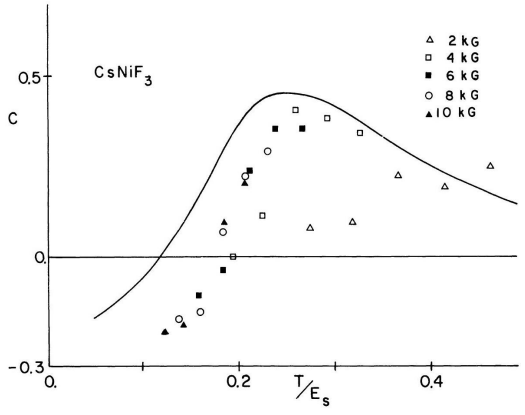


Fig. 7. The specific heat of $\mathrm{CsNiF
_{3}$ (planar ferromagnetic chain) in magnetic fields [90] are compared with the Bethe Ansatz calculation [91].}

3.5.4 4. Solitons in Conducting Systems

4.1. Peierls - Fröhlich Instability

In the following we shall describe solitons in conducting systems. We are interested mostly in quasi-one-dimensional systems, where the system undergoes a Peierls-Fröhlich transition [92, 93] at nonzero temperature; the resulting condensed state is called the PeierlsFröhlich state or the charge density wave (CDW) state. A recent work on low dimensional systems is found in [7]. We shall start with a one-dimensional system described by the Fröhlich Hamiltonian [93]

$$\mathcal{H} = \sum_{ks} \epsilon_k C_{ks}^{+} C_{ks} + \sum \omega_q^0 b_q^* b_q + ig \sum_q \left(\omega_q^0/2\right)^{1/2} C_{k+qs}^{+} C_{ks} \left(b_q + b_q^*\right) \tag{4.1}$$

where $C_{ks}^{+}$and b_q^* are the creation operators for a Bloch electron with momentum k and spin s and a longitudinal phonon with momentum q; and ϵ_k and ω_q^0 are bare energies of the electron and phonon, respectively. Furthermore the electron-phonon coupling constant g is taken to be constant for simplicity. Due to the electron-phonon interaction the phonon dispersion is modified from ω_q^0 [94, 95] as

$$\omega_q = \omega_q^0 (1 - \pi(q))^{1/2} \tag{4.2}$$

where

$$\begin{aligned} \pi(q) &= \frac{2q^2}{\pi} \int \mathrm{d}p \frac{f_p \left(1 - f_{p+q}\right)}{\epsilon_{p+q} - \epsilon_p} \\ &= \frac{1}{\pi v_F} g^2 \frac{1}{x} \ln \left| \frac{1+x}{1-x} \right| \quad \text{at} \quad T = 0 \text{ K} \end{aligned} \tag{4.3}$$

and $x = q/2P_F$.
Here f_p is the Fermi distribution function and

$$\epsilon_p = \frac{1}{2m} p^2 - \mu$$

is used in evaluating Equation (4.3). At $T = 0$ K, $\pi(q)$ diverges logarithmically for $q = 2P_F$ and P_F is the Fermi momentum. This singularity in the phonon dispersion indicates that the one-dimensional normal electron state becomes unstable at low temperatures. This instability is known as Peierls-Fröhlich instability [92, 93]. At high temperatures, the logarithmic divergence is completely smeared out by the temperature. As the temperature is decreased, the phonon dispersion starts to exhibit a sharp dip around $q = 2P_F$. This is the Kohn anomaly [95], and has been observed in a number of quasi-one-dimensional systems. See [96] for a review. With lowering temperature, this dip becomes sharper, and ultimately the system becomes unstable against formation of the charge density wave (CDW) state when $\omega_Q = 0$ with $Q = 2P_F$, within the mean field approximation.

Strictly speaking both the Midgal approximation and the mean field approximation are not valid in the one-dimensional system due to the fluctuations neglected in the mean field theory. However, no real physical systems are strictly one-dimensional. Furthermore, even in the one-dimensional system, the short-range correlation with the local order parameter close to the mean field value develops at low temperature, say below $T_c/4$ [97], where T_c is the transition temperature determined within the mean field theory. Therefore we shall continue to analyse the charge density wave (CDW) condensate in terms of the mean field theory in spite of its limitations.

4.2. The Charge Density Wave (cdw) State

The mean field theory of the charge density wave state is worked out in a classical paper by Lee et al. [98]. The order parameter describing the CDW condensate is introduced by

$$\Delta = g\left(2\omega_Q\right)^{1/2}\langle b_Q\rangle \tag{4.5}$$

Substituting this into Equation (4.2) where we replace b_Q by $\langle b_Q\rangle$, we obtain;

$$\mathscr{H}_{\mathrm{MF}} = g^{-2}|\Delta|^2 + \sum_S \int \mathrm{d}x \Psi_S^+(x)\left(-i\sigma_3 v_F\partial_x + \sigma_1\Delta_1 + \sigma_2\Delta_2\right)\Psi_S(x) \tag{4.6}$$

where we have introduced a spinor representation for electrons [99] as

$$\Psi_{ks} = \left\{ \begin{array}{l} C_k + \frac{1}{2}Qs \\ C_{k-\frac{1}{2}}Qs \end{array} \right\} \tag{4.7}$$

and $\Psi_s(x)$ is the Fourier transform of Ψ_{ks} and $\Delta = \Delta_1 + i\Delta_2$. Here σ_i are the Pauli matrices and we have neglected $k^2/(2m)$ in comparison with $v_F k$. The thermal Green's function for the electron is now given by

$$G\left(k,\omega_n\right) = \left(i\omega_n - \xi_k\sigma_3 - \Delta_1\sigma_1 - \Delta_2\sigma_2\right)^{-1} \tag{4.8}$$

where $\xi_k = v_F k$ and $\omega_n = (2n+1)\pi T$ is the Matsubara frequency. Then Δ is determined from the self-consistent equation

$$\begin{aligned} \Delta &= g^2 T\sum_n \int \frac{\mathrm{d}k}{2\pi}\,\mathrm{Tr}\left\{\left(\sigma_1 + i\sigma_2\right)G\left(k,\omega_n\right)\right\} \\ &= \frac{g^2}{2\pi}\Delta\int \mathrm{d}k \frac{\tanh\left(\frac{1}{2}\beta E_k\right)}{E_k} \end{aligned} \tag{4.9}$$

where

$$E_k = \left(\xi_k^2 + |\Delta|^2\right)^{1/2} \tag{4.10}$$

This is essentially the BCS gap equation [100]. In particular, at $T = 0$ K, we obtain

$$\Delta = 2We^{-1/\lambda} \tag{4.11}$$

with

$$\lambda = g^2\left(\pi v_F\right)^{-1} \quad \text{and} \quad W = Q^2/8m \tag{4.12}$$

where W is the half band width. Within the mean field theory the temperature dependence of Δ is the same as the BCS energy gap of a superconductor. Δ vanishes at T_c given by

$$T_c = \frac{2\pi}{\gamma}We^{-1/\lambda} \tag{4.13}$$

On the other hand, in the vicinity of the transition temeprature the prediction of the mean field theory becomes less reliable for the quasi-one-dimensional system.

In the CDW state, the electron charge density develops an oscillatory behavior given by

$$\rho_{\mathrm{CDW}}(x) = N_0\lambda^{-1}R_e[\Delta\exp(i(Qx+\phi))] = N_0\lambda^{-1}\Delta\cos(Qx+\phi) \tag{4.14}$$

where ϕ is the phase of Δ.

As in a superconductor, the Pauli susceptibility decreases rapidly in the CDW state [101]:

$$\chi_{\mathrm{CDW}} = \chi_N \left(1 - 2\pi T \sum_{n=0}^{\infty} \frac{\Delta^2}{\left(\omega_n^2 + \Delta^2\right)^{3/2}} \right) = \chi_N Y(T) \tag{4.15}$$

where $Y(T)$ is the Yosida function. Furthermore, the electric conductivity of the CDW state is approximately given by [102]

$$\sigma_{\mathrm{CDW}} = 2\sigma_n \left(1 + e^{\beta\Delta}\right)^{-1} \tag{4.16}$$

in the clean limit $l \gg \xi$, where l is the electron mean free path, $\xi = v_F/\Delta$ is the BCS coherence length and $\beta = (k_B T)^{-1}$. The temperature dependences of $\Delta, \chi_{\mathrm{CDW}}$ and σ_{CDW} are shown in Figure 8, where we made use of the table given by Mühlschlegel [103]

4.3. Phase (ϕ) - Hamiltonian

The dynamics of the CDW is described in terms of the time-dependent order parameter $\Delta(t)$. As has been pointed out by Lee et al. [98], the order parameter has two degrees of freedom in the linear regime; the phase mode and the amplitude mode, as in a superconductor. However, unlike the superconductor the former mode is gapless (i.e. the Goldstone mode) unless the CDW is pinned either by the commensuration energy or by the impurities.

The dynamic of $\Delta(x,t)$ can be formulated as follows [99]: Assuming that $\Delta(x,t)$ is given by

$$\Delta(x,t) = (\Delta + \delta)e^{i\phi} \tag{4.17}$$

where Δ is the equilibrium order parameter and δ and ϕ are fluctuations from the equilibrium value and depend on x and t.

In the absence of the pinning potential a constant ϕ is completely eliminated by a phase change in the electron field such as

$$\tilde{\Psi} = U^{+}\Psi U \tag{4.18}$$

with $U = \exp\left(\frac{1}{2}\sigma_3\phi\right)$, which is the consequence of the global gauge invariance. However, when ϕ depends both on x and t, the above transformation gives rise to the extra terms in the electronic part of the Hamiltonian (4.6); Equation (4.6) becomes

$$\mathcal{H}_e = \mathcal{H}_e^0 + \mathcal{H}_e^{\mathrm{fl}} \tag{4.19}$$

$$\mathcal{H}_e^0 = \sum_s \int \mathrm{d}x \Psi_s^{+}(x) \left\{ -iv_F \partial_x \sigma_3 + \Delta\sigma_1 \right\} \Psi_S(x) \tag{4.20}$$

$$\mathcal{H}_e^{\mathrm{fl}} = \sum_s \int \mathrm{d}x \Psi_s^{+}(x) \left\{ \delta(x,t)\sigma_1 + \frac{1}{2} v_F \phi_x + (i/2)\phi_t \sigma_3 \right\} \Psi_S(x) \tag{4.21}$$

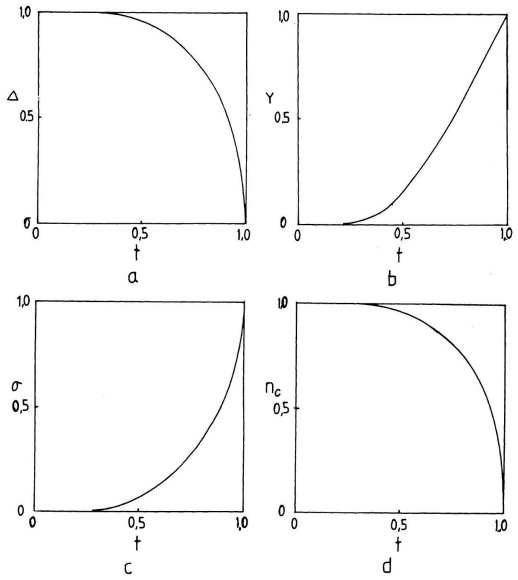


Fig. 8. The mean field theory results for the energy gap $\Delta(t)$, the Yosida function $Y(t)=1-n_{S}(t)$, the Ohmic conductivity $\sigma_a(t)$ and the condensate density $n_c(t)$ are shown as functions of reduced temperature $t = T/T_c$.}

Now assuming that δ and ϕ vary slowly both in space and time compared with the characteristic electronic length ξ and time Δ^{-1}, we can treat $\mathcal{H}_e^{\text{fl}}$ perturbationally. The secondorder perturbation yields an effective Hamiltonian

$$\mathscr{H}_{ph} = \frac{1}{\pi v_F \lambda \omega_Q^2} \int \mathrm{d}x \left(\delta_t^2 + \lambda \omega_Q^2 \delta^2 + \frac{1}{3} \lambda \omega_Q^2 v_F^2 (2\Delta)^{-2} \left(\frac{\partial \delta}{\partial x} \right)^2 + \Delta^2 \left[\phi_t^2 + c^2 \phi_x^2 \right] \right) \tag{4.22}$$

where

$$c^2 = \lambda \omega_Q^2 v_F^2 (2\Delta)^{-2} \tag{4.23}$$

at $T = 0$ K. More generally the coefficients of δ^2, δ_x^2 and ϕ_x^2 have an additional temperature dependence. The Hamiltonian (4.22) predicts the dispersions of the amplitude mode and the phase mode as

$$\begin{aligned} \omega_a^2 &= \lambda \omega_Q^2 \left[1 + \frac{1}{3} \left(\frac{v_F k}{2\Delta} \right)^2 \right] \\ \omega_{ph}^2 &= c^2 k^2 \end{aligned} \tag{4.24}$$

These results agree with those obtained by Lee et al. [98], while Equation (4.22) differs from that obtained by Brazovskii and Dzyaloshinskii [99], who did not include the spin degrees of freedom. Noting the fact that the electric current and the electric density operators are given by

$$j(x) = e v_F \Psi_S^+(x) \sigma_3 \Psi_S(x) \tag{4.25}$$

and

$$\rho(x) = e \Psi_s^+(x) \Psi_s(x)$$

the extra current and charge associated with ϕ_t and ϕ_x are given by

$$j(x) = \frac{e}{\pi} n_c(T)\phi_t \tag{4.26}$$

$$\rho(x) = -\frac{e}{\pi}(1 - Y(T))\phi_x \tag{4.27}$$

where [40]

$$n_c(T) = 1 - \frac{\beta}{4}\int_{-\infty}^{\infty} \mathrm{d}\xi \frac{\xi^2}{\xi^2 + \Delta^2} \operatorname{sech}^2\left(\frac{\beta}{2}\left(\xi^2 + \Delta^2\right)^{1/2}\right) \tag{4.28}$$

and $Y(T)$ is the Yosida function already defined in Equation (4.15). In particular, in the vicinity of $T = T_c, n_c(T)$ is given by $n_c(T) = \pi\Delta(T)/4T_c$ while at $T = 0$ K, $n_c(T) = 1$. The temperature dependence of $n_c(T)$ is shown in Figure 8(d).

4.4. Commensuration Energy

So far we have neglected the pinning potential which will pin the phase of the order parameter. In real quasi-one-dimensional systems, the phase always appears to be pinned. As discussed by Lee, Rice and Anderson [98], the pinning energy comes from the commensurability energy and the impurity potential. We shall consider here the commensurability energy. The effects of the impurity potential will be discussed in Section 6. When the period of the charge density wave is nearly commensurate with the periodicity of the underlying ionic lattice with degree M, there exists an extra energy, the commensurability
energy. First let us consider the case of the exact commensurability; the ionic lattice gives rise to a potential energy

$$V(x) = V\cos(Gx) \tag{4.29}$$

where $G = MQ$ and M is an integer. Then the potential energy

$$\mathscr{H}_c = \sum_s \int \mathrm{d}x V(x)\psi_s^+(x)\psi_s(x) \tag{4.30}$$

yields a commensuration energy in the CDW state of the form

$$E_{\mathrm{com}} = -\frac{A\omega_0^2}{M^2}\int \mathrm{d}x \cos(M\phi(x)) \tag{4.31}$$

where

$$A = \Delta^2/\left(\pi v_F \lambda \omega_Q^2\right) \quad \text{and} \quad \omega_0^2 \sim V\Delta^{M-2}/\epsilon_F^{M-1} \tag{4.32}$$

Combining the commensuration energy with the phase Hamiltonian (4.22), we obtain

$$\mathscr{H}_{ph} = \frac{A}{2}\int \mathrm{d}x \left\{\phi_t^2 + c^2\phi_x^2 + \frac{2\omega_0^2}{M^2}(1 - \cos M\phi)\right\} \tag{4.33}$$

where we have added a constant so that the ground state energy is zero.
Now in the nearly commensurate case, we replace the relation $G = MQ$ by

$$G = M(Q + q) \quad \text{with} \quad |q| \ll Q \tag{4.34}$$

In this more general situation Equation (4.33) is rewritten as

$$\mathscr{H}_{ph} = \frac{A}{2}\int \mathrm{d}x \left\{\theta_t^2 + c^2\left(\theta_x - q\right)^2 + \frac{2\omega_0^2}{M^2}(1-\cos M\theta)\right\} \tag{4.35}$$

where we have introduced a new phase by

$$\theta = \phi + qx \tag{4.36}$$

4.5. ϕ-solitons, Discommensurations

First consider the commensurate case ($q = 0$) where the phase Hamiltonian is given by Equation (4.33). As is easily seen, the ground state of the system is highly degenerate and is given by

$$\phi = 0, \pm\frac{2\pi}{M}, \pm\frac{4\pi}{M}, \ldots \tag{4.37}$$

Furthermore ϕ obeys a sine-Gordon equation

$$\phi_{tt} - c^2\phi_{xx} = -\frac{\omega_0^2}{M}\sin(M\phi) \tag{4.38}$$

The ϕ soliton is given by [33]

$$\phi(x,t) = \frac{4}{M}\tan^{-1}[\exp m\gamma(x-vt)] \tag{4.39}$$

with the soliton energy

$$E_S(v) = E_S\gamma = 8A\omega_0 cM^{-2}\gamma \tag{4.40}$$

where $m = \omega_0/c$ and $\gamma = (1 - v^2/c^2)^{-1/2}$

The soliton moves with uniform velocity v and carries charge given by

$$Q_s = \frac{e}{\pi}\int_{-\infty}^{\infty}\mathrm{d}x\phi_x = 2eM^{-1} \tag{4.42}$$

In general the ϕ soliton carries a fractional charge for $M \geqslant 3$. Indeed the fractional charge for $M = 3$ agrees with the charge of one type of solitons in the trimerized system considered by Su and Schrieffer [104]. Furthermore, as seen from Equation (4.27), the charge Q_s is not even simple fraction at nonzero temperatures. The soliton charge decreases continuously as the temperature is raised and vanishes when the CDW state disappears.

The soliton energy E_s is usually much smaller than the quasi-particle energy Δ. In this circumstance it is expected that the ϕ soliton is the dominant charge carrier at low temperature in the quasi-one dimensional conducting systems. For example it has been suggested in the past that the ϕ soliton would dominate the low temperature electric conductivity of TTF-TCNQ, KCP and TaS_3 [33, 105]. However, the author does not think that the evidence for the ϕ-soliton is very strong.

In the weakly incommensurate case the ground state of the Hamiltonian (4.35) is constructed in terms of a soliton lattice [106, 107].

$$\cos\left(\frac{1}{2}M\theta\right) = \mathrm{sn}\left(mk^{-1}x \mid k\right) \tag{4.43}$$

where $\mathrm{sn}(u \mid k)$ is the Jacobian elliptic function and k is a parameter. This describes a soliton lattice with the soliton lattice constant l;

$$l = 2kK(k)m^{-1} \tag{4.44}$$

and $K(k)$ is the complete elliptic integral. Substituting Equation (4.43) into Equation (4.35), the soliton lattice energy per unit length is calculated as

$$\begin{aligned} E_{sl} &= \frac{AC^2}{2l}\int_0^l \mathrm{d}x \left\{ \left(\frac{2m}{Mk}dn - q\right)^2 + \frac{4m^2}{M^2}(cn)^2 \right\} \\ &= \frac{E_S}{l}\left\{ \frac{1}{k}\left(E(k) - \frac{1}{2}\left(1-k^2\right)K(k)\right) - \frac{\pi}{4}(Mq/m) + \frac{1}{8}(Mq/m)^2 kK(k)\right\} \end{aligned} \tag{4.45}$$

where $E(k)$ is the complete elliptic integral.

$$\begin{aligned} E(k) &= \int_0^{\pi/2} \mathrm{d}\theta \left(1 - k^2\sin^2\theta\right)^{1/2} \\ K(k) &= \int_0^{\pi/2} \mathrm{d}\theta \left(1 - k^2\sin^2\theta\right)^{-1/2} \end{aligned} \tag{4.46}$$

Then the parameter k is chosen so as to minimize Equation (4.45). Although the general soliton can be found only numerically, the critical point where the soliton lattice disappears is studied analytically when q is changed. Indeed, for small l the ground state does not allow solitons; the ground state is commensurate. As q increases to a critical value q_c, the soliton lattice appears suddenly and the soliton density increases rapidly with $q - q_c$. Making use of the asymptotic expressions for the elliptic integrals for k approaching unity;

$$\begin{aligned} E(k) &= 1 + \frac{1}{2}k'^2\left(\ln\left(4/k'\right) - \frac{1}{2}\right) + \cdots \\ K(k) &= \ln\left(4/k'\right) + \frac{1}{4}k'^2\left(\ln\left(4/k'\right) - 1\right) + \cdots \end{aligned} \tag{4.47}$$

where $k' = \left(1-k^2\right)^{1/2}$, we can rewrite Equation (4.45) as

$$E_{Sl} \cong E_S\left[\left(\frac{M}{4}q^2\right)m^{-1} + l^{-1}\left(1 - \frac{\pi}{4}\frac{M}{m}q + 4e^{-ml}\right) + O\left(e^{-2ml}\right)\right] \tag{4.48}$$

where we made use of the relation

$$k = 1 - 8e^{-ml} \tag{4.49}$$

Equation (4.48) indicates that in the dilute limit solitons are interacting by a repulsive potential which decays exponentially with their separation l. Minimizing Equation (4.48) with l, we find

$$4(ml+1)e^{-ml} = \left(\frac{\pi}{4}\frac{M}{m}q - 1\right) \tag{4.50}$$

which implies that there is no soliton where $q < q_c = 4m/\pi M$. For $q > q_c$, the soliton lattice with the soliton density l^{-1} appears, where l increases as

$$l^{-1} \cong m\left[\ln\left(\frac{\pi}{4}\frac{M}{m}q - 1\right)\right]^{-1} \tag{4.51}$$

near the threshold.
In a three-dimensional system with weak interaction in the transverse direction, the soliton lattice is a parallel sheet of discommensurations which carry extra charge $Q = 2e/M$ for each chain [31, 32]. A possible charge transport due to moving discommensurations in the CDW state of the quasi-one-dimensional metals has been recently proposed by Bak [108]. However, it appears that discommensurations are not likely to give a periodically oscillating current in the CDW system because of their microscopic size. Another transport mechanism associated with discommensuration is proposed by Weger and Horovitz [109]. However the author believes that the model is unrealistic as they assumed that the discommensurations in TaS_3 are pinning free. The author does not know of any experiment which indicates pinning-free motion of solitons or discommensurations.

Even in polyacetylene, which we shall describe in the next section, solitons appear to be always pinned, as far as the infrared absorption experiment can tell us.

3.5.5 5. Solitons in Polyacetylene I

5.1. Dimerization of Polyacetylene

We shall now consider the electronic properties of polyacetylene. Polyacetylene is a chain-like molecule formed by carbon and hydrogen. Recent excitement concerning this system lies, on the one hand, in the ease of controlling the conductivity of polyacetylene by several orders of magnitude by simple doping with cation or anion and, on the other hand, in the theoretical elegance of the model describing it. Also, polyacetylene seems to provide the prototype of the organic conductors whose electronic properties are modified by doping. Also there is a close similarity between the CDW state we have discussed in Section 4 and the dimerization of polyacetylene. Indeed, the dimerization of conjugated chains is in most cases the simplest manifestation of the Peierls instability. For general information on polyacetylene we encourage readers to consult excellent reviews [110-114].

In the following we are primarily interested in trans- $(CH)_x$. Usually acetylene is polymerized into cis- $(CH)_x$ by making use of a catalytic reaction. Then cis- $(CH)_x$ is isomerized into trans- $(CH)_x$ either by thermalization or by doping with impurity, although the details of the isomerization are not well understood. Both cis- $(CH)_x$ and trans- $(CH)_x$ have planar configurations, as shown in Figure 9, where the back bone is formed by the carbon atoms. Furthermore, the σ electrons of the carbon atom form a closed shell while one π electron per carbon atom contributes to the bonding.

Both pristine (i.e. undoped) trans $-(CH)_x$ and doped trans $-(CH)_x$ exhibit unusual properties. First of all, polyacetylene cannot be dissolved in ordinary liquids like water or alcohol. On the other hand polyacetylene accepts a great variety of cations and anions as dopants. In the pristine state trans-polyacetylene is a good insulator with an energy gap $2\Delta \sim 1.5$eV. However, by doping polyacetylene with ions its conductivity increases rapidly, reaching the conductivity of metals like Cu or Al around a few percent doping of ions at room temperature. The extraordinary adjustability of conductivity by simple doping suggests some technical applications of polyacetylene.

Perhaps more puzzling are the free spins of $10^{-3} - 10^{-4}$ per carbon atom in transpolyacetylene, as seen by electron spin resonance (ESR) experiments [115-118], while in cis-polyacetylene the free spin density is one or two orders of magnitude lower. Apparently the free spins are generated in the process of isomerization. Furthermore, these

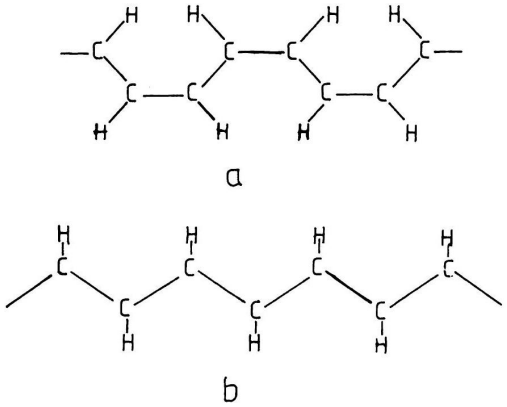


Fig. 9. Two chemical isomers of polyacetylene chain are shown (a) cis- \$(\mathrm{CH)_{x}\$, (b) trans- $(CH)_x$.}

spins appear to be quite mobile, at least at room temperature. In order to understand these puzzles a soliton model has been proposed by Su, Schrieffer and Heeger (SSH) [34] and by Rice [35]. In the following we shall describe in greater detail the SSH model.

5.2. Su, Schrieffer, Heeger Model

Although in general polyacetylene has a rather complicated morphology, at the microscopic level it looks like tangled spaghetti with a strand diameter of 200Å. Each strand of spaghetti then consists of bundles of $(CH)_x$-chains aligned parallel to the axis of the strand. Here we shall consider a single chain of trans-polyacetylene as shown in Figure 9b. The SSH model is given by the following Hamiltonian;

$$\mathcal{H} = \frac{1}{2}M\sum_n \dot{y}_n^2 + \frac{1}{2}K\sum_n (y_n - y_{n+1})^2 - \sum_{n,s} t_{n,n+1}\left(C_{ns}^+ C_{n+1s} + C_{n+1s}^+ C_{ns}\right) \tag{5.1}$$

and

$$t_{n,n+1} = t_0 - \alpha\,(u_{n+1} - u_n)$$

where y_n is the displacement of the nth CH ions from the equilibrium configuration corresponding to the undimerized state projected along the chain direction and $C_{ns}^+$is the creation operator of a π-electron at the nth site having spin s. We note that Equation (5.1) describes the simplest one-dimensional electron-phonon system, where the direct electron-electron interaction is neglected. SSH analysed the Hamiltonian (5.1) within the mean field approximation (i.e. the fluctuations in y_n 's are neglected) and found:

1. The ground state is dimerized and doubly degenerate. Two ground states which are referred as the A phase and the B phase are shown in Figure 10, where the double bond implies the distance between the adjacent carbon atoms is shorter than that with the single bond.

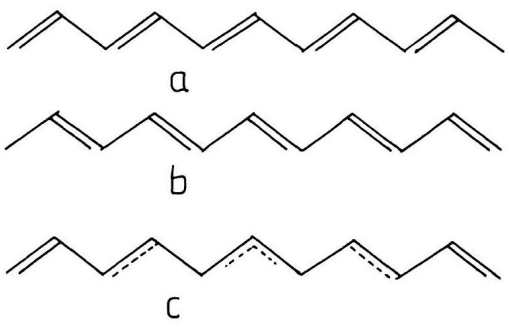


Fig. 10. Two ground state configurations of $\operatorname{trans -(\mathrm{CH})_{X}$ and a soliton configuration are shown in (a) (b) and (c).}

2. There are topological solitons (or kinks), which are the domain walls between two distinct ground states. Furthermore, the soliton energy E_S is independent of the charge of the soliton and smaller than the quasi-particle energy Δ. This implies that extra electrons or holes introduced by doping with impurities enter into polyacetylene as charged solitons rather than as quasi-particles (soliton doping).

3. The natural soliton carries spin $\frac{1}{2}$, while the charged soliton is spinless. (Spin charge anomaly.) We believe that this is the most beautiful consequence of the SSH model. Indeed this is the simple realization of the Jackiw and Rebbi mechanism [119] found in the quantum field theory in $1+1$ dimensions. In the Jackiw-Rebbi model they found that the soliton has a fractional (i.e. $\frac{1}{2}$) fermion charge. In the SSH model the spin degeneracy of the electron masks this anomaly but the same effect manifests as the spin charge anomaly.

This result indicates that the puzzling free spins found experimentally are neutral solitons. I would like to mention that a similar defect, though in a more crude form, has been already considered by Pople and Walmsley [120] long before the SSH model. How neutral solitons are produced in the process of isomerization is speculated by Su [121] as a finite-chain effect.

We shall derive the above results within the continuum version of the SSH model [122-124]. For example, the continuum model allows a number of exact solutions for the dimerization pattern, which are treated analytically.

5.3. Continuum Limit

Let us first introduce the staggered displacement by $\tilde{y}_n = (-)^n y_n$. In the equilibrium dimerized state $\tilde{y}_n$ is either y_0 or $-y_0$ corresponding to the A or the B phase. In more general situations $\tilde{y}_n$ is assumed to vary slowly with n. The SSH Hamiltonian in the continuum limit is then given by [123]

$$\mathcal{H}_c = \left(2g^2\right)^{-1} \int \mathrm{d}x \left(\dot{\Delta}^2 + \omega_0^2 \Delta^2(x)\right) + \sum_s \int \mathrm{d}x \psi_s^+(x) \left[-iv_F \sigma_3 \partial_x + \sigma_1 \Delta(x)\right] \psi_s(x) \qquad (5.2)$$

where

$$\begin{aligned} &\Delta(x) = 4\alpha\tilde{y}(x), \qquad g = 2\alpha\omega_Q (a/K)^{1/2} \\ &\omega_Q = 2(K/M)^{1/2}, \qquad v_F = 2t_0 a \end{aligned} \qquad (5.3)$$

$\tilde{y}(x)$ is the continuum version of $\tilde{y}_n$ and the spinor $\psi_s(x)$ consists of the right- and lefttravelling electrons, as in Equation (4.7)

$$\psi_s(x) = \left\{ \begin{array}{c} u_s(x) \\ v_s(x) \end{array} \right\}$$

with

$$c_{ns} \to a^{1/2} \left\{ \left[\exp\left(i n k_F a \right) \right] u(x) - i \left[\exp -i n k_F a \right] v(x) \right\} \tag{5.4}$$

Note also the similarity between Equations (5.2) and (4.20). Indeed, within the continuum limit, the SSH model describes a typical one-dimensional electron system with Peierls instability. However, the dimerization order parameter given in Equation (5.3) is real, unlike the general case described in Section 4. This is the particular feature of the half-filled band where $Q = 2k_F = \pi/a$.

The basic approximation introduced in Equation (5.2) is that the spatial variation of $\Delta(x)$ is slow compared with a, the lattice constant; we neglect all higher-order terms in a/ξ, where $\xi = v_F/\Delta$ is the characteristic length controlling the spatial variation of $\Delta(x)$. Then the mean field approximation is equivalent to $\dot{\Delta} = 0$; the ionic displacement is static. Then, minimizing Equation (5.2) with respect to $\Delta(x)$ and $\psi_s(x)$, we obtain a set of self-consistent equations;

$$\Delta(x) = g^2 \omega_Q^{-2} \sum_s \left\langle \psi_s^+(x) \sigma_1 \psi_s(x) \right\rangle = g^2 \omega_Q^{-2} {\sum_{sn}}' \left(u_{ns}^*(x) v_{ns}(x) + \text{c.c} \right) \tag{5.5}$$

$$\epsilon_n \psi_n(x) = \left(-i v_F \sigma_3 \partial_x + \sigma_1 \Delta(x) \right) \psi_n(x) \tag{5.6}$$

where

$$\psi_n(x) = \left\{ \begin{array}{c} u_n(x) \\ v_n(x) \end{array} \right\} \tag{5.7}$$

and the sum in Equation (5.5) is carried out up to the Fermi level, which we took to be $\epsilon_F = 0$.

The set of Equations (5.5) and (5.6) is very similar to the Bogoliubov-de Gennes (BdG) equation for inhomogeneous superconductors [125]. Furthermore, Equation (5.6) is the same as the equation which appears in the inverse scattering method for the sine-Gordon equation [17]. This allows us to find a number of exact solutions of Equations (5.5) and (5.6). Finally the mean field energy of the particular solution $\Delta(x)$ is given by

$$E_{\text{MF}}[\Delta(x)] = \left(2g^2 \right)^{-1} \omega_Q^2 \int \, \mathrm{d}x \Delta^2(x) + {\sum_{s,n}}' \epsilon_{ns} \tag{5.8}$$

where the sum over energy ϵ_{ns} is carried out up to the Fermi level $\epsilon_F = 0$.
The dimerized ground state is doubly degenerate and is described by $\Delta(x) = \Delta$ (or $-\Delta$) where Δ is a constant. The eigenvalues ϵ_n are then given by

$$\epsilon_k = \pm E_k, \quad E_k = \left(\left(v_F k \right)^2 + \Delta^2 \right)^{1/2} \tag{5.9}$$

and

$$\psi_k = \left\{ \begin{array}{c} u_k \\ v_k \end{array} \right\} \frac{1}{L^{1/2}} e^{ikx} \tag{5.10}$$

where

$$u_k = \left[\frac{1}{2}\left(1 + \frac{v_F k}{\epsilon_k}\right)\right]^{1/2}$$
$$v_k = \left[\frac{1}{2}\left(1 - \frac{v_F k}{\epsilon_k}\right)\right]^{1/2} \tag{5.11}$$

and L is the length of the polyacetylene chain and k is related to the total momentum of the quasi-particle P by $P = k_F \pm k$.

Here $\pm$ in Equation (5.9) refers to the electron state in the conduction band and that in the valence band, respectively. Substituting Equation (5.11) into Equation (5.5), we obtain

$$\Delta = 4g^2\omega_Q^{-2}\int_{-k_F}^{k_F}\frac{\mathrm{d}k}{2\pi}\frac{\Delta}{2E_k} = 2\lambda\Delta\ln\left(\frac{2W}{\Delta}\right) \tag{5.12}$$

where $W = v_F k_F$ is the band width and $\lambda = g^2/\pi v_F\omega_Q^2$. From Equation (5.12) we find the BCS expression

$$\Delta = 2We^{-1/2\lambda} \tag{5.13}$$

The ground state energy per unit length is similarly obtained as

$$E_{\mathrm{MF}}[\Delta]L^{-1} = -\frac{1}{\pi v_F}W\left(W^2 + \Delta^2\right)^{1/2} \cong -\frac{1}{\pi v_F}\left(W^2 + \frac{1}{2}\Delta^2\right) \tag{5.14}$$

where the second term in Equation (5.14) is the dimerization energy.

The electron density of states is obtained similarly as

$$N(\omega) = \int_{-k_F}^{k_F}\frac{\mathrm{d}k}{2\pi}\delta(E-\omega) = \frac{1}{\pi v_F}\frac{|\omega|}{\left(\omega^2 - \Delta^2\right)^{1/2}}\theta(|\omega| - \Delta) \tag{5.15}$$

for one spin component. The density of states is the same as in a superconductor with energy gap Δ. The frequency-dependent conductivity is also obtained from

$$\sigma(\omega) = \mathrm{Im}\left[\omega^{-1}\langle[j,j]\rangle(\omega)\right] \tag{5.16}$$

where $j = e\sigma_3 v_F$ and $\langle[A,B]\rangle(\omega)$ is the Fourier transform of the retarded product. Substituting the expression for j into Equation (5.16) we obtain [129, 130]

$$\begin{aligned}\sigma_0(\omega) &= 2\pi e^2 v_F\omega^{-2}\int \mathrm{d}k\frac{\Delta^2}{E_k}\delta(2E-\omega)\\ &= 4\pi e^2 v_F\omega^{-2}\left[(\omega/2)^2 - \Delta^2\right]^{-1/2}\theta(|\omega| - 2\Delta)\end{aligned} \tag{5.17}$$

There is no electromagnetic absorption for $|\omega| < 2\Delta$ implying that the dimerized state is an insulator. For $|\omega| > 2\Delta$ the conductivity has a square root singularity at the absorption threshold.

5.4. Solitons in Polyacetylene

Now we shall consider the soliton. A soliton localized at $x = 0$ is given by

$$\Delta(x) = \Delta\tanh(x/\xi) \tag{5.18}$$

which interpolates between the A and B phase smoothly (see Figure 10c). It is shown that Equation (5.18) with $\xi = v_F/\Delta$ satisfies the self-consistent set of Equations (5.5) and (5.6).

There is a bound state at the center of the energy gap with

$$\epsilon_B = 0, \quad \psi_B(x) = \left\{ \begin{array}{c} 1 \\ -i \end{array} \right\} \frac{1}{2}\xi^{-1/2}\,\mathrm{sech}(x/\xi) \tag{5.19}$$

Furthermore, the scattering states are given by

$$\epsilon_k = \pm E_k, \quad \Psi_k(x) = \frac{1}{2}\left(L - \xi\cos^2\phi_k\right)^{-1/2} \left\{ \begin{array}{c} 1 - \frac{v_F k + i\Delta(x)}{\epsilon_k} \\ -i\left(1 + \frac{v_F k + i\Delta(x)}{\epsilon_k}\right) \end{array} \right\} e^{ikx} \tag{5.20}$$

where $\phi_k = \tan^{-1}(v_F k/\Delta)$.

Then it is easy to verify that Equation (5.5) is satisfied independently of occupation of the midgap states at $\epsilon = 0$, since $u(x)$ and $v(x)$ are relatively pure imaginary. The soliton energy is calculated from Equation (5.8) as

$$E_s = E_{\mathrm{MF}}[\Delta(x))] - E_{\mathrm{MF}}[\Delta] = \frac{2}{\pi}\Delta \tag{5.21}$$

again independent of occupation of the midgap states, implying that E_S is independent of the charge of the soliton. We note in passing that $E_S < \Delta$ which implies soliton doping. The charge of the soliton is determined as follows. Since the midgap state associated with the soliton is composed of half of the state in the conduction band and half of the state in the valence band, a deficit of a half-electron state is created for both spin components in the valence band. This implies that the neutral soliton is obtained by singly occupying the midgap state, which compensates the one electron deficit of two spin states in the valence band. Since this electron in the midgap state can take the up or the down spin state, the neutral soliton has a spin $\frac{1}{2}$. On the other hand the positively charged soliton is obtained by emptying the midgap state, which corresponds to a spinless object. Similarly, the negatively charged soliton is obtained by doubly occupying the midgap state again resulting in a spinless object. This charge-spin anomaly is shown schematically in Figure 11. The extra spin or charge distribution associated with the neutral soliton or the charged soliton is given by

$$\rho_{\mathrm{spin}}(x) = (4\xi)^{-1}\,\mathrm{sech}^2(x/\xi)$$

or

$$\rho_{\mathrm{charge}}(x) = \pm e(4\xi)^{-1}\,\mathrm{sech}^2(x/\xi) \tag{5.22}$$

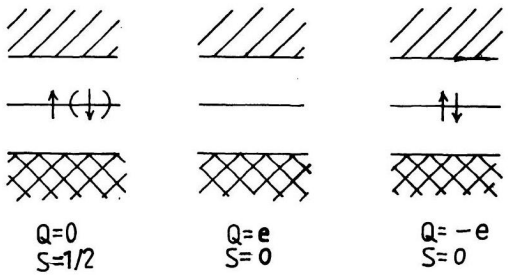


Fig. 11. The occupation of the midgap states for neutral and charged solitons are schematically shown. For neutral soliton a single electron occupies the midgap state resulting in the spin doublet, while the charged solitons have even electrons (0 or 2) in the midgap state resulting in the spin singlet state.

If we go back to the original discrete model, we discover that the spin or the charge resides only on the even or the odd lattice sites depending on the position of the center of the soliton [34], as the on-site density is given by $f_{\pm}(x)$ where $f_{\pm}(x) = u(x) \pm iv(x)$. For example for the spin density we have;

$$\rho_{\text{spin}}^{\text{even}}(x) = |f_{+}(x)|^2, \quad \rho_{\text{spin}}^{\text{odd}} = |f_{-}(x)|^2 \tag{5.23}$$

Substituting Equation (5.19) into Equation (5.23), we find

$$\rho_{\text{spin}}^{\text{even}}(x) = \xi^{-1}\,\text{sech}^2(x/\xi), \quad \rho_{\text{spin}}^{\text{odd}}(x) = 0 \tag{5.24}$$

The midgap state associated with the soliton is most readily seen by optical absorption as appearence of the midgap absorption [126-129]. Although the midgap absorption coefficient is easily obtained in terms of electronic wave functions given by Equations (5.19) and (5.20) [128], in the analysis of the interband absorption the boundary condition for the electronic wave functions plays the crucial role [130]. The boundary condition (BC) for the wave function is formulated as follows. Let us consider a polyacetylene ring which consists of even number N of the (CH)-site. In the absence of solitons we have

$$\Delta(x + L) = \Delta(x) \tag{5.25}$$

with $L = Na$. This leads to the ordinary boundary condition (BC) for electronic wave functions

$$\psi(x + L) = \psi(x) \tag{5.26}$$

In the presence of a single soliton the sign of $\Delta(x)$ is flipped after passing the soliton, resulting in

$$\Delta(x + L) = -\Delta(x) \tag{5.27}$$

Then the BC for electronic wave functions given by Equation (5.26) is no longer consistent with Equation (5.27). The BC consistent with a single soliton is given by

$$\psi(x + L) = \sigma_3\psi(x) \tag{5.28}$$

which gives rise to the same phase shift of ϕ_k for both $u(x)$ and $v(x)$ components in the presence of the soliton. On the other hand the k selection rules for electrons in the conduction band and those in the valence band are given by [130]

$$\begin{aligned} kL &= 2n\pi + \phi_k \quad \text{for} \quad \epsilon > 0 \\ kL &= (2n+1)\pi + \phi_k \quad \text{for} \quad \epsilon < 0 \end{aligned} \tag{5.29}$$

The above boundary condition is crucial not only for the calculation of the frequency dependent conductivity but also other two point correlation functions. We will not give the derivation of the frequency dependent conductivity here, but the final expression [130];

$$\sigma(\omega) = \sigma^{(1)}(\omega) + \sigma^{(2)}(\omega) \tag{5.30}$$

$$\sigma^{(1)}(\omega) = \frac{e^2 v_F}{4\Delta}\pi^2\xi n_s \left(z^2 - \frac{1}{4}\right)^{-1/2} \text{sech}^2\left[\pi\left(z^2 - \frac{1}{4}\right)^{1/2}\right] \tag{5.31}$$

$$\sigma^{(2)}(\omega) = \frac{e^2 v_F}{2\Delta} z^{-2}\left(z^2 - 1\right)^{-1/2}\left\{1 - \xi n_s\left(2 + z^{-2} + f(z)\right)\right\} \tag{5.32}$$

where

$$f(z) = -2\lim_{\epsilon\to 0}\left\{\pi\int_{\epsilon}^{\left(z^2-1\right)^{1/2}} \mathrm{d}y\,\mathrm{cosch}^2\,\pi y\frac{z^2}{\left(z^2-y^2\right)^2+y^2}\left(\frac{z^2-y^2}{z^2-y^2-1}\right)^{1/2} - \right.$$
$$\left. -\frac{1}{\epsilon}z^{-1}\left(z^2-1\right)^{-1/2}\right\} \tag{5.33}$$
$$z = \omega/(2\Delta)$$

and n_s is the soliton density on the $(CH)_x$ chain. The first term in Equation (5.30) involves the midgap state and has the threshold energy at $\omega = \Delta$, while the second term is due to the interband excitation. In the limit $n_s = 0$ Equation (5.30) reduces to Equation (5.17), the conductivity for the perfectly dimerized state. The frequency-dependent conductivity also satisfies the sum rule

$$\int_{-\infty}^{\infty}\mathrm{d}\omega\sigma(\omega) = e^2 v_F \tag{5.34}$$

independent of the soliton density.
Within the present model the soliton is considered to be extremely mobile [34]. For this purpose we shall estimate the soliton mass. Assuming that a moving soliton with velocity v is given by

$$\Delta(x,t) = \Delta\tanh[(x-vt)/\xi] \tag{5.35}$$

the first term of Equation (5.2) yields the kinetic energy

$$E_{\mathrm{kin}} = \frac{2}{3}(\Delta/g)^2\xi^{-1}v^2 \tag{5.36}$$

implying the soliton mass

$$m_s = \frac{4}{3}(\Delta/g)^2\xi^{-1} = \frac{2}{3\pi}\left(\Delta^3/\lambda\omega_Q^2\epsilon_F\right)m \tag{5.37}$$

Substituting appropriate values for Δ, ω_Q and ϵ_F, the soliton mass is found to be only a few times of the electron mass m. Therefore the soliton in polyacetylene looks like extremely mobile object within the SSH model.

5.5. Other Solutions

We shall consider some other exact solutions of Equations (5.5) and (5.6). The first is the soliton lattice, which is the solution with lowest energy when extra electrons or holes are added to the system. The second is the polaron, which is considered as a bound state of soliton and antisoliton.

A. Soliton Lattice

In the absence of external field, solitons of the same charge (positive or negative) on a single $(CH)_x$ chain form a soliton lattice in order to minimize the total energy. The corresponding solution is given in terms of Jacobian elliptic functions [131-133];

$$\Delta(x) = \Delta k\,\mathrm{sn}(u\mid k)\,\mathrm{sn}(u+K\mid k) \tag{5.38}$$

with $u = (k\xi)^{-1}x, an_s^{-1} = k\xi K(k)$
The soliton lattice energy per unit length is now given by

$$E_{Sl}L^{-1} = \frac{2\Delta_0}{\pi k} n_S \left[E(k) - \frac{1}{2} k'^2 K(k) \right] \tag{5.39}$$

where $E(z)$ and $K(z)$ are again complete elliptic integrals and Δ_0 is the dimerization order parameter of the perfectly dimerized state. From Equation (5.39) the chemical potential for the soliton is obtained as

$$\mu_s = \frac{\partial}{\partial n_s} E_{sl} = 2\Delta(\pi k)^{-1} E(k) \tag{5.40}$$

which is always smaller than the energy gap $E_{\text{gap}} = \Delta k^{-1}$. Therefore, within the continuum limit, electrons or holes are introduced as solitons independent of the soliton density. However, the continuum limit will be no longer valid for $n_s \xi > 1$. The density of states is found to be rather simple in the soliton lattice and is given by [133]

$$N(\epsilon) = \frac{1}{\pi v_F} \left(\frac{\epsilon^2}{\Delta^2} - \frac{E(k)}{K(k)} \right) \phi(\epsilon) \tag{5.41}$$

$$\phi(\epsilon) = \Delta^2 \,\mathrm{Re}\left[\left(\Delta'^2 - \epsilon^2 \right) \left(\Delta^2 - \epsilon^2 \right) \right]^{-1/2} \tag{5.42}$$

where

$$\Delta = k' \Delta_0 \quad \text{and} \quad \Delta' = \Delta_0 k' k^{-1} \tag{5.43}$$

The midgap states form an electron band which extends between $-\Delta' \leqslant \epsilon \leqslant \Delta'$.

B. Polaron

The existence of a polaron solution to the SSH model was first discovered by Su and Schrieffer [134] in their numerical analysis of one electron injected into the perfectly dimerized polyacetylene. The electron introduces a local depression of the dimerization order parameter $\Delta(x)$ and moves together with this depression. Subsequently the analytical solution within the continuum model was found by Brazovskii and Kirova and by Campbell and Bishop [135, 136]. Indeed such a solution has been considered much earlier within the Gross-Neveu model by Dashen et al. [137]. The semi-classical approximation of the Gross-Neveu model is identical to the mean field approximation of the continuum limit of the SSH model.

The solution is given by

$$\Delta(x) = \Delta_0 - \kappa_0 v_F \left(t_+ - t_- \right) \tag{5.44}$$

where

$$\begin{aligned} t_\pm &= \tanh\left[\kappa_0 \left(x \pm x_0 \right) / \xi \right] \\ \kappa_0 &= 1/\sqrt{2}, \quad x_0 = \sqrt{2}(\sqrt{2} - 1)\xi \end{aligned} \tag{5.45}$$

with

$$E_p = \frac{2\sqrt{2}}{\pi} \Delta_0 \sim 0.900 \Delta_0 \tag{5.46}$$

Note that $E_p < \Delta$ implying the quasi-particle is unstable against formation of the polaron. The analytic expressions for the electronic wave functions are also known [136]. We only remark here that the polaron introduces two bound states inside the energy gap with energy

$\pm\omega_0 = \pm\Delta_0/\sqrt{2}$. Unlike the soliton the polaron has the normal charge-spin relation and is devoid of topological charge. Therefore the polaron may play an important role in the soliton doping, since the solitons are created only by pairs on a single polyacetylene chain due to the topological constraint. On the other hand a single electron can be transformed into a polaron in polyacetylene with emission of phonons. In this circumstance if we limit ourselves to a single polyacetylene chain, the first electron enters the chain as polaron. The second electron then splits the polaron into a pair of negatively charged solitons. Recently an analysis has been reported, which indicates that a pair of polarons are unstable against formation of a pair of solitons [138]. More recently it has been reported that polarons are seen in the optical absorption spectrum of lightly doped polyacetylene around $\omega = 1.47$ and 1.6 eV [139], which is comparable to the optical structure calculated by Fesser et al. [140]. Absence of the topological constraint for polarons implies that the polaron does not require the degenerate ground state unlike the soliton. Therefore polarons can exist and will play an important role in many other polymers like cis- $(CH)_x$. [135] and polyparaphenylene [141]. This warrants a further study on polarons in polymers.

3.5.6 5. Solitons in Polyacetylene II

5.6. Comparison with Experiments

We shall describe briefly the properties of pristine and lightly doped trans-polyacetylene.

A. Magnetic Properties

As already mentioned the free spins seen by ESR [115-118] are identified with neutral solitons. Furthermore the width of the spin resonance in trans- $(CH)_x$ is found to change from 10 Gauss at low temperatures to less than 1 Gauss at room temperature, while that in cis- $(CH)_x$ is about 10 Gauss independent of the temperature. This can be interpreted as mobile spins in trans- $(CH)_x$ (motional narrowing), whereas the spins are immobile in cis- $(CH)_x$. This conclusion is strengthened by dynamic nuclear polarization measurements
by Nechtshein et al. [142]. The observed enhancement of the NMR amplitude in trans$(CH)_x$ by pumping at and near the electronic Larmor frequency $\nu_e = \gamma_e H$ exhibits the Overhauser effect, indicating that the spin in trans- $(CH)_x$ is mobile at room temperature. By contrast, the same experiments in cis- $(CH)_x$ indicate the existence of the localized spin. Furthermore measurements of the proton spin relaxation rate ${T_1}^{-1}$ show that ${T_1}^{-1}$ is proportional to ${\nu_n}^{-1/2}$ for pristine trans- $(CH)_x$ over the frequency range $10 - 340$ MHz , where ν_n is the proton Larmor frequency. If the proton spin relaxation is mainly due to the coupling to the electron spin, the above result indicates one dimensional electron spin diffusion with diffusion constant $D = 10^{-2}$ cm^2/sec. Furthermore, from the deviation from the ${\nu_N}^{-1/2}$ law, the anisotropy in D is inferred as 10^6. This result is readily interpreted as being due to the soliton diffusion along the $(CH)_x$ chain. However, more recent experiments on T_1 in deuterated polyacetylene [143] revealed that D depended strongly on the deuteron concentration, if the above interpretation is used. Since such a strong concentration dependence of D is quite unlikely, which suggests that the nuclear dipole interaction between proton spins plays a substantial role in T_1 in trans- $(CH)_x$. Furthermore, all the electron spins in trans- $(CH)_x$ appear to be immobilized below 10 K [143].

Within the SSH model the soliton interacts with both optical and acoustic phonons [144]. However, below the room temperature the scattering with the optical phonon becomes negligible as the thermal optical phonon population decreases exponentially. Then emission and absorption of the acoustic phonon gives rise to the soliton diffusion constant $D \propto T^{1/2}$, where T is the temperature. Therefore this model cannot account for the localization of spins at low

temperatures. At room temperature the theory predicts $D \simeq 10^{-1}$ cm^2/sec, which may be comparable to the one deduced from the T_1 measurement. However, besides the fact that the deduction suffers a criticism, a quite different value for $D = 10^{-5}$ cm^2/sec is obtained from the spin echo experiment [145]. Therefore the spin dynamics in undoped trans- $(CH)_x$ may be more complicated than originally thought.

The spin susceptibility of pristine trans- $(CH)_x$ follows the Curie law between 1.5 K and 300 K [146, 147]. Upon doping, the number of Curie law spins N_c decreases from 400 ppm for $y = 0$ to about 120 ppm for $y = 0.002$ and continues to fall rapidly to small density for $y = 0.05$, whereas the onset of Pauli susceptibility is not observed before $y = 0.07$ is reached [148]. Here y is the dopant (AsF_5) concentration. This behavior is of particular interest for the soliton model. The above result indicates that metallic electron band will develop only for $y > 0.07$, whereas the electric conductivity for polyacetylene becomes almost metallic for $y > 0.02$ at least at the room temperature [148]. This suggests strongly existence of a new conduction mechanism due to the charged soliton.

B. Optical Properies

The absorption spectrum of pristine $(CH)_x$ of the either isomeric form is typical for a semiconductor with well defined energy gap. The energy gap 2Δ for cis- $(CH)_x$ is above 2 eV , whereas that for trans- $(CH)_x$ is about 1.5 eV [149]. In contrast to the theoretical prediction Equation (5.17) the observed absorption spectrum does not exhibit the square root singularity at the threshold, most probably due to the interchain coupling. The absorption spectra in the visible and near infrared (IR) show drastic changes upon
doping [128, 129]. In general at low doping levels, a new absorption is built up in the region between 0.5 and 0.8 eV while the interband absorption is suppressed. This new absorption is interpreted as due to the midgap states introduced by solitons. Although the earlier result [128] appears to indicate that a dopant molecule introduces more than one soliton [126], the latter result obtained by the electrochemical doping is more consistent with the theoretical calculation [130] as far as relative intensities of the midgap absorption and the interband absorption are concerned. The observed spectrum shape of the midgap absorption is much broader than the SSH model prediction as in the case of the interband absorption.

Upon doping new infrared lines are generated at 1400 and 900 cm^{-1} in trans- $(CH)_x$. The position of lines are insensitive to dopants and the intensities increase linearly with dopant concentration [150,151]. Similar lines are found in $(CD)_x$ at 1120 and 780 cm^{-1} [152]. The phonon modes in the presence of a soliton has been analysed numerically by Mele and Rice [153], which describe most of the features observed experimentally. Now the lower modes are interpreted as being due to the sliding mode, which is pinned by the Coulomb potential of dopant molecule [154]. The author believes that the higher mode is nothing but the optical phonon with small wave vector k, which can couple to the IR wave due to the symmetry breaking introduced by soliton.

C. Transport Properties

The pristine trans- $(CH)_x$ is a semiconductor with well defined energy gap. Upon doping the electric conductivity increases dramatically and reaches the metallic conductivity for $y \simeq 0.01$ at room temperature [155]. However the nature of the transition from the semiconducting to the highly conducting state is not well understood, although experimentally it is found at $y \simeq 0.01$ [156].

For example as seen from the Pauli susceptibility [148], the density of states at the Fermi surface appears to be zero at the concentration $y = 0.01$. We shall limit ourselves to the dilute

concentration limit ($y < 0.01$) of dopants where solitons are expected to play an important role. An attractive model is proposed by Kivelson [157] where the electronic transport is controlled by phonon assisted hopping between the electronic midgap states associated with solitons. This model applies only when both neutral and charged solitons are present and therefore it is valid only for dilute concentration of dopants. With this model Kivelson finds the dc conductivity and the thermoelectric power;

$$\sigma_{\rm hop} = A\frac{e^2\gamma(T)}{k_BTN}\left(\frac{\xi}{R_0^2}\right)\frac{y_n y_{ch}}{(y_n+y_{ch})^2}\exp\left(-2BR_0/\xi\right) \tag{5.47}$$

and

$$S = K_B/e\left[\frac{1}{2}\left(3+T\frac{\partial}{\partial T}\ln\gamma(T)+\ln\left(y_n/y_{ch}\right)\right)\right] \tag{5.48}$$

where R_0 is the distance between charged impurities $C_{im} = \left(\frac{4}{3}\pi R_0^3\right)^{-1}$, and y_n and y_{ch} are the concentrations of the neutral and the charged solitons per carbon atom and A and B are constants of the order of unity Finally $\gamma(T)$ describes the temperature-dependent hopping rate. By assuming that $\gamma(T) \simeq 500\text{eV}(T/300\text{ K})$[10], Kivelson can account for the large and almost temperature-independent thermoelectric power observed experimentally [156]. The ac conductivity within this model gives a characteristic frequency dependence $\sigma_{\rm ac} \sim \omega[\ln(2\omega/T(T))]$,[4] where $\Gamma = y_n y_{ch}\left(y_n+y_{ch}\right)^{-2}\gamma(T)/N$. This frequency dependence is studied in detail by Epstein et al. [158] and they find that the model describes consistently both the dc conductivity and the ac conductivity of dilutely doped polyacetylene for $y_{ch} = 2.35\times10^{-4}$ and for $T = 300-84$ K, if $\gamma(T)$ is chosen as $\gamma(T) = 500\text{eV}(T/300\text{ K})^{14\cdot7}$.

D. Photogeneration of Soliton Pairs

Perhaps the most unambigious evidence for solitons is provided by photogeneration of solitons. In their numerical study of the SSH model, Su and Schrieffer [128] show that an electron-hole pair injected in the perfectly dimerized $(CH)_x$ is converted very rapidly within 10^{-13}sec into charged soliton pairs. This possibility for cis- $(CH)_x$ and trans- $(CH)_x$ is studied experimentally by Lauchlan et al. [159]. They discovered the photocurrent in trans- $(CH)_x$, which rises rapidly with the energy of exciting photon for $\hbar\nu \gtrsim 1$eV, while no photoconductivity is observed in cis- $(CH)_x$. On the other hand, a large photoluminescence with the peak value around $\hbar\nu \simeq 1.9$eV is observed in cis- $(CH)_x$, while only a neglible (at most two orders of magnitude smaller) photoluminescence is seen near 1.5 eV in trans $-(CH)_x$. The photoconductivity in trans $-(CH)_x$ is identified as due to the photogenerated charged solitons. On the other hand the absence of photoconductivity is interpreted as absence of free solitons in cis-$(CH)_x$. As the two dimerization configurations in cis- $(CH)_x$ are nondegenerate, the soliton pairs created in cis- $(CH)_x$ are confined; the pair acquires an additional energy associated with the difference in the energies of the two dimerization configurations per unit cell multiplied by their separation [135]. Therefore all photogenerated soliton pairs are in bound states in cis-$(CH)_x$ and they cannot contribute to the conductivity. Ultimately the pair of solitons in the bound state annihilate each other giving rise to the photoluminescence. Although this general picture is very plausible, it is not clear if the charge carriers in trans- $(CH)_x$ are indeed solitons, except the fact that the threshold energy for the photoconductivity is roughly 1eV $(= 2E_S)$ rather than 1.5eV$(= 2\Delta)$. Within the SSH model the photogeneration probability for solitons is calculated by Sethna and Kivelson [160] and Zhao-bin and Lu [161]. In spite of the difference in their assumption, they predict that the transition rate increases exponentially above the threshold $\hbar\nu = 2E_S$, which appears to describe qualitatively the frequency dependence of the photoconductivity.

The more direct evidence of the soliton pair creation is provided by detection of other characteristics associated with solitons; the appearance of the infrared active modes, the midgap absorption, and the reduction in the interband absorption. All of these characteristics have been seen in recent experiments [162-167]. The midgap absorption and the interband bleaching are observed within 10^{-13}sec after charged defects are generated by the photons with $h\nu$ from 1.2 to 1.9 eV [162-164]. Furthermore, from the time dependence of the photodichroism it is concluded that solitons are mobile with linear diffusion constant $D \simeq 10^{-2}$ cm^2/sec at room temperature [163]. Although the higher infrared mode with 1370 cm^{-1} has been observed, the infrared mode with 900 cm^{-1} is
shifted down to 500 cm^{-1} [166]. If we assume that this is the pinned sliding mode [154], the above experiment implies that the charged solitons in trans- $(CH)_x$ are still pinned in the absence of impurity. We shall discuss later the possible origin of this pinning. Therefore these experimental results appear to provide convincing evidence for solitons in trans- $(CH)_x$ polyacetylene. More recently whether these photogenerated charged defects carry spins or not is tested by ESR experiment [168]. Flood and Heeger find that the spin density is at most 10^{-2} of the charged carrier density. Since the conversion rate from the charge soliton pair $\mathbf{S}^+$and $\mathbf{S}^-$into the neutral soliton pair $\mathbf{S}^0{}_\uparrow$ and $\mathbf{S}^0{}_\downarrow$ appears to be extremely slow [169], the ESR result will provide the definitive evidence for solitons.

In summary there are bulk of experimental data, which are interpreted in terms of solitons. If we limit ourselves to an individual experiment like the appearence of the midgap states, for example, the electronic bound states introduced by impurities can mimic the absorption spectrum [170]. However, it is then difficult to understand how these bound states are created by photoexcitation.

5.7. Extension of the Model

We have seen that the SSH model can account for a vast variety of experimental results of pristine and dilutely doped trans-polyacetylene. However, from the theoretical point of view some drastic assumptions are introduced in constructing and solving the model. Major assumptions made in the SSH theory are;

1. The system is one-dimensional
2. The Coulomb interaction between electrons is neglected except possible renormalization effect on t_0 and K in Equation (5.1)
3. The quantum fluctuation of the lattice is ignored.

In order to remove the assumptions 1 and 2, the SSH model has to be modified, while the assumption 3 can be incorporated within. the SSH model. Therefore, we shall start with the assumption 3.

A. Quantum Fluctuations

The quantum fluctuations are studied both perturbationally and numerically [171-174]. The perturbation treatment indicates that the dimerization pattern is not destroyed by the quantum fluctuation of the ionic lattice. Furthermore, the soliton and the polaron are stable excitations even in the presence of quantum fluctuations [171]. The most comprehensive treatment on this question is done by Fradkin and Hirsch [174], who make use of the Monte Carlo method on the one hand and the ?enormalization method on the other hand. They have shown that the dimerized state in the SSH model is the ground state irrespective to the electron phonon coupling strength and the ion mass. For this stability the spin degree of freedom associated with

the electron is of crucial importance. For example for the hypothetical spinless electron, the dimerized state is not always the ground state. This result is not hard to understand, since in the extreme quantum limit, the continuum limit of the SSH model is exactly the Gross-Neveu model, of which exact results are known [175]. In this model for $N = 1$, the fermion does not have mass while, for $N \geqq 2$ the fermion becomes massive. Here N is the degrees of freedom associated with the fermion. Therefore, though quantum fluctuation may be important numerically, this does not destroy the general feature of the SSH theory.

B. Coulomb Correlation

Until recently, the effect of the Coulomb interaction is a most controversial subject. To begin with we do not know what is the proper potential to use. The long range potential used by quantum chemists to analyse short polyenes appears to lead to unacceptable results [176]. If we limit ourselves to the on-site Coulomb interaction of the Hubbard type, it was believed that the ground state becomes antiferromagnetic for moderate value of U. On the other hand the soliton like state appears to exist independent of the nature of the ground state [177, 178].

Recently it is shown that the on-site Coulomb potential has minor effect on the dimerization order parameter as long as U is less than the band width W [179,180]. From the experimental point of view, the on-site Coulomb energy of the order of $U = 3$eV is required to interpret a recent electron nuclear-nuclear triple resonance experiment [181] in terms of the neutral soliton. The above experiment indicates that the spin density at the odd and the even sites are of opposite sign and $\rho_+ = 0.06$ and $\rho_- = -0.02$ where ρ is normalized with the spin density of the single electron. In the original SSH model, the spin density of the nuetral solitons is located either on the odd carbon sites or the even carbon sites. Inclusion of the Coulomb term gives rise to a spin density on the alternate sites with opposite sign [182]. Indeed $U = 3$eV will give the observed spin density if the soliton is confined in a finite range of the order of fifty unit lattice [183].

Furthermore, the peak in the midgap absorption in the doped polyacetylene is shifted downward by about 0.2 eV . This is again consistent with $U = 3$eV, as the doubly occupied midgap state corresponding to the negatively charged soliton will be pushed up about $\Delta E = U/2\xi$ in comparison with the singly occupied midgap state [166].

C. Three Dimensional Order

A recent X-ray scattering experiment [184] suggests clearly that the dimerization pattern in trans- $(CH)_x$ exhibits three dimensional order. If the observed local order extends into the three dimensional space, there should be no free solitons; all solitons are confined. Therefore in order to estimate the confinement potential, it is very important to study the origin of this three dimensional order. The most likely candidate for this is the interchain electron hopping [185]. Within this model, we obtain the confinement energy

$$E_c(x) = W(x/a) \tag{5.49}$$

where

$$W = 4t_\perp^2/\pi t_0 \tag{5.50}$$

and $t_\perp$ is the interchain hopping integral while t_0 is the intrachain hopping integral given in Equation (5.2) and x is the distance between a pair of solitons on the same chain. Making use of $t_\perp$ used in band-structure calculation of polyacetylene [186] it is found that

$$W \simeq 30 - 3 \text{ K} \tag{5.51}$$

where $t_\perp/t_0 = 30^{-1} - 100^{-1}$. A very similar $t_\perp$ is deduced in a recent analysis of the pressure independent of interband transition energy [187]. It is noteworthy that a similar confinement energy $W \simeq 3.5$ K is obtained by Baughman and Moss [188], when modeling the interchain coupling in terms of Coulomb or dispersion force. Although the above value of W may be modified as in our model two chains of polyacetylene are assumed to lie on the same plane, whereas in reality they are not as seen in the X-ray scattering data [184], we believe that the above value is quite reliable. First of all, due to the confinement potential, all neutral solitons are confined near the edge of the polyacetylene crystal. This is not only consistent with the bond lengths determined by the nuclear spin nutation spectroscopy [189], but also the confinement potential provides the necessary potential well to localize the neutral soliton within 50 atomic units [183]. Indeed when $W = 3$ K, the neutral soliton is localized within 50a from the edge of polyacetylene [190]. Due to the confinement potential all photogenerated charged soliton pairs $S^+$and $S^-$are in the bound state. Then it is quite natural to identify the infrared mode with 500 cm^{-1} associated with the photogenerated solitons [166] to the excitation of the bound pair from the ground state to the first excited level. The potential energy between $S^+$and $S^-$is given by

$$V(x) = W\frac{x}{a} + \frac{8}{\pi}\Delta \exp(-2x/\xi) \tag{5.52}$$

where the second term arises from the repulsive potential between two solitons [191] as modified by Rice [192] who takes into account the proper symmetry of the electronic wave functions in the midgap states. Identifying $E_1 - E_0 = 500$ cm^{-1} yields now $W = 18$ K, where the soliton mass M_s is assumed to be twice the electron mass [190]. Although this W is still within the estimated range, it is six times larger than that deduced for the neutral soliton. We do not believe that this is a serious defect of the model, because it is quite likely that the neutral solitons reside in less crystalline area of polyacetylene and therefore they have a weaker confinement potential.

The presence of the confinement potential suggests that the physical properties of cis- $(CH)_x$ and trans- $(CH)_x$ are after all quite similar. The only difference is that the former has much stronger confinement potential resulting in no photoconductivity at room temperature. A recent experiment by Blanchet et al. [167] indeed shows that the photoconductivity in trans-$(CH)_x$ disappears quite suddenly below 150 K . Therefore we expect that below 150 K all photogenerated solitons are in the bound states and disappear by recombination. This implies that the photoluminescence should be observable for trans $-(CH)_x$ below 150 K with $\omega \simeq 200 - 300$ cm^{-1}. The fact that the infrared mode with $\omega = 500$ cm^{-1} disappears above 150 K [167] further confirms the general picture. The solitons in trans- $(CH)_x$ are confined below $T = 150$ K and are liberated and free above $T = 150$ K. This picture is also consistent with the disappearance of the solid state effect at 150 K in ESR signal of pristine trans- $(CH)_x$ [143]. The liberation of solitons at $T = 150$ K appears to be a collective effect, since it is very difficult to describe such a sudden transition in terms say of a single pair. Clearly a further work on the liberation of solitons is desirable.

5.8. Future Development

Some of the properties of trans- $(CH)_x$ described above are consequence of the halffilled band. When the Fermi momentum is 1/3 of π/a as studied by Su and Schrieffer [104], the solitons have fractional charges. The continuum model for the trimerized chain is considered recently by Hara et al. [193] and Gammel and Krumhansl [194]. Whether these fractionally charged solitons are observable by transport measurements is not known. Furthermore, the stability of the fractionally charged solitons in the presence of the Coulomb interaction appears to require further study.

A more rigorous analysis of the SSH model (Equation (5.1)) is done by Sutherland [195] for arbitrary electron filling factor. In particular, he finds that the solitons discussed above exist not only for the half-filled band but also for k_F close to the half-filled band. Furthermore, when the band is close to the third-filled he finds in general the solitons with fractional charge as in the Su-Schrieffer model.

A somewhat different model is considered by Brazovskii et al. [196]. The model is same as the SSH model (Equation (5.1)) except that $t_{n,n+1}$ is replaced by

$$t_{n,n+1} = t_0 \exp\left[-\alpha t_0^{-1}\left(u_{n+1} - u_n\right)\right] \tag{5.53}$$

Expanding the exponent in powers of α, the linear term gives the SSH model. They found that this model (the BDK model) is exactly solvable within the mean field approximation based on the exact result on the Toda lattice. In this model, the filling factor $\nu = 0$ (empty band), 1/2 (half filled band), and 1 (filled band) are the special points. Near $\nu = 1/2$ for example the ground state is described by the soliton lattice as described in Subsection 5.5. The electron energy spectrum consists of three disconnected bands. Furthermore, there is nothing special for $\nu = 1/3$ for example. When ν is close to 0 or 1 , the order parameter becomes complex and the sliding mode exists in the ideal chain. It is not well understood why the prediction of the BDK model is so different for $\nu = 1/3$ from that of the SS model.

More recent variants of the SSH model are proposed by Rice and Mele [197, 198] for diatomic polymers and by Rice et al. [199] for polyyne chains. The former model allows solitons with irrational charge, whereas the latter model is the SSH model but with electrons of 4 flavors. However we shall not go into application of these models.

The existence of degenerate ground states is of central importance for the physics of trans-polyacetylene. However, some of the ideas developed for polyacetylene are applicable to the polymer chains which do not have degenerate ground states but one of the low energy states is slightly lifted from the other. In these systems solitons are necessarily confined but polarons and bipolarons (i.e. polarons with charge $\pm 2e$ or bound state of pair of charged solitons) are considered as elementary excitations [135, 136, 141]. Recently optical absorption data of polypyrrole [200] and polythiophene [201] one analysed convincingly in terms of polarons and bipolarons in these systems. We present the chemical structure of polypyrrole (i.e. pyrrole polymer) and polythiophene in Figures 12 and 13 together with their polaron configurations.

Therefore, in spite of the unique position trans-polyacetylene occupies in the conducting polymers the concepts developed for the physics of polyacetylene will find wider and wider application in physics of the conducting polymers.

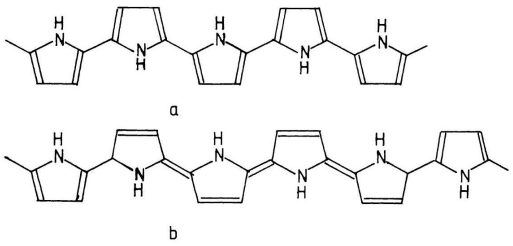


Fig. 12. The bond configurations of polypyrrole are shown. (a) the ground state, (b) the polaron (or bipolaron) state.

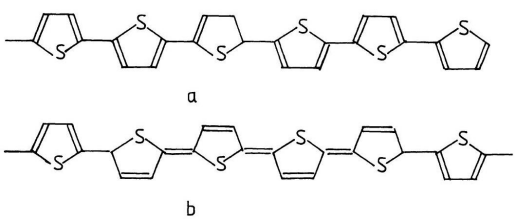


Fig. 13. The bond configurations of polythiophene are shown. (a) ground state, (b) the polaron (or bipolaron) state.

3.5.7 6. Sliding CDW Transport

6.1. Transport Properties

The discovery of non-Ohmic conductivity in $NbSe_3$ by Monceau et al. [202] opens up a new field. In the weak field limit the temperature dependence of the electric conductivity has two dips characteristic of the transition to the charge density wave (CDW) state [102]; the conductivity decreases as the quasi-particle number decreases due to the opening of the energy gap. However, Monceau et al. discovered that a moderate electric field $E \simeq 5\text{mV/cm}$ could eliminate these distinctive features. Now extensive studies establish that this non-Ohmic conductivity is due to the sliding of the CDW condensate. This possibility has been envisioned by Fröhlich [93] almost 30 years ago. Indeed the two features in the conductivity are associated with the two CDW transitions at $T = 144$ K and 59 K . The two CDW condensates are incommensurate but very close
to the $M = 4$ commensurability [203]. Later Fleming and Grimes [204] discovered that the nonlinearity in the conductivity requires a small threshold field $E_T(\sim$ a few mV/cm). Furthermore in the non-Ohmic regime a quasi-periodic current (narrow band noise) is generated [204]. The frequency dependent conductivity is very sensitive to the frequency. For an ac field of 10GHz(-0.5 K) the two CDW features seen in the dc conductivity almost disappear [205]. The smallness of the threshold field and the characteristic frequency rule out single particle interpretations (Zener tunneling, field ionization) for the anomaly. Furthermore independence of the CDW amplitude on the electric current as seen by X-ray even in the nonlinear regime [206] strengthens the idea that motion of the CDW condensate plays a crucial role in the nonlinear transport. More recently new systems like TaS_3 (orthorhombic and monoclinic) [207, 208], $(TaSe_4)_2\,I$, $(NbSe_4)_{10/3}\,I$ [209,210] and the blue bronze $K_{0.3}MoO_3$ and $Rb_{0.3}MoO_3$ [211] are found to exhibit similar anomalous transport. Therefore the anomalous transport observed in the CDW states of $NbSe_3$ is generic in a class of quasi-one dimensional compounds. Since a review on this subject will be given by Monceau in Part II and since a few excellent reviews [212-214] are already available, we shall summarize the principle experimental results in this subsection. Then we shall go on to describe the theoretical models to describe the anomalous transport from a solitonic point of view.

A. Field and Frequency Dependence of Conductivity

The dc conductivity in $NbSe_3$ in the CDW state is found to be strongly nonlinear [202]. While later the existence of a small linear regime is established [204]. Indeed Fleming and Grimes [204] suggested the following empirical expression

$$\sigma(E) = \sigma_a + \sigma_b(E) \tag{6.1}$$

$$\sigma_b(E) = \sigma_b\theta\left(E - E_T\right)\left(1 - \frac{E}{E_T}\right)\exp\left(-E_0/E - E_T\right) \tag{6.2}$$

where σ_a is the Ohmic component and E_T is the threshold field. E_0 is another field, which is $2-4E_T$ for very clean $NbSe_3$ [213]. Although Equation (6.2) suggests the Zener tunneling (if we put $E_T = 0$) in a semiconductor with the energy gap 2Δ, the smallness of E_0 excludes any process associated with the quasi-particles. For example if Δ for the CDW energy gap were substituted, E_0 would be of the order of 10^4 V/cm, whereas in the cleanest $NbSe_3$ samples, the observed $E_0 \simeq 5 \times 10^{-3}$ V/cm. Furthermore, the existence of the threshold field E_T is rather difficult to understand within the tunneling model. We note also that alternative forms for $\sigma_a(E)$,

$$\sigma_b(E) = \sigma_b\theta\left(E - E_T\right)\exp\left(-E_0/E - E_T\right)$$

and

$$= \sigma_b\theta\left(E - E_T\right)\left(1 - E/E_T\right)\exp\left(-E_0/E\right)$$

produce equally good fits to the observed nonlinear conductivity as long as $E \leqq 3E_0$ and therefore it is not useful to argue the precise form of the nonlinear conductivity at the present time.

As already mentioned Ong et al. [205, 216] showed the CDW features are removed from the conductivity for $\omega = 10$GHz. Grüner et al. [217] have determined the conductivity over an extended frequency range. The results may be summarized approximately as;

$$\sigma_1(\omega) - i\sigma_2(\omega) = \sigma_a + \sigma_b\frac{(\omega\eta)^2 - i(\omega\eta)}{1 + (\omega\eta)^2} \tag{6.3}$$

where $\eta = \tau\omega_0^2$.
Here Equation (6.3) is the one corresponding to an overdamped oscillator where τ is the relaxation time and ω_0 is the oscillator frequency. The experimental data are fitted with $\eta^{-1} = 3.6 \times 10^8$ Hz, although the observed frequency dependence is much broader than Equation (6.3) suggests. This result is interpreted in terms of the pinned overdamped phase modes suggested by Lee, Rice and Anderson [98]. Broadness of the frequency dependence may suggest a collection of the phase modes with different pinning frequencies and damping constants. We stress again that the smallness of both E_T and η^{-1} indicate strongly the collective origin of the E and ω dependence of the conductivity.

B. Quasi Periodic Oscillation in Transport Current

Perhaps the most spectacular transport phenomenon is the appearence of a quasi periodic oscillation in the conduction current in the nonlinear regime as discovered by Fleming and Grimes [204].

This oscillation is decomposed into narrow band noise and broad band noise when the voltage spectrum is Fourier analysed. Furthermore the narrow band noise consists of one fundamental and its harmonics, although sometimes a few fundamentals are observed. Subsequently Monceau et al [220] found that the frequency of the narrow band noise ν increases linearly with the CDW current J_{CDW}, where J_{CDW} is defined as

$$J_{\mathrm{CDW}} = \sigma_b(E)E = J\left(1 - \frac{\sigma(O)}{\sigma(E)}\right) \tag{6.4}$$

where $\sigma(E)$ is defined in Equation (6.1). This relation suggests strongly that both the narrow band noise and the broad band noise are associated with uniform motion of the CDW condensate. The uniformly sliding CDW is described in terms of the time dependent phase ϕ;

$$\phi(x,t) = -Qvt \tag{6.5}$$

with $Q = 2k_F$. For example Equation (6.5) gives rise to the uniformly moving charge density

$$\rho_{\rm CDW}(t) = N_0\lambda^{-1}\Delta\cos[Q(x-vt)] \tag{6.6}$$

where use is made of Equation (4.14). Equation (6.6) implies that the local charge oscillates with frequency

$$\nu = Qv \tag{6.6}$$

On the other hand substituting Equation (6.5) into Equation (4.26), we shall have the CDW current

$$J_{\rm CDW} = -en_c(T)v \tag{6.7}$$

Eliminating v from Equations (6.6) and (6.7), we obtain

$$|J_{\rm CDW}| = \frac{e}{Q}n_c(T)\nu \tag{6.8}$$

which is exactly what found by Monceau et al. [218] .
More recently the temperature dependence of the linear coefficient as well as N dependence of Equation (6.8) have been studied [219,220]. In the vicinity of $T = T_c$, it is found $n_c(T) \propto \Delta(T)$ [219] consistent with Equation (4.28). Although Monceau et al. [220] indicate that the experimental results for $NbSe_3, TaS_3$ (both orthorhombic and monoclinic) and $(TaSe_4)_2$ I are more consistent with Equation (6.8) but with e replaced by $2e$, we don't believe that there is any justification for such a relation. We think rather that the above analysis of Monceau et al. indicates the difficulty in estimating N, the density of conduction electrons, in these compounds.

C. Impurity Effects

As discussed by Lee, Rice, Anderson [98] the CDW is pinned either by impurities or by incommensurability potential. Therefore it is of great interest to study the origin of the threshold field E_T. In a series of experiments on $NbSe_3$ doped with Ta and Ti , Ong et al. [215, 216] established that both E_T and E_0 obey a y^2 relation where y is the Ta concentration. On the other hand for the Ti doped samples and the samples irradiated with high energy protons [221], E_T increases linearly with y the impurity concentration or the dosage of protons.

The observed concentration dependence of the threshold field not only indicates that the impurity pinning plays the central role in these compounds but also that the different y dependence of E_T for the Ta and Ti doping is interpreted with the concepts of the weak and the strong pinning developed by Fukuyama, Lee and Rice [40,222]. We shall describe the theoretical concepts in the following subsection.

D. Hysteresis, Memory Effects

Another remarkable feature of the nonlinear conduction is the appearance of a long relaxation time of the order of millisecond. When a dc pulse is applied the onset of nonOhmicity requires above a millisecond as first observed by Gill [223]. This relaxation time increases exponentially with energy gap 2Δ, as the temperature decreases, suggesting that the quasi-particle

pair creation plays an important role in the relaxation of the CDW. When a pulse field of alternative sign is applied the conduction current exhibits the memory effect with the same relaxation time. More recently Zettl and Grüner [224] reported a 'switching' phenomenon; the jump between the Ohmic and non-Ohmic regime
depends on the hysteresis in TaS_3. This implies that the underlying CDW state is not uniquely determined by the external electric field but passes through a multitude of quasi-equilibrium states before the final equilibrium configuration is reached.

6.2. Impurity Pinning and the Fukuyama Lee Rice Domain

From the observed impurity concentration dependence of the threshold field E_T [215], the impurities are clearly the dominant pinning centers. The interaction energy between electrons and impurities is given by

$$H_{\text{imp}} = \sum_i \int \mathrm{d}^3x \rho(\mathbf{x}) V(\mathbf{x} - \mathbf{R}_i) \tag{6.9}$$

where $\rho(\mathbf{x}) = \Sigma_i \psi_s^+(\mathbf{x})\psi_s(\mathbf{x})$ is the local electron density and the summation is over the impurity sites $\mathbf{R}_i$. In the following we approximate the impurity potential $V(\mathbf{x}) = V_0\delta(\mathbf{x})$. Substituting for $\rho(x)$ by $\langle\rho(x)\rangle = \rho_{\text{CDW}}(x)$ given in Equation (4.14), we find

$$H_{\text{imp}} = v_{\text{imp}} \sum_i \cos\left(Qx_i + \phi\left(\mathbf{x}_i\right)\right) \tag{6.10}$$

with

$$v_{\text{imp}} = N_0 \Delta V_0 \lambda^{-1} \tag{6.11}$$

Therefore in the presence of random impurities the equilibrium configuration for $\phi(x)$ is determined by the phase Hamiltonian

$$\mathcal{H}(\phi) = \frac{1}{2} A \int \mathrm{d}^3x \partial\phi \mathrm{c}^2 \partial\phi + v_{\text{imp}} \sum_i \cos\left(Qx_i + \phi\left(\mathbf{x}_i\right)\right) \tag{6.12}$$

where the first term is the phase elastic energy taken from Equation (4.22) with proper generalization to the three dimensional system. Here $\mathbf{c}^2$ is the square of the tensor of the phason velocity. Since the anisotropy in the phason velocity is easily eliminated from Equation (6.12) by appropriate length scale change [40], we shall consider in the following a slightly simpler version of Equation (6.12)

$$\mathcal{H}(\phi) = \frac{1}{4} N_0 v_F^2 \int \mathrm{d}^3x |\nabla\phi|^2 + v_{\text{imp}} \sum_i \cos\left(Qx_i + \phi\left(\mathbf{x}_i\right)\right) \tag{6.13}$$

where v_F is the Fermi velocity and N_0 is the electron density of states per spin at the Fermi surface. The Hamiltonian (6.13) has been extensively studied by Fukuyama, Lee and Rice [222,40]. We shall summarize here the principal results. From the outset it is important to distinguish two cases: the strong pinning case and the weak pinning case. In the strong pinning case the second term dominates Equation (6.13). Then the equilibrium configurations are determined by minimizing $\phi(\mathbf{x})$ at the impurity sites;

$$\begin{aligned} \phi\left(\mathbf{x}_i\right) &= \pi - Qx_i \quad \text{modulo } (2\pi) \quad \text{for} \quad V_0 > 0 \\ &= -Qx_i \quad \text{modulo } (2\pi) \quad \text{for} \quad V_0 < 0 \end{aligned}$$

Then the rest of $\phi(\mathbf{x}_i)$ are determined to minimize the elastic energy consistent with the boundary condition Equation (6.13). When the impurity concentration is y, the pinning energy per unit volume is estimated as

$$E_{\text{pin}} \simeq \frac{\pi^2}{4} N_0 E_F^2 y^{2/3} - y\,|v_{\text{imp}}| \tag{6.14}$$

Here we estimate the elastic energy from

$$\frac{\partial \phi}{\partial x} \simeq \frac{\pi}{a} y^{1/3} \tag{6.15}$$

where $ay^{-1/3}$ is the average distance between two impurities and a is the atomic distance. From Equation (6.14) we can deduce that the strong pinning limit applies when

$$V_0 \geqslant \lambda E_F^2/\Delta \sim 10 E_F \tag{6.16}$$

in the case of $NbSe_3$ for example.
In the weak pinning limit on the other hand a single impurity is not strong enough to pin the local phase. In this circumstance the CDW is split into domains with linear dimension L_0. Within each domain ϕ is fairly coherent; we can define an averaged $\bar{\phi} = \langle \phi \rangle_d$. The linear dimension of the domain L_0 as well as the pinning energy per unit volume in this case is estimated as follows;

$$E_{\text{pin}} = \frac{1}{4} N_0 v_F^2 L_0^{-2} - |v_{\text{imp}}|\, y^{1/2} \left(a/L_0\right)^{3/2} \tag{6.17}$$

where the first term is estimated from

$$\frac{\partial \phi}{\partial x} \sim L_0^{-1}$$

while the second term is obtained from by averaging $\cos\left(Qx_i + \phi(x_i)\right)$ within the domain

$$\left\langle \cos\left(Qx_i + \phi(x_i)\right)\right\rangle_d = \operatorname{Re}\left\langle \exp\left(i\left(Qx_i + \bar{\phi}\right)\right)\right\rangle_d = \left(y\left(L_0/a\right)^3\right)^{1/2} \left(L_0/a\right)^{-3} \cos\bar{\phi} \tag{6.18}$$

According to Fukuyama and Lee [222], the average can be considered as the random walk of a unit vector in the two-dimensional space with number of steps $y\left(L_0/a\right)^3$, the impurity number in the volume L_0^3. Here it is assumed that the variation in Qx_i dominates that of $\phi(x_i)$. Then minimizing Equation (6.17) for L_0, we find

$$L_0 = \left(N_0 v_F^2/3\,|v_{\text{imp}}|\right)^2 a^{-3} y^{-1} \tag{6.19}$$

and

$$E_{\text{pin}} = -\frac{27}{4} y^2 a^6\, |v_{\text{imp}}|^4 \left(N_0 v_F^2\right)^{-3} \tag{6.20}$$

In the weak pinning limit, the pinning energy is proportional to y^2. Furthermore, Equation (6.20) gives the correct order of magnitude of the pinning voltage. Note that Equations (6.19) and (6.20) yields:

$$L_0 \simeq (\lambda\xi/3)^2 a^{-1} y^{-1} \tag{6.21}$$

$$E_{\text{pin}} \simeq -(27/4)\lambda^{-4} y^2 (a/\xi)^2 N_0 \Delta^2 \tag{6.22}$$

for $V_0 \cong E_F$ and $\xi = v_F/\Delta(\sim 100\text{Å})$ is the BCS coherence distance for the CDW state. For $y = 0.1\%$ for example, we still have $L_0 \simeq 10\mu$ m and $|E_{\text{pin}}| \simeq 10^{-13} E_{\text{cond}}$. The latter implies the pinning frequency $\omega_0 = 10^{-6}\Delta$ consistent with the experiments described in the preceding subsection. Indeed the isoelectronic impurities like Ta in $NbSe_3$ give rise to the weak pinning, while the non-isoelectric impurities like Ti result in the strong pinning.

Although within the present approach it is difficult to calculate the effective phase potential $V(\bar{\phi})$ or to predict the E and ω dependence of the conductivity, the impurity pinning can interpret both the y dependence and the order of magnitude of E_T correctly. Furthermore within the mean field theory Equation (6.20) predicts that the pinning frequency ω_0 diverges like $(1 - T/T_c)^{-1/2}$ near the transition temperature which is also consistent with the observed temperature dependence of E_T [225]. On the other hand at low temperatures Equation (6.20) predicts a temperature independent pinning frequency whereas the observed E_T for $NbSe_3$ increases like $\exp(-aT)$ as the temperature decreases [225].

6.3. Tunneling Model

We shall now describe the theoretical models which attempt to understand the E and ω dependence of the conductivity and the origin of quasi-periodic current in the non-Ohmic regime.

The first of them is the tunneling model, which hypothesizes that the E dependence of the conductivity is due to the quantum mechanical tunneling of some sort of the CDW mode, which is suggested by similarity of Equation (6.2) with the Zener tunneling expression. The first of such a model is the soliton-pair creation proposed by Maki [226]. In spite of several difficulties this model encounters in applying to the CDW transport in $NbSe_3$, this model is still the simplest conceptually. We believe also that this model is extremely helpful to understand Bardeen's model which is free of some of the above difficulties [227].

In order for the soliton tunneling to apply the pinning potential has to be periodic in $\phi(\mathbf{x})$. The commensurability potential provides such a potential, although this may not be essential.

In the presence of a periodic potential the phase dynamics is controlled by Equation (4.33). In particular the system contains the ϕ-solitons [33] with charge $Q = \pm 2eM^{-1}$, where $M = 4$ in the case of the commensurability potential.

In the presence of an electric field E along the chain direction a soliton-antisoliton pair gains a potential energy of $2eM^{-1}Ed$ where d is the distance between the pair. Making use of the instanton technique, the probability of the soliton pair production
is readily obtained [226], which gives rise to a nonlinear component of the conductivity

$$\sigma_b(E) = 2(2e/M)^2 \frac{C_0}{\pi E_s} \frac{E_0}{E} \exp\left(-E_0/E\right) \tag{6.23}$$

where

$$E_0 = \pi M E_S^2 / (2eC_0) \tag{6.24}$$

and $E_S = 8AC_0\omega_0 M^{-2}$ the ϕ-soliton energy.
The principal difficulty of the model is that the soliton energies needed to account for the nonlinear conductivity in $NbSe_3$ are extremely small. For example in order to account for the nonlinear conductivity below T = 144 and 59 K in $NbSe_3$, E_S has to be 0.63 and 0.15 K respectively. If this were really the case, we would not expect any anomaly in the conductivity, since the thermally excited solitons will bring forth the normal conductivity except at extremely low temperatures ($T \leqslant E_S$).

A possible way out of this difficulty is to assume that these solitons are confined due to the interchain coupling. Indeed $NbSe_3$ appears to be three dimensional rather than one dimensional.

The confinement potential not only limits the density of thermally excited solitons but also gives rise to a threshold field to the tunneling process. If the confinement potential for soliton and antisoliton pair is given by

$$E_c(x) = W|x|/a \tag{6.25}$$

as in the case of polyacetylene (Equation (5.49)) where x is the distance between the pair, the probability of the pair production vanishes for $E \leqslant E_T = MW/(2ea)$, while for $E > E_T$ we shall have

$$\sigma_b(E) = 2(2e/m)^2 \frac{C_0}{\pi E_S} \frac{E_0}{E - E_T} \exp\left(-E_0/\left(E - E_T\right)\right) \tag{6.26}$$

Therefore in the presence of soliton confinement, the only strong objection to the ϕ-soliton model is how a periodic potential for ϕ can be obtained from the impurity pinning, since experimentally the soliton energy is determined by the impurity potential rather than the commensurability potential.

The Bardeen model [227,228] does not depend on detail of $V(\phi)$, the potential for ϕ. This is both an advantage and a difficulty in his theory. Since Bardeen describes his tunneling model in this volume, we shall limit ourselves to a few remarks on his model. Indeed, if the following two conditions are satisfied, the Bardeen model can be reinterpreted in terms of the ϕ-soliton pair production: (1) The impurity potential produces a quasi-periodic potential in ϕ. (2) The commensurability index M in this potential is extremely large: $M \sim 10^3$. By choosing an enormously large M the soliton charge Q becomes extremely small (note $Q = 2e/M$), therefore in this circumstance the soliton energies required to account for the nonlinear conductivity are comfortably large (i.e. comparable to the quasi-particle energy). Although Bardeen interpreted the existence
of a threshold field in terms of screening, this can be as well due to the confinement potential. Indeed from the topological point of view the soliton pair creation is rather generic as shown in Figure 14. The depinning starts as local phase around a point x changes from $\phi(x)$ to $\phi(x) \pm 2\pi/M$, as seen from some numerical analysis of the one dimensional model [229].

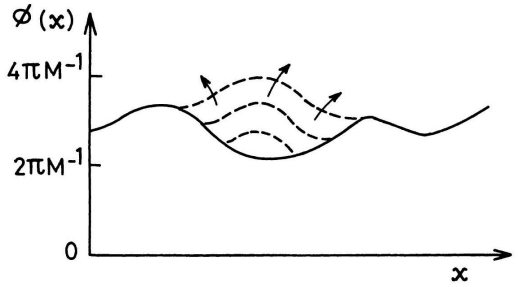


Fig. 14. The initial depinning of the phase $\phi(x)$ in the CDW is schematically shown.

Therefore the problem boils down on how to find a quasi-periodic potential for ϕ starting from the impurity potential. Perhaps a manybody approach to the Lee-Rice pinning by Klemm and Schrieffer [230] may throw light on this question. If the impurity distribution is not random but has a short range correlation, the impurity scattering might result in a quasi-periodic potential for ϕ with large M.

We shall conclude this subsection with two fundamental objections to all the tunneling models in the case of $NbSe_3$. First, to the extent that the tunneling is a purely quantum mechanical process, we expect that E_T becomes constant and independent of temperature at lower temperatures, where the pinning energy becomes temperature independent. However in

the case of $NbSe_3$ and TaS_3 (orthorhombic) the observed threshold field E_T increases as the temperature is lowered [225, 206]. This suggests rather strongly that the depinning is a thermal process rather than a quantum process. Indeed in the two dimensional system, the creation of a phase vortex ring results in a similar expression as Equation (6.23);

$$\sigma_{th}(E) \propto e^{-E_0/E} \tag{6.26}$$

where

$$E_0 = \pi M E_v^2 / 2ek_BT \tag{6.27}$$

and E_v is the vortex energy per unit length [231].

Again the three dimensional coupling introduces a threshold field in Equation (6.26). This model predicts that E_0 diverges as T^{-1} at low temperatures, which is not inconsistent with observed E_0. Indeed such a T^{-1} dependence of the threshold field has been observed recently for $(NbSe_4)_{10/3}$ I by Z. Z. Wang et al. [232]. However, how to relate E_T to the pinning potential has yet to be worked out. Second, the number of charged pairs tunneled increases gradually with E, whereas the observed $\sigma(E)$ near $E = E_T$ indicates that the charged carrier number is independent of E near $E = E_T$ [213].

Summing up, the thermal activation process may be dominant near the threshold. However, when the CDW condensate is once set in motion it appears that we need more global description of the CDW motion, whereas quantum or thermal process are only local processes. Also the temperature dependence of E_T in blue bronzes $K_{0.30}MoO_3$ appears to be quite different from those of $NbSe_3$ and TaS_3 described above [211]. Therefore even the threshold behavior of the nonlinear conductivity may be controlled by different mechanisms depending on the quasi-one dimensional systems.

6.4. Classical Particle Model

The second model to be described is the classical particle model or washboard model. We have seen already that in the weak pinning limit the CDW condensate is split into the Fukuyama, Lee, Rice (FLR) domains. Within a FLR domain an average phase $\bar{\phi}$ is assigned. We shall concentrate on the dynamics of $\bar{\phi}$, which we shall write ϕ hereafter for simplicity. The simplest equation for ϕ may be

$$\phi_{tt} + \tau^{-1}\phi_t + \frac{\mathrm{d}V(\phi)}{\mathrm{d}\phi} = -F \tag{6.28}$$

first proposed by Grüner et al. [233], where

$$F = ev_F\lambda(\omega Q/2\Delta)^2 n_s(T)E \tag{6.29}$$

and E is the electric field.

The effective phase potential $V(\phi)$ is assumed to be periodic in ϕ. The simplest choice is

$$V(\phi) = \omega_0^2 M^{-2}(1 - \cos(M\phi)) \tag{6.30}$$

where ω_0 is the pinning frequency.

In the presence of a small ac electric field with frequency ω, the induced CDW current is calculated as [233]

$$\begin{aligned} J_{\mathrm{CDW}} &= eQ^{-1}n_c(T)\frac{\partial\phi}{\partial t} \\ &= \sigma_{\mathrm{CDW}}(\omega)E_\omega \end{aligned} \tag{6.31}$$

where

$$\sigma_{\mathrm{CDW}}(\omega) = \sigma_b \frac{-i\omega\tau^{-1}}{\omega_0^2 - \omega^2 - i\omega\tau^{-1}} \tag{6.32}$$

and

$$\sigma_b = \tau e^2 v_F Q^{-1} n_s(T) \tag{6.33}$$

Comparing Equation (6.32) with the observed ac conductivity of $NbSe_3$ [217], it is concluded that the inertia term is of little importance; the first term in the left-hand side of Equation (6.28) can be neglected. Furthermore we can identify $\tau\omega_0^2 = \eta$ as defined, following Equation (6.3). Furthermore, since M in the potential (6.30) can be eliminated by rescaling ϕ completely, at least in the classical theory, we shall concentrate on

$$\tau^{-1}\phi_t + \omega_0^2 \sin\phi = -F \tag{6.34}$$

in the following.
Since Equation (6.34) is analysed in greater detail by Monceau et al. [218, 234], we shall summarize their results here. Equation (6.34) describes a motion of a viscous ball on a tilted washboard where the tilt angle is controlled by F. For $F < F_T = \omega_0^2$ the ball does not fall, implying $J_{\mathrm{CDW}} = 0$. When $F > F_T$, J_{CDW} is calculated as

$$J_{\mathrm{CDW}}(t) = eQ^{-1} n_c(T)\tau \left(F^2 - F_T^2\right) \left(F - F_T \cos(ut)\right)^{-1} \tag{6.35}$$

with

$$u = \frac{1}{2}\tau \left(F^2 - F_T^2\right)^{1/2} \tag{6.36}$$

First of all, Equation (6.35) gives the dc current

$$J_{\mathrm{CDW}}^{\mathrm{dc}}(t) = eQ^{-1} n_c(T)\tau \left(F^2 - F_T^2\right)^{1/2} \tag{6.37}$$

which increases as the square root of $F - F_T$. Furthermore, Equation (6.35) has a periodic component with frequency nu. The intensities of the nth harmonics decreases as K^n with $K = F/F_T - \left[(F/F_T)^2 - 1\right]^{1/2}$.

This model predicts the well defined threshold field F_T and the non-Ohmic behavior above the threshold. Furthermore, the appearance of an oscillatory current above the threshold with fundamental frequency u is predicted. However if you look into more detail at the prediction, it is clear that even the qualitative features of the nonlinear transport are missing from the model. In particular: (1) The dc component increases as $(F - F_T)^{1/2}$ near the threshold, whereas in most cases the experiment indicates that J_{CDW} increases linearly with $F - F_T$; (2) in the limit $F \gg F_T, \sigma_{\mathrm{CDW}}$ given by Equation (6.37) approaches a constant value as F^{-2}, while experimentally the approach to the constant value is slower, as F^{-1}; (3) the observed higher harmonic intensities decrease much slowly with n than the prediction [234]; (4) the predicted ac components are infinitely sharp. Furthermore, there is no room for the broad band noise. The origin of these difficulties most likely lies in the drastic simplification of the model. The actual CDW condensate contains large internal degrees of freedom associated with $\phi(\mathbf{x})$. Therefore, description of the collection of $\phi(\mathbf{x})$ by a single ϕ is obviously not adequate. Furthermore, a simple periodic potential $V(\phi)$ assumed here is never derived. In spite of these shortcomings the present model established convincingly the existence of the threshold field and the sliding of the CDW for $F > F_T$, the associated non-Ohmicity of conductivity and the appearence of the periodic oscillatory current. One way to improve the classical particle model is to

incorporate large degrees of freedom neglected in the model. There are several works in this direction. For example Sneddon et al. [235] considered the fluctuation of ϕ around $\bar{\phi}$ within a continuum model and found that the fluctuation gives rise to the nonlinear conductivity which decays like $F^{-1/2}$ in the limit $F \gg F_T$. Unfortunately, however there appears to be no experimental evidence for this slow decay term. Fisher [236] considered the behavior of the nonlinear conductivity near the threshold in analogy to a phase transition. He concluded that the characteristic length characterizing the domain size is no longer the FLR length L_0 but the coherence length, which diverges as $(F - F_T)^{-1/2}$ within the mean field approximation, which leads to $J_{\mathrm{CDW}} \propto (F - F_T)^{3/2}$ near the threshold. Again this result appears to contradict most of the experimental results. The second approach is to consider the one dimensional version of Equation (6.13). The corresponding equation of motion is;

$$\tau^{-1}\phi_t(x) - c_0^2\phi_{xx}(x) + \omega_0^2 \sum_i \delta(x - x_i) \sin(Qx_i + \phi(x_i)) = -F \tag{6.38}$$

where x_i 's are the impurity sites. The above equation is considered as a generalization of Equation (6.34), where the position of impurities are explicitly included. This type of equation has been sîudied numerically by Sokoloff [237] and Pietronero and Strässler [238]. Precisely speaking the latter authors studied a modified model where the first term in the left hand side of Equation (6.38) is replaced by local ones; $\tau^{-1}\phi_t(x) \to \Sigma_i \delta(x - x_i)\tau^{-1}\phi_t(x_i)$. Both of them found that in the limit of a large number of impurities the threshold behavior of J_{CDW} is broadened in the one dimensional model. On the other hand the calculated widths of the fundamental and the higher harmonics are much broader than those observed in the nonlinear regime of $NbSe_3$. However, these are certainly improvements over the classical model. The third approach will be to incorporate the remaining degrees of freedom in terms of phase vortices or dislocations in the CDW [41]. This model will be described in the following subsection.

The most crucial difficulty of the classical particle model is the origin of a periodic potential in ϕ. In the thermodynamic limit it is known that the impurity potential averages out completely. A more elaborate formulation of the FLR theory may produce such a potential [230]. As noted by Barnes and Zawadowski [239] the higher order terms of Equation (6.9) may produce also such a potential. A more careful exploration in this direction is also desirable.

6.5. Vortex Array Model

We shall describe here a recent model put forwards by Ong et al. [41] to account for the narrow band noise in the nonlinear regime of the CDW transport. The model is based on the experimental fact that sources of the narrow band noise are localized and probably near the contact [240]. Furthermore in most of experiments done on $NbSe_3$ contacts formed by silver paint are the major perturbation to a thin crystal of $NbSe_3$ as shown

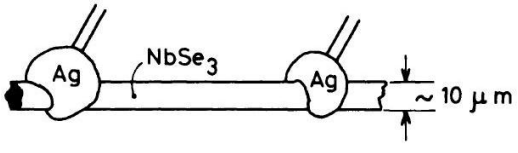


Fig. 15. $\mathrm{A
\mathrm{NbSe}_{3}$ crystal with two silver paint contacts is schematically shown.}

in Figure 15. Under this circumstance the electric field under the contacts is much smaller than that in the bulk of the sample as the contacts provide bypath for the electric current. When the electric field E in the bulk is larger than E_T, the CDW between the contacts slides

with velocity v; the phase of the CDW is increasing linearly with time t as $\phi = Qvt$. On the other hand since the electric field E' under a contact is much smaller the phase of the CDW under the contact is stagnant. This implies a clash between a sliding phase and a stagnant phase close under the contact. The clash is avoided, however, by introducing an array of phase vortices (or dislocations) which moves along the phase boundary perpendicular to v with velocity v_s;

$$v_s/l_v = v/\lambda_{\mathrm{CDW}} = v. \tag{6.39}$$

where l_v is the distance between two vortices in the array, $\lambda_{\mathrm{CDW}} = 2\pi Q^{-1}$ and ν is the frequency of the fundamental of the narrow band noise. To the extent that the array of vortices forms a regular lattice, the frequency of the noise agrees with the classical particle model. Making use of the Hamiltonian (6.13), the vortex energy per unit length is estimated as

$$E_v = \frac{1}{4} N_0 v_F^2 \int \mathrm{d}^2x \left(1/r^2\right) = \frac{1}{2}\pi N_0 v_F^2 \ln\left(L_0/\xi\right) \tag{6.40}$$

where

$$\phi = \tan^{-1}(y/x) \tag{6.41}$$

indicating a vortex at $(x, y) = (0, 0)$ is substituted, and the integral is cut off at L_0 the FLR length and ξ the coherence length. The free energy of an array of vortices is much less than the complete disruption of the CDW condensate at the phase boundary, since the ratio of two free energies $\Delta F_v/\Delta F_s = (\pi\xi/l_v)\ln(L_0/\xi)$ is always much less than unity. In the presence of an array of vortices at $x = 0$ and $y = y_i$, the extra CDW current associated with the array is calculated as follows.

Integrating Equation (4.26) around a loop enclosing the vortex array we obtain that the current difference between two sides of the array is

$$\begin{aligned} \Delta J &= J_{\mathrm{CDW}}(\text{ left }) - J_{\mathrm{CDW}}(\text{ right }) \\ &= -2\pi n_c(T) e Q^{-1} \sum_i \partial y_i/\partial t \end{aligned} \tag{6.42}$$

where we substituted

$$\phi = \sum_i \tan^{-1}\left(y - y_i/x\right) \tag{6.43}$$

in Equation (4.26). Taking the time average of Equation (6.42), the dc component is nothing but the difference of the local J_{CDW} between the two sides of the vortex array. The vortex array compensates the difference of the local CDW current and achieves the conservation of the CDW current throughout the sample whenever there are a few domains with different sliding velocities. On the other hand since the motion of vortices cannot be uniform, Equation (6.42) generates an ac component as well. The present model accounts easily for the experimental fact that three fundamentals instead of one fundamental are usually observed in the four probe experiment [234]. The major advantage of the present model over the classical particle model is that we do not need to have a periodic potential for ϕ generated from the impurity potential. In the vortex model the periodic potential for an array of vortices is provided by the walls where vortices enter and exit. The narrow band noise has always width due to fluctuation around the uniform motion of vortices. It is naturally expected the width of the narrow band noise increases with the transverse cross-section of the samples. On the other hand we expect that the noise amplitude is independent of the distance between two contacts. We will show

in Figure 16 the frequency spectrum of the observed current in $NbSe_3$ samples with different contact distance [241]. It is quite clear from Figure 16 that there is no appreciable change in the noise intensity for samples with contact distance between 0.07 mm and 1.6 mm , although there is a recent report contrary to the above result [242]. Indeed the predicted decrease of the noise intensity with the increasing transverse cross-section of $(TaSe_4)_2 I$ has recently been reported by Mozurkewich et al. [243]. In any case the size and the geometry dependence of the narrow band noise is of particular importance to understand the origin of the narrow band noise.

The vortex array model also resolves a standing puzzle why the cleaner sample has stronger and sharper noise spectrum, as the model does not require a periodic potential due to the impurity potential.

From the vortex array picture the CDW condensate in the sliding regime splits into three domains, two domains at two contacts and one sliding domain in between. It is very remarkable that the CDW in the region between two contacts is monodomain, which can be seen from the absence of the second fundamental. Within the present model each domain boundary generates noise with fundamental proportional to the difference of the sliding velocities of two domains involved. This implies that the phase coherence of the CDW extends much longer than the FLR length L_0 once the CDW is set into motion.

3.5.8 7. Summary

We have reviewed solitons in quasi-one-dimensional systems. In the magnetic systems there is clear indication that the low temperature properties of some of these systems are dominated by solitons. In the conducting systems the notion of solitons has played a central role in understanding the electronic properties of polyacetylene and other related compounds like polythiophene and pyrrole polymer. However a further study is clearly desirable to understand the soliton dynamics. Finally in the quasi-one dimensional CDW system the phase vortices (2 dimensional solitons) will play an important role in the CDW dynamics. On the other hand, direct evidence for the ϕ solitons in any of quasi-one dimensional conductors appear to be still lacking although discommensurations are

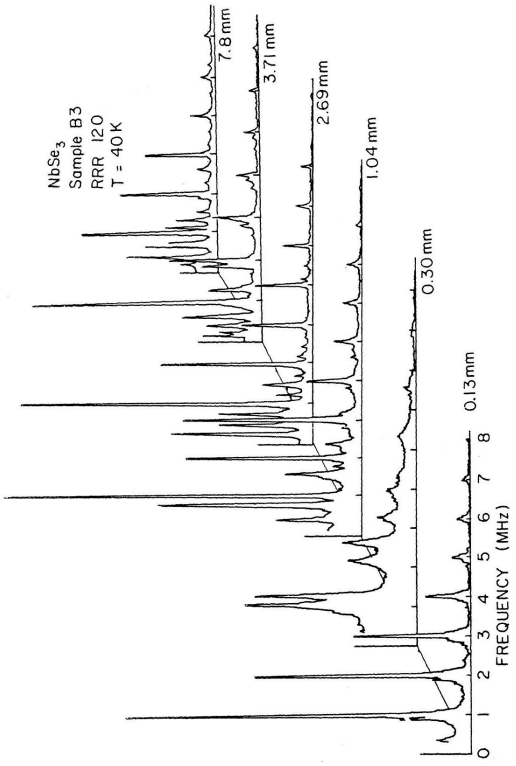


Fig. 16. A typical frequency spectrum of $\mathrm{NbSe
_{3}$ sample with different distance between contacts is shown. The intensity of the fundamental is almost independent of the distance for $d = 0.13$ mm $-$ 3.71 mm.}

observed, which are macroscopic objects. It is hoped that this review will provide a starting point for future study of the soliton dynamics in quasi-one dimensional conductors.

3.5.9 References

1. J. Scott-Russel, Proc. Roy. Soc. Edinburgh 319 (1844).
2. A. Barone, F. Esposito, C. F. Maggee and A. C. Scott, Riv. Nuovo Cimento 1, 227 (1971).
3. G. B. Whitham, Linear and Nonlinear waves (1974) John Wiley and Sons, New York.
4. A. R. Bishop and T. Schneider (eds.) Solitons in Condensed Matter Physics (1978) Springer Verlag, Berlin, Heidelberg, New York.
5. J. Bernasconi and T. Schneider (eds.) Physics in One Dimensional (1981) Springer Verlag, Berlin, Heidelberg, New York.
6. A. R. Bishop, J. A. Krumhansl and S. E. Trullinger, Physica 1D, 1 (1980).
7. J. de Physique (Paris) C3 (1983).
8. D. J. Kortweg and G. de Vries, Phil. Mag. 39, 422 (1895).
9. A. Kochendörfer and A. Seeger, Z. Phys. 127, 533 (1950).
10. J. Frenkel and T. Kontorova, J. Phys. USSR 1, 139 (1939).
11. E. Fermi, J. Pasta and S. Ulam, Los Alamos Report LA-1940 (1955); Collected papers of Enrico Fermi Vol. II, p. 978 (1965) University of Chicago Press, Chicago.

12. M. Toda, J. Phys. Soc. Japan Suppl. 26, 235 (1969).

13. N. J. Zabusky and M. D. Kruskal, Phys. Rev. Lett. 15, 240 (1965).

14. C. S. Gardner, J. M. Greene, M. D. Kruskal and R. M. Miura, Phys. Rev. Lett. 19, 1095 (1967).

15. P. D. Lax, Comm. Pure and Appl. Math. 21, 1095 (1968).

16. V. E. Zakharov and A. B. Shabat, Sov. Phys. JETP 34, 62 (1972).

17. M. J. Ablowitz, D. J. Kaup, A. C. Newell and H. Segur, Studies in Appl. Math 53, 249 (1974).

18. A. C. Scott, F. Y. F. Chu and D. W. McLaughlin, Proc. IEEE 61, 1443 (1973).

19. D. Finkelstein, J. Math. Phys. 7, 1218 (1966).

20. S. Coleman, in New Phenomena in Subnuclear Physics ed. A. Z. Zichichi (1977) Plenum, New York.

21. G. Toulouse and M. Kleman, J. Phys. (Paris) 37, L149 (1976).

22. V. P. Mineyev and G. E. Volovik, Phys. Rev. B18, 3197 (1978).

23. L. D. Landau and E. M. Lifshitz, Statistical Physics p. 430 (1959) Pergamon Press, London.

24. A. A. Abrikosov, Soviet Phys. JETP 5, 1174 (1957).

25. J. M. Kosterlitz and D. J. Thouless, J. Phys. C6, 1181 (1973).

26. J. M. Kosterlitz and D. J. Thouless, 'Two Dimensional Physics' in Prog. Low Temp. Phys. vol. 7B ed. D. F. Brewer (1978) North Holland, Amsterdam.

27. W. Döring, Z. Natur. 31, 373 (1948).

28. K. Maki and P. Kumar, Phys. Rev. B16, 182, 4805 (1977).

29. K. Maki and P. Kumar, Phys. Rev. B17, 1088 (1978).

30. K. Maki and Y. R. Lin-Liu, Phys. Rev. B17, 3558 (1978).

31. W. L. McMillan, Phys. Rev. B14, 1496 (1976).

32. P. Bak and V. J. Emery, Phys. Rev. Lett. 36, 978 (1976).

33. M. J. Rice, A. R. Bishop, J. A. Krumhansl and S. E. Trullinger, Phys. Rev. Lett. 36, 432 (1976).

34. W. P. Su, J. R. Schrieffer and A. J. Heeger, Phys. Rev. Lett. 42, 1698 (1979); Phys. Rev. B22, 1101 (1980).

35. M. J. Rice, Phys. Lett. 71A, 152 (1979).

36. J. A. Krumhansl and J. R. Schrieffer, Phys. Rev. B 11, 3535 (1975).

37. J. K. Kjems and M. Steiner, Phys. Rev. Lett. 41, 1137 (1978).

38. J. P. Boucher, L. P. Regnault, J. Rossat-Mignod, J. P. Renard, J. Bouillot and W. G. Stirling, Sol. Stat. Comm. 33, 171 (1980).

39. J. P. Boucher and J. P. Renard, Phys. Rev. Lett. 52, 663 (1984).

40. P. A. Lee and T. M. Rice, Phys. Rev. B19, 3970 (1979).

41. N. P. Ong, G. Verma and K. Maki, Phys. Rev. Lett. (in press).

42. R. F. Dashen, B. Hasslacher and A. Neveu, Phys. Rev. D10, 4114, 4130 (1974); D11, 3424 (1975).

43. S. Coleman, Phys. Rev. D11, 2088 (1975).

44. R. Jackiw, Rev. Mod. Phys. 49, 681 (1977).

45. H. Bergknoff and H. B. Thacker, Phys. Rev. Lett. 42, 135 (1979); Phys. Rev. D19, 3666 (1979).

46. H. J. Mikeska, J. Phys. C11, L29 (1978).

47. H. J. Mikeska, J. Phys. C13, 2913 (1980).

48. K. Maki, J. Low Temp. Phys. 41, 327 (1980).

49. K. M. Leung, D. Hone, D. L. Mills, P. S. Riseborough and S. E. Trullinger, Phys. Rev. B21, 4017 (1980).

50. A. Seeger, H. Donth and A. Kochendörfer, Z. Phys. 134, 173 (1953).

51. B. D. Josephson, Phys. Lett. 1, 251 (1962); Adv. Phys. 14, 419 (1965).

52. A. C. Scott, Nuovo Cimento 69B, 241 (1970).

53. K. Nakajima, Y. Onodera, T. Nakamura and R. Sato, J. Appl. Phys. 45, 4095 (1974).

54. J. K. Perring and T. H. R. Skyrme, Nucl. Phys. 31, 550 (1962).

55. K. Maki and H. Takayama, Phys. Rev. B20, 3223 (1979).

56. J. F. Currie, J. A. Krumhansl, A. R. Bishop and S. E. Trullinger, Phys. Rev. B22, 477 (1980).

57. D. J. Scalapino, M. Sears and R. A. Ferrell, Phys. Rev. B6, 3409 (1972).

58. N. Gupta and B. Sutherland, Phys. Rev. A14, 1790 (1976).

59. H. Takayama and K. Maki, Phys. Rev. B21, 4558 (1980).

60. T. Schneider and E. Stoll, Phys. Rev. B22, 5317 (1980).

61. K. Sasaki, Prog. Theor. Phys. (Kyoto) 68, 411 (1982).

62. H. Takayama and G. Sato, J. Phys. Soc. Japan 51, 3120 (1982).

63. K. Sasaki and T. Tsuzuki, J. Mag. Mag. Mat. 31-34, 1283 (1983).

64. T. Miyashita and K. Maki, Phys. Rev. B28, 6733 (1983).

65. J. L. Gervais and B. Sakita, Phys. Rev. D11, 2943 (1975).

66. K. Maki, Phys. Rev. B24, 3991 (1981).

67. A. Luther, Phys. Rev. B14, 2153 (1976).

68. J. D. Johnson, S. Krinsky and B. M. McCoy, Phys. Rev. A8, 2526 (1973).

69. M. Fowler and X. Zotos, Phys. Rev. B24, 2634 (1981); B25, 5806 (1982).

70. X. Zotos and M. Fowler, Phys. Rev. B26, 1430 (1982).

71. M. Imada, K. Hida and M. Ishikawa, Phys. Lett. 90A, 79 (1982).

72. M. Fowler, Phys. Rev. B26, 2514 (1982).

73. X. Zotos, Phys. Rev. B26, 2519 (1982).

74. M. Steiner, J. Villain and C. G. Windsor, Adv. in Phys. 25, 87 (1976).

75. J. Villain, Physica 79B, 1 (1975).

76. N. Ishimura and H. Shiba, Prog. Theor. Phys. (Kyoto) 63, 743 (1980).

77. H. Yoshizawa, K. Hirakawa, S. K. Satija and G. Shirane, Phys. Rev. B23, 2298 (1981).

78. S. E. Nagler, W. J. L. Buyers, R. L. Armstrong and B. Briat, Phys. Rev. Lett. 49, 590 (1982); Phys. Rev. B28, 3873 (1983).

79. K. Maki, Phys. Rev. B24, 335 (1981).

80. L. R. Walker, R. E. Dietz, K. Andres and S. Derek, Sol. St. Comm. 11593 (1972).

81. J. P. Boucher, L. P. Regnault, J. Rossat-Mignod and J. Villain, Sol. St. Comm. 31, 311 (1979).

82. L. P. Regnault, J. P. Boucher, J. Rossat-Mignod, J. R. Renard, J. Bouillot and W. G. Stirling, J. Phys. C15, 1261 (1982).

83. I. Harada, K. Sasaki and H. Shiba, Sol. St. Comm. 40, 29 (1981).

84. L. Gunther and Y. Imry, Phys. Rev. Lett. 44, 1225 (1980).

85. M. Büttiker and R. Landauer, J. Phys. C. 13, L325 (1980).

86. M. Imada, J. Phys. Soc. Japan 47, 699 (1979); 49, 1247 (1980).

87. J. P. Boucher, H. Benner, F. Devreux, L. P. Regnault, J. Rossat-Mignod, C. Dupas, J. P. Renard, J. Bouillot and W. G. Stirling, Phys. Rev. Lett. 48, 431 (1982).

88. F. Borsa, Phys. Rev. B25, 3430 (1982).

89. G. Reiter, Phys. Rev. Lett. 46, 202 (1981) (Errata 46, 518).

90. A. P. Ramirez and W. P. Wolf, Phys. Rev. Lett. 49, 227 (1982).

91. X. Zotos, J. de Phys. (Paris) C3-477 (1983).

92. R. E. Peierls, Quantum Theory of Solids (1955), Oxford University Press, Oxford.

93. H. Fröhlich, Proc. Roy. Soc. A223, 296 (1954).

94. A. B. Migdal, Sov. Phys. JETP 7, 996 (1958).

95. W. Kohn, Phys. Rev. Lett. 2, 393 (1959).

96. J. T. Devreese, R. P. Evard and V. E. van Doren (eds.) Highly Conducting One-Dimensional Solids (1979) Plenum Press, New York.

97. P. A. Lee, T. M. Rice, and P. W. Anderson, Phys. Rev. Lett. 31, 462 (1973).

98. P. A. Lee, T. M. Rice, P. W. Anderson, Sol. Stat. Commun. 14, 703 (1974).

99. S. A. Brazovskii and I. E. Dzyaloshinskii, Sov. Phys. JETP 44, 1233 (1976).

100. J. Bardeen, L. N. Cooper, and J. R. Schrieffer, Phys. Rev. 108, 1175 (1957).

101. K. Maki and M. Sakurai, Prog. Theor. Phys. 47, 1110 (1972).

102. J. Zittartz, Phys. Rev. 165, 605 (1568).

103. B. Mühlschlegel, Z. für Phys. 155, 313 (1959).

104. W. P. Su and J. R. Schrieffer, Phys. Rev. Lett. 46, 738 (1981).

105. T. Takoshima, M. Ido, K. Tsutsumi, T. Sambongi, S. Homma, K. Yamaya and Y. Abe, Sol. St. Comm. 35, 911 (1980).

106. A. L. Fetter and M. J. Stephen, Phys. Rev. 168, 475 (1968).

107. B. Sutherland, Phys. Rev. A8, 2514 (1973).

108. P. Bak, Phys. Rev. Lett. 48, 692 (1982).

109. M. Weger and B. Horovitz, Sol. St. Comm. 43, 583 (1982).

110. A. J. Heeger and A. G. MacDiarmid in [5] .

111. W. P. Su, S. Kivelson and J. R. Schrieffer in [5].

112. D. Baeriswyl, G. Harbeke, H. Kiess, and W. Mayer in Electronic Properties of Polymers ed. J. Mort and G. Pfister (1982) John Wiley & Sons, New York.

113. W. P. Su in Handbook on Conducting Polymers ed. Terje Skotheim, Marcel Dekker, New York, to be published.

114. A. J. Heeger and J. R. Schrieffer, Rev. Mod. Phys., to be published.

115. I. B. Goldberg, H. R. Crowe, P. R. Newman, A. J. Heeger, and A. G. MacDiarmid, J. Chem. Phys. 70, 1132 (1979).

116. Y. Tomkiewicz, T. D. Schultz, H. B. Brom, T. C. Clarke, and G. Street, Phys. Rev. Lett. 43, 1532 (1979).

117. B. Francois, M. Bernard, and J. J. André, J. Chem. Phys. 75, 4142 (1981).

118. B. R. Weinberger, E. Ehrenfreund, A. Pron, A. J. Heeger, and A. G. MacDiarmid, J. Chem. Phys. 72, 4749 (1980).

119. R. Jackiw and C. Rebbi, Phys. Rev. D13, 3398 (1976).

120. J. A. Pople and S. H. Walmsley, Mol. Phys. 5, 15 (1962).

121. W. P. Su, Sol. St. Comm. 35, 899 (1980).

122. S. A. Brazovskii, Sov. Phys. JETP Lett. 28, 606 (1979); Sov. Phys. JETP 51, 342 (1980).

123. H. Takayama, Y. R. Lin-Liu, and K. Maki, Phys. Rev. B21, 2388 (1980).

124. B. Horovitz, Phys. Rev. B22, 1101 (1980).

125. P. G. de Gennes, Superconductivity of Metals and Alloys (1966), Benjamin Inc., New York.

126. K. Maki and M. Nakahara, Phys. Rev. B23, 5005 (1981).

127. J. T. Gammel and J. A. Krumhansl, Phys. Rev. B24, 1035 (1981).

128. N. Suzuki, M. Ozaki, S. Etemad, A. J. Heeger and A. G. MacDiarmid, Phys. Rev. Lett. 45, 1483 (1980).

129. A. Feldblum, J. H. Kaufman, S. Etemad, A. J. Heeger, T.-C. Chung and A. G. MacDiarmid, Phys. Rev. B26, 815 (1982).

130. S. Kivelson, T.-K. Lee, Y. R. Lin-Liu, I. Peschel, and Yu Lu, Phys. Rev. B25, 4173 (1982).

131. S. A. Brazovskii, S. Gordyunin, and N. N. Kirova, Soviet Phys. JETP Lett. 31, 456 (1980).

132. B. Horovitz, Phys. Rev. Lett. 46, 742 (1981).

133. M. Nakahara and K. Maki, Phys. Rev. B24, 1045 (1981).

134. W. P. Su and J. R. Schrieffer, Proc. Natl. Acad. Sci USA 77, 5626 (1980).

135. S. A. Brazovskii and N. Kirova, Sov. Phys. JETP Lett. 33, 6 (1981).

136. D. K. Campbell and A. R. Bishop, Phys. Rev. B24, 4859 (1981) and Nucl. Phys. B200, 297 (1982).

137. R. Dashen, B. Hasslacher and A. Neveau, Phys. Rev. D12, 2443 (1975).

138. Y. Onodera and S. Okuno, J. Phys. Soc. Japan 52, 2478 (1983).

139. S. Etemad, A. Feldblum, A. G. MacDiarmid, T. C. Chung and A. J. Heeger, J. Phys. (Paris) C-3, 413 (1983).

140. K. Fesser, A. R. Bishop and D. K. Campbell, Phys. Rev. B27, 4804 (1983).

141. J. L. Brédas, R. R. Chance and R. Silbey, Phys. Rev. B26, 5843 (1982).

142. M. Nechtschein, F. Devreux, R. L. Greene, T. Clarke, and G. B. Street, Phys. Rev. Lett. 44, 356 (1980).

143. W. G. Clark, K. Glover, G. Mozurkewich, C. T. Murayama, J. Sanny, S. Etemad and M. Maxfield. J. de Phys. (Paris) C-3, 293 (1983).

144. K. Maki, Phys. Rev. B26, 2181; 2187 and 4539 (1983).

145. N. S. Shiren, Y. Tomkiewicz, T. G. Kazyaka, A. R. Taranko, H. Thomann, L. Dalton, and T. C. Clarke, Sol. St. Comm. 44, 1157 (1982).

146. H. Shirakawa, T. Ito and S. Ikeda, Makromol. Chem. 179, 1565 (1978).

147. M. Schwoerer, U. Lauterbach, W. Müller, and G. Wegner, Chem. Phys. Lett. 69, 359 (1980).

148. S. Ikehata, J. Kaufer, T. Woerner, A. Pron, M. A. Druy, A. Sivak, A. J. Heeger, and A. G. MacDiarmid, Phys. Rev. Lett. 45, 1123 (1980).

149. R. Fincher Jr., M. Ozaki, M. Tanaka, D. Peebles, L. Lauchlan, A. J. Heeger, and A. G. MacDiarmid, Phys. Rev. B20, 1589 (1979).

150. J. F. Rabolt, T. C. Clarke, and G. B. Street, J. Chem. Phys. 71, 4614 (1979).

151. C. R. Fincher, M. M. Ozaki, A. J. Heeger and A. G. MacDiarmid, Phys. Rev. B19, 4140 (1979).

152. S. Etemad, A. Pron, A. J. Heeger, and A. G. MacDiarmid, E. J. Mele and M. J. Rice, Phys. Rev. B23 5137 (1981).

153. E. J. Mele and M. J. Rice, Phys. Rev. Lett. 45, 926 (1980).

154. B. Horovitz, Sol. Stat. Commun. 41, 729 (1982).

155. C. K. Chiang, C. R. Fincher Y. W. Park, A. J. Heeger, H. Shirakawa, E. J. Louis, S. C. Gau, and A. G. MacDiarmid, Phys. Rev. Lett. 39, 1098 (1977).

156. Y. W. Park, A. J. Heeger, M. A. Druy, and A. G. MacDiarmid, J. Chem. Phys. 73, 946 (1980).

157. S. Kivelson, Phys. Rev. Lett. 46, 1344 (1981); Phys. Rev. B25, 3798 (1982).

158. A. J. Epstein, H. Rommelman, M. Abkowitz and H. W. Gibson, Phys. Rev. Lett. 47, 1549 (1981).

159. L. S. Lauchlan, S. Etemad, T.-C. Chung, A. J. Heeger, and A. G. MacDiarmid, Phys. Rev. B24, 3701 (1981).

160. J. P. Sethna and S. Kivelson, Phys. Rev. B26, 3513 (1982).

161. S. Zhao-bin and Yu Lu, Phys. Rev. B27, 5199 (1983).

162. J. Orenstein and G. Baker, Phys. Rev. Lett. 49, 1043 (1982).

163. Z. Vardeny, J. Strait, D. Moses, T.-C. Chung, and A. J. Heeger, Phys. Rev. Lett. 49, 1657 (1982).

164. C. V. Shank, R. Yen, R. L. Fork, J. Orenstein, and G. L. Baker, Phys. Rev. Lett. 49, 1660 (1982).

165. Z. Vardeny, J. Orenstein, and G. L. Baker, Phys. Rev. Lett. 50, 2032 (1983).

166. G. B. Blanchet, C. R. Fincher, T.-C. Chung, and A. J. Heeger, Phys. Rev. Lett. 50, 1938 (1983).

167. G. B. Blanchet, C. R. Fincher and A. J. Heeger, Phys. Rev. Lett. 51, 2132 (1983).

168. J. D. Flood and A. J. Heeger, J. Phys. (Paris) C3-397 (1983).

169. R. Ball, W. P. Su, and J. R. Schrieffer, J. Phys. (Paris) C3-429 (1983).

170. D. Baeriswyl, J. de Phys. C3-381 (1983).

171. M. Nakahara and K. Maki, Phys. Rev. B25, 7789 (1982).

172. W. P. Su, Sol. St. Comm. 42, 297 (1982).

173. J. E. Hirsch and E. Fradkin, Phys. Rev. Lett. 50, 420 (1982).

174. E. Fradkin and J. E. Hirsch, Phys. Rev. B27, 1680 (1983).

175. M. Karowski and H. J. Thun, Nucl. Phys. B190, 61 (1981).

176. H. Fukutome and M. Sasai, Prog. Theor. Phys. 67, 41 (1982); ibid. 69, 1, 373 (1983).

177. K. Takano, T. Nakano and H. Fukuyama, J. Phys. Soc. Japan 51, 336 (1982).

178. C. Aslangul and D. Saint-James, J. Phys. (Paris) 44, 953 (1983).

179. S. Mazumdar and S. N. Dixit, Phys. Rev. Lett. 51, 292 (1983).

180. J. E. Hirsch, Phys. Rev. Lett. 51, 296 (1983).

181. H. Thomann, L. R. Dalton, Y. Tomkiewicz, N. S. Shiren and T. C. Clarke, Phys. Rev. Lett. 50, 553 (1983).

182. K. R. Subbaswamy and M. Grabowski, Phys. Rev. B24, 2168 (1981).

183. A. Heeger and J. R. Schrieffer, preprint.

184. C. R. Fincher, C. E. Chen, A. J. Heeger, A. G. MacDiarmid, and J. B. Hastings, Phys. Rev. Lett. 48, 100 (1982).

185. D. Baeriswyl and K. Maki, Phys. Rev. B28, 2068 (1983).

186. P. M. Grant and I. P. Batra, Sol. St Comm. 29, 225 (1979); J. Phys. (Paris) C3-437 (1983).

187. D. Moses, A. Feldblum, E. Ehrenfreund, A. J. Heeger, T.-C. Chung, and A. G. MacDiarmid, Phys. Rev. B26, 3361 (1982).

188. R. H. Baughman and G. Moss, J. Chem. Phys. 77, 6321 (1982).

189. C. S. Yannoni and T. C. Clarke, Phys. Rev. Lett. 51, 1191 (1983).

190. K. Maki, Synthetic Metals 9, 185 (1984).

191. Y. R. Lin-Liu and K. Maki, Phys. Rev. B22, 5754 (1980).

192. M. J. Rice, Phys. Rev. Lett. 51, 142 (1983).

193. J. Hara, T. Nakano, and H. Fukuyama, J. Phys. Soc. Japan 51, 34 (1982).

194. J. T. Gammel and J. A. Krumhansl, Phys. Rev. B27, 7659 (1983).

195. B. Sutherland, Phys. Rev. B27, 7209 (1983).

196. S. A. Brazovskii, N. E. Dzyaloshinskii and I. M. Krichever, Sov. Phys. JETP 56, 212 (1982).

197. M. J. Rice and E. J. Mele, Phys. Rev. Lett. 49, 1455 (1982).

198. B. Horovitz and B. Schaub, Phys. Rev. Lett. 50, 1942 (1983).

199. M. J. Rice, A. R. Bishop and D. K. Campbell, Phys. Rev. Lett. 51, 2136 (1963).

200. J. C. Scott, J. L. Brédas, K. Yakushi, P. Pfluger and G. B. Street, Synthetic Metals (in press); J. L. Brédas, J. C. Scott, K. Yakushi and G. B. Street, preprint.

201. M. Kobayashi, J. Chen, T.-C. Chung, F. Moraes, A. J. Heeger and F. Wudl, preprint. T.-C. Chung, H. H. Kaufman, A. J. Heeger, and F. Wudle, preprint.

202. P. Monceau, N. P. Ong, A. M. Portis, A. Meerschaut, and J. Rouxel, Phys. Rev. Lett. 37, 602 (1977).

203. K. Tsutsumi, T. Takagaki, M. Yamamoto, Y. Shiozaki, M. Ido, T. Sambongi, K. Yamaya, and Y. Abe, Phys. Rev. Lett. 39, 1675 (1977).

204. R. M. Fleming and C. C. Grimes, Phys. Rev. Lett. 42, 1423 (1979).

205. N. P. Ong and P. Monceau, Phys. Rev. B16, 3443 (1977).

206. R. M. Fleming, D. C. Moncton and D. B. McWhan, Phys. Rev. B18, 5560 (1978).

207. A. H. Thompson, A. Zettl and G. Grüner, Phys. Rev. Lett. 47, 64 (1981); G. Grüner, A. Zettl, W. G. Clark, and A. H. Thompson, Phys. Rev. B23, 6813 (1981).

208. A. Meerschaut, J. Rouxel, P. Haen, P. Monceau and M. Nunez-Regueiro, J. Phys. Lett. 40, L157 (1979).

209. Z. Z. Wang, M. C. Saint-Lager, P. Monceau, M. Renard, P. Gressier, A. Meerschaut, L. Guemas, and J. Rouxel, Sol. St. Comm. 46, 325 (1983).

210. M. Maki, M. Kaizer, A. Zettl, and G. Grüner, Sol. St. Comm. 46, 497 (1983).

211. J. Dumas, C. Schlenker, J. Marcus and R. Buder, Phys. Rev. Lett. 50, 757 (1983); J. Dumas and C. Schlenker, Sol. St. Comm. 45, 885 (1983).

212. R. M. Fleming, in [5].

213. N. P. Ong, Can J. Phys. 60, 757 (1982).

214. G. Grüner, Physica 8D, 1 (1983).

215. J. W. Brill, N. P. Ong, J. C. Eckert, J. W. Savage, S. K. Khanna and R. B. Somoano, Phys. Rev. B23, 1517 (1981).

216. N. P. Ong, J. W. Brill, J. C. Eckert, J. W. Savage, S. K. Khanna, and R. B. Somoano, Phys. Rev. Lett. 42, 811 (1979).

217. G. Grüner, L. C. Tippie, J. Sanny, and W. G. Clark, Phys. Rev. Lett. 45, 935 (1980).

218. P. Monceau, J. Richard and J. Renard, Phys. Rev. Lett. 45, 43 (1980); Phys. Rev. B25, 931 (1982).

219. J. Bardeen, E. BenJacob, A. Zettl, and G. Grüner, Phys. Rev. Lett. 49, 493 (1982).

220. P. Monceau, M. Renard, J. Richard, M. C. Saint-Lager, H. Salva, and Z. Z. Wong, Phys. Rev. B28, 1646 (1983).

221. W. W. Fuller, P. M. Chaikin, and N. P. Ong, Sol. St. Comm. 39, 547 (1981); W. W. Fuller, G. Grüner, P. M. Chaikin, and N. P. Ong, Phys. Rev. B23, 6259 (1981).

222. H. Fukuyama and P. A. Lee, Phys. Rev. B17, 535 (1978).

223. J. C. Gill, Sol. St. Comm. 39, 1203 (1981).

224. A. Zettl and G. Grüner, Phys. Rev. B26, 2298 (1982).

225. N. P. Ong, Phys. Rev. B17, 3243 (1978).

226. K. Maki, Phys. Rev. Lett. 39, 46 (1977); Phys. Rev. B18, 1641 (1978).

227. J. Bardeen, Phys. Rev. Lett. 42, 1498 (1979); 46, 1978 (1980).

228. J. Bardeen, Lectures for International School of Physics 'Enrico Fermi', Varenna, Italy, July 4-6 (1983).

229. P. B. Littlewood and T. M. Rice, Phys. Rev. Lett. 48, 44 (1982).

230. R. A. Klemm and J. R. Schrieffer, Phys. Rev. Lett. 51, 47 (1983).

231. K. Maki, Phys. Lett. 70A, 449 (1979).

232. Z. Z. Wang, P. Monceau, M. Renard, P. Gressier, L. Guemas, A. Meerschaut, Sol. St. Comm. 47, 439 (1983).

233. G. Grüner, A. Zawadowski and P. M. Chaikin, Phys. Rev. Lett. 46, 511 (1981).

234. J. Richard, P. Monceau, and M. Renard, Phys. Rev. B25, 948 (1982).

235. L. Sneddon, M. C. Cross and D. S. Fisher, Phys. Rev. Lett. 49, 292 (1982).

236. D. S. Fisher, Phys. Rev. Lett. 50, 1486 (1983).

237. J. B. Sokoloff, Phys. Rev. B23, 1992 (1981).

238. L. Pietronero and S. Strässler, Phys. Rev. B28, 5863 (1983).

239. S. E. Barnes and A. Zawakowski, Phys. Rev. Lett. 51, 1003 (1983).

240. N. P. Ong and G. Verma, Phys. Rev. B27, 4495 (1983).

241. N. P. Ong and G. Verma, Proceedings of the international symposium on 'Nonlinear Transport and Related Phenomena in Inorganic Quasi-One Dimensional Conductors' Sapporo, Japan, October 20-22 (1983).

242. G. Mozurkewich and G. Grüner, Phys. Rev. Lett. 51, 2206 (1983).

243. G. Mozurkewich, M. Maki and G. Grüner, Sol. St. Comm. 48, 453 (1983).

3.6 Theory Of the Superconducting Properties of Quasi-1D Materials

3.6.1 1. Introduction

In recent years, there has been a continuing interest in the superconducting properties of materials that are nearly one-dimensional in their electronic properties [1-22]. A few materials have been found which exhibit strong anisotropy in their electron conduction, with one axis being a much better conduction direction than the others in the normal state. These materials have been of interest due to the strong anisotropies in the superconducting properties they exhibit, and the hope that materials of sufficiently strong superconducting anisotropy might exhibit novel behavior has been growing, as better crystals of highly anisotropic superconductors have been made.

1.1. General Features of a Quasi-one-dimensional Superconductor

Let us first define what is meant by a quasi-one-dimensional superconductor. First of all, it is a material that is metallic in the normal state, and exhibits a bulk superconducting transition at the critical temperature $T_c > 0$. Below T_c, the material is in the superconducting phase, and exhibits certain properties characteristic of all bulk superconductors: a Meissner effect in which the magnetic flux is excluded for fields less than the critical field H_c (or in the case of Type II superconductors, below the lower critical field H_{c1}), a supercurrent, and an upper critical field H_{c2} at which the superconductivity is destroyed [23-24]. In real systems, it may not always be possible to observe all of these phenomena conclusively, but they must exist in principle.

Secondly, the properties of a quasi-one-dimensional superconductor are very anisotropic. In the normal state, the conductivity in one direction is much larger than in the two other crystal directions. In the superconducting state, the critical fields are anisotropic, with H_{c2} in the highest conduction direction exceeding its value in the other two directions. This anisotropy is similar to that observed in quasi two-dimensional, or layered, superconductors, in which there is a highly conducting plane and hence H_{c2} in that plane exceeds its value normal to the highly conducting plane [25-27]. In addition, the lower critical fields for highly anisotropic materials should exhibit a kink in their angular dependence, as we shall see in Section 3.3.

Thirdly, one must make the distinction between a conventional anisotropic 'bulk' superconductor and a quasi-one-dimensional superconductor. Although both materials
exhibit superconducting order throughout the crystal, an anisotropic bulk superconductor should exhibit an anisotropy of H_{c2} that is relatively temperature independent below T_c, as its temperature dependence in a given field direction is essentially that expected for an isotropic superconductor. A quasi-one-dimensional superconductor, on the other hand, should exhibit 'dimensional crossover' in the temperature dependence of the upper critical field parallel to the highly conducting direction, as in the case of certain intercalated layered compounds and $Nb-Ge$ layered composites [26-27]. In addition, novel behavior in the temperature dependence of H parallel to the conducting axis is expected, as will be discussed later.

It should be noted that the above properties distinguish a quasi-one-dimensional superconductor from two other systems of interest: a purely one-dimensional 'superconductor', and a thin wire, which for widths less than the coherence length exhibits one-dimensional superconducting fluctuations. A purely one-dimensional conductor can, for attractive effective electron-electron interactions, exhibit a tendency for superconducting ordering at low temperature, but true long

range order only sets in at $T = 0$ [28]. A thin wire, on the other hand, may be made thick enough to exhibit true long range order. However, unless it is made of highly anisotropic material, it only exhibits critical field anisotropies due to its geometry, and would not exhibit the anomalies in the temperature dependence of H_{c2} and the angular dependence of H_{c1} that are predicted to occur in a quasi-one-dimensional superconductor [29]. This case will be examined in detail in Section 4.2.

To date, it has not been clearly established that any existing materials are truly quasi-one-dimensional superconductors. There have been a number of superconducting materials of strong filamentary anisotropy that have been made and studied, but none of them have exhibited the anomalies in the temperature dependence of H_{c2} that would characterize a truly quasi-one-dimensional superconductor [1-22]. In that sense, the existing materials are perhaps better described as bulk superconductors with strong filamentary anisotropy. By analogy with the temperature dependence of H_{c2} in the layered compounds, the superconductors with filamentary anisotropy such as $(SNBr_{0.4})_x$, $TaSe_3$, and $Tl_2Mo_6Se_6$ are more like the rather anisotropic unintercalated layered materials TaS_2 and $NbSe_2$ than the intercalated ones such as TaS_2 (pyridine) $_{1/2}$[5, 8, 20, 26]. On the other hand, the magnitude of the H_{c2} anisotropy in the latter two materials is similar to that observed in intercalated materials. Hence, it is possible that a more detailed study of the temperature dependence of H_{c2} in these materials might establish truly quasi-one-dimensional behavior. It is also possible in principle that intercalation compounds of these materials might be made. If so, such materials should exhibit the predicted anomalies in the temperature dependence of H_{c2}. Nevertheless, the existing materials are sufficiently anisotropic that the angular dependence of the lower critical field should exhibit a cusp, as has been seen in the unintercalated layered compound $NbSe_2$ [30].

In addition, there is a class of materials which appear to exhibit a great deal of disorder. In particular, $(SN)_x$ appears to be made of many strands or filaments [1]. Also, the samples of $NbSe_3$ which appear to exhibit superconductivity are also strand-like [3,22]. As we shall see in Section 4, this type of disorder would tend to disguise any anomalies in the critical field behavior characteristic of a true quasi-one-dimensional superconductor.

1.2. Preliminary Theoretical Considerations

Before we consider the properties of quasi-one-dimensional superconductors, we will first discuss the occurrence of superconductivity in such materials. There are two basic theoretical approaches to treating filamentary materials. The simplest approach is to assume that the material is similar to ordinary bulk materials except that the Fermi surface is anisotropic. This is often called the 'anisotropic mass' model, as the low energy single electron states are taken to have the form,

$$\epsilon\left(k_x, k_y, k_z\right) = \hbar^2 \left(k_x^2/m_x + k_y^2/m_y + k_z^2/m_z\right)/2 \tag{1.1}$$

where the three crystal axes are taken to be in the $\hat{x}, \hat{y}$, and $\hat{z}$ directions. The advantage of this approach is that it is possible to include any interaction that can be treated in an ordinary isotropic superconductor; among those of interest are Pauli paramagnetism, which can be responsible for the destruction of superconductivity at large magnetic fields, and impurity scattering such as spin-orbit scattering, which can tend to counteract the Pauli pair-breaking under appropriate circumstances. On the other hand, the above approach does not explicitly take the quasi-one-dimensionality into account, as the system is assumed to be inherently three-dimensional in nature [31].

The other basic approach is to treat the system as a lattice of weakly coupled onedimensional metallic chains. In this model, the single electron states are assumed to be free particle-lixe along the chains, and of the tight-binding form between chains,

$$\epsilon\left(k_x, k_y, k_z\right) = \hbar^2 k_z^2/2m + J_x \cos\left(k_x a\right) + J_y \cos\left(k_y b\right), \tag{1.2}$$

where J_x and J_y are the single particle energies for tunneling from one chain to the next in the x, y directions, and a and b are the respective lattice constants. The advantage of this approach is that it explicitly treats the quasi-one-dimensionality of the system, and hence the electron-electron interactions along the chain can be treated much better than in a three-dimensional system. In addition, the long-wavelength excitations are of the anisotropic mass form, so that this approach can treat both dimensionality regimes. Unfortunately, this model has the disadvantages that it is difficult to treat the impurity scattering for the technical reason that crossed impurity-averaging diagrams cannot be neglected [32, 33].

In addition, for very small interchain tunneling energies, the model described by Equation (1.2) is complicated by the competition of four types of pairing excitations: in addition to ordinary singlet pairing of two electrons (SS), there can be triplet superconducting pairing (TS), and electron-hole pairings of either the spin-density wave (SDW) or charge-density wave (CDW) types, depending upon the signs of the effective interactions between the charges and spins of the electrons [28]. Basically, when the effective interaction between the charges of two electrons is attractive, the electrons will tend to form pairs. Whether they form singlet or triplet pairs depends upon the sign of the effective interaction between their spins. By particle-hole symmetry, a repulsive interaction between electrons corresponds to an attractive interaction between a particle and a hole. Hence, particle-hole pairings are favored for repulsive interactions between
the charges of the electrons. Attractive electronic spin-spin interactions result in the favoring of SDW excitations, and repulsive electronic spin-spin interactions favor CDW excitations. This situation is pictured in Figure 1. It should be emphasized that in a

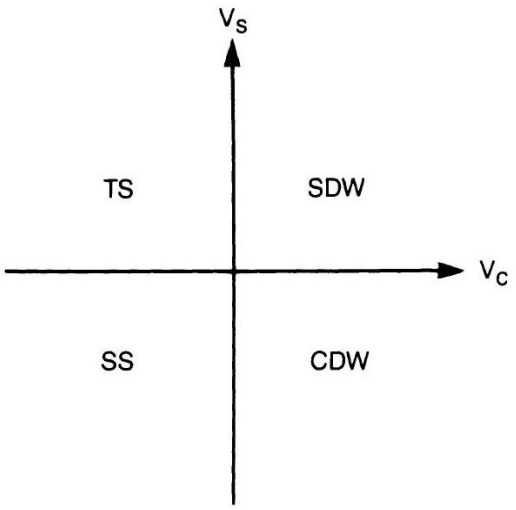


Fig. 1. The regions of different dominant two-body response functions at low temperature for a purely one-dimensional metal are shown. $V_{c
$ and V_S are the effective interactions between the charges and spins of the bodies, respectively. The four types of ordering are singlet and triplet superconductivity (SS and TS), and spin- and charge-density wave (SDW and CDW) ordering. A more detailed description is given in reference [28].}

one-dimensional electron gas, there is no long-range order; these regions in the phase diagram (Figure 1) merely indicate which types of two-particle excitations become important at low temperatures, as for $T > 0$ the one-dimensional system is a normal metal.

Although the phase diagram pictured in Figure 1 is that of a one-dimensional system, it also corresponds to three-dimensional metals that exhibit 'nesting' of the Fermi surface, as pictured in Figure 2. A Fermi surface exhibits 'nesting' if there is a particular wave

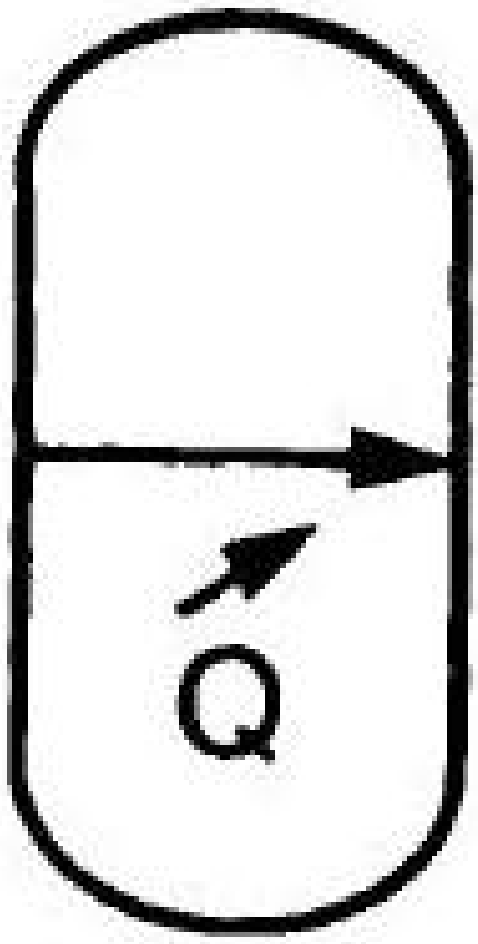


Fig. 2. An idealized Fermi surface cross-section exhibiting nesting over a finite fraction of its area is pictured.

vector **Q** that spans a finite fraction of the Fermi surface. In practice, it is not really necessary for a single wave vector to exactly span a finite fraction of the Fermi surface; a near-spanning of the Fermi surface over a few percent of the Fermi surface is usually sufficient for particle-hole excitations to be important, provided that the interactions are of the appropriate sign [34-35] .

As is indicated in Figure 1, there are regions in the phase diagram in which more than one type of pairing can be important. In particular, in the lower half of the diagram, there is a region in which both SS and CDW excitations are important. Assuming that interchain interactions can drive the CDW excitations in this region to a long-range CDW phase transition, it may still be possible for a superconducting transition to occur at a lower temperature, if the CDW transition creates a gap over only part of the Fermi surface (i.e., the region of 'nesting'), leaving a finite fraction of the Fermi surface available for superconducting pairing. This phenomenom is well-known in the layered compounds $NbSe_2$ and TaS_2 [34-36], and appears to play a role in the filamentary material $NbSe_3$ as well. In $NbSe_3$, there are two incommensurate CDWs that form at high temperatures [37], and at low temperatures the system appears to exhibit evidence for a tendency towards superconductivity [3]. In addition, in the region in which TS excitations predominate, SS excitations are also important. In the absence of impurities,

one would expect that interchain tunneling would prefer to drive a triplet rather than a superconducting transition. However, as triplet pairing is suppressed by normal as well as magnetic impurities, unless the crystal were made extremely pure, it is doubtful that a triplet transition would occur. On the other hand, singlet pairing is not substantially suppressed by normal impurities; hence in this region of the phase diagram, it is most likely that if a superconducting transition occurs, it is of the conventional BCS [38], or singlet, type.

Finally, we note that a lattice of coupled chains, a CDW transition can be driven by either interchain Coulomb interactions (i.e., interchain backscattering) or by interchain tunneling. Since superconducting pairing is not enhanced by interchain electron-electron interactions (unless interchain pairing is important), a superconducting transition can only be driven by interchain tunneling [32].

3.6.2 2. Anisotropic Mass Model

The simplest model of an anisotropic superconductor is represented by the standard Ginzburg-Landau (GL) free energy, modified to allow for anisotropy in the elastic energy of the order parameter [23,39,40]

$$F = \int \mathrm{d}^3 r \left\{ \alpha |\psi|^2 + \beta |\psi|^4/2 + b^2/8\pi + \sum_{\mu} \left| \left(-i\partial_\mu + 2ea_\mu\right) \psi \right|^2 / \left(2m_\mu\right) \right\}, \tag{2.1}$$

where $\mathbf{b}(r) = \nabla \times \mathbf{a}$ is the microscopic magnetic induction, $\mathbf{a}$ is the vector potential, e is the magnitude of the electronic charge, α and β are the usual Ginzburg-Landau parameters, $\psi(r)$ is the order parameter, $\partial_\mu \equiv \partial/\partial x_\mu, x_\mu$ is x, y, z for $\mu = 1, 2, 3$, respectively, and the integration extends over the volume V of the sample. We use the natural units $\hbar = c = k_B = 1$.

Equation (2.1) may be derived from microscopic theory, using the single particle states represented by Equation (1.1) [24]. It is valid for temperatures close to T_c ($|T - T_c| / T_c \ll 1$), and for fields small with respect to the Pauli-limiting field $H_p = \sqrt{2} T_c/\mu_B$, where μ_B is the Bohr magneton [41]. The third term in Equation (2.1) is the magnetic energy term, which is not important for calculating H_{c2}, but is important for calculating the other critical fields. In the absence of a field, the order parameter inside the sample may be taken to be the constant that minimizes the free energy, $\psi(r) = 0$ for $\alpha, \beta > 0$, and $\psi(r) = \psi_0 = (-\alpha/\beta)^{1/2}$ in equilibrium for $\alpha < 0, \beta > 0$. We always must have $\beta > 0$ for the superconducting state to be stable. This is pictured in Figure 3. Since

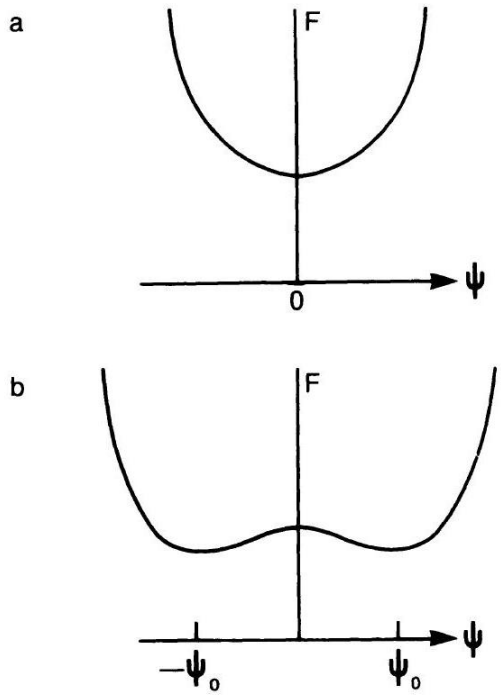


Fig. 3. Shown are schematic plots of the Ginzburg-Landau free energy for a spatially constant order parameter ψ. In (a), $T>T_{c}$. In (b), $T < T_c$, giving minima at $\pm\psi_0$.

$\psi(r)$ is the order parameter, we expect its mean-field value to be zero above T_c and non-zero below T_c. Assuming that the Ginzburg-Landau parameters α and β can be expanded in powers of $T - T_c$, this implies $\alpha \cong \alpha_0 (T - T_c)$ and $\beta \cong$ constant > 0 near to T_c. This temperature dependence of the Ginzburg-Landau parameters is consistent with that obtained from microscopic theory near to T_c [24].

2.1. The Upper Critical Field

The upper critical field is the largest field for which superconductivity can exist. In a homogeneous material, it is thus also the field at which the superconductivity is destroyed. It may be calculated by treating the magnetic field as uniform, and assuming ψ_0 to be very small. These assumptions are valid since the superconductivity is destroyed everywhere, and at the temperature for which a given field destroys the superconductivity, the order parameter vanishes. Hence, the upper critical field is a thermodynamic property of the specimen [23].

We assume the magnetic field (which at H_{c2} is equal to the magnetic induction) is constant in magnitude and directed arbitrarily with respect to the crystal axes,

$$\mathbf{b} = b(\sin\theta\cos\phi, \sin\theta\sin\phi, \cos\theta). \tag{2.2}$$

We now express all quantities in dimensionless form. First, we define a coherence length $\xi(T)$ and a penetration depth $\lambda(T)$ by [39]

$$\xi(T) = (-2m\alpha)^{-1/2} \tag{2.3}$$

and

$$\lambda(T) = \left(m/16\pi e^2\psi_0^2\right)^{1/2} \tag{2.4}$$

where

$$m = (m_1 m_2 m_3)^{1/3} \tag{2.5}$$

We then use the conventional normalization [23] in which length is measured in units of λ, magnetic field in units of $\sqrt{2}H = \Phi_0/(2\pi\xi\lambda)$, vector potential in units of $\lambda\sqrt{2}H = \Phi_0/(2\pi\xi)$, and energy density in units of $H^2/(4\pi) = \Phi_0^2/\left(32\pi^3\xi^2\lambda^2\right) = \alpha^2/\beta$, where the flux quantum $\Phi_0 = \pi/e$. The reduced free energy is then given by

$$F = \mathrm{d}^3 r \left\{ -|f|^2 + |f|^4/2 + b^2 + \sum_\mu (m/m_\mu) \left| (-i\partial_\mu/\kappa + a_\mu) f \right|^2 \right\} \tag{2.6}$$

where $f = \psi/\psi_0$ is the reduced order parameter and $\kappa = \lambda/\xi$ is the effective GinzburgLandau parameter. The cross-term in the last term in Equation (2.6) may be eliminated by making a gauge transformation,

$$f = f_0 \exp(i\gamma) \tag{2.7}$$

and choose a to eliminate the superfluid velocity,

$$\mathbf{a}_0 = \mathbf{a} + \nabla\gamma/\kappa. \tag{2.8}$$

The free energy may now be written as

$$F = \int \mathrm{d}^3 r \left\{ -f_0^2 + f_0^4/2 + \sum_\mu (m/m_\mu) \left[\left(\partial_\mu f_0\right)^2/\kappa^2 + a_0^2 f_0^2 \right] + b^2 \right\} \tag{2.9}$$

Equation (2.9) and $\mathbf{b} = \mathrm{curl}\ (\ \mathbf{a}_0\ )$ may now be used to calculate the upper and lower critical fields. The lower critical field will be found in Section 2.2. Because of its simplicity, the upper critical field may be found in a number of ways. The procedure that follows is probably the most straightforward.

The magnetic vector potential $\mathbf{a}_0$ is taken to be of the form,

$$\begin{aligned} \mathbf{a}_0 =& b\{z\sin\theta\sin\phi - y\cos\theta, x\cos\theta - z\sin\theta\cos\phi, y\sin\theta\cos\phi - \\ & - x\sin\theta\sin\phi\}/2 \end{aligned} \tag{2.10}$$

which clearly satisfies $\mathbf{b} = \mathrm{curl}\,(\mathbf{a}_0)$. Other forms for $\mathbf{a}_0$ satisfying this requirement are of course also acceptable, but the above form is chosen because of its symmetry. The upper critical field may now be calculated by minimizing the free energy as given by Equation (2.9) with respect to variations in ψ, neglecting the resulting term of order ψ^3 which is vanishingly small,

$$\sum_\mu \left\{ -{\partial_\mu}^2 f_0/\kappa^2 + a_0^2 f_0 \right\}/m_\mu - f_0/m = 0 \tag{2.11}$$

Equation (2.11) may be transformed into a one-dimensional harmonic oscillator form by first performing an anisotropic scale transformation to equalize the coefficients of the derivative terms, and then rotating the axes so that one of them is parallel to $\mathbf{b}$. In performing these transformation, the Maxwell relation $\mathbf{b} = \mathrm{curl}\ \mathbf{a}_0$ must be preserved. At $b = H_{c2}, \mathbf{b}$ is independent of position in the specimen, and the Maxwell relation will automatically be satisfied.

We first transform the scale of the system by

$$x_\mu = x'_\mu\,(m/m_\mu)^{1/2} \tag{2.12}$$

This changes Equation (2.11) to the form

$$-\nabla^2 f_0/\kappa^2 + \left\{ \left(b'_y z' - b'_z y'\right)^2 /4 + \left(b'_z x' - b'_x z'\right)^2 /4 + \right.$$
$$\left. + \left(b'_x y' - b'_y x'\right)^2 /4 \right\} f_0 - f_0 = 0 \tag{2.13}$$

where the scaled components of the magnetic induction b' are given by

$$b'_\mu = b_\mu \left(m_\mu/m\right)^{1/2} \tag{2.14}$$

and where the components of b are given by Equation (2.2). We then rotate about the z' axis by an angle $-\phi'$,

$$\begin{aligned} x' &= x'' \cos\phi' - y'' \sin\phi' \\ y' &= y'' \cos\phi' + x'' \sin\phi' \\ z' &= z''. \end{aligned} \tag{2.15}$$

The phase ϕ' is then chosen to eliminate the term proportional to $x''y''$. One such possible choice is

$$\tan\phi' = b'_y/b'_x \tag{2.16}$$

This choice of ϕ' also eliminates the term proportional to $y''z''$. The axes are now rotated by an angle $-\theta'$ about the y'' axis,

$$\begin{aligned} x &= x'' \cos\theta' + z'' \sin\theta' \\ z &= z'' \cos\theta' - x'' \sin\theta' \\ y &= y'' \end{aligned} \tag{2.17}$$

The phase θ' is chosen to eliminate the resulting xz term, which implies that

$$\cos\theta' = b'_z/[b\alpha(\theta,\phi)], \tag{2.18}$$

where the anisotropy factor $\alpha(\theta,\phi)$ is given by

$$\alpha(\theta,\phi) = \left[\sum_\mu b'^2_\mu\right]^{1/2} /b = \left[\sum_\mu \left(m_\mu/m\right)\left(\hat{e}_\mu \cdot \hat{b}\right)^2\right]^{1/2} \tag{2.19}$$

with the $\hat{e}_\mu \cdot \hat{b}$ being the direction cosines of b as given by Equation (2.2). This choice of the phase θ' diagonalizes the Ginzburg-Landau equation,

$$-\nabla^2 f_0/\kappa^2 + \alpha^2(\theta,\phi)\left(x^2+y^2\right) f_0/4 = f_0. \tag{2.20}$$

Clearly, this is the Schroedinger equation for an harmonic oscillator with cylindrical symmetry, and may readily be solved. The upper critical field is the largest field for which superconductivity can persist, and it is easily seen that in this case that it is obtained from the lowest eigenvalue of Equation (2.20),

$$b = \kappa/\alpha(\theta,\phi). \tag{2.21}$$

In Figure 4, we have plotted the anisotropy of H_{c2} as given by Equation (2.21) for the

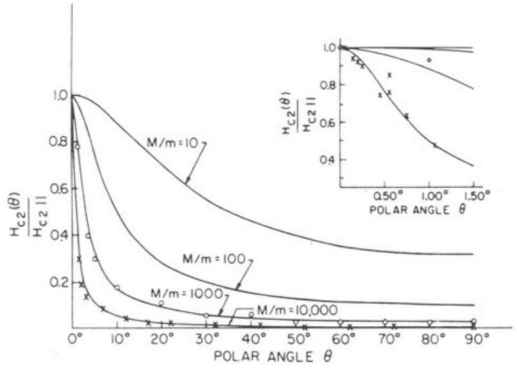


Fig. 4. Polar dependence of the upper critical field for various effective mass ratios [50]. Plotted also are the data points × for $(\mathrm{SN
)_{x}$ at $T = 0.255$ K [2], and the data points ° for $TaSe_3$ at $T = 1.73$ K [5] .}

field perpendicular to one of the crystal axis directions, for four different effective mass anisotropies. For comparison, data on $(SN)_x$ and $TaSe_3$ have been included. In Figures 5 and 6, the angular dependence of H_{c2} as given by Equation (2.21) is compared with data on $TaSe_3$ for two different azimuths. Finally, in Figure 7, the angular dependence of H_{c2} is compared with data on $Tl_2Mo_6Se_6$. The agreement is generally quite good.

The temperature dependence of H_{c2} as given by Equation (2.21) is linear, since κ is roughly temperature independent, and the magnetic field is measured in the standard fashion, indicated previously. As the GL theory is valid for small values of the magnetic field and ($T_c - T$), we expect deviations from linearity at low temperatures. At low

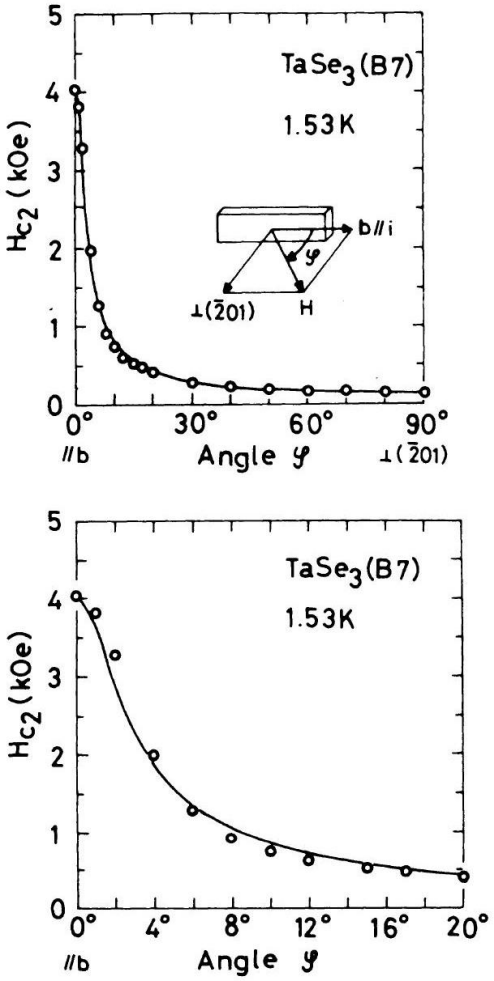


Fig. 5. Angular dependence of the upper critical field in $\mathrm{TaSe _{3}$ at 1.53 K [5]. The angle ϕ in this figure is the angle from the b axis in the plane including the b axis and the normal to the (201) plane. The solid line is the anisotropic mass formula (Equation (2.21)) with an effective mass anisotropy of 700.}

temperatures, the temperature dependence of H_{c2} for an isotropic superconductor flattens out, as predicted by Abrikosov and Gor'kov [42]. In Figure 8, the temperature dependence of H_{c2} for the parallel and perpendicular directions in the doped sample $Nb_{1-x}Ta_xSe_3$ is shown. The linear temperature dependence near to T_c is as expected, and the Abrikosov-Gor'kov theory fits quantitatively. In Figure 9, H_{c2} for the direction perpendicular to the filament is plotted for $(SN)_x$ and $(SNBr_{0.4})_x$. The brominated sample has the expected temperature dependence for a bulk material, exhibiting the linear temperature dependence near to T_c., and bending over at low temperatures. The sample of $(SN)_x$ studied, however, has a very different temperature dependence. This upward curvature of H_{c2} is not well understood (it is apparently not 'dimensional crossover', which will be discussed in Section 3), but it is similar to the upward curvature

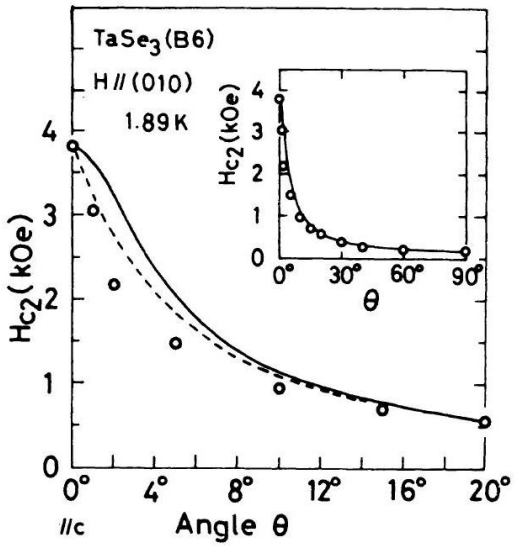


Fig. 6. Polar (θ) dependence of $H_{C 2 $ in $TaSe_3$ at 1.53 K . The angle θ is the angle between the b and c axes. The solid line is the anisotropic mass formula with a mass anisotropy of about 200 . The dashed curve is a fit to the Tinkham thin film formula [57]. The data is for a different sample from that in Figure 5 [5].}

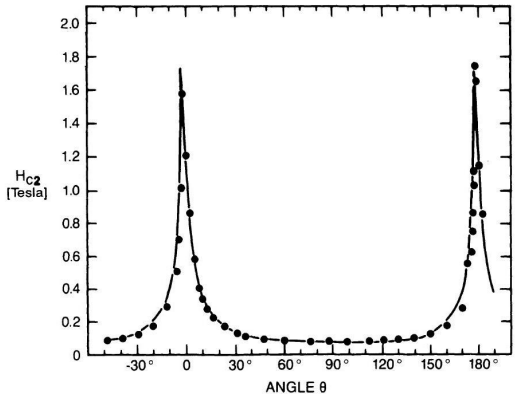


Fig. 7. Angular dependence of $H_{c 2 $ for $Tl_2Mo_6Se_6$ (after ref. [20]).}

observed in the layered superconductors for the field perpendicular to the layers [26]. This anomalous temperature dependence near to T_c seems to be a general feature of many, but not all highly anisotropic materials.

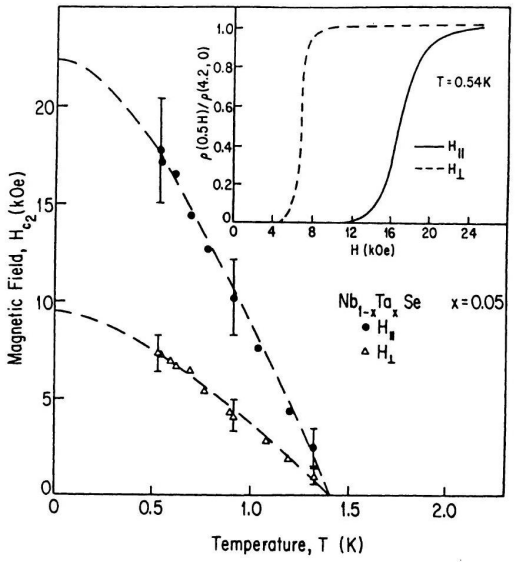


Fig. 8. Temperature dependence of $H_{c 2} in the doped sample $Nb_{1-x}Ta_xSe_3$ for $x = 0.05$, measured resistively [10]. The dashed curves are fits to the Abrikosov-Gorkov formula [42].}

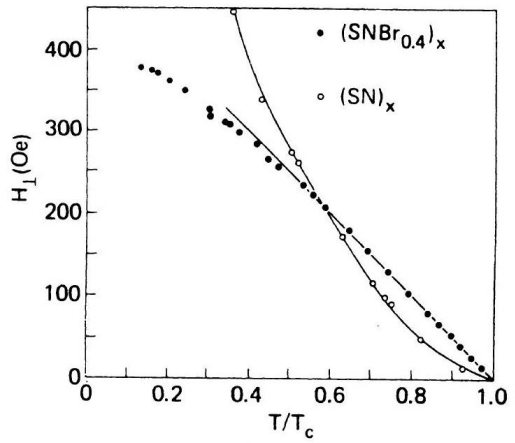


Fig. 9. Temperature dependence of the perpendicular $H_{c 2} in $(SN)_x$ and $(SNBr_{0.4})_x$. The data are for a single crystal before and after bromination, and the solid lines are guides to the eye [14].}

2.2. The Lower Critical Field

We now focus upon the lower critical field in the anisotropic mass model. Since below the upper critical field H_{c2}, the magnetic induction is not a constant, and the order parameter is not vanishingly small, one must keep the spatial dependence of the magnetic induction and the non-linear term in the free energy. Since the lower critical field is the field at which a single magnetic vortex enters the superconductor, we expect the magnetic induction to be largest in magnitude in the vortex core, and to vanish far from the vortex core. The order parameter, on the other hand, vanishes at the center of the vortex core, and reaches the constant value ψ_0 far from the vortex core. In general, the magnetic induction just outside the core will not be constant in direction. However, it is difficult to solve for the magnetic induction if both its magnitude and direction are allowed to vary in the sample. It is possible to solve for H_{c1}

analytically if one assumes that only the magnitude of the magnetic induction can vary in the sample; i.e., the direction of the magnetic induction is taken to be a constant [39],

$$\mathbf{b}(r) = b(r)(\sin\theta\cos\phi, \sin\theta\sin\phi, \cos\theta). \tag{2.22}$$

We then transform the free energy in exactly the same way as the linearized GinzburgLandau equation was previously transformed. After performing the scale and rotation transformation [Equations (2.12), (2.15) and (2.17)], the free energy is reduced to

$$F = \int \mathrm{d}^3 r \left\{ -f_0^2 + f_0^4/2 + \left(\nabla f_0\right)^2/\kappa^2 + a_0^2 f_0^2 + b^2/\alpha^2(\theta,\phi) \right\}. \tag{2.23}$$

As we might expect from the calculation of H_{c2}, which only depends upon the single parameter κ/α, the free energy can be further simplified by performing an isotropic scale transformation.

$$\begin{aligned} x_\mu &\to x_\mu/\alpha \\ \partial_\mu &\to \alpha\partial_\mu \\ a_{0\mu} &\to a_{0\mu} \\ b_\mu &\to \alpha b_\mu. \end{aligned} \tag{2.24}$$

This transformation satisfies Maxwell's equation, as required. The free energy becomes

$$F = \alpha^{-3} \int \mathrm{d}^3 r \left[-f_0^2 + f_0^4/2 + b^2 + a_0^2 f_0^2 + \tilde{\kappa}^{-2} \left(\nabla f_0\right)^2 \right] \tag{2.25}$$

where

$$\tilde{\kappa} = \kappa/\alpha. \tag{2.26}$$

The free energy is now just a function of $\tilde{\kappa}$ in this approximation, and the thermodynamic properties can thus be calculated. As we found previously, the upper critical field is given by $\tilde{\kappa}$, as should be expected since at H_{c2}, the direction and magnitude of the magnetic induction are constant. The lower critical field $\mathbf{H}_{c1}$, however, is not parallel to the magnetic induction except in an isotropic system, since in thermodynamic equilibrium the magnetic field $\mathbf{H}(\mathbf{B})$ is given by [23]

$$\mathbf{H}(\mathbf{B}) = \nabla_{\mathbf{B}} F(\mathbf{B})/2, \tag{2.27}$$

where H and B are the macroscopic field and induction, respectively, and $\mathbf{F}(\mathbf{B}) = F/V + 1/2$ is the Helmholtz free energy per unit volume of the superconducting relative to the Meissner state. As the Helmholtz free energy is the same as for an isotropic material with the replacement $\kappa \to \tilde{\kappa}$, the component of $\mathbf{H}_{c1}$ parallel to $\mathbf{B}$ will have the same functional dependence upon $\tilde{\kappa}$ as an isotropic material has upon κ. In the large $\tilde{\kappa}$ limit [43],

$$H_{\|\mathbf{B}} \cong (2\tilde{\kappa})^{-1}(\ln\tilde{\kappa} + 0.497). \tag{2.28}$$

From Equation (2.26), we obtain in the limit $B \to 0$,

$$\mathbf{H}_{c1}(\theta,\phi) = \left[\hat{B} + \hat{\theta}\partial/\partial\theta + \hat{\phi}(\sin\theta)^{-1}\partial/\partial\phi\right] H_{\|\mathbf{B}}(\theta,\phi). \tag{2.29}$$

In Figure 10, we have plotted the parallel and perpendicular components of $\mathbf{H}_{c1}$, along

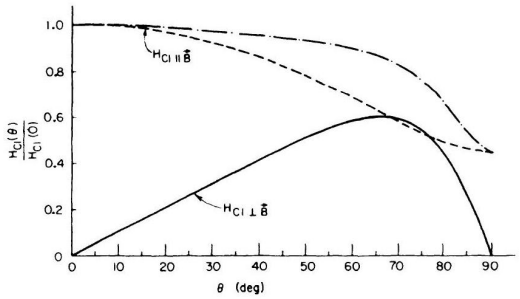


Fig. 10. Shown are the components of $H_{c 1} $ parallel and perpendicular to **B**, and the magnitude of $\mathbf{H}_{c1}$, as a function of the angle θ that **B** makes with the normal to the filament ($\hat{z}$) axis, for $\kappa = 10$ and effective mass anisotropy $\epsilon = 0.1$ [39].}

with its magnitude, for an anisotropic material of uniaxial symmetry with effective mass ratio $\epsilon = 0.1$, as a function of θ, the angle **B** makes with the normal to the filament ($\hat{z}$) axis. The curve for the magnitude of $\mathbf{H}_{c1}$ is redrawn in Figure 11, where we have plotted the dependence of H_{c1} on the angle θ that the field **H** makes with the normal to the filament axis. In this figure, curves for $\epsilon = 0.01$ and 0.001 are also shown. For those two curves, there is a region where the free energy is multiple-valued. The value of H_{c1} that is favored is the lowest value, and thus the angular dependence of H_{c1} will exhibit

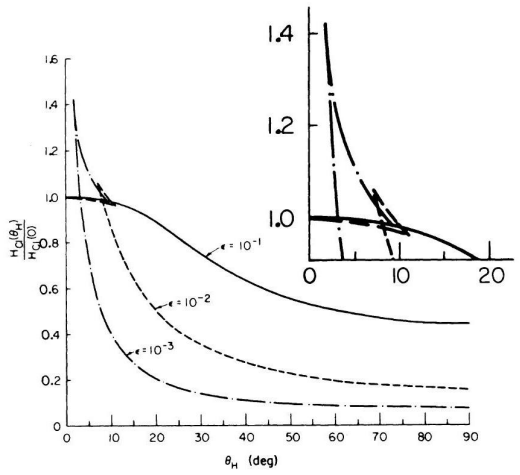


Fig. 11. The lower critical field $H_{c 1} $ for materials with filamentary symmetry with $\kappa = 10$, and effective mass ratios $\epsilon = 0.1, 0.01,$ and 0.001 , as a function of θ_H, the angle H makes with the normal to the filament ($\hat{z}$) axis. The inset is an enlargement of the upper-left-hand portion of the figure [39].}

a kink for sufficient anisotropy [39,44]. We note that the lower critical field in a real material is dependent upon the crystal shape, due to demagnetization effects [45]. Since nearly all of the quasi-one-dimensional superconductors are filamentary in shape, they can be approximated by elongated ellipsoids. In Figure 12, we have plotted the dependence of H_{c1} upon the external angle θ_e for the same uniaxial anisotropies as in Figure 11, but for a material that is much longer than it is wide, as is often the case experimentally [45]. We note that for the external field parallel to the long axis, there is no demagnetization correction. For the field perpendicular to the long axis, the demagnetization factor changes H_{c1} by a relative factor of 2 .

Although there have not yet been any experiments on the angular dependence of the lower critical field in inorganic quasi-one-dimensional superconductors, there have been measurements

on closely related materials. Schwenk, Andres, and Wudl [46] have recently measured the angular dependence of the lower critical field in the organic quasi-one-dimensional superconductor (TMTSF) ClO_4 in the basal plane, where demagnetization effects are not very pronounced. Their results are shown in Figure 13, and compared with the expected angular dependence calculated from the anisotropic mass theory assuming (as above) the direction of **B** to be a constant. Considering the difficulty in measuring H_{c1} precisely, the agreement appears to be reasonably good. There does not appear to be any obvious evidence of the kink in the angular dependence of H_{c1} predicted in the above discussion, but the experiments do not rule it out, either.

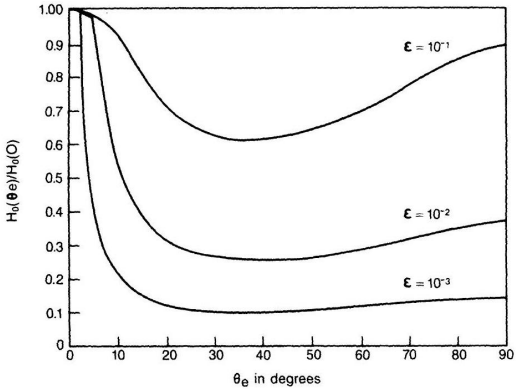


Fig. 12. The lower critical field $H_{C 1 $ for materials with filamentary symmetry with the length/ width $\to \infty$, as a function of θ_e, the angle the applied magnetic field makes with the normal to the filament ($\hat{z}$) axis, for various anisotropies.}

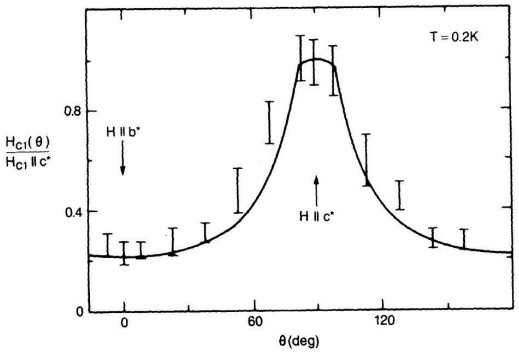


Fig. 13. The lower critical field for (TMTSF) $\mathbf{C l O _{\mathbf{4}}}$ in the basal plane, as a function of the angle the applied magnetic field makes with the $\hat{b}^*$ axis [46]. The solid line is a fit to the Klemm-Clem formula, given ty Equation (2.28 and 2.29).}

In addition, there have been measurements on the related material $NbSe_2$ by Denhoff and Gygax [30]. This material has a strong, uniaxial anisotropy, but is layered in structure. Although their measurements did not agree quantitatively with the above theory,
they did observe a kink in the angular dependence of H_{c1}. They were able to quantitatively fit their data by assuming that the direction of **B** was either parallel or perpendicular to the layers, and treating the value of H_{c1} in the parallel direction as an adjustable parameter. However, as their restriction upon the direction of **B** is even more stringent than in the above discussion,

it must correspond to a higher free energy. Although their experiments were very carefully performed, there appeared to be a great deal of flux pinning, which was most pronounced for an applied field in the direction of the kink [30].

In the above discussion, it was assumed that the direction of the magnetic induction B was a constant throughout the sample. This assumption has been questioned by Kogan [47] and by Kogan and Clem [48], who showed that the bulk free energy is minimized if the direction of **B** is not a constant. Exactly at H_{c2}, **B** is a constant in the sample, both in magnitude and in direction. Although the above discussion allows for the magnitude of **B** to vary locally in the sample (as it surely must near H_{c2}, where a single vortex has entered the sample, and the magnitude of **B** must decrease substantially as one moves away from the vortex core), it assumes that the direction of **B** is also constant in the sample. This assumption is strictly speaking only valid in the following limits [48]: (1) at H_{c2}; (2) when the vortex is parallel to a crystal axis; and (3) for $\tilde{\kappa} \gg 1$. At H_{c2}, the order parameter is a (small) constant, and the field is uniform, as we assumed above. However, Kogan and Clem showed that just below H_{c2}, there is a current parallel to the vortex axis in an anisotropic material, unless the vortex axis is parallel to a crystal axis. Unfortunately, they were not able to obtain the angular dependence of the magnetization near to H_{c2} in closed form [48].

Let us examine the conditions under which the vortex axis will be essentially parallel to a crystal axis. Assuming the direction of **B** to be a constant, as we have above, the kink in the angular dependence of H_{c1} predicted for highly anisotropic materials is due to a switching of the direction of **B** from being nearly parallel to one crystal axis to an angle nearly parallel to another crystal-axis. That is, the energy is lowered if the vortices lie parallel to the most highly conducting axis. It costs energy, however, if the vortices differ substantially from the direction of **H**. Hence, for applied fields nearly perpendicular to the most conducting axis, the vortices are forced to lie nearly parallel to **H**. However, as the direction of **H** is rotated towards the most conducting direction, the direction of **B** is always closer to the most conducting direction, and at a critical angle, jumps to an angle very close to the conducting axis direction. The position of this critical angle depends upon the anisotropy of the material. As can be seen from Figures 11 and 12, for anisotropy factor $\epsilon = 0.1$, there is no critical angle if the direction of **B** is restricted to being a constant. For very high anisotropies, however, the critical angle for **H** is very close to perpendicular to the most conducting axis. That is, **B** lies essentially parallel to the most conducting axis unless the applied field is very close to perpendicular to that direction, in which case **B** switches suddenly to the perpendicular direction.

The parameter $\tilde{\kappa}$ measures the stiffness of the vortices. For $\tilde{\kappa}$ small, it does not cost much energy to bend the vortex lines. For $\tilde{\kappa} \gg 1$, however, it costs a great deal of energy to bend the vortex lines. In the above discussion, it was found that $\tilde{\kappa}$ was a strong - function of the angle of **B**. In the fits to the experiments that we mentioned, however, the minimum values of $\tilde{\kappa}$ were on the order of 10 . This minimum value occurs for the
vortex near to perpendicular to the most conducting axis. For angles near to the conducting axis, $\tilde{\kappa}$ is considerably larger, at least for highly anisotropic materials. Hence, for these angles, **B** is nearly parallel to the most conducting axis, and hence nearly constant in direction. For applied fields near to perpendicular to the most conducting axis, the non-uniformity of the direction of **B** is the most pronounced.

Finally, the temperature dependence of the lower critical field in the GL model is linear, as for H_{c2}. Figure 14 exhibits data for the perpendicular 'lower critical field' in

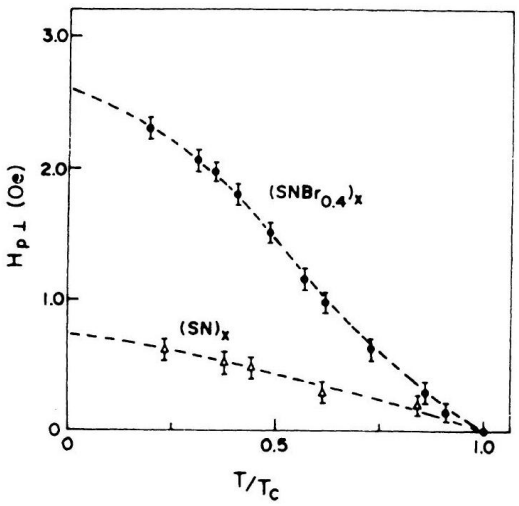


Fig. 14. Lower critical field as determined from the maxima in the magnetization curves for $(\mathrm{SN})_{x}$ and $(SNBr_{0.4})_x$ for fields in the direction perpendicular to the filaments, as a function of temperature. From [8].}

$(SN)_x$ and in $(SNBr_{0.4})_x$, as determined from the maximum in the magnetication curves (actually, the appropriate definition of H_{c1} is the field at which the magnetization curve first departs from linearity, but in these materials such well-defined points were difficult to ascertain [8]. Hence, the points plotted are really upper limits upon H_{c1}).

3.6.3 3. Josephson-coupled Chain Model

3.1. The Model

The model for the quasi-one-dimensional conductors that explicitly treats the lower dimensionality of the system arises from a single particle energy of the form given by Equation (1.2). That is, the crystcl is assumed to be made up of a rigid lattice of chains, and that the electrons propagate from chain to chain by single particle tunneling. By analogy with the layered superconductors, the superconducting properties of these systems near to T_c and for relatively small fields can be understood in terms of a Josephsoncoupled model. That is, the order parameters on adjacent chains are coupled by Josephson
tunneling, as in the Lawrence-Doniach theory [49] of coupling of the order parameters on adjacent layers of a layered superconductor [25,47].

In a layered superconductor, when a magnetic field is applied perpendicular to the layers, the Cooper pairs form Landau orbits within a given layer, and hence do not feel any interlayer phase difference. Thus, the vortex currents circulate freely within the layers (Figure 15a), and the normal vortex cores penetrate all of the layers, causing the

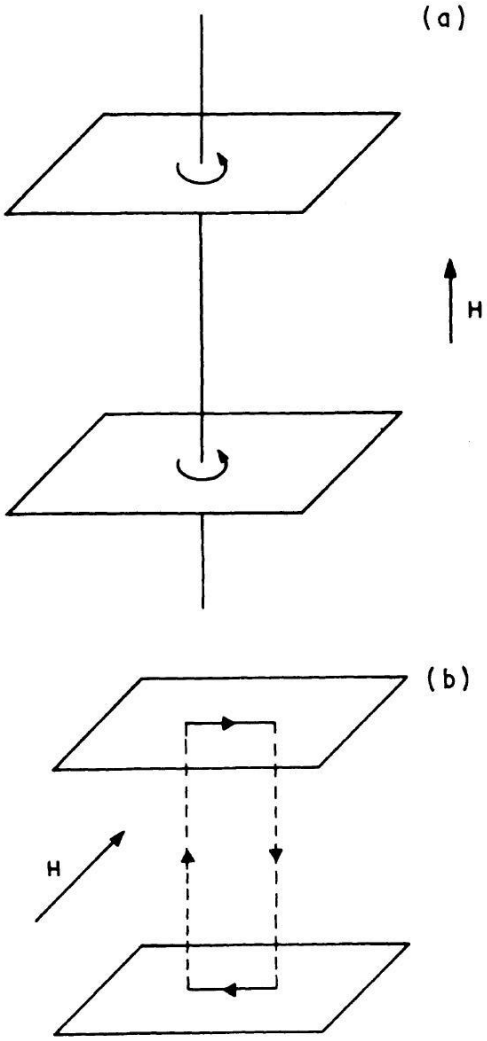


Fig. 15. (a). Field applied perpendicular to the layers in a layered superconductor. The vortex currents circulate within the layers. (b) Field parallel to the layers in a layered superconductor. The vortex currents partially circulate within the layers and partially Josephson tunnel from layer to layer. From [50].

perpendicular upper critical field H_{c2} to be essentially that of a bulk superconductor. However, when the magnetic field is applied parallel to the layers, the vortex currents complete orbits by both circulating within and tunneling between two different layers, as shown in Figure 15b. The system behaves as a series of coupled Josephson junctions.

There is a dimensional-crossover temperature T^*, at which the vortex currents propagate only between nearest-neighbor planes, the normal cores of the vortices (with diameter $\xi_\perp(T^*)/\sqrt{2}$ at the temperature T^* in the perpendicular direction) fitting between the adjacent layers, a distance s apart. Below T^*, the layers decouple, and the orbital pairbreaking is removed as a mechanism for the destruction of superconductivity in a layer. The layers then all behave as a thin film (of microscopic thickness) in a parallel field, which for a small thickness, can have a much higher H_{c2} than does a bulk superconductor; H_{c2} will be determined by other mechanisms such as Pauli paramagnetism and spin-orbit scattering.

Analogously for a quasi-one-dimensional superconductor consisting of a lattice of coupled superconducting chains, when the magnetic field is applied perpendicular to the chains, the vortex currents must tunnel at least twice from chain to chain in order to complete one orbit, as pictured in Figure 16a. We thus expect that H_{c2} for a quasi-one-

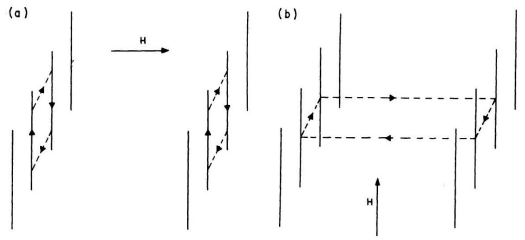


Fig. 16. (a) Field applied perpendicular to the chains in a filamentary superconductor. (b) Field applied parallel to the chains. From [50].

dimensional superconductor will behave just as H_{c2} for a layered superconductor. In particular, below a dimensional-crossover temperature T^*, the chains decouple, and H_{c2} diverges in the Ginzburg-Landau theory. It turns out, however, that this decoupling temperature T^* is a strong function of azimuthal angle ϕ. When the field is parallel to either chain lattice direction ($\phi = 0$ or $\pi/2$), only the vortex core diameter perpendicular to this direction need become smaller than the lattice dimension. When the field is not imposed along a crystal lattice direction, the vortex core crossection must fit between the chain lattice at that particular azimuthal angle, which implies that the vortex core crossection must be smaller than for a field in either direction of the crystal lattice directions; hence the decoupling temperature T^* for a general azimuthal angle is less than for the two lattice directions.

For a field parallel to the chains, the vortex currents propagate entirely by tunneling, as pictured in Figure 16b. The system behaves as a two-dimensional lattice of coupled Josephson junctions - a SQUID (superconducting quantum interference device) grid. As long as the chains are coupled, they cannot discriminate between different integral
numbers of flux quanta through each SQUID, resulting formally in a periodic $H_{c2,\|}$ at any temperature. As for the field in the perpendicular direction, there is a dimensionalcrossover temperature T^* at which the minimum vortex current path is obtained (the vortex core fitting entirely between neighboring chains). In addition, for temperatures above T^*, it turns out that it is energetically more favorable for the vortex lattice to fit commensurately with the chain lattice, so that cusps in the $H_{c2,\|}(T)$ curve result at temperatures corresponding to a commensurate fitting of the lattice; these cusps are most pronounced for a commensurability ratio of two small integers.

Let us now consider the Ginzburg-Landau model for a rectangular ($a \times b$) lattice of superconducting chains parallel to the z direction. We ignore the finite chain thickness, the interaction of the magnetic field with the electron spins, and the impurities. The free energy in gauge-invariant form is [53]

$$
\begin{aligned}
F = \int \mathrm{d}z ab \sum_{ij} \Big\{ & \alpha \left|\psi_j^i(z)\right|^2 + \beta \left|\psi_j^i(z)\right|^4 /2 + \\
& + \left|\left(i\partial/\partial z + 2eA_z(\mathbf{r})\right)\psi_j^i(z)\right|^2 /2m + \\
& + \zeta_x \left|\psi_j^{i+1}(z) \exp\left(-2ie\int_{ia}^{(i+1)a} \mathrm{d}x A_x(\mathbf{r})\right) - \psi_j^i(z)\right|^2 + \\
& + \zeta_y \left|\psi_{j+1}^i(z) \exp\left(-2ie\int_{jb}^{(j+1)b} \mathrm{d}y A_y(r)\right) - \psi_j^i(z)\right|^2 + \\
& + \left|\mathbf{H}(\mathbf{r}) - \mathbf{H}_a\right|^2 /(8\pi) \Big\}
\end{aligned}
\tag{3.1}
$$

where $\alpha = -\left(2m\xi^2(T)\right)^{-1} = \left(2m\xi^2(0)\right)^{-1}(T - T_c)/T_c$ is the usual Ginzburg-Landau parameter, and $\zeta_x = \left(2M_x a^2\right)^{-1}, \zeta_y = \left(2M_y b^2\right)^{-1}$ are the interchain coupling parameters due to the Josephson tunneling of electron pairs, written in terms of effective masses such that in the limits $a, b \to 0, F$ reduces to the anisotropic mass form. The magnetic field is taken to be in the direction (θ, ϕ) as given by Equation (2.2). The vector potential for this calculation is taken to be of the form [51],

$$\mathbf{A} = H_a(z\sin\theta\sin\phi, x\cos\theta - z\sin\theta\cos\phi, 0). \tag{3.2}$$

Note that the symmetry of the problem is different than in the anisotropic mass model, so it is simpler in practice to separate out the z axis from the others. Other forms for A are certainly possible, but this one is particularly useful for $\theta = 0$ and $\pi/2$, the two predominant angles of interest. We take the applied field $H_a = H$.

3.2. The Field Perpendicular to the Chains

Let us first consider the case of $H_{c2}(\theta = \pi/2)$. By varying the free energy and neglecting the term cubic in ψ (since $\psi \to 0$ as $H \to H_{c^2}$), we obtain
$\alpha\psi_l^k - (2m)^{-1}\ \mathrm{d}^2\psi_l^k/\mathrm{d}z^2 +$

$$+\zeta_x\left\{2\psi_l^k - \exp\left(2ihaz\sin\phi/d^2\right)\psi_l^{k-1} - \exp\left(-2ihaz\sin\phi/d^2\right)\psi_l^{k+1}\right\} + \tag{3.3}$$
$$+\zeta_y\left\{2\psi_l^k - \exp\left(2ihbz\cos\phi/d^2\right)\psi_{l-1}^k - \exp\left(-2ihbz\cos\phi/d^2\right)\psi_{l+1}^k\right\} = 0,$$

where $h \equiv eHd^2$ is the reduced field, and $d \equiv \left(a^2\cos^2\phi + b^2\sin^2\phi\right)^{1/2}$ is a characteristic length. We note that d does not enter any final expressions for H_{c2}. Fourier transformation of Equation (3.3) yields

$$\begin{aligned} &-(2m)^{-1}\ \mathrm{d}^2\psi/\mathrm{d}z^2 + 2\zeta_x\left\{1 - \cos\left(2haz\sin\phi/d^2\right)\right\}\psi + \\ &+ 2\zeta_y\left\{1 - \cos\left(2hbz\cos\phi/d^2\right)\right\}\psi = -\alpha\psi = E\psi \end{aligned} \tag{3.4}$$

where we have set the perpendicular Fourier wavevectors Q_x and Q_y equal to 0 in order to yield the lowest eigenvalue in Equation (3.4), corresponding to the largest h and hence the largest field H_{c2} for which superconductivity can persist. Equation (3.4) is in the form of the two-term Hill equation [52] and, for general ϕ, is complicated, as the two periodic potentials are incommensurate with respect to each other. Three values of ϕ lead immediatedly to a solution, however: $\phi = 0, \pi/2$, and $\tan^{-1}(b/a)$, for which the equation reduces to the Mathieu equation [53],

$$-(2m)^{-1}\ \mathrm{d}^2\psi/\mathrm{d}z^2 + \gamma(1 - \cos qz)\psi = E\psi = -\alpha\psi, \tag{3.5}$$

where for $\phi = 0, \gamma = 2\zeta_y, q = 2hb/d^2$; for $\phi = \pi/2, \gamma = 2\zeta_x, q = 2ha/d^2$; and for $\phi = \tan^{-1}(b/a), \gamma = 2\left(\zeta_x + \zeta_y\right), q = 2hab/\left\{d^2\left(a^2 + b^2\right)^{1/2}\right\}$. As $h \to \infty, q \to \infty$ and $\cos qz$ oscillates wildly. As this first happens when T approaches T^* from above, we see that T^* for $\theta = \pi/2$ is given by $-\alpha\left(T - T^*\right) = \gamma$. This implies that the three different ϕ values result in three distinct T^* values. In fact, it turns out that there are only these three T^* values; for $\phi \neq 0$ and $\phi \neq \pi/2, -\alpha\left(T - T^*\right) = 2\left(\zeta_x + \zeta_y\right)$, just as for $\phi = \tan^{-1}(b/a)$. The reason is that for ϕ unequal to either 0 or $\pi/2$, we have an equation of the form,

$$-(2m)^{-1}\ \mathrm{d}^2\psi/\mathrm{d}z^2 + \gamma_1\left(1 - \cos q_1 z\right)\psi + \gamma_2\left(1 - \cos q_2 z\right)\psi = -\alpha\psi. \tag{3.6}$$

Since as $H \to \infty$, both q_1 and $q_2 \to \infty$, and both $\cos q_1 z$ and $\cos q_2 z$ oscillate wildly. Hence, $-\alpha\left(T - T^*\right) = \gamma_1 + \gamma_2$. In short, we see that T^* is given by

$$T^*/T_c = \begin{cases} 1 - 2m\xi^2(0)/\left(M_y b^2\right) & \phi = 0 \\ 1 - 2m\xi^2(0)/\left(M_x a^2\right) & \phi = \pi/2 \\ 1 - 2m\xi^2(0)\left\{1/\left(M_x a^2\right) + 1/\left(M_y b^2\right)\right\} & \text{otherwise.} \end{cases} \tag{3.7}$$

Since T^* for $\phi = 0$ and $\pi/2$ is much larger than for the other directions, we expect that H_{c2} should show strong angular dependence near the lattice directions.

Before we include the full azimuthal dependence of the perpendicular ($\theta = \pi/2$) critical field, let us first examine Equation (3.5). This equation may be solved analytically for small and large q (i.e., small or large magnetic field). For small q, $\cos qz$ may be expanded in powers of $q; \cos qz \cong 1 - (qz)^2/2! + O(qz)^4$. The basis wavefunctions are parabolic cylinder functions, as the leading term in the potential is that of a harmonic oscillator. One may then carry out the calculation for the lowest eigenvalue order by order in perturbation theory.

For large but finite h, we may carry out the perturbation for H_{c2} above T^* by treating $1/q$ as a small parameter. To zeroth order in $1/q$, the wavefunction ψ_0 is a constant, and the lowest eigenvalue $E_0 = 0$. The leading nontrivial eigenvalue is of order $1/q^2$, yielding an H_{c2} that diverges as $(T - T^*)^{-1/2}$ from above.

Let us now examine the full ϕ dependence of H_{c2}. First, we consider the region just below T_c, where H_{c2} is small. As for the Mathieu equation, we may expand the potential in Equation (3.5) in powers of h. In leading order, we obtain the harmonic oscillator form,

$$-(2m)^{-1}\, \mathrm{d}^2\psi/\mathrm{d}z^2 + (1/2)(2h/d)^2 \left(M_y^{-1}\cos^2\phi + M_x^{-1}\sin^2\phi\right) z^2\psi = E\psi \tag{3.8}$$

From the lowest eigenvalue, we obtain the expected anisotropic mass result, obtained from Equation (2.21) by setting $\theta = \pi/2$,
$H_{c2}(T,\phi) = \Phi_0 \left|T - T_c\right| \left[(m/M_x)\sin^2\phi + (m/M_y)\cos^2\phi\right]^{-1/2} \left(2\pi\xi^2(0)T_c\right)^{-1}$.

By keeping higher order terms in the expansion of the two cosines, using perturbation theory in powers of h, and inverting the lowest eigenvalue, we obtain an expansion in powers of $\left|T - T_c\right|/T_{c'}$

$$\begin{aligned} H_{c2\perp}(T,\phi) =& \Phi_0 \left|\left(T - T_c\right)/T_c\right| \left\{(m/M_x)\sin^2\phi + \right. \\ & \left. + (m/M_y)\cos^2\phi\right\}^{-1/2} \sum_{n=0}^{\infty} a_n(\phi) \left|\left(T - T_c\right)/T_c\right|^n \end{aligned} \tag{3.10}$$

For the case of isotropic coupling $\left\{\zeta_x = \zeta_y; \xi_\perp^2 = m\xi_\parallel^2(0)/M\right\}$ we find these coefficients to be

$$\begin{aligned} a_0 &= 1 \\ a_1 &= \left(a/4\xi_\perp^2\right)^2 \left(\sin^4\phi + \cos^4\phi\right) \\ a_2 &= \left(a/4\xi_\perp^2\right)^4 \left\{(13/3)\left(\sin^4\phi + \cos^4\phi\right)^2 - (4/3)\left(\sin^6\phi + \cos^6\phi\right)\right\} \end{aligned} \tag{3.11}$$

It is easy to see that for $\phi = 0, \pi/2$, and $\pi/4$, these results reduce to those obtained from the Mathieu equation. It should be noted that even for isotropic coupling, there is some aximuthal anisotropy of H_{c2} (note that a_1 varies by a factor of 2). Also, since $a_1(\phi) > 0$ for all ϕ, H_{c2} exhibits positive curvature as the temperature is lowered from T, indicating the onset of decoupling of the chains. Complete decoupling occurs at T^*, of course.

We now consider the ϕ dependence of H_{c2} in the large field regime just above T^*. For $\phi = \pi/2$, Manneville found [54]

$$H_{c2}(\phi = \pi/2) \cong \Phi_0 m\xi(0) \left\{T_c/\left(T - T^*\right)\right\}^{1/2} / \left(\pi a^3\sqrt{2}M\right) \tag{3.12}$$

where T^* was given by Equation (3.7) for $\phi = \pi/2$. Similarly, for $\phi = 0, H_{c2}(\phi = 0)$ near to T^* is given by Equation (3.12) with $a \to b, M_x \to M_y$, and T^* given by Equation (3.7) for $\phi = 0$. However, the fact that T^* is substantially lower than those values for slightly different ϕ values indicates that H_{c2} should vary substantially near to $\phi = 0, \pi/2$ in the larger field regime.

Turkevich and Klemm showed that one could solve the general ϕ problem by assuming that the arguments of the cosine potentials are commensurate [50],

$$a\sin\phi = dn_x/N; \quad b\cos\phi = dn_y/N \tag{3.13}$$

for some integers n_x, n_y, N. By taking N extremely large, $n_{x,y}/N$ can cover all the rationals. The following procedure also works for arbitrary n_x, n_y, and N. By setting $x = hz/Nd$ and defining

$$\sigma_x = 2md^2\zeta_x, \quad \sigma_y = 2md^2\zeta_y \tag{3.14}$$

the Schroedinger equation takes the form of the two-term Hill equation [52],

$$\mathrm{d}^2\psi/\mathrm{d}x^2 + \sigma^2\psi + 2\lambda\left[\sigma_x\cos\left(2n_x x\right) + \sigma_y\cos\left(2n_y x\right)\right]\psi = 0 \tag{3.15}$$

where the eigenvalue is

$$\sigma^2 \equiv \lambda\epsilon = -\lambda 2md^2\left(\alpha + 2\zeta_x + 2\zeta_y\right) \tag{3.16}$$

and the small parameter $\lambda = (N/h)^2$. Since the potential is periodic, Bloch's theorem suggests we write ψ in the form [52]

$$\psi(x) = \exp(i\tau x)\left\{a_0 + \sum_n a_n \exp\left[i\left(p_n n_x + q_n n_y\right)x\right]\right\} \tag{3.17}$$

where p_n, q_n are integers and τ is a complex number. To leading non-trivial order in λ, this equation may be solved by expanding ψ and ϵ in powers of λ,

$$\begin{aligned} \psi &= \psi_0 + \lambda\psi_1 + \lambda^2\psi_2 + \ldots \\ \epsilon &= \epsilon_0 + \lambda\epsilon_1 + \lambda^2\epsilon_2 + \ldots \end{aligned} \tag{3.18}$$

In addition, we have the normalization condition

$$\int_0^L \mathrm{d}x L^{-1}|\psi|^2 = 1 \tag{3.19}$$

To zeroth order, we have $\psi_0 = 1$. To order λ,

$$\psi_1'' + \epsilon_0 + 2\left[\sigma_x\cos\left(2n_x x\right) + \sigma_y\cos\left(2n_y x\right)\right] = 0 \tag{3.20}$$

which implies

$$\epsilon_0 = 0, \quad \psi_1 = 2\left\{\sigma_x\left(2n_x\right)^{-2}\cos\left(2n_x x\right) + \sigma_y\left(2n_y\right)^{-2}\cos\left(2n_y x\right)\right\}, \tag{3.21}$$

since ψ_1 is periodic in x. The possible additional constant of integration must equal 0 to preserve the normalization condition above. The leading non-trivial result for the eigenvalue enters in order λ^2,

$$\psi_2'' + \epsilon_1 + 2\left[\sigma_x \cos\left(2n_x x\right) + \sigma_y \cos\left(2n_y x\right)\right]\psi_1 = 0, \tag{3.22}$$

which implies

$$\epsilon_1 = -(1/2)\left\{\left(\sigma_x/n_x\right)^2 + \left(\sigma_y/n_y\right)^2\right\} \tag{3.23}$$

in order that ψ_2 be periodic. We thus have

$$\lambda\epsilon - \lambda^2\epsilon_1 + \ldots = 0, \tag{3.24}$$

or

$$\lambda = \epsilon/\epsilon_1 \tag{3.25}$$

to this order, where ϵ is given by Equation (3.16). Since both sides of the equation are proportional to N^2, we may solve for h and hence H_{c2},

$$H_{c2}(T,\phi) \cong \Phi_0\xi(0)m(\sqrt{2}\pi)^{-1}\left\{\Gamma_c/\left(T - T^*\right)\right\}^{1/2}\left\{\left(M_x a^3 \sin\phi\right)^{-2} + \right.$$
$$\left. + \left(M_y b^3 \cos\phi\right)^{-2}\right\}^{1/2} \tag{3.26}$$

near to T^*, where T^* is given by Equation (3.7) for $\phi \neq 0, \pi/2$. We note that this expansion diverges as $\phi \to 0, \pi/2$, as expected. It should be noted that at $\phi = \tan^{-1}(b/a)$, it underestimates the exact expression obtained from the Mathieu equation by the factor $\left\{1 + 2\eta/\left(1+\eta^2\right)\right\}^{1/2}$, where $\eta = M_x a^2/M_y b^2$ (for isotropic coupling, this factor is $\sqrt{2}$). This factor arises from the commensurability of n_x and n_y; it can be understood by setting $n_x = n_y$ before performing the calculation for ϵ. It is easily seen that instead of Equation (3.25) [with ϵ_1 given by Equation (3.23)] for the eigenvalue λ, we obtain a similar equation with ϵ_1 given by

$$\epsilon_1 = -\left(\sigma_x + \sigma_y\right)^2 / \left(2n^2\right). \tag{3.27}$$

Turkevich and Klemm showed that by mapping the eigenvalue equation onto a twodimensional lattice problem and by summing over all equivalent starting points on the lattice, an expansion could be found which is exact near the desired (commensurate) value of ϕ[50]. Nevertheless, the procedure described here gives the correct T^* and the correct power of the divergence of H_{c2} above T^*. Similarly, in the vicinity of $\phi = 0$ or $\pi/2$, an infinite class of divergent terms must be summed in order to obtain a finite
answer. The results for the temperature dependence of H_{c2} for several azimuthal angles is shown in Figure (17) for the special case of isotropic coupling. The very strong azimuthal dependence near to $\phi = 0$ should be noted.

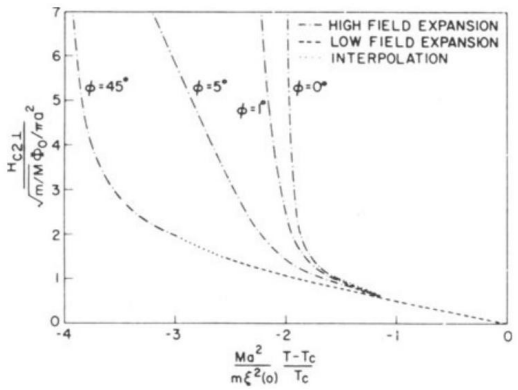


Fig. 17. Perpendicular upper critical field $H_{c 2 \perp}(T)$ for various azimuthal angles, for a square chain lattice. The azimuthal dependence is symmetric about $\phi = 45°$. There is pronounced azimuthal dependence near the lattice direction $\phi = 0°$. From [50].}

3.3. The Field Parallel to the Chains

We now consider the case of the magnetic field parallel to the superconducting chains. Using the vector potential as given by Equation (3.2) with $\theta = 0$, we minimize the free energy with respect to variations in the order parameter ψ, just as in leading up to Equation (3.3) for the perpendicular field direction. As the resulting potential is independent of l and z, we form the respective Fourier series and Fourier transform in those variables, setting the wavevectors Q_x and $Q_y = 0$, as we did in obtaining Equation (3.4) for the perpendicular direction. We obtain,

$$(\epsilon - 2\zeta_y \cos k\chi)\,\psi_k - \zeta_x\,(\psi_{k-1} + \psi_{k+1}) = 0, \tag{3.28}$$

where $\epsilon = \alpha + 2\zeta_x + 2\zeta_y$ is the eigenvalue of the difference equation, and the dimensionless variable $\chi = 2hab/d^2$. This difference equation may be solved in a manner analogous to the Mathieu equation. We note that ϵ and ψ are periodic in χ. Hence, ψ may be written in the form

$$\psi_k = \exp(ik\tau) \sum_{n=0}^{\infty} a_n \cos(nk\chi). \tag{3.29}$$

Substituting Equation (3.29) into Equation (3.28), equating the resulting coefficients of $\cos(mk\chi)$, and setting $\tau = 0$ (to give the lowest eigenvalue), one obtains the set of equations,

$$\epsilon a_0 = \zeta_y a_1 + 2\zeta_x a_0 \tag{3.30a}$$
$$\epsilon a_1 = 2\zeta_y a_0 + \zeta_y a_2 + 2\zeta_x a_1 \cos\chi \tag{3.30b}$$
$$\epsilon a_n = \zeta_y\,(a_{n-1} + a_{n+1}) + 2a_n\zeta_x \cos(n\chi), \quad n > 1 \tag{3.30c}$$

To solve this system of equations, we start with the top equation, writing a_0 in terms of a_1, which we write in terms of a_0 and a_2, etc. More explicitly, from Equation (3.30a) and (3.30b), we have,

$$(\epsilon - 2\zeta_x)\,a_0 = \zeta_y a_1 = \zeta_y^2\,(2a_0 + a_2)\,/\,(\epsilon - 2\zeta_x \cos\chi) \tag{3.31}$$

which implies

$$\left\{\epsilon - 2\zeta_x - 2\zeta_y^2/\,(\epsilon - 2\zeta_x \cos\chi)\right\} a_0 = a_2\zeta_y^2/\,(\epsilon - 2\zeta_x \cos\chi) = 0 \tag{3.32}$$

We then solve for a_2 in terms of a_0 and a_3 (by using Equation (3.30a) to write a_2 in terms of a_3 and a_1, and then using Equation (3.30b) to write a_1 in terms of a_0 and a_2. One may then solve for a_2 in terms of a_0 and a_3),

$$a_2 = \frac{\zeta_y \left\{a_3 + 2\zeta_y a_0 / \left(\epsilon - 2\zeta_x \cos\chi\right)\right\}}{\left\{\epsilon - 2\zeta_x \cos 2\chi - \zeta_y^2 / \left(\epsilon - 2\zeta_x \cos\chi\right)\right\}} \tag{3.33}$$

This expression may now be used in combination with Equation (3.32) to give a_0 in terms of a_3. This procedure may be carried on ad infinitum, and yields the continued fraction equation for the eigenvalue ϵ,

$$\epsilon - 2\zeta_x - \cfrac{2\zeta_y^2}{\epsilon - 2\zeta_x \cos\chi - \cfrac{\zeta_y^2}{\epsilon - 2\zeta_x \cos 2\chi - \cfrac{\zeta_y^2}{\epsilon - 2\zeta_x \cos 3\chi - \ldots}}} \tag{3.34}$$

This continued fraction must be solved for the eigenvalue $\epsilon(\chi)$ by truncating the denominator at some point, and then inverting the resulting expression to give χ (and hence H_{c2}) in terms of ϵ (and hence T). Turkevich and Klemm [50] performed this calculation numerically, obtaining the temperature dependence of H_{c2} shown in Figure 18. Note that the periodicity of $\epsilon(\chi)$ results in the figure being periodic in H_{c2} for a fixed temperature. Each repetition of the $T\,(H_{c2})$ curve arises from an additional flux quantum being placed in each unit cell of the chain lattice. The additional structure (or kinks) in the H_{c2} curve arises from a non-integral, commensurate fitting of the flux lattice into the chain lattice. The most striking anomaly is for one flux quantum in two unit cells. The next most important ones are for one or two flux quanta in three unit cells, and so on. However,

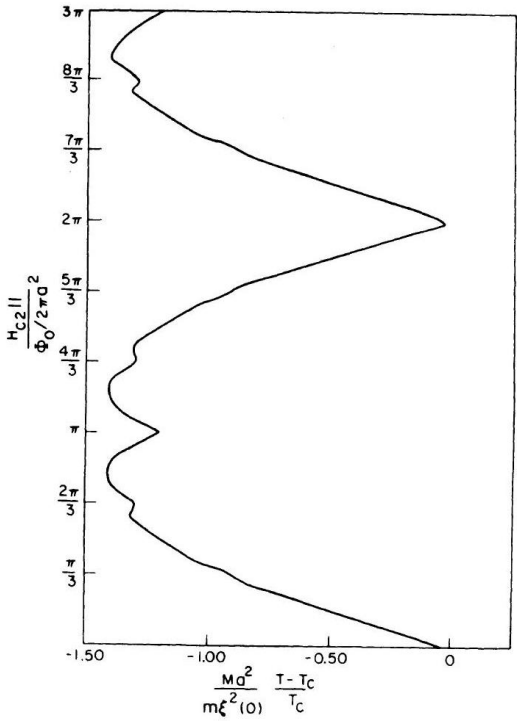


Fig. 18. Parallel upper critical field $H_{c 2 |}(T)$. This is periodic in H every time one flux quantum is inserted through the chain lattice. The additional kinks arise when a flux quantum is inserted into a section of the chain lattice larger than a single unit cell. From [50].}

it should be noted that the repeated structure will disappear when Pauli pairbreaking is

included in the theory [41], just as the apparent divergence of H_{c2} at T^* disappears in the layered compounds.

In a layered superconductor, the upper critical field is found from the usual pairbreaking equation [25],

$$\ln\left(T/T_{c0}\right) + \psi\left(1/2 + \alpha_{pb}/2\pi T\right) - \psi(1/2) = 0, \tag{3.35}$$

where $\psi(x)$ is the digamma function, and the pairbreaking parameter α_{pb} is given by

$$\alpha_{pb} = \epsilon + \tau_{so}\left(\mu_B H\right)^2, \tag{3.36}$$

with τ_{so} the spin-orbit scattering time (for two-dimensional scattering), and ϵ the eigenvalue of the Schroedinger equation with both harmonic and periodic potentials,

$$\left\{D\left[-\mathrm{d}^2/\mathrm{d}x^2 + (2eHx\cos\theta)^2\right] + J^2\tau[1 - \cos(2eHsx\sin\theta)]\right\}\phi = 2\epsilon\phi, \tag{3.37}$$

with $D = v^2\tau/2$ the two-dimensional diffusion constant and J the interlayer electron tunneling energy [55]. As an indication of the role of Pauli pairbreaking and spin-orbit scattering, Figure 19 exhibits the expected behavior in a layered superconductor in a parallel field.

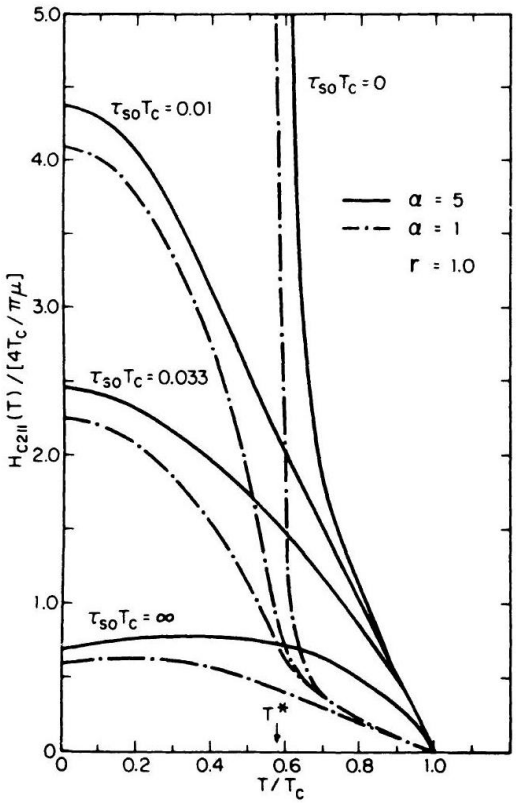


Fig. 19. Critical fields of layered compounds for modest ($\alpha = 1$) and strong ($\alpha = 5$) Pauli paramagnetic limiting and for various spin-orbit scattering rates. From [25].

3.6.4 4. Superconducting Networks

4.1. Some Puzzling Experimental Results

Although there are examples of materials that can be made in a crystalline form, some materials that exhibit quasi-one-dimensional superconductivity appear to be composed of bundles of fibers. Examination of $(SN)_x$ under a scanning electron microscope has revealed the

twisted, strandlike nature of the material [1]. This non-crystalline feature of the material results in critical field curves that are anomalous in their temperature dependence. The anomalous temperature dependence of H_{c2} in $(SN)_x$ is exhibited in Figure 9. For comparison, the same quantity is also displayed for the brominated material $(SNBr_{0.4})_x$, which behaves as an ordinary anisotropic bulk material.

Another puzzling experimental result is the low temperature superconductivity observed in $NbSe_3$. This material is known to have two incommensurate charge-density
waves, setting in at the temperatures 145 and 59 K , respectively [37]. However, low temperatures resistivity studies have shown a dramatic decrease in the resistivity [3], as pictured in Figure 20. More recent investigations have indicated that not all $NbSe_3$

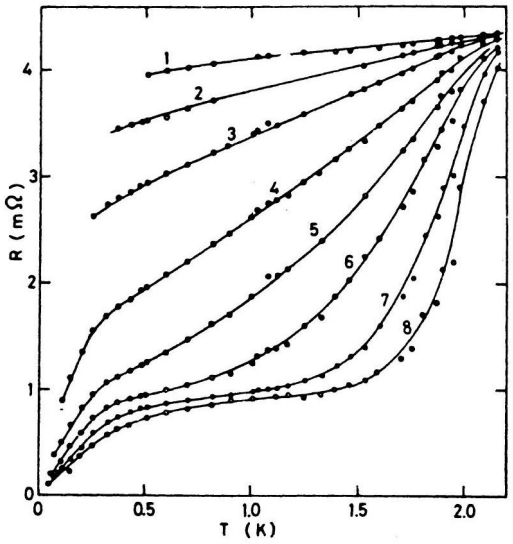


Fig. 20. Resistance of $\mathrm{NbSe
_{3}$ for sample A (with $R_{300}/R_{40} = 80$) vs temperature for different current densities. In A/mm^2, the current densities from Nos. $1 - 8$ are: $0.52, 0.26, 0.13, 0.052, 0.026, 0.013$, 0.0052 , and 0.0013 . From [12].}

samples exhibit this superconducting-like behavior. Apparently, single crystal samples do not show the behavior, whereas samples composed of many strands do [22]. This dramatic sample variation of the low temperature resistivity is pictured in Figure 21.

Very recently, yet another interesting feature has been observed in the highly anisotropic superconductor $TaSe_3$. Although this material has been known for some time to be a superconductor, and exhibits the angular and azimuthal dependence of the upper critical field characteristic of an anisotropic bulk material (e.g. Figure 5 and 6), it also exhibits extraordinary, novel resistivity behavior for low currents near to T_c, as pictured in Figure 22 [21]. These experiments are not yet understood, although the magnetic field dependence of the resistivity peak and the high anisotropy of the material are suggestive of a spin-density wave (e.g. see Figure 1), a fibrous structure such as has been observed in NbSe , has not yet been ruled out. It will be interesting to see how this material 'unravels'.

In this section, we will summarize the theoretical attempts to treat the strand-like nature of some of the materials. The most comprehensive treatment to date is by S . Alexander; hence most of what follows will be based upon his work [56].

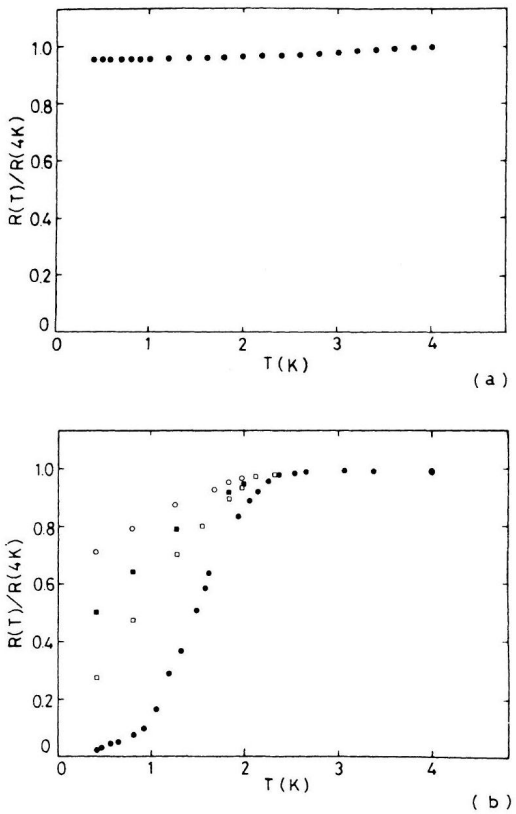


Fig. 21. Low temperature resistivity of different samples of $\mathrm{NbSe _{3}$. (a) Single crystal (non-superconducting). (b) material consisting of many fibers (exhibits apparent superconductivity). The different curves are from top to bottom for decreasing current densities, analogous to Figure 20. After [22].}

4.2. The Single Strand

The simplest model of a filamentary superconductor consisting of a number of strands is that of a single strand. The upper critical field of a single strand has been found in the Ginzburg-Landau regime (i.e., near to T_c) by several authors [29, 31, 50]. One might at first think that the upper critical field would be exactly that for an anisotropic bulk superconductor, as at H_{c2}, H and B are equal and there are no demagnetization effects. However, for filaments with a maximum cross-sectional diameter much less than the coherence length, the restricted geometry can influence the temperature and angular dependence of the upper critical field in a manner analogous to that of a thin film. For simplicity, the effective mass perpendicular to the highly conducting axis is assumed

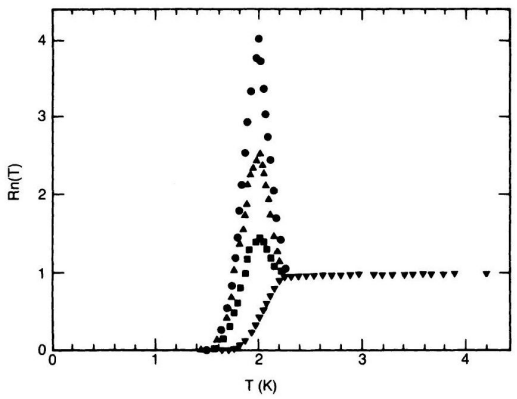


Fig. 22. Normalized resistance $R(T) / R(4.2 \mathrm{˜K)$ for a sample of $TaSe_3$ with room temperature resistance ratio = 167, as a function of current density. From top to bottom, the current density (A/cm^2) is $0.4, 0.7, 1.5$, and 2.2 , respectively. After [21].}

independent of azimuthal angle, $m_x = m_y = M, m_z = m$. The Ginzburg-Landau free energy appropriate for an uniaxially anisotropic superconductor of cylindrical shape is given by

$$F = \int_0^L \mathrm{d}z \int_0^R \rho \, \mathrm{d}\rho \int_0^{2\pi} \mathrm{d}\theta \left\{ \alpha|\psi|^2 + (\beta/2)|\psi|^4 + h^2/(8\pi) + \right.$$
$$\left. + (2m)^{-1} \left| \left(-i\frac{\partial}{\partial z} - 2eA_z \right) \psi \right|^2 + (2M)^{-1} \left| (-i\nabla_\perp - 2eA_\perp)\, \psi \right|^2 \right\} \tag{4.1}$$

A simplifying choice of the vector potential in cylindrical coordinates is

$$\mathbf{A} = (A_\rho, A_\theta, A_z) = H\rho \left\{ 0, (1/2)\cos\theta_0, -\sin\theta_0 \sin(\theta - \phi_0) \right\} \tag{4.2}$$

where the magnetic field has been taken to be in the direction

$$\mathbf{B} = H \left(\sin\theta_0 \cos\phi_0, \sin\theta_0 \sin\phi_0, \cos\theta_0 \right). \tag{4.3}$$

The relevant boundary condition is that there be no supercurrent across the boundary

$$\left.\frac{\partial\psi}{\partial\rho}\right|_R = \left.\frac{\partial\psi}{\partial z}\right|_{0,L} = 0. \tag{4.4}$$

Variation of the free energy [Equation (4.1)] with respect to ψ^* yields,

$$-(2M)^{-1} \left\{ \frac{\partial^2\psi}{\partial\rho^2} + \rho^{-1}\frac{\partial\psi}{\partial\rho} + \rho^{-2}\frac{\partial^2\psi}{\partial\theta^2} + (M/m)\frac{\partial^2\psi}{\partial z^2} \right\} +$$
$$+ (ieH/M) \left[\cos\theta_0 \frac{\partial\psi}{\partial\theta} + (M/m)2\rho \sin\theta_0 \sin(\theta - \phi_0) \frac{\partial\psi}{\partial z} \right] +$$
$$+ \left(2e^2H^2\rho^2/M \right) \left[(1/4)\cos^2\theta_0 + \sin^2\theta_0 \sin^2(\theta - \phi_0) \right] \psi = -\alpha\psi = E\psi. \tag{4.5}$$

Equation (4.5) is a Schroedinger equation, and may be solved for small magnetic field by perturbation theory. The unperturbed problem is

$$-(2M)^{-1} \left[\rho^{-1}\frac{\partial}{\partial\rho} \left(\rho\frac{\partial\psi}{\partial\rho} \right) + \rho^{-2}\frac{\partial^2\psi}{\partial\theta^2} + (M/m)\frac{\partial^2\psi}{\partial z^2} \right] = E_0\psi, \tag{4.6}$$

which is just the Laplace equation in cylindrical coordinates (provided the z axis is appropriately scaled to remove the anisotropy). The unperturbed eigenfunctions satisfying the boundary conditions [Equation (4.4)] are of the form

$$\psi_{kln} = \exp(ikz)\exp(ilq)J_l\left(x_{ln}/R\right), \tag{4.7}$$

where x_{ln} is the nth zero of the first derivative of the l th Bessel function, corresponding to the energies

$$E_0 = k^2/2m + \left(x_{ln}/R\right)^2/2M. \tag{4.8}$$

The lowest eigenvalue is for $k = 0$ and $x_{0,0} = 0$, corresponding to a constant order parameter across the strand. The remainder of the left-hand side of Equation (4.5) can be treated as a perturbation. To first order in H, there is no correction to the eigenvalue E. To second order in H, however, there is a correction arising from the part of the perturbation independent of spatial derivatives of ψ, yielding

$$E_2 = \left(e^2H^2R^2/2M\right)\left[(1/2)\cos^2\theta_0 + (M/m)\sin^2\theta_0\right]. \tag{4.9}$$

This second-order energy may be inverted to obtain the upper critical field

$$H_{c2} = M\Phi_0(m\pi R\xi(0))^{-1}\left|2\left(T - T_c\right)/T_c\right|^{1/2}\left(\cos^2\theta_0 + (M/m)\sin^2\theta_0\right)^{-1/2}. \tag{4.10}$$

We note that the angular dependence of H_{c2} in an isolated strand is very similar to that expected for an anisotropic bulk material (i.e. Equation (2.21)), and could be interpreted as identical to it, with a change in the definition of the effective mass anisotropy by a factory of 2 . This angular dependence is also much more gradual than the cusp at $\theta = 0$ given by the corresponding formula due to Tinkham for thin films [57]. In the thin-film case, the normal vortex cores can penetrate the film for a perpendicularly applied field, but get progressively 'squeezed out' as the external field is made more parallel. This results in a divergence of H_{c2} for an infinitely thin film. In the above thin-filament case,
the normal vortex cores have been 'squeezed out' for all orientations of the external field. Thus in the limit $R \to 0, H_{c2}$ diverges for all orientations. Note also that the temperature dependence near to T_c is proportional to $|T - T_c|^{1/2}$ for all angles, and hence exhibits downward curvature as the temperature is lowered, a result identical to the temperature dependence of H_{c2} for thin films [57].

4.3. General Network Equations

We now consider systems of superconducting filaments. We imagine that a particular material consists of a disordered lattice of chains. This disorder can take on many forms. Some chains may lie in an ordered fashion relative to the nearby chains. Others may be physically separated from the nearest chains, due perhaps to vacancies of chains. Still others may be twisted, ending with dead ends away from other chains. It may happen that the scale of chain vacancies is well-defined, or there may be no particular length scale, i.e., essentially all length scales less than the sample size may be present. Alexander [56] has studied these types of disorder by considering various networks of thin superconducting wires (or chains), as was first proposed by de Gennes and Deutscher et al. [58, 59]. They treated the linearized Ginzburg-Landau equations on networks of thin filaments by deriving linear-difference equations for the value of the order parameter at the junctions of the net, using the solutions along the filaments. He then solved for the upper critical field for several finite networks and for the Sierpinski

gasket, shown in Figure 23. The Sierpinski gasket represents a simplified model for a lattice of filaments

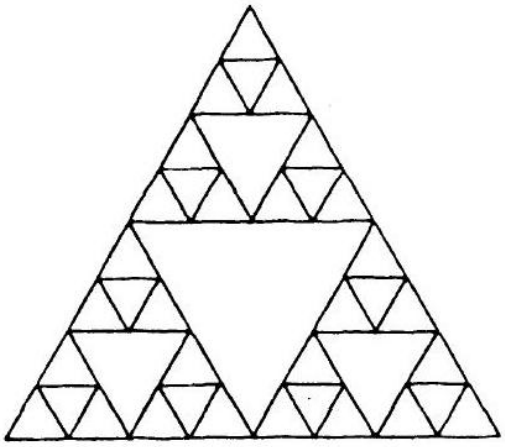


Fig. 23. A finite section of the triangular Sierpinski gasket. After [56].

with filament vacancies of all length scales, and leads to a new length scale proportional to a power of the bare (single strand) coherence length. The dead ends lead to a 'mass' or T^* renormalization.

The Ginzburg-Landau free energy for an infinitely thin strand at the upper critical field may be written [62]

$$F = \int \mathrm{d}s \left\{ A|\psi|^2 + (1/2)B|\psi|^4 + C|\hat{s} \cdot (i\nabla - 2e\mathbf{A})\psi|^2 \right\} \tag{4.11}$$

where $\hat{s}$ is a unit vector tangential to the stand, and the order parameter $\psi(s)$ is a function of the position along the strand. Equation (4.11) is obtained from Equation (4.1) by letting $R \to 0$, and the parameters A, B, C are proportional to α, β, and $(2m)^{-1}$, respectively. Minimizing Equation (4.11) with respect to variations in ψ leads to

$$\left\{ -1/\xi_s^2 + \left(i\frac{\partial}{\partial s} - a \right)^2 + b|\psi|^2 \right\} \psi = 0 \tag{4.12}$$

where $a = 2e\hat{s} \cdot \mathbf{A}$ is the reduced vector potential, $b = B/C$, and

$$1/\xi_s^2 = -A/C \propto (T_c - T)/TD_0, \tag{4.13}$$

where C has been taken to be proportional to the diffusion constant D_0 on the strand (i.e., the dirty limit has been assumed) [23]. To describe a network, each strand obeys the above GL equation, plus there are the appropriate boundary conditions at the junctions. We first generalize the order parameter ψ to a network, denoting $\psi_{ij}(s_{ij})$ as the order parameter at position s_{ij} on the strand with length l_{ij} between the connecting points (or junctions) s_i and s_j. Continuity of the order parameter at the junctions requires

$$\psi_{ij}(s_i) = \Delta_i, \quad \psi_{ij}(s_j) = \Delta_j \tag{4.14}$$

The surface term obtained from the free energy variation is of the form

$$\sum_j \left[\left(i\frac{\partial}{\partial s_{ij}} - a_{ij} \right) \psi_{ij}(s_{ij}) \right]_{s_i} = 0 \tag{4.15}$$

where a_{ij} is the vector potential on the strand between junctions i and j at the point s_{ij}, and all derivatives are in the outgoing directions on the respective branches. The summation is over all branches ending at the junction at s_j. The problem as stated by Equation (4.12-4.15) is well-posed, but the non-linearity in Equation (4.12) is important only for systems that are so inhomogeneous that, for a given external field H near to the macroscopic H_{c2}, some parts of the sample are far from their local H_{c2}. Hence, for most systems, it suffices to neglect the term in Equation (4.13) cubic in ψ. The linearized Equation (4.13) combined with the boundary conditions [Equation (4.14)] results in the solution

$$\psi_{ij}\left(s_{ij}\right) = \exp\left(-ia_{ij}s_{ij}\right)\left[\Delta_i \sin\left(\theta_{ij} - \phi_{ij}\right) + \Delta_j \exp\left(i\gamma_{ij}\right)\sin\phi_{ij}\right] / \sin\theta_{ij} \tag{4.16}$$

where

$$\theta_{ij} = l_{ij}/\xi_s, \quad \phi_{ij} = s_{ij}/\xi_s, \tag{4.17}$$

and

$$\gamma_{ij} = \int a_{ij}\, \mathrm{d}s_{ij} \cong a_{ij}l_{ij} \tag{4.18}$$

This equation combined with the 'Kirchoff' condition (Equation (4.14)) gives the set of coupled linear equations [58]

$$-\Delta_i \sum_j \cot\theta_{ij} + \sum_j \left[\Delta_j \exp\left(i\gamma_{ij}\right) / \sin\theta_{ij}\right] = 0. \tag{4.19}$$

This may be rewritten as

$$m_i\Delta_i/\xi_s^2 + \sum_j d_{ij}\left(\eta_{ij}\Delta_j - \Delta_i\right) = 0 \tag{4.20}$$

where $\eta_{ij} = \exp\left(i\gamma_{ij}\right)$ and the 'bond diffusivity' d_{ij} and mass m_i associated with the i th junction are given by

$$d_{ij} = \left(\xi_s \sin\theta_{ij}\right)^{-1} \tag{4.21}$$

and

$$m_i = \xi_s \sum_j \tan\left(\theta_{ij}/2\right) \tag{4.22}$$

The above equations have been studied by Alexander for a variety of network geometries [56].

4.4. Finite Networks

The first and simplest example considered by Alexander is that of a single superconducting ring of circumference L. A vortex can be formally introduced on the ring, and Equation (4.19) becomes [56]

$$\left(-2\cot\theta + 2\cos\gamma/\sin\theta\right)\Delta = 0 \tag{4.23}$$

which implies

$$\cos\theta = \cos\gamma \tag{4.24}$$

where $\theta = L/\xi_s$ and γ is the line integral of a around the ring, proportional to the flux through the ring. Equation (4.23) implies a solution (and hence an upper critical field) when

$$L/\xi_s < \pi. \tag{4.25}$$

For a larger ring, the vortex fits inside the ring, and hence does not destroy the superconductivity. If Equation (4.25) can be satisfied for some temperature > 0, then there will be a temperature T^* at which H_{c2} would diverge in the absence of other pairbreaking effects, given by

$$\xi_s(T^*) = L/\pi \tag{4.26}$$

Alexander next considered the case of a single ring of circumference L with an open side branch of length l attached to it. The two junctions are labelled 1 and 2 at the point where the branch is connected and at the end of the branch, respectively. The two equations obtained from Equation (4.19) are [56]

$$-\Delta_2 \cot\theta' + \Delta_1 \exp(i\gamma_{21}) / \sin\theta' = 0 \tag{4.27}$$

and

$$-\Delta_1 (2\cot\theta + \cot\theta') + 2\Delta_1 \cos\gamma / \sin\theta + \Delta_2 \exp(i\gamma_{12}) / \sin\theta' = 0, \tag{4.28}$$

where $\theta' = l/\xi_s$. Combination of the above two equations and using the fact that $\gamma_{12} = -\gamma_{21}$, one finds

$$\cos\theta - (1/2)\sin\theta\tan\theta' = \cos\gamma. \tag{4.29}$$

Near to T_c, one may expand for small θ, θ', and γ, and one finds

$$\gamma^2 = L(L+l)/\xi_S^2, \tag{4.30}$$

which implies that the critical field is increased by the addition of the side branch. The equation from which T^* is determined is Equation (4.29) with the right hand side replaced by -1 . As the side branch gets longer, T^* is increased from its single-ring value [Equation (4.26)], since the coherence length, proportional to the vortex core radius, is decreased.

It is easy to generalize the ring with one side branch to a ring with many side branches. Consider a ring of circumference L with N equally spaced side branches of length l, as pictured in Figure 24. We label the junctions on the ring $i = 1, \ldots, N$, and the dead ends

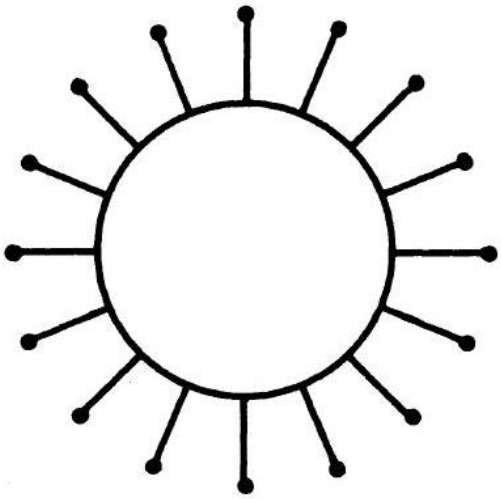


Fig. 24. Ring with N equally spaced dead-end side branches. After [56].

the corresponding $i' = 1', \ldots, N'$. The equations obtained from Equation (4.19) for the i th and i' th junctions are [56]

$$-2\cot\theta\Delta_i + \eta^*\Delta_{i-1}/\sin\theta + \eta\Delta_{i+1}/\sin\theta - \cot\theta'\Delta_i + \eta'\Delta_{i'}/\sin\theta' = 0 \tag{4.31}$$

and

$$\Delta_{i'}\cot\theta' - \eta'^*\Delta_i/\sin\theta' = 0, \tag{4.32}$$

where $\theta = L/\xi_s, \theta' = l/\xi_s, \eta = \exp(i\gamma_{ii+1}) = \exp(i\gamma/N)$ where γ is the flux in the ring, and $\eta' = \exp(i\gamma_{ii'})$. Using Equation (4.32) to solve for $\Delta_{i'}$ in terms of Δ_i, and noting that the periodicity of Δ_i requires Δ_i to be of the form,

$$\Delta_j = \Delta\exp(2\pi imj/N), \tag{4.33}$$

one finds immediately

$$\cos[(2\pi m + \gamma)/N] = \cos(\theta/N) - (1/2)\sin(\theta/N)\tan\theta'. \tag{4.34}$$

We note that Equation (4.34) reduces to Equation (4.29) for $N = 1$. For large N, one may expand Equation (4.34) and obtains [59]

$$(2\pi m + \gamma)^2 = L(L + Nl)/\xi_s^2, \tag{4.35}$$

which is valid for small θ, θ', and for γ and winding number $m \ll N$. By comparison with Equation (4.30), we see that the effective coherence length (proportional to the radius of the vortex cores) is progressively reduced as more side chains are added.

Although in the preceding example, the coherence length was found to be reduced by the addition of the dead-end side chains, the order parameter Δ_i was found to be uniform for winding number 0 . For $m \neq 0$, the phase of the order parameter was found to vary from junction to junction. This winding number m is related to flux quantization, which is also present in the single ring previously considered. However, in that system there was only one junction on the ring, so that this destruction of the phase coherence was not present. These two effects of the dead ends are quite general: the coherence length is reduced and the phase coherence is destroyed. Alexander has demonstrated the generality of this statement by considering a 'transmission line' strand with $N - 1$ sidebranches of variable length located at arbitrary

positions along the main strand. One would obtain this configuration by cutting the ring pictured in Figure 24 between two side chains, and making the lengths and positions of the side chains variable. The essential result of his calculation is that the diffusivity and the mass are both renormalized [56],

$$m/d = (L/\xi_L)^2 \,, \tag{4.36}$$

where ξ_L is the effective coherence length for the line on the scale L.
A distinctly different type of finite lattice is the double loop pictured in Figure 25.

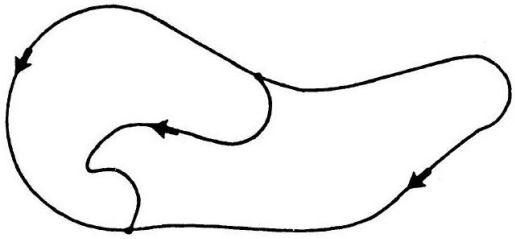


Fig. 25. Double loop. After [56] .

Since the general situation is rather complicated, Alexander considered only special cases. In the first case, the flux through each half loop was taken equal to γ, and the length of the left and right paths from the upper to the lower vertex equal to L. The length of the middle path is taken to be L', and setting $\theta = L/\xi_s$ and $\theta' = L'/\xi_s$, one finds from Equation (4.19) [56],

$$2\cot\theta + \cot\theta' = \pm\left[2\cos\gamma/\sin\theta + 1/\sin\theta'\right] \tag{4.37}$$

There are two situations. In the first situation, which is appropriate for θ' near to 0 , one has

$$\cos\theta - (1/2)\sin\theta\tan(\theta'/2) = \cos\gamma, \tag{4.38}$$

which corresponds to two independent half loops, each with a sidebranch of length $L'/2$. We note that when $\theta = \theta' \ll 1$, we have two (half) loops with flux γ and a (full) loop with no flux. In the second case, appropriate for θ' near to π, we have

$$\cos\theta + (1/2)\sin\theta\cot(\theta'/2) = -\cos\gamma, \tag{4.39}$$

which reduces to Equation (4.38) by $\theta \to \pi - \theta, \theta' \to \pi - \theta'$.
The second special case of the double loop considered by Alexander is that of all three paths from one junction to the other having the same length L, and the fulx in the left and right half loops being γ and 2γ, respectively, so that the total flux is 3γ. One finds [56]

$$9\cos^2\theta = 3 + 2(\cos\gamma + \cos 2\gamma + \cos 3\gamma). \tag{4.40}$$

Since this equation is cubic in $\cos\gamma$, there are several possibilities. First, for $\theta < 0.94$, there is only one critical field, as usual. However, for

$$0.94 < \theta < 1.23 \tag{4.41}$$

there are three critical fields. Superconductivity disappears at H_1, reappears at H_2, and disappears again at H_3. In the range

$$1.23 < \theta < 1.37 \tag{4.42}$$

there are two critical fields. Finally, for

$$1.37 < \theta \leq \pi/2 \tag{4.43}$$

there is no critical field. At the isolated points $\theta = 0.94$ and 1.37, there are two and one solutions, respectively. This pattern is symmetric about $\theta = \pi/2$. Thus, deformations in the lattice containing loops with different amounts of magnetic flux can give rise to 'reentrant' superconductivity, at least regarding the upper critical field.

4.5. The Sierpinski Gasket

The above networks considered were all finite in size, and are not easily generalized to infinite networks of a type that might simulate the effects of percolating clusters. However, a model for a network which can be solved and which contains some of the features of a percolating cluster is that of the Sierpinski gasket (Figure 23) [60,61]. This model is 'self-similar', that is, it looks the same on many different length scales. The smallest length scale is a, the side of one of the smallest triangles in the gasket pictured. The smallest network on this length scale consists of an equilateral triangle composed of three triangles of size a placed corner to corner in such a fashion that a triangular hole of equal size is formed in the center. This finite network can then be used to construct a network of the next hierarchical size: three such networks are placed together as before, yielding a triangular hole in the center the size of the previous network scale.

Let us first consider the smallest network, consisting of three triangles of size a (on a side) connected together at their vertices, yielding an equilateral triangle of size $2a$ with junctions in the middle of each side. Let us label the junctions 1,2 , and 3 , respectively. Use of Equation (4.19) results in the matrix equation [59],

$$p_0 T_{123} \Delta = 0 \tag{4.44}$$

where

$$p_0 = (\sin\theta_0)^{-1} \tag{4.45}$$

the vector Δ has components Δ_1, Δ_2, and Δ_3, respectively, and the T matrix is given by

$$T_{123} = \begin{bmatrix} -2t_0 & \eta_{12} & \eta_{13} \\ \eta_{21} & -2t_0 & \eta_{23} \\ \eta_{31} & \eta_{32} & -2t_0 \end{bmatrix} \tag{4.46}$$

where $t_0 = \cos\theta_0$ and $\eta_{ij} = \exp(i\gamma_{ij})$ are defined as before, with $\theta_0 = a/\xi_s$.
The simple network may be extended to include coupling to the adjacent networks by replacing the right hand side of Equation (4.44) by a vector F. Alexander has considered this problem in detail, by iterating to successively larger networks. He finds that after n iterations, the recursion relations for t and p become [56]

$$t_{n+1} = t_n (4t_n - 3) \tag{4.47}$$

and

$$p_{n+1}/p_n = (2t_n + 1) / [(4t_n + 1)(2t_n - 1)] \tag{4.48}$$

As can be immediately seen from Equation (4.47), there are two fixed points $t = 0$ and $t = 1$. Although both of these fixed points are unstable, the $n = 1$ fixed point is relevant to the resistor network, and is appropriate for small θ_0. The flux through the gasket is essentially just the added flux through all of the single triangles,

$$\gamma_n \cong 4^n \gamma_0 \tag{4.49}$$

where the single triangle flux $\gamma_0 = \eta_{12}\eta_{23}\eta_{31}$. The 'angle' θ is renormalized, however,

$$\theta_n \cong 5^n \theta_0 \tag{4.50}$$

Alexander showed that the above recursion relations could be used to solve for a finite gasket of size [56]

$$L = 2^n a \tag{4.51}$$

by renormalizing the gasket to a single triangle with parameters t_n and γ_n. Since there will be no external interactions with other vertices, the matrix equation is as given by Equation (4.44). Thus, the condition for a solution is

$$\det T_n = 0 = -8t_n^3 + 6t_n + 2\cos\theta_n \tag{4.52}$$

Since Equation (4.52) has solutions for t_n in the range -1 to 1 , we may write $t_n = \cos\theta_n$, and we find

$$\cos(3\theta_n) = \cos(\gamma_n) \tag{4.53}$$

Assuming we are near to the $n = 1$ fixed point, Equation (4.53) may be expanded for small θ_n and γ_n,

$$9\theta_n^2 \cong \gamma_n^2 \tag{4.54}$$

First, by defining θ_n to be

$$\theta_n = L/\bar{\xi}_s, \tag{4.55}$$

by using Equations (4.50) and (4.51) and the definition of θ_0, we have

$$\bar{\xi}_s^2 \cong (4/5)^n \xi_s^2 \propto L^{-\theta}\xi_s^2 \tag{4.56}$$

where

$$\theta = -2 + \ln 5/\ln 2 \cong 0.32 \tag{4.57}$$

Then, using Equation (4.54) and using the fact that $\gamma_0 = \sqrt{3}\pi H a^2/(2\Phi_0)$, where Φ_0 is the flux quantum, we have

$$H_{c^2} \cong \Phi_0/\left(L\bar{\xi}_s\right) \cong \Phi_0/\left(\xi_s L^{1-\theta/2}\right) \tag{4.58}$$

In the above equations, it has been assumed that the gasket is self-similar over its entire extent, i.e., on the scale L. For less perfect gaskets, which are self-similar on a scale $\lambda_s < L$, the linearized Ginzburg-Landau equations will break down, as the inhomogeneities will allow for variations in the order parameter on the scale λ_s. We then have Equation (4.56) with λ_s replacing L, and setting $\theta_s = \lambda_s/\bar{\xi}_s$, the requirement that θ_s be of order of magnitude unity gives

$$\lambda_s \propto {\xi_s}^{2/(2+\theta)}. \tag{4.59}$$

This length sets an upper bound on the upper critical field, obtained by setting $L \cong \lambda_s$ in Equation (4.56), and using Equation (4.59) for ξ_s in terms of λ_s,

$$H_s \cong \Phi_0/\lambda_s^2 \tag{4.60}$$

A lower limit for H_{c2} is simply obtained by assuming one flux quantum penetrates the entire sample,

$$H_L \cong \Phi_0/L^2. \tag{4.61}$$

By comparing Equations (4.60) and (4.61), we see that the upper critical field as a function of L can generally be written

$$H_{c2}(L) \propto \Phi_0 \left(L/\lambda_s\right)^y / L^2 \tag{4.62}$$

for $L > \lambda$, where $y < 2$ in order to satisfy the upper and lower limits. This implies that H_{c2} is a decreasing function of L in this regime.

4.6. Percolation Clusters

Finally, Alexander attempted to relate the above results to the case of percolation clusters of superconducting chains. He compared his results to the Skal-Shklovski-deGennes (SSG) model of percolation clusters [62] containing dead ends but no loops on a scale smaller than ξ_p. First, he neglected the effect of the dead ends. In the SSG model, the percolation length ξ_p is divergent at the percolation concentration p_c,

$$\xi_p \propto (p - p_c)^{-\nu}, \tag{4.63}$$

and the string length (or length of the backbone near to percolation) is

$$l_p \propto (p - p_c)^{-\xi}, \tag{4.64}$$

where the exponent ζ is related to the conductivity exponent t[61],

$$\sigma \propto (p - p_c)^{-t}, \quad \zeta = t - (d-2)\nu, \tag{4.65}$$

where d is the dimensionality. For a percolation cluster, the relevant lattice scale is ξ_p instead of a, so the appropriate γ is

$$\gamma \cong 2\pi H \xi_p^2/\Phi_0. \tag{4.66}$$

The strands connecting the junctions are not necessarily a distance ξ_p apart, but are a greater distance l_p apart, on the average, due to their wildly meandering paths. The relevant 'angle' to use in Equation (4.19) is

$$\theta = l_p/\xi_s \tag{4.67}$$

Assuming a square lattice such as that considered in Section 3, we find that for small $\theta, \gamma \cong \theta^2$, which implies

$$H_{c2} \propto \left(l_p/\xi_p\right)^2 \Phi_0/\xi_s^2 \tag{4.68}$$

This implies that there is an effective coherence length $\bar{\xi}_s$ such that $H_{c2} \propto {\xi_s}^{-2}$,

$$\bar{\xi}_s = \left(\xi_p/l_p\right) \xi_s. \tag{4.69}$$

When dead ends are considered, the effective coherence length is further modified. From Equation (4.36), setting $d = l_p^{-1}$ and $L = \xi_p$

$$\bar{\xi}_s \cong \xi_p \left(l_p m_p\right)^{-1/2} \tag{4.70}$$

where the 'mass' on the percolation lattice of scale ξ_p is given by

$$m_p \propto (p - p_c)^{\beta} \xi_p^d \tag{4.71}$$

where the exponent β is analogous with other critical phenomena in which the order parameter (e.g., spin density) exponent is β[61]. This implies

$$\bar{\xi}_s \cong \xi_s \left(p - p_c\right)^{(t-\beta)/2} \tag{4.72}$$

provided that $\bar{\xi}_s$ and λ_s are both greater than ξ_p, where

$$\theta = (t - \beta)/\nu \tag{4.73}$$

in the expression (Equation (4.59)) for λ_s. With this effective coherence length, the upper critical field is

$$H_{c2} \propto \left(\Phi_0/\pi\xi_s^2\right)\left(p - p_c\right)^{\beta - t}. \tag{4.74}$$

This expression is in reasonably good agreement with the experimental measurements of Deutscher et al. [59] on small particles in the small ξ_p regime, where $\xi_p < \lambda_s$. When $\xi_p \cong \lambda_s$, however, Alexander suggests that there should be a crossover regime, and that for larger ξ_p, H_{c2} should behave as

$$H_{c2} \sim \Phi_0/\xi_p^2 \tag{4.75}$$

although this is really only a lower limit result. In any event, the experiments show that there is a crossover, but that H_{c2} continues to increase as ξ_p increases, contrary to Alexander's arguments. He considers patching up the theory by including loops in a more reasonable fashion, but concludes that even such patch-ups will not give the experimentally observed behavior close to percolation [56].

3.6.5 5. Summary

We have seen that the expected behavior of quasi-one-dimensional superconductors is quite different from what one would expect in ordinary bulk materials. The temperature dependence of the upper critical field should show upward curvature indicative of dimensional crossover, regardless of the angle of the applied field, provided that the anisotropy is sufficiently great. For the field parallel to the chain lattice, the temperature dependence of H_{c2} should also exhibit kinks associated with a commensurate fitting to the vortex lattice into the chain lattice. These kinks are most likely to be pronounced for a fitting of a small number (e.g., 1 or 2) of flux quanta into a slightly larger small number of unit cells. If there is sufficient disorder in the material, similar anomalies in the upper critical field curves could arise from the fitting of flux quanta into rings or loops of the strands. However, if the strands form loops and rings of many different length scales, then there would be so many possibilities for the fitting of vortices into the rings or loops that the effective temperature dependence of H_{c2} would be altered to a non-trivial power of $T_c - T$. Near to the percolation threshold, the extreme inhomogeneities of the sample allow for an order parameter that is spatially non-uniform; some regions will have a very small order parameter near to H_{c2}, while others have a local order parameter that is non-vanishing at H_{c2}. This picture seems to be appropriate for materials such as $NbSe_3$, which is now fairly well-established as consisting of bundles of fibers, at least in the materials that exhibit superconductivity [22].

To date, no materials have been made with sufficient intrinsic anisotropy in addition to sufficient crystallinity to observe the kinks in the parallel upper critical field that have been predicted. It remains to be seen if existing materials can be structurally perfected, or if more anisotropic materials can be produced.

As regards the lower critical field, there does not appear to be much difference between a highly anisotropic bulk superconductor with filamentary symmetry and a quasi-onedimensional superconductor. For a material with sufficient anisotropy such that the kinks in the temperature dependence of the parallel upper critical field are observable, the angular dependence of the lower critical field should exhibit a kink, corresponding to the vortex cores preferring to lie parallel to the easy axis (i.e., parallel to the chains). Such behavior is not expected in a material with an effective mass anisotropy of roughly 10 or less, however.

It is worth noting that measurements of the lower critical field have been plagued with the difficulty in determining the field at which the departure from the linear magnetization versus field curve occurs. Unlike the case of $NbSe_2$, for which this field is rather well-defined [30], $(SN)_x$ did not appear to exhibit a well-defined H_{c1} [8]. The strand-like nature of that and other materials suggests that there are many possible easy ways in which to insert a single vortex into the material. For example, if the strands make a loop,
it is easier for the flux to penetrate that loop than the bulk of the sample. Unfortunately, calculations of the lower critical field for such geometries are generally non-trivial: the order parameter is large and non-uniform, and hence the GL equations are non-linear.

The organic material (TMTSF) $_2ClO_4$, however, has been made sufficiently crystalline that H_{c1} could reliably be determined [46]. Nevertheless, even in that material, the difficulty of measuring the lower critical field precisely proved to be sufficient as to preclude the determination of the existence of a kink in its angular dependence.

Finally, it is hoped that new materials will continue to be made, and existing materials will continue to be made better. It is quite likely, as we have seen, that novel behavior should be observed.

4 Charge Density Waves in Solids by L.P. Gor'kov, Gruner

(was Gorkov also an expert in this topic?)

4.0.1 Preface

The various chapters of this book cover a field which is, in general, referred to as charge density wave dynamics.

The materials which have been investigated in detail, are inorganic linearchain compounds with highly anisotropic electronic properties. Their structural properties, and normal-state metallic properties, together with their essential features which allow charge density waves to develop, are summarized by Rouxel and Schlenker.

The various aspects of the transition and of the charge density wave ground state are discussed by Pouget and Comes. The transition leads to a periodic lattice distortion, which can be studied by various scattering techniques. Neutron scattering leads, in addition, to a detailed picture of the excitations of the collective mode.

An overview of the dynamics of the charge density waves under the influence of applied DC and AC electric fields is given by Grüner and Monceau. The unusual electrical transport, electric-field induced changes in the thermoelectric and elastic properties, together with information provided by local probes give clear evidence for a novel type of collective transport

mechanism.

Experimental details of the depinning, and of the translational motion of the condensate is discussed by Nad', with a focus on the role played by local defects and boundaries, which, among others, can be controlled by doping and by the size of the specimens.

A variety of phenomena are observed when both DC and AC electric fields are applied. These are analogous to those observed in Josephsonjunctions. These interference phenomena, together with their interpretation are summarized by Brown and Zettl.

Impurities play an important role, both in the static properties and in the dynamics of charge density waves, and the various microscopic models of the impurity-collective mode interaction are discussed by Feigelman and Vinokur.

Due to the complexity of the problem, computer simulations, mostly based on one-dimensional models, play an important role. These, together with partial solutions of more realistic models are reviewed by Littlewood, with
emphasis on novel aspects of driven nonlinear many degree of freedom systems.

A different approach, which is based on the microscopic description of the collective mode in the presence of impurities, is given by Artemenko and Volkov. This approach, while not giving detailed account of the dynamics, is important and provides the basis for phenomenological descriptions.

Attempts to arrive at a realistic description of the behaviour under the influence of applied fields are summarized by Gor'kov, with emphasis on the role played by both amplitude and phase excitations in nonlinear conductivity due to slipping.

An overview by Brazovskii of the possible role of solitons in incommensurate charge density wave systems both for the static and for the dynamic properties of the materials, concludes the book.

4.1 1. Introduction by L.P. Gofkov and G. Grüner

4.1.1 1. Introduction

This book is devoted to a relatively new field of condensed matter physics. The subject is a new type of collective transport phenomenon, where electrical current is carried by a ground-state condensate, called the charge density wave (CDW). The formation of charge density waves was discussed by Peierls and by Fröhlich more than thirty years ago, they showed that a one-dimensional electron gas, coupled to a phonon system is unstable at low temperatures, and undergoes a phase transition to a nonconducting state. The ground state is a periodic lattice distortion and a periodic modulation of the charge density. The period λ is given by the Fermi wave vector, $\lambda = \pi/k_{\mathrm{F}}$. For a small lattice distortion, the charge density modulation is given by

$$\Delta\rho = \rho_1 \cos\left(2k_{\mathrm{F}}x + \phi\right), \tag{1}$$

with ρ_1 the amplitude and ϕ the phase of the condensate. In many of the cases studied so far, the period is not commensurate with the underlying lattice, and the phase can assume an arbitrary value. The Hamiltonian, which is in general used to establish the mean features of the phase transition and the ground state, is that of a one-dimensional (1D) coupled electron-phonon system

$$H = \sum_{k,q,\sigma} \epsilon_k c_{k\sigma} c^+_{k\sigma} + \sum_{k,\sigma} \hbar\omega_{q0} b^+_q b_q + \sum_{k,q,\sigma} g(k) c^+_{k+q,\sigma} c_{k,\sigma} \left(b_q + b^+_{-q}\right), \tag{2}$$

where $c^+_k\,(c_k)\,, b^+_q\,(b_q)$ are the electron and phonon creation (annihilation) operators with momenta k and q, σ is the spin, ϵ_k and ω_{q0} are the electron and phonon frequencies and $g(\boldsymbol{k})$

is the electron-phonon coupling constant. The mean field theory of the CDW formation is, from the mathematical point of view, analogous to that of the BCS theory of a superconductor. The ground state is composed of electron-hole pairs with a total momentum of $q = 2k_{\mathrm{F}}$, and similarly to superconductors the energy spectrum has a gap for charge excitations.

Issues like the thermodynamics of the phase transition, the direct observations of the periodic lattice distortion by various scattering techniques, the validity of the mean field treatment and the effect of fluctuations were
discussed extensively more than a decade ago, when organic linear chain conductors, like TTF-TCNO, were discovered and studied in detail.

Inorganic linear chain metals, which have a highly anisotropic band structure, received less attention although by now it is clear that they are perhaps simpler examples of the so-called one-dimensional phenomena which were so popular in the early seventies. The materials, like $NbSe_3$, TaS_3 and $K_{0.3}MoO_3$ (often called the blue bronze), show evidence for second-order phase transitions at T_{P} (T_{P} is the so-called Peierls transition temperature) and X-ray and neutron scattering studies establish clear evidence for an incommensurate charge density wave. Furthermore, transport, optical and magnetic properties clearly show the development of single-particle gaps. The materials also display novel frequency (ω) and electric field ($\boldsymbol{E}$) dependent transport properties at energy scales well below the energies associated with the single-particle gaps. This behavior is due to a new type of collective transport carried by moving charge density waves. The phenomenon was perhaps first observed in the material $K_{0.3}MoO_3$ as early as 1972, but the field was initiated by the observation of nonlinear transport and also by the observation of anomalous conductivity at microwave frequencies by Monceau, Ong and co-workers in 1975 in the material $NbSe_3$.

4.1.2 2. The dynamics of the CDW mode: Fundamental concepts

The dynamics of the collective mode is described in terms of a position- and time-dependent order parameter $\Delta(x,t)$. As $\Delta(x,t)$ is complex both amplitude and phase fluctuations occur. These can be described by assuming that the two types of fluctuations are decoupled and

$$\Delta(x,t) = (\Delta_0 + \delta)\,\mathrm{e}^{\mathrm{i}\phi'} \tag{3}$$

where Δ_0 is the equilibrium order parameter, δ and ϕ' are the fluctuations from the equilibrium value. Then, to lowest order in δ and ϕ', the amplitude mode corresponds to $\Delta_{2k_{\mathrm{F}}} + \Delta_{-2k_{\mathrm{F}}} = 2\Delta_0 + 2\delta$, and the phase mode to $\Delta_{2k_F} - \Delta_{-2k_F} = 2k_0\Delta\phi'$. The dispersion relations of these modes are given (in the long-wavelength $q^{-1} \gg \lambda$ limit) by

$$\Omega_+^2 = \lambda' \left(\omega_{2k_{\mathrm{F}}}\right)^2 + \frac{1}{3}\left(\frac{m}{m^*}\right)\left(v_{\mathrm{F}}q\right)^2 \tag{4a}$$

$$\Omega_-^2 = \left(\frac{m}{m^*}\right)\left(v_{\mathrm{F}}q\right)^2 = \left(c_0 q\right)^2 \tag{4b}$$

Here v_{F} is the Fermi velocity and $c_0 = \left(m/m^*\right)^{1/2} v_{\mathrm{F}}$ is the so-called phason velocity, λ' the dimensionless electron-phonon coupling constant, and $\omega_{2k_{\mathrm{F}}}$ the unrenormalized phonon frequency at wavevector $2k_{\mathrm{F}}$. The effective
mass m^* is given in terms of the fundamental parameters $\lambda', \omega_{2k_{\mathrm{F}}}$ and Δ (the single-particle gap at $T = 0$) by

$$\frac{m^*}{m} = 1 + \frac{4\Delta^2}{\hbar^2\lambda'\left(\omega_{2k_F}\right)^2} \tag{5}$$

With a characteristic Fermi energy $\epsilon_F \sim 1$eV, single-particle gap $\Delta \sim 0.1$ eV and phonon frequency $\omega_{2k_F} \sim 10^{-2}$eV, the electron-phonon coupling constant λ' is of the order of 0.5 and the single-particle gap $\Delta \sim 10^{-1}$eV. With these values, $\Omega_+(q=0) \sim 5 \times 10^{-3}$eV, which is smaller than Δ, and the effective mass is of the order of $m^*/m \sim 10^3$.

The amplitude mode is Raman active, and experiments, in particular in $K_{0.3}MoO_3$, and $(TaSe_4)_2\,I$, clearly establish the existence of this mode. The dispersion relations, eq. (4) have also been examined by neutron scattering studies in $K_{0.3}MoO_3$. The phase mode for $q = 0$ carries an electric current, and in the absence of pinning and damping it leads to a zero-frequency collective mode reminiscent of superconductivity. This was first suggested by Fröhlich in 1954.

As in a superconductor, the phase $\phi(x,t)$ plays an important role in the dynamics of the collective mode. $q = 0$ corresponds to the translational motion of the condensed electrons, with the ions oscillating around their equilibrium positions. A rigid translational motion of the CDW leads to an electric current, and the current density per chain $j_{\rm CDW} = -n_{\rm CDW}\, ev_d = n_{\rm CDW}\, e(\,{\rm d}\phi/{\rm d}t)$, where $n_{\rm CDW}$ is the number of electrons in the collective mode. With $\phi = 2k_{\rm F}x$ and $\lambda = \pi/k_{\rm F}$,

$$j_{\rm CDW} = \frac{e}{\pi}\frac{{\rm d}\phi}{{\rm d}t}. \tag{6}$$

It is important to note that, while the electrons execute a translational motion, the ions merely oscillate about their equilibrium position. A compression of the wave leads to a change of the electronic density, and therefore

$$n_{\rm CDW} = \frac{e}{\pi}\frac{{\rm d}\phi}{{\rm d}x}. \tag{7}$$

The picture described above is clearly an oversimplification. First of all, the materials in which the charge density wave ground state is established are not strictly one-dimensional, and the ground state is the result of the coupling of the fluctuations on the neighboring chains. This leads to a phase transition at finite temperatures. From the physical point of view, the important feature of the materials is that, above the phase transition, the Fermi surface is almost flat and consists of two sheets separated by $2\boldsymbol{k}_{\rm F}$. Depending on the extent of interchain bandwidth, the gap may develop along the whole Fermi surface or remove only part of it. These details
determine not only the details of the phase transition, but those of the dynamics as well. For a gap developing along the whole Fermi surface, a metal-insulator transition results, and a one-dimensional picture is an adequate starting point of a theoretical analysis.

4.1.3 3. Interaction with defects

Electrostatic potentials, which arise as the consequence of impurities, lattice defects, grain boundaries and discontinuities created by contacts, can have a profound influence on the charge density wave, and both the amplitude and the phase will be modified around the potential $V(r)$. In general, this leads to the loss of translational invariance, and the problem for a single impurity potential has been treated on the basis of microscopic models. The effect of a collection of impurities, which may lead to pinning of the collective mode, or boundary potentials have been treated using phenomenological models.

Weak perturbations keep the amplitude of the collective mode unchanged, and the problem can be treated by using a Ginzburg-Landau Hamiltonian, assuming a potential which couples directly to the phase of the CDW

$$\boldsymbol{H} = \frac{n\hbar v_{\mathrm{F}}}{4\pi} \int (\nabla\phi)^2 \, \mathrm{d}\boldsymbol{r} + \int \rho_1 V(\boldsymbol{r}) \cos\left(2\boldsymbol{k}_{\mathbf{F}} \cdot \boldsymbol{r} + \phi(\boldsymbol{r})\right) \mathrm{d}\boldsymbol{r} \tag{8}$$

The first term on the right-hand side represents the elastic energy associated with the long-wavelength phase deformations; the second represents the interaction of the collective mode with the pinning potential $V(r)$. The combined effect of elastic and potential energy terms in eq. (8) is a decrease of the total energy and, because the potential depends on the position $V(\boldsymbol{r})$, the interaction also leads to pinning of the phase, prohibiting translational motion of the charge density wave.

For random impurity potentials the problem has been treated in detail. There is no long-range order in presence of impurities, and the phase-phase correlation length L_0 is finite, given by

$$L_0^{-1} = \left(\frac{V_0\rho_1}{\pi\hbar v_{\mathrm{F}}}\right) n_i, \tag{9}$$

where n_i is the number of impurities in unit volume. The finite correlation length leads, in turn, to a finite frequency for the oscillations of the collective mode about the equilibrium position, with

$$\omega_0 = 2\pi \left(\frac{m}{m^*}\right)^{1/2} v_{\mathrm{F}} L_0^{-1} \tag{10}$$

as expected.

For strong potentials $V(r)$ both the amplitude and phase of the mode is modified around the impurities, leading also to the possibility of bound states below the single-particle gap.

4.1.4 4. Experiments

The existence of the single-particle gap and the collective mode is evident from frequency-dependent conductivity studies performed in various materials below the phase transition. As an example, $\sigma(\omega)$ extracted for $K_{0.3}MoO_3$ from studies as conducted by various groups in different spectral regions is displayed in fig. 1. The value of the single-particle gap, as obtained from the temperature dependence of the DC conductivity, is shown by the dotted arrow, and $\sigma(\omega)$ above this spectral range is due to single-particle excitations across the gap. The mode indicated by the full line is due to the collective response of the charge density wave, which oscillates under the influence of a small amplitude AC electric field about the equilibrium position, which is determined by the various pinning forces.

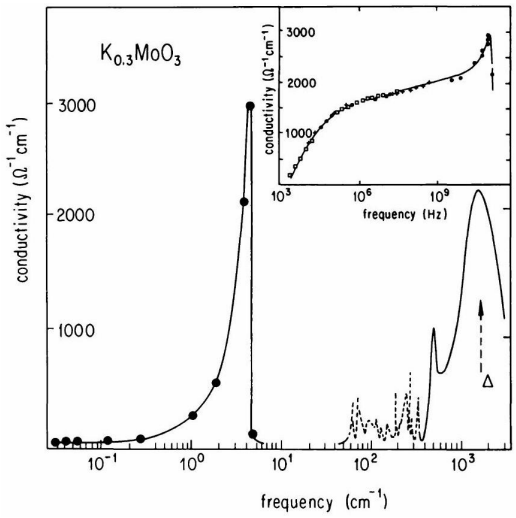


Fig. 1. Frequency-dependent conductivity $\sigma(\omega)$ in the CDW state of $\mathrm{K}_{0.3}\mathrm{MoO}_3$. The inset shows the low-frequency response in detail.

In the absence of a simple theoretical model the response is usually analyzed phenomenologically in terms of a harmonic oscillator response,

$$\ddot{x} + (1/\tau)\dot{x} + \omega_0^2 x = (eE/m^*)\,\mathrm{e}^{\mathrm{i}\omega t}, \tag{11}$$

and the parameters m^*, ω_0 and the damping time τ can be extracted. m^*/m agrees with the mean field expression, eq. (5), and the pinning frequency is also in broad qualitative agreement with a value which is given by eq. (9) and (10), assuming reasonable values for the pinning potential, Fermi velocity, single-particle gap and residual impurity concentration.

The spectrum at lower frequencies is due to internal excitations of the collective mode, and in the lower radiofrequency spectral range, behaviors typical of glasses or spin glasses are found. The response to a step excitation is not exponential, and displays a behavior which is characteristic to glasses and other random systems. The behavior has also been modeled by introducing a quantum-mechanical treatment of the low-energy charge fluctuations. Such a treatment accounts excellently for many experimental data concerning the presence of combined DC and AC electric fields.

The small pinning energy associated with the collective mode suggests that for small DC electric fields the collective mode can be driven into a current carrying state by executing a translational motion. Indeed, nonlinear conductivity has been observed in all the materials discussed before, with a sharp onset field, the so-called threshold field $\boldsymbol{E}_\mathrm{T}$, for the nonlinear conductivity. The detailed form of the nonlinear conduction varies depending on external factors such as temperature, impurity concentrations, or macroscopic inhomogeneities (such as grain boundaries) in the specimen.

The DC conductivity, defined as $j/\boldsymbol{E}$, where j is the total current density and $\boldsymbol{E}$ is the applied electric field is shown in orthorhombic TaS_3 in fig. 2. The electric field is applied along the chain direction, along which the CDW is incommensurate with the underlying lattice. For directions perpendicular to the chains non-linear and frequency dependent effects do not occur. Below the threshold field $\boldsymbol{E}_\mathrm{T}$, approximately 300mV/cm for this specimen, the conductivity obeys Ohm's law, and the temperature dependence of this component reflects the exponential freezing out of the uncondensed electrons. The onset of nonlinear conduction is smooth as evidenced by the current-voltage characteristics also displayed in the figure. A behavior, similar to that displayed in fig. 2, is, in general, found for the other compounds, and the existence of the sharp threshold field $\boldsymbol{E}_\mathrm{T}$ in the bulk is now well-established. The behavior in the figure is sometimes

described in terms of a two-fluid model, involving electrons excited across the gap and electrons concerned in the collective mode, and the total current can be written as

$$I_{\text{total}} = I_{\text{n}} + I_{\text{CDW}}, \tag{12}$$

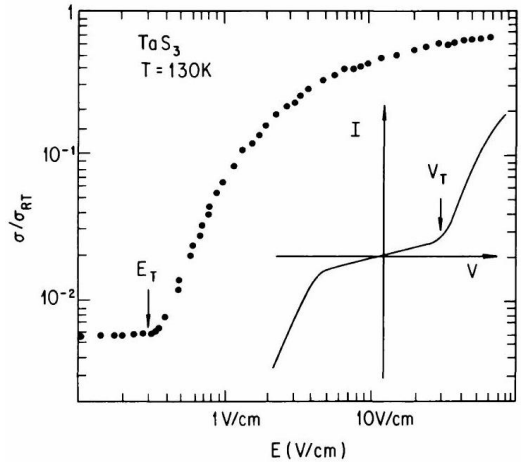


Fig. 2. Nonlinear conductivity $\sigma = j/E$, where j is the current density and E the applied electric field measured in TaS_3 in the charge density wave state. The inset shows the current-voltage characteristics.

where the subscripts n and CDW refer to current carried by the uncondensed and condensed electrons. This separation of the current, however, has no firm justification since mutual relaxation processes between the various electrons may be important. Direct evidence for the translational notion of the condensate comes from elegant nuclear magnetic resonance experiments, performed both on $NbSe_3$ and $K_{0.3}MoO_3$.

The onset of nonlinear conduction is often rather dramatic and is accompanied by switching and hysteresis effects, in particular in small specimens. These have been observed in $NbSe_3$, TaS_3, and $K_{0.3}MoO_3$; such effects usually become more pronounced with decreasing temperature. At higher temperatures, the onset of nonlinear conduction is accompanied by an oscillatory instability, which by lowering the temperature gradually evolves into a hysteretic current-voltage characteristic. This behavior is due to extended pinning centers in the materials, and this has been demonstrated directly by locating (by using moving contacts) the exact positions where such behavior is generated. At very low temperatures $T \ll T_{\text{P}}$, still a different type of nonlinearity, a rather steep current-voltage characteristic is observed with a threshold field one or two orders of magnitude larger than $\boldsymbol{E}_{\text{T}}$, where the smooth nonlinear conduction such as displayed in fig. 2 occurs. A typical current-voltage characteristic is displayed in fig. 3. This behavior most probably reflects the importance of Coulomb forces at low temperatures, they suppress the internal polarizations which can develop at high temperatures due to screening by normal electrons.

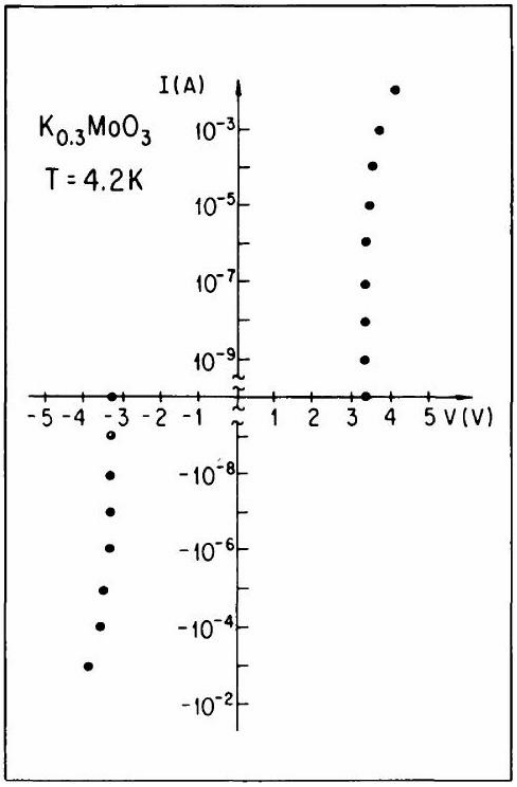


Fig. 3. Current-voltage characteristics measured in $\mathrm{K}\{0.3\}\ \mathrm{MoO}\{3\}$ at low temperatures. The threshold voltage corresponds to a threshold field of several volts per centimeter.

The observed field and frequency-dependent response is strongly related, and materials with smaller pinning frequency, or larger low-frequency dielectric constant lead to smaller threshold field $\boldsymbol{E}_{\mathrm{T}}$.

Perhaps the most spectacular observation in the field is the detection of current oscillations in the nonlinear conductivity region. The first experimental results of Fleming and Grimes, where the current oscillations were observed by employing a spectrum analyzer, are displayed in fig. 4. The sharp peaks in the observed spectral response indicate a periodic, nonsinusoidal contribution to the time-dependent current. This phenomenon, which has been studied both in the time and in the frequency domain, is often referred to as "narrow band noise". The term "noise" however, is misleading. Consequently, we refer to the phenomenon as current oscillations. The frequency of the oscillation is propotional to the curent carried by the collective mode, and normalizing to CDW current for one chain, the observations can be described as

$$\frac{j_{\mathrm{CDW}}}{f_0} = 2e\frac{n_{\mathrm{CDW}}(T)}{n_{\mathrm{CDW}}(0)}. \tag{13}$$

The above relation is associated with the fundamental periodicity of the phase ϕ. The CDW current, described in terms of the drift velocity $\boldsymbol{v}_{\mathrm{d}}$ of the (rigidly moving) condensate is given by $j_{\mathrm{CDW}} = n_{\mathrm{c}} e v_{\mathrm{d}}$. Associating the

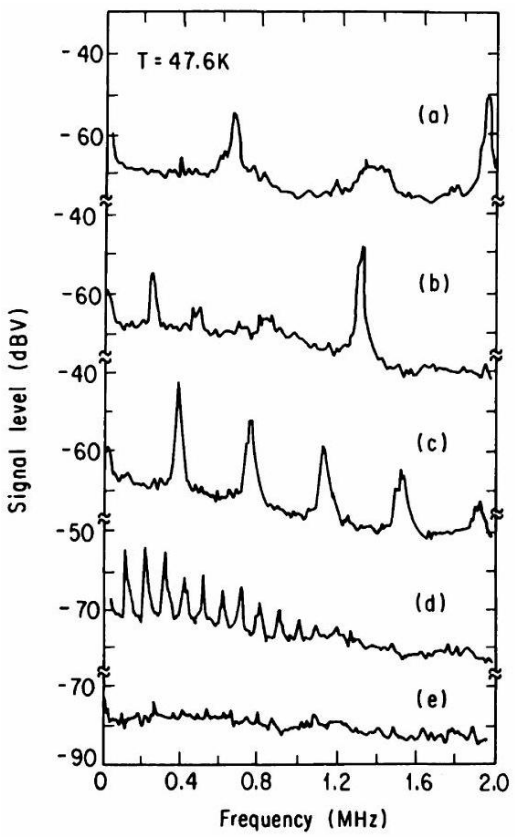


Fig. 4. Output of on-line spectrum analyzer for selected values of current. Increasing current from zero (e) to a value above threshold (d) results in an increase of broad-band noise plus a discrete frequency with numerous harmonics. The frequency increases with current and at higher currents (b) a second frequency appears. Currents and dc voltages (a) \$I=270 \mu \mathrm{˜A}\$, $V = 5.81$mV, (b) $I = 219\mu$ A, $V = 5.05$mV, (c) $I = 154\mu$ A, $V = 4.07$ V, (d) $I = 123\mu$ A, $V = 3.40$mV, (e) $I = V = 0$.

fundamental frequency with a CDW displacement by one period, $f_0 = v_\mathrm{d}/\lambda$, this then leads to

$$\frac{j_\mathrm{CDW}}{f_0} = n_c(T)e\lambda = 2e, \tag{14}$$

as $\lambda = \pi/k_\mathrm{F}$ and $n_c = 2k_\mathrm{F}/\pi$.

Several studies have been performed to establish the origin of the oscillating currents. It is by now clear, that current oscillations cannot be recovered in the thermodynamic infinite-volume limit, and that they are related to pinning effects. Evidence for both bulk and contact generated

oscillating currents were found, suggesting that various forms of defects can lead to current oscillation.

The oscillating current in the presence of a DC driving field is reminiscent of the AC Josephson effect, and a variety of experiments have been performed by examining various interference phenomena which arise in the presence of DC and AC fields. An oversimplified equation of motion

$$\ddot{x} + (1/\tau)\dot{x} + \omega_0^2 \sin 2k_\mathrm{F}x = eE/m^*, \quad E = E_\mathrm{DC} + E_\mathrm{AC}\cos\omega t \tag{15}$$

which is based on the assumption that the collective mode moves without distortion in a sinusoidal pinning potential, has been extensively used to account for many of the experimental

findings, including analogies to Shapiro steps, subharmonic steps, transitions to chaotic behavior, etc. More realistic models, based on the generation and dynamics of local deformations of the phase, vortex structures, etc., are also successful in describing a variety of observations.

While the current oscillations are indicative of a coherent CDW motion, the nonlinear conduction is also accompanied by a substantial broad band noise, with an effective noise temperature of several thousands degrees. This indicates that the dynamics of the internal degrees of freedom associated with the condensate are important.

4.1.5 5. Scope of the book and outstanding questions

This book summarizes the current state of affairs with the primary focus on the dynamics of the collective mode. While many features of the nonlinear and frequency dependent response are clearly established, there is a considerable controversy concerning the importance of dimensionality, and the relevance of one-dimensional models, the role of the internal deformations of the collective mode and classical versus quantum effects. These issues are discussed in depth in the various chapters in the book.

The reason why different models appear to be successful in interpreting different sets of experimental data, is most probably due to the complexity of pinning, and the broad variety of pinning centers. Because of this, different types of nonlinearities may occur, requiring different phenomenological equations of motion of the amplitude and phase of the condensate. The situation could be clarified only by systematic introduction of defects (both random and regular arrays) and by the study of their effect on the ω and $\boldsymbol{E}$ dependent response. Initial steps have recently been taken in this direction.

Relatively little is known about the behavior of parameters other than electrical conduction in the current carrying CDW state. For example, the description of the anomalous thermoelectric and elastic properties require,
most probably, microscopic models, and these models would also be needed to account for the damping which accompanies the nonlinear CDW conduction.
The universal features of the strongly nonlinear low-temperature response in materials where the gap develops along the entire Fermi surface have only recently emerged, and the phenomenon is related to the freezeout of normal carriers, which in turn enhances the long-range Coulomb forces. They may have a profound influence on the phason spectrum, and may establish long-range order even in the presence of random impurities. Also, in particular in pure specimens, the relaxation of momentum to the lattice due to Umklapp processes is reduced, leading to the possibility of various types of drag effects.

Relatively little is known about the various nonlinear excitations and "midgap" states which can arise as the consequence of the broken symmetry ground state or of impurities, and detailed optical studies, including photogeneration of carriers, will be required to establish the full optical spectrum in the spectral range between the collective mode and singleparticle response. This topic clearly requires the extension to higher dimensions of the concepts originally used for strictly one-dimensional situations, by including interchain interactions and interchain tunneling.

It is believed that the issues mentioned above will dominate the further development of the field.

This page intentionally left blank

4.2 Structural, Electronic Properties and Design of Quasi-One-Dimensional Inorganic Conductors by Schlenker

4.2.1 Introduction

There is an ever increasing need for new materials to support the growing theories, or illustrate new effects, in the field of low-dimensional conductors. Unfortunately the synthesis of low-dimensional solids can be difficult. It has to take into account many factors at the same time, some of these being largely conflicting. Among important factors are (i) a critical ionicity of the bonds allowing the structural type to be stable, (ii) the possible existence of polytypes, (iii) a redox competition between d cationic levels and sp anionic ones which may complicate the structures and give rise to instabilities, (iv) particular geometries, atomic distances, and electronic structures.

The transition metal chalcogenide families have provided most of the quasi-one-dimensional (1D) inorganic conductors showing charge density wave (CDW) instabilities and non-linear transport due to the sliding of CDW . Among them, $NbSe_3$ has an historical importance since it gave rise to the first experimental evidence for CDW transport. Since then, it has been the object of extensive studies. Later on, it was established that, among the families of the transition metal oxide bronzes, several compounds, such as the molybdenum blue bronze $K_{0.30}MoO_3$, are also lowdimensional conductors. Since comparatively large single crystals of the blue bronze could be grown, most of its physical properties have been studied. Also it is in the low temperature CDW state of the blue bronze, that extremely high velocities of the CDW (> 1 m/s) have now been observed. This may be related to the mechanism of Fröhlich superconductivity predicted long ago for CDW materials and should stimulate further work in quasi-1D conductors.

The interest in low-dimensional conductors lies in the anisotropy of the Fermi surface which, associated with some electron-phonon coupling, leads to instabilities of the Peierls type. Opening of energy gaps at the Fermi surface will decrease the electronic energy. If this decrease takes over the energy increase associated with the coupled lattice distortion, the so-called Peierls distorted state will be favored; this takes place below the Peierls critical temperature T_p. In the low temperature state, the modulation of the electron gas density or charge density wave coexists with the lattice
distortion. In ideal one-dimensional conductors, the Fermi surface is made of two parallel planes and the gap opening is expected to be complete, thus leading to a semiconducting CDW state. The situation is more complex in real materials. However, an important parameter governing the lowdimensional electronic properties is the transverse coupling between chains in the 1D case or between slabs in the 2D one. This depends critically on the crystal structure and chemistry of the compounds.

The van der Waals gap that separates slabs or fibers in low-dimensional solids has, on each side, atomic layers of the same nature, usually anionic layers. For a given structural type to be stable, it is necessary that the bonding through the van der Waals gap, however always weak, is sufficiently strong to maintain the structure against slab to slab coulombic repulsions. The more ionic the bonding inside a slab, the more important the slab to slab separation and, hence, the low-dimensional character. Such an evolution which associates the strongest 1D character to the most ionic chains places, of course, a limit on the stability of the overall structure. It can be said that the limit of low dimensionality is the intrinsic instability that it generates. There lies the difficulty of synthesis which can rely only on qualitative approaches. In addition the increased tendency of slabs or fibers to behave independently when the low-dimensional character increases leads possibly to polytypic species (which exist for example for TaS_3, more ionic, and not for $NbSe_3$).

In the case of oxides the repulsion is quite strong and very destabilizing and consequently

most of the MO_2 oxides have the rutile or fluorine structures and not the layered forms of the parent MS_2 chalcogenides. Layered oxides however can exist. They will be found for the highest oxidation states of transition metals because, in that case, the strong polarization of the oxygen electrons towards the inside of the slabs or fibers will largely decrease the repulsions (MoO_3 and V_2O_5 are examples of that situation). The structures can also be stabilized by counter-cations which will separate the slabs and, hence, minimize the repulsions, while introducing at the same time a stabilizing Madelung energy. This energy increases with the size of the counter-cation, and structures unstable by themselves and unknown with small alkali metals may become stable for the bigger ones. This is typically the case of transition metal bronzes such as $K_{0.30}MoO_3$. Interesting is also the fact that when slabs or fibers are to be built by mixed polyhedra, the most covalent ones are forming the outer layers. Tetrahedra will form the outer layers of mixed-polyhedra slabs or fibers.

Between the largely ionic oxides and the quasi-metallic, but usually tridimensional, tellurides, sulfides and selenides represent the best domain in chemistry where to design low-dimensional materials. But now, this evolution in the direction of sulfides or selenides brings new problems which
arise from a redox competition between d cationic levels and sp anionic levels as can be easily understood when looking at the usual and general band scheme for transition metal chalcogenides (fig. 1). It is well-known that between a valence band essentially sp anionic in character and antibonding levels mostly formed from the corresponding cationic levels, the d orbitals of the metal, split by the crystal field play an essential role

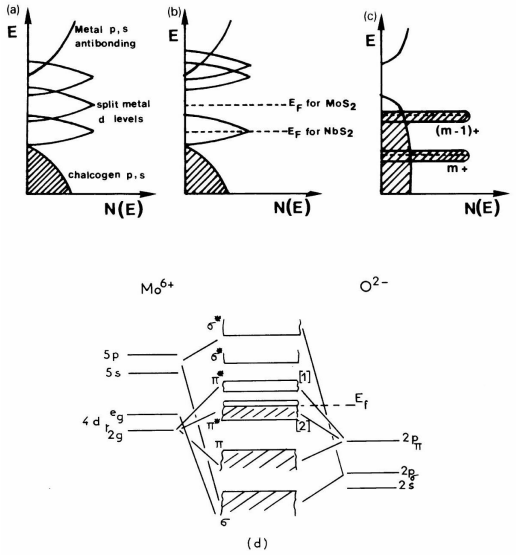


Fig. 1. Simplified band scheme for transition metal chalcogenides: (a) general, (b) half-filled d_{z^2} band in NbS_2 and filled in MoS_2, (c) situation at the end of a period. (d) Molybdenum blue bronze $K_{0.30}MoO_3$. The atomic levels of Mo^{6+} and O^{2-} are also shown. The antibondings π^* bands have a predominantly d character. They are split by the crystal.

concerning the physical properties, and also the behavior towards intercalation reactions. But the position of these d levels also governs redox processes inside the structure itself, which may induce drastic structural modifications. In front of sulfur a maximum cationic oxidation state of four is generally observed leading to $d^{(0)}$ configuration and no electronic conductivity in the case of IV A elements dichalcogenides with octahedral symmetry and a broad t_{2g} band. A d^1 configuration in the case of Nb and Ta is responsible for a stabilization through a lowering of the symmetry to a trigonal prismatic situation, with a half-filled d_{z^2} (a_1') band and a metallic

behavior. Immediately after, with a d^2 configuration and same symmetry, MoS_2 and WS_2 are semiconductors. Going further to the right one should come back to octahedral symmetry with half-filled t_{2g} band. But the expansion of the d levels decreases, reducing the chance of overlapping. Still more important is the fact that the d levels are progressively lowered and at a certain point will enter the sp anionic valence band. If a filled d level enters the valence band there is no drastic change in the properties. But if an empty d level is in this situation, it will fill up at the expense of the valence band at the top of which holes appear. Chemically speaking it means that the cation is reduced and the anion oxidized under the form of a polyanion. This is the case upon reduction of Fe^{3+} to Fe^{2+} in pyrite or marcasite with the occurrence of $(S_2)^{2-}$ pairs. This redox competition between cationic and anionic species will still become more important on going from sulfides to selenides, the top of the valence band being at a higher level. The very complex structure of $NbSe_3$ directly reflects that competition with three different chains corresponds to three different levels in the electronic exchange.

The geometry of low-dimensional chalcogenides with a surrounding of metal atom layers or rows by the non-metal element implies MX_n formulations with a rather high value of n, and going from 2D to 1D dimensionality will still increase the value of n. Up to now chain-like chalcogenides are associated to MX_3, MX_4, MX_5 formulations. However, partial or infinite condensation of polyhedra in a given chain, association of different chains and stabilization by counter-ions, considerably enlarge the description that can be given for one-dimensional chalcogenides.

The molybdenum blue bronze may be described with a band structure analogous to that of the chalcogenides. In this case, one may start from the electronic states of a MoO_3 oxide with empty antibonding hybridized $p-d$ states (fig. 1d). Since one expects a strong ionic character in $K_{0.30}MoO_3$, one assumes a complete charge transfer from the monovalent metal towards the antibonding conduction band. The filling of the conduction band can then be completely predicted and compared to various experimental data as will be discussed in section 8 .

4.2.2 1. Transition metal trichalcogenides

The quasi 1D transition metal trichalcogenides are built up from a chalcogen trigonal prismatic frame surrounding a metallic chain. Irregular MX_6 trigonal prisms are stacked on top of each other to form MX_3 chains which usually run parallel to the b axis of a monoclinic unit cell (fig. 2). The b parameter is therefore directly related to the metal-metal distance and eventually reflects, through a doubling of its value for example, the existence of any superstructure due to metal-metal pairing along the chains. Two other structural features are of importance (i) neighboring chains are translated by $b/2$, (ii) the prisms are irregular due to the presence of a chalcogen-chalcogen pair.

The former point allows a bonding between one metal atom and chalcogen atoms belonging to neighboring chains. Actually the coordination of the metal will be described as bicapped trigonal prismatic. In connection with the ionicity of the structure, such lateral bonds may be rather strong and imply a description of the structures in terms of two-dimensional zig-zag arrangements of MX_3 chains (fig. 3). The real dimensionality of trichacolgenides is fixed by this lateral coupling. Interactions between chains can be investigated through Raman or infrared studies. The strength of interchain M-X bonds appears to be a substantial fraction (0.15 to 0.28) of that of the intrachain M-X bond (Levy and Grisel 1985, Wieting et al. 1982, Zwick et al. 1982, 1980, Izumi et al. 1981).

The latter point allows to assign the general formulation $M^{4+}(S_2)^{2-}S^{2-}$ to

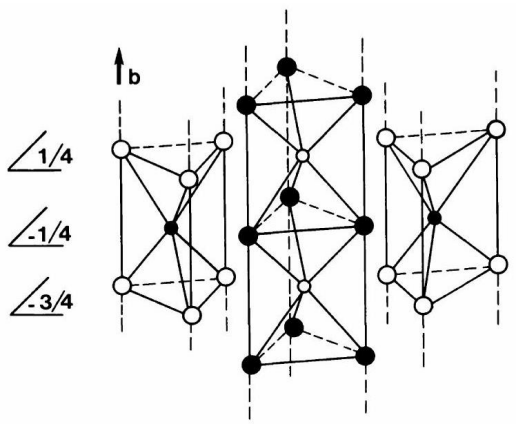


Fig. 2. MX_{3} chains running along the b monoclinic axis, two neighboring chains being displaced by $b/2$.

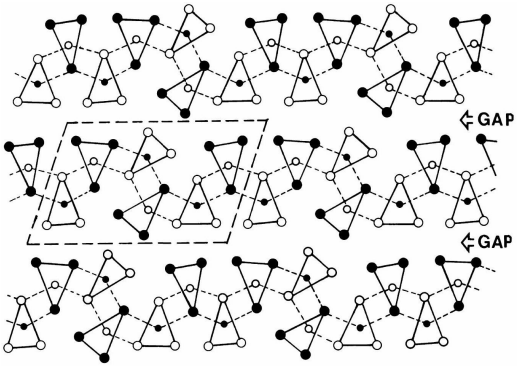


Fig. 3. Slabs made up from zig-zag arrangements of MX_{3} chains, after a projection of the $NbSe_3$ structure along [010] (cross section perpendicular to the chains).

these compounds. But things can be much more complicated due to the possible length change of the pair as a consequence of the already mentioned redox competition between cationic d levels and the top of the sp anionic valence band. A longer pair means that its antibonding states have been partially populated at the expense of the electronic density along the metallic chain. The chalcogen pair behaves as an electron reservoir which takes or gives less or more electrons to the adjacent metallic chain and governs its properties. From a structural point of view the existence of various chains directly reflects in the a and c unit cell parameters. Transition metal trichalcogenides are essentially represented by the derivatives of group IV A and V A elements (amorphous MoS_3, and WS_3 will be briefly discussed in section 1.5). They are prepared by direct combination of the elements in evacuated silica tubes at temperatures ranging from 500 to 700°C. At higher temperatures, they decompose to dichalcogenides. Needle shaped crystals or a cottonous mass of filamentary crystals ($NbSe_3$) are obtained. Crystal growth can be successfully tempted with a slight excess of

Table 1 Unit cell dimensions for $\mathbf{M X}_{\mathbf{3}}$ compounds

Compounds	a(Å)	b(Å)	c(Å)	$\boldsymbol{\beta}°$	Symmetry	Ref.
TiS_3	4.958	3.4006	8.778	97.32	Monoclinic	Furuseth et al. (1975)
ZrS_3	5.1243	3.6244	8.980	97.28	Monoclinic	Furuseth et al. (1975)
$ZrSe_3$	5.4109	3.7488	9.444	97.48	Monoclinic	Furuseth et al. (1975)
$ZrTe_3$	5.8939	3.9259	10.100	97.82	Monoclinic	Furuseth et al. (1975)
HfS_3	5.0923	3.5952	8.967	97.38	Monoclinic	Furuseth et al. (1975)
$HfSe_3$	5.388	3.7216	9.428	97.78	Monoclinic	Furuseth et al. (1975)
$HfTe_3$	5.879	3.9022	10.056	97.98	Monoclinic	
NbS_3	4.963	2×3.365	9.144	97.17	Triclinic ($\alpha = \gamma = 90°$)	Rijnsdorp and Jellinek (1
$NbSe_3$	10.006	3.478	15.626	109.30	Monoclinic	Meerschaut and Rouxel (
TaS_3	36.804	3.340	15.173		Orthorhombic	Bjerkelund and Kjekshus
TaS_3	9.515	3.3412	14.912	109.99	Monoclinic	Meerschaut et al. (1979)
$TaSe_3$	10.402	3.495	9.829	106.26	Monoclinic	Bjerkelund and Kjekshus

chalcogen, some bromine or iodine (Lieth and Torhell 1977). But the excess of chalcogen may favor the formation of a different form if there are polytypes (see below, the case of NbS_3), and iodine will lead to $(NbSe_4)_n I$ or $(TaSe_4)_n I$ phases in the cases of $NbSe_3$ and $TaSe_3$. When apparently nice big single crystals are obtained they often reveal to be aggregates of single crystals with a preferential orientation (b axis). Nevertheless they may allow some interesting NMR, neutron or vibrational studies.

Table 1 gives the unit cell dimension of MX_3 compounds. Three main structural arrangements exemplified by $ZrSe_3, TaSe_3$ and $NbSe_3$ are found. They correspond to an increased complexity of the structures with respectively one, two and three, different chains in the unit cell, each of them being repeated twice (fig. 4).

1.1. One type of chains

All the trichalcogenides of IV A transition metals ($M = \mathrm{Ti, Zr, Hf; X = S, Se, Te}$) can be described on the basis of variant A or variant B structural types of $ZrSe_3$ (Kröniert and Plieth 1965, Furuseth et al. 1975). Each unit cell contains only one type of chain with a true chalcogen pair ($d_{(\mathrm{Se\text{-}Se})} \approx 2.34\text{Å}, d_{(\mathrm{S-S})} \approx 2.04 - 2.09\text{Å}$). This chain is repeated twice. There are two main differences between variant A (Kröniert and Plieth 1965) and variant

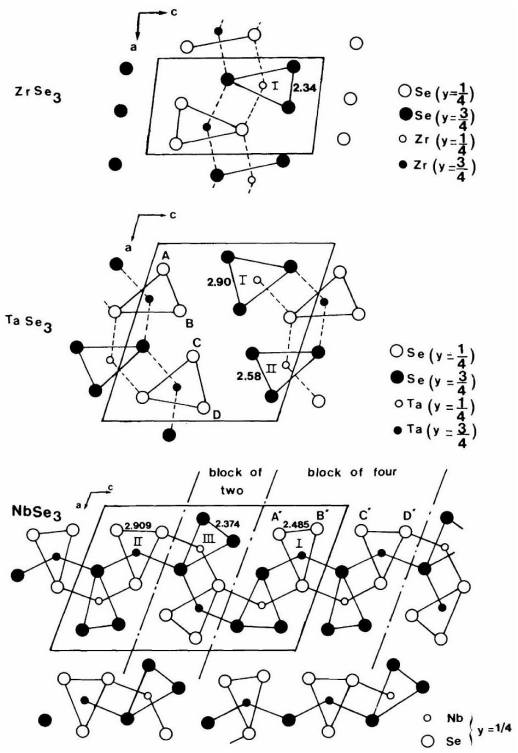


Fig. 4. One, two and three types of chains in the structures of $\mathrm{ZrSe}*{3}*, *mathrm{TaSe}*{3}$ and $NbSe_3$ (projections along [010]).

B (Furuseth et al. 1975) (fig. 5), (i) the shape of the triangular base is closer to an isosceles triangle in type A than in type B, (ii) the two interchain $M \ldots X$ distances are equivalent in variant A, while two inequivalent M...X distances exist in variant B. TiS_3 (Furuseth et al. 1975) belongs to B type and ZrS_3 (Furuseth et al. 1975) to A type. The presence of a true chalcogen pair in the basis of the prisms corresponds to a M^{4+} oxidation of

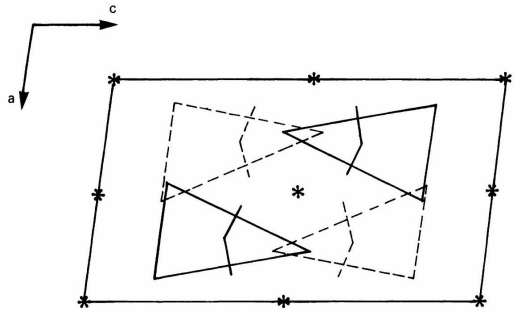


Fig. 5. Variant A (solid lines) and variant B (dashed lines) of ZrSe_{3}.

the metal (d^0 configuration). These chalcogenides are diamagnetic semiconductors. NbS_3 (Rijnsdorp and Jellinek 1978) presents also one type of chain in the unit cell with a true $(S_2)^{2-}$ pair ($d_{(S-S)} = 2.05$Å). However the d^1 configuration of Nb^{4+} does not lead to a metallic behavior due to the formation of Nb − Nb pairs along the chains, which results in an alternation of short (3.037Å) and long (3.693Å)Nb − Nb distances. The Nb − Nb pairing and the associated $2b$ superstructure illustrate a Peierls distortion. Upon heating it was not possible to reach the transition towards a metallic state before NbS_3 decomposes. However, Cornelissens et al. (1978), by heating the crystals in the electron microscope, were able to

observe pretransitional effects associated to a de-correlation of chains and manifested by a vanishing of the $2b$ superstructure spots into streaks.

In fact, concerning niobium trisulfide, the situation is rather complex and additional work is needed. In the course of the above studies a new type of NbS_3 called type II was found (Cornelissens et al. 1978, Boswell and Prodan 1980). Roucau et al. (1983) have shown the unit cell to be monoclinic with $a' = 2a, b' = b/2, c' = 2c, \beta' = \beta (a, b, c, \beta$ being type I parameters as shown in table 1). The disappearance of the pairing along the b axis (chain direction) and the doubling of the lattice parameters in the (a, c) plane, strongly suggests similarity with $NbSe_3$ as described below. The resistivity changes from 80Ω cm for NbS_3 type I to $8 \times 10^{-2}\Omega$ cm for NbS_3 type II, at room temperature. NbS_3 type II undergoes a Peierls transition at 330 K .

Superlattice spots appear as doublets near $\pm b^*/3$. Recent measurements by Wang et al. (1989) have led to different values of the corresponding q vectors than those reported previously (Cornelissens et al. 1978, Boswell and Prodan 1980). These values are: $\boldsymbol{q}_1\,(0.5\boldsymbol{a}^*, 0.298\boldsymbol{b}^*, 0\boldsymbol{c}^*)$ and $\boldsymbol{q}_2\,(0.5\boldsymbol{a}^*,\ 0.352\boldsymbol{b}^*, 0\boldsymbol{c}^*)$. When heating the samples q_1 spots progressively decrease in intensity and disappear at 340 K which means that $\boldsymbol{q}_1$ distortion is related to the transition observed in resistivity measurements. The origin of $\boldsymbol{q}_2$ is not clear. Anyway the doublet is probably related to different transitions.

The thermally activated conductivity (Haen et al. 1978) of NbS_3 type I with the $2b$ superstructure ($E_{ac} = 0.44$eV), could be changed into a metallic behavior when applying a pressure in order to suppress the $Nb - Nb$ alternation of bonds along the chain. A high pressure form of NbS_3 has indeed been reported (Kikhawa et al. 1982) with a monoclinic unit cell $\left(a = 9.68\text{Å}, b = 3.37\text{Å}, c = 14.83\text{Å}, \beta = 103.9^\circ\right)$. The $2b$ superstructure has disappeared but a semiconducting type of behavior is maintained, although the activation energy is reduced to 0.18 eV .

It is likely that there are still more types of NbS_3. Izumi et al. (1983) obtained metallic crystals with a wide range of homogeneity around the composition NbS_3. These undergo a superconducting transition at around 2 K . Another phase with approximate composition ($NbS_{3.5-4}$), occurring in two forms, is also mentioned. The first type of this sulfur-rich phase is a semiconductor with an anomaly at 140 K . The second type presents two successive anomalies at 140 and 235 K . A report by Zettl et al. (1978) of a new NbS_3 (named type III) may concern a phase similar to the sulfur-rich first type of phase. Further chemical and structural characterizations are needed to ensure that we are really dealing with new forms of NbS_3. It is rather difficult to consider that the NbS_3 structural type would allow a large non-stoichiometry. However extra cations or chalcogen bridges are both possible between chains and will respectively increase, or decrease, the metal versus chalcogen ratio. The X-ray powder data of the Zettl phase (NbS_3 type III) suggest a c axis similar to the c axis of NbS_3 type I, the a axis seems also to be similar but the monoclinic angle is increased to $98-99^\circ$. This suggests similar NbS_3 chains but with a different relative arrangement or separated by some chemical intercalant. Figure 6 shows the low field dc conductivity versus $10^3/T$. A broad peak in the derivative curve (see inset) is observed at 155 K . It is associated to a CDW which would condense all the electrons (semiconducting state below 150 K). Diffuse lines observed at room temperature lead to sharp spots on cooling but the components of the q vector associated to the CDW are not given. Depinning of the CDW has also been made above a threshold field of about 20 V/cm, i.e., one order of magnitude more than for o- TaS_3 which has a behavior allowing a good comparison (metal to non-metal transition at 210 K with important pretransitional effects). The higher threshold field is

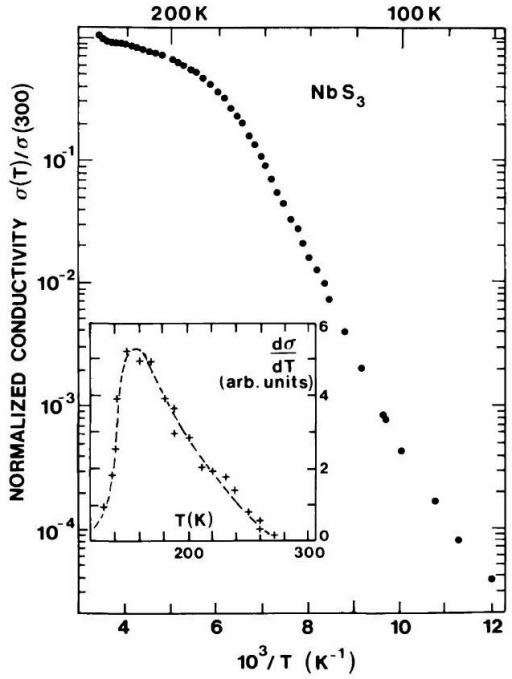


Fig. 6. Low field dc conductivity versus $10^{3} / T$ for NbS_3 type III.

associated to the presence of chemical impurities, which could support the non-stoichiometry inferred from the X-ray parameters.

1.2. Two types of chains

The above trichalcogenides show true chalcogen-chalcogen pairs as far as their structural determination was made. $TaSe_3$ has two groups of two types of chains in its monoclinic unit cell (Bjerkelund et al. 1966). The Se-Se bond lengths are respectively 2.576 and 2.896Å, both these values exceeding the normal bond length of a $Se - Se$ pair (fig. 4). One can recognize quasi-linear Se_4 groups (A-B-C-D) with successive Se-Se separations of 2.576Å (A-B), 2.653Å (B-C) and 2.896Å (C-D). The B-C bridge of 2.653Å determines a coupling of the two types of chains to form blocks of four $TaSe_3$ units.
$TaSe_3$ is metallic without any anomaly in the resistivity curve down to 4.2 K (Sambongi et al. 1977, Yamaya et al. 1979). No structural transition associated to the onset of the CDW has been observed. However resistivity anomalies have been found in the vicinity of a superconductive transition at 2 K (see for example Haen et al. 1978, Tajima and Yamaya 1984). This behavior has been associated (Tajima and Yamaya 1984) with the superconducting state itself rather than with other phase transitions such as CDW or SDW. The temperature onset is not affected by the change in current density (fig. 7).

A high pressure form of $TaSe_3$ apparently very similar to $NbSe_3$ ($a = 10.02$Å$, b = 3.48$Å$, c = 15.65$Å$, \beta = 109.6°$) has been prepared by Kikkawa et al. (1982) along with a non-stoichiometric form $TaSe_{2.80}$. The former has the same electrical behavior as the 'normal' $TaSe_3$. Once more precise structural and chemical determinations are needed. The non-stoichiometric form has not been prepared as a pure single phase (is it $TaSe_{3-y}$ or $Ta_{1+x}Se_3$?)
$Ta\,(Se_{1-x}\,S_x)_3$ samples, with $0 < x < 0.15$, have been studied by Yamaya and Abe (1982). The electrical resistivity changes gradually from a metallic to a semiconducting behavior and the superconducting transition disappears as sulfur concentration increases. Diffuse lines perpendicular to the b^* axis have been observed at $x = 0.15$ above 150 K and suggest the possible existence of a CDW in that case.

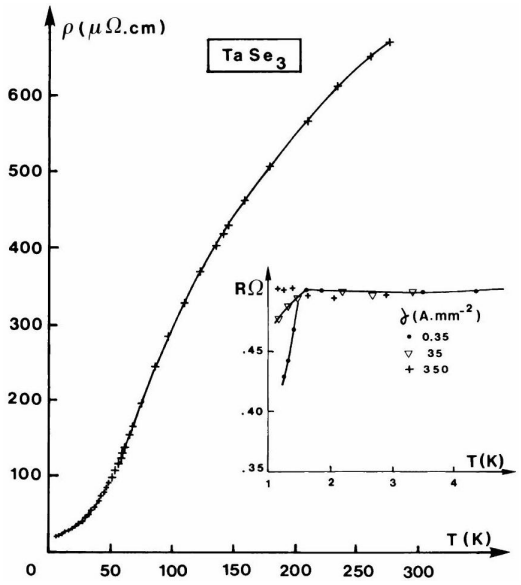


Fig. 7. Resistivity of TaSe_{3} as a function of temperature.

1.3. Three types of chains: niobium triselenide

$NbSe_3$ represents the most important compound as well as the most complicated structure (Meerschaut and Rouxel 1975, Hodeau et al. 1978). Three different chains, each being repeated twice (fig. 4), are found in the monoclinic unit cell (table 1), according to three different values taken by the $Se-Se$ bond length in their triangular basis (respectively 2.37, 2.48, 2.91Å). As usual, neighboring chains are displaced by $\boldsymbol{b}/2$: the first one corresponds to a true $(Se_2)^{2-}$ pair and reflects the situation $Nb^{4+}\,(Se_2)^{2-}\,Se^{2-}$. The longest distances in the two others mean that we have started to populate the antibonding level of the $(Se_2)^{2-}$ pair. Less than one electron per atom is left in the 2.48Å chain and probably none in the 2.91Å chain. This electronic exchange between the metallic chain and the chalcogen pair is the consequence of that redox competition already mentioned above. It can be illustrated by molecular orbital diagrams as built up by Hoffmann et al. (1980) in the two extreme cases of symmetry for a ($NbSe_6$) prism, i.e., $D_{3\,h}$ symmetry corresponding to a regular prism with an equilateral basis and no chalcogen pair, and C_{2v} symmetry associated to the isosceles situation brought by the presence of a $(Se_2)^{2-}$ pair. With the $D_{3\,h}$ symmetry (fig. 8) we have the classical splitting of the d orbitals with $a_1'\,(d_{z^2})$ and then $e'\,(d_{xy},\ d_{x^2-y^2})$ below $e''\,(d_{xz},\ d_{yz})$. The highest orbital set, e″, derived from the six selenium atoms is above a block of filled Se levels. The electronic situation of $[NbSe_6]^{6-}$ corresponds there to Nb^{5+} with all d levels being empty, and a hole in the Se e" levels. The distortion to C_{2v} symmetry illustrates the formation of a $Se-Se$ bond, with a stabilized $Se-Se$ bonding level and a destabilized antibonding Se-Se level. Now, one electron occupies the a_1' level of a cation reduced at the 4^+oxidation state. The 2.37Å chain reflects the latter situation. The 2.91Å is an insulating chain with Nb^{5+}, d^0 configuration. The 2.48Å chain represents an intermediate situation. Of course the extension of the calculations to the overall band structure of $NbSe_3$ will change this first approach, particularly because $NbSe_3$ with strong lateral bonds is not purely 1D. But this scheme shows nicely the complexity of things.

The arrangement of $NbSe_3$ chains with respect to each other in the unit cell reminds us of both the $TaSe_3$ and $ZrSe_3$ structures. Blocks of four chains similar to those of $TaSe_3$ are separated by groups of two chains of the $ZrSe_3$ type (fig. 4). In the four chain blocks, Se atoms form quasi-linear Se_4 units $A'B'C'D'(Se-Se = 2.48, 2.73$ and $2.91Å)$ as in $TaSe_3$. But instead of being repeated through an inversion center at ($0, 1/2, 1/2$), the four-chain group in $NbSe_3$ is interrupted by the two chains unit. The surface separating these blocks is parallel to the (

a, b) plane which explains the easy cleavage of the crystals parallel to this plane as well as to the (b, c) plane of the slabs.

The two charge density waves (Haen et al. 1975, Chaussy et al. 1976,

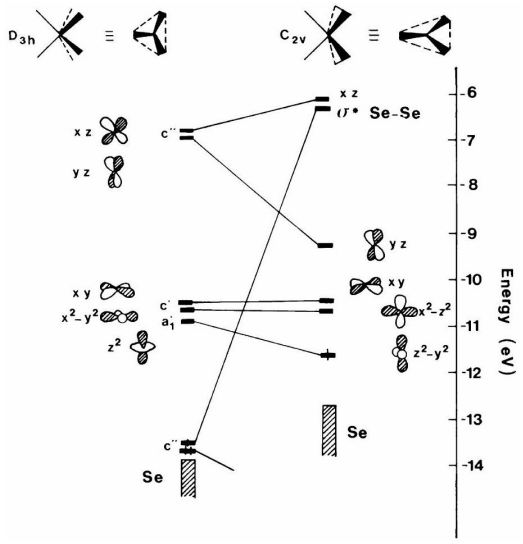


Fig. 8. The electronic structure of $\left(\mathrm{NbSe}_{6}\right)^{6-}$ in D_{3h} and C_{2v} geometries.

Ong and Brill 1978) in $NbSe_3$ ($T_c = 145$ and 59 K , as shown in fig. 9), occur in the two first types of chains (Wilson 1979). The third chain being very likely an insulating one. Electron diffraction studies, band calculations and also chemical developments, as we shall see later on, support this interpretation. Tsutsumi et al. (1977) and Hodeau et al. (1978) have determined the following components of the two wave vectors: at T_1(145 K), $\boldsymbol{q}_1(0, 0.243(3), 0)$, at T_2(59 K), $\boldsymbol{q}_1(0, 0.241(3), 0)$ and $\boldsymbol{q}_2(1/2, 0.259(3), 1/2)$.

It suggests indeed that the first distortion can be seated in the [2.37Å] chain which forms sheets parallel to the a axis. The second distortion could be present in the [2.48Å] chain since it forms sheets parallel to the [101] orientation. Calculations of the $2k_F$ values along the b axis and the analysis of the band orbital character at the Fermi level support these conclusions (Whangbo and Gressier 1984).

A charge density wave is a coupled modulation of both the conduction electron density and the lattice. The cost in elastic energy, due to the distortion of the lattice, is overcome by a gain in electronic energy in connection with the opening of gaps in the Fermi surface. Applying a

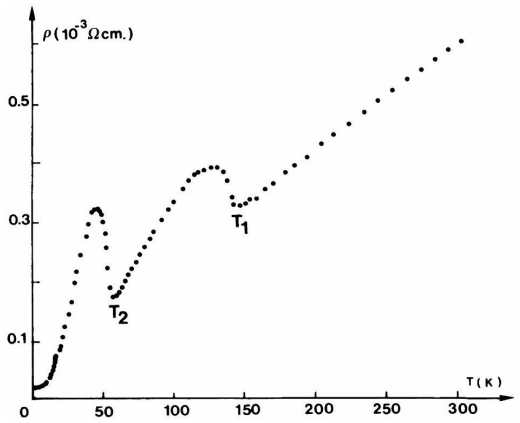


Fig. 9. The two charge density waves in NbSe_{3} (145 and 59 K) as manifested by resistivity measurements.

pressure increases the former term. The CDW will remain stable to the extent that the gain in electronic energy will exceed the new cost in elastic energy to be associated with the atomic displacements. Therefore the onset temperatures T_1 and T_2 should move towards lower temperatures which is, indeed, observed as shown in fig. 10 (Briggs et al. 1980). A similar study was done previously in the case of dichalcogenides by Delaplace et al. (1976). It was found that the T_c superconducting temperature was raised in temperature at the same time the CDW was progressively suppressed by the pressure effect. This is what is also observed (fig.11) in the case of $NbSe_3$ (Briggs et al. 1980). The mechanisms of the interplay of superconductivity enhancement and CDW suppression in $NbSe_3$ under pressure, or through doping by tantalum has been investigated by measurements of the ^{93}Nb spin-lattice relaxation time by Wada et al. (1987). In spite of an important increase of the temperature of the superconducting transition a significant decrease of density of states was found at the Fermi level. This unexpected result is interpreted as the recovery of the density of states at the bottom of the CDW gap near E_F within the CDW chains by the collapse of the gap with increasing pressure. Another mechanism, which works in the case of Ta doping as well as for the pressure experiments, originates in the peaks of DOS near the CDW gap edge within the BCS cut-off interval of the Debye energy. These peaks are raised when reducing the CDW gap width.

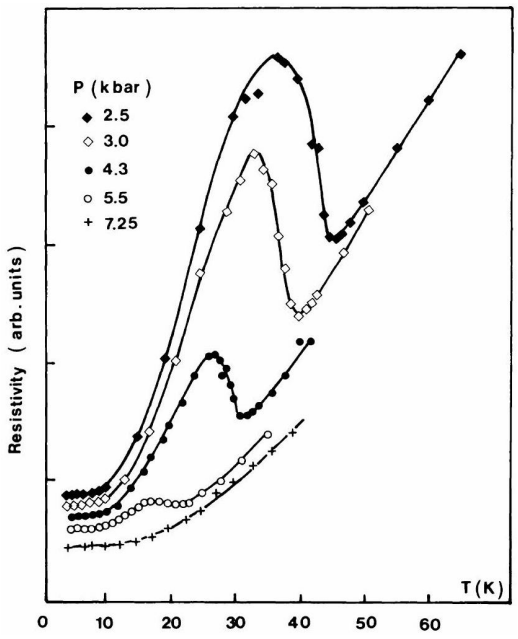


Fig. 10. Resistivity as a function of temperature at different pressures for the second anomaly ($T_{0}=59 \mathrm{˜K}$).

Hall effect measurements have been made as a function of temperature to depict the change in carriers at the transition. As mentioned by Ong and Monceau (1978) the sign of $R_{\mathbf{H}}(0)$ changes at 15 K (from p-type to n-type as T is increased). At both transitions, $R_{\mathbf{H}}(0)$ increases abruptly indicating a loss of carriers. This is well in connection with the opening of gaps at the Fermi surface when CDWs take place. But the sharp increase of $\boldsymbol{R}_{\mathbf{H}}(0)$ at both transitions is too large to be explained by a change in carriers only. A change in the mobility anisotropies is likely to occur simultaneously as an expected consequence of the appearance of a superlattice.

The measurements of the thermal properties give more accurate indications about the changes in carriers concentrations. Specific heat measurements by Tomic et al. (1981) are represented in fig. 12. They show the C_p variation as a function of temperature. Two anomalies are observed at 145 and 59 K . The total change in entropy at the transitions is estimated

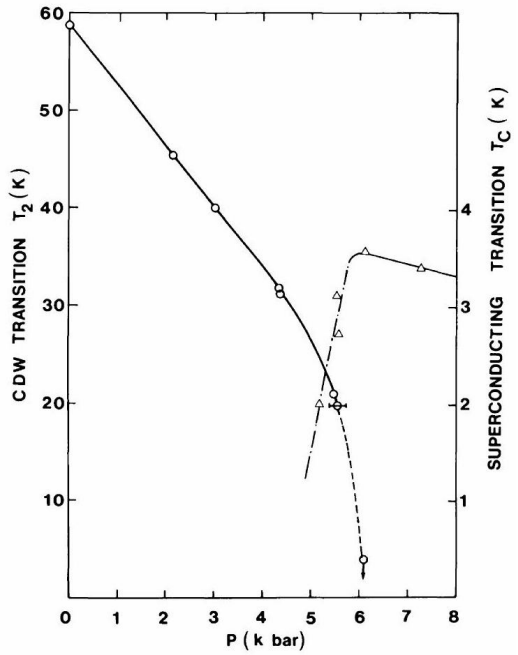


Fig. 11. Pressure effect on T_{2} CDW transition and the superconducting transition of $NbSe_3$.

from the areas under the peaks. It was found to be $\Delta S \approx 0.01 R_0$ at 145 K and $0.005 R_0$ at 59 K (R_0 is the value of the gas constant). On the other hand, the total conduction electron entropy at T_c (γT_c) calculated in R_0 units from densities of states given by Bullett (1979) is equal to 0.04 at 145 K and 0.016 at 59 K . This leads to an estimation that about 25% of the conduction electrons are condensed at T_1 and about 30% at T_2. From transport measurements in the non-ohmic regime, Ong and Monceau (1978) deduced that about 20% of the Fermi surface is destroyed at T_1 and 60% of the remaining area at T_2.

The role of chemical impurities or irradiation defects on the electrical properties has been extensively studied in the case of $NbSe_3$, essentially in connection with the pinning mechanism of the CDW. Doping has been achieved (Tagaki et al. 1978, Brill et al. 1981, Monceau 1982, Hsieh et al. 1983, Yamaya and Abe 1982, Nunez-Regueiro 1980) by substituting niobium atoms either by elements of the same column (Ta) or by other transition elements (Ti, Zr essentially). A sulfur-selenium exchange has also been considered. It has to be noticed that even in the case of substitution of

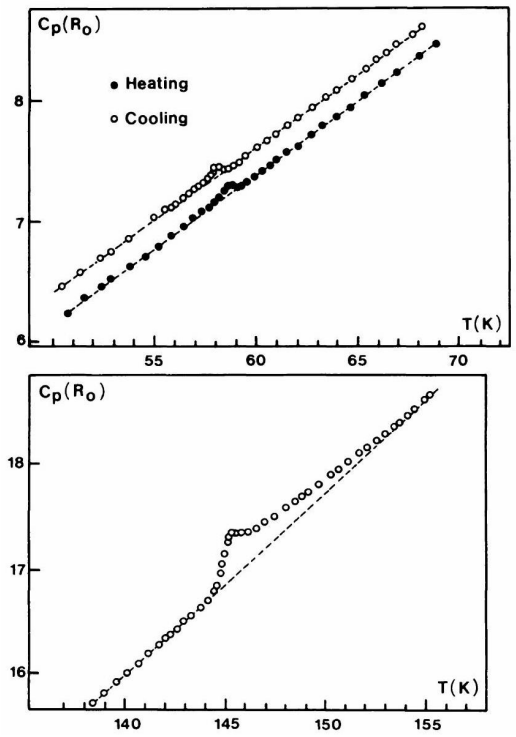
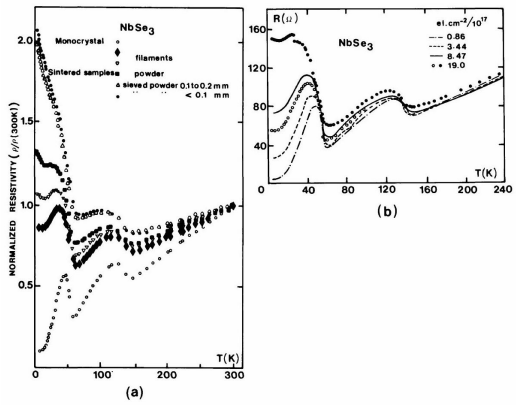


Fig. 12. Specific heat measurements around the two transitions.

niobium by tantalum (same column), a variation of the metal-chalcogen distances inside the prisms will lead to a small local change of charge. A common feature among the resistivity curves for samples containing chemical impurities, irradiation defects or sintered polycrystals is that the resistivity increases sharply at lower temperatures (figs. 13a and b). A similar behavior is found for $NbSe_3$ samples prepared under pressure (Kikkawa et al. 1982). Besides a residual impurity effect, these features have to be associated with a shortening of the length of the conducting chains, since a similar feature is observed when the conductivity is measured on samples made of small grains (Briggs et al. 1981).

Substitution of selenium for sulfur in $Ta\,(S_x\ S_{1-x})_3$ samples shows a



(a)

Fig. 13. Normalized resistivity versus temperature for sintered samples (a) and irradiated samples (b) of NbSe_{3}.

semiconducting behavior when $x > 0.06$. A Peierls transition seems to occur around 70 K in the same series when $x = 0.15$, as suggested by the observation of diffuse lines (Yamaya and

Abe 1982). Doping $NbSe_3$ with group IV elements affects noticeably the T_1 and T_2 transition temperatures. For example 500 ppm of Ti decreases T_1 by 9 K and T_2 by 11 K (NunezRegueiro 1980). A superconducting transition at 2 K has been observed in $NbSe_3$ samples doped with Ta, Zr or Ti .

Irradiation is probably a more reliable technique to create defects and disorder in trichalcogenides. The concentration of chemical impurities introduced in MX_3 phases is very weak. It is difficult to characterize the structural localization of the impurities as well as their real concentration (which is a great difference as compared with dichalcogenides). In contrast, the irradiation technique creates, at low irradiation doses, a number of defects which is proportional to the dose. High energy electrons (3 MeV) create in $NbSe_3$ stable defects which are displaced transition metal atoms and the associated vacancies. Figure 13b shows that the T_1 and T_2 temperature are not affected when $NbSe_3$ samples are irradiated with doses
up to $19 \times 10^{17} \mathrm{ecm}^{-2}$ (Monceau et al. 1981). The transitions are smoothened, with a strong increase of resistivity at low temperature. Using 2.5 MeV protons leads to similar results (Fuller et al. 1981). The difference in nature of defects created by doping or by irradiation is directly reflected by the fact that irradiated samples do not show any superconducting transition, in contrast to doped samples or samples under pressure.

1.4. Tantalum trisulfide

In order to get a more one-dimensional compound it is necessary to increase the ionicity of the chemical bonds. Starting from $NbSe_3$ this will be achieved by changing niobium for the more electropositive tantalum and selenium for the more electronegative sulfur. TaS_3, which was already known with an orthorhombic unit cell (Bjerkelund and Kjekshus 1964), testifies effectively of the increased 1D character in three ways: (i) a transition at 210 K which goes as far as a metal to insulator transition (Sambongi et al. 1977), (ii) important pretransitional effects manifested by diffuse lines which condense at the transition into spots between the main Bragg rows of spots, (iii) the existence of polytypic forms.

In the original work by Bjerkelund and Kjekshus (1964), only the unit cell parameters of orthorhombic TaS_3 were given (table 1). A new variety with a monoclinic unit cell was found later on by Meerschaut et al. (1981) and completely characterized through single-crystal X-ray diffraction data. As in the case of the other trichalcogenides, it is obtained by direct combination of the elements in sealed silica tubes, after a slow increase of temperature up to 650°C. The needle shaped crystals of monoclinic TaS_3 are mixed with the fibrous orthorhombic variety. A careful separation is needed. Under pressure Kikkawa et al. (1981) obtained a powder which is purely monoclinic TaS_3.

Like $NbSe_3$, monoclinic TaS_3 (Meerschaut et al. 1981) presents three types of chains according to the S-S pair bond length (fig. 14). In fact two chains are related to short S-S distances of 2.068 and 2.105Å very close to the usual distance in $(S_2)^{2-}$ anions (2.05Å) in NbS_3. The third chain corresponds to a much larger value (2.83Å) although somewhat smaller than the S-S separation of 3.315Å in $2HTaS_2$.

Monoclinic TaS_3 undergoes two phase transitions (Meerschaut et al. 1979, Roucau et al. 1980) as shown in fig. 15. The first one at 240 K , is a metal-semiconductor transition, the second one at 160 K appears in the semiconducting state. TaS_3 becomes a semiconductor after the transitions, in contrast to $NbSe_3$ which remains metallic. Electron diffraction studies show important pretransitional effects manifested by diffuse lines that can already be seen at room temperature (Roucau et al. 1980). On decreasing the temperature, they condense into spots at 240 K . The wave vector

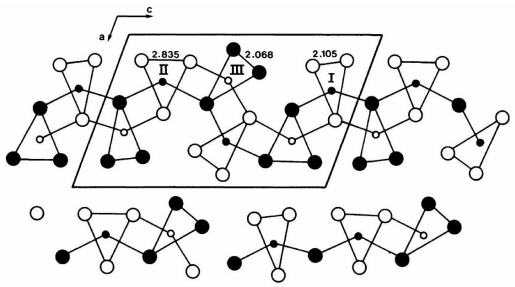


Fig. 14. Projection along [010] of the structure of monoclinic TaS_{3}.

components of the associated distortion are $(0, 0.254(3), 0)$. A second set of superlattice spots appears below 160 K with wave vector components ($1/2, 0.245(3), 1/2$). The occurrence of these satellite spots is well connected with the two features observed in the resistivity curves. The q vectors of the incommensurate distortions are given in table 2 along with those of other trichalcogenides.

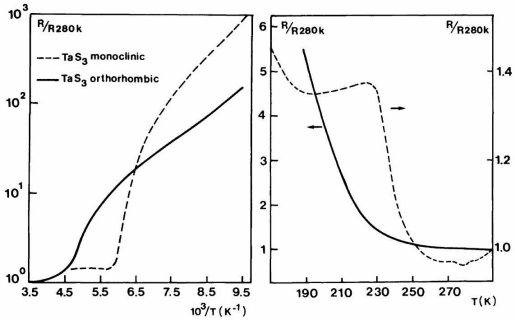


Fig. 15. Variation of the normalized resistances of monoclinic and orthorhombic TaS_{3} as a function of temperature.

		Table 2 Distortion wave vectors in NbS
$NbSe_3$	$T_2 = 59$ K 0, 0.241(3), 0 $1/2, 0.259(3), 1/2$	$T_1 = 145$ K 0, 0.243(3), 0
TaS_3 (monoclinic)	$T_2 = 160$ K 0, 0.254(3), 0 1/2, 0.245(3), 1/2	$T_1 = 240$ K 0, 0.254(3), 0
TaS_3 (orthorhombic)	$T \leqslant 130$ K Commensurate	$T \leqslant 210$ K Incommensurate 1/2
$FeNb_3Se_{10}$ (monoclinic)	$T = 140$ K 0, 0.270(3), 0	

A comparison of the unit cell parameters of the two types of TaS_3 shows that b mono $\approx c$ ortho. The corresponding value (3.34Å) expresses the height of one $[TaS_6]$ trigonal prism or, equivalently, the Ta-Ta distance along the chain axis. The two structures clearly refer to different arrangements of the same, or very similar, chains of trigonal prisms. It is the classical situation of polytypes in low-dimensional chalcogenides systems. Figure 16 gives the relative orientation of the two unit cells (Roucau et al. 1980). The exact structure of orthorhombic TaS_3 is still unknown but Meerschaut and Rouxel (1986) were able to propose a model which is very likely according to (i) the use of Patterson maps (not good enough to allow by themselves a complete structural determination), (ii) symmetry considerations, (iii) the reference to the monoclinic form. It shows at first that Cmcm space group is more suitable than C222 frequently reported. Then, the description of the unit cell should deal with four slabs built up from TaS_3 chains associated in a zig-zag manner. Figure 17 shows how these slabs are made from similar units of four chains like in monoclinic TaS_3.

The electrical properties of orthorhombic tantalum trisulfide seem to be strongly altered by doping or irradiation effects. $Ta(S_xSe_{1-x})_3$ samples have a semiconducting behavior for $x > 0.06$. Diffuse lines observed in samples with $x = 0.15$ suggest a Peierls transition around 70 K in that case (Yamaya and Abe 1982). When orthorhombic TaS_3 is irradiated by high energy electrons the Peierls transition decreases and the peak in $\mathrm{d}\log R/\mathrm{d}(1/T)$ at the transition progressively vanishes. However the onset temperature does not vary linearly with the defect concentration. A decrease of 15 K has

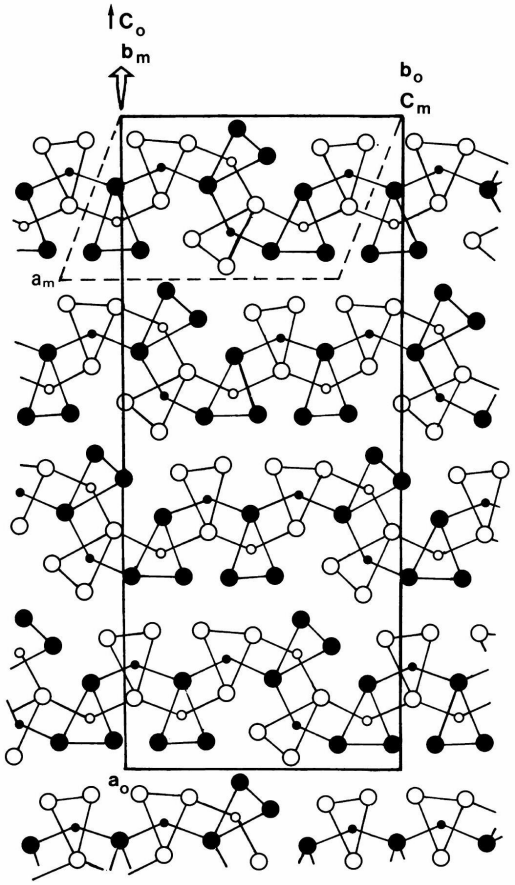


Fig. 16. Unit cell of orthorhombic TaS_{3} with respect to monoclinic TaS_3.b_m and C_0 are perpendicular to the figure.

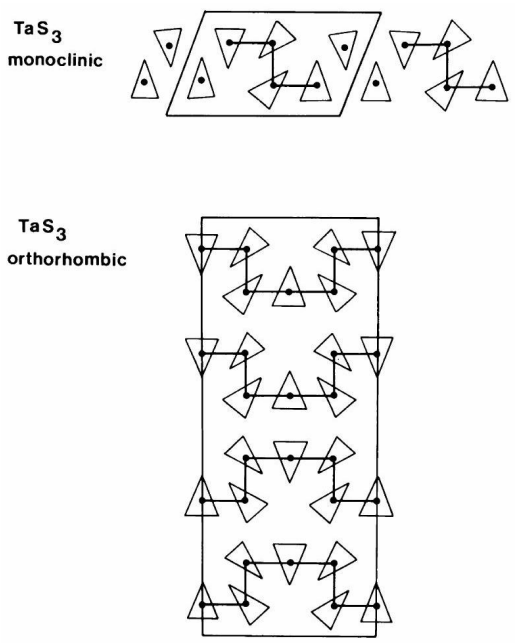


Fig. 17. Arrangement of chains in the two forms of TaS_{3}.

been measured for a dose of 3×10^{-3} displacements per atom (Mutka et al. 1984). Now, in the case of monoclinic TaS_3, irradiation with electrons suppresses the plateau in the resistivity variation between the two Peierls transitions and gives rise to a progressive increase in resistance when T decreases (Mihaly et al. 1981, Salva et al. 1984). Finally, for both TaS_3 the coherence length of the CDWs is much affected by irradiation (Mutka et al. 1984, Mihaly et al. 1981). Diffuse rings replace superlattice spots. Experiments in dark field imaging, to observe the CDW domain structure, show the transverse size of the domains to be very sensitive to irradiation (Chen and Fleming 1983).

1.5. Amorphous MX_3

The thermal decomposition of ammonium thio-salts, the chemical treatment by H_2 S, or Li_2 S, of solutions of salts in water or organic solvents, lead to amorphous trichalcogenides (Dieman and Müller 1973, Prasad et al. 1973, Liang et al. 1980). MoS_3 and WS_3 can only be obtained under this form.

The use of hexamethyl-disylthiane was recently proposed to get chalcogenrich chalcogenides from salt solutions in organic solvents at room temperature (Auborn et al. 1987). These quasi-crystalline materials have not been considered in the scope of the properties described in this book and therefore a detailed report will not be given here. However it is worth noticing that once more a chain-like structure is proposed for MoS_3 and WS_3 from various techniques such as EXAFS and XPS (Liang et al. 1980, Dieman 1977). There are two types of chalcogen species, i.e., $(X_2)^{2-}$ and X^{2-} as in other trichalcogenides. The Mo-S and W-S distances are found to be close to 2.40Å in the chains and 2.75Å between them. A dimerization of the metal atoms along the chains gives rise to alternating short and long metal-metal distances (2.8 and 3.2Å for example in the case of MoS_3). The main difference with other MX_3 compounds is that along the chains one finds successively $[MX_6]$ octahedra and trigonal prisms. Such a complicated building may explain the bad crystallization of these materials.

4.2.3 2. Pentachalcogenides: a bridged MX_3 structure

This class of chalcogenides is represented by $HfTe_5$ (Brattas and Kjekshus 1971) and $ZrTe_5$ (Furuseth et al. 1973) obtained by Kjekshus et al. from direct combination of the elements in evacuated silica tubes at temperatures

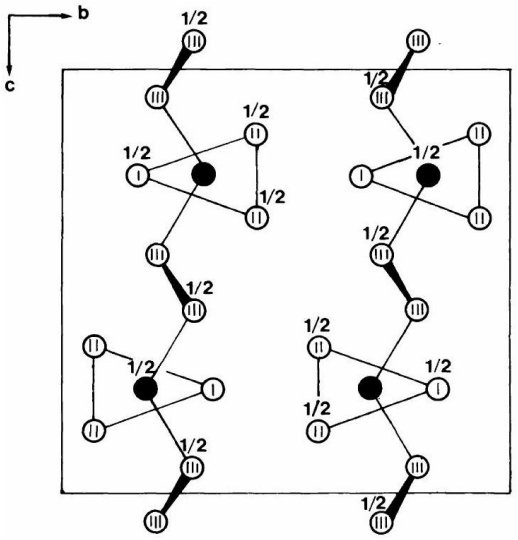


Fig. 18. Structural type of pentatellurides.

ranging from 450 to 800°C. The structure can be described on the basis of trichalcogenides prismatic chains bonded by tellurium bridges (fig. 18). A short $Te-Te$ bond in the triangular basis of the prisms (TeII-TeII = 2.763Å) is almost equal to the typical value (2.74Å) proposed by Pauling (1960)) for the $Te-Te$ bond. The Te bridge between chains is a bit longer (TeIII-TeIII = 2.908Å). The unit cell is orthorhombic.

Pentatellurides of zirconium and hafnium present very striking phase transitions manifested by large anomalies in the transport properties. They

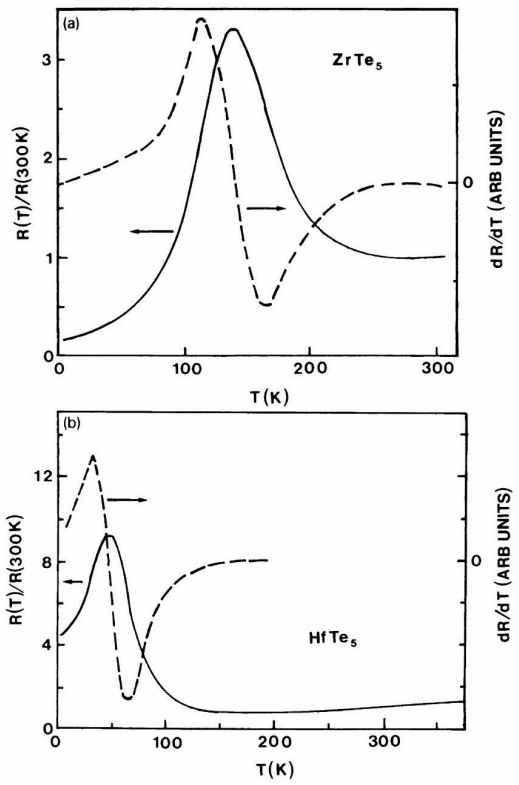


Fig. 19. Variation of the resistance (solid line) and of its derivative (dashed line) for (a) ZrTe_{5}, and (b) $HfTe_5$.

also show various kinds of structural modulations (Di Salvo et al. 1981, Okada et al. 1982, Sambongi et al. 1985, Sambongi 1986).

An exhaustive discussion of the physical properties has been given by Sambongi (1986). Figure 19 illustrates the resistance anomalies in $ZrTe_5$ and $HfTe_5$. There is a strong dependence of the resistivity on frequency (Skelton et al. 1982, Jackson et al. 1983). For $HfTe_5$ the peak vanishes at 9.1 GHz. For $ZrTe_5$ it is largely suppressed. This dependence on frequency suggests the condensation of a collective mode. The formation of a CDW of the excitonic insulating state and a band Jahn-Teller mechanism have been proposed, but, in spite of the large amount of work which has been done, there is not yet any complete explanation of things.

4.2.4 3. One-dimensional chalcogenides from condensation of different chains

In the course of the studies about the role of chemical impurities, new compounds were isolated. Niobium can be substituted in $NbSe_3$ by very slight amounts of other transition metals. But a complete study of Nb− (S-Se)-transition metal systems, showed many new compounds to exist. $FeNb_3Se_{10}$ is the prototype of this new class of compounds (Meerschaut et al. 1981, Cava et al. 1981). Fibrous and needle-like crystals are obtained by heating the elements in silica tubes at about $650 - 700°C$.$FeNb_3Se_{10}$ has a very particular structure (fig. 20) with two types of chains running along the b axis of a monoclinic unit cell, each chain being repeated twice. One chain corresponds to a trigonal prismatic frame of selenium atoms around a first type of niobium atoms, the other develops an octahedral arrangement of selenium atoms around both iron atoms and a second type of niobium atoms. Iron is octahedrally coordinated whereas niobium occurs with both types of coordination. A variation of the Fe/Nb ratio in the octahedral chains accounts for deviations from the stoichiometric formulation which should be

replaced by the expression $Fe_{1+x}Nb_{3-x}Se_{10}$ with $0.25 < x < 0.40$ (Whangbo et al. 1982). The trigonal prismatic chain exhibits a short $Se - Se$ distance of 2.348Å and is almost identical to the MX_3 chain with the shortest $Se-Se$ bond in $NbSe_3$. Resistivity measurements show a metal to non-metal transition at 140 K when temperature is decreased. Superlattice peaks appear below the transition and characterize a distortion, the wave vector of which being slightly temperature dependent with values of $q(0, 0.270(3), 0)$ near 140 K , and ($0, 0.258(3), 0$) near 6 K . The fact that the CDW has nearly the same wave vector components as those of the first CDW in $NbSe_3$, can be taken as a proof that the CDW is related to the [$NbSe_3$] type of chain within the structure. On the other hand, it also

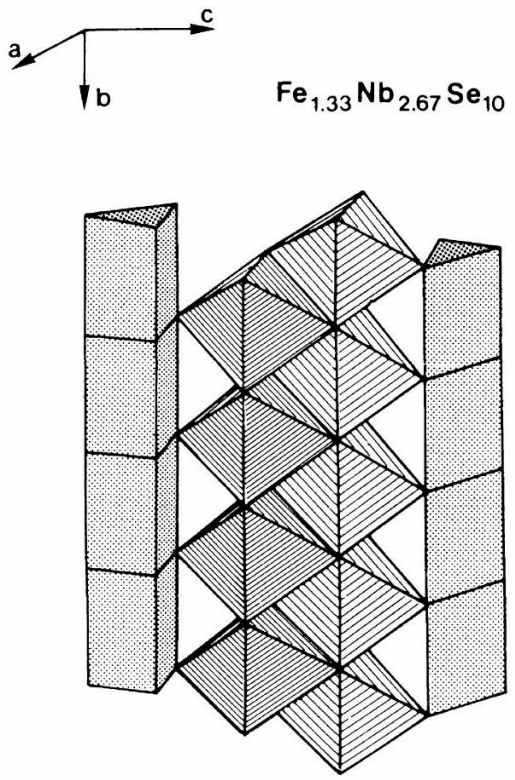


Fig. 20. ' $\mathrm{FeNb}*{3}* \mathrm{Se}{10}$ ' structural type.

suggests that the first CDW in niobium triselenide is seated in the $NbSe_3$ chain with the shortest Se-Se distance (chain III in fig. 4). The random potential created by the disordered adjacent $Fe - Nb$ octahedral chain may explain that an insulating state is reached in the case of $FeNb_3Se_{10}$.

Ben Salem et al. (1984) along with Cava et al. (1983) have prepared isotypic compounds by replacing niobium atoms in octahedral sites by other transition metal elements such as V, Cr, Ta. All these compounds show the transition around 140 K , but the resistance rise below the transition can differ drastically (Ben Salem et al. 1984).

The $FeNb_3Se_{10}$ structural type can be regarded as the result of condensations in a given structure of various chains, each of them corresponding to the usual coordination of a given element. This concept has been nicely extended by Ibers to condensations of the trigonal prismatic chains with chains having a square planar section as in $Nb_2Pd_3Se_8$ (Keszler and Ibers 1984), or chains built up from tetrahedra as in Ta_2NiS_5 (Sunshine and Ibers 1985).

4.2.5 4. One-dimensional chains stabilized by counter ions: halogenotetrachalcogenides

The mineral patronite, VS_4, presents a 1D organization with S_4 rectangles, built up from two true $(S_2)^{2-}$ pairs rotating around $-V-V-$ chains and giving a rectangular antiprismatic coordination to the metal atoms. Vanadium is at the $+4$ oxidation state but the remaining delectron on the metal is used in a V-V pairing which leads to a diamagnetic semiconducting behavior. Long (3.241Å) and short (2.841Å) V-V distances alternate along the c axis (parallel to the chains) of a monoclinic unit cell (Allman et al. 1964). Figure 21 represents the projection of the structure along [001]. Up to now attempts to change the properties by applying a pressure have been unsuccessful, and heating the samples does not allow to remove this Peierls distortion before the compound decomposes.

It was of interest to prepare niobium and tantalum homologues of VS_4. More expanded d orbitals could help to get an electronic delocalization along the chains. Attempts have been unsuccessful and this is probably due to an increased ionicity which destablizes the one-dimensional arrangement. The way to manage is to prepare selenides or tellurides. Selenides have not

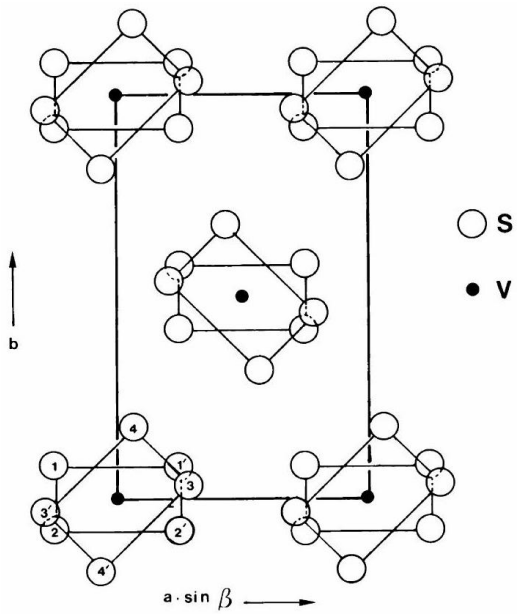


Fig. 21. Projection of the VS_{4} structure along [001].

yet been obtained but tellurides with a structure related to the VS_4 arrangement are known and will be discussed in the next section. MX_4 chains can also become stable with respect to each other when separated by counter-ions. This is the case of halogenotetrachalcogenides.

Needle-shaped single crystals of $(MSe_4)_n I$ phases ($M = Nb, Ta; n = 2, 3, 10/3, \ldots$) are obtained (Gressier et al. 1984) by heating mixtures of the elements in evacuated and sealed glass tubes at temperatures ranging from 400 to 550°C. The common structural type of these phases can be illustrated by considering $(NbSe_4)_3 I$ (Meerschaut et al. 1977). With a tetragonal symmetry (P4/mnc) the structure is composed of ($NbSe_4$) chains and iodine columns which are both parallel to the c axis (fig. 22). The

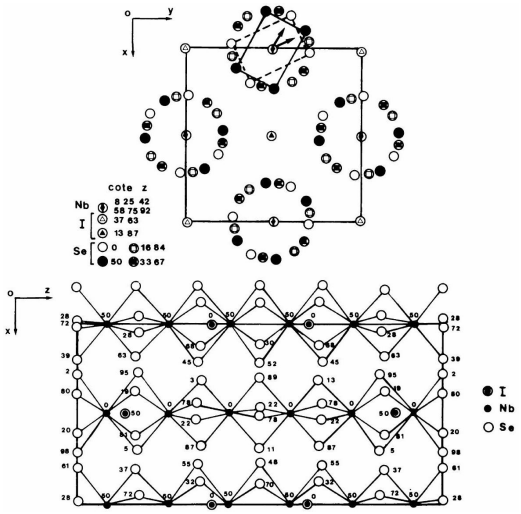


Fig. 22. $\left(\mathrm{NbSe}\right)_{3}\mathrm{I}$ structural type.

metallic chains are widely separated: two niobium atoms having the same z value, but belonging to different chains are 6.70Å apart. Along the chains $\mathrm{Nb}-\mathrm{Nb}$ interatomic distances alternate in the sequence of two long (3.25Å) and one short (3.06Å). Simply writing down the most likely formal valences, one obtains the $\left(\mathrm{Nb}^{4+}\right)_2\mathrm{Nb}^{5+}\left(\mathrm{Se}_2^{2-}\right)_6\mathrm{I}^-$formulation which may account for the alternation of long and short metal-metal distances according to: $\ldots\mathrm{Nb}^{4+}-\mathrm{Nb}^{4+}\ldots\mathrm{Nb}^{5+}\ldots\mathrm{Nb}^{4+}-\mathrm{Nb}^{4+}\ldots\mathrm{Nb}^{5+}\ldots$. The shortest distance corresponds to a $\mathrm{Nb}^{4+}-\mathrm{Nb}^{4+}$ association. Nb^{5+} separates two Nb^{4+} by two longer distances.

From one compound to another this sequence changes according to the amount of counter-ion (table 3). A second difference concerns the way the Se_4 rectangles, made of two true $\left(\mathrm{Se}_2\right)^{2-}$ pairs ($\mathrm{Se}-\mathrm{Se}\approx 2.35$Å) and surrounding Nb or Ta in an antiprismatic manner, turn around the axis of the chains. Indeed the [MSe_8] rectangular antiprisms are stacked along the c axis in a screw-like arrangement characterized by the relative position of the arrows pointing from the center to the middle of the edges (fig. 22, table 3, and Gressier et al. 1984, Meerschaut et al. 1977, Fujishita et al. 1984, Meerschaut et al. 1984, Gressier et al. 1982). Every two adjacent $\left(\mathrm{Se}_4\right)^{4-}$ units have a dihedral angle θ of about 45°. This value corresponds to a minimization of the energy of a MSe_8 'molecular' group (minimization of the repulsion between π and π^* orbitals of two successive Se_4 rectangles, along with the obtainment of the best set of symmetry adapted orbitals to interact with the metal orbitals). But the displacement of such successive rectangles can refer to a right- or left-handed rotation. For example, in that respect, $\left(\mathrm{NbSe}_4\right)_3\mathrm{I}$ is a 123432 tetrachalcogenide, $\left(\mathrm{TaSe}_4\right)_2\mathrm{I}$ is 1234 and

Table Structural characterization of $\left(\mathrm{MX}\right)_{n}\mathrm{I}$ phases

Compound reference	Unit cell	M-M sequence
$\left(\mathrm{NbSe}_4\right)_2\mathrm{I}$	$a=9.515$Å, $c=12.80$Å	like $\left(\mathrm{TaSe}_4\right)_2\mathrm{I}$
$\left(\mathrm{NbSe}_4\right)_3\mathrm{I}$	quadratic P4/ mnc $a=9.489$Å, $c=19.13$Å$Z=4$	(3.25)(3.25)(3.06)
$\left(\mathrm{NbSe}_4\right)_{10/3}\mathrm{I}$	$a=9.464$Å, $c=31.91$Å	(3.23)(3.17)(3.17) (3.23)(3.15
$\left(\mathrm{TaSe}_4\right)_2\mathrm{I}$	$a=9.531$Å, $c=12.824$Å	3.206Å
$\left(\mathrm{TASe}_4\right)_3\mathrm{I}$		like $\left(\mathrm{NbSe}_4\right)_3\mathrm{I}$

$\left(\mathrm{NbSe}_4\right)_{10/3}\mathrm{I}$ is a 1234565432 chalcogenide. In the M-Se combination all the metal orbitals

are concerned, except d_{z^2} which remains isolated and built a d_{z^2} band along the chain. This band governs the electronic properties of each system (Gressier et al. 1984). Assuming in a first approach that each iodine takes one electron, the average number of d electrons per metal is $(n-1)/n$ with a corresponding filling of the d_{z^2} band of $f = (n-1)/2n$, possibly leading to a distortion increasing the repeat distance by a factor $1/f$. As n increases the d_{z^2} band of $(MSe_4)_n I$ becomes closer to half filled. Vanadium tetrasulfide constitutes finally an example of the $n \to \infty$ limit. It has consequently the $2c$ insulating Peierls distortion. More precisely, band structure calculations have been performed (Gressier et al. 1984), which slightly modify the rough approach mentioned just above. They are in rather good agreement with the observed distortions. For example the calculations on $(TaSe_4)_2 I$ lead to an estimation of $2k_F = 0.88c^*$ and the distortion is observed at $0.94c^*$ by Roucau et al. (1984) and $0.91c^*$ by Fujishita et al. (1984).

Indeed these materials present interesting phase transitions. Not all of them are of CDW origin. $(TaSe_4)_2 I$ presents a transition at 263 K manifested by a sharp peak in the logarithmic derivative curve $\mathrm{d}\log(R/R_0)/\mathrm{d}(1/T)$. The CDW origin is demonstrated by the depinning which is possible above a threshold field (Wang et al. 1983, Maki et al. 1983). Electron diffraction studies (at 90 K) reveal satellite spots very close to the main Bragg spots (Roucau et al. 1984). The components of the distortion vector q are found equal to $(1, 0, 0.94)$. The temperature dependence of peak intensity of superlattice reflections clearly indicates a secondorder transition (Fujishita et al. 1984). The phase transition in $(TaSe_4)_2 I$ was recently studied by Raman scattering (Ohana et al. 1985, Sekine et al. 1985). An important result is that polarized Raman spectra (Sekine et al. 1985) present a peak at about 90 cm^{-1} with anomalous temperature dependence in its frequency and its damping constant. It can be seen from the temperature dependence of the coupling coefficient that it is related to the CDW transition. On the other hand the temperature dependence of the damping constant agrees with that of the amplitude mode in KCP. Therefore it is suggested that the 90 cm^{-1} phonon is the amplitude mode.

$(NbSe_4)_2 I$ crystals have been obtained by Fujishita (1984). According to the unit cell parameters (table 3), there is no doubt that $(NbSe_4)_2 I$ is isostructural with $(TaSe_4)_2 I$. Measurements of resistivity show a phase transition at about 210 K with a non-linear conduction below T_c. The threshold field necessary to observe the non-linear effects increases with decreasing temperature far below T_c. Superlattice reflections observed by X-rays in the low temperature phase appear at $\boldsymbol{q}(\pm 0.065, \pm 0.065, \pm 0.159)$. This gives direct evidence of a CDW state. Continuous variation of the intensity of superlattice reflections proves the transition to be second order (Fujishita et al. 1989). Recently, magnetic susceptibility measurements by Sato and Nishihara (1989) and Johnston et al. (1985) have shown an important and unexpected difference between $(TaSe_4)_2 I$ and $(NbSe_4)_2 I$. In both cases a $\chi(T)$ anomaly is observed around the transitions. But in the case of $(TaSe_4)_2 I$ the anomaly is sharp and coincides well with the transition temperature, whereas in $(NbSe_4)_2 I$ the anomaly is not sharp and has a clear maximum above the transition temperature. The 'anomalous' behavior of the latter compound is explained with the same concepts as those proposed by Nagasawa (Nagasawa et al. 1983) for the transition observed at 200 K in $Na_{0.4}\ V_2O_5$. The explanation of the transition involves the concept of ordering of bipolarons, singlet pairs of electrons at the neighboring sites. This kind of localized electron pair is to be considered in the limit of strong electron-phonon coupling whereas a Cooper pair in superconductors is in the limit of wide spread band electrons. Large local fluctuations above T_c may suppress (like in $Na_{(0.4}V_2O_5$) or smear ($(NbSe_4)_2 I$) the anomalies. The bipolaron interpretation suggests that the electron localization is smaller in $(TaSe_4)_2 I$, which is indeed in agreement with more extended d orbitals.

$(NbSe_4)_{10/3} I$ is the third compound to exhibit a CDW transition. The transition, manifested by a peak in the logarithmic derivative curve $\mathrm{d}\log(R/R_0)/\mathrm{d}(1/T)$, is observed at 285 K (Wang et

al. 1983). Electron diffraction studies (Roucau et al. 1984) show satellite spots on patterns of the (a^*, c^*) plane. They appear below T_c and are located along the c^* axis with no component along the a^* or b^* axis (in fact satellite spots are elongated along a^* in the (a^*, c^*) plane). The q vector is ($0, 0, 0.487$). Non-linear transport properties are observed below the transition temperature if the applied field exceeds a threshold value (fig. 23). But, in addition, an hysteresis phenomenon takes place in the $285 - 220$ K temperature range (Wang et al. 1983). Such a memory effect has also been observed in o-TaS_3 (Mihaly and Mihaly 1983) and $NbSe_3$ (Gill 1981), and will be also described for the blue bronze $K_{0.30}MoO_3$. There is a threshold field when the field is increased and a different one when it is decreased.

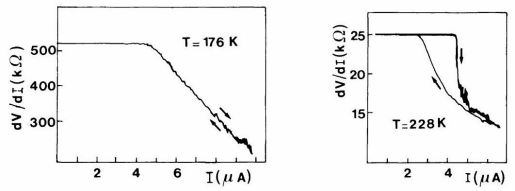


Fig. 23. Non-linear transport properties at 176 K and hysteresis at 228 K for \$\left(\mathrm{NbSe}*{4}*\right)*{10 / 3} \mathrm{I}\$.

Such a situation, which may depend on the electrical history of the sample, implies that, probably, closely related metastable states of comparable energy are involved in the depinning of the CDW.

The CDW transition at 285 K in $(NbSe_4)_{10/3}I$ has been studied by pulsed NMR of the ^{93}Nb nucleus (Butaud et al. 1984). The onset of the incommensurate state is followed on the $(1/2, -1/2)$ transition resonance line. The temperature dependence of the lineshape is in agreement with that expected from a purely plane wave CDW. This allows the determination of the temperature dependence of the CDW which gives the order parameter of the transition (fig. 24).

$(NbSe_4)_3I$ has been deeply investigated. Resistivity measurements (Gressier et al. 1984) indicate semiconducting behavior above room temperature with a gap of 4400 K (room temperature resistivity $\approx 1\Omega$ cm). A transition is manifested at 275 K by a sharp decrease in the activation energy. Then, at lower temperatures two types of behavior have been observed on crystals named type I or type II, which could not be distinguished by X-ray techniques (fig. 25). Type I behavior is characterized by a very small semiconducting gap below 275 K . In contrast type II crystals, after a decrease of the gap near 275 K , show again an increase in resistivity at lower temperature with a typical semiconducting behavior ($E_g \approx 3000$ K). This non-unique behavior of crtystals which are supposed to be $(NbSe_4)_3 I$ was observed by various groups involved in the study of the properties of low-dimensional chalcogenides. It may have to deal with a slight variation of the chemical composition, particularly of the iodine content (Grüner 1984). This point will be considered below in a more general discussion. Roucau et al. (1984) have performed an electron diffraction study. It appears that the phase transition is not related to the onset of a CDW but is a second-order displacive phase transition to which is associated a change of space group corresponding to the disappearing of the glide plane n (i.e.,

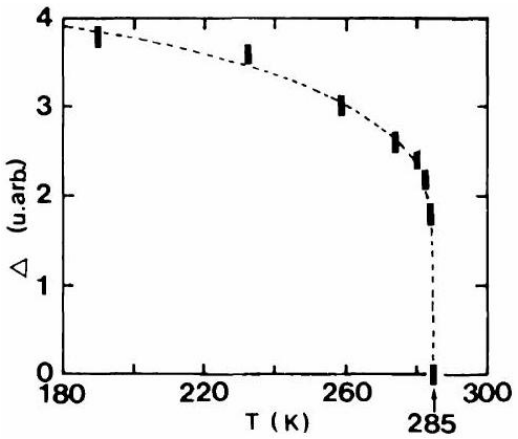


Fig. 24. Temperature dependence of the order parameter Δ of the transition in $\left(\mathrm{NbSe}_{4}\right)_{10 / 3} \mathrm{I}$ assuming the amplitude of the frequency distribution associated with the CDW is linear with Δ.

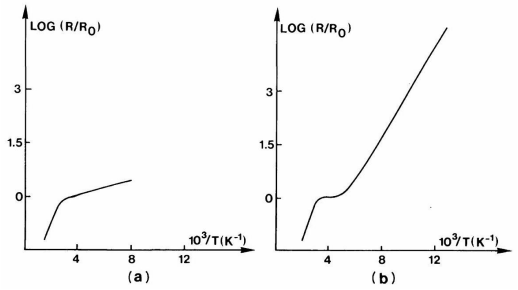


Fig. 25. The two types of electrical behavior observed on $\left(\mathrm{NbSe}_{4}\right)_{3} \mathrm{I}$ crystals.

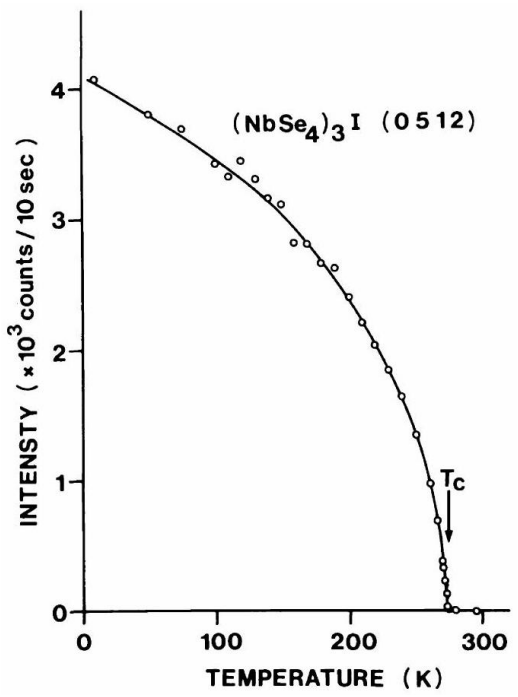


Fig. 26. Variation of the intensity of the $(0, 5, 12)$ reflection below the structural transition of \$\left(\mathrm{NbSe}\{4\}\right)\{3\} \mathrm{I}\$.

the $h()l$ spots are visible at all values of the sum $h + l$, the limiting condition $0kl$ such as $k + l = 2n$ disappearing in the low temperature form). Thus reflections with $0kl$ such as $k + l = 2n$ are typical of the low-temperature phase. Following their intensity as a function of temperature [$(0, 5, 12)$ reflection], Izumi et al. do not observe any hysteresis or jump (fig. 26) which clearly establishes the phase transition to be second order (Izumi et al. 1984).

The phase transition has also been followed by pulsed NMR studies of the ^{93}Nb nuclei. Above 275 K the spectra performed on a single crystal are temperature independent. Below the phase transition, each resonance line splits into two, corresponding to the doubling of the number of inequivalent sites. The temperature dependence of the splitting is another access to the order parameter of the transition (Butaud et al. 1984).
$(TaSe_4)_3\,I$ is very similar to $(NbSe_4)_3\,I$ with a similar second-order displacive phase transition (Gressier et al. 1984) observed at a lower temperature ($T \approx 200$ K).

4.2.6 5. The particular case of $TaTe_4$ and $NbTe_4$

As mentioned above $NbTe_4$ and $TaTe_4$ are stable with a structural arrangement of the VS_4 type. However, if the average structure is clearly ascertained from the early work of Kjekshus (Selte and Kjekshus 1964), the detailed structure is a rather complicated incommensurate one, which has just been solved recently.

To the average structure of $NbTe_4$ was associated a tetragonal unit cell (P4/mcc, $Z = 24$) with $a = b = 2 \times 6.466$Å and $c = 3 \times 6.837$Å (Fig. 27), niobium being surrounded by a square antiprism of tellurium. It was shown later (Boswell et al. 1983, Boswell and Prodan 1984, Malvy et al. 1984), that the superstructure along c is an incommensurate one. In fact the reflection pattern of $NbTe_4$ presents two classes of reflections: (i) a group of strong reflections at the nodes of the reciprocal lattice spanned by the vectors $\boldsymbol{a}^*, \boldsymbol{b}^*, \boldsymbol{c}^*$, (ii) a group of weaker reflections which can be described with the above reciprocal lattice and a fourth vector:

$$\boldsymbol{q}' = \frac{1}{2}\boldsymbol{a}^* + \frac{1}{2}\boldsymbol{b}^* + 0.309\boldsymbol{c}^*,$$

according to an integral linear combination $\boldsymbol{\delta} = \boldsymbol{ha}^* + \boldsymbol{kb}^* + \boldsymbol{lc}^* + \boldsymbol{mq}'$. This modulated structure recently solved (Böhn and von Schnering 1983, van Smaalen and Bronsema 1986) shows that the modulation wave resides mainly on the Nb atoms which have an amplitude of 0.33Å. Between each pair of Nb atoms there are four Te atoms with the same z coordinate, the average positions of which are related to each other by the fourfold axis (equal displacements along c, equal magnitudes but different orientations in

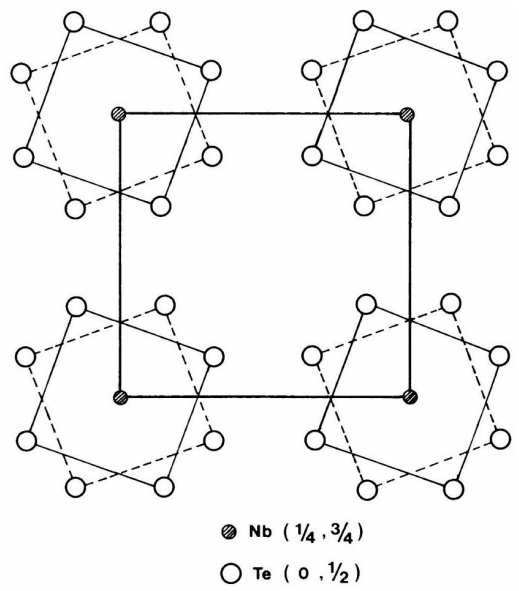


Fig. 27. Average structure of NbTe_{4} and $TaTe_4$.

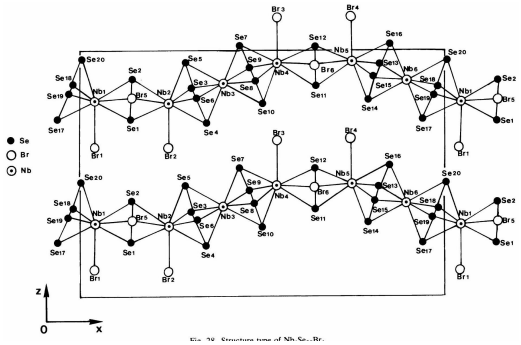
the (a, b) plane). As a whole the square of Te atoms can have a displacement along c. In addition there are the shrinking and expansion of the square and its rotations around c. This form of displacement established by van Smaalen (van Smaalen and Bronsema 1986) was already suggested by Böhn and von Schnering. Whangbo (1986) gives an attractive explanation. The experimental value close to $c^*/3$ means that the d_{z^2} bands along the Nb chains are 1/3 filled. Now, an ideal $NbTe_4$ structure made of undistorted Te square planes implies the formal oxidation state $Nb^{4+}\left(Te_2^{2-}\right)_2$ and a half-filled d_{z^2} band. The discrepancy between the two values should be resolved through Te^{2-} species, which are produced by lengthening the $Te-Te$ bonds. As the formula unit is represented by $Nb_{24}\left(Te_2\right)_{48}$ for the real unit cell ($2a, 2a, 3c$), it is necessary to assume an increase of $4Te-Te$ bonds out of 48 , corresponding to a change from $4\left(Te_2\right)^{2-}$ to $8Te^{2-}$. In this way 16 d electrons, instead of 24 , are available for 24 Nb , which will lead to a 1/3 filled d_{z^2} band. The fundamental question which remains is to know the origin of the distortion. A CDW transition has probably not to be considered due to the importance of the distortion.

4.2.7 6. New trends: chain-chain stabilization, waved structures, clusters condensation

A first evolution, starting from $\left(MX_4\right)_n$ I phases would be to replace I^-ions by other types of counter ions. Replacement of iodine by other halogens may lead to two types of predictions: (i) If the structural type is maintained it will be less stable (increased overall charge on the chains due to a more electronegative halogen and, at the same time smaller separation between chains). This may allow one to solve the $\left(NbX_4\right)_x$ chains in solvents. Considering the work done by Tarascon and di Salvo (Tarascon et al. 1985) on the $M_2Mo_6Se_6$ phases to get Mo_6Se_6

chains dispersion in organic solvent, a recombination could be attempted to get a mixed chain structure associating (MX_4) and (Mo_6Se_6) chains. All the attempts have been, up to now, unsuccessful. Soft chemistry processes such as the action of chlorine diluted in argon at room temperature allows to remove iodine (ICl and ICl_3 are formed) but the MX_4 framework is also attacked. Direct reaction between the elements do not lead to $(MX_4)_n Cl$ phases. Only a few bromine derivatives (Guemas et al. 1981), badly crystallized, have been obtained. This is clearly related to the loss of stability of the structure.
(ii) Working at higher temperature one can expect new structural arrangements in which a more electronegative halogen will tend to participate directly in the coordination polyhedra of the metal by pushing apart the selenium framework. This has been realized in a series of materials in which niobium atoms directly bonded to the halogen are found along with niobium atoms that are still in $(Se_4)_2$ rectangular antiprismatic coordination. In fact a more correct approach is to consider M_2X_4 bipyramids. $Nb_6Se_{20}Br_6$ (Meerschaut et al. 1986) with a nice wave structure (fig. 28), and $Nb_4Se_{16}Br_2$ (Meerschaut et al. 1987), appear then to derive from a partial condensation of these bipyramids in (Nb_3Se_8) and (Nb_4Se_{12}) groups separated by the halogen-bonded niobium atoms. The same bipyramids are found isolated in NbS_2Cl_2 (Rijnsdorp et al. 1969) or Nb_2Se_9 (Meerschaut et al. 1979) where they are separated by chlorine atoms or by a (Se_5) group. On the other hand, they give rise to an infinite condensation in VS_4 where the (MX_4) chains are isolated or in $(MSe_4)_n I$ where they are separated by halogen atoms (fig. 29).

A way to stabilize chains is to separate them by counter-ions. Another solution would be to play with two types of chains. This is illustrated by the very new compound $Nb_3Se_{10}Br_2$, the structure of which (Meerschaut et al. 1987) is built from an alternation of ($NbSe_4$) chains centered along a twofold axis and ($NbSe_3Br$) chains running along a 2_1 axis parallel to the former one ($Se - Br$ exchanges on certain sites explains the rather complicated formulation) studies on these materials are in progress (fig. 30).



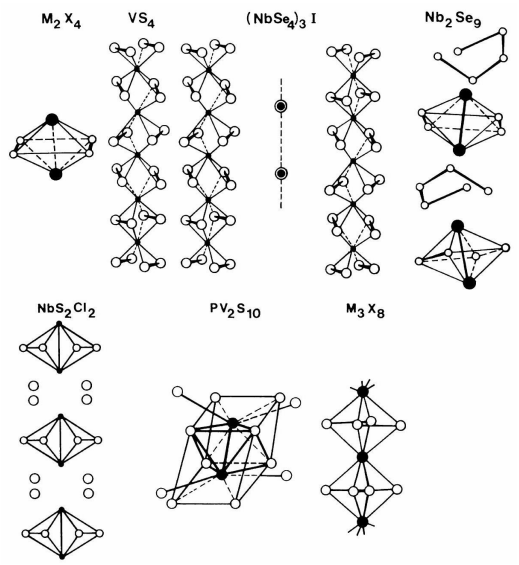


Fig. 29. 1D structures from finite or infinite condensation of $\mathrm{Nb}*{2}* *mathrm{X}*{4}$ bipyramids.

The Chevrel phases (Chevrel et al. 1971) are built up from Mo octahedral clusters enclosed in a pseudo-cube of chalcogen atoms. These Mo_6X_8 units, usually isolated, can accept between them extra cations and particularly rare earth cations. But it has been shown also that the clusters can condense to form infinite chains. This is the case for $M_2Mo_6Se_6$ phases (fig. 31), the chains being separated by M^+cations ($M = Tl, K, Rb, Cs, \ldots$). Among these compounds, $Tl_2Mo_6Se_6$ (Potel et al. 1980) which is metallic, is still being extensively investigated, largely in connection with its superconductive transition around 3 K . The $M_2Mo_6X_6$ compounds, although no

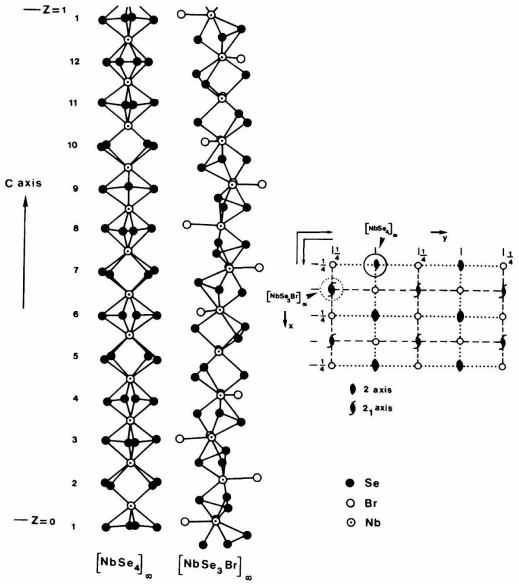


Fig. 30. Structural type of $\mathrm{Nb}*{3}* *mathrm{Se}*{10} \mathrm{Br}_{2}$.

sharp Peierls transition has been seen, are remarkable 1D materials because of the very high anisotropy of their transport properties (Lepetit et al. 1984) and also because of the anisotropy of their polarized reflectance spectra (Geserich 1985). The architecture of chain-like $M_2Mo_6X_6$

compounds is very attractive because of its extreme sensitivity to the interchain coupling which suggests many chemical developments.

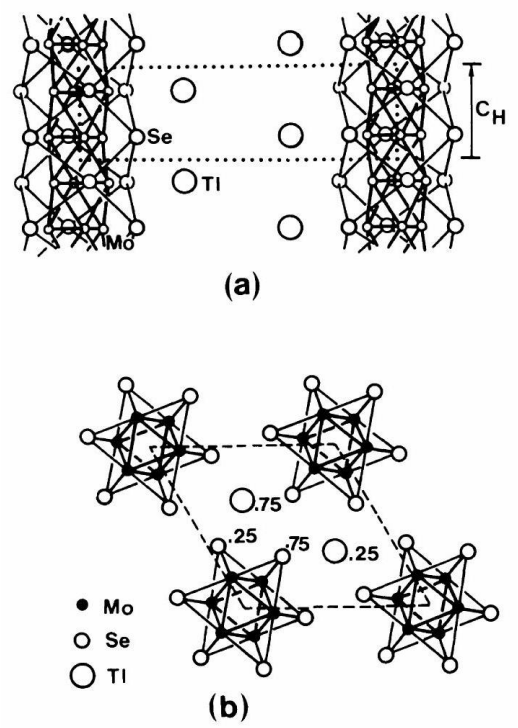


Fig. 31. $\mathrm{Tl}{2} \mathrm{Mo}{6} \mathrm{Se}_{6}$ structural type.

4.2.8 7. Quasi-one-dimensional oxides: the molybdenum blue bronze $A_{0.30}MoO_3$

Several molybdenum oxide bronzes can be synthesized with low-dimensional character: the blue bronzes $A_{0.30}MoO_3$, the red bronzes $A_{0.33}MoO_3$ and the purple bronzes $A_{0.9}Mo_6O_{17}$. A is in all cases monovalent, being either an alkali metal or thallium. The red bronzes are insulators (Stephenson and Wadsley 1965). The purple bronzes are layered and quasi-2D compounds (Schlenker et al. 1985, NATO-ASI 1987, Schlenker and Dumas 1986, Schlenker 1989). Only the lithium compound has been reported to have some 1D character (Onoda et al. 1987). Most of these compounds show CDW instabilities. But up to now no evidence for CDW transport has been found in the red or purple bronzes. We will therefore not consider them further here.

One should also note that one Vanadium bronze, $Na_x\ V_2O_5 - \beta$, is a chain-like compound and therefore quasi-1D. However, it is semiconducting and has been described in terms of bipolarons rather than CDW (Nagasawa et al. 1983, Nagasawa et al. 1987).

Molybdenum blue bronze single crystals are synthetized by the electrocrystallization technique (Wold et al. 1964). Up to now, only three compounds have been grown with A being K, Rb, or Tl . Most of the physical properties are strikingly similar for these three bronzes. The Peierls transition from a metallic to a semiconducting state is found at 180 K in the three cases (fig. 32). This corroborates that the A counter-ion does not play an important direct role: it mainly provides conduction electrons for the conduction band.

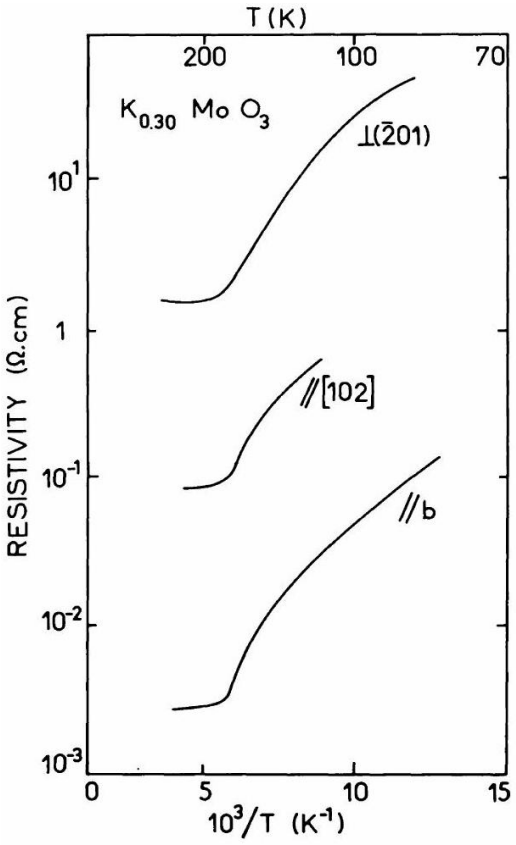


Fig. 32. Resistivity of $\mathrm{K}_{0.30}\mathrm{MoO}_3$ as a function of reciprocal temperature along the b-chain axis, along [102] and perpendicular to the octahedra slabs ($\bar{2}, 0, 1$ plane).

7.1. Structural aspects

The crystal structure of the blue bronze is primarily layered-type. It is built with clusters of the distorted MoO_6 octahedra linked together via corner sharing into infinite slabs (fig. 33a and b). The slabs are separated by the A counter-ions. The quasi 1D character of the electronic properties is due to the presence of infinite chains of MoO_6 octahedra clusters along the monoclinic b axis (fig. 33c). Similar results have been found at room temperature for the potassium (Graham and Wadsley 1966), rubidium (Ghedira et al. 1985) and thallium (Ganne et al. 1985) blue bronzes with neighbouring lattice parameters, in spite of some difference in the A^+ionic radii (table 4). This corroborates that the A counter-ion does not play a dominant role in the properties, except for partially filling the conduction band through charge transfer.

Precursor effects to the Peierls transition are clearly seen at room temperature by X-ray diffuse scattering (Pouget et al. 1983, 1985, Fleming et al. 1985): the diffuse streaks are characteristic of two-dimensional correlations at 300 K , as expected from the crystal structure (fig. 34a). They condense into satellites at the Peierls transition, with a wave vector $q\,(0, 1 - q_b, 0.5)$. The b^* component is found close to 0.75 , but always smaller: this corresponds to an incommensurate CDW along the 1D-axis (fig. 34b).

The temperature dependence of the q_b wave vector (fig. 34b) has to be attributed to a change of the total number of electrons in the two conduction bands. It has been proposed that this change is due to the presence of the third band lying just above the Fermi level (Pouget et al. 1985). The experimental data would be consistent with a narrow band located ~ 650 K above the Fermi level, in agreement with the band structure calculation.

The order parameter, proportional to the square of the intensity of the satellite does not

follow exactly a BCS law, as expected in the simple mean field approximation (fig. 34c). Close to T_P, the critical exponent seems to be ~ 0.31 which rather corresponds to an XY Ising model. This is consistent with a two component order parameter, $\Delta e^{i\varphi}$, taking into account the phase φ of the CDW (Girault 1987, Girault et al. 1988). Similar results have been obtained from the temperature dependence of the quadrupole splitting of the ^{87}Rb NMR lines in $Rb_{0.30}MoO_3$ (Butaud et al. 1985, Butaud 1987).

In the low temperature incommensurate CDW state, the modulated structure obtained by taking into account the satellite reflections has also been refined in the blue bronze (Schutte and de Boer 1988, Girault 1987, Girault et al. 1988): the modulation is important principally for the Mo sites involved in the 1D chains and is mainly transverse, perpendicular to the 1D b axis, but parallel to the octahedra layers. This is not inconsistent with

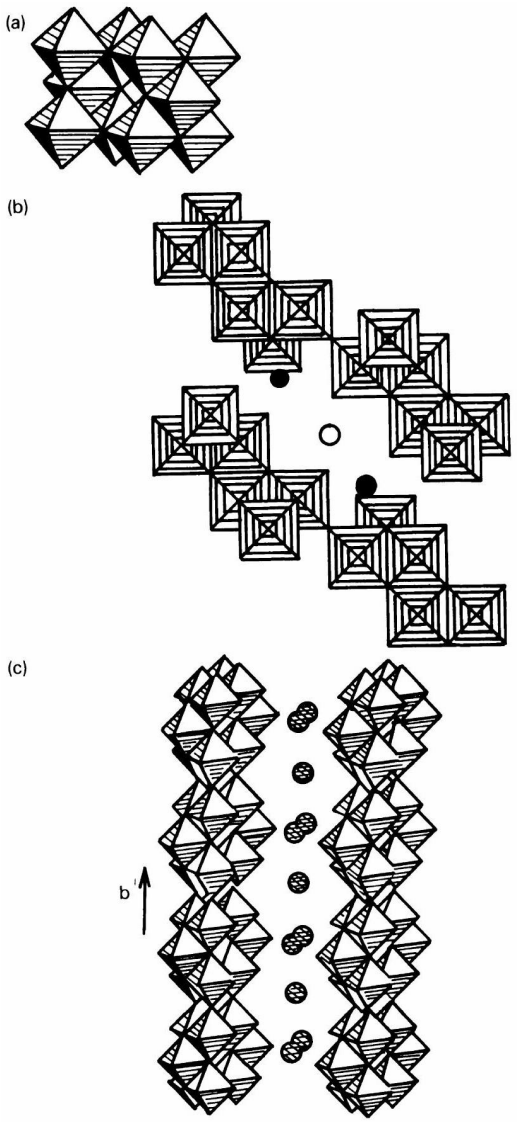


Fig. 33. Crystal structure of the blue bronze $\mathrm{A}_{0.30}MoO_3$. (a) The ten-octahedra clusters. (b) The octahedral slabs separated by the A ions. (c) The infinite MoO_6 octahedra chains along the monoclinic b axis.

Table 4 Unit cell parameters for $\mathrm{A}*{0.30}*\mathrm{MoO}*{3}$ blue bronzes. The structure is monoclinic, space group C2/m

Compound	a(Å)	b(Å)	c(Å)	β (degrees)	A^+ionic radii (Å)	Ref.
$K_{0.30}MoO_3$	18.25	7.56	9.85	117.5	1.33	Dumas et al. (1987)
$Rb_{0.30}MoO_3$	18.94	7.56	10.04	118.8	1.47	Janossy et al. (1987)
$Tl_{0.30}MoO_3$	18.54	7.57	10.07	118.4	1.47	Mihaly (1987), Mihaly et al. (19

results obtained for the Kohn anomaly from neutron inelastic scattering (Pouget et al. 1985, Escribe-Filippini et al. 1987).

EPR studies have also been performed on the blue bronzes in order to study the low temperature ($T < 20$ K) CDW state. EPR centers are very likely due to a stoichiometry defect and are Mo^{5+} in small concentrations (100 ppm) (Brusetti et al. 1981, Bouchard Jr et al. 1976). A remarkable time dependence of the spectra reflects the metastability and relaxation of the CDW state (Dumas et al. 1987). Recent results on the splitting of the EPR line indicate that commensurate domains exist in part of the crystal in the low temperature state (Janossy et al. 1987). This may hinder the 'fast' Fröhlich conductivity observed in the same state (Mihaly et al. 1988) and should be explored further.

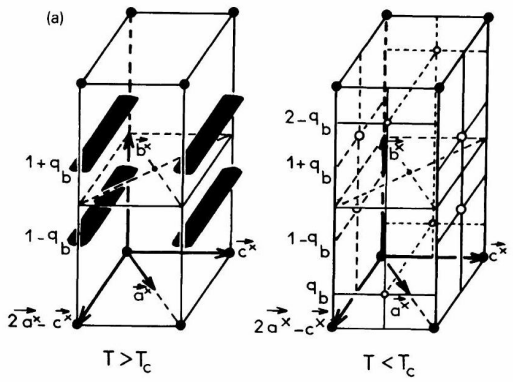


Fig. 34a.

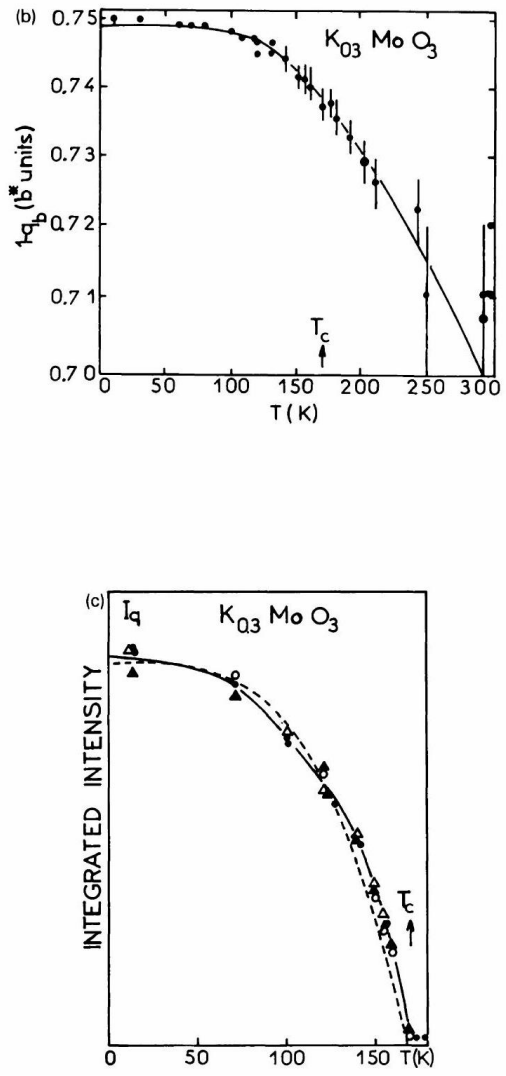


Fig. 34. (a) Schematic representation for the blue bronze in the reciprocal space of the diffuse streaks for $T>T_{\mathrm{p}}$ and of the satellite reflections for $T < T_{\mathrm{p}}$ (from Pouget et al. 1983). (b) Temperature dependence of the incommensurate component $1 - q_b\,(= 2k_{\mathrm{F}})$ of the satellite reflections (below T_{c}) and of the diffuse scattering (above T_{c}). (c) Normalized integrated intensity of the ($17, +1 \pm q_b, 8.5$) and ($17, \pm 1 \pm q_b, 8.5$) satellite reflections as a function of the temperature. The dotted line gives the temperature dependence of the square of the BCS order parameter (from Pouget et al. 1985).

7.2. Spectroscopic studies and band structure

Optical reflectivity studies performed with polarized light first established that the blue bronze is a genuine 1D conductor since the anisotropy of the plasma frequency for directions parallel and perpendicular to the 1D axis in the plane of the slabs was found larger than 100 . The corresponding anisotropy of the optical conductivity was estimated to be larger than 10^4 (Travaglini et al. 1981) (fig. 35). The spectra were consistent with the scheme of the band structure given in fig. 1d.

X-ray and ultraviolet photoemission spectroscopy studies corroborate the band structure calculations (Veuillen et al. 1987, Whangbo and Schneemeeyer 1986). A remarkable result has also been obtained by angle resolved UV photoemission on $(2, 0, 1)$ cleavage plane: the strong anisotropy of the spectrum obtained with respect to the angle θ between the collected photoelectrons and the normal incident photons allows a direct measurement of the Fermi wave

vector (fig. 36). It is found to be $0.31 \pm 0.05 \text{Å}^{-1}$, in good agreement with the value of 0.312Å^{-1} obtained from the q_b component of the satellite $\left(2k_{\mathrm{F}} \sim \frac{3}{4}b^*\right)$ (Veuillen et al. 1987).

The band structure has been calculated with the tight binding approximation for real chains and for a slab of $Mo_{10}O_{30}$ clusters for the bands

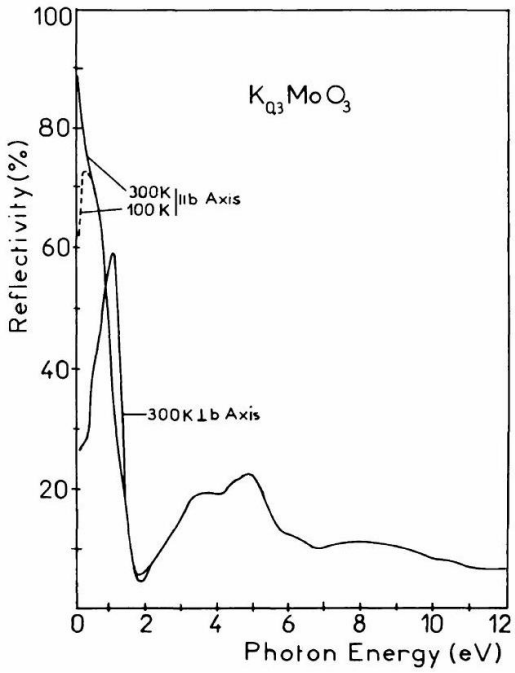


Fig. 35. Optical reflectivity of $\mathrm{K}_{0.30}\mathrm{MoO}_3$ with light polarized either along b or along [102] (perpendicular to b in the plane of the slabs at 300 K) (from Travaglini et al. 1981).

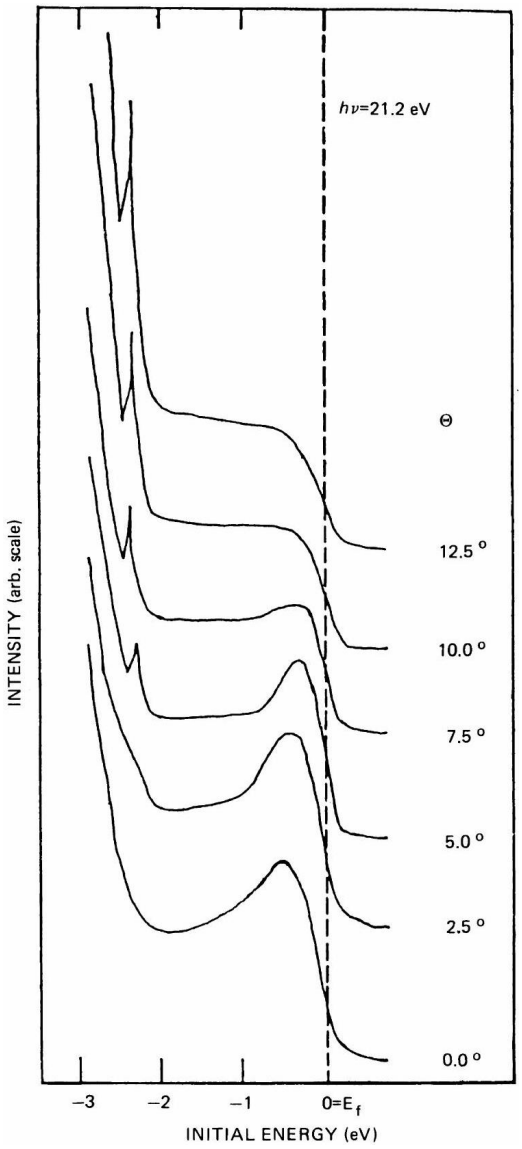


Fig. 36. Angle resolved ultraviolet photoemission spectra taken on $\mathrm{K}_{0.30}\mathrm{MoO}_3$ with 21.2 eV photons for $k_{\|}$along b^* showing the conduction band peak just below E_{F} (from Veuillen et al. 1987). $k_{\|}$is the component of the photoelectron wave vector k parallel to the surface $(2,0,1)$ crystallographic plane. Photoelectrons are collected in the plane defined by the normal to the $(2,0,1)$ plane and the b axis, at an angle θ from the normal.

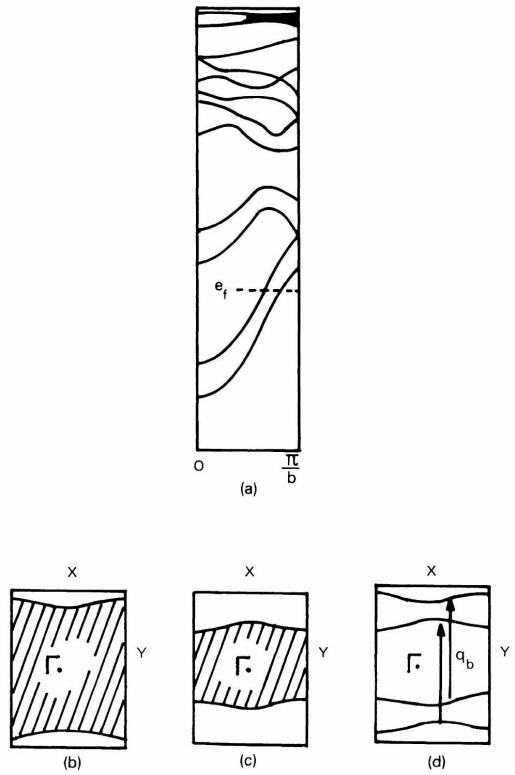


Fig. 37. Band structure calculated for the blue bronze. (a) Tight binding calculation for a chain of clusters of MoO_{6} octahedra showing two bands overlapping at the Fermi level (e_f). (b), (c), (d), Fermi surfaces associated with two partially filled d-block bands of a real $Mo_{10}O_{30}$ slab: (b) Fermi surface of the first band, where the wave vectors of the shaded and unshaded regions lead to occupied and unoccupied band levels respectively, (c) Fermi surface of the second band, (d) nesting of the Fermi surfaces of the first and second bands (from Whangbo and Schneemeyer 1986).

close to the Fermi level (Whangbo and Schneemeeyer 1986) (fig. 37a). The results are consistent with the presence of two overlapping bands roughly three quarters filled. They also show that a third band lies higher, close to the Fermi level. Figures 37b,c,d show the Fermi surfaces (FS) deduced from this calculation for the two bands and the predicted nesting of the FS along b^* : the upper FS of the first band is nested to the lower FS of the second band and reciprocally, with a wave vector $0.75b^*$. This is in agreement with the existence in the blue bronze of one CDW only.

7.3. The Peierls transition

Various physical properties, including transport, magnetic, thermal and elastic properties have been studied in the blue bronze: they show drastic changes or anomalies at the Peierls transition in the blue bronzes.

The electrical resistivity shows metal-non-metal transition at the Peierls transition (Fogle and Perlstein 1972). The anisotropy is consistent with a quasi-1D behaviour (fig. 32). This establishes that the Fermi surface is not far from being planar in the metallic state and is completely destroyed by the CDW instability. Both Hall effect (Bervas 1984) (fig. 38) and thermopower (Brusetti et al. 1981) (fig. 39) data show that the dominant carriers are holes above the Peierls transition and electrons below. At

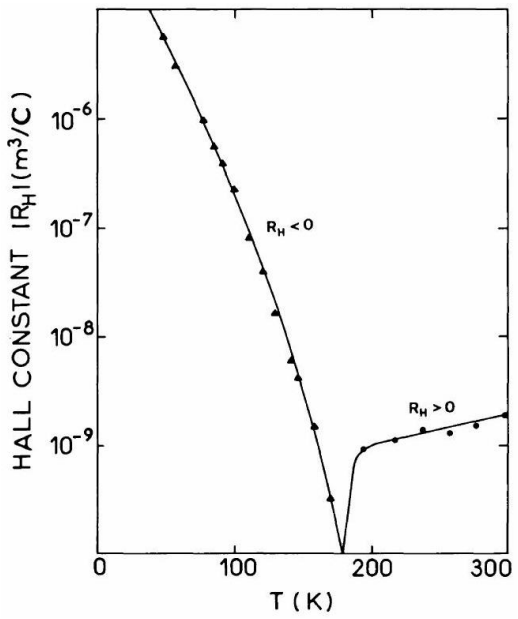


Fig. 38. Hall constant of $\mathrm{K}_{0.30}\mathrm{MoO}_3$ as a function of temperature (from Bervas 1984).

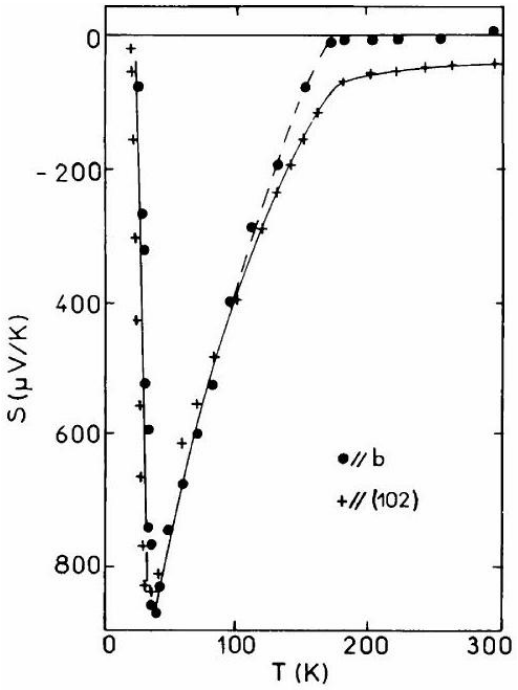


Fig. 39. Thermopower of $\mathrm{K}_{0.30}\mathrm{MoO}_3$ as a function of temperature, with the temperature gradient either along b or along [102] (from Brusetti et al. 1981).

300 K , the carrier concentration is roughly consistent in a simple Drude model, with a complete charge transfer from the A metal to the conduction band. Since the order parameter and therefore the Peierls gap is increasing with decreasing temperatures down to ~ 50 K (see fig. 34b), one does not expect a simple activated law for the transport properties above 50 K . In fact, the electrical resistivity shows an activation energy of ~ 0.03eV in the range $30 - 70$ K (Brusetti et al. 1981). As the Peierls gap has been estimated from optical reflectivity data to be 0.15 eV (Travaglini et al. 1981), this indicates that the blue bronze is not an intrinsic

semiconductor and that the transport properties at low temperatures are due to the presence of defects or impurity levels in the Peierls gap. The corresponding localized states may result from a stoichiometry defect giving rise to Mo^{5+} $\left(4\ d^1\right)$ localized states, as seen by EPR (Bang and Sperlich 1975, Dumas et al. 1987). One should note that the ratio of the Peierls gap to kT_P is found to be ~ 9, much larger than the mean field value 3.5. This feature is common to all CDW materials showing a Peierls transition.

The magnetic susceptibility of $K_{0.30}MoO_3$ (Brusetti et al. 1981, Bouchard Jr et al. 1967, Schneemeyer et al. 1984, Johnston 1984) is found to be anisotropic between the $(2, 0, 1)$ plane of the layers and the perpendicular orientation (fig. 40). Although the observed susceptibility is the result of several contributions, ($\chi = \chi_{\text{dia}} + \chi_{\text{Pauli}} + \chi_{\text{van vleck}}$), the anisotropy is mainly due to the Van Vleck paramagnetism, related to the anisotropy of the band structure. The decrease of x with decreasing temperature corresponds to

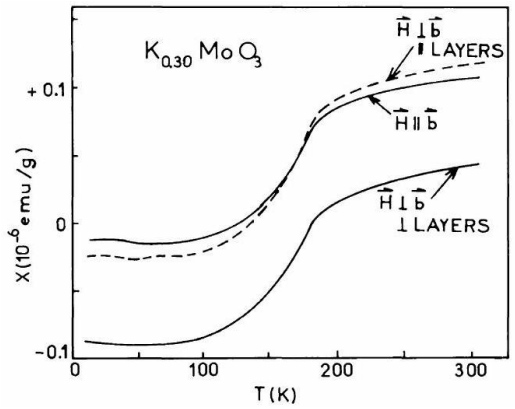


Fig. 40. Magnetic susceptibility of $\mathrm{K}\{0.30\}\ \mathrm{MoO}\{3\}$ as a function of temperature for different orientations of the magnetic field (from Schneemeyer et al. 1984).

the opening of the Peierls gap and to the vanishing of the Pauli contribution. This result has been analyzed by Johnston by taking into account the fluctuations (Johnston 1984). A pseudogap of 200 K is found above T_P. The obtained zero-temperature Peierls gap is of the order of 1200 K , not too far from the value obtained from optical reflectivity studies.

From specific heat studies, the Debye temperature for the potassium and the rubidium bronzes has been found to be close to 320 K(320 ± 10 K for $K_{0.30}MoO_3$ and 310 ± 10 K for $Rb_{0.30}MoO_3$) (Konaté 1984). This value is similar to what has been obtained either for MoO_3(340 ± 10 K), for the purple bronze $K_{0.9}Mo_6O_{17}$ and for the oxides η - Mo_4O_{11} and $\gamma - Mo_4O_{11}$ (Konaté 1984). This shows that the Debye temperature is mainly determined by the presence of the MoO_6 octahedra in all these materials.

A specific heat anomaly, found in both bronzes between approximately 150 and 190 K , corresponds to an enthalpy of ~ 25 J mole^{-1} and an entropy change of the order of 150 mJ mole^{-1} K^{-1} (fig. 41). This leads to a value for the density of states in the metallic phase of the order of 0.3eV^{-1} mole^{-1}, if all the entropy is attributed to the conduction electrons. One also obtains from these data a value of roughly $0.24R$ for the discontinuity in the electronic specific heat at the transition. This, compared to the entropy change, suggests that 1D fluctuations are important in this system (Johnston 1984, Konaté 1984).

At low temperatures ($0.1\ \text{K} < T < 1\ \text{K}$), the specific heat shows an excess contribution linear in temperature (Dahlhauser et al. 1986) and is time dependent at the lowest temperatures. This has been attributed to some low energy excitations due to the phase distortions of the randomly pinned CDW. However, the thermal conductivity shows no anomalous behavior in

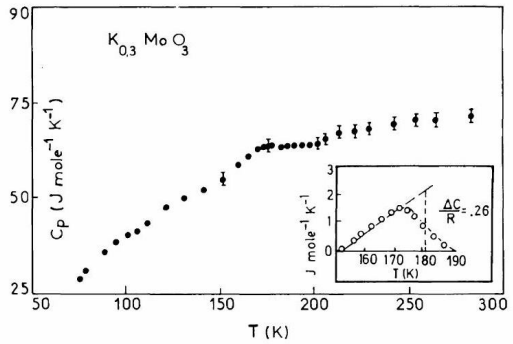


Fig. 41. Specific heat of $\mathrm{K}{0.30} \mathrm{MoO}{3}$ as a function of temperature in the vicinity of the Peierls transition (from Konaté 1984).

the same temperature range (Dahlhauser et al. 1986). The Young's modulus has been measured in the vicinity of the Peierls transition, both parallel and perpendicular to the b-axis (Bourne and Zettl 1986) (fig. 42). A strong anomaly is found near T_{P} in the perpendicular case and a weak one in the parallel orientation. These results are consistent with a second-order phase transition at T_{P}, connected with a considerable lattice softening.

7.4. Role of defects: impurities and irradiation

The ion channeling technique, using 1 MeV protons, has been used to study the role of impurities or lattice imperfections in the blue bronze (Daudin et al. 1987). Figure 43 shows the minimum backscattering yield obtained on

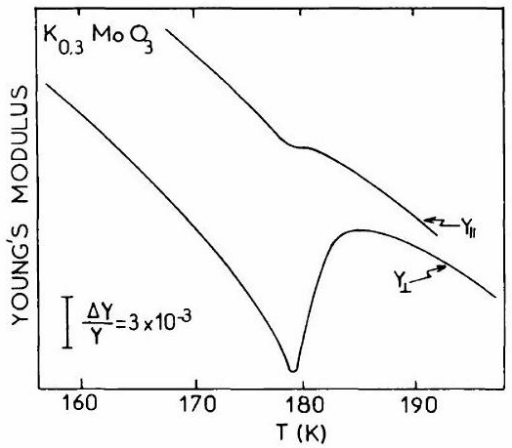


Fig. 42. Young's modulus measured parallel ($Y_{\|}$) and perpendicular ($Y_{\perp}$) to the b axis as a function of temperature near the Peierls transition in $\mathrm{K}_{0.30}\mathrm{MoO}_3$ (from Brown and Zettl 1986).

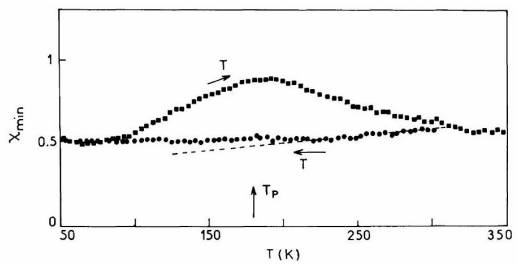


Fig. 43. Minimum backscattering yield $\chi_{\text {min }}$ obtained by proton channeling experiments on $K_{0.30}MoO_3$ as a function of temperature for successive cooling and heating cycles (1 K/min). The Peierls temperature (T_P) is indicated. The dotted line is a guide for the eye (from Daudin et al. 1987).

$A_{0.30}MoO_3$ between 350 and 50 K by successive heating and cooling. An anomalous increase of $\chi_{\min}$, starting around 100 K , is found with increasing temperatures only. These results have been attributed to the interaction of CDW defects or domains interacting with lattice defects. The hysteresis and peculiar temperature dependence of $\chi_{\min}$ on the heating cycle eliminate a simple relation with the CDW order parameter. They rather correspond to an out of equilibrium CDW state, possibly CDW domains, slowly rearranging as a function of temperature and time. The existence of hysteresis above the Peierls transition supports the existence of short-range order above T_{P}.

Various experiments have been performed on doped samples. Doping with isoelectronic impurities such as W substituted onto Mo sites or Rb onto K sites acts differently on the Peierls transition temperature (Schneemeyer et al. 1985). Very large effects are found by tungsten substitution whereas alkali substitution produces minor effects. The resistivity in the semiconducting phase is strongly decreased by doping with W and the low temperature activation energy changes from 35 meV down to 15 meV for doping concentrations reaching 12at%. This indicates that the W impurities lead to the formation of an impurity band in the Peierls gap.

Similarly, the Peierls temperature seems to be insensitive to a stoichiometry defect for the alkali metal. In order to clarify this point, the b^* satellite wave vector component has been measured in samples with different stoichiometries ($A_{0.28}MoO_3$ and $A_{0.30}MoO$) : q_b seems to be insensitive to the stoichiometry (Girault et al. 1987). In fact, it has been shown that the stoichiometry defect on the alkali metal is associated to oxygen vacancies in such a way that the filling of the conduction band is approximately constant (Girault et al. 1987, 1989).

Interesting results have been obtained by doping with V : in this case, a change of the b-component of the satellite wave vector has been found as a function of V concentration, as expected from the different numbers of outer electrons in V (Izumi et al. 1981) and Mo (Lieth and Torhell 1977), if V is substituted onto Mo sites (Girault et al. 1987, 1989). At the same time, V doping possibly induces disorder and Anderson localization, resulting in a semiconductor type behaviour.

The effect of Fe doping has been investigated by Mössbauer studies performed between 6 and 300 K on single crystals of ^{57}Fe-doped $K_{0.30}MoO_3$ containing about 300 ppm atomic of iron (Veuillen et al. 1987). The Peierls transition was not displaced by such a low concentration of impurities. Figure 44 shows that the Mössbauer linewidth shows an interesting temperature dependence: it shows little change between 200 and 120 K , around the Peierls temperature and increases steeply only below 120 K . This has been attributed to the pinning of CDW by the Fe impurities. The absence of broadening between 180 and 120 K shows that just below T_{P} the phase of the CDW at the impurity site is determined by Fe itself: the Fe ions act as strong pinning centers for the CDW . CDW domains are therefore nucleated around each

impurity. Below approximately 120 K , the steep increase of the linewidth suggests that the Fe progressively become weak pinning centers. In the limit of very weak pinning and in the incommensurate phase, the CDW phase would be random at each Fe site (Veuillen et al. 1987, Veuillen 1986).
Such a temperature dependence for the pinning of CDW by impurities is consistent with the predictions of the Lee and Rice model (Lee and Rice 1979). In this model, the pinning properties depend on the dimensionless

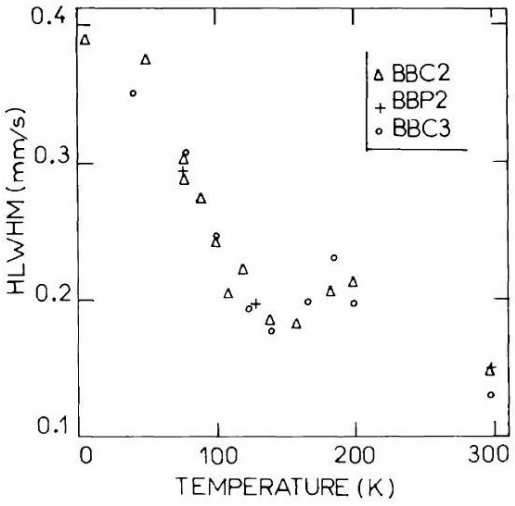


Fig. 44. Mössbauer linewidth as a function of temperature for several samples (single crystals and powder) of ${ }^{57} \mathrm{Fe}$ doped $K_{0.30}MoO_3$ (from Veuillen et al. 1986).

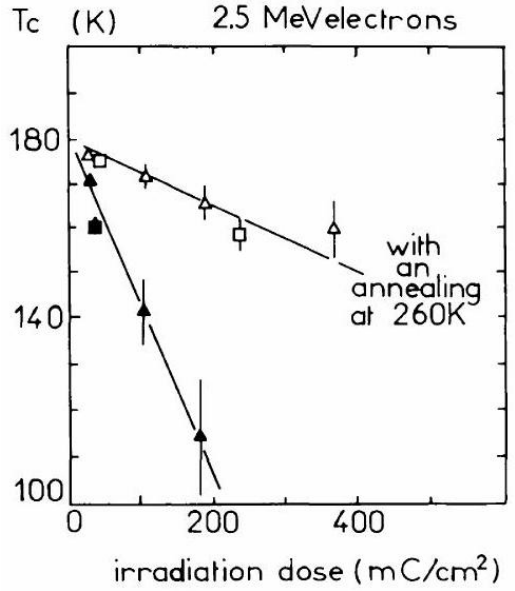


Fig. 45. Effect of electron irradiation on the Peierls transition of the blue bronze (from Mutka et al. 1984).

parameter ϵ which is related to the ratio of the pinning energy to the elastic energy associated to the pinning. At non-zero temperature, the strong pinning case corresponds in a first approximation to $\epsilon > \left[\left(T_P - T\right)/T_P\right]^{1/2}$ and the weak pinning one to the opposite. The

Mössbauer data on the blue bronze indicate that the transition between the two regimes takes place near 100 K and that ϵ may be of the order of 0.5 to 0.7 for Fe impurities.

Defects created by electron irradiation have a strong effect on the Peierls temperature and on the Peierls gap (Mutka et al. 1984, 1985) (fig. 45). Rather strong irradiation doses ($\approx 0.3 C/cm^2$) seem to smear out the Peierls gap, probably because of the induced disorder. In spite of the numerous results already obtained on doped blue bronzes, systematic studies especially at very low doping and for non-isoelectronic impurities, remain still to be done. It is clear that the CDW semiconducting state is sensitive to small impurities concentrations (less than 1%). It is only at this small doping level that the competing effects of a change of electron concentration and of the induced disorder could be elucidated. The role of the impurities in the pinning of CDW in relation with CDW transport is also not well understood at the moment and further work in that direction would be welcome.

4.2.9 8. Conclusions

8.1. A critical discussion of the chemical approaches of 1D inorganic chalcogenides

A way to modify the electronic properties of low-dimensional chalcogenides is to change their chemical composition either by atomic substitutions in the chains or by intercalation between them. Intercalation of lithium in transition metal trichalcogenides is easy to perform through the butyl-lithium technique, liquid ammonia solutions or electrochemical ways (Chianelli and Dines 1975, Murphy and Trumbore 1976, Whittingham 1977). The geometrical conditions governing the intercalation of Li^+ions have been discussed (Hodeau et al. 1978) and also, concerning the electrons transferred to the host, a nice connection was made between the discharge curve of $Li - NbSe_3$ batteries, for example, and the band structure of the chalcogenide (Ben Salem et al. 1989). It shows the progressive filling of the levels by the electrons with pseudo-plateaus in the discharge curve associated to high density of states regions. Unfortunately the crystals one gets after intercalation are of a poor quality (cracks and defects) and do not allow to practice reliable physical measurements. Besides its use in batteries, intercalation remains however, from a theoretical point of view, a convenient way to check the nature of the redox centers present in the structure (chalcogen pairs, high oxidation states of the transition metal).

Chemical substitutions are not easy to perform in trichalcogenides. Problems arise about the real amount of substitution and perhaps, even more important, about the position and distribution of impurities. Irradiation by electrons, protons or neutrons is often more reliable than doping to create controlled disorder in the structures.

Besides a strong increase of the residual resistance at low temperature, disorder lowers and may suppress Peierls transitions. Bulaevskii and Sadovskii (1974a,b) have shown that disorder has qualitatively the same effect on the Peierls transition as magnetic impurities on a superconducting transition. The increase in resistance at low temperature is to be related to a localization of the electrons which are not affected by the CDWs as well as to an interruption of the conducting chains which are cut in small onedimensional boxes. The electrons may have to jump from one chain to a neighboring one instead of crossing the interruption. The fact that polycrystalline samples made of pressed powders show similar curves as the doped or irradiated samples is much in favor with that hypothesis in $NbSe_3$. Surprisingly, cations and anions disorder in $Ta_{1-x}Nb_x\ S_3$ and $TaS_{3-x}Se_x$ show very similar effects although the cationic disorder was expected to bring more important modifications to a d band phenomenon.

Tri- and tetrachalcogenides of transition metals represent a large group of CDW materials. During the past few years (1985-1987) new developments in chemistry have been more concerned with an extension of crystal chemistry concepts to series involving stabilization of chains by other chains, waved structures or construction of chains from partial or infinite condensation of clusters, than that they have been dealing with the synthesis of new CDW compounds. Besides

the strong fundamental interest in solid state chemistry to reach a better understanding of the design, stability and
electronic properties of low-dimensional solids, it appears also that, perhaps, one needs probably to deepen the knowledge of the already known CDW materials rather than preparing new ones. This comes largely from the problems that have been raised by the depinning of charge density waves. The physics of CDW dynamics is largely developed in the various chapters of this book. But Solid State Chemistry is also largely concerned through the role of structural defects.

Concerning trichalcogenides, and especially $NbSe_3$, it is not to be excluded that pieces of one MX_3 chain are incorporated in another one. The redox competition between d cationic levels and the sp anionic band is at the origin of the formation of chalcogen pairs. Lateral couplings from chain to chain complicate the situation and do not allow an easy prediction of the structural type to be formed. The length of the chalcogen pairs depends on those couplings as well as on the $d - sp$ competition. In the sulfides, which are more 1D in character, the structures are less complicated than in selenides. Most of the trichalcogenides have to be regarded as metastable phases. Very likely under high temperature and high pressure conditions, a unique chain would be present in $NbSe_3$ like in $ZrSe_3$. The question is also posed why the existence of different [MX_6] polyhedra results in a segregation in three different chains in $NbSe_3$ and not in an alternation of different polyhedra in the same chain like in MoS_3 (which makes the latter compound to be quasi-amorphous).

In the case of tetrachalcogenides the situation is still more complicated. The $(MX_4)_n$ I phases are obtained in sealed tubes, i.e., under thermodynamic conditions that are difficult to ascertain. With the same elements (Nb, Se, I, for example) one can get various phases. A small range of temperatures is associated with particular starting conditions (volume of the tube, quantities) in order to get a given compound. However, most of the time, different phases are obtained in the same tube, each crystal having to be checked carefully. In addition, all the phases have very closely related structures which makes it possible to observe an intergrowth phenomenon. This would simply result in slight local metal and iodine displacements in their respective chains. The two types of $(NbSe_4)_3$ **I** crystals illustrate probably the possible presence of $(NbSe_4)_{10/3}$ I microdomains along the $(NbSe_4)_3$ I structure in type II crystals. The low temperature resistivity of this phase strongly recalls the behavior of $(NbSe_4)_{10/3}$ I at these temperatures ($E_g \approx 3000$ K instead of 4000 K for $(NbSe_4)_3$ I). These stacking faults form defects perpendicular to the chain axis. Electron diffraction studies are in progress to get a better characterization. One can also think of defects in the way the (Se_4) planes rotate around the metallic chain.
$(MX_4)_n$ I phases remind us of most of the other families of 1D conductors. They are chains of metal atoms enclosed in a chalcogen framework like trichalcogenides. But these chains are stabilized by counter ions and, from
that point of view, represent a symmetrical situation with respect to blue bronzes. Iodine columns and conducting chains also alternate in some organic conductors such as (TSeT)I_x phases (tetraselenotetracene $\mathbf{I}_x$ which presents $\mathbf{I}^-$ions and not $\mathbf{I}_3^-$ions like most of the organic materials). Finally, the sequence of long and short metal-metal distances along the metallic chains reminds us of some chain polymers. Indeed the electrical behavior shows also here that the highest room temperature resistivity is to be associated with the systems showing the largest distribution of metal-metal distances. $(TaSe_4)_2$ I with only one metal-metal distance is the most conducting phase at room temperature.

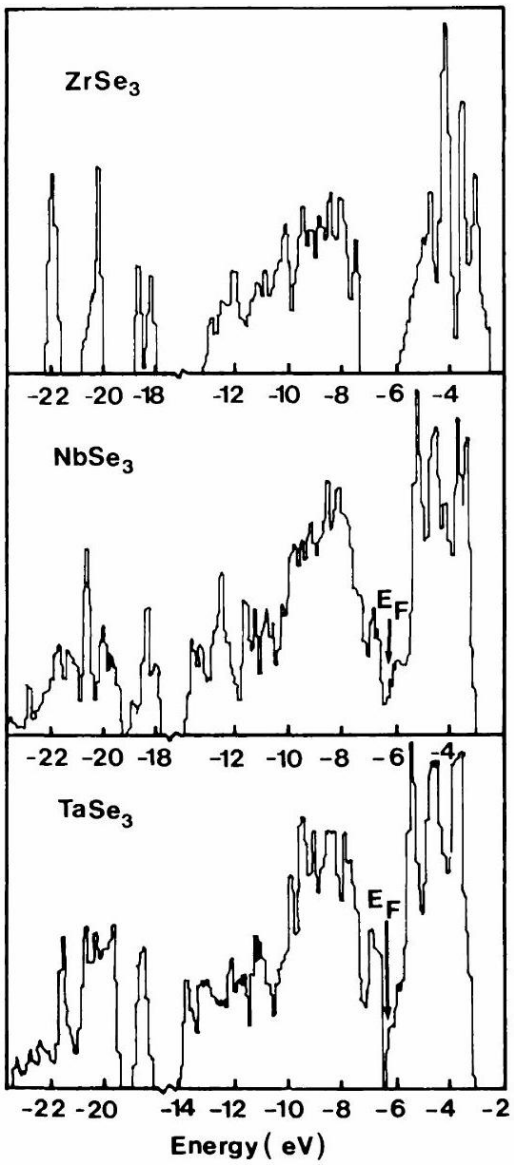


Fig. 46. Electron densities of states in the valence and conduction bands of $\mathrm{ZrSe}*{3}*, *mathrm{NbSe}*{3}$ and $TaSe_3$.

The real dimensionality of a given trichalcogenide is related to the ionicity of the metal-chalcogen bonds. It directly reflects in the crystal chemistry and properties of the materials (occurrence of polytypes in the more 1D sulfides as compared to selenides, important pre-transitional effects, metal to non-metal transitions at higher temperatures). Extended band calculations such as the ones made by Bullett (Bullett 1979) allow more quantitative comparisons among trichalcogenides. They are in good agreement with experimental XPS studies by Endo et al. (1981). Figures 46 and 47 show respectively the density of states diagrams for $ZrSe_3, NbSe_3$, $TaSe_3$ and the dispersion parallel to the chain direction for bands near the Fermi energy in $NbSe_3$ and $TaSe_3$ along (a) $(0, k_2, 0)$; (b) $(\pi/a, k_2, 0)$; (c) $(0, k_2, \pi/c)$. Of course the semiconducting behavior of $ZrSe_3$ appears clearly and the experimental gap of 1.8 eV (Schairer and Shafer 1973, Jellinek et al. 1974) fits well with the calculation results ($\approx$ 1.6eV), so does the main valence band width ($\sim$ 6eV) with the X-ray photoemission spectra (Jellinek et al. 1974). But more important is a possible explanation of the existence of phase transitions in $NbSe_3$ and not in $TaSe_3$. This comes from an examination of the energy bands at the Fermi level (fig. 47). In niobium trichalcogenide six ($NbSe_3$) groups are found per unit cell, 69 energy bands are filled but there is a sharp separation between the 68th band relatively

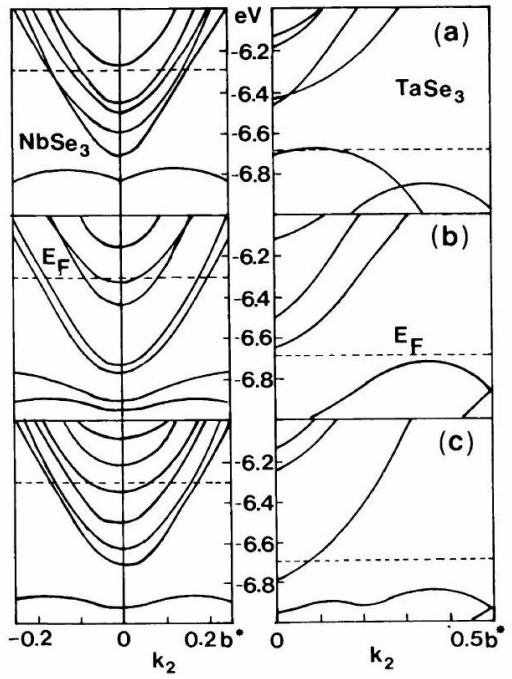


Fig. 47. Dispersion parallel to the chain direction for bands near the Fermi energy in NbSe_{3} and $TaSe_3$ along (a) $(0, k_2, 0)$; (b) $(\pi/a, k_2, 0)$; (c) $(0, k_2, \pi/c)$.

flat and the 69th which belongs to a group of four, almost dispersionless in the (a, c) plane but rising rapidly as k moves away in the chain direction. This level has a strong d_{z^2} component along the b axis. The result is a pseudo-1D metal with four energy levels crossing the Fermi energy. A Peierls transition with $\frac{1}{4}b^*$ is expected. Now, in the case of $TaSe_3$, 46 energy levels are filled but there is a slight semi-metallic overlap with the next higher band. No CDW is expected because of the much stronger dispersion in the (a^*, c^*) plane of the relevant bands.

8.2. Towards solving some problems related to the physics of CDW in quasi-1D inorganic conductors

Although a considerable amount of work has been done these last years on quasi-1D inorganic conductors in relation with the CDW state, several important problems are not solved yet.

For example, the origin of the metastability of the CDW state remains unclear. What is the role of the impurities and other crystal defects? How important is the intrinsic competition between the lattice periodicity and the CDW modulation directly related to the Fermi wave vector k_{F}. Since changing the Fermi wave vector is in principle possible through changing stoichiometry or impurity concentration, it is clear that separating both mechanisms will be difficult. As discussed at the end of section 7, one should systematically study the effect of doping as a function of concentration. But bulk properties will not be sufficient. Local tools should be explored in detail. For example, for transition metal impurities, EPR is a powerful technique, since the paramagnetic impurities should act either as probes sensitive to modifications of the surrounding or as 'active' centers coupled to the CDW.

Another important problem which remains unsolved is the role of the electrical contacts in CDW transport. Although the description of CDW transport is not the purpose of this chapter, we may suggest some hints. One should note that, in the case of the blue bronze, the 'fast' Fröhlich conductivity at low temperature is observed only when special care is taken for the realization of contacts. It is certainly not clear whether this is a side effect or central to the

problem of CDW transport, in relation with the conversion of CDW condensed carriers into normal carriers at the ends of the sample. Of course, systematic studies of the influence of the nature of the electrical contact could be performed. But one probably needs more refined tools of surface physics to understand this point. It is clear that the interface between the CDW material and the metallic contact should be studied in detail, using for example photoelectron spectroscopies. One would certainly need some knowledge of the electron states at the interface. The blue bronze may be one of the 1D materials well adapted for these studies, since photoemission techniques have already been used successfully in this case.

4.2.10 References

Allman, R., L. Bauman, A. Kutoglu, H. Rösch and E. Hellner, 1964, Naturwissenschaften 51, 263.

Auborn, J.J., Y.L. Barbiero, K.J. Hanson, D. Schleich and M.J. Martin, 1987, J. Electrochem. Soc. 134-3, 580.

Bang, G., and G. Sperlich, 1975, Z. Phys. B 22, 1.

Ben Salem, A., A. Meerschaut, H. Salva, Z.Z. Wang and T. Sambongi, 1984, J. Phys. (France) 45, 771.

Ben Salem, A., M.H. Whangbo, A. Meerschaut and J. Rouxel, 1989, Inorg. Chem. (to be submitted).

Bervas, E., 1984, Thèse d'Ingénieur-Docteur (Université Scientifique Technologique et Médicale de Grenoble).

Bjerkelund, E., and A. Kjekshus, 1964, Z. Anorg. & Allg. Chem. B 328, 235.

Bjerkelund, E., J.H. Fermor and A. Kjekshus, 1966, Acta Chem. Scand. 20, 1836.

Böhn, H., and H.G. van Schnering, 1983, Z. Kristallogr. 162, 26.

Boswell, F.W., and A. Prodan, 1980, Physica B 99, 361.

Boswell, F.W., and A. Prodan, 1984, Mater. Res. Bull. 19, 93.

Boswell, F.W., A. Prodan and J.K. Brandon, 1983, J. Phys. C 16, 1067.

Bouchard Jr, G.H., J.H. Perlstein and M.J. Sienko, 1967, Inorg. Chem. 6, 1682.

Bourne, L.C., and A. Zettl, 1986, Solid State Commun. 60, 789.

Brattas, L., and A. Kjekshus, 1971, Acta Chem. Scand. 25, 2783.

Briggs, A., P. Monceau, M. Nunez-Regueiro, J. Peyrand, M. Ribault and J. Richard, 1980, J. Phys. C 13, 2117.

Briggs, A., P. Monceau, M. Nunez-Regueiro, M. Ribault and J. Richard, 1981, J. Phys. (France) 42, 1453.

Brill, J.W., N.P. Ong, J.C. Eckert, J.W. Savage, S.K. Khanna and R.B. Somsans, 1981, Phys. Rev. B 23, 1517.

Brusetti, R., B.K. Chakraverty, J. Devenyi, J. Dumas, J. Marcus and C. Schlenker, 1981, in: Recent Development in Condensed Matter Physics, Vol. 2, eds J.T. Devreese, L.F. Lemmens, V.E. Van Doren and J. Van Royen (Plenum Press, New York) p. 181.

Bulaevskii, L.N., and M.V. Sadovskii, 1974a, Fiz. Tverd. Tela 16, 1159.

Bulaevskii, L.N., and M.V. Sadovskii, 1974b, Sov. Phys.-Solid State 16, 743.

Bullett, D.W., 1979, J. Phys. C 12, 277.

Butaud, P., 1987, Thèse de l'Université Scientifique, Technologique et Médicale de Grenoble.

Butaud, P., P. Segransan, C. Berthier and A. Meerschaut, eds, 1984, in: Proc. Conf. on Charge Density Waves in Solids, XII Congress, Budapest, 1984.

Butaud, P., P. Ségransan, C. Berthier, J. Dumas and C. Schlenker, 1985, Phys. Rev. Lett. 55, 253.

Cava, R.J., V.L. Hines, A.D. Mighell and R.S. Roth, 1981, Phys. Rev. B 24, 3634.

Cava, R.J., F.J. Di Salvo, M. Eibschutz and J.V. Waszczak, 1983, Phys. Rev. B 27, 7412.

Chaussy, J., P. Haen, J.C. Lasjaunias, P. Monceau, G. Waysand, A. Waintal, A. Meerschaut, P. Molinié and J. Rouxel, 1976, Solid State Commun. 20, 759.

Chen, C.H., and R.M. Fleming, 1983, Solid State Commun. 48, 777.

Chevrel, R., M. Sergent and J. Prigent, 1971, J. Solid State Chem. 3, 515.

Chianelli, R.R., and M.B. Dines, 1975, Inorg. Chem. 14, 2419.

Cornelissens, T., G. Tendeloo, J. Landuyt and S. Amelinckx, 1978, Phys. Status Solidi 48, K5.

Dahlhauser, K.J., A.C. Anderson and G. Mozurkewich, 1986, Phys. Rev. B 34, 4432.

Daudin, B., M. Dubus, J. Dumas and J. Marcus, 1987, J. Phys. (France) 48, 1779.

Delaplace, R., P. Molinié and D. Jérome, 1976, J. Phys. Lett. 37, L13.

Di Salvo, F.J., R.M. Fleming and J.V. Waszczak, 1981, Phys. Rev. B 24, 2935.

Dieman, E., 1977, Z. Anorg. & Allg. Chem. 432, 127.

Dieman, E., and A. Müller, 1973, Coord. Chem. Rev. 10, 79.

Dumas, J., C. Schlenker, J.Y. Veuillen, R. Chevalier, J. Marcus, R.J. Cinti and E. Al Khoury Nemeh, 1987, Synth. Met. 19, 937.

Endo, K., H. Ihara, S. Gorda and K. Watanabe, 1981, Physica B 105, 159.

Escribe-Filippini, C., J.P. Pouget, B. Hennion and M. Sato, 1987, Synth. Met. 19, 931.

Fleming, R.M., L.F. Schneemeyer and D.E. Moncton, 1985, Phys. Rev. B 32, 3568.

Fogle, W., and J.H. Perlstein, 1972, Phys. Rev. B 6, 1402.

Fujishita, H., M. Sato, S. Sato and S. Hoshino, ????, J. Phys. C????.

Fujishita, H., M. Sato and S. Hoshius, 1984, Solid State Commun. 49, 313.

Fuller, W.W., G. Grüner, P.M. Chaikin and N.P. Ong, 1981, Phys. Rev. B 23, 6259.

Furuseth, S., L. Brattas and A. Kjekshus, 1973, Acta Chem. Scand. 27, 2367.

Furuseth, S., L. Brattas and A. Kjekshus, 1975, Acta Chem. Scand. A 29, 623.

Ganne, M., A. Boumaza and M. Dion, 1985, Mater. Res. Bull. 20, 1297.

Geserich, P., 1985, in: Electronic Properties of Inorganic Quasi 1D Materials, Part II, ed. P. Monceau (Reidel, Dordrecht) pp. 111-138.

Ghedira, M., J. Chenavas, M. Marezio and J. Marcus, 1985, J. Solid State Chem. 57, 300.

Gill, J.C., 1981, Solid State Commun. 39, 1203.

Girault, S., 1987, Thèse de l'Université de Paris XI - Orsay.

Girault, S., A.H. Moudden, G. Collin, J.P. Pouget and R. Comès, 1987, Solid State Commun. 63, 17.

Girault, S., A.H. Moudden, J.P. Pouget and J.M. Godard, 1988, Phys. Rev. B 38, 7980.

Graham, J., and A.D. Wadsley, 1966, Acta Crystallogr. 20, 93.

Gressier, P., L. Guemas and A. Meerschaut, 1982, Acta Crystallogr. Sect. B 38, 2877.

Gressier, P., A. Meerschaut, L. Guemas, J. Rouxel and P. Monceau, 1984a, J. Solid State Chem. 51, 141.

Gressier, P., M.H. Whangbo, A. Meerschaut and J. Rouxel, 1984b, Inorg. Chem. 23, 1221.

Grüner, G., 1984, (personal communication, ABANO Congress on Low-dimensional Solids).

Guemas, L., P. Gressier, A. Meerschaut and D. Grandjean, 1981, Rev. Chim. Miner. 18, 91.

Haen, P., P. Monceau, B. Tissier, G. Waysand, A. Meerschaut, P. Molinié and J. Rouxel, 1975, in: Proc. 14th Int. Conf. on Low Temperature Physics, Otaniemi, Finland, p. 445.

Haen, P., J.M. Mignot, P. Monceau, M. Nunez-Regueiro and J. Richard, 1978, Lect. Notes Phys. 95, 323.

Hodeau, J.L., M. Marezio, C. Roucau, R. Ayroles, A. Meerschaut, J. Rouxel and P. Monceau, 1978, J. Phys. C 11, 4117.

Hoffmann, R., S. Shaik, J.C. Scott, M.H. Whangbo and M.J. Foshee, 1980, J. Solid State Chem. 34, 263.

Hsieh, P.L., F. De Czito, A. Janossy and G. Grüner, 1983, J. Phys. (France) 44-C3, 1753.

Izumi, M., K. Uchinokura and E. Matsuura, 1981, Solid State Commun. 37, 641.

Izumi, M., T. Nakayama, R. Yoshizaki, K. Uchinokura, T. Iwazumi, T. Seino and E. Matsuura, 1983, in: Proc. Int. Symp. on Nonlinear Transport and Related Phenomena in Quasi-One-Dimensional Inorganic Conductors, Sapporo, Japan, October 20-22, 1983, p. 301.

Izumi, M., T. Iwazumi, K. Uchinokura, R. Yoskizaki and E. Matsuura, 1984, Solid State Commun. 51, 191.

Jackson, C.M., A. Zettl, G. Grüner and F.J. Di Salvo, 1983, Solid State Commun. 45, 247.

Janossy, A., C. Berthier, P. Ségransan and P. Butaud, 1987, Phys. Rev. Lett. 59, 2348.

Jellinek, F., R.A. Pollack and M.W. Shafer, 1974, Mater. Res. Bull. 9, 845.

Johnston, D.C., 1984, Phys. Rev. Lett. 52, 2049.

Johnston, D.C., M. Maki and G. Grüner, 1985, Solid State Commun. 53, 5.

Keszler, D.A., and J.A. Ibers, 1984, J. Solid State Chem. 52, 73.

Kikkawa, S., M. Koizumi, S. Yamanaka, Y. Onuki, R. Inada and S. Tanuma, 1981, J. Solid State Chem. 40, 28.

Kikkawa, S., N. Ogawa, M. Koizumi and Y. Onuki, 1982a, J. Solid State Chem. 41, 315.

Kikkawa, S., K. Shinya and M. Koizumi, 1982b, J. Solid State Chem. 41, 323.

Konaté, K., 1984, Thèse de 3ème Cycle (Université Scientifique, Technologique et Médicale de Grenoble).

Kröniert, W., and K. Plieth, 1965, Z. Anorg. & Allg. Chem. 336, 207.

Lee, P.A., and T.M. Rice, 1979, Phys. Rev. B 19, 3970.

Lepetit, R., P. Monceau, M. Potel, P. Goujeon and M. Sergent, 1984, J. Low Temp. Phys. 56, 219.

Levy, F., and A. Grisel, 1985, in: Electronic Properties of Inorganic Quasi-One-Dimensional Compounds, ed. P. Monceau (Reidel, Dordrecht) pp. 269-308.

Liang, K.S., S.P. Cramer, D.C. Johston, C.H. Chang, A.J. Jacobson, J.P. Neufville and R.R. Chianelli, 1980, J. Non-Cryst. Solids 42, 345.

Lieth, R.M.A., and J.C.J.M. Torhell, 1977, in: Preparation and Crystal Growth of Materials with Layered Structures, ed. R.M.A. Lieth (Reidel, Dordrecht) pp. 141-223.

Maki, M., M. Kaiser, A. Zettl and G. Grüner, 1983, Solid State Commun. 46, 497.

Malvy, J., G.A. Wiegers, J. van Landuyt and S. Amelinckx, 1984, Mater. Res. Soc. Symp. Proc. 21, 181.

Meerschaut, A., and J. Rouxel, 1975, J. Less Common Met. 39, 197.

Meerschaut, A., and J. Rouxel, 1986, in: Crystal Chemistry and Properties of Materials with Quasi-One-Dimensional Structures, ed. J. Rouxel (Reidel, Dordrecht) pp. 205-279.

Meerschaut, A., P. Palvadeau and J. Rouxel, 1977, J. Solid State Chem. 20, 21.

Meerschaut, A., J. Rouxel, P. Haen, P. Monceau and M. Nunez-Regueiro, 1979a, J. Phys. Lett. 40, L-157.

Meerschaut, A., L. Guemas, R. Berger and J. Rouxel, 1979b, Acta Crystallogr. Sect. B 35, 1747.

Meerschaut, A., L. Guemas and J. Rouxel, 1981a, J. Solid State Chem. 36, 118.

Meerschaut, A., P. Gressier, L. Guemas and J. Rouxel, 1981b, Mater. Res. Bull. 16, 1035.

Meerschaut, A., P. Gressier, L. Guemas and J. Rouxel, 1984, J. Solid State Chem. 51, 307.

Meerschaut, A., P. Grenouilleau and J. Rouxel, 1986, J. Solid State Chem. 61, 90.

Meerschaut, A., P. Grenouilleau and J. Rouxel, 1987a, J. Solid State Chem. 66, 293.

Meerschaut, A., P. Grenouilleau, L. Guemas and J. Rouxel, 1987b, J. Solid State Chem. 70, 36.

Mihaly, G., and P. Beauchêne, 1987, Solid State Commun. 63, 911.

Mihaly, G., and L. Mihaly, 1983, Solid State Commun. 48, 449.

Mihaly, G., N. Housseau, H. Mutka, L. Zuppiroli, J. Pélissier, P. Gressier, A. Meerschaut and J. Rouxel, 1981, J. Phys. Lett. 42, L-263.

Mihaly, G., P. Beauchêne and J. Marcus, 1988a, Solid State Commun. 66, 149.

Mihaly, G., P. Beauchêne, J. Dumas, J. Marcus and C. Schlenker, 1988b, Phys. Rev. B 37, 1047.

Monceau, P., 1982, Physica B 109&110, 1890.

Monceau, P., J. Richard and P. Lagnier, 1981, J. Phys. C 14, 2995.

Murphy, D.W., and F.A. Trumbore, 1976, J. Electrochem. Soc. 123, 960.

Mutka, H., S. Bouffard, G. Mihaly and L. Mihaly, 1984, J. Phys. Lett. 45, L-113.

Mutka, H., S. Bouffard, J. Dumas and C. Schlenker, 1984, J. Phys. Lett. 45, L729.

Mutka, H., S. Bouffard, M. Sanquer, J. Dumas and C. Schlenker, 1985, Mol. Cryst. & Liq. Cryst. 121, 133.

Nagasawa, H., T. Erata, M. Onoda, H. Suzuki, Y. Kanai and S. Kagoshima, 1983, J. Phys. (France) C3, 1737.

Nagasawa, H., M. Onoda, Y. Kanai and S. Kagoshima, 1987, ICSM 86, Synth. Met. 19, 971.

NATO-ASI on Low-Dimensional Conductors, and Superconductors, 1987, Magog, Quebec (Plenum Press, New York).

Nunez-Regueiro, N., 1980, Thesis, Grenoble.

Ohana, I., D. Schmeltzer, D. Shaltiel, Y. Yacoby and A. Mustachi, 1985, Solid State Commun. 54, 747.

Okada, S., T. Sambongi, M. Ido, Y. Tazuke, R. Ashi and O. Fujita, 1982, J. Phys. Soc. Jpn. 51, 460.

Ong, N.P., and J.W. Brill, 1978, Phys. Rev. B 18, 5265.

Ong, N.P., and P. Monceau, 1978, Solid State Commun. 26, 487.

Onoda, M., K. Toriumi, Y. Matsuda and M. Sato, 1987, J. Solid State Chem. 69, 67.

Pauling, L., 1960, The Nature of the Chemical Bond (Cornell Univ. Press, Ithaca, NY).

Potel, M., R. Chevrel and M. Sergent, 1980, Acta Crystallogr. Sect. B 36, 1545.

Pouget, J.P., S. Kagoshima, C. Schlenker and J. Marcus, 1983, J. Phys. Lett. 44, L-113.

Pouget, J.P., C. Eporibe-Filippini, B. Hennion, R. Currat, A.H. Moudden, R. Mozet, J. Marcus and C. Schlenker, 1985a, Mol. Cryst. Liq. Cryst. 121, 111.

Pouget, J.P., C. Noguera, A.H. Moudden and R. Moret, 1985b, J. Phys. (France) 46, 1731.

Prasad, T.P., E. Dieman and A. Müller, 1973, J. Inorg. & Nucl. Chem. 35, 1895.

Rijnsdorp, J., and F. Jellinek, 1978, J. Solid State Chem. 25, 325.

Rijnsdorp, J., G.J. Delange and G.A. Weigers, 1969, J. Solid State Chem. 30, 365.

Ritsma, J., G. Demazeau and J. Rouxel, (unpublished results).

Roucau, C., R. Ayroles, P. Monceau, L. Guemas, A. Meerschaut and J. Rouxel, 1980, Phys. Status Solidi 62, 483.

Roucau, C., T. Granier and R. Ayroles, 1983, J. Phys. C 3-44, 1725.

Roucau, C., R. Ayroles, P. Gressier and A. Meerschaut, 1984, J. Phys. C 17, 2993.

Salva, H., Z.Z. Wang, P. Monceau, J. Richard and M. Renard, 1984, Philos. Mag. 49, 385.

Sambongi, T., 1986, in: Crystal Chemistry and Physical Properties of Quasi 1D Structures, ed. J. Rouxel (Reidel, Dordrecht) pp. 281-313.

Sambongi, T., M. Yamamoto, K. Tsutsumi, Y. Shiozaki, K. Yamaya and Y. Abe, 1977a, J. Phys. Soc. Jpn. 42-4, 1421.

Sambongi, T., K. Tsutsumi, Y. Shiozaki, M. Yamamoto, K. Yamaya and Y. Abe, 1977b, Solid State Commun. 22, 729.

Sambongi, T., K. Biljakovic, A. Smontara and L. Guemas, 1985, Synth. Met. 10, 161.

Sato, M., and H. Nishihara, 1985, J. Phys. C 18, 2145.

Schairer, W., and M.W. Shafer, 1973, Phys. Status Solidi a 17, 181.

Schlenker, C., ed., 1989, Low Dimensional Electronic Properties of Molybdenum Bronzes and Oxides (Kluwer).

Schlenker, C., and J. Dumas, 1986, in: Crystal Chemistry and Properties of Materials with Quasi-One Dimensional Structures, ed. J. Rouxel (Reidel, Dordrecht) p. 135.

Schlenker, C., J. Dumas, C. Escribe-Filippini, H. Guyot and J. Marcus, 1985, Philos. Mag. B 52, 643.
Schneemeyer, L.F., F.J. Di Salvo, R.M. Fleming and J.V. Waszczak, 1984, J. Solid State Chem. 54, 358.
Schneemeyer, L.F., S.E. Sprengler, F.J. Di Salvo and J.V. Waszczak, 1985, Mol. Cryst. & Liq. Cryst. 125, 41.
Schutte, W.J., and J.L. de Boer, Acta Crystallogr. Sect. B, submitted 1988.
Sekine, T., T. Seino, M. Izumi and E. Matsuura, 1985, Solid State Commun. 53, 767.
Selte, K., and A. Kjekshus, 1964, Acta Chem. Scand. 18, 690.
Skelton, E.F., T.J. Wieting, S.A. Wolf, W.W. Fuller, D.U. Gubser, T.L. Francaville and F. Levy, 1982, Solid State Commun. 41, 1.
Stephenson, N.C., and A.D. Wadsley, 1965, Acta Crystallogr. 18, 241.
Sunshine, S.A., and J.A. Ibers, 1985, Inorg. Chem. 24, 3611.
Tagaki, T., M. Ido and T. Sambongi, 1978, J. Phys. Soc. Jpn. Lett. 45, 2039.
Tajima, Y., and K. Yamaya, 1984, J. Phys. Soc. Jpn. 53, 495.
Tarascon, J.M., F.J. Di Salvo, C.H. Chen, P.J. Carroll, M. Walsh and L. Rupp, 1985, J. Solid State Chem. 58, 290.
Tomic, S., K. Biljakovic, D. Djurek, J.R. Cooper, P. Monceau and A. Meerschaut, 1981, Solid State Commun. 38, 109.
Travaglini, G., P. Wachter, J. Marcus and C. Schlenker, 1981, Solid State Commun. 37, 599.
Tsutsumi, K., T. Tagagaki, M. Yamamoto, Y. Shiozaki, M. Ido, T. Sambongi, K. Yamaya and Y. Abe, 1977, Phys. Rev. Lett. 39, 1675.
van Smaalen, S., and K.D. Bronsema, 1986, Acta Crystallogr. Sect. B 42, 43.
Veuillen, J.Y., 1986, Thèse de l'Université Scientifique, Technologique et Médicale de Grenoble.
Veuillen, J.Y., R.C. Cinti and E. Al Khoury Nemeh, 1987, Europhys. Lett. 3, 355.
Veuillen, J.Y., R. Chevalier, J. Marcus and C. Schlenker, 1987, Solid State Commun. 63, 587.
Vincent, H., and M. Marezio, 1986, in: Crystal Chemistry and Properties of Materials with Quasi One-Dimensional Structures, ed. J. Rouxel (Reidel, Dordrecht).
Wada, S., M. Kaburagi, Y. Saito and R. Aoki, 1988, J. Phys. F 18(6), 1231.
Wang, Z.Z., M.C. Saint Lager, P. Monceau, M. Renard, P. Gressier, A. Meerschaut and J. Rouxel, 1983a, Solid State Commun. 46, 325.
Wang, Z.Z., P. Monceau, M. Renard, P. Gressier, L. Guemas and A. Meerschaut, 1983b, Solid State Commun. 47, 439.
Wang, Z.Z., H. Salva, P. Monceau, C. Roucau, L. Guemas and A. Meerschaut, 1989, Phys. Rev., submitted.
Wertheim, G.K., L.F. Schneemeyer and D.N.E. Buchanan, 1985, Phys. Rev. B 32, 3568.
Whangbo, M.H., 1986, in: Crystal Chemistry and Properties of Materials with Quasi 1D Structures, ed. J. Rouxel (Reidel, Dordrecht) pp. 27-85.
Whangbo, M.H., and P. Gressier, 1984, Inorg. Chem. 23, 1305.
Whangbo, M.H., and L.F. Schneemeyer, 1986, Inorg. Chem. 25, 2424.
Whangbo, M.H., R.J. Cava, F.J. Di Salvo and R.M. Fleming, 1982, Solid State Commun. 43, 277.
Whittingham, M.S., 1977, in: Electrode Materials and Processes for Energy Conservation and Storage, ed. J.D. MacIntyre (Princeton Univ. Press, Princeton, NJ).
Wieting, J., A. Grisel and F. Levy, 1982, Mol. Cryst. & Liq. Cryst. C 81, 835.
Wilson, J.A., 1979, Phys. Rev. B 19, 6456.
Wold, A., W. Kunnmann, R.J. Arnott and A. Ferreti, 1964, Inorg. Chem. 3, 545.
Yamaya, K., and Y. Abe, 1982, Mol. Cryst. & Liq. Cryst. 81, 133.
Yamaya, K., T.H. Geballe, J.F. Kwach and R.L. Greene, 1979, Solid State Commun. 31, 627.
Zettl, A., C.M. Jackson, A. Janossy, G. Grüner, A. Jacobsen and A.H. Thompson, 1978, Solid

State Commun. 26, 725.
Zwick, A., M.A. Renucci and A. Kjekshus, 1980, J. Phys. C 13, 5603.
Zwick, A., G. Landa, R. Carles and M.A. Renucci, 1982, Solid State Commun. 44, 89.

This page intentionally left blank
CHAPTER 3

4.3 The CDW Transition, Structural Studies by Pouget, Comes

4.3.1 1. Introduction

Since the pioneering observation, more than 15 years ago, by X-ray diffuse scattering techniques of the structural features of the charge density wave (CDW) instability and the Peierls transition in the one-dimensional (1D) inorganic conductor $K_2Pt(CN)_4 0.3Br \cdot xH_2O$(KCP) (Comes et al. 1973) and the organic charge transfer salt TTF-TCNQ (Denoyer et al. 1975, Kagoshima et al. 1975), a considerable number of studies has been devoted to the physics of the CDW transition and to the manifestation of collective behaviour of the CDW in the electronic properties of these materials. These various aspects are covered by several chapters of this book. The present chapter attempts to survey the main results brought by X-ray, electron and neutron scattering studies, which directly probe the lattice counterpart of the CDW instability. Our aim is not to provide an exhaustive review of all the structural manifestations of the CDW instability, but to illustrate some key features of this instability on materials like transition metal trichalcogenides ($NbSe_3$), blue bronzes ($K_{0.3}MoO_3$) and charge transfer salts (TTF-TCNQ), which exhibit a well-established sliding CDW transport. More specific reviews on the structural instabilities of these materials can be found in Comes and Shirame (1979) (KCP, TTF-TCNQ), Monceau (1985) (transition metal tri- and tetra-chalcogenides), Pouget (1988) (organic charge transfer salts) and Pouget (1989) (molybdenum bronzes). The present chapter also completes general reviews (Kagoshima 1982, Moret and Pouget 1986) on the structural aspects of the CDW instability.

The matter of this chapter is organized as follows. A general presentation of the CDW instability will be given in section 2 . The electronic structure and the specific critical CDW wave vector of the 1D conductors considered here will be presented in section 3 . The spatial and dynamical aspects of the CDW fluctuations above the Peierls transition will be the object of section 4. Because of their importance in non-linear transport properties, the effects of disorder will be explicitly considered in section 5 . Sections 6 and 7 will respectively present the main interchain CDW coupling mechanisms and some simple resulting phase diagrams. A special attention will be paid in section 8 to the complex phase diagram shown by TTF-TCNQ. The lattice distortions observed at the Peierls transition and its relation with the electron-phonon coupling will be presented in section 9 . Finally the experimental observations of the phase and the amplitude excitations of the incommensurate CDW ordered state will be reviewed in section 10 .

4.3.2 2. The charge density wave instability

2.1. Electronic polarizability

A 1D electron gas exhibits an instability toward either a CDW, a spin density wave or a superconducting ground state depending on the strength and the range of the electron-electron interactions, and the detailed band filling (Solyom 1979, Emery 1979). Below, we shall consider only the case where the CDW instability is dominant and driven, through the electronphonon coupling, by the divergence of the electron-hole response function, $\chi_e(q)$, of the 1D electron gas. In the case of a gas of non-interacting electrons $\chi_e(q)$ shows a maximum for the wave

vector $2k_F$ which connects occupied electronic states to unoccupied states at the Fermi level (the Fermi surface is composed of two points at $\pm k_F$, where k_F, expressed in reciprocal wave vector unit of the chain, is simply related to the band filling ρ by $4k_F = \rho$). As illustrated by fig. 1, this maximum diverges logarithmically for decreasing temperatures as:

$$\chi_e(2k_F) = N(E_f) \log \frac{E_0}{k_B T}, \tag{1}$$

where E_0 is a cut-off energy of the order of the Fermi energy and $N(E_F)$ is

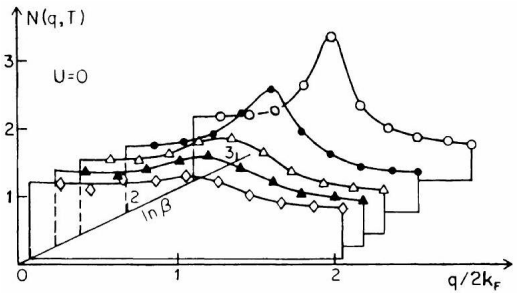


Fig.1. The charge density polarizability $N(q)$ for a non-interacting ($U = V = 0$) 1D electron gas versus q for various reduced temperatures $\left(\beta t_{|}=3,3.75,4.5,7.25,14.5\right.$ corresponding for $4t_{\|} = 0.5$eV to temperatures approximately of $500, 400, 300, 200, 100$ K, respectively). Here $N(q)$ has been normalized by its low temperature $q = 0$ value: $N(0) = 2/\pi v_F$. Notice the asymmetric q dependence of $N(q)$ with respect to $2k_F$.$t_{\|}$is the hopping matrix element, V_F the Fermi velocity and $\beta = 1/k_B T$ (from Scalapino and Hirsch 1983).

the density of states at the Fermi energy. If the strength of the electronelectron interactions progressively increases, for example by the increase of the on-site Coulomb interaction U, the $2k_F$ maximum vanishes and an additional maximum progressively develops for the $4k_F$ wave vector (see fig. 2). In the limit $U \to \infty, \chi_e(4k_F)$ also exhibits the logarithmic divergence in temperature given by eq. (1). This divergence corresponds to the electron-hole instability of a spinless non-interacting Fermi gas of Fermi wave vector $k_F^{\infty} = 2k_F$. In realistic situations both U and V (nearest neighbour) Coulomb interaction terms must be considered. When V is comparable to U, numerical calculations (Scalapino and Hirsch 1983, Hirsch and Scalapino 1984) show that the $4k_F$ maximum is strongly enhanced and that $\chi_e(q)$ can present (at low temperature) two well-defined maxima for $q = 2k_F$ and $4k_F$. Figure 3 shows also that the $\chi_e(2k_F)$ maximum is strongly temperature dependent. Its divergence, for decreasing temperature, is much stronger than the (quasi-logarithmic) one of $\chi_e(4k_F)$. This divergence can be expressed under the form of a power law:

$$\chi_e(2k_F) \sim (E_0/k_B T)^{\gamma}, \tag{2}$$

where the exponent γ depends on the Coulomb interaction parameters U and V (or on their Fourier transform g_1 and g_2, for $q = 2k_F$ and $q = 0$, respectively) (Solyom 1979, Emery 1979)..

The observation of a structural instability at the $4k_F$ wave vector (in

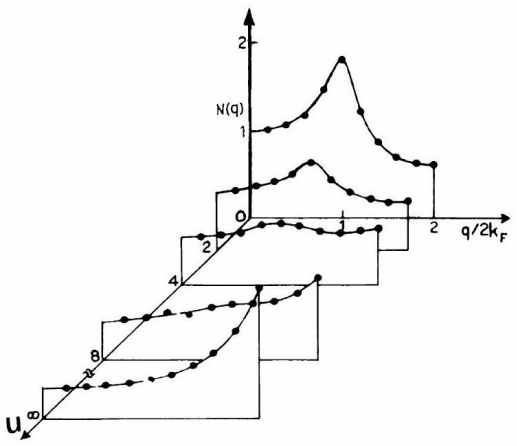


Fig. 2. Charge density polarizability $N(q)$ versus q for various values of U at $\beta t_{|}=7.25$ ($T = 200$ K). U is expressed in units of t (from Scalapino and Hirsch 1983).

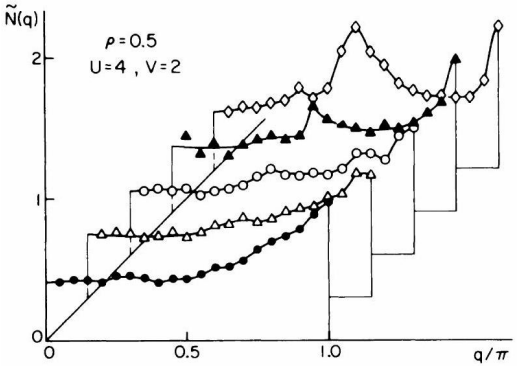


Fig. 3. Charge transfer polarizability $\tilde{N}(q)$ versus q for $\rho = 0.5, U = 4$ and $V = 2$ for the same reduced temperatures as in fig. 1. U and V are expressed in units of $t_{\|}$. With $\rho = 0.5$, the $4k_{\mathrm{F}}$ peak is in $q = \pi$ and the $2k_{\mathrm{F}}$ peak in $\pi/2$ (from Scalapino and Hirsch 1984).

addition to that at $2k_{\mathrm{F}}$) in several charge transfer salts of the TTF-TCNQ family (Epstein et al. 1981, Khanna et al. 1977, Pouget et al. 1976, Kagoshima et al. 1976) (see for example fig. 6) suggests that the 1D electron gas of organic material experiences quite substantial electronelectron interactions. In the case of TTF-TCNQ various estimates (Barisic and Bjelis 1985, Hubbard 1978, Mazumdar and Soos 1981) and physical measurements (Takahashi et al. 1984, Jacobsen 1986) give electron-electron interactions of intermediate strength: typically $U/2 \sim V \sim 4t_{\|}(\sim 0.5\mathrm{eV})$. The finding of an on-site Coulomb repulsion comparable to the nearest neighbour one is expected in organic materials, because the intrastack distance is comparable to the intramolecular distances. On the contrary, it has been argued (Barisic 1985) that inorganic conductors (KCP, $NbSe_3$, $K_{0.3}MoO_3$), showing only a weakly temperature dependent $2k_{\mathrm{F}}$ instability (see section 4.1), are close to the weak Coulomb interactions limit ($U < 4t_{\|}$). The relative weakness of Coulomb interactions is not obvious in the case of $K_{0.3}MoO_3$ and $NbSe_3$, for which band calculations (see section 3) give transfer integrals ($t_{\|} \sim 0.2 - 0.4\mathrm{eV}$) only slightly larger than that of organic materials. However an efficient screening mechanism of U could be due to the presence of several conduction bands originating from the same chain (or pair of strongly coupled chains) in these inorganic materials.

2.2. Electron-phonon coupling

Via the electron-phonon coupling, the $2k_F$ or $4k_F$ electronic polarizability instability leads to a lattice instability. This instability generally appears
under the form of a (Kohn) anomaly in the q dependence of the frequency of a particular phonon branch, which mode is linearly coupled to the 1D electron gas. Within the RPA approximation, the electron-phonon coupling changes the bare phonon dispersion frequency Ω_q to ω_q according to:

$$\omega_q^2 = \Omega_q^2 \left[1 - \lambda_q \chi_e(q)\right] \tag{3}$$

where λ_q is the electron-phonon coupling constant. The electronic polarizability $\chi_e(q)$ which enters in (3) depends on the electronic parameter which is at first order modulated by the phonon field (Scalapino and Hirsch 1983, Hirsch and Scalapino 1984). For example the on-site energy (and thus its charge density) is directly coupled to intramolecular distortions but also to changes of intermolecular (interatomic) coordinates through the crystalline field. In these cases $\chi_e(q)$ is the electronic charge density polarizability ($N(q)$ in figs. 1 and 2). The hopping matrix element, $t_\parallel$, is directly affected by a change of intermolecular (interatomic) coordinates, but also by intramolecular distortions changing the molecular orbital wave functions. In these cases $\chi_e(q)$ is the charge transfer polarizability ($\tilde{N}(q)$ in fig. 3). Numerical calculations show that $N(q)$ and $\tilde{N}(q)$ do not behave identically as a function of U, V and temperature.

The electronic instability coupled to the phonon field leads to the formation of CDW, whose dynamics is controlled by ω_q. When ω_q vanishes at the Peierls transition temperature, a periodic lattice distortion (PLD) is established. Below this temperature the average electronic density, ρ, in chain direction (y) is modulated according to:

$$\rho(y) = \rho + \delta\rho \cos\left(2k_F y + \phi\right) \tag{4}$$

where it is assumed that the critical instability occurs for the wave vector $2k_F$. In the mean field approximation the Peierls transition occurs at the vanishing of (3). In the case of a $2k_F$CDW instability of a gas of non-interacting electrons, (1) and (3) give:

$$k_B T_c^{MF} = E_0 \exp - \left(\frac{1}{N\left(E_F\right)\lambda_{2k_F}}\right) \tag{5}$$

The temperature dependence of ω_q is thus simply given by:

$$\omega_q^2 = \Omega_q^2 \log\left(T/T_c^{MF}\right). \tag{5}$$

The RPA approximation neglects fluctuations and it is well known that, because of the associated entropy terms, no true phase transition can occur at finite temperature in a purely 1D system. In 1D conductors the longrange order is destroyed by the fluctuations of the phase ϕ and the amplitude $\delta\rho$ of the CDW (here we assume, as is generally the case, that $2k_F$ or $4k_F$ are incommensurate numbers). The thermodynamic properties resulting from such fluctuations can be calculated in the framework of the

Landau-Ginzburg theory for a non-interacting electron gas (Scalapino et al. 1972), see also the reviews (Dieterich 1976, Schulz 1987); the case of interacting electrons is also considered in Barisic and Bjelis (1985) and Menyhard 1978. At low temperature the amplitude fluctuations are frozen and, in the phase fluctuation regime, ω_{2k_F} behaves like T. In the vicinity of T_c^{MF}, the amplitude fluctuations dominate. A 'Hartree-Fock' treatment of these fluctuations shows that the behaviour of $\omega_{2k_F}^2$ is still given by RPA result (5)', where T_c^{MF} is replaced by T_{eff} $\left(< T_c^{MF}\right)$ which depends on the various coefficients entering in the Landau-Ginzburg expansion. Because of the flucutations, the CDW keeps a finite spatial coherence in chain direction. However at low

temperature the CDW correlation length becomes so long that a modest interchain coupling is sufficient to drive (at $T_c \ll T_c^{MF}$) the PLD in real materials (see for example the reviews by Dieterich (1976) and Schulz (1987)).

The best way to measure the spatial aspect of the CDW fluctuations is through X-ray diffuse scattering experiments. Generally a phonon instability at a wave vector $\boldsymbol{Q}$ gives rise to an extra diffuse scattering at the same wave vector $\boldsymbol{Q}$ in reciprocal space (Comes and Shirane 1979):

$$I_d(\boldsymbol{Q}) \propto |F_d(\boldsymbol{Q})|^2 \, S(\boldsymbol{q}) \tag{6}$$

where $F_d(\boldsymbol{Q})$ is the diffuse structure factor and $S(\boldsymbol{q})$ is the instantaneous displacement-displacement correlation function of the unstable lattice mode ($\boldsymbol{Q} = \boldsymbol{G} + \boldsymbol{q}$ where $\boldsymbol{G}$ is a reciprocal lattice wave vector). In the classical limit and for an electron-phonon coupled system, one has (Pouget 1988):

$$S(\boldsymbol{q}) \propto \lambda_q k_B T \chi_\rho(\boldsymbol{q}), \tag{7}$$

where $\chi_\rho(q)$ is the CDW response function; which, in the RPA approximation of the electron-phonon coupling, is given by:

$$\chi_\rho(\boldsymbol{q}) = \frac{\chi_e(\boldsymbol{q})}{1 - \lambda_q \chi_e(\boldsymbol{q})} \tag{8}$$

This extra intensity $I_d(\boldsymbol{Q})$ shows a peak at the wave vector $2k_F$ or $4k_F$ for which $\chi_e(\boldsymbol{q})$ exhibits a well-defined maximum. It can even present an asymmetric profile, with a long tail for $q < 2k_F$ or $4k_F$ (see fig. 4) because $\chi_e(q)$ (see fig. 1) and thus $\chi_\rho(q)$, given by (8), have such an asymmetry in their q dependence.

In the temperature range $T > T^*$, where the fluctuations are dominated by the intrachain quantities, the extra X-ray diffuse scattering appears in the form of diffuse sheets (perpendicular to the chain direction) in reciprocal space. The intersection of such sheets with the Ewald sphere gives rise to diffuse lines (modulated in intensity by the diffuse structure factor $F_d(\boldsymbol{Q})$).

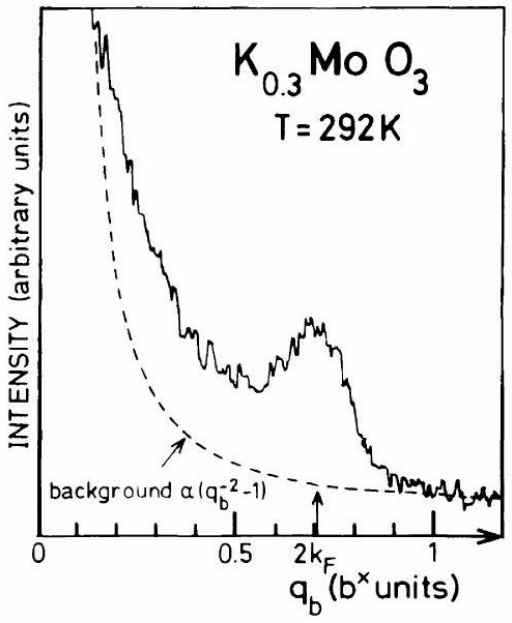


Fig. 4. Microdensitometer scan in chain direction b through the $2 k_{\mathrm{F}}$ scattering of $K_{0.3}MoO_3$ at room temperature. Note the asymmetric profile of the $2k_{\mathbf{F}}$ scattering (for $q_{\mathbf{b}} < 2k_{\mathbf{F}}$) (the dashed line is an estimation of the background).

The following X-ray patterns clearly show such lines due to:

- the $2k_F$ CDW fluctuations of KCP (fig. 5)
- the $2k_F$ and $4k_F$ CDW fluctuations of the charge transfer organic salt TMTSF-DMTCNQ (fig. 6)
  -the two kinds of $2k_F$CDW fluctuations of $NbSe_3$ (fig. 7).
  As schematically shown on fig. 8 one generally observes:
- A true regime of 1D fluctuations where the continuous diffuse lines are separated from the layers of main Bragg reflections by the wave vector $2k_F$ or $4k_F$; this is observed between T_{1D} (onset of 1D CDW fluctuations) and T^* (crossover towards a regime of 2D or 3D fluctuations). In this regime the only relevant spatial scale is the CDW correlation length in chain direction, $\xi_{\|}$, measured by the half width at half maximum of the diffuse sheets, with a profile which has generally a Lorentzian shape.
- A regime of short-range interchain coupling between T^* and T_c. The lateral coupling between CDW (see section 6) leads to a modulation of the diffuse intensity within the sheets (T^* is more precisely the temperature at which the transverse correlation length amounts to the interchain spacing $d_\perp$; in the case of strong anisotropy one has to distinguish between T^*_{3D} and T^*_{2D}).
- The PLD below the Peierls critical temperature T_c. This transition is characterized by the formation of sharp satellite reflections indicating a long-range transverse order (described by the transverse wave vector component $\boldsymbol{q}_\perp$) between long-range ordered 1D CDW.

These different regimes can be more quantitatively defined by the

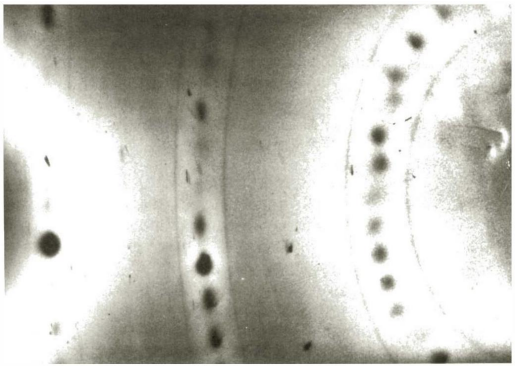


Fig. 5. X-ray pattern from $\mathrm{K}_{2}\mathrm{Pt}(\mathrm{CN})_{4}\mathrm{O}.3\mathrm{Br}\cdot x\mathrm{H}_{2}\mathrm{O}$ at room temperature. The thin and continuous $2k_F$ diffuse lines are clearly visible. The chain axis c is horizontal (the periodicity of intense Bragg reflection is $c^* = c^*/2$) (from Emery 1979).

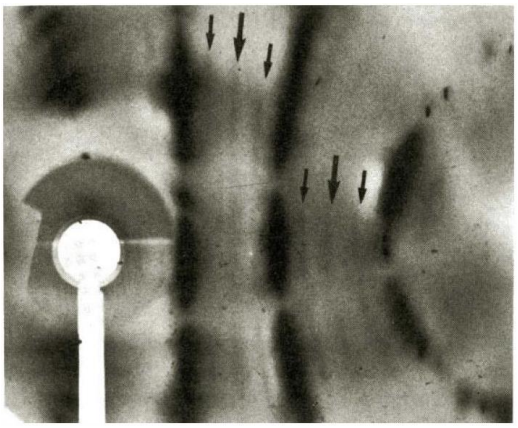


Fig. 6. X-ray pattern from TMTSF-DMTCNQ at 125 K showing the \$2 k_{\mathrm{F}}\$ (thin arrows) and $4k_{\mathrm{F}}$ (thick arrows) diffuse scatterings. The chain axis a is horizontal.

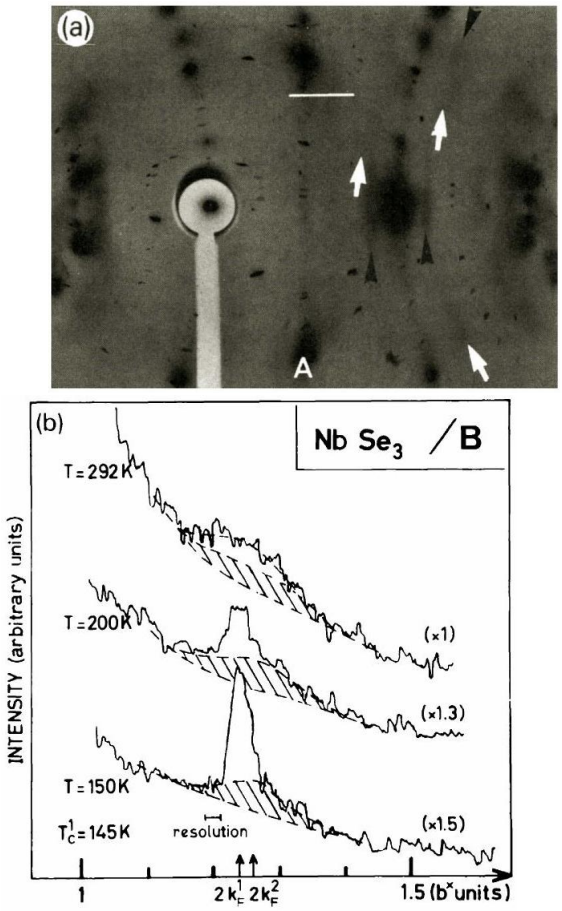


Fig. 7. (a) X-ray pattern from $NbSe_3$ at room temperature showing the two kinds (q_1 black arrows, and q_2 white arrows) of $2k_{\mathrm{F}}$ diffuse scattering. The thin white line shows the scan performed in (b). The chain axis b is horizontal (from Pouget et al. 1983). (b) Microdensitometer reading in chain direction showing more precisely the $2k_{\mathrm{F}}^1\,(q_1)$ and $2k_{\mathrm{F}}^2\,(q_2)$ scatterings and their temperature dependence above T_c^1. The extra intensity related to the q_2 scattering, which is broad and weakly temperature dependent in that temperature range, has been shaded.

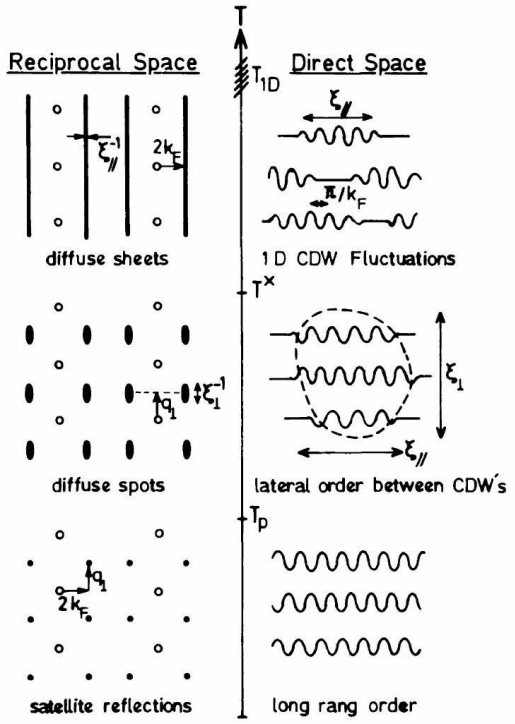


Fig. 8. Schematic representation of the diffraction (reciprocal space) from a 1D conductor showing a $2 k_{\mathrm{F}}$ CDW instability in the 3 temperature ranges discussed in the text. The corresponding instantaneous position-position correlation of the CDW lattice (in direct space) is shown on the right side.

measurement of the temperature dependence of $\chi_\rho, \xi_\parallel$and $\xi_\perp$. They are illustrated by fig. 9 in the case of the $2k_{\mathrm{F}}$ scattering of TMTSF-DMTCNQ. At T^* a change in the temperature dependence of χ_ρ^{-1} and $\xi_\parallel^{-1}$ is observed and $\xi_\perp \approx d_\perp$. At T_{c}, as expected for a second-order phase transition, χ_ρ^{-1}, $\xi_\parallel^{-1}$ and $\xi_\perp^{-1}$ vanish.

Table 1 summarizes the results of similar measurements performed on the other materials considered in this review.

In the classical approximation, the ratio of I_{d}/T gives a direct access to the CDW response function χ_ρ. Generally, because of the electron-phonon coupling induced fluctuations, χ_ρ differs from the electron-hole response function χ_{e} considered in section 2.1. It is only well above the lattice mean field critical temperature $T_{\mathrm{c}}^{\mathrm{MF}}$, that $\chi_\rho(q)$ is close to $\chi_{\mathrm{e}}(q)$; in that case (8) becomes:

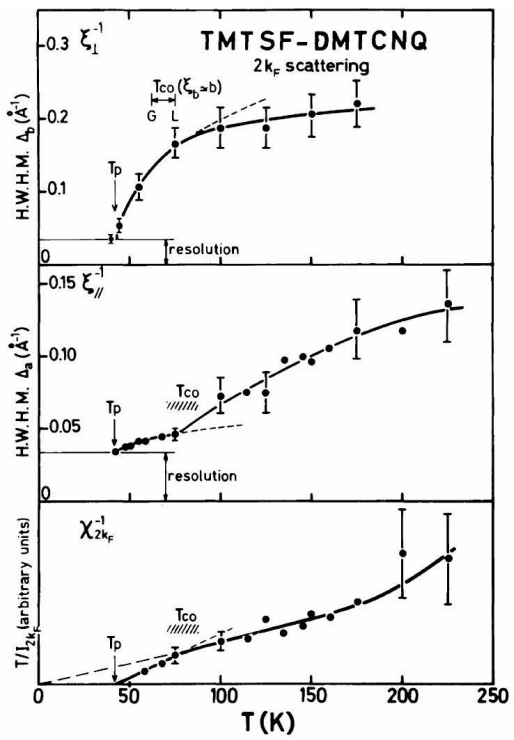


Fig. 9. Temperature dependence of the half width at half maximum (HWHM) along b and a (related to $\xi_{\perp}^{-1}$ and $\xi_{\parallel}^{-1}$) and of the inverse peak intensity divided by the temperature (related to χ_{ρ}^{-1}) for the $2k_{\mathrm{F}}$ scattering of TMTSF-DMTCNQ. The temperatures delimiting the various regimes of fluctuations defined by fig. 8 are $T_{1\mathrm{D}} \sim 230$ K, $T^{*}\,(T_{\mathrm{co}}) \sim 75$ K and $T_{\mathrm{c}}\,(T_{\mathrm{P}}) = 42$ K (from Pouget 1988).

$$\chi_{\rho}(q) \approx \chi_{\mathrm{e}}(q)\,[1 + \lambda_q \chi_{\mathrm{e}}(q)] \approx \chi_{\mathrm{e}}(q) \tag{9}$$

Around $T_{\mathrm{c}}^{\mathrm{MF}}$, when the fluctuations of the amplitude of the CDW dominate, it is possible to show (Pouget 1989) that with a good approximation, the CDW susceptibility of a non-interacting electron gas behaves as:

$$\chi_{\rho}\,(2k_{\mathrm{F}}) \approx \frac{\log\,(E_{\mathrm{o}}/T)}{\log\,(T/T_{\mathrm{eff}})}, \tag{10}$$

and similarly that the CDW inverse correlation length is given by:

$$\xi_{\parallel}^{-1} \approx \xi_{\mathrm{e}}^{-1}\,[\log\,(E_0/T)\log\,(T/T_{\mathrm{eff}})]^{1/2} \tag{11}$$

Table 1
Phase diagram and $2 k_{\mathrm{F}}$ fluctuation regime of several quasi-1D conductors at ambient pressure (+ means incomplete long-range order in one or two transverse directions)

Salts	PLD wave vector	T_{c}
$K_2Pt(CN)_4 0.3Br \cdot xH_2O$	$(\ 1/2, 1/2, 2k_{\mathbf{F}})^{+}$	$100 - 120$ K
$A_{0.3}MoO_3$ (A = K, Rb, Tl)	$(\ 1, 2k_F, 1/2)^{+}$	183 K
$NbSe_3$	$(\ 0, 2k_F^1, 0\ )\ (\ 1/2, 2k_F^2, 1/2\ )$	145 K (T_{c}^1) 59 K $(T_{\mathrm{c}}^2$
TTF-TCNQ (D)	$(1/4, 2k_{\mathrm{F}}, 0)$ 38 K $(q_a(T), 2k_{\mathrm{F}}, 0)^{+}$ 49 K $(1/2, 2k_{\mathrm{F}}, 0)^{+}$	54 K
TSF-TCNQ	$(\ 1/2, 2k_{\mathbf{F}}, 0)$	3D short-range orde

where:

$$\xi_e = \frac{\hbar V_F}{\pi\sqrt{2}k_B T} \tag{11}$$

is the electronic thermal length and V_F the Fermi velocity.

4.3.3 3. Electronic structure of some quasi-one-dimensional conductors

The observation of a structural instability, occurring for the wave vector $2k_F$ (or $4k_F$), furnishes a very simple measurement of the Fermi wave vector k_F of the quasi-1D electron gas. This determination is straightforward for a single 1D conduction band. It is generally delicate in the case of several conduction bands, when several wave vectors k_F can be connected by the CDW instability. Here we shall illustrate these various aspects by reviewing the electronic structure of some 1 D conductors and their $2k_F$ CDW instability.

The simplest band structure is shown by $K_2Pt(CN)_40.3Br \cdot xH_2O$ where there is only one conduction band from the d_{z^2} orbital of the $Pt(CN)_4$ planar complex (fig. 10). Without the Br this band is completely filled. In KCP , the Br takes 0.3 electron per $Pt(CN)_4$. With two $Pt(CN)_4$ units per

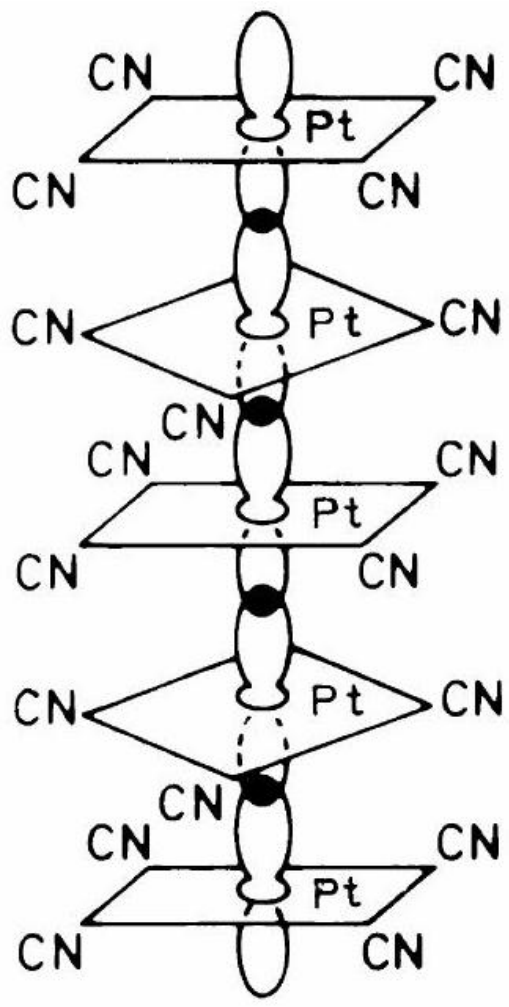


Fig. 10. Overlap of $\mathrm{d}_{z^{2}}$ orbitals between stacked $Pt(CN)_4$ complex ions. The ions are staggered to reduce the Coulomb repulsion between CN ligands. Thus the real chain periodicity c is twice the $Pt(CN)_4$ nearest neighbour distance, c'.

repeat distance c in chain direction, the conduction band is emptied by 0.6 holes, leading to a $2k_{\mathrm{F}} = \rho/2 = 0.3c^*$. This wave vector is directly obtained from the position in reciprocal space of the diffuse lines shown by the X-ray pattern of fig. 5 (Comes et al. 1973).

The organic charge transfer salts are composed of segregated stacks of donor (D) and acceptor (A) molecules, as shown in fig. 11 for TTF-TCNQ. There is overlap between the P_π molecular orbitals in stacking direction ($\boldsymbol{b}$ in the case of TTF-TCNQ). Thus two systems of bands originating respectively from D and A stacks are formed. If these bands overlap there is a partial charge transfer from D to A in order to establish a common Fermi level. A priori the degree of charge transfer ρ is unknown. It can be obtained either, with good accuracy, from the measurement of the $2k_{\mathrm{F}}$ or $4k_{\mathrm{F}}$ critical wave vector (see table 2) or, with less accuracy, by measuring directly the charge per molecule or the relative change of an intramolecular parameter sensitive to this charge (for comparison of both kinds of determination see Pouget (1988)). Two examples, corresponding to the different amount of electrons to share between D and A are here very illustrative:

(a) TTF-TCNQ and its family, with two electrons to share. In that case the number of electrons transferred to the acceptor is equal to the number of holes created on the donor. k_{F} which is consequently common to the two bands (fig. 12), can be easily obtained from the critical wave vector of the structural instability. On the other hand it is difficult to know which stack

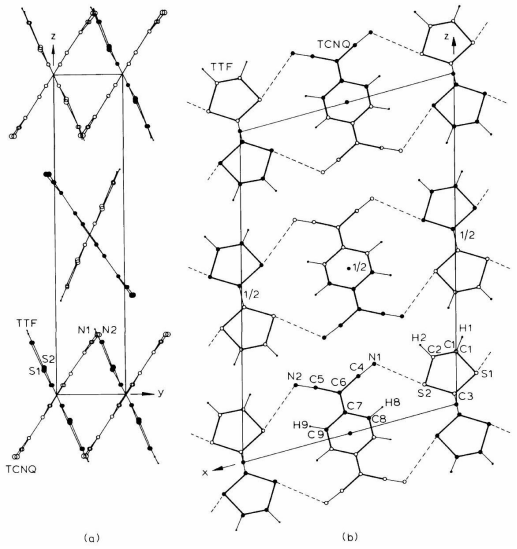


Fig. 11. Projected structure of TTF-TCNQ along the a-axis (a) and b-axis (b). In (b) the short contact distances $\mathrm{S} \cdots \mathrm{N}$ are indicated by the dashed lines. In (a) these distances are practically suited within the plane of the TTF molecules.

presents the structural instability. Its assignment requires either the analysis of the intensity distribution of the diffuse scattering through the $\boldsymbol{Q}$ dependence of $F_{\mathrm{d}}(\boldsymbol{Q})$ (as done for TSF-TCNQ (Yamaji et al. 1981)), or the study of solid solutions where a given stack is selectively perturbated upon alloying (case of $\mathrm{TTF}_{1-x}\mathrm{TSF}_x\mathrm{TCNQ}$ (Pouget 1988)).

(b) NMP-TCNQ, with one electron to share. In that case the Fermi wave vector differs on the D and A stacks. $k_{\mathrm{F}}^{\mathrm{A}}$ and $k_{\mathrm{F}}^{\mathrm{D}}$ are, however, related by the charge conservation relationship: $\rho_{\mathrm{NMP}} + \rho_{\mathrm{TCNO}} = 1$. In the case of

Table 2
Charge transfer and stack bearing the $2 k_{\mathrm{F}}$ or $4k_{\mathrm{F}}$ instability of some organic one-dimensional conductors

Salts	Charge transfer	Instability	
	ρ	$2\boldsymbol{k_{\mathrm{F}}}$	$\boldsymbol{4k_{\mathrm{F}}}$
TTF-TCNQ	0.59	TCNQ ($T < 150$ K)	TTF ($T <$ above RT)
TSF-TCNQ	0.63	TSF ($T < 250$ K)	-
TMTSF-DMTCNQ	0.50	TMTSF ($T < 225$ K)	TMTSF ($T <$ above RT)
NMP-TCNQ	0.67	TCNQ $\left(2k_{\mathrm{F}}^1 = \rho/2\right)$ ($T <$ above RT) NMP $\left(2k_{\mathrm{F}}^2 = (1-\rho)/2\right)$ ($T < 70$ K)	
			?

NMP-TCNQ, because of the commensurate value of ρ_{TCNO} ($\approx 2/3$), the ambiguity of the assignment could only be resolved by the study of $\mathrm{NMP}_{1-x}\mathrm{Phen}_x$ TCNQ solid solution, where the amount of electrons to share, $1-x$, varies with the Phen content (Epstein et al. 1981).

As the charge transfer of organic materials results from a delicate balance between the various contributions to the cohesion energy, ρ changes when external parameters like the pressure or the temperature are varied (Megtert et al. 1982).

The blue bronzes ($\mathrm{A}_{0.3}\mathrm{MoO}_3$ where $\mathrm{A} = \mathrm{K}, \mathrm{Rb}, \mathrm{Tl}$) are built with clusters containing $10\mathrm{MoO}_6$ octahedra. These clusters are stacked on top of each other in the b (1D) direction, while they share corners in the [102] direction. In the perpendicular direction, the layers of octahedra are

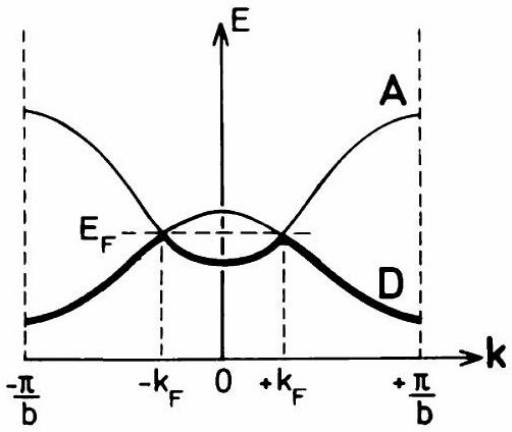


Fig. 12. Schematic one-electron D and A band structure dispersion of charge transfer salts like TTF-TCNQ.

separated by the monovalent metals A . Band calculations (Whangbo and Schneemeyer 1986) show that two quasi-1D conduction bands originate from the molecular orbitals of each cluster. These bands are respectively of the bonding and antibonding type as shown by fig. 13. They are filled by the 3 electrons provided by the monovalent metals to each cluster repeat unit (the 6 electrons from each Mo go into the bonding states of the oxygens). This gives an average $2k_{\mathrm{F}}$ of $\frac{3}{4}b^*$ which has been directly measured by means of angle-resolved ultraviolet photoemission spectroscopy (Veuillen et al. 1987). The metal-insulator phase transition which

accompanies the PLD requires a complete removal of the Fermi surface at $T_c = 183$ K. This can only be achieved by the nesting of one band (of Fermi wave vector k_F^1) into the other (of Fermi wave vector k_F^{II}) (Pouget et al. 1986, also see fig. 28 b). In that case the critical wave vector is: $2k_F = k_F^I + k_F^{II}$. It amounts to $0.75b^*$ for stoichiometric $A_{0.3}MoO_3$, a value which is observed at low temperature (at higher temperatures the $2k_F$ wave vector curiously decreases, taking the value $2k_F = 0.71b^*$ at room temperature - see fig. 4). The proof that the low-temperature value of $2k_F$ is really given by the number of conduction electrons is brought by the study of the solid solution $K_{0.3}Mo_{1-x}\ V_xO_3$ (Girault et al. 1988), where $2k_F$ shifts as predicted by stoichiometry: each V atom reduces by one the electrons transfered to the oxygens, and thus $2k_F = ((3 - 10x)/4)b^*$.

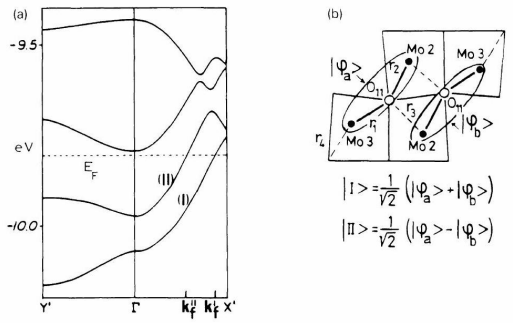


Fig. 13. (a) Dispersion of the one-electron bands of $\mathrm{K}\{0.3\}\ \mathrm{MoO}\{3\}$ in the vicinity of E_F for the wave vector (nearly) in chain direction ($\Gamma X'$) and in transverse direction ($\Gamma Y'$). I and II correspond respectively to the bonding and antibonding states defined in (b) (adapted from Whangbo and Schneemeyer 1986). (b) Projection along the 1D direction of the psuedo cluster of 400 octahedra forming the infinite chains running along b and from which the orbitals $|\varphi_a\rangle$ and $|\varphi_b\rangle$ generate the two conduction bands shown in (a).

The band structure of transition metal chalcogenides MX_3 ($NbSe_3$, TaS_3) is still more complex. These materials are made of trigonal prismatic chains where every metal atom M is sandwiched between two X_3 triangles. In the monoclinic variety (fig. 14a) there are 6 chains, running along the b direction, per unit cell. Three different kinds of chains are formed: chains II, where X_3 forms a triangle with long bond lengths, and chains I and III, where X_3 forms a triangle with a short X−X bond length. Chains I (and III) are grouped by pairs separated from each other by a type II chain. The appropriate oxidation state of the X_3 triangle is $X^{2-}\ (X_2)^{2-}$ and $(X^{2-})_3$ for chains I (III) and II, respectively (Wilson 1979). After filling of the bonding states, 2 electrons remain (among the 30 provided by the metal atoms per unit cell) to fill the conduction bands. Band calculations show that 4 bands cross the Fermi level (fig. 14b) (there is still a controversy concerning the presence (Bullett 1982, Shima 1983), or not (Whangbo and Gressier 1984) of a fifth conduction band in $NbSe_3$). Two bands mainly originate from chain III (bands d and e in fig. 14b) and two bands mainly from chain I (bands c and f). There is an average of 0.5 conduction electron per band. ^{93}Nb NMR provides evidence (Devreux 1982, Ross Jr et al. 1986) that chains III are involved in the upper phase transition (T_c^1) and that chains I are involved in the lower phase transition (T_c^2) of $NbSe_3$. The simplest interpretation is that these two phase transitions are associated with two decoupled CDW instabilities originating mainly from the pair of chains III

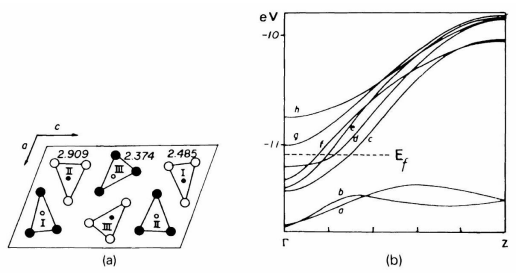


Fig. 14. (a) Projection of the structure of NbSe_{3} along the monoclinic axis b. The 3 kinds of chain are clearly indicated (Nb : small circle, Se: large circles; empty circles ($y = 0$), filled circles ($y = 1/2$)). (b) Electron band structure of $NbSe_3$ in the vicinity of E_F for wave vectors parallel to b^* (from Whangbo and Gressier 1984). Bands c and f are mostly due to chain I orbitals, bands d and e to chain III orbitals and bands g and h to chain II orbitals.

and the pair of chains I, respectively. As the Fermi surface is completely removed below T_c^2 in TaS_3 (Monceau 1985), the two CDW instabilities must affect the 4 conduction bands. As each pair of chains gives rise to 2 bands these CDW are more likely due to the nesting of one sheet of the Fermi surface into the other as in the blue bronze. One should therefore have $2k_F^1 = k_F^d + k_F^e$ for the T_c^1 instability and $2k_F^2 = k_F^c + k_F^f$ for the T_c^2 instability. For open Fermi surfaces (and ignoring the presence of an eventual fifth band), a simple electron count gives $4\,(2k_F^1 + 2k_F^2) = 2$. From the wave vectors quoted in table 3 this equality is followed for TaS_3 and deviates by about 0.3% for $NbSe_3$ (this difference could be due to the fact that for a warped open Fermi surface the component in chain direction of the best nesting wave vector can differ from the Fermi vector averaged on the transverse components of the Fermi surface; this last quantity determining the number of conduction electrons).

A simpler situation should in principle occur in $(Fe_{1+x}Nb_{1-x})\,Nb_2Se_{10}$ with only two type III prismatic $NbSe_3$ chains per unit cell (the remaining Fe and Nb atoms belong to octahedral chains). In agreement with the description

Table 3
Structural parameters, CDW correlation lengths in chain direction and CDW anisotropy in the 3D regime of fluctuations for $\mathrm{K}_{0.3}\mathrm{MoO}_3$, NbSe_3 and TaS_3

	$\mathrm{K}_{0.3}\mathrm{MoO}_3$	NbSe_3	TaS_3
Space group	C2/m	$\mathrm{P2}_1/\mathrm{m}$	$\mathrm{P2}_1/\mathrm{m}$
Lattice parameters (292 K)	$a = 18.260$Å $b = 7.548$Å $c = 9.858$Å $\beta = 116.52°$	$a = 10.006$Å $b = 3.478$Å $c = 15.626$Å $\beta = 109.30°$	$a = 9.515$Å $b = 3.341$Å $c = 14.912$Å $\beta = 109.99°$
T_c	183 K	(1) : 145 K (2) : 59 K	(1) : 240 K (2) : 160 K
Modulation wave vector	$q = (1, 0.75 - \delta(T), 0.5)$ $0 \leqslant \delta(T) \leqslant 0.05$	$\boldsymbol{q}_1 = (0, 0.241, 0)$ $\boldsymbol{q}_2 = (0.5, 0.260, 0.5)$	$\boldsymbol{q}_1 = (0, 0.253, 0)$ $\boldsymbol{q}_2 = (0.5, 0.247, 0.5)$
CDW $\xi_{\|\|}$(292 K)	$\xi_b = 25 \pm 3$Å	$\xi_b^{(1)} = 13 \pm 4$Å $\xi_b^{(2)} \sim 10$Å	$\xi_b^{(1)} = 25 \pm 5$Å $\xi_b^{(2)} \sim 20$Å
CDW anisotropy (above T_c)	$\frac{\xi_b}{\xi_{a+2c}} \simeq 4$	$\left(\frac{\xi_b}{\xi_{a^x}}\right)_{(1)} \simeq 7$ $\left(\frac{\xi_b}{\xi_c}\right)_{(1)} \simeq 13$	not determined

given for NbSe_3, only the CDW instability with the q_1 wave vector remains (it leads to a smooth metal transition at about $T_c \approx 140$ K (Monceau 1985)). However, as in these materials x is supposed to deviate significantly from 0 , the $2k_F^1$ component in chain direction ($\approx 0.26b^*$) cannot be explained by a simple electron count (Whangbo 1986).

An orthorhombic variety of imperfectly known structure also exists for TaS_3. It contains 24 chains per unit cell. The most probable array (Meerschaut and Rouxel 1986) is composed of pairs of chains with a short X-X bond length separated by single chains with long X_3 bond lengths. All these pairs are equivalent by symmetry, but each pair is not necessarily formed by identical entities. If each pair of chains gives rise to two conduction bands, the average $2k_F$ is thus 0.25 , as for the monoclinic variety. This value agrees with the c^* component of the single CDW critical wave vector observed at low temperature: $\left(\frac{1}{2}, \frac{1}{8}, \frac{1}{4}\right)$. This wave vector component is certainly stabilized, as for the monoclinic variety, by the nesting of one conduction band into the other. This instability removes the Fermi surface; the 215 K Peierls transition being accompanied by a metal insulator phase transition (Monceau 1985).

4.3.4 4. Charge density wave fluctuations above the Peierls transition

4.1. Spatial fluctuations

As mentioned in section 2, it is important to distinguish between inorganic and organic materials. Figure 15 compares, on a reduced scale, the temperature dependence of the CDW response function and of the correlation length in chain direction of the $2k_F$ scattering from $\mathrm{K}_{0.3}\mathrm{MoO}_3$ above $T_c = 183$ K and of the $2k_F^1$ scattering from NbSe_3 above $T_c^1 = 145$ K. Within the experimental errors the $2k_F$ CDW fluctuations of these two materials behave similarly. For $T/T_c > 1.15$ the temperature dependence of $\chi_\rho(2k_F)$ can be roughly accounted for by

the $\log(T/T_{\rm eff})$ term (with $T_{\rm eff} \approx 0.93T_{\rm c}$) in expression (10) which is valid in the amplitude fluctuation regime. This means that the electron-phonon coupling certainly drives the CDW instability of these inorganic materials. A detailed analysis (Pouget 1989, Pouget et al. 1989) of the structural fluctuations of $K_{0.3}MoO_3$ shows that the electron-phonon coupling is quite strong taking the reduced value: $\lambda_{2k_{\rm F}} N(E_{\rm F}) \approx 0.55$, with $N(E_{\rm F}) \approx 0.8$ state per eV and per Mo (corresponding to an average Fermi velocity $V_{\rm F} \approx 2.10^5$ m/s in chain direction). Independently the average Fermi velocity of the nested bands (or more likely $V_{\rm F}/\sqrt{\log(E_0/T)}$) can be estimated from the absolute value of $\xi_{\|}$using (11). The value thus deduced from the room temperature data of fig. 15 (i.e., for which the $\log(E_0/T)$ correction is the lowest) is 2.6×10^5 m/s for $K_{0.3}MoO_3$

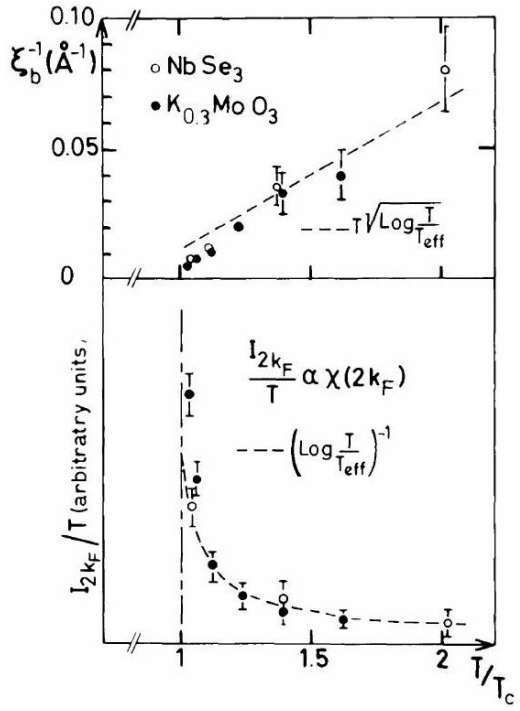


Fig. 15. Temperature dependence of the response function $\chi_{\rho}(2k_{\rm F})$ and of the inverse correlation length in chain direction ξ_b^{-1} for the $2k_{\rm F}$CDW of $K_{0.3}MoO_3$ and for the $2k_{\rm F}^1$CDW of $NbSe_3$ in the reduced temperature scale $T/T_{\rm c}$, where $T_{\rm c}$ is the Peierls transition temperature. The $K_{0.3}MoO_3$ data are from Pouget et al. (1986), the $NbSe_3$ data are from Pouget et al. (1983) and Fleming et al. (1978) and fig. 7b. The CDW correlation lengths have been obtained after a Gaussian resolution correction. The dashed line is a fit of χ_ρ and $\xi_{\|}^{-1}$ according to expressions (10) and (11), respectively, where the temperature dependence of $\log(E_0/T)$ has been neglected.

(2×10^5 m/s from band calculation (Whangbo and Schneemeyer 1986) and Pauli paramagnetism (Johnston 1984)) and 2.3×10^5 m/s for the $2k_{\rm F}^1$CDW of $NbSe_3$ ($\approx 3 \times 10^5$ m/s estimated from the average slope at $E_{\rm F}$ of bands d and e (Bullett 1982, Whangbo and Gressier 1984)). Below $T_{\rm 3D}^*$, critical fluctuations leading to the divergence of ξ and χ at $T_{\rm c}$ with non-classical exponents have been observed in $K_{0.3}MoO_3$ (Girault et al. 1989). The non-classical behaviour of the CDW fluctuations of the blue bronze should be contrasted with the harmonic one observed below $T_{\rm 3D}^*$ in KCP (Soda et al. 1987). In the last material the classical region of fluctuations is certainly enhanced by the larger value of the in-chain thermal length ξ_e and by the pertinent effect of the disorder.

Differently, the $2k_{\rm F}$CDW response function in the regime of 1D structural fluctuations varies

appreciably among the series of organic conductors. Two extreme situations are shown by TSF-TCNQ (fig. 16) and TTF-TCNQ (fig. 17). In the case of TSF-TCNQ, $\chi_\rho\,(2k_\mathrm{F})$ follows rela-

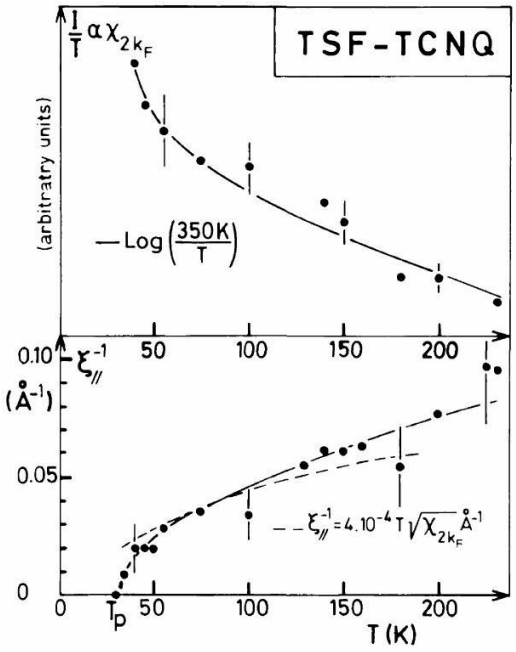


Fig. 16. Temperature dependence of the response function $\chi_\rho\left(2 k_\mathrm{F}\right)$ and of the inverse correlation length in chain direction ξ_b^{-1} for the $2k_\mathrm{F}$ CDW on the TSF stack in the quasi-1D regime of fluctuations of TSF-TCNQ. The data are from Pouget (1988). The CDW correlation lengths have been obtained after a Gaussian resolution correction. The continuous line of the upper part of the figure and the dashed lines of the lower part of the figure are fit according to expressions (10) and (11), respectively, where the temperature dependence of $\log\left(T/T_\mathrm{eff}\right)$ has been neglected. Note that no parameter adjustment has been made for the fit by expression
(11): V_F has been taken from the literature.

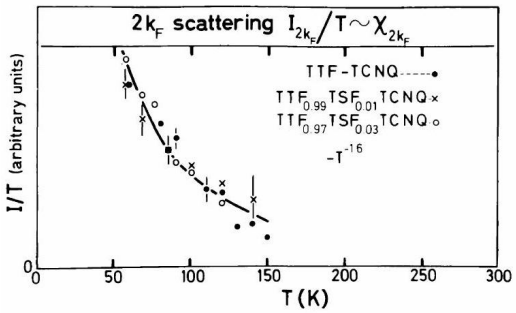


Fig. 17. Temperature dependence of the $2 k_\mathrm{F}$ CDW response function $\chi_\rho\,(2k_\mathrm{F})$ of $\mathrm{TTF}_{1-x}\mathrm{TSF}_x\mathrm{TCNQ}$ for $x = 0, 0.01$ and 0.03 in the 1D regime of fluctuations. Note that within experimental errors $\chi_\rho\,(2k_\mathrm{F})$ of the 3 compounds behave similarly in temperature. The full line is the best fit of the data with a single power law divergence $T^{-\alpha}(\alpha \sim 1.6)$ (data from Khana et al. 1977, Thielemans et al. 1976).

tively well a $\log\left(E_0/T\right)$ law (no good fit can be obtained from the $\log\left(T/T_\mathrm{eff}\right)$ expression). As $\chi_\rho\,(2k_\mathrm{F})$ behaves as the electron-hole response function $\chi_\mathrm{c}\,(2k_\mathrm{F})$ of a gas of independent

electrons (see (1)), the CDW instability of TSF-TCNQ seems to be mainly driven by the electron gas. However, as the cut-off frequency obtained from the data of fig. 16 ($E_0 \approx 350$ K), is about 4 times less than that expected from the Fermi energy of the TSF stack, perturbative corrections from the electronelectron interactions and the electron-phonon coupling must be certainly included in a correct description of the fluctuations. However, it is interesting to remark that the absolute value and the temperature dependence of $\xi_{\|}$can be relatively well accounted for between 50 and 200 K by expression (11), with $\log(T/T_{\text{eff}})$ neglected (the dashed curve shown in fig. 16, has been obtained with $\log(E_0/T)$ taken from the temperature dependence of $\chi_{\text{p}}(2k_{\text{F}})$ and ξ_{e} calculated from (11)' where V_{F} is deduced from the TSF band width $4t_{\|} = 0.6$eV (Herman 1977, Jacobsen 1985) and the charge transfer $\rho = 0.63$ (table 2) according to: $\hbar V_{\text{F}} = 2t_{\|} b \sin \pi\rho/2$).

In the case of TTF-TCNQ the strong divergence in temperature of $\chi_{\rho}(2k_{\text{F}})$ can be fitted by a power law with an exponent $\alpha \approx 1.6$. In this salt the $2k_{\text{F}}$ instability arises on the TCNO stack (as shown by the unchanged temperature dependence of the $2k_{\text{F}}$ fluctuations upon TTF/TSF substitution, for low amounts of TSF see fig. 17). Compared to the TSFTCNQ case, such a large increase of the temperature dependence of $\chi_{\rho}(2k_{\text{F}})$ is certainly due to the enhancement of the electron-electron interactions. The divergence of the $4k_{\text{F}}$CDW response function is found to be always weaker than that of the $2k_{\text{F}}$ one, as expected from electronic polarizability calculations (see section 2). This behaviour is illustrated by fig. 18 showing the quasi-logarithmic temperature dependence of the $4k_{\text{F}}$ CDW response function of TTF-TCNQ. This last instability arises mainly

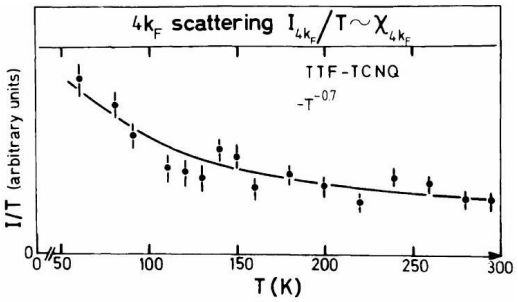


Fig. 18. Temperature dependence of the $4 k_{\mathrm{F}} \mathrm{CDW}$ response function $\chi_{\rho}(4k_{\text{F}})$ in the 1D regime of fluctuations of TTF-TCNQ. The full line is the best fit of the data with a single power law divergence $T^{-\alpha}(\alpha \sim 0.7)$ (data from Khana et al. 1977).

on the TTF stacks which is also shown by the above quoted effect of TTF/TSF substitution (see also section 4).

4.2. Dynamical fluctuations

In section 4.1 we have considered X-ray diffuse scattering experiments which measure the instantaneous displacement-displacement correlation function of the unstable lattice mode. This quantity defined by (6) can be expressed in the fluctuation of the order parameter $\boldsymbol{\eta_q}$ as:

$$S(\boldsymbol{q}, t = 0) = \langle |\eta_{\boldsymbol{q}}|^2 \rangle$$

where $\rangle$ means a thermodynamical average. The dynamical fluctuations of the order parameter, described by the correlation function:

$$S(\boldsymbol{q}, t) = \langle \eta_{\boldsymbol{q}}(t = 0)\eta_{-\boldsymbol{q}}(t) \rangle \tag{12}$$

are probed by inelastic neutron scattering experiments which directly measure $S(\boldsymbol{q}, \boldsymbol{\omega})$, the frequency Fourier transform of (12). In the RPA approximation, used in section 2.2, these fluctuations are controlled by the formation of a Kohn anomaly in the phonon spectrum, with a softening for $q = 2k_{\mathrm{F}}$ given by (3).

In its 1D fluctuation regime, KCP exhibits a giant Kohn anomaly in the acoustic branch polarized in chain direction (fig. 19) (Comes et al. 1975, Carneiro et al. 1976). This anomaly is well peaked at the $2k_{\mathrm{F}}$ wave vector. The ω and q dependence of the Kohn anomaly is more precisely shown by the constant intensity contours of fig. 20. It consists mainly in an intensity

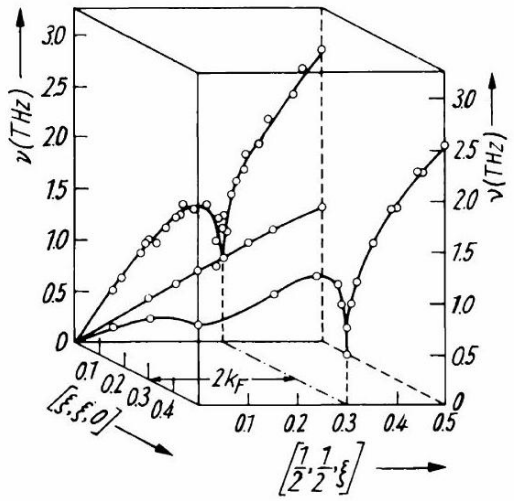


Fig. 19. Room temperature phonon dispersion surface of \$\mathrm{K}*{2}* *mathrm{Pt}(*mathrm{CN})*{4} \mathrm{˜B}*{0.3}* *cdot x* *mathrm{H}*{2} \mathrm{O}\$ showing the 1D giant Kohn anomaly in the acoustic branch polarized along the chain direction (from Comes 1975).

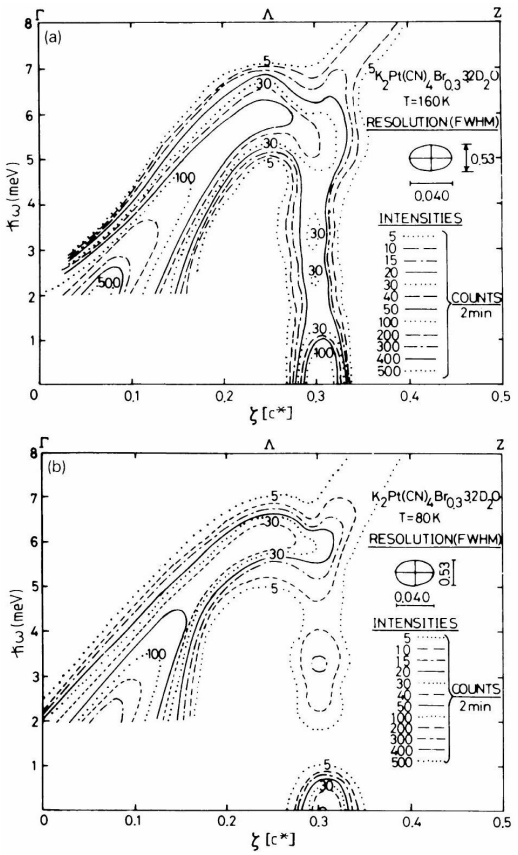


Fig. 20. Normalized ($\omega, \boldsymbol{q}$) intensity contours of the neutron scattering from the excitation of wave vectors $\boldsymbol{q} = \zeta c^*$ above (160 K) and below (80 K) the 'Peierls' transition of $K_2Pt(CN)_4 0.3Br \cdot xH_2O$. The elastic incoherent scattering and the inelastic background have been subtracted (from Carneiro et al. 1976).

ridge from the acoustic frequency ($\omega \approx 6$meV) to about $\omega \approx 0$, where an extra intensity centered at about $\omega \approx 0$ (central peak) develops. The inelastic features are weakly temperature dependent. The intensity of the quasi-elastic peak begins to increase appreciably below about 120 K , taken as the 'Peierls' transition temperature. In this material, the long-range

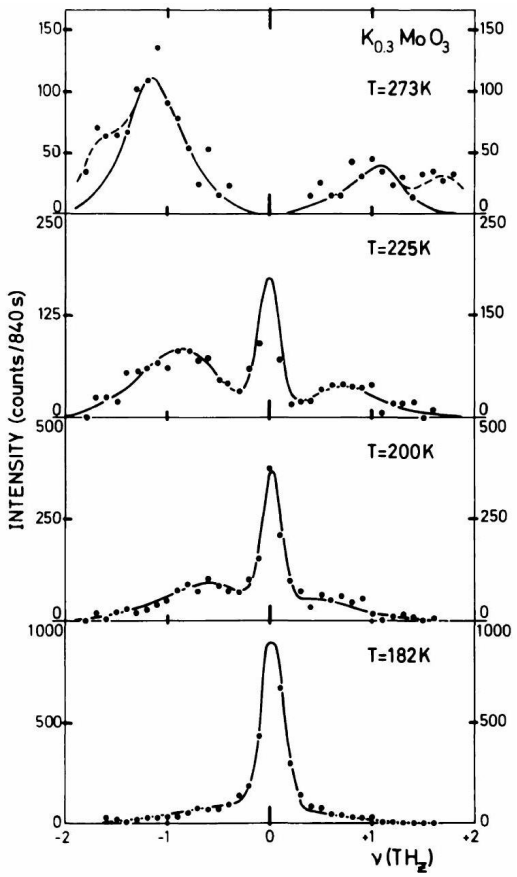


Fig. 21. Neutron scattering from \$\mathrm{K}*{0.3}* *mathrm{MoO}*{3}\$ at $\boldsymbol{q}_c = (1, 2k_\mathrm{F}, 0.5)$ as a function of the transferred frequency $\nu = \omega/2\pi$ for different temperatures above T_c. The background has been subtracted. The full line is the result of a fit of the cross section by the sum of two damped harmonic oscillator response functions centered at $\pm\omega_{q_c}$ and of a $\delta(\omega)$ central peak response function convoluted by the experimental resolution (from Pouget et al. 1985).

transverse CDW order is however, never achieved at atmospheric pressure, which was usually attributed to disorder effects (Br disorder).

In contrast to KCP which has frozen CDW dynamics possibly related to disorder effects, $A_{0.3}MoO_3$, which is a well-ordered material, clearly shows the phonon softening expected in the case of a displacive structural instability (Sato et al. 1983, Pouget et al. 1985). The softening of the frequency of the Kohn anomaly at $2k_\mathrm{F}$ as T approaches T_c from above, is well illustrated by the frequency scans of fig. 21 . The frequency softening, shown in fig. 22, is also accompanied by an increase of the damping of the $2k_\mathrm{F}$ mode, due to anharmonicity. However, the main evolution of $S(\boldsymbol{q}, \omega)$ near T_c is the critical growth of a central peak. A substantial contribution to this scattering is certainly due to the $2k_\mathrm{F}$ CDW Friedel oscillations induced in the vicinity of impurities or defects, as shown by the anomalous broadening of the ^{87}Rb NMR line width above T_c (Butaud et al. 1985) (see also section 5).

The time dependent CDW fluctuations (at the Larmor frequency) can be probed by spin-lattice relaxation time T_1 nuclear magnetic resonance (NMR) measurements. An enhancement of T_1^{-1} is clearly observed between T_c and T_3D^* in the 3D critical region for KCP (^{195}Pt (Niedoba et al. 1974) and ^{14} N (Soda et al. 1987)) and for $Rb_{0.3}MoO_3$ (^{87}Rb (Berthier and Segransan 1987)). In these materials T_3D^* is about 200 K (see table 1).

In TTF-TCNQ the $2k_\mathrm{F}$ CDW pretransitional dynamics consists, in the development below about 150 K , (in agreement with the X-ray results of fig. 17) of a weak Kohn anomaly in

the acoustic phonon branch polarized along the long direction of the molecules, c^* (Shirane et al. 1976). At the difference of $K_{0.3}MoO_3$ the Kohn anomaly does not soften appreciably when T_c is approached from above (fig. 22). The divergence of $S(2k_F)$ at T_c, as expected for a second-order phase transition, could be achieved by a

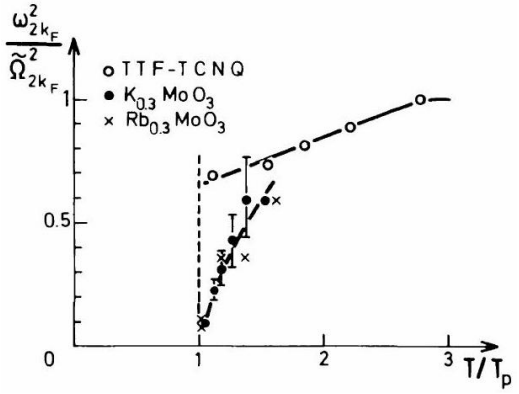


Fig. 22. Temperature dependence of $\omega_{2k_F}^2$, in reduced units, for TTF-TCNO and the blue bronzes $A_{0.3}MoO_3$(A = K, Rb) (from Pouget 1987a).

critical growth of the quasi-elastic component, $S(2k_F, \omega \approx 0)$, of the dynamic response function observed below T^*_{3D} (Comes et al. 1976). The relaxational character of the dynamics of the $2k_F$ Peierls transition of TTF-TCNQ could be due to electron-electron interactions or to strong anharmonicity (Barisic and Bjelis 1985). The pretransitional dynamics of the $4k_F$ CDW instability of TTF-TCNQ is not known. The $4k_F$ instability does not arise in the acoustic phonon spectrum (Pouget et al. 1979). It could have a purely relaxational dynamics due to sizeable electron-electron interactions.

4.3.5 5. Disorder

In the presence of disorder (defects, impurities, etc.) the 3D long-range CDW order is suppressed. With respect to the regular array, these defects create a potential V^D which is linearly coupled to the CDW, $\delta\rho(r)$. Its main effect is to induce local CDW (i.e. Friedel oscillations) and, at low temperature, to pin the phase of the already established CDW. In both cases, because of the random distribution of disorder centers: (i) the CDW coherence length is broken in chain direction and (ii) a periodic ordering of the phase of the CDW cannot be established in transverse directions. With the suppression of the long-range PLD, the manifestations of the Peierls transition on the electronic properties are either suppressed in the case of strong disorder or smoothened in the case of weak disorder. More quantitatively, the effect of disorder depends upon the number of defects and upon the strength of the perturbating potential. The weaker potentials are produced by disorders which are external to the conducting chains such as Br and H_2O disorder in $K_2Pt(CN)_40.3Br \cdot xH_2O$, K/Rb substitution in $A_{0.3}MoO_3$, Fe/Nb incomplete ordering in $(Fe_{1+x}Nb_{1-x})\,Nb_2Se_{10}$, TTF/TSF substitution for the $2k_F$ CDW of TTF-TCNQ. The strongest potentials occur when the disorder directly affects the conducting chains: Mo/V or W substitution in $K_{0.3}MoO_3$, TTF/TSF substitution for the $4k_F$ CDW of TTF-TCNQ and generally this is also true for defects created by irradiation (Zuppiroli 1988).

A very important effect of the disorder, which can be tested by X-ray diffuse scattering, consists of the formation of CDW Friedel oscillations around impurity centers. These oscillations create local lattice distortions and thus an extra X-ray intensity proportional to (Pouget 1988, Girault et al. 1988, Sham 1979):

$$\delta S^{\mathrm{D}}(q) \propto \lambda_q \chi_\rho^2(q) x \left|V_q^{\mathrm{D}}\right|^2, \tag{13}$$

where x is the impurity concentration (assumed to be small enough to prevent overlap between perturbed regions) and $\left|V_q^{\mathrm{D}}\right|^2$ is the mean square q
component of the impurity potential averaged on the sample. Contribution (13) must be added to the termal fluctuation term (7). The enhancement of the X-ray diffuse scattering intensity wich results from the contribution (13) has been quantitatively measured in $K_{0.3}Mo_{1-x}\ V_xO_3$ (Girault et al. 1988). In addition the extra contribution (13) changes appreciably the temperature dependence of the X-ray diffuse intensity, especially at low temperatures when χ_ρ diverges. This effect is clearly illustrated by fig. 23, showing, as predicted by (13), a dramatic enhancement in the temperature dependence of the $4k_{\mathrm{F}}$ peak intensity of irradiated TTF-TCNO (5% mol defects) with respect to that of non-irradiated TTF-TCNQ. The impurity induced nature of the Friedel oscillations is clearly proved by the particular features shown by the $4k_{\mathrm{F}}$ scattering in the $TTF_{1-x}TSF_x$ TCNQ alloy. Figure 24 shows, for the sample with $x = 0.03$, the progressive formation with temperature of destructive (at $1 + 4k_{\mathrm{F}}$) and constructive (at $2 - 4k_{\mathrm{F}}$) interferences between the $4k_{\mathrm{F}}$ scattering and the contribution to the X-ray background coming from the Laue or (and) Huang scattering due to the TTF/TSF random substitution, which is at the origin of the impurity potential inducing the $4k_{\mathrm{F}}$CDW on the D stacks.

Apart from the observation (Forro et al. 1983, Tamegai et al. 1987) of a broadening of the CDW scattering in q space, due to the disorder induced reduction of the correlation lengths at low temperature, no detailed analysis of the profile of the X-ray scattering in terms of the superposition of the contributions (7) and (13) has been done. Here let us just add that because

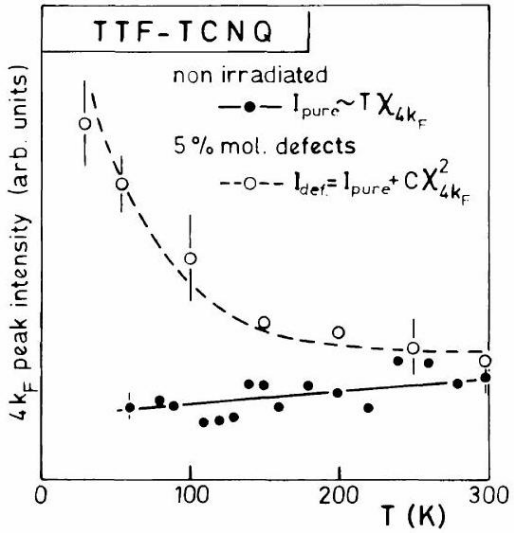


Fig. 23. Temperature dependence of the $4 k_{\mathrm{F}}$ peak intensity of pure TTF-TCNO and of TTF-TCNQ with 5% mol irradiation defects (from data of Khanna et al. 1977 and Forro et al. 1984). The relative scale between the 2 intensities has been adjusted in order to have the best fit between the experimental data and the expression described in the text. χ_{4kF} has been taken from fig. 18.

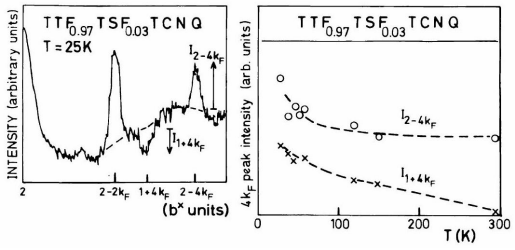


Fig. 24. (left) Microdensitometer reading from $\mathrm{TTF}*{0.97}*\mathrm{TSF}*{0.03}\mathrm{TCNQ}$ at 25 K showing the interferences in $2-4k_{\mathrm{F}}$ and $1+4k_{\mathrm{F}}$ between the $4k_{\mathrm{F}}$ scattering and the Laue or (and) Huang scattering, which q dependence is materialized by the dashed line. (right) Temperature dependence of the $4k_{\mathrm{F}}$ positive and negative peak intensities: $I_{2-4k\ \mathrm{F}}$ and $I_{1+4k\ \mathrm{F}}$, respectively.

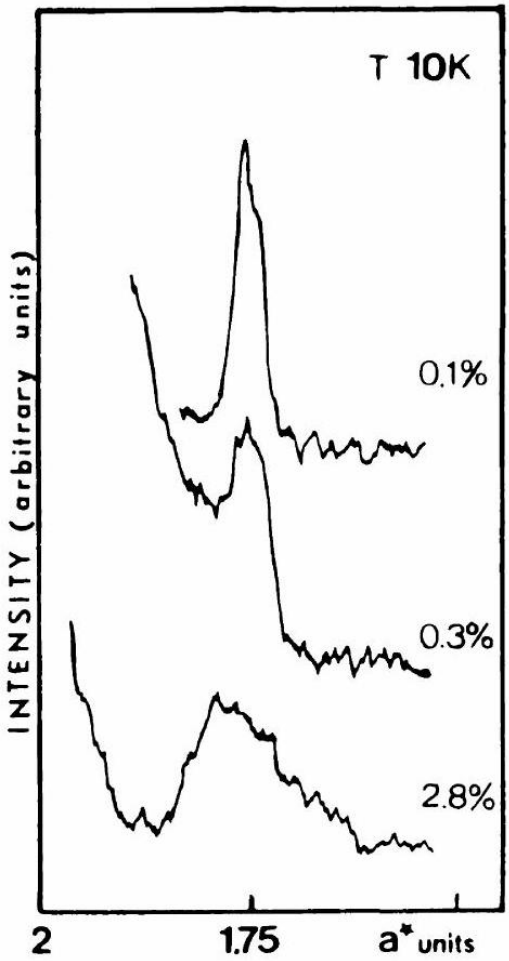


Fig. 25. Microdensitometer reading along the chain direction of the profile of the $2 k_{\mathbf{F}}$ scattering of TMTSF-DMTCNQ for different irradiation doses. Note the long tail of scattering for $q > 0.25a^*$ in the sample with 2.8 mol% defects. As the $2k_{\mathrm{F}}$ X-ray intensity originates mostly from the TMTSF stack where $2k_{\mathrm{F}} = 0.75a^*$, it is easy to see that the asymmetric broadening occurs for $q < 2k_{\mathrm{F}}$ (from Forro et al. 1983).

of the asymmetric q dependence of $\chi_{\mathrm{e}}(q)$ and thus of $\chi_{\rho}(q)$ (see (8)) with respect to, let us say, $2k_{\mathrm{F}}$, the X-ray scattering, when broadened enough, develops a long tail for in-chain wave

vectors $q < 2k_F$. The asymmetric broadening has been clearly observed for the $2k_F$ scattering of $K_{0.3}Mo_{1-x}\ V_xO_3$ (Girault et al. 1988) and irradiated TMTSF-DMTCNQ (see fig. 25).

4.3.6 6. Interchain CDW coupling

The two main coupling mechanisms between 1D CDW are the Coulomb interaction between the modulated part of electronic density ($\delta\rho(r)$ term in (4)) (Saub et al. 1976) and the nesting effect when, because of electron tunneling between chains, the shape of the Fermi surface is warped (Horowitz et al. 1975). These couplings fix the transverse component $q_\perp$ of the modulation wave vector of the PLD. Its effect on CDW fluctuations is only relevant below T^*. The crossover temperature may differ between the two lateral directions if the coupling is very anisotropic, as in $A_{0.3}MoO_3$. The interchain coupling is generally very weak, but it manifests itself for temperatures where the in-chain correlation length is relatively well developed. It leads to a rapid increase of the lateral CDW correlation length, as the temperature decreases towards T_c. This is illustrated by fig. 26 in the case of the $\boldsymbol{q}_1$CDW of $NbSe_3$. The interchain coupling energies can be deduced from such measurements. Only a detailed analysis has been performed for $K_{0.3}MoO_3$ (Abrahams et al. 1977, Pouget et al. 1989).

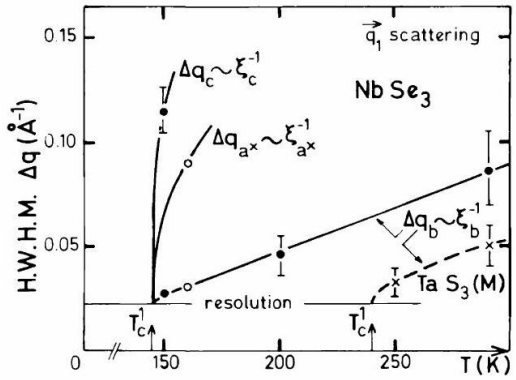


Fig. 26. Half width at half maximum (HWHM) of the $\boldsymbol{q}_1$ scattering, $\Delta\boldsymbol{q}$, from $NbSe_3$ measured along the b, c and a^* directions which are the 3 main directions of anisotropy of the structure (the full circles are from Pouget et al. (1983) and the empty one from Fleming et al. (1978)). This figure reports also the behaviour of Δq_b in monoclinic TaS_3 (R. Moret, unpublished results).

However, a rough analysis of the anisotropy of the CDW correlation lengths (table 3) shows that the fluctuations are more anisotropic in $NbSe_3$ than in $K_{0.3}MoO_3$.

In the case of simple orthorhombic arrays both the Coulomb and the tunneling coupling lead to an out of phase ordering of CDW ($q_\perp = \pi/d_\perp$) as schematically shown in fig. 27. Table 1 shows that this wave vector component is observed in the tetragonal directions of KCP, between layers of MoO_3 octahedra in the blue bronzes ($2\boldsymbol{a}^* - \boldsymbol{c}^*$ direction), in the direction (a) along which D and A stacks alternate for TTF-TCNQ (between 54 K (T_H) and 49 K (T_M)), and for TSF-TCNQ. In principle pressure experiments may help to discriminate between these two kinds of coupling because with the decrease of the interchain distances one expects:

- an enhancement of the Coulomb coupling and thus an increase of T_c.
- a deterioration of the nesting properties of the Fermi surface (by the addition of other sinusoidal components to its shape) and thus a decrease of T_c.

Experimentally the observation of an increase of T_{H} in TTF-TCNO at a rate of 0.5 K/kbar (fig. 32) and of the enhancement under pressure of the

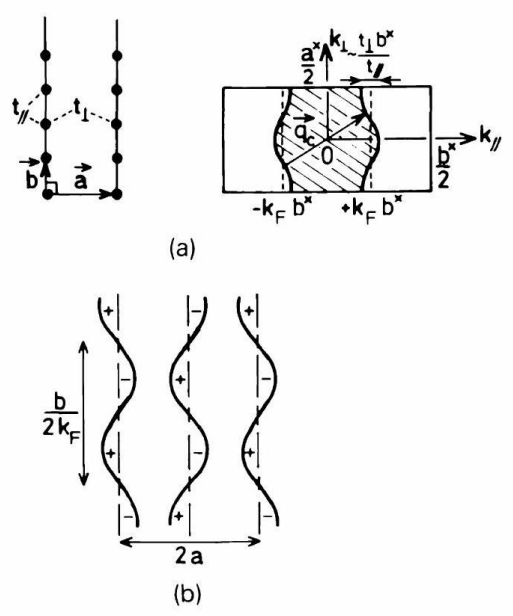


Fig. 27. (a) Warped sinusoidal Fermi surface resulting from finite tunneling coupling ($t_{\perp}$) between chains. The best nesting wave vector $\left(\frac{1}{2}, 2k_{\mathrm{F}}\right)$ of the Fermi surface is shown. (b) Out of phase coupling between like CDW which minimizes the direct Coulomb coupling. The sign of the $\delta\rho$ term is indicated.

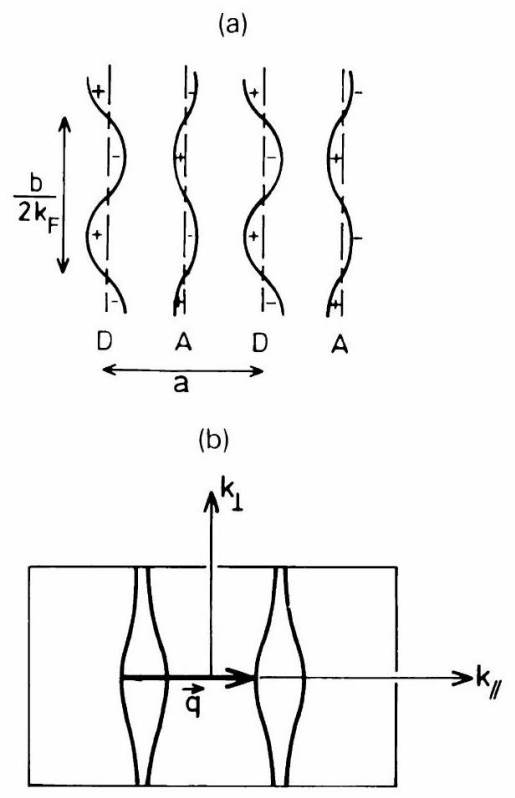


Fig. 28. (a) Ordering of D and A CDW for dominant Coulomb interactions between nearest neighbour stacks. (b) Nesting between bonding and antibonding like parts of a Fermi surface composed of two sheets, leading to the stabilization of the ($k_{\mathrm{F}}^{\mathrm{I}}+k_{\mathrm{F}}^{\mathrm{II}}, 0$) wave vector.

resistivity anomaly at T_c for KCP (Thielemans et al. 1976) are in favour of a CDW Coulomb coupling mechanism in these materials.

In the case of CDW of different nature, or of a Fermi surface composed of several sheets, different values of $q_\perp$ are expected. Figure 28 shows two important situations leading to, at $q_\perp = 0$:
(a) strong Coulomb coupling between D and A CDW (case of TTFTCNQ under pressure),
(b) nesting between sheets of the Fermi surface of opposite curvature (case of $A_{0.3}MoO_3$ along the ($\boldsymbol{b}, \boldsymbol{a} + 2\boldsymbol{c}$) layer direction).

The deterioration of the nesting is probably responsible for the decrease of T_c for $K_{0.3}MoO_3$ under pressure ($\mathrm{d}T_c/\mathrm{d}P = -1.5$ K/kbar (Brussetti et al. 1982)). Similar effects could explain the large decrease under pressure of both T_c^1 and T_c^2 of $NbSe_3$: ($\mathrm{d}T_c^1/\mathrm{d}p = -4$ K/kbar and $\mathrm{d}T_c^2/\mathrm{d}p = -6.25$ K/kbar (Monceau 1985)).

An interesting situation occurs in TSF-TCNQ with the competition in temperature between the out of phase ($q_a = \frac{1}{2}a^*$) and in phase ($q_a = 0a^*$) ordering along a of the $2k_F$CDW (table 1) (Kagoshima (1982)). This could be caused by a subtle balance between the like and unlike interstack interactions (Pouget 1988) (see also section 8).

It should be remarked that below T_c, anomalies occur in electronic properties, an incomplete ordering can still be present in directions of the crystal where the coupling is especially weak. This is the case for TTFTCNQ at ambient pressure in the a direction where D and A molecules alternate, and for $K_{0.3}MoO_3$ in the $2\boldsymbol{a}^* - \boldsymbol{c}^*$ direction perpendicular to the layers of octahedra. Just below T_c, the coherence length of the CDW ordered domains is about 150Å along a in TTF-TCNQ (Pouget et al. 1979) and 1000Å along $2\boldsymbol{a}^* - \boldsymbol{c}^*$ in $K_{0.3}MoO_3$ (Fleming et al. 1985).

4.3.7 7. Phase diagrams

The structural phase diagram is generally very simple when there is a single CDW instability. This is the case of KCP and $K_{0.3}MoO_3$, exhibiting a single $2k_F$ Peierls transition. However, because of fluctuations, the Peierls transition occurs at a temperature (T_c) largely depressed with respect to the mean field one T_c^{MF}. This last quantity is related, in the weak electronphonon coupling case, to the value of the Peierls gap at 0 K, $2\Delta_0$, by the well-known BCS relationship:

$$3.5k_B T_c^{MF} = 2\Delta_0$$

With T_c^{MF} deduced from the measurement of Δ_0, it is estimated that $T_c^{MF}/T_c \sim 3-6$ for KCP and $T_c^{MF}/T_c \sim 2-3$ for $K_{0.3}MoO_3$ (the inaccuracy is due to the fact that transport, magnetic and optical measurements give different values of Δ_0). The orthorhombic variety of TaS_3 also enters in the class of salts showing a single CDW instability. Surprisingly this compound seems to exhibit two phase transitions. Firstly at 215 K (the Peierls transition) a weakly incommensurate modulation develops. Then around 130 K the wave vector seems to lock at the commensurate value $\left(\frac{1}{2}, \frac{1}{8}, \frac{1}{4}\right)$ (Wang et al. 1983). To some extent the temperature dependent behaviour of the $2k_F$ component (along c^*) reminds one of that observed in $K_{0.3}MoO_3$, although in this latter material the existence of a true incommensurate-commensurate transition, sometimes claimed to occur around 100 K , is not experimentally proven.

In materials containing inequivalent chains or group of chains developing their own CDW instability like the monoclinic varieties of $NbSe_3$ or TaS_3, the phase diagram is the succession of the Peierls transitions of each kind of independent CDW (table 3). For instance in $NbSe_3$ the temperature dependence of the q_1 CDW order parameter which develops below T_{c1} is not significantly affected by the onset, at T_{c2}, of the q_2 CDW (Fleming et al. 1978). This decoupled behaviour is probably due to the fact that the $\boldsymbol{q}_1$ and $\boldsymbol{q}_2$ CDW differ appreciably by their wave vector and that they belong mainly to type III and type I chains respectively, which are relatively well separated in the crystal structure by the insulating chains of type II.

Complex phase diagrams can be observed among the organic charge transfer salts like TTF-TCNQ when, by charge conservation, the Fermi wave vector is the same on the D and A stacks and when each kind of stack develops its own $2k_F$ instability. Thus a competition arises between the transverse ordering wave vectors of each CDW sublattice. It has been analyzed in detail for Coulomb interactions on an orthorhombic array of D and A CDW (Bjelis and Barisic 1977, 1978). In the next section we shall illustrate this situation with TTF-TCNQ.

4.3.8 8. Example of a complex phase diagram: $TTF-TCNQ$

At ambient pressure TTF-TCNQ undergoes 3 structural phases transitions at 54 K (T_H) , 49 K (T_M) and 38 K (T_L). Between these phases the q_a component of the wave vector of modulation ($q_a, 2k_F, 0$) changes with

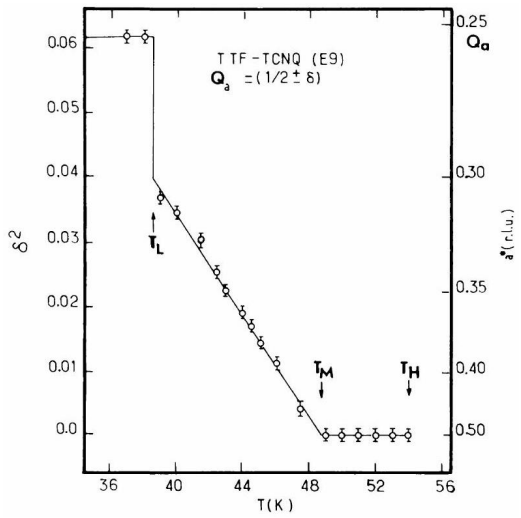


Fig. 29. Temperature dependence of the q_{a} component of the modulation wave vector of TTF-TCNQ (right scale) and of the square of its deviation, δ, at the value 1/2 (left scale) (from Ellenson et al. 1976). The transition temperature to the 3 modulated phases of TTF-TCNQ is indicated.

temperature, as shown by fig. 29 (Ellenson et al. 1976, Kagoshima et al. 1976). The T_{H} and T_{M} transitions are second-order phase transitions:
(a) The T_{H} transition is driven by the $2k_{\mathrm{F}}$ CDW instability on the TCNQ stacks. The modulation wave vector $\boldsymbol{q_{\mathrm{H}}} = \left(\frac{1}{2}, 2k_{\mathbf{F}}, 0\right)$ consists mainly in an out of phase ordering of CDW belonging to the TCNQ sublattice (fig. 30b), a type of order well explained by Coulomb interactions between like CDW (fig. 27b). However because of the monoclinic symmetry of the array of chains the ordering of the TCNQ sublattice can induce a distortion of the TTF sublattice (let us say of T^{+}symmetry according to the notations of Megtert et al. (1985), Abrahams et al. (1977)), but with a phase shift in quadrature with that of the TCNQ sublattice (see fig. 30b and Pouget (1988) for a physical explanation). NMR, EPR and optical measurements (Tomkiewicz et al. 1976, Rybaczowski et al. 1976, Bozio and Pecile 1981) show that at T_{H} the Peierls gap mainly opens on the TCNQ stacks and that the induced CDW distortion of the TTF stacks, not yet detected, must be extremely weak.
(b) The T_{M} transition is driven by the $2k_{\mathrm{F}}$ CDW instability on the TTF stacks. Interchain interactions lead to an out of phase ordering of the TTF CDW (i.e. of T^{-}symmetry (Megtert et al. 1985, Abrahams et al. 1977)) which enters in conflict with the preexisting ordering of T^{+}symmetry. It induces a continuous shift of the q_a component of the ordering wave vector by a quantity proportional to the TTF order parameter ψ_{F} (Bak and Emery 1976, Bjelis and Barisic 1977), which thus behaves in the mean field

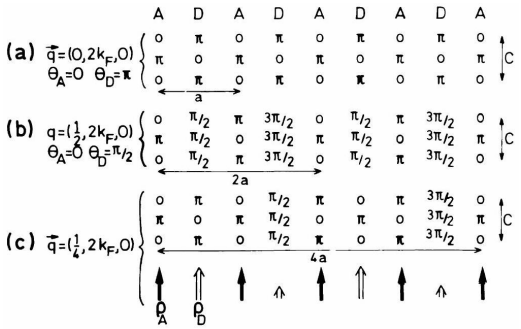


Fig. 30. Phase shifts in the (a, c) plane for (a) the (\$0,2 k_{\mathbf{F}}, 0\$), (b) the ($\frac{1}{2}, 2k_{\mathbf{F}}, 0$) and (c) the ($\frac{1}{4}, 2K_{\mathrm{F}}\mathrm{M}0$) CDW orderings. In (b) and (c) the dominant instability is assumed to be on the A stacks. In (c) the modulation of the amplitude of D and A CDW corresponding to the ordering $\left(\frac{1}{4}, 2k_F, 0\right)$ is also shown (from Pouget 1988).

approximation as

$$\delta\left(\equiv q_a - \frac{1}{2}\right) \propto \psi^{\mathrm{F}} \sim \sqrt{T_{\mathrm{M}} - T}.$$

This temperature dependence of q_a is well accounted for experimentally (fig. 29). The start of the TTF distortion at T_{M} has been observed by vibronic absorption (Bozio and Pecile 1981). However the gap on the TTF chains, not detected by EPR and NMR (Takahashi et al. 1984), must be very small between T_M and T_L. Below T_M, the CDW ordering can be described by plane waves with the wave vectors $\boldsymbol{q}^1_{\mathbf{M}} = (\pm \boldsymbol{q}_a(T), \pm 2k_{\mathbf{F}}, 0)$ and $\boldsymbol{q}^2_{\mathrm{M}} = (\mp q_a(T), \pm 2k_{\mathrm{F}}, 0)$. It has not been established experimentally if below T_{M} the CDW pattern of TTF-TCNQ consists of a single q modulation (in that case $\boldsymbol{q}^1_{\mathrm{M}}$ and $\boldsymbol{q}^2_{\mathrm{M}}$ belong to different domains of the crystal) or a double q modulation (in that case $\boldsymbol{q}^1_{\mathrm{M}}$ and $\boldsymbol{q}^2_{\mathrm{M}}$ coexist microscopically). However it has been shown (Barisic and Bjelis 1985, Abrahams et al. 1977) that in the limit $\delta \to 0$, compatible with the second-order nature of the T_{M} transition, the single- q modulation (i.e. phase modulation) has a lower free energy than the double- q modulation (i.e. amplitude modulation). For this reason TTF-TCNQ will certainly adopt a domain structure, with a local coexistence of the two modulation wave vectors $\boldsymbol{q}^1_{\mathrm{M}}$ and $\boldsymbol{q}^2_{\mathrm{M}}$ in the domain walls. This particular domain pattern could be the clue to understand the unusual global hysteresis of about 1.5 K , shown by $q_a(T)$ between T_{M} and T_{L} (Ellenson et al. 1977) (see for example Barisic and Bjelis (1985) and Bjelis and Barasic (1982a,b) for its description in the framework of the Landau-Ginzburg theory).

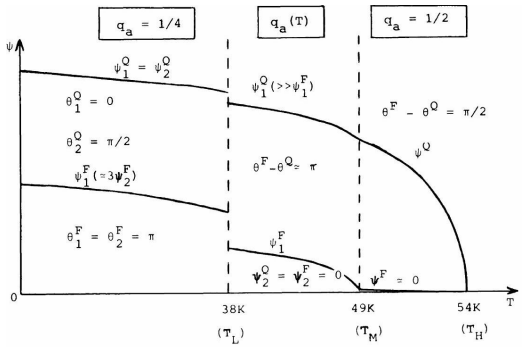
At 38 K (T_{L}) TTF-TCNQ undergoes a first-order phase transition where the component q_a locks at the commensurate value $\frac{1}{4}a^*$. It was soon realized, from the observation of interference between the $\boldsymbol{q}^1_{\mathrm{L}}$ and $\boldsymbol{q}^2_{\mathrm{L}}$ wave vector (Kagoshima et al. 1976), that below T_{L} the two waves coexist microscopically and thus modulate the amplitude of the $2k_{\mathrm{F}}$CDW. This was definitively shown by recent structural analysis (Coppens et al. 1987, Bouveret and Megtert 1989). At T_L, the growth of the order parameter $\psi(\boldsymbol{q}^2)$ in domains where the order parameter $\psi(\boldsymbol{q}^1)$ is well developed and vice versa, necessitates a nucleation process which probably takes place in the domain walls, giving rise to a first-order phase transition (in this respect it is interesting to note that the hysteresis at T_{L} has the same temperature extent as the global hysteresis of $q_a(T)$ in the sliding phase (Ellenson et al. 1977)). This transition has been described in the framework of the Landau theory using fourth-order umklapp terms in the free energy (Abrahams et al. 1977, Bjelis and Barisic 1976). When the dominant order parameter is on the TCNQ stacks, in agreement with the electronic properties (i.e., at T_{L} the gap on the TCNQ stack is well developed while the gap on the TTF stacks begins to grow (Takahashi et al. 1984)), and when the monoclinic symmetry of the chain array is considered (Pouget 1988), the A and D

CDW patterns take the phase shifts shown in fig. 30c. This phase shift pattern has been recently confirmed by an analysis of the low-temperature distortion of TTF-TCNQ (Bouveret and Megtert 1989). The ($\frac{1}{4}, 2k_{\mathrm{F}}, 0$) CDW array can be viewed as composed of a sequence of 4 domains, each of period a, where the elementary phase shifts of the ($0, 2k_{\mathrm{F}}, 0$) and ($\frac{1}{2}, 2k_{\mathrm{F}}, 0$) CDW structures alternate. It is easy to see from fig. 30c that, with the same environment, all the CDW on the TCNQ sublattice, possess the same amplitude, while with two different environments (i.e. a favourable one in the ($0, 2k_{\mathrm{F}}, 0$) domain and an unfavourable one in the ($\frac{1}{2}, 2k_{\mathrm{F}}, 0$) domain), the TTF CDWs have different amplitudes (experimentally in the ratio 2 to 1 (Bouveret and Megtert 1989)). It should be noted that the modulation of the TTF sublattice should deviate slightly from this description when the ($\frac{1}{2}, 4k_{\mathrm{F}}, 0$) Fourier component of the distortion, due to the 3D ordering of the $4k_{\mathrm{F}}$CDW is taken into account.

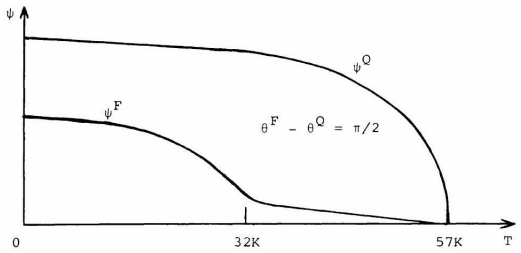
Figure 31(a) summarizes the evolution of the amplitude ψ and of the phase θ (along a) for the two components order parameter on the D and A stacks in the 3 modulated phases shown by TTF-TCNQ at ambient pressure.

The phase diagram of TTF-TCNO changes significantly under pressure (fig. 32) (Megtert et al. 1982) and upon alloying with TSF-TCNQ (fig. 33) (Sakai et al. 1983). The pressure and the alloying act differently on the phase diagram of TTF-TCNQ. While a modest pressure ($P \sim 5$kbar) leads to the stabilization of the $\left(\frac{1}{2}, 2k_F, 0\right)$ modulation at all temperatures, this modulation is replaced upon alloying (for $x < 0.9$) by the ($0, 2k_{\mathrm{F}}, 0$) one (fig. 30a). When the instability is driven by a single stack (here the TCNQ), such different orderings result from the delicate balance between like and unlike interstack coupling (see for example Pouget (1988), Bjelis and Barisic (1977) and Jerome and Schulz (1982)). In the case of TTF-TCNQ the stabilization of the ($\frac{1}{2}, 2k_{\mathrm{F}}, 0$) ordering together with the increase of T_{H} ($\equiv T_{\mathrm{O}}$ temperature at which the TCNQ stacks distort) under pressure results probably from the expected increase of the like interstack coupling and from the unexpected decrease of the unlike interstack coupling (for a possible explanation of this last feature, see section 9). The pressure dependence of these couplings is probably also the clue to understand the sequence of low-temperature phase transitions of TTF-TCNQ (fig. 32) where the CDW ordering wave vector changes from ($\frac{1}{4}, 2k_F, 0$) to $\left(\sim \frac{1}{3}, 2k_{\mathrm{F}}, 0\right)$ and then to $\left(\frac{1}{2}, 2k_{\mathrm{F}}, 0\right)$. In this respect, starting from the structure of the $\left(\frac{1}{4}, 2k_{\mathrm{F}}, 0\right)$ phase, shown in fig. 30(c), the $\left(\frac{1}{3}, 2k_{\mathrm{F}}, 0\right)$ ordering can be obtained by the removing of one half of the ($0, 2k_{\mathrm{F}}, 0$) CDW ordered domains, then the $\left(\frac{1}{2}, 2k_{\mathrm{F}}, 0\right)$ ordering by removing the remaining ($0, 2k_F, 0$) domains (Pouget 1988). In the case of the solid solution $\mathrm{TTF}_{1-x}\mathrm{TSF}_x\mathrm{TCNQ}$ the stabilization of the ($0, 2k_{\mathrm{F}}, 0$) phase, together with the decrease of $T_{\mathrm{H}} (\equiv T_{\mathrm{Q}})$ for increasing x, probably originates from the

$$\psi(n, m, o) = \mathrm{Re}\left\{\left[\psi_1 e^{i(2\pi q_a n + \theta_1)} + \psi_2 e^{-i(2\pi q_a n - \theta_2)}\right] e^{i4\pi k_F m}\right\}$$



(a) \$\quad \mathrm{P}=1 \mathrm{~atm}:: \overrightarrow{\mathrm{q}}=\left(\mathrm{q}{*mathrm{a}}, 2 *mathrm{k}{\mathrm{F}}, 0\right)\$



(b) $\quad P=5 \mathrm{Kbar}: \vec{q}=\left(\frac{1}{2}, 2 \mathrm{k}_{\mathrm{F}}, 0\right)$

Fig. 31. (a) Temperature dependence of the amplitudes (ψ_1, ψ_2) and phases (θ_1, θ_2) along a of respectively the order parameter $\psi(\boldsymbol{q}_1)$ and $\psi(\boldsymbol{q}_2)$ describing the CDW ordering (in the (a, b) plane) of the TTF(F) and TCNQ(Q) stacks in the 3 modulated phases of TTF-TCNO at ambient pressure (the ratio ψ_1^F/ψ_2^F, for $T < T_{\mathrm{L}}$, has been taken from Bouveret and Megtert (1989)). (b) Possible temperature dependence of the TCNQ and TTF order parameters (ψ^{O} and ψ^{F} respectively) in the ($\frac{1}{2}, 2k_{\mathrm{F}}, 0$) modulated phase of TTF-TCNQ at 5 kbar .

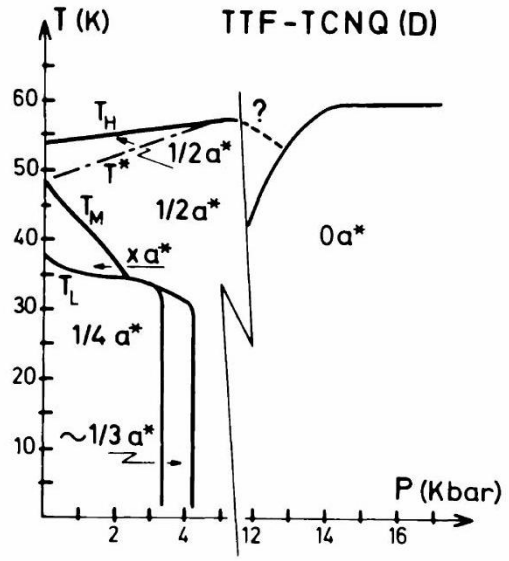


Fig. 32. Phase diagram of TTF-TCNQ deduced from neutron elastic scattering measurements performed on fully deuterated single crysal (adapted from Megtert et al. (1984)). The various phases are characterized by the $\hat{a}^*$ component, q_a, of the modulation wave vector.

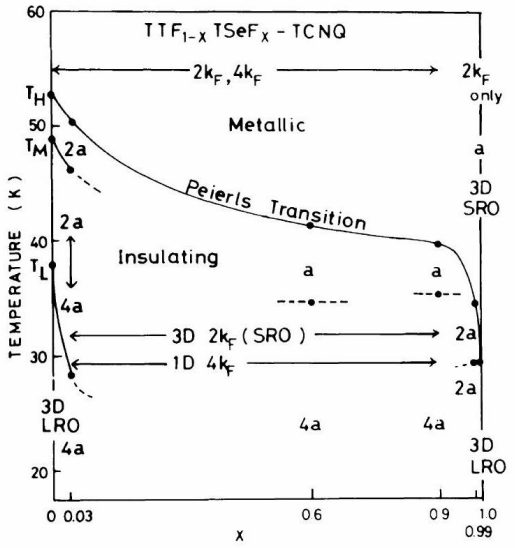


Fig. 33. Phase diagram of the solid solution $\mathrm{TTF}*{1-x}\mathrm{TSF}_x\mathrm{TCNQ}$. The various phases are characterized by the wave length on the modulation along a ($\lambda_a = 2\pi/q_a$). The long-range order (LRO) and short-range order (SRO) nature of the 3D coupling between $2k_\mathrm{F}$CDW, as well as the 1D nature of the $4k_\mathrm{F}$ CDW are indicated (from Sakai et al. 1983).

decrease of the like interstack coupling (increase of the lattice parameters) and from the increase of the unlike interstack coupling (strengthening of the N...S/Se interactions by the progressive replacement of the TTF molecules by the TSF ones).

Under pressure and upon TSF alloying the sliding phase of TTF-TCNQ disappears. However the D stacks still undergo a $2k_\mathrm{F}$ distortion through a first-order phase transition leading, at about 35 K , to the $\left(\frac{1}{4}, 2k_\mathrm{F}, 0\right)$ or to the $\left(\sim \frac{1}{3}, 2k_\mathrm{F}, 0\right)$ modulated phases. This distortion still persists at low temperature in the $(\frac{1}{2}, 2k_\mathrm{F}, 0)$ modulated phase, because transport measurements shows the opening of an electrical gap on the TTF stack below about 32 K (T_F) at 5 kbar (Jerome and Schulz 1982). However the coupling between the $2k_\mathrm{F}$ TTF CDWs is certainly not strong enough in this pressure range to change the ordering wave vector of the TCNQ CDWs which is well established below T_O. The temperature dependence of the TCNQ and TTF order parameters in the $(\frac{1}{2}, 2k_\mathrm{F}, 0)$ phase, compatible with electronic transport (Jerome and Schulz 1982) and structural (Megtert et al. 1982) measurements, is shown on fig. 31b.

Under higher pressure the evolution of the interstack coupling of TTFTCNQ is certainly further changed: T_Q slightly decreases while T_F increases until about $13 - 15$kbar where the TCNQ and TTF transitions merge together. Above this pressure the Peierls transition temperature, now common to both kinds of stack, increases (Jerome and Schulz 1982). The $(0, 2k_\mathrm{F}, 0)$ modulated structure is then observed (Megtert et al. 1982). This ordering is certainly stabilized by the increase of the coupling between unlike stacks.

The phase diagram is also changed in $\mathrm{TTF}_{1-x}\mathrm{TSF}_x\mathrm{TCNQ}$ for $x > 0.9$. With the disappearance of the $4k_\mathrm{F}$ CDW instability the donor stack shows certainly a more pronounced $2k_\mathrm{F}$ CDW instability. With increasing x this instability rapidly gets the dominant role, driving the Peierls transition for pure TSF-TCNQ. In this respect it is interesting to notice that for $x > 0.9$, T_O sharply decreases. However in TSF-TCNQ, the competition between like and unlike interstack CDW coupling still leads to the coexistence of $(0, 2k_F, 0)$ and $(\frac{1}{2}, 2k_F, 0)$ local CDW ordering (Kagoshima 1982). The out of phase ordering between TSF CDWs becomes long-range ordered below 29 K in TSF-TCNQ. However, local fluctuations towards the in-phase ordering $(0, 2k_\mathrm{F}, 0)$ still subsists below 29 K (Pouget 1988).

4.3.9 9. Lattice distortion and electron-phonon coupling

Until now we have mostly discussed the Peierls transition with the CDW (or the Peierls gap) as a scalar order parameter. In fact, from the structural point of view, the order parameter is a lattice displacement, and generally,
when the PLD is described by a displacive mode of a given polarization, there is a one to one correspondence between the CDW and the lattice displacement via the linear electron-phonon coupling (see section 2.2). However, in some complex cases like TTF-TCNQ it is necessary to consider the vectorial nature of the displacement field; i.e., a given CDW may be coupled to several lattice modes. The linear electron-phonon coupling also imposes that the critical lattice mode must at first order change the parameters of the 1D electron gas like the site energy or the transfer integral $t_{\|}$(the nature of the CDW response function χ_ρ depends also on the physical quantity which is modulated by the phonon field, see section 2.2).

In 1D conductors where stacks are made of piles of molecules or complexes, the easiest way to produce a first-order electron-phonon coupling is to modulate the repeat distance in chain direction by an acoustic displacement of the constituting entities. This is achieved in KCP by translation of the $Pt(CN)_4$ complexes in the direction perpendicular to their plane (fig. 34a), in agreement with the finding of a Kohn anomaly in the

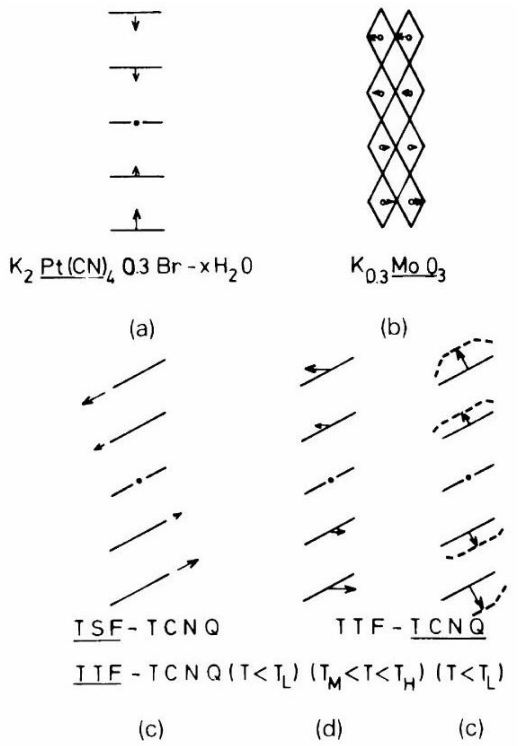


Fig. 34. Schematic representation of the polarization of the $2 k_{\mathrm{F}} \mathrm{CDW}$ of $K_2Pt(CN)_40.3Br \cdot xH_2O$ (a), $K_{0.3}MoO_3$ (b), TSF-TCNQ (c), TTF-TCNQ for $T_H > T > T_M$ (d) and for $T < T_L$ ((c) and (e)). The entity mainly modulated is underlined. In (e) the internal distortion of the TCNQ molecule found in the structural refinement of Bouveret and Megtert (1989) is schematically shown.

acoustic branch polarized along c (fig. 19). The amplitude of the longitudinal displacement is about 0.025Å, below 60 K (Lynn et al. 1975). In charge transfer salts, because of the tilting of the organic molecules with respect to the chain direction, any translation of the molecules in the symmetry plane of the stack produces a first-order modulation of the electron gas parameters. It is found in TSF-TCNQ (Yamaji et al. 1981) that, probably because of steric interactions

between donors, the unstable mode of TSF stacks consists in a rigid slip of the D molecule along its long direction (fig. 34c). In TTF-TCNQ the maximum displacement of the TTF amounts to about 0.03Å along this direction below T_L (Coppens et al. 1987, Bouveret and Megtert 1989). The direction of polarization of the distortion of the TCNQ stack is not so rigidly fixed by the angle of tilt of the A molecule. Structural measurements provide evidence that the polarization seems to rotate as a function of the temperature. At ambient pressure, the displacement of the TCNQ molecules is found to be polarized transversally (along c^*) above T_M (fig. 34d), in agreement with the finding of the Kohn anomaly in a transverse acoustic branch (Shirane et al. 1976), but in a direction perpendicular to the TCNQ plane (fig. 34e) below T_L (here the distortion of the TCNQ stack consists of a displacement of the benzenoid cycle by about 0.04Å and in a boat-like internal deformation of the molecule (Bouveret and Megtert 1989), probably due to short contact forces linking the C ≡ N terminal groups to the neighbouring TTF). There are experimental evidences that a similar rotation of the polarization occurs also under pressure by the addition below T^* (defined in fig. 32) in the ($\frac{1}{2}, 2k_F, 0$) modulated phase of TTF-TCNQ of a longitudinal component of distortion on the TCNO stack (Megtert et al. 1985). More likely, the increase of short-contact intrastack steric repulsions under pressure tends also to align the polarization of the TCNO displacement with the long axis of the molecule, as found for the donors at ambient pressure. Here we want only to suggest that the change of direction of polarization of the distortion of the TCNO sublattice could be a key feature to understand the subtle phase diagram of TTF-TCNQ. In particular since the variations of the D-A short contact distances (shown in fig. 11) between S and C ≡ N entities, which bear a maximum of electronic density, depend on the direction of the relative displacement of the molecules, one expects a substantial dependence of the D-A first-neighbour CDW multipolar Coulomb coupling with the nature of the polarization (such a contribution to the interstack coupling has been considered by Weger and Friedel (1977) and Hartzstein et al. (1980) both for translational and librational modes of the TTF and TCNQ molecules). Thus the rotation of the polarization of the TCNQ displacements could explain the unexpected decrease of the interstack coupling under pressure (in this respect it is interesting to remark in fig. 32 that the $\left(\frac{1}{2}, 2k_F, 0\right)$ phase is stabilized in all the temperature ranges when, at 4kbar, T^* and T_M merge together).

Until now we have considered the effect of the electron-phonon coupling in a single conduction band. In section 3 we have seen that in the case of $K_{0.3}MoO_3, NbSe_3$ and TaS_3 several conduction bands cross the Fermi level. With such a band structure several " $2k_F$ " instabilities can occur, depending if the critical wave vector links the $\pm k_F$ wave vectors of a given band or the $-k_F^I$ to the $+k_F^{II}$ wave vectors belonging to different bands. In the case of a band structure composed of bonding (B) and antibonding (AB) combinations of molecular orbitals, as in the compounds quoted above, a first-order electron-phonon coupling requires a phonon field of different symmetry for the coupling between the B − B (or AB − AB) and the B − AB orbitals at the Fermi level (Noguera 1986). The latter coupling, which opens simultaneously a gap at the Fermi level on B and AB bands, requires an out of phase modulation of the two chains or entities involved in the band structure. Such a phase shift is observed at the T_c^1 transition of $NbSe_3$, where the distortion mainly involves chains III (fig. 14) (Moudden et al. 1987) and at the Peierls transition of $K_{0.3}MoO_3$, where it involves mainly the " Mo(2) − O(11) − Mo(3) " entities defined in fig. 13. In the latter case, where the entities are related by an inversion center, the out of phase modulation is brought by the instability of an acoustic phonon mode (Pouget 1989). Structural determinations (Sato et al. 1986, Schutte and de Boer 1989, Girault 1987) show that the distortion of $K_{0.3}MoO_3$ consists mainly of a transverse displacement of the Mo(2) and Mo(3) atoms, forming the infinite chains of octahedra, towards the bridging oxygen O(11) (fig. 34b) by about 0.06Å at low temperature. This leads to a modulation of the Mo-O distances which change at first-order both the site energy and the in-chain tunneling integrals

(Pouget et al. 1989, Barisic 1985).

4.3.10 10. Excitations of the incommensurate *CDW* ordered state

In a single- q incommensurate modulated structure the low-frequency excitations are those of the phase and of the amplitude of the order parameter. They have been clearly observed for the $2k_F$CDW of $K_{0.3}MoO_3$.

Figure 35 provides evidence below T_c for a new acoustic-like phonon branch starting from the satellite reflections associated to the incommensurate modulation of $K_{0.3}MoO_3$ (Escribe-Filippini et al. 1987). This excitation branch, which originates from the softened Kohn anomaly, involves the phase of the CDW. The corresponding velocity is quite high: $v_p = (3.3 \pm 0.5) \times 10^3$ m/s. However, as q tends towards $2k_F$ the phason frequency does not reach exactly the value zero. Between T_c and 130 K

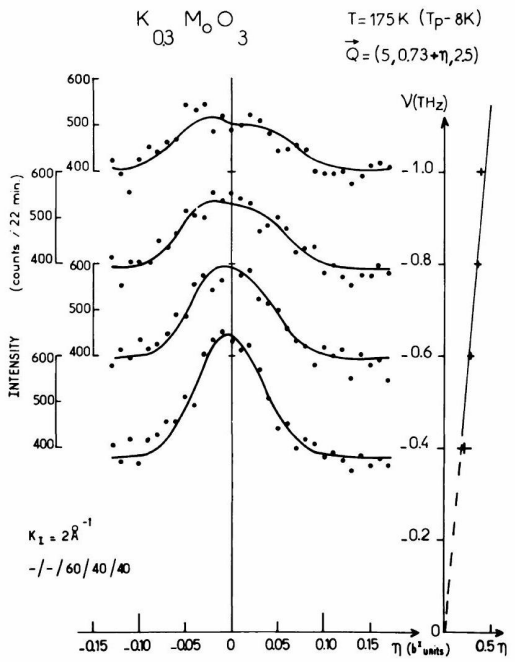


Fig. 35. Constant frequency scans (left scan) and dispersion (right side) of the phase mode branch of $\mathrm{K}\{0.3\}\ \mathrm{MoO}\{3\}$ at $T = 175$ K. The slope gives a phason velocity $v_p = 3.3 \pm 0.5 \times 10^3$ m/s in the chain direction (adapted from Escribe-Filippini et al. (1987)).

a damped harmonic oscillator fit of the phase mode excitations at $2k_F$ provides evidence for an overdamped response ($\Gamma_p = 0.8 \pm 0.2$THz) together with a small frequency gap of about 0.2 ± 0.1THz (Pouget et al. 1989). A gap of about this frequency (0.1 THz) has also been detected at very low temperature by far infrared absorption (Ng et al. 1986). It can be associated with the high frequency CDW pinning mode of $K_{0.3}MoO_3$ (a lower frequeny, temperature dependent, pinning mode is also obtained from the analysis of the frequency dependence of the CDW conductivity - see for example Mihaly (1989)). In absence of pinning the charged CDW should move collectively under the action of an external electric field applied in chain direction. In presence of pinning a threshold electric field must be overcome in order to observe clearly the manifestation of the CDW phase sliding on electronic transport properties (see chapter 4). However, below
this threshold, the field is expected to move locally the CDW or to deform it. It is only recently

that these field-induced motional deformations have been detected directly in $K_{0.3}MoO_3$ by means of X-ray diffraction, in the form of:

- A transverse broadening of the satellite reflections as soon as the field is applied. An effect which could be interpreted as the break into domains of the CDW sublattice due to the relative motion of pieces of differently pinned CDW (Tamegai et al. 1984, Fleming et al. 1985).
- A longitudinal broadening of the satellite reflections for large electric fields: an effect which can be associated with the polarization of the CDW sublattice (Mihaly et al. 1987).

To the displacive nature of the Peierls transition corresponds below T_c a new phonon branch involving the fluctuations of the amplitude of the CDW . The frequency ω_A of this mode at $2k_F$ is generally detected by means of Raman scattering. In the case of $K_{0.3}MoO_3$ the Raman data (Travaglini et al. 1983) are corroborated by inelastic neutron scattering experiments (Pouget et al. 1989, Sato et al. 1985). Furthermore, as shown by fig. 36, it is interesting to note that the frequency of the amplitude mode does not soften at T_c(183 K), as expected for a mean-field-like secondorder tansition. The extrapolation given by fig. 3b leads to its complete softening at the mean-field Peierls temperature ($T_c^{MF} \approx 320$ K). Between

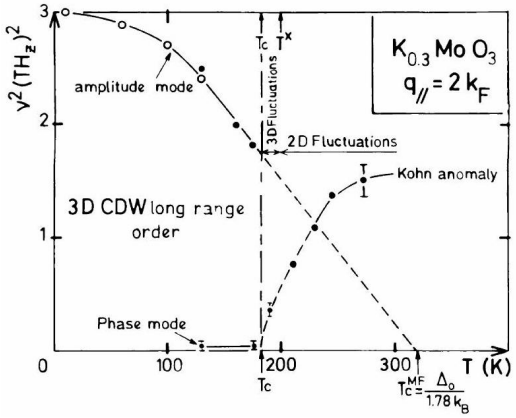


Fig. 36. Temperature dependence of the square of the frequency, ν, of the low-frequency structural excitations involved in the $2 k_{\mathrm{F}}$ CDW transition of $K_{0.3}MoO_3$. The mean field Peierls temperature T_c^{MF}, deduced from gap measurements (Johnston 1984) is indicated. The interrupted line is an extrapolation of the temperature dependence of the amplitude mode assuming a mean field behaviour: $\omega_A^2 \propto \left(T_c^{MF} - T\right)$. (Full symbols: neutron data, empty symbols: Raman data) (from Pouget et al. 1989).

T_c^{MF} and T_c the electron-phonon coupled system is strongly anharmonic. Numerical simulations of the dynamics of purely 1D systems (Tutis 1989) show that well below T_c^{MF}, amplitude and phase damped responses progressively emerge, at finite and zero frequencies respectively, by splitting of the overdamped response of the $2k_F$ Kohn anomaly. In 3D real systems, the basic features of the numerical calculations are qualitatively kept. In $K_{0.3}MoO_3$ the amplitude mode begins to be observed in the near vicinity of T_c, while it is seen well above " T_c " in KCP. In this 1D conductor inelastic neutron measurements (see fig. 20) provide evidence of two responses at about 1.3THz(5.5meV) and 0.6THz(2.5meV) not only below " T_c " $\sim$ 120 K but also on a large temperature range above " T_c " (Comes and Shirane 1979). These responses, also observed on Raman (Steigmeier et al. 1975) and infrared (Bruesch and Zeller 1974) data, have been assigned respectively to the amplitude and (pinned) phase modes of the CDW.

4.3.11 11. Concluding remarks

In this review we have only considered quasi-1D organic and inorganic conductors showing a CDW Peierls instability. Via the electron-phonon coupling this instability is related to the $2k_F$ or the $4k_F$ intrachain instability of the 1D electron-hole response function. A Peierls-like insulating state can be also stabilized through the CDW electronic response function of the 1D lattice coupled to an external potential provided by charged molecular entities external to the chain (Pouget 1987a,b). One of its clearer manifestations occurs when these entities possess orientational (case of noncentrosymmetrical anions X in (TMTSF)$_2$X or (TMTTF)$_2$X (Moret and Pouget 1986)) or positional (case of iodine chains in DIPS $\phi_4 (I_3)_{0.76}$ (Albouy et al. 1987, Noguera and Le Guennec 1988)) degrees of freedom. In these cases the metal-insulator transition is accompanied by the ordering, with the $2k_F$ or $4k_F$ wave vector, of these degrees of freedom. In all the 1D conductors considered in this review, the $2k_F$ CDW instability drives the metal insulator Peierls transition. This is not a general rule and several organic conductors like MEM (TCNQ) $_2$ (Huizinga et al. 1979) or (DMDCNQI) $_2$Ag (Moret et al. 1988) show first a $4k_F$CDW transition, localizing the charge degrees of freedom, then a $2k_F$ (spin-Peierls) transition leading to a pairing of the spin degrees of freedom in a non-magnetic state.

It is now clearly established that the 1D conductors can also exhibit, instead of the CDW ground state extensively discussed in this review, a spin density wave (SDW) or a superconducting ground state. The most familiar manifestation of these two last kinds of instabilities are found among the Bechgaard salts (TMTSF) $_2$X (Jerome and Schulz 1982). Furthermore in the case of salts with centrosymmetric anions (X = PF_6, AsF_6) it is found that
the pressure induces a change from the SDW to the superconducting ground states. The stabilization under pressure of a superconducting phase in materials, like $NbSe_3$ (Monceau 1985) or TTF [M(amit)$_2$] (M = Pd, Ni) (Brossard et al. 1989, Ravy et al. 1989) showing $2k_F$ CDW instability at atmospheric pressure is also observed.

In conclusion, the structural aspects of the Peierls transition shown by 1D conductors are now relatively well established. The nature of the interactions controlling the CDW instability is basically understood. But less is known about their evolution among the various families of 1D conductors and their change under the action of an external parameter. This is particularly true for the materials showing a competition between several ground states, where a detailed knowledge of the interactions is still lacking to understand the phase diagram.

4.3.12 References

Bouveret, Y., and S. Megtert, 1989, J. Phys. (France), (1st July).
Bozio, R., and C. Pecile, 1981, Solid State Commun. 37, 193.
Brossard, L., M. Ribault, L. Valade and P. Cassoux, 1989, in: J. Phys. (France) (June).

[0]Abrahams, E., J. Solyom and F. Woynarovich, 1977, Phys. Rev. B 16, 5238.
Albouy, P.A., J.P. Pouget and H. Strzelecka, 1987, Phys. Rev. B 35, 173.
Bak, P., and V.J. Emery, 1976, Phys. Rev. Lett. 36, 978.
Barisic, S., 1985, in: Electronic Properties of Inorganic Quasi One Dimensional Materials I, ed. P. Monceau (Reidel, Dordrecht, The Netherlands) p. 1.
Barisic, S., and A. Bjelis, 1985, in: Theoretical Aspects of Band Structures and Electronic Properties of Pseudo-One-Dimensional Solids, ed. H. Kanimura (Reidel, Dordrecht, The Netherlands) p. 49.
Berthier, C., and P. Segransan, 1987, in: Low Dimensional Conductors and Superconductors, NATO ASI No. B 155, eds D. Jerome and L.G. Caron (Plenum Press, New York) p. 455.
Bjelis, A., and S. Barisic, 1976, Phys. Rev. Lett. 37, 1517.
Bjelis, A., and S. Barisic, 1977, in: Organic Conductors and Semiconductors, Lecture Notes in Physics, Vol. 65, eds L. Pal, G. Grüner, A. Janossy and J. Solyom (Springer, Berlin) p. 291.
Bjelis, A., and S. Barisic, 1978, J. Phys. (France) Lett. 39, L 347.
Bjelis, A., and S. Barisic, 1982a, Phys. Rev. Lett. 48, 684.
Bjelis, A., and S. Barisic, 1982b, Mol. Cryst. & Liq. Cryst. 85, 151.

Brown, S.E., and A. Zettl, 1989, to be supplied by authors.
Bruesch, P., and H.R. Zeller, 1974, Solid State Commun. 14, 1037.
Brusetti, R., B.K. Chakraverty, J. Devenyi, J. Dumas, J. Marcus and C. Schlenker, 1982, in: Recent Developments in Condensed Matter Physics, Vol. 2, eds J.T. Devreese, L.F. Lemmens, V.E. van Doren and J. van Royen (Plenum Press, New York) p. 181.
Bullett, D.W., 1982, J. Phys. C 15, 3069.
Butaud, P., P. Segransan, C. Berthier, J. Dumas and C. Schlenker, 1985, Phys. Rev. Lett. 55, 253.

Carneiro, K., G. Shirane, S.A. Werner and S. Kaiser, 1976, Phys. Rev. B 13, 4258.
Comes, R., and G. Shirane, 1979, in: Highly Conducting One Dimensional Solids, eds J.T. Devreese, R.P. Evrard and V.E. van Doren (Plenum Press, New York) p. 17.
Comes, R., M. Lambert, H. Launois and H.R. Zeller, 1973, Phys. Rev. B 8, 571.
Comes, R., B. Renker, L. Pintschovius, R. Currat, W. Glaser and G. Scheiber, 1975, Phys. Status Solidi B 71, 171.
Comes, R., G. Shirane, S.M. Shapiro, A.F. Garito and A.J. Heeger, 1976, Phys. Rev. B 14, 2376.

Coppens, P., V. Petricek, F. Levendis, K. Finn, F.K. Larsen, A. Paturle, G. Yan and N.D. Le Grand, 1987, Phys. Rev. Lett. 59, 1695.
Denoyer, F., R. Comes, A.F. Garito and A.J. Heeger, 1975, Phys. Rev. Lett. 35, 445.
Devreux, F., 1982, J. Phys. (France) 43, 1489.
Dieterich, W., 1976, Adv. Phys. 25, 615.
Ellenson, W.D., R. Comes, S.M. Shapiro, G. Shirane, A.F. Garito and A.J. Heeger, 1976, Solid State Commun. 20, 53.
Ellenson, W.D., S.M. Shapiro, G. Shirane and A.F. Garito, 1977, Phys. Rev. B 16, 3244.
Emery, V.J., 1979, in: Highly Conducting One Dimensional Solids, eds J.T. Devreese, R.P. Evrard and V.E. van Doren (Plenum Press, New York) p. 247.
Epstein, A.J., J.S. Miller, J.P. Pouget and R. Comes, 1981, Phys. Rev. Lett. 47, 741.
Escribe-Filippini, C., J.P. Pouget, B. Hennion and M. Sato, 1987, Synth. Met. 19, 931.
Fleming, R.M., D.E. Moncton and D.B. McWhan, 1978, Phys. Rev. B 18, 5560.
Fleming, R.M., R.G. Dunn and L.F. Schneemeyer, 1985, Phys. Rev. B 31, 4099.
Forro, L., L. Zuppiroli, J.P. Pouget and K. Bechgaard, 1983, Phys. Rev. B 27, 7600.
Forro, L., S. Bouffard and J.P. Pouget, 1984, J. Phys. (France) Lett. 45, L 343.
Girault, S., 1987, Thesis Paris-Sud University (unpublished).
Girault, S., A.H. Moudden, J.P. Pouget and J.M. Godard, 1988, Phys. Rev. B 38, 7980.
Girault, S., A.H. Moudden and J.P. Pouget, 1989, Phys. Rev. B 39 (1st March).
Hartzstein, C., V. Zevin and M. Weger, 1980, J. Phys. (France) 41, 677.
Herman, F., 1977, Phys. Scr. 16, 303.
Hirsch, J.E., and D.J. Scalapino, 1984, Phys. Rev. B 29, 5554.
Horowitz, B., H. Gutfreund and M. Weger, 1975, Phys. Rev. B 8, 3174.
Hubbard, J., 1978, Phys. Rev. B 17, 494.
Huizinga, S., J. Kommandeur, G.A. Sawatzky, K. Kopinga and W.K.M. de Jonge, 1979, in: Quasi One Dimensional Conductors II, Lecture Notes in Physics, Vol. 96, p. 45.
Jacobsen, C.S., 1985, Mat.-Fys. Medd. Dan. Vidensk. Selsk. 41, 251.
Jacobsen, C.S., 1986, J. Phys. C 19, 5643.
Jerome, D., and H.J. Schulz, 1982a, in: Extended Linear Chain Compounds, Vol. 2, ed. J.S. Miller (Plenum Press, New York) p. 159.
Jerome, D., and H.J. Schulz, 1982b, Adv. Phys. 31, 299.
Johnston, D.C., 1984, Phys. Rev. Lett. 52, 2049.

Kagoshima, S., 1982, in: Extended Linear Chain Compounds II, ed. J.S. Miller (Plenum Press, New York) p. 303.

Kagoshima, S., H. Anzai, K. Kajimura and T. Ishiguro, 1975, J. Phys. Soc. Jpn. 39, 1143.
Kagoshima, S., T. Ishiguro and H. Anzai, 1976, J. Phys. Soc. Jpn. 41, 2061.
Khanna, S.K., J.P. Pouget, R. Comes, A.F. Garito and A.J. Heeger, 1977, Phys. Rev. B 16, 1468.

Lynn, J.W., M. Izumi, G. Shirane, S.A. Werner and R.B. Saillant, 1975, Phys. Rev. B 12, 1154.

Mazumdar, S., and Z. Soos, 1981, Phys. Rev. B 23, 2810.
Meerschaut, A., and J. Rouxel, 1986, in: Crystal Chemistry and Properties of Materials with Quasi One Dimensional Structures, ed. J. Rouxel (Reidel, Dordrecht, The Netherlands) p. 222.

Megtert, S., R. Comes, C. Vettier, R. Pynn and A.F. Garito, 1982, Mol. Cryst. & Liq. Cryst. 85, 159.
Megtert, S., A. Bjelis, J. Przystawa and S. Barisic, 1985, Phys. Rev. B 32, 6692.
Menyhard, N., 1978, J. Phys. C 11, 2207.
Mihaly, G., 1989, in: Proceedings of the 9th General Conference of the Condensed Matter Division of the E.P.S. (Nice-France). To be published in Physica Scripta.
Mihaly, L., K.B. Lee and P.W. Stephens, 1987, Phys. Rev. B 36, 1793.
Monceau, P., 1985, in: Electronic Properties of Inorganic Quasi One Dimensional Materials II, ed. P. Monceau (Reidel, Dordrecht, The Netherlands) p. 139.
Moret, R., and J.P. Pouget, 1986, in: Crystal Chemistry and Properties of Materials with Quasi One Dimensional Structure, ed. J. Rouxel (Reidel, Dordrecht, The Netherlands) p. 87.
Moret, R., P. Erk, S. Hünig and J.U. Von Schütz, 1988, J. Phys. (France) 49, 1925.
Moudden, A.H., S. Girault, J.P. Pouget, P. Monceau and F. Levy, 1987, in: Proc. 2nd European Workshop on Charge Density Waves, Aussois, 1987, p. 74 (unpublished).
Ng, H.K., G.A. Thomas and L.F. Schneemeyer, 1986, Phys. Rev. B 33, 8755.
Niedoba, H., H. Launois, D. Brinkmann and H.U. Keller, 1974, J. Phys. (France) Lett. 35, L 251.

Noguera, C., 1986, J. Phys. C 19, 2161.
Noguera, C., and P. Le Guennec, 1988, Phys. Rev. B 37, 492.
Pouget, J.P., 1987a, in: Low Dimensional Conductors and Superconductors, NATO ASI No. B 155, eds D. Jerome and L.G. Caron (Plenum Press, New York) p. 17.
Pouget, J.P., 1987b, in: Organic and Inorganic Low-Dimensional Crystalline Materials, NATO ASI No. B 168, eds P. Delhaes and M. Drillon (Plenum Press, New York) p. 185.
Pouget, J.P., 1988, in: Highly Conducting Quasi One Dimensional Organic Crystal Semiconductors and Semimetals, Vol. 27, ed. E.M. Conwell (Pergamon Press, New York) p. 87.
Pouget, J.P., 1989, in: Low Dimensional Electronic Properties of Molybdenum Bronzes and Oxides, ed. C. Schlenker (Reidel, Dordrecht, The Netherlands) (in press).
Pouget, J.P., S.K. Khanna, F. Denoyer, R. Comes, A.F. Garito and A.J. Heeger, 1976, Phys. Rev. Lett. 37, 437.
Pouget, J.P., S.M. Shapiro, G. Shirane, A.F. Garito and A.J. Heeger, 1979, Phys. Rev. B 19, 1792.

Pouget, J.P., R. Moret, A. Meerschaut, L. Guemas and J. Rouxel, 1983, J. Phys. (France) Colloq. 44, C3-1729.
Pouget, J.P., C. Noguera, A.H. Moudden and R. Moret, 1985a, J. Phys. (France) 46, 1731 [1986, erratum J. Phys. (France) 47, 145].
Pouget, J.P., C. Escribe-Filippini, B. Hennion, R. Currat, A.H. Moudden, R. Moret, J. Marcus and C. Schlenker, 1985b, Mol. Cryst. & Liq. Cryst. 121, 111.
Pouget, J.P., S. Girault, A.H. Moudden, B. Hennion, C. Escribe-Filippini and M. Sato, 1989, Phys. Scr. T 25, 58.

Ravy, S., J.P. Pouget, L. Valade and J.P. Legros, 1989, Europhys. Lett. (in press).
Ross Jr, J.H., Z. Wang and C.P. Slichter, 1986, Phys. Rev. Lett. 56, 663.

Rybaczewski, E.F., E.S. Smith, A.F. Garito, A.J. Heeger and B. Silbernagel, 1976, Phys. Rev. B 14, 2746.
Sakai, M., S. Kagoshima and E.M. Engler, 1983, J. Phys. (France) Colloq. 44, C3-1313.
Sato, M., H. Fujishita and S. Hoshino, 1983, J. Phys. C 16, L-877.
Sato, M., H. Fujishita, S. Sato and S. Hoshino, 1985, J. Phys. C 18, 2603.
Sato, M., M. Fujishita, S. Sato and S. Hoshino, 1986, J. Phys. C 19, 3059.
Saub, K., S. Barisic and J. Friedel, 1976, Phys. Lett. A 56, 302.
Scalapino, D.J., and J.E. Hirsch, 1983, J. Phys. (France) Colloq. 44, C3-1507.
Scalapino, D.J., M. Sears and R.A. Ferrell, 1972, Phys. Rev. B 6, 3409.
Schulz, H.J., 1987, in: Low-Dimensional Conductors and Superconductors, NATO ASI, No. B 155, eds D. Jerome and L.G. Caron (Plenum Press, New York) p. 95.
Schutte, W.J., and J.L. de Boer, 1989, Acta Crystallogr. (in press).
Sham, L.J., 1979, in: Highly Conducting One Dimensional Solids, eds J.T. Devreese, R.P. Evrard and V.E. van Doren (Plenum Press, New York) p. 227.
Shima, N., 1983, J. Phys. Soc. Jpn. 52, 578.
Shirane, G., S.M. Shapiro, R. Comes, A.F. Garito and A.J. Heeger, 1976, Phys. Rev. B 14, 2325.
Soda, G., C. Bourbonnais and D. Jerome, 1987, J. Phys. Soc. Jpn. 56, 3951.
Solyom, J., 1979, Adv. Phys. 28, 101.
Steigmeier, E.F., R. Loudon, G. Harbeke, H. Auderset and G. Scheiber, 1975, Solid State Commun. 17, 1447.
Takahashi, T., D. Jerome, F. Masin, J.M. Fabre and L. Giral, 1984, J. Phys. C 17, 3777.
Tamegai, T., K. Tsutsumi, S. Kagoshima, Y. Kanai, M. Tani, M. Tomozawa, M. Sato, K. Tsuji, J. Harada, M. Sakata and T. Nakajima, 1984, Solid State Commun. 51, 585.
Tamegai, T., K. Tsutsumi and S. Kagoshima, 1987, Synth. Met. 19, 923.
Thielemans, M., R. Deltour, D. Jerome and J.R. Cooper, 1976, Solid State Commun. 19, 21.
Tomkiewicz, Y., A.R. Taranko and J.B. Torrance, 1976, Phys. Rev. Lett. 36, 751.
Travaglini, G., I. Morke and P. Wachter, 1983, Solid State Commun. 45, 289.
Tutis, E., 1989, Thesis (Zagreb, Yugoslavia) unpublished.
Veuillen, J.Y., R. Chevalier, J. Marcus and C. Schlenker, 1986, Phys. Rev. B 143, 186.
Veuillen, J.Y., R.C. Cinti and E. Al Khoury Nemeh, 1987, Europhys. Lett. 3, 355.
Wang, Z.Z., H. Salva, P. Monceau, M. Renard, C. Roucau, R. Ayroles, F. Levy, L. Guemas and A. Meerschaut, 1983, J. Phys. (France) Lett. 44, L 311.
Weger, M., and J. Friedel, 1977, J. Phys. (France) 38, 241 and 881.
Whangbo, M.H., 1986, in: Crystal Chemistry and Properties of Materials with Quasi One Dimensional Structure, ed. J. Rouxel (Reidel, Dordrecht, The Netherlands) p. 27.
Whangbo, M.H., and P. Gressier, 1984, Inorg. Chem. 23, 1305.
Whangbo, M.H., and L.F. Schneemeyer, 1986, Inorg. Chem. 25, 2424.
Wilson, J.A., 1979, Phys. Rev. B 19, 6456.
Yamaji, K., S. Megtert and R. Comes, 1981, J. Phys. (France) 42, 1327.
Zuppiroli, L., 1988, in: Highly Conducting Quasi One Dimensional Organic Crystal Semiconductors and Semimetals, Vol. 27, ed. E.M. Conwell (Pergamon Press, New York) p. 437.

4.4 4 Dynamical Properties of Charge Density Waves

and
P. MONCEAU
Centre de Recherches sur les Très Basses Températures
C.N.R.S., BP 166 X, 38042 Grenoble-Cedex, France
L.P. Gor'kov and G. Grüner

4.4.1 1. Introduction

Although predicted nearly thirty years ago, electronic transport due to moving charge density waves (CDW) was demonstrated experimentally only in the last decade when the properties of various organic and inorganic linear chain conductors have been explored. Collective charge density wave response was first investigated in the materials TTF-TCNQ, and KCP, and the anomalous low-frequency response of these materials was claimed to be due to the oscillating motion of pinned charge density waves.

Clear evidence for collective mode dynamics was first provided by nonlinear conductivity studies on the inorganic linear chain compound $NbSe_3$. The observation was followed by the discovery of other materials with a CDW ground state and by the observation of a variety of phenomena which can be attributed to the collective response of the condensate. The observations can be accounted for by various models, these all are based on the original idea of Fröhlich, that the electric current is carried by the translational motion of the CDW ground state. In contrast to the prediction, however, various forces can pin the collective mode to the underlying lattice, and in the current carrying state, damping effects are important. In other words, Fröhlich superconductivity is not realized in the materials studied so far.

The field has also broadened considerably in recent years. Depending on the mechanism of pinning, and also by crystal perfection, impurity content and temperature, the details of the dynamics are different, and the nonlinear $I-V$ curves, the details of the frequency dependent response can be modelled by different assumptions. The variety of observations is also a source of controversies, in many cases, not entirely resolved at present.

In this paper we give a short review of the various observations which have been made on various inorganic linear chain compounds in their charge density wave ground states. Although mainly the electrical properties of the various materials have been studied in detail, the dynamics of the collective mode leads to unusual other transport phenomena and also to unusual elastic properties. While these can all be consistently attributed to the dynamical response of the collective CDW mode, direct evidence comes from local probes, such as nuclear magnetic resonance. We do not
attempt to describe the theoretical state of affairs. The various points of view are summarized by Littlewood and by Gorkov, in this volume.

4.4.2 2. Some basic notions on charge density waves

The Peierls transition, and the various inorganic linear chain compounds have been discussed elsewhere in this volume, and consequently, we only briefly mention some of the basic observations. The metal-insulator transition, signalling the onset of the charge density wave ground state has been observed in a variety of materials with linear chain structure, and the compounds TaS_3 (both the orthorhombic and the monoclinic form), $(TaSe_4)_2\,I$, $(NbSe_4)_2\,I$, $(NbSe_4)_{3.33}\,I$ and $K_{0.3}MoO_3$ are also prototype examples for the dynamics of charge density waves. (For a review of the structural features and static properties see, Rouxel and Schlenker, this volume).

The Hamiltonian, which leads to the Peierls transition and to the CDW ground state is given, in one dimension, by

$$\mathscr{H} = \sum_{k,\sigma} \epsilon_k c^+_{k\sigma} c_{k\sigma} + \sum_{k,\sigma} \hbar\omega^0_q b^+_q b_q + \sum_{k,q,\sigma} g(k) c^+_{k+q,\sigma} c_{k,\sigma} \left(b_q + b^+_q\right), \tag{2.1}$$

where $c^+_k\,(c_k)\,, b^+_q\,(b_q)$ are the electron and phonon creation (annihilation) operators with momenta k and q, σ denotes the spin, ϵ_k and ω^0_q are the electron and phonon dispersions and $g(k)$ is the electron-phonon coupling constant. The ground state in the weak coupling limit, leads to a periodically modulated charge density $\Delta\rho$,

$$\Delta\rho = \rho_1 \cos\left(2k_{\mathrm{F}}r + \phi\right), \tag{2.2}$$

where ρ_1 is the amplitude and ϕ the phase of the condensate. The period $\lambda = \pi/k_{\mathrm{F}}$.

The development of the incommensurate CDW is directly observed by X-ray scattering which gives the wavevector k, or CDW periodicity λ. In all cases, λ is close to a commensurate period of $4a$ where a is the lattice constant in the chain direction (Pouget and Comes, this volume).

In the Peierls state the various transport properties are expected to be determined by carrier excitations across the single-particle gap. The dc resistivity due to these excitations displays an exponential temperature dependence. This is shown in fig. 1 for some of the materials with a CDW ground state. The gaps are larger than which would correspond to the BCS relation $2\Delta/\left(k_{\mathrm{B}}T_{\mathrm{c}}\right) = 3.5$ (Monceau et al. 1985). This is either due to strong electron-phonon coupling or due to low-dimensional effects. The material $NbSe_3$ has two phase transitions (see fig. 2), and at both only part of the Fermi surface is removed. Here again $2\Delta/\left(k_{\mathrm{B}}T_{\mathrm{c}}\right)$ is significantly larger than 3.5 (Fournel et al. 1986). The optical properties are also determined by the

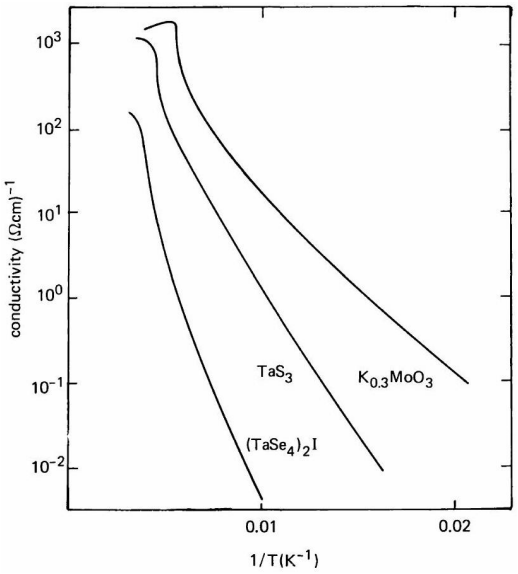


Fig. 1. Temperature dependence of the electrical conductivity in $\mathrm{o}-\mathrm{TaS}_3$, in $(TaSe_4)_2\,I$ and in $K_{0.3}MoO_3$. The arrows represent the Peierls transition temperatures; they are evident by examining the temperature derivatives $\mathrm{d}R/\mathrm{d}T$.

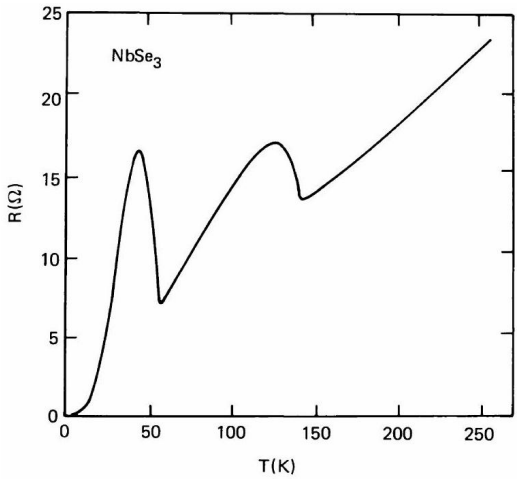


Fig. 2. Temperature dependence of the electrical resistance of NbSe_{3}. Sharp increases of $\rho(T)$ at 144 K and 59 K signal the onset of two phase transitions involving different chains.

gap, which in general, corresponds to $\hbar\omega$ in the visible to infrared spectral range. In addition to these single-particle phenomena, the coupled elec-tron-phonon system can contribute to charge transport by moving the CDW rigidly, while the ions which are involved in the periodic lattice distribution execute only oscillatory motion. The energy of an incommensurate CDW is independent of the phase ϕ, and consequently the translational motion could be induced by small dc electric fields. In the absence of damping, this also would lead to a supercurrent, as described by Fröhlich (1954).

No evidence for such anomalous conductivity is found when the experiments are performed in small dc fields; under such circumstances all transport coefficients can be described in terms of standard single-particle transport theories appropriate for a band semiconductor. It has been first emphasized by Lee, Rice and Anderson (1974) that, in contrast to superconductors, the phase of the CDW condensate can be pinned to the lattice through the interaction with impurities, lattice imperfections, grain boundaries, commensurability effects, etc. Consequently, the collective mode contribution to the dc conductivity measured at low electric fields is zero. However, the pinning energy per electron can be much smaller than the single-particle energies Δ and ϵ_{F}, and consequently the response to finite amplitude dc and to ac excitations is dominated by the dynamics of the collective mode.

2.1. The dynamics of the collective mode: fundamental concepts

The dynamics of the collective mode is described in terms of a position and time dependent order parameter $\Delta(x,t)$. As $\Delta(x,t)$ is complex, both amplitude and phase fluctuations occur. These can be described by assuming that the two types of fluctuations are decoupled and

$$\Delta(x,t) = (\Delta_0 + \delta)\,\mathrm{e}^{\mathrm{i}\phi'},$$

where Δ_0 is the equilibrium order parameter, δ and ϕ' are the fluctuations from the equilibrium value. Then to lowest order in δ and ϕ' the amplitude mode corresponds to $\Delta_{2k_{\mathrm{F}}}+\Delta_{-2k_{\mathrm{F}}} = 2\Delta_0+2\delta$, and the phase mode corresponds to $\Delta_{2k_{\mathrm{F}}}-\Delta_{-2k_F} = 2\mathrm{i}\Delta\phi'$. The dispersion relations of these modes were first calculated by Lee, Rice and Anderson (1974), using the electronphonon Hamiltonian of eq. (2.1). The electron-phonon interaction transforms the acoustic phonons near the new zone boundary into an optical and an acoustic branch with frequencies

$$\Omega_+^2 = \lambda' \left(\omega_{2k_\mathrm{F}}\right)^2 + \frac{1}{3}\left(m/m^*\right)\left(v_\mathrm{F} q_x\right)^2, \tag{2.3a}$$

$$\Omega_-^2 = \left(m/m^*\right)\left(v_\mathrm{F} q_x\right)^2 = \left(c_0 q_x\right)^2, \tag{2.3b}$$

with q_x the wavevector along the chain direction, λ' the dimensionless electron-phonon coupling constant and $\boldsymbol{\omega_{2\mathbf{k}_\mathbf{F}}}$ the phonon frequency at $q = 2k_\mathrm{F}$. The Ω_+mode is called the amplitude, the Ω_-mode the phase mode. The effective mass m^* is given in terms of fundamental parameters of the problem, $\lambda', \omega_{2k_\mathrm{F}}$ and Δ, by

$$\frac{m^*}{m} = 1 + \frac{4\Delta^2}{\hbar^2 \lambda' \left(\omega_{2k_\mathbf{F}}\right)^2} \tag{2.4a}$$

at $T = 0$. Both modes soften with increasing temperature, while the temperature dependence of the effective mass is given by

$$\frac{m^*}{m} = 1 + \frac{4\Delta^2}{\hbar^2 \lambda' \left(\omega_{2k_\mathrm{F}}\right)^2} \frac{n_\mathrm{c}(T)}{n_\mathrm{c}(T=0)}. \tag{2.4b}$$

with the temperature dependent carrier density n_c given by the BCS expression. While the amplitude mode has a gap, the phase mode is gapless, and the $q = 0$ translational mode corresponds to zero excitation energy. The dispersion relation for $\Omega_+$and $\Omega_-$is shown in fig. 3. The large effective mass m^* is the consequence of the coupled dynamics of the electrons and phonons, as the total kinetic energy includes both that of the electrons which execute translational motion and the ions which oscillate about their equilibrium positions. The amplitude mode, Ω_+, is expected to be Raman active, while the phase mode carries a dipole moment, as it involves the motion of condensed electrons in respect of the background of the position changes of the ions. Consequently, the $q = 0$ phase mode carries a current. Equation (2.3) is appropriate in the long-wavelength $q^{-1} \gg \lambda$ limit. For short-wavelength fluctuations, deviations from the above dispersion relation occur that are similar to those which arise for optical and acoustical phonons near to a zone boundary. Also, Coulomb interactions may shift

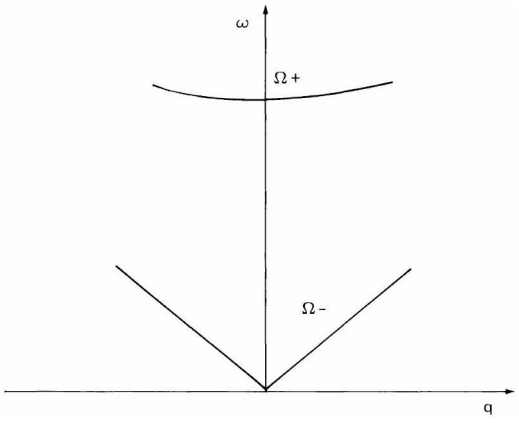


Fig. 3. Phase and amplitude mode dispersion relations.

the Ω_-branch up to optical frequencies. Uncondensed electrons, however, most likely screen the Coulomb interactions and eq. (2.3) is expected to be appropriate. With a characteristic Fermi energy $\epsilon_\mathrm{F} \sim 1\mathrm{eV}$, single-particle gap $\Delta \sim 0.1\mathrm{eV}$ and phonon frequency $\omega_{2k_\mathrm{F}} \sim 10^{-2}\mathrm{eV}$, the electron-phonon coupling constant λ' is of the order of 0.5 . With these values, $\Omega_+(q = 0) \sim 5 \times 10^{-3}\mathrm{eV}$, which is smaller than Δ, and the effective mass is of the order of $m^*/m \sim 10^3$.

This picture has to be modified at low temperatures when the screening of the CDW deformations by the quasiparticles is suppressed. In this case the dispersion law of the phase mode has been calculated by Lee and Fukuyama (1978), Kurihara (1980), Barisic (1985, 1987), Nakane and Takada (1985), and Wong and Takada (1987). Longitudinal and transverse modes have to be analyzed separately: a longitudinal compression of the CDW implies a charge redistribution leading to long-range Coulomb forces. This raises the Ω-phase mode to a finite frequency given by $1.5\lambda'^{1/2}\omega_{2k_F}$ (Lee, Rice and Anderson 1974). On the contrary a transverse shear only implies a dephasing of the CDW between adjacent chains but not a charge redistribution, and this preserves the acoustic character of the phase mode. With Coulomb interactions, the dispersion relation (2.3b) for the longitudinal modes becomes (Wong and Takada 1987)

$$\Omega_-^2 = \left(c_0^2 + \frac{\Omega_p^2 q_x^2}{\epsilon_z q_x^2 + q_0^2} \right) q_x^2 \tag{2.5a}$$

with two limits

$$\Omega_-^2 = \left(c_0^2 + \Omega_p^2/q_0^2 \right) q_x^2 \text{ for } q_x^2 \ll q_0^2/\epsilon_z, \tag{2.5b}$$

$$\Omega_-^2 = \frac{3}{2}\lambda' \omega_{2k_F}^2 + c_0^2 q_x^2 \text{ for } q_x^2 \gg q_0^2/\epsilon_z. \tag{2.5c}$$

Here $\Omega_p^2 = 4\pi n e^2/m^*$ is the CDW plasma frequency, ϵ_z the screening dielectric constant, $\epsilon_z = 1 + (4\pi n e^2/m)\,(1/6\Delta^2)$, and $q_0^2 = 4\pi e^2 n_{qp}/T$ the square of the Thomas-Fermi screening wave number with the quasiparticle density n_{qp}. Because of the single-particle gap, this quasiparticle concentration is thermally activated. The crossover between the regimes (2.5 b) and (2.5c) is given by the phase mode length and the Thomas-Fermi screening length. When $|q_x| \ll q_0 \epsilon_z^{-1/2}$, the phase mode length is much larger than the Thomas-Fermi screening length, there is no local charge density in the scale of a phase mode length and the excitations remain acoustic. However, the phason velocity increases. On the other hand when $|q_x| \gg q_0 \epsilon_z^{-1/2}$ the quasiparticles are unable to screen any charge fluctuation in the scale of the phase mode length and the spectrum shows an optical mode for $q \to 0$, which has been given by Lee, Rice and Anderson (1974).

Due to the gap in the dispersion relation for the amplitude mode, amplitude fluctuations do not play an important role at temperatures $kT \ll \Omega_+$. Therefore, most of the descriptions of dynamical collective
phenomena to be discussed are in terms of the dynamics of the phase only. Such a description may be appropriate at low temperatures, but close to the Peierls transition important effects coming from the dynamics of the amplitude mode are expected to occur. For phase dynamics the Lagrangian density in one dimension can be written (Fukuyama and Lee 1978, Brasovskii and Dzyaloshinskii 1976)

$$\mathscr{L} = \frac{n_c}{4\hbar} \frac{m^*}{m v_F} \left(\frac{\mathrm{d}\phi}{\mathrm{d}t} \right)^2 - n_c k \left(\frac{\mathrm{d}\phi}{\mathrm{d}x} \right)^2 \tag{2.6}$$

to lowest order in the derivatives, with n_c the one-dimensional carrier density. The first term on the right-hand side corresponds to the kinetic energy of a line of mass $m^* n_c$ per unit length with $n_0 = n_c n_\perp$ the number of chains per cross section. The second term represents the potential energy associated with the distortions of the collective mode, with a phenomenological elastic constant κ. The equation of motion corresponding to the above Lagrangian is

$$\frac{\mathrm{d}^2\phi}{\mathrm{d}t^2} = \frac{4k_F\kappa}{m^*} \frac{\mathrm{d}^2\phi}{\mathrm{d}x^2}. \tag{2.7}$$

The solutions of eq. (2.7) are of the form $\exp(\mathrm{i}\omega t - qx)$ with the dispersion relation

$$\Omega^2 = (\kappa/m^*)\,(2k_{\mathrm{F}}q)^2 \tag{2.8}$$

and comparison with eq. (2.3) gives the phenomenological elastic constant in terms of v_{F} as

$$\kappa = \hbar v_{\mathrm{F}}/2\pi \tag{2.9}$$

The plane wave solutions represent the periodic compression and expansion of the CDW, these excitations are called phasons. The dispersion relation (2.3b) also defines a phason velocity

$$c_0 = (m/m^*)^{1/2}\, v_{\mathrm{F}} \tag{2.10}$$

which gives, for $v_{\mathrm{F}} \sim 3 \times 10^7$ cm/s, and for $m^*/m \sim 10^3, c_0$ as approximately 10^6 cm/s.

As in a superconductor, the phase $\phi(x,t)$ plays an important role in the dynamics of the collective mode. The $q = 0$ phase mode corresponds to the translational motion of the condensed electrons, with the ions oscillating around their equilibrium positions. A rigid displacement of the CDW leads to an electric current, and the current density per chain $j_{\mathrm{CDW}} = -n_{\mathrm{c}} e v_{\mathrm{d}} = -n_{\mathrm{c}} e(\,\mathrm{d}x/\mathrm{d}t)$. With $\phi = 2k_{\mathrm{F}}x$ and $\lambda = \pi/k_{\mathrm{F}}$,

$$j_{\mathrm{CDW}} = -\frac{e}{\pi}\frac{\mathrm{d}\phi}{\mathrm{d}t} \tag{2.10a}$$

A compression of the wave leads to a change of the electronic density, and therefore

$$n_{\mathrm{c}} = \frac{1}{\pi}\frac{\mathrm{d}\phi}{\mathrm{d}x} \tag{2.10b}$$

at zero temperature. The cross derivatives of the above equations lead to the equation of continuity

$$\mathrm{d}j_{\mathrm{CDW}}/\mathrm{d}x + \mathrm{d}n_{\mathrm{c}}/\mathrm{d}t = 0. \tag{2.11}$$

Equation (2.11) is more general than implied by its derivation, and is valid to all orders in the derivative expansion of the phase (Horovitz 1985). Here and in the previous formulas, the subscript refers to the current carried by the CDW. Subsequently, the subscript will be used only if the effect of normal electrons, leading to normal current is also important. Otherwise all quantities (current, current density, cordial and differential conductivity etc.) refer to transport carried by the collective mode.

The above relations can also be derived by considering the modification of the dispersion relation of electrons in momentum space. As in a superconductor for a slowly varying $\phi(x,t)$ the Fermi surface is tied to the position and time dependent condensate. Consider first a slowly varying $\phi(x)$, for which $(1/k_{\mathrm{F}})\,(\mathrm{d}\phi/\mathrm{d}x) \ll 1$. This can be described as a change in the wavevector $2k_{\mathrm{F}} + \mathrm{d}\phi/\mathrm{d}x$, and consequently the single-particle gap is shifted from $\pm k_{\mathrm{F}}$ to $\pm\left(k_{\mathrm{F}} + \frac{1}{2}(\,\mathrm{d}\phi/\mathrm{d}x)\right)$, as shown in fig. 4 a . If the electrons do not change their density then the gap is removed from the Fermi surface. This leads to electrons in states above the gap, and to a large increase of the total electronic energy. A change of the electron density, by tying the gap to the Fermi surface involves less energy. As $\rho(x) = 2k_{\mathrm{F}}(x)/2\pi$, the gap is at the Fermi level if

$$\rho(x) = \rho_0 + \frac{1}{\pi}\frac{\mathrm{d}\phi}{\mathrm{d}x}, \tag{2.12}$$

the same relation as eq. (2.10b).

For a time dependent phase $\phi(t)$ the inversion symmetry is broken and the dispersion relation becomes asymmetric as shown in fig. 4b. The electronic energies are given by

$$\epsilon_{\pm k} = \left[v_{\mathrm{F}} k \pm \frac{1}{2}\, \mathrm{d}\phi/\mathrm{d}t + \Delta^2 \right]^{1/2} \tag{2.13}$$

near the gap. The energies corresponding to the displaced Fermi surface are given by

$$E_{\pm k} = -\Delta \pm \frac{1}{2}\, \mathrm{d}\phi/\mathrm{d}t, \tag{2.14}$$

and the total current

$$j_{\mathrm{CDW}} = 2e \int \frac{\mathrm{d}\epsilon}{\mathrm{d}k} \frac{\mathrm{d}k}{2\pi} = \frac{\epsilon_{+k} - \epsilon_{-k}}{\pi} = -\frac{e}{\pi} \frac{\mathrm{d}\phi}{\mathrm{d}t}, \tag{2.15}$$

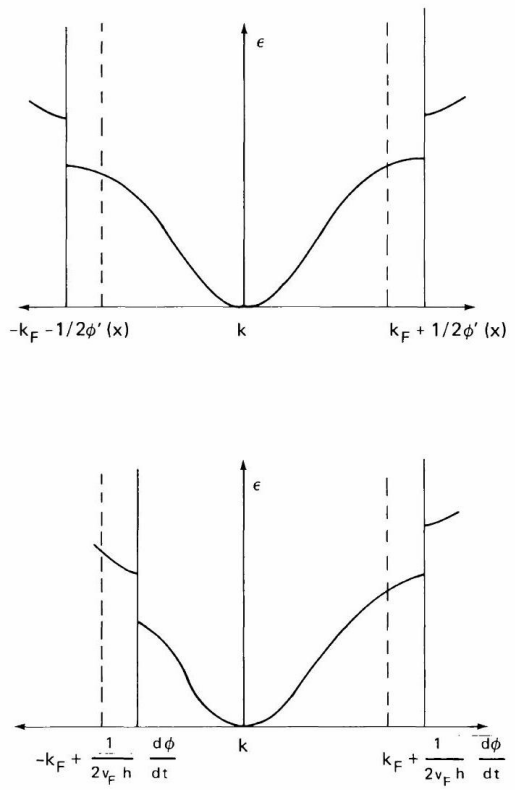


Fig. 4. Displaced Fermi surface for a position (fig. 4a) and for a time dependent (fig. 4b) phase. The states are filled up to the Fermi level, $\pm\left(k_{\mathrm{F}}+\frac{1}{2}\mathrm{\tilde{d}}\,\phi(x)/\mathrm{d}\,x\right)$ in fig. 4 a , and up to $\pm\,[k_{\mathrm{F}}+\,(1/2v_{\mathrm{F}}h)\,(\mathrm{d}\phi/\mathrm{d}t)]$ in fig. 4 b . The dotted lines refer to the original Fermi surface at $\pm k_{\mathrm{F}}$.

the same as eq. (2.10a). This relation, and also eq. (2.12), break down for strong local distortions of the condensate. In such cases both the amplitude and phase perturbations have to be included. The relation which connects the electric current and condensate density to the time and spatial derivative of the phase $\phi(x,t)$ of the condensate is different from the relations which are appropriate for a superconductor, namely $p_{\mathrm{s}} = \mathrm{i}\hbar(\mathrm{d}\phi/\mathrm{d}x)$ and $\mu = \mathrm{i}\hbar(\mathrm{d}\phi/\mathrm{d}t)$, where p_{s} and μ are the momentum and the chemical potential. This arises because, in contrast to the superconducting ground state, the charge density wave condensate is formed by electron-hole pairs, and pairing also involves the wavevector $2k_{\mathrm{F}}$.

In the presence of an applied electric field $E(\omega) = E_0 \mathrm{e}^{\mathrm{i}\omega t}$, the equation of motion becomes

$$\frac{\mathrm{d}^2\phi}{\mathrm{d}t^2} + \frac{m}{m^*}\hbar v_\mathrm{F}^2 \frac{\mathrm{d}^2\phi}{\mathrm{d}x^2} = \frac{2k_\mathrm{F}eE(\omega)}{m^*}, \tag{2.16}$$

and the frequency-dependent conductivity

$$\sigma(\omega) = \frac{j(\omega)}{E(\omega)} = \frac{m}{m^*}\frac{\mathrm{i}\omega_\mathrm{p}^2}{4\pi(\omega + \mathrm{i}\delta)}, \tag{2.17}$$

where $\omega_\mathrm{p}^2 = 8v_\mathrm{F}e^2$ is the plasma frequency. The real part of the conductivity

$$\mathrm{Re}\,\sigma(\omega) = \frac{m}{4m^*}\omega_\mathrm{p}^2\delta(\omega) \tag{2.18}$$

has a Dirac delta singularity at $\omega = 0$, with an oscillator strength $f = \pi ne^2/m^*$. This oscillator strength is removed from the single-particle excitations and the square-root singularity which should appear at $\omega = 2\Delta$ is replaced by a square root edge as shown in fig. 5.

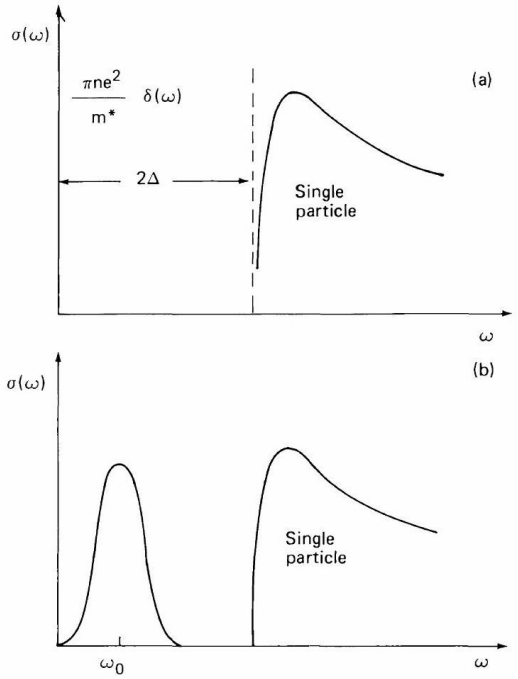


Fig. 5. Frequency dependent response of the collective mode (a) without pinning, and (b) with pinning and damping. The response at frequencies $\omega > 2\Delta/\hbar$ is due to single-particle excitations.

2.2. The mechanisms of pinning

Both the frequency and electric field dependent conduction observed in materials with incommensurate charge density wave ground state are the consequence of the interaction between the collective mode and the lattice irregularities. The interaction leads to a finite pinning energy, and this in turn shifts the oscillator strength to finite frequencies and also results in a finite dc threshold for nonlinear conduction. Pinning effects together with the fundamental $2k_\mathrm{F}$ periodicity of the problem are also responsible for the current oscillation phenomena.

Because the phason mode with the dispersion relation (2.8) is gapless, the collective mode can distort around potentials represented by $V(\boldsymbol{r})$, thus lowering the total energy of the collective mode. The Ginzburg-Landau Hamiltonian for a potential which couples directly to the phase of the CDW is

$$\mathscr{H} = \frac{n_c \hbar v_F}{4\pi} \int (\nabla\phi)^2 \, d\boldsymbol{r} + \int V(\boldsymbol{r}) \cos\left(2\boldsymbol{k}_F \cdot \boldsymbol{r} + \phi(\boldsymbol{r})\right) d\boldsymbol{r} \tag{2.19}$$

The first term on the right-hand side represents the elastic energy associated with the long-wavelength phase deformations; the second represents the interaction of the collective mode with the pinning potential. It is assumed that the amplitude of the collective mode is not perturbed by the interaction between the collective mode and the potential $V(\boldsymbol{r})$. Consequently, eq. (2.19) is expected to be appropriate for relatively weak potentials, which are substantially smaller than the bandgap Δ. The combined effect of elastic and potential energy terms in eq. (2.19) is a decrease of the total energy, also because the potential depends on the position $V(\boldsymbol{r})$, the interaction also leads to pinning of the collective mode. For small amplitude displacements the pinning energy is given by $E_{pin} = K\,(x - x_0)^{1/2}$, where K is the restoring force constant and $(x - x_0)$ is the rigid displacement of the mode from the equilibrium position x_0 which is established as a result of the potential $V(\boldsymbol{r})$. With pinning described in terms of a restoring force, it can be represented by an average pinning frequency $\omega_0^2 = K/m^*$ and also including a phenomenological damping term $(1/\tau)(d\phi/dt)$, the equation of motion becomes for small amplitude displacements

$$\frac{d^2\phi}{dt^2} + \frac{1}{\tau}\frac{d\phi}{dt} + \omega_0^2\phi = \frac{2k_F eE}{m^*} \tag{2.20}$$

The frequency dependent conductivity which corresponds to eq. (2.20) is given by

$$\sigma(\omega) = \frac{n_c e^2}{i\omega m^*} \frac{\omega^2}{\omega_0^2 - \omega^2 - i\omega/\tau} \tag{2.21}$$

and is that of an optical mode centered around the frequency ω_0. The dc conductivity, $\mathrm{Re}\,\sigma_{CDW}(\omega = 0) = 0$, and the zero frequency dielectric constant is given (including the contribution from quasiparticle excitations across the gap Δ) as

$$\epsilon(\omega = 0) = 1 + \frac{4\pi n_c e^2}{m^*\omega_0^2} + \frac{4\pi n_c^2 \hbar^2}{6m\Delta^2}. \tag{2.22}$$

The second term on the right-hand side describes the contribution of the collective mode, the third term represents the contribution of single-particle excitations. For weak pinning, where $\hbar\omega_0 \ll \Delta$, eq. (2.21) leads to the conductivity shown in fig. 5b, with the contribution of the pinned mode appearing well within the single-particle gap. This also leads to a giant dielectric constant at low frequencies and to zero crossing at $\omega = \omega_0$.

A dc electric field leads to the translational motion of the condensate, and consequently to a current carrying state when the energy provided by the dc field over one CDW period λ is larger than E_{pin} . The condition which follows from this argument

$$eE_T\lambda > \frac{1}{2}K\lambda^2 \tag{2.23a}$$

leads to a threshold field

$$E_T = \frac{1}{2}\lambda K/e. \tag{2.23b}$$

The ω and E dependent response of the pinned mode are strongly related. By taking $K = m^*\omega_0^2$, the relation between E_T and the characteristic pinning frequency ω_0 is

$$E_T = \frac{1}{2}\lambda m^*\omega_0^2/e, \tag{2.24}$$

and the dielectric constant is related to E_T through the relation

$$E_{\mathrm{T}}\epsilon(\omega \to 0) = 4\pi e n_{\perp}, \tag{2.25}$$

where $n_{\perp}$ is the number of chains per unit area. These arguments completely neglect the role played by the internal modes of the condensate in the dynamics. It is assumed that, after the long-wavelength deformations around the pinning potentials are established, the response to external dc and ac driving forces is accounted for by considering the time dependence of the average phase. The internal deformations, however, remain unchanged when going from the pinned to the current carrying state.

Since the restoring force drops out in eqs. (2.24) and (2.25), they are expected to be appropriate for any pinning mechanism. Impurities, grain boundaries, lattice defects and even the boundaries of the specimens may contribute to the overall restoring force. Because of early experimental evidence suggesting that impurities play an important role in pinning the collective mode, only impurity pinning has been considered in detail.

Recently it has become increasingly more evident however, that pinning by macroscopic defects and surfaces may also be important under certain circumstances.

The interaction between impurities and the CDW has fundamental consequences on both the static and dynamic properties. As first argued by Sham and Patton (1976), Imry and Ma (1975) and by Efetov and Larkin (1977), long-range order is destroyed by randomly positioned impurities, and, in less than four dimensions, the phase-phase correlation function has the form

$$\exp\{\mathrm{i}[\phi(\boldsymbol{r}) - \phi(0)]\} \approx \exp\left(-\boldsymbol{r}/L_0\right) \tag{2.26}$$

where the characteristic length scale L_0 depends on the strength of the impurity potential and on the elastic properties of the condensate. L_0 can be evaluated using scaling arguments (Fukuyama and Lee 1978). For a random impurity distribution, with impurity potential $V(\boldsymbol{r}) = V_0\delta(\boldsymbol{r})$, eq. (2.19) reads

$$\mathscr{H} = \frac{n_{\perp}\hbar v_{\mathrm{F}}}{4\pi}\int(\nabla\phi)^2\,\mathrm{d}\boldsymbol{r} + V_0\rho_1\sum_{\mathrm{i}}\cos\left(2\boldsymbol{k}_{\mathrm{F}}\cdot\boldsymbol{r}_{\mathrm{i}} + \phi\left(\boldsymbol{r}_{\mathrm{i}}\right)\right) \tag{2.27}$$

with i referring to random impurity sites. In eq. (2.27) it is assumed that spatial fluctuations of the phase $\phi(\boldsymbol{r})$ occur for wavelengths large compared to the amplitude coherence length $\xi_{\mathrm{a}} = \hbar v_{\mathrm{F}}/kT_{\mathrm{p}}$, of the order of 100Å for typical materials. Also, amplitude fluctuations of the collective mode, together with quantum and finite temperature effects, are neglected. The first term favors a spatially homogeneous phase, while the second term favors local distortions of the condensate where the phase is fully adjusted at every impurity site to obtain a maximum decrease of the potential energy. The ratio

$$\epsilon' = \frac{V_0\rho_1}{\pi\hbar v_{\mathrm{F}} n_i} \tag{2.28}$$

tells whether the potential energy on elastic distortions are more important, and $\epsilon' > 1$ is called strong, $\epsilon' < 1$ weak impurity pinning. For $\epsilon' \gg 1$ where the elastic energy can be totally neglected, the pinning energy is simply to total energy gain due to the electrostatic interaction with the impurities in $\epsilon = V_0\rho_1 n_{\mathrm{i}}$ and consequently the pinning energy

$$\epsilon_{\mathrm{pin}} = V_0\rho_1 n_{\mathrm{i}}\frac{\lambda^2}{2} \tag{2.29}$$

and the restoring force constant $K = V_0\rho_1 n_{\mathrm{i}}$. All the arguments advanced earlier apply, and eq. (2.23b) with eq. (2.29) leads to a threshold field proportional to the impurity concentration. The phase-phase correlation

length is expected to be of the order of the distance between impurities, as each impurity completely breaks the phase of the condensate.

The case of $\epsilon \ll 1$ (weak impurity pinning) is more interesting and scaling arguments can be used to evaluate the phase-phase correlation length. In d dimensions one can define a volume $(L_0)^d$ over which the phase varies less than π but is adjusted to impurity fluctuations to have a maximum decrease of the potential energy. This argument (Fukuyama 1978, Fukuyama and Lee 1978) leads to the potential energy density

$$\epsilon_{\rm pot} = -V_0\rho_1 \left(n_{\rm i}/L_0^d\right)^{1/2}. \tag{2.30}$$

The elastic energy of the domain, using eq. (2.27) is given by

$$\epsilon_{\rm elastic} = \frac{n_\perp \hbar v_{\rm F}}{4\pi} L_0^d \left(\frac{\pi}{L_0}\right)^2 d \tag{2.31}$$

where $n_\perp$ is the number of chains per unit area. Minimizing the total energy density of the domain with respect to L_0 leads to a finite phase-phase correlation length for any dimension $d < 4$. In three dimensions

$$L_0^{-1} = \left(\frac{V_0\rho_1}{\pi\hbar v_{\rm F}}\right) n_{\rm i} \tag{2.32}$$

and the pinning energy

$$\epsilon_{\rm pin} = -\frac{1}{4}\left(\frac{V_0\rho_i}{\pi\hbar v_{\rm F} n_{\rm i}}\right). \tag{2.33}$$

An anisotropic band structure also leads to an anisotropic phase-phase correlation length. As L_0 is proportional to $v_{\rm F}$, see eq. (2.32), the correlation length in the various directions scales with the anisotropy of the single-particle band. With typical single-particle band anisotropies of the order of 10, L_0 is expected to be approximately ten times larger along the chain direction than perpendicular to the chains. The anisotropy of L_0 can be included in expressions of $\epsilon_{\rm pin}$ and $E_{\rm T}$ by appropriate scaling. Such a procedure leads to additional numerical factors of the order of $(v_z v_y/v_x^2)$ where x refers to the chain direction. The concentration dependence of the parameter remains, however, unchanged. Arguments similar to those used before lead to $\omega_0, \epsilon(\omega \to 0)$ and to $E_{\rm T}$ with the following results

$$\omega_0 = 2\pi \left(\frac{m}{m^*}\right)^{1/2} v_{\rm F} L_0^{-1} \tag{2.34}$$

$$\epsilon(\omega \to 0) = 1 + \frac{n_\perp^4 \hbar^4 \pi^3 v_{\rm F}^2 n_c e^2}{m^* V_0^4 \rho_1^4 n_{\rm i}^2} \tag{2.35}$$

$$E_{\rm T} = \frac{\pi\hbar v_{\rm F}}{8e}\left(\frac{V_0\rho_1}{\pi\hbar v_{\rm F} n_\perp}\right)^4 n_{\rm i}^2 \tag{2.36}$$

In contrast to the strong pinning case, $E_{\rm T}$ is proportional to the square of the impurity concentration, while $\epsilon(\omega \to 0) \sim n_{\rm i}^{-2}$.

For a typical impurity potential of $V_0 = 10^{-2}$eV, with $v_{\rm F} = 3 \times 10^7$ cm/s, and a CDW amplitude $\rho_1 = 0.1$, an impurity concentration of 1000 ppm leads to $\epsilon' \sim 2$ suggesting that for relatively pure specimens strong impurity pinning is appropriate, while for alloys, with a substantial amount of impurities, the weak impurity pinning limit occurs. From eq. (2.32) the phase-phase correlation length $L_{0x} \sim 1$ mm in three dimensions, comparable with the length of the specimens investigated. With a typical bandwidth anisotropy of 10, the correlation length perpendicular to the chain direction is of the order of 0.1 mm , which is also comparable to the

dimensions of the typical specimens in this direction. This suggests that for pure specimens the phase is approximately constant over the volume, and also that pinning by sources other than impurities (such as the surface or contacts) may also contribute. The pinning energy, for strong impurity pinning is of the order of 10^{-2} K with the above parameters.

4.4.3 3. Electrical transport: frequency and electric field dependent conductivity

For band semiconductors the electrical conductivity is independent of frequency for $\omega < \Delta/\hbar$ and is also independent of electric field for applied fields $eEl < \Delta$ where l is the mean free path. For a typical gap of the order of 0.1 eV , nonlinear conduction occurs in the kV range, with frequency dependent conduction observed at optical (infrared) frequencies. In contrast, in the materials discussed before, in the CDW ground state σ is both strongly nonlinear and also frequency dependent. In fig. 6, the frequency dependent conductivity $\mathrm{Re}\,\sigma(\omega)$ measured along the chain direction, is displayed for several compounds. Only experimental results in the region of the single-particle gaps (shown by full lines) and in the DC to millimeter wave spectral range are displayed for clarity. The full lines are the results of optical experiments, and the strong decrease of the conductivity with decreasing frequency demonstrates the existence of the single-particle gaps. The gap values evaluated from the optical (Geserich et al. 1986), experiments compare, in general, favorably with the gaps evaluated from the dc conductivity below T_p. The strong resonances observed in the millimeter wave spectral range (Sridhar et al. 1986, Reagor et al. 1986, Ng et al. 1986) indicate a collective response associated with the charge density wave ground state, as it is evident that the frequency dependent response such as displayed in the figure cannot arise from a single-particle transport mechanism. The energy which corresponds to the frequency where $\mathrm{Re}\,\sigma(\omega)$ has a maximum is orders of magnitude smaller than the single-particle gap

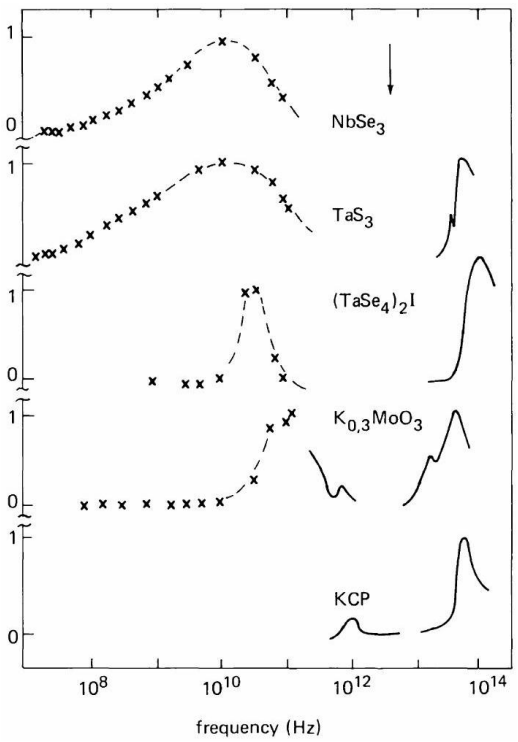


Fig. 6. The frequency dependent conductivity of $\mathrm{NbSe}\{3\}, \mathrm{o}-\mathrm{TaS}\{3\}$ and $(TaSe_4)_2 I$, and $K_{0.3}MoO_3$. The full lines represent the regions where the drop signals the single-particle gaps, the strong peaks in the millimeter wave spectral range are due to the response of the pinned collective mode.

and also the thermal energy kT. The oscillator strength which appears at finite frequency (in contrast to what is observed in a superconductor) suggests that the collective mode is pinned to the underlying lattice, and this is borne out by detailed investigations on specimens where the impurity concentration is varied. The peak frequency ω_0 can be associated with the pinning frequency ω_0 as discussed in section 3 . The finite width of the resonances observed may be due to damping effects associated with the dynamics of the collective mode, or alternatively can be the consequence of inhomogeneous broadening brought about by randomly positioned impurity pinning centers. Alternatively, a band of heavy carriers with a small gap would also lead to an overall behavior which is displayed in fig. 6.

The low frequency dielectric constant is enormous, in general of the order of 10^7 or more and this is the consequence of the large oscillator
strength at low frequencies. The zero frequency dielectric constant is given by

$$\epsilon(\omega) = \frac{4\pi n e^2}{m^*} \int_0^\infty \frac{\mathrm{Re}\,\sigma(\omega)}{\omega^2}\,\mathrm{d}\omega, \tag{3.1}$$

which for a narrow resonance reduces to $\epsilon \sim 1 + 4\pi n e^2/(m^*\omega_0^2)$.
The ω dependent response can be described in terms of eq. (2.21) and, in general, good fits to the harmonic oscillator response are obtained. An example is shown in fig. 7, where both $\mathrm{Re}\,\sigma(\omega)$ and $\mathrm{Im}\,\sigma(\omega)$ are contrasted with the expression which follows from a single degree of freedom description, shown by the full line in the figure. Fits as shown in fig. 7 lead to the fundamental values $\omega_0, 1/\tau$ and m^*/m, and in fig. 8, the effective mass values are plotted as a function of the single-particle gaps. The gap values are obtained from optical studies or from the temperature dependence of

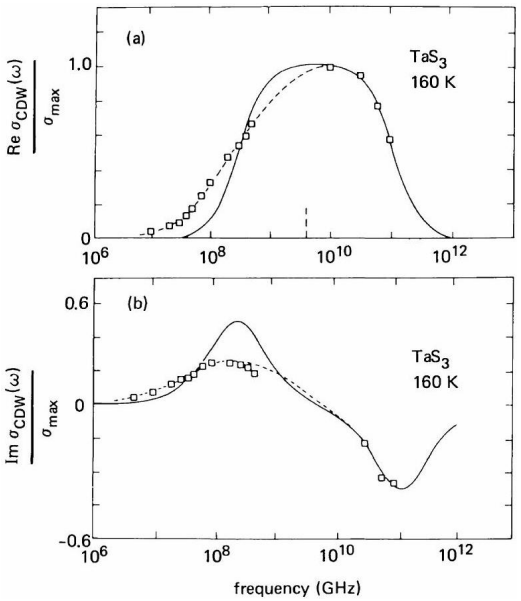


Fig. 7. Frequency dependent conductivity, $\operatorname{Re} \sigma(\omega)$ and $\operatorname{Im} \sigma(\omega)$ in TaS_3. The full line is a harmonic oscillator description. The dotted line takes a distribution of pinning frequenciees into account (Wu et al. 1986).

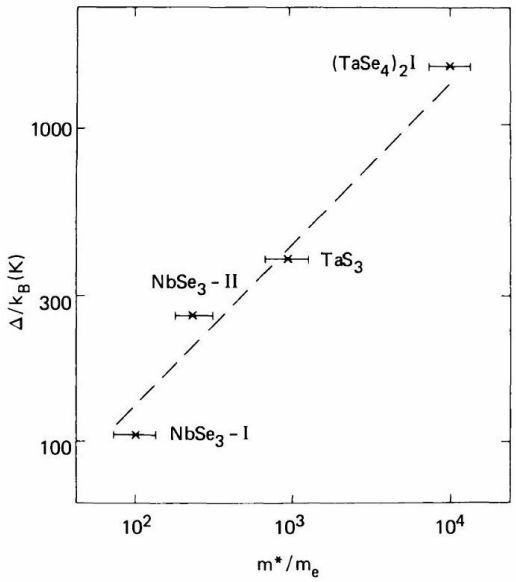


Fig. 8. Effective mass versus single-particle gaps in various compounds.

the DC resistivity below the Peierls transition; for $NbSe_3$ it is assumed that the BCS relation is appropriate, and $\Delta = 1.72 k_B T_p$ for both CDW phases. The full line is expression (2.4a) with $\lambda = 0.5$ and $\omega_{2k_F} = 100$ K, both reasonable values. However, if for the lower CDW in $NbSe_3$ one takes the value of the gap measured by tunneling spectra ($2\Delta/kT_p = 12$, Fournel et al. 1986) the agreement with expression (2.4a) is less convincing.

The temperature corresponding to the pinned mode is in the range of a few K , and this may allow the detection of CDW excitations by thermodynamical measurements. The heat capacity of $(TaSe_4)_2$ I measured down to 0.1 K has shown an excess heat capacity with a peak at $T = 1.75$ K (Biljakovic et al. 1986). If the CDW phase excitations were gapless, we have shown that a supplementary term proportional to T^3 is expected to occur at low temperature

(Boriack and Overhauser 1978). Figure 9 shows the residual heat capacity of $(TaSe_4)_2I$ after subtraction of the phonon contribution. The excess heat capacity has been analyzed with a modified Debye spectrum with two cut-off frequencies - the pinned mode frequency and a higher cut-off when the phason modes cannot be distinguished from the phonon modes. Excellent agreement has been found between the pinned mode frequency of $(TaSe_4)_2I$ which gives best fit in fig. 8 and the value measured by millimeter conductivity measurements (Reagor et al. 1985a) and the TA mode frequency measured by inelastic neutron scatter-

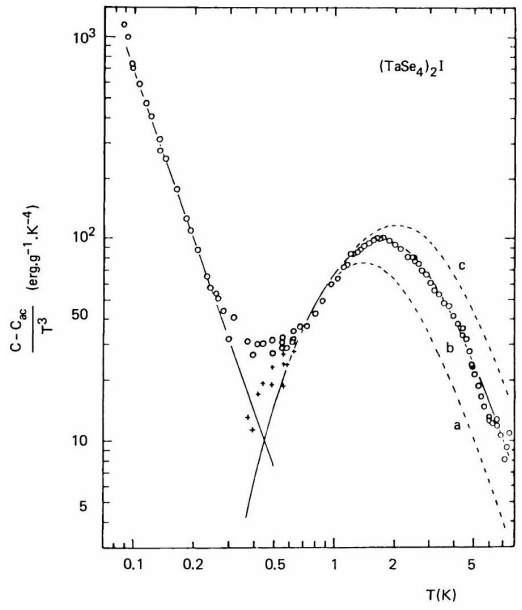


Fig. 9. Residual specific heat of $\left(\mathrm{TaSe}\right)_2 \mathrm{I}$ after subtraction of the phonon contribution divided by T^3. The anomaly around 2 K is assigned to the phason contribution with a pinning frequency of 45 GHz and a phason Debye temperature of 10 K in (a), 13 K in (b), 16 K in (c). The solid straight line at low temperatures corresponds to a $T^{-2.78}$ variation (Biljakovic et al.

ing at the CDW satellite position (Monceau et al. 1986a). Moreover, below $T = 0.4$ K the specific heat follows the $T^{0.2}$ law which is reminiscent of the results in amorphous materials. This extra contribution has been attributed to phonon-activated excitations between two CDW metastable energy levels. A similar excess in heat capacity has also been measured in $K_{0.3}MoO_3$ (Dahlhauser et al. 1986), and the effect of impurities on the temperature thermal properties has been examined by Brown et al. (1988).

It is evident from fig. 7 that the low-frequency response does not follow eq. (2.21) where the dynamics of a single degree of freedom is considered. Low-frequency measurements of the dielectric constant have been performed on TaS_3 (Zhilinskii et al. 1984, Wu et al. 1986, Cava et al. 1985),
on $(TaSe_4)_2I$ (Cava et al. 1986) and on $K_{0.3}MoO_3$ (Cava et al. 1984). In general the relaxation does not follow the simple exponential (Debye) law, empirical laws previously employed for other disordered systems such as:

$$\epsilon(\omega) = \epsilon_\infty + \frac{\epsilon_0 - \epsilon_\infty}{\left[1 + (\mathrm{i}\omega\tau_0)^{1-\alpha}\right]^\beta} \tag{3.2}$$

have been used to account for the low-frequency response. Here τ_0 is the average relaxation time.

For $\omega \gg 1/\tau_0$ eq. (3.2) can be written as

$$\epsilon \sim (\mathrm{i}\omega)^{\beta(1-\alpha)}, \tag{3.3}$$

i.e., a power law found experimentally in many CDW systems (Wu et al. 1986). Figure 10 shows such a power law $\sigma_{\mathrm{ac}}(\omega) \sim \omega^s$ for o- TaS_3 in the liquid helium temperature range with $s \sim 0.8$. τ_0 given by eq. (3.2) was found to be thermally activated with an activation energy in the range of the Peierls gap (Cava et al. 1984, 1985, 1986). This low frequency dielectric response has been claimed to be due to the coupling with longitudinal screened collective modes of the CDW (Littlewood 1987). For frequencies close to the pinning frequency the coupling is essentially to transverse CDW modes which are unscreened and consequently much less damped, as observed experimentally.

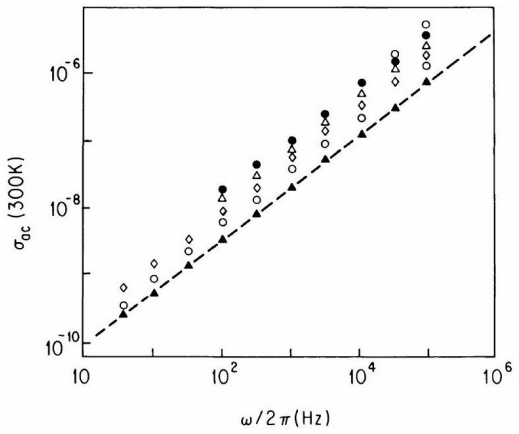


Fig. 10. Frequency dependence of $\sigma_{\mathrm{ac}} / \sigma_{300\ \mathrm{K}}$ of o $-$ TaS_3 at temperatures ($\triangle$) 4.22 K , (O) 6.15 K, (+)9.95 K, (Δ)14.0 K, (Δ)18.3 K, ($>$) 35.4 K . The dashed line represents the law $\sigma_{\mathrm{ac}} \sim \omega^{\mathrm{s}}$ with $s = 0.77$ (from Zhilinskii et al. 1984).

The small pinning energy associated with the collective mode suggests that for small DC electric field, the collective mode can be driven into a current carrying state with possibly nonlinear current-voltage characteristics. Indeed, nonlinear conductivity has been observed in all the materials discussed before, with a sharp onset field, called the threshold E_{T} for the nonlinear conductivity. The detailed form of the nonlinear conduction varies depending on external factors such as temperature, impurity concentration, or macroscopic inhomogeneities (such as grain boundaries) in the specimen.

The DC conductivity, defined as j/E where j is the total current density and E is the applied electric field is shown in orthorhombic TaS_3 in fig. 11. Below a threshold field E_{T}, approximately 300mV/cm the conductivity obeys Ohm's law, and the temperature dependence of this component reflects the exponential freezing out of the electrons excited across the single-particle gap. The onset of nonlinear conduction is smooth as evidenced by the current-voltage characteristics also displayed in the figure. A behavior, similar to that displayed in fig. 11, is found in general for the other compounds, and the existence of the sharp threshold field E_{T} is well established. The behavior in the figure can be described in terms of a two fluid model involving electrons excited across the gap and electrons concerned in the collective mode. Such a division is expected to be valid, except perhaps in the vicinity of the Peierls transition. The total current can

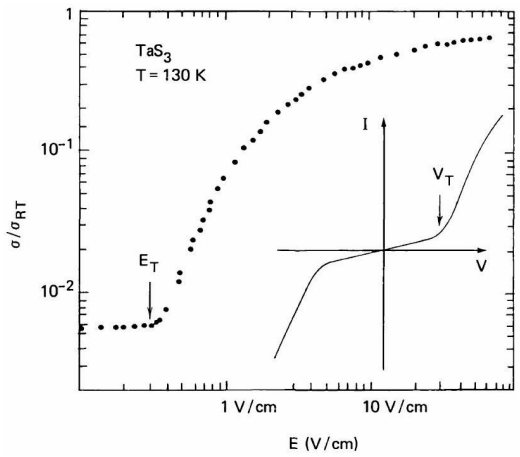


Fig. 11. Electric field dependent conductivity in $\mathrm{o}-\mathrm{TaS}_{3}$. The data are normalized to the room temperature conductivity. The inset shows typical DC $I-V$ characteristics on the same material.

be written as

$$I_{\text{total}} = I_{\text{n}} + I_{\text{CDW}}, \tag{3.4}$$

where the subscripts n and CDW refer to current carried by the uncondensed and condensed electrons. The validity of such a two-fluid description has been clearly demonstrated recently by generating nonlinear current-voltage characteristics in an open circuit configuration ($I_{\text{total}} = 0$) where the voltage was generated through the thermoelectric effect (Beyermann et al. 1986). The current-voltage characteristic is also often explored by measuring the differential resistance $\mathrm{d}V/\mathrm{d}I$, employing lowfrequency lock-in techniques. While the method cannot be used at high fields because of heating effects, it is advantageous to study the behavior near threshold.

The frequency and field dependent response is strongly related, and a smaller pinning frequency, and consequently larger dielectric constant, leads to a smaller threshold field. In general, a larger low-frequency dielectric constant and smaller characteristic pinning frequency are associated with a smaller threshold electric field, suggesting that both are related to an overall energy which characterizes the pinning of the collective mode.

At high temperatures, the conductivities of various materials, when extrapolated to the infinite electric field limit, or measured at frequencies $\omega_{\max}$ where $\mathrm{Re}\,\sigma(\omega)$ is maximum, are finite, and are close to the conductivities which would be observed in the absence of the phase transitions. In terms of a relaxation time τ, the conductivity at high fields or frequencies is written as

$$\sigma_{\text{CDW}}\,(E \to \infty, \quad \text{or} \quad \omega = \omega_{\max}) = ne^2\tau/m^*. \tag{3.5}$$

This is approximately observed in $NbSe_3$ (Ong and Monceau 1977), in o- TaS_3 (Sridhar et al. 1986) in $(TaSe_4)_2\,I$ (Reagor et al. 1986) and in $K_{0.3}MoO_3$ (Reagor and Mozurkewich 1985) at temperatures where the CDWs are incommensurate with the lattice. The high-field conductivity is weakly depressed by small amounts of impurities in $NbSe_3$ (Oda and Ido (1985) in o- TaS_3 the high-frequency conductivity is also fairly insensitive to impurity effects (Sridhar et al. 1986). Both suggest that even for a 'perfect' crystal, without impurities sliding charge density waves would lead to a finite conductivity. Moreover the variation as a function of temperature of the linear and the nonlinear portion of the current in $(TaSe_4)_2\,I$, (TaS_3), $K_{0.3}MoO_3$ show an activated behavior with approximately the same activation energy as the Peierls gap (Fleming et al. 1986). Again as for the dielectric measurements, these results indicate that at low temperatures the

CDW is strongly damped. Such an increase of the damping frequency has been predicted by Sneddon (1985) by taking into account the electrostatic screening and Coulomb interactions.

The onset of nonlinear conduction is often rather dramatic and is accompanied by switching and hysteresis effects. These have been observed in $NbSe_3$ (Zettl and Grüner 1982, Saint-Lager 1983), TaS_3 (Mihaly and Grüner 1984), and $K_{0.3}MoO_3$ (Maeda et al. 1986), such effects usually become more pronounced with decreasing temperature. An example is shown in fig. 12, where $I-V$ curves recorded in $NbSe_3$ at different temperatures are displayed. At higher temperatures the onset of nonlinear conduction is accompanied by an oscillatory instability, which by lowering the temperature gradually evolves into a hysteretic current-voltage characteristic. The behavior is due to extended pinning centers in the materials, and this has been demonstrated directly by locating (by using moving contacts) the exact positions where such behavior is generated (Brown and Mihaly 1985, Hall et al. 1986). In the range of liquid helium temperature, still a different type of nonlinearity, has been observed with a sharp step current-voltage characteristic. In $K_{0.3}MoO_3$ (Tessema et al. 1985, Mihaly and Beauchêne 1987) and other materials zero differential resistance has been measured at a threshold field which is one or two orders of magnitude

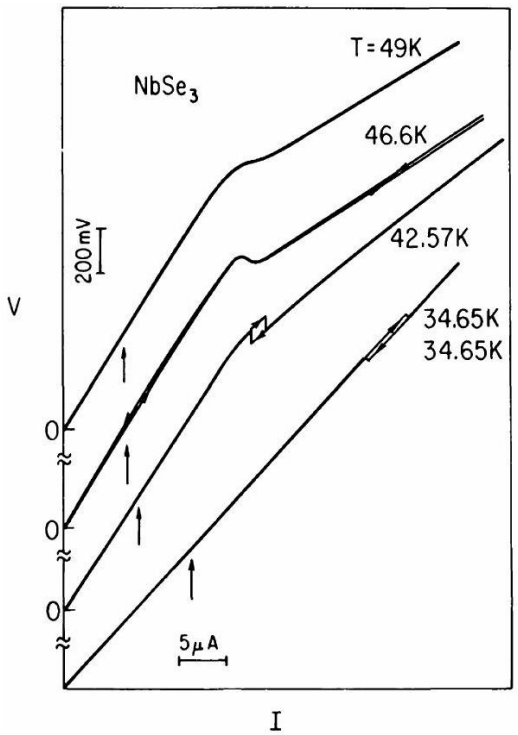


Fig. 12. Current-voltage characteristics of NbSe_{3} at several temperatures showing the switching effect. Arrows indicate the value at which the differential resistance $\mathrm{d}V/\mathrm{d}I$ starts slightly to decrease (Saint-Lager 1983).

larger than E_{T} where the smooth nonlinear conduction occurs. It appears that in this limited temperature range the CDW can move without damping. The coexistence between a strongly damped regime and a free sliding regime as shown in fig. 13 at higher temperatures is, however, unexplained. The overall behavior of the current-voltage characteristics, shown in fig. 13 and also the threshold field is similar to those observed in ordinary semiconductors where the effect is due to hot electrons. Consequently, the behavior may in principle be of single-particle origin, and not related to the onset of charge density wave transport. However, strong polarization effects (Chen et al. 1988) certainly due to deformations of the CDW are observed below $V_{\mathbf{T}}$ and this would suggest that the nonlinear conduction and charge density

wave dynamics are intimately related. A zero differential resistance has also been measured in extremely pure $NbSe_3$ (resistance ratio between room temperature and helium temperature larger than 250) at $T = 1.1$ K under a field of 22 T (Coleman et al. 1986). High magnetic fields allow one to study CDW dynamics of $NbSe_3$ which remains metallic down to the

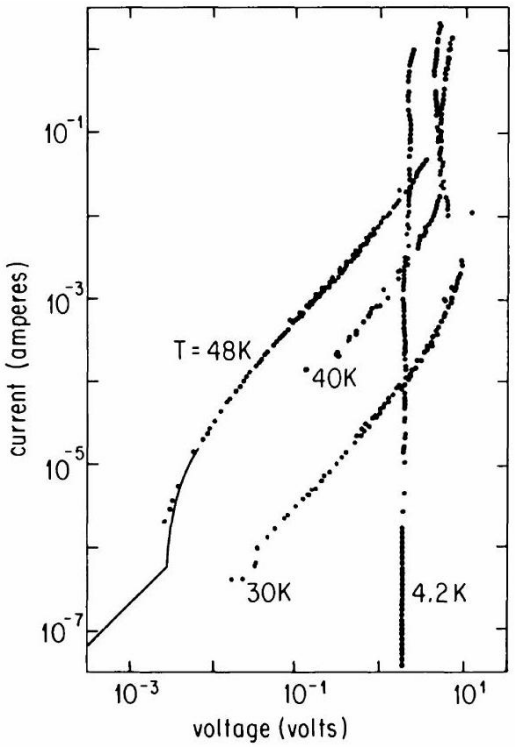


Fig. 13. Current-voltage characteristics $I(V)$ measured in $\mathrm{K}\{0.3\}\mathrm{MoO}\{3\}$ at low temperatures. Above a few volts zero differential resistance is observable at 4.2 K and also at 40 K and 48 K (Mihaly and Beauchêne 1987).

lowest temperatures by the increase of the normal electron resistance and the lowering of the threshold field (Coleman et al. 1985, Monceau and Richard 1988).

The fact that the charge density wave is not destroyed, but contributes to the DC current for $E > E_{\mathbf{T}}$, in experiments such as displayed in figs. 10-12 has been demonstrated by performing X-ray experiments in the nonlinear conduction region (Fleming et al. 1978, 1984, Mihaly et al. 1987b). In these experiments superlattice reflections were found in the current carrying regime with intensities equal to those measured without an applied field. The observation demonstrates that the charge density wave executes a translational motion in the presence of an applied electric field. This has later been confirmed by a series of NMR experiments to be discussed later. X-ray scattering experiments, while showing that the CDW motion does not induce any change in the longitudinal line width, were unable to reveal any structure due to metastable states. However extremely small modifications of the Fermi surface can be detected by the study of quantum Shubnikovde Haas oscillations in the magnetoresistance of $NbSe_3$. For this compound the CDW gaps do not occur on the whole Fermi surface and a small electron pocket, with approximately 10^{18} carriers /cm^3, remains, as is deduced from measurements of the period of the magnetoresistance oscillations for different orientations of the magnetic field. The magnetoresistance of $NbSe_3$ in the virgin state (α) (after cooling in zero field) and after a depinning and a repinning of the CDW (curves β) are shown in fig. 14 for both orientations of H (Richard et al. 1987). In state α with H parallel to (b, c) the period of oscillations may vary from sample to sample between (). 30 to 0.35 MG , but after the depinning-repinning process

the period is always equal to 0.28 MG . Therefore it can be concluded that, when the sample is cooled from room temperature, the CDW is locally distorted at strong pinning centers or at the electrodes and that these distortions are relaxed after the CDW has been depinned. These local distortions at the Fermi surface are very small: a decrease of 10% in the electron pocket (10^{17} electrons /cm^3) would induce a relative increase of the longitudinal CDW wavevector of 10^{-4} (there are 10^{21} electrons /cm^3 in the band affected by the CDW).

Other types of experiments also suggest that the CDW is, by the application of electric fields, driven out of the pinned configuration, and furthermore they suggest that the dynamics of the internal deformation of the mode is important. Here, the relaxation back to a pinned state is monitored through the measurement of the normal (ohmic) resistance. Making the natural assumption that local changes of the CDW phase around pinning centers also lead to the changes in the resistance $R_{\rm n}$ of the normal electrons which are excited across the gap, the time evolution of this quantity can be used as a measure of the above relaxation process. In

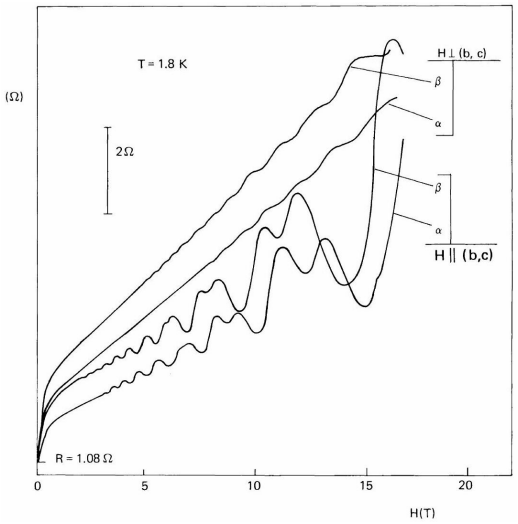


Fig. 14. Variation of the magnetoresistance of NbSe_{3} at $T = 1.8$ K with H parallel and perpendicular to the (b, c) plans. Curves α correspond to the virgin state when the sample has been cooled from room temperature. Curves β are recorded after the CDW has been depinned and repinned (Richard et al. 1987).

general a slow, logarithmic time decay

$$R_{\rm n}(t) - R_{\rm n0} = A_0 \log\left(t/t_0\right), \tag{3.6}$$

or alternatively a stretched exponential behavior

$$R_{\rm n}(t) - R_{\rm n0} = A \exp(t/\tau)^{\alpha}, \tag{3.7}$$

with $\alpha < 1$ is observed. Measurements of the relaxation of these metastable states on a large time scale has been extensively studied. Kriza and Mihaly (1986) have reported a decay of the polarization in $K_{0.3}MoO_3$ in terms of a stretched-exponential relaxation

$$P(t) = P_0 \exp[-(t/\tau)]^{1-n} \tag{3.8}$$

over six decades. Following the description of Ngai (1979) for glassy materials, such a nonexponential decay indicates the coupling of the relaxing modes to low-energy excitations. This approach has been questioned by Littlewood and Rammal (1987) who, using eq. (3.2) for the dielectric constant, have shown that the experimental data can also be fit with power laws

and that the processes involving thermally activated hopping between metastable states should therefore only appear on much longer time scales. These observations are qualitatively similar to those made on spin glasses after an applied magnetic field. This similarity is not accidental, and suggests the absence of long-range order (and consequently a broadly defined 'glassy' behavior) for a CDW which is pinned by randomly positioned impurities. More complicated phenomena, such as remanent dielectric polarization are related to the above observations. The long-time effects associated with these relaxation phenomena may also play a role in the details of the depinning process, and therefore also in determining current-voltage characteristics in the nonlinear conductivity region.

The parameters which characterize the frequency and field dependent conductivity vary from material to material, and they also display a characteristic temperature dependence. While in the majority of cases pinning by impurities plays the most important role (except in rather pure specimens with small dimensions where boundary effects may be important), the threshold electric field E_{T} is smaller, and the low-frequency dielectric constant ϵ is larger in materials with smaller Peierls transition temperature. In fig. 15 these two parameters are displayed for various materials as a function of temperature. The decrease of ϵ and increase of E_{T} near T_{P} is most probably related to the strongly temperature dependent condensate density, but the low-temperature behavior of these parameters is still not completely understood. Maki (1986a) has shown that the incorporation of the thermal fluctuations of the CDW phase yields a variation of E_{T} with an $\exp(-T_0/T)$ law where T_0 is proportional to the maximum amplitude of the pinning potential. This is in qualitative agreement with the results of fig. 15.

The importance of impurity pinning is confirmed by a broad range of studies where the electric field and frequency dependent response is investigated in alloys or on specimens where impurities are created by irradiation. Early experiments (Ong et al. 1979, Brill et al. 1981) on $NbSe_3$ alloys suggested that E_{T} is proportional to n_{i}^2, in agreement with weak impurity pinning.

Experiments performed on alloys in a broad concentration range (Monceau 1982, Underweiser et al. 1987) however, indicate that the situation is more complicated than that suggested by the scaling approach of Fukuyama and Lee (1978). In fig. 16, E_{T} measured below the second phase transition is displayed as a function of the reciprocal Residual Resistivity Ratio $(\mathrm{RRR})^{-1}$. The latter is proportional to the total strength of the impurity

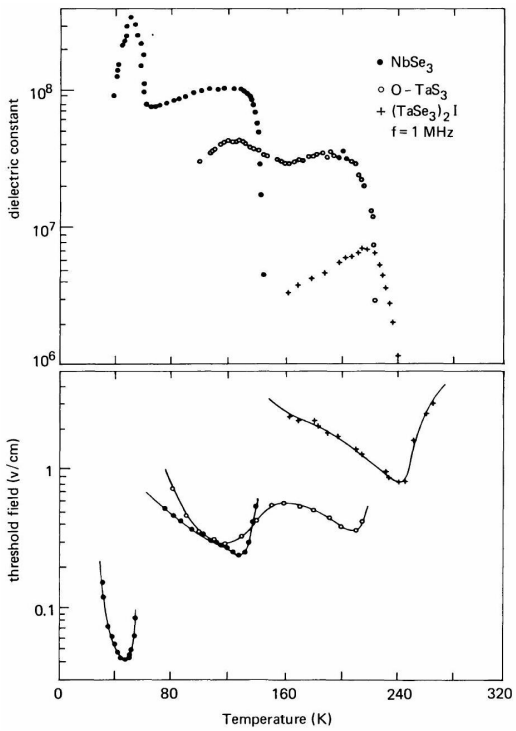


Fig. 15. Temperature dependence of the threshold electric field $E_{\mathbf{T}}$ and low-frequency dielectric constant (ϵ measured at $f = 1$MHz) in various materials. The full lines are guides to the eye.

scattering and can consequently be regarded as a scaled impurity concentration n_{i}. While E_{T} strongly increases with increasing n_{i}, the functional dependence is somewhat stronger than linear, but weaker than n_{i}^2. The behavior is not understood at present. It may be the consequence of a crossover between strong impurity pinning for small, and weak impurity pinning for large concentration of impurities. Alternatively, finite size effects may play an important role for small impurity concentrations where

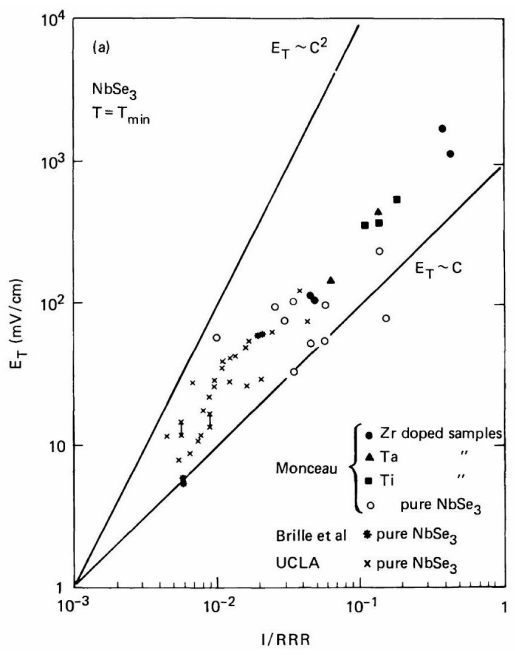


Fig. 16. Threshold electric field versus residual resistivity ratio in pure NbSe_{3} and in alloys. The straight line represents the linear and the quadratic concentration dependence of E_{T}, $E_{\mathrm{T}} \sim n_i^m$ (Monceau 1982, M. Maki 1986).

the phase-phase correlation length becomes comparable to the dimension of the specimens. The large scatter of the data for relatively pure specimens also indicates that pinning centers other than impurities may become important. In contrast, in the upper CDW state of $NbSe_3$, E_{T} was found to be a linear function of n_{i} suggesting that the strong impurity limit is appropriate even for small impurity potentials such as represented by the Ta atoms. In materials where defects are introduced by irradiation ($NbSe_3$: Fuller et al. 1981, TaS_3 : Mihaly et al. 1984a, $K_{0.3}MoO_3$: Mutka et al. 1984), E_{T} is proportional to the defect concentration suggesting strong impurity pinning. Such behavior, observed in electron irradiated $Rb_{0.3}MoO_3$ and $K_{0.3}MoO_3$ (Mutka et al. 1984) is displayed in fig. 17, the full line corresponding to $E_{\mathrm{T}} \sim n_{\mathrm{i}}.E_{\mathrm{T}}$ also increases with alloying for TaS_3, and this

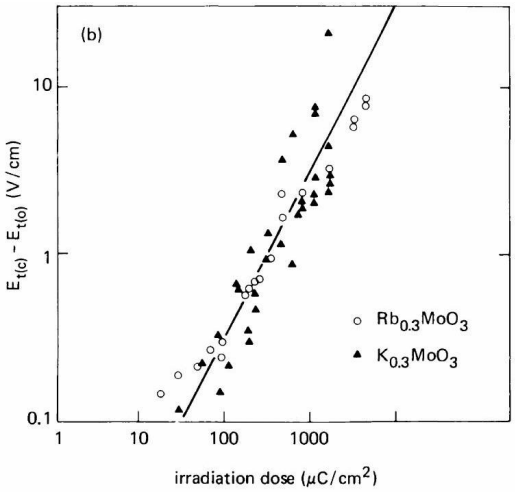


Fig. 17. Threshold electric field versus irradiation dose in $\mathrm{K}_{0.3}\mathrm{MoO}_{3}$, and $Rb_{0.3}MoO_3$ (from Mutka et al. 1984).

increase is proportional to the square of ΔT_{P}, the change of the Peierls transition temperature with alloying (Hsieh et al. 1983). As ΔT_{p} is proportional to $n_i^{1/2}$ (Mihaly et al. 1984b), E_{T} increases linearly with the impurity concentration. In $Rb_{0.3}MoO_3$ doping increases E_{T}, roughly proportional to the square of the dopant concentration, suggesting that in this material doping the Rb chain may lead to weak impurity pinning effects (Schneemeyer et al. 1985). The strongly concentration dependent threshold field is accompanied by corresponding changes in the frequency dependent response. The pinning frequency has been measured directly by investigating the ω dependent response both in TaS_3 (Sridhar et al. 1986) and in $(TaSe_4)_2\,I$, but in the absence of the precise impurity concentrations, the functional dependence of ω_0 on n_i could not be evaluated. The relation between $\epsilon(\omega \to 0)$ and E_{T} has, however, been investigated by measuring both parameters on the same specimens of alloys $Ta_{1-x}Nb_x\,S_3$ (Wu et al. 1984). The results are shown in fig. 18. The full line gives

$$\epsilon(\omega \to 0)E_{\mathrm{T}} = 0.75 e n_{\perp}, \tag{3.9}$$

which is within order of magnitude agreement with eq. (2.25). Although the frequency dependent response has not been investigated in detail, the relation $E_T \sim \omega_0^2$ was also confirmed by frequency dependent studies performed at microwave frequencies in irradiated o-TaS_3 (Mihaly et al. 1984a).

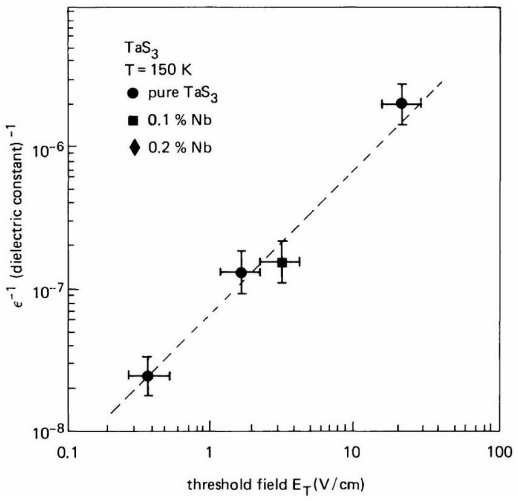


Fig. 18. Inverse low frequency dielectric constant $\epsilon(4\ \mathrm{MHz})$ versus threshold field E_{T} in o- TaS_3 alloys (Wu et al. 1984).

Random impurity pinning also leads to finite phase-phase correlation lengths which, in view of the band anisotropy, are different in different crystallographic orientations.

The static phase-phase coherence length L_0 is related to the overall pinning energy and eq. (2.34), which is expected to be model independent, relates L_0 to the pinning frequency ω_0. With the parameters used before, $m^*/m \approx 10^3$ and $v_{\mathrm{F}} = 3 \times 10^7$ cm/s, a characteristic pinning frequency (derived from the frequency dependent response, see fig. 9) of approximately 10^{10} s^{-1}, leads to L_0 in the order of 10μ m. Equation (2.34) refers to the correlation length along the chain direction L_{0x}, while because of the anisotropic Fermi surface, the correlation lengths in the perpendicular directions L_{0y} and L_{0z} are one to two orders of magnitude less than the above estimate.

The finite static correlation length leads to a broadening of the superlattice reflections, and thus could in principle by determined by scattering experiments. Due to the limited resolution of scattering experiments, such studies give only a lower bound on the range of phase correlations

both parallel to the chains and in the perpendicular directions. Both in $NbSe_3$ and in $K_{0.3}MoO_3$, the diffraction peaks are resolution limited (Fleming

1982, Fleming and Schneemeyer 1984). This sets a lower bound of $L_{0x} > 0.4\mu$ m in $NbSe_3$ and > 0.7 in $K_{0.3}MoO_3$ the phase coherence perpendicular to the chains extends over a distance of approximately 0.2μ m.

For relatively pure specimens where the overall impurity potential $\sum_i V_i$ is weak, other defects such as dislocations and grain boundaries may also play an important role, while in small specimens, the surface of the specimens or the contacts may act as pinning centers. The latter has been investigated in several materials by measuring the threshold field as the function of the dimension of the specimens.

The total pinning energy in the case of boundary effects may come from pinning centers in the bulk, from the surface and also from the pinning by the contacts placed (ideally) at the end of the specimens. These have different dependence on the sample dimensions, and in general, in terms of restoring forces which act on the collective mode, can be written as

$$K = K_{\text{bulk}} + K_{\text{surface}} + K_{\text{contact}} = t_1 AL + t_2 SL + t_3 A \tag{3.10}$$

where A, L and S refer to the cross section, length and surface (per unit length) of the specimen. The constants t_1, t_2 and t_3 refer to the pinning strengths for unit dimensions. The threshold electric field is given in the presence of the various contribution to pinning by

$$E_{\text{T}} = \frac{V_{\text{T}}}{L} = \frac{\lambda K}{2eA} = \frac{\lambda}{2e}\left(t_1 + t_2\frac{S}{A} + \frac{t_3}{L}\right). \tag{3.11}$$

In the thermodynamic limit with boundary effects neglected, E_{T} is independent of the dimensions of the specimen. For surface pinning it increases with decreasing cross section (for a square cross section $E_{\text{T}} \sim A^{-1/2}$) and for contact pinning it increases with decreasing length. The relative importance of these effects is determined by the constants t_1, t_2 and t_3.

Various experiments indicate that pinning by the contacts is important for short specimens. The threshold field E_{T} has been investigated as the function of length L of the specimens in $NbSe_3$ (Zettl and Grüner 1984, Gill 1985, Prester 1985, Monceau et al. 1986b) and in TaS_3 (Mihaly et al. 1983) and it was shown that there was a large increase of E_{T} when L was reduced (below 1 mm). Figure 19 shows the differential resistance of $NbSe_3$ with electrodes 8μ m wide separated by a distance indicated in the figure. The critical current for the onset of the nonlinearity is clearly increased when L is reduced.

Another way for explaining these results is to analyse (Gill 1986a, Monceau et al. 1986b, Nad' 1985) the influence of L on the onset of the depinning on short samples as the voltage necessary for creating or maintaining phase slip centers at the electrodes. The essential role of boundary conditions in CDW motion has been first recognized independently by Ong

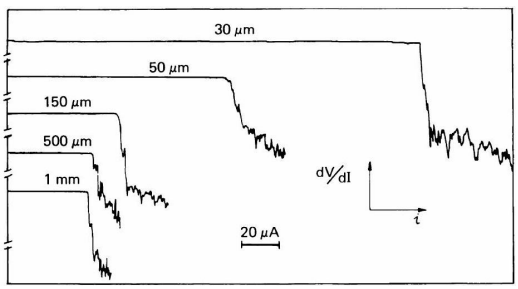


Fig. 19. Variation of the differential resistance $\mathrm{d} V / \mathrm{d} I$ of a $NbSe_3$ sample at $T = 50$ K as a function of the current with voltage electrodes of 8μ m wide separated by the indicated distance L. The threshold current is strongly increasing when L is reduced.

and Maki (1986b) and by Gorkov (1983). When a current lead brings electrons at the electrodes they have to be injected as excitations. The conversion of these electronic excitations into the collective mode can only occur at places where the gap $\Delta = 0$ through topological defects as phase slip centers or phase vortices. For a given length, the threshold voltage can be written as

$$V_{\mathrm{T}}(L) = E_{\mathrm{T}}L + V_0, \tag{3.12}$$

where the first term is the bulk pinning provided by impurities which is independent of L at least down to distances of $\sim 10\mu$ m and V_0, the extra potential for the conversion of normal electrons-CDW condensate at the electrodes. For the lower CDW in $NbSe_3(T < 59$ K$)V_0$ is found temperature dependent but typically of around 0.2 mV (Saint-Lager 1983, Monceau et al. 1986b). If this voltage is thought as due to bulk pining it would correspond to a length of around 100μ m. This voltage is too small for the creation of a normal hard core of a vortex but appropriate for an enlargement of a vortex ring acting as a Franck-Read source (Lee and Rice 1979). At higher temperatures for the upper CDW in $NbSe_3$ (Gill 1986a,b) or for o-TaS above 150 K there is no need of a critical strain for the initiation of the phase slippage (at least if the contacts are not disturbing too much the equipotentials near the interfaces) but in the nonlinear state for a given CDW current it remains a finite voltage for maintaining phase slip. This voltage has been found to be thermally activated similarly to phase slippage in small superconducting wires (Tinkham 1975).

Careful experiments have been reported recently also on specimens with small cross section (Borodin et al. 1986, Gill 1986a,b). In both o-TaS $_3$ and in $NbSe_3$, the threshold field scales with the cross section A of the specimens as $E_{\mathrm{T}} \sim A^{-1/2}$, a clear indication for the importance of surface pinning in specimens where the cross section is smaller than approximately 100μ m^2. A simple estimate suggests that the pinning potential due to surface is approximately the same as an impurity potential, the above critical cross section is not unreasonable. For a specimen of square cross section with $A = 100\mu$ m^2, the ratio of the surface to bulk atomic sites is approximately 10^2. If $t_1 \cong t_2$ then an impurity concentration of 1% leads to an equal contribution to the pinning for impurities and for the surface. Careful experiments on specimens with different impurity concentrations are required to test the above observations. It is clear, however, that for sample dimensions of $A \cong 100\mu$ m^2 and $l \cong 100\mu$ m pinning by surfaces plays an important role.

4.4.4 4. Electrical transport: spectral features

Perhaps the most spectacular observation in the field is the detection of current oscillations in the nonlinear conductivity region. The phenomenon, which has been studied both in the time and in the frequency domain, is often referred to as 'narrow band noise'. The term 'noise', however, is misleading. Consequently, we refer to the phenomenon as current oscillations.

Depending on the experimental arrangement either an oscillating current or an oscillating voltage is detected, the former for a constant voltage, the latter for a constant current drive. Due to the presence of normal electrons which lead to a normal component to the total current, and thus contribute to the voltage drop across the specimen, the usual experimental configuration represents an intermediate situation. To first approximation, the current oscillation amplitude Δj_1 and the oscillating voltage ΔV_1 are related by $\Delta J_1 = \Delta V_1/R$, where R is the measured resistance of the specimen at a frequency which corresponds to the frequency of the oscillations.

The first observation has been made by Fleming and Grimes (1979) on $NbSe_3$, where the time dependent voltage has been recorded by a spectrum analyzer. For electric fields below threshold only a structureless broad band noise was observed but for $E > E_{\mathrm{T}}$ sharp peaks, superimposed on a large amplitude broad band noise, are evident. The spectrum consists of a

fundamental frequency and of several harmonics with slowly decaying intensity. With increasing electric fields, the amplitude and also the frequencies increase. The quality of the spectra is strongly dependent of mounting, contact procedures and thermal cycling which can produce damage to the crystal, and fig. 20 shows a particularly good spectrum with a single frequency and 23 harmonics as measured by Thorne et al. (1987).

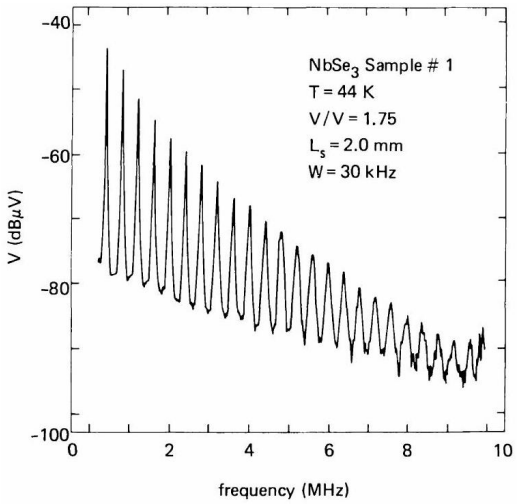


Fig. 20. Fourier transformed spectrum of the time dependent voltage measured in response to an applied current for NbSe_{3} (Thorne et al. 1987).

Current oscillations have subsequently been found by studies in real time domain, following a pulse applied to the specimens (Fleming 1983, Bardeen et al. 1982). Spectra, similar to those shown in fig. 20 have been also observed in all materials where nonlinear conduction occurs; in TaS_3 (Grüner et al. 1981a), in (TaSe4)2I (Wang et al. 1983a), in $(NbSe_4)_{3.33}$ I (Wang et al. 1983b) and $K_{0.3}MoO_3$ (Dumas et al. 1983), and consequently is a characteristic overall feature which accompanies the nonlinear conduction process.

The frequency of the oscillations is approximately proportional to the excess current carried by the CDW (Monceau et al. 1980), and furthermore, the ratio of the excess current to the frequency varies with temperature, approximately as the number of condensed electrons n_{CDW} (Bardeen et al. 1982). Figure 21 displays the linear relation between the current density carried by the CDW in motion and f_0 in a wide frequency range for a pure TaS_3 specimen (Monceau and Renard 1986c). Normalizing to CDW current for one chain, the above observations can be described as

$$\frac{j_{\mathrm{CDW}}}{f_0} = C \times e \times \frac{n_{\mathrm{c}}(T)}{n_{\mathrm{c}}(T=0)}, \tag{4.1}$$

where j_{CDW} refers to the current per chain. While the precise value of the

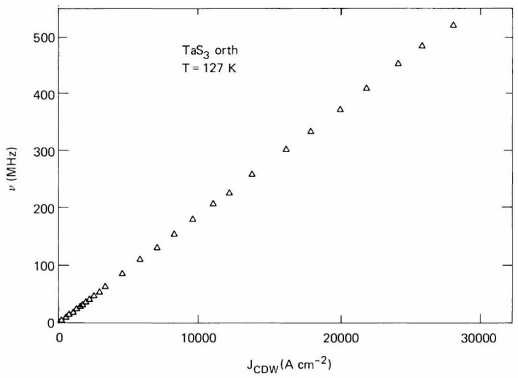


Fig. 21. Variation of the fundamental frequency measured in spectra as shown in fig. 20 as a function of the density of current carried by the charge density wave for a sample of $\mathrm{o}-\mathrm{TaS}_{3}$ at $T = 127$ K. The relation $J = nev$ is obeyed up to very high velocities (Monceau and Renard 1986).

constant in eq. (4.1) is still debated it is between 1 and 2 for a broad range of materials.

The above relation between the current and oscillation frequency is associated with the fundamental periodicity associated with the phase ϕ. The CDW current, described in terms of drift velocity v_{d} of the (rigidly moving) condensate is given by $j_{\mathrm{CDW}} = n_{\mathrm{c}} e v_{\mathrm{d}}$. Associating the fundamental frequency with a CDW displacement by one period, $f_0 = v_{\mathrm{d}}/\lambda$, this then leads to

$$j_{\mathrm{CDW}}/f_0 = n_{\mathrm{c}}(T) e \lambda, \tag{4.2}$$

with $\lambda = \pi/k_{\mathrm{F}}$ and $n_{\mathrm{c}} = 2k_{\mathrm{F}}/\pi$. Equation (4.1) with a constant $c = 2$ is then recovered. Alternatively, the fundamental frequency can be related to the energy difference ΔE between the two sides of the displaced Fermi surface shown in fig. 4. With

$$\Delta E \sim \frac{\partial E}{\partial v} v_{\mathrm{d}} = \frac{\partial E}{\partial k} \frac{\partial k}{\partial v} v_{\mathrm{d}} = 2 v_{\mathrm{F}} v_{\mathrm{d}} \tag{4.3}$$

$\Delta E = h f_0$ and $j_{\mathrm{CDW}} = n_{\mathrm{c}} e v_{\mathrm{d}}$ also leads to eq. (4.1) with $c = 2$ (Grüner et al. 1981b). The strictly linear relation between j_{CDW} and f_0 as displayed in fig.

21, also suggests that the CDW velocity is constant throughout the specimen. Indeed j_{CDW} is proportional to f_0 over a broad range of currents and frequencies only in high quality specimens. In materials where evidence suggests that disorder plays an important role, deviations from the linear relation between j_{CDW} and f_0 are observed (likely related to finite velocityvelocity correlation lengths).

The question whether current oscillations are generated in the bulk or at boundaries, and whether current contacts are important has been hotly debated and a variety of experiments have been designed to test the validity of both assumptions. While it is generally agreed that current oscillations are a finite size effect and do not occur in the thermodynamic limit, the issue of current generation has not yet been resolved. Experiments where the noise amplitude is measured as the function of dimensions of the specimens (Mozurkewich and Grüner 1983, Ong et al. 1984) led to contradictory results. Experiments involving nonperturbative contacts which also can be moved along the length of the specimens favor bulk noise generation (Brown and Mihaly 1985). Various experiments have also been performed in the presence of a temperature gradient, which leads to different temperatures T_1 and T_2 at the site of the current contacts, placed in general at the ends of the specimens. In case of oscillating current generation at the contacts, under certain circumstances a splitting of the oscillation frequencies is expected. While the first experiments (Zettl et al. 1984) did not show such splitting, in subsequent measurements (Verma and Ong 1986, Ong et al. 1984, Ong and Maki 1985) such splitting has indeed been

detected. It has, however later been shown, that a further increase of the temperature gradient leads to further splitting of the oscillation frequencies (Brown et al. 1985, Lyding et al. 1986). The multiple splittings suggest the formation of velocity coherent regions with a minimum length of the order of 100μ m. While these experiments do not answer the question on current generation, they raise the important question of topological defects in charge density waves and the possibility of phenomena associated with the dynamics of the amplitude of the order parameter (Ong et al. 1984, Gorkov 1983, Ong and Maki 1985).

In addition to the current oscillations, the nonlinear conduction is also accompanied by a substantial broad band noise, with an effective noise temperature of several thousand degrees (Richard et al. 1982a). The spectral dependence can be well described by an $f^{-\alpha}$ behavior (Bhattacharya et al. 1985, Maeda et al. 1986) and the amplitude of the noise voltage is inversely proportional to the square root volume, suggestive of fluctuations generated by independent pinning centers in the bulk (Richard et al. 1982a, Bhattacharya et al. 1985). It has also been suggested, on the basis of experiments on intentionally damaged specimens (Thorne et al. 1987), that broad band noise is either generated by macroscopic defects, or
it mainly reflects the distribution of various current oscillation components. The $1/f^{\alpha}$ spectrum then may represent the distribution of beat frequencies between various coherent regions separated by macroscopic defects. The phenomena have also been interpreted as due to a current noise, generated at various pinning centers (Wonneberger and Breymayer 1984).

The combination of AC and DC electric fields leads also to various interference effects (Monceau et al. 1980, Richard et al. 1982b, Zettl and Grüner 1984). This mode locking has been intensively studied in recent years (see the review by Brown and Zettl, in this volume and the review by Grüner 1989). The phenomenon is due to the interaction between two frequencies, one the intrinsic oscillation frequency f_0 (and its harmonics), the other the externally applied frequency f_{ext} . Mode locking occurs in general, whenever p and q are integers, and they show up for $pf_0 = qf_{\text{ext}}$ in the DC $I - V$ characteristics (Monceau et al. 1980, Zettl and Grüner 1984) and in the AC response (Zettl and Grüner 1984).

4.4.5 5. Other transport coefficients and elastic properties

While the low field DC conductivity provides clear evidence for the metal-to-semiconductor transition associated with the development of the CDW ground state, other transport coefficients, such as thermoelectric power (TEP) and Hall effect also reflect the removal of the Fermi surface by the transition. A small, and metallic-like TEP above T_{P} is usually followed by a strong rise below the transition. This is accompanied by similar changes in the Hall constant. At temperatures below T_{P} these parameters can, in general, be accounted for by formulas developed for ordinary band semiconductors, with a temperature dependent gap $\Delta(T)$ which has the BCS form and disappears at the transition. At low temperatures, where also the DC conductivity deviates from the exponential form, anomalies in the TEP and Hall effect can also be found. It is likely that these reflect the contribution of impurity states to the transport coefficients.

Expression (3.4) implies a two band model where the normal electrons and electrons in the CDW condensate provide separate and independent channels for the conduction process. While this description is suggestive of a collective transport carried by the CDW when electric fields exceed threshold, other transport measurements performed in the nonlinear conductivity region provide direct evidence that the current at high fields is carried by a ground state condensate.

Early measurements (Dee et al. 1979) of the thermoelectric power in $NbSe_3$ are in apparent conflict with the Fröhlich conduction mechanism. Detailed measurements on o-TaS_3 (Stokes et al. 1984) (and subsequently on other materials) indicate that in the current carrying state the thermoelec-

tric effects are fundamentally different from that of simple metals or semiconductors. Both the measurement and the analysis of TEP experiments, when extended to investigate nonlinear phenomena, require special care. First, conventional experiments use an open circuit, $J = 0$ configuration. In order to detect a contribution to the thermopower in the nonlinear regime a finite current has to be applied. Second, conventional discussions of thermoelectric effects consider only small thermal and electric gradients in cases of systems initially in thermal equilibrium. For a system initially in a nonequilibrium steady state (driven by an electric field E) at a uniform temperature T the electric and heat current densities δJ and δU are given by

$$\delta J(E) = \left.\frac{\mathrm{d}J}{\mathrm{d}E}\right|_{E=E_0} \delta E + \frac{L_{12}\left(E_0\right)}{T^2}\nabla T, \tag{5.1}$$

$$\delta U(E) = \left.\frac{\mathrm{d}U}{\mathrm{d}E}\right|_{E=E_0} \delta E + \frac{L_{22}\left(E_0\right)}{T^2}\nabla T, \tag{5.2}$$

where ∇T is the applied (small) temperature gradient, L_{12} and L_{22} are Onsager coefficients. The thermoelectric power, for constant current density, is given by

$$S\left(E_0\right) = \frac{-L_{12}}{T^2 \left.\frac{dJ}{\mathrm{d}E}\right|_{E=E_0}} \tag{5.3}$$

For a two fluid model of the normal electrons and the CDW condensate as suggested by eq. (3.4), the TEP is given by

$$S\left(E_0\right) = \left(S_{\mathrm{N}} \left.\frac{\mathrm{d}J}{\mathrm{d}E}\right|_{\mathrm{normal}} + S_{\mathrm{CDW}} \left.\frac{\mathrm{d}J}{\mathrm{d}E}\right|_{\mathrm{CDW}}\right) / \left(\left.\frac{\mathrm{d}J}{\mathrm{d}E}\right|_{\mathrm{normal}} + \left.\frac{\mathrm{d}J}{\mathrm{d}E}\right|_{\mathrm{CDW}}\right). \tag{5.4}$$

where the subscripts refer to the differential conductivities for the normal and condensed electrons. For the case $S_{\mathrm{CDW}} = 0$, the above equation reduces to

$$\frac{S\left(E_0\right)}{S_{\mathrm{N}}} = \frac{\sigma'_{\mathrm{N}}(E)}{\sigma'_{\mathrm{N}}(E) + \sigma'_{\mathrm{CDW}}(E)} \tag{5.5}$$

Here $\sigma' = \mathrm{d}J/\mathrm{d}E$ is the differential conductivity. Therefore, for $S_{\mathrm{CDW}} = 0$ the electric field dependence of the total measured thermopower S is expected to be the same as that of the inverse differential conductivity. In fig. 22 these parameters measured in o- TaS_3 are displayed as a function of electric field. Within experimental error eq. (5.5) is obeyed over a moderate range of applied fields confirming that (to within the experimental error) $S_{\mathrm{CDW}} = 0$.

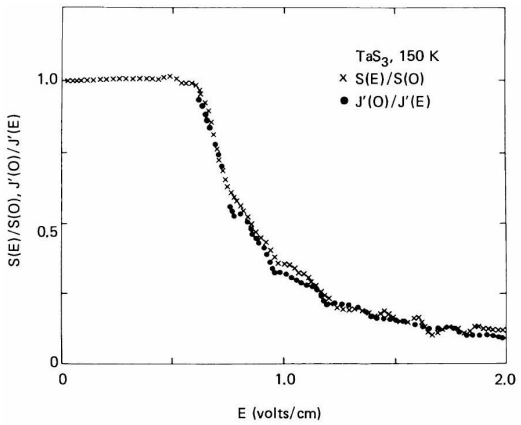


Fig. 22. Electric field dependence of the thermopower S and differential conductivity $I^{\prime}= \mathrm{d} I / \mathrm{d} V$ in o-TaS $_3$ (Stokes et al. 1984).

The Peltier heat is related to the thermoelectric power by

$$\Pi(E) = TS(E_0)\left[\sigma'(E_0)\,E_0\,(J(E_0))^{-1}\right], \tag{5.6}$$

and consequently $\Pi(E)$ associated with the nonlinear conduction is also close to zero. This analysis suggests that in contrast to single-particle transport where the Wiedeman-Franz law applies, no or very little entropy transport is associated with the nonlinear electric conduction. Slight deviations from eq. (5.5) observed at low temperatures can be accounted for by phonon-drag phenomena (Stokes et al. 1984). Similar conclusions are reached for $(TaSe_4)_2\,I$ and in the upper transition of $NbSe_3$ (Stokes, unpublished) while at the lower phase transition in $NbSe_3$ the anomalous behavior (Dee et al. 1979) suggests that phonon-drag effects may be dominant. Such effects were studied subsequently by Kriza et al. (1989) who extended the early experiments on TaS_3 at higher electric fields, and have found deviations from eq. (5.5) which became more important at lower temperatures both in TaS_3 and in $K_{0.3}MoO_3$. By extending the experiments to high electric fields by employing a pulse technique, it was established, that the condensate carries heat, together with the electric current. Furthermore, the heat carried was found to be proportional to the Joule heat generated by the moving condensate at high electric fields. The length scale which relates
the heat transport to heat generation is comparable to L_0 discussed in section 2, but the observation is unaccounted at the moment.

Within the framework of the two fluid model, the Hall voltage $V_{\mathbf{H}}$, for a magnetic field H perpendicular to the chain direction is given by

$$V_{\mathbf{H}} = \frac{\sigma_N \mu_{N\perp} + \sigma_{CDW}\mu_{CDW\perp}}{(\sigma_N + \sigma_{CDW})_\perp} HE \tag{5.7}$$

where E is the electric field applied along the chain direction. $\mu_{N\perp}$ and $\mu_{CDW\perp}$ are the contributions of the normal and CDW electrons, respectively, to the mobility perpendicular to the chain direction at electric field E, while $(\ \sigma_N + \sigma_{CDW})_\perp$ refers to the total perpendicular conductivity which corresponds to the Hall voltage. Measurements, performed in $NbSe_3$ (Kawabata et al. 1981, Tessema and Ong 1981) lead to a Hall voltage which is proportional to the electric field up to fields of $E \sim 2E_T$; for such electric field values $V_{\mathbf{H}}$ is smaller than the threshold field E_T. Consequently the current associated with the nonlinear conduction is extremely anisotropic, and is not influenced by the Lorentz force. This was subsequently confirmed in TaS_3 (Latyshev et al. 1983) for electric fields slightly exceeding E_T, but, for larger electric field, deviations from $V_H \sim E$ have been found in TaS_3 (Artemenko et al. 1984), in $K_{0.3}MoO_3$ (Forro et al. 1986) and in $(TaSe_4)_2\,I$ (Forro et al. 1987). These results have been explained by taking into account the deviation from equilibrium of the distribution function of quasiparticles drifting with the CDW under the influence of the applied electric fields (Artemenko et al. 1984). One should then subtract from the normal current in eq. (2.4) a quantity proportional to the charge density wave current. These experiments point out the breakdown of the oversimplified two fluid description as that had already been stressed by Rice et al. (1979) earlier on theoretical grounds.

The metal-to-semiconductor transition is associated with pronounced anomalies of the elastic properties. The Young's modulus has a large dip and the internal friction increases at T_P (Brill and Ong 1978, Brill 1982, Mozurkewich et al. 1985a,b). These anomalies, not unexpected for a structural phase transition, are related to specific heat anomalies within the framework of the Clausius-Clapeyron equation, which account for the changes in the elastic constant. Corresponding changes in the internal friction are unexplained at present.

Both the Young's modulus and the internal friction show large anomalies in the nonlinear conductivity region. This was first investigated in o- TaS_3 (Brill and Roark 1984, Brill et al. 1986), in $(TaSe_4)_2\,I$ and in $NbSe_3$ (Mozurkewich et al. 1985a,b). Experimental results for the

elecric field dependence of the elastic modulus $\Delta E'/E'$ and internal friction $\delta' \sim Q^{-1}$ (where Q is the quality factor of the elastic resonance) measured in TaS_3 are displayed in fig. 23. The onset of nonlinear conduction leads to a

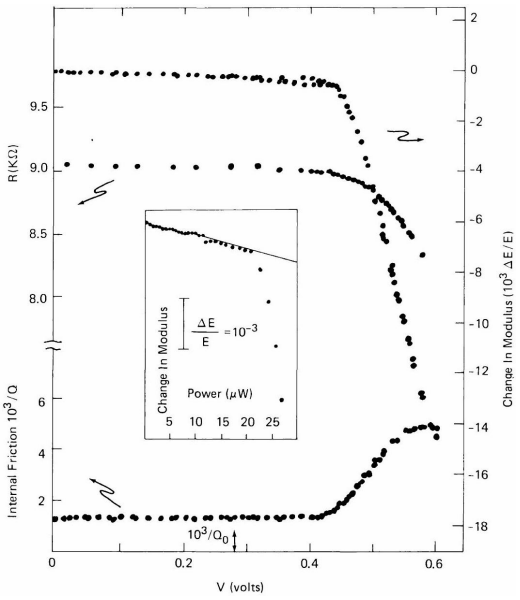


Fig. 23. Resistance, 1/(quality factor), and relative change in modulus $\Delta E / E_{0}=2 \Delta f / f_{0}$ versus voltage at 149 K in TaS_3.Q_0 is the quality factor in vacuum at zero voltage. Inset: $\Delta E/E_0$ versus power dissipated in the sample at 149 K . The line shows the proportionality below threshold (Brill and Roark 1984).

decrease of E' and increase of δ'. Similar behavior was found in $NbSe_3$ and in $(TaSe_4)_2I$ (Mozurkewich et al. 1985a,b, Suzuki et al. 1986), but no effect was observed in $K_{0.3}MoO_3$ (Bourne et al. 1986). The shear modulus was also measured recently and also shows significant anomalies as a function of applied electric field (Xiang and Brill 1987).

While the detailed underlying mechanism for the observed effect is not clear, it is expected that a pinned CDW would contribute to the elastic
constant while for a completely unpinned mode such contribution would be negligible. Also, damping effects associated with the dynamics of the internal modes can be responsible for the increased internal friction observed. The change of the elastic constant can be estimated by a mode coupling approach where the phonon and phason branches are coupled through Coulomb forces (Mozurkewich et al. 1985a,b), or by calculating the longitudinal sound velocity (Coppersmith and Varma 1984, Sneddon 1986). Such calculations lead to the softening of the lattice in the sliding conductivity region but fail to account for the magnitude or for the electric field dependence of the elastic properties. It has also been suggested (Maki and Virosztek 1988) that pinning effects have a profound influence on the sound velocity in the CDW state, and such effects may also account for the observed field dependent effects.

4.4.6 6. Local probes

Various local probes such as Mössbauer, EPR and NMR techniques have also been used to study the dynamics of the collective mode. Mössbauer spectra on ^{57}Fe doped $K_{0.3}MoO_3$ (Veuillen et al. 1986) and EPR experiments (Rouxel and Schlenker, chapter 2, this volume) give at present little information on the coupling between the collective mode and impurities. In contrast, nuclear magnetic resonance (NMR) has been proven to be extremely valuable in exploring both the static and dynamic properties of the CDW ground state.

Although current oscillations with the relation given by eq. (4.1) are regarded as evidence for the collective motion of the CDW condensate, the most direct evidence for moving charge density waves comes from NMR experiments (for a review see Berthier and Segranson 1987). The effect of a quadrupolar interaction is to lift the degeneracy between the transitions corresponding to the different nuclear levels.

$$\Delta\nu^0_{m\to m+1}(\boldsymbol{R}) = \frac{2m+1}{4}\nu(Q)f(\theta), \tag{6.1}$$

where

$$\nu(Q) = \frac{3e^2qQ}{2I(2I-1)} \tag{6.2}$$

with Q the quadrupole moment, eq the main component of the electric field gradient (EFG) tensor produced by the charges external to the nuclei, I the spin of the nucleus, and where $f(\theta)$ depends on the orientation of the (EFG) principal axis with respect to the external applied magnetic field. Below the Peierls transition, the electronic charge is modulated, see eq. (2.2) and this
leads to the modulation of the electric field gradient tensor. With this modulation eq. (6.1) becomes

$$\begin{aligned}\Delta\nu_{m\to m+1}(\boldsymbol{R}) =& \Delta\nu^0_{m\to m+1}(\boldsymbol{R}) + \frac{\omega_1}{2\pi}\left[\cos\left(2k_{\mathrm{F}}\boldsymbol{R}+\phi\right)\right] \\ &+ \frac{\omega_2}{2\pi}\left[\cos^2\left(2k_{\mathrm{F}}\boldsymbol{R}+\phi\right]\right.\!.\end{aligned}$$

where ω_1 and ω_2 depend on the amplitude of the CDW and factors characterizing the nuclei. The incommensurate CDW transition yields an infinite number of inequivalent sites and therefore broadens the $m \to m+1$ transition and the lineshape becomes double-peaked as shown in fig. 24 for

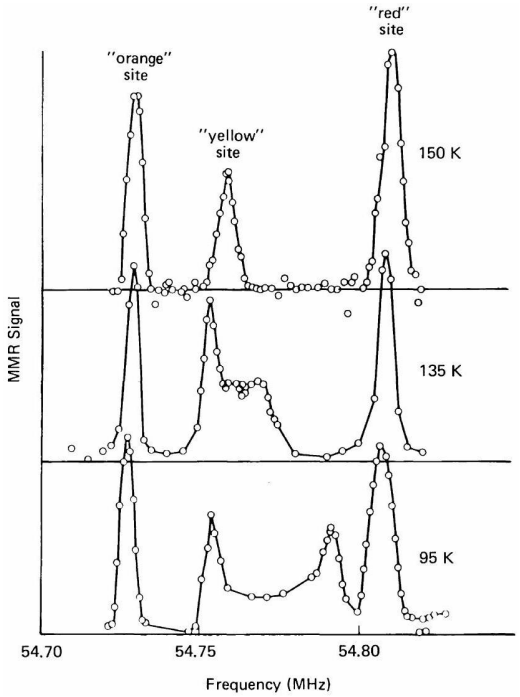


Fig. 24. NMR spectra showing the $\mathrm{NbSe}_{3}{ }^{93} \mathrm{Nb}$ central transitions at 52.478 kG with H_0 parallel to the chain axis as a function of temperature. The unit cell has three inequivalent Nb sites and the CDW at $T = 145$ K occurs only on one site as seen by the broadening of the NMR lineshape (Ross et al. 1986).

$NbSe_3$ (Ross Jr et al. 1986). The three inequivalent niobium sites correspond to the three chains in the unit cell and the CDW which appears at $T = 145$ K sets only on the chain with the strongest Se-Se coupling called yellow site (Devreux 1982, Wilson 1979). The lineshape can also be calculated in the case of non-sinusoidal perturbation, and it has been shown (Ross Jr et al. 1986), that the experimental lineshape cannot be fitted with a regular array of discommensurations separated by commensurate domains.

The theory of the NMR lineshape in the presence of a uniform sliding CDW has been worked out by Kogoj et al. (1984). If the CDW moves with a constant velocity v, the time evolution of the CDW phase will be $\phi = -\Omega t$

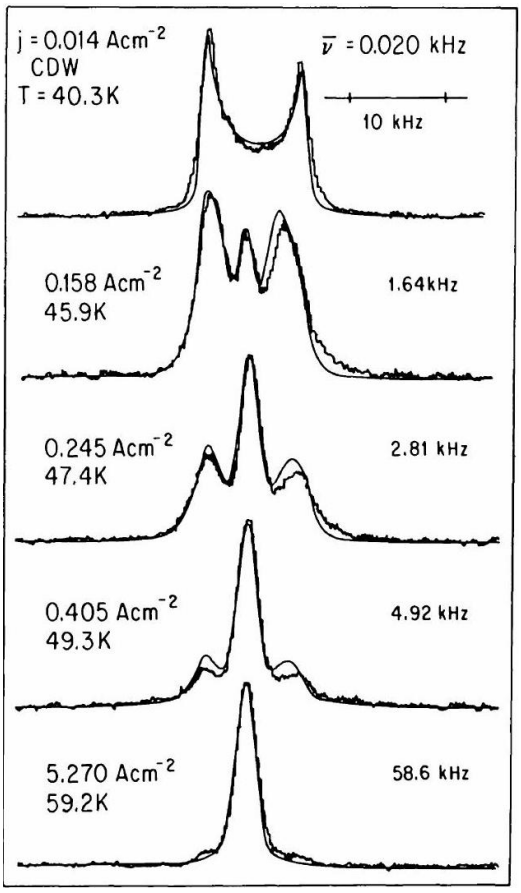


Fig. 25. Variation of the NMR lineshape for a $\mathrm{R}\{0.3\}\ \mathrm{MoO}\{3\}$ sample as a function of the charge density wave current J_{CDW} for a given applied electric field E ($E \sim 15$ times the threshold). A motional narrowing of the central line is apparent as two sidebands oberved at $T = 49.3$ K (Janossy et al. 1987).

with $\Omega = v/\lambda_{\mathrm{CDW}}$. The NMR lineshape is then found to be:

$$g(\omega) = \sum_{n=-x}^{+\infty} \left[J_n \left(\omega_1/\Omega\right)^2 \delta(\omega - n\Omega) h(\omega) \right]$$

The main effect of the CDW motion is the motional narrowing and the observation of a central line corresponding to $n = 0$. But well-defined sidebands also appear for $\omega = \pm n\Omega$.

The first evidence of a motional narrowing has been presented by Nomura and Kume (1985) on $K_{0.3}MoO_3$ and confirmed immediately later by Segransan et al. (1986) on $K_{0.3}MoO_3$ and by Ross Jr et al. (1986) on $NbSe_3$. Figure 25 shows the NMR lineshape for $K_{0.3}MoO_3$ at 40 K for several currents above threshold. Clearly the central line dominates the spectra at high currents. From the sidebands observed for the current density of 0.405Å cm^{-2} the CDW velocity was calculated, and it was found to be in good agreement with the general expression $J_{\mathrm{CDW}}/f = ce$ with $c = 2$ in agreement with arguments advanced earlier, see eqs. (4.1) and (4.2).

4.4.7 7. Conclusions

In this review we have described some of the anomalous properties associated with the dynamics of charge density waves. The experiments clearly establish this novel type of collective transport phenomenon, as envisioned by Fröhlich (1954) several years ago. The field appears to

be much broader than anticipated, this is related to the breadth of the observations, which vary from specimen to specimen and which also depend on several external factors. The nonlinear conductivity, observed in the CDW state is a typical example. In the majority of cases a smooth onset of nonlinear $I-V$ characteristics, such as shown in fig. 11, is observed. Switching effects which arise as the consequence of macroscopic defects in the specimens, can be modelled in a different way, while at low temperatures the nonlinear characteristic with practically zero differential resistance also requires a different explanation. Such differences most probably show up in other properties, these, however have not been explored in detail.

Nonlinear, and frequency dependent conduction has also been recently observed in other systems, also with a broken symmetry ground state. The organic conductor TTF-TCNQ (Lacoe 1986) where the CDW is more complicated than in the inorganic linear chain compounds also display E and ω dependent transport, clearly associated with the dynamics of the collective mode. Similar $I-V$ curves were also found in graphite at high magnetic field (Iye and Dresselhaus 1985), and in HgCdTe , where a Wigner crystal ground state is proposed (Field et al. 1986). Finally, nonlinear
(Osada et al. 1987) and frequency dependent (Hajiseyewadi et al. 1986) transport has recently been found in the spin density wave (SDW) ground states of organic linear chain compounds. While these initial results are promising, clearly further studies, involving experiments including other transport coefficients and the spectral response, are required to clarify the state of affairs in these materials.

4.4.8 References

Artemenko, S.N., E.N. Dolgov, A.N. Kruglov, Y.I. Latyshev, Ya.S. Savitskaya and V.V. Frolov, 1984, Pis'ma v Zh. Eksp. & Teor. Fiz. 39, 258.
Bardeen, J., E. Ben-Jacob, A. Zettl and G. Grüner, 1982, Phys. Rev. Lett. 49, 493.
Barisic, S., 1985, Mol. Cryst. & Liq. Cryst. 119, 413.
Barisic, S., 1986, in: Electronic Properties of Inorganic Materials with Quasi-One-Dimensional Structures, ed. P. Monceau (Reidel, Dordrecht).
Barisic, S., 1987, in: Low Dimensional Conductors and Superconductors, NATO ASI Series, Vol. 155, eds D. Jerome and L.G. Caron (Plenum Press, New York) p. 395.
Berthier, C., and P. Segransan, 1987, in: Low Dimensional Conductors and Superconductors, NATO ASI Series, Vol. 155, eds D. Jerome and L.G. Caron (Plenum Press, New York) p. 455
.
Beyermann, W.P., L. Mihaly and G. Grüner, 1986, Phys. Rev. Lett. 56, 1689.
Bhattacharya, S., J.P. Stokes, M.O. Robbins and R.A. Klemm, 1985, Phys. Rev. Lett. 54, 2453.
Biljakovic, K., J.C. Lasjaunias, F. Zougmore, P. Monceau, F. Levy, L. Bernard and R. Currat, 1986, Phys. Rev. Lett. 57, 1907.
Boriack, M.L., and A.W. Overhauser, 1978, Phys. Rev. B 18, 6454.
Borodin, D.V., S.V. Zeitsev-Zolov and F.Ya. Nad', 1986, Sov. Phys.-JETP 63, 1984.
Bourne, L.C., M.S. Sherwin and A. Zettl, 1986, Phys. Rev. Lett. 56, 1952.
Brazovskii, S., and I.E. Dzyaloshinskii, 1976, Sov. Phys.-JETP 44, 1233.
Brill, J.W., 1982, Solid State Commun. 41, 925.
Brill, J.W., and N.P. Ong, 1978, Solid State Commun. 25, 1075.
Brill, J.W., and W. Roark, 1984, Phys. Rev. Lett. 53, 846.
Brill, J.W., N.P. Ong, J.C. Eckert, J.W. Savage, S.K. Khanna and R.B. Somoano, 1981, Phys. Rev. B 23, 1517.
Brill, J.W., W. Roark and G. Minton, 1986, Phys. Rev. B 33, 6831.
Brown, S.E., and L. Mihaly, 1985, Phys. Rev. Lett. 55, 742.

Brown, S.E., G. Mozurkewich and G. Grüner, 1985, Solid State Commun. 54, 23.
Brown, S.E., J.O. Willis, B. Alavi and G. Grüner, 1988, Phys. Rev. B 37, 6551.
Cava, R.J., R.M. Fleming, P.B. Littlewood, E.A. Rietman, L.F. Schneemeyer and R.G. Dunn, 1984, Phys. Rev. B 30, 3228.
Cava, R.J., R.M. Fleming, R.G. Dunn and E.A. Rietman, 1985, Phys. Rev. B 31, 8325.
Cava, R.J., P.B. Littlewood, R.M. Fleming, R.G. Dunn and E.A. Rietman, 1986, Phys. Rev. B 33, 2439.
Chen, T., L. Mihaly and G. Grüner, 1988, Phys. Rev. Lett. 60, 464.
Coleman, R.V., M.P. Everson, G. Eiserman and A. Johnson, 1985, Phys. Rev. B 32, 537.
Coleman, R.V., M.P. Everson, G. Eiserman and A. Johnson, 1986, Physica B 143, 33.
Coppersmith, S.N., and C.M. Varma, 1984, Phys. Rev. B 30, 3566.
Dahlhauser, K.J., A.C. Anderson and G. Mozurkewich, 1986, Phys. Rev. B 34, 4432.
Dee, R.H., P.M. Chaikin and N.P. Ong, 1979, Phys. Rev. Lett. 42, 1234.
Devreux, I., 1982, J. Phys. (Paris) 43, 14.
Dumas, J., C. Schlenker, J. Marcus and R. Buder, 1983, Phys. Rev. Lett. 50, 757.
Efetov, K.B., and A.I. Larkin, 1977, Zh. Eksp. & Teor. Fiz. 72, 2350.
Field, S.B., D.H. Reich, B.S. Shivaram, R.F. Rosenbaum, D.A. Nelson and P.B. Littlewood, 1986, Phys. Rev. B 33, 5082.
Fleming, R.M., 1982, in: Physics in One Dimension, eds J. Bernasconi and T. Scheider (Springer, Berlin).
Fleming, R.M., 1983, Solid State Commun. 43, 169.
Fleming, R.M., and C.C. Grimes, 1979, Phys. Rev. Lett. 42, 1423.
Fleming, R.M., and L.F. Schneemeyer, 1984, Bull. Am. Phys. Soc. 29, 470.
Fleming, R.M., D.E. Moncton and D.B. McWhan, 1978, Phys. Rev. B 18, 5560.
Fleming, R.M., D.E. Moncton, J.D. Axe and G.S. Brown, 1984, Phys. Rev. B 30, 1877.
Fleming, R.M., R.J. Cava, L.F. Schneemeyer, E.A. Rietman and R.G. Dunn, 1986, Phys. Rev. B 33, 5082.
Forro, L., J.R. Cooper, A. Janossy and K. Kamaras, 1986, Phys. Rev. B 34, 9047.
Forro, L., J.R. Cooper, A. Janossy and M. Maki, 1987, Solid State Commun. 62, 715.
Fournel, A., J.P. Sorbier, M. Konczykowski and P. Monceau, 1986, Phys. Rev. Lett. 57, 2199.
Fröhlich, H., 1954, Proc. R. Soc. London Ser. A 223, 296.
Fukuyama, H., 1978, J. Phys. Soc. Jpn. 45, 1474.
Fukuyama, H., and P.A. Lee, 1978, Phys. Rev. B 17, 535.
Fuller, W.W., G. Grüner, P.M. Chaikin and N.P. Ong, 1981, Phys. Rev. B 23, 6259.
Geserich, H.P., G. Scheiber, M. Durrer, F. Levy and P. Monceau, 1986, Physica B 143, 198.
Gill, J.C., 1985, in: Proc. Int. Conf. on Charge Density Waves in Solids, Lecture Notes in Physics, Vol. 217, eds Gy. Hutiray and J. Sólyom (Springer, Berlin).
Gill, J.C., 1986a, J. Phys. C 19, 6589.
Gill, J.C., 1986b, Contemp. Phys. 27, 37.
Gor'kov, L.P., 1983, Sov. Phys.-JETP Lett. 38, 87.
Grüner, G., 1988, The Dynamics of Charge Density Waves in: Review of Modern Physics, Vol. qz60, No. 4.
Grüner, G., 1989, in: Progress in Low Temperature Physics, Vol. 12, ed. D.F. Brewer (North-Holland, Amsterdam) to be published.
Grüner, G., A. Zettl, W.G. Clark and A.H. Thompson, 1981a, Phys. Rev. B 23, 6813.
Grüner, G., A. Zawadowski and P.M. Chaikin, 1981b, Phys. Rev. Lett. 46, 511.
Hajiseyevadi, H., S. Sridhar, G. Grüner, L. Chiang and F. Wudl, 1986, Phys. Rev. Lett. 55, 1216.
Hall, R.P., M.F. Hundley and A. Zettl, 1986, Physica B 143, 152.
Horowitz, B., 1985, in: Solitons, Modern Problems in Condensed Matter Sciences, Vol. 17, eds

S.E. Trullinger and V. Zakharov (North-Holland, Amsterdam).

Hsieh, P.L., F. De Czito, A. Jánossy and G. Grüner, 1983, J. Phys. Colloq. 44, C3-1753.

Ido, M., Y. Okajima, H. Wakimoto and M. Oda, 1987, Physica B 143, 54.

Imry, Y., and S. Ma, 1975, Phys. Rev. Lett. 35, 1392.

Iye, Y., and G. Dresselhaus, 1985, Phys. Rev. Lett. 54, 1182.

Janossy, A., C. Bathier and P. Segransan, 1987, Phys. Scr. Vol. T, Sweden, Vol. T 19B, 578.

Kawabata, K., M. Ido and T. Sambongi, 1981, J. Phys. Soc. Jpn. 50, 739.

Kim, Tae Wan, W. Beyermann and G. Grüner, ????, .

Kogoj, M., S. Zumer and R. Blinz, 1984, J. Phys. C 17, 2415.

Kriza, G., and G. Mihaly, 1986, Phys. Rev. Lett. 56, 2529.

Kriza, G., G. Mihaly and G. Grüner, 1989, (to be published).

Kurihara, Y., 1980, J. Phys. Soc. Jpn. 49, 852.

Lacoe, R.C., H.J. Schulz, D. Jerome, K. Bechgaard and I. Johannsen, 1985, Phys. Rev. Lett. 55, 2351.

Latyshev, Y.I., Ya.S. Savitskaya and V.V. Frolov, 1983, Pis'ma v Zh. Eksp. & Teor. Fiz. 38, 446 [Sov. Phys.-JETP Lett. 38, 541].

Lee, P.A., and H. Fukuyama, 1978, Phys. Rev. B 17, 542.

Lee, P.A., and T.M. Rice, 1979, Phys. Rev. B 19, 3970.

Lee, P.A., T.M. Rice and P.W. Anderson, 1974, Solid State Commun. 14, 703.

Littlewood, P.B., 1987, Phys. Rev. B 36, 3108.

Littlewood, P.B., and R. Rammal, 1987, Phys. Rev. Lett. 58, 524.

Lyding, J.W., J.S. Hubacek, G. Gammie and R.E. Thorne, 1986, Phys. Rev. B 33, 4341.

Maeda, A., T. Fukayama, K. Uchinokura and S. Tanaka, 1986, Solid State Commun. B 58, 25.

Maki, K., 1986a, Phys. Rev. B 33, 2852.

Maki, K., 1986b, Physica B 143, 59.

Maki, K., and A. Virosztek, 1988, (to be published).

Maki, M., 1986, unpublished data.

Mihaly, G., and P. Beauchêne, 1987, Solid State Commun. 63, 911.

Mihaly, G., Gy. Hutiray and L. Mihaly, 1983, Phys. Rev. B 28, 4896.

Mihaly, G., L. Mihaly and H. Mutka, 1984, Solid State Commun. 49, 1009.

Mihaly, L., and G. Grüner, 1984, Solid State Commun. 50, 807.

Mihaly, L., Ki-Bong Lee and P.W. Stephens, 1987a, Phys. Rev. B 36, 1793.

Mihaly, L., T. Chen and G. Grüner, 1987b, Solid State Commun. 61, 751.

Monceau, P., 1982, Physica B + C 109&110, 1890.

Monceau, P., and M. Renard, 1986, Europhys. News 17, 99.

Monceau, P., and J. Richard, 1988, Phys. Rev. B 37, 7982.

Monceau, P., J. Richard and M. Renard, 1980, Phys. Rev. Lett. 45, 43.

Monceau, P., M. Renard, J. Richard, M.C. Saint-Lager and Z.Z. Wang, 1985, in: Proc. Int. Conf. on Charge Density Waves in Solids, Lecture Notes in Physics, Vol. 217, eds Gy. Hutiray and J. Sólyom (Springer, Berlin).

Monceau, P., L. Bernard, R. Currat, F. Levy and J. Rouxel, 1986a, Physica B 136, 352.

Monceau, P., M. Renard, J. Richard and M.C. Saint-Lager, 1986b, Physica B 143, 64.

Mozurkewich, G., and G. Grüner, 1983, Phys. Rev. Lett. 51, 2206.

Mozurkewich, G., P.M. Chaikin, W.G. Clark and G. Grüner, 1985a, Solid State Commun. 56, 421.

Mozurkewich, G., P.M. Chaikin, W.G. Clark and G. Grüner, 1985b, in: Proc. Int. Conf. on Charge Density Waves in Solids, Lecture Notes in Physics, Vol. 217, eds J. Solyom and Gy. Hutiray (Springer, Berlin).

Mutka, H., S. Bouffard, J. Dumas and C. Schlenker, 1984, J. Phys. Lett. 45, L729.

Nad', F.Ya., 1985, in: Proc. Int. Conf. on Charge Density Waves in Solids, Lecture Notes in

Physics, Vol. 217, eds Gy. Hutiray and J. S'olyom (Springer, Berlin) p. 286.
Nakane, Y., and S. Takada, 1985, J. Phys. Soc. Jpn. 54, 977.
Ng, H.K., G.A. Thomas and L.F. Schneemeyer, 1986, Phys. Rev. B ???, 8755.
Ngai, K.L., 1979, Comm. Solid State Phys. 9, 127.

Nomura, K., and K. Kume, 1985, in: 1st European Workshop on Charge Density Waves in Solids, Zagreb, Yugoslavia (unpublished).
Nomura, K., K. Kume and M. Sato, 1986, J. Phys. C 19, L289.
Oda, M., and M. Ido, 1982, Solid State Commun. 44, 1535.
Oda, M., and M. Ido, 1985, Solid State Commun. 50, 879.
Ong, N.P., and K. Maki, 1985, Phys. Rev. B 32, 6582.
Ong, N.P., and P. Monceau, 1977, Phys. Rev. B 16, 3443.
Ong, N.P., and G. Verma, 1983, Phys. Rev. B 27, 4495.
Ong, N.P., J.W. Brill, J.C. Eckert, J.W. Savage, S.K. Khanna and R.B. Somoano, 1979, Phys. Rev. Lett. 42, 811.
Ong, N.P., G. Verma and K. Maki, 1984, Phys. Rev. Lett. 52, 663.
Osada, T., N. Miura and G. Saito, 1987, Solid State Commun. 60, 441.
Prester, M., 1985, Phys. Rev. B 32, 2621.
Reagor, D., and G. Grüner, 1986, Phys. Rev. Lett. 56, 659.
Reagor, D., and G. Mozurkewich, 1985, private communication.
Reagor, D., S. Sridhar, M. Maki and G. Grüner, 1985a, Phys. Rev. B 32, 8445.
Reagor, D., S. Sridhar and G. Grüner, 1985b, in: Proc. Int. Conf. on Charge Density Waves in Solids, Lecture Notes in Physics, Vol. 217, eds J. Solyom and Gy. Hutiray (Springer, Berlin).
Reagor, D., S. Sridhar and G. Grüner, 1986, Phys. Rev. B 34, 2212.
Rice, T.M., P.A. Lee and M.C. Cross, 1979, Phys. Rev. B 20, 1345.
Richard, J., P. Monceau, M. Popoular and M. Renard, 1982a, J. Phys. C 15, 7157.
Richard, J.. P. Monceau and M. Renard, 1982b, Phys. Rev. B 25, 948.
Richard, J., P. Monceau and M. Renard, 1987, Phys. Rev. B 35, 4533.
Ross Jr. J.H., Z. Wang and C.P. Schlichter, 1986, Phys. Rev. Lett. 56, 663.
Saint-Lager, M.C., 1983, Thesis 3ème Cycle (University of Grenoble).
Schlenker, C., and J. Dumas, 1986, Physica B 143, 103.
Schneemeyer, L.F., R.M. Fleming and S.E. Sprenger, 1985, Solid State Commun. 53, 505.
Segransan, P., A. Janossy, C. Berthier, J. Marcus and P. Butaud, 1986, Phys. Rev. Lett. 56, 1854.

Sham, L.J., and B.R. Patton, 1976, Phys. Rev. B 13, 2151.
Sneddon, L., 1985, Phys. Rev. B 29, 719.
Sneddon, L., 1986, Phys. Rev. Lett. 55, 1194.
Sridhar, S., D. Reagor and G. Grüner, 1986, Phys. Rev. B 34, 2223.
Stokes, J.P., A.N. Bloch, A. Janossy and G. Grüner, 1984, Phys. Rev. Lett. 52, 372.
Suzuki, A., H. Mizebayashi, S. Okuda and M. Domaya, 1986, Phys. Rev. B 143, 161.
Tessema, G.X., and N.P. Ong, 1981, Phys. Rev. B 23, 5607.
Tessema, G.X., B. Alavi and L. Mihaly, 1985, Phys. Rev. B 31, 6878.
Testardi, L.R., 1975, Phys. Rev. B 12, 3849.
Thorne, R.E., W.G. Lyons, J.W. Lyding, J.R. Tucker and J. Bardeen, 1987, Phys. Rev. B 35, 6348.

Tinkham, M., 1975, Introduction to Superconductivity (McGraw-Hill, New York) p. 231.
Travaglini, G., and P. Wachter, 1984, Phys. Rev. B 30, 1971.
Underweiser, M., M. Maki, B. Alavi and G. Grüner, 1987, Solid State Commun. 64, 181.
Verma, G., and N.P. Ong, 1986, Physica B 143, 100.
Veuillen, J.Y., R. Chevalier, J. Marcus and C. Schlenker, 1986, Phys. Rev. B 143, 186.
Wang, Z.Z., M.C. Saint-Lager, P. Monceau, M. Renard, P. Gressier, A. Meerschaut, L. Guemas

and J. Rouxel, 1983a, Solid State Commun. 46, 325.
Wang, Z.Z., K. Salva, P. Monceau, M. Renard, C. Roncan, R. Ayroles, I. Levy, L. Guemas and A. Meerschaut, 1983b, J. Phys. Lett. 44, L311.
Wilson, J.A., 1979, Phys. Rev. B 19, 6456.
Wong, K.Y., and S. Takada, 1987, Phys. Rev. B 36, 5476.
Wonneberger, W., and H.J. Breymayer, 1984, Z. Phys. B 56, 241.
Wu, Wei-Yu, A. Janossy and G. Grüner, 1984, Solid State Commun. 49, 11.
Wu, Wei-Yu, L. Mihaly, G. Mozurkewich and G. Grüner, 1986, Phys. Rev. B 33, 2444.
Xiang, X.D., and J.W. Brill, 1987, Phys. Rev. B 36, 2969.
Zettl, A., and G. Grüner, 1982, Phys. Rev. B 26, 2298.
Zettl, A., and G. Grüner, 1983, Phys. Rev. B 28, 2091.
Zettl, A., and G. Grüner, 1984, Phys. Rev. B 29, 755.
Zettl, A., M. Kaiser and G. Grüner, 1984, Bull. Am. Phys. Soc. ????.
Zhilinskii, S.K., M.E. Itkis and F.Ya. Nad', 1984, Phys. Status Solidi a 81, 367.

This page intentionally left blank

4.5 5 Deformation and Phase-slip in Charge Density Waves in Quasi-One-Dimensional Conductors

4.5.1 1. Introduction

In many of the quasi-one-dimensional conductors at sufficiently low temperature the electron-phonon interaction leads to the development of a periodic superstructure, which is a spatially periodic distortion of the crystal lattice and a corresponding spatial modulation of the free electron density, which is known as charge density wave (CDW). A CDW has a number of unusual properties which are due to the cooperative motion of the electrons included in CDW (Hutiray and Sólyom eds. 1985, Grüner and Zettl 1985, Monceau 1985). The study of these properties has been going on for over ten years, but still their physical nature is not completely understood. Initially a CDW was treated as some rigid object which can move in an underlying crystal lattice, as soon as the pinning on the impurities and defects (when the CDW is incommensurate with the underlying lattice) was overcome.

Later it was understood that the internal degrees of freedom of the CDW - deformations, strains and nonlinear excitations have a considerable effect on the properties of the CDW. The CDW deformation can be defined in terms of the space-depending shift of one part of the periodic superstructure (CDW) with respect to another part under the influence of the external forces. In this case the wave vector q and phase φ of the CDW become coordinate dependent. The main directions of the studies in this field are the following:
(1) The static and dynamic interactions of the deformable CDW with free carriers.
(2) The phenomena, which are connected with the interactions of the CDW with the centers of the pinning, including the memory effects and metastable states, the remanent deformation of the CDW, 'overshoot' phenomenon and soliton-like states.
(3) The processes which provide removal of excess deformation of the CDW (phase-slip centers and vortices) and manifest themselves in the generation of the narrow band noise, in the threshold field dependence on the length of the sample and etc. (Hutiray and Sólyom eds. 1985, Grüner and Zettl 1985, Monceau 1985).

The experimental studies connected with these phenomena were carried
out on sufficiently large samples of quasi-one-dimensional conductors, in which the phase coherence was not maintained throughout the whole volume of the samples. Only the short-range order with the finite phase coherence length exists in actual crystals containing impurities and defects (Efetov and Larkin 1977, Fukuyama and Lee 1978, Lee and Rice 1979). For example,

in accordance with estimates in orthorhombic TaS_3 the longitudinal phase coherence length $l_{\|}$is typically $\sim 10\mu$ m, but transversal phase coherence length $l_{\perp}$ is one or two orders smaller (Grüner and Zettl 1985, Monceau 1985, Mihaly and Grüner 1984, Borodin et al. 1986a). After the beginning of the CDW motion the phase coherence length can grow (Fisher 1985). The characteristic distance of CDW amplitude variation - correlation length ξ is ≈ 30Å (Grüner and Zettl 1985, Monceau 1985). TaS_3 samples usually studied (with length $L \simeq 1$ mm and crosssectional area $S = 10 - 100\mu$ m^2) are considerably larger in size than the phase coherence region (domain) and contain a lot of domains ($\sim 10^6$). In this case in experiments we observe the properties which are the result of averaging of uncorrelated phase variations in separate domains throughout the sample volume.

It is natural to suppose that the effects caused by deformations and excitations of CDW will reveal themselves more clearly in the samples, in which the phase coherence is maintained throughout the whole volume, i.e., in the samples whose size is of the order of phase coherence length.

For this reason we carried out a systematic study of variations of the properties of quasi-one-dimensional conductors TaS_3 as a function of the longitudinal and transverse sizes of the samples down to very small values (Borodin et al. 1986b,c,d, 1987a,b). The study of small size TaS_3 samples revealed a number of new features typical for a completely coherent deformable CDW. A simple model of such CDW and its distortions including phase-slip due to external forces (temperature and electric field) is discussed. On the basis of this model an explanation of the experimental data is suggested. Results obtained make it possible to achieve a more clear understanding of the physical nature of the phenomena in quasi-onedimensional conductors with deformable coherent CDW.

4.5.2 2. Phase coherence of the *CDW*

2.1. The samples

The majority of results reported in this paper was obtained using crystal samples of orthorhombic TaS_3 with sizes varying in a wide range: the length L varies from several millimeters to 5μ m, and the cross-sectional area S from $10^2\mu$ m^2 to $\sim 10^{-3}\mu$ m^2. It turned out that a decrease in S resulted in a
variation of the sample properties. All samples under investigation can be arbitrarily divided into three groups. The first group contains large samples with $S = 1 - 100\mu$ m^2 and $L = 300 - 1000\mu$ m, the second group samples with $S = 0.1 - 1\mu$ m^2 and $L = 5 - 800\mu$ m, the third group samples with $S = 10^{-1} - 10^{-3}\mu$ m^2 and $L = 6 - 120\mu$ m. The samples were placed on the substrates of crystal quartz or sapphire. The electrical contacts were prepared by vacuum deposition of several (about 6) narrow ($\approx 10\mu$ m) metal strips (indium, gold) with a distance between them (L) varying from 5 to 1000μ m (Borodin et al. 1986b). The contacts obtained were ohmic, their resistance being about $10\Omega(T \simeq 100$ K). The sizes of the samples were derived from their room temperature resistance and measured also by optical and electron microscopes. The comparison of the lengths of the sample sections derived from the resistance L_r and optical measurements of L_0 showed that in the thick samples ($S \geqslant 1\mu$ m^2) $L_r > L_0$ due to the contact spreading resistance r, whereas in the thin samples ($S < 1\mu$ m^2) the contribution of r can be neglected and $L_0 = L_r$ (Borodin et al. 1986a, 1987b). Below the sample length L is treated as the distance between the edges of the contact strips measured by microscope. The initial thick samples ($S \simeq 100\mu$ m^2), from which we obtained thin samples of the second and third groups by cleavage (Borodin et al. 1986b), were adequately pure with a temperature of threedimensional ordering $T_{\mathrm{p}} = 225$ K and the threshold electric field $E_{\mathrm{T}} = 0.3$ V/cm$(T = 120$ K).

2.2. Temperature dependence of the resistance

Measurement of the dependence of the resistance on temperature $R(T)$ showed that the form of this dependence varied with decreasing crosssectional area S of the samples (Borodin et al. 1986c,d). For samples with $S > 0.1\mu$ m^2 (groups 1 and 2) the dependence $R(T)$ has the usual form with a sharp increase of the resistance near $T = T_\mathrm{p}$ and with an activation region corresponding to the energy gap $\Delta \simeq 800$ K (fig. 1) (Nad' 1985). In the temperature range $200 - 77$ K a hysteresis is observed on $R(T)$: with decreasing temperature the $R(T)$ curve is situated lower than the curve with increasing temperature (Higgs and Gill 1983). In group 3 samples a slight decrease of T_p and some broadening of the Peierls transition became noticeable beginning from $S \simeq 0.1\mu$ m^2. A further decrease of S led to a noticeable shift of the $R(T)$ curves toward low temperature and to a large broadening of the Peierls transition (fig. 1, samples 10 and 12a). These variations become more distinct in fig. 2 which shows a temperature dependence of the logarithmic derivative $\mathrm{d}\lg(R/R_{300})/\mathrm{d}(10^3/T)$ for several samples with different cross-sectional area. Also visible is the shift of maxima of the curves corresponding to $T = T_\mathrm{p}(S)$, their broadening and reduction, especially pronounced for thin and short samples (samples 12

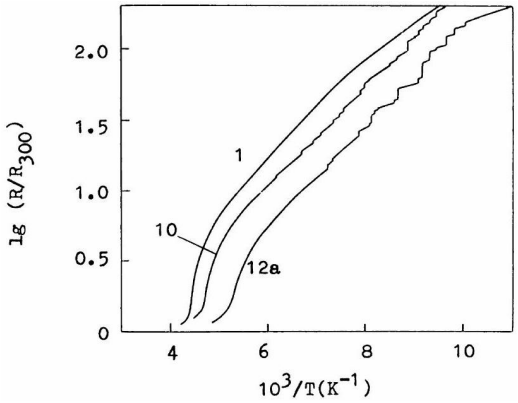


Fig. 1. The dependence of the resistance on temperature for the samples of orthorhombic \$\mathrm{TaS}_{3}\$. Samples: 1, $L = 1160\mu$ m, $S = 66\mu$ m^2 (group 1); 10, $L = 24\mu$ m, $S = 0.033\mu$ m^2; 12a, $L = 8\mu$ m, $S = 0.017\mu$ m^2 (group 3).

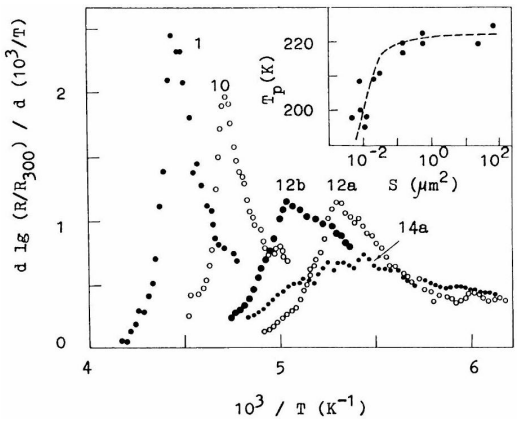


Fig. 2. The dependence of the logarithmic derivative of the resistance on temperature for \$\mathrm{TaS}_{3}\$ samples. The numbers of samples are indicated at the curves. Samples: 12b, $L = 24\mu$ m, $S = 0.017\mu$ m^2; 14a, $L = 6\mu$ m, $S = 0.005\mu$ m^2. The sizes of samples 1,10 , 12a are given in fig. 1.

and 14a). The inset in fig. 2 shows that the decrease of $T_{\rm p}$ may be as great as ≈ 30 K.

As S decreases the $R(T)$ curve displays qualitatively important new features. Beginning from $S \approx 0.3 - 0.4\mu$ m^2 the $R(T)$ dependence takes a step-like form with jumps in the temperature range $T \leqslant 150$ K (fig. 1). More distinctly this pattern is observed in samples with $S \sim 10^{-2}\mu$ m^2. Figure 3 shows a fragment of the $R(T)$ curve for a sample with $S \simeq 10^{-2}\mu$ m^2 as a comparison with a similar fragment of the $R(T)$ curve for a sample with $S \simeq 40\mu$ m^2 (in the inset). Both dependences show the hysteretic form. However in thick samples the $R(T)$ curve is smooth, but in thin samples it has a step-like form and consists of short, nearly linear regions with 'activation energy' $\mathrm{d}\ln R/\mathrm{d}(1/T) \simeq 200$ K, which is smaller than the average activation energy Δ obtained from a large temperature range (fig. 1). The transitions between these regions are going by jumps and their relative amplitudes $\Delta R/R$ are about $1 - 10\%$. The amplitudes of jumps ΔR and the temperature ranges ΔT between them depend on the ambient temperature and decrease with growing temperature (fig. 1). Slight fluctuations of the jump temperatures are observed in repeated temperature cycling. However the regions of the smooth variation of $R(T)$ between jumps are fairly well reproducible, which means that they are stable hysteresisless states.

Figure 4 shows on a large scale the variation of R through the states (indicated by numbers) which are occupied successively with repeated

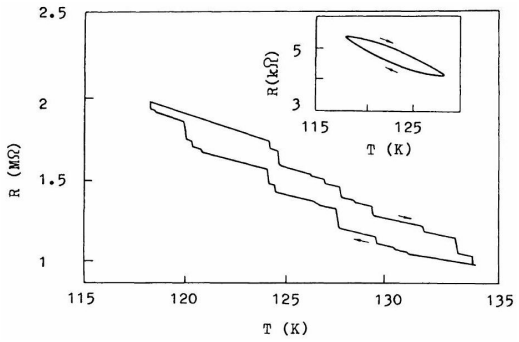


Fig. 3. The dependence of the resistance on temperature for samples with small cross-sectional area \$S \simeq 10\^{-2} \mu \mathrm{\~m}\^{2}, L \simeq 20 \mu \mathrm{\~m}\$. The inset shows a similar dependence for a large sample with $S \simeq 40\mu$ m$^2, L \simeq 1$ mm. The amplitude of the modulation current $I = 10^{-2} I_{\rm T}$.

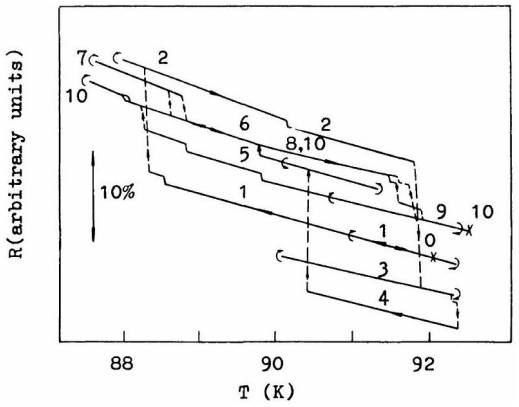


Fig. 4. The region of the dependence of resistance on repeated temperature cycling in the range \$88-92 \mathrm{\~K}\$ for group 3 samples ($11, S = 0.02\mu$ m$^2, L = 24\mu$ m). The numbers indicate the sequence of occupied states.

temperature cycling in the range $88-92$ K. As can be seen from fig. 4 the sample resistance takes up one of these discrete approximately equidistant states ($\Delta R/R = 4\%$). In a number of cases the sample repeatedly gets to the same states (states $6, 8, 10$). The variation of R within these states was approximately linear. Within these states both with increasing or decreasing temperature of approximately $\Delta T = 2 - 5$ K after jump no hysteresis of the $R(T)$ curve was observed within our experimental accuracy (0.3%). In thick samples (group 1) at the same range of temperature cycling ($\Delta T \approx 5$ K)$R(T)$ dependence has a pronounced hysteretic form which persists down to the smallest ranges $\Delta T \leqslant 0.2$ K measured by us.

In the thinnest samples studied with $S \sim 10^{-3}\mu$ m^2 the amplitude of hysteretic loop and the temperature range of its existence tend to become narrow, the jumps become less distinct and their amplitude diminishes. This tendency becomes especially pronounced in short samples ($L \leqslant 10\mu$ m).

2.3. Electric field dependence of the resistance

As the sample's cross-sectional area S decreases some remarkable variations including quite new features appear on the $I - V$ curve. Figure 5 shows a series of typical dependences of conductivity ($\sigma = I/U$) on the electric field $E\,(E > E_{\mathrm{T}})$ normalized to its value σ_0 in the ohmic region ($E \ll E_{\mathrm{T}}$), fairly long samples ($L \geqslant 100\mu$ m) with different S. First of all as can be seen from fig. 5 the threshold field E_{T} for the beginning of nonlinear conductivity grows with decreasing S. Figure 6 shows the $E_{\mathrm{T}}(S)$ dependence, with

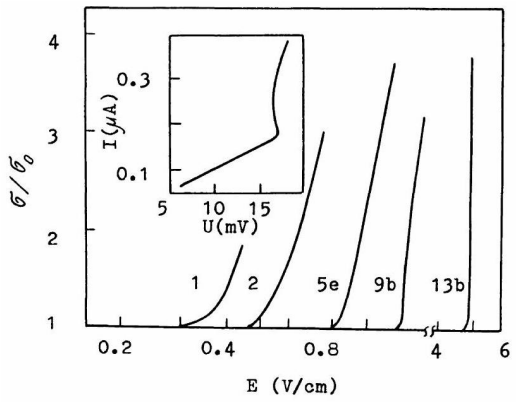


Fig. 5. The dependence of conductivity normalized to its value at $E<E_{\mathrm{T}}$ on the electric field for samples with various cross-sectional area: $1, S = 66\mu$ m$^2, L = 1160\mu$ m; $2, S = 24\mu$ m^2, $L = 105\mu$ m; $5, S = 0.6\mu$ m$^2, L = 790\mu$ m; 9 b, $S = 0.15\mu$ m$^2, L = 105\mu$ m; 13 b, $S = 0.008\mu$ m^2, $L = 114\mu$ m($T = 120$ K). The inset shows the region of the $I - V$ curve of sample 9 b ($T = 140$ K).

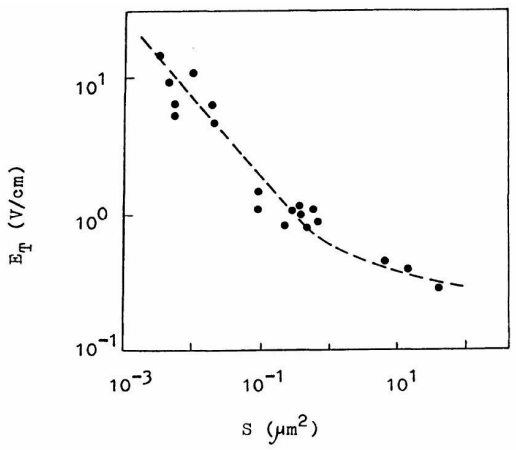


Fig. 6. The dependence of threshold field E_{T} on the cross-sectional area for various samples ($T = 120$ K).

S decreasing by more than four orders of magnitude from $S = 10\mu$ m^2 to $S < 10^{-2}\mu$ m^2 (Borodin et al. 1986c,d). The scatter of data points in fig. 6 appears to be due to variations in the forms of the cross sections of our samples. Nevertheless as can be seen from fig. 6 the value of E_{T} changes slightly with decreasing S down to 1μ m^2 (group 1). In the range $S < 1\mu$ m^2 the experimental points can be approximated by the dependence $E_{\mathrm{T}} \simeq V_{\mathrm{s}} S^{-1/2}$ at $V_{\mathrm{s}} = 0.1$mV, i.e., roughly speaking E_{T} grows inversely proportional to transversal sizes of the sample. A similar growth of E_{T} was observed in $NbSe_3$ samples with decreasing cross-sectional area (Yetman and Gill 1987, Chen et al. 1987).

At the same time the form of the $I - V$ curve varies considerably with decreasing S (fig. 5). A number of characteristic features of these variations can be seen more clearly from the dependence of the differential resistance ($R_{\mathrm{d}} = \mathrm{d}U/\mathrm{d}I$) on current I (fig. 7). Figures 5 and 7 show that in the samples of the first group (samples 1 and 2) with increasing E and I the conduction grows gradually which is usually attributed to the uncorrelated motion of

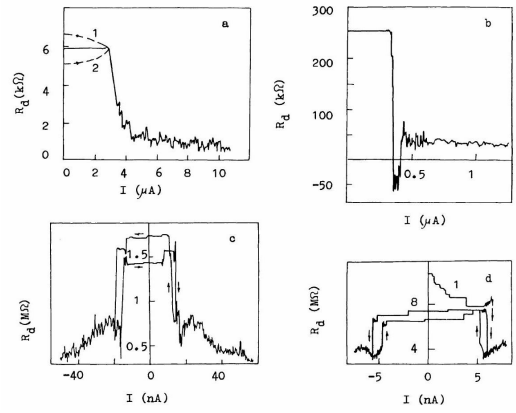


Fig. 7. The dependence of the differential resistance on the current. (a) sample 2, $T=120$ K; (b) sample 5, $T = 137$ K; (c) sample 11, $T = 98$ K; (d) sample 14 b, $S = 0.005\mu$ m^2, $L = 24\mu$ m, $T = 98$ K. The sizes of the other samples are given in the captions of figs. 2, 4, 5.

CDWs in the multidomain samples (Fisher, D. 1983). In the samples of the second group (samples 5 and 9) the conduction increases more sharply with growing E. The region of the positive curvature ($\mathrm{d}^2U/\mathrm{d}I^2 > 0$) appears on the $I - V$ curve near $E > E_{\mathrm{T}}$ and in a

number of cases we can see the region of the negative differential resistance (NDR) in the range $130 < T < 150$ K. The inset in fig. 5 shows the $I - V$ curve of sample 9 b at $T = 140$ K. The form of the curve is S-like with a fairly large region of NDR. Figure 7b unambiguously shows the appearance of NDR at $I > I_{\mathrm{T}}$ with R_{d} reaching the plateau where narrow band noise generation becomes visible. These curves have been measured when the current was regulated and they retained their form regardless of the direction of current variation and its polarity. With decreasing temperature below ≈ 130 K NDR disappears gradually whereas the transition region of the positive curvature does not disappear down to $T = 100$ K. The NDR disappears also with increasing temperature above 150 K . The NDR was sensitive to the thermal cycling. After several cycles of temperature reduction down to 100 K and temperature raising up to 300 K the NDR as a rule disappears but the $I - V$ curve retained its general form described above.

In samples with $S < 10^{-1}\mu$ m^2 (group 3) the region of positive curvature becomes wider and a fourfold growth of conduction at practically constant voltage is observed, for example, in sample 13b ($S = 8 \times 10^{-3}\mu$ m^2) (fig. 5). A detailed study shows that in this case the $I - V$ curve retains its S -like shape.

It was also found that the resistance of group 3 samples changed by jumps with current variation. If the sample was initially in the metastable state, determined by the temperature prehistory, during the first current increase the removal of metastable states proceeds in a step-like form (curve 1, fig. 7d), rather than smoothly (Hutiray et al. 1983) as in group 1 samples (curves 1 and 2, fig. 7a). With repeated plotting the $R_{\mathrm{d}}(I)$ dependence has a reproducible hysteretic form with a characteristic R_{d} maximum near $I \geqslant I_{\mathrm{T}}$ and a smaller I_{T} value on the curve representing a decreasing current. In small (group 3) samples the R_{d} value was not constant even when the current did not reach its threshold value. In this range one can observe jump-like transitions between states with different resistance and, as a rule, oscillatory growth of R_{d} with a current approaching I_{T} from below (fig. 7c and 7d) (Borodin et al. 1986a, 1987b).

2.4. Narrow band noise

Information about the degree of the CDW coherence in the volume of the sample can also be obtained by investigating the narrow band generation resulting from the CDW motion. The narrow band generation in small samples was studied by Borodin et al. (1985, 1986 d) and it was shown that

the amplitude of the periodic voltage oscillations allowed their frequency dependence to be registered directly. It was found that the form and width of the generation lines changed greatly depending on the size of the sample. The fundamental lines of the generation spectrum in group 1 samples had an irregular form and were comparatively wide ($\Delta f \sim 1$MHz) (fig. 8a). With decreasing cross-sectional area the fundamental line breaks up into several narrow lines. In samples with $S \leqslant 1\mu$ m^2 we observed several lines ~ 100kHz wide placed close to each other, and this pattern was harmonically repeated. When the cross-sectional area was further reduced the number of the fundamental lines and their width decreased. In samples with $S \sim 0.1\mu$ m^2 very few fundamental lines with a width $\Delta f < 100$kHz are observed (fig. 8b).

The spectrum of some of the most perfect and rather short samples consists of only one fundamental line with a width smaller than 10 kHz at $T = 120$ K (fig. 8c). In such samples low frequency noise, which is imposed on the narrow band generation, was relatively smaller than in thick samples. Moreover the narrow band generation was observed beginning from low frequency $f \simeq 50$kHz and the $I - V$ curve of such samples shows a sharp bend at $I = I_{\mathrm{T}}$. In the temperature range $100 - 160$ K the width of the lines

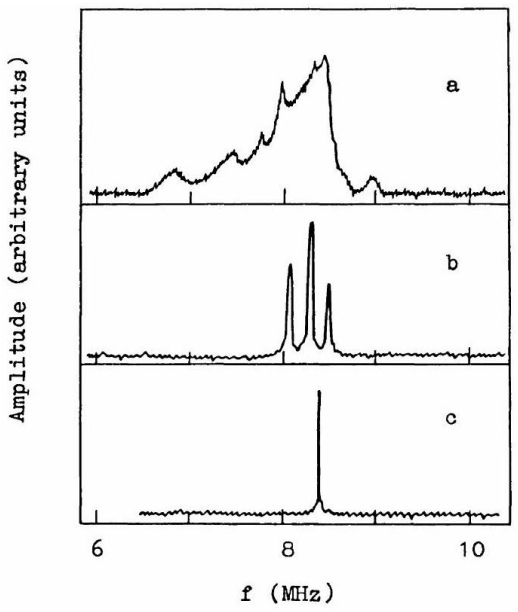


Fig. 8. The form of narrow band generation lines for the samples of the various cross-sectional area: (a) sample 2 , (b) sample $8, S=0.3 \mu \mathrm{~m}^{2}, L=45 \mu \mathrm{~m}$; (c) sample 10, $S = 0.033\mu$ m^2, $L = 24\mu$ m.

grew and at $T > 170$ K the narrow band generation vanished in the wideband noise.

In thinner samples with $S \sim 10^{-2}\mu$ m^2 the width of the generation lines gradually increased and their amplitudes decreased. Finally in samples with $S < 10^{-2}\mu$ m^2 at $I > I_{\mathrm{T}}$ we could see only low frequency noise with spectral density $f^{\alpha}(\alpha \sim 1)$ but no lines of the narrow band generation were obtained. In group 2 samples ($1 > S > 0.1\mu$ m^2) in which, as mentioned above, the spectrum contained several rather narrow fundamental lines the shift of one group of lines relative to the second group was effected by passing an additional direct current through a neighbouring section (Borodin et al. 1985). Line splitting and frequency locking were also observed. Similar effects were observed in a $NbSe_3$ sample when one of its ends was heated while the other one was kept at constant temperature (Verma and Ong 1984, Zhang and Ong 1984, Saint-Lager et al. 1987a).

2.5. Discussion

The outlined results are considered to be a strong experimental evidence for the existence of the coherent CDW through the whole volume of small samples of rather pure TaS_3. Indeed the form of the $I - V$ curve with a bend near $E \geqslant E_{\mathrm{T}}$ and NDR are typical for the coherent CDW under conditions when its phase coherence length approached the sizes of the samples. In this case the long-wave variation of the phase can be limited by these sizes (Klemm and Robbins 1986).

Hysteresisless regions and jump-like transitions between them observed on $R(T)$ correspond to the set of metastable states of the coherent CDW pinned on the centers of the strong pinning, for example, on the contacts (see below). In large samples containing a lot of uncorrelated domains these effects are averaged, which leads to the smooth $R(T)$ dependence. The fact that the number of fundamental lines is reduced to one and its width becomes very narrow is also in favour of the high degree of CDW coherence in small samples. The variation of the condition of the CDW pinning on one contact by temperature increase (Verma and Ong 1984, Zhang and Ong 1984, Saint-Lager et al. 1987a) or by passing the current through a neighbouring section (Borodin et al. 1985) can result in disturbing the CDW coherence throughout the whole sample

and splitting of the initially synchronized frequencies of narrow band oscillations. On the other hand, when several domains with uncorrelated phase exist in the samples, variation of the conditions of the CDW motion at a contact can promote the increase of the degree of CDW coherence and frequency locking of initially different frequencies of oscillations. Apparently the externally applied electromagnetic field with a frequency, which is close to the frequency of CDW
oscillations, can also promote the enhancement of CDW coherence (Sherwin and Zettl 1985, Sneddon 1984).

The optimal sizes of TaS_3 samples to observe the effects of total phase coherency of CDW are $L = 10 - 100\mu$ m and $S = 10^{-1}\mu$ m^2. We attribute the effects observed to the finite size of the samples, i.e., as a matter of fact they are the size effects. It means that the phase coherence lengths of CDW in our samples, in order of magnitude, are $l_{\|} = 10 - 100\mu$ m and $L_{\perp} = 10^{-1}\mu$ m. The reduction of the sample length down to $L < 10\mu$ m does not result in any increase of the CDW coherence, since the contacts and nonuniformity of the electric field near them have a growing effect on the CDW formation (Borodin et al. 1986a). The decrease of the cross-sectional area to a value smaller than $10^{-2}\mu$ m^2 does not appear to enhance the CDW coherence either. In such small samples the role of the three-dimensional effects, which are essential for the existence of the actual phase transition, is reduced while the influence of the sample surface and fluctuations is increased. The broadening of the Peierls transition on the $R(T)$ curve with a significant decrease of $T_{\rm p}$ (fig. 2), the reduction of the intensity of step-like structure, the sharp growth of the threshold field $E_{\rm T}$ (fig. 6) and also the gradual disappearance of the narrow band generation in the thinnest samples provide evidence for the above mentioned suggestions. It should be noted that doping with strong impurities has a qualitatively similar effect on the CDW properties (the broadening of transition, decrease of $T_{\rm p}$, growth of $E_{\rm T}$) (Mutka et al. 1984). In both cases with decreasing distance between pinning centers (impurities, contacts or surface) the phase coherence length is reduced, which results in the above mentioned effects. On the other hand the increase of purity and structural perfection of the material would promote the increase of the phase coherence lengths and would make it possible to observe above mentioned size effects in the samples with larger cross-sectional area and length.

4.5.3 3. Model of deformations and strains in the CDW

In order to explain the observed phenomena let us consider the behaviour of the coherent deformable CDW, which is pinned at the contacts of the sample with finite length. In such an elastic CDW the deformation and strains can arise, which correspond to the variations of the CDW phase $\delta\varphi$ and the wave vector $\delta q \sim \delta\varphi/L_0$, where L_0 is characteristic length of the phase growth (for example, the Fukuyama-Lee-Rice length or sample length L at $L < L_0$).

In the majority of actively studied quasi-one-dimensional conductors ($NbSe_3$, TaS_3, $K_{0.3}MoO_3$ and so on) CDW is incommensurate with pristine lattice, but is close to commensurability. The incommensurate superlattice
corresponding to CDW is softer than the rigid pristine lattice. Under the influence of the external forces the incommensurate CDW can be deformed with the appropriate variation of q and some nonlinear excitations can develop in the CDW. For example, it was shown by direct measurements that the application of electric field leads to the variation of q by several percent in the sample of $K_{0.3}MoO_3$ (Tamegai et al. 1984). In many onedimensional conductors q depends on the temperature and the CDW approaches commensurability with decreasing temperature (Monceau 1985). For instance in orthorhombic TaS_3 in the range $200 - 100$ K the longitudinal and transversal components of q varied approximately by 2% approaching fourfold commensurability (Wang et al. 1983). However according to recent results a

possibility of approaching the total commensurability is questionable. This may well be caused by the presence of impurities and defects in actual crystals, which prevents the CDW from approaching the total commensurability throughout the whole sample (Littlewood 1985).

It seems that the electronic properties of small samples can be described in terms of a two-liquid model, according to which the sample is assumed to consist of two interacting subsystems: coherent deformable CDW and quasiparticles. Strictly speaking such a model can be valid for stationary CDW, but for the moving CDW it can be valid only at the existence of a single relaxation time (Rice et al. 1979). In the case of the nonuniform deformation of the CDW space-dependent variation of its charge density $\delta\rho(x)$ appears in the sample, which is proportional to the gradient of the CDW phase $\mathrm{d}\varphi/\mathrm{d}x$. These local variations of charge density must be screened by free carriers (Rice et al. 1979, Artemenko and Volkov 1981, Artemenko et al. 1986, Sneddon 1984, Itkis et al. 1986, Borodin et al. 1986c,d, 1987a,b). As a result of these variations chemical potential level ζ will be shifted with respect to the middle of the energy gap (band bending) which will be also proportional to the gradient of the CDW phase $\mathrm{d}\varphi/\mathrm{d}x \sim \delta q \ll q$. The corresponding variation of the Peierls gap is proportional to $(\mathrm{d}\varphi/\mathrm{d}x)^2$, and at $\zeta \ll \Delta$ it is negligible (Itkis et al. 1986, Artemenko et al. 1986). Generally speaking as a result of Coulomb effects and electroneutrality any departure of CDW and q from thermodynamical equilibrium leads to the variation of the properties of one-dimensional conductors, determined by quasiparticles, for example, the sample conductance at $E < E_{\mathrm{T}}$ (Gill 1981, Itkis et al. 1986, Artemenko et al. 1986, Borodin et al. 1986c,d, 1987a,b, Barišić 1987).
The strains and deformations are reversible only at small values of $\delta q \ll q$. While large deformations, exceeding some threshold value, seem to favour a jump-like local change of the CDW phase by 2π, which releases the accumulated deformation (Itkis et al. 1986, Artemenko et al. 1986, Borodin et al. 1987b). These effects must manifest themselves most clearly
in the case of coherent CDWs in quasi-one-dimensional conductors with a totally dielectrified energy spectrum, which for example occurs in TaS_3.

The phenomenological equations, which describe such phenomena in terms of the one-dimensional model of a Peierls conductor, were obtained by Borodin et al. (1986c,d, 1987a,b). The CDW excess charge due to the departure of the CDW wave vector q from the equilibrium value q_0 is compensated by an appropriate change of the electron (n) and hole (p) concentrations:

$$n_0 \left(q - q_0\right) / q_0 + n = p, \tag{3.1}$$

where q_0 is determined by the linear electron concentration $n_0 = q_0/\pi$. In the case of weak interchain interaction this equation is also valid for volume concentrations which are equal to the linear concentrations multiplied by the number of chains within a unit cross-sectional area. Substituting the usual expression for n and p in eq. (3.1), we obtain (Borodin et al. 1987b):

$$n_0 \left(q - q_0\right) / q_0 = -2Ne^{-\Delta/T} \sinh(\zeta/T), \tag{3.2}$$

where ζ is the energy of the chemical potential level measured from the middle of the Peierls gap, N is the effective state density, which is assumed to be equal for electrons and holes. This equation expresses the relationship between ζ and q. The weak field conductivity is determined by free electrons and holes and according to eqs. (3.1) and (3.2) it is equal to

$$\sigma = 2e\mu N \mathrm{e}^{-\Delta/T} \cosh(\zeta/T) = en_0\mu \left(q - q_0\right) / q_0 \coth(\zeta/T), \tag{3.3}$$

where the mobilities of electrons and holes are assumed to be equal to $\mu = \mu_{\mathrm{n}} = \mu_{\mathrm{p}}$.

The model outlined above together with eqs. (3.2) and (3.3) can be used for the analysis of the step-like temperature dependence $R(T)$ of small samples (figs. 1 and 3). In small samples with coherent CDW pinned at contacts there is a set of discrete values of $q = q_{\mathrm{m}} \simeq 2\pi m/L$,

each corresponding to a certain metastable state of CDW. As a result of the variation of q with temperature the sample repeatedly finds itself in one of these states at $q = q_{\rm m} = \text{const}$, and within a certain temperature range ΔT between jumps it can be in it (fig. 4). Since within this range, ΔT, the magnitude of q does not change, the dependence of R on T is hysteresisless. However, as can be seen from eq. (3.2), at $q - q_0 = \text{const}$ the value of ζ must change with temperature. This change of ζ corresponds to the onset of internal uniform reversible CDW strain and the change in the free energy of the electron system. In a sense this is similar to the behaviour of an elastic spring when heated with both ends fixed.

The activation energy of conductivity in accordance with (3.3) at constant Δ is equal to

$$\epsilon = \Delta - \tanh(\zeta/T)\mathrm{d}(\zeta/T)/\mathrm{d}(1/T). \tag{3.4}$$

As can be seen from eq. (3.4) ϵ depends on the position of the chemical potential level and the velocity of its variation as a function of temperature. In the range between jumps at $q - q_0 = \text{const}$ the activation energy is equal to $\epsilon^* = \Delta\left(1 - \tanh^2(\zeta/T)\right)$ and is always smaller than in the sample with large cross-sectional area. Indeed in the experiment we obtain $\epsilon^* \simeq 200$ K (fig. 3). Using this value of ϵ^* and the value of $\Delta = 800$ K we can determine the shift of the chemical potential level $\zeta/T = -1.3$. The negative sign of ζ is obtained from (3.2) at $q - q_0 > 0$, which is characteristic for orthorhombic TaS_3 (Wang et al. 1983). This means that in orthorhombic TaS_3 the chemical potential level at $T \approx 100$ K is shifted from the middle of the gap by a value larger than kT. This result is in good agreement with data on the thermopower (Fisher B. 1983, Higgs 1985, Itkis et al. 1986) and Hall effect (Latyshev et al. 1983) which both correspond to p-type conductivity.

Upon subsequent change of temperature beyond the range ΔT the departure of q from the thermodynamic equilibrium value exceeds the value $\delta q = \pm 2\pi/L$ and CDW passes into a new metastable state by a jump-like change of the CDW phase difference by 2π. This corresponds to the creation (or disappearance) of one new CDW period in the sample. Knowing from experiment the temperature dependence of $\tilde{q}(T)$, averaged throughout a large sample (Wang et al. 1983), we can estimate the magnitude of temperature interval between jumps $\Delta T = \delta q(\ \mathrm{d}\tilde{q}/\mathrm{d}T)^{-1}$. The substitution of the data obtained by Wang et al. (1983) gives for $\delta q = 2\pi/L (L = 20\mu\ \mathrm{m}) T = 1$ K which is in good agreement with the values of ΔT observed by us (fig. 3). Similarly the jump magnitude can be estimated from eq. (3.3). At $|\zeta|T \gg 1, \delta\sigma/\sigma_0 = \delta q/(q - q_0)$. For a sample 20μ m long and $q - q_0 = 2 \times 10^{-3} q_0$ at $T = 100$ K (Wang et al. 1983) we obtain $\delta\sigma/\sigma = 3\%$ which is also in good agreement with experiment. Thus the appearance (or disappearance) of one CDW period in the sample, with a corresponding appearance of $2e$ charge per each chain, can be revealed by an approximately ten percent change in the resistance of small samples, while the relative change of q after jump is very small $\delta q/q_0 \sim 10^{-4}$. Figure 4 shows that at a fixed temperature in actual samples some metastable state exist and the transitions can occur not only in the nearest but also in one of the neighbouring states (states 2 and 4).

A similar jump-like transition between metastable states, releasing the strains and deformations of CDW, can take place under the influence of current I but at constant temperature. This effect occurs also in the range of currents smaller than threshold current $I_{\rm T}$ (fig. 7). The effect of external electric field on CDW and q is similar to the effect of temperature in that it promotes the transition between metastable states (see also Ong et al. 1985a). In the samples containing a certain small number of domains the system of jumps on the $R(T)$ curve corresponds to the possibility of several spatial phase distributions being realized, which reflect the individual features of domain distribution and pinning forces in them. In a sense this case is analogous to the dependence of conductivity of a mesoscopic sample on the spatial distribution of impurities.

The first studies of CDW deformation and its influence on the properties of quasi-one-dimensional conductors were carried out using samples with a large cross-sectional area (see Monceau 1985). It was found for example that the resistance of TaS_3 samples, measured after cooling or heating can differ by about 10% from a certain equilibrium value, which was obtained after application of the voltage pulse $V \geqslant 4V_\Gamma$ (Hutiray et al. 1983). This effect can be accounted for by the fact that the CDW after a change in temperature is in some nonequilibrium deformable metastable state with an average value of q differing from the thermodynamic equilibrium value for a given temperature. At the same time as was suggested by Hutiray et al. (1983) the value of the Peierls gap changes too, which results in a change of the weak field conductivity. The application of the pulse of voltage $V \geqslant 4V_T$ removes this deformation.

After a more thorough study, however, it turned out that the sample resistance measured after the application of a pulse of voltage $V > V_T$ depends on the sign of this voltage. The subsequent investigations lead to the suggestion that under the influence of the electric field CDW deforms so that it is compressed in the vicinity of one current contact and stretched near the other (Janossy et al. 1984, Mihaly and Janossy 1984). When the electric field is removed this CDW deformation is pinned on the impurities and is gradually relaxed to the equilibrium. However at low temperatures relaxation times are very large (G. Mihaly and L. Mihaly 1984, Ong et al. 1985a) and the change of the sample properties is negligible during the time of the usual measurement. As a result of direct (Mihaly and Janossy 1984) and indirect (Janossy et al. 1984) measurements it was found that the resistance of one half of the sample increases while that of the other half decreases. The total effect of these changes on the sample resistance is small and depends on the asymmetry of the CDW deformation in the halves of the sample. However at that time the physical nature of such variation of the sample resistance was not completely understood, and the question of the character of the CDW deformation and the appropriate characteristic lengths was also unclear.

In order to decide on these questions we used a new method to study the deformations in CDW (Itkis et al. 1986). As was shown before the variation of conductivity in the range of deformation of the CDW seems to be due to the shift of the chemical potential level, which can be determined by the change in the differential thermopower $\delta S \sim \delta\zeta/T$ (Itkis et al. 1986). The experiment was carried out as follows. The nonuniformity of the sample properties due to remanent deformation of the CDW was revealed by producing two temperature gradients with opposite sign in the sample. For
this, TaS_3 samples fixed over the substrate were illuminated by laser beam with approximately 10μ m in diameter. The temperature under the light spot could increase by several degrees and decreased linearly towards the contacts. It was observed that the value of some background thermopower E_0 significantly changed as a result of passing the pulses of voltage V_p above threshold voltage V_T (fig. 9). The magnitudes of these changes E_1 and E_2 depend on the value and the sign of the V_p. Moreover this dependence had a hysteretic form. When the laser beam moved along the sample we obtained the dependence of the magnitude of the hysteretic loop $E_v = E_1 - E_2$ on the position of the illumination point x_0. From simple calculations it follows that $\mathrm{d}E_v(x_0)/\mathrm{d}x_0 = \delta S(x_0)$-const, where $\delta S(x_0)$ is the local change of differential thermopower and the magnitude of the constant is independent of x_0. Figure 10 shows the experimental dependences $E_v(x_0)$ (a), $\mathrm{d}E_v/\mathrm{d}x_0 \sim \delta S(x_0)$ (b) as well as a diagram of the corresponding band bending (c). As can be seen from fig. 10 CDW is compressed near one contact and stretched near the other. The deformation is maximal in the vicinity of the contacts and extends within the sample over a macroscopic distance of $\approx 300\mu$ m. Qualitatively similar results were obtained by Brown et al. (1986), when they measured the spatial distribution of the remanent deformation with a moving electric contact. In our $\sim$ 1 mm long samples according to estimates the difference between the CDW phase in the middle of the sample and

at the contacts was as large as 30π. The spatial phase

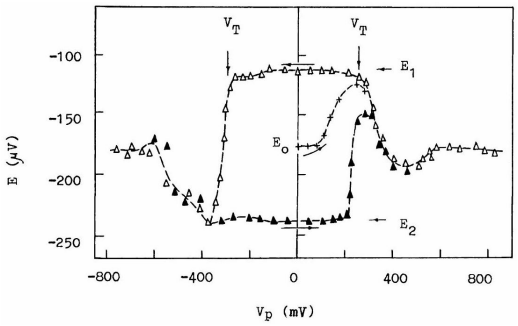


Fig. 9. The dependence of thermopower on the previously applied voltage V_{p} .($\mathbf{\Delta}$) V_{p} varies from -800 to +800 mV and (△) from +800 to -800 mV , (+) with variation of V_{p} from the initial state at E_0.$T = 125$ K.

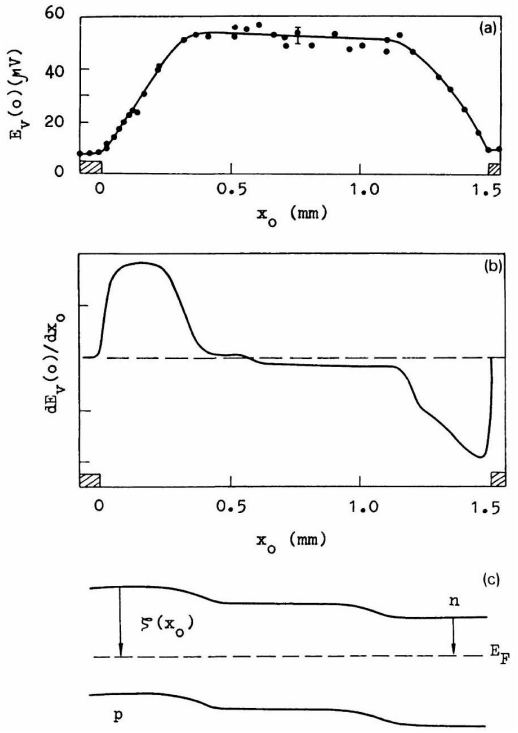


Fig. 10. (a) The dependence of the half-width of the hysteretic loop $E_{\mathrm{v}}(0)=\left(E_{1}-E_{2}\right) / 2$ (fig. 9) on the coordinate of the point at which the sample is illuminated; (b) the dependence of $\mathrm{d}E_{\mathrm{v}}(0)/\mathrm{d}x_0$ on x_0, which determined the spatial distribution of the remanent CDW deformation; (c) the schematic diagram of the corresponding band bending.

variation by successive 2π jumps helps the total energy of the system to be maintained at the minimum. In this case in our samples the characteristic length of a phase variation of 2π (domain length) was equal to $\approx 20\mu$ m. In the case of large concentrations of weak impurities this length corresponds to the Fukuyama-Lee-Rice length. In the case of rare strong impurities it corresponds to the average distance between them. It seems most probable that the latter case takes place in our samples with small impurity concentrations (the average distance between impurities along the chain is approximately $\approx 10\mu$ m).

As can be seen this length is not small and its value corresponds to the above mentioned estimates and the result of the measurements of the phase coherence length $l_{\|}$of the stationary CDW. In the moving CDW this length can considerably grow (Fisher D. 1985), i.e., the coupling between phases of different points of the CDW can exist over large distances ~ 0.1 mm. Accordingly the nonlocal effects can be observed over the same distances (Gill 1982, Artemenko et al. 1986). At low temperatures, when the length of the electrical screening by quasiparticles grows considerably, the possibility of observation of nonlocal effects due to deformation and polarization of the CDW are also growing. Indeed as was shown (Saint-Lager et al. 1987b, Zaitsev-Zotov 1987) the distortion of the CDW in one part of the sample resulted in the variation of the sample properties in the other part ~ 0.1 mm away.

4.5.4 4. Phase-slip in the CDW

As was mentioned above the samples of TaS_3 commonly investigated contain a lot of phase coherent regions (domains) and in the experiment we can usually observe the properties averaged through the whole volume of the sample. After the reduction of the sample sizes we can reveal the discontinuous jump-like nature of the variation of the quasi-one-dimensional conductor properties, which is due to the discontinuous change of a phase difference in each domain by 2π.

What is the physical mechanism of the jump itself? From the data presented here it follows that the deformation of the CDW precedes the jumps and these jumps correspond to an appearance of the discontinuity within the phase coherent CDW, the change of the phase difference by 2π providing a quantitative explanation of the observed variation of R. All this unambiguously indicates that the observable jump-like changes in R are due to the phase-slip process in the CDW.

The concept of phase-slip in reference to quasi-one-dimensional conductors with CDW was initially introduced to explain the mechanism of narrow band generation (Gor'kov 1983, 1984, Ong and Verma 1983, Ong et al. 1984) and subsequently it was developed in a number of theoretical (Batistić et al. 1984, Artemenko et al. 1986) and experimental works (Verma and Ong 1984, Zhang and Ong 1984, Borodin et al. 1985, 1986a,c,d, 1987a,b, Hall et al. 1986, Gill 1986a,b). This phenomenon can be qualitatively visualized as follows. In a quasi-one-dimensional conductor with coherent CDW the growth of the gradient of the CDW phase $\mathrm{d}\varphi/\mathrm{d}x$, arising from the deformation of the CDW in the electric field, can only be
possible up to a certain critical value. This will inevitably be followed by a local (over length ξ) suppression of the order parameter (the energy gap), the disconnection of the phase coherence and the removal of the accumulative phase difference by 2π, after which the state with indeformable CDW is recovered. Further the process is periodically repeated. Moreover the phase-slip can in principle occur either over all the sample cross sections (Gor'kov 1983, 1984) or by a creation of a phase vortex and its subsequent motion across the sample (Ong and Verma 1983, Ong et al. 1984). It turned out that these processes are in many respects similar to the processes of phase-slip in narrow superconducting channels (Langer and Ambegaokar 1967, Ivlev and Kopnin 1984).

The phase-slip repeated periodically provides the conversion of the quasiparticle current into the CDW current near contacts and results in the generation of the periodic voltage oscillations when the current is regulated. Recently a number of experimental results were obtained which confirm the existence of such a mechanism. It was shown, for example, that the voltage oscillations originate in the regions of strong pinning of the CDW at the contacts. The frequency of these oscillations can be controlled by varying the temperature at one contact (Verma and Ong 1984, Zhang and Ong 1984) or by passing the d.c. current through the sample sector adjacent to this contact (Borodin et al. 1985) (see section 2.4). It was also suggested that

the additional voltage V_{ps} independent of the sample length must exist near contacts to maintain the process of phase-slip. This ought to lead to the growth of the threshold field E_T when the sample length is decreased (Gor'kov 1983, 1984, Ong and Verma 1983, Ong et al. 1984, Batistić et al. 1984). In several experiments the growth of E_T in short samples with length $L \leqslant 100\mu$ m was indeed observed (Mihaly G. et al. 1983a,b). These investigations were usually carried out in quasi-onedimensional conductors with great anisotropy, of conductivity $A = \sigma_{\parallel}/\sigma_{\perp} \sim 100$, with rather large cross-sectional areas ($10 - 100\mu$ m^2). As a result a significant region of nonuniform electric field $L \sim (SA)^{1/2} \approx 10 - 100\mu$ m existed in the vicinity of the lateral contacts, which was equivalent to the appearance of an additional resistance r and voltage near contacts (Borodin et al. 1986a). This prevented the unambiguous establishment of the fact of the existence of V_{ps} (Borodin et al. 1986a, Gill 1986a,b). The use of samples of transversal sizes $\sim ().1\mu$ m allowed us to reduce significantly the region of nonuniform electric field near contacts, to establish the existence of V_{ps}, to obtain the dependence of V_{ps} on temperature and CDW current and thus to determine the main characteristics of the phase-slip process (Borodin et al. 1987a,b). Similar results were obtained by Gill for $NbSe_3$ (Gill 1986a,b).

The current flowing through a quasi-one-dimensional conductor is due to the motion both of the quasiparticles and the CDW. With an electric field
below the threshold field in the steady regime the current is transported by quasiparticles with the CDW pinned. Both the pinned CDW and the moving CDW at $E > E_T$ can be influenced by forces of different origin. They are the forces of the pinning of the impurities and defects within the volume of the sample, on its surface (that force is especially essential in thin samples) and finally on the contacts. Besides it is necessary to take into account a definite friction force resulting from the interaction between the moving CDW and the quasiparticles. The ratio between these forces, which determine the value of E_T and the character of the CDW motion, depends on the purity and the sizes of the samples. For example in samples, where E_T is largely determined by the pinning of the CDW on the surface or at the contacts, the CDW before the threshold can become free from the pinning in the volume, and can slightly change its phase configuration and begin to deform. Perhaps the variation of the differential resistance in the region $I < I_T$ observed by us in small samples (fig. 7) is accounted for these effects. The pinning forces in the volume and on the surface of a homogeneous sample and the corresponding field E_T are independent of the sample length L. While the additional voltage V_{ps} resulting from the phase-slip process and the conversion of the CDW current into a quasiparticle current is independent of L. When the CDW moves, the voltage, which is equal to the sum of the above mentioned contributions, will exist on the sample and this voltage itself will affect the quasiparticles:

$$U = E_c\,(I_c)\,L + V_{ps}\,(I_c) = \rho L I_q, \tag{4.1}$$

where ρ is the resistance per unit length of the sample at $I < I_T, I_c = I - U/R$ is the current arising from the motion of the CDW, I_q is the quasiparticle current. The approximate equivalent circuit of the sample is shown in the inset in fig. 11. The threshold current I_T can be determined as the current corresponding to some minimal CDW current $I_c^* \ll I_T$ which first became detectable. Then from eq. (4.1) we can obtain the dependence of I_T on the sample length:

$$I_T = V_{ps}\,(I_c^*)\,/\rho L + E_c\,(I_c^*)\,/\rho. \tag{4.2}$$

As was shown (Borodin et al. 1987b) the dependence $I_T(L)$ does not include the spreading resistance near the contacts, due to the nonuniformity of the electric field, and the growth of $\boldsymbol{I}_T$ resulting from eq. (4.2) as L is reduced provides stronger evidence for the existence of the V_{ps} (Borodin et al. 1986a, Monceau et al. 1986). The dependence of I_T on L measured by us

in thin samples is shown in fig. 11. As can be seen from fig. 11 in samples with length which is smaller than $\approx 50\mu$ m a significant growth of I_{T} is observed. The dependence $I_{\mathrm{T}}(L)$ which is calculated in accordance with eq. (4.2) and shown in the same figure (dashed line) is consistent with the experiment. As follows from eqs. (4.1) and (4.2) the contributions from the

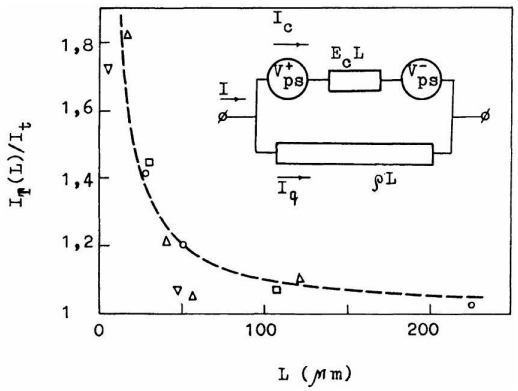


Fig. 11. The dependence of threshold current I_{T} on the length of the section L for various samples. The value of I_{T} is normalized by the value of threshold current I_{t} for the longest section of each sample. The dashed curve shows the calculated dependence according to eq. (4.2) at $V_{\mathrm{ps}} = 1\mathrm{mV}, E_{\mathrm{c}} = 1$ V/cm. The inset shows the equivalent circuit for a one-dimensional conductor with coherent CDW. L is the sample length, ρ the linear resistivity at $I < I_{\mathrm{T}}, E_{\mathrm{c}}(I_{\mathrm{c}})$ the electric field corresponding to the CDW motion in the volume of the sample at current I_{c}; V_{ps}^{+} and V_{ps}^{-} are the voltages due to the phase-slip of the CDW and the conversion of the CDW current into the quasiparticle current I_{q}.

uniform pinning (volume, surface) and from the local pinning on the contacts become comparable at $L = V_{\mathrm{ps}}/E_{\mathrm{c}}$, which corresponds to the sample length $L \approx 10\mu$ m at the above mentioned values of V_{ps} and E_{c}. Since the lengths of many of our samples were of the order of 10μ m it is necessary in the analysis of their properties to take into account both contributions to the value of I_{T}.

In order to pick up the contribution of V_{ps} only, and to determine its dependence on I_{c} and temperature, it is necessary to 'subtract' $I - V$ curves of two sections of the same sample with different lengths L_1 and L_2 :

$$V_{\mathrm{ps}}(I_{\mathrm{c}}) = (U_1 R_2 - U_2 R_1) / (R_2 - R_1), \tag{4.3}$$

where R_1 and R_2 are the resistances of the sections at $I < I_{\mathrm{T}}$. In eq. (4.3) we must use the values of voltage U_1 and U_2 at the same CDW current I_{c}. As was shown (Borodin et al. 1987b) the error in the determination of the V_{ps} from eq. (4.3), which is due to the nonuniformity of the electric field near the contacts, is within 1% in our case of thin samples with coherent CDW. Figure 12 shows the typical set of dependences $V_{\mathrm{ps}}(I_{\mathrm{c}})$ at different temperatures obtained from eq. (4.3) for two sections $L_1 = 30\mu$ m and $L_2 = 105\mu$ m of sample 9 with cross-sectional area $S = 0.15\mu$ m^2. As can be seen

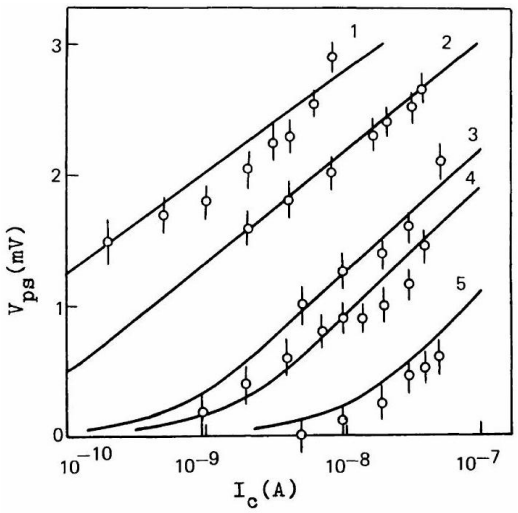


Fig. 12. The dependence of V_{ps} on CDW current I_{c} at various temperatures for sample 9. Solid lines: the dependences $V_{\mathrm{ps}}(I_{\mathrm{c}})$ calculated from eq. (4.4) at $F = 2500$ K, $\eta = 60e$, $I_0 = 3.5$ A. Temperatures: (1) 100 K , (2) 111 K , (3) 128 K , (4) 134 K , (5) 151 K .

from fig. 12 the dependence of V_{ps} on I_{c} is not strong $-V_{\mathrm{ps}}$ grows approximately logarithmically with increasing I_c. At the same time the values of V_{ps} obtained at a given current I_{c} varies significantly with temperature. For instance at $I_{\mathrm{c}} = 10^{-8}$ A, V_{ps} decreases approximately by a factor of 10 while the temperature increases only by a factor of 1.5 (fig. 12). The observed strong dependence of V_{ps} on T points to the essential importance of the thermal activation in the phase-slip process.

As was noted the phase-slip can occur only in a case when the energy gap in some local region of the sample becomes equal to zero. This requires a certain energy F, which is the energy barrier between the states of CDW before phase-slip and after it, i.e., before and after creation (or disappearance) of one CDW period. The probability of overcoming such a barrier by thermodynamical fluctuations is proportional to $\mathrm{e}^{-F/T}$. Moreover the variation of temperature apart from the activation effect can induce the internal strain in the pinned CDW (for example due to the dependence of q on T) and thereby it results in the decrease of the barrier height. The application of the voltage reduces the effective height of the barrier by $\sim \eta V_{\mathrm{ps}}$, where η is the charge which passes during phase-slip by 2π. Taking into account of the foregoing and the deep physical analogy between phase-slip processes in superconductors and quasi-one-dimensional conductors it is possible to write the following expression for the current I_{c}, which is attributed to this process (Langer and Ambegaokar 1967, Ivlev and Kopnin 1984, Gill 1986a,b, Borodin et al. 1987a,b):

$$I_{\mathrm{c}} = I_0 \mathrm{e}^{-F/T} \sinh\left(\eta V_{\mathrm{ps}}/2T\right), \tag{4.4}$$

Using this equation the values of parameters η and F can be estimated from the experimental data of fig. 12. The value of η can be derived from the slope of the linear regions of $I_{\mathrm{c}}(V_{\mathrm{ps}})$ curves at a constant temperature assuming η and F are not dependent on I_{c}. Owning to a certain scattering of experimental points we give the average value of $\eta = 60e$, where e is the electron charge. The value of F can be derived, for example, from either the dependence of V_{ps} on T for a given I_{c} or from the activation dependence of I_{c} on T for a given V_{ps}. In both cases from fig. 12 we can obtain some average value of $F = 2500$ K. Substituting these values in eq. (4.4) and taking $I_0 = 3.5$ A as a fitted parameter we can obtain the dependences which are shown by solid lines in fig. 12. As can be seen from fig. 12 the experimental data for small samples of TaS_3 are well described by eq. (4.4) for the temperature range measured.

The values of parameter η/e, which were derived from five $V_{\rm ps}\,(I_{\rm c})$ curves for sections of different lengths in three samples are within $30-80$. The value of the energy barrier per one electron, which is of the order of the condensation energy per one electron eF/η, is within $4-6$meV$(40-60$ K). Assuming the value of η/e is equal to the number of electrons which were transformed from condensed state to normal and passed through the range of the phase-slip, we can estimate the volume of this range $v_\lambda = \eta/en$, where n is the concentration of carriers in the normal state. Substituting $n \simeq 10^{21}$ cm^{-3} for TaS_3 we obtain $v_\lambda = 6\times10^{-20}$ cm^{-3}. Dividing v_λ by the length of the CDW period (period of the superlattice) $\lambda = 4c \simeq 13.4$Å we obtain the cross-sectional area of the phase-slip region $S_{\rm ps} = 4.5\times10^{-13}$ cm^2 and the appropriate transverse size of this region ≈ 70 A. Generally speaking the possibility of existence of such transversal correlation lengths of the CDW cannot be excluded. It should be noted, however, that the value of $S_{\rm ps}$ is quite close to the value of the transversal area of the unit cell of the CDW superlattice in $TaS_3, 9\times10^{-13}$ cm^2 (Monceau 1985), especially taking into account that the CDW can be formed only on half of the number of the chains of the unit cell as it takes place in $NbSe_3$. In this case the same electron concentration would correspond to a twice greater cross-sectional area $S_{\rm ps} \simeq 9\times10^{-13}$ cm^2.

The value of $S_{\rm ps}$ is approximately the $10^{-2}-10^{-3}$ part of the crosssectional area of our samples. In the case when only a single phase-slip center (PSC) exists in the whole cross section of the sample it would be impossible to notice the appropriate jump-like change of the sample resistance with variation of the electric field or temperature. Therefore most probably the PSC outlined above nucleates in a small part of the sample
cross section of the order of the size of the unit cell as a nucleus or a dislocation, and then propagates in the phase coherent CDW through the whole of the crystal cross section (Ong and Verma 1983, Ong et al. 1984, Gill 1986a,b, Borodin et al. 1987b). Indeed, the coherent CDW with the appropriate superlattice is a kind of 'electron crystal', in which deformations and dislocations can be produced by external forces similarly to the usual crystal solid. These deformations and dislocations will determine the yield point of this electron crystal (Lee and Rice 1979, Feinberg and Friedel 1988). The greatest deformations and strains in CDW arise at the contacts, perhaps at the impurity centers of strong pinning and on the roughness of the sample surface (Borodin et al. 1987b, Yetman and Gill 1987, Feinberg and Friedel 1988). Just at that spot the distortion of the CDW lattice (PSC) will be produced by the electric field and thermodynamical fluctuations. They can be considered as edge or screw dislocations (Feinberg and Friedel 1988). These dislocations (PSC) will propagate across the electronic crystal (CDW), providing an abrupt decrease of the phase difference. The energy needed to start their motion is a hundred times smaller than for the phase shift of one part of the crystal relative to the other (Feinberg and Friedel 1988). The slope of the CDW wave vector q in TaS_3 with respect to the greatest conductivity axis can also make a contribution. In accordance with the estimates made for TaS_3 (Feinberg and Friedel 1988) the critical voltage at the contacts needed to initiate dislocation motion is equal to $V = 2.5$mV, which is surprisingly close to the values $V_{\rm ps}$ obtained by us.

When the barrier blocking the motion of dislocations has been surmounted the subsequence of their motion can occur with smaller friction with a reduced voltage on the sample. This suggestion can be one of the possible explanations of the negative differential resistance observed by us (fig. 7). The motion of dislocations can be rather synchronized which accounts for the observed narrow band generation. At the fairly strong electric field the shearing movement of the CDW as a whole evidently becomes possible at least in some part of the sample volume.

It is natural that similar processes of removal of strains owing to the creation of the PSC can occur with variation of the temperature in the CDW pinned on the contacts, the wave vector of which depends on temperature. With variation of q versus T the value $q = q_m$ fixed in the sample departs more and more from the equilibrium value at a given temperature. As a

result the internal strains in the CDW are growing. This case is similar to the effect of external forces on the CDW. On reaching some critical strain in the CDW the production of the PSC will occur with the assistance of thermodynamical fluctuations. The PSC propagates across the sample cross section and results in the jump-like change of its resistance. The quantitative calculations carried out above confirm this qualitative picture. The phase-slips in the separate domains provide the relaxation
of the metastable states in the sample with remanent deformation of the CDW under the influence of thermodynamical fluctuations at $E = 0$ and $T = \text{const}$ (Borodin et al. 1986c, Gill 1986a,b). This process has a cascade character and as a result the relaxation turns out to be proportional to $\lg t$ (Mihaly G. and Mihaly L. 1984, Ong et al. 1985a, Gill 1986a,b), but with the finite height of the barrier for the PSC nucleation the stable state can be reached within a finite time t_0 (Ong et al. 1985a). Naturally the increase of temperature and the application of electric field accelerate the process of relaxation (Mihaly G. and Mihaly L. 1984, Ong et al. 1985a).

4.5.5 5. Conclusion

The total combination of the data obtained by us gives a strong evidence for the existence of the phase coherent CDW within the whole volume of small TaS_3 samples under investigation. If the coherent CDW is pinned on the contacts variation of temperature and electric field leads to a creation of strain and deformation, a shift of the chemical potential level and variations in conductivity and differential thermopower. On reaching the critical deformations in the coherent CDW similar to the electron crystal, the nucleation of the PSCs (dislocations) and their subsequent motion occurs. These processes determine the threshold properties of the CDW, the conversion of the quasiparticle current into the CDW current and the narrow band generation. In pure homogeneous samples with a great electron mean free path length and a large phase coherence length a single domain case can be realized with rather large sizes of samples. Perhaps these conditions are easier to achieve in such material as $NbSe_3$ whose phase coherence length is larger than in TaS_3. In such samples at the electric field above the threshold field the motion of the CDW will be determined by the processes of the PSC nucleation at the contacts, and the spectra of narrow band generation will contain one fundamental line and its harmonics.

The results obtained by us extend the application of the concept of the phase-slip. Besides the previous interpretation of phenomena in the electric field above threshold E_T in terms of PSC, it turns out that their role in the processes at $E < E_T$ - the jump-like change of the resistance with variation of current and temperature is also important. In this case PSC is the result of the thermoactivation process. In small samples it is possible to record directly the resistance change owing to the single act of phase-slip by 2π. In large samples, which contain a lot of domains, similar jumps can occur in each of them.

The concept of deformation and phase-slip of the CDW proves to be useful in explaining many other effects which are observed in quasi-one-
dimensional conductors. For example, the observation only of integral numbers of periods of the voltage oscillations at the application of repetitive current pulses (Ido et al. 1986, Fleming and Schneemeyer 1986a) is probably associated with the possibility of the generation only of integral numbers of the PSC, i.e., with the discreteness of its nucleation process. From the result obtained it also follows that it is not quite correct to speak of independent separate contributions to the conductivity on the part of quasiparticles and on the part of the CDW together with its nonlinear excitations. We see that in reality they are closely connected and are dynamically interacting systems. Any motions of the CDW are accompanied by the motion of the quasiparticle and to a great extent are determined by them. For example in reality the

so-called CDW current I_c depends significantly on the quasiparticle motion both at the moment of phase-slip (when the energy gap is equal to zero) and during deformations and scattering of the CDW on quasiparticles. This is the cause of the observed scaling between the value of the ohmic conductivity ($E < E_T$) and the differential conductivity at $E > E_T$ (Ong et al. 1985b) and this is also the cause of similarity of their activation dependencies on temperature (Fleming and Schneemeyer 1986b). Perhaps the variation of the Hall coefficient after the beginning of the CDW motion is explained in the same manner (Artemenko et al. 1984, Forro et al. 1986).

With decreasing temperature the number of free carriers decreases significantly, the Thomas-Fermi screening length grows and simultaneously the electron mean free path length can decrease due to the enhancement of the electron localization. In this case the effective screening of charges arising from CDW deformation and polarization becomes difficult and they can be directly revealed in the experiment. This accounts for the observed remanent polarization in blue bronze (Cava et al. 1984) and probably also in the nonlocal effects in $NbSe_3$ (Gill 1982, Saint-Lager et al. 1987b) and TaS_3 (Zaitsev-Zotov 1987). At the same low temperatures the phase jumps on the domain boundary can be important for electrical conductivity and its frequency dependence and also for the optical properties of large samples (Zhilinskii et al. 1983, Littlewood 1985, Nad' 1985). In the many quasi-onedimensional materials the CDW approaches to commensurability with decreasing temperature. The deformation of such a CDW and the nucleation of the PSC in it become difficult and the nonlinear effects weaken. This is confirmed by experiments on elongation of TaS_3 crystals bringing them into commensurate state (Preobrazhensky 1985).

The data presented in this paper are the result of a number of collaborations with D.V. Borodin, M.E. Itkis, V.Ya. Pokrovskii and S.V. Zaitsev-Zotov. I would like to thank them for their collaboration. I would also like to thank Ya.S. Savitskaya and V.V. Frolov for providing the samples.

4.5.6 References

Artemenko, S.N., and A.F. Volkov, 1981, Sov. Phys.-JETP 54, 992.
Artemenko, S.N., E.N. Dolgov, A.N. Kruglov, Y.I. Latyshev, Ya.S. Savitskaya and V.V. Frolov, 1984, JETP Lett. 46, 891.
Artemenko, S.N., A.F. Volkov and A.N. Kruglov, 1986, Sov. Phys.-JETP 64, 906.
Barišić, S., 1987, Low Dimensional Conductors and Superconductors, Series B Physics, Vol. 155, eds D. Jérome and L.G. Caron (Plenum Press, New York) p. 395.
Batistić, I., A. Bjeliš and L.P. Gor'kov, 1984, J. Phys. (France) 45, 1049.
Borodin, D.V., S.V. Zaitsev-Zotov and F.Ya. Nad', 1985, JETP Lett. 41, 416.
Borodin, D.V., S.V. Zaitsev-Zotov and F.Ya. Nad', 1986a, Sov. Phys.-JETP 63, 184.
Borodin, D.V., S.V. Zaitsev-Zotov and F.Ya. Nad', 1986b, Preprint IRE, No. 4.
Borodin, D.V., S.V. Zaitsev-Zotov and F.Ya. Nad', 1986c, JETP Lett. 43, 625.
Borodin, D.V., F.Ya. Nad', Ya.S. Savitskaya and S.V. Zaitsev-Zotov, 1986d, Physica B 143, 73.
Borodin, D.V., S.V. Zaitsev-Zotov and F.Ya. Nad', 1987a, in: Proc. 2nd All-Union Symp. on Nonuniform Electronic States, Novosibirsk, 1987, ed. L.A. Boyarskii, pp. 12 and 14 (Scientific Council USSR Academy of Science Low Temperature Physics).
Borodin, D.V., S.V. Zaitsev-Zotov and F.Ya. Nad', 1987b, Zh. Eksp. & Teor. Fiz. 93, 1394.
Brown, S.E., L. Mihaly and G. Grüner, 1986, Solid State Commun. 58, 231.
Cava, R.J., R.M. Fleming, E.A. Rietman, R.G. Dunn and L.F. Schneemeyer, 1984, Phys. Rev. Lett. 53, 1677.
Chen, J., M.C. Saint-Lager and P. Monceau, 1987, in: 2nd European Workshop on CDW, Aussois, Abstracts, p. 14.

Efetov, K.B., and A.I. Larkin, 1977, Sov. Phys.-JETP 45, 1243.
Feinberg, D., and J. Friedel, 1988, J. Phys. (France) 49, 485.
Fisher, B., 1983, Solid State Commun. 46, 227.
Fisher, D.S., 1983, Phys. Rev. Lett. 50, 1486.
Fisher, D.S., 1985, Phys. Rev. B 31, 1396.
Fleming, R.M., and L.F. Schneemeyer, 1986a, Phys. Rev. B 33, 2930.
Fleming, R.M., and L.F. Schneemeyer, 1986b, Phys. Rev. B 33, 5450.
Forro, L., J.R. Cooper, A. Janossy and K. Kamaras, 1986, Phys. Rev. B 34, 9047.
Fukuyama, H., and P.A. Lee, 1978, Phys. Rev. B 17, 535.
Gill, J.C., 1981, Physica B 108, 1033.
Gill, J.C., 1982, Solid State Commun. 44, 1041.
Gill, J.C., 1986a, Physica B 143, 49.
Gill, J.C., 1986b, J. Phys. C 19, 6589.
Gor'kov, L.P., 1983, JETP Lett. 38, 67.
Gor'kov, L.P., 1984, Sov. Phys.-JETP 59, 1057.
Grüner, G., and A. Zettl, 1985, Phys. Rep. 119, 117.
Hall, R.P., M.F. Hundley and A. Zettl, 1986, Physica B 143, 152.
Higgs, A.W., 1985, in: Charge Density Waves in Solids, Lecture Notes in Physics, Vol. 217, eds Gy. Hutiray and J. Sólyom (Springer, Berlin) p. 442.
Higgs, A.W., and J.C. Gill, 1983, Solid State Commun. 47, 737.
Hutiray, Gy., and J. Sólyom, eds, 1985, Charge Density Waves in Solids, Lecture Notes in Physics, Vol. 217 (Springer, Berlin).
Hutiray, Gy., G. Mihaly and L. Mihaly, 1983, Solid State Commun. 47, 121; 737.
Ido, M., Y. Okajima and M. Oda, 1986, Phys. Soc. Jpn. 55, 2106.
Itkis, M.E., F.Ya. Nad' and V.Ya. Pokrovskii, 1986, Sov. Phys.-JETP 63, 177.
Ivlev, B.I., and N.B. Kopnin, 1984, Usp. Fiz. Nauk 142, 435.
Janossy, A., G. Mihaly and G. Kriza, 1984, Solid State Commun. 51, 63.
Klemm, R.A., and M.O. Robbins, 1986, Physica B 143, 76.
Langer, J.S., and V. Ambegaokar, 1967, Phys. Rev. 164, 498.
Latyshev, Y.I., Ya.S. Savitskaya and V.V. Frolov, 1983, JETP Lett. 38, 541.
Lee, P.A., and T.M. Rice, 1979, Phys. Rev. B 19, 3970.
Mihaly, G., and L. Mihaly, 1984, Phys. Rev. Lett. 52, 149.
Mihaly, G., Gy. Hutiray and L. Mihaly, 1983a, Phys. Rev. B 28, 4894.
Mihaly, G., Gy. Hutiray and L. Mihaly, 1983b, Solid State Commun. 48, 203.
Mihaly, L., and G. Grüner, 1984, Solid State Commun. 50, 807.
Mihaly, L., and A. Janossy, 1984, Phys. Rev. B 30, 3530.
Monceau, P., ed., 1985, Electronic Properties of Inorganic Quasi-One-Dimensional Compounds, Part II (Reidel, Dordrecht) p. 139.
Monceau, P., M. Renard, J. Richard and M.C. Saint-Lager, 1986, Physica B 143, 64.
Mutka, H., S. Bouffard, G. Mihaly and L. Mihaly, 1984, J. Phys. (France) 45, L-113.
Nad', F.Ya., 1985, in: Charge Density Waves in Solids, Lecture Notes in Physics, Vol. 217, eds Gy. Hutiray and J. Sólyom (Springer, Berlin) p. 286.
Ong, N.P., and G. Verma, 1983, Phys. Rev. B 27, 4495.
Ong, N.P., G. Verma and K. Maki, 1984, Phys. Rev. Lett. 52, 663.
Ong, N.P., D.D. Duggan, C.B. Kalem and T.W. Jing, 1985a, in: Charge Density Waves in Solids, Lecture Notes in Physics, Vol. 217, eds Gy. Hutiray and J. Sólyom (Springer, Berlin) p. 387.
Ong, N.P., C.B. Kalem and J.C. Eckert, 1985b, Phys. Rev. B 30, 2902.
Preobrazhensky, V.B., A.N. Taldenkov and S.Yu. Shabanov, 1985, Solid State Commun. 54, 399.

Rice, T.M., P.A. Lee and M.C. Cross, 1979, Phys. Rev. B 20, 1345.
Saint-Lager, M.C., M. Prester, P. Monceau and M. Renard, 1987a, in: 2nd European Workshop on CDW, Aussois, Abstracts, p. 30.
Saint-Lager, M.C., M. Renard and P. Monceau, 1987b, in: 2nd European Workshop on CDW, Aussois, Abstracts, p. 32.
Sherwin, M.S., and A. Zettl, 1985, Phys. Rev. B 32, 5536.
Sneddon, L., 1984, Phys. Rev. B 29, 719.
Tamegai, T., K. Tsutsumi, S. Kagoshima, Y. Kanai, M. Tani, M. Tomozawa, M. Sato, K. Tsuji, J. Harada, M. Sakata and T. Nakajima, 1984, Solid State Commun. 51, 585.
Verma, G., and N.P. Ong, 1984, Phys. Rev. B 30, 2928.
Wang, Z.Z., H. Salva, P. Monceau, M. Renard, C. Roucau, R. Ayroles, F. Levy, L. Guemas and A. Meerschaut, 1983, J. Phys. (France) 44, L-311.
Yetman, P.J., and J.C. Gill, 1987, Solid State Commun. 62, 201.
Zaitsev-Zotov, S.V., 1987, Pis'ma v Zh. Eksp. & Teor. Fiz. 46, 453.
Zhang, X.J., and N.P. Ong, 1984, Phys. Rev. B 30, 7343.
Zhilinskii, S.K., M.E. Itkis, I.Yu. Kal'nova, F.Ya. Nad' and V.B. Preobrazhensky, 1983, Sov. Phys.-JETP 58, 211.

This page intentionally left blank

4.6 6 Charge Density Wave Current Oscillations and Interference Effects by Zettl

Department of Physics
University of California at Berkeley
Berkeley, California 94720, USA
L.P. Gor'kov and G. Grüner

4.6.1 Contents

1. Introduction 225

2. Models of CDW motion and oscillation phenomena 229
   2.1. Single degree of freedom models 229
   2.2. Classical models with many degrees of freedom 231
   2.3. Current oscillations and microscopic pinning 233
   2.4. The tunneling model and current oscillations 235
   2.5. Phase-slip processes 237

3. Experimental issues pertaining to the narrow-band noise 238
   3.1. Volume dependence of the oscillations 238
   3.2. Periodicity of the potential 242
   3.3. Statistical measurement of the narrow-band noise 245

4. Electronic interference effects 246
   4.1. Shapiro steps 247
   4.2. Single degree of freedom models for the interference 254
   4.3. Internal modes and relevant time scales 257
   4.4. Many degree of freedom models for the interference 262

5. Driven CDWs and the theory of nonlinear dynamics 266
   5.1. Competing periodicities: the circle map 266

5.2. CDW switching and transitions to chaos 269
5.2.1. Mode locking and chaos ..... 27()
5.2.2. Models for the switching and chaotic response 272

6. Relevant length scales and domain structure 278
6.1. Intrinsic phase and velocity domains 278
6.2. Temperature gradient effects 281

7. Electro-elastic interference 284
7.1. Elastic mode locking 284
7.2. Models for the elastic mode locking 285

8. Conclusion 288
References 289

4.6.2 1. Introduction

One of the more interesting and controversial discoveries associated with transport by charge-density waves (CDWs) was the observation of distinct oscillations in the linear-chain compound $NbSe_3$ (Fleming and Grimes 1979). The oscillations have become known as narrow-band noise (NBN) because of the fluctuating character of the response and to contrast it with a broad-band component that also characterizes CDW response. Rich harmonic content is typical for the oscillatory behavior and is illustrated in the spectral analysis of fig. 1.1 (taken from the original paper by Fleming and Grimes). Also seen is the $1/f$-like behavior at lower frequencies that became known as broad-band noise (BBN). The current oscillations appear only above a sharp threshold electric field E_T that also signifies the onset of the non-Ohmic conductivity. As the dc field is increased, the fundamental frequency increases monotonically from zero. CDW conduction noise can be similarly observed if a constant total current is applied to the crystal and the response voltage is monitored. This is in fact the more usual experimental situation for ease of detection and was the method used to generate the traces of fig. 1.1.

Conduction noise, either in the form of the oscillations or the broad-band noise, has become an accepted signature of collective dc transport in density-wave systems. Other CDW materials displaying the oscillations include TaS_3 in two forms (monoclinic and orthorhombic), $(TaSe_4)_2I$ and related materials, and the blue bronzes $K_{0.3}MoO_3$ and $Rb_{0.3}MoO_3$.

To illustrate why the oscillations are significant for these systems, we begin with a brief description of Fröhlich superconductivity. It was proposed by Fröhlich (1954) that superconductivity could result from the Peierls semiconducting (CDW) state in a one-dimensional metal by moving the distortion. In a system where the CDW and the lattice are commensurate, it costs energy to translate the distortion (often referred to as commensurability pinning), whereas the incommensurate CDW has no preferred position. Therefore, the CDW can move freely provided that it is incommensurate. The energy gap at the Fermi level prevents any damping from taking place by scattering of single electrons.

While all of the materials referred to above have incommensurate CDWs,

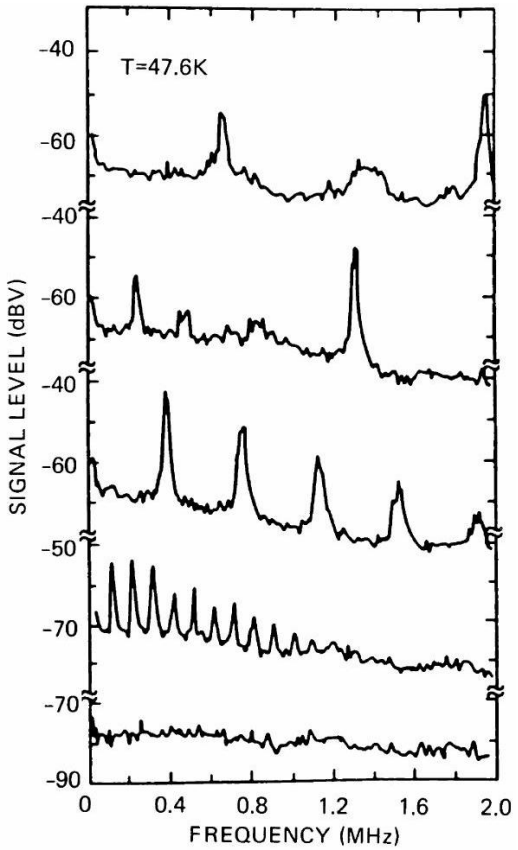


Fig. 1.1. Spectrum analysis of the voltage response for a series of current levels. (Fleming et al. 1979).

Fröhlich superconductivity is not observed for a variety of reasons. In real systems, the translational symmetry will be broken by impurities and other crystal defects, and presumably also by thermal phonons. These defects act to pin the phase of the charge-density wave, and to some degree must be responsible for a finite phase-phase coherence length. If the impurity concentration in the real CDW crystal is sufficiently small then the total pinning force may be quite weak, allowing for depinning by a modest dc electric field $E_{\rm dc}$ exceeding the depinning threshold $E_{\rm T}$. In addition to allowing for the development of a pinning force, the low-energy phase distortions provide a possible mechanism for the dissipation of energy from the CDW. Pinning and damping are always observed experimentally.

Following the discovery of the narrow-band noise, it was conjectured that the velocity of the periodic charge-density wave was modulated because of the potential created by the pinning centers (Monceau et al. 1982, Grüner et al. 1981). The time-varying velocity was responsible for the measured oscillations. Associated with this intuitive interpretation is the postulate that sliding CDW conduction and current oscillations are inseparable. In support is the observation that the excess (CDW) current and the fundamental frequency of the current oscillations are proportional. The relation is well established in $NbSe_3$ (Monceau et al. 1982, Zettl and Grüner 1984), TaS_3 (Brown and Grüner 1985), and $K_{0.3}MoO_3$. Figure 1.2 is an example depicting the linearity from Zettl and Grüner (1984).

It is often convenient to draw analogies to systems exhibiting similar behavior to CDWs, summarized by a dc threshold field for nonlinear conduction and oscillation phenomena above that threshold. Superconducting tunnel junctions and the damped, driven pendulum both share these properties. A finite current can flow at zero voltage in the junctions up to a critical density J_c. Above J_c, the dc voltage is a monotonically increasing function of the current; small voltage oscillations in addition to the dc are the ac Josephson effect. The frequency of

the oscillations is linearly proportional to the dc voltage.

Measurements of the dc current-voltage ($I-V$) curves of the junctions when microwaves are applied is fundamentally important because constant voltage steps can be observed (Shapiro 1963) whenever the condition

$$n\hbar\omega_{\text{app}} = 2eV \tag{1.1}$$

is met, giving to a high precision the ratio $\hbar/e$. In eq. (1.1), V is the dc voltage across the junction, ω_{app} is the applied microwave frequency, and n is an integer. The name Shapiro step is often associated with this interference effect.

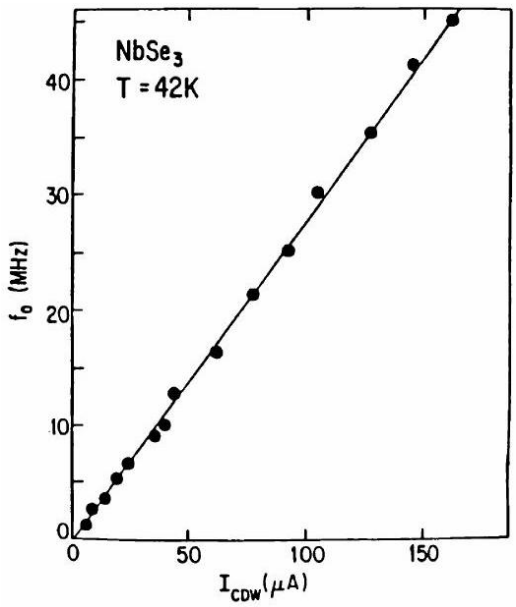


Fig. 1.2. Fundamental frequency of the oscillation response versus dc current level. (From Zettl and Grüner 1984).

The linear relationship between excess current and frequency of the oscillations for CDWs suggests that similar behavior may be realized for this system. First observed by Monceau et al. (1983), fig. 1.3 is a recording of differential resistance $\delta V/\delta I$ versus V for $NbSe_3$ from their paper. A peak in the differential resistance that increases to the Ohmic value below the threshold would indicate that the excess current does not change over the span in voltage where $\delta V/\delta I$ is high. The circumstances for which complete locking ($\delta V/\delta I$ = Ohmic value) occurs will be described in more detail in section 4 . Complete locking can often be observed at harmonic steps, which correspond to the situation

$$p\omega_{\text{app}} = \omega_0, \tag{1.2}$$

where ω_0 is the fundamental angular frequency of the oscillations and p is an integer. Experimentally, ω_0 is determined by measuring the excess current and converting that to the equivalent fundamental frequency.

In addition to the harmonic steps, there has been considerable interest in the subharmonic steps, which satisfy $(p/q)\omega_{\text{app}} = \omega_0$. This is because of general interest in nonlinear driven systems, as well as being significant for the physics pertaining to sliding CDWs. These aspects will be described in sections 4 and 5. Results of mode-locking experiments in the presence of a temperature gradient in the context of velocity domain formation will be reviewed in section 6.

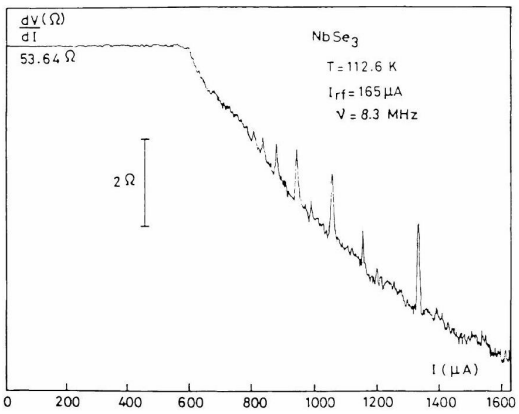


Fig. 1.3. Differential resistance versus dc current in the presence of a large radiofrequency ($\nu=8.3 \mathrm{MHz}$) drive. The peaks in the trace are the interference effects (from Monceau et al. 1982).

Physical properties of materials not directly associated with electronic transport can also be dramatically altered by sliding CDWs. The Young's modulus actually softens in several materials when the threshold field is exceeded. The application of an ac field complicates the situation still further, as steps are observed in the Young's modulus that correspond to the steps in the $I-V$ curve itself. The experiments and interpretation will be reviewed in section 7 .

4.6.3 2. Models of CDW motion and oscillation phenomena

The reason for the current oscillations remains a controversial issue in the field of charge-density waves. Because the models that attempt to explain the conduction noise and interference effects appear elsewhere in this book, we give only a brief description as a way of introduction for the experiments.

2.1. Single degree of freedom models

The simplest model which includes most of the basic features of CDW conduction is a particle sitting in a washboard potential (Grüner et al. 1981, Monceau et al. 1980). An important neglection are the CDW internal degrees of freedom; for the moment we consider the CDW as a large, but finite sized, rigid object. It is pinned by anything that disrupts the translational invariance of the system (in the limit that the rigid CDW becomes infinite in extent, the total pinning force approaches zero). The electric field couples to the effective charge density ρ_0, defined by the spatially varying charge density $\rho(x)$

$$\rho(x) = \rho_0 + \rho_1 \cos\left[2k_{\mathrm{F}}x + \phi(x)\right], \tag{2.1}$$

with k_{F} the Fermi wavevector, $\phi(x)$ the location of the CDW relative to the lab frame, and ρ_1 the amplitude of the charge modulation. The onedimensional (1D) equation of motion can be written

$$m^* \frac{\mathrm{d}^2x}{\mathrm{d}t^2} + \Gamma \frac{\mathrm{d}x}{\mathrm{d}t} + \frac{\mathrm{d}V}{\mathrm{d}x} = eE(t), \tag{2.2}$$

where m^* is the effective mass of the CDW and Γ is a phenomenological damping constant. It is expected that m^* is much larger than the electron mass because the lattice distortion must

move with the CDW. The simplest periodic potential is the cosine (also appropriate for the Josephson junction), for which eq. (2.2) becomes

$$m^* \frac{\mathrm{d}^2 x}{\mathrm{d}t^2} + \Gamma \frac{\mathrm{d}x}{\mathrm{d}t} - 2k_\mathrm{F} V_0 \sin(2k_\mathrm{F} x) = eE(t) \tag{2.3}$$

Equation (2.3) contains many of the important features of CDW response: a finite threshold field $E_\mathrm{T} = 2k_\mathrm{F} V_\mathrm{O}/e$, strong frequency-dependent conductivity, and a modulated drift velocity v_d under constant applied electric field. The CDW current density is given by

$$j_\mathrm{CDW} = n_\mathrm{CDW} e \bar{v}_\mathrm{d} = n_\mathrm{CDW} e \lambda f_0, \tag{2.4}$$

where n_CDw is the condensate density, $\bar{v}_\mathrm{d}$ is the time-average velocity, λ is the CDW wavelength and f_0 is the fundamental frequency of the response oscillations. On a per chain basis, eq. (2.4) gives

$$j_\mathrm{c}/f_0 = 2e \tag{2.5}$$

at $T = 0$.j_c is the CDW current carried on each chain, $\lambda = 2\pi/2k_\mathrm{F}$ and the condensate density is $2k_\mathrm{F}/\pi$ for one chain.

Failures of the single-particle model prompted more sophisticated treatment. With respect to the current oscillations and behavior around threshold there are several obvious problems. First, the ratio of the amplitude of the voltage oscillations δV to the threshold voltage V_T is far too small. Because it is the strength of the pinning leading to both effects, it is expected that $\delta V/V_\mathbf{T}$ is on the order of unity. For example, in the high-field overdamped limit, the time-dependent velocity $\mathrm{d}x/\mathrm{d}t$ is given by

$$\begin{aligned} \frac{\mathrm{d}x}{\mathrm{d}t} &= (e/\Gamma)\left(E - E_\mathrm{T} \sin(2k_\mathrm{F} x)\right) \\ &= (eE/\Gamma)\left(1 - (E_\mathrm{T}/E)\sin(2k_\mathrm{F} x)\right) \end{aligned} \tag{2.6}$$

with E the dc driving field. It follows that the oscillating current density $\delta j \sim \sigma_\mathrm{b} E_\mathrm{T}$ and therefore $\delta V \sim V_\mathrm{T}$ (where σ_b is the high field conductivity of the CDW). Experimentally $NbSe_3$ shows the strongest current oscillation phenomena and smallest threshold field but still $\delta V/V_\mathbf{T} \sim \mathrm{O}(10^{-3})$ (Grüner and Zettl 1985). This can be explained by assuming that the pinning force somehow becomes reduced when the CDW is moving. However, it is important to note that this hypothesis requires giving up the main assumption that the CDW is rigid. Another feature of the single-particle model is the very different behavior produced when driven by a voltage or current. Graphed in fig. 2.1 are the two cases. A conductance from normal electrons is the reason for the current carried below threshold. However, the experiments never show any change as the source impedance is varied. Furthermore, the shape of the $I-V$ curve is always concave up rather than down. Although it is possible that the curvature changes in the limit of high fields, that has never been observed.

The overdamped sinusoidal washboard model does not result in any subharmonic steps whatsoever. Attempts to explain them rely either on hypothesizing an effective potential with rich harmonic content or invoking

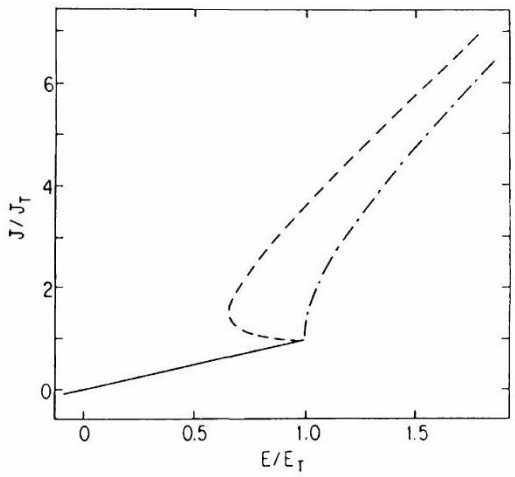


Fig. 2.1. Current-voltage ($I - V$) curve for the single-particle model. The presence of a channel for normal electrons accounts for the conductivity below the threshold field E_{T}. Note that the current drive (dashed curve) is double-valued with respect to the field. The dashdotted curve denotes voltage drive.

a model that includes phase degrees of freedom. Because some unique aspects of the interference effects (section 4) share features with models that contain many effective degrees of freedom, we proceed to describe this modification of the classical transport model.

2.2. Classical models with many degrees of freedom

Near threshold, it is expected that impurity pinning of the phase will have very strong distortive effects on the CDW, so the easiest situation to handle is in the high-velocity limit, when the pinning centers can be treated perturbatively. Sneddon, Cross and Fisher (1982) (SCF) demonstrated that for this case the high field velocity takes the form:

$$j_{\mathrm{c}} = \sigma_{\mathrm{b}} E - c\sqrt{E}. \tag{2.7}$$

It was assumed that only long-wavelength distortions of the phase are important and therefore macroscopic equations are still appropriate. Adding an elasticity term to the equation of motion allows the CDW to distort as it moves over the impurities. That energy can be dissipated to other degrees of freedom in the crystal. It is important to note that the concave up form for the differential conductance is qualitatively consistent with the data.

Another significant feature that emerged from this treatment was that the velocity of the CDW was not modulated in time, so perhaps the observations are attributable to finite size effects. The argument in support of finite size can be put in simple terms by considering correlations of the

CDW between different regions. At zero velocity, the phase will be distorted by the impurities. The approximate distance over which the phase is nearly constant is the phase-phase correlation length $\langle\phi(0)\phi(x)\rangle$. Equivalently, a moving CDW described by a deformable model must have a finite velocity-velocity correlation length. Time-dependent velocities from different regions will have a random relative phase. The resulting sum over all the regions as the number of regions grows infinitely large has zero velocity modulation amplitude.

Fisher (1985) extended the work of SCF to lower velocities by treating the depinning of the CDW as a critical phenomenon. The model incorporates a CDW elasticity through the effective interactions $\boldsymbol{J}_{ij}$ between the phases ϕ_i and ϕ_j at impurity sites $\boldsymbol{R}_i$ and $\boldsymbol{R}_j$:

$$H_0 = -\sum_j h_j \cos\left(\phi_j - \beta_j\right) + \frac{1}{2}\sum_{ij} J_{ij}\left(\phi_i - \phi_j\right)^2 \tag{2.8}$$

The preferred phase at $\boldsymbol{R}_j$ is $\boldsymbol{\beta}_j$ and the pinning strength is h_j. For convenience the strength of the pinning potential is always the same: $h_j = h$. In the mean field (infinite range) approximation N phases are coupled by $J_{ij} = J/N$. The equation of motion is written

$$\frac{\mathrm{d}\phi_j}{\mathrm{d}t} = -\frac{\delta H_0}{\delta \phi_j} + F, \tag{2.9}$$

where the inertial term has been neglected and F is the driving field. The narrow-band noise amplitude is obtained from the velocity-velocity correlation function. As in critical phenomena, the appropriate length scale diverges at the transition between the moving and non-moving state,

$$\xi(F) \sim \xi_0 \left(\frac{F - F_\mathrm{T}}{F_\mathrm{T}}\right)^{-\nu} \tag{2.10}$$

with F_T the threshold, ξ_0 the phase-phase correlation length, and $\nu = 1/2$ in the mean field calculation. The important result to emerge from the mean field calculation is the jerkiness of the motion on the length scale of $\xi(F)$. This result is surprising, because each phase is coupled to the mean velocity field,

$$\bar{\phi}(t) = \frac{1}{2N}\sum_j \phi_j(t) \tag{2.11}$$

so that eq. (2.8) is rewritten

$$H_0(MF) = \frac{J}{2N}\sum_j \left(\phi_j - \bar{\phi}\right)^2 - \sum_j h_j \cos\left(\phi_j - \beta_j\right) \tag{2.12}$$

The equation of motion for the phase at the j th impurity is

$$\frac{\mathrm{d}\phi_j}{\mathrm{d}t} = J\left(\phi_j - \bar{\phi}\right) - \sum_j h_j \cos\left(\phi_j - \beta_j\right) \tag{2.13}$$

In the limit of an infinite number of impurities, we can write $\bar{\phi}(t) = vt$. Although far above threshold the motion of individual phases will be relatively smooth, at smaller electric fields the relative phase velocities become more 'jerky'.

Fisher argues that short-range interactions will only enhance the jerkiness of the motion. Far above threshold ξ is comparable to ξ_0, but closer to threshold ξ diverges according to eq. (2.10). Here as in the single-phase model, the CDW spends most of the time almost pinned (moving very slowly), then quickly advances a large fraction of 2π. The important consequence of the divergence is an enhanced ac noise amplitude near to the threshold

$$\left\langle j_\mathrm{ac}^2 \right\rangle^{1/2} / j_\mathrm{dc} \sim \left(\frac{F - F_\mathrm{T}}{F_\mathrm{T}}\right)^{\nu/2(d-4+\eta)} \left(\frac{\xi_\mathrm{d}}{V}\right)^{1/2} \tag{2.14}$$

Contained in eq. (2.43) is the volume incoherence factor $\left\langle j_\mathrm{ac}^2 \right\rangle^{1/2} \sim V^{-1/2}$ that can be tested experimentally.

2.3. Current oscillations and microscopic pinning

Many of the attempts to determine the pinning forces on a microscopic level have been led by Zawadowski. Barnes and Zawadowski (1983) have calculated the effect of scattering of electron-hole pairs by impurities and implications for pinning of the CDW and narrow-band noise. Later, the interaction of the CDW and Friedel oscillations created near the impurity was investigated by Tutto and Zawadowski (1985) to higher orders in the perturbation. It is important to mention these results because any form obtained from the microscopic theory can in turn be used in the macroscopic equations of motion. For convenience, only a one-dimensional segment is considered and the phase is coherent over that segment.

The charge-density wave is formed by two macroscopic quantum states consisting of electron-hole pairs with momentum $\pm 2k_{\mathrm{F}}$ and spin zero. It is the interference of the two states which results in the gap formation and thus the CDW. To second order in the acceleration (scattering) of the CDW by a single impurity, a transition takes place in which two electrons are scattered from the same side of the dispersion curve to the opposite. In turn, the position (phase) of the two states combine to form the CDW position $\phi = \phi_{\mathrm{L}} - \phi_{\mathrm{R}}$, and the transition rate depends on position as $\sin\left[2\left(\phi - \phi_0\right)\right]$, where ϕ_0 is the preferred position. Therefore, the scattering rate due to the impurity oscillates in time and may be a contributing source
of the oscillation phenomena. The second-order results predict a pinning wavelength that is half the CDW wavelength. If no more terms were important, the ratio of j_c/f_0 would be half that predicted from the phenomenological treatments above.

Higher-order processes are also possible, and it turns out significant. The origin of the terms comes from scattering of electrons that move in the effective potential induced by the CDW; they are shown in fig. 2.2. Perhaps an easier way to visualize the impurity pinning to nth order is to describe the interference between the charge-density wave and the Friedel oscillation formed about the impurity. The electron density is either maximal or minimal at the impurity, with periodicity $2k_{\mathrm{F}}$ just as the CDW. The phase of the CDW is mismatched with the Friedel oscillation in general, so there must be a crossover region around the impurity (in a volume x_0).

Since the volume over which the amplitude can vary (ξ_0) usually satisfies $\xi_0 \gg x_0$, the phase on two sides of the impurity cannot change by much. Long-range deformations act to minimize the overall energy in the regions around the impurities. The effective potential V_0 at the impurity site can be borrowed from the microscopic description mentioned here and incorporated into any calculations using a phase Hamiltonian such as eq. (2.8). Tutto and Zawadowski predict that at temperatures close to the CDW phase transition the effective potential becomes more sinusoidal. Shown in fig. 2.3 is an example of the potential. The harmonic content of the NBN, as in the classical theories depends on the velocity; any shape of the potential gives 'spike-like' behavior very close to threshold. For overdamped motion at high velocities, it is the spatial derivative of the potential that directly gives the velocity and therefore the harmonic content. Sinusoidal behavior near T_{p} results from the higher-order perturbation terms exerting a force

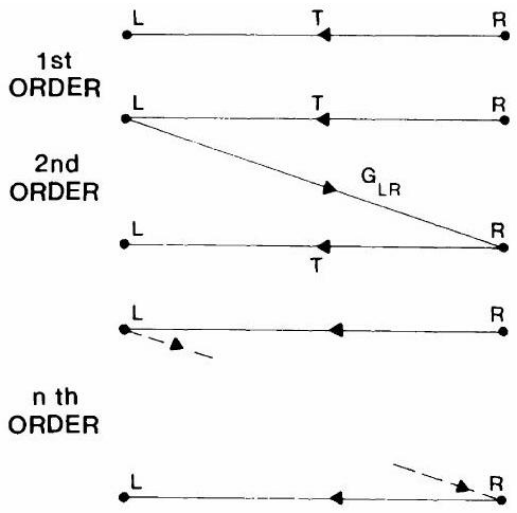


Fig. 2.2. Higher-order electron-hole scattering processes as described by Barnes and Zawadowski (1983).

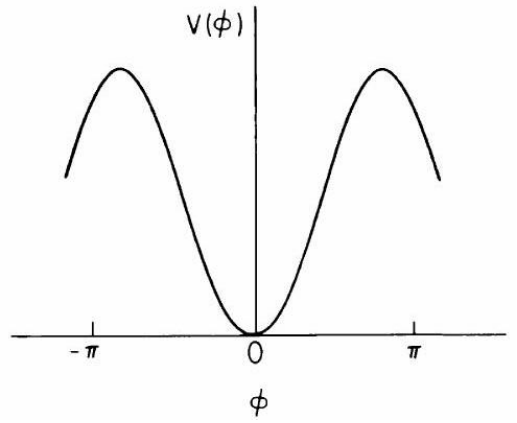


Fig. 2.3. Potential as created by impurities in the model calculated by Tutto and Zawadowski (1985).

on the CDW that decreases faster than the order parameter, which in turn determines the first-order term through, for example, Coulomb interactions.

2.4. The tunneling model and current oscillations

Bardeen (1985) has proposed a mechanism for CDW transport which involves the coherent macroscopic tunneling between two energetically equivalent states $\phi_{\mathrm{A}}(x)$ and $\phi_{\mathrm{B}}(x)$. One important difference between models described previously and the tunneling model is the alternation between the two states. In the presence of an electric field, a CDW in state ϕ_{A} will move from its optimal position at the average rate $-v_{\mathrm{d}}t$. When the spatial average position is $\pi/2, \phi_{\mathrm{A}}$ and ϕ_{B} are equivalent in energy but separated by a barrier. At phases $\phi > \pi/2, \phi_{\mathrm{B}}$ is favorable. The effective potential, as shown in fig. 2.4, can be written

$$V(\theta) = \begin{cases} -\cos\theta, & -\pi/2 < \theta < \pi/2, \\ \cos\theta, & \pi/2 < \theta < 3\pi/2. \end{cases} \tag{2.15}$$

The CDW current is determined by the transition rate between the two states. The effective potential is similar in shape to that calculated by Tutto and Zawadowski (1985) but is shorter

in spatial periodicity by a factor of two. Similar to the deformable classical models, it is the ability for the CDW to change its form to best accommodate the impurity potential that allows for sliding motion.

The motion of the CDW as described in the tunneling model can be discussed classically (Mihaly 1986) as illustrated in fig. 2.5 (using the strong pinning limit for convenience). Similar to the idealized case of Bardeen, place pinning centers an integral number of wavelengths apart at regular intervals. Halfway in between each of these, place another set of strong pinning centers. The phase distorts to accommodate the new centers and therefore the lowest energy state is that shown in fig. 2.5b. Application of

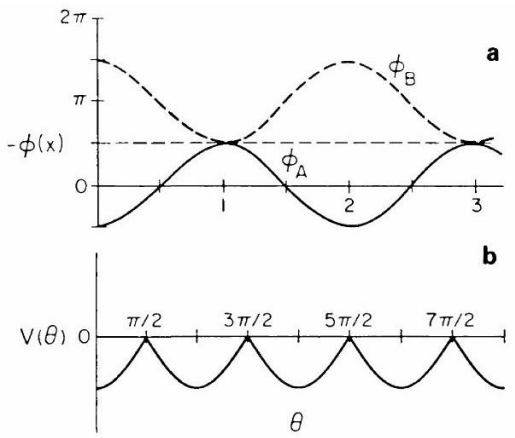


Fig. 2.4. (a) The two states ϕ_{A} and ϕ_{B} in the tunneling model. (b) Effective potential. Note that the periodicity is half that of classical pinning models (Bardeen 1985).

an electric field moves the compressed region to the position of fig. 2.5c, so that the CDW is always pinned at one half of the sites. The repetition of this process gives an average phase advance of π per cycle, as in the tunneling picture. Forcing the CDW to move in this manner retains the potential of eq. (2.15); the rich harmonic content of the oscillations persists to high fields. Similar to the classical phase treatments of CDW sliding motion, the

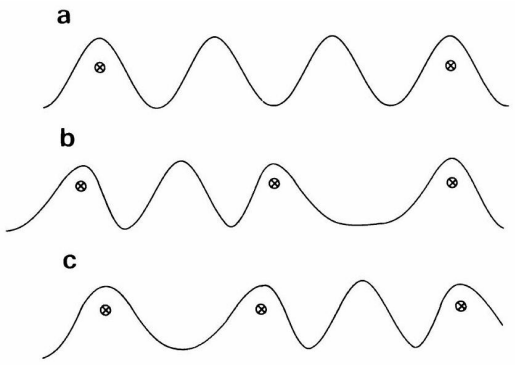


Fig. 2.5. Classical analogy to the tunneling model, strong pinning limit. (a) The CDW is pinned by two impurities an integral number of wavelengths apart. (b) Insertion of an impurity midway between causes a compression in one half and an extention in the other. (c) An electric field shifts the compressed region.

source of the narrow-band noise is a bulk phenomenon due to impurity pinning.

2.5. Phase-slip processes

All of the models described above have the common feature that the narrow-band noise arises from bulk pinning effects, so in that sense they are indistinguishable. However, because the ratio $\delta V/V_{\mathrm{T}}$ is so small the connection is not straightforward; indeed, experiments addressing this issue are a main topic of this chapter. It can also lead one to search for other explanations regarding the source of the noise.

Up until now, only phase excitations have been considered. Amplitude fluctuations are completely neglected. In some limits this is acceptable, but at least in one case for every sample, amplitude excitations have to be included. In the presence of a very weak pinning center, the CDW phase will be distorted a small amount and the size of the gap will remain large; the density of condensed carriers remains constant near the pinning center. However, in the limit when a dislocation or chemical impurity has such a strong effect to completely block the sliding mode, then the order parameter will decrease near the impurity. The only way for current to pass is by normal single-particle transport.

This process must occur at the contacts for every sample. Ong, Verma, and Maki (1984) and independently Gor'kov (1983) have developed a theory describing the conversion of CDW carriers to normal carriers at the terminals of the sample. The spatially periodic charge modulation leads to the oscillating voltages picked up in the experimenters' detection circuits. Their proposal depends on the creation of an array of vortices at the sample ends, or anywhere there is a phase discontinuity. Included is the assumption that the static phase-phase coherence length is much shorter than any dynamical phase coherence lengths, which may be on the order of the total length of the sample. This supposition leads to a uniform CDW velocity in time and space in the bulk of the sample. The creation of vortices at one end of the sample and the annihilation at the other is the source of the ac conduction noise. Conservation of charge requires us to write

$$v_{\mathrm{d}} l_{\mathrm{v}} = v_{\mathrm{s}} \lambda_{\mathrm{CDW}}, \tag{2.16}$$

where l_{v} is the vortex spacing and v_{s} the velocity.
The phase-slip process can be thought of as the way the sample reduces stress that is built up by the dc electric field. The phase is considered to be fixed at the end of the sample. A sliding charge-density wave moving towards the contact tries to compress the CDW near the contact because of this boundary condition. By letting the phase change by an amount 2π the energy stored in the system is released, like shorting out a capacitor. The
amplitude fluctuations discussed earlier are from the requirement that the discharge be in the form of 'normal electrons', able to propagate outside of the sample into the measuring leads.

The current oscillations become a modulated chemical potential difference in the experiment through an effective resistance that is independent of sample length but inversely proportional to the sample width. Therefore, it is expected that the voltage amplitude $U_0 \sim R_{\mathrm{eff}}$.

The important length scale in the vortex model is the distance over which the CDW velocity decreases to zero at the contact. We expect that the oscillations decay exponentially over the phase-slip length ξ; therefore the ac electric field is given by

$$E(x) = E_\omega \left(\mathrm{e}^{-x/\xi} + \mathrm{e}^{\mathrm{i}\phi} \mathrm{e}^{-(f-x)/\xi} \right) \tag{2.17}$$

where ϕ is the random phase between the noise sources at the two ends of the sample. Integrating eq. (2.17) over the length of the sample gives the total measured ac voltage.

4.6.4 3. Experimental issues pertaining to the narrow-band noise

Experimentalists have investigated several aspects of CDW motion via measurements of the oscillation phenomena and the related observations of the interference effects upon application of an ac electric field.

3.1. Volume dependence of the oscillations

One of the controversial issues is the origin of the oscillations and its relation to CDW motion, as discussed in section 2 . The experiments can be divided into two classes: those that address the volume dependence and others where it is attempted to separate the signals coming from each end (for example, through the use of a temperature gradient). Here we discuss the results of three of those experiments as performed by Mozurkewich and Grüner (1983), Jing and Ong (1986) and Brown and Mihaly (1985).

First, however, it should be emphasized that these measurements are difficult to draw conclusions from. The reason is a lack of reproducibility that has been noted by several authors. The material of choice is $NbSe_3$ where the NBN peaks are extremely sharp, usually much less than 10 kHz wide. Typically the drive is a constant dc current and the voltage is measured as a function of time. This signal is in turn fed to a spectrum analyzer (different than a Fast Fourier Transform). The fundamental peak in the spectrum is arbitrarily selected for the measurements. It is assumed that any information contained in the higher harmonics is obtained by measuring the fundamental only and does not change from crystal to crystal.

The next difficulty arises from fluctuations in the spectrum. In the time domain a periodic signal that fluctuates considerably is observed. On the trace of a spectrum analyzer, the height of the peaks vary in time and the finite widths in frequency space also vary. A good simulation of the signal can be constructed by feeding a white noise source to the VoltageControlled Oscillator input of a function generator. The output of the generator looks similar to the response from a $NbSe_3$ crystal. When measuring the oscillations a bandwidth must be chosen along with a method for signal averaging. The choice of measurement bandwidth becomes significant when signal to noise ratios are marginal and when the fluctuations change from one experimental run to another.

Mozurkewich and Grüner (1983) tried to overcome these difficulties by keeping the measurement bandwidth larger than the signal and the fundamental centered around 10 MHz . In this way, they measured the root-mean-square (rms) voltage $V_{\rm rms} \equiv \Delta V$ of the fundamental frequency peak. The dependence on cross-sectional area was made by applying two contacts to the sample and measuring. Then the contacts were removed and the sample was cleaved along the direction of CDW current. The process was repeated as many times as feasible. The length dependence was measured in a similar fashion except that the cuts were made orthogonal to the direction of current. Their results are summarized in fig. 3.1, where $\Delta j \equiv \Delta V/RA = \Delta V/\rho\ell$ is plotted versus sample volume (A is the cross-sectional area, ρ is the resistivity, and ℓ is the length of the sample). The quantity Δj is assumed to be the oscillating current that would be detected if the drive was voltage rather than current. Technically this is valid only for a non-

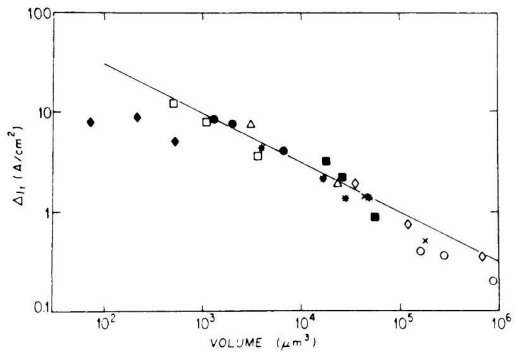


Fig. 3.1. Volume dependence of the amplitude of the fundamental oscillation frequency (Mozurkewich and Grüner 1983).

interacting two-fluid model (representing the CDW electrons and the 'normal' electrons). The solid line has a slope of $-1/2$, which would indicate a vanishing current oscillation amplitude in the infinite volume limit.

The $1/($ volume $)^{1/2}$ behavior is the result one obtains for the two-dimensional random walk. Consider a circuit consisting of a string of independent ac voltage sources all of the same frequency and amplitude V_0. The rms voltage measured at the ends, because the relative phases are uncorrelated, is proportional to the square root of the number of oscillators N :

$$V_{\mathrm{rms}} = V_0\sqrt{N}. \tag{3.1}$$

Normalizing to obtain the current and associating a length with each oscillator gives an ac current that varies as $1/($ length $)^{1/2}$. Of course the damping must be included, so phenomenologically we associate a resistance that may be field dependent with each oscillator. Similarly, the crosssectional area dependence can be modelled by placing oscillator-resistor pairs in parallel. In that case $\Delta j \sim \Delta V \sim 1/($ area $)^{1/2}$. It was found using an overdamped oscillator model for the fit that the appropriate domain volume $V_{\mathrm{d}} \geqslant 0.2\mu$ m^3. It is possible that the domain volume depends on the CDW velocity, as described by Fisher (1985).

The measurements of Mozurkewich and Grüner remained controversial, as Ong, Verma and Maki (1984) presented a study that showed no length dependence at all, but with a considerable amount of scatter in the data. Brown and Mihaly (1985) attempted a different type of experiment, where the length dependence could be measured without cutting the sample. The main idea was to first make a contact to the sample that did not reduce the electric field in the sample very much directly under it. Usually, silver paste or some other conductor is used to make contact to the sample which reduces the electric field and therefore 'stops' the CDW in that region (Ong and Verma 1983). The required conversion to normal current is the process that generates the narrow-band noise in the contact models, thereby effecting the measurement. What they used was another $NbSe_3$ fiber that could be pressed lightly against the sample as a third contact, with the additional capability that it could be moved during the experimental run. The movable 'middle' contact allowed for three measurements to be made for each position: the voltage between both ends V_{13}, and the voltage from each end to the middle V_{12} and V_{23}. The results from that experiment are shown in fig. 3.2. Data taken from three samples are shown in the figure, for which the lengths varied $0.6 - 1.1$ mm. The length is normalized to one, and the position of the middle contact is the distance between contacts 1 and 2 . The general trend is that the noise amplitude increases with contact separation, but not in a linear fashion. In fact, the results are consistent with the model described above by the string of random-phase oscillators. For entirely random phases, one expects $(V_{12} + V_{23})/V_{13} = \sqrt{2}$ when contact 2 is

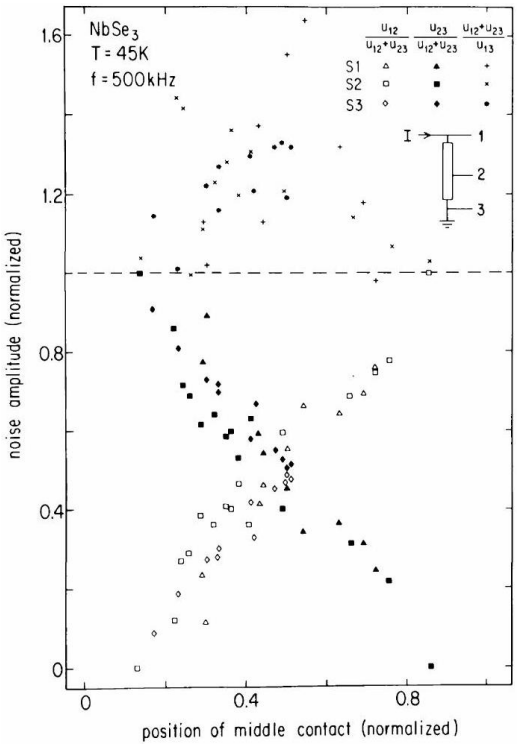


Fig. 3.2. Noise amplitude versus position of the middle contact. The solid symbols represent the signal between contacts 2 and 3 (inset) and the open symbols are between contacts 1 and 2 . Also plotted is the sum (above the dashed line) (Brown and Mihaly 1985).

at the center of the sample. The hypothesis that the voltage oscillations are generated in the bulk of the sample is further supported by their observation of the relative phase of the narrow-band noise on the two sides of the sample. Brown and Mihaly (1985) reported that there was no observable correlation, indicating a fluctuating relative phase on a very fast time scale.

The study was extended to include samples of a broader range in length (up to 1.7 mm long), with the results plotted in fig. 3.3. Fits were generated using eq. (2.17) of the vortex model for each sample with a constant $\xi = 0.3$ mm, and the phases of the oscillations at each end are random and fluctuating. The dashed line is a fit to the random-phase oscillator model. From the three plots, it is clear that the only way to consistently explain the results using the contact description is to keep the ratio ξ/ℓ a constant (solid line). Physically, ξ represents the appropriate length scale for screening of the vortex array, and reflects the velocity correlation function. As

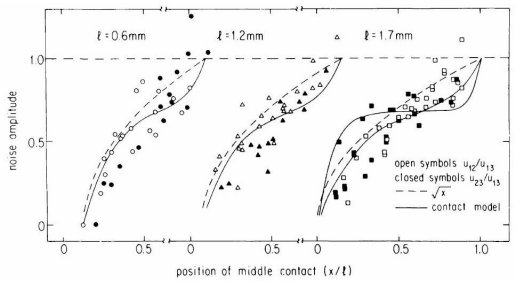


Fig. 3.3. Noise amplitude versus position of middle contact. The signal from the two sides of the sample are plotted on top of each other for convenience. The dashed lines are a fit to the random-phase oscillator model. The solid lines are a fit to eq. (2.17) with $\xi/\ell =$ constant. The longest sample also has been fit with $\xi = 0.3$ mm.

discussed by Fisher (1985), the velocity correlation length is larger than the Lee-Rice phase coherence length. Also, since the velocity is zero at the contact, it is the small velocity length which is important. There is no reason why ξ should change with sample length when $\ell > \xi$. In all of the experiments this condition should hold, since the shortest sample for which we have a fit $\xi \sim 0.3$ mm, with no phase coherence to the oscillations between the two sides of the sample.

More recently, Jing and Ong (1986) have reported a length dependent ac amplitude that indicates $\xi \sim 0.26$ mm. It appears difficult to simultaneously explain the results from the two experiments. However, we point out that there are some indications from experiments performed in the presence of a temperature gradient that the noise generation is a phenomenon resulting from bulk pinning of the charge-density wave (Lyding et al. 1986).

3.2. Periodicity of the potential

Provided that the narrow-band noise actually reflects bulk pinning, one can learn something about the effective potential by studying the harmonic content of the oscillatory response and from the constant ratio of excess current density to fundamental frequency f_0.

As presented in section 2, the time-average current density j_{CDW} is

$$j_{\mathrm{CDW}} = n_{\mathrm{CDW}} e \lambda f_0, \tag{3.2}$$

where n_{CDW} is the density of the condensed electrons and λ is the effective pinning wavelength. The density can be considered to be an order

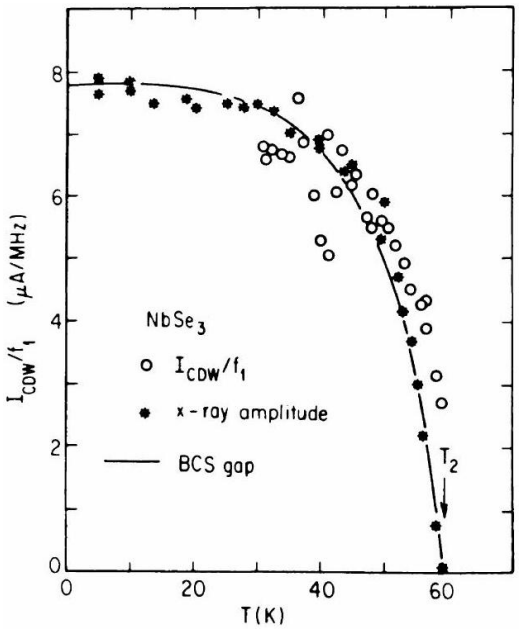


Fig. 3.4. Ratio $I_{\text {CDW }} / f_{0}$ versus temperature for $NbSe_3$ (open circles (Zettl and Grüner 1985)) and compared to the X-ray data of Fleming et al. (1978).

parameter as demonstrated by Zettl and Grüner (1984) and illustrated in fig. 3.4. The open circles are I_{CDW} / f_0 directly, and the asterisks are taken from X-ray diffraction experiments (Fleming et al. 1978) (the intensity of the satellite peaks). Normalizing the current to a single chain gives

$$j_{\mathrm{c}} = q \quad \text{per chain}, \tag{3.3}$$

where q is the net charge transported per chain per ac cycle. Experimentally, this number has been controversial for various reasons. First, the number of condensed electrons in $NbSe_3$ for each CDW is not known. The semiconducting materials are more difficult to get clean measurements from, because typically there is a significant spread in the fundamental frequency (indicating a corresponding distribution of CDW velocity in the sample). Plots constructed from CDW current and fundamental frequency where there are such distributions are not linear (Brown et al. 1985). This effect is illustrated in fig. 3.5, where at $T = 164$ K for this orthorhombic TaS_3 ($o - TaS_3$) sample there is a pronounced curvature. However, the slope tends toward a constant as the frequency is increased. Also plotted is the same quantity, but using the interference phenomena (Shapiro steps) as frequency markers (recall that steps are observed in the $I - V$ curve whenever the NBN frequency is an integer multiple of an external drive

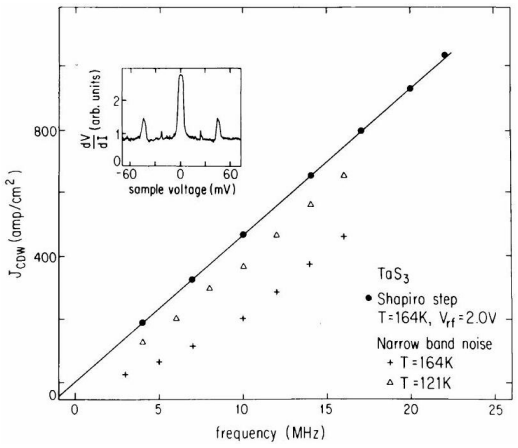


Fig. 3.5. Excess current versus fundamental oscillation frequency in $\mathrm{TaS}_{3}.The(,+ \Delta$) symbols are taken from direct measurements of the oscillations. The solid circles are from the Shapiro steps.

frequency). The data fit an excellent straight line with intercept at zero, as would be expected for a coherent sample response.

Because the Shapiro step curve and the NBN curve do not coincide, the CDW current at a step should depend on the rf power applied. This can be understood, if, for example, there is a distribution of threshold fields within the sample. The large amplitude ac may act to reduce the importance of that distribution for at least two possible reasons. If the significant parameter is $E - E_{\mathbf{T}}$, then sufficiently large fields reduce the importance of a distribution of E_{T}. For some samples, the steps are observed to become sharper with increased amplitude of the ac driving field, indicating increased synchronization of the sample response.

Electron diffraction experiments (Wang et al. 1983) show that the temperature dependence of the superlattice wavevector is weak, and therefore any observed temperature dependence of the slope $j_{\mathrm{CDW}}\,/f_0$ can be attributed to a change in the CDW electron density $n(T)$. The results from the temperature dependence study appear in fig. 3.6, showing almost no change over the range $115-200$ K. Above 200 K the value drops quickly towards zero as the transition temperature $T_{\mathrm{p}} \sim 220$ K is approached. Compared to similar results for $NbSe_3$, the development of the order parameter occurs over a much smaller range in temperatures (non-BCS behavior). It may be a result of the more one-dimensional nature of TaS_3 that the mean-field theory is less appropriate.

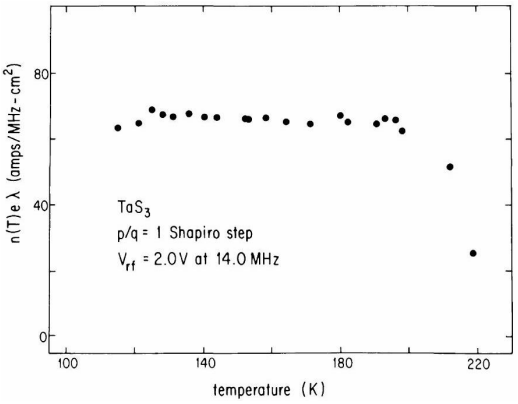


Fig. 3.6. Temperature dependence of the ratio $J_{\text {CDW }} / f_{0}$.

Evaluation of the temperature independent region gives

$$j_c/f_0 = (2.0 \pm 0.2)e, \tag{3.4}$$

consistent with those models where the energy periodicity related to the phase of the condensate is just the wavelength of the CDW distortion. The issue is not considered closed because estimates from other materials disagree. Recent measurements (Hundley et al. 1988) in the blue bronze $K_{0.3}MoO_3$ are consistent with that reported here. However, the semimetals $NbSe_3$ and monoclinic TaS_3 seem to yield results more consistent with a pinning wavelength that is half of the CDW wavelength (Monceau et al. 1983).

3.3. Statistical measurements of the narrow-band noise

We mentioned earlier the difficulty of doing measurements of the NBN because of fluctuations in the detected signal. Link and Mozurkewich (1988) performed a statistical study of those fluctuations and found the distribution of voltages corresponding to the fundamental frequency to be Gaussian in shape and centered about zero. This is the same distribution one obtains for Johnson noise in resistors. There is a time scale which serves as a crossover to the Gaussian behavior; when the voltages are recorded over a short enough interval, a bimodal distribution, as in fig. 3.7, is observed. Link and Mozurkewich found the crossover time τ to the Gaussian shape to be as short as 10μ s. When continually longer intervals are

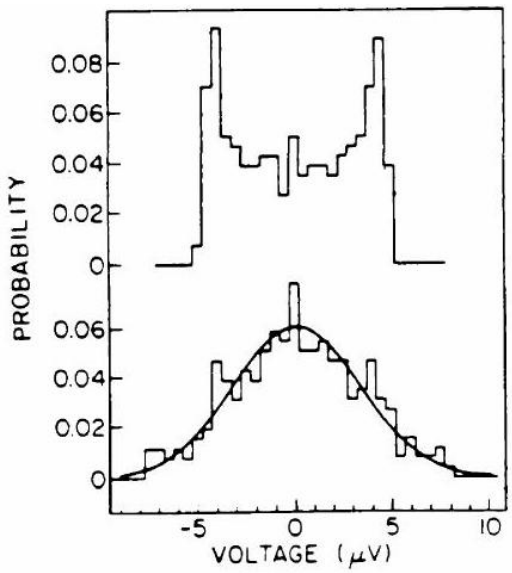


Fig. 3.7. Histograms of the voltage response of NbSe_{3} above threshold. At short times the structure is bimodal (top), whereas longer records reveal the unimodal shape (bottom) (Link and Mozurkewich 1988).

used the distribution becomes unimodal, with τ varying from record to record. It is possible the variation is a result of finite-size effects. It was demonstrated in a study of the fluctuations in the higher harmonics of the NBN that the fundamental and first harmonic signals are uncorrelated. This may be considered surprising because empirically the spectral widths of the various harmonics scale with each other.

Their observations put constraints on possible models for the noise generation. Any model with a unique sliding state can be eliminated. One possibility is to allow the relative phase among various regions of the sample to vary (Brown et al. 1985). We note, however, that various aspects of pinning in sliding CDW systems are not understood, since none of the available calculations of the phase Hamiltonians reproduce the fluctuations.

4.6.5 4. Electronic interference effects

The coexistence of an intrinsic narrow band noise frequency and the inherent nonlinear CDW $I-V$ characteristic sets the stage for a number of spectacular electronic interference effects in sliding CDW conductors. The CDW may be driven by an electric field of the form

$$E = E_{\rm dc} + E_{\rm ac}P(t), \tag{4.1}$$

where $E_{\rm dc}$ represents a dc bias offset and $E_{\rm ac}$ is the amplitude of the ac component $P(t)$. In practice, the drive is more often a total current, similar in form to eq. (4.1). In either case, the system response is not a smooth function of the drive parameters, but shows anomalous 'interference' structure. The response is determined by measuring the current through (or voltage across) the sample. The response signal may be viewed in real time (as in pulse synchronization and transient ringing experiments), viewed in the frequency domain (as in frequency locking and chaos experiments), or filtered for a single frequency (as in ac conductivity measurements and dc $I-V$ curves). In all cases, interference usually occurs whenever the internal narrow band noise frequency $\omega_{\rm NBN}$ is equal to or simply related to a characteristic frequency of the ac drive. $P(t)$ is a periodic function of time t and may, for example, be a sinusoid, square wave, or train of rectangular pulses. In $NbSe_3$, TaS_3, and $K_{0.3}MoO_3$, interference has been observed in the dc conductivity (Monceau et al. 1980, Brown et al. 1985, Zettl and Grüner 1983, Hall and Zettl 1984, Brown et al. 1984, Sherwin and Zettl 1985, Thorne et al. 1987, Hundley and Zettl 1988), ac conductivity (Zettl and Grüner 1984, Cava et al. 1984, Hundley and Zettl 1988), and real time transient response (Fleming 1982, Brown et al. 1986, Fleming et al. 1985). $NbSe_3$ shows the strongest interference effects, presumably because the CDW response is most coherent in that material.

4.1. Shapiro steps

One of the most dramatic CDW interference effects and the one emphasized in this review is a modification of the sample $I-V$ characteristics in the presence of a superposed ac drive field. In the most common experimental situation, the ac field is a sinusoid and hence the total applied field is of the form

$$E = E_{\rm dc} + E_{\rm ac}\cos(\omega_{\rm ex}t) \tag{4.2}$$

Under these conditions, anomalies occur in the dc $I-V$ characteristics whenever the narrow band noise frequency and applied frequency are related by

$$\omega_{\rm NBN}/\omega_{\rm ex} = p/q \tag{4.3}$$

with p and q integers. Figure 4.1 shows an early observation (Monceau et al. 1980) of such interference in the differential resistance of $NbSe_3$. The sharp spikes in dV/dI occur when $\omega_{\rm NBN}/\omega_{\rm ex} = 1, 2, 3$, etc. Similar interference is obtained in TaS_3 (Brown et al. 1985) and $K_{0.3}MoO_3$ (Hundley and Zettl 1988). Figure 4.2 shows that the interference peaks in dV/dI correspond to actual 'steps' in the direct $I-V$ characteristics (Zettl and Grüner 1983). The magnitude of the steps, δV, is a strong function of external ac frequency and amplitude. The steps observed in CDW materials are similar to those observed in the $I-V$ characteristics of dc biased Josephson junctions in the presence of microwave radiation, as originally studied by Shapiro (1963). In the Josephson junction case, the steps reflect interference between the internal ac Josephson oscillations and the exter-

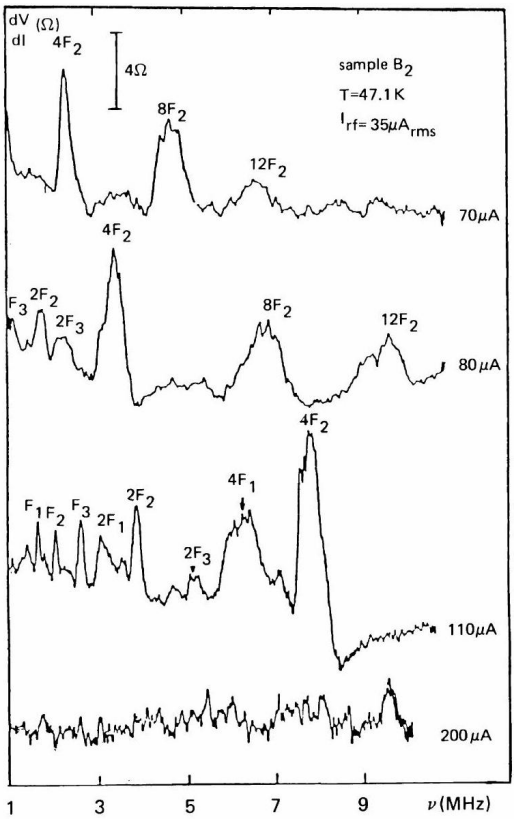


Fig. 4.1. Differential resistance in NbSe_{3} measured in the presence of a superposed rf electric field. The sharp peaks represent interference structure. (From Monceau et al. 1980.)

nally applied microwave oscillations. Both the Josephson interference and CDW interference steps have become known as 'Shapiro steps'.

Similar interference effects are also observed in the dc $I-V$ characteristics of type II superconductors with flux vortex flow in the presence of rf radiation (Fiory 1971). Indeed, the close analogy between flux flow in superconductors and CDW motion, together with the previous observation of interference effects in type II superconductors, provided initial motivation for study of interference effects in $NbSe_3$.

Steps corresponding to integral values of $n \equiv p/q$ (eq. (4.3)) are commonly referred to as harmonic steps, while steps corresponding to non-

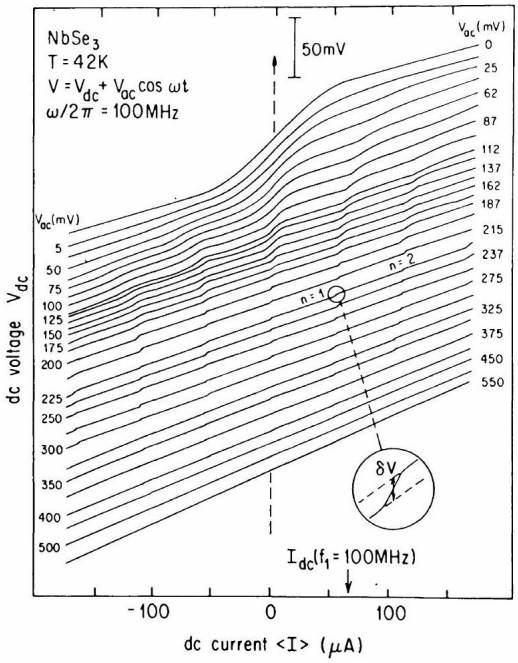


Fig. 4.2. Shapiro steps in direct $I - V$ curves of NbSe_{3}. The inset defines the step height δV.
(From Zettl and Grüner 1983.)

integral n are referred to as subharmonic steps. Although early reports of Shapiro step interference in $NbSe_3$ made note (Monceau et al. 1980, Zettl and Grüner 1983) of the presence of subharmonic steps, more careful differential resistance measurements on CDW systems have since demonstrated an astoundingly rich subharmonic spectrum (Hall and Zettl 1984, Brown et al. 1984, Thorne et al. 1987). It is not uncommon to observe as many as 50 to 100 subharmonic steps between successive harmonic steps. Figure 4.3a shows a typical $\mathrm{d}V/\mathrm{d}I$ interference plot for $NbSe_3$, with some dominant interference peaks identified with p/q values (Hall and Zettl 1984). The interference pattern displays self-similar structure, suggestive of fractal geometry (see section 5.1). Figures 4.3b,c show Shapiro step d $V/\mathrm{d}I$ plots for TaS_3 and $K_{0.3}MoO_3$, respectively (Brown et al. 1985, Hundley and Zettl 1988). Similar peak structure is observed, though the peaks are less sharp and smaller in relative height than those seen in $NbSe_3$.

Figure 4.3a shows that for the dominant interference peaks in $NbSe_3$, the differential resistance $\mathrm{d}V/\mathrm{d}I$ is flat over a substantial range of dc bias and achieves nearly the pinned, zero bias value. The CDW condensate is mode locked (Hall and Zettl 1984, Sherwin and Zettl 1985) during the interference, and does not contribute to the differential conductance of the sample (i.e. during mode locking only the normal, uncondensed electrons respond to small low-frequency ac perturbations of the electric field drive). The fact that $\mathrm{d}V/\mathrm{d}I$ remains flat over a range of dc bias implies that near the step edges ω_{NBN} is pulled substantially away from its 'natural' value. The Shapiro step width or magnitude δV is a measure of over what range ω_{NBN} will track ω_{ex} due to mode locking. In an experimental $\mathrm{d}V/\mathrm{d}I$ versus

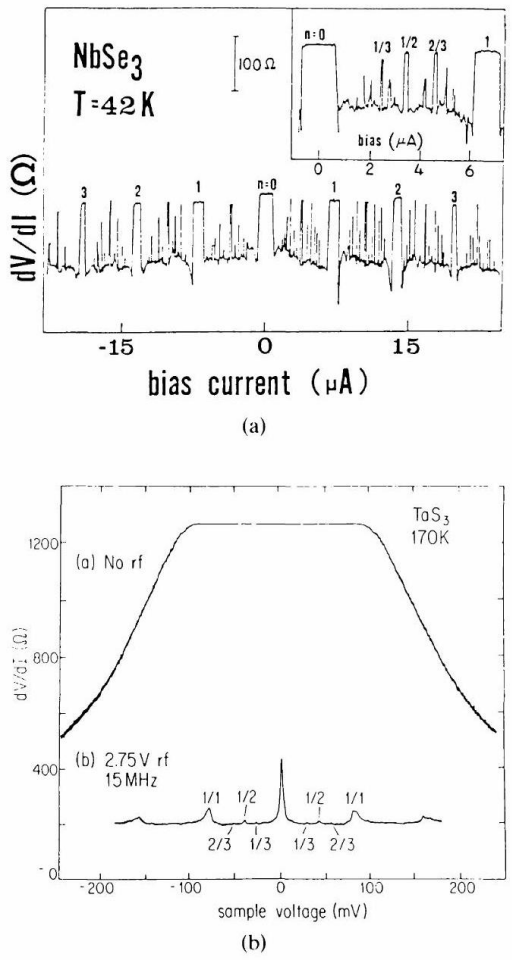
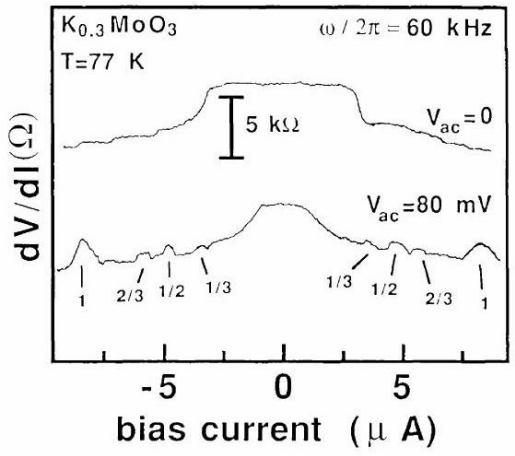


Fig. 4.3a,b.



(c)

Fig. 4.3. (a) Shapiro step interference in dV/dI traces of $NbSe_3$.$n = p/q$ is the step index. The inset identifies some subharmonic steps. (From Hall and Zettl 1984.) (b) Harmonic and subharmonic Shapiro step interference peaks in TaS_3. (From Brown et al. 1985.) (c) Harmonic and subharmonic Shapiro step interference peaks in $K_{0.3}MoO_3$. (From Hundley and Zettl 1988.) $I_{\rm dc}$ (not $E_{\rm dc}$) plot, δV is found by integrating the area under the rectangular interference peak. Experimentally (Zettl and Grüner 1983, Thorne et al. 1987), δV is a strong function of the

ac drive amplitude $E_{\rm ac}$ and frequency $\omega_{\rm ex}$. Figure 4.4 shows δV versus $E_{\rm ac}$ for the $n = 1/1$ Shapiro step in $NbSe_3$. For low values of $E_{\rm ac}, \delta V$ increases rapidly with increasing $E_{\rm ac}$, but at higher ac drive oscillatory behavior is obtained.

As is to be expected, Shapiro step interference in the dc $I - V$ characteristics similar to that shown in figs. 4.1 to 4.3 (sinusoidal drive) also occurs for non-sinusoidal ac excitation (Brown et al. 1986). Figure 4.5 compares $\mathrm{d}V/\mathrm{d}I$ of $NbSe_3$ measured in the presence of a low-frequency sinusoidal drive with dc bias (upper trace), to that measured in the presence of a low-frequency square wave drive with dc bias (lower trace). For relatively large dc bias values, the two interference date sets look very similar. On the other hand, for very low values of $E_{\rm dc}$, the square wave drive data shows suppressed interference peaks.

A more interesting situation occurs (Brown et al. 1986) if the square wave drive is asymmetric, as shown in fig. 4.6. In this drive configuration, the sample spends a waiting time t_1 below threshold and a time t_2 above threshold. The dc bias is defined as the time averaged response voltage measured experimentally. The inset to fig. 4.7 shows a typical $\mathrm{d}V/\mathrm{d}I$ interference plot thus obtained (with the sample actually current, not voltage, driven). The interference peaks are closer together on the negative bias side, where the system spends a longer time above threshold. The

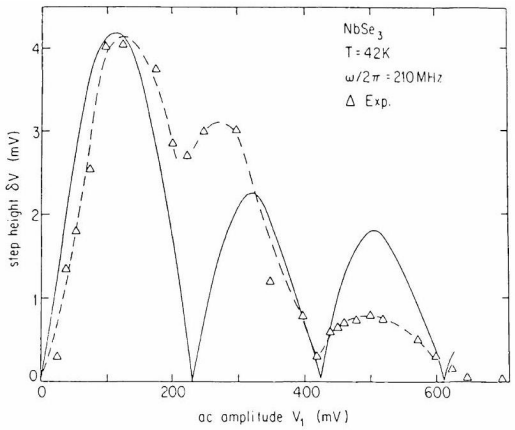


Fig. 4.4. Alternating current amplitude dependence of Shapiro step height δV in NbSe_3. The dashed lines are a guide to the eye for the experimental data. The solid line is eq. (4.9). (From Zettl and Grüner 1983.)

Shapiro step width δV is plotted in fig. 4.7 for different ac drive amplitudes and different t_1 and t_2 values. For short $t_1, \delta V$ increases roughly linearly with t_1 and the relative slope of δV versus t_1 varies approximately as $1/t_2$. Saturation of δV occurs for large values of t_1.

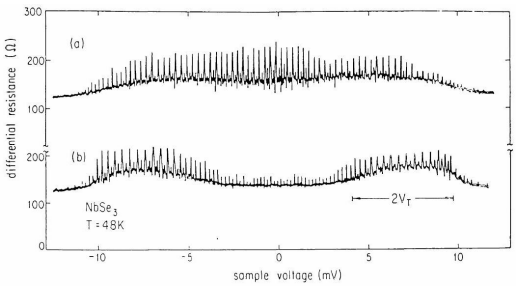


Fig. 4.5. Shapiro step interference in NbSe_3 for (a) sinusoidal ac drive and (b) square wave drive. The ac amplitude and frequency are identical in both traces. (From Brown et al. 1986.)

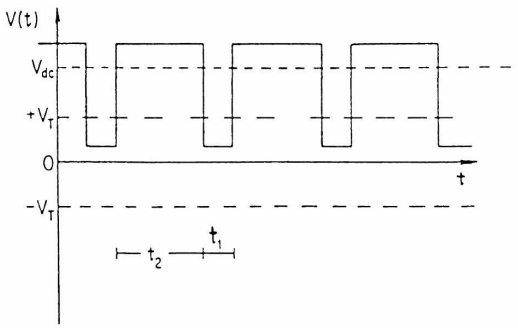


Fig. 4.6. Representative drive waveform for non-sinusoidal Shapiro steps experiments. (From Brown et al. 1986.)

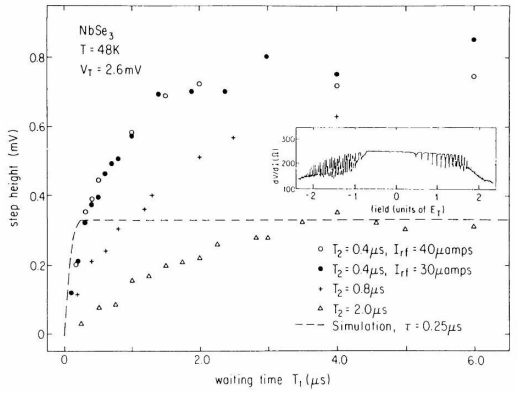


Fig. 4.7. Shapiro step magnitude in NbSe_{3} for non-sinusoidal and non-symmetric ac drive. The times T_1 and T_2 correspond respectively to t_1 and t_2 in fig. 4.6. The dashed line is the prediction of eq. (4.6). The inset shows a typical Shapiro steps $\mathrm{d}V/\mathrm{d}I$ trace for this type of ac drive. (From Brown et al. 1986.)

4.2. Single degree of freedom models for the interference

In a single-particle picture, Shapiro step interference and mode locking can be described in very simple terms. We first consider the motion of a charged particle in a periodic (e.g. sinusoidal) pinning potential. The most elementary electric field drive that satisfies eq. (4.1) is one where E switches periodically between two constant levels: $E = E_2 > E_\mathrm{T}$ for a time duration t_2, followed by $E = E_1 = 0$ for a time duration t_1 (see fig. 4.6). In this special case, the particle begins to move from the bottom of a potential well when E_2 is applied. Provided the t_2 is sufficiently long, the particle will move out of the original well and into the next, or a more distant, well. After the field switches off to $E_1 = 0$, the particle relaxes to the bottom of the nearest well and remains there for the remainder of time t_1, until the field switches once again to E_2, etc. In the steady state, the ac-sensitive time averaged CDW current will be (Brown et al. 1986)

$$\langle j(t) \rangle \approx p\lambda / (t_1 + t_2)\,, \tag{4.4}$$

where p is an integer and λ is the periodicity of the pinning potential. The dominant frequency of the external ac drive corresponds to a time period ($t_1 + t_2$), hence we identify $\omega_\mathrm{ex}/2\pi = (t_1 + t_2)^{-1}$. Together with eq. (4.4), this implies

$$\langle j(t) \rangle \approx p\lambda\omega_\mathrm{ex}/2\pi, \tag{4.5}$$

i.e., the CDW current is locked to ω_{ex} and hence the particle is mode locked. A similar situation will occur even if $E_2 \neq 0$, since this simply redefines the dynamic minimum in the potential. An alternative but equivalent description of the locking involves energy considerations (Thorne et al. 1986). With only a dc bias applied above threshold, the moving particle has a potential energy that corresponds to its average height in the well. For the case of a sinusoidal pinning potential this will be halfway up the well. When the particle becomes phase locked, more time will be spent near the potential minima and the mean potential energy will decrease. This is a more favorable dynamic situation.

In the interference data of fig. 4.5, there is a strong cutoff for the interference at approximately ±10mV dc bias, for both sinusoid and square wave ac drive. This cutoff corresponds to the situation where the drive signal no longer goes below threshold at any instance. This suggests that for Shapiro step interference to occur, the CDW system must spend some time below threshold during any one period of the ac drive. Further evidence for this is observed in the square wave data, for dc bias between approximately -4 mV and +4 mV . Here the external drive switches the sample between levels that are both larger than the threshold for depinning, but with opposite signs. Hence for this set of drive parameters the sample spends virtually no time below threshold, and the Shapiro step interference is greatly suppressed. The corresponding sine wave drive data shows no such suppression, because for a sinusoidal drive of similar amplitude there is always a non-negligible time spent below threshold.

In the case of rectangular pulse ac drive with two relevant times t_1 and t_2 (see fig. 4.6), a single-particle calculation yields for two limiting cases the following expressions for the Shapiro step magnitude (Brown et al. 1986):

$$\begin{aligned} \delta V &= V_{\mathbf{T}}\tau/t_2, \quad && t_1 \gg t, \\ \delta V &= 2V_{\mathbf{T}}t_1/t_2, \quad && t_1 \ll \tau, \end{aligned} \tag{4.6b}$$

where τ is the CDW damping time. Equations (4.6a,b) are independent of the specific form of the pinning potential. Physically, the forms of eqs. (4.6a,b) can be understood by considering t_1, the time spent below threshold. When t_1 is long, the CDW current is always locked because a minimum in the potential can always be reached. For large E_{ac}, the steps will be equal in size and fill the E_{dc} axis, which means the step magnitudes vary as $1/t_2$. In the limit $t_1 \ll \tau$, the step width is limited by t_1.

Figure 4.7 shows as a dashed line the behavior predicted by this simple single-particle description. A fit to the data of δV versus t_1 at long t_1 yields $\tau = 0.25\mu$ s (eq. (4.6a)). At short t_1, the fit is not quantitatively consistent with experiment.

It should also be noted that recent Shapiro step interference experiments (Thorne et al. 1987) on $NbSe_3$ in the upper CDW state have demonstrated that, for samples with unusually sharp breaks in the $I-V$ characteristics at threshold (measured in the absence of rf radiation), Shapiro step interference with complete mode locking does obtain at high frequencies even if the CDW is never driven into the pinned state. It would appear inconsistent to describe these results in terms of a slow relaxation to the pinned state. Whether the unusual dc $I-V$ characteristics of these samples (suggestive of switching behavior, see below) is related to this 'enhanced' mode locking, is not clear.

We now examine more closely the case of sinusoidal ac drive fields where $E = E_{dc} + E_{ac}\cos(\omega_{ex}t)$. The highly oversimplified model of 'rigid' classical CDW motion described by the damped pendulum equation (Grüner et al. 1981)

$$\mathrm{d}^2x/\mathrm{d}t^2 + \tau^{-1}\,\mathrm{d}x/\mathrm{d}t + Q^{-1}\omega_0^2\sin(Qx) = eE/m^* \tag{4.7}$$

and introduced in section 2.1 is here surprisingly successful in providing qualitative and even quantitative fits to many features of the Shapiro step interference. In dimensionless form eq. (4.7) reads (Zettl and Grüner 1983)

$$\mathrm{d}^2\theta/\mathrm{d}t^2 + G\ \mathrm{d}\theta/\mathrm{d}t + \sin\theta = E/E_\mathrm{T}, \tag{4.8}$$

where $G = (\omega_0\tau)$ and time is measured in units of ω_0^{-1}. Equation (4.8) is well known in the Josephson junction literature (Lindelof et al. 1981), where it describes the phase difference between superconductors comprising a resistively shunted junction (RSJ). In the current-driven Josephson junction case, E/E_T is replaced by I/I_T, and G is related to junction resistance R, capacitance C, and plasma frequency ω_J by $G = (RC\omega_\mathrm{J})^{-1}$. In the overdamped and high-frequency limit ($\omega_\mathrm{ex} \gg \omega_0^2\tau$), eq. (4.8) predicts Shapiro steps in the $I-V$ characteristics whose magnitude for the $n = 1/1$ step is given (Zettl and Grüner 1983) by

$$\delta V = 2\alpha V_\mathrm{T}(\omega = 0)\left|J_1\left(\omega_0^2\tau E_\mathrm{ac}/\omega_\mathrm{ex}E_\mathrm{T}(\omega = 0)\right)\right|, \tag{4.9}$$

where α represents the CDW volume fraction locked to the external signal and J_1 is the first-order Bessel function. In the low-frequency limit ($\omega_\mathrm{ex} \leqslant \omega_0^2\tau$), a modified Bessel-like solution for δV can be obtained numerically (Fack and Kose 1971). In the extreme low-frequency limit ($\omega_\mathrm{ex} \ll \omega_0^2\tau$), the numerical solution predicts that δV has a maximum at $E_\mathrm{ac} = E_\mathrm{T}$ where $\delta V = (\omega_\mathrm{ex}/\omega_0^2\tau)\, V_\mathrm{T}$.

The solid line in fig. 4.4 is the prediction of eq. (4.9) for δV versus E_ac, with no fitting parameters except for α, which sets the vertical scale (in fig. 4.4, $\alpha = 0.6$, suggesting for this sample 60% volume phase coherence). Although the fit in fig. 4.4 is surprisingly good, lending credibility to eq. (4.8), there are notable discrepancies between the Shapiro step data and the predictions of eq. (4.8). First, δV is predicted to vanish at the zeroes of J_1, while the experimental data suggest finite δV for all finite E_ac . This is shown more clearly in fig. 4.8. A second and perhaps more serious difficulty is that in the overdamped limit eq. (4.8) predicts no subharmonic interference. In $NbSe_3$, TaS_3 and $K_{0.3}MoO_3$ the ac conductivity suggests overdamped behavior, yet subharmonic Shapiro step interference is consistently observed. Hence, single-particle rigid motion in a sinusoidal potential cannot account for all aspects of Shapiro step interference.

The simplest correction to the deficiencies of eq. (4.7) or (4.8) is to retain the general form of the equation of motion but introduce a non-sinusoidal pinning potential. The expression for the Shapiro step magnitude then becomes (Thorne et al. 1987)

$$\delta V = V_\mathrm{T}\,(\omega_\mathrm{ex} = 0)\,\mathrm{Max}_\theta\left\{2\sum(q\beta)a_q J_p\left[q\beta\omega_1/\omega_\mathrm{ex}\right]\sin(q\beta\theta)\right\}, \tag{4.10}$$

where $(q\beta)a_q$ is the q th Fourier component of the pinning force, J_p is the p th-order Bessel function, ω_1 is proportional to E_ac, and β is 1 or 2 for pinning periodicities 2π or π, respectively. Higher harmonics in the nonsinusoidal pinning potential lead to subharmonic interference steps, and the summation of Bessel functions in eq. (4.10) eliminates zeroes in the predicted δV, consistent with experiment. However, as shown in fig. 4.8, detailed measurements of δV versus E_ac on $NbSe_3$ samples indicate that δV exhibits

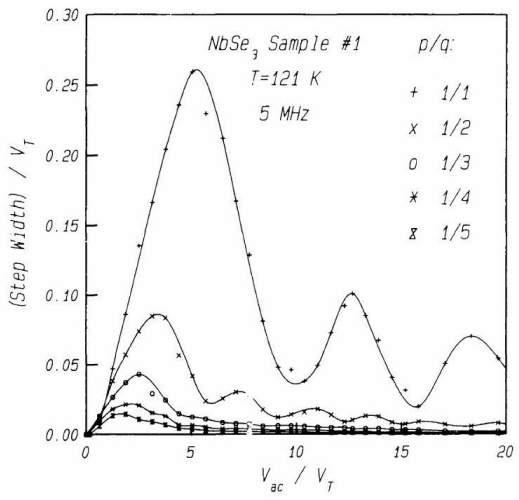


Fig. 4.8. Shapiro step magnitude versus ac drive amplitude in upper CDW state of NbSe_{3}. (From Thorne et al. 1987.)

smooth minima with increasing E_{ac}, while eq. (4.10) predicts sharp downward pointing cusps at the minima. This problem is generic to rigid particle classical models, regardless of the form of the pinning potential. In terms of generating narrow band noise spectra and harmonic and subharmonic Shapiro step interference most consistent with experiment, the best singleparticle periodic potential appears to be cusped (Thorne et al. 1987), similar to that discussed by Tutto and Zawadowski (1985) and predicted by Bardeen's tunneling model (Bardeen 1985).

In Bardeen's tunneling model discussed previously in section 2.4, the electrons and macroscopically occupied phonons in the CDW are treated as a macroscopic quantum system with only one thermal degree of freedom in a large phase-coherent volume. The model is consistent with narrow band noise generation and nonlinear CDW $I-V$ characteristics and should, therefore, account at least to first order for Shapiro step interference. However, no specific form for δV or subharmonic interference structure has been calculated for the tunneling model.

4.3. Internal modes and relevant time scales

An increasing number of transport, structural, and NMR experiments on CDW conductors suggest that CDW internal degrees of freedom play a
central role in CDW dynamics. We will examine the relevance of internal modes to electronic interference effects.

Below threshold, the pinned CDW displays rich metastable state structure with both short and long characteristic time scales for decay. The long time scales can be on the order of thousands of years for a true equilibrium state to be reached. Metastable states correspond to different local configurations of CDW phase which results from the interaction of the condensate with crystal impurities. The states may correspond to an extremely polarized CDW, where the Q-vector (and hence single-particle gap) varies significantly over the length of the crystal.

Metastable state structure is well demonstrated by the so-called pulsememory effect, first observed in $NbSe_3$ by Gill (1981) and subsequently identified in other CDW materials (Janossy et al. 1985, Fleming and Schneemeyer 1983). The effect is observed by exciting the CDW with a series of rectangular current pulses. If the amplitude of the pulses I_{p} exceeds the threshold I_{T}, then during the time between pulses the static CDW 'remembers' the polarity of the previous pulse. If a particular current pulse is of opposite polarity to the previous pulse, the voltage response of the system shows a slow 'charging' transient. This transient is interpreted as

reflecting the nonequilibrium metastable state induced by repeatedly driving the CDW above threshold and quenching it to rest. As the CDW is excited by a series of unipolar pulses with $I_P > I_T$, the trained static configuration between pulses will reflect a highly distorted CDW, with the phase 'stretched' near one end of the sample and 'compressed' near the other end. A sudden reversal of pulse polarity initially results in the CDW unleashing this stored phase, leading to a sudden anomalously large phase velocity transient with a correspondingly small voltage response. Once the stored phase is exhausted, the CDW assumes a steady state velocity limited by damping. The time scale for CDW depolarization is on the order of $5 - 20\mu$ s in $NbSe_3$ (Gill 1981) and $100 - 500\mu$ s in $K_{0.3}MoO_3$ (Fleming and Schneemeyer 1983).

A closely related memory effect concerns the phase of the coherent noise oscillations. To observe the effect, the CDW is excited by a steady state current with $I_s > I_T$, and the noise oscillations riding on the voltage response are observed in real time. The current is then suddenly driven to zero at time t' and reinstated at a later time t''. The phase with which the oscillations resume at t'' is found (Gill and Higgs 1983) to be exactly the same as the phase with which the oscillations ceased at t'. Hence, during the zero drive static situation between t' and t'', the CDW is in a metastable state which retains the phase information of the earlier sliding state. Variations in temperature during the static situation erase the phase memory.

Both of the above-mentioned memory effects are closely related to 'pulse synchronization', a form of Shapiro step interference viewed in the realtime domain. Pulse synchronization was first observed by Fleming (1982). A train of unipolar rectangular current pulses is applied to the sample and the voltage response is observed in real time on an oscilloscope. As the amplitude of the current pulse I_P exceeds I_T, narrow-band noise oscillations are directly observed. For a given $\boldsymbol{I_P > I_T}$, it is found that the noise oscillations can be enhanced by 'synchronizing' their period to the pulse width. This is accomplished by fine tuning either I_P or the pulse width such that an integral number of noise oscillations 'fit' into the length of the pulse. Causality is satisfied since the memory effect during a particular pulse reflects only the width of the previous identical pulses. An example of pulse synchronization in $NbSe_3$ is shown in fig. 4.9.

During a pulse synchronization experiment, the drive field applied to the sample is precisely of the form eq. (4.1), where E_{dc} is interpreted as the time-average drive signal, and $P(t)$ reflects the positive and negative excursions from E_{dc}. Pulse synchronization may thus be identified as the phenomenon of Shapiro step interference viewed in the time domain. The criterion for pulse synchronization is the same as for Shapiro step interference, eq. (4.3).

From figs. 4.2 and 4.3a, it is apparent that the width of the Shapiro step interference peaks can be substantial, which implies significant noise frequency pulling near the step edges. Analogous frequency pulling can be observed in time domain pulse synchronization experiments on $NbSe_3$ and $K_{0.3}MoO_3$. Figure 4.10 shows the real-time response of $K_{0.3}MoO_3$ to rectangular current pulses. In trace (a), the noise oscillations are clearly visible, and an integral number of oscillations occupy the pulse width. As the pulse width is increased, the noise frequency changes (even though the

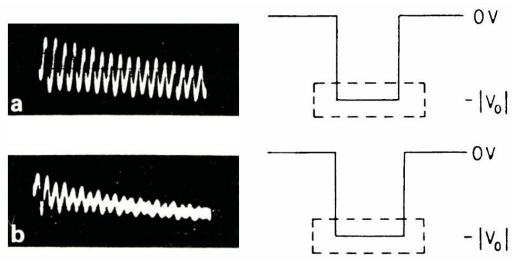


Fig. 4.9. Example of pulse synchronization effect in NbSe_{3} : (a) synchronized; (b) unsynchronized. (From Brown et al. 1986.)

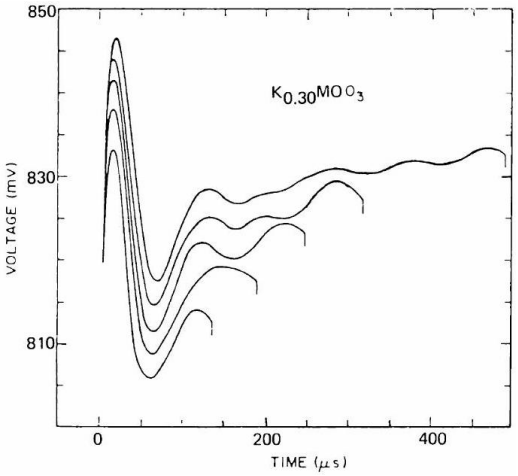


Fig. 4.10. Pulse width memory effect in $\mathrm{K}\mathit{0.3}\mathrm{MoO}_{3}$ at 45 K . The pulses have a period of 10 mS ; different traces correspond to different pulse widths. (From Fleming et al. 1985.)

height of the current drive pulse remains constant) so that an integral number of oscillations still occupies the new pulse width. In other words, changing the ac drive frequency (by changing the drive pulse width) results in a pulling of the noise frequency. Over a substantial range of ω_{ex}, the noise frequency remains locked to a harmonic of ω_{ex} .

In the pulse-induced Shapiro step described in fig. 4.7, saturation of δV occurs for t_1 above approximately 4μ s. This independently identifies a relaxation time comparable to that obtained from pulse memory experiments. The fit of eq. (4.6) to experimental data in fig. 4.7 suggests that a distribution of relaxation times may be more approporiate than a single time scale. The spectrum of times is associated with the development of the pinned state after the high field is turned off. In this sense the behavior is similar to the stretched exponential or logarithmic decay of CDW polarization following a current pulse. However, both the Shapiro step experiments and polarization relaxation experiments probably reflect more a sampling of a large number of metastable states rather than a simple distribution of relaxation times.

A feature of CDW response again related to internal modes, memory, and Shapiro step interference is that of transient ringing, first identified in NbSe_3 (Zettl 1983). Ringing refers to the strong decrease in the amplitude of the narrow-band noise oscillations following the start of a current pulse which drives the CDW from below threshold to above threshold. The ringing resembles an inertial effect, not expected in an overdamped system. Ringing only occurs if the CDW is initially started from a static configuration below threshold, and hence does not simply reflect response to a dramatically changing

drive (i.e. step function with the associated high harmonic frequency content). The amplitude of the transient after the start of the pulse is also strongly dependent upon the dc bias of the pinned CDW prior to the pulse. This strong sensitivity to initial metastable (pinned) state has been exploited to determine CDW relaxation rates between different

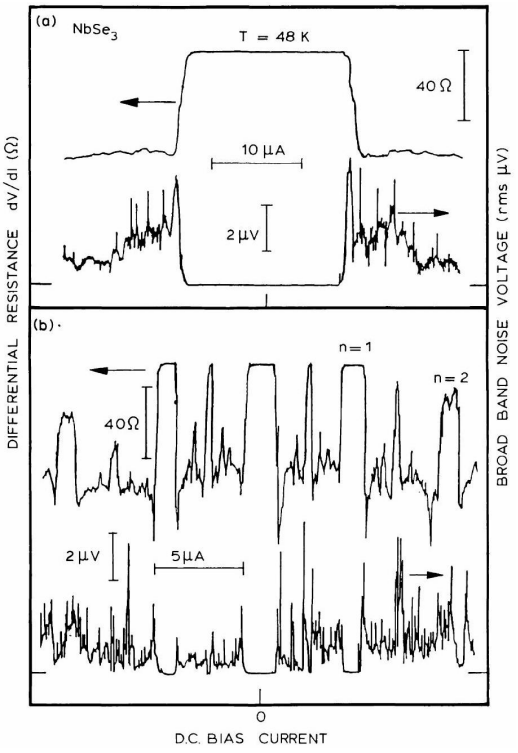


Fig. 4.11. $\mathrm{d} V / \mathrm{d} I$ and broad-band noise amplitude in $NbSe_3$: (a) no rf, (b) with superposed rf drive. Complete electronic locking is associated with a suppression of broad band noise. (From Sherwin and Zettl 1985.)

metastable pinned states. For $NbSe_3$, it is found (Parilla and Zettl 1985) that relaxation from the metastable state just below threshold to the (polarized) metastable state associated with an unbiased (but trained) CDW takes on the order of $50 - 100$ ns. This relaxation is exceptionally fast and distinct from that associated with the 'waiting time' of Shapiro steps experiments.

It has been suggested that the broad-band noise generated by a sliding CDW reflects directly internal CDW degrees of freedom. In the absence of rf radiation, the broad band noise amplitude is a well-defined function of CDW phase velocity. Figure 4.11a shows, for $NbSe_3$, the broad-band noise amplitude as a function of dc bias. In the presence of rf radiation, the CDW phase velocity on a mode locked Shapiro step becomes fixed. Surprisingly, in this locked state the sliding CDW generates no broad band noise (Sherwin and Zettl 1985). This is demonstrated in fig. 4.11b. It has been suggested that during mode locking, the internal degrees of freedom responsible for broad-band noise generation are 'frozen out'. This interpretation suggests that the CDW condensate is exceptionally coherent during mode locking, which has implications for elastic CDW response (see section 7).

4.4. Many degree of freedom models for the interference

Single degree of freedom models have not been fully successful in describing Shapiro step interference phenomena. It appears necessary to explicitly treat the CDW as a many degree of freedom system. The hydrodynamical approach of Sneddon, Cross and Fisher (1982) (see

section 2.2) predicts (to all orders in perturbation theory) no steady state narrow band noise oscillations. In the presence of ac and dc drive fields, however, interference is obtained. The form of the interference in the $I-V$ characteristics is predicted to be (Sneddon et al. 1982)

$$\mathrm{d}I/\mathrm{d}E \approx v_{\mathrm{d}}^{-1} J_n^2 \left(gV_{\mathrm{ac}}/\omega_{\mathrm{ex}}\right) G\left[\left(gv_{\mathrm{d}} - n\omega_{\mathrm{ex}}\right)/v_{\mathrm{d}}^2\right], \tag{4.11}$$

where v_{d} is the dc drift velocity of the condensate, g represents a reciprocal lattice vector, and $G(z)$ is a function peaked at $z = 0$. The model of Sneddon et al. does not predict true mode locking during interference; rather, interference occurs whenever the intrinsic and applied frequencies are relatively close. In addition, the interference features predicted by eq. (4.11) are smooth functions of dc bias, in contrast to the rather sharp Shapiro step interference peaks experimentally observed. Sneddon has extended the classical deformable model to include electrostatic interactions of the CDW with itself (Sneddon 1984), conduction electrons, and the host lattice with defects. The model suggests an important role played by free electron screening. For TaS_3, for example, it is predicted that the wings of the $\mathrm{d}V/\mathrm{d}I$ interference peaks will be strongly enhanced and that
the peak heights will change little as the temperature is lowered in the CDW state. Experimentally, the interference peaks in TaS_3 are observed to broaden with decreasing temperature. Sneddon has further studied (Sneddon 1984) interference effects by extensions of the Frenkel-Kontorova model, where the CDW is treated as interacting discretized units in a periodic potential. The model accounts well for dc field-induced interference structure in the complex ac conductivity of $NbSe_3$ and TaS_3.

Coppersmith and Littlewood (1986) have reexamined the deformable CDW model of Sneddon, Cross and Fisher. The system is discretized and the phase $\phi_i = Qu_i$ at the impurity site becomes

$$\begin{aligned}\mathrm{d}\phi_i/\mathrm{d}t =& \left[\left(\phi_{i+1} - \phi_i\right)/L_i - \left(\phi_i - \phi_{i-1}\right)/L_{i-1}\right] + U\sin\left(\phi_i + \phi_j\right) \\ &+ \frac{1}{2}E(t)\left(L_i + L_{i-1}\right),\end{aligned} \tag{4.12}$$

where $\phi_i = QR_i$ is the undistorted phase and $L_i = R_{i+1} - R_i$ is the distance between the impurities. A sinusoidal pinning potential is assumed. In the low-field regime, eq. (4.12) does predict true mode locking when ω_{ex} is small and $E_{\mathrm{dc}} = E_{\mathrm{ac}}$ such that significant relaxation takes place while the drive field is below threshold. Subharmonic mode locking arises from the presence of many pinned metastable states. The experiments of Brown et al. (1986) discussed in section 4.1 (see fig. 4.5) support this model, i.e., it appears that the CDW needs to spend time below threshold for true mode locking to occur. Figure 4.12 shows mode locking predicted by the deformable CDW model with different numbers of random impurities. Both harmonic and subharmonic interference is observed; the appearance of high-order subharmonics is associated with an increase in the number of degrees of freedom. It is interesting to note that, for a drive configuration where the time the CDW is at rest is long compared to the time above threshold ($t_1 \gg t_2$ in fig. 4.6), a single degree of freedom model with any potential will yield (even with CDW inertia) only harmonic mode locking. This is in contrast to experimental observations, and supports a many degree of freedom model for the Shapiro step interference.

A very large number of degrees of freedom is not necessary to generate subharmonic as well as harmonic mode locking in a classical CDW dynamics model. Matsukawa and Takayama (1987) have considered the case of a set of overdamped coupled oscillators each independently obeying eq. (4.7). Subharmonic interference is obtained for as few as two coupled oscillators. For two linearly coupled oscillators in a sinusoidal potential, the equations of motion are

$$\mathrm{d}\phi_1/\mathrm{d}t = \phi_2 - \phi_1 + \sin\phi_1 + E_{\mathrm{dc}} + E_{\mathrm{ac}}\cos\omega_{\mathrm{ex}}t \tag{4.13a}$$

$$\mathrm{d}\phi_2/\mathrm{d}t = \phi_1 - \phi_2 + \sin(\phi_2 + \delta) + E_{\mathrm{dc}} + E_{\mathrm{ac}}\cos\omega_{\mathrm{ex}}t. \tag{4.13b}$$

Equation (4.13a,b) predict subharmonic mode locking unless $\delta = 0$. Figure

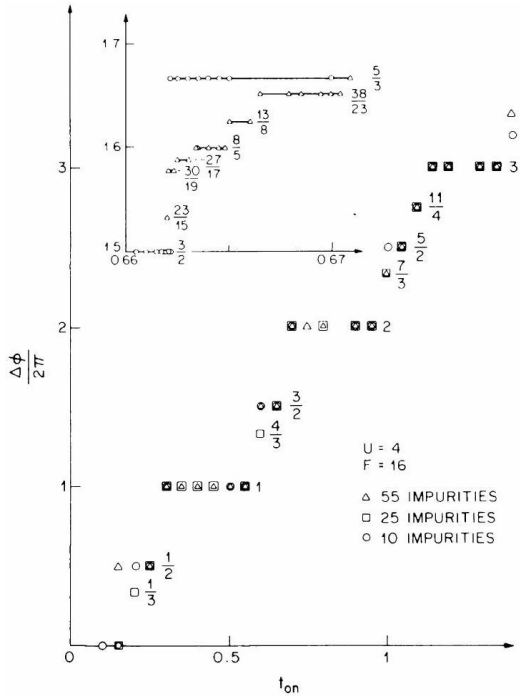


Fig. 4.12. Mode locking in the many-degree-of-freedom model of eq. (4.12). The vertical axis is the number of wavelengths moved per pulse, plotted versus the pulse duration t_{on} with a fixed $E_{\mathrm{on}} = 16$ and $U = 4$. Three different numbers of degrees of freedom are shown: 10,25 or 55. Locking is demonstrated because the number of wavelengths moved is always a rational fraction. Inset: magnified portion of the plot, demonstrating that increasing the number of degrees of freedom causes the appearance of high-order subharmonics (from Coppersmith and Littlewood 1986).

4.13a shows the $I - V$ characteristics of this model with $\delta = \pi/2$. A rich spectrum of mode locking is observed, in good qualitative agreement with experiment. No chaos is predicted, even for large E_{ac}, again consistent with experiments on conventional $NbSe_3$ samples. Figure 4.13b shows mode locking in the $E_{\mathrm{ac}} - E_{\mathrm{dc}}$ plane predicted by eqs. (4.13a,b). The decrease in δV at large ac drive is similar to that observed experimentally (see fig. 4.8).

Recently, it was suggested that CDW memory and associated interference phenomena may be an example of universal 'phase organization'. Tang et al. (1987) consider a 'soft' system with many effective degrees of freedom (such as the Frenkel-Kontorova model with many balls connected with weak springs). If the system driven by a train of rectangular force pulses, the system can be 'trained' such that, at the end of a driving pulse,

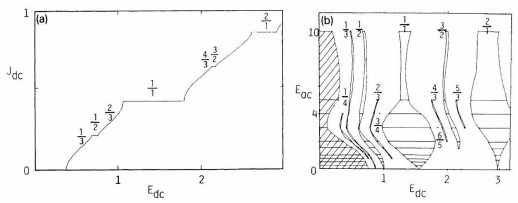


Fig. 4.13. Mode locking for a set of coupled oscillators described by eq. (4.13). (a) Interference in the direct $I - V$ characteristics. The lockings at $q = 1, 2$, and 3 are appreciable. (b) Locking regions in the E_{dc}-E_{ac} plane. (From Matsukawa and Takayama 1987.)

the system will be in a self-organized state. This state can be one that appears least likely for the system, e.g., all balls at the tops of the potential peaks! Figure 4.14 shows an example of a phase organized state. The dynamics of the system self-selects certain metastable states; in a CDW experiment, these states may be those most important for strong interference. Hence, universal phase organization provides a natural account of the pulse duration memory effect (fig. 4.10) and associated mode locking in CDW conductors. Central to the phenomenon of phase organization is the presence of many degrees of freedom. This is in contrast to nonlinear dynamics analyses based, for example, on the circle map (see section 5.1), or a small number of coupled oscillators, e.g. eq. (4.13).

Recently, Dong and Yu (1988) have suggested that many 'pseudoinertial' aspects of CDW dynamics are well described by a single degree of freedom model such as eq. (4.7) with inertia included only for the sliding CDW state. Such a description provides good fits to, for example, transient ringing experiments (Parilla and Zettl 1985). On the other hand, the model cannot account well for metastable state structure.



Fig. 4.14. Snapshot of phase organized state of weakly coupled balls in a sinusoidal potential, just prior to the drive field being turned off. (From Tang et al. 1987.)

4.6.6 5. Driven CDWs and the theory of nonlinear dynamics

A driven CDW comprises an exceedingly complex nonlinear system, with many degrees of freedom. The conventional approach in dealing with dynamical systems is to derive a set of differential equations which describes the system, and then integrate the equations to extract the motion. Often, however, the equations of motion are unknown, or, once established, very difficult to solve.

In many systems with a large number of degrees of freedom (such as a fluid), the complex dynamics are actually well described by only a few active degrees of freedom. In such cases it is often advantageous to describe the dynamics in terms of a low-dimensional discrete mapping, rather than by differential equations of motion. A return map relates the state of the system at index $m+1$ (m could be a time unit) to the state of the system at index m. If the points on the mapping fall on a smooth line, the return map is termed one-dimensional. Once the return map for a system has been identified, the evolution of the system can be tracked by simply iterating the map, which in general is far easier than integrating complex equations of motion. Even exceedingly complex system response (such as chaos) is well described by maps. Return maps find a natural application in the description of nonlinear CDW dynamics (Zettl 1988).

5.1. Competing periodicities: the circle map

Interference in CDW systems results directly from the interaction of two competing periodicities, one defined by the narrow-band noise frequency ω_{NBN} and the other defined by the frequency of the external ac drive ω_{ex}. The general phenomenon of competing periodicities has been extensively studied from the point of view of nonlinear dynamics theory (Aizawa and Kobatake 1975, Jensen et al. 1983a,b, 1984, Bohr et al. 1984, Bak et al. 1984).

Consider the quasiperiodic behavior of a system with internal frequency $\omega_{\mathrm{NBN}} = \mathrm{d}\theta_1/\mathrm{d}t$ driven by an incommensurate source at frequency $\omega_{\mathrm{ex}} = \mathrm{d}\theta_2/\mathrm{d}t$. The evolution of the system in phase space can be represented as motion on a two-dimensional torus, as illustrated in fig. 5.1. A particular plane cutting through the torus defines a Poincaré section; in fig. 5.1 the plane has been chosen at $\theta_2 = 0$. The intersection points of the system trajectory with the chosen plane may be obtained by 'strobing' the system at 'times' $\theta_2 = 0, 2\pi, 4\pi$, etc., and recording the intersection points in the plane. The series of points thus obtained clearly lie on the intersection of the torus surface with the plane; this intersection is topologically equivalent to a circle. As the system evolves and points accumulate, points on the circle generated during one pass of the system are mapped to another part

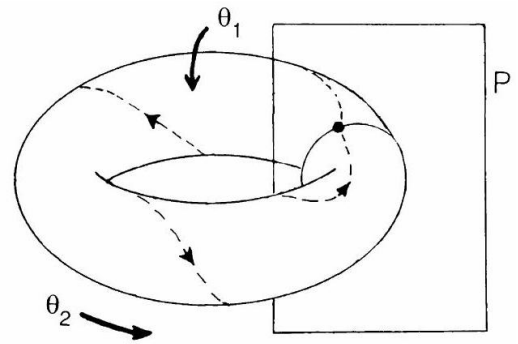


Fig. 5.1. Motion on a 2D torus for a system with two competing periodicities. Phase 1 represents the intrinsic system periodicity; phase 2 represents the external drive periodicity. The dashed line is the trajectory for a $p/q = 3/1$ mode locked state. The Poincaré section contains a single point.

of the circle during the next pass. This defines a nonlinear map of the 'circle onto itself'. One such mapping of the invariant circle is the sine circle map,

$$\theta_{m+1} = \theta_m + \Omega + (K/2\pi)\sin(2\pi\theta_m)\,, \tag{5.1}$$

a discrete mapping which has been used extensively to describe many natural systems with two competing periodicities (Aizawa and Kobatake 1975, Jensen et al. 1983a,b, 1984, Bohr et al. 1984, Bak et al. 1984). Here $\theta_m = \theta(t = mT)$ with m an integer and $T = 2\pi/\omega_{\mathrm{ex}}$ .K represents the strength of the coupling between the external drive and the system, and Ω is the ratio of the two characteristic frequencies in the absence of interference (i.e. $\Omega = \omega_{\mathrm{NBN}}/\omega_{\mathrm{ex}}$). The sine circle map predicts mode locking, subharmonic interference, and a quasiperiodic transition to chaos. Figure 5.2 shows some of the more prominent mode locked regions for the sine circle map in $K - \Omega$ space. For $K < 1$, the mode locked steps form an (incomplete) devil's staircase of dimension $d = 1$. Just at $K = 1$, the staircase is complete with a fractal dimension (Jensen et al. 1983a,b, 1984, Bohr et al. 1984, Bak et al. 1984) $d = 0.870$. This is the Hausdorff dimension of the complementary Cantor set for the mode locked region. For $K > 1$, resonances overlap and the map is no longer invertable, hence chaos is possible.

There are two motivations for analyzing CDW interference phenomena in the context of the sine circle map. First, the sine circle map has been found to give a surprisingly accurate account of mode locking in several physical systems with competing periodicities (examples being barium sodium niobate (Martin and Martienssen 1986) and germanium (Gwinn and Westervelt 1987). A second motivation is that detailed numerical and

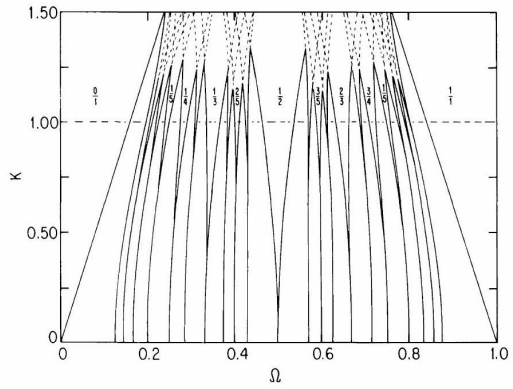


Fig. 5.2. Mode locked regions in the sine circle map. Only a selected set of locked regions is shown. The critical line is at $K = 1$. (From Jensen et al. 1983a,b, 1984, Bohr et al. 1984, Bak et al. 1984.)

analytic calculations (Jensen et al. 1983a,b, 1984, Bohr et al. 1984, Bak et al. 1984) have demonstrated that, for a certain parameter range, the sine circle map is the appropriate return map for the damped pendulum equation, eq. (4.7), which forms the basis of the rigid particle classical model of CDW motion.

The first analysis (Brown et al. 1984) of CDW interference in terms of the circle map addressed the fractal dimension of the locked and unlocked region in a Shapiro steps experiment. To analyze experimental data such as shown in fig. 4.3a, one could count up the widths of all mode locked regions in Ω space, and to test for completeness of the devil's staircase determine if the quasiperiodic orbits (gaps) are confined to a Cantor set of zero measure. A more practical (finite resolution) method is to consider the behavior of the gaps (Brown et al. 1984, Jensen et al. 1983a,b, 1984, Bohr et al. 1984, Bak et al. 1984). Given a scale r, the total measure of the gaps between the mode locked steps is $1 - S(r)$, and the number of holes $N(r) = [1 - S(r)]/r$. If $rN(r) \to 0$ as $r \to 0$, the staircase is complete, with fractal dimension d given by

$$N(r) \propto r^{-d}. \tag{5.2}$$

Such an analysis for $NbSe_3$ by Brown et al. (1984) is shown in fig. 5.3. The data lie on a line whose slope indicates a fractal dimension $d = 0.91$, close to the expected value of 0.87 and hence suggestive that the system is close

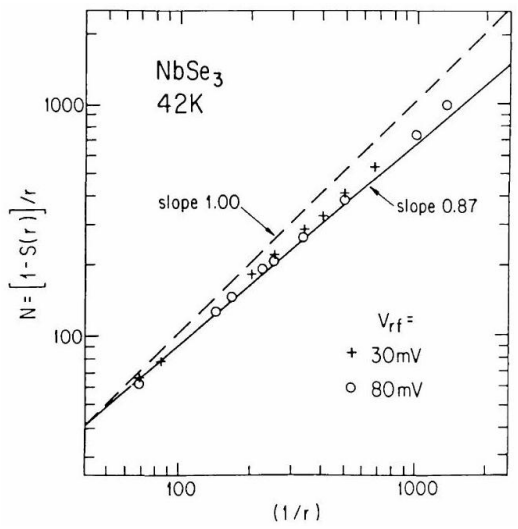


Fig. 5.3. Fractal dimension determination of Shapiro step locking in NbSe_{3}. The data lies close to $d = 0.87$ expected from the circle map at the critical line. (From Brown et al. 1984.)

to criticality and chaotic response. However, no critical line or chaotic response has been identified, even for a large range of ac drive amplitudes. More systematic studies by Sherwin et al. (1988) have also demonstrated that d is strongly ac amplitude dependent in $NbSe_3$, and tends to approach 1 for large ac drive. In the context of the circle map, mode locking in $NbSe_3$ is always subcritical (i.e. $K < 1$).

In comparing the predictions of the sine circle map to CDW response, it seems natural to associate K in eq. (5.1) directly with $E_{\rm ac}$, and Ω with $E_{\rm dc}$. A plot of mode locking in the $E_{\rm ac} - E_{\rm dc}$ plane for a CDW system might then be analogous to fig. 5.2 for the circle map. Such direct comparison, however, reveals serious discrepancies, such as the experimentally observed oscillatory behavior of δV with increasing $E_{\rm ac}$ (see figs. 4.4 and 4.8), and the lack of chaotic response at high ac drive. These problems suggest that the driven CDW condensate is not the best physical realization of the sine circle map, at least not if K is directly associated with $E_{\rm ac}$ (in section 5.2.2, it is argued that this direct association is flawed). The physical significance of a well-defined fractal dimension corresponding to the mode locking in $NbSe_3$ is not clear.

5.2. CDW switching and transitions to chaos

For most CDW crystals the CDW condensate depins smoothly as an applied dc bias exceeds threshold $E_{\rm T}$; the functional form of the $I - V$ characteristic
is similar to the Zener tunneling expression. However, not all samples of a given material display smooth depinning. In selected crystals of $NbSe_3$, TaS_3, $K_{0.3}MoO_3$, and $(NbSe_4)_{3.33}I$, the CDW depins in a sharp, hysteretic manner which results in a strong discontinuity in the dc $I - V$ characteristics. This phenomenon was first observed in the lower CDW state of $NbSe_3$ by Zettl and Grüner (Zettl and Grüner 1982), and it is referred to as switching.

Switching typically occurs only over a limited temperature range for a given sample. The switching state is characterized by a temperature independent depinning field (Hall and Zettl 1984), $I - V$ hysteresis (Zettl and Grüner 1982), negative differential resistance (Hall et al. 1984), inductive ac response (Hall and Zettl 1985), and large phase polarization (Hall et al. 1988). In the presence of combined ac and dc drive fields, switching samples show unusual Shapiro step structure and period doubling routes to chaos (Hall et al. 1984). Switching can be induced by strong impurity doping or irradiation, and it appears to arise from isolated 'ultrastrong' impurity pinning within the crystal bulk (Hall et al. 1988). The observed velocity

discontinuities (Hall et al. 1986) in switching crystals imply local, periodic collapse of the CDW amplitude at phase slip centers. Consequently, one of the most interesting aspects of CDW switching is that to successfully model the phenomenon, it is necessary to include degrees of freedom for both the CDW amplitude and phase. This is in contrast to most models of CDW conduction (see section 2) which treat the CDW amplitude as rigid and assign degrees of freedom only to the CDW phase. Switching in $NbSe_3$ has been extensively studied experimentally (Sherwin et al. 1988, Hall and Zettl 1985, Hall et al. 1988) and theoretically (Inui et al. 1988).

5.2.1. Mode locking and chaos

Figure 5.4 shows Shapiro steps interference phenomena in a switching crystal of $NbSe_3$ (Hall et al. 1984). The interference steps in this voltagedriven experiment are the roughly horizontal plateaus whose differential resistance is equal to the low-field pinned state differential resistance. Switching samples show dramatic mode locking. In the trace corresponding to $V_{\rm rf} = 28$mV in fig. 5.4, for example, complete mode locking, with little space between harmonic mode locked steps, is observed over a large range of dc bias.

On any particular mode locked Shapiro step shown in fig. 5.4, the time averaged dc CDW velocity is constant and insensitive to dc bias. One might expect, on a mode locked step, that higher frequency fluctuations are suppressed, as is the case for non-switching samples (Sherwin and Zettl 1985). For switching samples, however, the situation is quite different; indeed, some of the most complex CDW response occurs precisely when the condensate is mode locked in the dc limit! Figure 5.5a shows an expanded view of mode locked Shapiro steps in switching $NbSe_3$ similar to

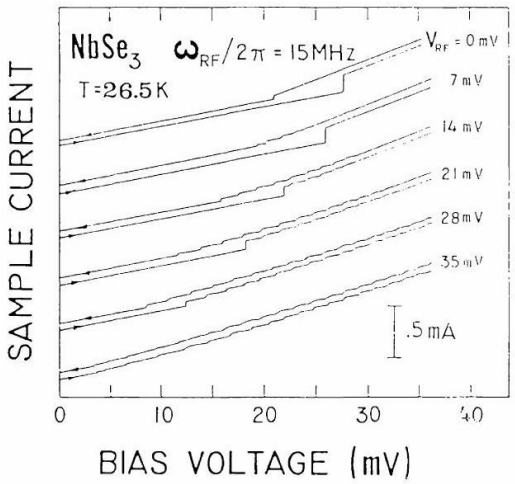


Fig. 5.4. Mode locking in direct $I-V$ traces of switching \$\mathrm{NbSe}_{3}\$. (From Hall et al. 1984.)

those seen in fig. 5.4. The solid line response is measured at zero frequency. The arrows indicate forward and reverse voltage bias sweep direction, and the traces have been vertically offset for clarity. The CDW is nearly always harmonically mode locked. Figure 5.5b shows the corresponding response spectrum in the frequency domain, for selected dc bias voltages on a particular mode locked step. Complex response is obtained, with an apparent period doubling route to chaos with increasing dc bias. The first frequency spectrum shows only the fundamental of the rf drive at frequency $f = \omega_{\rm ex}/2\pi = 5$MHz, and higher harmonics of f due to the non-linearity of the CDW system. In the second spectrum, peaks appear at $f/2$, indicating that a period doubling bifurcation has occurred. The third spectrum shows a generally elevated noise level and new frequency structure indicative of a second period doubling bifurcation. The final

spectrum shows broad-band chaotic response. The bifurcation points are shown schematically in fig. 5.5a as vertical lines separating different response forms. It is apparent that on each mode locked step, there is a period doubling route to chaos. Such behavior is only observed in switching samples, and thus far it has only been observed in $NbSe_3$ although it probably exists in other switching CDW materials as well.

Figure 5.6a shows the structure of mode locking in the $E_{ac} - E_{dc}$ plane for switching $NbSe_3$ (Sherwin et al. 1988). At the lowest value of ac drive shown (top of fig. 5.6a) there is a hysteretic transition between the $n = p/q = 0/1$ and $1/1$ steps, and the $n = 1/2$ step is eclipsed. There is no gap between the $0/1$ and $1/1$ steps. The period doubling route to chaos is most strongly developed in this region of very hysteretic mode locking. At higher values of ac drive (lower in fig. 5.6a), the $n = 1/2$ step emerges and a

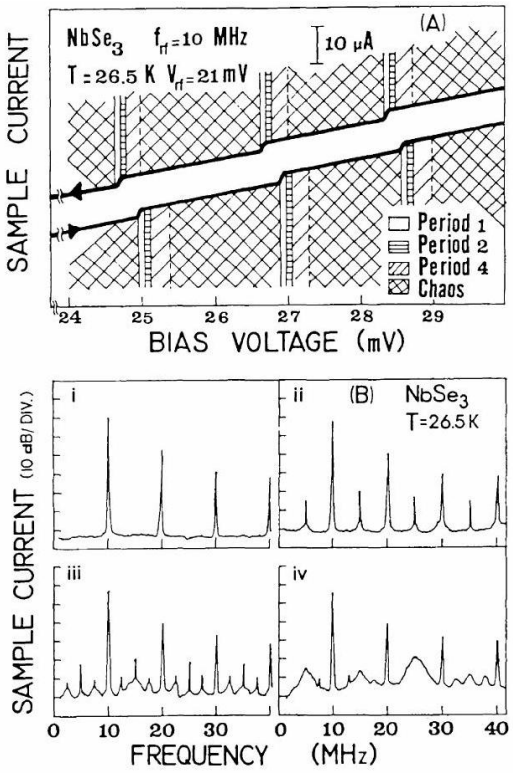


Fig. 5.5. (a) Schematic representation of current response in voltage-driven Shapiro step region of switching \$\mathrm{NbSe}_{3}\$. The heavy solid lines are the $I - V$ characteristics. A period doubling route to chaos is observed on each mode locked step. Forward and reverse current sweeps have been vertically offset for clarity. (b) Frequency spectrum of current response for selected dc bias. External rf drive frequency and amplitude as in (a). (i) $V_{dc} = 25$mV, period 1; (ii) $V_{dc} = 25.1$mV, period 2; (iii) $V_{dc} = 25.2$mV, period 4; (iv) $V_{dc} = 25.5$mV, chaos. (From Hall et al. 1984.)

smaller fraction of parameter space is occupied by the mode locked regions. Some period doubling instabilities still exist, but they occur less frequently. Below the critical line identified at $V_{rf}/V_c = 0.97$, period doubling instabilities are no longer observed, and the $n = 1/2$ step shrinks in relative magnitude. In general the response is a very complicated function of ac amplitude and frequency, dc bias, and temperature.

5.2.2. Models for the switching and chaotic response

Mode locking in switching CDWs has many of the characteristics of inertial, underdamped motion. Another way of writing eq. (4.4) in dimensionless form is (Hall et al. 1984, D'Humieres et al. 1982)

$$\beta \mathrm{d}^2\varphi/\mathrm{d}t^2 + \mathrm{d}\varphi/\mathrm{d}t + \sin\varphi = e_{\mathrm{dc}} + e_{\mathrm{ac}} \sin(\Omega_{\mathrm{s}} t)\,, \tag{5.3}$$

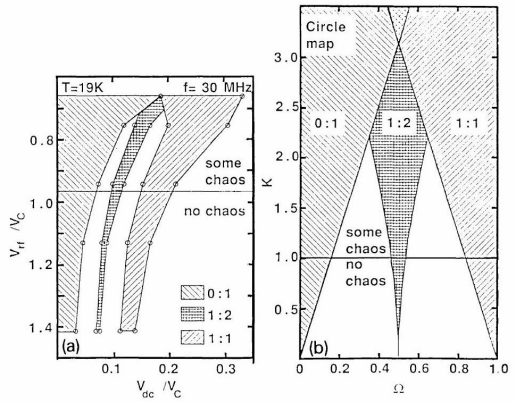


Fig. 5.6. (a) $p/q = 0/1, 1/2$, and $1/1$ mode locked regions of switching NbSe_3. Period doubling and chaos are observed only above the solid horizontal line at $V_{\mathrm{rf}}/V_{\mathrm{c}} = 0.97$. (b) Predictions of the sine circle map. Note the similarity to (a). (From Sherwin et al. 1988).

where β quantifies system inertia, e_{dc} and e_{ac} are dc and ac drive fields normalized to the threshold field E_{T}, and Ω_{s} is the ac drive frequency scaled to $\omega_0^2\tau$. In this representation the inertial parameter is more transparent. The solutions of eq. (5.3) with finite β show (D'Humieres et al. 1982, Kautz 1981) many of the features of driven switching CDWs, including hysteresis, mode locking, and chaos. For $\beta > 1$ (underdamped motion), hysteretic Shapiro steps are predicted, and period doubling routes to chaos are observed on some of the mode locked steps (Kautz 1981). However, eq. (5.3) fails to account in detail for switching CDW response. For example, the ac conductivity of a switching CDW with no applied dc field appears overdamped, inconsistent with eq. (5.3) when β is extracted from the switching $I-V$ characteristics. Equation (5.3) also predicts chaotic response for the limited frequency range $\beta^{-1} < \omega_{\mathrm{ex}} < \beta^{-1/2}$, inconsistent with experimental observations of chaos in NbSe_3 over a much larger frequency range (Hall et al. 1984). Finally, the period doubling route to chaos of eq. (5.3) is not periodic in dc bias, in contrast to the experimental data of fig. 5.4 Thus eq. (5.3) does not provide an entirely satisfactory description of CDW dynamics in either switching or non-switching CDWs.

Recent studies (Sherwin et al. 1988) have re-examined the applicability of the sine circle to CDW dynamics. Although the circle map does not provide
a good description for mode locking in non-switching CDWs, it is surprisingly successful in describing the complex behavior of switching CDWs! Figure 5.6b shows for the sine circle map the mode locked regions $p/q = 0/1, 1/2$ and $1/1$ in $K-\Omega$ space. The critical line at $K = 1$ is indicated. For $K < 1$, the circle map predicts distinct mode locked, and quasiperiodic, solutions, but no period doubling or chaos. For $K > 1$, the circle map has a local maximum, with different possible states of the system for a given set of drive parameters. At the edges of the $p/1$ and $p/2$ regions for $K > 1$, the solutions represent simple mode locking. However, as Ω is swept toward the center of the mode locked regions, period doubling instabilities and chaos occur for this range of K. For both the CDW and the circle map, the structure of mode locking and the period doubling route to chaos are periodic in dc bias.

A comparison between figs. 5.6a and 5.6b shows a surprising correspondence between the CDW response and behavior predicted by the circle map. It is interesting that the data indicate that K is inversely related to $E_{\rm ac}$, i.e. large $E_{\rm ac}$ corresponds to small K. This inverse relation reflects a general feature of many nonlinear systems: when forced sufficiently strongly, the nonlinearity of the system becomes a mere perturbation to a linear system. This 'linearizing' effect accounts for the decreasing widths of Shapiro steps with increasing ac drive for both switching and nonswitching CDWs.

The observation of period doubling in mode locked switching CDWs indicates that mode locking in this system can be supercritical, i.e. $K > 1$. The critical line in fig. 5.6a separates regions in which period doubling (not necessarily chaos) is and is not observed experimentally in $NbSe_3$. The dimension of the mode locked regions along this line should be a lower bound to the dimension predicted by the circle map at $K = 1$. Sherwin et al. (1988) have found that $d = 0.85 \pm 0.05$ at the critical line of switching $NbSe_3$, in agreement with the circle map predictions.

The structure of mode locking in switching CDWs is seen to be consistent with the predictions of the circle map in nontrivial ways: (1) The presence of dynamical instabilities is correlated with the width of mode locked steps. (2) The structure of mode locking and the period doubling route to chaos are periodic in dc bias. (3) The period doubling cascade occurs as the system is pushed from the edge of mode locked regions toward the middle of those regions. (4) The fractal dimension of the devil's staircase (Cantor set complementary to the mode locked regions) at the critical line is within experimental error of theoretical predictions.

The success of the circle map in describing the complex response of switching CDWs in the presence of ac and dc drive fields unfortunately gives no insight into the microscopic origins of the unusual dynamics. It has been demonstrated by Hall et al. (1986, 1988) that phase slip processes
within the crystalline bulk are integral to the switching process. Phase slip gives rise to an apparent motion-dependent inertia which can qualitatively account (Inui et al. 1988) for harmonic and subharmonic mode locking, and period doubling routes to chaos. The phase slip process requires a macroscopic polarization of the CDW prior to the collapse of the CDW amplitude. After the amplitude collapses, a finite time is needed for the CDW to depolarize before it can slide. This lag in the response resembles system inertia (response lags the force). When the phase slip process is entrained at a frequency of order the inverse of the relaxation time, the tendency of the CDW to follow the external forcing may compete with the requirement that the CDW 'remember' its previous polarization state (see section 4.3). This competition leads to a frustrated subharmonic or chaotic response.

The detailed dynamics of a CDW condensate with associated phase slip centers has been examined by Hall et al. (1986) and Inui et al. (1988). In simplified form, the equations of motion for the CDW condensate are

$$\mathrm{d}\phi_{\rm bulk}/\mathrm{d}t = e - \sin\phi_{\rm bulk} - \alpha\Delta\left(\phi_{\rm bulk} - \phi_{\rm psc}\right), \tag{5.4a}$$

$$\kappa\mathrm{d}\Delta/\mathrm{d}t = -\left(\Delta + \left[\phi_{\rm bulk} - \phi_{\rm psc}\right]^2/\Theta^2 - 1\right), \tag{5.4b}$$

$$\phi_{\rm psc} \to \phi_{\rm psc} \quad \text{if} \quad \Delta > 0, \quad \phi_{\rm psc} \to \phi_{\rm psc} \pm 2\pi \quad \text{if} \quad \Delta \leqslant 0, \tag{5.4c}$$

where $\phi_{\rm bulk}$ represents the bulk CDW phase. $\phi_{\rm bulk}$ couples to a normalized electric field e, an impurity pinning potential $\sin\phi_{\rm bulk}$, and a strongly pinned phase $\phi_{\rm psc}$ at the phase slip center. $\phi_{\rm psc}$ changes by hops of 2π when the CDW amplitude Δ at the strong pinning site collapses, and Δ obeys simple relaxational dynamics driven by the square of the phase polarization, $(\phi_{\rm bulk} - \phi_{\rm psc})^2$. α represents the stiffness of the phase mode, κ is the ratio of phase to amplitude relaxation rates; and Θ is the stiffness of the amplitude mode.

Equations (5.4a)-(5.4c) are intractable analytically, but solutions have been obtained by numerical integration on a digital computer (Inui et al. 1988). Figure 5.7 shows the predicted response for a Shapiro step experiment in the $E_{\rm ac} - E_{\rm dc}$ plane. The amplitude relaxation rate has been fixed at $\kappa = 0.5$. Typically, solutions in fig. 5.7 are periodic and mode locked to harmonic (p/q = integer) Shapiro steps. The solutions are identified with the step index n and period P as (n, P). The blank areas in fig. 5.7 represent quasi-periodic or subharmonically mode locked solutions. In typical CDW experiments, the ac field amplitude is held constant and the dc bias is swept through a range of values. The horizontal line in fig. 5.7 corresponds to an analogous sweep. As $e_{\rm dc}$ increases along this line, solutions move through the third harmonic Shapiro step, then through the fourth harmonic Shapiro step, and finally through an unlocked region to the fifth harmonic Shapiro step. Figure 5.8 shows the details of this sweep. The dashed line in the figure represents the entrainment ratio (Shapiro step

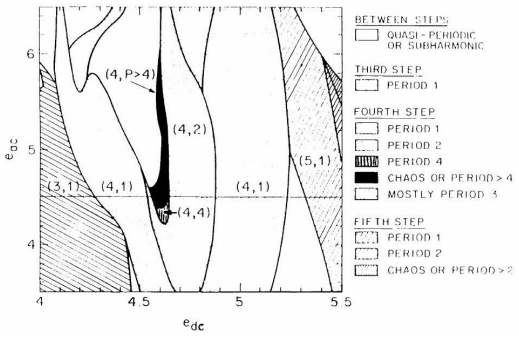


Fig. 5.7. Predicted response of phase-slip model of switching, eqs. (5.4a)-(5.4c). Harmonically mode locked solutions are characterized by an index pair (n, P) which represents their entrainment n and periodicity P. (Boundaries between different regions are approximate). (From Inui et al. 1988.)

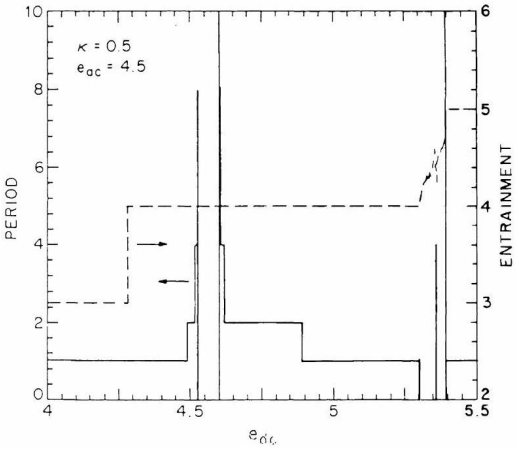


Fig. 5.8. A dc sweep along the solid horizontal line of fig. 5.7. The dashed and solid lines respectively indicate the entrainment and periodicity of solutions found in this range of dc bias. (From Inui et al. 1988.)

order). Over most of the figure, solutions are mode-locked to a harmonic step, similar to what is observed experimentally in the switching regime of $NbSe_3$ (figs. 5.4 and 5.5a). For example, the third Shapiro step in fig. 5.8 extends from $e_{\rm dc} = 4.0$ to 4.3 ; the fourth step from 4.3 to 5.3, and the fifth step from 5.4 to 5.5 .

The solid line in fig. 5.8 represents the periodicity index P (quasi-periodic and chaotic solutions are assigned $P = 0$). Even though solutions are usually mode-locked at dc in fig. 5.8, the periodicities of the solutions are often not one. For example, on the fourth Shapiro step, a period doubling cascade to chaos is observed. The corresponding response in the frequency domain is shown in fig. 5.9 for selected values of dc bias in this cascade. The behavior on this step is remarkably similar to that observed in $NbSe_3$, as shown in fig. 5.5b. Nearly all of the unusual mode locking and chaotic response features of switching CDWs are, at least qualitatively, well accounted for by the phase slip model of switching.

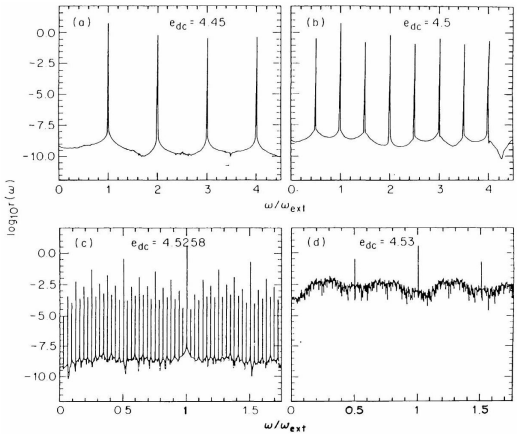


Fig. 5.9. Period doubling route to chaos in the phase slip model of switching induced by increasing dc bias on a particular mode locked step. (From Inui et al. 1988.)

4.6.7 6. Relevant length scales and domain structure

6.1. Intrinsic phase and velocity domains

The static CDW is characterized by a finite static phase coherence length given by the Fukuyama-Lee-Rice length (Lee and Rice 1979)

$$L_s = 2\pi/n_i V_0^2 \tag{6.1}$$

where V_0 is the strength of the impurity potential and n_i is the impurity concentration. L_s is roughly the length over which the phase fluctuations $\langle \delta\phi^2 \rangle^{1/2}$ is less than 2π. For most CDW conductors, L_s is estimated to be on the order of one micron or less, consistent with lower bounds extracted from X-ray scattering measurements. For a dynamic CDW, several new length scales come into play. The dynamic phase-phase correlation length $\langle \phi(0)\phi(x) \rangle$ of a dc-driven sliding CDW condensate has been estimated (Mozurkewich and Grüner 1983) from the narrow-band noise studies, and implies a microscopic domain volume $\Omega_d = 0.2\mu$ m^3. Within this domain the phase of the CDW behaves more or less as a rigid entity. As the sample volume increases, different microscopic domains oscillate out of phase, and the narrow band noise amplitude falls as $\Omega_d^{-1/2}$, vanishing in the thermodynamic limit. In this interpretation, the noise is a finite-size effect. The recent observation (Hundley and Zettl 1988) of very coherent and large amplitude narrow-band noise response in ultra-thin $K_{0.3}MoO_3$ crystals supports this interpretation.

The time derivative of the CDW phase defines a CDW phase velocity with an associated narrow band noise frequency. Since mode locking experiments reflect interaction between an external rf field and the narrowband noise frequency, Shapiro step interference is a useful method to investigate CDW phase velocity coherence and its sensitivity to external ac fields. The phase velocity-velocity correlation function

$$\langle (\mathrm{d}\phi(0)/\mathrm{d}t)(\mathrm{d}\phi(x)/\mathrm{d}t)\rangle \tag{6.2}$$

defines an ac-sensitive dynamic velocity coherence length ξ_{D} which may greatly exceed $L_{\mathrm{s}}.\xi_{\mathrm{D}}$ is dependent on the CDW velocity and the amplitude and frequency of externally applied electric fields (Hall et al. 1987).

In a $\mathrm{d}V/\mathrm{d}I$ Shapiro step mode locking experiment, the height of the interference peak during mode locking will coincide with the pinned differential resistance only if the entire CDW condensate takes part in the interference. Such 'complete' locking is, however, not always observed (compare, for example, figs. 4.3a,b and c). The completeness of mode locking can be influenced by changing sample dimensions (Hall et al. 1987). Figure 6.1a shows Shapiro step interference for a relatively long and thick $NbSe_3$ sample. The height of the $n = 1$ step indicates incomplete locking. If

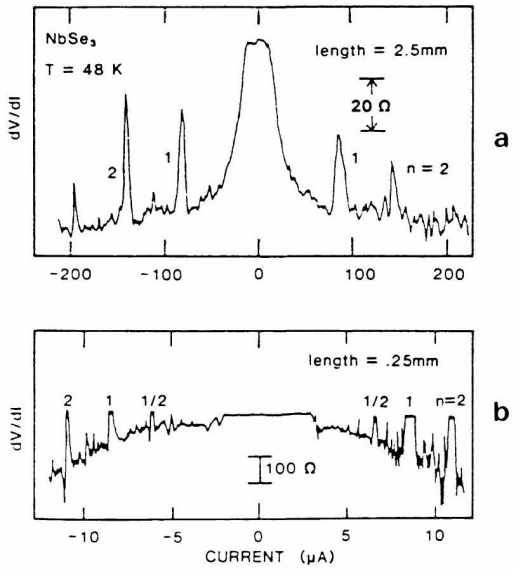


Fig. 6.1. Shapiro step spectrum of NbSe_{3} crystal. rf frequency is 5 MHz and rf amplitude has been adjusted to maximize the $n = 1$ step height. (a) Original crystal, incomplete locking; (b) Spectrum for a sample cleaved from original crystal. Here sample length and cross-sectional area have both been reduced by a factor of 10 . The smaller sample displays complete locking.
(From Hall et al. 1987.)

the sample is reduced in volume by decreasing its length and cross sectional area by factors of 10 , the interference structure of fig. 6.1 b results. Complete locking is now observed. This suggests that large samples are composed of a number of large, macroscopic velocity-coherent domains, which may oscillate at independent frequencies for a given set of drive parameters. The volume of these macroscopic domains may be determined from the Shapiro step interference spectrum.

The height h of the interference peak, measured from the effective base line (or saturated $\mathrm{d}V/\mathrm{d}I$ value) represents the volume fraction of the CDW condensate mode locked to the external ac drive (Hundley and Zettl 1986, Zettl 1986). This is simply understood if one considers the thin CDW conductor as a linear series of domains. Each domain consists of an independent CDW condensate in parallel with a resistance R_{n} representing normal electrons. Differences in CDW phase velocity from one domain to the next are compensated for by carrier conversion at domain interfaces.

The CDW associated with each domain has a differential resistance $R_{\rm CDW}$, where $R_{\rm CDW} \to \infty$ if the domain is mode locked, and $R_{\rm CDW} \to R_{\rm c}$ (a constant) in the conduction saturated (unlocked) limit. In this model, the total differential resistance for the sample is (Zettl 1986)

$$\mathrm{d}V/\mathrm{d}I = \sum_{j=1}^{N} R_{\rm n} R_{\rm CDW} / \left(R_{\rm n} + R_{\rm CDW}\right), \tag{6.3}$$

where j indexes the domain and N is the total number of domains in the crystal. If all N domains are mode locked, $\mathrm{d}V/\mathrm{d}I = \sum_{j=1}^{N} R_{\rm n} = \mathrm{d}V/\mathrm{d}I\,(I_{\rm dc} = 0)$, and

$$h = h_{\rm max} = \sum_{j=1}^{N} R_{\rm n} - \sum_{j=1}^{N} R_{\rm n} R_{\rm c} / \left(R_{\rm n} + R_{\rm c}\right).$$

If, on the other hand, only M of the N domains are mode locked,

$$h = \sum_{j=1}^{M} R_{\rm n} + \sum_{j=M+1}^{N} R_{\rm n} R_{\rm c} / \left(R_{\rm n} + R_{\rm c}\right) - \sum_{j=1}^{N} R_{\rm n} R_{\rm c} / \left(R_{\rm n} + R_{\rm c}\right).$$

This implies that the experimentally determined ratio $h/h_{\rm max} = M/N$, the locked volume fraction.

For a given Shapiro step (indexed by n), the ratio $h/h_{\rm max}$ depends on both the ac electric field amplitude and frequency, and of course the size of the crystal.

To determine $\xi_{\rm D}$(ac) explicitly, one may explore mode locking for a single large crystal over different spatial ranges. Figure 6.2 shows the results for such an experiment (Hall et al. 1987) in $NbSe_3$, where non-perturbative 'sliding' voltage sensing probes were used to determine $h/h_{\rm max}$ for the $n = 1$ Shapiro step, as a function of distance d between voltage probes. The

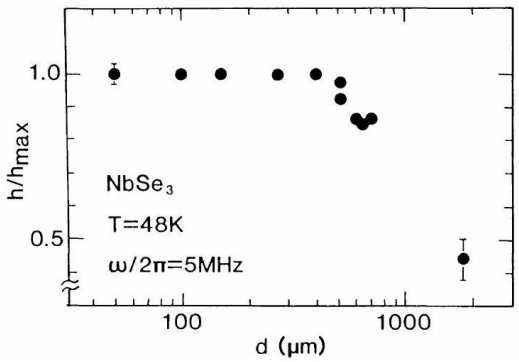


Fig. 6.2. Ratio of h / h_{max} for mode locking in $NbSe_3$ crystal. d is the distance between voltage sensing probes on the crystal surface (from Hall et al. 1987).

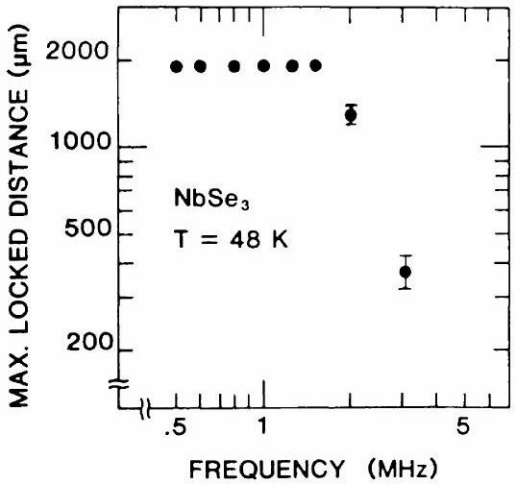


Fig. 6.3. Maximum linear domain size versus rf frequency in NbSe_{3}. For applied frequency less than 2 MHz , the domain size equals the entire sample volume. (From Hall et al. 1987.)

external ac frequency is 5 MHz , and the ac amplitude has been chosen to maximize $h/h_{\max}$. For $d > 500\mu$ m, $h/h_{\max}$ decreases with increasing probe separation, while $h/h_{\max} = 1$ for $d < 500\mu$ m. This determines $\xi_{\mathrm{D}} = 500\mu$ m for relatively pure specimens of $NbSe_3$. Within a length on the order of 500μ m, all microscopic domains may be fully mode locked by an external ac electric field of frequency 5 MHz .

Using a similar sliding voltage probe method, the frequency dependence of ξ_{D} has also been explicitly determined (Hall et al. 1987) for $NbSe_3$. For low $\omega_{\mathrm{ex}}, \xi_{\mathrm{D}}$ may be very large, exceeding the sample length of 0.2 mm in fig. 6.3. Above 2MHz, ξ_{D} is seen to drop dramatically with increasing ω_{ex}. Hence at high CDW velocities, the CDW condensate is broken into numerous macroscopic regions with independent phase velocities. Even a very large amplitude rf field is unable to synchronize the regions.

6.2. Temperature gradient effects

An interesting aspect of phase velocity coherence is the effect of an applied uniform temperature gradient. Experiments (Lyding et al. 1986, Ong et al. 1984) have demonstrated that a temperature gradient may split the narrowband noise spectrum into two or more seemingly independent spectra, with no smearing of the noise peaks. Although such splitting was originally taken as evidence for noise generation at sample contacts (see section 2.5), most experiments point to an interpretation in which the CDW breaks into macroscopic domains, each with a different characteristic phase velocity and oscillation frequency.

The splitting of the noise spectrum in a temperature gradient is reflected also in the Shapiro step spectrum. Figure 6.4 shows the results of such an

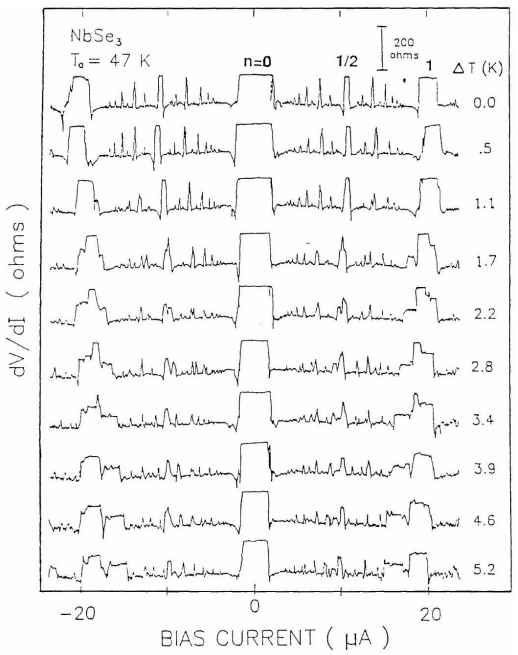


Fig. 6.4. Shapiro step interference in NbSe_{3} in the presence of an applied temperature gradient. For finite gradient, the sample breaks into independent phase-velocity coherent domains with independent Shapiro step spectra. (From Hundley and Zettl 1986.)

interference experiment (Hundley and Zettl 1986) on $NbSe_3$ performed in the presence of a temperature gradient. Independent interference peaks, associated with mode locking to different macroscopic regions within the sample, are observed. From the ratio $h/h_{\max}$ associated with each set of interference peaks, the volumes of the independent regions can be evaluated. The data of fig. 6.4 suggests that the sample has split into two
independent macroscopic domains, with the 'hot' domain comprising 40% of the sample volume and the 'cold' domain comprising 60% of the sample volume. This accounts for 100% of the sample volume. The interface between the macroscopic domains must consist of a phase slip center.

The total number of macroscopic domains within a sample subjected to a temperature gradient represents a competition between the tendency to decrease CDW elastic energy by forming more domains, and the tendency to increase phase slip energy when more domains are formed (with the associated formation of more domain interfaces). A simple model has been proposed by Hundley et al. (unpublished) which explicitly evaluates the balance of elastic and phase slip energy in terms of measurable CDW parameters. Figure 6.5 shows the calculated strain energy, phase slip energy, and total CDW energy as a function of the number of macroscopic domains in a CDW crystal subject to a temperature gradient. The parameters used in the calculation represent those expected for a $NbSe_3$ crystal of length 1 mm and cross-sectional area 5×10^{-7} cm^2, at temperature $T_0 = 48$ K (cold end) with a gradient of 6 K across the sample, and subject to a dc bias current $I_0 = 100\mu$ A. The total energy is minimized if the sample breaks into three domains, consistent with the number of domains observed in a real $NbSe_3$ crystal under similar experimental conditions (Hundley and Zettl 1986, Lyding et al. 1986).

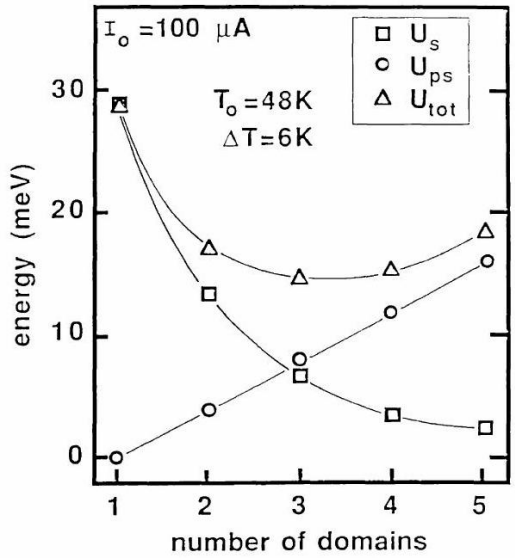


Fig. 6.5. Predicted number of domains for an assumed NbSe_{3} sample in a temperature gradient. Energy considerations suggest for the indicated set of parameters that the sample should break into three domains (min. energy). (From Hundley et al. unpublished.)

4.6.8 7. Electro-elastic interference

7.1. Elastic mode locking

Electronic mode locking in CDW conductors directly affects the CDW velocity in the interference regime. As discussed in section 4.3, internal degrees of freedom play an important role in the mode locking. Although most attention has been focused on the electronic response of CDW materials, experiments have demonstrated that the elastic response of CDW materials is sensitive to CDW motion. Since elastic response involves internal degrees of freedom of the CDW and underlying lattice, it is a useful probe of CDW dynamics, including those of an electronically mode locked condensate.

For most sliding CDW materials (such as $NbSe_3$, TaS_3 and $(TaSe_4)_2$ I), the Young's modulus Y and internal friction δ of the crystal change smoothly following CDW depinning (Brill and Roark 1984, Mozurkewich et al. 1985). As first demonstrated by Brill and Roark (1984) for TaS_3, Y decreases with increasing $E_{\mathrm{dc}} > E_{\mathrm{T}}$ and eventually saturates; similarly δ increases with increasing $E_{\mathrm{dc}} > E_{\mathrm{T}}$ and either saturates or eventually turns over at high field. A simple interpretation of these results is that in the pinned state, the stiffness of the CDW adds to that of the lattice, while a depinned CDW is decoupled from the lattice, and hence the stiffness of the lattice is reduced. Such arguments lead to order of magnitude estimates (Mozurkewich et al. 1985) in changes of Y upon depinning, which are in rough agreement with experiment.

In the region of ac-induced electronic mode locking, where the CDW drift velocity v_{d} is fixed over a finite range in E_{dc}, one might expect Y and δ to display no more than 'regions of constancy' during mode locking. This would occur if Y and δ were strictly functions of v_{d}. Alternatively, one might imagine that during mode locking, the CDW would fully decouple from the underlying lattice. In this case, Y and δ would, during electronic mode locking, assume their high field, saturated values.

Figure 7.1 shows that an entirely different behavior is observed (Bourne et al. 1986) for Y and δ during mode locking in TaS_3 and $NbSe_3$. During the Shapiro step interference, Y and δ both tend toward their zero-field, pinned values. This occurs for harmonic as well as subharmonic electronic mode locking. The effect is more dramatic for $NbSe_3$, for which the

electronic locking is nearly complete for the $n = 1$ interference step. For both TaS_3 and $NbSe_3$, a rough scaling exists between the degree of electronic mode lock (i.e. $h/h_{\max}$) and the size of the anomaly in Y and δ during mode lock. The anomalies in Y and δ during electronic interference reflect 'elastic mode locking', since here the velocity of sound is locked to a value dictated only by $(\mathrm{d}/\mathrm{d}t)[\langle \mathrm{d}\phi/\mathrm{d}t\rangle]$, assuming complete electronic mode locking.

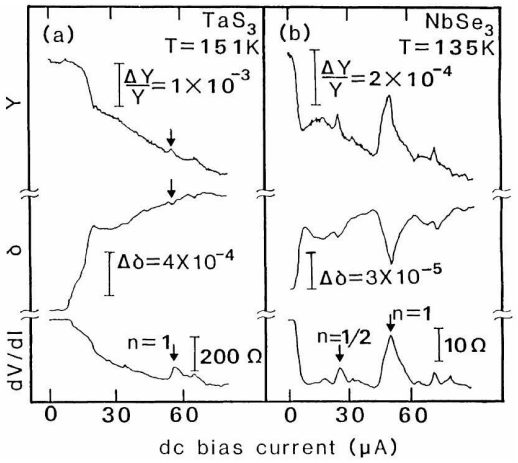


Fig. 7.1. Young's modulus, internal friction, and differential resistance for TaS_3 and $NbSe_3$ in presence of ac + dc electric field drive. Electronic Shapiro step interference is reflected in the elastic constants. (From Bourne et al. 1986.)

7.2. Models for the elastic mode locking

The theoretical models of CDW transport discussed in sections 2 and 4 in general consider only the electronic response, and assume a fully rigid CDW pinning potential. Hence these models fail to account for any elastic properties of the crystal.

Sherwin and Zettl (1986) have attempted to account for elastic mode locking in CDW conductors by an extension of the Frenkel-Kontorova model. The theory treats the CDW condensate and underlying lattice as coupled elastic media obeying classical mechanics. Elasticity of the underlying lattice is incorporated by a discretization which breaks the lattice and associated pinning potential into rigid units of mass M coupled harmonically by springs with spring constant K. The CDW is represented by discrete particles of mass m coupled harmonically to nearest neighbors by spring constant k. Both commensurate and incommensurate CDW cases can be described, and the model is easily extended to the random pinning case. Figure 7.2a shows a mechanical analog representation of the model. The particles in the potential wells are charged CDW 'particles'. Equations of

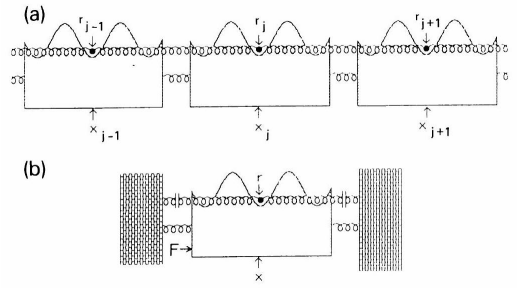


Fig. 7.2. Mechanical analog of electro-elastic coupling model of Sherwin and Zettl: (a) analog of eq. (7.1); (b) analog of eq. (7.2). (From Sherwin and Zettl 1986.)

motion for the model are

$$m\ \mathrm{d}^2 r_j/\mathrm{d}t^2 + \gamma \mathrm{d}\left(r_j - x_j\right)/\mathrm{d}t + k\left(2r_j - r_{j+1} - r_{j-1}\right) + QV\sin\left[Q\left(r_j - x_j\right)\right] = f_j(t)$$

$$M\ \mathrm{d}^2 x_j/\mathrm{d}t^2 + \Gamma \mathrm{d}\left(2x_j - x_{j-1} - x_{j+1}\right)/\mathrm{d}t + \gamma \mathrm{d}$$

(7.1a)

$$+ K\left(2x_j - x_{j-1} - x_{j+1}\right) + QV$$

where r_j and x_j are respectively the (laboratory frame) positions of the j th CDW mass and j th lattice unit, V is the strength of the impurity pinning potential, and $Q = 2\pi/\lambda$, with λ the CDW wavelength. Γ is the internal friction of the lattice and γ is a frictional coupling between the CDW and lattice. $f_j(t)$ is the force applied to the j th CDW particle by external electric fields, and $F_j(t)$ is the external mechanical force applied to the j th lattice unit. In the limit $K \to \infty$, eqs. (7.1a) and (7.1b) reduce to the discretized Sine-Gordon equation.

A great simplification occurs if the infinite set of CDW particles and lattice units is truncated to three units. This retains the essential physics by preserving internal degrees of freedom and CDW-lattice interactions. With clamped-clamped boundary conditions (appropriate to experimental conditions), the model is reduced to a single renormalized CDW particle interacting with a single renormalized lattice unit. The mechanical analog to the renormalized system is shown in fig. 7.2b. The corresponding equations of motion are (Bourne et al. 1986, Sherwin and Zettl 1986)

$$m^*\ \mathrm{d}^2 r/\mathrm{d}t^2 + \gamma_\mathrm{c}\ \mathrm{d}(r-x)/\mathrm{d}t + k_\mathrm{c} r + eE_\mathrm{T}\sin\left[2k_\mathrm{F}(r-x)\right] = e\left[E_\mathrm{dc} + E_\mathrm{ac}\cos\left(\omega_\mathrm{ex}t\right)\right] \quad (7.2a)$$

$$M\ \mathrm{d}^2 x/\mathrm{d}t^2 + \Gamma_\mathrm{L}\ \mathrm{d}x/\mathrm{d}t + \gamma_\mathrm{c}\ \mathrm{d}(r-x)/\mathrm{d}t + K_\mathrm{L} x + eE_\mathrm{T}\sin\left[2k_\mathrm{F}(x-r)\right] = F\cos\left(\omega_\mathrm{r}t\right) \quad (7.2b)$$

where r and x are, respectively, the laboratory positions of the CDW center of mass and lattice, m^* is the total CDW effective mass in the crystal, e the total charge of the CDW, M_L the lattice mass, γ_c and Γ_L respectively the total CDW damping and internal lattice friction, and k_F the Fermi wavevector. k_c and K_L parameterize, respectively, the total elasticity of the CDW and underlying lattice, and $F\cos\left(\omega_\mathrm{r}t\right)$ is the mechanical force applied to the lattice, the response to which determines the elastic properties of the system. In order for the CDW to slide continuously through the lattice while retaining the periodicity of the pinning potential, k_c is restricted to respond only to ac excitations.

Equations (7.2a,b) have been solved for in the regime of electronic Shapiro step mode locking by an analog computer using parameters appropriate to $NbSe_3$ or TaS_3. Figure 7.3 shows the predicted Y, δ, and $\mathrm{d}V/\mathrm{d}I$ curves as functions of dc bias. Complete Shapiro step mode locking is obtained, with corresponding elastic mode locking in striking agreement with the behavior observed in fig. 7.1. Hence, the mode locking of the elastic response follows directly from a simple model where CDW internal degrees of freedom are taken into account. A model similar to eqs. (7.1a,b)

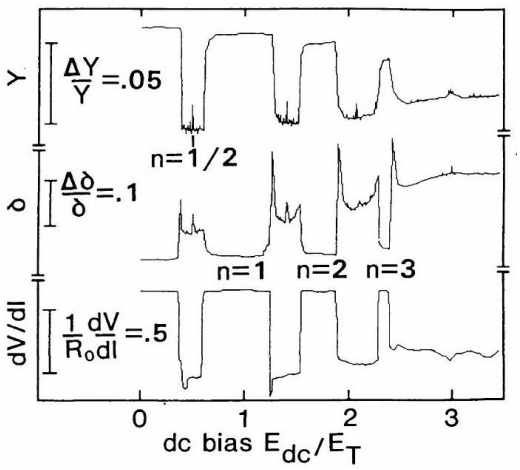


Fig. 7.3. Elastic and electronic response predictions of eq. (7.2) during mode locking. The results agree qualitatively with those observed experimentally in TaS_{3} and $NbSe_3$ (fig. 7.1). (From Sherwin and Zettl 1986.)

has been independently proposed by Sneddon (1986), but solved only in the limit of finite $E_{\rm dc}$, with $E_{\rm ac} = 0$.

4.6.9 8. Conclusion

The intrinsic current oscillations and related ac-dc interference effects in sliding CDW conductors remain among the most fascinating aspects of CDW dynamics. The study of these phenomena is a valuable tool in gaining an understanding of the CDW state. Most experimental evidence points to the narrow band noise oscillations as originating in the bulk. However, phase slip processes cannot be neglected, in particular when they occur at strong pinning sites and lead to switching and related chaotic response, etc. CDW mode locking is one of the most dramatic consequences of CDW nonlinearity and metastability, with many applications to the universal study of competing periodicities and phase organization.

Some of the classical models presented in this review have been surprisingly successful in accounting for very complex CDW response. Models which explicitly take CDW internal degrees of freedom into account are more realistic. The CDW cannot in general be treated as a rigid object in a periodic potential, since in this treatment metastability is lost. Elasticity measurements demonstrate a strong coupling between the CDW electronic response and the underlying phonon structure of the host lattice.

Despite much apparent success of classical models of CDW transport, controversy remains about the applicability of classical concepts to the CDW condensate. Bardeen (unpublished) has strongly criticised all classical approaches to CDW dynamics, and suggests that it is absolutely necessary to treat CDW metals as macroscopic quantum systems with quantum tunneling as an essential feature. Classical concepts are demonstrated to be useful only in the low-frequency response of the pinned CDW or for phenomena on large length scales in the sliding CDW state. Although this criterion puts many CDW interference phenomena into the classical regime, it is expected that, for certain parameter ranges, CDW interference reflects quantum effects. In Bardeen's view, the CDW is not 'like an elastic rug sliding down a staircase with stick-slip friction', but is rather 'a beautiful example of macroscopic quantum mechanics (with many analogies to superconductivity)' (Bardeen unpublished). In either case, CDW dynamics is a unique conduction mechanism with an exceptionally rich spectrum of exotic structural, transport, and mechanical properties.

4.6.10 References

Aizawa, Y., and Y. Kobatake, 1975, Prog. Theor. Phys. 53, 305; A.T. Winfree, 1967, J. Theor. Biol. 16, 15.
Bak, P., T. Bohr and M.H. Jensen, 1984, in: Proc. 54th Nobel Symp. "The Physics of Chaos and Related Phenomena", Graftaavallen, Sweden.
Bardeen, J., Phys. Rev. B (submitted).
Bardeen, J., 1985, Phys. Rev. Lett. 55, 1010.
Barnes, S.E., and A. Zawadowski, 1983, Phys. Rev. Lett. 51, 1003.
Bohr, T., P. Bak and M.H. Jensen, 1984b, Phys. Rev. A 30, 1970.
Bourne, L.C., and A. Zettl, 1987, Phys. Rev. B 36, 2626.
Bourne, L.C., M.S. Sherwin and A. Zettl, 1986, Phys. Rev. Lett. 56, 1963; L.C. Bourne and A. Zettl, 1987, Phys. Rev. B 36, 2626.
Brill, J.W., and W. Roark, 1984, Phys. Rev. Lett. 53, 846.
Brown, S.E., and G. Grüner, 1985, Phys. Rev. B 31, 8302.
Brown, S.E., and L. Mihaly, 1985, Phys. Rev. Lett. 55, 742.
Brown, S.E., G. Mozurkewich and G. Grüner, 1984, Phys. Rev. Lett. 52, 2277.
Brown, S.E., G. Mozurkewich and G. Grüner, 1985a, Solid State Commun. 54, 23.
Brown, S.E., G. Mozurkewich and G. Grüner, 1985b, in: Charge Density Waves in Solids, Lecture Notes in Physics, Vol. 217, eds Gy. Hutiray and J. Sólyom (Springer, Berlin) p. 318.
Brown, S.E., G. Grüner and L. Mihaly, 1986, Solid State Commun. 57, 165.
Cava, R.J., R.M. Fleming, P.B. Littlewood, E.A. Rietman, L.F. Schneemeyer and R.G. Dunn, 1984, Phys. Rev. B 30, 3228.
Coppersmith, S.N., and P.B. Littlewood, 1986, Phys. Rev. Lett. 57, 1927.
D'Humieres, D., M.R. Beasley, B.A. Huberman and A. Libchaber, 1982, Phys. Rev. A 26, 3483.
Dong, J., and L. Yu, 1988, Phys. Rev. B 37, 6667.
Fack, H., and V. Kose, 1971, J. Appl. Phys. 42, 320.
Fiory, A.T., 1971, Phys. Rev. Lett. 27, 501.
Fiory, A.T., 1973a, Phys. Rev. B 8, 5039.
Fiory, A.T., 1973b, Phys. rev. B 7, 1881.
Fisher, D.S., 1985, Phys. Rev. B 31, 1396.
Fleming, R.M., 1982, Solid State Commun. 43, 167.
Fleming, R.M., and C.C. Grimes, 1979, Phys. Rev. Lett. 42, 1423.
Fleming, R.M., and L.F. Schneemeyer, 1983, Phys. Rev. B 28, 6996.
Fleming, R.M., D.E. Moncton and D.B. McWhan, 1978, Phys. Rev. B 18, 5560.
Fleming, R.M., L.F. Schneemeyer and R.J. Cava, 1985, Phys. Rev. B 33, 2930.
Fröhlich, H., 1954, Proc. R. Soc. London Ser. A 223, 296.
Gill, J.C., 1981, Solid State Commun. 39, 1203.
Gill, J.C., and A.W. Higgs, 1983, Solid State Commun. 48, 709.
Gor'kov, L.P., 1983, JETP Lett. 38, 87.
Grüner, G., and A. Zettl, 1985, Phys. Rep. 119, 117.
Grüner, G., A. Zawadowski and P.M. Chaikin, 1981, Phys. Rev. Lett. 46, 511.
Gwinn, E.G., and R.M. Westervelt, 1987, Phys. Rev. Lett. 59, 157.
Hall, R.P., and A. Zettl, 1984a, Phys. Rev. B 30, 2279.
Hall, R.P., and A. Zettl, 1984b, Solid State Commun. 50, 813.
Hall, R.P., and A. Zettl, 1985, Solid State Commun. 55, 307; R.P. Hall and A. Zettl, Phys. Rev. B (in press).
Hall, R.P., M.S. Sherwin and A. Zettl, 1984a, Phys. Rev. Lett. 52, 2293.
Hall, R.P., M.S. Sherwin and A. Zettl, 1984b, Phys. Rev. B 29, 7076.
Hall, R.P., M.F. Hundley and A. Zettl, 1986a, Phys. Rev. Lett. 56, 2399.

Hall, R.P., M.F. Hundley and A. Zettl, 1986b, Physica B 143, 152.
Hall, R.P., M.F. Hundley and A. Zettl, 1987, Synth. Met. 19, 813.
Hall, R.P., M.F. Hundley and A. Zettl, 1988, Phys. Rev. B 38, 13002.
Held, G.A., 1985, Ph.D. Thesis (Univ. of California) [Lawrence Berkeley Laboratory Report No. LBL-20626].
Hundley, M.F., and A. Zettl, (unpublished).
Hundley, M.F., and A. Zettl, 1986, Phys. Rev. B 33, 2883.
Hundley, M.F., and A. Zettl, 1988, Solid State Commun. (in press); also unpublished work.
Hundley, M.F., P. Parilla and A. Zettl, (unpublished).
Hundley, M.F., W.N. Craeger and A. Zettl, 1988, Bull. Am. Phys. Soc. 33, 425.
Inui, M., R.P. Hall, S. Doniach and A. Zettl, 1988, Phys. Rev. B 38, 13047.
Janossy, A., G. Mihaly and L. Mihaly, 1985, in: Charge Density Waves in Solids, Lecture Notes in Physics, Vol. 217, eds Gy. Hutiray and J. Sólyom (Springer, Berlin) p. 412.
Jensen, M.H., P. Bak and T. Bohr, 1983a, Phys. Rev. Lett. 50, 1637.
Jensen, M.H., T. Bohr, P.V. Christiansen and P. Bak, 1983b, Brookhaven National Laboratory Report No. 33495.
Jensen, M.H., P. Bak and T. Bohr, 1984, Phys. Rev. A 30, 1960.
Jing, T.W., and N.P. Ong, 1986, Phys. Rev. B 33, 5841.
Kautz, R.L., 1981, J. Appl. Phys. 52, 6241.
Lee, P.A., and T.M. Rice, 1979, Phys. Rev. B 19, 3970; H. Fukuyama and P.A. Lee, 1978, Phys. Rev. B 17, 535.
Lindelof, P., 1981, Rep. Prog. Phys. 44, 949.
Link, G.L., and G. Mozurkewich, 1988, Solid State Commun. 65, 15.
Lyding, J.W., J.S. Hubacek, G. Gammie and R.E. Thorne, 1986, Phys. Rev. B 33, 4341.
Martin, S., and W. Martienssen, 1986, Phys. Rev. Lett. 56, 1522.
Matsukawa, H., and H. Takayama, 1984, Solid State Commun. 50, 283.
Matsukawa, H., and H. Takayama, 1987, Synth. Met. 19, 7.
Mihaly, L., (private communication).
Monceau, P., J. Richard and M. Renard, 1980, Phys. Rev. Lett. 45, 43.
Monceau, P., J. Richard and M. Renard, 1982, Phys. Rev. B 25, 931.
Monceau, P., M. Renard, J. Richard, M.C. Saint-Lager, H. Salva and Z.Z. Wang, 1983, Phys. Rev. B 28, 1646.
Mozurkewich, G., and G. Grüner, 1983, Phys. Rev. Lett. 51, 2206.
Mozurkewich, G., P.M. Chaikin, W.G. Clark and G. Grüner, 1985, in the volume of ref. 46, p. 353; Solid State Commun. 56, 421.
Ong, N.P., and G. Verma, 1983, Phys. Rev. B 27, 4495.
Ong, N.P., G. Verma and K. Maki, 1984, Phys. Rev. Lett. 52, 663.
Parilla, P., and A. Zettl, 1985, Phys. Rev. B 32, 8427.
Shapiro, S.M., 1963, Phys. Rev. Lett. 11, 80.
Sherwin, M.S., and A. Zettl, 1985, Phys. Rev. B 32, 5536.
Sherwin, M.S., and A. Zettl, 1986, Physica D 23, 62.
Sherwin, M.S., A. Zettl and R.P. Hall, 1988, Phys. Rev. B 38, 13028; see also ref. 77.
Sneddon, L., 1984a, Phys. Rev. B 29, 719 and 725.
Sneddon, L., 1984b, Phys. Rev. Lett. 52, 65.
Sneddon, L., 1986, Phys. Rev. Lett. 56, 1194.
Sneddon, L., M.C. Cross and D.S. Fisher, 1982, Phys. Rev. Lett. 49, 292.
Tang, C., K. Wiesenfeld, P. Bak, S.N. Coppersmith and P.B. Littlewood, 1987, Phys. Rev. Lett. 58, 1161.
Thorne, R.E., W.G. Lyons, J.W. Lyding, J.R. Tucker, J. Bardeen, S.E. Brown and G. Grüner, 1986, Phys. Rev. B 33, 7342.

Thorne, R.E., W.G. Lyons, J.W. Lyding, J.R. Tucker and J. Bardeen, 1987, Phys. Rev. B 35, 6360.

Tutto, I., and A. Zawadowski, 1985, Phys. Rev. B 32, 2449.

Wang, Z.Z., H. Salva, P. Monceau, M. Renard, C. Roucau, R. Ayroles, F. Levy, L. Guemas and A. Meerschaut, 1983, J. Phys. (France) Lett. 44, L-311.

Zettl, A., 1983, in: Proc. Int. Symp. on Nonlinear Transport and Related Phenomena in Inorganic Quasi-One-Dimensional Conductors, Sapporo, Japan, p. 41.

Zettl, A., 1986, Physica D 23, 155.

Zettl, A., 1988, in: Methods and Applications in Nonlinear Dynamics, ACIF Series, Vol. 7, ed. A. Saenz (World Scientific, Singapore) p. 203.

Zettl, A., and G. Grüner, 1982, Phys. Rev. B 26, 2298.

Zettl, A., and G. Grüner, 1983, Solid State Commun. 46, 501.

Zettl, A., and G. Grüner, 1984, Phys. Rev. B 29, 755.

This page intentionally left blank

4.7 7 Theory of CDW Pinning by Weak Impurities by Vinokur

4.7.1 1. Introduction

1.1. Large-scale CDW Hamiltonian

The theoretical and experimental study of the quasi-one-dimensional compounds which demonstrate anomalous electronic properties has aroused a great deal of interest over the past decades. The remarkable properties of those compounds such as extremely large static and low-frequency dielectric susceptibility (from 10^4 up to 10^7), nonlinear transport properties, memory and hysteretic effects are now associated with the formation of charge-density-waves (CDW) at low temperatures, below the Peierls transition. The electron density modulated by lattice distortions is commonly given as

$$\delta\rho = \rho_0 \cos\left(2k_{\mathrm{F}}x + \varphi\right) \tag{1.1}$$

where ρ_0 and φ are the amplitude and phase of the CDW, k_{F} is the Fermi vector, and collective modes corresponding to the phase and amplitude oscillations are described (Lee, Rice and Anderson 1974) as

$$\omega_- = \sqrt{\frac{m}{m^*}} v_{\mathrm{F}} q$$

$$\omega_+ = \lambda\omega_0^2\left(2k_{\mathrm{F}}\right) + \frac{3}{4}\frac{m}{m^*}v_{\mathrm{F}}^2 q^2$$

respectively, where m^* is the CDW effective mass, $\omega_0\left(2k_{\mathrm{F}}\right)$ is the bare phonon frequency corresponding to the phonon momentum of $2k_{\mathrm{F}}$.λ is the electron-phonon interaction constant. It is generally agreed that it is the acoustic phase mode which provides the anomalous electric properties mentioned above.

The presence of the commensurability or the impurity potential results in the removing of the degeneracy of the CDW ground state in phase and, as a consequence, in the appearance of the gap, ω_{p}, in the acoustic spectrum. This effect is known as pinning of the CDW (Lee, Rice and Anderson 1974, Gor'kov 1977, Efetov and Larkin 1977).

The point to be noted here is that, strictly speaking, there is no Peierls transition as well as any other transitions in the one-dimensional systems. Nevertheless, as there exists interchain interaction in real systems, CDW formation takes place when interchain phase correlation suppresses intrachain one-dimensional phase fluctuations. If the interchain interaction, $E_\perp$ is sufficiently small, $E_\perp \ll T_{\mathbf{p}}^2/\epsilon_{\mathbf{F}}$, where $T_{\mathbf{p}}$ is the Peierls transition temperature,

then the potential barrier for charge amplitude fluctuations is large near the transition point (one says that the charge amplitude is frozen) and the CDW free energy near the transition is determined by phase fluctuations only. Note that the potential barrier for phase fluctuations caused by CDW commensurability (or impurity) pinning is much smaller (provided the order of commensurability $m > 2$) than the amplitude barrier. Hence, the CDW free energy near the Peierls transition is given by Lee, Rice and Anderson (1974), Gor'kov (1977) and Brazovskii (1979):

$$F[\varphi] = \int \mathrm{d}\boldsymbol{r} \left\{ \frac{\bar{v}_\mathrm{F}}{2a_y a_z} \left[\left(\frac{\partial \varphi}{\partial x} \right)^2 + \frac{\xi_y^2}{\xi_x^2} \left(\frac{\partial \varphi}{\partial y} \right)^2 + \frac{\xi_z^2}{\xi_x^2} \left(\frac{\partial \varphi}{\partial z} \right)^2 \right] \right.$$
$$+ V_\mathrm{b}(\boldsymbol{r}) \cos\left(\varphi + 2\boldsymbol{k}_\mathrm{F}\boldsymbol{r}\right) + V_\mathrm{f}(x) \frac{\partial \varphi}{\partial x}$$
$$\left. + V_0 \cos\left[m\varphi + \left(2\boldsymbol{k}_\mathrm{F} m - \boldsymbol{Q}\right)\boldsymbol{r}\right] - \left(e/\pi a_y a_z\right)\varphi E \right\} \tag{1.2}$$

We assume conductivity chains to lie along the x-axis. Here $\bar{v}_\mathrm{F} = \hbar v_\mathrm{F}/2\pi$ is the reduced Fermi velocity, we put $\hbar = 1$ here and below; a_x, a_y, a_z are the lattice parameters, ξ_x, ξ_y, ξ_z are the coherence lengths. The second and third terms describe impurity pinning, the fourth term is due to commensurability effect ($\boldsymbol{Q}$ is the reciprocal lattice vector). The commensurability potential is $V_0 = \left(\Delta^2/\epsilon_\mathrm{F}\right)\left(e\Delta/D\right)^{m-2}$ (Lee, Rice and Anderson 1974), where Δ is the Peierls gap in the electron spectrum, D is the width of the 1D electron band. $V_\mathrm{b}(\boldsymbol{r}) = V_\mathrm{b}\sum_i \delta\left(\boldsymbol{r} - \boldsymbol{r}_i\right)$ is the short-range part of the impurity potential which describes backward electron scattering, $V_\mathrm{f}(x)$ is the long-range impurity potential which is responsible for forward electron scattering (we neglect fluctuations of $V_\mathrm{b}(\boldsymbol{r})$ magnitude, its temperature dependence follows from the relation $V_\mathrm{b} \propto \Delta$, Lee and Rice (1979)). The last term accounts for the external electric field in the chain direction.

1.2. Strong and weak impurities

Impurities in CDW systems perturb CDW phase configurations in order to minimize the free energy (1.2). Local deformation of the CDW phase near impurities destroys a long-range ordering and gives rise to the appearance of the finite pinning energy. Note that in the absence of a commensurability potential only back-scattering impurities cause the CDW pinning. The forward-scattering impurities do not break the translational invariance of the system and as a consequence cannot pin CDW (the combined action of the commensurability potential and forward scattering impurity potential does lead to pinning, see section 2.3). The gain in impurity energy is maximal when $\varphi + 2\boldsymbol{k}_\mathrm{F}\boldsymbol{r} = \pi$ at impurities. If the impurity potential is large enough to overcome elasticity of the CDW and fix the CDW phase, then these impurities are called strong impurities. One can easily see that strong impurities should satisfy the following condition (Lee and Rice 1979)

$$c\bar{v}_\mathrm{F} \ll V_\mathrm{b}, \tag{1.3}$$

where $c = n_i \cdot \min\left(a_\perp^2, \xi_\perp^2\right)$ is the number of impurities per unit length of the chain, n_i is the impurity volume concentration, $a_\perp$ and $\xi_\perp$ are the interchain spacing and transverse coherence length, respectively. Strong pinning of one-dimensional CDW was explored by Gor'kov (1977).

In the opposite limit of weak pinning

$$c\bar{v}_\mathrm{F} \gg V_\mathrm{b} \tag{1.4}$$

the single impurity cannot fix CDW phase and CDW pinning arises from collective action of weak impurities. In this case CDW configuration $\varphi(x)$ minimizes the energy in the domains

with linear sizes well exceeding the mean distance between impurities. The study of weak pinning problem was initiated by Fukuyama and Lee (1978) (1D model) and Efetov and Larkin (1977), Lee and Rice (1979). Below we restrict ourselves to the weak pinning limit.

1.3. Three- and one-dimensional pinning by impurities

Experimental studies of CDW pinning are usually performed in the temperature region $T < T_{\mathrm{P}}$ where the pronounced 3D coherent structure exists. It was shown (Efetov and Larkin 1977) that in the incommensurate phase the long-range-order (LRO) is broken by impurities no matter how weak they are. The longitudinal, $L_{\parallel}$, and transverse, $L_{\perp}$ correlation lengths were estimated by Efetov and Larkin (1977) and Lee and Rice (1979) as

$$L_{\parallel} \simeq \frac{8\pi \bar{v}_{\mathbf{F}}^2}{n_i V_{\mathbf{b}}^2 a_{\perp}^2} \left(\frac{\xi_{\perp}}{\xi_{\parallel}}\right)^2, \quad L_{\perp} \simeq \frac{\xi_{\perp}}{\xi_{\parallel}} L_{\parallel} \tag{1.5}$$

where we have neglected the possible anisotropy in the (x, y) plane. The pinning strength is characterized by the values of the static dielectric permeability $\epsilon_{\parallel}(\mathrm{O})$ and the threshold depinning field E_{p} (i.e. the electric field that leads to the motion of CDWs as a whole) and both $\epsilon_{\parallel}(\mathcal{O})$ and E_{Γ} can be
expressed through the correlation length $L_{\parallel}$:

$$\epsilon_{\parallel}(0) \approx \left(\frac{e}{\pi}\right)^2 \frac{L_{\parallel}^2}{a_{\perp}^4} \frac{a_{\perp}^2}{\bar{v}_{\mathrm{F}}} = \left(\frac{e}{\pi}\right)^2 \frac{1}{a_{\perp}^4} \left(\frac{8\pi}{n_i V_{\mathrm{b}}^2}\right)^2 \left(\frac{\bar{v}_{\mathrm{F}}}{a_{\perp}^2}\right)^3 \left(\frac{\xi_{\perp}}{\xi_{\parallel}}\right)^4 \tag{1.6a}$$

$$E_{\mathrm{p}} \approx \frac{e}{a_{\perp}^2} \frac{1}{\epsilon_{\parallel}(0)} \simeq \frac{\bar{v}_{\mathrm{F}}}{e L_{\parallel}^2} \tag{1.6 b}$$

Characteristic scale of pinning frequency is given by

$$\omega_{\mathrm{p}} \simeq u / L_{\parallel} \tag{1.7}$$

in the case of weak dissipation (u is the phase velocity of the CDW) and by

$$\Omega_{\mathrm{p}} \simeq \frac{1}{\lambda} \omega_{\mathrm{p}}^2 = \frac{1}{\lambda} \frac{m}{m^*} \left(e E_{\mathrm{p}} \bar{v}_{\mathrm{F}}\right) \tag{1.8}$$

in the overdamped limit, where λ is the dissipation rate and m^* is the effective CDW mass $\left(m/m^* = (u/\bar{v}_{\mathrm{F}})^2\right)$. The analogous estimates were obtained by Efetov and Larkin (1977) for the case of the strong Coulomb interactions where the problem is formally equivalent to the local one in the four-dimensional space and pinning appears to be exponentially weak.

Unfortunately the perturbation theory developed by Efetov and Larkin (1977) as well as the scaling estimates by Lee and Rice (1979) cannot be applied for the investigations of pinning properties in the most interesting region $\omega \leqslant \Omega_{\mathrm{p}}, E \leqslant E_{\mathrm{p}}$ hence, low-frequency conductivity as well as nonlinear dielectric response appear to lie beyond the scope of that qualitative theory. Therefore, it seems to be interesting to consider one-dimensional models of impurity pinning which are more tractable by analytic methods. The model of the 1D pinning in the weak impurity limit was studied by Fukuyama and Lee (1978) who considered the free energy

$$F_{1\mathrm{D}}[\varphi] = \int \mathrm{d}x \left[\frac{\bar{v}_{\mathrm{F}}}{2} \left(\frac{\mathrm{d}\varphi}{\mathrm{d}x}\right)^2 + \sum_k V_{\mathrm{b}} \delta\left(x - x_k\right) \cos(\varphi + Qx) - \frac{e}{\pi} \varphi E\right] \tag{1.9}$$

where x_k are the positions of backward scatterers randomly distributed with concentration c. The scale of pinning energy, U_1, at $E = 0$ can be estimated as the elastic energy $\bar{v}_{\mathrm{F}}/L_1$

(where L_1 is the correlation length, i.e., 1D analogue of $L_\parallel$)moreover, $U_1 \simeq V_b\sqrt{cL_1}$, that is the energy gain produced from the coupling with impurities. Equating these estimates we obtain

$$U_1 \simeq \left(\bar{v}_\mathrm{F} c V_\mathrm{b}^2\right)^{1/3}; \quad L_1 \simeq \bar{v}_\mathrm{F}^{2/3}\left(cV_\mathrm{b}^2\right)^{-1/3}; \quad \omega_\mathrm{p} \simeq (u/\bar{v}_\mathrm{F})\, U_1 \tag{1.10}$$

where the last estimate is analogous to (1.7). The above consideration is the special example of the general arguments (Imry and Ma 1975) for the absence of LRO in the degenerate systems with random fields in $D \leqslant 4$ space dimensions; the estimates (1.5)-(1.6) for the 3D case can also be obtained by similar arguments. It follows from eqs. (1.5) and (1.10) that at $T < T_\mathrm{P}$ the interchain coupling is strongly relevant. Indeed, using the relation $c = n_i a_\perp^2$ and the obvious inequality $\xi_\perp \geqslant a_\perp$, we arrive at

$$L_\parallel = L_1^3\left(\frac{\xi_\perp}{\xi_\parallel a_\perp}\right)^2 > \frac{L_1^3}{\xi_\parallel^2} \gg L_1 \tag{1.11}$$

(the last inequality is obviously fulfilled in the weak pinning region). Therefore, the picture of 1D pinning can be applied literally at $T > T_\mathrm{P}$ only, where the coupling can be neglected. For most of the CDW compounds studied up to now, $U_1 \ll T_\mathrm{P}$, i.e., pinning is completely destroyed by thermal fluctuations. The intermediate situation in fact takes place in the new compound $(TaSe_4)_2\,I$ with the characteristic pinning frequency, ω_p, of the order $\omega_\mathrm{p}/2\pi = 35\mathrm{GHz}$ corresponding to the pinning energy $U_1 \simeq (\bar{v}_\mathrm{F}/u)\,\omega_\mathrm{p} \approx 170$ K (due to the enormous value of the effective mass: $\bar{v}_\mathrm{F}/u = (m^*/m)^{1/2} \simeq 10^2$) (Reagor et al. 1985). The pinning energy, thus, is comparable to $T_\mathrm{P} \approx 260$ K, so the existence of systems with $U_1 \gg T_\mathrm{P}$ seems to be possible (the simplest way of fabricating such systems might be to dope $(TaSe_4)_2\,I$ with extra defects). Nevertheless, at present the most effective feature of the approach presented is that the 1D pinning model permits a detailed theoretical treatment to be carried out which can provide a better qualitative understanding of the 3D case. The following sections of our review are devoted to the semi-quantitative theory of 1D pinning.

4.7.2 2. Weak pinning in 1D CDW systems. Static properties

2.1. General approach

The essential feature of the weakly disordered system is that its ground state is formed at distances much larger than the mean impurity spacing. The ground state itself appears to be multiple degenerate. As the usual perturbation theory (with respect to disorder) cannot be employed in the investigation of such systems the new method, that is, the generalization of the transfer matrix for the case of a disordered system, has been proposed by one of the authors (Feigel'man 1980). Now we turn to the description of this method which has been developed in the subsequent paper by Vinokur, Mineev and Feigel'man (1981).

To begin with we discuss a purely incommensurate system, generalization to the commensurability effects will be performed in the course of expounding. So, let us consider one-dimensional incommensurate CDW in the potential of back-scattering impurities (we would like to remind that forward-scattering cannot pin incommensurate CDW). The Hamiltonian is determined by long-wave phase deformations and is as follows:

$$H = \int \mathrm{d}x \left[\frac{\bar{v}_\mathrm{F}}{2}\left(\frac{\mathrm{d}\varphi}{\mathrm{d}x}\right)^2 - V\sum_i \delta\left(x - x_i\right)\cos(\varphi + Qx)\right] \tag{2.1}$$

(the subscript ' b ', the impurity potential symbol in V_b is omitted). $Q/c \equiv 2k_\mathrm{F}/c$ is supposed to be much larger than unity so Qx_i (where x_i is the impurity position) are random uncorrelated quantities. The partition function, corresponding to the Hamiltonian (2.1) is

$$Z = \int \prod_i \frac{\mathrm{d}\varphi_i}{2\pi} \exp\left\{ -\frac{1}{T} \sum_i \left[\frac{\bar{v}_\mathrm{F}}{2} \frac{(\varphi_i - \varphi_{i-1})^2}{x_i - x_{i-1}} - V \cos(\varphi_i + Q x_i) \right] \right\} \tag{2.2}$$

(the Gaussian integration over all impurity-free points has been performed).
Let us suppose that the distribution of the phase, $\varphi(x)$ minimizing the system energy, the value of the phase of the N th impurity φ_N, given, has already been found. Then one can write the total system energy, $\epsilon_N(\varphi)$, as

$$\epsilon_N(\varphi_N) = \epsilon_N^<(\varphi_N) + \epsilon_N^>(\varphi_N)$$

where $\epsilon_N^<(\varphi)$ and $\epsilon_N^>(\varphi)$ are the energies of the left-hand and right-hand parts of the system, respectively. It should be noted that the parts of the system 'know' nothing about each other, the phase at the point N is fixed. So one can investigate the properties of the functions $\epsilon_N^<(\varphi)$ and $\epsilon_N^>(\varphi)$ independently assuming the N th impurity to be the end point of the semi-infinite system.

Let the normalized partition function of the semi-infinite system, $\Psi_N(\varphi)$, depending on the phase φ at the end point be of the form

$$\Psi_N(\varphi_N) = \text{ const } \times \exp\left[-\epsilon_N(\varphi_N)/T\right]$$

(the integration over all $\varphi_k, k < N$ has been performed). Then

$$\begin{aligned} \lambda_{N+1}\Psi_{N+1}(\varphi_{N+1}) &= \exp\left[\frac{V}{T}\cos(\varphi_{N+1} + Q x_{N+1})\right] \\ &\times \int \frac{\mathrm{d}\varphi_N}{2\pi} \Psi_N(\varphi_N) \exp\left[-\frac{\bar{v}_\mathrm{F}}{2T} \frac{(\varphi_{N+1} - \varphi_N)^2}{l_{N+1}}\right] \end{aligned} \tag{2.3}$$

where λ_{N+1} is the normalization factor and $l_{N+1} = x_{N+1} - x_N$.
Assuming the changes of the phase and energy of the chain to be small at any step

$$|\varphi_{N+1} - \varphi_N| < 1, \quad \left|\boldsymbol{\epsilon}_N(\varphi_N) - \boldsymbol{\epsilon}_{N+1}^<(\varphi_{N+1})\right| < \boldsymbol{\epsilon}_N^<(\varphi_N), \tag{2.4}$$

one can obtain easily the recurrent relation for $\epsilon_N(\varphi)$:

$$\begin{aligned} \epsilon_{N+1}^<(\varphi) - \epsilon_N^<(\varphi) = &-\frac{1}{2}\frac{l_{N+1}}{\bar{v}_\mathrm{F}} \left(\frac{\partial \epsilon_N^<}{\partial \varphi}\right)^2 + \frac{T}{2}\frac{l_{N+1}}{\bar{v}_\mathrm{F}} \left(\frac{\partial^2 \epsilon_N}{\partial \varphi^2}\right) \\ &- V\cos(\varphi + Q x_{N+1}) \end{aligned} \tag{2.5}$$

The stochastic equation (2.5) (x_{N+1} is the random parameter) determining the Markovian process for a 2π-periodic function $\epsilon_N(\varphi)$ will be our basic relation. The weak pinning condition, $V \ll c\bar{v}_\mathbf{F}$, provides the smallness of the changes when shifting over the impurity spacing. We shall consider the low-temperature limit and neglect the second term of the right-hand side of eq. (2.5). Then eq. (2.5) is reduced to the Hamilton-Jacobi equation with imaginary discrete time, N, corresponding to the Hamiltonian (2.1). Employing eq. (2.5) instead of the commonly used equation of motion for the phase φ, one investigates the solutions which are sure to be local minima of the energy functional and takes the definite value of the phase at point N. The method generally adopted and based on the solution of the equation would lead to the necessity of averaging over all solutions with equal weight, including the ones which are unstable and well far from the ground state.

Our aim is to calculate average values of various physical quantities and to find them, we begin with the calculation of the distribution function of the parameter β_N defined as

$$\beta_x^< = \left(\frac{\partial^2 \epsilon_x^<}{\partial \varphi^2}\right)_{\partial \epsilon^</\partial \varphi = 0} \tag{2.6}$$

The importance of the quantity β_N is that the ground state energy, correlation length and other physical quantities can be expressed in terms of the distribution function $W^< (\beta^<)$. The characteristic scale, β_0, of the β variation determines the scale of the pinning energy per correlation length. The local value of the phase, that minimizes energy $\epsilon_N^< (\varphi_N)$ will be denoted as γ_N :

$$\left.\frac{\partial \epsilon_N^<(\varphi)}{\partial \varphi}\right|_{\varphi=\gamma_N} = 0. \tag{2.7}$$

Now expanding $\boldsymbol{\epsilon}_N^<(\boldsymbol{\varphi})$ into a Taylor series near the minimum

$$\begin{aligned} \epsilon_N^<(\varphi) &= \epsilon_N^< (\gamma_N) + \sum_{n=2}^{\infty} \frac{\beta_N^{(n)}}{n!} (\varphi - \gamma_N)^n \\ \beta_N^{(2)} &\equiv \beta_N \end{aligned} \tag{2.8}$$

and differentiating consequently with respect to φ at the point $\varphi = \gamma_{N+1}$ one can obtain the infinite chain of the coupled recurrent equations (Vinokur, Mineev and Feigel'man 1981):

$$\begin{aligned} \Delta\gamma \equiv& \gamma_N - \gamma_{N+1} = \frac{V}{\beta_N} \sin(\gamma_{N+1} + Q x_{N+1}) \\ \Delta\beta \equiv& \beta_N - \beta_{N+1} = \beta_N^2 \frac{l_{N+1}}{\bar{v}_F} - V \cos(\gamma_{N+1} + Q x_{N+1}) + \beta_N^{(3)} \Delta\gamma \\ & - \frac{1}{2} \beta_N^{(4)} (\Delta\gamma)^2 \\ \Delta\beta^{(3)} \equiv& \beta_N^{(3)} - \beta_{N+1}^{(3)} = 3\beta_N \beta_N^{(3)} \frac{l_{N+1}}{\bar{v}_{\mathrm{F}}} + \beta_N^{(4)} \Delta\gamma \\ & - \frac{1}{2} \beta_N^{(5)} (\Delta\gamma)^2 + V \sin(\gamma_{N+1} + Q x_{N+1}), \\ \Delta\beta^{(4)} \equiv& \beta_N^{(4)} - \beta_{N+1}^{(4)} = 4\beta_N \beta_N^{(4)} \frac{l_{N+1}}{\bar{v}_{\mathrm{F}}} + \beta_N^{(5)} \Delta\gamma - \frac{1}{2} \beta_N^{(6)} (\Delta\gamma)^2 \\ & + V \cos(\gamma_{N+1} + Q x_{N+1}), \end{aligned} \tag{2.9}$$

Averaging these equations with respect to x_{N+1} and with (unknown) distribution function $W\left(\gamma, \beta, \beta^{(3)}, \ldots\right)$ one can be convinced that all average values of $\beta^{(2n)}$ are of the order of β_0, where

$$\beta_0 = \left(\bar{v}_{\mathbf{F}} c V^2\right)^{1/3}, \tag{2.10}$$

and all the $\beta^{(2n+1)}$ averages are of much smaller order of magnitude (note, however, that $\left\langle \left(\beta^{(2n+1)}\right)^2 \right\rangle \simeq \beta_0^2$). As γ_{N+1} depends on x_{N+1}, γ_{N+1} should be expressed through γ_N, then one can perform averaging over x_{N+1} and γ_N independently. We would like to note again that all the results are applicable when $T \ll \beta_0$.

Equations (2.9) are in fact the Langevin equations for a stochastic vector $\xi = \left(\gamma, \beta, \beta^{(3)}, \ldots\right)$ with infinite numbers of the components. The distribution function $W^< \left(\gamma^<, \beta^<, \beta^{<(3)}, \ldots\right)$

obeys the corresponding FokkerPlanck equation (FPE). The distribution function of interest, $W^{<}(\beta^{<})$, is obtained from $W^{<}(\gamma^{<}, \beta^{<}, \ldots)$ by averaging over $\gamma^{<}, \beta^{<(3)}, \beta^{<(4)}, \ldots$. The FPE derived from eqs. (2.9) possesses the determination of the asymptotic form of $W^{<}(\beta^{<})$at $\beta^{<} \gg \beta_0$. To get the distribution function $W^{<}(\beta^{<})$in the region $V \ll \beta^{<} \ll \beta_0$ it is convenient to expand $\epsilon_N^{<}(\varphi)$ into the Fourier series. Finally, we find (Vinokur, Mineev and Feigel'man 1981):

$$W^{<}(\beta^{<}) = (a/\beta_0)(\beta^{<}/\beta_0)\ln(\beta_0/\beta^{<}), \quad \beta^{<} \ll \beta_0, \tag{2.11a}$$

$$W^{<}(\beta^{<}) = (a/\beta_0)(\beta^{<}/\beta_0)^{8/5}\exp\left[-\frac{4}{3}(\beta^{<}/\beta_0)^3\right], \quad \beta^{<} > \beta_0, \quad a \simeq 1. \tag{2.1lb}$$

(Note that the condition $V \ll \beta^{<}$provides the smallness in the change of all quantities when shifting over one step along the chain; at $\beta^{<} \ll V$, $W^{<}(\beta^{<}) \simeq \exp(-c/\beta^{<})$.) Obviously just the same result is derived for $W^{>}(\beta^{>})$.

We shall further need the distribution function $W(\beta)$ of the quantity β_x, corresponding to the arbitrary point x in the interior of the system (far from the ends). To get the asymptotics of $W(\beta)$ one can use the 'averaged' relation $\beta_x \cong \beta_x^{<} + \beta_x^{>}$, where $\beta_x^{<}$and $\beta_x^{>}$correspond to the left hand part and right hand part of the system, separated by point x with the fixed phase φ_x. Then one obtains

$$W(\beta) \simeq (a/\beta_0)(\beta/\beta_0)^3\ln^2(\beta_0/\beta), \quad V \ll \beta \ll \beta_0, \tag{2.12a}$$

$$W(\beta) \simeq (a/\beta_0)(\beta/\beta_0)^{27/10}\exp\left[-\frac{1}{3}(\beta/\beta_0)^3\right], \quad \beta \gg \beta_0. \tag{2.12b}$$

It is to be noted that β_x is nothing but the inverse Green function:

$$G^{-1}(x,x) = \frac{\partial^2\epsilon(\varphi)}{\partial\varphi_x^2} = \beta_x \tag{2.13}$$

The characteristic length of the domain where the pinning is weaker than the average value (i.e. $\beta_x \ll \beta_0$) can be estimated as

$$l(\beta_x) \simeq \bar{v}_F/\beta_x \tag{2.14}$$

Equation (2.14) also gives the size of the region where the coherent response to a small $\varphi(x)$ variation takes place.

2.2. Incommensurate *CDW*

2.2.1. Pinning energy and correlation length

The total energy of the ground state of the chain containing N impurities is (by definition) $\epsilon_N^{<}(\gamma_N)$. The mean energy density per site is

$$E_{\mathrm{p}} = c\left\langle\epsilon_{N+1}^{<}(\gamma_{N+1}) - \epsilon_N^{<}(\gamma_N)\right\rangle. \tag{2.15}$$

Making use of (2.5) and (2.9) one obtains immediately:

$$E_{\mathrm{p}} = \frac{cV^2}{4}\int_0^x W^{<}(\beta)\frac{\mathrm{d}\beta}{\beta} \simeq \epsilon_{\mathrm{F}}\left(cV^2/\epsilon_{\mathrm{F}}\right)^{2/3} \tag{2.16}$$

The correlation function of CDW

$$K(x) = \langle \delta\rho(x)\delta\rho(0)\rangle = \text{const}\langle\cos[\varphi(x) - \varphi(0)]\rangle \tag{2.17}$$

is reduced to the functions

$$K_{\parallel}(N) = \langle \cos\gamma_N \cos\gamma_0\rangle \tag{2.17a}$$
$$K_{\perp}(N) = \langle \sin\gamma_N \sin\gamma_0\rangle \tag{2.17b}$$

In the incommensurate phase $K_{\parallel} = K_{\perp}$. Then $K_{\parallel}(N,0)$ can be defined as

$$K_{\parallel}(N,0) = \frac{\int \mathrm{d}\gamma_0\ \mathrm{d}\gamma_N\ \mathrm{d}\beta_0\ \mathrm{d}\beta_N \cos\gamma_N \cos\gamma_0 \mathscr{P}\left(\gamma_N, \beta_N; \gamma_0, \beta_0\right)}{\int \mathrm{d}\gamma_0\ \mathrm{d}\gamma_N\ \mathrm{d}\beta_0\ \mathrm{d}\beta_N \mathscr{P}\left(\gamma_N, \beta_N; \gamma_0, \beta_0\right)} \tag{2.18}$$

due to the fact that random variations of β_N and γ_N are determined by the Markovian process

$$\mathscr{P}\left(\gamma_N, \beta_N; \gamma_0, \beta_0\right) = P\left(\gamma_N, \beta_N; N \mid \gamma_0, \beta_0\right) W\left(\gamma_0, \beta_0\right), \tag{2.19}$$

where $P(\ldots \mid \ldots)$ is the conditional probability density for β and γ to take the values of β_N and γ_N at site N provided $\beta = \beta_0$ and $\gamma = \gamma_0$ at the initial site.

Conditional probability density P obeys the nonstationary Fokker-Planck equation with the corresponding initial conditions:

$$\begin{aligned}
&\frac{\partial P}{\partial t} - \tilde{L}P = \delta\left(\gamma - \gamma_0\right)\delta\left(\beta - \beta_0\right)\delta(t),\\
&\tilde{L} = \frac{\partial}{\partial x}\left(\frac{\partial}{\partial x} + \frac{\partial \Phi}{\partial x}\right) + \frac{1}{x^2}\frac{\partial^2}{\partial \gamma^2},\\
&x = \beta/\beta_0, \quad t = \left(cV^2/4\beta_0^2\right)N,\\
&\Phi(x) = -\frac{2}{x^2} + \frac{4x^3}{3} + \int^x \frac{\mathrm{d}x'}{x'} f\left(x'\right),\\
&f(x) = \begin{cases} 1 + 1/\ln\left(x^{-1}\right), & x \ll 1,\\ \frac{2}{5}, & x \gg 1. \end{cases}
\end{aligned} \tag{2.20}$$

Making use of the transformation $L = \mathrm{e}^{\Phi/2}\tilde{L}\mathrm{e}^{-\Phi/2}$ one can express the correlation function in terms of the eigenfunctions, Ψ_ν, and the eigenvalues, λ_ν, of the operator L :

$$K_{\parallel} = \sum_{\nu} |f_\nu|^2 \exp\left(-\lambda_\nu t\right) \tag{2.21}$$
$$f_\nu = \int \mathrm{d}x\ \mathrm{d}\gamma \mathrm{e}^{-\Phi/2}\psi_\nu(x,\gamma)\cos\gamma$$

As the eigenvalue corresponding to the equilibrium solution $\lambda_0 = 0$, one needs only the first nonzero eigenvalue λ_1. Numerical solution gives $\lambda_1 \approx 3.22$, so the correlation length R_{c}, is:

$$R_{\mathrm{c}} \approx 1.24\left(\bar{v}_{\mathrm{F}}^2/cV^2\right)^{1/3}, \tag{2.22}$$

which coincides with the accuracy of the numerical factor with the scaling estimate (Fukuyama and Lee 1978).

2.2.2. Static susceptibility, threshold field and nonlinearity

The external electric field, E, is accounted for by the extra term $-\mathscr{E}\varphi$, where $\mathscr{E} = (e/\pi)E$, in the right hand side of Hamiltonian (2.1) and in turn in the right hand side of eq. (2.5). It should be noted that at $T \neq 0$ and $\mathscr{E} \neq 0$ there is no ground state in the system. If, however, $T \ll \beta_0$, the time of the transitions between metastable states is sufficiently large and a quasiequilibrium consideration neglecting these rare transitions is possible. The only quantity one needs in order to calculate static characteristics with the accuracy of the numerical factor is then the pinning energy β_0.
The bulk dielectric susceptibility is defined as

$$\chi_0 = -\frac{1}{4\pi S_\perp}\left(\frac{e}{\pi}\right)^2\left(\frac{\partial^2 E_{\rm p}}{\partial \mathscr{C}^2}\right)_{\mathscr{C}\to 0} \tag{2.23}$$

where $E_{\mathbf{p}}$ is the pinning energy density from (2.15) and $S_\perp$ is the area per one CDW chain.

Making use of (2.23) one can show that the dielectric constant, $\epsilon_0 = 1 + 4\pi\chi_0$, is estimated as

$$\epsilon_0 \simeq \frac{C}{S_\perp}\left(\frac{e}{\pi}\right)^2 \frac{\bar{v}_{\rm F}^{1/3}}{(cV^2)^{2/3}}, \quad C \approx 1 \tag{2.24}$$

(for the derivation of the relation analogous to (2.24) for a slightly different model, see Feigel'man and Vinokur 1983a). The electric field scale, $\mathscr{E}_0$, is determined from the Fokker-Planck equation for $W(\beta, \gamma, \ldots)$, the electric field being taken into account and is as follows:

$$\mathscr{E}_0 = \beta_0^2/\epsilon_{\rm F} = \left(cV^2\right)^{2/3}/\bar{v}_{\rm F}^{1/3}. \tag{2.25}$$

The quantity $\mathscr{E}_0$ coincides up to the order of magnitude with the threshold field $\mathscr{E}_{\rm T}$ of CDW depinning. At electric fields $E > E_{\rm T}$CDW moves as a whole carrying a current. One can estimate the value of $\mathscr{E}_T$ assuming the gain in the energy due to the shift of CDW over its period to be (at $\mathscr{E} \approx \mathscr{E}_{\rm T}$) of the order of the pinning energy (we mean the pinning energy per correlation length $R_{\rm c}$), i.e.,

$$\mathscr{E}_T \simeq \beta_0/R_c,$$

this relation leads immediately to (2.25). Estimates (2.24)-(2.25) coincide with those by Lee and Rice (1979).

It is interesting to calculate nonlinear corrections to a dielectric response arising from polarization in the domains with a relatively weak pinning. Let this weak-pinning be characterized by pinning energy $\beta \ll \beta_0$, its length $l(\beta) \simeq \bar{v}_{\rm F}/\beta$ (cf. (2.14)). Then the field $\mathscr{E} > \beta/l(\beta)$ is strong enough to reconstruct the ground state of that region (note that in the regions with $\beta \ll \beta_0$ the whole scale of $\epsilon(\varphi)$ variation per period ($0, 2\pi$) is also of the order of β (Vinokur, Mineev and Feigel'man 1981)). Let us estimate the contribution of this reconstruction to $\chi(\mathscr{E})$. The change in phase $\Delta\varphi$ associated with the applied field is determined by the estimate

$$(\Delta\varphi)^2\bar{v}_{\rm F}/l(\beta) \simeq \mathscr{E}\Delta\varphi l(\beta)$$

Thus, the contribution to the polarization density, ΔP, is

$$\Delta P \simeq \frac{e}{\pi S_\perp}\Delta\varphi \simeq \frac{e}{\pi S_\perp}\mathscr{E}\frac{l^2(\beta)}{\bar{v}_{\rm F}} \simeq \frac{e}{\pi S_\perp}\bar{v}_{\rm F}\frac{\mathscr{E}}{\beta^2} \tag{2.26}$$

This expression should be averaged over the distribution $W(\beta)$. Bearing in mind that reconstruction takes place in the regions with $\beta^2 < \mathscr{E}\bar{v}_{\rm F}$, we obtain at $\mathscr{E} \ll \mathscr{E}_{\rm T}$:

$$P_{\text{nonlinear}} \simeq \frac{e}{\pi S_\perp}\mathscr{E}\bar{v}_{\text{F}}\int_0^{\sqrt{\mathscr{E}\bar{v}_{\text{F}}}} W(\beta)\frac{\mathrm{d}\beta}{\beta^2} \simeq \frac{e}{\pi S_\perp}\left(\frac{E}{E_{\text{T}}}\right)^2 \ln^2\left(\frac{E_{\text{T}}}{E}\right) \tag{2.27}$$

where eq. (2.12a) for $W(\beta)$ has been used and a physical threshold field $E_{\text{T}} = (\pi/e)\mathscr{E}_{\text{T}}$ has been introduced. Hence, nonlinear contribution to the polarization is strongly nonanalytic:

$$\frac{P_{\text{nonlinear}}\,(E)}{P_0(E)} \simeq \frac{|E|}{E_{\text{T}}}\ln^2\left(\frac{E_{\text{T}}}{|E|}\right). \tag{2.28}$$

The circumstantial experimental evidence in favour of this result one can perceive in the data obtained by Stokes et al. (1985), where a strong nonlinearity in the a.c. response of the pinned CDW has been found for the amplitudes well below the threshold field. Note that the fact of the nonanalytical behavior of $P(E)$ was also obtained by Fisher (1985).

2.3. Commensurability and random forward scattering

The effects of commensurability are known to be relevant for most of the CDW systems explored. Sometimes they result in the locking of the CDW wavevector leading to the commensurate state. The transition between commensurate and incommensurate states (C – I transition) can be driven by temperature or external pressure. Therefore, below we consider CDW pinning caused by impurities with the commensurability potential $V_0\cos m\varphi$ and incommensurability term $h(\,\mathrm{d}\varphi/\mathrm{d}x)$ taken into account.

Moreover, we should generalize our treatment of the CDW interactions with impurities. The point is that in some cases the amplitude of the electron forward scattering on the impurity potential can be much larger than the backward scattering amplitude (this is possible, e.g., if the scatterers are charged and located between the conducting chains, see Brasovzkii (1979)).

Random forward scattering leads to the term $V_{\text{f}}(x)(\mathrm{d}\varphi/\mathrm{d}x)$ in the CDW Hamiltonian, which does lead to CDW pinning when its interference with the commensurate potential is taken into account.

Below we consider the dielectric susceptibility and correlation length behavior of pinned CDWs in commensurate as well as incommensurate states at different relations between disorder parameters.

2.3.1. Strong forward scattering

The Hamiltonian of the system at low temperatures is as follows (Feigel'man and Vinokur 1983a):

$$H(\varphi) = \int \mathrm{d}x\left[\frac{\bar{v}_{\text{F}}}{2}\left(\frac{\mathrm{d}\varphi}{\mathrm{d}x}\right)^2 - h\frac{\mathrm{d}\varphi}{\mathrm{d}x} + V_{\text{f}}(x)\frac{\mathrm{d}\varphi}{\mathrm{d}x} - V_0\cos m\varphi - \mathscr{E}\varphi\right] \tag{2.29}$$

where again φ is the CDW phase, $\bar{v}_{\text{F}} = v_{\text{F}}/2\pi$ is the reduced Fermi velocity, $V_{\text{f}}(x)$ is the random potential describing forward-scattering impurities, statistical properties of $V_{\text{f}}(x)$ are given by

$$\overline{V_{\text{f}}(x)V_{\text{f}}\,(x')} = \mu^2\delta\,(x - x') \tag{2.30}$$

m is the order of commensurability, h is the incommensurability parameter, $\mathscr{E} = (e/\pi)E$ is the reduced external electric field. We introduce the dimensionless parameter, α_{f},

$$\alpha_{\text{f}} = \frac{\mu^2}{m\bar{v}_{\text{F}}^{3/2}V_0^{1/2}} \tag{2.31}$$

characterizing the degree of disorder. In this section we shall study the limiting case of a strong disorder $\alpha_f \gg 1$. Note that $\alpha_f = 2R_0/R_1$, where $R_1 = 2\bar{v}_F^2/\mu^2$ is the correlation length in the incommensurate system ($V_0 = 0$) and $R_0 = (\bar{v}_F/m^2V_0)^{1/2}$ is the size of the soliton in the regular system. It appears that the essential dependence of the system on h appears at $h \geqslant \mu^2/v_F$ so we consider the situations $h = 0$ (commensurate state) and $h \gg \mu^2/v_F$ separately.
Commensurate state ($h = 0$)
The basic equation (2.5) for the free energy of the semi-infinite system (say, from $-\infty$ to x) is now of the form

$$\frac{\partial \epsilon_x^>}{\partial x} = -\frac{1}{2v_F}\left(\frac{\partial \epsilon_x^>}{\partial \varphi} + V_f(x)\right)^2 - V_0 \cos m\varphi - \mathscr{E}\varphi + \frac{T}{2\bar{v}_F}\frac{\partial^2 \epsilon_x^>}{\partial \varphi^2} \tag{2.32}$$

and a similar equation can be written down for the right-hand side of the system.
At $T \neq 0, \mathscr{E} \neq 0$ the system has no equilibrium ground state, but at $T \ll \beta_0$ (where β_0 is the characteristic scale of $\epsilon^>(\varphi)$ variation), the time needed for a transition between two metastable states is rather long. It is reasonable, thus, to consider the quasiequilibrium problem where these transitions are neglected. Further on, we shall omit the last term in (2.32) assuming the condition $T \ll \beta_0$ to be satisfied.
Somewhat unexpectedly the nature of pinning is rather similar to that previously considered in section 2.2. The characteristic scale β_0 is estimated at $\mathscr{E} = 0$ as (Feigel'man and Vinokur 1983a):*

$$\beta_0 = \bar{v}_F\,(V_0 m/\mu)^{2/3} \tag{2.33}$$

Moreover, the form of small- β asymptotics of the distribution function $W^>(\beta^>)$coincides with the one presented in (2.11a). To derive this result we represent $\epsilon^>(\varphi)$ in the form ($\mathscr{E} \equiv 0$):

$$\epsilon_x^>(\varphi) = -\frac{\beta_x^>}{m^2}\cos m\,(\varphi - \gamma_x^>)\,, \tag{2.34}$$

and derive a stochastic equation for $\beta_x^>$and $\gamma_x^>$(the higher order harmonics are generated due to a nonlinear character of eq. (2.32), but their amplitudes are small as long as condition $\beta^> \ll \beta_0$ is satisfied):

$$\frac{\partial \beta_x^>}{\partial x} = m^2 V_0 \cos m\gamma_x^>, \quad \frac{\partial \gamma_x^>}{\partial x} = -\frac{V_f(x)}{\bar{v}_F} - \frac{mV_0}{\beta_x^>}\sin m\gamma_x^>. \tag{2.35}$$

Introducing the variable $u = \beta^>/\beta_0$ and the parameter $\zeta = \alpha_f^{-2/3} \ll 1$ one gets the corresponding Fokker-Planck equation

$$\frac{\partial}{\partial u}\left(-W^> \cos m\gamma^>\right) + \frac{\partial}{\partial \gamma^>}\left(\frac{1}{2m^{2/3}\zeta}\frac{\partial W^>}{\partial \gamma^>} + \frac{1}{u}\frac{\sin m\gamma^>}{m}W^>\right) = 0. \tag{2.36}$$

We look for the solution of eq. (2.36) in the form

$$\begin{aligned} W^>(u,\gamma) =& W_0^>(u) + \frac{\zeta}{m^{4/3}}W_1^>(u)\cos m\gamma^> \\ &+ \left(\frac{\zeta}{m^{4/3}}\right)^2 W_2^>(u)\cos 2m\gamma^> + \cdots \end{aligned} \tag{2.37}$$

and find

[0]*It was an error in that paper where m^2 was written instead of m.

$$W_0^> = Cu\ln(1/u); \quad W_1^> = 2C; \quad W_2^> = C/u; \ldots, \tag{2.38}$$

where the constant $C \approx 1$ remains undetermined by the presented method. It follows from (2.38) that the expansion in eq. (2.37) is in fact an expansion in powers of ζ/u, hence, the solution holds at $\zeta \ll u \ll 1$.

Thus, we obtain the distribution density $W^>(\beta^>)$in the form coinciding with (2.11a):

$$W^>(\beta^>) = C\frac{\beta^>}{\beta_0^2}\ln\left(\frac{\beta_0}{\beta^>}\right), \quad \zeta\beta_0 < \beta^> \ll \beta_0. \tag{2.39}$$

One can see from (2.37) and (2.38) that the average value of the commensurate parameter is strongly reduced by disorder:

$$\langle\cos m\gamma\rangle \approx \frac{1}{m^{4/3}}\zeta = \bar{v}_\mathrm{F}\left(\frac{m^2V_0}{\mu^4}\right)^{1/3}\frac{1}{m^{4/3}}. \tag{2.40}$$

Moreover, one can show that the correlation function

$$K(x) = \langle\cos(\varphi(x) - \varphi(0))\rangle \quad \text{at} \quad \zeta \ll 1$$

is the same as at $\zeta = 0$:

$$K(x) = \mathrm{e}^{-|x|/R_1}, \quad R_1 = 2\bar{v}_\mathrm{F}^2/\mu^2 \tag{2.41}$$

To obtain the estimate for the dielectric susceptibility we use eq. (2.23) and get

$$\chi_0 = \frac{2}{4\pi S_\perp}\left(\frac{e}{\pi}\right)^2\left[\langle\xi_0\rangle - 2m^2V_0\left\langle\xi^2\cos m\gamma\right\rangle_0\right] \tag{2.42}$$

where the variable $\xi_x = \partial\gamma_x/\partial\mathscr{E}$ is introduced and brackets $\langle\ldots\rangle_0$ mean the average over the distribution $P(\beta,\gamma,\xi)$ obtained at $\mathscr{E} = 0$. The result is (Feigel'man and Vinokur 1983a)

$$\chi_0 \simeq \tilde{c}\frac{1}{4\pi S_\perp}\left(\frac{e}{\pi}\right)^2\left(\frac{\mu}{mV_0}\right)^{4/3}\frac{1}{\bar{v}_\mathrm{F}}; \quad \tilde{c} \approx 1. \tag{2.43}$$

The threshold field E_T can be estimated similarly to (2.25):

$$E_\mathrm{T} \simeq \frac{\pi}{e}\bar{v}_\mathrm{F}\left(\frac{mV_0}{\mu}\right)^{4/3} \tag{2.44}$$

Note now that the characteristic pinning length (i.e., the length of the domain that reacts coherently upon any disturbance in the system) $l_0 \simeq \bar{v}_\mathrm{F}/\beta_0 = (\mu/mV_0)^{2/3}$ is much larger than the structure correlation length R_1.

The analysis of the nonlinear response at $E \ll E_\mathrm{T}$ is carried out as in section 2.2.2, the result coincides with (2.28) in the field range $\zeta^2E_\mathrm{T} \leqslant E \ll E_\mathrm{T}$. At lower values of E we expect analytic dependence.

Strongly incommensurate state

Now we discuss a strong incommensurability case when the average phase gradient $h/\bar{v}_\mathrm{F}$ is much larger than the inverse correlation length R_1^{-1}. We shall see that the values of the main quantities characterizing pinning (i.e. $\beta_0, \chi_0, E_\mathrm{T}$) match smoothly their values calculated at $h = 0$. Obviously, the commensurability order parameter $\langle\cos m\varphi\rangle$ should disappear at $h \simeq \sqrt{\bar{v}_\mathrm{F}V_0} \ll \mu^2/\bar{v}_\mathrm{F}$, but we shall not dwell upon this question.

It is convenient to introduce a new collective variable θ according to the formula

$$\varphi = \frac{hx}{\bar{v}_\mathrm{F}} + \theta - \frac{\bar{v}_\mathrm{F} V_0}{mh^2} \sin\left(\frac{mhx}{\bar{v}_\mathrm{F}} + m\theta\right). \tag{2.45}$$

At $V_\mathrm{f}(x) = 0$ the energy of the system is invariant with respect to translation $\theta \to \theta +$ const. Substituting (2.45) into (2.29) we obtain

$$H[\theta] = \int \mathrm{d}x \left[\frac{\bar{v}_\mathrm{F}}{2}\left(\frac{\mathrm{d}\theta}{\mathrm{d}x}\right)^2 + V_\mathrm{f}(x)\frac{\mathrm{d}\theta}{\mathrm{d}x} - \frac{V_\mathrm{f}(x)V_0}{h}\cos\left(\frac{mhx}{\bar{v}_\mathrm{F}} + m\theta\right) - \mathscr{E}\theta\right], \tag{2.46}$$

where we have omitted rapidly oscillating terms which do not contain $V_\mathrm{f}(x)$. The Hamiltonian (2.46) is just the continuum version of the Hamiltonian (2.2). The only difference is produced by the second term which does not contribute to pinning but determines the correlation length coinciding with the result (2.41) for $h = 0$. The estimates for $\beta_0(h)$ and $\chi_0(h)$ can be written down immediately:

$$\begin{aligned}
\beta_0(h) &\simeq \left(\frac{\mu V_0}{h}\right)^{2/3} m^{4/3} \bar{v}_\mathrm{F}^{1/3}, \\
\chi_0(h) &\simeq \frac{1}{4\pi S_\perp}\left(\frac{e}{\pi}\right)^2 \frac{\bar{v}_\mathrm{F}^{1/3}}{m^{8/3}}\left(\frac{h}{mV_0}\right)^{4/3}.
\end{aligned} \tag{2.47}$$

At $h \approx h_\mathrm{cross} = m\mu^2/\bar{v}_\mathrm{F}$ the crossover from eq. (2.47) to the results (2.33), (2.43) takes place. The distribution function $W^{>}(\beta^{>})$is given by eq. (2.39), but instead of β_0 one should use $\beta_0(h)$ from (2.47) and also the inequality $\beta > \zeta\beta_0$, relevant in the commensurate state, should be omitted.

In order to take backward scattering into account, the term

$$H_\mathrm{b} = \int \mathrm{d}x V_\mathrm{b}(x)\cos(\varphi + Qx); \quad \overline{V_\mathrm{b}(x)V_\mathrm{b}(x')} = cV_\mathrm{b}^2 \delta(x - x'), \tag{2.48}$$

should be added to (2.32). $\chi(h)$ and $\beta_0(h)$ behaviors depend on the relation between the parameters cV_b^2 and $(\bar{v}_\mathrm{F}V_0/\mu)^2$, the results can be found in Feigel'man and Vinokur (1983a).

2.3.2. $C - I$ transition in the presence of weak disorder

Now we discuss the situation when both types of impurities are present, but weak with respect to the commensurability potential (Feigel'man and Vinokur 1983b). The Hamiltonian is the sum of (2.29) and (2.48). The conditions of disorder weakness read:

$$\alpha_\mathrm{f} = \frac{\mu^2}{\bar{v}_\mathrm{F}^{3/2} V_0^{1/2} m} \ll 1, \quad \alpha_\mathrm{b} = \frac{cV_\mathrm{b}^2}{\bar{v}_\mathrm{F}^{1/2} V_0^{3/2} m^3} \ll 1. \tag{2.49}$$

The static properties of the commensurate state are weakly affected by disorder if the conditions (2.49) are fulfilled. The properties of a strongly incommensurate state $h \gg h_\mathrm{c} = (4/\pi)\sqrt{V_0 \bar{v}_\mathrm{F}}$ have been already discussed in the preceding section 2.3.1. Therefore, here we shall discuss the region near the C-I transition, where the disorder leads to substantial effects despite the fact that conditions (2.49) are fulfilled. In the absence of disorder the ground-state configuration $\varphi_0(x)$ slightly above the commensurability threshold ($h \geqslant h_\mathrm{c}$) can be represented as:

$$\varphi_0(x) = \frac{1}{m}\sum_{h=-\infty}^{\infty}\left\{4\,\mathrm{arctg}\exp\left[\frac{\pi}{2k\mathbb{K}(k)}\left(xm\sqrt{\frac{V_0}{\bar{v}_\mathrm{F}}} + k\xi\right) - 2nk\mathbb{K}(k)\right] - \pi\right\}, \tag{2.50}$$

where the elliptic modulus k is given by the relation $h/h_c = (4/\pi)\mathbb{E}(k)/k$, $K(k), \mathbb{E}(k)$ are complete elliptic integrals of the first and second kind, and ξ is the integration constant. Near the threshold $\delta = h/h_c - 1 \ll 1$(2.50) corresponds to the soliton lattice with the period $b = (2/m)k\mathbb{K}(k)\sqrt{\bar{v}_F/V_0}$, much larger than the soliton width $(1/m)\sqrt{\bar{v}_F/V_0}$. Introducing the collective phase variable $\theta_n = (x_n - nb)/b$ that describes the deformations of the soliton lattice (x_n is the coordinate of the nth soliton), we arrive at the following Hamiltonian

$$H[\theta_n] = \sum_n \left[\frac{s}{2b}(\theta_n - \theta_{n-1})^2 + U_f(\theta_n) + U_b(\theta_n) - \frac{2e}{m} b\theta_n E \right] \tag{2.51}$$

where $s \simeq (\bar{v}_F/m^2)\,\delta \ln^2 \delta$ is the elasticity modulus of the soliton lattice, $2e/m$ is the soliton charge, $U_{f,b}(\theta_n)$ are produced by random potentials:

$$U_f(\theta_n) = 2\sqrt{\frac{V_0}{\bar{v}_F}} \int \frac{dy V_f(y + b\theta_n)}{ch\left(my\sqrt{V_0/\bar{v}_F}\right)} \tag{2.52}$$

$$U_b(\theta_n) = \int dy V_b(y + b\theta_n) \cos\left\{ 4\,\mathrm{arctg}\exp\left[my\sqrt{\frac{V_0}{\bar{v}_F}} + 2k_F(y + b\theta_n) \right] \right\}. \tag{2.53}$$

Now strong- and weak-pinning dilemma (cf. section 1.2) arises anew at the level of the effective Hamiltonian (2.51). Weak pinning of the soliton lattice takes place at

$$\delta \gg \delta^* = \left(\alpha_b + m^2\alpha_f\right)^{1/2} \ln \frac{1}{\alpha_b + m^2\alpha_f} \tag{2.54}$$

In the region (2.54) the correlation length, R_c and dielectric susceptibility, χ, are (Feigel'man and Vinokur 1983b)

$$R_c = \frac{1}{m}\sqrt{\frac{\bar{v}_F}{V_0}}\delta^{2/3}\left(\ln\frac{1}{\delta}\right)^{7/3}\left(\alpha_b + m^2\alpha_f\right)^{-1/3} \gg b \tag{2.55}$$

$$\chi \simeq \chi_0\delta^{1/3}\left(\ln\frac{1}{\delta}\right)^{-4/3}\left(\alpha_b + m^2\alpha_f\right)^{-2/3} \tag{2.56}$$

where $\chi_0 = (4\pi S_\perp)^{-1}(e/\pi)^2(m^2V_0)^{-1}$ is the susceptibility of the commensurate state. The above results at sufficiently low temperatures hold,

$$T \ll T^*(\delta) = m\sqrt{\bar{v}_F V_0}\,\delta^{1/3}\left(\alpha_b + m^2\alpha_f\right)^{1/3}\left(\ln\frac{1}{\delta}\right)^{5/3} \tag{2.57}$$

at $T \geqslant T^*(\delta)$ soliton lattice pinning is destroyed by thermal fluctuations.
In the region $\delta \leqslant \delta^*$ pinning of individual solitons takes place; their density $n_s = 1/b$ is low $(n_s l_0 \gg 1)$ so that there is a large number of different
soliton configurations. The system properties in that region were studied by Talapov (1981).

The fluctuations of disorder lead to the appearance of the finite soliton density at $h < h_c(\delta < ())$ as well. At large enough $|\delta|$ the fluctuations leading to the formation of the soliton are exponentially rare (Balatsky and Vinokur 1984):

$$n_s \simeq \exp\left(-\delta^2/\alpha\right), \quad \alpha = \alpha_b + m^2\alpha_f. \tag{2.58}$$

This estimate holds for $|\delta| \geqslant \delta^{**} = \alpha^{1/2}\ln|\ln\alpha|$. Moreover, the temperature should be low enough:

$$T < T^{**}(\delta) = \alpha/4\delta$$

otherwise the soliton density is determined by thermal fluctuations:

$$n_{\mathrm{s}} \approx \exp\left(-\frac{|\delta| h_{\mathrm{c}}}{T} + \frac{\alpha h_{\mathrm{c}}^2}{2T^2}\right). \tag{2.59}$$

To conclude this subsection we note, that when passing the commensurability threshold, the dielectric susceptibility grows rapidly from χ_0 at $\delta \ll -\delta^{**}$ to $\chi \simeq \chi_0 \alpha^{-1/2} |\ln \alpha|$ at $\delta \simeq \delta^*$. At further δ increase χ grows according to (2.55) up to $\delta \simeq 1$; its behavior at $\delta \gg 1$ resembles that considered in section 2.3.1 (see Feigel'man and Vinokur (1983b) for more details).

4.7.3 3. Low-frequency conductivity of 1 D strongly disordered *CDW*

3.1. Underdamped dynamics: Mott-Berezinskii law

In the absence of thermal activation or tunneling processes the static CDW conductivity vanishes in the low-frequency limit due to the pinning phenomenon. The same is true for the classical problem of one-electron localization in the random potential. In that case the low-frequency conductivity is known to obey the famous Mott-Berezinskii law in one dimension (Mott and Twose 1961; Berezinskii 1973): $\sigma(\omega) - \omega^2 \ln^2 \omega$ (whose generalization for higher dimension was argued (Mott and Twose 1961) to be $\sigma(\omega) \sim \omega^2 \ln^{d+1} \omega$.

We shall see now that this result is more general and holds as well for a strongly correlated electron system such as one-dimensional CDW pinned by disorder if the CDW dynamics is underdamped (Feigel'man and Vinokur 1981). It should be noted that experimentally this last condition is not fulfilled usually (the only exception known is probably $(TaSe_4)_2$ I). Nevertheless, the problem considered looks rather exciting even from a purely theoretical viewpoint.

The undamped dynamics is governed by the Lagrangian

$$\mathscr{L}[\varphi] = \int \mathrm{d}x \left\{ \frac{\bar{v}_{\mathrm{F}}}{u^2}\dot{\varphi}^2 - \frac{\bar{v}_{\mathrm{F}}}{2}\left(\frac{\mathrm{d}\varphi}{\mathrm{d}x}\right)^2 + V_{\mathrm{f}}(x)\frac{\mathrm{d}\varphi}{\mathrm{d}x} + h\frac{\mathrm{d}\varphi}{\mathrm{d}x} + V_0 \cos m\varphi + V_{\mathrm{b}}(x)\cos\left(2k_{\mathrm{F}}x + \varphi\right)\right\}, \tag{3.1}$$

where u is the phase velocity of the CDW and all other notations coincide with that of section 2 . The disorder parameters α_{f} and α_{b} are assumed to be large: $\alpha_{\mathrm{f}}, \alpha_{\mathrm{b}} \gg 1$ (cf. (2.52)). The density of phason states, $\rho(\omega)$, and the conductivity, $\sigma(\omega)$, are connected with the Green function $G_\omega(x, x')$ of the equation of small oscillation of CDW phase $\boldsymbol{\theta}(x, t)$, near the ground state, $\varphi(x)$:

$$\begin{aligned} &\frac{\bar{v}_{\mathrm{F}}}{u^2}\omega^2\theta = -\bar{v}_{\mathrm{F}}\theta'' + \mathscr{V}(x)\theta \\ &\mathscr{V}(x) = V_{\mathrm{b}}(x)\cos\left(2k_{\mathrm{F}}x + \varphi(x)\right) + m^2 V_0 \cos(m\varphi(x)) \end{aligned} \tag{3.2}$$

Then the retarded Green function, $G_\omega^{\mathrm{R}}(x, x')$ is

$$G_\omega^{\mathrm{R}}(x, x') = \frac{u^2}{\bar{v}_{\mathrm{F}}} \sum_n \frac{\psi_n(x)\psi_n(x')}{\omega^2 - \omega_n^2 + \mathrm{i}\delta\omega} \tag{3.3}$$

where ψ_n are eigenfunctions of the Schrödinger equation (3.2). Further on, density of states and conductivity can be expressed in terms of the Green function (3.3):

$$\rho(\omega) = -\frac{2}{\pi}\frac{\omega\bar{v}_{\mathrm{F}}}{u^2}\left\langle \operatorname{Im} G^{\mathrm{R}}_{\omega}(x,x')\right\rangle, \tag{3.4}$$

$$\sigma(\omega) = -\frac{e^2\omega}{\pi^2}\left\langle \int \mathrm{d}x' \operatorname{Im} G^{\mathrm{R}}_{\omega}(x,x')\right\rangle, \tag{3.5}$$

where the symbol $\langle\cdots\rangle$ means averaging over random potential.
We are interested in the low-frequency system behavior at $\omega \ll \omega_{\mathrm{p}}$, where ω_{p} is the characteristic pinning frequency. The phason modes are well localized; their spectrum is discrete and localization lengths can be estimated as $l(\omega) \simeq u/\omega$. Thus, comparing spectral representation (3.3) with the definition of the quantity β_x (cf. eq. (2.13)):

$$\beta_x = \frac{\partial^2 \epsilon_x(\varphi)}{\partial \varphi_x^2} = G^{-1}_{\omega=0}(x,x) \tag{3.6}$$

(here x is any point in the middle of the system) we obtain

$$\omega_x = (u/\bar{v}_F)\,\beta_x \tag{3.7}$$

where ω_x is the energy of the state localizing near the point x. Making use of eq. (3.7) and definition of density of states, $\rho(\omega) = \langle\delta(\omega-\omega_n)\rangle$, (3.5), we get

$$\begin{aligned}\rho(\omega)\mathrm{d}\omega &= (a/R_{\mathrm{c}})\,W(\beta)\mathrm{d}\beta \\ &= (\beta_0/\epsilon_{\mathrm{F}})\,W\left(\frac{\bar{v}_{\mathrm{F}}\omega}{u}\right)\frac{\bar{v}_{\mathrm{F}}}{u}\,\mathrm{d}\omega\end{aligned} \tag{3.8}$$

where $W(\beta)$ is the probability density of the pinning energy, β, per correlation length (see section 2).

The factor $a/R_{\mathrm{c}} = \beta_0/\epsilon_{\mathrm{F}}$ has arisen due to the fact that the density of states $\rho(\omega)$ is normalized to the single lattice site (the lattice spacing is a) whereas $W(\beta)$ is normalized to the correlation length R_{c}.

Equation (3.6) can be rewritten in the form

$$\begin{aligned}\sigma(\omega) &= \frac{e^2u^2}{2\pi\bar{v}_{\mathrm{F}}}\left\langle\int \mathrm{d}x' \sum_n \psi_n(x)\psi_n(x')\,\delta(\omega-\omega_n)\right\rangle \\ &= \frac{e^2u^2}{2\pi\bar{v}_{\mathrm{F}}}\int\frac{\mathrm{d}x}{L}\int \mathrm{d}x' \sum_n \psi_n(x)\psi_n(x')\,\delta(\omega-\omega_n)\end{aligned} \tag{3.9}$$

It is important that for a fixed value of ω_n integration is performed over the localization region of the length of $l(\omega_n) \simeq u/\omega_n$, so

$$\begin{aligned}\sigma(\omega) &\simeq \frac{e^2u^2}{2\pi\bar{v}_{\mathrm{F}}S_\perp}\frac{1}{L}\sum_n l(\omega_n)\,\delta(\omega-\omega_n) \\ &\simeq \frac{e^2u^2}{2\pi\bar{v}_{\mathrm{F}}S_\perp}\frac{u}{a}\frac{1}{\omega}\rho(\omega)\end{aligned} \tag{3.10}$$

As has been discussed in section 2 in the case of strong forward, $\alpha_{\mathrm{f}} \gg 1$ and/or backward, $\alpha_{\mathrm{b}} \gg 1$, scattering, the distribution function

$$W(\beta) = C\left(\beta^3/\beta_0^4\right)\ln^2\left(\beta_0/\beta\right) \qquad (3.11)$$
$$C \simeq 1$$

for $\beta \ll \beta_0$, where β_0 is the scale of the pinning energy.
Then one obtains from (3.8), (3.10), (3.11)

$$\rho(\omega) = \frac{c_1}{\omega_\mathrm{m}}\left(\frac{\omega}{\omega_\mathrm{p}}\right)^3 \ln^2\left(\frac{\omega_\mathrm{p}}{\omega}\right) \qquad (3.12)$$

$$\sigma(\omega) = c_2\frac{e^2u^2}{\bar{v}_\mathrm{F}\omega_\mathrm{p}S_\perp}\left(\frac{\omega}{\omega_\mathrm{p}}\right)^2 \ln^2\left(\frac{\omega_\mathrm{p}}{\omega}\right) \qquad (3.13)$$

where $\omega_\mathrm{m} = u/a, c_1, c_2 \simeq 1$. The characteristic pinning frequency $\omega_\mathrm{p} = (u/\bar{v}_\mathrm{F})\,\beta_0$ where β_0 is the scale of the pinning energy, determined in section
2. For the generic model (2.1) one obtains with eq. (2.10) that

$$\omega_\mathrm{p} = \frac{u}{\bar{v}_\mathrm{F}}\left(\bar{v}_\mathrm{F}cV_\mathrm{b}^2\right)^{1/3}, \qquad (3.14)$$

whereas in the general case (Feigel'man and Vinokur 1983c)

$$\omega_\mathrm{p} = \omega_0\begin{cases}\left(\alpha_\mathrm{f}^{-1}+\alpha_\mathrm{b}\right)^{1/3}, & h \leqslant \mu^2/\bar{v}_\mathrm{F}\\ \left[\alpha_\mathrm{f}m^2\left(h_\mathrm{c}/h\right)^2+\alpha_\mathrm{b}\right]^{1/3}, & h \gg \mu^2/\bar{v}_\mathrm{F},\end{cases} \qquad (3.15)$$

where $\omega_0 = (u/\bar{v}_\mathrm{F})\,m\sqrt{\bar{v}_\mathrm{F}V_0}$ is the pinning frequency in the pure commensurate system. The results (3.12) and (3.13) are valid at $\Omega_\mathrm{min} \ll \omega \ll \omega_\mathrm{p}$, where the lower bound $\Omega_\mathrm{min} \simeq (u/\bar{v}_\mathrm{F})\,\beta_\mathrm{m}$ is due to deviation of the distribution function $W(\beta)$ from the form (3.11) at $\beta \simeq \beta_\mathrm{m} \ll \beta_0$ (cf. eqs. (2.12a), (2.42)). The lowest eigenstates with $\omega \leqslant \Omega_\mathrm{min}$ originate from large 'Poissonian' fluctuations of random potential, so we believe that at $\omega \to 0\sigma(\omega) \propto \exp\left(-\omega_\mathrm{p}/\omega\right)$.

The point to be noted here is that conductivity can be expressed in the form

$$\sigma(\omega) = \frac{ne^2\tau}{m^*}f(\omega\tau), \quad f(x) = x^2\ln^2 x, \qquad (3.16)$$

where n is the electron density, $m^* = (v_\mathrm{F}/u)\,m$ is the CDW effective mass, $\tau = \omega_\mathrm{p}^{-1}$. We see that the dimensionless function $f(\omega\tau)$ describing lowfrequency CDW conductivity is identical to that of the localization theory (Berezinskii 1973).

To understand the meaning of this remarkable coincidence it is instructive to express the CDW Lagrangian

$$\mathscr{L} = \frac{\bar{v}_\mathrm{F}}{2u^2}\left(\frac{\partial\varphi}{\mathrm{d}t}\right)^2 - \frac{\bar{v}_\mathrm{F}}{2}\left(\frac{\partial\varphi}{\partial x}\right)^2 + V_\mathrm{b}(x)\cos(\varphi + Qx), \qquad (3.17)$$

in terms of the fermionic variables (we preserve only back-scattering potential for brevity). Making use of the well-known bosonization formulae (Coleman 1975, Mandelstam 1975) we get the Thirring model Lagrangian with the additional term due to random scattering:

$$\mathscr{L}_\mathbf{F} = \mathrm{i}\bar{\psi}\gamma_\mu\partial_\mu\psi - \frac{1}{2}g\left(\bar{\psi}\gamma_\mu\psi\right)^2 - \bar{\psi}\left[\xi_1(x) + \mathrm{i}\gamma_5\xi_2(x)\right]\psi, \qquad (3.18)$$

where

$$\begin{aligned}\langle\xi_1(x)\xi_2(x')\rangle &= 0\\ \langle\xi_1(x)\xi_1(x')\rangle &= \langle\xi_2(x)\xi_2(x')\rangle\\ &= \frac{cV_{\mathbf{b}}^2}{\omega_{\mathrm{m}}^2}\delta(x-x')\end{aligned} \tag{3.19}$$

Note that (3.18) can be regarded as an approximated Lagrangian for the 1D nonrelativistic Fermi gas in the random potential. The quasiclassical limit $u/v_{\mathrm{F}} \ll 1$ corresponds to a very strong repulsion ($g \gg 1$) in this Fermi gas. So our result (3.13) means that the low-frequency dependence of the conductivity $\sigma(\omega)$ of 1D Fermi system is not affected by the fermionic interaction. The change is that localization time, $\tau \simeq (cV_{\mathrm{b}}^2)^{-1}$ at $g = 0$ is replaced by $\tau \simeq (cV_b^2)^{-1/3}$ as $g \to \infty$.

3.2. Overdamped dynamics

In most of the CDW systems phason modes undergo a substantial dissipation that originates mainly from the interaction with thermal phonons of the underlying lattice (Brazovskii 1979). Thus, eq. (3.2) for low-frequency small oscillations should be supplemented by linear friction term and then reads

$$\frac{\bar{v}_{\mathrm{F}}}{u^2}\left(\omega^2 + \mathrm{i}\lambda\omega\right)\theta = -\bar{v}_{\mathrm{F}}\theta'' + \mathscr{V}(x)\theta \tag{3.20}$$

The corresponding expression for the Green function is (cf. (3.4)):

$$G_\omega^{\mathrm{R}}(x,x') = \frac{u^2}{\bar{v}_{\mathrm{F}}}\sum_n \frac{\psi_n(x)\psi_n(x')}{\omega^2 + \mathrm{i}\lambda\omega - \omega_n^2} \tag{3.21}$$

Below we consider the overdamped limit $\lambda \gg \omega$ so that the first term in the denumerator in (3.21) can be neglected. Equation (3.5) can be now rewritten as

$$\sigma(\omega) = \frac{u^2e^2}{\pi^2\bar{v}_{\mathrm{F}}}\lambda\omega^2\int\frac{\mathrm{d}x'}{L}\int\mathrm{d}x\sum_n\frac{\psi_n(x)\psi_n(x')}{\omega_n^4 + \lambda^2\omega^2} \tag{3.22}$$

where $\psi_n(x)$ and ω_n coincide with that of section 3.1. Thus, analogues of eqs. (3.10) and (3.13) can be easily derived:

$$\begin{aligned}\sigma(\omega) &= \frac{e^2u^2}{\bar{v}_{\mathrm{F}}S_\perp}\frac{\omega}{L}\sum_n l(\omega_n)\frac{\lambda\omega}{\lambda^2\omega^2 + \omega_n^4}\\ &= c_\sigma\frac{e^2u^2}{S_\perp\bar{v}_{\mathrm{F}}\lambda}\left(\frac{\omega}{\Omega_{\mathrm{p}}}\right)^{3/2}\ln^2\left(\frac{\Omega_{\mathrm{p}}}{\omega}\right), \quad \omega \ll \Omega_{\mathrm{p}},\end{aligned} \tag{3.23}$$

where $\Omega_{\mathrm{p}} = \omega_{\mathrm{p}}^2/\lambda$ is the characteristic pinning frequency in the overdamped limit, ω_{p} is defined in (3.14) and $c_\sigma \simeq 1$. The imaginary part of the dielectric permeability follows immediately from (3.23):

$$\begin{aligned}\mathrm{Im}\,\epsilon(\omega) = \frac{4\pi\sigma(\omega)}{\omega} &= 4\pi c_\sigma\frac{e^2u^2}{\overline{v_{\mathrm{F}}}\omega_{\mathrm{p}}^2S_\perp}\left(\frac{\omega}{\Omega_{\mathrm{p}}}\right)^{1/2}\ln^2\left(\frac{\Omega_{\mathrm{p}}}{\omega}\right),\\ &\simeq c_\epsilon\epsilon_0\left(\omega/\Omega_{\mathrm{p}}\right)^{1/2}\ln^2\left(\Omega_{\mathrm{p}}/\omega\right); \quad \omega \ll \Omega_{\mathrm{p}},\end{aligned} \tag{3.24}$$

where ϵ_0 is a static permeability (see section 2) and $c_\epsilon \simeq 1$. For the real part of $\epsilon(\omega)$ at low frequency $\omega \ll \Omega_\mathrm{p}$ one gets:

$$\epsilon_0 - \mathrm{Re}\,\epsilon(\omega) = -\frac{1}{\pi}\omega \left\{ \frac{\mathrm{Im}\,\epsilon\,(\omega')\,\mathrm{d}\omega'}{(\omega'-\omega)\,\omega'} = \mathrm{Im}\,\epsilon(\omega). \right. \tag{3.25}$$

We would like to emphasize that relation (3.25) between $\mathrm{Im}\,\epsilon(\omega)$ and $\mathrm{Re}\,\epsilon(\omega)$ is exact, not withstanding that both quantities are calculated with the order-of-magnitude accuracy only (the order-of-magnitude relation between $\epsilon_0 - \mathrm{Re}\,\epsilon(\omega)$ and $\mathrm{Im}\,\epsilon(\omega)$ would be a general consequence of the broad spectrum of relaxation rates in the disordered system).

3.3. Intervalley transitions

It is commonly believed that disordered systems at low temperatures are characterized by a vast amount of metastable states (valleys in the configuration space). The transitions between these states are slow and the corresponding relaxation times are distributed over huge time intervals (e.g., from 10^{-10} up to 10^5 s or more in spin glasses (Binder and Young 1986)) leading to remarkable phenomena of non-ergodicity, memory dependence and ageing. These phenomena are well-known experimentally in CDW systems as well (see Grüner and Zettl 1985). Unfortunately, their quantitative theoretical description is absent up to now. Here we discuss one of the simplest related problems, i.e., the transition-induced contribution to the low-frequency CDW conductivity.

We shall study the region of intermediate frequencies where it is sufficient to consider transitions between neighbouring metastable states (the discussion of longer time intervals within mean-field theory can be found in a recent paper by Littlewood and Rammal (1987)). That means that relaxation is governed by the distribution of 'two-level systems'. Any two-level system (TLS) is characterized by the barrier energy U and level splitting Δ. In the case considered the values of these both quantities are of the order of local value of (note again that β_x is the scale of variation of the function $\epsilon\,(\varphi_x)$). The contribution of a set TLS to the imaginary part of a dielectric response can be estimated (see Mott and Davis 1971, Ioffe and Vinokur 1987) as

$$\mathrm{Im}\,\epsilon(\omega) \simeq \frac{e^2}{4\pi S_\perp} \int \mathrm{d}U\ \mathrm{d}\Delta \frac{R(U,\Delta) l_U}{T\,\mathrm{ch}^2(\Delta/2T)} \frac{\omega\tau(U)}{1+\omega^2\tau^2(U)} \tag{3.26}$$

where we suppose TLS to be classical and $R(U,\Delta)$ is their distribution density; $\tau(U) \simeq \Omega_\mathrm{p}^{-1}\exp(U/T)$ is the time associated with thermal activation over the barrier $U \gg T$; $l_U \simeq \bar{v}_\mathrm{F}/U$ is the length associated with a given TLS (cf. eqs. (3.10) and (3.23) where the analogous factors appear).

The characteristic scales of Δ and U are of the order of β, so that

$$\int \mathrm{d}\Delta \frac{R(U,\Delta)}{T\mathrm{ch}^2(\Delta/2T)} \simeq \frac{W(U)}{U} \tag{3.27}$$

where the $W(U)$ function coincides with $W(\beta)$ from eq. (2.12). Due to a very sharp $\tau(U)$ dependence, the main contribution to the integral over U in (3.26) comes from TLS with $\omega\tau(U) \simeq 1$. Finally, we get

$$\mathrm{Im}\,\epsilon(\omega) \simeq \frac{e^2}{4\pi S_\perp} \frac{\bar{v}_\mathrm{F} T^2}{\beta_0^4} \ln\left(\frac{\Omega_\mathrm{p}}{\omega}\right) \simeq \epsilon_0 \left(\frac{T}{\beta_0}\right)^2 \ln\left(\frac{\Omega_\mathrm{p}}{\omega}\right) \tag{3.28}$$

The result (3.18) is valid in the frequency domain $\Omega_\mathrm{p}\exp\left(-\beta_0/T\right) \leqslant \omega \leqslant \Omega_\mathrm{p}$ where small-TLS participate (relevant $\beta \ll \beta_0$). Note that $\mathrm{Im}\,\epsilon(\omega)$ grows with ω decrease and is of the order of $(T/\beta_0)\,\epsilon_0$ at the frequency $\omega \simeq \Omega_\mathrm{p}\exp\left(-\beta_\mathrm{o}/T\right) = \Omega_\mathrm{min}$ which is the transition rate corresponding to the transitions between average barriers.

The expression for the conductivity $\sigma_{\rm tr}(\omega)$ immediately follows from (3.28)

$$\sigma_{\rm tr}(\omega) \simeq \epsilon_0 \omega \left(T/\beta_0\right)^2 \ln\left(\Omega_{\rm p}/\omega\right); \quad \Omega_{\rm min} \leqslant \omega \leqslant \Omega_{\rm p}. \tag{3.29}$$

In the lowest frequency region $\omega \ll \Omega_{\rm min}$ the pinning is effectively lost (the density of high barriers $\beta \gg \beta_0$ decreases too rapidly to be relevant, cf. (2.12b)), therefore, we speculate that

$$\sigma_{\rm tr}(\omega \to 0) \simeq \sigma_{\rm tr}\left(\omega \simeq \Omega_{\rm min}\right) \simeq \frac{T}{\beta_0}\sigma_0 \exp\left(-\beta_0/T\right) \tag{3.30}$$

where $\sigma_0 = u^2/\lambda \bar{v}_{\rm F}$ is the static conductivity in the absence of the pinning potential $\mathscr{V}(x)$.

In conclusion we note that the low-frequency behavior of conductivity depends strongly on the ratio between pinning frequency, $\omega_{\rm p}$, and damping constant, λ. If (i) $\lambda \gtrsim \omega_{\rm p}$ (strong dissipation limit), a two-frequency region can be distinguished. At $\Omega_{\rm p} \gg \omega \gg \Omega_{\rm tr} \cong \frac{1}{4}\Omega_{\rm p}\left(T/\beta_0\right)^4 \left[\ln\left(\beta_0/T\right)\right]^{-1}$ the main contribution arises from intravalley relaxation processes and conductivity is given by (3.23). At lower frequencies $\Omega_{\rm tr} \gg \omega \gg \Omega_{\rm min}$ intervalley transitions dominate and conductivity should be described by eq. (3.29). (ii) In the limit of a weak dissipation $\omega_{\rm p} \gg \lambda$ there are three characteristic ranges of ω. For ω contained in the interval $\omega_{\rm p} \gg \omega \gg \lambda$ conductivity is described by underdamped Berezinsky-Mott formula (3.13). At $\lambda \gg \omega \gg \Omega_{\rm tr}$ dissipation becomes essential and conductivity takes the form (3.23) and for lower
$(\Omega_{\rm tr} \gg \omega \gg \Omega_{\rm min}\,)\,\omega$ intervalley transitions are switched on again leading to (3.29).

4.7.4 4. Conclusions

CDW pinning impurity is mainly a three-dimensional problem which is rather far from being solved theoretically. In this review we have discussed its one-dimensional version that is more amenable for theoretical study. The method of a stochastic transfer matrix developed makes it possible to advance beyond simple scaling estimates known for the 3D case and to obtain some new results for both static and dynamic CDW properties. The former concern nonanalytic nonlinear dielectric response (section 2.2.2). The latter refer to a low-frequency conductivity in the underdamped and overdamped regimes (section 3). For most of these results, the structure and probability distribution of relatively soft localized phason modes are relevant. The term 'soft' we use for the modes with frequencies well less than the average pinning frequency $\omega_{\rm p}$. The important feature of a weak impurity pinning is that 'quasigap' in the density of states at $\omega < \omega_{\rm p}$ is a power-law which leads to strong frequency and field dependences of the dielectric response. It is unclear whether the same picture should hold for a 3D model, though the experimental data seem to agree with it. Nevertheless, two other features of soft modes are probably retained in 3D case, namely: (i) in the domains with a low local gap ($\omega \ll \omega_{\rm p}$), the total scale of pinning energy (i.e. the scale of the $\epsilon(\varphi)$ function variation) is small, and (ii) the characteristic lengths of these domains are large: $l(\omega) \sim \omega^{-1}$ (cf. (2.14)). Note that in a recent qualitative study of 3D weak pinning (Littlewood and Rammal 1987) both these features were overlooked, therefore, some results of their paper (e.g. eqs. (2.13), (2.14)) contradict our conclusions.

We believe that the study of the 1D pinning model is useful for a qualitative understanding of the real 3D situation. Moreover some of the 1D results can possibly be applied to the $(TaSe_4)_2$ I system slightly above the 3D Peierls transition.

4.7.5 References

[0]Balatsky, A.V., and V.M. Vinokur, 1984, Solid State Commun. 52, 847.

Feigel'man, M.V., 1980, Zh. Eksp. & Teor. Fiz. 79, 1095 [Sov. Phys.-JETP 52, 555].
Feigel'man, M.V., and V.M. Vinokur, 1983a, Solid State Commun. 45, 595.
Feigel'man, M.V., and V.M. Vinokur, 1983b, Solid State Commun. 45, 599.
Feigel'man, M.V., and V.M. Vinokur, 1983c, Solid State Commun. 45, 603.
Feigel'man, M.V., and V.M. Vinokur, 1987, Phys. Lett. A 81, 53.
Fisher, D.S., 1985, Phys. Rev. B 31, 1396.
Fukuyama, H., and P.A. Lee, 1978, Phys. Rev. B 17, 535.
Gor'kov, L.P., 1977, Pis'mav Zh. Eksp. & Teor. Fiz. 25, 384 [JETP Lett. 25, 358].
Grüner, G., and A. Zettl, 1985, Phys. Rep. 119, 117.
Imry, Y., and S.-K. Ma, 1975, Phys. Rev. Lett. 35, 1399.
Ioffe, L.B., and V.M. Vinokur, 1987, J. Phys. C 20, 6149.
Lee, P.A., and T.M. Rice, 1979, Phys. Rev. B 19, 3970.
Lee, P.A., T.M. Rice and P.W. Anderson, 1974, Solid State Commun. 14, 703.
Littlewood, P., and L.P. Rammal, 1987, preprint CRTBT-CNRS.
Mandelstam, S., 1975, Phys. Rev. D 11, 3026.
Mott, N.F., and E.A. Davis, 1971, Electronic Processes in Non-Crystalline Materials (Clarendon Press, Oxford) p. 58.
Mott, N.F., and W.D. Twose, 1961, Adv. Phys. 10, 107.
Reagor, D., S. Sridhar, M. Maki and G. Grüner, 1985, Phys. Rev. B 32, 8445.
Stokes, J.P., O.M. Robbins and S. Bhattacharya, ?????, Phys. Rev. B 32, 6939.
Talapov, A.L., 1981, Zh. Eksp. & Teor. Fiz. 81, 1980.
Vinokur, V.M., M.B. Mineev and M.V. Feigel'man, 1981, Zh. Eksp. & Teor. Fiz. 81, 2142 [Sov. Phys.-JETP 54, 1138].

4.8 8 Computer Simulations of CDW Dynamics by Littlewood

4.8.1 1. Introduction

Numerical methods have come to play an increasingly important role in the study of many complex physical models. While the growth in the use of computational methods has been encouraged by the wide availability of high-speed computers, numerical techniques are well-suited for many problems of current interest.

One common feature of those problems for which numerical techniques have proved invaluable is that their dynamics are inherently complex, involving many degrees of freedom, although complicated systems do not necessarily possess complex dynamical behavior. Although most non-trivial models may apparently involve many interacting degrees of freedom, their behavior may often be described by the low-dimensional dynamics of only a few effective degrees of freedom (EDF) - for example roll formation (though not turbulence) in Rayleigh-Benard convection cells. In complex systems, the many-EDF nature is crucial.

The classic case where many interacting modes remain relevant is that of critical phenomena. In spatially uniform systems, the ideas of scaling and the techniques of the renormalization group can be applied to systematically integrate out the high-energy degrees of freedom. In non-linear systems, or where disorder or frustration is present and relevant, such techniques cannot be simply applied. Here, numerical simulations can show the way forward.

The thrust of a numerical simulation is generally threefold. Firstly, one hopes to check that the specified model and dynamics faithfully reproduce the behavior of the real system. In cases

Berezinskii, V.L., 1973, Zh. Eksp. & Teor. Fiz. 65, 1251 [1974, Sov. Phys.-JETP 38, 620]. Binder, K., and A.P. Young, 1986, Rev. Mod. Phys. 58, 765. Brazovskii, S.A., 1979, Zh. Eksp. & Teor. Fiz. 76, 1000 [Sov. Phys.-JETP 49, 504]. Chen, T., L. Mihaly and G. Grüner, 1988, Phys. Rev. Lett. 60, 464. Coleman, S., 1975, Phys. Rev. D 11, 2088. Efetov, K.B., and A.I. Larkin, 1977, Zh. Eksp. & Teor. Fiz. 72, 2350.

where the validity of the underlying model is in doubt this may be the most important function. Usually the full model is too complicated to be simulated in its entirety, and one must make judicious approximations to study various aspects of the behavior. Secondly, one can inspect the details of the simulation in a fashion that is generally impossible for the real system. Thus one can extract features of the behavior which are inaccessible to macroscopic measurements in order to simplify the behavior to its essentials, to compare with analytic approximations or scaling theories, and to suggest further approximate schemes. This has been the prime function of numerical simulations of

CDWs, because little experimental information has been available on a microscopic or mesoscopic length scale. Thirdly one may indeed be able to obtain quantitative results for comparison with experiment (as opposed to the essentially qualitative agreement which is a test of the theory).

The most enduring model for the dynamics of CDWs has been the model of Fukuyama, Lee and Rice (FLR) describing an elastically deformable CDW pinned by impurities (Fukuyama and Lee 1977, Efetov and Larkin 1977, Lee and Rice 1979). It has been introduced elsewhere in this volume, and will be the central focus of this chapter. The FLR model is analytically rather intractable; difficulties with an analytic solution can be traced, in perturbation theory (Sneddon et al. 1982), to the presence of many interacting spatial modes especially in the region close to the sliding threshold (Sneddon 1984, Coppersmith and Littlewood 1985, Matsukawa and Takayama 1987, Matsukawa 1987). Support for the idea that the behavior close to threshold can be treated as a critical phenomenon comes both from the high-field perturbation theory, as well as a mean field theory (Fisher 1983, 1985, Sneddon 1984), the only version of the model for which a full analytic treatment is possible. Below threshold, the model has many metastable states, so that controlled analytic work is difficult (Feigel'man and Vinokur 1981, 1983).
Simulations of the FLR model can be extremely time-consuming, especially in large systems, and it has (with some exceptions) been studied numerically only in one dimension (Teranishi and Kubo 1979, Sokoloff 1981, 1985, Sokoloff and Horowitz 1983, Pietronero and Strässler 1983, Matsukawa and Takayama 1984, 1986, 1987, Abe 1987, 1985, 1986, Littlewood and Rice 1982, Littlewood 1986a,b, 1987). Thus for certain aspects of the dynamics it is often advantageous to make further simplifications, or to study closely related simpler models which include the relevant physics. The Frenkel-Kontorova model of a CDW with incommensurate, rather than random, pinning is another system where many degrees of freedom are relevant. Its properties above threshold are very similar to those of the FLR model, and it is possible to make some analytic headway before being reduced to purely numerical methods (Coppersmith and Fisher 1983, Peyraud and Aubry 1983, Coppersmith 1984, Sneddon 1984). A model of stick-slip friction (instead of a conservative pinning potential) yields polarization hysteresis below threshold in a fashion reminiscent of experiment (Mihaly et al. 1987). Some of the qualitative features of the behavior under pulsed driving fields are also present in a two-stage cellular automaton which can be approximately derived from the FLR model in certain limits (Coppersmith and Littlewood 1987, Coppersmith 1987a,b, Tang et al. 1987). Mode-locking has also been studied in a coupled domain model (Tua and Ruvalds 1985) and within few degree-offreedom models (Inui and Doniach 1987, Matsukawa and Takayama 1987).

And of course a single degree of freedom model (Grüner et al. 1981) is useful to make an order of magnitude comparison of experimental quantities to check the approximate self-consistency of the theory.

The FLR model treats the CDW as an elastically deformable sheet, and neglects processes of phase slip involving amplitude fluctuations. Phase slip must certainly occur at the contacts even if nowhere else in the sample (Ong 1989). Aside from providing an extra source of pinning (which might be included in the FLR model by adding a few strong pinning centers) the dynamics of the CDW amplitude may need to be taken into account. On a microscopic level,

amplitude fluctuations may involve the creation and motion of vortices or their condensation into sheets of phase slip (running either parallel or perpendicular to the CDW axis). In many, perhaps all, of the semiconducting CDW materials it is clear that the CDW does break up into domains with phase slip parallel to the direction of sliding, as would be expected from the crystalline anisotropy. Vortex arrays, or sheets of phase slip, running perpendicularly to the CDW sliding direction must occur in the vicinity of the current contacts; such phase breaking can also be deliberately induced in the bulk by applying a large temperature gradient. Furthermore, samples which have been deliberately strongly disordered show a class of 'switching' phenomena which are generally ascribed to the effects of amplitude fluctuations (Zettl and Grüner 1982, Hall et al. 1988, Inui et al. 1988). However, the very fact that a large perturbation is required to induce phase slippage in the bulk gives confidence that this is not an over-riding phenomenon, at least in $NbSe_3$.
'Switching' samples have hysteresis in their IV characteristics as well as a qualitatively different a.c. response from non-switching materials. In joint a.c. and d.c. electric fields they display a period doubling transition to chaos with a different character from the quasiperiodic mode-locking of nonswitching samples (which do not show chaos). None of these phenomena occur in the FLR model, but they can be reproduced successfully in a model with coupled dynamics of the amplitude and phase (Inui et al. 1988).

The diversity of physical phenomena associated with sliding CDWs imposes stringent tests on any theory. The phenomena range from 'glassy' dielectric relaxation to a highly coherent response in joint a.c. and d.c. driving fields. An overview of the experiments has been given in the article by Grüner and Monceau; we shall comment on the comparison between some of the experiments and the numerical models further in this chapter.

The interest in all of these models is not restricted to their application to sliding charge density waves, but also in their behavior as prototypical examples of the properties of many-EDF systems. Complexity introduces new features into the dynamics which are not found in few-EDF models; sliding CDWs may be useful as a laboratory in which to study these phenomena.

4.8.2 2. Models for classical CDW dynamics

2.1. Dynamics of the CDW phase

We shall discuss CDW dynamics within the framework of a GinzburgLandau expansion of the free energy in terms of the CDW order parameter $\rho(\boldsymbol{r}) = \rho_c + \rho_0 \cos(\boldsymbol{Q} \cdot \boldsymbol{r} + \phi(\boldsymbol{r}))$. This approach is originally due to McMillan (1975, 1976) and was extended by others after the discovery of CDW transport (Fukuyama and Lee 1977, Efetov and Larkin 1977, Lee and Rice 1979). To simplify the analysis, we have assumed a single purely sinusoidal CDW; we also assume that the CDW is free to slide only in the incommensurate z-direction of $\boldsymbol{Q}$. A more significant approximation is to neglect fluctuations in the CDW amplitude ρ_0, so that solely elastic deformations of the CDW are allowed. The energy of the CDW can be written

$$H = H_{\rm el} + H_{\rm imp} + H_{\rm field} \,. \tag{2.1}$$

The elastic energy can be written (after rescaling lengths to make the elastic constants isotropic)

$$H_{\rm el} = \frac{1}{2} \int \mathrm{d}\boldsymbol{r} K (\nabla \phi)^2. \tag{2.2}$$

Because the sliding CDW carries a current

$$j_{\rm CDW} = \rho_c \dot{\phi} / Q_z, \tag{2.3}$$

the polarization energy in an electric field $\boldsymbol{E}$ is

$$H_{\text{field}} = \int \mathrm{d}\boldsymbol{r}\rho_{\text{c}}E_z\phi/Q_z. \tag{2.4}$$

The interaction with the underlying lattice or with impurities is assumed to be via an electrostatic potential, leading to

$$H_{\text{imp}} = \sum_i \int \mathrm{d}\boldsymbol{r}V\left(\boldsymbol{r}-\boldsymbol{R}_i\right)\rho(\boldsymbol{r}). \tag{2.5}$$

Other forms of interaction are possible but will lead to much the same physics. With the addition of an effective mass m^* and a damping parameter γ_0 for the CDW, we have the equation of motion

$$m^*\ddot{\phi}+\gamma_0\dot{\phi}-K\nabla^2\phi+\sum_i \rho_0 V\left(\boldsymbol{r}-\boldsymbol{R}_i\right)\sin(\boldsymbol{Q}\cdot\boldsymbol{r}+\phi)=\rho_{\text{c}}E_z/Q_z. \tag{2.6}$$

A fuller discussion of the model can be found in the article by Lee and Rice (1979) and references therein.

It should be recognized that the electric field in eq. (2.6) is not the applied field but the internal field, and thus subject to screening by
uncondensed carriers, and therefore to spatial and temporal fluctuations (Sneddon 1984). While this is not directly related to the rest of the material in this chapter, it has very important consequences in real materials, and in setting the value of the damping parameter γ at low frequency (Littlewood 1987, 1988, Tucker et al. unpublished). Taking a simple two-fluid model (Rice et al. 1979), the total current (including displacement, polarization and conduction currents of both the CDW and uncondensed carriers) is

$$\boldsymbol{j}(\boldsymbol{r},t)=\boldsymbol{\epsilon}\boldsymbol{\epsilon}_0\dot{\boldsymbol{E}}+\sigma\boldsymbol{E}+\rho_{\text{c}}\dot{\boldsymbol{\phi}}Q_z^{-1}\hat{\boldsymbol{z}} \tag{2.7}$$

and satisfies $\boldsymbol{\nabla}\cdot\boldsymbol{j}=0$. Here $\boldsymbol{\epsilon}$ is the background dielectric constant of the medium and σ the linear conductivity of the normal carriers. The relevant time scale for the CDW dynamics is set by the CDW washboard frequency $\omega_0=Q_zv$, with v the CDW velocity. Thus if $\omega_0 \ll \sigma/\epsilon\epsilon_0$, charge conservation guarantees that spatial fluctuations in the electric field will be screened, with

$$E_z(\boldsymbol{r},t)=E_0(t)-\rho_{\text{c}}\dot{\phi}/\sigma Q_z \tag{2.8}$$

where $E_0(t)$ is the uniform applied field. At low enough frequencies, any local fluctuation in the CDW current is exactly counterbalanced by a 'backflow' of normal carriers. Substituting eq. (2.8) into (2.6) leads to an equation of motion with identical form, but with a uniform applied field E_0 and an enhanced damping constant $\gamma=\gamma_0+\rho_{\text{c}}^2/\sigma Q_z^2$. This result was first written down by McMillan (1975, 1976), and established more carefully by Sneddon (1984) who pointed out its importance in semiconducting CDWs where σ has an Arrhenius temperature-dependence; at sufficiently high frequency the condition for full screening fails and the character of the response will change. Further ramifications for the details of the dynamical behavior have been worked out elsewhere (Littlewood 1987).

2.2. Approximations for numerical work

Equation (2.6) is still rather too complex for efficient numerical simulation and a number of further approximations are conventional.

(i) Neglect of inertia. This is possible for frequencies $\ll \gamma/m^*$, which is typically several GHz

or higher.
(ii) Because we are not concerned with behavior on short length scales, the impurity interaction is taken to be a δ-function.
(iii) Most numerical work is carried out on one-dimensional models, although real systems have three-dimensional coherence. This should not be important for qualitative descriptions of the dynamics because a weak impurity interaction is relevant in all dimensions below 4 (see section 2.4). Of course, details of the behavior will be different, and in particular values
of critical exponents close to threshold are changed, but such features will not be of primary concern.
(iv) A common, but not universal, approximation is to evaluate the damping term only at the impurity positions, and to assume that the CDW phase responds instantaneously in between the impurity sites. This neglects the dynamic degrees of freedom on short length scales, but should not be a serious difficulty for the consideration of the low-frequency response involving characteristic lengths much larger than the typical impurity separation.
(v) Notwithstanding the previous point, simulations are frequently performed in the strong pinning limit where the CDW phase fluctuation takes place on a scale comparable to the impurity separation. This has the practical advantage of suppressing finite size fluctuations and allowing simulations to be carried out on system sizes containing many correlation lengths. A single 'impurity' should be considered here more as a characteristic Lee-Rice 'domain'. There is no evidence that any qualitative difference exists between strong- and weak-pinning versions of the model, unlike the case of the Frenkel-Kontorova model (see section 2.3) for which special considerations apply.

After some further rescaling of parameters, and setting the average distance between impurities to unity, we then have the following equation of motion for the phase $\phi_i \equiv \phi(R_i)$:

$$\dot{\phi}_i = \Delta^2 \phi_i + \frac{1}{2} E\left(R_{i+1} - R_{i-1}\right) + V \sin\left(\theta_i + \phi_i\right), \tag{2.9}$$

where Δ^2 is the discrete second derivative

$$\Delta^2 \phi_i = \left(\phi_{i+1} - \phi_i\right)/l_i - \left(\phi_i - \phi_{i-1}\right)/l_{i-1}, \tag{2.10}$$

and $\theta_i = QR_i$ varies randomly from site to site, with $l_i = R_{i+1} - R_i, \langle l_i \rangle = 1$.
The problem has now been reduced to a set of coupled first-order non-linear differential equations, which can be analyzed by conventional techniques. The only parameter in the problem is the scaled pinning strength V with the weak and strong pinning limits corresponding to $V \ll 1$ and $V \gg 1$ respectively. It is indeed possible to take a distribution of pinning strengths, although randomness in V_i seems not to change the model's behavior in any essential fashion.

2.3. Related models

It is generally found that the most important aspects of the physics arise from randomness in θ_i, so a further simplifying approximation is to take the impurity spacing to be a constant ($l_i = 1$), while preserving the uniform random distribution for θ. If one instead takes $\theta_i = Qi$, with Q not rational,
one recovers the overdamped Frenkel-Kontorova (FK) model,

$$\dot{\phi}_i = \phi_{i+1} - 2\phi_i + \phi_{i-1} + E(t) + V \sin\left(Qi + \phi_i\right). \tag{2.11}$$

The static properties of the FK model are susceptible to analytic treatment, and there has been considerable effort given to simulation of the dynamics (Coppersmith and Fisher 1983, Peyraud and Aubry 1983, Coppersmith 1984, Sneddon 1984). In a d.c. field the periodic

nature of the pinning can be used to advantage to construct a perturbation series which can be numerically evaluated to high order (Sneddon 1984).

It is clearly straightforward in principle to add an inertial term $m^*\ddot{\phi}_i$ to either (2.9) or (2.11), although we argued above that the effective mass in CDWs is too small to be relevant except at very high frequencies. A continuum version of (2.11) in a commensurate potential is of course the damped driven sine-Gordon equation

$$\ddot{\phi} + \lambda\dot{\phi} = \nabla^2\phi + V\sin\phi + E. \tag{2.12}$$

For $\lambda \to 0$ this equation has travelling soliton solutions and the behavior for small λ has been extensively analyzed (Christiansen 1986, Eykholt et al. 1986). This limit of the model can be physically realized in superconducting Josephson transmission lines.

A closely-related physical model is the random-field XY Hamiltonian

$$H = \sum_{i>j} J_{ij}\boldsymbol{S}_i \cdot \boldsymbol{S}_j + \sum_i \boldsymbol{h}_i \cdot \boldsymbol{S}_i \tag{2.13}$$

$$= \sum_{i>j} J_{ij}\cos\left(\phi_i - \phi_j\right) + \sum_i h_i \cos\left(\theta_i - \phi_i\right), \tag{2.14}$$

where ϕ_i is the angle between a fixed length spin and an arbitrary axis. For nearest neighbor interactions, and with $J \gg h$ so that the spins rotate smoothly, this becomes identical to the Hamiltonian from which (2.9) is derived. There is no physical analogue in the XY model to the electric field in the FLR model, whereas a uniform magnetic field translates to a commensurate potential. Note also that the cosine interaction in (2.14) is insensitive to 2π twists, whereas these contribute to the elastic energy in (2.9) because the phase is a continuous variable. This distinction is unimportant if the CDW is stiff, or if the impurity pinning is weak (i.e., $V \sim h/J \ll 1$); however in strong pinning a periodic form of the interaction is more plausible because it allows for amplitude collapse leading to phase slip.

For a single degree of freedom eq. (2.12) is just the equation of motion of a damped pendulum, and was introduced some time ago as a qualitative description of CDW dynamics by Grüner, Zawadowski and Chaikin (GZC) (1981). With joint a.c. and d.c. driving fields this is known to have a very rich structure of mode-locking of the fundamental CDW period to a harmonic or subharmonic of the frequency of the driving field (Bak 1985). Such structure has indeed been observed in CDWs (Richard et al. 1982, Brown et al. 1984, 1986, Hall and Zettl 1984, Thorne et al. 1986, 1987, Bhattacharya et al. 1987) although the interpretation given here for these phenomena will be based on the overdamped many-EDF model of eq. (2.9), which has very different characteristic behavior (Coppersmith and Littlewood 1987, Coppersmith 1987a,b, Tang et al. 1987, Coppersmith and Littlewood 1986).

The last immediate relative of the FLR model is a mean field theory, where the elastic interactions are taken to be of infinite range, leading to the equation of motion

$$\dot{\phi}_i = \langle\phi\rangle - \phi_i + E + V_i\sin\left(\theta_i + \phi_i\right), \tag{2.15}$$

where the brackets $\langle\ \rangle$ denote an average over the sites. Despite its apparent simplicity, this model has non-trivial critical behavior with a rich structure of metastable states below threshold (Fisher 1983, 1985), in sharp contrast to the single-particle GZC model (Grüner et al. 1981).

Although we shall be mostly concerned with simulations of the FLR model, many of the related models do provide useful insight into CDW behavior, especially if they allow analytic treatment.

2.4. Qualitative features of the FLR model

Some simple arguments can be applied to the FLR model to estimate the relative energy and length scales, as well as to understand the qualitative behavior (Lee and Rice 1979). The CDW phase fluctuates on a characteristic length scale L_0 (often called the Lee-Rice length), which is determined by competition between the elastic energy and the impurity pinning energy. If $V \ll 1$, the CDW phase is not pinned to individual impurities but can pin to fluctuations in the preferred phase θ_i over the region L_0, gaining an energy $\sim -VL_0^{-d/2}$ (in d dimensions). Comparing this to the elastic energy cost $\sim L_0^{-2}$ and minimizing leads to $L_0 \sim V^{-2/(4-d)}$; the correlation length becomes very long if the pinning is weak. L_0 can be determined by X-ray diffraction, although this has proved very difficult because the correlation length is typically very large especially along the chains where the CDW is stiff.

Because the CDW is now pinned to the lattice there will be a finite threshold field for sliding E_T. If the deformed, pinned CDW is displaced by a multiple of its wavelength (i.e. $\phi(r) \to \phi(r) + 2n\pi$), the CDW is of course in an identical state. The typical barrier E_B to be overcome for the CDW to slide is that to move a domain of size $\sim L_0$ by one wavelength, so that $E_\mathrm{B} \sim \pi L_0^{d-2}$. Hence the threshold field will be of order $E_\mathrm{T} \approx L_0^{-2} \approx V^{4/(4-d)}$ provided $V \ll 1$.

In the physical case of three dimensions, the barrier between different metastable states ($\sim E_\mathbf{B}$) is very large in the weak pinning limit when L_0 is large, and thermal effects resulting from hopping over barriers will not be important. The situation is changed for dimensions $d < 2$, where thermal effects will be important in the weak pinning limit. It is of course straightforward to add a thermal noise term to the equation of motion (2.9) to simulate the effect of a finite temperature, but the results of a finite temperature 1D simulation may be misleading as to the realistic threedimensional case.

As in any random field system, there will be many metastable states. Although there is locally (on a length scale $\leqslant L_0$) a preferred choice of phase, there are many possible arrangements of the relative phases modulo 2π of neighboring regions. An estimate of the total number of metastable states N_s is that $\log N_\mathrm{s} \approx A\,(L/L_0)^d$, where L is the linear dimension of the sample, and A a constant of order unity. A typical pinned configuration will wander randomly on scales $> L_0$ and resemble a rough d-dimensional interface.

The pinned configurations are stable to small perturbations and the response to a small a.c. field will be that of a collection of damped oscillators with a characteristic lifetime inversely proportional to E_T; on account of the randomness in the pinning the distribution of lifetimes may be broad, and this distribution will reflect the properties of the particular state.

2.5. Amplitude dynamics and phase slip

At the current contacts it is clear that the CDW amplitude must periodically collapse in the conversion of CDW to normal carriers. When strong pinning centers are introduced into the bulk, CDWs depin abruptly and hysteretically (Zettl and Grüner 1982, Hall et al. 1988); in these 'switching' samples measurements of the local CDW conductivity have shown that the CDW breaks up into regions of uniform phase velocity (Hall et al. 1986).

A model to describe the dynamics of the amplitude collapse was introduced by Inui et al. (1988). In this picture the elastic strain of the CDW is not allowed to build up indefinitely by allowing the CDW amplitude to be reduced by a large amount of phase polarization. At strong pinning centers, this can lead to a transient collapse of the CDW amplitude with a rapid $\sim 2\pi$ phase slip to reduce the CDW elastic strain. It is in fact already clear from the derivation of the FLR equations from a Ginzburg-Landau expansion that the CDW elasticity K (eq. (2.6)) is proportional to the CDW amplitude. A more complete GL expansion including the amplitude terms would lead to a Hamiltonian

$$H = H_{\rm el} + H_\rho + H_{\rm field} + H_{\rm imp}, \tag{2.16}$$

with the coupling to impurities and to the electric field as before, but with a gradient energy

$$\begin{aligned} H_{\rm el} &= \frac{1}{2}\int \mathrm{d}\boldsymbol{r} Y \left|\nabla\rho \mathrm{e}^{\mathrm{i}\phi}\right|^2 \\ &= \frac{1}{2}\int \mathrm{d}\boldsymbol{r} Y(\nabla\rho)^2 + u^2(\nabla\phi)^2 \end{aligned} \tag{2.17}$$

Below $T_{\rm c}$, the energy for small amplitude fluctuations is quadratic:

$$H_\rho = \frac{1}{2}a\int \mathrm{d}r\,(\rho-\rho_0)^2 \tag{2.18}$$

Here ρ_0 is the equilibrium value of the order parameter. From (2.17) and (2.18) it is clear that spatial fluctuations of the order parameter will be on the scale of the coherence length $\xi_0 = (Y/a)^{1/2}$ which is a microscopic length scale, so that the gradient term in the amplitude can be neglected. Both amplitude and phase dynamics are taken to be overdamped.

With the same approximations which led previously to eq. (2.9), the first two terms in (2.16) become

$$H_{\rm el} + H_\rho = \frac{1}{2}\sum_i \left[Y\rho_{i+1}\rho_i\left(\phi_{i+1}-\phi_i\right)^2/l_i + a\left(\rho_i-\rho_0\right)^2\right] \tag{2.19}$$

The quadratic form for the last term in (2.19) is only appropriate for $\rho_i/\rho_0 \ll 1$ but this is probably sufficient here (it could easily be improved by the inclusion of higher-order terms). The whole complicated mess of dynamics on a microscopic length scale $\sim \xi_0$ is replaced in this model by a simple prescription: if $\rho_i \to 0$ then one assumes a rapid phase slip $\sim 2\pi$ takes place at the site, at which point the amplitude is allowed to regenerate. Providing this conversion process is fast enough the detailed dynamics should be irrelevant.

This model has in fact been studied only in the approximation of a single strong impurity site coupled to a single weakly-pinned FLR domain, such as might apply to phase slippage at a contact. For this two-degree of freedom system, the reduced equations become

$$\dot{\phi} = E - \sin\phi - \alpha\Delta\left(\phi-\phi_0\right) \tag{2.20}$$

$$\kappa\dot{\Delta} = -\Delta + 1 - \left(\left(\phi-\phi_0\right)/\theta\right)^2 \tag{2.21}$$

where $\Delta = \rho/\rho_0$ and ϕ_0 is assumed to jump by 2π if Δ is driven negative. This is the GZC model for the phase coupled to amplitude fluctuations; the parameter κ is proportional to the relative relaxation rates of the phase and
amplitude. Real systems are expected to correspond to $\alpha\theta \gg 1$ (highly polarizable phase) and $\kappa \ll 1$ (fast amplitude relaxation).

These equations can be shown to lead to hysteresis in the current-voltage characteristics provided $\boldsymbol{\theta}$ (the amount of CDW polarization necessary to cause CDW amplitude collapse) is large enough. The results of simulations of the dynamical properties of this model will be discussed in section 3.5.

When the phase pinning is dominated by a single strong pinning site, it is also necessary to take into account the screening effects due to free carrier 'backflow' in the insulating materials. Here it has been shown that 'switching', with characteristics similar to those observed experimentally, can be produced within the two-fluid picture discussed briefly in section 2.1 (Mihaly et al. 1987, Littlewood 1988).

4.8.3 3. Numerical simulations

The major area of activity of numerical simulations of CDW dynamics has revolved around the ID FLR model with the equation of motion (2.9); as discussed in the last section, there are a number of variants. Of course simulations have not been the only source of information about the behavior of this model, and results from perturbation theory, mean field theory, and various other analytic approximations will be folded into the results presented here.

In this section are reviewed the major properties of the phase-pinning models in the various regimes: metastable states (section 3.1); the small amplitude (linear and non-linear) a.c. response (section 3.2); motion in a d.c. field including equilibrium critical behavior as $E \to E_{\mathrm{T}}$ as well as long-time transients and noise (section 3.3); the joint response to large amplitude a.c. and d.c. fields (section 3.4). As a contrast to the behavior of the many-EDF model section 3.5 discusses simulations of the model of section 2.5 with contact or strong pinning and amplitude dynamics.

3.1. Metastable states

At fields below threshold, metastable solutions can be obtained by relaxing a chosen initial configuration to equilibrium via eq. (2.9). Two such solutions are shown in fig. 1 for an identical realization of 200 randomly positioned impurities and $V = 0.1$. (Periodic boundary conditions were employed.) While both states are clearly disordered, they are nearly identical except within two short regions (the difference between the two solutions is plotted as the dashed line in fig. 1). The existence of such soliton-like excitations is very easily understood (Littlewood and Rice 1982) from eq. (2.9) (for simplicity we return to the continuum version). Suppose

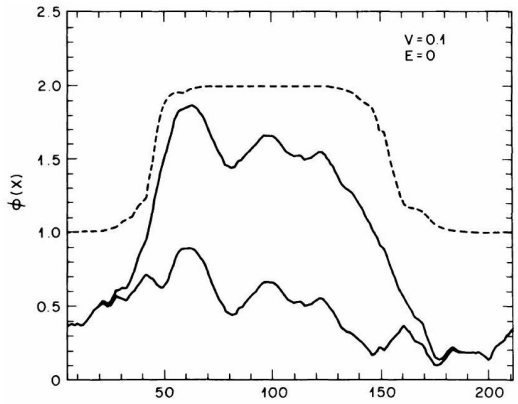


Fig. 1. Two metastable solutions (Littlewood 1986a) $\phi(x)/2\pi$ for the same configuration of $N = 200$ randomly placed impurities, with $V = 0.1$ (solid lines) and their phase difference (dashed line).

we have found a static (metastable) solution of (2.9), satisfying

$$\nabla^2\phi_0 + \sum_i V \sin\left(\theta_i + \phi_0(x)\right) \delta\left(x - R_i\right) = 0. \tag{3.1}$$

Writing $\phi(x) = \phi_0(x) + \psi(x)$ we then look for solutions of

$$\nabla^2\psi + \sum_i V\delta\left(x - R_i\right) \left[\sin\left(\theta_i + \phi_0\right)\left(\cos\psi - 1\right) + \cos\left(\theta_i + \phi_0\right)\sin\psi\right] = 0. \tag{3.2}$$

If we approximate the spatially varying coefficients in (3.2) by their averages (which amounts to neglecting fluctuations in the pinning potential), then (3.2) becomes

$$\nabla^2\psi - E_{\mathrm{T}} \sin\psi = 0, \tag{3.3}$$

where $E_{\mathrm{T}} = L_0^{-2} \sim V^{4/3}$ as before. Equation (3.3) is the sine-Gordon equation, in which there are soliton solutions with a characteristic width $E_{\mathrm{T}}^{-1/2} = L_0$.

While this is qualitatively correct, as can be seen from the example of fig. 1 , the width of the soliton is comparable to the correlation length of the initial solution ϕ_0, so the averaging procedure is invalid (Littlewood and Rice 1982). Nevertheless, this is a useful way to look at 'nearby' metastable states.

The importance of soliton-antisoliton pair creation becomes apparent

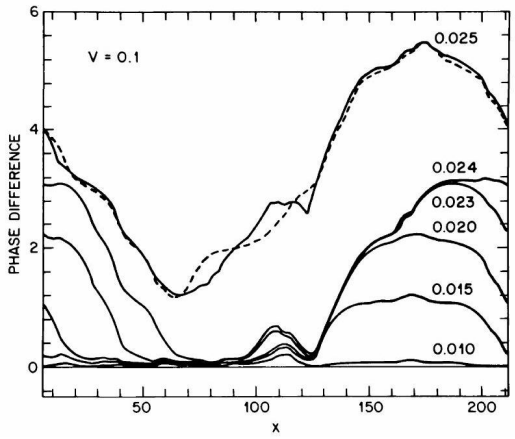


Fig. 2. Equilibrium solutions at different fields (values in figure) relative to the initial solution at $E = 0$. The topmost curve is a snapshot of a moving solution at $E>E_{\mathrm{T}}$ and the dashed curve the static pinned solution at $E = 0$ obtained after the field is turned off (Littlewood 1986b, 1987).

when the applied field is increased. Figure 2 shows a sequence of pinned configurations obtained by increasing the d.c. field in small increments and allowing the system to reach static equilibrium at each field, for the same impurity configuration and strength as in fig. 1. Plotted here is the difference $\phi_E(x) - \phi_0(x)$ measured from the initial pinned configuration at zero field. For fields < 0.01, the CDW is weakly polarized in its original potential well, but as the field increases 2π phase slip is generated at some weak point in the sample and the CDW becomes strongly distorted. Even though the 'local' threshold field may be exceeded in some part of the sample, there is only a transient current because the CDW is not allowed to break in this model. For this simulation the bulk threshold field is between 0.024 and 0.025 , and the topmost solid curve in fig. 2 is a snapshot of the sliding solution after the phase breaks free. At this point in the simulation the field was reduced to zero, and the dotted line is the final configuration reached.

There are already a number of lessons to be drawn from these simple simulations. Firstly, it is clear that there are many metastable states - so many, in fact, that there is always a pinned metastable configuration close (i.e. within $\delta\phi \sim \pi$) to any smooth enough (i.e. $|\nabla\phi| \leqslant L_0^{-1}$) configuration of the CDW. This is exemplified by the topmost solid curve ($E > E_{\mathrm{T}}$) and the dashed curve $E = 0$ in fig. 2. Secondly, the CDW can undergo a sizeable
polarization for fields below threshold; increasing and then decreasing the electric field can shift the CDW between metastable states even if the applied field never exceeds $E_{\mathbf{T}}$. Finally, the many-EDF nature of the model is crucial to its behavior, and the system cannot be described by a collection of independent oscillators. It is already evident from fig. 2 that the sliding is a cooperative phenomenon, with polarization fluctuations developing on a long length scale (

$\gg L_0$) close to threshold. The characteristic length L_0 sets the 'microscopic' scale for the problem, and fluctuations on scale shorter than this cost a large energy and will be suppressed. Thus it is convenient to perform simulations in the strong pinning limit with $V \approx L_0 \approx E_T \sim 1$.

A question which immediately arises is whether all metastable states have similar properties, and if not, what is the characteristic generic behavior of the system. In systems where temperature plays an important role, one expects that states of low energy will be the most important. At very low temperature, where there is a negligible chance of thermal activation over barriers between neighboring states, the relevant metastable configurations will be determined by the sample history, and by the accessibility of the states in question. This rather obvious point has important ramifications for CDWs.

If we drive the system far from static equilibrium (typically by applying a large field) and then turn off the driving, the phase configuration will relax down the energy surface until it finds the first static equilibrium configuration. This process can be envisaged schematically in fig. 3. Provided the

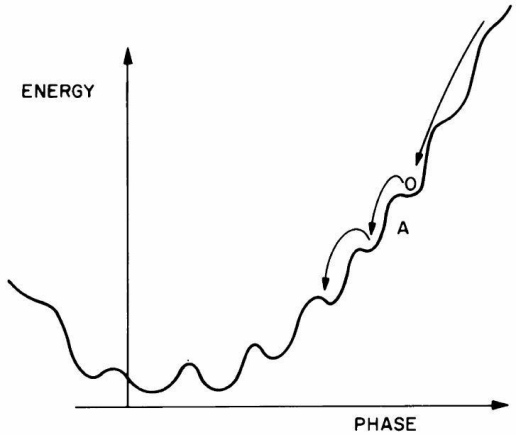


Fig. 3. Schematic picture of a cross section of the energy surface, with the CDW configuration represented by a ball. From a non-equilibrium initial state, the CDW relaxes to the first available state (A), which is only weakly stable to small perturbations and is of high energy. Further relaxation can take place only via thermal activation.

region of metastable states in configuration space is closed (which is guaranteed by the convexity of the elastic energy) the first stable state reached will not only by of high energy but also very weakly stable to small perturbations. Such a configuration will have smaller than average barriers to nearby states, and will be very easily polarized within its well. This characteristic 'softness' leads to unusual behavior of the low-frequency a.c. linear response, which can be studied experimentally.

3.2. Small amplitude a.c. response

The linear response of a pinned state to an infinitesimal a.c. field $E(\omega)$ at frequency ω is easily calculated by linearizing about the pinned solution, as in eq. (3.2). The response to a small field defines the frequency-dependent dielectric function for the uniform response

$$\epsilon(\omega) = N^{-1} \sum_i \frac{\mathrm{d}\psi_i(\omega)}{\mathrm{d}E(\omega)} \tag{3.4}$$

Another quantity of interest, although difficult to measure experimentally, is the fluctuation response

$$C(\omega) = N^{-1} \sum_i \left| \frac{\mathrm{d}\psi_i(\omega)}{\mathrm{d}E(\omega)} \right|^2 - |\epsilon(\omega)|^2 \tag{3.5}$$

$C(\omega)$ will be non-zero only by virtue of the non-uniformity in the response; this quantity is thus a test of the significance of the random pinning in the FLR model. Both (3.4) and (3.5) can be written in terms of the Green function

$$G_{ij}(\omega) = \sum_k y_i^{(k)} y_j^{(k)} / \left(\mathrm{i}\omega + W_k\right) \tag{3.6}$$

where $y_i^{(k)}$ is the k th eigenvector of the linearized problem with mode energy W_k. We have

$$\epsilon(\omega) = N^{-1} \sum_{ij} G_{ij}(\omega) \tag{3.7}$$

$$C(\omega) = N^{-1} \sum_{ijk} G_{ij}(\omega) G_{ik}(-\omega) - |\epsilon(\omega)|^2 \tag{3.8}$$

In fig. 4 we plot the a.c. response of a state obtained by relaxation in zero field from a sliding state with $E \approx 2E_\mathrm{T}$; for this simulation $N = 400, V = 2$. A striking feature is the cusp-like rise in $\mathrm{Re}\,\epsilon(\omega)$ at low frequencies, and a strong enhancement of the fluctuation response $C(\omega)$. The anomalous low-frequency response can be traced to the existence of very many low-energy modes of oscillation, the distribution of which is shown as $n(W)$

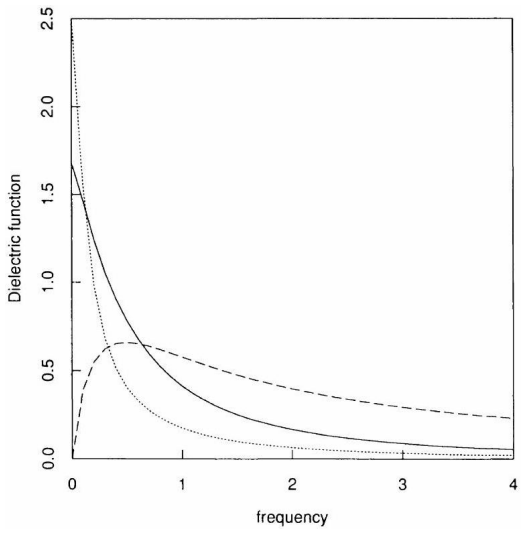


Fig. 4. $\operatorname{Re} \epsilon(\omega)$ (solid line), $\mathrm{Im}\,\epsilon(\omega)$ (dashed line) and the fluctuation response $C(\omega)$ (dotted line) calculated for a single configuration ($N = 400, V = 2$) in a pinned state obtained by relaxation to equilibrium of a sliding state with $E \approx 2E_\mathrm{T}$.

in fig. 5. If matrix-element effects can be neglected, eqs. (3.7) and (3.8) can be written

$$\epsilon(\omega) = \int \mathrm{d}W \frac{n(W)}{\mathrm{i}\omega + W} \tag{3.9}$$

$$C(\omega) = \omega^{-1}\,\mathrm{Im}\,\epsilon(\omega) - |\epsilon(\omega)|^2 \tag{3.10}$$

The relatively sparse numerical data, but also mean field theory (Fisher 1983, 1985) and a self-consistent field approximation (Littlewood and Varma 1987), suggest the generic behavior

of the density of states is $n(W) \sim W^{\alpha} g\left(W/W_0\right), 0 < \alpha < 1$. Here $g(x)$ is a monotonically decreasing function of $x; g(x \to 0) = 1, g(x \to \infty) = 0$. Such a form produces a $|\omega|^{\alpha}$ cusp in $\mathrm{Re}\,\epsilon$, and a $|\omega|^{\alpha-1}$ divergence in $C(\omega)$. This result is to be contrasted with the Lorentzian form which would be found if all the eigenmodes were degenerate, as in a single-particle model (Grüner et al. 1981).

The existence of a cusp in the low-frequency dielectric function is confirmed by experiment (Cava et al. 1984) (although one group (Wu et al. 1984) has reported a divergence, i.e. $\alpha < 0$). A convenient parameterization (Cava et al. 1984) of the data over a wide frequency range has been found

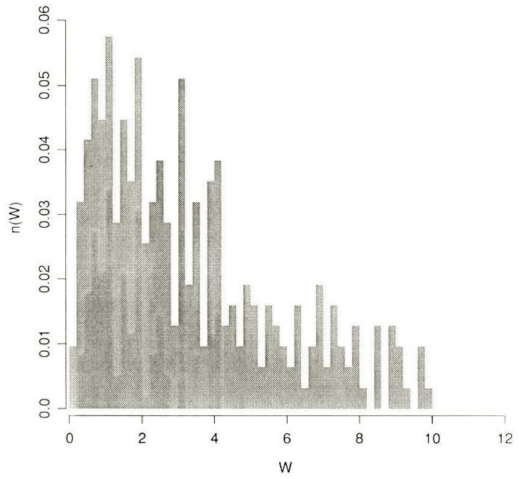


Fig. 5. Density of states of linear modes of oscillation for the pinned configuration whose dielectric response was shown in fig. 4.

to be the Havriliak-Negami formula (fig. 6)

$$\epsilon(\omega) = \epsilon(0) / \left[1 + (\mathrm{i}\omega\tau)^{\alpha}\right]^{\beta} . \tag{3.11}$$

The measured value of α is typically in the range 0.5 to 1 , varying somewhat with both impurity concentration and temperature. The product $\alpha\beta$ is about 0.7 , and describes the high frequency ($\leqslant$ 10MHz) roll over in the dielectric constant; because this number is less than unity, it is clear that spectral weight is still to be found even at the highest frequencies of the electrical measurements. The enormous dynamic range (continuing into the microwave region) (Reagor et al. 1985, 1986, Sridhar et al. 1985, 1986) results not only from a broad distribution of modes, but also from an inherent frequency-dependence to the damping parameter τ (Littlewood 1987). In insulating CDWs at low temperatures, this can lead to the existence of two peaks in $\mathrm{Im}\,\epsilon(\omega)$ as a result of a crossover in the damping mechanism, and is not to be attributed to a double-peaked distribution of pinning energies.

It is important to realize that the 'gapless' distribution of modes in fig. 5 is not the typical behavior of a metastable state-most metastable states have a gap- but that this behavior is that of a marginally stable configuration which is the most likely to be found in an experiment where the CDW is far from its low-energy configurations. In a state of marginal stability the response is

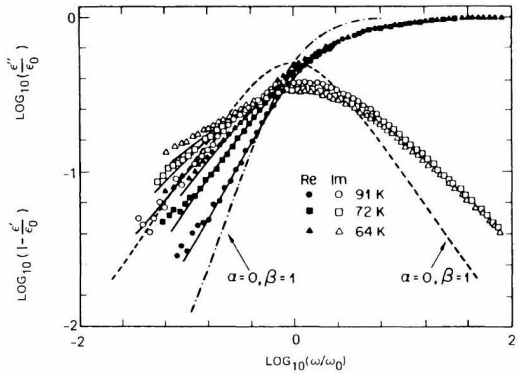


Fig. 6. Scaled dielectric response functions measured in $\mathrm{K}{0.3}\mathrm{MoO}{3}$ by Cava et al. (1984) at three different temperatures, and fit to the formula of eq. (3.11). The harmonic oscillator form is shown for comparison.

inherently non-linear. Because the distribution of mode energies tends to zero, there will be arbitrarily small barriers to nearby states. Hence the response to an infinitesimal d.c. field will differ from the $\omega \to 0$ limit of the a.c. response, because there will always be some part of the system 'on the edge', where $\psi_i(E) \sim \mathrm{O}(1)$ even for infinitesimal E. The d.c. response will be

$$\langle \mathrm{d}\psi/\mathrm{d}E \rangle_{\mathrm{d.c.}} = \lim_{\omega \to 0} \epsilon(\omega) + \mathrm{d}f(E)/\mathrm{d}E, \tag{3.12}$$

where $f(E)$ is the fraction of the sample where the phase jumps are large. If the distribution of barrier heights is controlled by the mode distribution, it is easy to show that $f(E) \sim E^{(\alpha+1)/2}$. With a further assumption that the non-linear soft modes do not interact strongly, and requiring that the distribution $n(W)$ is unchanged by a small change in field, one obtains $\alpha = 1$ (i.e., a linear cusp in $\epsilon(\omega)$). This is the same as the result of mean field theory (Fisher 1983, 1985), and is consistent with the numerical results in one dimension (Littlewood 1986a), although a self-consistent field theory (Littlewood and Varma 1987) gives $\alpha = \frac{1}{2}$. There is of course no universal form for the distribution $n(W)$ - the power law behavior represents only the generic behavior of the characteristic CDW configuration.

Furthermore, if there are indeed arbitrarily small barriers in the system, thermal effects will eventually become important on a low enough energy scale. In this event, the dielectric constant will be time-dependent, because a gap will open up in the spectrum following the preparation of the initial
state (Littlewood and Rammal 1988). There is no unambiguous evidence for this, but it may be responsible for some of the apparent temperature dependence (Cava et al. 1984) in the exponent α. Clearer checks for thermal effects would be to study the low-frequency small-amplitude nonlinear response, which is predicted by this picture to have a divergent power-law dependence on frequency at zero temperature. Indeed, there is good evidence that the low-frequency response is indeed strongly nonlinear (Cava et al. 1985, Stokes et al. 1985) even for a.c. amplitudes $\sim 10\%$ of threshold.

3.3. Sliding in a d.c. field

The collective character of CDW motion is most evident when the CDW is moving. Whether the narrow band noise is a bulk phenomenon or is generated at strong pinning centers (either within the sample or at the contacts), the existence of such a well defined (quasi-) periodic component of the current implies a sizeable coherence to the velocity of the CDW. Moreover, the velocity-coherence can be made complete by the imposition of an a.c. field in addition to the d.c.

driving, a subject which will be addressed in section 3.4. Although there are many metastable pinned states, a perhaps surprising feature of the FLR model is that there is a unique (time-dependent) sliding solution in dynamic equilibrium. However, the state of dynamic equilibrium is established only after very long times ($\sim L^{1/2}$, where L is the linear dimension of the system) allowing considerable hysteresis and memory of the CDW configuration.

3.3.1. Sliding in dynamic equilibrium

If one monitors the CDW configuration while simulating the FLR equation of motion (2.9) in a field $E > E_{\mathrm{T}}$, after some considerable time the configuration settles down to be periodic in time: $\phi_{\mathrm{eq}}(x,t) = \phi_{\mathrm{eq}}(x, t+nT) + 2\pi n$, where the period is $T = 2\pi/\nu$, with ν the CDW velocity. This periodicity is displayed (fig. 7) by a sequence of snapshots of an equilibrium solution at a set of times, and has been made more evident by plotting the difference $[\phi_{\mathrm{eq}}(x,t) - \phi_{\mathrm{eq}}(x,t_0)]/2\pi$ relative to the configuration at some arbitrary starting time t_0.

The motion is clearly neriodic in time; in consequence the Fourier spectrum of the mean current $I(\omega) = \int \mathrm{d}t \mathrm{e}^{\mathrm{i}\omega t} \left\langle \dot{\phi}_{\mathrm{eq}}(x,t) \right\rangle$ will be a set of δ-functions at harmonics of the washboard frequency $\nu : I(\omega) = \sum_n A_n \delta(\omega - n\nu)$. Because the relative phases of the velocity oscillations are uncorrelated at large distances, the amplitudes A_n will be of order $(\xi_\nu/L)^{1/2}$ (multiplied by a velocity-dependent prefactor), where ξ_ν is the velocity correlation length and is on the scale of L_0. We also remark that there is of course no broad band noise, the motion being periodic.

The configurations may be quantitatively characterized by measurements

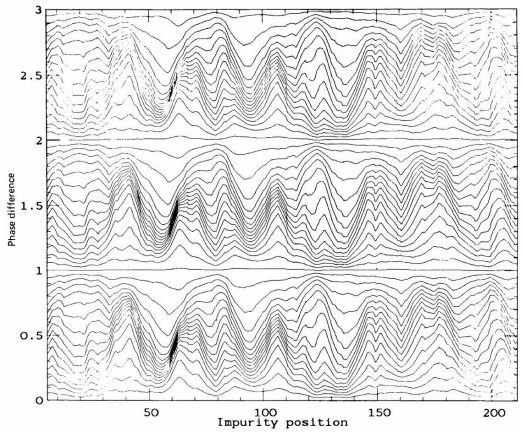


Fig. 7. Snapshots of an equilibrium sliding configuration at several different times measured (in units of 2π) relative to the configuration at an arbitrary initial time ($N = 200, V = 0.1$) (From Littlewood 1986.)

of various correlation functions, the most obvious being the equal time phase-phase and velocity-velocity correlation functions

$$C_\phi(r) = \langle \phi(r',t)\, \phi(r+r',t) \rangle - \langle \phi(r',t) \rangle^2 , \tag{3.13}$$

$$C_\nu(r) = \left\langle \dot{\phi}(r',t)\, \dot{\phi}(r+r',t) \right\rangle - \left\langle \dot{\phi}(r',t) \right\rangle^2 . \tag{3.14}$$

The angular brackets represent spatial averages over r', a time average being unnecessary in an infinite system. For the finite systems studied here, a time average is performed as well.

In fig. 8 is plotted the rms values of the phase fluctuations $\Delta_\phi = [C_\phi(0)]^{1/2}$ and velocity fluctuation $\Delta_\nu = [C_\nu(0)]^{1/2}$, for equilibrium sliding configurations with $E > E_{\mathbf{T}}$ (we choose

here $N = 200, V = 1$). The phase fluctuations are large (we should expect $\Delta_\phi \sim L^{1/2}$), but they also grow approximately linearly with increasing field for $E \gg E_{\mathrm{T}}$. In fig. 9 are shown snapshots of the phase configurations at different fields; the large polarization fluctuations are quite evident. In contrast, the velocity fluctuations grow much more slowly with increasing field.

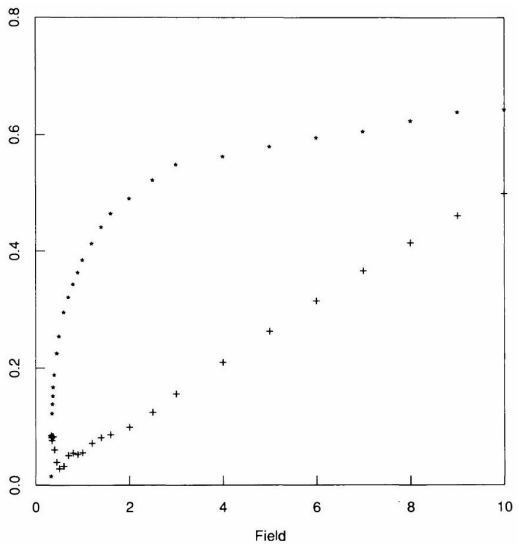


Fig. 8. Values of the rms phase fluctuation Δ_{ϕ} (crosses, arbitrary units) and the rms velocity fluctuation Δ_ν (asterisks, left scale) for equilibrium sliding configurations at fixed d.c. field ($N = 200, V = 1$) greater than threshold.

The behavior at large velocities was earlier (Sneddon et al. 1982, Sneddon 1984) analyzed by a perturbation theory in inverse powers of the CDW velocity. If the CDW slides very fast, it has no time to relax in response to the pinning potential, and the leading order corrections to free sliding of the CDW give (Sneddon et al. 1982)

$$\nu = E - CE^{(d-2)/2} + \cdots \tag{3.15}$$

in d dimensions, where C is a constant. These results are borne out by numerical simulations (Matsukawa and Takayama 1984, 1986) in $d = 1, 2$ or 3 dimensions, shown in fig. 10. Note that although the high-field state is weakly coupled to the impurities, it is far from uniform, as can be seen in fig. 9.

It has been generally believed that the threshold behavior can be described as a critical phenomenon (Fisher 1983, 1985). This has only been studied within mean field theory (Fisher 1983, 1985) for the FLR model, but the critical behavior of the closely related one-dimensional Frenkel-

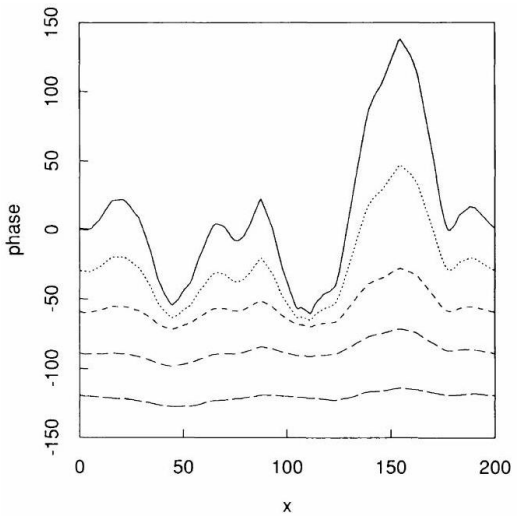


Fig. 9. Snapshots of equilibrium sliding configurations at different d.c. fields $E = 0.5, 1, 2, 5,$ 10 ; phases are measured in units of 2π and the order of the curves is increasing fields from bottom to top of the figure ($N = 200, V = 1$).

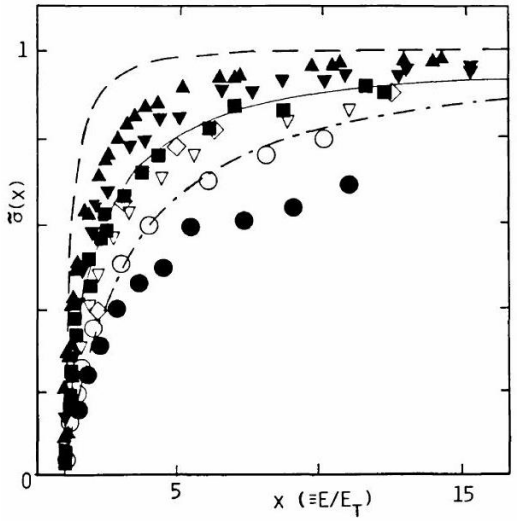


Fig. 10. Normalized non-linear d.c. conductivity in different dimensions from Matsukawa and Takayama (1984, 1986). Solid triangles ($d = 1, V < 10$); inverted solid triangles ($d = 1$, $V = 100, 400$); solid squares ($d = 2, 0.25 < V < 25$); solid circles and open symbols ($d = 3$, $V = 4$, varying impurity concentration). Single particle model (Grüner et al. 1981) (dashed line); tunneling model (chain line); $1 - 1/x$ (solid line)

Kontorova (FK) model is well established (Coppersmith and Fisher 1983, Peyraud and Aubry 1983, Coppersmith 1984, Sneddon 1984).

Within the critical region, we expect to find $\nu \sim e^{\zeta}$ ($e = (E/E_{\mathbf{T}} - 1)$ is the reduced field) and a diverging length scale for the velocity fluctuations, $C_\nu(r) \approx \Delta_\nu^2 f\,(r/\xi_\nu)\,; \xi_\nu \sim e^{-\nu}$. Figure 11 is an attempt to analyze the results from a single-impurity configuration ($N = 200, V = 1$) within this framework.

In fig. 11 is plotted the equilibrium velocity ν and the amplitude of the velocity fluctuations Δ_ν as a function of field close to $E_{\mathrm{T}} (= 0.336 \pm 0.0005$ for this sample). The critical region should be roughly where $\Delta_\nu/\nu \sim 1$. The length scaling $\xi_\nu(e)$ necessary to collapse the plots of $C_\nu(r)$

for different fields on to the same scaling form is determined; the scaling function is shown in fig. 12. This procedure is quite successful in that it leads to a well-behaved scaling function, as well as a correlation length which grows as $e \to 0$. The values of the exponents are very small and cannot be determined reliably from a single simulation; neither have we made any attempt to control the finite size effects. As estimates, we give: $\zeta = 0.85 \pm 0.15; \nu = 0.2 \pm 0.1$; and $\Delta_\nu \sim e^g$ with $g = 0.3 \pm 0.1$. For comparison in mean field theory (Fisher 1983, 1985) $\zeta = \frac{3}{2}, \nu = \frac{1}{2}$, and for a singleparticle model (Grüner et al. 1981) $\zeta = \frac{1}{2}, \quad \nu = 0, \quad g = \frac{1}{2}$. The overall behavior, and the magnitude of the exponents, are similar to the onedimensional FK model (Coppersmith and Fisher 1983, Peyraud and Aubry 1983, Coppersmith 1984, Sneddon 1984).

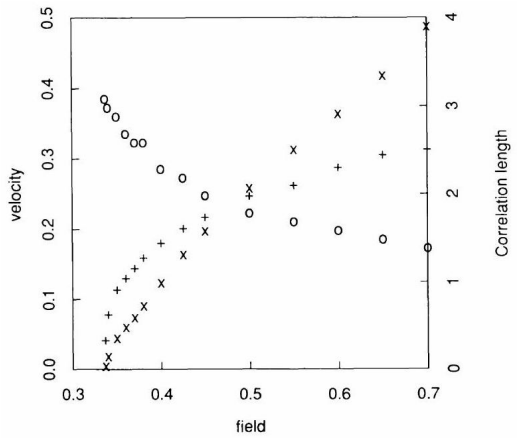


Fig. 11. Behavior of the velocity (x) and rms velocity fluctuations \$\Delta_{\nu}(+)\$ (left scale) and the velocity correlation length $\xi_\nu(0)$ (right scale) close to threshold.

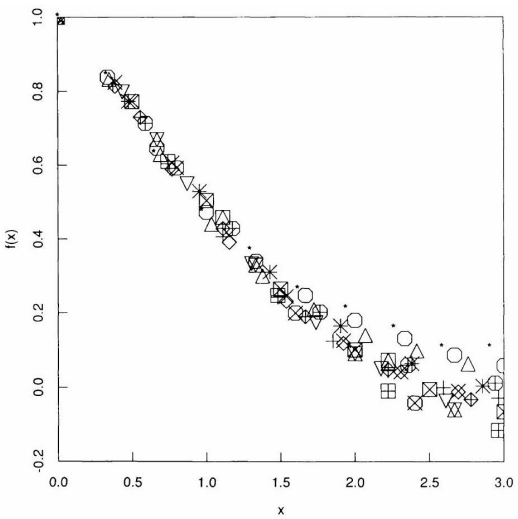


Fig. 12. Scaling function \$f\left(x=r / \xi_{\nu}\right)\$ for the velocity-velocity correlation function extracted for different fields for ($E/E_\mathrm{T} - 1$) in the range 0.002 to 1 . Different symbols correspond to different values of the field.

The typical amplitude of the narrow band noise will become very large close to E_T, when taken as a ratio to the d.c. current. We should expect that

$$|j_\mathrm{a.c.}\,|/j_\mathrm{d.c.} \sim (\Delta_\nu/\nu)\,(\xi_\nu/L)^{1/2} \sim e^{g-\zeta-\nu/2}. \tag{3.16}$$

In (3.16) $|j_{\mathrm{a.c.}}|$ represents the total a.c. response, which consists of very many harmonics close to threshold; the amplitude of any individual harmonic must scale to zero faster (Fisher 1985) than the velocity exponent ζ.

Experimentally, reported values for ζ are in the range of $1 - 1.5$ (Grüner and Monceau 1989) with perhaps the cleanest results obtained at low temperatures (Mihaly and Beauchêne 1987) where the critical region is expected to be large (Littlewood 1988). An attempt to extract the correlation length exponent ν was made by studying the amplitude of the BBN close to threshold (Robbins et al. 1985). As there is no BBN in dynamic equilibrium, further assumptions have to be made about the origin of the noise (see section 3.3.2 for a discussion of how this might occur in the FLR model). Even then, the ratio of the BBN amplitude to the d.c. current is not
simply proportional to $(\xi_\nu/L)^{d/2}$; see eq. (3.16) above. Neither will this ratio necessarily be given by $e^{g-\zeta-d\nu/2}$, because the different harmonics of the noise will scale with possibly different exponents (Fisher 1983, 1985).

3.3.2. Long-time transients, noise and hysteresis

We remarked earlier that it is quite difficult to reach dynamic equilibrium in a simulation - the data shown in figs. 11 and 12 required equilibration times of several hundred periods of each field. The long times required are a result of the large polarizations which build up in the CDW at fields close to and above threshold (Matsukawa and Takayama 1984, 1986, Littlewood 1986a).

The polarization build-up is similar to charging a capacitor although the CDW polarization does not relax when the field is turned off. The classic experiment to demonstrate this phenomenon is the pulse sign memory effect (Gill 1981, Fleming et al. 1985), whereby the shape of the response to a field depends on the sign of the preceding pulse, illustrated in fig. 13.

Within the transient regime (and in fact for times well after the average velocity has stabilized) there is generation of broad band noise (BBN) in the CDW current (Littlewood 1986a, 1986b, 1987). At the same time, the narrow band noise (NBN) frequency and amplitude are both 'wandering'. In fig. 14 is plotted the Fourier spectrum

$$I(\omega, T) = (2\Delta T)^{-1} \int_{T-\Delta T}^{T+\Delta T} \mathrm{d}t \mathrm{e}^{\mathrm{i}\omega t} \langle \dot{\phi}(t) \rangle \tag{3.17}$$

at two different times T, over a window of width ΔT, following the turning on of a field at $t = 0$. As the simulation proceeds to later times, the NBN

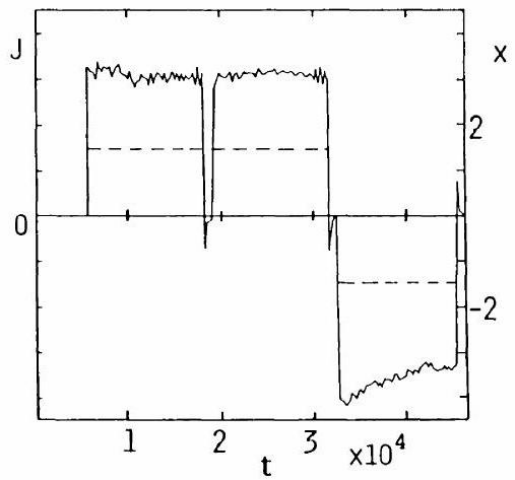


Fig. 13. Pulse sign memory from simulations by Matsukawa and Takayama (1987).

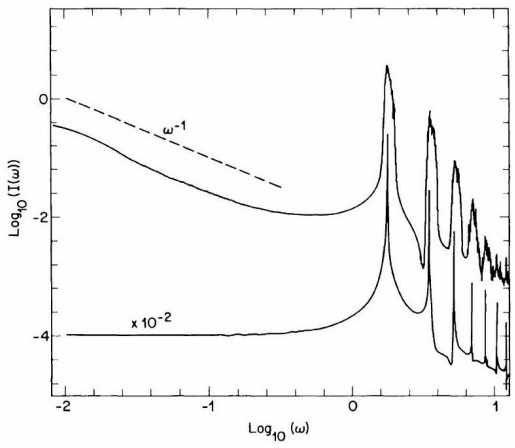


Fig. 14. Current noise from a numerical simulation ($N = 500, V = 1, E = 2$) at times $T = 5000$ (upper trace) and $T = 30000$ (lower trace) over a window $2\Delta T = 1000$. An ω^{-1} behavior is shown for comparison (dashed line). (From Littlewood 1986, 1987.)

becomes sharply defined and the amplitude of the BBN (which has a roughly ' $1/f$ ' character) decays. Figure 15 shows a typical trace of the CDW current in the transient regime; the wandering in amplitude and frequency of the NBN is due to slow dephasing of regions in the sample moving at slightly different velocities.

It has been known for some time that the NBN in sliding CDWs has a variable amplitude (Ong et al. 1984, Jing and Ong 1986), even in samples which have a single frequency component to the noise; recent analysis suggests that both the amplitude and frequency have Gaussian statistics (Link and Mozurkewich, unpublished). The obvious difficulty in interpreting the NBN and its variability as a bulk (finite size) phenomenon is that in dynamic equilibrium (for the FLR model) there is no BBN, and the NBN has a sharply defined periodicity and amplitude for a given sample. No experiment is free from external sources of noise, and some preliminary work (Miyashita and Takayama 1986) on the FLR model has shown that an additional source of 'white' noise is amplified by the system to yield BBN in the response with a ' $1/f$ ' character. This can be interpreted simply; any additional noise in the equations of motion will prevent the system from reaching a state of dynamic equilibrium, and the behavior will then be similar to that in the transient regime. The noise source need not be thermal; for example voltage fluctuations may be generated at the contacts during the conversion of CDW to normal carriers.

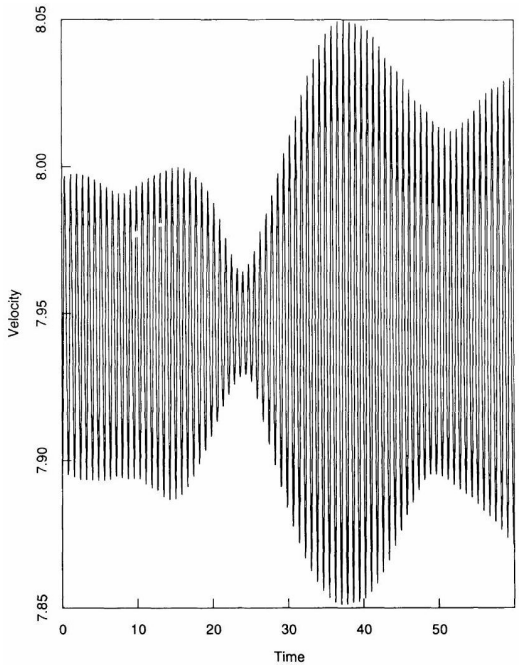


Fig. 15. Typical trace of the CDW current $I(t)$ in the transient regime ($N = 200, V = 1$, $E = 8$).

3.4. Response to joint a.c. and d.c. fields

The low frequency and low field response of CDWs is dominated by hysteresis and memory effects. Remarkably the response to large a.c. fields is much more uniform, and the non-linear aspects of the dynamics dominate the effects of disorder (Brown and Zettl 1989). In this section, we shall discuss how this might come about.

There are several experimental features associated with joint a.c./d.c. driving, and we mention here three:
(i) In a field $E(t) = E_0 + E_1 \cos(\omega t)$, the derivative current-voltage characteristic $\mathrm{d}I/\mathrm{d}V$ develops peaks whenever the CDW washboard frequency is close to a harmonic or subharmonic of the driving frequency ω; under favorable circumstances, true locking (i.e. plateaux in $\mathrm{d}V/\mathrm{d}I$) may occur, so that the CDW velocity $v = (p/q)\omega$ for a range of d.c. bias
(Richard et al. 1982, Brown et al. 1984, 1986, Hall and Zettl 1984, Thorne et al. 1986, 1987, Bhattacharya et al. 1987).
(ii) In a purely a.c. field, the hysteresis loops (i.e. plots of $I(t)$ versus $V(t)$) are purely capacitative when $E_1 < E_\mathrm{T}$, as would be expected from an overdamped model. For amplitudes greater than threshold, inductive character appears, mimicking the behavior of an inertial term in the equation of motion (Tessema and Ong 1983, 1985).
(iii) Closely related to (ii) is the observation (Fleming et al. 1985) of transient 'ringing' oscillations (at, or close to, the washboard frequency) superimposed on the response to a square wave pulse. An unusual feature was seen in conjunction with this phenomenon; if a train of identical square-wave pulses was applied, the phase of the ringing oscillations becomes synchronized with the end of the pulse, so that the current is always rising as the pulse ends, independent of the pulse length or height (Fleming and Schneemeyer 1986, Brown et al. 1986). This has been dubbed 'pulse duration memory'.

The phenomena of mode-locking (i) and inductive hysteresis (ii) or ringing oscillations can be found within a single degree of freedom model with inertia. However the size of the inertial term required to explain the transient ringing is much larger than that estimated from measurements of the linear a.c. response (Tessema and Ong 1983, 1985). Harmonic locking does occur in an

overdamped single degree of freedom model (e.g. eq. (2.12)), but subharmonic locking (i.e. $v = (p/q)\omega$ with $q \neq 1$) will be pronounced only if the pinning potential is far from sinusoidal. (There is of course nothing sacred about a sinusoidal form (Thorne et al. 1987 have interpreted their results in this fashion).) However no low-EDF model can give rise to the remarkable phenomenon of "pulse duration memory" so far as is known.

Calculations within the FLR model via a high-field perturbation expansion demonstrated the existence of interference features in the linear a.c. response $\sigma(\omega)|_{E_0}$ when $\omega \approx v$ (Sneddon 1984, Coppersmith and Littlewood 1985, Matsukawa and Takayama 1987, Matsukawa 1987). This feature would indeed lead to a transient ringing oscillation for a small step-like change in the d.c. bias (Coppersmith and Littlewood 1985). The effect is anyway a small one, with the calculations only being valid for $E_0 \gg E_{\mathrm{T}}$ (Coppersmith 1986a,b). Calculations (again within perturbation theory) for the d.c. conductance in the presence of an a.c. field display anomalies in $\mathrm{d}I/\mathrm{d}V$ at both harmonics and subharmonics (Sneddon et al. 1982, Sneddon 1984, Matsukawa and Takayama 1987, Matsukawa 1987). These anomalies have the form of sharp cusps in $\mathrm{d}I/\mathrm{d}V$, and no true mode locking is predicted within perturbation theory (at least with a hydrodynamic form for the relaxation as used by Sneddon, Cross and Fisher (SCF) (1982) - the FLR model neglects a convective derivative so that the perturbation theory goes unstable when $\omega = v$ (Matsukawa and Takayama 1987, Matsukawa 1987, Coppersmith 1986a,b). The subtle difference between the FLR model and the SCF model is not generally important, except perhaps in this specific circumstance; it has been argued that the SCF model is stable against mode-locking to all orders in perturbation theory (Coppersmith and Littlewood 1986) whereas the FLR model is not (Matsukawa and Takayama 1987). In practice, this will likely mean that mode-locking is only to be expected when the total field $E(t)$ is below threshold for enough time in some part of the cycle; even if $E_1 \gg E_0$ true mode-locking will not occur when $E_{\mathrm{T}}/\omega E_1$ is small (Coppersmith and Littlewood 1986). In the FLR model, a narrow mode-locked region will persist even in the limit of high a.c. frequency and small a.c. amplitude. That mode-locking is experimentally enhanced when $\min|E(t)| < E_{\mathrm{T}}$ is indicated by experiments on $NbSe_3$ with square-wave (Brown et al. 1986) (rather than pure a.c.) driving. However, in some samples there remains a narrow window of mode-locking even in the high-frequency limit (Thorne et al. 1987).

A further complication to the numerical results is that finite-size effects will also lead to a narrow range of mode-locking in the high-frequency limit, a range which vanishes as $L \to \infty$, as shown by Tua and Ruvalds (1985) within a different but closely related model.

We remarked above that the GZC model (Grüner et al. 1981) (an overdamped pendulum) displays only harmonic locking. Subharmonic locking does appear as soon as several degrees of freedom are coupled, high-order ($q = 5$) steps existing even for a model of two coupled pendula (Inui and Doniach 1987, Matsukawa and Takayama 1987). The behavior of a large system has some features which are not present in few-EDF models.

Figure 16 shows a plot of the locked regions obtained from simulations by Matsukawa and Takayama (1987) on the FLR model for a fixed a.c.

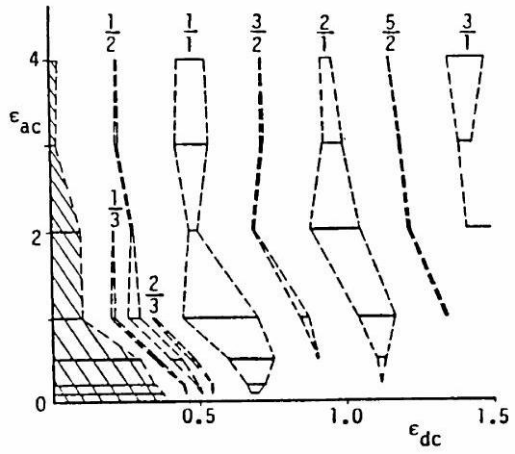


Fig. 16. Phase diagram of mode-locked regions in the FLR model ($\omega = 0.15\pi, V = 0.1$). (From Matsukawa and Takayama 1987.)

frequency $\omega = 0.15\pi$, and $V = 0.1$; by studying sample sizes ranging from $N = 100$ to $N = 800$ they determined that the mode-locking persisted in the infinite-length limit. The mode-locked widths are largest when $E_1 \approx E_0$, although they persist even for small a.c. amplitudes. There is also some evidence for oscillatory dependence of the locking widths on both a.c. amplitude and frequency. The oscillation is to be expected because already in perturbation theory (Sneddon et al. 1982) it was found that the differential conductance near the harmonic ($p/1$) interference features was proportional to $J_p^2\,(E_1/\omega)$ (J_p is a Bessel function of the first kind). Subharmonic locking was found (Matsukawa and Takayama 1987) only for low-order subharmonics, although there are interference features at all values of p/q.

All of the above features can be reproduced by a simple overdamped single-EDF model with a non-sinusoidal pinning potential. Thus we must ask if there are any qualitative differences between the behavior of lowEDF models and the many-degree of freedom FLR model.

In fact the very existence of mode-locking in the FLR model is surprising. It is clear that in the simulations the mode-locking is most predominant when $E_1 \approx E_0$. The total field is thus below threshold for a large fraction of the cycle, and the CDW must be relaxing toward some nearby pinned state. There are so many such states that it is remarkable that mode-locking can exist at all.

The behavior of the FLR model is easiest to understand by considering the response to repeated pulses, rather than to a sinusoidal time-dependent field (Coppersmith and Littlewood 1987, Coppersmith 1987a,b, Tang et al. 1987, Coppersmith and Littlewood 1986). We consider a repeated train of pulses at a field $E > E_{\mathrm{T}}$ for a time t_{on}, separated by a time t_{off} where the field is zero. If the time t_{off} is very long in comparison to the time needed to relax to a metastable state, the effect of a single pulse is to translate the CDW from one metastable configuration to another, which we may represent as a mapping $\mathrm{F} : \left\{\phi_j^{\mathrm{A}}\right\} \rightarrow \left\{\phi_j^{\mathrm{B}}\right\}$. Because the equations are deterministic, the state reached long after the pulse is turned off is uniquely determined by the configuration $\left\{\phi_j^{\mathbf{B}'}\right\}$ at the very end of the pulse (see fig. 17). Because there are so many metastable states, one might expect that enormously many pulses would be necessary to have a configuration repeat (once a repetition occurs, the sequence will repeat indefinitely). The simulations show, however, that following a short transient the system always locks into a finite, short sequence of states. The configurations repeat periodically so that after q pulses, the CDW has moved forward by precisely p wavelengths.

The results of a simulation with fixed pulse height and varying t_{on} are shown in fig. 18. The system always locks, with narrow high-order subharmonic steps appearing as the system size is increased. This behavior is very different from a single degree of freedom model, where only

harmonic

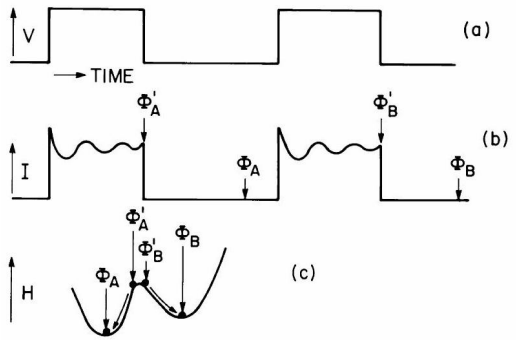


Fig. 17. The pulse duration memory effect, showing schematically the locking of the phase of the transient current oscillations (b) to the end of the voltage pulse (a).

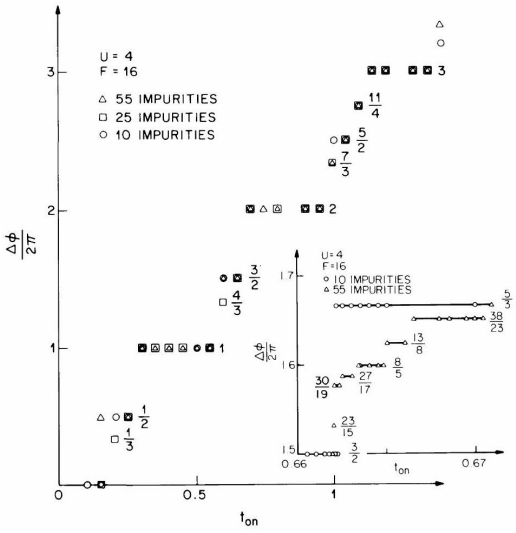


Fig. 18. Numerical simulations under pulsed driving (Coppersmith and Littlewood 1987) for fixed pulse height and varying t_{on}, showing the average number of wavelengths $\Delta\phi/2\pi$ moved per pulse. The inset shows a magnification of the region between 3/2 and 5/3.

locking can exist (for the trivial reason that there exists only a single pinned state).

If one looks at the current response to a single pulse, well-defined ringing oscillations are seen; for a single long pulse these decay with time to the finite size NBN amplitude (fig. 19). The transient oscillations exist for an infinite system, unlike the NBN in the FLR model. For a periodic application of short pulses, the phase of the transient oscillations locks to the end of the pulse, so that the current is always rising as the pulse ends, independent of the pulse length (Littlewood 1986b, 1987, Coppersmith and Littlewood 1987, Coppersmith 1987a,b, Tang et al. 1987). This 'pulse duration memory' is clearly displayed by the experimental data shown in fig. 20 ; it is evident, though less apparent in the results of numerical simulation on a small system shown in the same figure. Both in experiment and simulation a sequence of a few training pulses is necessary to achieve memory. The numerical results shown in fig. 20 are in fact from locked configurations, although this is not strictly necessary to develop the effect.

The pulse duration memory is the key to the understanding of the mode-locking behavior of the FLR model. The transient oscillations occur because the system begins in a pinned

configuration ϕ^{A} where all the degrees of freedom lie at minima of the potential energy. After the field is turned on, the local velocities are somewhat inhomogeneous (the system is not necessarily close to the equilibrium sliding state) and individual domains generate current oscillations with slightly different periods. As the oscillations dephase, the overall amplitude decays. Note that the existence of a rising cusp in the current at the end of the pulse would imply (for a single degree of freedom) that the local phase was at a maximum of the potential. However for a single degree of freedom this would occur only for special

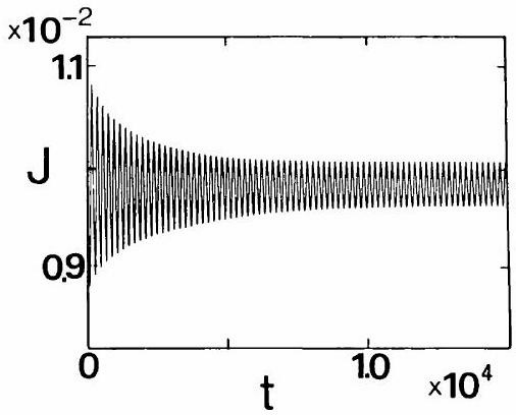


Fig. 19. Ringing oscillations decaying to finite size effect NBN in a numerical simulation of the response to a single pulse (Matsukawa and Takayama 1984, 1986).

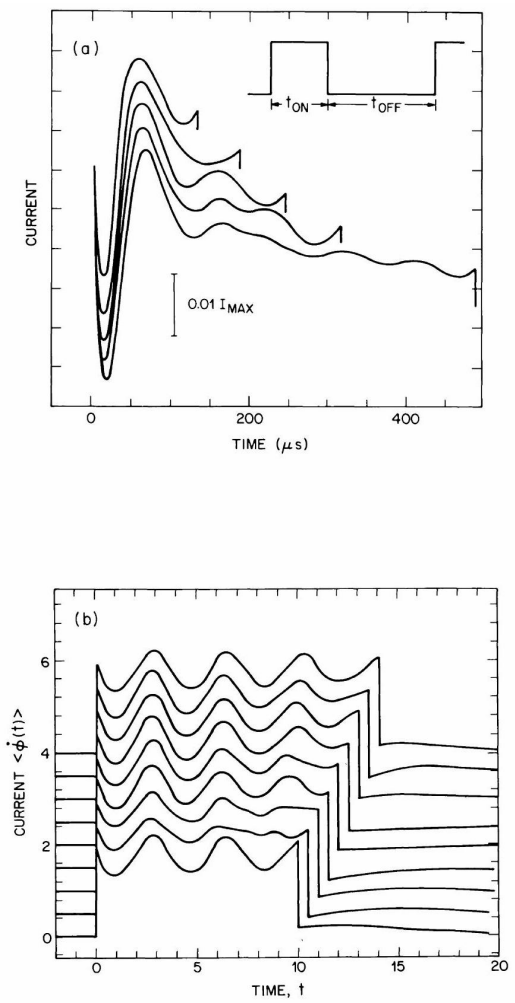


Fig. 20. The pulse duration memory effect. (a) Experimental data of Fleming et al. (1985) and (b) numerical simulations of Coppersmith and Littlewood (1987) (curves displaced vertically for clarity).

values of the pulse length and height; nevertheless, the existence of such a cusp requires that a disproportionate number of the degrees of freedom do reach the maximum of their local potentials, precisely as the field is turned off. That such a confluence does occur is easiest to demonstrate in the FK model of particles connected by springs in an incommensurate sinusoidal potential (Tang et al. 1987). Figure 21 shows the configuration at the very end of the pulse after the system has been trained; indeed almost all of the particles do lie on the very top of the potential well.

The condition that a given state will repeat after a single pulse can be phrased in terms of the width of the initial velocity distribution Δv in a given applied field. If the width $\Delta v \leqslant 2\pi/t_{\rm on}$ and the average velocity is such that $vt_{\rm on}(\mathrm{mod}2\pi)$ is close to zero, it is very likely that the system will relax to the same initial state, and will thus be harmonically locked. But one can imagine preparing many states which will have a narrow distribution of velocities in a given field; in fact there must be many different states which all mode lock under identical driving conditions. Starting from an arbitrary initial condition, the system will lock in the first of the many possible states which it finds. For a given value of the pulse height and length we may picture the possible locked states clustered together in a closed region of configuration space. As the configuration evolves slowly toward the cluster, it will be first captured by states which lie on the cluster boundary, and these generic configurations will control the observed behavior. But precisely because the generic configurations are on the boundary of the cluster, they will

be only marginally stable to changes in the driving. (For example in the configuration of fig. 21 each particle has to choose whether to relax to the left or the right well - if the pulse were only very slightly different the delicate balance required for repetition would be destroyed.) Marginal stability of the locked sequence yields automatically the pulse duration memory with a rising current cusp; the basins of attraction of the local minima of the potential are divided by local maxima.

One can simplify this problem still further by specifying the mapping from one state into another not by a differential equation but by a cellular automaton (Coppersmith and Littlewood 1987, Coppersmith 1987a,b, Tang et al. 1987). One of the simplest cases that can be studied (Coppersmith

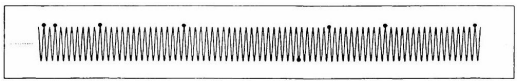


Fig. 21. Configuration of particles in the FK model at the very end of the voltage pulse after the system has been trained (only an eight-ball sequence of a long chain is shown). (From Tang et al. 1987.)

1987. is the two-stage map $\mathrm{F} : \left\{x_j^n\right\} \to \left\{x_j^{n+1}\right\}$ with the defining equations

$$y_j^n = k\left(x_{j+1}^n - 2x_j^n + x_{j-1}^n\right) + E + d_j, \tag{3.18}$$

$$x_j^{n+1} = \mathrm{int}\left(y_j^n + \frac{1}{2}\right), \tag{3.19}$$

where the d_j may be taken to be random variables. The two equations can be considered to model the two stages of coupled motion in the field, followed by relaxation to the bottom of the nearest well (in this case, the nearest integer). This map has been shown to exhibit the same phenomenon of pulse duration memory as the FLR model simulations. As the system evolves toward the region of fixed points ('locked states') the distribution of the intermediate variables $\{y_j\}$ develops a sharp peak where the fractional part of the y_j is close to $\frac{1}{2}$, exactly the boundary of the basins of attraction of the integers.

The advantage of studying the mapping equations rather than the full equation of motion is that the maps can be completely characterized, while the essential features of the full dynamics are preserved. The special properties of many-EDF systems are not restricted to a single model. We have here a general mechanism for pattern selection and a general principle which we have already seen for the static properties: when there are enough choices of configurations, a system will find those which are most easily accessible - and such states will generally be those which are the least stable.

3.5. Amplitude dynamics

A simple model including coupled dynamics for the amplitude and phase was discussed in section 2.5 (Inui et al. 1988). In the form of eq. (2.19) it involves many degrees of freedom and is a straightforward extension of the FLR model. However this model has been examined in detail only with a single amplitude and phase degree of freedom (eqs. (2.20) and (2.21)).

The most important new piece of physics is that elastic strain in the CDW phase cannot build up indefinitely; once the strain exceeds a critical value the amplitude collapses and rapid phase slip takes place to relieve the strain. This model was set up to describe 'switching' samples, where the d.c. current-voltage characteristics are hysteretic. Figure 22 shows d.c. hysteresis

curves obtained for monotonically increasing (dashed line) and decreasing (solid line) applied field. Hysteresis exists for sufficiently large κ and for a sufficiently large value of θ (which measures the polarization of the CDW necessary to cause phase slip).

In combined a.c. and d.c. fields this model displays complicated behavior with mode-locking (both harmonic and subharmonic) as well as quasiperiodicity and chaos. When the parameters are such that d.c. switching

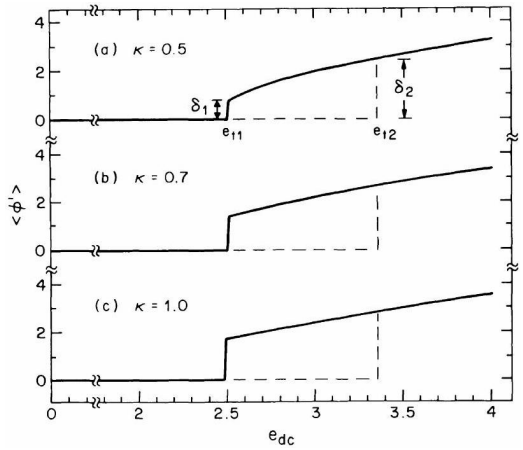


Fig. 22. Hysteretic IV characteristics for increasing (dashed line) and decreasing (solid line) d.c. field for three different values of κ, the amplitude relaxation rate. (From Inui et al. 1988).

occurs, harmonic mode-locking is dominant; for a fixed a.c. field and sweeping d.c. bias the system is nearly everywhere locked to a harmonic of the driving frequency. The gaps between these integer Shapiro steps are small, and the subharmonic steps or quasiperiodic regimes in between are narrow; experimentally this is also the case, with the gaps often too narrow to characterize the behavior (Inui et al. 1988, Zettl and Grüner 1982, Hall et al. 1988). A qualitatively new feature of the model is that it exhibits a period-doubling route to chaos while the system remains harmonically mode-locked on a Shapiro step. This behavior is graphically illustrated in fig. 23, which is a spectral analysis of the CDW current for different d.c. biases with the average current locked to the fourth Shapiro step.

The small amplitude a.c. response is similar to the FLR case in that it shows inductive dips in the conductance at frequencies close to the washboard frequency. However, in this model the widths of the anomalies are considerably broader than in the FLR model. There is a similar difference in the experimental magnitude of these features between switching and nonswitching samples.

The qualitative agreement between the behavior of the model and experiments on switching samples is good, although there are a few discrepancies which have been argued to result from the neglect of many degrees of freedom for the phase. A full discussion can be found in the article by Inui et al. (1988). The difference between the behavior of the

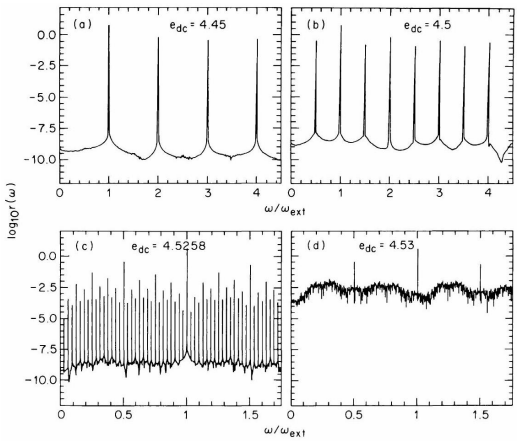


Fig. 23. Alternating current noise $I(\omega)$ for fixed a.c. amplitude and frequency and varying the d.c. bias on the fourth mode-locked step, showing periods 1 (a), 2 (b), 32 (c) and chaos (d). (From Inui et al. 1988).

reduced equations (2.20) and (2.21) and that of the FLR model results not only from the inclusion of phase slip, but also from the low dimensionality of the model. It is not clear whether the full many-degree of freedom model (2.19) will retain these low-dimensional feaures - in particular the perioddoubling route to chaos, and this should be checked. If switching samples are indeed dominated by contact pinning, or by a few strong pinning centers, a low-EDF model is indeed appropriate; the behavior of a model system with distributed amplitude fluctuations is not yet understood.

4.8.4 4. Conclusions

This article has focussed on the many-EDF properties of CDWs treated as a dynamical system, for which the FLR model is a useful starting point. The FLR model is one of the simplest models which contains the features of
spatially distributed non-linear pinning which seems to be necessary to understand the bulk properties of sliding CDWs. The picture is more than just phenomenological, because the model can be justified within a Ginz-burg-Landau expansion which has been very successful in understanding the static properties of many charge density wave transitions. The underlying assumption is that microscopic details should not be relevant for the behavior on long length scales and at low frequency; all that matters is the structure of the underlying theory.

In order to perform numerical simulations we are forced to this point of view anyway to avoid unnecessary complexity. Thus the justification of the model (by comparison to experiment) should be not in terms of any detailed fit to an individual piece of data but in terms of how well the model does overall in explaining a large number of different experiments. It is not difficult to produce a simple phenomenological model to fit a single experiment. Single-degree of freedom models work very well to explain the high-frequency a.c. conductivity, produce large NBN, and will lead to mode-locking similar to that observed experimentally; they of course cannot produce hysteresis and memory effects, and fail to adequately describe the IV characteristics close to threshold. Models for the low-field glassy behavior can also be constructed for the purpose of modelling hysteresis effects and the pinned low-frequency dynamics. The FLR model is more general in that it includes all these effects; and because it is expected to describe a large class of phenomena, it is indeed possible to test whether or not its description is accurate.

The most important feature of the FLR model is not that it has many metastable states, but that those states which are generically observed should have a special property, namely

marginal, or minimal stability. Because the configurations which are observed are controlled by their accessibility, the system always organizes itself to be on the edge of the region of stability; such configurations are in no sense typical and are in fact extremely rare in a statistical sense. This is in complete contrast to Hamiltonian systems at a finite temperature, where one expects that the system is dominated by states of low energy.

The two most compelling experiments on CDWs which indicate that such marginal states are in fact observed are: (i) the cusp-like low-frequency dependence of the dielectric function $\epsilon(\omega)$ (section 3.2) and (ii) the 'pulse duration memory' effect observed in dynamics (section 3.4). Neither of these phenomena are expected to be restricted to the FLR model, but the ingredients of spatially-distributed pinning and the relevance of many degrees of freedom are essential.

Not all the model predictions have been adequately tested. In particular the a.c. response at low frequencies is predicted to diverge in the pinned state. The non-linear a.c. response has been studied in $K_{0.3}MoO_3$ at low
temperatures, but at a frequency higher than the screened relaxation rate (Mihaly et al. 1988). In fact the unusual dynamics associated with the high-field 'threshold' (Fogle and Perlstein 1972, Maeda et al. 1985, Mihaly and Tessema 1986) in $K_{0.3}MoO_3$ at low temperatures may have to do with a crossover in the mechanism of CDW damping, rather than intrinsically a behavior of the model. But at higher temperatures, experimental disagreement over the form (Cava et al. 1984, Wu et al. 1984) of the low-frequency dependence in $\epsilon(\omega)$ may be a result of inadvertent contamination by the non-linear response. This question deserves further study.

There has been considerable disagreement over the interpretation of the mode-locking experiments in joint a.c. and d.c. fields, which lies partly in real differences between the experimental data of different groups. At least one group observes narrow mode-locked steps in a field and frequency range where a model with hydrodynamic damping (although not the FLR model) would predict mode-locking not to occur (Thorne et al. 1987). The samples in question were chosen for their highly coherent NBN, but it is noticeable that the d.c. characteristics close to threshold display a downward cusp in $\mathrm{d}I/\mathrm{d}V$ (Thorne et al. 1987), quite different from what would have been expected from the FLR model in three dimensions. The FLR model does make a specific prediction that under pulsed driving, with a long time in between pulses when the field is below threshold, CDWs should exhibit subharmonic as well as harmonic locking (Coppersmith and Littlewood 1986); only harmonic locking will be produced in a single degree of freedom model (provided that the pinning potential is single-valued over 2π).
The NBN itself is open to other interpretations than as a finite size bulk effect (Gor'kov 1989, Ong 1989), and experiments to determine the origin of the NBN have not been conclusive. The temporal variability of the NBN as well as the existence of low-frequency broadband noise can be explained within the FLR model only with the addition of some external weak source of noise in the driving field, quite possibly arising at the contacts.

This critical behavior, and the shape of the IV characteristics even well above threshold provide strong evidence for the importance of many degrees of freedom. The width of the critical region is controlled not so much by the applied field as by the resultant velocity. It is then fortunate that the effective velocity-dependence of the damping parameter which occurs in insulators at low temperature should lead to an unusually large range of field for the critical region in these materials (Littlewood 1988). Indeed, the CDW current can be fit to a power-law form $I \propto (V - V_{\mathrm{T}})^{\zeta}$ over several decades in voltage in $K_{0.3}MoO_3$ at low temperature, with $\zeta \approx 1.2$. Such a value for the critical exponent in three-dimensions seems roughly appropriate for the FLR model, although it has not been calculated. ζ should of course be temperature-independent in the model, although a
weak temperature-dependence was reported. Provided difficulties with inhomogeneous (filamentary) conduction can be overcome, the semiconducting materials offer a good possibility to

study the predicted critical phenomena.

Amplitude fluctuations must certainly occur at contacts and possibly in the bulk at strong pinning centers. The existence of amplitude fluctuations does not per se invalidate the FLR model; it is only if the dynamics of these fluctuations are important that there will be any qualitative change in the behavior of the system. The dynamics of amplitude collapse is a plausible mechanism for the generation of NBN, and is probably relevant to the behavior of switching samples. It appears that the behavior of switching samples can indeed be quite well understood within a low-EDF model (Inui et al. 1988) (section 3.5) which may imply that the behavior of such samples is indeed contact-dominated and thus low-dimensional. An open question remains the behavior of a model with distributed amplitude fluctuations and many degrees of freedom - and in particular whether low-EDF phenomena such as a period doubling cascade to chaos will persist.

4.8.5 References

Abe, S., 1985, J. Phys. Soc. Jpn. 54, 3494.
Abe, S., 1986, in: Proc. Yamada Conf. XV, Physica B 143.
Abe, S., 1987, J. Phys. Soc. Jpn. 55, 1987.
Bak, P., 1985, in: Charge Density Waves in Solids, Lecture Notes in Physics, Vol. 217, eds Gy. Hutiray and J. Sólyom (Springer, Berlin).
Bhattacharya, S., J.P. Stokes, M.J. Higgins and R.A. Klemm, 1987, Phys. Rev. Lett. 59, 1849.
Brown, S.E., and A. Zettl, 1989, this volume.
Brown, S.E., G. Mozurkewich and G. Grüner, 1984, Phys. Rev. Lett. 52, 2277.
Brown, S.E., G. Grüner and L. Mihaly, 1986, Solid State Commun. 57, 165.
Cava, R.J., R.M. Fleming, P.B. Littlewood, E.A. Rietman, L.F. Schneemeyer and R.G. Dunn, 1984, Phys. Rev. B 30, 3228.
Cava, R.J., R.M. Fleming, R.G. Dunn and L.F. Schneemeyer, 1985, Phys. Rev. B 31, 8325.
Christiansen, P.L., 1986, Physica D 23, 68.
Coppersmith, S.N., 1984, Phys. Rev. B 30, 410.
Coppersmith, S.N., 1986a, Physica D 23, 54.
Coppersmith, S.N., 1986b, Phys. Rev. B 34, 2073.
Coppersmith, S.N., 1987a, Phys. Rev. A 36, 3375.
Coppersmith, S.N., 1987b, Phys. Lett. A 125, 473.
Coppersmith, S.N., 1987c, Phys. Rev. A 36, 3375; and to be published.
Coppersmith, S.N., and D.S. Fisher, 1983, Phys. Rev. B 28, 2566; and to be published.
Coppersmith, S.N., and P.B. Littlewood, 1985, Phys. Rev. B 31, 4049.
Coppersmith, S.N., and P.B. Littlewood, 1986, Phys. Rev. Lett. 57, 1927.
Coppersmith, S.N., and P.B. Littlewood, 1987, Phys. Rev. B 36, 311.
Efetov, K.B., and A.I. Larkin, 1977, Zh. Eksp. & Teor. Fiz. 72, 2350 [Sov. Phys.-JETP 45, 1236].
Eykholt, R., A.R. Bishop, P.S. Lomdahl and E. Damany, 1986, Physica D 23, 102.
Feigel'man, M.V., and V.M. Vinokur, 1981, Phys. Lett. A 87, 53.
Feigel'man, M.V., and V.M. Vinokur, 1983, Solid State Commun. 45, 603; and this volume.
Fisher, D.S., 1983, Phys. Rev. Lett. 50, 1486.
Fisher, D.S., 1985, Phys. Rev. B 31, 1396.
Fleming, R.M., and L.F. Schneemeyer, 1986, Phys. Rev. B 33, 2930.
Fleming, R.M., R.J. Cava and L.F. Schneemeyer, 1985, Phys. Rev. B 31, 1181.
Fogle, W., and J.H. Perlstein, 1972, Phys. Rev. B 6, 1402.
Fukuyama, H., and P.A. Lee, 1977, Phys. Rev. B 17, 535.
Gill, J.C., 1981, Solid State Commun. 39, 1203.

Gor'kov, L.P., 1989, this volume.
Grüner, G., and P. Monceau, 1989, this volume.
Grüner, G., A. Zawadowski and P.M. Chaikin, 1981, Phys. Rev. Lett. 46, 511.
Hall, R.P., and A. Zettl, 1984, Phys. Rev. B 30, 2279.
Hall, R.P., M.F. Hundley and A. Zettl, 1986, Phys. Rev. Lett. 56, 2399.
Hall, R.P., M.F. Hundley and A. Zettl, 1988, Phys. Rev. B 38, 13002;13019.
Inui, M., and S. Doniach, 1987, Phys. Rev. B 35, 6244.
Inui, M., R.P. Hall, S. Doniach and A. Zettl, 1988, Phys. Rev. B 38, 13047.
Jing, T.W., and N.P. Ong, 1986, Phys. Rev. B 33, 5841.
Lee, P.A., and T.M. Rice, 1979, Phys. Rev. B 19, 3970.
Link, G.L., and G. Mozurkewich, (unpublished).
Littlewood, P.B., 1986a, Phys. Rev. B 33, 6694.
Littlewood, P.B., 1986b, Physica D 23, 45.
Littlewood, P.B., 1987a, Jpn. J. Appl. Phys. 26 (Suppl. 26-3) 1901.
Littlewood, P.B., 1987b, Phys. Rev. B 36, 3108.
Littlewood, P.B., 1988, Solid State Commun. 65, 1347.
Littlewood, P.B., and R. Rammal, 1988, Phys. Rev. B 38, 2675.
Littlewood, P.B., and T.M. Rice, 1982, Phys. Rev. Lett. 48, 44.
Littlewood, P.B., and C.M. Varma, 1987, Phys. Rev. B 36, 480.
Maeda, A., T. Fukuyama and S. Tanaka, 1985, Solid State Commun. 55, 951.
Matsukawa, H., 1987, J. Phys. Soc. Jpn. 56, 1522.
Matsukawa, H., and H. Takayama, 1984, Solid State Commun. 50, 283.
Matsukawa, H., and H. Takayama, 1986, in: Proc. Yamada Conf. XV, Physica B 143, 80.
Matsukawa, H., and H. Takayama, 1987a, J. Phys. Soc. Jpn. 56, 1507.
Matsukawa, H., and H. Takayama, 1987b, Jpn. J. Appl. Phys. 26 (Suppl. 26-3) 601.
Matsukawa, H., and H. Takayama, 1987c, Synth. Met. 19, 7.
McMillan, W.L., 1975, Phys. Rev. B 12, 1187; 1197.
McMillan, W.L., 1976, Phys. Rev. B 14, 1496.
Mihaly, G., and P. Beauchêne, 1987, Solid State Commun. 63, 911.
Mihaly, G., T. Chen, T.W. Kim and G. Grüner, 1988, Phys. Rev. B 38, 3602.
Mihaly, L., and G.X. Tessema, 1986, Phys. Rev. B 33, 5858.
Mihaly, L., M. Crommie and G. Grüner, 1987a, Europhys. Lett. 4, 103.
Mihaly, L., T. Chen and G. Grüner, 1987b, Solid State Commun. 61, 751.
Miyashita, T., and H. Takayama, 1986, in: Proc. 18th Int. Conf. on Low Temperature Physics, Jpn. J. Appl. Phys. 26 (Suppl. 26-3) 603.
Ong, N.P., 1989a, article in this volume.
Ong, N.P., 1989b, this volume.
Ong, N.P., G. Verma and K. Maki, 1984, Phys. Rev. Lett. 52, 663.
Peyraud, M., and S. Aubry, 1983, J. Phys. C 16, 1593.
Pietronero, L., and S. Strässler, 1983, Phys. Rev. B 28, 5863.
Reagor, D., S. Sridhar, M. Maki and G. Grüner, 1985, Phys. Rev. B 32, 8445.
Reagor, D., S. Sridhar and G. Grüner, 1986, Phys. Rev. B 34, 2212.
Rice, T.M., P.A. Lee and M.C. Cross, 1979, Phys. Rev. B 20, 1345.
Richard, J., P. Monceau and M. Renard, 1982, Phys. Rev. B 25, 948.
Robbins, M.O., J.P. Stokes and S. Bhattacharya, 1985, Phys. Rev. Lett. 55, 2822.
Sneddon, L., 1984, Phys. Rev. Lett. 52, 65.
Sneddon, L., 1984a, Phys. Rev. B 29, 719; 725.
Sneddon, L., 1984b, Phys. Rev. B 30, 2974.
Sneddon, L., M.C. Cross and D.S. Fisher, 1982, Phys. Rev. Lett. 49, 292.
Sokoloff, J.B., 1981, Phys. Rev. B 23, 1992.

Sokoloff, J.B., 1985, Phys. Rev. B 31, 2270.
Sokoloff, J.B., and B. Horowitz, 1983, J. Phys. (France) 44, C3-1667.
Sridhar, S., D. Reagor and G. Grüner, 1985, Phys. Rev. Lett. 55, 1196.
Sridhar, S., D. Reagor and G. Grüner, 1986, Phys. Rev. B 34, 2223.
Stokes, J.P., M.O. Robbins and S. Bhattacharya, 1985, Phys. Rev. B 32, 6939.
Tang, C., K. Wiesenfeld, P. Bak, S.N. Coppersmith and P.B. Littlewood, 1987, Phys. Rev. Lett. 58, 1161.
Teranishi, N., and R. Kubo, 1979, J. Phys. Soc. Jpn. 47, 720.
Tessema, G.X., and N.P. Ong, 1983, Phys. Rev. B 27, 1417.
Tessema, G.X., and N.P. Ong, 1985, Phys. Rev. B 31, 1055.
Thorne, R.E., J.R. Tucker, J. Bardeen, S.E. Brown and G. Grüner, 1986, Phys. Rev. B 33, 7342.
Thorne, R.E., J.R. Tucker and J. Bardeen, 1987, Phys. Rev. Lett. 58, 828.
Tua, P.F., and J. Ruvalds, 1985, Solid State Commun. 54, 471.
Tucker, J.R., W.G. Lyons and G. Gammie, (to be published).
Wu, Wei-Yu, L. Mihaly, G. Mozurkewich and G. Grüner, 1984, Phys. Rev. Lett. 52, 2382.
Zettl, A., and G. Grüner, 1982, Phys. Rev. B 26, 2298.

4.9 9 Transport Phenomena in CDW Conductors Microscopic Approach

4.9.1 1. Introduction

Experimental investigations of quasi-one-dimensional conductors with charge density wave (CDW) revealed many interesting phenomena such as: (a) Nonlinearity of the current-voltage characteristic (CVC) in electrical fields E exceeding a threshold value E_{T} (for example, in typical conductors with CDWNbSe$_3$ and TaS$_3$ the threshold field $E_{\mathrm{T}}, E_{\mathrm{T}} \geqslant 0.01$ V/cm and $E_{\mathrm{T}} \geqslant 0.1$ V/cm, respectively); (b) Generation of electrical oscillations at $E > E_{\mathrm{T}}$ with field dependent frequencies reaching magnitudes up to $\sim 10^8$ Hz; (c) Hysteresis and memory effects at $E < E_{\mathrm{T}}$ when the voltage response to applied current pulses depends on the magnitude and sign of the preceding pulses; (d) Large value of dielectric constant ($\epsilon \geqslant 10^6 - 10^8$), and others (for details, see review articles by Grüner and Zettl 1985, Monceau 1985). These phenomena, showing significant distinction between conductors with CDW and ordinary metals or semiconductors, allowed one to come to the conclusion that, besides the usual conduction mechanism related to the motion of free carriers, i.e. carriers situated above the Peierls gap (Peierls 1930), there is a new mechanism caused by a collective response of the CDW to an external perturbation. Fröhlich was the first who showed in 1954 that the charge transfer in conductors with CDW can be realized by carriers condensed in the CDW (Fröhlich 1954).

Thus, there arose the problem how to describe transport phenomena in conductors with the CDW. In this connection, it is useful to recall the analogy between CDW conductors and superconductors which was noted many times in different papers. Besides the quasiparticles, in both cases there is an additional degree of freedom characterized by the amplitude Δ and the phase φ of the order parameter $\hat{\Delta}$. So equations describing the behaviour of this collective variable (the condensate) must be incorporated into the full set of kinetic equations. Of course, there is an essential difference between the CDW and the condensate in superconductors which is connected with different symmetry of the order parameter: in the first case $\hat{\Delta}_p \sim \langle a_{p\uparrow} a^+_{p+Q\uparrow} \rangle \sim \langle a_{p\downarrow} a^+_{p+Q\downarrow} \rangle$while in the second case $\hat{\Delta}_p \sim \langle a^+_{p\uparrow} a^+_{-p\downarrow} \rangle$(here $Q = 2p_{\mathrm{F}}; p_{\mathrm{F}}$ is the Fermi momentum). From a different symmetry of the order parameter, it follows that the phase of the superconducting order parameter has the meaning of the quantum mechanical phase, and the CDW phase characterizes the position of the CDW. This distinction shows up in

the Meissner effect and in nondissipative current flows in superconductors, and in the absence of similar effects in conductors with the CDW. Besides, the interaction of the condensate with impurities in these cases is different: the ordinary (nonmagnetic) impurities in superconductors do not affect the order parameter $\hat{\Delta}$ and do not break the translational invariance of the system, while such impurities in CDW conductors suppress Δ and break the translational invariance; they cause, in particular, pinning of the CDW.

In spite of the difference between superconductors and CDW conductors, there is an analogy in, for example, the description of their kinetic properties. It is known that, in the simplest approach to the description of kinetic phenomena in superconductors, one uses so-called time-dependent Ginz-burg-Landau equations (TDGL) (see e.g. De Lozanne and Beasley 1986). As was shown by Gor'kov and Eliashberg (1968), these equations can be obtained in the case of superconductors with a large concentration of magnetic impurities when the energy gap is suppressed (gapless case). Similar equations were derived for conductors with CDW by Gor'kov (1984). Again, the necessary condition of the applicability of these equations is the absence of a gap in the excitation spectrum. This happens when the concentration of ordinary impurities is sufficiently large, i.e., when the parameter $\Delta\tau$ is small: $\Delta\tau \ll 1$, where τ is the momemtum relaxation time*. Although the TDGL equations are rather complicated nonlinear differential equations, they are simpler than kinetic equations because they contain the macroscopic variables only: complex order parameter $\hat{\Delta} = \Delta \exp(\mathrm{i}\varphi)$, electrical field E and current j. Different problems of the theory of nonequilibrium processes can be analyzed with the help of these equations.

In a more general case the energy gap is not equal to zero, and the TDGL equations cannot be used. In this case, one needs to address more complicated kinetic equations. We derive here the kinetic equations for Peierls conductors and apply them to the analysis of some important phenomena in CDW systems. We will assume that the interchain coupling strength is not negligible and, hence, the CDW phase on different chains in the crystal is correlated.

Most general equations are the equations for matrix Green functions. One part of them describes the dynamics of excitation spectrum, and the other one, containing the Keldysh function determines the kinetics of the system. In the next section, after some general remarks (section 2.1) we will discuss microscopic equations for the Green functions (section 2.2). On the basis of these equations we will derive in quasiclassical approximation

($\omega, kv \ll \Delta$) simpler kinetic equations for distribution functions n_1 and n_z which allow one to find macroscopic characteristics such as charge density ρ, current density j and CDW phase φ.

In many cases kinetic equations can be further simplified and reduced to equations for macroscopic variables. Further, we consider different problems which can be solved with the help of these simplified equations. For example, in sections 3.1 and 3.2, we calculate d.c. and a.c. conductivities. Formulae for σ_{dc} will be presented both for the case when the behaviour of a system is semiconducting (TaS_3, $K_{0.3}MoO_3$, etc.) and for the case of metallic Peierls conductors (for example, $NbSe_3$).

Analysis of nonuniform CDW deformations will be carried out in section 4 (phason spectrum, deformable CDW sliding, etc.). In this case it is very important to take into account the screening of the CDW charge by free carriers which modify, for example, the spectrum of the long-wavelength phasons. Screening effects will be discussed in different subsections of section 4. Note that the screening effects show up most essentially in Peierls conductors with semiconducting energy spectrum. In this case some measurable characteristics depend drastically (exponentially) on the temperature because the free carriers concentration diminishes exponentially on cooling at $T < T_{\mathrm{p}}$ (T_{p} is the Peierls transition temperature). Most attention

[0]*Note that the momentum relaxation rate is caused by impurity scattering or by phonon scattering if the latter is more effective.

in this review is paid just to the case of low temperatures and Peierls conductors with a semiconducting energy gap. Note that most materials studied experimentally belongs to this type (TaS_3, $K_{0.3}MoO_3$, $(TaSe_4)\,I$, $(NbSe_4)_{10}\,I_3$ and others).

Finally, in section 5 we present the main results concerning the experimental and theoretical study of the Hall effect in conductors with sliding CDW. In the Conclusion, we list several unresolved problems of the CDW kinetics.

4.9.2 2. Kinetic equations

2.1. Phenomenological approach

Many problems connected with the CDW dynamics were solved on the basis of phenomenological equations (see e.g. Grüner and Zettl 1985, Monceau 1985). The CDW is considered as an anisotropic elastic medium moving with friction under the action of an electric field. The interaction of the CDW with randomly distributed impurities is described by a sum of δ-functions. Thus, the equation of CDW motion has the form

$$-\hat{K}\nabla^2 u + m^*\ddot{u} + \tilde{\gamma}\dot{u} + V_{\text{im}}\sum_i \delta\left(\boldsymbol{r} - \boldsymbol{r}_i\right)\sin\left[Q\left(r_i + u\right)\right] = eE. \tag{2.1}$$

Here $u = \varphi/Q$ is a displacement of the CDW, $\hat{K}$ is the tensor of elastic moduli, $\tilde{\gamma}$ is the friction coefficient, V_{im} is the Fourier component of the potential of CDW interaction with impurities. This equation is supplemented with an expression for the current density

$$j = j_q + j_{\text{CDW}}, \quad j_q = \sigma_1 E, \quad j_{\text{CDW}} = \sigma_2\dot{u}/elQ \tag{2.2}$$

where σ_1 is the quasiparticle conductivity, σ_2 is the CDW conductivity, $Q = 2p_{\text{F}}$ is the wave vector of the CDW.

A large number of papers is devoted to studies of the phenomenological equations (2.1)-(2.2) (see, e.g. Littlewood (1987) and articles cited in his paper). The results obtained in this way allow one to explain many experimental data (hysteretic phenomena, pinning, anomalous behaviour of the a.c. conductivity $\sigma(\omega)$, etc.). However, in some cases these equations are not sufficient for a complete description of the system under consideration. For instance, if the level of chemical potential μ or the gap Δ are changed for some reasons, it is necessary to take into account a modification of the quasiparticle distribution function which determines the change of μ and Δ. In other words, the full theoretical description should contain generalized kinetic equations for the quasiparticles. Besides, the microscopic theory allows one to calculate coefficients in equations like eqs. (2.1)-(2.2) (for example, $\hat{K}, \tilde{\gamma}, \sigma_{1,2}$, etc.) and to determine the limits of applicability of these equations.

2.2. Microscopic equations

In deriving kinetic equations for a CDW system we can utilize an approach used in the theory of nonequilibrium phenomena in superconductors (see, e.g. Larkin and Ovchinnikov 1986). In this theory, describing the dynamics of the quasiparticles and the condensate, the matrix Green functions are introduced which consist of ordinary functions G and anomalous functions F. As in the case of superconductors, anomalous Green functions are proportional to the amplitude of the order parameter Δ, and differ from zero at $T < T_{\text{p}}$. The order parameter Δ in Peierls conductors is related to a static lattice deformation $\hat{\Delta} = g_{\text{e-ph}}\left\langle b_Q + b_{-Q}^+\right\rangle$, where $b_Q^+$is the operator of phonon creation.

We will use the mean-field approximation and neglect thermal and quantum fluctuations assuming that the condition $m^*/m \sim \Delta^2/\left(\lambda\omega_Q^2\right) \gg 1$ is fulfilled (Efetov and Larkin 1977, Brazovskii 1979); here λ is the dimensionless electron-phonon coupling constant, ω_Q is the frequency

of phonons with momentum Q. In most Peierls conductors ($K_{0.3}MoO_3$, TaS_3, $(NbSe_4)_{10}I_3$, etc.) this condition is fulfilled sufficiently well because typical values of phonon frequencies are in the temperature range of $50-100$ K (Sekine et al. 1987, Escribe-Fillipini et al. 1987, Monceau et al. 1987) while
$\Delta \sim 1000$ K. In addition, in order to neglect thermal fluctuations we should assume that the dispersion of electron or phonon spectra in directions perpendicular to the chain direction is not negligibly small, i.e., $T < \max\{\eta_0, |\omega_\perp| m^*/m\}$, where η_0 and $\omega_\perp$ are the widths of electron and phonon spectra in transverse direction, respectively.

The retarded G^{R} and advanced G^{A} Green functions determine the excitation spectrum of the system and the response of the CDW to an external perturbation. The Green function G, introduced by Keldysh (1964), describes the kinetics of the system. Thus, the full set of equations derived in the mean-field approximation includes dynamical equations for $G^{\mathrm{R(A)}}$ and G which describe the response of the system to an external perturbation in the presence of interaction with impurities (see Appendix).

This rather complicated set of equations may be simplified considerably, if one makes use of the quasi-one-dimensionality of the spectrum (Artemenko and Volkov 1981b, Eckern 1986). We consider a model of a CDW conductor used earlier by Gor'kov and Dolgov (1979), that is, we assume that the spectrum of a quasi-one-dimensional metal at $T > T_{\mathrm{p}}$ has the form

$$\epsilon_{\mathrm{p}} = p_\parallel^2/2m + \eta(p_\perp) - \epsilon_{\mathrm{F}}, \tag{2.3}$$

where $p_{\parallel,\perp}$ are the momenta parallel and perpendicular to the chain direction, the function $\eta(p_\perp)$ describing a curvature of the Fermi sheets is assumed to be small as compared to the Fermi energy: $\eta_0 = \max|\eta(p_\perp)| \ll \epsilon_{\mathrm{F}}$. In compounds with a semiconducting spectrum at $T < T_{\mathrm{p}}$ (TaS_3, $K_{0.3}MoO_3$, etc.) one has $\eta_0 < \Delta$, whereas in compounds with a metallic spectrum at $T < T_{\mathrm{p}}$ (for example, $NbSe_3$) one has $\eta_0 > \Delta$. On the other hand, the magnitude of η should not be too small because at too small η it is necessary to take into account thermal fluctuations or localization effects. The latter ones are unimportant when $\tau\eta_0 > 1$. In this case, the equations for the Green functions can be simplified by integration over the variable $\xi_p = p_\parallel^2/2m - \epsilon_{\mathrm{F}} = (p_\parallel - p_{\mathrm{F}})v$. Doing so, we obtain equations for the Green functions $\hat{g}$ integrated over the variable ξ_p

$$\hat{g}(t,t';R) = \frac{\mathrm{i}}{\pi}\int \mathrm{d}\xi_p G(p_\parallel, t, t'; R)$$

An analogous method of averaging over the modulus of the momentum p near the Fermi surface was used in the theory of superconductivity (see, e.g. Larkin and Ovchinnikov 1986). Equations for the functions $\hat{g}$ integrated over ξ_p are more compact and simple than initial equations. In some cases (for example, for the calculation of linear response) they may be solved directly. Nevertheless, being quite general (it is required only that a characteristic length of a perturbation is large with respect to the period of the CDW, Q^{-1}), they remain to be rather complicated.

Further simplification of these equations may be achieved in the quasi-classical limit when frequencies ω and wave vector k are not too large, i.e. when $\omega, kv \ll \Delta$. Then, the equations for $\hat{g}^{\mathrm{R(A)}}$ can be solved by means of perturbation theory, and the equation for $\hat{g}$ is reduced to kinetic equations for distribution functions n_1 and n_z. The function $\hat{g}$ is expressed through n_1 and n_z in the following form (see Appendix):

$$\hat{g} = \hat{g}^{\mathrm{R}}\hat{n} - \hat{n}\hat{g}^{\mathrm{A}}, \quad \hat{n} = n_z\hat{\sigma}_z + n_1\hat{1}, \tag{2.4}$$

where $\hat{\sigma}_z$ is the Pauli matrix.
The kinetic equations for n_z and n_1 acquire the simplest form when the bending of the Fermi

surface is small: $\eta_0 \ll \Delta$ (semiconducting spectrum of excitation). In this case one has (Artemenko et al. 1986)

$$\left(\frac{\epsilon^2}{\xi^2(\tilde{\epsilon})}\frac{\partial}{\partial t}+\frac{2\mathrm{i}\Delta}{G_-}F_+ +\nu_\mathrm{b}G_-\right)n_z+v\frac{\partial n_1}{\partial x}=\left(ev\tilde{E}-\frac{\nu_\mathrm{b}}{2}\dot{\varphi}G_-\right)\frac{\partial n_1}{\partial\epsilon} \tag{2.5a}$$

$$\frac{\partial n_1}{\partial t}+v\frac{\partial n_z}{\partial x}+v_\perp\frac{\partial n_1}{\partial r_\perp}+\left[\nu_\mathrm{f}\left(G_-^2+F_-^2\right)+\nu_\mathrm{b}\left(G_-^2-F_-^2\right)\right]\left(n_1-\langle n_1\rangle\right)/\left(2G_-\right)$$
$$=\left[(ev_\perp\boldsymbol{E})\frac{\partial\left(n_1G_-\right)}{\partial\epsilon}+e\boldsymbol{E}\frac{\partial\left(n_1G_-\right)}{\partial p_\perp}\right]/G_- \tag{2.5b}$$

Here $\xi(\tilde{\boldsymbol{\epsilon}})=\sqrt{\tilde{\boldsymbol{\epsilon}}^2-\Delta^2},\tilde{\boldsymbol{\epsilon}}=\boldsymbol{\epsilon}-\eta\left(p_\perp\right),F_+=f^{\mathbf{R}}+f^{\mathbf{A}}=-2\mathrm{i}\nu_0\Delta\tilde{\boldsymbol{\epsilon}}^2/\xi^4(\tilde{\boldsymbol{\epsilon}}),F_-=\Delta/\tilde{\epsilon}G_-,\quad G_-=g^\mathrm{R}-g^\mathrm{A}=(2\tilde{\epsilon}/\xi)\theta(|\tilde{\epsilon}|-\Delta),\quad \nu_0=\nu_\mathrm{f}+\nu_\mathrm{b}/2,\quad \nu_\mathrm{f,b}$ are the frequencies of forward- and backward-scattering rates, $\tilde{E}=E+v\varphi'/2$, $\varphi'=\partial\varphi/\partial x$. The angular brackets mean the averaging over momenta $p_\perp$ in transverse direction, the x-axis is directed along chains.

We dropped here terms describing the heating effects and inelastic electron-phonon collisions. For example, in eq. (2.5b) the terms $[evE+(\nu_\mathrm{b}/2)\,\partial\varphi/\partial t]\,G_-^{-1}\partial\left(n_zG_-\right)/\partial\epsilon+I_\mathrm{e-ph}$ are dropped.

Current and charge density are expressed through the functions n_1 and n_z in the following way:

$$\boldsymbol{j}_\parallel=\left(\sigma_{\parallel\mathrm{N}}/l\right)\left(\int\mathrm{d}\epsilon G_-n_z+\dot{\varphi}\right)+\left(\epsilon_\Delta/4\pi\right)\frac{\partial E}{\partial t} \tag{2.6a}$$

$$\boldsymbol{j}_\perp=\left(\sigma_{\perp\mathrm{N}}/l\right)\frac{\nu_\mathrm{f}+\nu_\mathrm{b}}{4\left\langle v_\perp^2\right\rangle}\int\mathrm{d}\epsilon\left\langle v_\perp G_-n_1\right\rangle \tag{2.6b}$$

$$\rho=\left(\sigma_{\parallel\mathrm{N}}/vl\right)\left(\int\mathrm{d}\epsilon G_-n_1-v\frac{\partial\varphi}{\partial x}\right)-\left(\epsilon_\Delta/4\pi\right)\frac{\partial E}{\partial x} \tag{2.7}$$

where $\sigma_{\parallel,\perp\mathrm{N}}$ is the longitudinal (transverse) conductivity in normal state, $l=v/\nu_\mathrm{b}$ is the mean-free-path length, $\epsilon_\Delta=\left(4\pi\sigma_{\parallel\mathrm{N}}\nu_\mathrm{b}\Delta/\sigma\right)\left|\partial\left(N_\mathrm{s}/\Delta^2\right)/\partial\Delta\right|,N_\mathrm{s}$ is the dimensionless density of condensed electrons

$$N_\mathrm{s}=-\frac{\Delta^2}{2}\int\mathrm{d}\epsilon\left[\left(\xi^\mathrm{R}\right)^{-3}-\left(\xi^\mathrm{A}\right)^{-3}\right]\tanh\left(\frac{\epsilon}{2T}\right)$$
$$=\begin{cases}1-\sqrt{\frac{2\pi\Delta}{T}}\exp\left(-\frac{\Delta}{T}\right), & \Delta\gg T\\ \frac{7\zeta(3)}{8\pi^2}\frac{\Delta^2}{T^2}, & \Delta\ll T\end{cases}$$

The last terms in eqs. (2.6)-(2.7) describe the renormalization of the dielectric constant due to the appearance of the Peierls gap. At $\Delta\gg T$ one has $\epsilon_\Delta\sim\omega_\mathrm{p}^2/\Delta^2,\omega_\mathrm{p}$ being the plasma frequency. The charge conservation equation follows from expressions (2.6)-(2.7) and eq. (2.5). If frequencies and characteristic gradients are small enough, the last terms in eqs. (2.6a) and (2.7) are also small corrections.

Finally, we write down equations for modulus Δ and phase φ of the order parameter which follow from the selfconsistency equation (see, eq. (A.9))

$$\omega_0^{-2}\left[\frac{1}{\Delta}\frac{\partial^2\Delta}{\partial t^2}-\left(\frac{\partial\varphi}{\partial t}\right)^2\right]=\int \mathrm{d}\epsilon\left[n_1-\tanh\left(\frac{\epsilon}{2T}\right)\right]\frac{G_-}{\tilde{\epsilon}} \tag{2.8}$$

$$\omega_0^{-2}\left[\frac{\partial^2\varphi}{\partial t^2}+\frac{2}{\Delta}\frac{\partial\varphi}{\partial t}\frac{\partial\Delta}{\partial t}-s^2\nabla_\perp^2\varphi\right]$$
$$=\frac{2ev\tilde{E}}{\Delta^2}-\frac{ev\tilde{E}}{2\Delta^2}\int \mathrm{d}\epsilon G_-\frac{\partial n_1}{\partial\tilde{\epsilon}}+2\nu_0\int \mathrm{d}\epsilon\frac{\epsilon^2}{\left(\epsilon^2-\Delta^2\right)^4}n_z \tag{2.9}$$

where $\omega_0^2 = \lambda\omega_Q^2$, ω_Q is the 'bare' phonon frequency, $s^2=\left(\partial^2\omega_q^2/\partial q^2\right)(q=Q)-\langle v_\perp^2\rangle\,\omega_0^2/2\Delta^2$, $v_\perp$ is the transverse electron velocity.

It is worth noting that if the magnitude $\langle v_\perp^2\rangle$ is large enough, the value of s^2 is negative. It means that in equilibrium (when $\tilde{E}=0$) the system is unstable with respect to transverse fluctuations of the CDW phase φ. Then, the stable state of the system is a state with a vector Q having a component in transverse direction. Taking into account this component we may obtain again an equation for the phase φ like eq. (2.9) where the coefficient s^2 is positive. We will suppose in the following that $Q\|x$ and $s^2>0$.

The eqs. (2.5)-(2.9) are valid if $\omega, kv \ll \Delta$ and $\eta_0<\Delta$. The latter condition allows one to simplify the collision term by integration of it over $p_\perp$. Note also that when deriving the equation for the phase φ(2.9), we used two approximations. First, only one dissipation mechanism of sliding CDW was taken into account - the friction of the CDW due to its interaction with quasiparticles (another multiphonon mechanism will be discussed later). Second (and it is very important), the term describing pinning of the CDW is absent. If pinning is caused by the interaction of the CDW with im-
purities, then to the right-hand-side of eq. (2.9) one should add the term (Efetov and Larkin 1977, Lee and Rice 1979, see also Artemenko and Kruglov 1982, who obtained this term for the equation used here)

$$-\sum_i V_O\delta\left(\boldsymbol{r}-\boldsymbol{r}_i\right)\sin\left(\varphi+Qr_i\right) \tag{2.10}$$

where V_Q is the Fourier component of impurity interaction potential. If the CDW is commensurate with the underlying lattice, then the term,

$$-\kappa_\mathrm{T}\Delta\sin(M\varphi) \tag{2.11}$$

should be added to the right-hand-side of eq. (2.9); where $\kappa_\mathrm{T}\sim\left(\Delta/\epsilon_\mathrm{F}\right)^M$; $M=3,4$, etc. M is the order of commensurability.

This result may be obtained if one takes into account mixing of states on the Fermi surface with momenta p and $p+M_1Q$ (where $M_1\leqslant M$) (Lee et al. 1974, see also Artemenko and Volkov 1981c). In many compounds vector Q has components in transverse directions. For example, in the commensurate state of o-TaS $3Q=\left(\frac{1}{2}a,\frac{1}{8}b,\frac{1}{4}c\right)$ (the c-axis is parallel to the chain direction). In this and similar cases the states with momenta p and $p+4Q$ do not coincide. Hence, in order to reach the initial state we need to take into account 8 states, four of which are close to the Fermi surface. As a result, a small parameter determining the threshold field due to commensurability becomes still smaller, and instead of the factor $\left(\Delta/\epsilon_\mathrm{F}\right)^2$, we get

$$\kappa_\mathrm{T}=\left(\Delta^3/\epsilon_\mathrm{F}^4\right)\max\{T,\eta\} \tag{2.12}$$

The region of applicability of the equations given above is sufficiently wide. As it will be shown later, in many cases they are reduced to phenomenological eqs. (1.1) and (1.2). Equations (2.5)-(2.11) can be used for the analysis of different problems related to the kinetics of the CDW. We begin with the simplest case of uniformly sliding CDW in a constant field E.

4.9.3 3. Uniform sliding of the CDW

3.1. Stationary case

Let us consider the current-carrying state of a CDW conductor when an applied electric field exceeds the threshold value significantly ($E \gg E_{\mathrm{T}}$), and the pinning effects may be neglected. Suppose that the gap is opened at the whole Fermi surface ($\eta < \Delta$), and we can use eqs. (2.5a,b). Then, the function n_1 has the equilibrium form $n_1 = \tanh(\epsilon/2T)^*$, and n_z is deter-

mined from eq. (2.5a) immediately,

$$n_z = (evE - \nu_{\mathrm{b}} G_- \dot{\varphi}/2)\, \frac{\partial n_1}{\partial \epsilon}/\nu(\epsilon), \tag{3.1}$$

where $\nu(\epsilon) = 2\,[\nu_{\mathrm{b}}\epsilon/\xi + \nu_0 \Delta^2 \epsilon/\xi^3]$.
Using this expression, we find the current density

$$j = \sigma_1 E + \sigma_2 \dot{\varphi}/el \tag{3.2}$$

from eq. (2.6a), and the relation between CDW velocity and field E

$$\gamma \dot{\varphi}/l = eE \tag{3.3}$$

from eq. (2.9). Here $l = v/\nu_{\mathrm{b}}$ is the mean-free-path length. The coefficients in eqs. (3.2) and (3.3) can be calculated in limiting cases of low ($T \ll \Delta$) and high ($T \gg \Delta$) temperatures (Artemenko and Volkov 1981a): (a) $T \ll \Delta$; $\sigma_1 = \sigma_{\mathrm{N}} 2\sqrt{\pi} T\Delta\,(\nu_{\mathrm{b}}/\nu_0)\exp(-\Delta/T)$, $\sigma_2 = \sigma_{\mathrm{N}}$, $\gamma^{-1} = (T/\Delta)\ln(T/\eta_0) \times \exp(\Delta/T)$; (b) $T \gg \Delta$; $\sigma_1 = \sigma_{\mathrm{N}}$, $\sigma_2 = (\pi/4)(\Delta/T)\sqrt{\nu_0/\nu_{\mathrm{b}}}\,\sigma_{\mathrm{N}}$, $\gamma^{-1} = \frac{1}{2}\pi \ln(\Delta/\eta_0)$. Calculating the coefficient γ we cut the diverging integrals at energies $\epsilon - \Delta \approx \eta_0$.

It follows from the expressions given above that the contribution of the CDW to the conductivity is small if the temperature T is close to the temperature of the Peierls transition T_{p} (i.e. $\Delta \ll T$). The conductivity of free carriers σ_1 in this case is nearly the same as in the normal state σ_{N}. At low temperatures ($T \ll \Delta$) the conductivity of free carriers is exponentially small as it should be in the semiconducting state. The CDW conductivity is exponentially large in this case because the only friction mechanism we have taken into account is the interaction of the CDW with quasiparticles, the number of which is exponentially small at low temperatures so that the friction coefficient γ is also small: $\gamma \sim \exp(-\Delta/T)$.

Actually, there exist another friction mechanism contributing to γ. In particular at temperatures lower than Δ but higher than the characteristic phonon frequencies ($\sim 50 - 100$ K (Sekine et al. 1987, Escribe-Filippini et al. 1987, Monceau et al. 1987)), an effective friction mechanism is the interaction of the CDW with phonons. For example, Brazovskii (1979) calculated phasons damping due to multiphonons processes. The phason damping coefficient at $\omega \to 0$ and $k \to 0$ coincides with γ because the uniformly sliding CDW corresponds to phasons with $\{\omega, k\} \to 0$. But Brazovskii studied the case of uncorrelated phases on different chains; hence, his results can not be applied directly to those materials where the CDW phase φ is ordered in transverse directions.

Analogous processes of CDW damping were analysed by Takada et al. (1985). Supposing that the phasons spectrum has a sound-like form, they obtained the result $\gamma \sim T^2$. But, at $T < \Delta$ the phasons spectrum is more complicated (see section 4.1). This circumstance may change the tem-

perature dependence of γ. The requirement that the temperature should be high enough for

[0]*The function n_1 is related to the ordinary Fermi distribution function f : $n_1 = 1 - 2f$.

thermal excitation of short-wave phonons is necessary because only in this case the Umklapp-processes providing relaxation of the total momentum of the electron-phonon system are possible. The situation here is just the same as in normal metals with closed Fermi surface (see, for example, section 4.4 in Abrikosov's book 1987). At temperatures lower than phonon energies near the Brillouin zone boundary $\hbar\omega_{\rm ph} = T_0$ the phonon contribution to γ should be exponentially small $\sim \exp(-T/T_0)$ because the Umklapp-processes become very weak. It means that at $T < T_0$ the velocity of the CDW and the CDW contribution to the current (see eq. (3.2)) should be very large. Perhaps, this is the reason of sharp current rise at $E > E_{\rm T}$ which was observed in blue bronze at helium temperatures (Mihaly and Beauchene 1987) and in $NbSe_3$ in strong magnetic fields opening the gap at the Fermi surface (Coleman et al. 1987).

Ong and Zhang (1986) observed a relation between the conductivity in low fields σ_1 and the conductivity σ^* in high fields $E \gg E_{\rm T}$. It was established, for example, that in the semiconducting material TaS_3, where σ_1 diminishes as T decreased, $\sigma_1 \sim \sigma^*$. Such a proportionality is not described by the theory presented above. If one takes into account nonuniform deformations of the CDW during its sliding, one may obtain corrections to σ_∞ (note, that $\sigma_\infty = \sigma(E \to \infty)$) which are temperature dependent (see section 4.3.1).

Let us consider now the CDW sliding in a system with metallic conductivity at $T < T_{\rm p}$ (for instance, $NbSe_3$). In this case $\eta_0 > \Delta$; hence, to calculate the CDW conductivity, it is necessary to use the microscopic equations for the Green functions (see Appendix) (Gor'kov and Dolgov 1979, Artemenko and Volkov 1981b). Calculation gives for the current density the following result:

$$j = \sigma_{\rm N} E(1-a) + \sigma_{\rm N}(\dot\varphi/el)(a + |b|/2)$$

and for the relation between the field E and the CDW velocity

$$\dot\varphi/el = E(1 + |b|/2a)$$

where

$$a = \int {\rm d}\epsilon \frac{{\rm i}\Delta \langle F_+ \rangle}{8T\nu_{\rm b}\cosh^2(\epsilon/2T)}, \quad b = -\int {\rm d}\epsilon \frac{\partial \langle G_- \rangle}{\partial \epsilon}\frac{\tanh(\epsilon/2T)}{2}$$

the angular brackets mean the averaging over transverse momentum $p_\perp$, $F_+ = f^{\rm R} + f^{\rm A}, G_- = g^{\rm R} - g^{\rm A}$. The conductivity is equal to $\sigma_1 = \sigma_{\rm N}(1-a)$ in weak fields, and $\sigma_\infty = \sigma_{\rm N}[1 + |b| + b^2/4a]$ in strong fields. For the case of a spectrum in transverse direction $\eta(p_\perp) = \eta_0 \cos(\boldsymbol{p}_\perp \boldsymbol{a})$, estimations give for a and b : $a \sim \Delta^2/\nu_{\rm b}T, |b| \sim \Delta^2/T$ if $\nu \ll \eta_0 \ll T$ (Gor'kov and Dolgov 1979), and $a \sim \Delta^2/\nu_0\eta_0, |b| \sim \Delta^2/\eta_0^2$ if $\nu, T \ll \eta_0$ (Artemenko and Volkov 1981b).

In both cases $a \gg |b|$. It means that when the temperature is decreased below $T_{\rm p}$, the conductivity in weak fields is diminished by the magnitude $(\sigma_{\rm N} a)$ due to gap appearance on the Fermi surface. The CDW sliding compensates this decrease of σ and leads to a slight increase (by $\sigma_{\rm N}|b|$) in σ with respect to $\sigma_{\rm N}$. Such a behaviour of the conductivity was observed in $NbSe_3$ (Ong and Monceau 1977) and was explained for the first time by Gor'kov and Dolgov (1979).

We turn now to the CDW sliding in moderate fields $E \geqslant E_{\rm T}$.

3.2. Nonstationary case

The problem of developing a theory of the CDW sliding in arbitrary fields $E \geqslant E_{\rm T}$ is much more difficult. This is related to the fact that the CDW in most materials is not commensurate, and CDW pinning is caused by an interaction of the deformed CDW with impurities randomly distributed in the crystal. The problem is simplified essentially in the case of the commensurate CDW which can be considered as being spatially uniform. Then, the expression for the current (3.2) remains to be valid, and the relation for the CDW velocity should be modified by taking

into account the CDW interaction with the underlying lattice (eq. (2.11)). Instead of eq. (3.3), we have

$$\gamma\dot{\varphi}/el = E - E_{\mathrm{T}}\sin(M\varphi), \tag{3.3'}$$

where $E_{\mathrm{T}} = 2\Delta^2\kappa_{\mathrm{T}}/\lambda v$ at $T \ll \Delta$ and $E_{\mathrm{T}} = 8\Delta T\sqrt{\nu_{\mathrm{b}}/\nu_0}\kappa_{\mathrm{T}}/\lambda\pi v$ at $T \gg \Delta$.
The model of the CDW conductor described by eqs. (3.2) and (3.3') is known as the rigid CDW model (Grüner et al. 1981, Artemenko and Volkov 1981a, Monceau et al. 1982). Strictly speaking, this model is applicable only to the commensurate case (Artemenko and Volkov 1981a), but it is used also for the qualitative description of the CDW which is pinned by impurities; in this case one assumes $M = 1$ (Grüner et al. 1981). The applicability of this model to the last case may be justified for short samples and weak pinning (Klemm and Schriffer 1983, Robbins and Klemm 1986).

As was mentioned above, pinning of the CDW in available materials with Fröhlich conductivity is determined by impurities, but not by commensurability effects which turn out to be unimportant. The matter is that the most materials are not commensurate ($NbSe_3$, $m-TaS_3$, blue bronze, etc.). The transition to a state with commensurate CDW occurs in $o-TaS_3$ as temperature decreases (see, for example, Grüner and Zettl 1985, Monceau 1985). Let us estimate the magnitude of the threshold field for commensurate o- TaS_3 using eq. (2.12). Taking the values $\Delta \sim 0.1\mathrm{eV}, \Delta/\epsilon_{\mathrm{F}} \sim T/\Delta \sim 0.1, v \sim 10^7$ cm/s, we get $E_{\mathrm{T}} \sim 10^{-2}$ V/cm. This value is less than the
field $E_{\mathrm{T}} \sim 0.1-1$ V/cm which is observed in $o-TaS_3$ and seems to be determined by impurity pinning.

Equations (3.2) and (3.3) describing the rigid CDW are analogous to equations for a Josephson contact (see, e.g. Aslamazov and Volkov 1986). Performing the integration of these equations, one can obtain the rate of the phase increase $\dot{\varphi}$ which is proportional to the CDW velocity. If we have the voltage-biased case, then the solution for $\dot{\varphi}$ at $E \geqslant E_{\mathrm{T}}$ is

$$\gamma\dot{\varphi}/el = \left(E^2 - E_{\mathrm{T}}^2\right) / \left[E + E_{\mathrm{T}}\sin\left(\left(el\sqrt{E^2 - E_{\mathrm{T}}^2}/\gamma\right)t\right)\right]. \tag{3.4}$$

We put here, for brevity, $M = 1$. Therefore, the CDW moves with temporally variable velocity. The form of the current-voltage characteristic (CVC) is obtained by averaging eqs. (3.2) and (3.4) over time

$$\bar{j} = \sigma_1 E + (\sigma_2/\gamma)\sqrt{E^2 - E_{\mathrm{T}}^2} \tag{3.5}$$

The CDW conductivity σ_{CDW} at high fields is determined by expansion of eq. (3.5)

$$\sigma_{\mathrm{CDW}}(E) = (\sigma_2/\gamma)\left(1 - \frac{1}{2}E_{\mathrm{T}}^2/E^2\right) \tag{3.6}$$

The correction to $\sigma_{\mathrm{CDW}}(\infty) = \sigma_2/\gamma$ determined by the second term diminishes as E increases, and weakly depends on the temperature T if the dependence $\gamma(T)$ is weak (for example, when CDW damping is due to phonon mechanism).

In the current-biased case* the CVC has an s-shaped form (Artemenko and Volkov 1981b, Monceau 1985)

$$j = \sigma_1\bar{E} + \left[j^2 - \left(\sigma_1\bar{E}\right)^2\right]^{1/2} / (1 + \gamma\sigma_1/\sigma_2) \tag{3.7}$$

and the CDW conductivity at large currents equals to

$$\sigma_{\mathrm{CDW}}(\bar{E}) = (\sigma_2/\gamma) - \frac{1}{2}\sigma_1\left(E_{\mathrm{T}}/\bar{E}\right)^2 / (1 + \gamma\sigma_1/\sigma_2). \tag{3.8}$$

Now the frequency of oscillations is equal to

$$\omega_{\rm os} = el\frac{\left[j^2 - \left(\sigma_1\bar{E}\right)^2\right]^{1/2}}{\sigma_2\left(1+\gamma\sigma_1/\sigma_2\right)} \tag{3.9}$$

It is interesting to note that in this case the correction to $\sigma_{\rm CDW}(x)$ has another form. In particular, at low temperatures, when $\sigma_1 \ll \sigma_2/\gamma$, one has $\sigma_{\rm CDW}(E) - \sigma_{\rm CDW}(\infty) = -\sigma_2 E_{\rm T}^2/\left(2\gamma_{\rm eff}\bar{E}^2\right)$, where the effective damping coefficient $\gamma_{\rm eff} = \gamma\sigma_2/\sigma_1$ increases exponentially with decreasing temperature. This fact, being related to the appearance of oscillations of the

quasiparticle current, plays an important role when the CDW moves nonuniformly (see section 4.3).

In the current-biased case, voltage oscillations with frequency (3.9) take place, and in the voltage-biased case there are current oscillations with frequency el $\left(E^2 - E_{\rm T}^2\right)^{1/2}/\gamma$.

The model of the rigid CDW sliding in a periodical potential was used for the explanation of oscillations in CDW conductors (bulk mechanism of generation).

Under the influence of an external a.c. signal $E = E_{\rm b} + E_\Omega\sin(\Omega t)$, Shapiro steps appear on the CVC, their amplitudes varying according to the formula $\Delta E_n = J_n\left(eE_\Omega l/\Omega\right)$, where J_n is the Bessel function of the nth order. For example, to find the dependence of the threshold field $E_{\rm T}$ on the amplitude E_Ω one can present the phase φ in the form $\varphi = \varphi_0 + \psi$, where ψ is a small function oscillating with frequency Ω. At $\Omega \gg elE_{\rm T}$ it equals to $\psi = -(elE/\Omega)\cos(\Omega t)$. Then, we perform an averaging over rapid oscillations with frequency Ω in the equation for the slowly varying function φ_0 with frequency $\omega_{\rm os}$:

$$E_{\rm T}\overline{\sin\left(\varphi_0 - (elE_\Omega/\Omega)\cos(\Omega t)\right)} = E_{\rm T}J_0\left(elE_\Omega/\Omega\right)\sin\varphi_0.$$

Hence, the threshold field of an irradiated sample is diminished. Such a behaviour was observed in $NbSe_3$ (Latyshev et al. 1987, Thorn et al. 1987).

4.9.4 4. Nonuniform distortions of the *CDW*

If the electric field E is not much larger than the threshold value $E_{\rm T}$ and the interaction with impurities is the main mechanism of pinning, then the CDW moves like a deformable object which experiences nonuniform deformations leading to a change of the effective friction coefficient. In order to understand the role of nonuniform deformations, it is useful to analyze small nonuniform perturbations of the CDW in frames of the 'classical' model. In fact, small perturbations of the CDW can be regarded as collective excitations of the system, so-called phasons. These excitations are coupled oscillations of electron and phonon systems, and can be detected by means of inelastic neutron scattering (Escribe-Fillipini et al. 1987, Monceau et al. 1986, Monceau et al. 1987), Raman scattering (Sekine et al. 1987) and measurements of their contribution to heat capacity at low temperatures (Biljakovic et al. 1986).

4.1. Phasons

The phason spectrum can be determined from eqs. (2.4)-(2.9). We consider the case when the electronic spectrum is almost one-dimensional, so we
neglect the transverse electron velocity in eqs. (2.4)-(2.9): $\langle v_\perp^2\rangle = 0$. Linearizing eqs. (2.4)-(2.5) with respect to small perturbations $\delta n = n - n_{\rm eq} \sim \exp(+{\rm i}\omega t - {\rm i}\boldsymbol{kr})\delta n$ we get $\omega\delta n_1 = (kv)\delta n_z$,

[0*] This case is realized when the value of an external impedance $Z_{\rm ext}$ ($\omega_{\rm os}$) at characteristic frequency of oscillations $\omega_{\rm os} = el\left(E^2 - E_{\rm T}^2\right)^{1/2}/\gamma$ is large, or depinning, and oscillations occur only in a part of the sample. In the last case the resistance of the other part of the sample plays the role of $Z_{\rm ext}$.

where k is the component of the wave vector parallel to the chain direction, $n_{\rm eq} = \tanh(\epsilon/2T)$ for n_1 and $n_{\rm eq} = 0$ for n_z. Provided the condition $\omega \ll \nu_{\rm f,b}$ is fulfilled, we obtain for n_z an expression of the type of eq. (3.1) with the substitution $E \to \tilde{E} \equiv E - k^2 v\varphi/2$ and $\nu(\epsilon) \to \nu(\epsilon) + (kv)^2/{\rm i}\omega$ in it.

Consider for simplicity the case of low temperatures when $\sigma_1/\sigma_2 \ll 1$. From eq. (2.6) we obtain for the current density along the chains

$$j = \sigma_1 \tilde{E} F_1 + \sigma_2 {\rm i}\omega\varphi/el + (\epsilon_\Delta/4\pi)\, {\rm i}\omega E \tag{4.1}$$

where a function F_1 can be written schematically as $F_1 = {\rm i}\omega/({\rm i}\omega + k^2 D)$. It describes quasiparticle diffusion in the case of nonuniform CDW distortion. In particular, it describes the screening of these deformations by quasiparticles. The expression for F_1 can be calculated exactly in limiting cases: $F_1 = 1$ when $\omega \gg k^2 D$ and $F = {\rm i}\omega/k^2 D$ when $\omega \ll k^2 D$, where $D = (v^2/\nu_0)\sqrt{2/\pi}(T/\Delta)^{3/2}$.

Starting from eq. (2.9), we get for the CDW phase

$$\varphi\left[4\frac{-\omega^2 + k_\perp^2 s^2}{\omega_0^2} + \frac{k^2 v^2}{\Delta^2}\right] = \frac{2ve}{\Delta^2}\left[E - E_{\rm T}\varphi - \gamma {\rm i}\omega/el\right] \tag{4.2}$$

where it is assumed that the pinning is caused by the commensurability effects described by eq. (2.11) with $M = 1, \omega_0^2 = \lambda\omega_Q^2, \gamma$ describes the CDW damping discussed in section 3.1.

In order to obtain the spectrum of oscillations, we find a relation between E and φ equating j to zero. This is equivalent to the quasineutrality condition which is valid in virtue of large values of $\epsilon_\Delta \sim \omega_{\rm p}^2/\Delta^2$ (where $\omega_{\rm p} = e^2 n/m, n$ is the free electrons density at $T > T_{\rm p}$). Neglecting unimportant terms which are small at low temperatures, we write down the dispersion relation in the following form:

$$\frac{\omega^2}{\omega_0^2} = \frac{\kappa_{\rm T}}{\lambda} + \frac{{\rm i}\omega\gamma}{\omega_1} + \frac{k_\perp^2 s^2}{\omega_0^2} + \frac{3}{2}\left[1 + \frac{3}{2}\frac{\tilde{\sigma}_1\omega_1}{{\rm i}\omega + k^2 D}\right]^{-1} \tag{4.3}$$

where $\omega_1 = 2\Delta^2/\nu_{\rm b} \gg \Delta, \tilde{\sigma}_1 = \sigma_1/\sigma_2 \approx \sigma_1/\sigma_{\rm N}$. Since $E_{\rm T} \leqslant 1$ V/cm, and $\Delta \sim 1000$ K (for example, in $TaS_3 \Delta = 800$ K), then $\kappa_{\rm T} \sim 10^{-5} - 10^{-6} \ll 1$.

The phason spectrum determined by eq. (4.3) has a different form depending on the ratio $\tilde{\sigma}_1\omega_1/\omega_0$.

(a) $\omega_0 \gg \tilde{\sigma}_1\omega_1$

This case is realized at sufficiently low temperatures. Then, we have for $\omega' = {\rm Re}\,\omega$

$$\omega'^2 = \omega_0^2\left(\frac{3}{2} + \kappa_{\mathbf{T}}\right) + k_\perp^2 s^2/\omega_0^2 \tag{4.4}$$

Hence, at $k \to 0$ there is a threshold frequency $\sqrt{3/2}\omega_0$ even in the absence of pinning (Lee et al. 1974). The phason damping is weak provided the condition ${\rm Im}\,\omega = \omega'' = \omega\,(\gamma/\omega_1 + \tilde{\sigma}_1\omega_1/\omega^2) \ll \omega'$ is valid, that is, $\tilde{\sigma}_1\omega_1 < \omega_0 < \omega_1/\gamma$.

(b) $\omega_0 \ll \tilde{\sigma}_1\omega_1$.

In this case the dispersion relation has the following form

$$\frac{\omega^2}{\omega_0^2} = \frac{\kappa_{\rm T}}{\lambda} + \frac{k_\perp^2 s^2}{\omega_0^2} + \frac{k^2 D}{\omega_1\tilde{\sigma}_1} + \frac{{\rm i}\omega}{\omega_1}\left(\gamma + \frac{1}{\tilde{\sigma}_1}\right), \tag{4.5}$$

provided $|{\rm i}\omega + k^2 D_1| \ll \tilde{\sigma}_1\omega_1$.

We note two most important features following from eq. (4.5). Firstly, the phason velocity $\omega'/k \sim (D/\omega_1\tilde{\sigma}_1)^{1/2} \sim (\omega_0\xi)\,(T/\Delta)^{1/4}\exp(\Delta/2T)$ increases exponentially with decreasing temperature. Secondly, the damping constant is changed, and increases on cooling also: $\gamma_{\rm eff} = \gamma + 1/\tilde{\sigma}_1$ (compare with section 3.2). Both these features are related to the role of

quasi-particles which screen out nonuniform deformations of the phase with characteristic relaxation time σ_1^{-1}. The damping of oscillations with the spectrum (4.5) is weak at frequencies $\omega \gg \gamma\left(\omega_0^2/\omega_1\right) + \omega_0^2/\left(\tilde{\sigma}_1\omega_1\right)$.

At $|\mathrm{i}\omega + k^2 D| \gg \tilde{\sigma}_1\omega_1$, i.e. at $k^2 D \gg \tilde{\sigma}_1\omega_1$, formula (4.5) is not valid, and the dependence $\omega'(k)$ is described again by eq. (4.4). The dependence $\omega'(k)$ is shown qualitatively for both cases in figs. 1a and 1b.

The phason spectrum changes with increasing temperature. Near the transition temperature $T_\mathrm{p}, \sigma_1 \sim \sigma_\mathrm{N}$ and $\sigma_2 \sim \sigma_\mathrm{N}(\Delta/T) \ll \sigma_1$. Thus, nonuniform phase perturbations are easily screened by free carriers. This leads to a softening of the phase mode, and the phason spectrum in this case may be

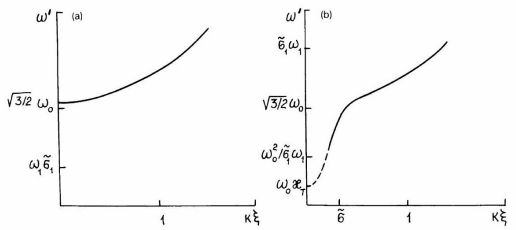


Fig. 1. Phason spectrum (a) for the case $\omega_{0} \equiv \sqrt{\lambda} \omega_{O} \gg \tilde{\sigma}_{1} \omega_{1} \equiv \Delta^{2} \tau\left(\sigma_{1} / \sigma_{N}\right)$; and (b) for the case $\omega_0 \ll \tilde{\sigma}_1\omega_1$ and $\xi = v/\Delta$.

written as

$$\omega^2 = \omega_0^2\left[\frac{\kappa_\mathrm{T}}{\lambda} + \frac{\pi}{16}\sqrt{\frac{\nu_0}{\nu_\mathrm{b}}}\frac{k^2v^2}{\Delta T} + \mathrm{i}\omega\frac{\nu_\mathrm{b}}{4\Delta T}\ln\left(\Delta/\eta_0\right)\right] + k_\perp^2 s^2.$$

In the limit of a pure conductor ($\nu \to 0$)

$$\omega^2 = \omega_0^2\left[\frac{\kappa_\mathrm{T}}{\lambda} + \frac{7\zeta(3)}{32\pi^2}\frac{k^2v^2}{T^2}\right].$$

Thus, near T_p the threshold frequency is caused by pinning only (Artemenko and Volkov 1981b).

4.2. Nonlinear screening

The dependence of the phason spectrum on σ_1 found in the preceding section, originates from the screening of nonuniform perturbations of the CDW by free carriers, their density being exponentially small at low temperatures. Using eq. (2.7) or starting from eq. (4.1) and continuity equation $-\mathrm{i}\omega\rho + \mathrm{i}kj = 0$, we can obtain an expression for the charge density in a low-frequency limit (Artemenko and Volkov 1981c)

$$\rho = -\frac{k_0^2}{4\pi}\left[\Phi\left(1 - N_\mathrm{s}\right) + \frac{1}{2}N_\mathrm{s}v\frac{\partial\varphi}{\partial x} - \frac{v^2\Delta}{3}\frac{\partial}{\partial\Delta}\left(\frac{N_\mathrm{s}}{\Delta^2}\right)\frac{\partial^2\Phi}{\partial x^2}\right] \tag{4.6}$$

where Φ is the electrostatic potential, k_0^{-1} is the Thomas-Fermi screening length in a normal state, N_s is the normalized condensate density. This expression, being valid for arbitrary temperatures, determines the charge density in the case of small CDW deformations. The first term on the right-hand side of eq. (4.6) is the contribution due to the charge density of free carriers, the second term determines the charge density created by CDW deformation, and the third term ascribes the modification of the dielectric constant $\epsilon_\Delta \sim \omega_\mathrm{p}^2/\Delta^2 \gg 1$ due to the

deformation of the Peierls gap. The expression (4.6) can be generalized to the case of a strong CDW deformation, when the deviation of the free carriers density from equilibrium is not small. To make this, we use eqs. (2.4) and (2.5). In the limit of low frequencies ($\omega\tau_\epsilon \ll 1, \tau_\epsilon$ is the energy relaxation time) the distribution function n_1 should have an equilibrium form with the chemical potential μ shifted from the center of the Peierls gap

$$n_1 = \tanh\left(\frac{\epsilon - \mu}{2T}\right), \tag{4.7}$$

where μ is, generally speaking, a spatially dependent function arisen due to screening of nonuniform CDW deformations by free carriers. The magnitude of μ is determined by the local quasineutrality condition $\rho = 0$,
where the charge density ρ is given by eq. (2.7) with n_1 determined by eq. (4.7). Thus we obtain (Artemenko et al. 1986)

$$2T\,(1 - N_\mathrm{s}) \sinh\left(\frac{\mu}{T}\right) = -v\frac{\partial\varphi}{\partial x} \tag{4.8}$$

It should be noted that eq. (4.8) holds for the case $k^2\xi^2 \ll 1 - N_\mathrm{s}$ only, because we omitted the third term in eq. (4.6). Inserting eq. (4.7) into eq. (2.5a), we obtain distribution function n_z, and then, using eqs. (2.6) we can calculate the current density

$$\dot{j}_\parallel = \sigma_1 \cosh\left(\frac{\mu}{T}\right)\mathscr{E}_\parallel + \sigma_2\dot{\varphi}/el + \frac{\epsilon_\Delta}{4\pi}\dot{E} \tag{4.9a}$$

$$\dot{j}_\perp = \sigma_\perp \cosh\left(\frac{\mu}{T}\right)\mathscr{E}_\perp \tag{4.9b}$$

where $\mathscr{E} = -\nabla\,(\Phi - \mu - v\varphi'/2)$ is the gradient of the electrochemical potential, $\sigma_\perp = 2\sigma_{\perp\mathrm{N}}\mathrm{e}^{-\Delta/T}\,(\nu_\mathrm{f} + \nu_\mathrm{b})\,/\nu_\mathrm{f}$ is the conductivity in transverse direction.

The equation for the phase, derived from eq. (2.9), has a form similar to eq. (4.2)

$$\frac{\Delta^2}{2v}\left[\frac{4}{\omega_0^2}\left(\frac{\partial^2}{\partial t^2} - s^2\nabla_\perp^2\right) - \xi^2\frac{\partial^2}{\partial x^2}\right]\varphi = e\,(E - E_\mathrm{T}\sin\varphi) + \mu'\,(1 - N_\mathrm{s} - A)$$
$$\times \cosh\left(\frac{\mu}{T}\right) + \Gamma\dot{\varphi}/l - \frac{2}{\lambda\xi}\sum_i V_Q\delta\,(r - r_i)\sin\,(\varphi - Qr_i) \tag{4.10}$$

with

$$A = \sqrt{2T/\Delta}\,(\nu_\mathrm{b}/\nu_0)\exp(-\Delta/T), \quad \Gamma = \gamma\cosh(\mu/T), \quad \xi = v/\Delta$$

The physical meaning of the nonlinear terms containing μ is rather simple. The free charge carriers in CDW conductors are analogous to the electrons and holes in usual semiconductors. If a nonuniform perturbation is static or quasistatic, then the electron and the hole densities are determined in the same manner as in equilibrium state: $n = N_0\exp(\mu/T)$ and $p = N_0\exp(-\mu/T)$.* Then, in accordance with eq. (4.8) $\rho = e(p - n) = -2eN_0\sinh(\mu/T)$. Therefore, the electron and hole current densities with the help of Einstein's relation $D_e = \mu_e T/e$ (where μ_e is quasiparticle mobility) can be presented in a form

$$j = j_\mathrm{n} + j_\mathrm{p} = -e\mu_\mathrm{e}n\frac{\partial\Phi}{\partial x} + eD_\mathrm{e}\frac{\partial n}{\partial x} - e\mu_\mathrm{p}p\frac{\partial\Phi}{\partial x} - eD_\mathrm{e}\frac{\partial p}{\partial x}$$
$$= -2e\mu_\mathrm{e}N_0\cosh\left(\frac{\mu}{T}\right)\frac{\partial}{\partial x}(\Phi - \mu/e)$$

This expression differs from the first term of eq. (4.9a) by $v\varphi'/2$ in brackets. This difference originates in the shift of the energy by $v\varphi'/2$ (see Appendix). The chemical potential μ determines a band bending caused by the internal electric field. Some effects, interpreted as a band bending, were observed in thermopower experiments by Itkis et al. (1986) and in the experiment in which the threshold field was spatially dependent (Latyshev et al. 1989), see also fig. 2.

Nonlinear screening results in various effects. For instance, screening of the CDW charge by quasiparticles influences the form and the length of a phase soliton (the discommensuration). An equation for the phase soliton, forming a domain wall (i.e. the phase does not depend on coordinates which are perpendicular to the chain direction), can be obtained from eqs. (4.8)-(4.10) with $j = 0$, and φ independent on time,

$$L_0^2\varphi'' - \sin\varphi\cosh(\mu/T) = 0 \tag{4.11}$$

with $L_0^2 = v/\left(eE_{\mathrm{T}}\left(1 - N_{\mathrm{s}}\right)\right)$. In the limit of small μ/T the solution of eq. (4.11) is $\varphi = 4\tan^{-1}\left(\mathrm{e}^{x/L_{\mathrm{o}}}\right)$. If $\mu \geqslant T$, one should exclude $\cosh(\mu/T)$ from eq. (4.11) with the help of eq. (4.8). Then the solution of eq. (4.11) becomes

$$\varphi = -2\tan^{-1}\left[1 + \frac{\left(L_0 eE_{\mathrm{T}}\right)^2}{T^2}\sinh\left(\frac{x}{L_0}\right)\right].$$

In this case the characteristic soliton length is $L_{\mathrm{s}} = L_0/\left[1 + \left(L_0 eE_{\mathrm{T}}/T\right)^2\right]^{1/2}$. The dependence of L_{s} on temperature is not monotonous. At low temperatures $L_{\mathrm{s}} \sim T/E_{\mathrm{T}}$, that is, L_{s} increases with increasing T, but at some temperature T_{m}, determined by equality $eL_0E_{\mathrm{T}} = (T\Delta/2)^{1/2}$, L_{s} reaches the maximum value $eL_{\mathrm{s}} \sim T_{\mathrm{m}}/E_{\mathrm{T}}$, and then L_{s} diminishes with further increase of T. The estimation for TaS_3 gives the value $L_{\mathrm{s\,max}} \sim 60\mu$ m at $T_{\mathrm{m}} \sim 75$ K.

It should be noted that we have considered the simplest model with symmetric electron spectrum and the Fermi level, situated at the center of the energy gap. Then, any CDW phase deformation increases the quasiparticle conductivity because $\sigma_1 \cosh \mu/T > \sigma_1$. If there is a deviation from the electron-hole symmetry (and this is a realistic experimental situation, see e.g. Borodin et al. 1986a), the CDW deformations, corresponding to the opposite signs of μ lead to an increase or decrease of the quasiparticle conductivity. Various hysteresis phenomena, observed in electric fields $E < E_{\mathrm{T}}$ (Higgs and Gill 1983, Mihaly and Mihaly 1984, Borodin et al. 1986b, Ong and Wang 1987) may be explained as a manifestation of CDW phase deformations leading to local conductivity variations.

As noted above, practically in all CDW conductors pinning is caused by the interaction of the CDW with impurities. Thus, the description of the pinning with the help of eq. (2.11) is only a crude approximation, in spite of the fact, that many phenomena in Peierls conductors may be explained qualitatively on this ground. Thus, to describe pinning effects we have to use eq. (2.10), which not only breaks the homogeneity of the CDW phase, but destroys the long-range order of the CDW phase (Efetov and Larkin 1977). In this case nonuniform deformations and screening effects in a moving CDW play the major role. In the next section we shall analyze the contribution of the CDW deformations and of the screening effects to the CDW conductivity in static electric field $\sigma_{\mathrm{CDW}}(E)$ and a.c. conductivity $\sigma_{\mathrm{CDW}}(\omega)$.

4.3. The sliding of the deformed *CDW*

Theoretical analysis of the CDW, interacting with random impurity pinning centers, is a much more complicated problem than the analysis of the uniform CDW. Nevertheless, many results, concerning the system with impurity pinning were obtained theoretically. For example,

[0]*We assume a symmetrical case, when mobilities, densities of states, etc., for electrons and holes are equal.

Lee and Rice (1979) estimated the threshold field E_{T} for the incommensurate CDW, pinned by impurities, Efetov and Larkin (1977) calculated the phase correlation length L_φ strictly summing up an expansion for the phase in powers of V_Q. Robbins and Klemm (1986) explained the dependence of the CVC shape on the relation between L_φ and sample length. Many results were obtained numerically (see e.g. Littlewood 1987). An analytical solution for the CDW phase and for the CVC form at $E \gg E_{\mathrm{T}}$ was obtained by Sneddon et al. (1982).

Equations which describe sliding of the deformable CDW can be obtained either directly from eqs. (2.4)-(2.7) in the limit of $\omega\tau_\epsilon \gg 1$, when one can drop $I_{\text{e-ph}}$ in eq. (2.5b) as in section 4.1, or with the help of eqs. (4.8)-(4.10) with $\mu \ll T$ for the case of low frequencies, $\omega \ll 1/\tau_\epsilon$. In both cases the final results are close. For instance, in the second case the current density is expressed by eqs. (4.9) and the equation for the phase has the form (4.10) with an electric field E, created both by an external applied field and by the field, induced by the CDW phase deformations. We exclude potentials Φ and μ using continuity and neutrality equations. Then considering sufficiently low frequencies and neglecting the displacement current in eq. (4.9a) and the inertia term in eq. (4.10), we obtain for the Fourier transform of the phase the following equation

$$\left[\hat{D}k^2 + \gamma_k \frac{\partial}{\partial t}\right] \varphi_k - \tilde{\sigma}_1 elE_{\mathrm{T}} (\sin\varphi)_k - U_{\mathrm{im}}\tilde{\sigma}_1 \times \sum_i \exp(\mathrm{i}kr_i) \sin(\varphi_i + Qr_i) = I_0\delta_{k,0} \tag{4.12a}$$

with

$$\hat{D}k^2 = \left(\tilde{\sigma}_1 D_{\parallel\mathrm{p}} + D_{\parallel\mathrm{e}}\right) k_\parallel^2 + \tilde{\sigma}_1 D_{\perp\mathrm{p}} k_\perp^2, \quad \gamma_k = \gamma\tilde{\sigma}_1 + \frac{D_{\parallel\mathrm{e}}k_\parallel^2}{D_{\parallel\mathrm{e}}k_\parallel^2 + D_{\perp\mathrm{e}}k_\perp^2}$$
$$D_{\parallel\mathrm{p}} = vlT\nu_{\mathrm{b}}/\Delta\nu_0; \qquad U_{\mathrm{im}} = eV_Q/(\xi\lambda);$$

$\langle j\rangle$ is the spatial average of the current density along the chains.

It is seen from eq. (4.12a) that both the damping rate and the stiffness of the CDW are renormalized by the terms containing electronic diffusion coefficients. Note that at low temperatures $\tilde{\sigma}_1 D_{\parallel\mathrm{p}} \ll D_{\parallel\mathrm{e}}$, but we shall retain $\tilde{\sigma}_1 D_{\parallel\mathrm{p}}$ as a semiphenomenological parameter in order to discuss different limiting cases at the end of the next subsection.

The main distinction of eq. (4.12a) from the phenomenological eq. (2.1) is a temperature dependence of the factors, containing $\tilde{\sigma}_1 \sim \exp(-\Delta/T)$, which leads, for example, to a renormalization of the phase coherence length L_φ and to a temperature dependence of the threshold field E_{T} for the case of weak impurity pinning, if one calculates E_{T} in the frame of approaches by Lee and Rice (1979) or by Klemm and Schrieffer (1983). The investigation of the CDW dynamics on the basis of eq. (4.12a) is rather complicated. Therefore we shall use a simplified form for a pinning term, which will permit us to reproduce the main results of the papers, quoted above. Thus, we will use a simplified version of eq. (4.12a)

$$\left(\hat{D}k^2 + \gamma_k \frac{\partial}{\partial t}\right) \varphi_k + \tilde{\sigma}_1 \left[(V_{\mathrm{T}} + V_{\mathrm{f}}) \sin\varphi\right]_k = I_0\delta_{k,0} \tag{4.12b}$$

The threshold field ('field' inside the round brackets) consists of two parts, one of them is the average value $V_{\mathrm{T}} = eE_{\mathrm{T}}l$, and the second, V_{f}, determines the fluctuating part, its average value $\langle V_{\mathrm{f}}(\boldsymbol{r})\rangle = 0$, but the correlator differs from zero

$$\langle V_{\mathrm{f}}(\boldsymbol{r}) V_{\mathrm{f}}(\boldsymbol{r}')\rangle = \int \frac{\mathrm{d}\boldsymbol{k}}{(2\pi)^3} \exp\left[\mathrm{i}\boldsymbol{k}(\boldsymbol{r} - \boldsymbol{r}')\right] V_{\mathrm{f}}^2(\boldsymbol{k}) \neq 0 \tag{4.13}$$

For the spectral density V_{f}^2 we use the Gaussian distribution

$$V_{\mathrm{f}}^2(\boldsymbol{k}) = (2\pi)^2 V_{\mathrm{fo}}^2 \exp\left(-k_{\parallel}^2 R_{\parallel}^2 - k_{\perp}^2 R_{\perp}^2\right)$$

The correlation radii $R_{\parallel}$and $R_{\perp}$ at $E \ll E_{\mathrm{T}}$ may be related to the Lee-Rice domain dimensions (Lee and Rice 1979). At $E \geqslant E_{\mathrm{T}}$ the magnitude of the correlation length changes (this problem is discussed by Fisher (1983, 1985)). As was shown by Littlewood and Varma (1987) the equations for the CDW, interacting with pinning centers according to eq. (2.10), can be reduced to an equation similar to eqs. (4.12b) and (4.13) with $R_{\parallel}, R_{\perp} = 0$. However, we will retain a finite value of R in order to reproduce finite-size effects analyzed by Robbins and Klemm (1986). That is, we shall study both the single-domain case, when the CDW phase is coherent in the whole volume, and the multiple-domain case, when the size of a sample is large in comparison with the phase coherence length.

4.3.1. *CDW* sliding in strong d.c. field $E \gg E_{\mathrm{T}}$

Starting from eq. (4.12b), we shall calculate the $I - V$ curve in the high field limit $V_0 = E_0 el \gg V_{\mathrm{T}}$ $\left(E_0 = \langle \bar{E} \rangle\right.$ is the spatially and temporally averaged
field. We seek the solution of eq. (4.12b) in a form $\varphi_k = \varphi_0 \delta_{k,0} + \psi_k$, $\varphi_0 = \Omega t + \psi_0$ is the spatially averaged phase, the functions ψ_0 and ψ_k are small as long as $E \gg E_{\mathrm{T}}$. The frequency Ω is determined by I_0 and V_0 (see eq. (4.9a))

$$I_0 = \tilde{\sigma}_1 V_0 + \overline{\dot{\varphi}}_0, \quad \overline{\dot{\varphi}_0} = \Omega \tag{4.14a}$$

Using eqs. (4.14a) and (4.12a) we obtain the relation between I_0 and V_0

$$I_0 = \left(\tilde{\sigma}_1 + \gamma^{-1}\right) V_0 - \frac{V_{\mathbf{T}}}{\gamma} \overline{\sin \varphi_0} - \gamma^{-1} \int \frac{\mathrm{d}\boldsymbol{k}_1}{(2\pi)^3} \overline{\langle V_{\mathbf{f}}\left(\boldsymbol{k} - \boldsymbol{k}_1\right) \psi\left(\boldsymbol{k}_1\right)\rangle \cos \varphi_0} \tag{4.14b}$$

The first term in eq. (4.14b) is the sum of the quasiparticle and the CDW current at $E \to \infty$. The second term is the correction to the CDW current due to pinning effects in the frame of the rigid CDW model, it was calculated in section 3.2 (eqs. (3.6) and (3.8)). The last term (we shall denote it δI) describes the contribution of the CDW deformations to the conductivity. Expressing ψ_k from (4.12b) in the first order in V_f, and averaging δI in (4.14b) by means of (4.13), we find the contribution to the current from nonuniform perturbation of the CDW

$$\delta I = -\frac{1}{\gamma} \int \frac{\mathrm{d}\boldsymbol{k}_1}{(2\pi)^3} \langle V_{\mathrm{f}}\left(\boldsymbol{k} - \boldsymbol{k}_1\right) \psi\left(\boldsymbol{k}_1\right)\rangle = -\frac{\tilde{\sigma}_1 \Omega V_{\mathrm{fo}}^2}{2\gamma} F_2(\Omega), \tag{4.15a}$$

with

$$F_2 = \int \frac{\mathrm{d}\boldsymbol{k}}{(2\pi)} \gamma_k \left[\left(\hat{D} k^2\right)^2 + \left(\gamma_k \Omega\right)^2\right]^{-1}$$

We used here the relation $\Omega = V_0/\gamma$, which is valid when $\gamma \tilde{\sigma}_1 \ll 1$. The form of the function $F_2(\Omega)$ depends on the relation between the characteristic time of the diffusion over the domain of phase coherence $\tau_0 = R_{\parallel}^2/D_{\parallel \mathrm{e}} = R_{\perp}^2/D_{\perp \mathrm{e}}$ and the oscillation period $2\pi/\Omega$. If the size of the domain is large enough ($\Omega\tau_0 \gg 1 + \beta_{\perp}/\gamma$, where $\beta_{\perp} = \tilde{\sigma}_1 D_{\perp \mathrm{p}}/D_{\parallel \mathrm{e}}$), then the function F_2 is given by

$$F_2(\Omega) = \frac{\pi\sqrt{\pi}}{8} \frac{1}{D_{\perp \mathrm{e}} \tau_0 \sqrt{D_{\parallel \mathrm{e}} \tau_0} \Omega^2} \tag{4.15b}$$

If $\Omega\tau_0 \ll 1 + \beta_{\perp}/\gamma$, then

$$F_2(\Omega) = \frac{f_2}{D_{\perp e}\sqrt{D_{\|e}\Omega}}$$

with f_2 calculated for two limiting cases

$$\begin{aligned} f_2 =& \frac{\pi}{\sqrt{2}} \int_0^1 \mathrm{d}x \frac{\sqrt{x^2 + \tilde{\sigma}_1\gamma}}{\left[\beta_\perp + x^2\left(1 + \beta_\| - \beta_\perp\right)\right]^{3/2}} \\ =& \frac{\pi}{\sqrt{2}} \begin{cases} \frac{2\left[\sqrt{1+\beta_\|}+\sqrt{\beta_\perp}\right]^{-1}}{\sqrt{\beta_\perp}\sqrt{1+\beta_\|}}, & \gamma\tilde{\sigma}_1 \ll \beta^2 \\ \frac{\sqrt{\tilde{\sigma}_1\gamma}}{\beta_\perp\sqrt{1+\beta_\|-\beta_\perp}}, & \beta^2 \ll \tilde{\sigma}_1\gamma \ll 1 \end{cases} \end{aligned} \tag{4.15c}$$

where $\beta_\| = \tilde{\sigma}_1 D_{\|p}/D_{\|e}, \beta^2 = \beta_\perp/\left(1 + \beta_\| - \beta_\perp\right)$.
It follows from (4.15b) that, in the case of the large characteristic length of the threshold field variation ($\Omega\tau_0 \gg 1$), fluctuations of E_T result in a contribution to the CVC, similar to the contribution in the case of a rigid CDW mdel (see eqs. (3.6) and (3.8)) $\delta I \sim -\tilde{\sigma}_1/V_0$. It is worth to note the following. While the CDW contribution to the current in the rigid CDW model depends on whether we have the current- or voltage-biased case (see section 3.2), the contribution δI in the model of deformable CDW does not depend on this. As follows from eq. (4.15b), this contribution corresponds to the current-biased case always because δI is caused by phase fluctuations in a small part of the sample with the volume $\sim D_{\perp e}\sqrt{D_{\|e}}\Omega^{3/2}$ while the other part of the sample plays a role of large external resistance fixing the current.

If the size of a domain, in which the threshold field may be regarded as constant, is small enough ($\Omega\tau_0 \ll 1$), then the major contribution to the nonlinear part of the current is created by the fluctuations of $E_T : \delta I \sim -\sqrt{V_0}$. In this case the nonlinear correction to the conductivity of the CDW $\delta\sigma_{CDW} = \mathrm{d}\delta I/\mathrm{d}V_0 = -1/\sqrt{V_0}$ has a sign, opposite to the sign of the corresponding term in the rigid CDW model $\delta\sigma_{CDW} \sim 1/V^2$ (Sneddon et al. 1982).

According to (4.15) $\delta\sigma_{CDW}$ decreases as the temperature decreases, with the exception of the case of eq. (4.15c), if, in addition, one assumes $\beta_\| = \tilde{\sigma}_1\left(D_{\|p}/D_{\|e}\right) \gg 1$. This inequality can be satisfied only in the case when the diffusion of the quasiparticles is suppressed for some reasons, and effective stiffness of the CDW along the chains is not affected by the diffusion of free electrons. In this limit $\delta I \sim -\sqrt{V}/\sqrt{\tilde{\sigma}_1}$, which is in a qualitative agreement with experimental data. This result corresponds to the case when the damping rate is affected, but the stiffness of the CDW is not affected by the quasiparticle contribution (Sneddon 1984, Littlewood 1987).

Comparing the expression for δI at $V_0 \gg V_T$ and $\Omega\tau_0 \ll 1$ with the
corresponding result of Sneddon et al. (1982) we find that $V_f^2 \sim U_{im}^2 N_{im}$, where N_{im} is the impurity concentration.
The transition from a single-domain model ($\Omega\tau_0 \gg 1$) to a multipledomain model was studied theoretically by Robbins and Klemm (1986).

4.3.2. CDW conductivity in weak a.c. field

Now we calculate the CDW conductivity $\sigma_{CDW}(\omega) = \sigma_R + \mathrm{i}\sigma_I$ in a weak a.c. field. We confine ourselves to the case of low frequencies $\omega \ll \omega_0$ and temperature $T \ll \Delta$. On the basis of eq. (4.12b) we shall obtain results, explaining qualitatively some experimental data. From linearized eq. (4.12b) for the spatially averaged values of the current I_ω and voltage V_ω we obtain

$$I_\omega = \left[\tilde{\sigma}_1 V_T + \mathrm{i}\omega\left(1 + \gamma\tilde{\sigma}_1\right)\right]\varphi_\omega(0) + \tilde{\sigma}_1 \int \frac{\mathrm{d}\boldsymbol{k}_1}{(2\pi)^3} V_f\left(\boldsymbol{k} - \boldsymbol{k}_1\right)\varphi_\omega\left(\boldsymbol{k}_1\right) \tag{4.16}$$

with $\varphi_\omega(0) = \langle\varphi_\omega(r)\rangle$. Here we used eq. (4.1), neglecting the displacement current. Fourier-transform of the phase $\varphi_\omega(\boldsymbol{k})$ is calculated from eq. (4.12b) in linear approximation in V_f,

$$\varphi_\omega^{(1)}(\boldsymbol{k}) = -\frac{\tilde{\sigma}_1 V_\mathrm{f}(\boldsymbol{k}) V_\omega}{(\mathrm{i}\omega\gamma + V_\mathrm{T})\left(\hat{D}k^2 + \mathrm{i}\omega\gamma_k + \tilde{\sigma}_1 V_\mathrm{T}\right)} \tag{4.17}$$

Substituting eq. (4.17) into eq. (4.16) and using eq. (4.13), we get

$$\tilde{\sigma}_\mathrm{CDW}(\omega) \equiv \sigma_\mathrm{CDW}(\omega)/\sigma_\mathrm{N} = \tilde{\sigma}_\mathrm{cl}(\omega) + \frac{\mathrm{i}\omega\tilde{\sigma}_1}{(\mathrm{i}\omega\gamma + V_\mathrm{T})^2}\left[F_3(\omega) - F_3(0)\right] \tag{4.18a}$$

where $\tilde{\sigma}_\mathrm{cl} = \mathrm{i}\omega/\left(\mathrm{i}\omega\gamma + \tilde{V}_\mathrm{T}\right)$ is the a.c. conductivity of the rigid CDW, $\tilde{V}_\mathrm{T} = V_\mathrm{T}(1-\delta)$, $\delta = \tilde{\sigma}_1 F_3(0)/V_\mathrm{T}$ characterizes renormalization of the threshold field by the phase fluctuations (Artemenko and Kruglov 1982, Littlewood and Varma 1987). $F_3(\omega)$ is defined by

$$F_3(\omega) = \int \frac{\mathrm{d}\boldsymbol{k}}{(2\pi)^3} \frac{V_\mathrm{f}^2(\boldsymbol{k})}{\hat{D}k^2 + \mathrm{i}\omega\gamma_k + \tilde{\sigma}_1 V_\mathrm{T}} \tag{4.18b}$$

The second term in eq. (4.18a), caused by the fluctuations of E_T, may be calculated again for the single-domain ($\omega\tau_0 \gg 1$) and for the multipledomain ($\omega\tau_0 \ll 1$) case. In addition to the characteristic frequency $\omega_1 = \tilde{V}_\mathrm{T}/\gamma$, in both cases $\delta\sigma_\mathrm{CDW}$ contains one more characteristic frequency $\omega_\mathrm{c} \sim \tilde{\sigma}_1 V_\mathrm{T} \ll V_\mathrm{T}$ (Sridhar et al. 1986, Littlewood 1987). For example, for the multiple-domain case

$$\delta\tilde{\sigma}_\mathrm{CDW} = \frac{\omega^2\tilde{\sigma}_1 V_\mathrm{fO}^2}{\left(\mathrm{i}\omega\gamma + \tilde{V}_\mathrm{T}\right)^2 D_{\perp\mathrm{e}}\sqrt{D_{\|\mathrm{e}}}\omega} \begin{cases} \frac{\pi\sqrt{\omega}\beta^3}{4\sqrt{V_\mathrm{T}\tilde{\sigma}_1}\beta_\perp^{3/2}}\left[\ln(\beta^{-2}) - \frac{\mathrm{i}}{4}\sqrt{\frac{\omega}{\tilde{\sigma}_1 V_\mathrm{T}}}\right] \\ \omega \ll \omega_\mathrm{c} = 8\tilde{\sigma}_1 V_\mathrm{T}\ln 1/\beta \\ \frac{\pi}{\sqrt{2}}(1-\mathrm{i})f_2, \quad \omega \gg \omega_\mathrm{c} \end{cases}$$

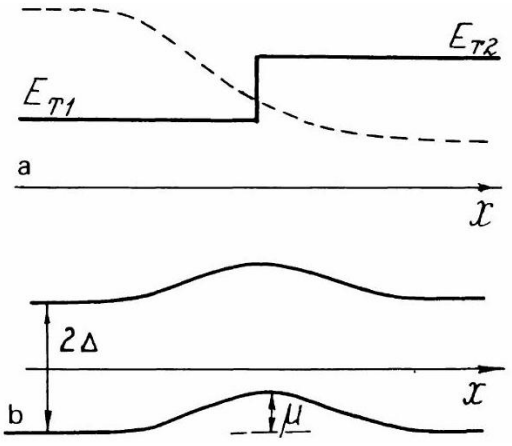


Fig. 2. Spatial dependence of the CDW phase φ (dashed line) in a sample with nonuniform threshold field E_{T} (solid line) (a) at $E < E_{\mathrm{T1}} < E_{\mathrm{T2}}$; (b) shows the band bending arising due to the screening of the CDW charge.

with f_2 and β determined in (4.15c,d). Frequency dependence of two parts of $\sigma_\mathrm{CDW}(\omega)$ is shown schematically in fig. 3. As was noted many times dependences of $\delta\sigma_\mathrm{CDW}(\omega)$ and $\sigma_\mathrm{CDW}(\Omega)$ (see eq. (4.15)) at large ω and $\Omega = V_0/\gamma$ have the same form.

Now we shall analyze another case of the nonuniform phase perturbation, when the screening of the CDW charge by free carriers plays an important role.

\{}paragraph4.3.3. Motion of phase solitons If the CDW period is close to the commensurate value, then a onedimensional lattice of phase solitons (discommensurations) appears (McMillan 1976). Phase solitons in a form of domain walls may be created also near the contacts by the current flow (Artemenko and Volkov 1985).

Under the action of an electric field solitons can move and contribute to the conductivity both in the case when they are charged (Rice et al. 1976, Burkov et al. 1981, Burkov and Pokrovsky 1983) and in the case when they are neutral due to screening effects (Artemenko and Volkov 1981b). As long as phase solitons are spatially nonuniform distortions of the CDW phase, they are screened out by free carriers (see section 4.2) and, therefore, their contribution to the conductivity depends on σ_1.

Soliton velocity and contribution to the conductivity can be calculated from eqs. (4.9) and (4.12) in which we neglect impurity pinning. Considering domain walls perpendicular to the chain direction in the limit $\mu \ll T$ we get in coordinate representation

$$I = \tilde{\sigma}_1 V_{\mathrm{T}} \sin\varphi + (1+\gamma\tilde{\sigma}_1)\,\dot{\varphi} - D_{\|\mathrm{e}} \frac{\partial^2\varphi}{\partial x^2}. \tag{4.19a}$$

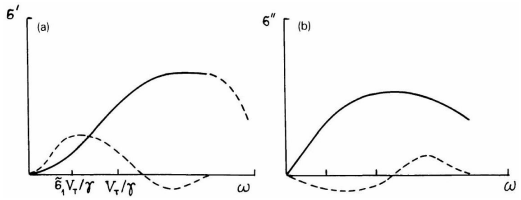


Fig. 3. Frequency dependence of: (a) the real σ' and (b) imaginary σ'' part of the CDW conductivity. Solid lines represent the result of the classical model with a constant threshold field $E_{\mathrm{T}} = V_{\mathrm{T}}/l$ (l is the mean free path length). Dashed lines are the contributions due to the fluctuations of the threshold field.

At small currents the soliton velocity s can be calculated perturbatively under the assumption that the soliton shape is stationary and independent of the current. Multiplying eq. (4.19a) by $\partial\varphi/\partial x$ with $\varphi = \varphi(x - st)$ and carrying out the integration of the obtained equation over the coordinate x, we get for the soliton velocity

$$s = \frac{2\pi I}{(1+\gamma\tilde{\sigma}_1)\left\langle(\varphi')^2\right\rangle}, \tag{4.19b}$$

where $\left\langle(\varphi')^2\right\rangle$ is $(\partial\varphi/\partial x)^2$ averaged over the period of the soliton lattice. Introducing into eq. (4.19b) a solution for the soliton lattice at $I = 0$, and using eq. (4.14a), we get a relation between an average voltage V and current I

$$V = \frac{I}{\tilde{\sigma}_1}\left[1 - \frac{\pi^2}{4\,(1+\gamma\tilde{\sigma}_1)\,K(k)E(k)}\right], \tag{4.20}$$

K and E are the elliptical integrals with the parameter k determined by the period of the soliton lattice d according to the relation $\mathrm{d}L_0 = 2k \cdot K(k)$. The second term in eq. (4.20) describes a decrease of the resistivity caused by the soliton motion.

In the limit of high soliton density($d \ll L_0, k \to 0$) the CDW with soliton lattice is close to the weakly modulated incommensurate CDW. That is why the conductivity of the system

$$\frac{I}{V} = \frac{1}{\gamma} - \frac{1}{32\gamma\tilde{\sigma}_1}\left(\frac{d}{\pi L_0}\right)^4 \tag{4.21}$$

is close to the conductivity of the rigid CDW at high fields.

In the limit of low soliton density ($d \gg L_0, k \to 1$) eq. (4.20) yields

$$\frac{I}{V} = \tilde{\sigma}_1 \left[1 + \frac{\pi^2 L_0}{d} \right]. \tag{4.22}$$

The first term in eq. (4.22) is the quasiparticle conductivity, and the second term describes the contribution from the moving solitons. Since the soliton density is proportional to L/d, the contribution of a single soliton to the conductivity is proportional to σ_1. This is consistent with the result of section 4.1, according to which an effective damping rate of nonuniform CDW phase perturbations increases and their contribution to the current decreases with decreasing temperature.

It is worth to note that Preobrazhenskii et al. (1985), who studied the influence of stretching on the conductivity of orthorhombic TaS_3, interpreted their results as an evidence of the contribution to the conductivity due to phase solitons. If we accept this point of view and assume that the soliton density is small, we come to the conclusion that the CDW conductivity is proportional to the quasiparticle conductivity. Dependence of this type was observed by Ong and Zhang (1986) in TaS_3 at fields E much larger than E_T. To make a final conclusion about the existence of phase solitons and their contribution to the conductivity, additional investigations are needed.

4.9.5 5. Hall effect

The well-known fact that, in the presence of an electric field, the CDW in a linear-chain conductor can slide along the chain direction, is reflected in equations of motion for the CDW phase (see eqs. (2.1) and (2.9)), according to which the phase is affected only by the component of the electric field E parallel to the conducting chains.* Thus, one may expect that, as long as the sliding of the CDW is a one-dimensional phenomenon, there should be no detectable Hall voltage due to the sliding CDW in the sample when the magnetic field is applied perpendicularly to the chains. The first experiments by Tessema and Ong (1981) and Kawabata et al. (1981) seemed to confirm the idea of the absence of the contribution of the sliding CDW to the Hall voltage. However, the theoretical calculations have predicted that the Hall voltage contains terms proportional to the CDW velocity $u = \dot{\varphi}/Q$ both in semiconducting CDW conductors like TaS_3, etc. (Artemenko and Kruglov 1984) and in metallic CDW conductors like $NbSe_3$ (Dolgov 1984).

[0]*If the CDW wave vector is not parallel to a chain direction, then equations of motion for the phase contain components parallel to Q (Artemenko and Kruglov 1985).

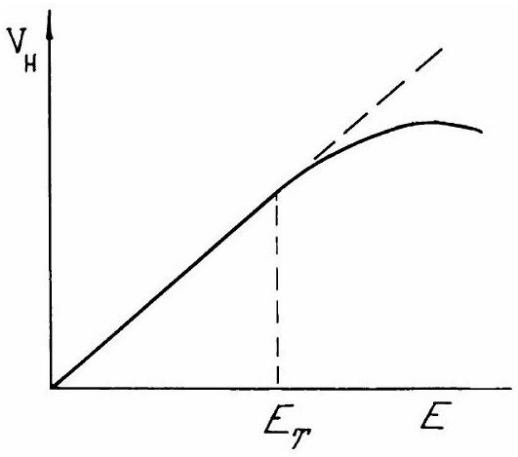


Fig. 4. Hall voltage dependence on the applied electric field.

Experiments on TaS_3 (Latyshev et al. 1985), blue bronze (Forró et al. 1986), $(TaSe_4)_2$ I (Forró et al. 1987) proved the existence of nonlinear Hall effect due to the sliding CDW. All these compounds are semiconductors below T_p. Thus, here we shall analyze the Hall effect for this case, when $\Delta > \eta_0$ and the quasiparticle density is small ($\Delta > T$).

In some cases calculations based on the kinetic equations for the Green functions are too cumbersome. Therefore, to calculate the contribution of the CDW to the Hall voltage it is more convenient to use a kinetic Bolzmann-type equation for a quasiparticle distribution function n_p, depending on the electron momentum (see Appendix). This equation, like eqs. (2.5) for distribution functions depending on energy ϵ, can be derived under the quasiclassical condition $\omega, kv \ll \Delta$, and in the case when the energy gap is not suppressed by momentum scattering ($\nu \ll \Delta$). In this limit the quasiparticle spectrum consists of two branches $\epsilon^{(1)}(p)$ and $\epsilon^{(2)}(p)$, and depends on the local value of the electric potential Φ and on the spatial and temporal derivatives of the CDW phase

$$\epsilon^{(1,2)} = \Phi(r,t) + \eta\left(p_\perp\right) - \frac{v\varphi'}{2} \pm \sqrt{\tilde{\xi}_p^2 + \Delta^2}, \tag{5.1}$$

where $\tilde{\xi}_p = \xi_p + \dot{\varphi}/2, \xi_p = v\left(p - p_\mathrm{F}\right)$. Kinetic equations for distribution functions n_1 and n_2 for the quasiparticles with energies $\epsilon^{(1)}$ and $\epsilon^{(2)}$, respectively, are presented in the Appendix (eq. (A.10)). The current density in the direction parallel ($\boldsymbol{j}_\parallel$) and perpendicular ($\boldsymbol{j}_\perp$) to the chains are expressed in terms of n_1 and n_2 according to eqs. (A.1) and (A.12).

The magnitude of the Hall current $j_\mathbf{H}$ depends both on the shape of $\boldsymbol{\eta}\left(\boldsymbol{p}_\perp\right)$ and on the relation between η_0 and T. We shall restrict our analysis to the most obvious case of low temperatures $T \ll \eta_0 \ll \Delta$, when the major contribution to the current comes from the region of momentum space near the extrema of $\eta\left(\boldsymbol{p}_\perp\right)$. In this case we can use the expansion for $\eta\left(\boldsymbol{p}_\perp\right)$ near its
maximum (η_1) and minimum (η_2) values

$$\eta_{1,2}\left(\boldsymbol{p}_\perp\right) = \eta_{1,2} \pm \frac{\left(\boldsymbol{p}_\perp - \boldsymbol{p}_{1,2}\right)^2}{2m_{1,2}}$$

Furthermore, at $T \ll \Delta$ we have $\sqrt{\Delta^2 + \xi_p^2} = \Delta + \frac{1}{2}\xi_p^2/\Delta = \Delta + \left(v^2/2\Delta\right)\left(p - p_\mathrm{F}\right)^2$. Thus, the problem of calculation of the Hall current in CDW conductors becomes analogous to a corresponding problem for the case of ordinary semiconductors. To calculate j_H, it is necessary to solve the kinetic equation perturbatively for the stationary case up to terms of the order of EH and $\dot{\varphi}H$. As a result we obtain for the parallel component of the current density

$$j_{\parallel} = \sigma_1^{(1)} \left(E - \alpha_1^{(1)} \dot{\varphi} \right) + \sigma_1^{(2)} \left(E - \alpha_2^{(2)} \dot{\varphi} \right) + \sigma_2 \dot{\varphi}/el, \tag{5.2}$$

where

$$\sigma^{(i)} = \frac{1}{6\pi^2} \frac{T}{\Delta} \frac{Sv}{\nu} \exp\left(-\frac{\Delta - \eta_i}{T} \right)$$

is the conductivity from electrons ($i = 1$) and holes ($i = 2$). S is the area of the Brillouin zone cross section at $|\boldsymbol{p}| = p_{\mathrm{F}}$, $\boldsymbol{\alpha}^{(i)} = \frac{3}{8}\sqrt{2\pi}\nu_b m_i \sqrt{T\Delta}/vS$. The second terms in brackets in eq. (5.2) arises from the scattering processes, which take place when the CDW moves in an electric field. At low temperatures a decrease of the CDW current described by these terms is small in comparison with the last term in eq. (5.2), but we single it out, because just that part of $j_{\parallel}$gives rise to a contribution to the Hall current, proportional to $\dot{\varphi}$.

The Hall current consists of two parts, corresponding to contributions of electrons and holes: $j_{\mathbf{H}}^{(1)} + j_{\mathbf{H}}^{(2)}$. If the contributions of the electrons and holes are equal, they compensate each other in a similar fashion as in ordinary semiconductors. The explicit calculation for j_{H} yields

$$\begin{aligned} j_{\mathrm{H}}^{(i)} &= j_{\mathrm{EH}}^{(i)} + j_{\mathrm{uH}}^{(i)}, \\ j_{\mathrm{EH}}^{(i)} &= A^{(i)} EH, \quad A^{(i)} = (-1)^{i+1} \sqrt{\frac{T}{\Delta}} \frac{S^2 v \exp\left[(\eta_i - \Delta)/T \right]}{8\sqrt{2\pi}\pi^3 c \nu^2 m_i^2}, \end{aligned} \tag{5.3}$$

$$j_{\mathrm{uH}}^{(i)} = -\frac{16}{3} \alpha^{(i)} A^{(i)} \dot{\varphi}_{\mathrm{H}}. \tag{5.4}$$

We see that the contributions to j_{H} due to the sliding CDW j_{uH} and due to the ordinary Ohmic current j_{EH} have opposite signs, and both contributions are proportional to a small density of thermally excited quasiparticles.

Since eqs. (5.3) and (5.4) are obtained from the kinetic equation, they can be easily interpreted in terms of the electron distribution functions. According to eq. (5.1) the CDW motion with velocity $u = \dot{\varphi}/2p_{\mathrm{F}}$ corresponds to a shift of the quasielectron 'momentum' ξ_p by $\dot{\varphi}/2$. But the motion of
electrons, which can be described as a change of the quasiparticle energy, does not contribute to a Hall current by itself. This fact is well known from the theory of the Hall effect in ordinary semiconductors. In this case a term in kinetic equation (A.10), describing an action of the Lorentz force on electron distribution, is equal to zero,

$$[\boldsymbol{v}_{\mathrm{g}} \times \boldsymbol{H}] \frac{\partial n\left(\epsilon_p\right)}{\partial \boldsymbol{p}} = [\boldsymbol{v}_{\mathrm{g}} \times \boldsymbol{H}] \cdot \boldsymbol{v}_{\mathrm{g}} \frac{\partial n}{\partial \epsilon} = 0,$$

where $\boldsymbol{v}_{\mathrm{g}} = \partial \epsilon_p / \partial \boldsymbol{p}$ is a group velocity of the quasiparticles.
However, the CDW motion is accompanied by scattering, which alters the quasiparticle distribution and gives rise to a decrease of the nonlinear current proportional to $\dot{\varphi}$ (see eq. (5.2)). This decrease may be regarded as an effective quasiparticle back-flow current. In kinetic equation this process originates from the collision term with δ-functions of energies, containing the change of the quasiparticle energy in a collision process by $\dot{\varphi}$. Therefore, the factor α in eqs. (5.2) and (5.4) is proportional to a backward scattering rate ν_{b}. The Lorentz force, acting on this back-flow current, gives rise to a contribution j_{uH} in eq. (5.4), namely, to a decrease in the Hall current above the threshold voltage.

Experiments performed by Latyshev et al. (1985) for o- TaS_3, Forró et al. (1986) for blue bronze, and Forró et al. (1987) for ($TaSe)_2$I confirm that the sliding of the CDW reduces the Hall voltage and this reduction is proportional to a small factor $\exp(-\Delta/T)$. More detailed comparison of the theoretical predictions with the experimental data (e.g. the preexponential

factors in eq. (5.4)) is rather difficult because a precise form of the function $\eta(\boldsymbol{p}_\perp)$, the relation between η and T, etc., are needed.

4.9.6 6. Conclusion

The microscopic theory, presented here, permits one to elucidate the limits of validity of phenomenological equation (2.1) of the CDW motion, and to connect the coefficients of this equation with the parameters of the material. In some cases equations, describing the CDW conductors are more complicated than eq. (2.1). This takes place, for example, if nonlinear screening is important, i.e. when the fields, arising due to screening of the CDW phase distortions by free carriers, shift electrochemical potential by the value $\mu \geqslant T$ (see eqs. (4.8)-(4.10)). Then, the free carrier density $n_q(\boldsymbol{r})$ varies with the coordinate drastically, and the form of the function $n_q(\boldsymbol{r})$ at $E < E_\mathrm{T}$ may depend on the prehistory of the phase variation in the sample. As a result, the quasiparticle conductivity at $E < E_\mathrm{T}$ will also depend on the prehistory, and this dependence will show up in hysteretic phenomena (Higgs and Gill 1983, Mihaly and Mihaly 1984, Borodin et al. 1986a,b).

Screening of nonuniform CDW deformations by free carriers is important not only for the quasiparticle conductivity but for the CDW conductivity too. Since the sliding of the CDW at fields $E > E_\mathbf{T}$ is accompanied by the phase deformations due to interaction with defects, nonuniform quasiparticle density which screens the charge, created by the CDW deformation, appears. The characteristic time of the quasiparticle density redistribution, being equal to $1/\sigma_1$, depends strongly on the temperature ($\sigma_1 \sim \exp(-\Delta/T)$ at $\Delta > T, \eta_0$). Hence, the response of the CDW to the self-consistent field, created by perturbations of the CDW and of the quasiparticle density, varies strongly with temperature too. Thus, the CDW moves not only under the action of an external electric field and friction force, but also under the action of a field created by quasiparticle charge. This self-consistent motion of two subsystems, i.e. of the CDW and the quasiparticles, leads to a modification of the CDW response, to an appearance of new characteristic frequencies depending on the quasiparticle conductivity σ_1, and to a modification of the phason spectrum.

Many experimental results are explained by the existing theory; in particular, among them are, for example, the general form of the CVC, and the frequency dependence of the CDW conductivity. Nevertheless, some problems are not solved yet. For example, there is no complete explanation for the frequency dependence of the $\sigma_\mathrm{CDW}(\omega) \sim \omega^{0.8}$ at low frequencies (Zhilinski et al. 1984, Sridhar et al. 1986, Bleher 1987) and for a correlation which seems to be established between σ_CDW at fields $E \gg E_\mathrm{T}$ and quasiparticle conductivity σ_1 (Ong and Zhang 1986).

Another interesting question to be investigated is the difference between photoelectric phenomena in CDW conductors at $E < E_\mathrm{T}$, and photoelectric phenomena in ordinary semiconductors. So, there are no data on the lifetime of the nonequilibrium charge carriers, and on the processes of their annihilation in CDW conductors. Presumably, as a result of these processes, amplitude solitons (see, for a review, Brazovskii and Kirova 1984) may be created (at least in the conductors with sufficiently weak interchain interaction). By now, no convincing evidence is present for the existence of the amplitude solitons in CDW conductors (we do not mean polymers, like polyacetylene).

We note that the analysis presented in this review describes the motion of the CDW and its depinning as a classical process. There is a different theoretical approach by Bardeen (1985), based on treating CDW conductors as macroscopic quantum systems. This approach seems to be valid at low temperatures in the case of sufficiently weak interchain coupling. We hope that the kinetic approach, presented in this review, may be used as an effective tool for the investigation of the problems remaining to be solved in the CDW dynamics in existing quasi-one-dimensional materials.

4.9.7 Appendix

A periodic lattice distortion caused by the Peierls transition leads to a mixing of states in the different parts of the Fermi surface. Thus, we introduce the electron Green functions in Keldysh's (1964) technique by the expression

$$G^{ij}_{\alpha\beta}\left(t,t';\boldsymbol{k},k'\right)=\frac{1}{\mathrm{i}}\left\langle a_{\alpha p_{\mathrm{F}}+k}\left(t_i\right)a^{+}_{\beta p_{\mathrm{F}}+k'}\left(t'_j\right)\right\rangle, \tag{A.1}$$

with $\alpha,\beta=\pm1,|k|,|k'|\ll p_{\mathrm{F}}$. Indices i and j correspond to a different part of the time contour. The Hamiltonian of the system has a form

$$H=H_{\mathrm{e}}+H_{\mathrm{ph}}+H_{\mathrm{e-ph}} \tag{A.2}$$

where

$$H_{\mathrm{e}}=\sum_{p}\epsilon_p a^{+}_p a_p+\sum_{p,q}V_q a^{+}_{p+q}a_p,$$
$$H_{\mathrm{ph}}=\sum_{q}\omega_q b^{+}_q b_q,\quad H_{\mathrm{e-ph}}=\sum g\left(a^{+}_{p+Q}a_p\Delta+\text{ c.c. }\right).$$

Potential V_q is a sum of the potential of the interaction with impurities and of the electrostatic potential Φ. Using (A.2), we can derive the equation of motion for the operators a_p and $a^{+}_p$and obtain equations for the Green functions. For example, for a function $\hat{G}=\hat{G}^{12}+\hat{G}^{21}$, introduced by Keldysh, we obtain

$$\hat{G}^{-1}_0(1)\hat{G}\left(1,1'\right)-\Phi(1)\hat{G}\left(1,1'\right)=\hat{\Sigma}\hat{G} \tag{A.3a}$$
$$\hat{G}\left(1,1'\right)G^{-1}_0\left(1'\right)-\hat{G}\left(1,1'\right)\Phi\left(1'\right)=\hat{G}\hat{\Sigma} \tag{A.3b}$$

where

$$\hat{G}^{-1}_0=\mathrm{i}\frac{\partial}{\partial t}-(\hat{\epsilon}+\hat{\Delta}),$$
$$\hat{\epsilon}=\begin{pmatrix}\epsilon(p+Q/2) & 0\\ 0 & \epsilon(p-Q/2)\end{pmatrix},\quad \hat{\Delta}=\begin{pmatrix}0 & \Delta\\ \Delta^{*} & 0\end{pmatrix}.$$

The self-energy $\hat{\Sigma}$ describes an elastic scattering

$$\hat{\Sigma}\left(k,\boldsymbol{p}_{\perp}\right)=\frac{1}{2\pi}\int \mathrm{d}\xi\frac{\mathrm{d}\boldsymbol{p}'_{\perp}}{S}\left\{\nu_{\mathrm{f}}\left(\boldsymbol{p}_{\perp}-\boldsymbol{p}'_{\perp}\right)\hat{\boldsymbol{G}}\left(k,\boldsymbol{p}_{\perp},\boldsymbol{R}\right)+\frac{1}{2}\nu_{\mathrm{b}}\left(\boldsymbol{p}_{\perp}-\boldsymbol{p}'_{\perp}\right)\right.$$
$$\left.\times\left[\hat{\sigma}_x\hat{G}\left(k,\boldsymbol{p}_{\perp},\boldsymbol{R}\right)\hat{\sigma}_x+\hat{\sigma}_y\hat{G}\left(k,\boldsymbol{p}_{\perp},\boldsymbol{R}\right)\hat{\sigma}_y\right]\right\}$$

where ν_{f} and ν_{b} are the forward and backward scattering rates, respectively, $\hat{\sigma}_x$ and $\hat{\sigma}_y$ are Pauli matrices. Then, we multiply eq. (A.3a) by Pauli matrix $\hat{\sigma}_z$ from the left, and subtract from it eq. (A.3b), multiplied by $\hat{\sigma}_z$ from the right. The resulting equation does not contain the variable $\xi_p=\frac{1}{2}[\boldsymbol{\epsilon}(\boldsymbol{k}+\boldsymbol{Q})-\boldsymbol{\epsilon}(\boldsymbol{k}-\boldsymbol{Q})]\approx vk$ and can be integrated over ξ_p. An analogous equation can be obtained for the retarded and advanced Green functions $\hat{G}^{\mathrm{R}}$ and $\hat{G}^{\mathrm{A}}$. Then, introducing a supermatrix

$$\check{G}=\begin{pmatrix}\hat{G}^{\mathrm{R}} & \hat{G}\\ 0 & \hat{G}^{\mathrm{A}}\end{pmatrix}$$

we obtain an equation for a matrix Green function $\check{g}=(\mathrm{i}\sigma_z/2\pi)\int\mathrm{d}\xi\check{G}$, which can be presented in a compact form

$$\tilde{\epsilon}\check{\sigma}_z\check{g} - \check{g}\sigma_z\tilde{\epsilon}' + \left[\check{\Delta} - \Phi\check{\sigma}_z, g\right]_- + \frac{\dot{\mathrm{i}}}{2}[\check{v}, \nabla\check{g}]_+ = [\check{\Sigma}, \check{g}]_-, \tag{A.4}$$

where

$$\tilde{\boldsymbol{\epsilon}} = \boldsymbol{\epsilon} - \eta\left(\boldsymbol{p}_\perp\right), \quad \eta = [\boldsymbol{\epsilon}(\boldsymbol{k} + \boldsymbol{Q}/2) + \boldsymbol{\epsilon}(\boldsymbol{k} - \boldsymbol{Q}/2)]/2,$$
$$\check{\boldsymbol{v}} = \boldsymbol{v}_1 + \hat{\boldsymbol{\sigma}}_z\boldsymbol{v}_z, \quad \boldsymbol{v}_1 = \partial\xi_p/\partial\boldsymbol{k}, \quad \boldsymbol{v}_z = \partial\eta/\partial\boldsymbol{k},$$
$$\check{\Delta} = \begin{pmatrix} \hat{\Delta} & 0 \\ 0 & \hat{\Delta} \end{pmatrix}, \quad \hat{\Delta} = \begin{pmatrix} 0 & \Delta \\ -\Delta^* & 0 \end{pmatrix}, \quad \check{\sigma}_z = \begin{pmatrix} \hat{\sigma}_z & 0 \\ 0 & \hat{\sigma}_z \end{pmatrix}, \quad \check{\Sigma} = \begin{pmatrix} \hat{\Sigma}^{\mathrm{R}} & \hat{\Sigma} \\ 0 & \hat{\Sigma}^{\mathrm{A}} \end{pmatrix},$$

$[\,\check{\Sigma}\check{g}\,]_-$ means the anticommutator and the convolution with respect to energy $\boldsymbol{\epsilon}$ and $\boldsymbol{p}_\perp$.$\Sigma^{\check{x}}$ is determined by the expression, following from eq. (A.3),

$$\check{\Sigma} = -\frac{\mathrm{i}}{2}\int\frac{\mathrm{d}\boldsymbol{p}'_\perp}{S}\left\{\nu_{\mathrm{f}}\left(\boldsymbol{p}_\perp - \boldsymbol{p}'_\perp\right)\check{\sigma}_z\check{g}\left(\boldsymbol{p}'_\perp\right)\check{\sigma}_z - \frac{1}{2}\nu_{\mathrm{b}}\left(\boldsymbol{p}_\perp - \boldsymbol{p}'_\perp\right)\right.$$
$$\left.\times\left[\check{\sigma}_x\check{g}\left(\boldsymbol{p}'_\perp\right)\check{\sigma}_x + \check{\sigma}_y g\left(\boldsymbol{p}'_\perp\right)\check{\sigma}_y\right]\right\}.$$

In a similar way as was done in the theory of superconductivity (Larkin and Ovchinnikov 1986), one can obtain a normalization condition

$$\int\frac{\mathrm{d}\boldsymbol{\epsilon}_1}{(2\pi)}\int\frac{\mathrm{d}\boldsymbol{p}_{\perp 1}}{(2\pi)^2}\check{g}\left(\boldsymbol{\epsilon}, \boldsymbol{p}_\perp; \boldsymbol{\epsilon}_1, \boldsymbol{p}_{\perp 1}\right)\check{g}\left(\boldsymbol{\epsilon}_1, \boldsymbol{p}_{\perp 1}; \boldsymbol{\epsilon}', \boldsymbol{p}'_\perp\right) = \check{1}\delta\left(\boldsymbol{\epsilon} - \boldsymbol{\epsilon}'\right)\delta\left(\boldsymbol{p}_\perp - \boldsymbol{p}'_\perp\right). \tag{A.5}$$

Current and charge densities are expressed as follows

$$j = \frac{1}{v}\int\,\mathrm{d}\epsilon\int\frac{\mathrm{d}\boldsymbol{p}_\perp}{(2\pi)^3}\left[\boldsymbol{v}_1\,\mathrm{Sp}\,\hat{g} + \boldsymbol{v}_z\,\mathrm{Sp}\left(\hat{\sigma}_z\hat{g}\right)\right] \tag{A.6}$$

$$\rho = \frac{1}{v}\int\frac{\mathrm{d}\boldsymbol{p}_\perp}{(2\pi)^3}\left[\int\,\mathrm{d}\epsilon\,\mathrm{Sp}\left(\hat{\sigma}_z\hat{g}\right) - \Phi\right] \tag{A.7}$$

For simplicity in this review we consider the case of the CDW wave vector parallel to a chain direction. Then, the first term in eq. (A.6) corresponds to a current parallel to the chains, and the second term with $\boldsymbol{v}_z = \boldsymbol{v}_\perp$ describes the current density in perpendicular direction.

To obtain quasiclassic kinetic equation for distribution functions, it is convenient to make the transformation

$$\check{g}\left(t, t'\right) \Rightarrow \check{S}(t)\check{g}\left(t, t'\right)\check{S}^+\left(t'\right)\exp\left[\mathrm{i}\tilde{\Phi}\left(t - t'\right)\right]$$

with

$$\check{S}(t) = \cos(\varphi/2) + \mathrm{i}\check{\sigma}_z\sin(\varphi/2), \quad \tilde{\Phi} = \Phi - v\varphi'/2.$$

Then, we calculate $\hat{g}^{\mathrm{R}}$ in the quasiclassical approximation $kv, k_\perp v_\perp \ll \Delta$, and obtain the following expression:

$$\hat{g}^{\mathrm{R}} = \left(\epsilon\hat{\sigma}_z + \mathrm{i}\hat{\sigma}_y\Delta\right)/\xi^{\mathrm{R}} - \mathrm{i}v\Delta\tilde{E}\hat{\sigma}_x/2\left(\xi^{\mathrm{R}}\right)^3 - \frac{v^2\Delta^2}{\left(\xi^{\mathrm{R}}\right)^2}\frac{\partial\tilde{E}}{\partial x}\hat{\sigma}_z$$
$$+\frac{\nu\Delta}{\left(\xi^{\mathrm{R}}\right)^2}\hat{\sigma}_y - \frac{v\Delta^2}{4\left(\xi^{\mathrm{R}}\right)^5}\hat{1}\frac{\partial E}{\partial t} + \frac{\mathrm{i}\varphi\Delta\epsilon}{4\left(\xi^{\mathrm{R}}\right)^2}\left\langle\mathbf{v}_\perp^2\right\rangle\nabla_\perp^2\varphi\hat{\sigma}_x \tag{A.8}$$

with

$$\tilde{E} = -\delta\tilde{\Phi}/\partial x, \quad \xi^{\mathrm{R}}(\epsilon) = \sqrt{(\epsilon + \mathrm{i}0)^2 - \Delta^2}, \quad \langle \cdots \rangle = \int \frac{\mathrm{d}\boldsymbol{p}_\perp}{S}(\cdots)$$

we represent the function $\hat{g}$ in a form

$$\hat{g} = \hat{g}^{\mathrm{R}}\hat{n} - \hat{n}\hat{g}^{\mathrm{A}}, \quad \hat{n} = n_1\hat{1} + n_z\hat{\sigma}_z$$

Using eq. (A.4) and taking into account eq. (A.8), we obtain eqs. (2.5) for distribution functions n_1 and n_2.

Kinetic equations should be supplemented by the expressions connecting Green functions and distribution functions with the order parameter $\hat{\Delta}$. Since $\hat{\Delta}$ is determined by the periodic lattice distortion with the wave vector $\boldsymbol{Q}$, an equation for $\hat{\Delta}$ can be derived from the equation of evolution for the phonon field operators b_Q and b^+_{-Q}. Combining equations for b_Q and b^+_{-Q}, we obtain the equation expressing Δ and Δ^* via the Green function $\hat{g}$,

$$\left(1 + \frac{1}{\omega_Q^2}\frac{\partial^2}{\partial t^2}\right)\hat{\Delta} = \frac{\lambda}{2}\int \mathrm{d}\epsilon \, \langle \hat{g} - \hat{\sigma}_z\hat{g}\hat{\sigma}_z \rangle \, . \tag{A.9}$$

If the external perturbation acting on a CDW conductor is quasiclassical ($\omega, kv \ll \Delta$), and the scattering is weak ($\Delta \gg \nu$), then the method for the derivation of the kinetic Boltzmann equation used by Keldysh (1964) in the case of normal conductors, may be extended to the case of the CDW conductor. In this method one uses the fact that the solution of eq. (A.3) for G can be found easily in the zeroth approximation to $\nu/\Delta, \omega/\Delta$, and kv/Δ. For example, for a diagonal compound of the Keldysh function, G_{11},
corresponding to momenta $p \approx p_{\mathrm{F}}$ we have

$$G_{11} = 2\pi\mathrm{i}\left[u_\xi^2\left(1 - 2n_1\right)\delta\left(\epsilon - \epsilon_p^{(1)}\right) + v_\xi^2\left(1 - 2n_2\right)\delta\left(\epsilon - \epsilon_p^{(2)}\right)\right],$$

where $\epsilon_p^{(1,2)}$ are the quasiparticle energies given by eq. (5.1), n_1 and n_2 are distribution functions for these quasiparticles. Field operators of quasiparticles are related to the electron field operators in eq. (A.1) via the Bogolyubov transformation with the amplitudes

$$u_\xi^2 = \frac{1}{2}(1 + \xi/\epsilon), \quad v_\xi^2 = \frac{1}{2}(1 - \xi/\epsilon), \quad \tilde{\epsilon} = \sqrt{\Delta^2 + \tilde{\xi}^2}$$

In order to exclude factor ϵ on the left-hand side of eqs. (A.3) we subtract these equations one from another, and take into account that in the quasiclassic limit $\hat{G}$ is a slowly varying function of the coordinate $\frac{1}{2}(1 + 1')$ and a rapidly varying function of ($1 - 1'$) (Fourier transformation from ($1 - 1'$) yields energy ϵ and momentum of the electron). After an integration over ϵ we obtain the kinetic equation (Artemenko and Kruglov 1984) for the distribution functions n_1 and n_2,

$$\begin{aligned}
&\frac{\partial n_i}{\partial t} + \frac{\partial \boldsymbol{\epsilon}_p^{(i)}}{\partial \boldsymbol{p}}\frac{\partial n_i}{\partial \boldsymbol{r}} - \frac{\partial \epsilon^{(i)}}{\partial \boldsymbol{r}}\frac{\partial n_i}{\partial \boldsymbol{p}} + \boldsymbol{E}\frac{\partial n_i}{\partial \boldsymbol{p}} - \frac{1}{c}\left(\left[\frac{\partial n_i}{\partial \boldsymbol{p}} \times \boldsymbol{H}\right] \cdot \frac{\partial \epsilon^{(i)}}{\partial \boldsymbol{p}}\right) \\
&\quad = \int \frac{\mathrm{d}\boldsymbol{p}'_\perp}{S}\int \mathrm{d}\xi' \left[n_i\left(\xi, \boldsymbol{p}_\perp\right) - n_i\left(\xi', \boldsymbol{p}'_\perp\right)\right]\Big[\nu_{\mathrm{f}}\left(u_\xi u_{\xi'} + v_\xi v_{\xi'}\right)^2\delta\left(\epsilon_p^{(i)} - \epsilon_{p'}^{(i)}\right) \\
&\qquad + \nu_{\mathrm{b}}u_{\xi'}^2 v_\xi^2\delta\left(\epsilon_p^{(i)} - \epsilon_{p'}^{(i)} - (-1)^i\dot{\varphi}\right) + \nu_{\mathrm{b}}u_\xi^2 v_{\xi'}^2\delta\left(\epsilon_p^{(i)} - \epsilon_{p'}^{(i)} + (-1)^i\dot{\varphi}\right)\Big] \\
&\qquad + \int \frac{\mathrm{d}\boldsymbol{p}'_\perp}{S}\int \mathrm{d}\xi' \left[n_i\left(\xi, \boldsymbol{p}_\perp\right) - n_j\left(\xi', \boldsymbol{p}'_\perp\right)\right]\Big[\nu_{\mathrm{f}}\left(u_\xi v_{\xi'} - u_{\xi'}v_\xi\right)^2\delta\left(\epsilon_p^{(i)} - \epsilon_{p'}^{(j)}\right) \\
&\qquad + \nu_{\mathrm{b}}v_\xi^2 v_{\xi'}^2\delta\left(\epsilon_p^{(i)} - \epsilon_{p'}^{(j)} - (-1)^i\dot{\varphi}\right) + \nu_{\mathrm{b}}u_\xi^2 u_{\xi'}^2\delta\left(\epsilon_p^{(i)} - \epsilon_{p'}^{(j)} + (-1)^i\dot{\varphi}\right)\Big]
\end{aligned} \tag{A.10}$$

with $i = 1, 2, j = 3 - i$.
Starting from the expression, defining the current density via the Green function, we obtain the equations for the currents in terms of n_1 and n_2. The current density along the chains is

$$j_{\parallel} = \int \frac{\mathrm{d}\boldsymbol{p}_{\perp}}{(2\pi)^3} \int \mathrm{d}\xi \frac{\tilde{\xi}}{\tilde{\epsilon}} (n_1 - n_2) + \sigma_{\mathrm{N}} \dot{\varphi}/l \tag{A.11}$$

where the last term originates from the region of the momentum space far below the Fermi surface. For the current perpendicular to the chain direction we obtain

$$\boldsymbol{j}_{\perp} = -\frac{1}{4\pi^3} \int \mathrm{d}\boldsymbol{p} \boldsymbol{v}_{\perp} (n_1 + n_2) \,. \tag{A.12}$$

4.9.8 References

Abrikosov, A.A., 1987, Introduction to the Theory of Metals (Nauka, Moscow).
Artemenko, S.N., and A.N. Kruglov, 1982, Zh. Eksp. & Teor. Fiz. 83, 1134 [Sov. Phys.-JETP 56, 643].
Artemenko, S.N., and A.N. Kruglov, 1984, Fiz. Tverd. Tela 26, 239.
Artemenko, S.N., and A.N. Kruglov, 1985, in: Lecture Notes in Physics, Vol. 336, Proc. Int. Conf. on Charge Density Waves in Solids, Budapest, 1984 (Springer, Berlin).
Artemenko, S.N., and A.F. Volkov, 1981a, Pis'ma v Zh. Eksp. & Teor. Fiz. 33, 155 [JETP Lett. 33, 147].
Artemenko, S.N., and A.F. Volkov, 1981b, Zh. Eksp. & Teor. Fiz. 80, 2018 [Sov. Phys.-JETP 53, 1050].
Artemenko, S.N., and A.F. Volkov, 1981c, Zh. Eksp. & Teor. Fiz. 81, 1872 [Sov. Phys.-JETP 54, 992].
Artemenko, S.N., and A.F. Volkov, 1985, in: Lecture Notes in Physics, Vol. 336, Proc. Int. Conf. on Charge Density Waves in Solids, Budapest, 1984 (Springer, Berlin).
Artemenko, S.N., A.F. Volkov and A.N. Kruglov, 1986, Zh. Eksp. & Teor. Fiz. 91, 1537 [Sov. Phys.-JETP 64, 906].
Aslamazov, L.G., and A.F. Volkov, 1986, in: Nonequilibrium Superconductivity, eds D. Langenberg and A. Larkin (North-Holland, Amsterdam) p. 65.
Bardeen, J., 1985, in: Hightlights of Condensed Matter Theory, Proc. Int. School of Physics "Enrico Fermi", Course LXXXIX, eds F. Bassani, F. Fumi and M. Tosi (North-Holland, Amsterdam).
Biljaković, K., J.C. Lasjaunias, F. Zongmore, P. Monceau, F. Levy, L. Bernard and R. Currat, 1986, Phys. Rev. Lett. 57, 1907.
Bleher, M., 1987, Solid State Commun. 63, 1071.
Borodin, D.V., S.V. Zaitsev-Zotov and F.Ya. Nad', 1986a, Pis'ma v Zh. Eksp. & Teor. Fiz. 43, 485 [JETP Lett. 43, 625].
Borodin, D.V., S.V. Zaitsev-Zotov and F.Ya. Nad', 1986b, Zh. Eksp. & Teor. Fiz. 90, 318 [Sov. Phys.-JETP 63, 184].
Brazovskii, S., 1979, Zh. Eksp. & Teor. Fiz. 76, 300.
Brazovskii, S., and N.N. Kirova, 1984, Sov. Sci. Rev. A, Phys. Rev. 5, 100.
Burkov, S.E., and V.L. Pokrovsky, 1983, Solid State Commun. 46, 609.
Burkov, S.E., V.L. Pokrovsky and G.V. Uimin, 1981, Solid State Commun. 40, 363.
Coleman, R.V., M.P. Everson, G. Eiserman, A. Johnson and Hao-An Lu, 1987, Synth. Met. 19, 795.
De Lozanne, A.L., and M.R. Beasley, 1986, in: Nonequilibrium Superconductivity, eds D. Langenberg and A. Larkin (North-Holland, Amsterdam) p. 111.

Dolgov, E.N., 1984, Solid State Commun. 50, 405.
Eckern, U., 1986, J. Low Temp. Phys. 62, 525.
Efetov, K.B., and A.I. Larkin, 1977, Zh. Eksp. & Teor. Fiz. 72, 2350 [Sov. Phys.-JETP 45, 1236].
Escribe-Filippini, C., J.P. Pouget, B. Mennion and H. Sato, 1987, Synth. Met. 19, 931.
Fisher, D.S., 1983, Phys. Rev. Lett. 50, 1486.
Fisher, D.S., 1985, Phys. Rev. B 31, 1396.
Forró, L., J.R. Cooper, A. Janossy and K. Kamaras, 1986, Phys. Rev. B 34, 9047.
Forró, L., J.R. Cooper, A. Janossy and M. Maki, 1987, Solid State Commun. 62, 715.
Fröhlich, H., 1954, Proc. R. Soc. London Ser. A 223, 296.
Gor'kov, L.P., 1984, Zh. Eksp. & Teor. Fiz. 86, 1818 [Sov. Phys.-JETP 59, 1057].
Gor'kov, L.P., and E.N. Dolgov, 1979, Zh. Eksp. & Teor. Fiz. 77, 396 [Sov. Phys.-JETP 50, 203].
Gor'kov, L.P., and G.M. Eliashberg, 1968, Zh. Eksp. & Teor. Fiz. 55, 2430 [Sov. Phys.-JETP 27, 328].
Grüner, G., and A. Zettl, 1985, Phys. Rep. 119, 117.
Grüner, G., A. Zawadowski and P.M. Chaikin, 1981, Phys. Rev. Lett. 46, 511.
Higgs, A.W., and J.C. Gill, 1983, Solid State Commun. 47, 737.
Itkis, M.E., F.Ya. Nad' and V.Ya. Pokrovskii, 1986, Zh. Eksp. & Teor. Fiz. 90, 307 [Sov. Phys.-JETP 63, 177].
Kawabata, K., M. Ido and T. Sambongi, 1981, J. Phys. Soc. Jpn. 50, 1992.
Keldysh, L.V., 1964, Zh. Eksp. & Teor. Fiz. 47, 1515 [1965, Sov. Phys.-JETP 20, 1018].
Klemm, R.A., and J.R. Schrieffer, 1983, Phys. Rev. Lett. 51, 47.
Larkin, A.I., and Yu.N. Ovchinnikov, 1986, in: Nonequilibrium Superconductivity, eds D. Langenberg and A. Larkin (North-Holland, Amsterdam) p. 493.
Latyshev, Y.I., Ya.S. Savitskaya and V.V. Frolov, 1985, in: Lecture Notes in Physics, Vol. 336, Proc. Int. Conf. on Charge Density Waves in Solids, Budapest, 1984 (Springer, Berlin).
Latyshev, Y.I., B.E. Minakova and Yu.A. Rzhanov, 1987, Pis'ma v Zh. Eksp. & Teor. Fiz. 46, 391.
Latyshev, Y.I., N.P. Pogotovskii and S.N. Artemenko, 1989, Synthetic Metals 29, F415.
Lee, P.A., and T.M. Rice, 1979, Phys. Rev. B 19, 3970.
Lee, P.A., T.M. Rice and P.W. Anderson, 1974, Solid State Commun. 14, 703.
Littlewood, P.B., 1987, Phys. Rev. B 36, 3108.
Littlewood, P.B., and C.M. Varma, 1987, Phys. Rev. B 36, 480.
MacMillan, W.L., 1976, Phys. Rev. B 14, 1496.
Mihaly, G., and P. Beauchene, 1987, Solid State Commun. 63, 911.
Mihaly, G., and L. Mihaly, 1984, Phys. Rev. Lett. 52, 149.
Monceau, P., ed., 1985, in: Electronic Properties in Inorganic Quasi-One-Dimensional Materials, Part II (Reidel, Dordrecht).
Monceau, P., J. Richard and M. Renard, 1982, Phys. Rev. B 25, 931.
Monceau, P., L. Bernard, R. Currat, F. Levy and J. Rouxel, 1986, Physica B 136, 352.
Monceau, P., L. Bernard, R. Currat, F. Levy and J. Rouxel, 1987, Synth. Met. 19, 819.
Ong, N.P., and P. Monceau, 1977, Phys. Rev. B 16, 3443.
Ong, N.P., and Z.Z. Wang, 1987, Nonlinearity in condensed matter, in: Proc. 6th Ann. Conf., Los Alamos, 1986 (Springer-Verlag, Berlin).
Ong, N.P., and X.J. Zhang, 1986, Physica B 143, 3.
Peierls, R., 1930, Ann. Phys. 4, 121.
Preobrazhensky, V.B., A.N. Taldenkov and S.Yu. Shabanov, 1985, Solid State Commun. 54, 399.
Rice, M.J., A.R. Bishop, J.A. Krumhansl and S.E. Trullinger, 1976, Phys. Rev. Lett. 36,

432.
Robbins, M.O., and R.A. Klemm, 1986, Phys. Rev. B 34, 8496.
Sekine, T., M. Izumi and E. Matsuura, 1987, Synth. Met. 19, 869.
Sneddon, L., 1984, Phys. Rev. B 29, 719.
Sneddon, L., M.C. Cross and D.S. Fisher, 1982, Phys. Rev. 49, 292.
Sridhar, S., D. Reagor and G. Grüner, 1986, Phys. Rev. B 34, 2212.
Takada, S., K.Y.M. Wong and T. Holstein, 1985, Phys. Rev. B 32, 4639.
Tessema, G.X., and N.P. Ong, 1981, Phys. Rev. B 23, 5607.
Thorne, R.E., J.R. Tucker and J. Bardeen, 1987, Phys. Rev. Lett. 58, 828.
Zhilinskii, S.K., M.E. Itkis and F.Ya. Nad', 1984, Phys. Status Solidi a 81, 367.

4.10 Phase Slipping Processes and the Generation of Narrow-Band Oscillations by Charge Density Waves by Gorkov

4.10.1 1. Introduction

Fröhlich (1954) first showed that lattice distortion (or charge density wave (CDW)) with an incommensurate wave vector, $2k_{\mathrm{F}}$, resulting at the Peierls instability in one-dimensional conductors, can freely slide along the host lattice carrying the electric current if pinning mechanisms are weak and may be neglected. Later the 'Fröhlich-conductivity' has been realized experimentally in numerous organic and inorganic linear chain materials. The Fröhlich conductivity mechanism is now the well-established phenomenon which, for instance, is responsible for the nonlinearity of the current-voltage characteristics in these materials.

Nevertheless, there are features of this phenomenon which remain unexplained. Among them the generation of quasi-periodic oscillations by the running CDW is probably one of the most interesting problems. Experimentally the effect is that under conditions of, say, a prescribed current a periodic component of the measurable voltage potential appears in the regime of running CDW. The phenomenon has first been discovered and investigated in $NbSe_3$ (Fleming and Grimes 1979, Monceau et al. 1980). It turned out later on that such oscillations are a general phenomenon which has been observed in TaS_3 (Grüner et al. 1981a,b), in the so-called blue bronze $K_{0.30}MoO_3$ and $Rb_{0.30}MoO_3$ (Dumas et al. 1983), in Ta_2Se_8I (Gressier et al. 1983). The very fact that the generation is connected with the CDW motion is now well confirmed. Thus, the generation appears only if the applied electric field exceeds some threshold value, E_t; the fundamental frequency and the harmonics are proportional to the so-called excess current (Monceau et al. 1980, 1982). In other words, there are now no doubts that this generation is directly connected with the Fröhlich conductivity mechanism. It should be mentioned, however, that while in the majority of cases the Peierls structural transition is due to the quasi-onedimensional nature of the electronic spectrum, it may be not so for $NbSe_3$ where the electronic properties are much less anisotropic (see Fleming et al. 1978).

Since then, various theoretical interpretations of the generation by the moving CDW have been suggested. However, most of the proposed mechanisms meet with difficulties when attempts are made to explain the
small width of the excited spectrum lines. In fact, in these theories the generation phenomena is usually related with the very existence of the threshold field, E_{t}. The pinning of the CDW in the incommensurate case is a volume effect, and is due to the defects or impurities, which primarily fix the phase of the wave (Gor'kov 1977, Fukuyama and Lee 1978, Lee and Rice 1979). If the electric field is strong enough to overcome the pinning forces (i.e. $E > E_{\mathrm{t}}$), and the CDW superstructure moves, the randomness of the single-impurity positions would lead to the excitation by them of an incoherent broad-band noise. In other words. the generation occurs only in the electric field exceeding the threshold value, E_{t}, because otherwise there were no

motion of the CDW as a whole, however, its mechanism should have some collective origin.

The goal of this paper is to describe the concept of phase slipping centers (PSC) which was introduced into the problem independently by the two groups of authors. Thus, Ong and Verma (1983) have argued that, because of the higher effective conductivity and, consequently, weaker electric field near a measuring contact, the CDW moves far from the contact but is pinned in the immediate vicinity of the contact. The two regimes merge due to a 'phase slipping' process. A similar idea (Gor'kov 1983) is that at the interface between two metals, one of which is a Fröhlich conductor, the lattice distortion is always pinned, and the conversion of the current transported by the CDW into the current of ordinary carriers occurs by the stoppage of the CDW-phase transport in the periodic phase slipping process. There are now numerous experimental observations indicating that under the specific geometric conditions the generation is really of local origin.

The generation by the moving CDW due to the PSC mechanism is, however, a more general phenomenon, and has, as we shall see, much in common with the analogous processes that determine the resistive currentvoltage characteristics in thin superconducting channels (Langer and Ambegaokar 1967, Ivlev and Kopnin 1978, 1980).

The interpretation of the experimental data on the generation spectra is usually based on the phenomenological use of a damped pendulum equation with an electric field as the driving force (Weger et al. 1980, Grüner et al. 1981a). Actually the growth and annihilation of the phase slipping center is a very complicated nonlinear periodic process. The microscopic physics underlaying this phenomenon in the general case leads to the set of equations which would rather obscure the main features. Therefore, in what follows, we shall mainly discuss results obtained in the framework of the microscopic model where the corresponding equations acquire a simple form (Gor'kov 1983, 1984). As we shall see, the generation may be due to the inherent nonlinear periodic solutions of these equations which have nothing in common with the excitation of the CDW vibrations by single
impurities. This also explains qualitatively the narrowness of the generated spectral lines.

4.10.2 2. Phenomenological discussion

The lattice superstructure that appears below the Peierls transition temperature T_{P} is usually expressed as a deformation $u(x) = u_0 \cos(2k_{\mathrm{F}}x + \varphi)$ that develops during the transition due to a softening of the frequency of the active phonon mode. In principle, the transition may be due to an electronic mechanism (thus, the electron-hole pairing gives rise to the charge density wave or even to the spin density wave). Therefore it is convenient to introduce the order parameter of the new phase as the 'gap' in the electron spectrum:

$$\Delta = |\Delta| \mathrm{e}^{\mathrm{i}\varphi}. \tag{2.1}$$

In the case of a structural transition the magnitude $|\Delta|$ of the gap is proportional to the amplitude of the structural deformation: $|\Delta^2| = g_{\mathrm{ph}}^2 u_0^2$ (g_{ph}^2 is the electron-phonon interaction constant which figures below in a dimensionless form). The arbitrary phase in eq. (2.1) is often written as $\varphi = -2k_{\mathrm{F}}x_0$ to emphasize the possibility of a shift of the CDW as a whole in the absence of the pinning forces. The charge density connected with the CDW is proportional to the gradient of the phase. Hence the phase is connected with the CDW charge. In a weak enough electric field E the equation for the phase, which describes the linear response of the system to the field, has the form

$$\Gamma\dot{\varphi} = aE + \xi_{\parallel}^2 \nabla_{\parallel}^2 \varphi + \xi_{\perp}^2 \nabla_{\perp}^2 \varphi, \tag{2.2}$$

where $\xi_{\parallel} \sim \hbar v_{\mathrm{F}}/T_{\mathrm{P}}$, and the value of the transverse correlation length $\xi_{\perp}$ depends on the interaction or the tunneling overlap between neighbouring chains. In eq. (2.2) the lattice kinetic

contribution $\ddot{\varphi}$ is omitted, and the dependence of the modulus of the order parameter on a weak field is assumed to be negligibly small. The friction coefficient Γ and the charge density, which is proportional to a^{-1}, are known for simple models. Thus, near $T_{\mathbf{P}}$ (but for $\Delta\tau \geqslant 1$) one has

$$a \sim e\xi_{\|}/T_{\mathrm{P}}, \quad \Gamma \sim 1/T_{\mathrm{P}}^2\tau. \tag{2.3}$$

while at a lower temperature ($T \leqslant T_{\mathrm{P}}$)

$$a \sim e\xi_{\|}/T_{\mathrm{P}}, \quad \Gamma \sim 1/T_{\mathrm{P}}^2\tau. \tag{2.3'}$$

The expressions (2.3) and (2.3') are obtained with the assumption that there remain below the transition temperature considerable electron-hole Fermi surfaces ('pockets') with normal carriers (Gor'kov and Dolgov 1979, 1981). Estimates similar to (2.3') are valid at $T \sim T_{\mathrm{P}} \sim |\Delta|$ and for the model
in which at zero temperature there are no pockets present in the electronic spectrum, and the normal carriers are due to electrons and holes thermally activated across the gap (Artemenko and Volkov 1981). In eqs. (2.3) and (2.3') the relaxation may be due to either elastic scattering by phonons ($1/\tau \sim T_{\mathrm{P}}$), or scattering by static defects. For the results of this section, the anisotropy ($\xi_{\perp} < \xi_{\|}$) is not essential, since it is assumed that the field E is applied along the conducting chains. Correspondingly, we have

$$\Gamma\dot{\varphi} = aE + \xi_{\|}^2 \frac{\partial^2\varphi}{\partial x^2}. \tag{2.2'}$$

One of the solutions to (2.2') is $\dot{\varphi} = \Omega$ where

$$\Omega = a\Gamma^{-1}E \sim eEl. \tag{2.4}$$

The static solution $\dot{\varphi} = 0$ is possible in the interior provided the body force exerted by the field is compensated by the pinning forces. Otherwise the static solution of the form

$$Q = \nabla_{\|}\varphi = -aE\xi_{\|}^{-2}x \tag{2.5}$$

would imply the variation of the superstructure with the coordinate. This is energetically unfavourable. Thus, when the electric field in the conductor exceeds the pinning threshold field ($E > E_{\mathrm{t}}$) the order parameter 'vector' (2.1) rotates uniformly with angular frequency Ω given by eq. (2.4), or which is the same thing, the superstructure moves as a whole with velocity

$$2k_{\mathrm{F}}u = \Omega. \tag{2.4'}$$

The natural question is how the solution (2.4) can be matched to the boundary conditions that arise either at the interface with an ordinary conductor, in which the Peierls distortion does not appear at all, or to the solution for the region where the local fields are below the threshold values and the CDW remains to be fixed.

Physical phenomena at the interface between two different metals are somewhat more complicated in the sense that the boundary introduces by itself distortions of atomic order of magnitude that decay as we go from the boundary towards the interior. In this case the structural distortions exist even above the Peierls transition temperature T_P, and are, in the vicinity of the boundary, little affected by the low-temperature (~ 100 K) structural transition. Therefore, below T_P the structural deformation (2.1) in the interior should be matched with the distortion already present near the boundary (for a more detailed discussion, see Gor'kov 1984). However, for phenomenological purposes, in both the cases the fixation of the CDW can be formulated as being the condition that the parameter (2.1) has a given value ($\varphi_0 = 0$) at $x = 0$:

$$\Delta(x=0)=\Delta_0. \tag{2.6}$$

Equation (2.2) may be illustrated by the convenient mechanical analogy shown in fig. 1. A long elastic spring secured at $x=0$ rotates in a viscous medium, the term with the electric field being the applied body torque. A steady-state behaviour is possible only if at some section, say, at $x=x_0$, because of the accumulating stresses, the coupling between the two parts of the spring periodically breaks, so that a slip (by, say, $[\varphi]=2\pi$) of the phase occurs. From the mathematical point of view, eq. (2.2') is a parabolic equation in which the term with the field plays the role of a spatially homogeneous source. The phase slipping process provides a 'sink', which can be formally described by including in eq. (2.2') the additional terms:

$$-2\pi\Gamma\delta\left(x-x_0\right)\delta\left(t-t_n\right), \quad t_n=2\pi\Omega^{-1}n.$$

After each slip the phase relaxes over distances:

$$|x-x_0|\sim\xi_{\|}(\Gamma\Omega)^{-1/2}\sim\xi_{\|}\left(\frac{T_{\mathrm{P}}}{eE\xi_{\|}}\right)^{1/2}. \tag{2.7}$$

In weak fields the distances (2.7) would be macroscopically large. So, taking some values, typical for $NbSe_3, T_{\mathrm{P}}\approx 50\ \mathrm{K}, v_{\mathrm{F}}\sim 10^7\ \mathrm{cm/s}\left(\xi_{\|}\sim 10^{-6}\ \mathrm{cm}\right)$, and $E\approx 10\mathrm{mV/cm}$, we find from (3.7) that $|x-x_0|\sim 10^{-3}-10^{-4}$ cm. The slipping process leads to greater or smaller oscillations of the phase in the vicinity of the boundary, depending on the relation between (2.7) and the position, x_0. Finally, the slipping process repeats itself with periodicity $\omega_0^{-1}=t_n$ which must be compared with the characteristic frequency Ω from eq. (2.4).

The various properties of CDW (pinning, motion in weak fields) are usually described in terms of the variation of the phase in (2.1). This is not the adequate approximation for the description of the phase slipping process: during this process the amplitude $|\Delta|$ in (2.1) periodically vanishes.

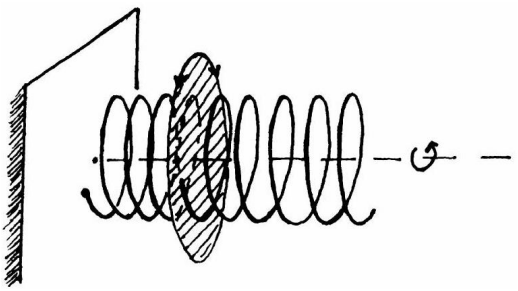


Fig. 1. A mechanical model for the phase slipping center.

4.10.3 3. Microscopic model

In real quasi-one-dimensional conductors the numerous complications due to the electron energy spectrum and the specific features of the onedimensional problem (fluctuations, localization of the electronic states in the presence of impurities, etc.) make the microscopic description of the transition into the CDW state extremely difficult. At the same time, as explained above, here we are primarily interested in the qualitative characteristics of the mechanism underlying the so-called Fröhlich conduction which is due to the motion of an incommensurate CDW. In order to avoid the superfluous difficulties of the problem we have chosen for the investigation of a three-dimensional model with an electronic spectrum possessing the 'nesting' property: $\boldsymbol{\epsilon}(\boldsymbol{p}+\boldsymbol{Q})=-\boldsymbol{\epsilon}(\boldsymbol{p})$, a model studied in detail by Keldysh and Kopaev (1964). The

one-dimensional features are now reflected in the only assumption that Fermi surfaces, though three dimensional, are open, and consist of two separate sections positioned on the right and left in the Brillouin zone near the $p_\parallel = \pm k_\mathrm{F}$ planes. The two sections have a congruous form and get superimposed on each other upon translation by the vector $\boldsymbol{Q}$ (such a property is possessed, for example, by the quasi-one-dimensional electron spectrum in the tight-binding approximation for simple chain structures (Horovitz et al. 1981)).

The 'nesting' of the Fermi surfaces results in the formation of a lowtemperature dielectric phase, with the superstructure wave vector Q. If the longitudinal component, $\boldsymbol{Q}_\parallel = 2k_F$, is incommensurate with the host lattice constant, then the system evidently exhibits the principal features of the Fröhlich-conduction phenomenon, i.e., the sliding CDW. Experience gained in the investigations of the kinetic phenomena occurring in superconductors suggests that even in this approximation, the problem remains too complicated, since, in the presence of the energy gap, the relaxation of excitations and its effect on the CDW motion in an electric field are described by very nontrivial kinetic processes. For the subsequent simplification of the model we take into account the fact that ordinary impurity scattering has a destructive effect on the structural transition, depressing the transition temperature, as it takes place in superconductors with paramagnetic impurities.

In what follows, to describe the nonlinear regime we shall use the dynamical microscopic equations which are valid in the region of defect concentrations close to the so-called critical concentration, where the dielectric phase is strongly suppressed and exists only at low temperatures $T_\mathrm{P} \ll T_\mathrm{P0}$ (here T_P0 is the critical temperature of the dielectric transition occurring in the same model in the absence of defects). The three-dimensional character of the model guarantees the existence of a long-range order even in this defect concentration region. It can also be shown
(Gor'kov 1984) that the threshold field, E_t, estimated in the common manner (Lee and Rice 1979), as a result of the impurity pinning, contains a small parameter, which allows one to study the CDW motion in both weak and strong electric fields. (The natural physical measure of the electric field strength is given by the value of the ratio: $eE\xi_\parallel/T_\mathrm{P}$.)

In mathematical respect the aforementioned dielectric transition model is close to the theory of superconductivity, and the derivation of the nonlinear dynamical equations in the indicated region is rather similar to the derivation of the dynamical equations for superconductors with paramagnetic impurities (Gor'kov and Eliashberg 1968).

The resulting equations (Gor'kov 1983) can be written out in the form of a time-dependent generalization of the Ginzburg-Landau equation for the parameter Δ :

$$\frac{2}{3}\tau_\mathrm{c}\dot{\Delta} + \frac{8}{27}\pi^2\tau_\mathrm{c}^2\left(T^2 - T_\mathrm{P}^2\right)\Delta + \frac{16}{9}\mathrm{i}\tau_\mathrm{c}^2\bar{v}eE_x\Delta - 4\tau_\mathrm{c}^2(\kappa\nabla)^2\Delta + \frac{20}{81}\tau_\mathrm{c}^2|\Delta|^2\Delta = 0. \tag{3.1}$$

Here $1/\tau$ is the total reciprocal lifetime of the electrons with respect to scattering by defects. For simplicity, it was assumed that the electron scattering is 'isotropic': $1/\tau_{++} = 1/\tau_{--} = 1/\tau_{+-} = 1/2\tau$, where $\pm$ correspond to the two parts of the Fermi surface at $\pm k_\mathrm{F}$. The critical concentration is determined by the relation $\tau_\mathrm{c} = 4\gamma/3\pi T_\mathrm{P}$ (γ is the Euler constant); T_P is the structural transition temperature ($T_\mathrm{P} \ll T_\mathrm{P0}$ in the concentration region under investigation). Equation (3.1) contains $\bar{v}$, which is nonzero only for the longitudinal component of the electron velocity (the averaging is performed over one section of the Fermi surface, say, the right-hand part at $+k_\mathrm{F}$). Finally, the form of the term with the space gradients exhibits an anisotropy in the longitudinal and transverse directions:

$$\boldsymbol{\kappa}_x^2 = \overline{v_x^2}\left[\ln\frac{3}{2} - \frac{1}{3} - \frac{\bar{v}^2}{v_x^2}\left(\ln\frac{3}{2} - \frac{7}{18}\right)\right]$$
$$\boldsymbol{\kappa}_{y,z}^2 = \overline{v_{y,z}^2}\left[\ln\frac{3}{2} - \frac{1}{3}\right] \tag{3.2}$$

The third term in (3.1) contains only the longitudinal component of the electric field, which reflects the fact that the CDW can move only along the incommensurate direction.

The simplicity of these equations lies in the form of the expression for the electric current. In fact, because of the small fraction of the electrons participating in the phase transition at $T_\mathrm{P} \ll T_\mathrm{PO}$, the dominant contribution to the current is made by the normal carriers. The presence of CDW gives rise to correction terms only of two types: the first is due to the decrease in the number of normal carriers, while the second gives the small increase in the current resulting from the CDW motion. Correspondingly, the current
has the form:

$$j_\parallel = \frac{\sigma_\parallel}{e}\left\{eE_x - \frac{8}{3}eE_x\tau_\mathrm{c}^2|\Delta|^2 + i\frac{8}{9}\tau_\mathrm{c}\frac{\bar{v}}{v_x^2}\left(\dot{\Delta}\Delta^* - \Delta\dot{\Delta}^*\right)\right\} \tag{3.3}$$

The transverse components of the current do not contain a third contribution, and are obtained by means of the substitution $\sigma_\parallel \to \sigma_\perp$.

The smallness of both corrections makes eqs. (3.1) and (3.3) independent of each other. In fact, the electric field in the first approximation is prescribed. The time behaviour of Δ is determined by the constant field E. The time dependence of Δ in our problem would give rise to small corrections to the current (3.3) or the field E_x, depending on the conditions imposed.

For the analysis it is convenient to simplify the equations obtained by going over to dimensionless variables. To do this, let us set:

$$|\Delta_0|^2 = \frac{6}{5}\pi^2 T_\mathrm{P}^2\left(1 - T^2/T_\mathrm{P}^2\right) \equiv \frac{6}{5}\pi^2 T_\mathrm{P}^2\delta,$$
$$\Delta = |\Delta_0|\,\Delta', \quad \omega_0 = \frac{4}{9}\pi^2 T_\mathrm{P}^2\tau_\mathrm{c}\delta,$$
$$\frac{6\bar{v}eE}{\pi^2\delta T_\mathrm{P}^2} = E', \quad x = \xi_\parallel x', \quad y, z = \xi_\perp y', \xi_\perp z', \tag{3.4}$$
$$\xi_{\parallel,\perp}^2 = \frac{27\kappa_{\parallel,\perp}^2}{2\pi^2 T_\mathrm{P}^2\delta}, \quad \lambda = \frac{16}{5}\pi^2\left(T_\mathrm{P}\tau_\mathrm{c}\right)^2\delta, \quad \epsilon = \bar{v}^2/\overline{v_x^2}$$

(notice that, according to (3.1), $\delta \sim 1$).
The set of equations (3.1) and (3.3), as rewritten for the dimensionless variables, has finally the following simple form:

$$\dot{\Delta} - \Delta + \mathrm{i}E\Delta - \nabla^2\Delta + |\Delta|^2\Delta = 0$$
$$\dot{j}_\parallel = \frac{\sigma_\parallel}{e}\frac{\pi^2 T_\mathrm{P}^2\delta}{6e\bar{v}}\left\{E - \lambda|\Delta|^2 E + \mathrm{i}\,\frac{8}{9}\,\epsilon\lambda\left(\dot{\Delta}\Delta^* - \Delta\dot{\Delta}^*\right)\right\} \tag{3.5}$$

(For convenience, the primes on the dimensionless variables have now been dropped. The inverse transition to the notation in (3.1) and (3.3) can always be done if needed, in accordance with definition (3.4)).

4.10.4 4. Some features of phase slipping processes

For any realistic experimental set-up the nonlinear equations (3.5) can be only solved numerically. In spite of all the simplifications introduced by the model considered above, the two coupled nonlinear equations for the real and imaginary parts of $\Delta = \Delta_1 + \mathrm{i}\Delta_2$ contain, in the general case, the space and time dependence and cannot be integrated for arbitrary geometry even
by numerical methods. Thus, in Ong et al. (1984) it is assumed that the phase slip takes place at an effective boundary between the moving CDW and the region near the measuring contacts. It is obvious, indeed, that if contacts possess a high conductivity, they shunt the sample currents in the contact vicinity giving rise to the local electric field values lower than the threshold field. However in general, the shape of such a boundary surface is quite complicated introducing an additional space dependence in eqs. (3.5). Therefore, quantitatively the problem may be formulated for channels which are long enough and where the phase slipping process occurs far enough from the contacts, i.e., on distances larger than the contact sizes. If so, the periodic phase slipping becomes the inherent nonlinear periodic process which is not strongly influenced by the details of how contacts are made. It seems that this assumption is qualitatively correct. If it is so, this would also explain the quasi-coherent character of the generated pulses.

4.1. Narrow channels

By definition, a long sample can be treated as a narrow channel if its thickness is less than the transverse coherence length. This is, of course, not so for most of the experimental situations. However, this assumption introduces the considerable simplification in the system of eqs. (3.5), since now they contain the dependence on only one of the space variables. It is expedient for what follows to write eqs. (3.5) also in the form of two equations determining the modulus and phase of the order parameter (2.1):

$$\begin{aligned} &|\dot{\Delta}| - \left(1 - \mathbf{Q}^2 - |\Delta|^2\right)|\Delta| + \nabla^2|\Delta| = 0 \\ &(\dot{\varphi} + E)|\Delta|^2 - \operatorname{div}\left(|\Delta|^2 \boldsymbol{Q}\right) = 0 \end{aligned} \tag{4.1}$$

where $\boldsymbol{Q} = \boldsymbol{\nabla}\boldsymbol{\varphi}$.

4.1.1. Dynamical character of phase slipping centers

From the definition of the phase

$$\varphi = \arctan \frac{\Delta_2}{\Delta_1}$$

it follows that the single PSC corresponds to the point where $|\Delta(x_0, t_n)| = 0$. The contribution made by the CDW motion to the longitudinal component of the current (the third term in eq. (3.3)) could vanish continuously if $\Delta \equiv 0$ at some point $x = x_0$. The static solution of this type is well known:

$$\Delta(x) = \tanh \frac{(x - x_0)}{\sqrt{2}}. \tag{4.2}$$

However, the formation of such a stationary soliton wall gives rise to an
additional surface energy, which, in any case, is disadvantageous in weak fields. As to the symmetric solution, it reduces in the vicinity of x_0 at the moment $t = 0$ to the form:

$$\Delta(x) \simeq a\,|x - x_0|\,. \tag{4.3}$$

Linearizing eq. (3.5)

$$\dot{\Delta} + \mathrm{i}E\Delta - \Delta - \nabla^2\Delta = 0,$$

we find:

$$\Delta(x,t) = a\frac{\exp[(1-\mathrm{i}E)t]}{2(\pi t)^{1/2}}\int_{-\infty}^{+\infty}|x'-x_0|\exp\left[-\frac{(x-x')^2}{4t}\right]\mathrm{d}x'.$$

Thus, the symmetric solution (4.3) vanishes, and $\Delta\,(x_0,t)$ increases with time. Therefore, as in superconductors (Ivlev and Kopnin 1980), a phaseslipping center turns out to be a dynamical object: $\Delta(x,t)$ can vanish only at specific moments of time, and this corresponds to a nonlinear periodic regime.

4.1.2. Location of phase slipping centers

In the phenomenological description presented above there was nothing to fix the location of the phase slipping center (the point x_0). The numerical solution would determine this position with the help of the boundary condition (2.6), selecting the most stable regime out of all conceivable regimes. Of course, it may turn out that, even in weak fields $E \ll 1$, the distance x_0 is of the order of the coherence length (in dimensionless units $\sim \xi_{\|}\big)$. But the fact that, in weak fields, the experimentally generated noise has the character of the discrete bursts (Monceau et al. 1980, Ong et al. 1984) and the spectrum consists of a large number of narrow lines, indicates that x_0 can be fairly large. For instance, Gill (1982) and Ong et al. (1984) have given as estimates for the effective distance over which the role of the contacts is important, values of the order of a fraction of a millimeter. However, their estimates are too large and reflect, probably, the mutual interaction of contacts (see section 5.1). The final answer in the framework of our scheme will be given by the numerical solution (Batistić et al. 1984). However, the upper estimation for the PSC position follows from arguments given in section 2: in the steady-state periodic regime the phase stops regularly interact with the boundary on distances given by eq. (2.7), i.e., at least on the diffusion width of the phase slip process.

\{}paragraph4.1.3. Strong electric fields ($E \gg 1$) In this case it is possible to obtain closed formulas for the phase slipping centers although, experimentally, this field region is evidently not of current interest. In the region $x \ll 1\,\big(x \sim E^{-1/2}\big)$ eqs. (3.5) for the complex Δ can be simplified.

$$\dot{\Delta} + \mathrm{i}E\Delta - \frac{\partial^2\Delta}{\partial x^2} = 0$$

The exact solution, satisfying the condition (2.6) at $x = 0$, to this equation is the superposition

$$\Delta = \Delta(0)\exp\left[-x(\mathrm{i}E)^{1/2}\right] + \frac{x}{\sqrt{2}}\exp(-\mathrm{i}Et) \tag{4.4}$$

The term linear in x has been chosen such that (4.4) can be matched with that solution to the nonlinear equation (3.5) which has the form

$$\Delta(x,t) = \tanh\left(\frac{x}{\sqrt{2}}\right)\exp(-\mathrm{i}Et)$$

in the region $x \gg E^{-1/2}$. Let us choose the simplest example in (2.6): $\Delta(0) = 1$. (The thermodynamic value of the gap is preserved near the boundary.) Using the condition $\Delta(x,t) = 0$ in expression (4.4), we easily find that

$$x_0 \approx (2E)^{-1/2} \ln E, \quad x_0 - Et_n = 2\pi n.$$

Integrating the oscillating component of the field in (3.3) over the coordinate, we obtain (in dimensionless units)

$$\delta V(t) = \sqrt{2}\lambda \left(1 - \frac{8}{9}\epsilon\right) \sin Et.$$

The amplitude of the potential oscillations does not depend on the electric field, and the position of the phase slipping center is clamped to the boundary at distances smaller than the coherence length.

4.1.4. Finite samples

In most cases real samples are rather small. Therefore some of the experimental results may depend on the length of the sample. In this section we shall show that in finite samples the threshold field for the CDW motion can be controlled by the boundary conditions on the sample ends.

According to the previous discussion, if the CDW moves inside the sample, this motion is to be accompanied by 'kinks' on both sides of the finite channel. This costs some energy, and at weak enough electric fields the stationary solutions of eqs. (3.5) or (4.1) may be preferable. The solution would have the form of the twisted spring in Fig. 1. To show that there is an upper limit for the field value above which the stationary solution is never stable, we consider eqs. (4.1) in the limit of low enough fields, $E \ll 1$. The contribution from the term with the second derivative (i.e. $\partial^2|\Delta|/\partial x^2$ in the first of eqs. (4.1)) is small and can be neglected since $|\Delta|$ varies slowly:

$$|\Delta|^2 = 1 - Q^2. \tag{4.5}$$

Substituting this into the second of eqs. (4.1) we obtain after integration:

$$3Q - \operatorname{arctanh} Q \simeq Ex \tag{4.6}$$

The left-hand side of eq. (4.6) has the form of a function with a maximum at $|Q|_{\max} = 1/\sqrt{3}$. In other words, the solution (4.6) is two-valued. The straightforward calculation with the use of eq. (3.5) shows that only the branch with $|Q| < 1/\sqrt{3}$ corresponds to the linearly stable solution. Therefore, at a given value of E, the solutions (4.5) and (4.6) become absolutely unstable for a long enough channel ($L > L_{\mathrm{c}}(E)$).

The nonstationary solution which develops above $E_{\mathrm{t}}(L)$ for a channel of length L, can not be found from the perturbative considerations. However, it is instructive to make, the following semiquantitative estimate. At small x, Q increases as $|Q| = Ex$. This corresponds to the additional contribution into the gradient term of the free energy expansion, $\sim Q^2|\Delta|^2$. Integrating over x (from $x = 0$ to $x = L$) one gets the energy loss due to increase of Q :

$$E^2 L^3$$

This energy may be compared with the energy needed for the formation of a 'kink' - the phase slipping center, in which $|\Delta|$ changes on the unit (or $\xi_{\|}$) scale. In this approach the stationary state with the growing gradient Q gets metastable already at the length of the channel

$$L_c \sim E^{-2/3} \tag{4.7}$$

These arguments have, of course, only the leading character. Nevertheless, they show that the threshold field $E_t(L)$ for the short channels does exist independently of the presence of the impurity pinning. Since, however, the new periodic regime which appears at $E > E_t(L)$, is stabilized by the strong nonlinearity of the equations describing the phase slipping process, the true threshold field $E_t(L)$ is to be found by the numerical methods.

4.2. Thick channels

Thus far we have investigated only the one-dimensional regime, in which the order parameter vanishes in the entire plane (at $x = x_0$) at t_n. In the case of a sufficiently thick sample the more stable solution could have a different form. For instance, this solution can look as the periodic (in the y-direction) array of 'vortices' that move in some plane $x = x_0$ in a direction, perpendicular to the current, with velocity $u_\perp$ (Gor'kov 1983, Ong et al. 1984). The periodicity along the y-direction, $\mathscr{D}$, is connected with the 'vortex' velocity by the trivial relation:

$$2\pi u_\perp = \Omega \mathscr{D}.$$

The physical meaning of such a 'vortex' structure is illustrated schema-

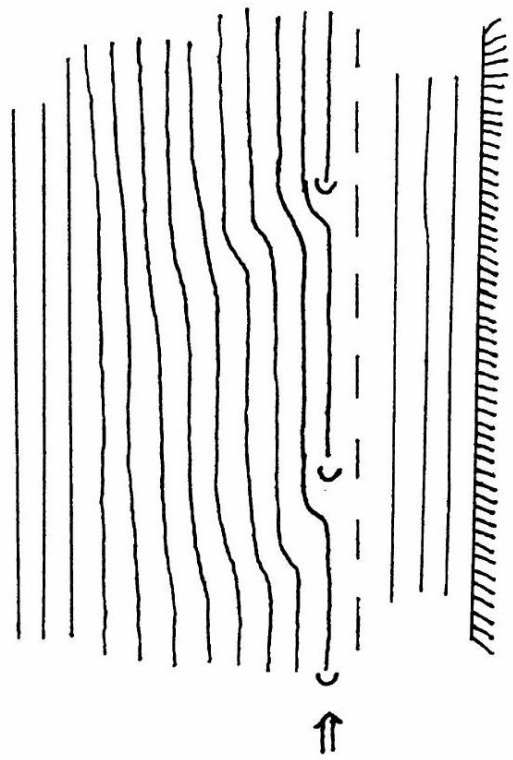


Fig. 2. The 'vortex' trail - dislocations in the superstructure lattice, running in the perpendicular direction to match the region of the fixed CDW with the one where the CDW is moving.

tically in fig. 2. The 'vortex' track corresponds to a 'train' of dislocations in the Peierls superstructure running in a perpendicular direction to compensate the phase transported by the CDW.

The old problems concerning the position of the $x = x_0$ plane in weak fields remain unanswered. In its turn, the distance between the dislocations is to be large in weak fields, i.e., the

system of dislocations corresponds to widely spaced, almost isolated lines. Assuming the form of the solution $\Delta(x, y - u_\perp t)$, we can estimate from eq. (3.5) the order of magnitude of the transverse velocity with the aid of (3.4):

$$u_\perp \sim \xi_\perp \omega_0 \sim \left(\overline{v_\perp^2}\right)^{1/2} (T_\mathrm{P}\tau_\mathrm{c})\,.$$

On applying the model to the relatively isotropic $NbSe_3$ we would obviously obtain overestimated values for the velocity $u_\perp$. Therefore, both the velocity $u_\perp$ and the periodicity $\mathscr{D}$ are, probably, field dependent. Besides, the result may also depend on the actual location of the $x = x_0$ plane. So far no attempts have been made to investigate these questions even numerically. One reason for this is that here the problem becomes more complicated since the single 'vortex' has a two-dimensional structure (in the x, y plane). Secondly, it is not clear at what sample thickness the plane regime is
replaced by the 'dislocation-trail' regime: the sample inhomogeneities and the surface barriers against the entry of the dislocation inevitably play an important role in this case (Fung and Steeds 1980). These factors may also give rise to some hysteretic features in the entire behaviour.

4.10.5 5. Some results of the numerical analysis

The numerical solution of eqs. (3.5) has been undertaken by Batistić et al. (1984) for narrow channels. No attempts have been made to compare the results of the solution quantitatively with the available experimental data since, firstly, it was clear from the very beginning that the chosen microscopic model oversimplifies the relaxation processes between excitations in the investigated, comparatively pure materials. Secondly, the samples used in the experimental works have had thicknesses much larger than the transverse coherence length.

5.1. Finite samples

The space and time variations of the CDW in the sample of finite length L were calculated with the assumption that the amplitude and the phase of the CDW remain fixed at $x = 0$ and $x = L$, and vary gradually towards the interior of the sample. The solution of the first equation in (3.5) were calculated for 'samples' with lengths L up to 100 at different values $E \ll 1$ (the lowest values for E were $\simeq 10^{-2}$).

The periodic behaviour $\Delta(x, t + t_\mathrm{p}) = \Delta(x, t)$ has always appeared at some fields $E > E_\mathrm{t}(L)$. The dependence of the threshold field on the sample length (already for $L \geqslant 15$) is well described by the power law:

$$E_\mathrm{t}(L) \simeq 2.55 L^{-\alpha},$$

with $\alpha = 1.23 \pm 0.05$. This result differs from our expectation (eq. (4.7)) obtained using energy balance considerations which are not expected to be quite correct in the nonlinear dissipative system.

At $E > E_\mathrm{t}(L)$ there are usually two phase slipping centers which gradually shift towards the sample edges with a further increase of the fields. The interference effects between them become relatively weak, and for large enough L the E-dependence of the PSC distance, x_ps, from the sample edge is indistinguishable from that obtained for a semi-infinite system (see the next subsection). The phase slip is a rather fast process, although the definite but rather weak minimum in $|\Delta|$ is present almost all the time. The position of the minimum moves from one side to another along the sample but the phase slip ($\Delta \equiv 0$) occurs each time in the same points, x_ps.

The time period of one cycle, t_p, may be rather long. In fact, the
dependence of t_p on the electric field can be fitted rather well by the square root law:

$$t_\mathrm{p} \sim \left(E^2 - E_\mathrm{t}^2\right)^{-1/2}$$

and this form does not depend on the specific value of L. On the other hand, as E increases, the time period approaches the asymptotic behaviour $t_\mathrm{p} \simeq 2\pi/E$, as is expected for infinite systems.

All the results are not strongly influenced by the asymmetry between the two sample edges if such an asymmetry is present. Only one time period has always been observed in all the numerical experiments described.

5.2. Semi-infinite channel

In this case CDW is taken to be fixed at the contact ($x = 0$), while far enough from the contact ($x \to \infty$) it acquires the form of the simple translational solution:

$$|\Delta| = 1, \quad \varphi = Et.$$

The range of investigated fields went from $E = 10$ down to $E = 10^{-2}$ and thus includes the analytical solution described in section 4.1.3. While the results for $E \geqslant 1$ reproduce well this solution, the range of small fields $E \leqslant 1$ is characterized by the power law

$$x_0 \equiv x_\mathrm{ps}(E) \simeq 1.15E^{-\gamma}$$

with

$$\gamma = 0.284 \pm 0.004$$

The time and space dependence of $\Delta(x,t)$ in the vicinity of x_0 is equivalent to that obtained for the long finite samples. As E decreases, the phase slipping process becomes more and more rapid and sharp on both x and t scales. The numerical analysis for fields weaker than $E \approx 10^{-2}$, was not possible. As above, all numerical solution after some time interval needed for stabilization, show the one-period behaviour. As a result, all the phase slipping processes always occur at the same positions on the x variable and in the equidistant time intervals.

To conclude this section it is expedient to write the explicit expression for the voltage oscillations, say, under the condition of a specified current. Thus, from (3.5) one immediately gets for the oscillating field component the following expression:

$$\delta E(x,t) = \lambda E\left(|\Delta|^2 - \overline{|\Delta|^2}\right) + \frac{16}{9}\lambda\epsilon\overline{|\Delta|^2}\dot{\varphi}$$

The voltage component is obtained by space integration.
The main characteristic feature of the phase slipping process in the model
under investigation (Batistić et al. 1984) is that the generated voltage contains many harmonics. This reflects the fact that the phase slip is a fast and well isolated process as has been emphasized above. Qualitatively, the basic properties of the quasi-coherent oscillations (field dependence, number of harmonics, etc.) obtained by Batistić et al. (1984), do correspond to the experimental observations.

4.10.6 6. Possible generalizations

To the best of the author's knowledge, there is so far only one serious attempt to generalize the equations describing the phase slipping centers (Artemenko et al. 1986a,b). As

we have mentioned in the very beginning, among numerous materials possessing the Fröhlich-conductivity mechanism, the case of $NbSe_3$ is an exception. Most of the others manifest a rather strong anisotropy in the electronic properties (especially, the conductivity) and therefore are better described by a more one-dimensional approach. In the low temperature Peierls state there is no free electrons, and the spectrum is characterized by a large gap. The system of the dynamical equations for this case is extremely complicated. However, it is still possible to formulate a set of equations for the isolated phase slipping center (i.e. at low enough electric fields) making use of the fact that the time and space scale for the gap variation are very short. Therefore, the solution for the PSC can be written separately in the form of an amplitude soliton with variable energy level. This solution serves then as a boundary condition for the effective kinetic equations (Artemenko et al. 1986a,b). The detailed numerical analysis in the framework of this scheme is so far absent.

4.10.7 7. Concluding remarks

The main part of this paper has been devoted to the discussion of the simple model for the CDW dynamical behaviour. This model, however, includes the phase slip. We have had no intention to provide an exhaustive review of all the peculiarities known for the so-called narrow-band spectrum generated by running CDW. The entire phenomenon is not completely understood. Even the experimental situation remains contradictory (the reader can find some discussion of this side of the problem in Thorne et al. (1987a,b,c, 1988)).

It seems to us that the importance of the phase slip concept stays underestimated, while so far it is the only microscopic mechanism providing a plausible explanation for this interesting phenomenon. In general terms
this mechanism can be formulated as the spontaneous conversion of the current carried by running CDW, into the current of ordinary carriers, giving rise to local oscillations of the electric field. During this process the local values of the order parameter drastically change near the phase slipping center, and this behaviour is described by dynamical nonlinear equations. From the mathematical point of view, the corresponding periodic behaviour is a cycle, i.e., it is the solution which is inherent in the physical nature of the equations.

At the discussion of the experimental situation the main attention is usually paid to the question where the oscillations are generated: in the interior of the sample or in the vicinity of contacts. First the idea of the phase slipping centers came from the analysis of processes occurring for running CDW in the vicinity of contacts with a normal metal. Correspondingly, some experiments have indicated in favour of the local origin of the generation mechanism and could be explained by the contact phenomena (Mozurkevich and Grüner 1983, Verma and Ong 1984, Zhang and Ong 1984, Brown and Mihaly 1985, Zhang et al. 1986). Subsequent experiments (Brown et al. 1985, Lyding et al. 1986, Monceau et al. 1986) called this statement in question. The experiments by Thorne et al. (1987a,b,c, 1988) quoted above, which have been done using rather perfect $NbSe_3$ crystals, also seem to favor the bulk character of the generation observed.

Two points attract attention in the generation phenomenon. The spectrum of oscillation consists of one fundamental frequency and many higher harmonics. The line, corresponding to the main frequency is very narrow and its width decreases with the improving of the sample quality. In the series of paper by Thorne et al. (1987a,b,c, 1988) these results are interpreted in terms of the so-called 'tunneling model' (see in Bardeen (1986) and references therein). This model has a definite achievement in the interpretation of the current-voltage characteristic behaviour in strong electric fields or in the presence of the alternating field of high frequency. To explain the above-mentioned peculiarities this model introduces, however, the idea of an average coherent potential of a complicated nonsinusoidal form, which is due to the background

of pinning impurities. It is rather difficult for us to accept such a picture.

The concept of the phase slipping centers realizing the periodical cyclic solutions of the dynamical equation, looks in all respects more plausible. So far, in this paper only those solutions have been described which correspond to the matched regions of the moving and fixed CDW. A natural generalization of this would be a solution for the region merging two parts of the CDW moving with different velocities. Such a situation seems to be inevitable in the interior of inhomogeneous samples. (As for the overall synchronization, we have seen in section 5.1 that even in the simple model described above, such a synchronization is already present between the two
sides of a rather long channel.) It seems that in the above model the translational solution $\varphi = Et$ remains stable with respect to the formation of the phase slipping centers in the interior of the semi-infinite channel, though, strictly speaking, such analysis has not been done. Meanwhile, solutions with the phase slipping centers, periodic both in the time and space coordinates, are well known in the theory of the so-called resistive state of superconductors (see in Ivlev and Kopnin (1978)). In this connection the study of the dynamical equations derived for the more realistic model, like the model mentioned in section 6 , is of the utmost interest.

To conclude, we believe that the concept of the phase slipping center as a nonlinear periodic regime for the corresponding dynamical equations is the most important one for understanding the origin of the quasi-coherent oscillations in the regime of running CDW. Unfortunately, not too much has been done in this direction so far. Why this is so, is quite clear - the dynamical equations based on the microscopical approach, are not simple. On the other hand, even for $NbSe_3$ eqs. (3.6) investigated above, have mainly an illustrative character because the region of their applicability (large concentrations of defects) does not correspond to the experimental situation.

4.10.8 References

Artemenko, S.N., and A.F. Volkov, 1981, Zh. Eksp. & Teor. Fiz. 81, 1872 [Sov. Phys.-JETP 54, 992].
Artemenko, S.N., A.F. Volkov and A.N. Kruglov, 1986a, Zh. Eksp. & Teor. Fiz. 91, 1536 [Sov. Phys.-JETP 64, 906].
Artemenko, S.N., A.F. Volkov and A.N. Kruglov, 1986b, Physica B 143, 146.
Bardeen, J., 1986, Physica B 143, 14.
Batistić, I., A. Bjelis and L.P. Gor'kov, 1984, J. Phys. (France) 45, 1049.
Brown, S.E., and L. Mihaly, 1985, Phys. Rev. Lett. 55, 742.
Brown, S.E., A. Janossy and G. Grüner, 1985, Phys. Rev. B 31, 6869.
Dumas, J., C. Schlenker, J. Marcus and R. Burder, 1983, Phys. Rev. Lett. 50, 757.
Fleming, R.M., and C.C. Grimes, 1979, Phys. Rev. Lett. 42, 1423.
Fleming, R.M., D.E. Moncton and D.B. McWhan, 1978, Phys. Rev. B 18, 5560.
Fröhlich, H., 1954, Proc. R. Soc. London Ser. A 223, 296.
Fukuyama, H., and P.A. Lee, 1978, Phys. Rev. B 17, 535.
Fung, K.K., and J.W. Steeds, 1980, Phys. Rev. Lett. 45, 1696.
Gill, J.C., 1982, Solid State Commun. 44, 1041.
Gor'kov, L.P., 1977, Pis'ma v Zh. Eksp. & Teor. Fiz. 25, 384 [Sov. Phys.-JETP Lett. 25, 358].
Gor'kov, L.P., 1983, Pis'ma v Zh. Eksp. & Teor. Fiz. 38, 76 [Sov. Phys.-JETP Lett. 38, 87].
Gor'kov, L.P., 1984, Zh. Eksp. & Teor. Fiz. 86, 1818 [Sov. Phys.-JETP 59, 1057].
Gor'kov, L.P., and E.N. Dolgov, 1979, Zh. Eksp. & Teor. Fiz. 77, 396 [Sov. Phys.-JETP 50, 203].
Gor'kov, L.P., and E.N. Dolgov, 1981, J. Low Temp. Phys. 24, 101.

Gor'kov, L.P., and G.M. Eliashberg, 1968, Zh. Eksp. & Teor. Fiz. 54, 612 [Sov. Phys.-JETP 27, 328].

Gressier, P., A. Meerschaut, L. Guemas, J. Rouxel and P. Monceau, 1983, J. Phys. (France) 1741.

Grüner, G., A. Zawadowski and P.M. Chaikin, 1981a, Phys. Rev. Lett. 46, 511.

Grüner, G., A. Zettl, W.G. Clark and A.H. Thompson, 1981b, Phys. Rev. B 23, 6823.

Horowitz, B., H. Gutfreund and M. Weger, 1981, Solid State Commun. 39, 541.

Ivlev, B.I., and N.B. Kopnin, 1978, Pis'ma v Zh. Eksp. & Teor. Fiz. 28, 640 [Sov. Phys.-JETP Lett. 28, 592].

Ivlev, B.I., and N.B. Kopnin, 1980, J. Low Temp. Phys. 44, 453.

Keldysh, L.V., and Yu.V. Kopaev, 1964, Fiz. Tverd. Tela 6, 2791.

Langer, J.S., and V. Ambegaokar, 1967, Phys. Rev. 164, 498.

Lee, P.A., and T.M. Rice, 1979, Phys. Rev. B 19, 3970.

Lyding, J.W., J.S. Hubacek, G. Gammie and R.E. Thorne, 1986, Phys. Rev. B 33, 4341.

Monceau, P., J. Richard and M. Renard, 1980, Phys. Rev. Lett. 45, 43.

Monceau, P., J. Richard and M. Renard, 1982, Phys. Rev. B 25, 931.

Monceau, P., M. Renard, J. Richard and M.C. Saint-Lager, 1986, Physica B 143, 64.

Mozurkewich, G., and G. Grüner, 1983, Phys. Rev. Lett. 51, 2206.

Ong, N.P., and G. Verma, 1983, Phys. Rev. B 27, 4495.

Ong, N.P., G. Verma and K. Maki, 1984, Phys. Rev. Lett. 52, 663.

Thorne, R.E., W.G. Lyons, J.W. Lyding, J.R. Tucker and J. Bardeen, 1987a, Phys. Rev. B 35, 6348.

Thorne, R.E., W.G. Lyons, J.W. Lyding, J.R. Tucker and J. Bardeen, 1987b, Phys. Rev. B 35, 6360.

Thorne, R.E., J.R. Tucker and J. Bardeen, 1987c, Phys. Rev. Lett. 58, 828.

Thorne, R.E., J.S. Hubacek, W.G. Lyons, J.W. Lyding and J.R. Tucker, 1989, Phys. Rev. B (to be published).

Verma, G., and N.P. Ong, 1984, Phys. Rev. B 30, 2928.

Weger, M., G. Grüner and W.G. Clark, 1980, Solid State Commun. 35, 243.

Zhang, X.J., and N.P. Ong, 1984, Phys. Rev. B 30, 7343.

Zhang, X.J., N.P. Ong and J.C. Eckart, 1986, Phys. Rev. Lett. 56, 1206.

This page intentionally left blank

4.11 11 Solitons in Crystals of Charge Density Waves by Brazovskii

4.11.1 1. Electrons and *CDW*

4.11.2 1.1. The selftrapping in a 1D model

Electronic properties of the charge density waves in quasi-1D conductors are so peculiar due to two reasons. The first one is the translational degeneracy which leads to phenomena of the Fröhlich conductivity (Fröhlich 1954, Lee, Rice and Anderson 1975). It shows itself in the giant dielectric susceptibility, in nonlinear and in nonstationary effects.* They are considered in most contributions in this volume. The second reason is a strong interaction of CDW deformations with excited electrons. It leads to the instability of electrons against a fast selftrapping which ends up as their conversion into various kinds of solitons.

From the point of view of semiconductor physics, the specific characteristics of a Peierls-Fröhlich state can be explained following Brazovskii (1978). In all semiconductors the interaction of the electrons (e) and the holes (h) with phonons leads to polaron effects and determines the structure of the fundamental edge. Among the three-dimensional substances this interaction can lead to selftrapping, i.e., to the formation of a tight-binding polaron only in ionic and

narrow-band dielectrics. A common feature of 1D systems is that the selftrapping effects take place at any type of electronphonon interactions (Rashba 1957). It is important that in a 1D system there is no barrier to selftrapping, so that the free electrons and holes are absolutely unstable. Among the 1D dielectrics in general a distinguishing feature of the Peierls-Fröhlich state is that for stationary interaction of the electron excitation with the amplitude and phase phonons, expressed in the scale of the gap $2\Delta_0$ for the energy and $\xi_0 = \hbar v_\mathrm{F}/\Delta_0$ for the length,** there is no small parameter. As a result a polaron state is produced with a characteristic dimension ξ_0 and the binding energy $\Delta_0 - E_\mathrm{s}$ and the depth of the local level $\delta E_0 = \Delta_0 - E_0$ turn out to be of the order of Δ_0. Thus the free

electrons in a quasi-1D Peierls-Fröhlich can be observed only in light absorption effects when, according to the Franck-Condon principle lattice deformations have low probability. All the long-lived excitations, i.e., all the intrinsic thermally activated charge and spin carriers and the extrinsic carriers produced as a result of charge transfer, doping, injection or optical pumping should be regarded as stationary states of a system with a deformed superstructure. They should be determined from the condition that the system energy has a local minimum when account is taken of the interaction of the electrons with the lattice deformations. In view of the deep selftrapping it is necessary to start out with the complete many-electron problem, which takes into account also the delocalized states of the valence electrons. The solutions of these problems (see Brazovskii and Kirova (1984) and the literature therein) have shown that the result of selftrapping differs strikingly in many cases from normal polarons. The resultant states have the character of topological solitons which connect various equivalent ground states of the system. These solitons have anomalous quantum numbers that result from total or partial cancellation of the charge density of the localized electrons and from the local perturbation of the electron density of the nonlocalized electrons of the continuous spectrum.

We attempt now to describe states assuming that the scale of the significant changes of δ and φ and of the wave functions of the electrons ψ is large compared with ξ_0, and the value of δ and the depth of the electron level $\epsilon = E - \Delta_0$ are small compared with Δ_0 :

$$\xi \gg \xi_0; \quad |\epsilon| \propto |\delta(x)| \ll \Delta_0.$$

The interaction of the electron e or of the hole h with the amplitude δ or phase phonons φ is determined by the Lagrangian

$$L\{\delta, \varphi, \psi\} = L_\delta + L_\varphi - \hat{\mathscr{H}} \tag{1.1}$$

where

$$\begin{aligned} L_\delta &= (2/\hbar v_\mathrm{F}\pi) \int \mathrm{d}x \left[\dot{\delta}^2/\omega_0^2 - \delta^2\right], & \omega_0 &= \lambda^{1/2}\bar{\omega}/2 \\ L_\varphi &= \int \mathrm{d}x \, (\hbar v_\mathrm{F}/4\pi) \left[\dot{\varphi}^2/u^2 - \varphi'^2\right], & u &= \omega_0 \xi_0/8 \\ \hat{\mathscr{H}} &= \int \mathrm{d}x \psi^*(x) \hat{H} \psi(x), & \hat{H} &= p^2/2m + \Delta_0 + \delta \pm \varphi' \hbar v_\mathrm{F}/2 \end{aligned} \tag{1.4}$$

The signs $\pm$ correspond to e and h, $\bar{\omega} = \omega\,(2k_\mathrm{F})$ is the bare phonon frequency, $m = \Delta_0/v_\mathrm{F}^2$.

We consider first the state with a short lifetime $\tau \ll \omega_0^{-1}$. In this case the fluctuations of δ and φ' constitute for the electron a Gaussian-white-noise
random potential being determined by the correlations at coincident instants of time. Then we arrive at the result that the absorption edge at $2\Delta_0$ is smeared on the scale $\epsilon_1 \propto (\omega_0^2 \Delta_0)^{1/3}$. Keeping in mind the definition of the Peierls model, i.e., $\Delta_0 \gg \omega_0$, we obtain that $\Delta_0 \gg \epsilon_1 \gg \omega_0$. This condition must be satisfied in the polyacethylene. But for CDW systems especially in

[0]*The comprehensive reviews were given by Monceau (1958) and by Grüner and Zettl (1985).

**$v_\mathrm{F}, k_\mathrm{F}$ and ϵ_F are the velocity, the momentum and the energy at the Fermi level of a metallic state. In the following text we put $\hbar = 1$.

organic materials we find commonly that $\omega_0 < \Delta_0$, so that $\epsilon_1 \leqslant \Delta_0$ and the optical edge would be smeared down. This conclusion seems to correspond to TaS_3. The general conclusion is that strong smearing of the fundamental edge in a Peierls dielectric is a particularly pronounced Urbach phenomenon and is not specially connected with the absence of long-range order in the 1D system.

A long-lived excited electron causes static distortion of the lattice. It can be seen from (1.1)-(1.4) that we have a typical polaron problem. Inasmuch for a polaron at rest the dynamical parameters u and ω_0 drop out of the problem the binding energy is $E_\mathrm{b} \propto \Delta_0$, i.e., we encounter the deep-level problem which is outside the scope of the approximation (1.1)-(1.4). At any rate it can be stated that the polaron size $\propto \xi_0 = hv_\mathrm{F}/\Delta_0$, and its mass is $m_\mathrm{p} \propto m\Delta_0^2/\omega_0^2$. An investigation of such a strongly selftrapped state calls for an exact solution which will be described in section 2 .

The intensity I_p of the optical excitation of a pair of selftrapped states can be estimated as:

$$\ln I_\mathrm{p} \propto -\left(\epsilon_0/\epsilon_1\right)^{3/2} \propto -\Delta_0/\omega_0.$$

In analogy the probability of the pure electronic mechanism for the transition of a polaron between chains should be small. The polaron effect explains the usual lowering of the activation energies and of the longitudinal conductivity compared with E_α for the transverse conductivity and with the value of $E_\mathrm{g}/2$ determined from the absorption edge.

In the approximation (1.1)-(1.4) we encounter the problem of total screening of the charge. An extremum solution for (1.3) and (1.4) yields

$$\rho(x) = \pi^{-1}\varphi'(x) + \psi^*(x)\psi(x) = 0, \quad \varphi(+\infty) - \varphi(-\infty) = -\pi, \tag{1.5}$$

so that it follows from the properties of the phase (Rice et al. 1976) that a charge is produced in the deformed CDW that screens completely the charge of the introduced electron. This result is confirmed by the exact solution discussed in section 2.

4.11.3 1.2. Electrons and polarons in a quasi-1D CDW system

One may anticipate that in a crystalline d-dimensional system of coupled CDW electronic excitations will become stable or metastable at least. Now we must distinguish (Brazovskii, Kirova and Yakovenko 1983) between the cases of weak and strong interchain coupling. Let us first consider weakly
coupled chains at low temperature, when they are perfectly coherent. We examine effects of interchain hopping which is characterized by the transfer integrals t. Let the particles wave function ψ and the CDW deformation δ to be distributed over the $N \gg 1$ chains. There are four terms:

$$-\delta, \quad 1/m^*l^2, \quad Nl\delta^2/v_\mathrm{F}, \quad t/N^{2/(d-1)}$$

which contribute to the total energy W. The first three of them correspond to the 1D problem (1.1)-(1.4) and the last one comes from the transfer part of the particle spectrum $t\left(k_\perp\right)$. Minimizing over δ and l we find that

$$l \propto N\xi_0, \quad \delta \propto \Delta_0/N^2, \quad W(N) \propto t/N^{2/(d-1)} - \Delta_0/N^2.$$

A layered system of chains like in MX_3 compounds is characterized by $d = 2$. Then we see that $W(N) < 0$ and it decreases for smaller N. We conclude that for $d = 2$ there are no barriers for the selftrapping. Eventually the result is the same as for a 1D model.

For a general case $d = 3$ we see that the band state is metastable: the barrier appears with scales l_0, N_0 and with a height V_0 :

$$l_0 \propto \xi_0 \Delta_0/t_\perp, \quad N_0 \propto \Delta_0/t_\perp, \quad V_0 \propto t_\perp^2/\Delta_0.$$

As soon as the chain incoherence (see below) of the impurities trap the particle under the region (l_0, N_0). The selftrapping goes on spontaneously with the result of a 1D model. We note that $V_0 \propto T_c$ - the 3D ordering temperature - so that the barrier is efficient only at $T \ll T_\mathrm{c}$.

There is a more important reason for the trapping and the subsequent selftrapping at $T \propto T_\mathrm{c}$. In a wide temperature range the phase difference $\varphi_\alpha - \varphi_\beta$ fluctuates strongly even if for nonzero order parameter $\langle \cos \varphi_\alpha \rangle = 0$ at $T < T_\mathrm{c}$. Then the single particle Hamiltonian

$$\left(\Delta_0 - \frac{1}{2m^*} \frac{\mathrm{d}^2}{\mathrm{d}x^2} \right) \delta_{\alpha\beta} + t_{\alpha\beta} \cos \frac{\varphi_\alpha - \varphi_\beta}{2}$$

shows a strong nondiagonal disorder in perpendicular directions unless $T \ll T_\mathrm{c}$. At $T \sim T_\mathrm{c}$ all eigenstates are localized on few chains so that the selftrapping is inevitable. The eigenstates become metastable at decreasing T when the localization length exceeds $N_0^{1/2}$.

We conclude that typically there are only hot particles with energy exceeding Δ_0 by $t_\perp$ or $m^* u^2$ which temporarily avoid the selftrapping. They will determine the transversal conductivity $\sigma_\perp$ while the longitudinal conductivity $\sigma_\parallel$and the thermodynamics will be determined by the selftrapped states - solitons. The coexistence of electrons and solitons is plausibly demonstrated in TaS_3 where the activation energies $E_{\mathrm{a}\parallel}$ and $E_{\mathrm{a}\perp}$ for $\sigma_\parallel$and $\sigma_\perp$ coincide at $T > T_\mathrm{c} \cong 200$ K where $E_{\mathrm{a}\parallel} \cong E_{\mathrm{a}\perp} \cong 750$ K which means that the single-particle transport dominates. For $T < T_\mathrm{c}, E_{\mathrm{a}\perp}$ is not changed essentially while $E_{\mathrm{a}\parallel}$ drops down to $\tilde{E}_\mathrm{a} \cong 200$ K. The last value may be
interpreted as the energy for a charge carrying soliton - presumably the 2π kink (see section 3.1) which can not carry the charge between the chains. (In this way the data for K(def)CP have been discussed by Brazovskii and Gordjunin 1980). Meanwhile the activation energy for the spin susceptibility in TaS_3 is characterized (Johnston et al. 1983) by an intermediate value $E_{\mathrm{a,sp}} \cong 600$ K which fits well the energy of the spin-carrying amplitude soliton (see sections 2 and 3). The discussion of experimental data on TaS_3 in terms of a concept of solitons was suggested by Nad' (1985).

The strong coupling case is defined by the inequality $\alpha/\lambda \gg 1$ where α is the degree of the anisotropy of interactions $\lambda(q_\perp)$ in the plane $(2k_\mathrm{F}, q_\perp)$. This case can be recognized experimentally, e.g., in $NbSe_3$, unlike TaS_3, since the same condition guarantees the mean field character of the phase transition (Gor'kov and Dzjaloshinskii 1974) at T_c - the absence of a precursion scattering, a pseudogap formation, etc.

Once again we consider the stationary problem (1.1)-(1.4) for a shallow state with $\delta \Rightarrow \delta_\alpha, \psi \Rightarrow \psi_{\alpha n}, \alpha$ and n being the indexes of a chain and of an eigenstate. The lattice energy must be generalized as

$$\frac{1}{\pi v_\mathbf{F}} \sum_{\boldsymbol{q}} (1 + f(\boldsymbol{q})) \delta_{\boldsymbol{q}}(x) \delta_{-\boldsymbol{q}}(x), \tag{1.6}$$
$$f(\boldsymbol{q}) = \lambda^{-1}(\boldsymbol{q}_\perp) - \lambda^{-1}, \quad \lambda = \lambda(\boldsymbol{q}_0) = \max_{\boldsymbol{q}_\perp} \lambda(\boldsymbol{q}_\perp),$$

where $\delta_{\boldsymbol{q}_\perp}(x)$ is a Fourier transformation of $\delta_\alpha(x)$. A variation of (1.1)-(1.4) and (1.6) gives

$$\delta_\alpha = \frac{1}{8\pi} v_\mathrm{F} S_\perp \int \mathrm{d}^2 \boldsymbol{q}_\perp \left[1 + f(\boldsymbol{q}_\perp)\right]^{-1} \exp\left[\mathrm{i}\boldsymbol{q}_\perp (\boldsymbol{R}_\alpha - \boldsymbol{R}_\beta)\right] \rho_\beta(x) \tag{1.7}$$
$$\rho_\beta(x) = \sum_n \psi^*_{\beta n} \psi_{\beta n}, \quad S_\perp = a_1 a_2; \quad \boldsymbol{R} = (R_1, R_2)$$

By definition $f(\boldsymbol{q}_\perp)$ has a sharp minimum at $\boldsymbol{q}_\perp = \boldsymbol{q}_0$:

$$f(\boldsymbol{q}_\perp) = b_1\kappa_1^2 + b_2\kappa_2^2, \quad \boldsymbol{q} = \boldsymbol{q}_0 + \left(\frac{\pi}{a_1}\kappa_1, \frac{\pi}{a_2}\kappa_2\right), \quad \kappa_{1,2} \ll 1,$$

b_1 and/or $b_2 \propto \alpha/\lambda \gg 1$.
Again we shall consider the two cases: $d = 2, b_1 \gg 1, b_2 \leqslant 1$ and $d = 3$, $b_1 \propto b_2 \gg 1$.

We see from (1.7) that the deformation spreads over a large number $N_\mathrm{d} \gg 1$ of chains, while it varies slowly ($\delta_\alpha(x) \cong \delta_0(x)$) at the central chains where few $N \ll N_\mathrm{d}$ electrons are localized. Hence the eigenstates may be approximated as $\psi_{n\alpha}(x) \cong \psi_0\delta_{n\alpha}$ where ψ_0 and its eigenvalue $\epsilon = \epsilon(N)$ is to
be found from the equations

$$\left[\frac{-1}{2m^*}\frac{\mathrm{d}^2}{\mathrm{d}x^2} + \delta_0(x) - \epsilon\right]\psi_0(x) = 0, \tag{1.8}$$

$$\delta_0(x) = -\pi^2 A_\mathrm{d} N v_\mathrm{F}\psi_0^2/2, \quad A_\mathrm{d} \propto N_\mathrm{d}^{-1} \ll 1,$$

$$A_3 \approx \ln(b_1b_2)/(b_1b_2)^{1/2}, \quad A_2 \approx b_\mathrm{d}^{1/2}. \tag{1.9}$$

Finally we arrive at the following values for the total energy $W(N)$ of the N-particle polaron, for $\epsilon(N)$ and for the localization length $l(N)$,

$$W(N)/\Delta_0 = N\epsilon(N)/3\Delta_0 = -N\xi_0^2/6l^2(N) = -\pi^2N^3A_\mathrm{d}^2/24. \tag{1.10}$$

The chemical potential of electrons is $\mu = \Delta_0 + \partial W/\partial N$. The values (1.10) as functions of N saturate at $N \propto N_\mathrm{d}$ on the scale of a 1D model and our approximation fails. (Also we can not neglect the phase deformations (1.3) anymore.) Keeping in mind that always $\Delta_0/\epsilon_\mathrm{F} > 10^{-2}$, i.e. $\lambda > 1/5$, and that $\alpha < 1$ we see that $b < 5$, so that $N_\mathrm{d} \leqq 4$. Hence the selftrapping becomes deep already for $2-4$ particles which form the droplet on the neighboring chains, while it is negligible for a single particle. One can show that Coulomb repulsion does not change these estimations under the condition $(e^2/\hbar v_\mathrm{F})(\xi_0^2/S_\perp) \gg 1$ which always takes place.

In conclusion the strong interchain structural coupling of CDW stabilizes electrons as intrinsic carriers (ones with a minimal E_a). At the same time extrinsic carriers (ones with a minimal μ) are unstable against aggregation in a droplet where the phase-slip is finally formed.

4.11.4 2. Amplitude spin carrying solitons in a 1D model

In this section we construct the terms for a complete selftrapping of the particles. We describe in detail a nearly amplitude spin carrying soliton which appears as a result of the selftrapping of a single electron or a hole.

The exact energy functional $W\{\Delta\}$ can be written in a form:

$$W\{\Delta\} = \int \mathrm{d}x \left[\frac{\Delta^2}{\pi v_\mathrm{F}\lambda} - \mathrm{i}B\right)\left(\Delta^*\frac{\mathrm{d}\Delta}{\mathrm{d}x} - \Delta\frac{\mathrm{d}\Delta^*}{\mathrm{d}x}\right)\Big] + \sum E\{\Delta\}, \tag{2.1}$$

where $\Delta(x)$ is a complex field of lattice deformations $\zeta(x)$:

$$\zeta(x) = \Delta(x)\exp(\mathrm{i}2k_\mathrm{F}x) + \Delta^*(x)\exp(-\mathrm{i}2k_\mathrm{F}x), \quad \Delta(\pm\infty) = \Delta_0 \sim \epsilon_\mathrm{F}\mathrm{e}^{-1/\lambda}.$$

The first term in (2.1) is the lattice energy which takes into account the dispersion of phonons (Brazovskii 1980, Brazovskii and Matveenko 1984).

$$\omega(2k_\mathrm{F} + q) = \bar{\omega} + sq, \quad s = \pi\lambda v_\mathrm{F}\bar{\omega}B, \quad B \propto 1/\lambda\epsilon_\mathrm{F}. \tag{2.2}$$

The eigenvalues $E = E\{\Delta\}$ correspond to those states which are twofold filled for the continuum spectrum $E < \Delta_0$ and ν-fold filled ($\nu = 0, 1, 2$) for the local level $E_0, \Delta_0 \geqslant E_0 \geqslant -\Delta_0$. They have to be determined by the equations for the eigenfunctions $\psi(x)$:

$$\begin{pmatrix} -\mathrm{i}v_\mathrm{F}\frac{\mathrm{d}}{\mathrm{d}x} - E & \Delta \\ \Delta^* & \mathrm{i}v_\mathrm{F}\frac{\mathrm{d}}{\mathrm{d}x} - E \end{pmatrix} \begin{pmatrix} \psi_+ \\ \psi \end{pmatrix} = 0$$

$$\psi(x) = \psi_+(x)\exp(\mathrm{i}k_\mathrm{F}x) + \psi_-(x)\exp(-\mathrm{i}k_\mathrm{F}x) \tag{2.3}$$

There is an adequate parameterization of the selftrapping process which gives the exact solution for the equilibrium state. We obtain it by introducing a 'chord-like soliton' $\Delta(x) = \Delta_1 + \mathrm{i}\Delta_2(x)$ as shown in the fig. 1 . Here the points $\pm\infty$ show the asymptotical configurations far from the soliton, $x \Rightarrow \pm\infty$, which must be settled at the circle $\Delta = \Delta_0$. For an unperturbed CDW they coincide at the same point which may be either $\mathrm{O}, \theta = 0$, or O', $\theta = \pi$. There is just one localized eigenstate ψ_0 with an eigenvalue E_0. For a onefold filling, $\nu = 1$, it gives the distribution of the spin: $\rho_0(x) = \psi_0^2(x)$. Concerning the charge distribution $\rho(x)$ there are also the distorted continuous states contributing to it. (In the shallow approximation (1.1)-(1.4) this effect has been taken into account in (1.5) via φ'.)

For a soliton with a given θ one finds the following parameters:

$$E_0 = \Delta_1 = \pm\Delta_0\cos\theta, \quad \Delta_2 = \mp k_0\tanh(k_0x), \quad k_0 = \Delta_0\sin\theta,$$

$$\rho_0(x) = k_0/2\cosh^2(k_0x), \quad \rho(x) = (\nu - 2\theta/\pi)\rho_0(x), \tag{2.4}$$

$$W_\nu(\theta) = \Delta_0[(\nu - 2\theta/\pi)\cos\theta + (2/\pi)\sin\theta] + B\Delta_0^2\sin 2\theta. \tag{2.5}$$

The energies for the three selftrapping terms are plotted in fig. 2. The minima $W_\nu(\theta)$ give as the following equilibrium states:

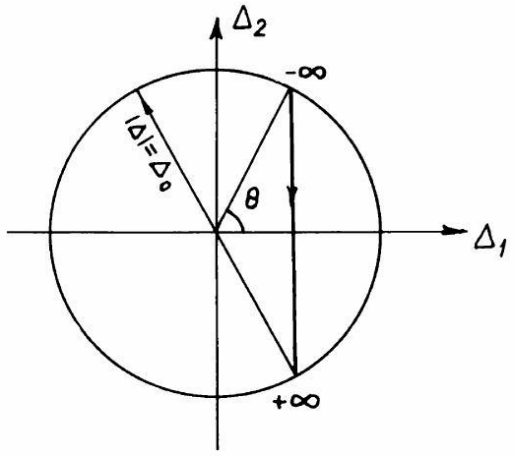


Fig. 1. The soliton trajectory on the plain of complex order parameter.

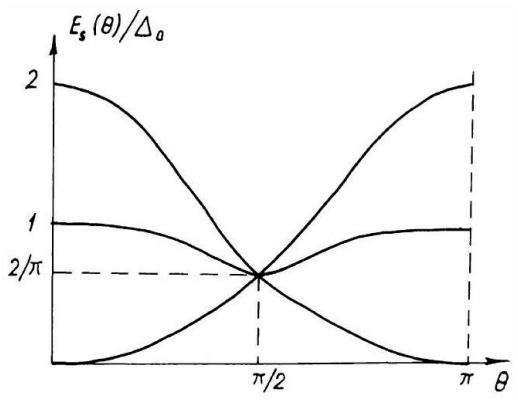


Fig. 2. The selftrapping terms for ν particles. $\nu = 0, 1, 2 \cdot 2\theta$ is a chiral angle.

(i) $\nu = 0, \theta = 0, W_0 = 0$. This is the homogeneous CDW in the ground state.
(ii) $\nu = 2, \theta = \pi, W_0 = 0$. This is a system with an additional filled level in an extended homogeneous ground state.

We conclude that there are no singlet ($\nu = 0, \nu = 2$) stationary excited states. Any excited pair of electrons or holes will be absorbed in the ground state without a barrier after a time $\tau \propto \omega_0^{-1}$. This nonradiative recombination, in accordance with a qualitative analysis given in section 1 goes through intermediate nonstationary polaron states.
(iii) We consider now the case of one electron. We have here an already nontrivial stationary state:

$$\nu = 1, \quad \theta = \pi/2, \quad k_0 = \Delta_0/v_\mathrm{F}, \quad E_0 = \Delta_1 = 0, \quad W_1 = 2\Delta_0/\pi, \tag{2.6}$$

which we shall investigate hereafter.
We note that this solution with $\theta = \pi/2$ has electron-hole symmetry, i.e., the selftrapping of either electron or a hole leads to the same result. It is not surprising therefore that the total electron density remains homogeneous and that the local charge of the soliton is zero.

The injected charge e is distributed homogeneously over the whole length L of a chain with a density e/L which does not depend on the soliton coordinate x_0. Consequently it cannot correspond to the current.

It is noteworthy that the energy of the amplitude soliton is completely delocalized (Brazovskii 1978, 1980). Evidently there are the lattice $w_\mathrm{lat}\,(x)$ and the bound state $w_\nu(x)$ counterparts of the energy density

$$w_\mathrm{lat}\,(x) = \left[\Delta^2(x) - \Delta_0^2\right]/\pi v_\mathrm{F}\lambda, \quad w_\nu(x) = \nu E_0 \rho_0(x).$$

Also there is a counterpart from the continuous spectrum which happens to be $w_\mathrm{c}(x) = -2\theta E_0\rho_0(x)/\pi$. The total energy density is finally

$$w(x) = w_\mathrm{lat} + w_\nu + w_\mathrm{c} = \Delta_0(\nu - 2\theta/\pi)\rho_0(x)\cos\theta + \mathrm{O}(1/L) \tag{2.7}$$

At the equilibrium (2.6) we find that $w(x) = \mathrm{const} \times 1/L$, i.e. $w(x) = 2\Delta_0/\pi L$. Thus the local changes of electron and lattice energies cancel each other completely.

The lattice dispersion term B in (2.1) preserves the general chord-like form (2.4) of the soliton to be an exact solution (Brazovskii and Matveenko 1984). It leads to the additional last term $\sim B\Delta_0^2 \sim \Delta_0^2/\epsilon_\mathrm{F}$ in the energy (2.5). This in part does not affect the equilibrium points for $\nu = 0$, 2, i.e. the homogeneous CDW . At $\nu = 1$ the equilibrium point of the spin soliton is slightly changed: $\boldsymbol{\theta} < \pi/2$. It results in the appearance of a small charge q and in shifting of the midgap level E_0 :

$$\theta = (\pi/2) - \alpha, \quad q_s = \alpha e/\pi, \quad E_0 \simeq \alpha\Delta_0, \quad \alpha \simeq \pi B\Delta_0, \tag{2.8}$$

Altogether with a charge a local energy (2.4) appears $w_{\text{lok}}(x) = 2\Delta_0\alpha^2/\pi$. In some materials like MX_4-based compounds (see Monceau 1985) the ratio Δ_0/ϵ_F may not be small so that qualitative effects of the phonon dispersion can be observed. For example the shifting of E_0 splits the midgap absorption peak.

In conclusion the single electronic excitations of a 1D CDW are transformed into the amplitude solitons which are the main spin carriers in the system. Unlike electrons their couplings to electric field and to the thermal gradients are very small being related to the effects of the lattice dispersion.

4.11.5 3. Spin carrying solitons in a system of coupled chains

3.1. The adaptation of a soliton

All perturbations that lowered the degeneracy of the ground state of the single chain exert a strong influence on the soliton structure. Such perturbations are the commensurability effects, the interactions between the chains and with impurities. Their role manifests itself at large distances $x \gg \xi_0$, where account need be taken of only the change of the phase φ_α of the field $\Delta_\alpha(x)$, where α is the chain index. The state of the system outside the core ($x \leqq \xi_0$) of the amplitude soliton can be determined from the condition that the phase energy functional $\mathscr{H} = \mathscr{H}\{\varphi_\alpha(x)\}$ be a minimum:

$$\mathscr{H} = \int \mathrm{d}x \left[\sum_\alpha \left(v_F \frac{\varphi'^2_\alpha}{4\pi} - \frac{T_P^2}{v_F} \cos n\varphi_\alpha \right) - \sum_{\alpha,\beta} \frac{CT_c^2}{v_F} \cos(\varphi_\alpha - \varphi_\beta) \right] \tag{3.1}$$

$T_c, T_p \ll \Delta_0, C \propto 1$. Here T_c is the temperature of the three-dimensional ordering of the system, T_p is the pinning temperature, α and β are the indexes of the neighboring chains. The Hamiltonian (3.1) determines the structure of the system for selftrapping of two particles, distorting the term $\nu = 2$, fig. 2 in the region $\theta = \pi$. In place of the new homogeneous state expanded to cover two particles, we obtain now a set of solitons that connect equivalent states with $\varphi = 2k\pi/n, k = 0, 1, \ldots$ (Rice et al. 1976). For the correlated chains their interaction $\propto T_c^2$ in (3.1) can be qualitatively considered as a commensurability of the order $n = 1$. Then the selftrapping along the term $\nu = 2$ in fig. 2 results in a formation of a 'phase-slip center', where the phase of one chain changes by 2π relative to the surrounding ones. The charge of the center is $q = 2e$ and its energy is $E_s \propto \max(T_c, nT_p)$. These excitations probably determine the small lowtemperature activation energies and conductivities observed in many materials, as has been discussed, in section 2 .

The amplitude solitons take the system out of the equilibrium determined by the minimum of the Hamiltonian (3.1). It makes them incompatible with all odd n since there are no pairs of equilibrium points which differ by $\pm\pi$. Nevertheless the system adopts itself to the appearance of the amplitude soliton by the equalization of the phase in a region of dimensions $l \propto v_F/T_c$; or $l \propto v_F/T_p, l \gg \xi_0$ on the tails of the soliton. The electron density becomes perturbed in this region, and as a result a spin soliton can acquire an electric

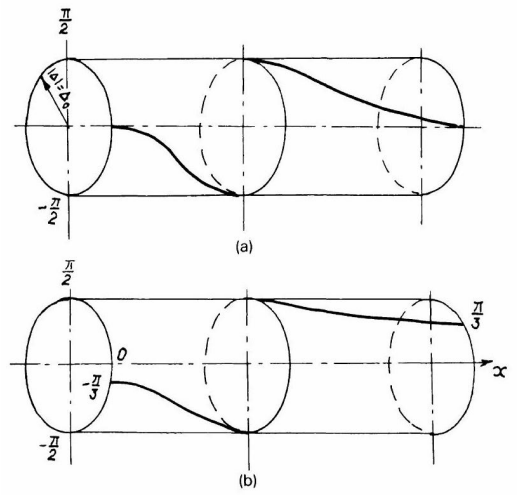


Fig. 3. The trajectories of adaptation case. (a) The case of interchain ordering. (b) The case of a threefold commensurability.

charge. This phenomenon is investigated in detail below in sections 3.2-3.4 with the interaction between chains as an example. The commensurability effects are investigated similarly. The plots of the complex function $\Delta(x)$ are shown in fig. 3a for $n = 1$ and fig. 3b for $n = 3$. A change in $\Delta(x)$ takes place near the surface of the cylinder $|\Delta(x)| = \Delta_0$ at $|x| \gg \xi_0$ and near its diametrical plane at $|x| \ll \xi_0$ in accordance with fig. 1. The function $\varphi(x)$ is plottted in fig. 4a as $\varphi_0(x)$. At $n = 3$ we have $\varphi(\pm\infty) = 0, 2\pi$. In the vicinity of the core of the amplitude soliton $\varphi(x) \simeq (\pi/2)\,\mathrm{sgn}\,(x - x_0)$ the charge of the soliton is

$$q_\mathrm{s} = e\left[(\varphi(+\infty) - \varphi\,(x_0 + 0)) + (\varphi\,(x_0 - 0) - \varphi(-\infty))\right]. \tag{3.2}$$

We obtain

$$n = 1: \quad q_\mathrm{s} = e; \quad n = 3; \quad q_\mathrm{s} = e/3.$$

A fractional charge for spin solitons at $n = 3$ was obtained by Brazovskii (1980). In another way it was considered by Su and Schrieffer (1981) and in subsequent publications (see Yu Lu 1988 for a detailed review).

3.2. The cluster model for a short-range order

In a system of weakly coupled chains, $T_\mathrm{c} \ll \Delta_0$, the soliton formation due to the selftrapping of an electron takes place mainly independently on the surrounding chains. As a result, however, the sign of the parameter $\Delta(x)$ is reversed on the central chain ($\alpha = 0$) on going through the region of the soliton with the center at the point $x_0 = 0$. Inasmuch as originally the chains have been correlated, the change of the sign of $\Delta(x)$ far from the soliton becomes equalized. To describe the effect we consider the cluster model of the nearest chain coordination. In the limit $Z \Rightarrow 0$ we arrive at the MF approximation for the 3D ordered phase. We take into account the chain with $\alpha = 0$, which carries the soliton, and its Z nearest neighbors. Since the equalization will take place at a distance $l \propto \hbar v_\mathrm{F}/T_\mathrm{c} \gg \xi_0$ we can use a quasiclassical description in terms of the phases φ_α on the chains, assuming that $|\Delta_\alpha(x)| \equiv \Delta_0$. The presence of the soliton is taken into account here by the discontinuity of the phase $\varphi_0(x)$

$$\varphi_0\,(x_0 + 0) - \varphi_0\,(x_0 - 0) = \pi \tag{3.3}$$

at continuous phases $\varphi_\alpha(x), \alpha \neq 0$, see fig. 4a.
The described model is characterized by an energy functional which follows from (3.1) for identical φ_α :

$$\mathscr{H}\{\varphi_\alpha\} = \frac{Z}{4\pi\hbar v_\mathrm{F}}\left[\varphi_\alpha'^2 - \frac{1}{(Z+1)l^2}\cos(\varphi_\alpha - \varphi_0)\right], \tag{3.4}$$
$$\varphi_\alpha = \varphi_0 + \psi, \quad l \propto \hbar v_\mathrm{F}/T_\mathrm{c}.$$

The equilibrium state of the system is described by the extremals of the functional (3.4) with the supplementary condition (3.3). The functions φ_0 and ψ satisfy the equations

$$(Z+1)\varphi_0'' + Z\psi'' = 0 \tag{3.5}$$
$$(Z+1)\psi'' + (Z+1)\varphi_0'' - l^{-2}\sin\psi = 0$$

with the boundary conditions

$$\psi(x), \psi'(x), \varphi_0(x) \to 0, \quad \text{at } x \to \pm\infty, \tag{3.6a}$$
$$\varphi_0(x) = -\psi(x) = \frac{1}{2}\pi\,\mathrm{sgn}(x - x_0), \quad \text{at} \quad x \to x_0. \tag{3.6b}$$

From (3.5) and (3.6) we obtain the following solutions:

$$\psi(x) = -4\,\mathrm{arctg}\left[\exp\frac{l_0 - |x - x_0|}{l}\right]\mathrm{sgn}(x - x_0)$$
$$\varphi_0(x) = \frac{1}{Z+1}\left[\frac{\pi}{2}\,\mathrm{sgn}\,x - Z\psi(x)\right] \tag{3.7}$$
$$\varphi_\alpha(x) = \frac{1}{Z+1}\left[\frac{\pi}{2}\,\mathrm{sgn}\,x + \psi(x)\right]$$

where $l_0 = l\ln[\mathrm{tg}(\pi/8)]$. Plots of $\varphi_0(x)$ and $\varphi_\alpha(x)$ are shown in fig. 4a.
Although the core of the soliton is not charged, in the region of phase relaxation $\xi_0 \ll |x - x_0| \leqslant l$ there appear charges q_α with density $\rho_\alpha(x) = e_\alpha\varphi_\alpha'(x)/\pi$, where $e_\alpha = \pm e$ is a carrier charge for a chain α in the metallic phase

$$q_0 = 2\frac{e}{\pi}\left[\varphi_\alpha(\infty) - \varphi_\alpha(0)\right] = -eZ/(Z+1)$$
$$q_\alpha = \frac{en}{\pi}\left[\varphi_\alpha(+\infty) - \varphi_\alpha(-\infty)\right] = e_\alpha/(Z+1) \tag{3.8}$$

We note that here the sign of q_0 is opposite to the sign of the charge $e_0 = \pm e$ of the initial carriers. For the opposite choice of the sign of the right-hand sides of eq. (3.3) and (3.6b) the sign of the charge q_0 in (3.3) will also be changed. This case will correspond to the direction of the trajectories which have been chosen on fig. 1 and fig. 3 to describe the electron selftrapping. The former boundary conditions (3.3) and (3.3b) correspond to the hole selftrapping. We conclude, that the charge q_0 in the tails of the amplitude soliton has the same sign as for the original carrier. The magnitude of q_0 tends to $\pm e$ only for $Z \Rightarrow \infty$. In the limit $Z \Rightarrow \infty$ the charge of every neighboring chain $q_\alpha, \alpha \neq 0$ is zero. Nevertheless their integral charge remains finite, so that the total charge of the system q

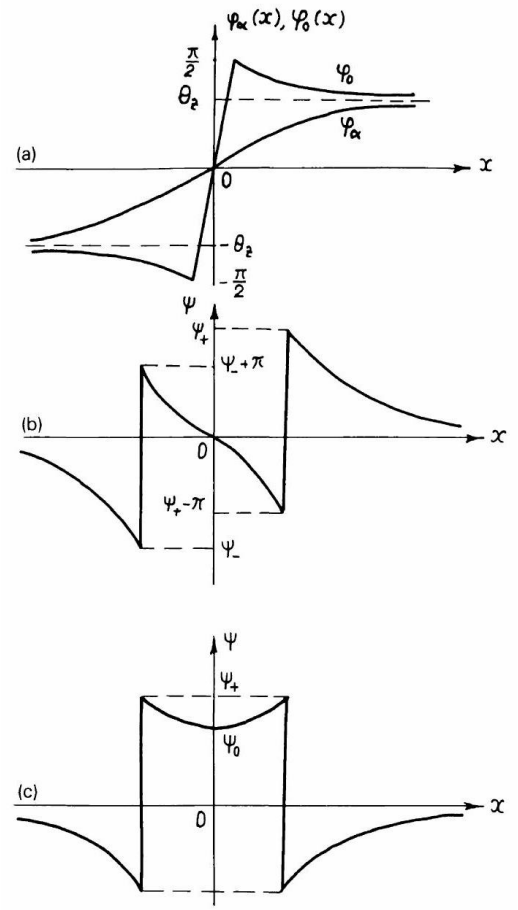


Fig. 4. The plots of phases for central φ_{0}, and surrounding φ_α chains. $\psi = \varphi - \varphi_0$: (a) a single soliton, (b) two solitons of the same signs, (c) two solitons of opposite signs.

depends on the signs of the charges of the carriers $\boldsymbol{e_\alpha}$. The following three cases are possible:
(a) All of the chains have the same charges - the single type of CDW,

$$e_\alpha = e_0, \quad q = q_0 + Zq_\alpha = 0$$

(b) The surrounding chains have charges opposite to that of the central chain - the two types of CDW alternating in both directions,

$$e_\alpha = -e_0, \quad q = q_0 - Zq_\alpha = -2Ze_0/(Z+1).$$

As $Z \to \infty$ we have $q \to -2e$, the charge is doubled.
(c) The charges of the chains alternate - the two types of CDW alternating across the layers, e.g. TTF-TCNQ,

$$\sum_{\alpha \neq 0} e_\alpha = 0, \quad q = q_0 = -Ze/(Z+1)$$

As $Z \to 0$ we have $q \to -e$, and the system has a single charge.

3.3. Interaction of solitons

The interchain coupling leads also to the most substantial interaction between the solitons. As indicated above, we can speak of solitons having two signs, $\psi(x) \cong \pm(\pi/2)\,\mathrm{sgn}\,(x - x_i)$ at $x \to x_i$ which have been originated by electron or hole selftrapping respectively. We consider

two solitons of the same sign, located at the points $x_{1,2} = \pm d/2$. The boundary condition (3.6b) is generalized in accordance with fig. 4b:

$$\psi\left(-\frac{1}{2}d - 0\right) = \pi + \psi\left(-\frac{1}{2}d + 0\right) = \psi_-$$
$$\psi\left(\frac{1}{2}d + 0\right) = -\pi + \psi\left(-\frac{1}{2}d - 0\right) = \psi_+ \tag{3.9}$$

The solutions of eqs. (3.5) outside the discontinuity points $x = \pm d/2$ are characterized by first integrals H or parameters k :

$$l^2\psi'^2 - 2(1 - \cos\psi) = 2H, \quad H = 2\left(1 - k^2\right)/k^2 \tag{3.10}$$

It follows from (3.6a) that at $|x| > d/2$ we have $H = 0$ and $k = 1$. At $|x| < d/2$ there is a point $x = 0$ where $\psi = 0, \psi' \neq 0$, so that $H > 0, k < 1$. According to the least-action principle for the functional (2) the quantity $H = H(d)$ is proportional to the force $\mathscr{F}$ of the interaction between the solitons:

$$\mathscr{F} = -\partial\mathscr{H}/\partial d = \left(v_{\mathrm{F}}H/2\pi^2 l\right) Z/(Z+1) \tag{3.11}$$

We obtain that the interaction is repulsive. The value of $\mathscr{H}$ on the extremal (3.5) is equal to

$$\frac{2\pi}{v_{\mathrm{F}}} l^2 \frac{Z+1}{Z}\mathscr{H} = \int_{\psi_-}^{\psi_+} \left[H + 4\sin^2\psi/2\right] + \int_{\psi_+ - \pi}^{\psi_- + \pi} 2|\sin\psi/2|\mathrm{d}\psi - Hd. \tag{3.12}$$

Varying (3.7) with respect to $\psi_+$and ψ_-at a specified H, we find that the solution is antisymmetric and

$$\cos\psi_\pm/2 = 1/\sqrt{2}k, \quad \psi_+ = -\psi_-, \quad 1/\sqrt{2} \leqslant k \leqslant 1$$

The solution of eqs. (3.5) can be written in the form

$$\cos\psi/2 = \mathrm{sn}[K(k) - x/kl; k]$$

where $K(k)$ is a complete elliptic integral of the first kind. The value of k is determined according to (3.4) from the equation

$$\mathrm{sn}(K(k) - d/2kl; k) = 1/\sqrt{2}k,$$

at large distances

$$d \gg l, \quad k \to 1, \quad \psi_\pm \to \pi/2 \quad \text{and} \quad H \cong \left[32/(\sqrt{2}+1)^2\right] e^{-d}. \tag{3.13}$$

We have found, in particular, that for a single soliton the phase relaxation proceeds antisymmetrically. At $d \ll 1$ we have $k \to 1/\sqrt{2}, \psi_\pm \to 0$ and $H \to 0$, i.e., the repulsion force is finite.

We consider now the case of solitons of opposite sign. In place of (3.9) we have, in accordance with fig. 4c,

$$\psi\left(-\frac{1}{2}d + 0\right) = \psi\left(\frac{1}{2}d - 0\right) = \psi_+,$$
$$\psi\left(-\frac{1}{2}d - 0\right) = \psi\left(\frac{1}{2}d + 0\right) = \pi - \psi_+.$$

Since $\psi'(0) = 0$ and $\psi(0) \neq 0$ we now have in (3.10) $H < 0$ i.e., attraction takes place. In place of (3.12) we have

$$\frac{2\pi}{v_{\mathrm{F}}} l^2 \frac{Z+1}{Z} \mathscr{H} = 2 \int_{\psi_0}^{\psi_+} \left[2\mathscr{H} + 4 \sin^2 \psi/2 \right] \mathrm{d}\psi + 4 \int_{\psi_+ - \pi}^{0} \sin^2 \psi/2 \; \mathrm{d}\psi - Hd. \tag{3.14}$$

Varying (3.15) with respect to ψ_0 and ψ_+we obtain

$$\cos \psi_+ = -\sin^2 \psi_0/2, \quad H = -2 \sin^2 \psi_0/2 \tag{3.15}$$

The solution of eq. (3.10) is now

$$\cos \psi/2 = \cos(\psi_0/2) \, \mathrm{sn} \left[K(\cos \psi_0/2) - x/l; \cos \psi_0/2 \right] \tag{3.16}$$

According to (3.15) and (3.16) the value of ψ_0 is determined from the equation

$$\mathrm{sn} \left[K(\cos \psi_0/2) - d/2l; \cos \psi_0/2 \right] = 1/\sqrt{2}$$

Its solution has a continuous singularity at the point $d/l = \pi/2$. At $d \gg l$ we have $\psi_0 \to 0, \psi_+ \to \pi/2$ and H coincides with (3.13) changing the sign. At $d \leqslant \pi l/2$ we have $\psi_0 = \psi_+ = \pi$ and $H = 2$.

The repulsion of solitons due to the interchain interaction is somewhat unexpected. Really if we quench the phase degree of freedom like in polyacetylene we shall always find the attraction with a constant confinement force $\propto T_{\mathrm{c}}^2/v_{\mathrm{F}}$. In our case of incommensurate CDW the phase φ is free locally but the total shift $\Delta\varphi$ is invariant being determined by the injected electrons. For a pair of solitons we have

$$\Delta\varphi = 0 \quad \text{or} \quad \Delta\varphi = 2\pi$$

depending on their charges being opposite or identical, correspondingly. The two well separated solitons have four tails altogether. The phase changes in an interval $(\, 0, \pm\pi/2 \,)$ in each tail. When two solitons of the same sign come close, $d \Rightarrow 0$, the phases $\psi_+ - \pi$ and $\psi_- + \pi$ at the internal edges of the interval $(\, -d/2, d/2 \,)$ must coincide (see fig. 4b) otherwise the energy (3.5) would grow as $(\psi_+ - \psi_- - 2\pi)^2 / d$. So at $d \propto \xi_0$ we find the two tails of the type $(0, \pi)$. Finally the amplitudinal nuclei of solitons annihilate due to electronic transitions to the term $\nu = 2$, fig. 2 , and we are left with one phase soliton of the type $(0, 2\pi)$. One can easily obtain that the total energy E_n of n phase tails of $(\, 0, 2\pi/n \,)$-type is

$$E_n = E_1 n \sin^2(\pi/2n), \quad E_1 \propto T_c. \tag{3.17}$$

We see that the tails of well separated solitons, $n = 4$, have lower energy $E_4 = (2 - \sqrt{2}) E_1 \simeq 0.6 E_1$ than the tails of the closely situated solitons, $n = 2$, $E_2 = 2E_1 > E_4$. This effect is a reason for soliton repulsion. We can also study analogously solitons situated on different neighboring chains to come to the following general conclusions.

(i) The solitons of the opposite signs on the same chain and of the same signs on different chains are attractive.

(ii) The solitons of the same sign on the same chain and of the opposite sign on different chains are repulsive.

It is important that Coulomb forces have the same effect for the solitons on one chain and the opposite effect for the solitons on different chains. Therefore the solitons of the opposite sign on the same chain will always attract each other and glue together. Then the electronic transition from the two stable, $\nu = 1$, into the two unstable, $\nu = 0, \nu = 2$, terms takes place and

the system relaxes to the ground state. This process ends up the nonradiative recombination of an initial electron-hole pair.

On the contrary the repulsion of solitons of the same sign will inhibit the electronic transitions. Consequently the conversion into the 2π-phase soliton, i.e., the final state of the phase slip is slowed down as $\exp(-A)$, $A \propto I/\xi_0 \propto \Delta_0/T_c$. The metastability of a gas of unipolar amplitude solitons is of importance in the conversion process of a normal current to the CDW sliding.

3.4. The continual model for the adaptation in the 3D long-range order

Here we return to the problems of a single soliton adaptation to analyze the system with the long-range order. Our study in section 3.2 has left us with a contradiction concerning the total charge carried by the soliton. Remember that under the interchain coupling the central chain which carries an amplitude soliton acquired a charge e. But the surrounding chains have been deformed so as to compensate it. The total complex is neutral and
cannot carry a charge current. It interacts with a homogeneous external field via the quadrupole moment only. These results are model independent following a more general theorem (Brazovskii 1980).

To understand the underlying physics we shall go from the cluster model of section 3.2 to an infinite system with a long-range order. Now a cluster of chains cannot have a finite asymptotical deviation θ_z (see fig. 4a) relative to the media of CDW chains. Nevertheless eq. (3.1) gives

$$\sum_{\alpha} \varphi_\alpha(x) \equiv -\varphi_0(x) \tag{3.18}$$

so that passing through the 'solitons plane' $x = 0$ the left-hand side of eq. (3.18) must acquire the shift $\pm\pi$, following the right-hand side (with eq. (3.2)). This phase shift can appear only after the summation of infinite amount ($Z \to \infty$) of infinitesimal ($\propto 1/Z$ to compare with (3.8)) quantities $\Delta\varphi_\alpha(x) = \varphi_\alpha(+\infty) - \varphi_\alpha(-\infty), \alpha \neq 0$. It means that we are allowed to go to the continuum model.

$$\varphi_\alpha(x) \to \varphi\,(x, r_\perp) = \varphi(r), \quad r = (x, r_\perp)\,, \quad \sum_{\alpha\neq 0} \Rightarrow \int \frac{\mathrm{d}r_\perp}{S_\perp}\varphi(r).$$

The effect of the discontinuous phase $\varphi_0(x)$ can be taken into account via the local source at $x = 0, r_\perp = 0$ which has to simulate the sum rule (3.18). Then we arrive at the model, which is described by the following equation:

$$\begin{aligned} &\partial^2\varphi/\partial x^2 + C\partial^2\varphi/\partial \boldsymbol{r}_\perp^2 = \pi S_\perp \delta(\boldsymbol{r})\partial\delta(x)/\partial x \\ &C \propto S_\perp/l^2 \ll 1, \quad l \propto v_\mathrm{F}/T_c \end{aligned} \tag{3.19}$$

The coefficient in the right-hand side of eq. (3.19) is found by the requirement to satisfy the conditions (3.18) and (3.3) which now read

$$\Delta\bar{\varphi}(x) = -\Delta\varphi_0(x) = \pi, \quad \bar{\varphi}(x) = \int \varphi(\boldsymbol{r})\mathrm{d}\boldsymbol{r}_\perp/S_\perp$$

Note that unlike the models of sections $3.1 - 3.3$ here the point source is the hole region $\propto l$ rather then ξ_0. We obtain from (3.19) that $\varphi(r)$ is a kind of a potential of a dipole source in some equivalent Coulomb problems:

$$\varphi(r) = \frac{S_\perp}{4C}\frac{x}{|r|^3}, \quad r = \left(x, r_\perp/\sqrt{C}\right) \tag{3.20}$$

One can easily check that (3.20) gives us $\bar{\varphi}(x) = (\pi/2)\,\mathrm{sgn}\,x$ to satisfy the requirements of eqs. (3.18) and (3.3). The charge density distribution in the media is found to be:

$$\rho(x) = \frac{e}{\pi}\frac{1}{S_\perp}\frac{\partial\varphi}{\partial x} = \frac{e}{4\pi C}\left[\frac{1}{|r|^3} - \frac{3x^2}{|r|^5}\right] \tag{3.21}$$

We can see from (3.21) that the charges of any finite layer, $|\boldsymbol{r}_\perp| < \infty$, are exactly zero. It means that the charge (3.2) of the solitonic tails at the central chain is not compensated with respect to its interaction with a local field. In this sense the soliton carries a charge $\pm e$. At the same time the interaction with a plain field, independent of $\boldsymbol{r}_\perp$, is compensated exactly. This result means firstly that the excess concentration of amplitude solitons with a spin 1/2 in their nuclei and the charges in their tails automatically appear altogether with a homogeneous countercharge background so that fluctuations of their concentration stand by the Coulomb forces. One can show that the effect of the homogeneous compensation disappears altogether with a Fröhlich conductivity as soon as the pinning is introduced. For example the additional term $P^2\varphi, P = \omega_\mathrm{p}/u \propto T_\mathrm{p}/v_\mathrm{F}$, where ω_p is the pinning frequency, in eq. (3.19) will lead to the 'screening factors' $\propto \exp(-P|\boldsymbol{r}|)$ in formulae (3.20) and (3.21). Then $\varphi(x)$ has no increment $\varphi(+\infty) - \varphi(-\infty) = 0$ and the central charge is not compensated.

Finally the structural interaction $U(\boldsymbol{r})$ of the two solitons is not exponential any more. Keeping in mind (3.4) we find from (3.19) that

$$U(\boldsymbol{r}) = \mp\,(v_\mathrm{F}/4)\,\partial\varphi(\boldsymbol{r})/\partial x = \mp\frac{v_\mathrm{F}S_\perp}{16}\left[\frac{1}{|\boldsymbol{r}|^3} - \frac{3x^2}{|\boldsymbol{r}|^5}\right] \tag{3.22}$$

The signs $\pm$ correspond to the solitons of the same or of the opposite signs. Note that the interaction changes the sign when the solitons are situated on essentially different chains, outside the cone $|x|/|r| < 1/\sqrt{3}$.

3.5. The adaptation near the transition temperature

We have considered above the solitons in the ordered system of chains at zero temperature. Now we give a brief account of the peculiarities near the transition temperature T_c for the 3D ordering: $T \leqslant T_\mathrm{c} \ll \Delta_0$. We shall use the MF approximation for the interchain coupling which assumes a large number Z of interacting chains. For consistency we must neglect the influence of the central soliton carrying chain on the neighboring ones. Then we can describe the system in terms of the order parameters $\eta_\alpha(x)$,

$$\eta_\alpha(x) = \langle\cos\rho_\alpha(x)\rangle\,, \quad \eta_\alpha(x) \ll 1$$

We shall use also the correlation function for an isolated chain taken at $T = T_\mathrm{c}$,

$$K(x-y) = \langle\cos\varphi(x), \cos\varphi(y)\rangle = \exp(-|x-y|/\xi), \quad \xi \propto v_\mathrm{F}/T_\mathrm{c}$$

We must consider the partition function for the Hamiltonian (3.1) with an additional condition (3.3). After a conventional procedure we arrive at the
selfconsistent equations

$$\eta_\alpha(x) = \frac{1}{T}\sum J_{\alpha,\beta}\int \mathrm{d}y K(x-y)\eta_\beta(y)\chi_\beta(y) \tag{3.23}$$

where $\chi_0(y) = \mathrm{sgn}\,y, \chi_\beta(y) = 1$ if $\beta \neq 0$.
Equation (3.22) differs from the common MF equations by the new factor $\chi_\beta(y)$ which takes into

account the presence of a solition on a chain $\beta = 0$. To use the MF approximation consistently in zero order in $1/Z$ we must neglect the term with $\beta = 0$ in equations for $\alpha \neq 0$. For $\alpha = 0$ we find the relative shape of the order parameter

$$\frac{\eta_0(x)}{\eta(x)} = \frac{\int \mathrm{d}y K(x-y) \operatorname{sgn} y}{\int \mathrm{d}y K(x-y)} = \operatorname{sgn} x \left[1 - \exp\left(-|x|/\xi_0\right)\right] \tag{3.24}$$

which is our final result. We see that the adaptation to the soliton develops on the same scale $\xi \propto l$ as at zero temperature. In the vicinity of the soliton, the order parameter passes through zero.

4.11.6 Note added in proof

The new results of sections 3.4 and 3.5 together with their subsequent development give a new insight to the microscopical picture for the conversion of the normal current into the Fröhlich one and for nucleation of the CDW phase-slippage in the volume. The important new ingredient is the equivalence between the dipole of section 3.4 and the loop of dislocations with half-integer vorticity. This loop cannot expand its area S because the confinement energy is proportional to S. The 2π-solitons create a dipole with a double amplitude but also with a different topological nature. It is equivalent to the loop of integer vorticity whose expansion costs only the energy of the order of its length, i.e. $\propto S^{1/2}$.

Now we can look at the principal steps of the current conversion at low temperatures. The normal carriers penetrate through the sample being either hot after injection or being stabilized temporarily by a weak barrier described in section 1.2. Eventually every carrier experiences the selftrapping (section 2) into the amplitude soliton with the charged tails of section 3.1 and the long range dipole distortion of section 3.4. This configuration is equivalent to the half-integer dislocation loop. Being repulsive along the chain these dipoles avoid recombination and form a long living gas drifting along the field which is a quasi stationary intermediate stage of the conversion. There is an eventual transformation of amplitude solitons in the nuclei of the dipoles into 2π-solitons which strengthens the dipoles by a factor 2 and eliminates the spins. Most probably, it proceeds by elecronic transferers which switch the two solitons
from a term $\nu = 1$ to terms $\nu = 0$ and $\nu = 2$, see section 2 and fig. 2. The double dipoles with 2π-nuclei gradually glue together and expand to give the aggregation of the microscopical integer dislocations into the macroscopical vortex ring which is the final process of conversion. More details like the effects of Coulomb interactions will be published elsewhere (Brasovskii 1989, JEPT and Solid State Commun., to be published).

4.11.7 References

Brazovskii, S., 1978, Pis'ma v Zh. Eksp. & Teor. Fiz. 28, 677 [Sov. Phys.-JETP Lett. 28, 606].
Brazovskii, S., 1980, Zh. Eksp. & Teor. Fiz. 78, 677 [Sov. Phys.-JETP 51, 342].
Brazovskii, S., and S. Gordjunin, 1980, Pis'ma v Zh. Eksp. & Teor. Fiz. 31, 399 [Sov. Phys.-JETP Lett. 31, 371].
Brazovskii, S., and N.N. Kirova, 1984, Electron selflocalization and periodic superstructures in quasi-one-dimensional dielectrics, in: Soviet Scientific Reviews, Sect. A, Physics Reports, Vol. 6, ed. I.M. Khalatnikov (Harwood, New York).
Brazovskii, S., and S. Matveenko, 1984, Zh. Eksp. & Teor. Fiz. 87, 1400 [Sov. Phys.-JETP 60, 804].
Brazovskii, S., N.N. Kirova and V. Yakovenko, 1983, J. Phys. Colloq. 44, C3-1525.
Fröhlich, H., 1954, Proc. R. Soc. London Ser. A 223, 292.

Gor'kov, L.P., and I.E. Dzyaloshinskii, 1974, Zh. Exp. & Teor. Fiz. 67, 397 [Sov. Phys.-JETP 40, 198].
Grüner, R.E., and A. Zettl, 1985, Phys. Rep. 119, 117.
Johnston, D.C., J.P. Stokes, Pei-Ling Hseih and G. Grüner, 1983, J. Phys. Colloq. 44, C3-1743.
Lee, P.A., T.M. Rice and P.W. Anderson, 1975, Solid State Commun. 17, 1089.
Monceau, P., 1985, in: Electronic Properties of Inorganic Quasi-One-Dimensional Materials, Vol. 2, ed. P. Monceau (Reidel, Dordrecht) p. 139.
Nad', F.Ya., 1985, in: Charge Density Waves in Solids, Lecture Notes in Physics, Vol. 217, eds Gy. Hutiray and J. Sólyom (Springer, Berlin) p. 286.
Rashba, E., 1957, Opt. Spectrosc. 2, 88.
Rice, M.J., A.R. Bishop, J.A. Krumhansl and S.E. Trullinger, 1976, Phys. Rev. Lett. 36, 432.
Su, W.P., and J.R. Schrieffer, 1981, Phys. Rev. Lett. 46, 738.
Su, W.P., J.R. Schrieffer and A.J. Heeger, 1979, Phys. Rev. Lett. 42, 1698.
Takoshima, T., M. Ido, K. Tsutsumi, T. Sambongi, S. Honma, K. Yamaya and Y. Abe, 1980, Solid State Commun. 35, 911.
Yu, Lu, 1988, Solitons and Polarons in Conducting Polymers (World Scientific Publishing, Singapore).

Part V
Old, Fundamental Theories

Part VI
Special Effects, Properties: Main Articles

Part VII
Experiments: Main Articles

Part VIII
Other Theories in a Nutshell

5 title

5.0.1 title

Part IX
Other theories

Part X
Other, Non-Typical Theory

6 CDW state high magnetic field quasi-1D mean field by Grigoriev, Lyubshin

0..1 Main idea of the article and what is important here?

(????)

0..2 Introduction

The phase diagram and the structure of CDW state in high magnetic field in quasi-1D materials: mean-field approach

P. D. Grigoriev
D. S. Lyubshin

Abstract

We develop the mean-field theory of a charge-density wave (CDW) state in magnetic field and study the properties of this state below the transition temperature. We show that the CDW state with shifted wave vector in high magnetic field (CDW_x phase) has at least double harmonic modulation on the most part of the phase diagram. In the perfect nesting case the single harmonic CDW state with shifted wave vector exists only in a very narrow region near the tricritical point where the fluctuations are very strong. We show that the transition from CDW_0 to CDW_x state below the critical temperature is accompanied by a jump of the CDW order parameter and of the wave vector rather than by their continuous increase. This implies a first order transition between these CDW states and explains the strong hysteresis accompanying this transition in many experiments. We examine how the phase diagram changes in the case of imperfect nesting.

The properties of metals with a charge-density-wave (CDW) ground state attract great attention since the fifties (see, e.g., monographs [[? ?]]). In quasi-1D metals, the Fermi surface (FS) consists of two slightly warped sheets separated by $2k_F$ and roughly possesses the nesting property that leads to the Peierls instability and favors the formation of the charge- or spin-density-wave (SDW) state at low temperature.

The mean-field description is known to be unable to describe strictly 1D conductors, where the non-perturbative methods and exactly solvable models are of great importance.[?] However, in most materials manifesting CDW or SDW phenomena the nonzero value of the electron transfer integral between conducting chains and the 3D character of the electron-electron interactions and lattice elasticity reduce the deviations from the mean-field solution and also make most of the methods and exactly solvable models developed for strictly 1D case inapplicable.[?] The effect of fluctuations in Q1D metals and their influence on the mean-field description of the Peierls transition in these metals has been considered in a number of papers (see e.g. [[? ?]] and references therein). It was shown that the interchain dispersion of electrons strongly damps the fluctuation and validate the mean-field description. In Q1D organic metals,[?] at which our present study is mainly aimed, the free electron dispersion near the Fermi level is, approximately, given by

$$\varepsilon_\sigma(\boldsymbol{k}) = \hbar v_F(|k_x| - k_F) - t_\perp)\boldsymbol{k}_\perp) - \sigma H, \tag{6.1}$$

where v_F and k_F are the Fermi velocity and Fermi momentum in the chain (x) direction, $H \equiv \mu_B B$ is the Zeeman energy, μ_B is the Bohr magneton and B is the external magnetic field. The perpendicular-to-chain term, $t_\perp)\mathbf{k}_\perp)$, is much greater than the energy scale of the CDW(SDW) transition temperature, T_{c0}. Only the "imperfect nesting" part, t'_b, of $t_\perp)\mathbf{k}_\perp)$ is of the order of T_{c0} (see Eqs. (6.2), (6.3)). Hence, the criterion for the mean-field theory to be applicable,[? ?] $t_\perp \gg T_{c0}$, is reliably satisfied in most Q1D organic metals.

The mean-field description of the CDW properties is, in many aspects, very similar to the BCS theory. The pairing of two electrons in superconductors is replaced in CDW by the pairing of an electron with the hole on the opposite sheet of the Fermi surface. The charge and spin coupling constants in CDW (see interaction Hamiltonian (6.5)) are analogous to coupling constants in spin-singlet and spin-triplet channels in superconductivity. The CDW phase with shifted nesting vector is similar to the non-uniform superconducting phase (LOFF phase).[? ?] However, there are several important differences between these two many-particle effects. The first difference is that the formation of a gap in the electron spectrum in CDW leads to an insulating rather than superconducting state. This happens due to the pinning of the CDW condensate by crystal imperfections. Hence, the CDW state does not reveal a superfluid current.[? ?] Other differences appear, e.g., in the excitation spectrum. In particular, the lowest energy excitations in magnetic field or at imperfect nesting are not always the electron pairs as in BCS theory but may be the "soliton kinks".[? ? ? ? ?]

The theoretical investigation of the CDW/SDW properties at a mean-field level comprises two main branches. The first focuses on the transition line from the metallic states to CDW/SDW state using susceptibility calculations. This allows to include many additional factors into the theoretical model, such as different free electron dispersion relations, spin and orbital effects of the external magnetic field, applied pressure etc. It helped to discover and to explain many beautiful effects such as the field-induced spin- and charge-density waves (FISDW),[? ? ? ?] the increase of the transition temperature due to the one-dimensionization of the electron spectrum in high magnetic field,[? ?] the CDW state with shifted nesting vector [? ?]) etc. However, all these results cannot be continued below the transition temperature since they are based on the electron susceptibility calculations using metallic-state electron Green's functions. In particular, the calculation of [[?]] predicts an appearance of the CDW$_x$ phase with shifted wave vector as the magnetic field exceeds some critical value. This calculation gives the metal-CDW$_x$ transition line, $T_c(H)$, and the dependence of the optimal shift $q_x(H)$ of CDW wave vector on magnetic field at this transition line. However, this calculation does not extend below the transition temperature, and, hence, cannot be used to describe the properties and the phase diagram inside the CDW phase. For example, it neither describes the structure of the CDW$_x$ phase below $T_c(H)$ nor gives the CDW$_0$-CDW$_x$ transition line $H_{c1}(T)$ or the kind of this transition. The mean-field study of CDW in Ref. [[?]] is applicable only in weak field when the CDW wave vector does not shift from its zero-field value.

The second branch of investigation involves the soliton physics. It appeared first to describe the ground state of polyacetylene [? ?] and then developed into a rather large activity (see Refs. [[? ?]] for a review). In particular, the soliton structure and the energy spectrum of CDW state in external magnetic field were considered [?]. However, all these results were only derived at zero temperature and perfect nesting and are not applicable at temperatures of the order of transition temperature, $T \sim T_c$. The finite-temperature phase transition to soliton phase has been considered in Ref. [[?]]. However, that phase diagram refers to zero field and finite shift of the chemical potential from the value μ_0 corresponding to the commensurate CDW.[?] The analysis of the CDW phase diagram in magnetic field has been performed in the case of perfect nesting and at the electron density close to half-filling.[?] However, this approach is also unable to describe the incommensurate case far from half-filling. In particular, it suggests the one-harmonic modulation of charge density, which is usually unstable in high

magnetic field (see below).

Further theoretical description of the CDW state in magnetic field became important last years because of the intensive experimental study of the CDW state in strongly anisotropic organic metals. [? ? ? ? ? ? ? ? ? ? ?]

In the present paper we study the CDW phase diagram and the properties of the CDW state at finite temperature below the transition point in the mean-field approximation. This study links the results of susceptibility calculations and the results from the soliton approach. We take into account the spin effect of the external magnetic field and consider the CDW phase with shifted nesting vector. The "antinesting" term in the electron dispersion is also taken into account. We show that the CDW_x state with shifted wave vector, proposed in Ref. [[?]], has double harmonic modulation almost everywhere in the phase diagram (see Fig. 6.3,6.5). At perfect nesting, $t'_b = 0$, the single harmonic CDW_x state exists only in a very narrow region near the tricritical point. We show that the transition from CDW_0 to CDW_x state below the critical temperature is accompanied by a jump of the CDW wave vector rather than by its continuous increase. This implies a first order transition between the CDW states and explains the strong hysteresis observed at the kink transition.[? ? ? ?]

Besides the Zeeman splitting, external magnetic field affects the orbital electron motion. First, an external magnetic field perpendicular to conducting layers leads to one-dimensionization of the electron spectrum in quasi-1D metals [?] that improves the nesting property of the Fermi surface. Second, due to the strong scattering by the nesting vector, electrons in quasi-1D metal in magnetic field may form close orbits in momentum space [?]. These orbital effects increase the CDW or SDW transition temperature and may lead to the field-induced spin-density waves [?] (for a review, see [[?]]). A similar effect for the charge density waves was also proposed [?]. The interplay between spin and orbital effects of the magnetic field is quite interesting. It leads, for example, to a series of phase transitions between the CDW states with quantized nesting vector.[?]

In our present study we disregard the orbital effects of magnetic field. This limitation, however, is not very restrictive. If the magnetic field is parallel to the conducting layers, it produces only the Zeeman splitting and no orbital effect. The orbital quantization effects are, usually, more subtle than the spin effect. As an illustration, the quantized nesting phases can be observed only at very low temperature [?] because the effects of nesting quantization are strongly damped at $\hbar\omega_c = e\hbar H/m^*c \ll 2\pi T, 2\pi\hbar/\tau, \Delta$. This damping is somewhat similar to that of the magnetic quantum oscillations. The one-dimensionalization of electron spectrum in magnetic field can be effectively taken into account in the present study by introducing the magnetic field dependence of the imperfect nesting transfer integral, $t'(H)$, in the electron dispersion relation (6.2). A situation which is mathematically equivalent to the Zeeman splitting of magnetic field without its orbital effect arises when there are two slightly different Q1D chain system in the same compound with coupling between the chains of different type. The quantities $U_c + U_s$ and $U_c - U_s$ play the role of the electron coupling constant inside the chains and between the chains of different type, respectively. Such a system occurs in many compounds as TTF-type organic metals (see, e.g., the discussion on page 196 in [[?]]). Two slightly different types of chains occur also in α-$(\mathrm{Per})_2\mathrm{M}(\mathrm{mnt})_2$.[? ? ?] In the systems with molecular chains of two types, however, the difference between optimal CDW wave vectors on different chains is fixed by the molecular structure and does not vary as in the case of external magnetic field which gradually separates the Fermi surfaces with two different spin components.

1. The Model and the mean-field theory of CDW in magnetic field.

1..1 The model

We consider a quasi-1D metal with dispersion (6.1) and $t_\perp)\boldsymbol{k}_\perp)$ given by the tight-binding model:

$$t_\perp)\boldsymbol{k}_\perp) = -2t_b\cos(k_y b) - 2t'_b\cos(2k_y b) - 2t_c\cos(k_z c_z), \tag{6.2}$$

where b and c_z are the lattice constants in y- and z-directions respectively. The dispersion along the z-axis is assumed to be much weaker than the dispersion along y-direction. Therefore, we omit the second harmonic $\propto \cos(2k_z c_z)$ in the dispersion relation (6.2). Since the terms $2t_c\cos(k_z c_z)$ and $2t_b\cos(k_y b)$ do not violate the perfect nesting condition

$$\varepsilon(\boldsymbol{p}+\boldsymbol{Q}) = -\varepsilon(\boldsymbol{p}), \tag{6.3}$$

they do not influence the physics discussed below unless the nesting vector become shifted in y-z plane. We do not consider such a shift in the present study.

The electron Hamiltonian is

$$\hat{H} = \hat{H}_0 + \hat{H}_{\rm int},$$

with the free-electron part

$$\hat{H}_0 = \sum_{\boldsymbol{k}\sigma} \varepsilon_\sigma(\boldsymbol{k}) a^\dagger_\sigma(\boldsymbol{k}) a_\sigma(\boldsymbol{k}) \tag{6.4}$$

and the interaction part

$$\hat{H}_{\rm int} = \frac{1}{2}\sum_{\boldsymbol{k}\boldsymbol{k}'\boldsymbol{Q}\sigma\sigma'} V_{\sigma\,\sigma'}(\boldsymbol{Q}) a^\dagger_\sigma(\boldsymbol{k}+\boldsymbol{Q}) a_\sigma(\boldsymbol{k}) \times a^\dagger_{\sigma'}(\boldsymbol{k}'-\boldsymbol{Q}) a_{\sigma'}(\boldsymbol{k}'). \tag{6.5}$$

This Hamiltonian does not include the orbital effect of magnetic field on quasi-1D electron spectrum which may be important in the case of substantially imperfect nesting and strong magnetic field perpendicular to the easy-conducting plane (see introduction). Later on we will be interested mainly in the interaction at the wave vector $\boldsymbol{Q}$ close to the so-called nesting vector $\boldsymbol{Q}_0$, which is usually chosen as

$$\boldsymbol{Q}_0 = (\pm 2k_F, \pi/b, \pi/c). \tag{6.6}$$

The deviations $\boldsymbol{Q}-\boldsymbol{Q}_0$ that will be considered below are of the order of $\max\{H, t'_b\}/\hbar v_F \ll k_F$, so that for such small deviations the interaction function

$$V_{\sigma\,\sigma'}(\boldsymbol{Q}) \approx V_{\sigma\,\sigma'}(\boldsymbol{Q}=\boldsymbol{Q}_0) = U_c - U_s\sigma\sigma' \tag{6.7}$$

The coupling constants U_c and U_s are the same as in Ref. [[?]]. Subscripts c and s distinguish charge and spin coupling constants. The Hamiltonian (6.5) can be obtained from the extended Hubbard model when the e-e scattering by the momenta close to the nesting wave vector $\boldsymbol{Q}_0$ is only taken in to account.

1..2 Mean field approach

First, we note that the terms with $\boldsymbol{Q}=0$ in (6.5) only renormalizes the chemical potential and will not be omitted in subsequent calculations (all sums over $\boldsymbol{Q}$ do not include $\boldsymbol{Q}=0$. We introduce the thermodynamic Green's function

$$g_\sigma(\boldsymbol{k}', \boldsymbol{k}, \tau-\tau') = \langle T_\tau\{a^\dagger_\sigma(\boldsymbol{k}', \tau') a_\sigma(\boldsymbol{k}, \tau)\}\rangle, \tag{6.8}$$

where the operators are taken in the Heisenberg representation, and the average

$$D_{\boldsymbol{Q}\sigma} = \sum_{\boldsymbol{k}} g_\sigma(\boldsymbol{k}-\boldsymbol{Q}, \boldsymbol{k}, -0) - \delta(\boldsymbol{Q}, 0) n_\sigma. \tag{6.9}$$

After defining

$$\Delta_{\boldsymbol{Q}\sigma} = \sum_{\sigma'} (U_c - U_s \sigma\sigma') D_{\boldsymbol{Q}\sigma'} \tag{6.10}$$

one obtains in the mean-field approximation

$$\hat{H}_{\text{int}} = \sum_{\boldsymbol{Q}\boldsymbol{k}\sigma} a_\sigma^\dagger(\boldsymbol{k}+\boldsymbol{Q}) a_\sigma(\boldsymbol{k}) \Delta_{\boldsymbol{Q}\sigma} - \frac{1}{2} \sum_{\boldsymbol{Q}\sigma} D_{-\boldsymbol{Q}\sigma} \Delta_{\boldsymbol{Q}\sigma}. \tag{6.11}$$

Hermiticy of the Hamiltonian requires $\Delta_{-\boldsymbol{Q}\sigma} = \Delta^*_{\boldsymbol{Q}\sigma}$. It is now straightforward to write down the equations of motion which in the frequency representation take the form

$$[i\omega - \varepsilon_\sigma(\boldsymbol{k})] g_\sigma(\boldsymbol{k}', \boldsymbol{k}, \omega) - \sum_{\boldsymbol{Q}} \Delta_{\boldsymbol{Q}\sigma} g_\sigma(\boldsymbol{k}', \boldsymbol{k}-\boldsymbol{Q}, \omega) = \delta(\boldsymbol{k}', \boldsymbol{k}). \tag{6.12}$$

1..3 The Cosine Phase

Now we consider the solution with $\Delta_{\boldsymbol{k}\sigma} \neq 0$ only for $\boldsymbol{k} = \pm\boldsymbol{Q}$, where $\boldsymbol{Q} = 2k_F \boldsymbol{e}_x + (\pi/b)\boldsymbol{e}_y + \boldsymbol{q}$ with $|\boldsymbol{q}| \ll k_F$. If we neglect the scattering into the states with $|k_x| \gtrsim 2k_F$, the equations (6.12) decouple: for $k_x > 0$ one has

$$\begin{pmatrix} i\omega - \varepsilon_\sigma(\boldsymbol{k}) & -\Delta_{\boldsymbol{Q}\sigma} \\ -\Delta_{-\boldsymbol{Q}\sigma} & i\omega - \varepsilon_\sigma(\boldsymbol{k}-\boldsymbol{Q}) \end{pmatrix} \hat{G} = \hat{I}, \tag{6.13}$$

where

$$\hat{G} \equiv \begin{pmatrix} g_\sigma(\boldsymbol{k}, \boldsymbol{k}, \omega) & g_\sigma(\boldsymbol{k}-\boldsymbol{Q}, \boldsymbol{k}, \omega) \\ g_\sigma(\boldsymbol{k}, \boldsymbol{k}-\boldsymbol{Q}, \omega) & g_\sigma(\boldsymbol{k}-\boldsymbol{Q}, \boldsymbol{k}-\boldsymbol{Q}, \omega) \end{pmatrix} \tag{6.14}$$

and $\hat{I}$ is the 2×2 identity matrix. The equation for $k_x < 0$ may be obtained via a substitution $\boldsymbol{Q} \to -\boldsymbol{Q}$. Introducing the notations

$$\varepsilon^\pm_\sigma(\boldsymbol{k}', \boldsymbol{k}) = \frac{\varepsilon_\sigma(\boldsymbol{k}'(\pm\varepsilon_\sigma(\boldsymbol{k})}{2} \tag{6.15}$$

and using $\Delta_{\boldsymbol{Q}\sigma}\Delta_{-\boldsymbol{Q}\sigma} = |\Delta_{\boldsymbol{Q}\sigma}|^2$ from (6.13) one has

$$\begin{aligned} g_\sigma(\boldsymbol{k}-\boldsymbol{Q}, \boldsymbol{k}, \omega) &= -\frac{\Delta_{\boldsymbol{Q}\sigma}}{[\omega + i\varepsilon_\sigma(\boldsymbol{k})][\omega + i\varepsilon_\sigma(\boldsymbol{k}-\boldsymbol{Q})] + |\Delta_{\boldsymbol{Q}\sigma}|^2} \\ &= -\frac{\Delta_{\boldsymbol{Q}\sigma}}{[\omega + i\varepsilon^+_\sigma(\boldsymbol{k}, \boldsymbol{k}-\boldsymbol{Q})]^2 + [\varepsilon^-_\sigma(\boldsymbol{k}, \boldsymbol{k}-\boldsymbol{Q})]^2 + |\Delta_{\boldsymbol{Q}\sigma}|^2}. \end{aligned} \tag{6.16}$$

The consistency equation therefore is

$$\Delta_{\boldsymbol{Q}\sigma'} = -T \sum_{\boldsymbol{k}\omega\sigma} \frac{(U_c - U_s\sigma\sigma')\Delta_{\boldsymbol{Q}\sigma}}{[\omega + i\varepsilon^+_\sigma(\boldsymbol{k}, \boldsymbol{k}-\boldsymbol{Q})]^2 + [\varepsilon^-_\sigma(\boldsymbol{k}, \boldsymbol{k}-\boldsymbol{Q})]^2 + |\Delta_{\boldsymbol{Q}\sigma}|^2}. \tag{6.17}$$

where ω takes the values $\pi T(2n+1)$, $n \in Z$. Using the identity

$$T \sum_\omega \frac{1}{(\omega - i\alpha)^2 + a^2} = \frac{1}{4a} \left\{ \text{th}\, \frac{a-\alpha}{2T} + \text{th}\, \frac{a+\alpha}{2T} \right\}$$

this may be rewritten as

$$\Delta_{\boldsymbol{Q}\sigma'} = -\frac{1}{4}\sum_{\boldsymbol{k}\sigma} \frac{(U_c - U_s\sigma\sigma')\Delta_{\boldsymbol{Q}\sigma}}{\sqrt{|\Delta_{\boldsymbol{Q}\sigma}|^2 + [\varepsilon_\sigma^-(\boldsymbol{k}, \boldsymbol{k}-\boldsymbol{Q})]^2}} \Big\{ \mathrm{th}\,\frac{E_{\sigma,+}(\boldsymbol{k})}{2T} - \mathrm{th}\,\frac{E_{\sigma,-}(\boldsymbol{k})}{2T} \Big\}, \tag{6.18}$$

where

$$E_{\sigma,\pm}(\boldsymbol{k}) = \varepsilon_\sigma^+(\boldsymbol{k}, \boldsymbol{k}-\boldsymbol{Q}(\pm\sqrt{|\Delta_{\boldsymbol{Q}\sigma}|^2 + [\varepsilon_\sigma^-(\boldsymbol{k}, \boldsymbol{k}-\boldsymbol{Q})]^2} \tag{6.19}$$

is the energy spectrum in the cosine phase. From (6.2) it follows that for the right-moving electrons

$$\varepsilon_\sigma^+(\boldsymbol{k}, \boldsymbol{k}-\boldsymbol{Q}) = \frac{\hbar v_F q_x}{2} + 2t_b \sin\frac{q_y b}{2} \sin\left(k_y b - \frac{q_y b}{2}\right) - 2t_b' \cos q_y b \cos(2k_y b - q_y b) - \sigma H, \tag{6.20}$$

$$\varepsilon_\sigma^-(\boldsymbol{k}, \boldsymbol{k}-\boldsymbol{Q}) = \hbar v_F(k_x - k_F - q_x/2) - 2t_b \cos\frac{q_y b}{2} \cos\left(k_y b - \frac{q_y b}{2}\right) + 2t_b' \sin q_y b \sin(2k_y b - q_y b)\,. \tag{6.21}$$

It is, however, more convenient to perform the momentum summation in Eq. (6.17) first. Extending the limits of the summation over k_x to infinity, one has

$$\Delta_{\boldsymbol{Q}\sigma'} = \frac{\pi\nu_F|U_c|T}{2} \sum_{\omega\sigma} \left\langle \frac{(1+\nu\sigma\sigma')\Delta_{\boldsymbol{Q}\sigma}}{\sqrt{[\omega + i\varepsilon_\sigma^+(\boldsymbol{k}, \boldsymbol{k}-\boldsymbol{Q})]^2 + |\Delta_{\boldsymbol{Q}\sigma}|^2}} \right\rangle_{k_y}, \tag{6.22}$$

where the branch of the square root with positive real part is implied, the angular brackets stand for the averaging over all values of k_y, and we introduced the standard notation

$$\nu = -U_s/U_c \tag{6.23}$$

for the coupling ratio and

$$\nu_F = \frac{L_x}{\pi\hbar v_F} \tag{6.24}$$

for the density of states on the Fermi level per one spin component.

Expansion to the third order in $\Delta_{\boldsymbol{Q}\sigma}$ yields

$$\Delta_{\boldsymbol{Q}\sigma'} = \sum_\sigma \frac{1+\nu\sigma\sigma'}{2} \left(K_\sigma^{(1)} - |\Delta_{\boldsymbol{Q}\sigma}|^2 K_\sigma^{(3)c}\right) \Delta_{\boldsymbol{Q}\sigma} \tag{6.25}$$

(the superscript "c" stands for "cosine") with

$$K_\sigma^{(1)} = \pi\nu_F|U_c|T \sum_\omega \left\langle \frac{\operatorname{sign}\omega}{\omega + i\varepsilon_\sigma^+(\boldsymbol{k}, \boldsymbol{k}-\boldsymbol{Q})} \right\rangle_{k_y}, \tag{6.26}$$

$$K_\sigma^{(3)c} = \frac{\pi\nu_F|U_c|T}{2} \sum_\omega \left\langle \frac{\operatorname{sign}\omega}{(\omega + i\varepsilon_\sigma^+(\boldsymbol{k}, \boldsymbol{k}-\boldsymbol{Q}))^3} \right\rangle_{k_y}. \tag{6.27}$$

The second-order transition line corresponds to

$$\det \begin{pmatrix} \frac{1+\nu}{2}K_+^{(1)} - 1 & \frac{1-\nu}{2}K_-^{(1)} \\ \frac{1-\nu}{2}K_+^{(1)} & \frac{1+\nu}{2}K_-^{(1)} - 1 \end{pmatrix} = 0. \tag{6.28}$$

The left hand side of this equation is a function of ν, T, H and $\boldsymbol{q}$. The normal to CDW phase transition occurs at some optimal value of $\boldsymbol{q}$ which corresponds to the minimum of the free energy of the CDW state, that at the transition point is equivalent to the maximum of T_c or to the minimum of l.h.s. of Eq. (6.28).

Unrestricted summation over k_x introduced divergence into the summation over ω in $K_\sigma^{(1)}$, which may be renormalized by introducing the zero-field and zero-t_b' transition temperature T_{c0}. To obtain a closed expression for the latter, we note that for $H = 0$ one has $K_+^{(1)} = K_-^{(1)}$, and the matrix in (6.28) has eigenvalues $K_\sigma^{(1)} - 1$ and $\nu K_\sigma^{(1)} - 1$. Therefore, at $H = 0$ $K_\sigma^{(1)}(T = T_c(t_b'), H = 0) = 1$. From (6.26) at $t_b' = 0$ after imposing a cutoff at $\omega \sim E_F$ one obtains $K^{(1)} = \nu_F |U_c| \ln(2\gamma E_F/\pi T)$, and

$$T_{c0} = \frac{2\gamma E_F}{\pi} \exp\left(-\frac{1}{\nu_F |U_c|}\right), \tag{6.29}$$

in agreement with Ref. [[?]] and with the usual BCS expression. We may now write

$$K_\sigma^{(1)} = 1 + \nu_F |U_c| \left[\ln\frac{T_{c0}}{T} + \pi T \sum_\omega \left(\left\langle \frac{\operatorname{sign}\omega}{\omega + i\varepsilon_\sigma^+(\boldsymbol{k}, \boldsymbol{k} - \boldsymbol{Q})}\right\rangle_{k_y} - \frac{\operatorname{sign}\omega}{\omega}\right)\right]. \tag{6.30}$$

The kernels $K_\sigma^{(1)}$ and $K_\sigma^{(3)c}$ can be further simplified in terms of the digamma function $\psi(x) = \frac{d}{dx}\ln\Gamma(x)$:

$$K_\sigma^{(1)} = 1 + \nu_F |U_c| \left[\ln\frac{T_{c0}}{T} + \psi\left(\frac{1}{2}\right) - \left\langle \operatorname{Re}\psi\left(\frac{1}{2} + \frac{i\varepsilon_\sigma^+(\boldsymbol{k}, \boldsymbol{k} - \boldsymbol{Q})}{2\pi T}\right)\right\rangle_{k_y}\right], \tag{6.31}$$

$$K_\sigma^{(3)c} = -\frac{\nu_F |U_c|}{16\pi^2 T^2} \left\langle \operatorname{Re}\psi''\left(\frac{1}{2} + \frac{i\varepsilon_\sigma^+(\boldsymbol{k}, \boldsymbol{k} - \boldsymbol{Q})}{2\pi T}\right)\right\rangle_{k_y}. \tag{6.32}$$

To actually find the fields $\Delta_{\boldsymbol{Q}\sigma}$ just below the transition point to the leading order, one has to make the substitution $K_\sigma^{(1)} \to K_\sigma^{(1)} - |\Delta_{\boldsymbol{Q}\sigma}|^2 K_\sigma^{(3)c}$ in (6.28). The ratio $\Delta_{\boldsymbol{Q}-} : \Delta_{\boldsymbol{Q}+}$ is real and at the transition point is the column ratio in (6.28),

$$\Delta_{\boldsymbol{Q}-} : \Delta_{\boldsymbol{Q}+} = \left(\frac{1+\nu}{2} K_+^{(1)} - 1\right) : \left(\frac{\nu - 1}{2} K_-^{(1)}\right) = \left(\frac{\nu - 1}{2} K_+^{(1)}\right) : \left(\frac{1+\nu}{2} K_-^{(1)} - 1\right). \tag{6.33}$$

Introducing the (real) ratio $\alpha \equiv |\Delta_{\mathbf{Q}-}|^2 : |\Delta_{\mathbf{Q}+}|^2$ we get

$$|\Delta_{\boldsymbol{Q}\sigma}^c|^2 = \frac{\alpha^{(1-\sigma)/2}\left(\nu K_+^{(1)} K_-^{(1)} - \frac{\nu+1}{2}(K_+^{(1)} + K_-^{(1)}) + 1\right)}{K_+^{(3)c}\left(\nu K_-^{(1)} - \frac{\nu+1}{2}\right) + \alpha K_-^{(3)c}\left(\nu K_+^{(1)} - \frac{\nu+1}{2}\right)}. \tag{6.34}$$

The superscript "c" stands for the cosine phase. The CDW cosine phase with $q_x \neq 0$ was analyzed at the transition line by means of the susceptibility calculation and called the CDW$_x$ phase, while the phase with $q_x = 0$ was called CDW$_0$ [?].

1..4 The Double Cosine Phase

Now we consider the solution with $\Delta_{\boldsymbol{k}\sigma} \neq 0$ for $\boldsymbol{k} = \pm\boldsymbol{Q}_0 \pm \boldsymbol{q}$, where $\boldsymbol{Q}_0 = 2k_F\boldsymbol{e}_x + (\pi/b)\boldsymbol{e}_y$ and $q \ll k_F$. Strictly speaking, there exist no self-consistent solutions with only four harmonics present or all others damped by a factor of $\Delta_{\boldsymbol{Q}\sigma}/E_F$. However, the modulations given above

have equal second-order transition temperatures, and immediately below the transition point other harmonics are damped by a factor of $\Delta_{\boldsymbol{Q}\sigma}/T$ or $\Delta_{\boldsymbol{Q}\sigma}/H$.

To obtain the leading-order expressions for the fields $\Delta_{\boldsymbol{Q}\sigma}$ in the vicinity of the transition line, we rewrite the equations (6.12) in the "matrix" form

$$GG_0^{-1} - GF = I, \tag{6.35}$$

where

$$\begin{aligned} &G(\boldsymbol{k}', \boldsymbol{k}) = g_\sigma(\boldsymbol{k}', \boldsymbol{k}), \quad G_0(\boldsymbol{k}', \boldsymbol{k}) = \frac{\delta(\boldsymbol{k}', \boldsymbol{k})}{i\omega - \varepsilon_\sigma(\boldsymbol{k})}, \\ &F(\boldsymbol{k}', \boldsymbol{k}) = \sum_Q \Delta_{\boldsymbol{Q}\sigma}\delta(\boldsymbol{k}', \boldsymbol{k} - \boldsymbol{Q}). \end{aligned} \tag{6.36}$$

The solution is

$$G = G_0 + G_0FG_0 + G_0FG_0FG_0 + \ldots \tag{6.37}$$

Omitting the contribution from the virtual states with the momentum $|k_x| \gtrsim 2k_F$, we obtain the consistency equation to the third order in $\Delta_{\boldsymbol{Q}\sigma}$:

$$\begin{aligned} \Delta_{\boldsymbol{Q}_0+\boldsymbol{q},\sigma'} =& T\sum_{\boldsymbol{k}\omega\sigma}(U_c - U_s\sigma\sigma') \times \left[\frac{\Delta_{\boldsymbol{Q}_0+\boldsymbol{q},\sigma}}{(i\omega - \varepsilon_\sigma(\boldsymbol{k}))(i\omega - \varepsilon_\sigma(\boldsymbol{k} - \boldsymbol{Q}_0 - \boldsymbol{q}))} + \right. \\ &+ \frac{\Delta_{\boldsymbol{Q}_0+\boldsymbol{q},\sigma}|\Delta_{\boldsymbol{Q}_0+\boldsymbol{q},\sigma}|^2}{(i\omega - \varepsilon_\sigma(\boldsymbol{k}))(i\omega - \varepsilon_\sigma(\boldsymbol{k} - \boldsymbol{Q}_0 - \boldsymbol{q}))(i\omega - \varepsilon_\sigma(\boldsymbol{k}))(i\omega - \varepsilon_\sigma(\boldsymbol{k} - \boldsymbol{Q}_0 - \boldsymbol{q}))} + \\ &+ \frac{\Delta_{\boldsymbol{Q}_0+\boldsymbol{q},\sigma}|\Delta_{\boldsymbol{Q}_0-\boldsymbol{q},\sigma}|^2}{(i\omega - \varepsilon_\sigma(\boldsymbol{k}))(i\omega - \varepsilon_\sigma(\boldsymbol{k} - \boldsymbol{Q}_0 - \boldsymbol{q}))(i\omega - \varepsilon_\sigma(\boldsymbol{k} - 2\boldsymbol{q}))(i\omega - \varepsilon_\sigma(\boldsymbol{k} - \boldsymbol{Q}_0 - \boldsymbol{q}))} + \\ &+ \left.\frac{\Delta_{\boldsymbol{Q}_0+\boldsymbol{q},\sigma}|\Delta_{\boldsymbol{Q}_0-\boldsymbol{q},\sigma}|^2}{(i\omega - \varepsilon_\sigma(\boldsymbol{k}))(i\omega - \varepsilon_\sigma(\boldsymbol{k} - \boldsymbol{Q}_0 + \boldsymbol{q}))(i\omega - \varepsilon_\sigma(\boldsymbol{k}))(i\omega - \varepsilon_\sigma(\boldsymbol{k} - \boldsymbol{Q}_0 - \boldsymbol{q}))}\right]. \end{aligned} \tag{6.38}$$

The equation for the other two harmonics may be obtained via a substitution $\boldsymbol{q} \to -\boldsymbol{q}$.

Performing the integration over k_x, we arrive at

$$\Delta_{\boldsymbol{Q}_0+\boldsymbol{q},\sigma'} = \sum_\sigma \frac{1 + \nu\sigma\sigma'}{2}\Big)K_\sigma^{(1)} - |\Delta_{\boldsymbol{Q}_0+\boldsymbol{q},\sigma}|^2K_\sigma^{(3)c} - |\Delta_{\boldsymbol{Q}_0-\boldsymbol{q},\sigma}|^2K_\sigma^{(3)d}\Big)\Delta_{\boldsymbol{Q}_0+\boldsymbol{q},\sigma} \tag{6.39}$$

(the superscript "d" stands for "double cosine") with $K^{(1)}$ and $K^{(3)c}$ given by (6.31) and (6.32), and

$$\begin{aligned} K_\sigma^{(3)d} &= \pi\nu_F|U_c|T\sum_\omega \left\langle \frac{(\omega - i\sigma H)\operatorname{sign}\omega}{[(\omega + i\varepsilon_\sigma^+(\boldsymbol{k}, \boldsymbol{k} - \boldsymbol{Q}))(\omega - i\varepsilon_{-\sigma}^+(\boldsymbol{k}, \boldsymbol{k} - \boldsymbol{Q}))]^2}\right\rangle_{k_y} = \\ &= -\frac{\nu_F|U_c|}{4\pi\hbar v_F q_x T}\left\langle \left[\operatorname{Im}\psi'\left(\frac{1}{2} + \frac{i\varepsilon_\sigma^+(\boldsymbol{k}, \boldsymbol{k} - \boldsymbol{Q})}{2\pi T}\right) + \operatorname{Im}\psi'\left(\frac{1}{2} + \frac{i\varepsilon_{-\sigma}^+(\boldsymbol{k}, \boldsymbol{k} - \boldsymbol{Q})}{2\pi T}\right)\right]\right\rangle_{k_y}. \end{aligned} \tag{6.40}$$

The function $K_\sigma^{(3)d}$ does not depend on σ and in what follows we omit this subscript.

At only a longitudinal shift of the CDW wave vector ($q_y = 0$) the k_y-dependence of $\varepsilon_{-\sigma}^+(\boldsymbol{k}, \boldsymbol{k} - \boldsymbol{Q})$ is symmetric, and the functions $K_\sigma^{(1)}$, $K_\sigma^{(3)c}$ and $K^{(3)d}$ (being dependent only on the shift wave vector q_x) possess the symmetry:

$$\begin{aligned} K_\sigma^{(1)}(q_x) &= K_{-\sigma}^{(1)}(-q_x), \\ K_\sigma^{(3)c}(q_x) &= K_{-\sigma}^{(3)c}(-q_x), \\ K^{(3)d}(-q_x) &= K^{(3)d}(q_x). \end{aligned} \tag{6.41}$$

This symmetry follows directly from Eqs. (6.31), (6.32) and (6.40) and the properties of digamma function: $\mathrm{Re}\,\psi^{(n)}(a+ib) = \mathrm{Re}\,\psi^{(n)}(a-ib)$, $\mathrm{Im}\,\psi^{(n)}(a+ib) = -\mathrm{Im}\,\psi^{(n)}(a-ib)$. This symmetry is not a consequence of the expansion in powers of Δ_σ: the consistency equation (6.22) also does not change under the transformation

$$q_x \to -q_x, \sigma \to -\sigma. \tag{6.42}$$

The ratio $|\Delta_{\boldsymbol{Q}_0+\boldsymbol{q},\sigma}|^2 : |\Delta_{\boldsymbol{Q}_0+\boldsymbol{q},-\sigma}|^2$ near the transition point is still given by (6.33) accounting for the property (6.41). Hence, $|\Delta_{\boldsymbol{Q}_0-\boldsymbol{q},\sigma}|^2 : |\Delta_{\boldsymbol{Q}_0-\boldsymbol{q},-\sigma}|^2 = |\Delta_{\boldsymbol{Q}_0+\boldsymbol{q},-\sigma}|^2 : |\Delta_{\boldsymbol{Q}_0+\boldsymbol{q},\sigma}|^2 \equiv \alpha$. As in derivation of (6.34) one may rewrite the system of equations (6.39) on Δ as two equations (6.28) with replacement $K_\sigma^{(1)}(\boldsymbol{Q}_0 \pm \boldsymbol{q}_x) \to K_{\pm\sigma}^{(1)} - |\Delta_{\boldsymbol{Q}_0\pm\boldsymbol{q},\sigma}|^2 K_{\pm\sigma}^{(3)c} - |\Delta_{\boldsymbol{Q}_0\mp\boldsymbol{q},\sigma}|^2 K^{(3)d}$.

Defining the ratio $\beta \equiv |\Delta_{\boldsymbol{Q}_0-\boldsymbol{q},-}|^2 : |\Delta_{\boldsymbol{Q}_0+\boldsymbol{q},+}|^2$ we can extend the derivation of (6.34) to get

$$|\Delta_{\boldsymbol{Q}_0+\boldsymbol{q},+}|^2 = \frac{\left(\nu K_+^{(1)} K_-^{(1)} - \frac{\nu+1}{2}(K_+^{(1)} + K_-^{(1)}) + 1\right)}{\left(K_+^{(3)c} + \alpha\beta K^{(3)d}\right)\left(\nu K_-^{(1)} - \frac{\nu+1}{2}\right) + \left(\alpha K_-^{(3)c} + \beta K^{(3)d}\right)\left(\nu K_+^{(1)} - \frac{\nu+1}{2}\right)}, \tag{6.43}$$

and from the $\boldsymbol{Q}_0 - \boldsymbol{q}$ part of (6.39)

$$|\Delta_{\boldsymbol{Q}_0-\boldsymbol{q},-}|^2 = \frac{\beta\left(\nu K_+^{(1)} K_-^{(1)} - \frac{\nu+1}{2}(K_+^{(1)} + K_-^{(1)}) + 1\right)}{\left(\beta K_+^{(3)c} + \alpha K^{(3)d}\right)\left(\nu K_-^{(1)} - \frac{\nu+1}{2}\right) + \left(\alpha\beta K_-^{(3)c} + K^{(3)d}\right)\left(\nu K_+^{(1)} - \frac{\nu+1}{2}\right)}. \tag{6.44}$$

Dividing (6.43) by (6.44) we obtain a linear equation on β:

$$\frac{\left(\beta K_+^{(3)c} + \alpha K^{(3)d}\right)\left(\nu K_-^{(1)} - \frac{\nu+1}{2}\right) + \left(\alpha\beta K_-^{(3)c} + K^{(3)d}\right)\left(\nu K_+^{(1)} - \frac{\nu+1}{2}\right)}{\left(K_+^{(3)c} + \alpha\beta K^{(3)d}\right)\left(\nu K_-^{(1)} - \frac{\nu+1}{2}\right) + \left(\alpha K_-^{(3)c} + \beta K^{(3)d}\right)\left(\nu K_+^{(1)} - \frac{\nu+1}{2}\right)} = 1, \tag{6.45}$$

which gives $\beta = 1$. The values $\beta = 0$ or $\beta = \infty$ in (6.43) and (6.44) correspond to cosine phase. Hence, in the double cosine phase the symmetry (6.42) is not broken, while the transition to cosine phase breaks this symmetry.

1..5 Free energy of cosine and double-cosine phases

One can easily write down the expressions for the free energies of cosine and double-cosine phases valid to the second order in the energy gap $|\Delta_\sigma|$.

From (6.11) we have for the free energy

$$F_{\mathrm{CDW}} - F_n = \frac{1}{2}\sum_{\boldsymbol{Q}\sigma} D_{-\boldsymbol{Q}\sigma}\Delta_{\boldsymbol{Q}\sigma}. \tag{6.46}$$

To the second order in $\Delta_{\boldsymbol{Q}\sigma}$ this rewrites as

$$\begin{aligned} F_{\mathrm{CDW}} - F_n &= -\frac{\pi\nu_F T}{4}\sum_{\boldsymbol{Q}\omega\sigma}\left\langle \frac{\Delta_{\boldsymbol{Q}\sigma}\Delta_{-\boldsymbol{Q}\sigma}\,\mathrm{sign}\,\omega}{\omega + i\varepsilon_\sigma^+(\boldsymbol{k}, \boldsymbol{k}-\boldsymbol{Q})}\right\rangle_{k_y} \\ &= -\frac{1}{4|U_c|}\sum_{\boldsymbol{Q}\sigma} K_\sigma^{(1)}|\Delta_{\boldsymbol{Q}\sigma}|^2. \end{aligned} \tag{6.47}$$

The phase with the most negative r.h.s of (6.46) wins; positive values of the r.h.s. correspond to first-order transitions. From Eq. (6.47) using Eq. (6.41) we have

$$F_c - F_n = -\frac{K_+^{(1)} + \alpha K_-^{(1)}}{2|U_c|} |\Delta^c_{\mathbf{Q_0}+\mathbf{q_x},+}|^2 \tag{6.48}$$

and

$$F_{2c} - F_n = -\frac{K_+^{(1)} + \alpha K_-^{(1)}}{|U_c|} |\Delta^{2c}_{\mathbf{Q_0}+\mathbf{q'_x},+}|^2. \tag{6.49}$$

The quantity $K_+^{(1)} + \alpha K_-^{(1)}$ depends on $\boldsymbol{q}$ but is always positive near the metal-CDW transition line $T_c(H)$ where this transition is of the second kind.

Since CDW_c and CDW_{2c} phases have the same transition temperature, the only way to determine which phase takes place is to compare their free energies, that near the transition line $T_c(H)$ are given by the formulas (6.48) and (6.49). The double cosine phase wins if the ratio

$$r_F \equiv \frac{F_{2c} - F_n)}{(F_c - F_n)} > 1, \tag{6.50}$$

where the values of the functions $F_{2c}(T, H, \boldsymbol{q})$ and $F_c(T, H, \boldsymbol{q})$ must be taken at the optimal value of the wave vector $\boldsymbol{q}$, that should be found by minimization of these free energy functions at each point of T, H phase diagram and for each of the two phases (CDW_c and CDW_{2c}) separately.

Below the transition temperature the optimal shift vectors $\boldsymbol{q}$ could be different for the cosine and double cosine phases (they minimize different free energy functions F_c and F_{2c}). However, at the transition temperature $T_c(H)$ the CDW_c and CDW_{2c} phases have the same optimal value of $\boldsymbol{q}$ which is determined by the minimum of the left-hand side of Eq. (6.28). Hence, on the transition line $T_c(H)$ Eq. (6.50) simplifies to

$$r_F = \frac{2|\Delta^{2c}_{\mathbf{Q_0}+\mathbf{q_x},+}|^2}{|\Delta^c_{\mathbf{Q_0}+\mathbf{q_x},+}|^2} > 1, \tag{6.51}$$

or after substitution of (6.34) and (6.43)

$$r_F = \frac{2\left[K_+^{(3)c}\left(\nu K_-^{(1)} - \frac{\nu+1}{2}\right) + \alpha K_-^{(3)c}\left(\nu K_+^{(1)} - \frac{\nu+1}{2}\right)\right]}{\left(K_+^{(3)c} + \alpha K^{(3)d}\right)\left(\nu K_-^{(1)} - \frac{\nu+1}{2}\right) + \left(\alpha K_-^{(3)c} + K^{(3)d}\right)\left(\nu K_+^{(1)} - \frac{\nu+1}{2}\right)} > 1. \tag{6.52}$$

These formulas will be used later to determine the phase diagram.

2. The phase diagram

In this section we only consider the longitudinal modulation ($q_y = 0$) of the CDW wave vector. The CDW phase with $q_y \neq 0$ (CDW_y phase) may appear for certain dispersion functions $t_\perp(\boldsymbol{k}_\perp)$. However, for the tight-binding model (6.2) the CDW_y phase is not expected to take place near the transition temperature. Near the critical pressure (when $t'_b \approx t'^*_b$ and the SDW-metal phase transition takes place) in zero field the SDW_2 phase was predicted using the susceptibility calculation from the normal state.[**?**] However, this phase was predicted only near $T = 0$. Moreover, the absolute instability line calculated in [[**?**]] does not give the actual transition line at low temperature since this transition takes place as the first-order phase transition.

To be more sure that we can disregard appearance of the CDW_y phase in our consideration near the transition temperature we performed the calculation of the optimal shift vector $\boldsymbol{q}$ at the transition line $T_c(H)$ in a large range of parameters. We swept the following three-dimensional range of parameters: $-0.3 \le \nu \le 0.9, 0 \le t_b'/t_b'^* < 1$ and $0 \le \mu_B H \le 2T_{c0}$ and have not found that the shift of Q_y leads to higher T_c anywhere inside this range.

This does not contradict the prediction of the CDW_y [**?**], since according to this paper the CDW_y phase appears at $\nu < 0$ essentially due to the orbital effect of the magnetic field (see Fig. 7d of Ref. [[**?**]]). Below we will only consider the range $0 \le \nu < 1$ which is close to the experimental situation in organic metals and disregard the appearance of CDW_y phase.

2..1 Transition line $T_c(H)$ and the normal-CDW_0-CDW_x tricritical point

The normal-to-CDW phase transition line is given by Eq. (6.28) irrespective of to which CDW phase this transition occurs. The shift of the wave vector q_x which enters Eq. (6.28) corresponds to the maximum value of T_c at given magnetic field H. The behavior of $T_c(H)$ and $q_x(H)$ at the transition temperature has been analyzed in Ref. [[**?**]]. Diagonalization of the M_3, M_4 part of the susceptibility matrix (6) in Ref. [[**?**]] corresponds to the diagonalization of the matrix in Eq. (6.28). On the transition line one of the eigenvalues of these matrices is zero. In the case of perfect nesting equation (6.28) gives the same result for $T_c(H)$ as Eq. (17) of Ref. [[**?**]] (see fig. 7(a) of [[**?**]]).

For $q_x = 0$ (CDW_0 phase) $K_+^{(1)} = K_-^{(1)}$ and Eq. (6.28) simplifies to $K_+^{(1)} = 1$, that gives for the transition temperature $T_c = T_c(H)$ the well-known equation

$$\ln\left(\frac{T_c(H,t_b')}{T_{c0}}\right) = \psi\left(\frac{1}{2}\right) - \\ - \left\langle \operatorname{Re}\psi\left(\frac{1}{2} - \frac{i\varepsilon_\sigma^+(\boldsymbol{k},\boldsymbol{k}-\boldsymbol{Q}_0)}{2\pi T_c}\right)\right\rangle_{k_y}, \tag{6.53}$$

where

$$\varepsilon_\sigma^+(\boldsymbol{k},\boldsymbol{k}-\boldsymbol{Q}_0) = -2t_b'\cos(2k_y b) - \sigma H. \tag{6.54}$$

In the Eq. (6.53) one can take either of the values $\sigma = \pm 1$ since this equation does not depend on the sign of σ. The transition line $T_c(H)$ from normal to CDW_0 phase does not depend on the value of ν.

The tricritical point (where the CDW_0 and CDW_x phases have the same transition temperature) is given by equation $\partial^2 D(\nu,T,H,q_x)/\partial q_x^2 = 0$, where $D(\nu,T,H,q_x)$ is the left-hand side of Eq. (6.28). At this point $q_x = 0, \Rightarrow\ K_+^{(1)} = K_-^{(1)} = 1$ and $\partial^n K_+^{(1)}/\partial q_x^n = (-1)^n \partial^n K_-^{(1)}/\partial q_x^n$, and the equation for the tricritical point becomes

$$\frac{\partial^2 K^{(1)}}{(\partial q_x)^2} = -\frac{2\nu}{1-\nu}\left(\frac{\partial K^{(1)}}{\partial q_x}\right)^2. \tag{6.55}$$

Substituting (6.31) and (6.32) this equation rewrites as

$$-\left\langle \operatorname{Re}\psi''\left(\frac{1}{2} - \frac{i\varepsilon_\uparrow^+(\boldsymbol{k},\boldsymbol{k}-\boldsymbol{Q}_0)}{2\pi T_c}\right)\right\rangle_{k_y} = \\ \eta\left[\left\langle \operatorname{Im}\psi'\left(\frac{1}{2} - \frac{i\varepsilon_\uparrow^+(\boldsymbol{k},\boldsymbol{k}-\boldsymbol{Q}_0)}{2\pi T_c}\right)\right\rangle_{k_y}\right]^2, \tag{6.56}$$

where

$$\eta = 2\nu\nu_F|U_c|/(1-\nu). \tag{6.57}$$

Together with Eq. (6.53) this equation allows to find the tricritical point.

2..2 $T_c(H)$ transition line at perfect nesting

The case of perfect nesting ($t_b' = 0$) is equivalent to the strictly 1D case in many mathematical aspects. However, the 3D nature of the compound (its energy spectrum, e-e interaction and lattice elasticity) preserves, and the mean-field approach still works. The analysis in this subsection (at $t_b' = 0$) is simple and performed analytically. It helps to understand some qualitative features of the CDW phase diagram in magnetic field.

At perfect nesting and purely longitudinal modulation of CDW ($q_y = 0$) the expressions for $K_\sigma^{(1)}$, $K^{(3)d}$ and $K_\sigma^{(3)c}$ simplify to

$$K_{\sigma 0}^{(1)} = 1 + \nu_F|U_c|\left[\ln\frac{T_{c0}}{T} + \psi\left(\frac{1}{2}\right) - \operatorname{Re}\psi\left(\frac{1}{2} + \frac{ih_\sigma}{2\pi T}\right)\right], \tag{6.58}$$

$$K_0^{(3)d} = -\frac{\nu_F|U_c|}{4\pi\hbar v_F q_x T}\left[\operatorname{Im}\psi'\left(\frac{1}{2} + \frac{ih_\sigma}{2\pi T}\right) + \operatorname{Im}\psi'\left(\frac{1}{2} + \frac{ih_{-\sigma}}{2\pi T}\right)\right], \tag{6.59}$$

and

$$K_{\sigma 0}^{(3)c} = -\frac{\nu_F|U_c|}{16\pi^2 T^2}\operatorname{Re}\psi''\left(\frac{1}{2} + \frac{ih_\sigma}{2\pi T}\right), \tag{6.60}$$

where

$$h_\sigma = \frac{\hbar v_F q_x}{2} - \sigma H. \tag{6.61}$$

At $q_x = 0$, Eq. (6.59) even more simplifies:

$$K_{00}^{(3)d} = -\frac{\nu_F|U_c|}{8\pi^2 T^2}\operatorname{Re}\psi''\left(\frac{1}{2} - \frac{iH}{2\pi T}\right) = 2K_{\sigma\,00}^{(3)c}. \tag{6.62}$$

One can now derive a simple formula for the transition line $T_c(H)$ in the high field limit $H \gg T_c(H)$. As $H \to \infty$, h_σ in (6.61) goes to zero for one spin component and to $-2\sigma H$ for the other. Using the limit expansion of the digamma function, $\operatorname{Re}\psi(1/2+ix) = \ln x + O(1/x)$, $x \to \infty$, from (6.58) we have at $H/\pi T_c(H) \gg 1$

$$\begin{aligned} K_+^{(1)} &\approx 1 + \nu_F|U_c|\ln(T_{c0}/T) \\ K_-^{(1)} &\approx 1 + \nu_F|U_c|\ln(\pi T_{c0}/4\gamma H). \end{aligned} \tag{6.63}$$

Equation (6.28) rewrites as

$$K_+^1 = \frac{(1+\nu)K_-^{(1)}/2 - 1}{\nu K_-^{(1)} - (1+\nu)/2},$$

that in the limit $H/\pi T_c(H) \gg 1$ becomes

$$\ln(T_{c0}/T) = \frac{\ln(4\gamma H/\pi T_{c0})}{\eta\ln(4\gamma H/\pi T_{c0}) + 1}. \tag{6.64}$$

At $\eta\ln(4\gamma H/\pi T_{c0}) \gg 1$ this simplifies to

$$T_c(H \to \infty) = T_{c0}\exp(-1/\eta). \tag{6.65}$$

In the intermediate interval $\pi T_c(H) \ll 4\gamma H \ll \pi T_{c0}\exp(1/\eta)$ we get

$$T_c(H) \approx \pi T_{c0}^2/(4\gamma H). \tag{6.66}$$

Hence, at perfect nesting in the limit $H \to \infty$ the transition temperature tends to a finite value which is natural since it corresponds to the CDW instability for only one spin component.

However, the behavior of $T_c(H)$ given by formulas (6.64), (6.65) and (6.66) strongly changes at finite "antinesting" term t_b' (see below).

2..3 Metal-CDW transition lines and tricritical points at finite t_b'

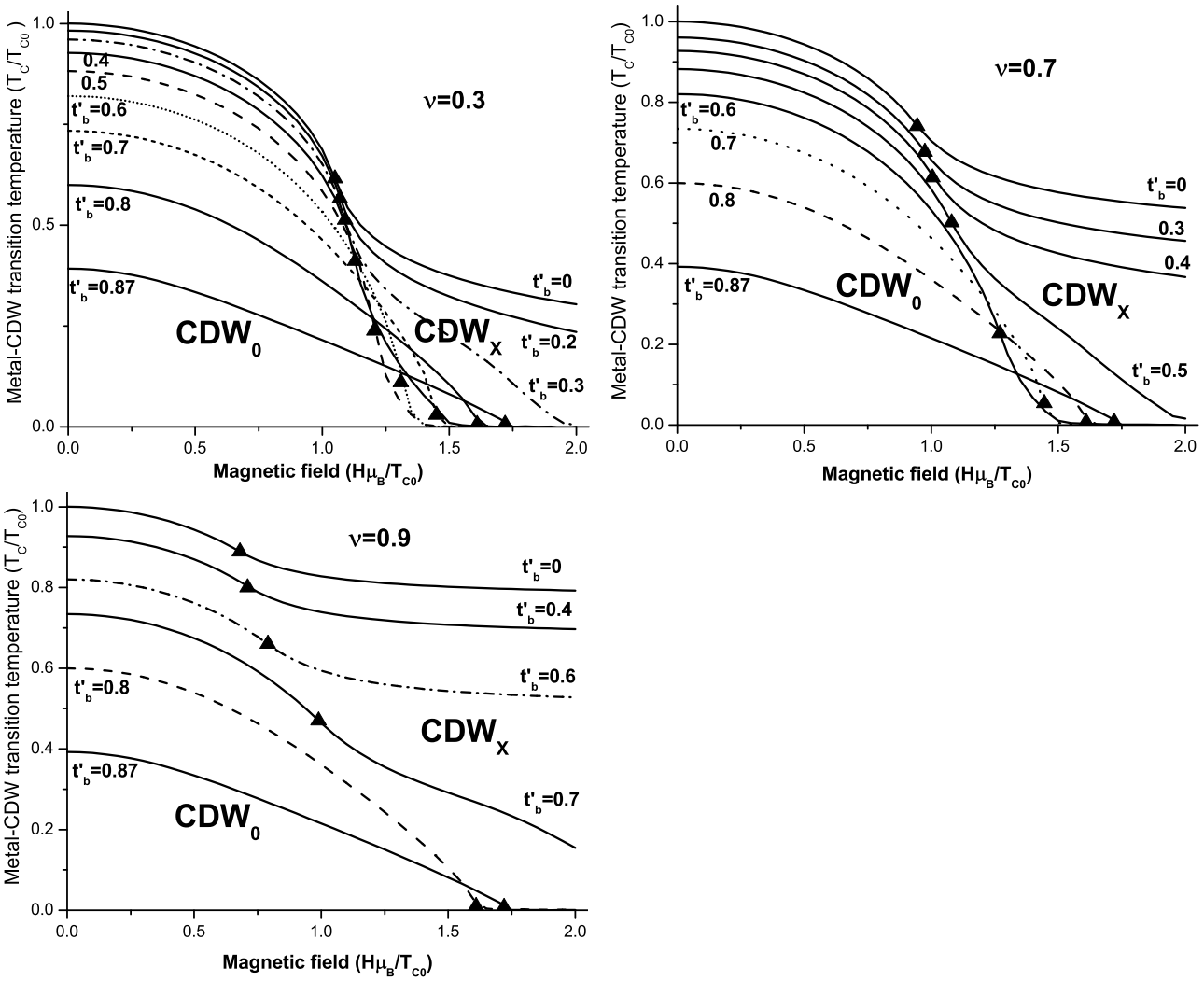


Figure 6.1: Transition lines $T_c(H)$ at different values of t_b' at three different values of the coupling constant ratio ν. The values of t_b' is given on the figures in units of T_{c0}; for the tight-binding dispersion (6.2) the critical value of t_b' at which CDW disappears without magnetic field is $t_b'^* = \Delta_0/2 \approx 0.88T_{c0}$. The triangles show the tricritical points Normal-CDW$_0$-CDW$_x$.

Using the Eq. (6.28) and Eq. (6.56) we calculated the transition lines $T_c(H)$ and the tricritical points at different values of t_b' and ν. The results are shown in Fig. 6.1. From this figure we see that the transition line $T_c(H)$ depends strongly on the both parameters t_b' and ν, and one cannot determine the value of t_b' from the $T_c(H)$ transition line if one does not know the value of ν. Hence, to determine experimentally what values take t_b' and ν in a particular compound, one has to perform two independent tests. For example, one can

study the pressure dependence of the $T_c(H)$ lines at two different tilt angles of magnetic field: the first measurement when the magnetic field is parallel to the conducting x-y plane and the formulas derived above in neglect of orbital effects are valid, the second measurement in the very strong magnetic field perpendicular to the conducting x-y plane, when the orbital effects are so strong that the one-dimensionization of the electron dispersion takes place and the formulas for perfect nesting (see sec. 3.2) become approximately valid. One can also determine the value of t_b' independently from the transport measurement and then compare it to the critical value of $t_b'^* = \Delta_0/2 \approx 0.88 T_{c0}$ at which the CDW state is damped without magnetic field.

There is one interesting common feature on all diagrams in Figs. 6.1. At each value of ν there is a critical value of $t_b' < t_b'^*$ above which the CDW_x phase disappears, i.e. as magnetic field increases the transition from CDW_0 to metal state instead of the CDW_x phase takes place up to the lowest temperature. This critical value of t_b' may shift due to the "one-dimensionization" effect of magnetic field.

We have also checked if the region of cosine phase increases considerably after finite "antinesting" term is taken into account. The results of this study at the transition line are given in Fig. 6.2. These results indicate that the region of cosine phase does not increase considerably at finite t_b' for the tight-binding dispersion.

2..4 Cosine and double-cosine phases at perfect nesting

To determine which of the two phases (CDW_c or CDW_{2c}) wins we have to compare their free energies given in section 2.5.

On the transition line this reduces to the evaluation of the ratio (6.52). At the tricritical point (when $q_x = 0$) this ratio can be easily evaluated using Eq. (6.62):

$$r_{Ftriple} = 2/3 < 1. \tag{6.67}$$

Hence, near the tricritical point the cosine phase wins. In the limit of high field ($H \gg T_c$) one has $\hbar v_F q_x \to 2H$ and $h_\sigma \to (1-\sigma)H$. In this limit $K_+^{(3)c} \approx -(\nu_F |U_c|/16\pi^2 T^2)\,\mathrm{Re}\,\psi''(1/2) \gg K_-^{(3)c}, K^{(3)d}$, and from (6.52) we get

$$r_F \to 2 \text{ at } H/T_c \to \infty. \tag{6.68}$$

Hence, at high magnetic field the double cosine phase wins. These two simple estimates suggest that the cosine and double-cosine phases both appear on the phase diagram.

The boundary between CDW_c and CDW_{2c} phases on the transition line $T_c(H)$ is given by the equation $r_F(T, H, \nu) = 1$, which rewrites as

$$\begin{aligned} &\left(K_+^{(3)c} - \alpha K^{(3)d}\right)\left(\nu K_-^{(1)} - \frac{\nu+1}{2}\right) = \\ &= \left(K^{(3)d} - \alpha K_-^{(3)c}\right)\left(\nu K_+^{(1)} - \frac{\nu+1}{2}\right). \end{aligned} \tag{6.69}$$

This equation is valid also for nonzero t_b' and together with Eq. (6.28) allows to determine the second tricritical point $(H_{c2}(\nu), T_c(H_{c2}))$ where the normal, CDW_c and CDW_{2c} phases meet.

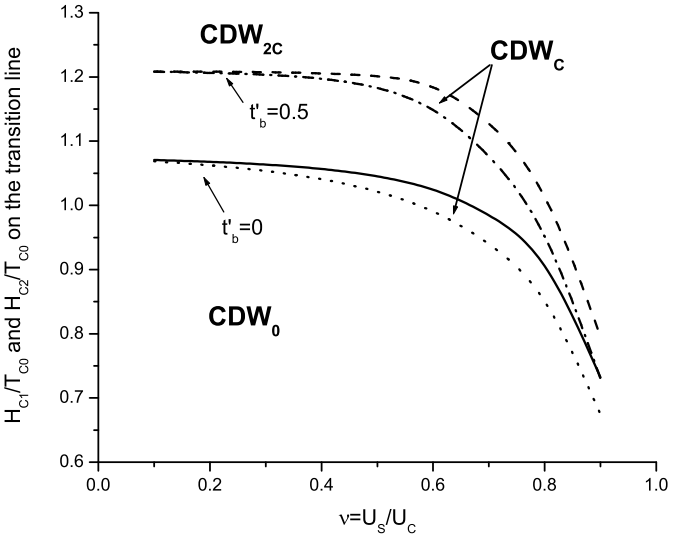


Figure 6.2: The magnetic field values $H_{c1}(\nu)$ and $H_{c2}(\nu)$ at two tricritical points Normal-CDW_0-CDW_c and Normal-CDW_c-CDW_{2c} correspondingly as function of coupling constant ratio $\nu = U_s/U_c$ for two different values of t'_b. The solid and dot lines denote $H_{c2}(\nu)$ and $H_{c1}(\nu)$ at perfect nesting ($t'_b = 0$) while the dash and dash-dot lines denote $H_{c2}(\nu)$ and $H_{c1}(\nu)$ at finite value of the "antinesting" term ($t'_b = 0.5T_{c0}$). The cosine phase exists in the areas between $H_{c1}(\nu)$ and $H_{c2}(\nu)$ lines at the same value of t'_b.

In Fig. 6.2 we plot two triple-point values $H_{c1}(\nu)$ and $H_{c2}(\nu)$ of magnetic field which are given by equations (6.56) and (6.69) correspondingly (together with Eq. (6.28)) at two different values of $t'_b = 0$ and $t'_b = 0.5T_{c0}$. $H_{c1}(\nu)$ and $H_{c2}(\nu)$ determine the tricritical points Normal-CDW_0-CDW_c and Normal-CDW_c-CDW_{2c}. From this figure we see that the range of the cosine phase is very narrow (the difference $H_{c2} - H_{c1}$ does not exceed 5% of H_{c1}) and strongly depends on ν.

At perfect nesting two tricritical points H_{c1} and H_{c2} coincide at $\nu = 0$. At this "double-triple" point the denominator in formulas (6.34) and (6.43) is zero. This means, that one should expand up to the higher orders in $|\Delta^2|$ than fourth and that at this point the critical fluctuations are very strong.

From Fig. 6.2 we see that (i) on the phase diagram of CDW in magnetic field there are at least 3 different CDW states: CDW_0, CDW_c and CDW_{2c}, (ii) at the transition line $T_c(H)$ the region of the CDW_c phase is quite narrow for various values of t'_b and is usually sandwiched between the CDW_0 and CDW_{2c} phases as the magnetic field increases.

To analyze how this picture evolves below the transition line $T_c(H)$ we performed a numerical calculation of the free energies of CDW_c and CDW_{2c} phases using formulas (6.48),(6.49),(6.43),(6.34). These formulas are valid if $\Delta \ll \pi T, H$, that covers a narrow region below $T_c(H)$.

The computation performed in the case of perfect nesting shows that the region of the CDW_c phase becomes even more narrow as the temperature decreases and disappears at $T \approx 0.95T_c(H)$ (see Fig. 6.3). Hence, the cosine phase at perfect nesting exists only in a very small region of the phase diagram where it is strongly smeared by the critical fluctuations.

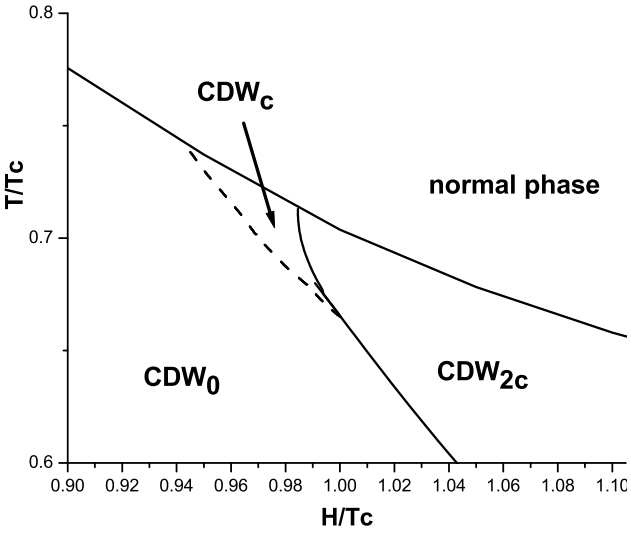


Figure 6.3: Phase diagram in $H-T$ coordinates at $\nu = 0.7$ at perfect nesting near the tricritical point. The CDW$_c$ region disappears rapidly as temperature decreases below T_c.

The similar phase diagram appears in surface superconductors in parallel magnetic field.[**?**] The cosine and double-cosine CDW phases correspond to the helical and cosine (stripe) superconducting phases respectively, and the total CDW$_x$ phase corresponds to the non-uniform superconducting LOFF state.[**?** **?**] However, our situation differs from that in Ref. [[**?**]], where the Rashba term in the electron dispersion relation plays an important role in obtaining the phase diagram similar to that on Fig. 6.3. The number of harmonics and coupling constant in our case is twice larger than that in Ref. [[**?**]]. However, the analogy between CDW and surface superconductors in magnetic field is rather deep (see the discussion section).

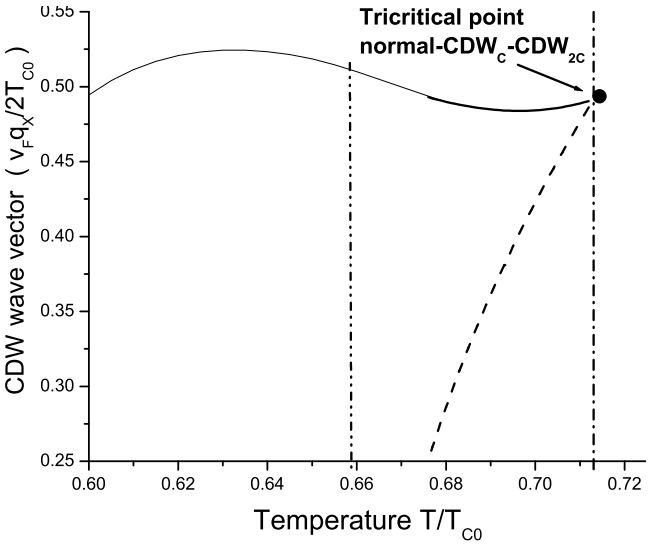


Figure 6.4: The shifts q_x of wave vectors of the phases CDW$_{2c}$ (solid line) and CDW$_c$ (dash line) along the CDW$_c$-CDW$_{2c}$ transition line (at $0.713 > T/T_{c0} > 0.66$) or CDW$_0$-CDW$_{2c}$ transition line (at $T/T_{c0} < 0.66$) as function of temperature. These shifts coincide only at the normal-CDW$_c$-CDW$_{2c}$ tricritical point at $T/T_{c0} = 0.713$. The difference between the solid and dash lines gives the jump of the CDW wave vector on the CDW$_c$-CDW$_{2c}$ transition line that makes this transition of the first kind and leads to hysteresis.The dash-dot line stands for the normal-CDW transition temperature, and the dash-double-dot line shows the temperature of CDW$_0$-CDW$_c$-CDW$_{2c}$ tricritical point.

On the transition line CDW$_c$-CDW$_{2c}$ the energy gaps and the optimal shifts q_x of the CDW

wave vectors of these two phases become substantially different as the temperature decreases below T_c (see Figs. 6.4). This means that the transition from CDW_c to CDW_{2c} is of the first order. The transition line between CDW_0 and CDW_{2c} is also of the first order, and the CDW_{2c} nesting vector differs from $Q_0 = 2k_F$ already on the transition line (see Fig. 6.4). This fact explains the huge hysteresis in magnetization and magnetoresistance observed in α-(BEDT-TTF)$_2$KHg(SCN)$_4$ at the kink transition.[**? ? ?**] The first-order phase transition driven by magnetic field is usually accompanied by hysteresis. The jump of the nesting vector on the CDW_0-CDW_{2c} transition line itself leads to huge hysteresis. The CDW and its wave vector are pinned by the impurities and crystal imperfections.[**?**] As magnetic field increases through the kink transition point $H = H_c(T)$, the jump of the CDW wave vector forces the CDW condensate to move. Due to the pinning this motion is hysteretic since at each time moment the CDW condensate finds some local minimum of the impurity potential. The larger jump of the CDW wave vector at the kink transition the greater the hysteresis is. This jump decreases with increasing temperature and comes to zero on the transition line $T_c(H)$. The hysteresis shows a similar temperature dependence. The hysteresis reduces with heating also due to the thermal activation processes which reduce the pinning.

3. Discussion

The electron charge and spin densities and the lattice distortion differ considerably in the cosine CDW_c and double-cosine CDW_{2c} phases that can help to distinguish these two states experimentally. In the double-cosine phase the charge modulation is the sum of two cosine distortions that leads to the beats of the charge density wave:

$$\begin{aligned}\rho_C^{2c}(x) &= \nu_F(\Delta_+ + \Delta_-)\{\cos[(Q_0 + q_x)x + \phi_1] \\ &\quad + \cos[(Q_0 - q_x)x + \phi_2]\} \\ &= 2\nu_F(\Delta_+ + \Delta_-)\cos[Q_0 x + (\phi_1 + \phi_2)/2] \\ &\quad \times \cos[q_x x + (\phi_1 - \phi_2)/2]. \end{aligned} \tag{6.70}$$

The phase shifts ϕ_1 and ϕ_2 may depend on coordinate because of the pinning of CDW by impurities. Usually, $\Delta_+(Q)$ and $\Delta_-(Q)$ in CDW_{2c} state differ substantially, and the charge density wave in magnetic field is accompanied by a spin density wave. The spin-density modulation in the double-cosine phase is given by

$$\begin{aligned}\rho_S^{2c}(x) &= \nu_F(\Delta_+ - \Delta_-)\{\cos[(Q_0 + q_x)x + \phi_1] \\ &\quad - \cos[(Q_0 - q_x)x + \phi_2]\} \\ &= -2\nu_F(\Delta_+ - \Delta_-)\sin[Q_0 x + (\phi_1 + \phi_2)/2] \\ &\quad \times \sin[q_x x + (\phi_1 - \phi_2)/2]. \end{aligned} \tag{6.71}$$

In the cosine phase both charge and spin densities have one-cosine modulations,

$$\begin{aligned}\rho_C^{c}(x) &= \nu_F(\Delta_+ + \Delta_-)\cos[(Q_0 + q_x)x + \phi_1] \\ \rho_S^{c}(x) &= \nu_F(\Delta_+ - \Delta_-)\cos[(Q_0 + q_x)x + \phi_1]. \end{aligned} \tag{6.72}$$

Thus, the charge modulations in the cosine and double-cosine phases can be experimentally distinguished by X-ray or Raman scattering, and the spin modulation can be detected by muon or neutron scattering experiments.

The energy spectrum in the cosine and double-cosine phases also differ strongly. In the cosine phase the energy spectrum (6.19) is asymmetric with respect to the spin components since the energy gaps Δ_σ differ for two spin components σ. This means that under external

electric field the spin current is produced in addition to the charge current since the charge is transferred by electrons with predominantly one spin component. The degree of current polarization depends on the shift of CDW wave vector, and, hence, can be controlled by the external magnetic field. This property of the cosine phase may find applications in spintronics. The double-cosine phase is symmetric in spin components, and its energy spectrum has at least two gaps for each spin component. The symmetry (6.42) preserves in the double-cosine phase while in the cosine phase it is spontaneously broken. Thus, the one-cosine and double-cosine CDW states differ substantially in their thermodynamic, transport and optical properties.

At low temperature $T \ll T_c$ the expansion in (6.37) is not applicable and the additional harmonics $\mathbf{Q}+(2n+1)\mathbf{q_x}$ with integer n appear in the double-cosine solution of the consistency equation. These harmonics make the charge modulation in the CDW_{2c} phase at low temperature essentially nonsinusoidal in space and, possibly, containing soliton walls. At low temperature the quasi-particles differs substantially from the pair excitations with activation energy 2Δ suggested by the simple mean-field description. Even at finite inter-chain electron dispersion the variational methods using the soliton solutions of the consistency equations show [**?**] that the lowest-energy excitations do not resemble the one-electron-type quasi-particles but involve many electrons and are accompanied by a "soliton" kinks in the coordinate dependence of the order-parameter $\Delta_\sigma(x)$. These excitations in the incommensurate CDW have spin 1/2, zero charge and the energy $2\Delta/\pi$ for a 1D chain without magnetic field. In external magnetic field their activation may become energetically favorable at $H > 2\Delta_0/\pi$ [**?**] that corresponds to the phase-transition from CDW_0 to the CDW_x phase. Unfortunately, there is no a complete solution of this problem at nonzero temperature at present time. The calculation at the electron density close to half-filling [**?**] does not describe properly the incommensurate case far from the half-filling. In particular, it considers only the one-cosine modulation of the charge density. As we have seen, it is usually energetically less favorable than the double-cosine phase in high magnetic field. Therefore, we do not present an exact phase diagram in the whole temperature and magnetic field range.

Qualitatively, for the tight-binding dispersion one may expect the following picture. The cosine phase does not appear on the phase diagram besides the small region near the tricritical point as shown on Fig. 6.3. One can easily show that in the case of perfect nesting at $T \to 0$ the cosine phase is always unstable toward the formation of the double-cosine modulation. However, an observation of the cosine phase would be very interesting because of its spin asymmetry in thermodynamic and transport properties. For this reason some further calculation of the phase diagram for various electron dispersion relations would be interesting. The transition from CDW_0 to CDW_{2c} phase at low temperature comes about as the appearance of soliton kinks (or soliton walls). [**?**] The soliton phase described in Ref. [[**?**]] has two forbidden bands (energy gaps) which makes it similar to the double-cosine phase. With increase of magnetic field the density of kinks increases, and the order parameter comes continuously to the sinusoidal modulation close to that in the double-cosine phase. At perfect nesting the CDW_0-CDW_{2c} boundary may be obtained qualitatively at arbitrary temperature as a smooth link between Fig. 6.3 and the point $H_c = 2\Delta_0/\pi \approx 1.1T_{c0}$ (see Fig. 6.5).

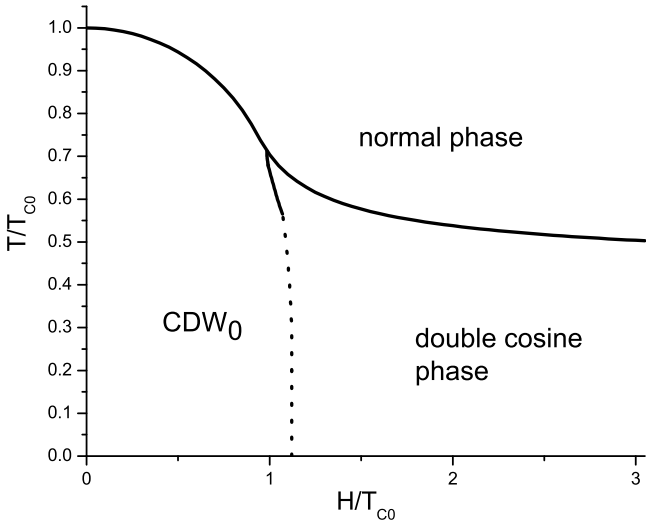


Figure 6.5: Phase diagram in $H-T$ coordinates at perfect nesting in the whole essential region of CDW at $\nu = 0.7$. The solid lines have been calculated from Eqs. (6.28), (6.48),(6.49),(6.34) and (6.43). The CDW_c region is so narrow that it can hardly be distinguished on the total phase diagram. The dot line is a smooth link between the CDW_0-CDW_{2c} boundary near T_c and its value $H_c = 2\Delta_0/\pi \approx 1.12T_{c0}$ at $T = 0$.

In the case of non-uniform LOFF state the susceptibility calculation in metal phase only gives the length of the optimal wave vector $|\boldsymbol{q}_{opt}|$ of the order-parameter modulation. To determine the most energetically favorable combination of $\boldsymbol{q}$: $|\boldsymbol{q}| = |\boldsymbol{q}_{opt}|$ one has to consider the third-order terms in $|\Delta|$ in the consistency equation. To determine which phase, CDW_c or CDW_{2c}, wins we performed the similar procedure. Our procedure takes into account some peculiarities of the CDW state such as the influence of the "antinesting" harmonic in the electron dispersion.

We have already mentioned the resemblance of the phase diagram obtained for CDW (Fig. 6.3) with that of layered superconductors with Rashba term.[**?**] The CDW_0-CDW_{2c} transition at low temperature also has many common features with the transition from uniform superconducting state to LOFF state in layered superconductors.[**?**] In that case at the first critical field H_{c1} the formation of a single soliton kink also becomes energetically favorable, and the functional shape of this soliton is well approximated by $\Delta(x) = \Delta_0 \tanh(x/x_0)$ both in CDW_{2c} and LOFF states at low temperature. However, there are some important differences between these two systems. In the case of superconductivity the phase transition to the LOFF state was predicted to be of the second kind [**?**], and the concentration of soliton walls increases gradually from zero with the increase of the magnetic field. In Ref. [[**?**]] the first-order phase transition was predicted between the uniform CDW and soliton phases. Our calculation also suggests the first-order transition between CDW_0 and CDW_{2c} phases. The first-order phase transition from metal to the LOFF phase was predicted by both the mean-field [**?**] and renormalization-group studies.[**?**] The renormalization group analysis suggests [**?**] that the enhanced fluctuations of the LOFF state, associated with additional broken symmetries, are important to make this transition of the first order. We do not consider the effect of fluctuations. According to the criterion in Refs. [[**? ?**]] the effects of fluctuations must not destroy the mean-field solution in organic metals where the interlayer transfer integral t_b is, usually, much larger than T_{c0}. The transition from the normal state to the CDW_x phase observed on experiments [**? ? ? ? ? ? ? ? ? ? ?**] seems also to be of the second order. Further analysis of the CDW_0-CDW_x phase diagram in the case of imperfect nesting at other dispersion relation can give more accurate description and even new qualitative features.

Our results are aimed to help to analyze the rather complicated phase diagram of CDW

state in high magnetic field observed in a number of organic metals, such as α-(BEDT-TTF)$_2$KHg(SCN)$_4$ [? ? ? ? ? ? ? ? ? ?] (see also a discussion in [[?]]), (Per)$_2$M(mnt)$_2$ (M being Au,Pt,Cu) [? ? ?] etc, where the transition from CDW$_0$ to high-field CDW$_x$ phase is within the experimentally achievable magnetic fields. The above investigation may also be applied to analyze the phase diagram in nonorganic compounds with CDW ground state [?] (the attainable magnetic field in pulsed magnets is already comparable to the transition temperatures in some of these compounds). An accurate quantitative description and comparison with the experimental observations in Refs. [[? ? ? ? ? ? ? ? ? ? ?]] may require the substitution of a more realistic electron dispersion relation for each compound in the formulas derived above. With the two-harmonic tight-binding dispersion our study already explains several qualitative features of the CDW state in high magnetic field. First, we show that the transition from CDW$_0$ to CDW$_x$ state is of the first kind and is accompanied by the substantial jumps of the energy gap in electron spectrum and of the nesting vector that results in strong hysteresis. This fact being observed in many experiments on α-(BEDT-TTF)$_2$KHg(SCN)$_4$ has not received a theoretical substantiation before. Second, we propose and prove the appearance of double-cosine CDW above the kink field which is consistent with the low temperature soliton solution. Third, we describe some properties of the cosine and double-cosine phases.

To summarize, we have developed a mean-field theory of the CDW state in magnetic field which takes into account imperfect nesting and the shift of the CDW wave vector. This allows a detailed study of the CDW properties and the phase diagram in high magnetic field below the transition temperature. Our analysis gives the link between the previous theoretical results based on the susceptibility calculation [?] and the soliton solutions at zero temperature.[? ?] Although our study of the CDW$_{2c}$ state is only applicable close to the transition line $T_c(H)$ where the ration Δ_σ/T_c can be considered as a small parameter, even an investigation in this region allows to make some important conclusions about the structure of CDW at high magnetic field. We have shown that the CDW$_x$ state at high magnetic field has predominantly a double-cosine modulation with wave vectors $\boldsymbol{Q}_\pm = \boldsymbol{Q}_0 \pm q_x$. At perfect nesting the one-cosine CDW with shifted wave vector exists (according to the mean-field calculations) only in a very narrow region near the tricritical point (see Fig. 6.3 and Fig. 6.5). The finite second ("antinesting") harmonic in the electron dispersion (6.2) does not change this picture considerably. However, more specific dispersions or other perturbations may substantially change the phase diagram. We also suggest an interesting peculiarity of the cosine phase — its spin asymmetry that allows to make a controllable spin current.

Part XI
Typical Theory: Another Explanations

Part XII
Articles about Potential Applications

Part XIII
Other Experiments

Part XIV
Appendix

.1 Appendix

.1.1 Introductions from Books

Preface from Density Waves in Solids by Gruiner

(nothing is important here, just general statements)

Density waves are broken symmetry states of metals (why??), brought about by electron-phonon or by electron-electron interactions.

The ground states are the coherent superposition of electron-hole pairs, and, as the name implies, the charge density or spin density is not uniform but displays a periodic spatial variation. The former is called the charge density wave (CDW), the latter the spin density wave (SDW) state of metals.

Charge density waves were first discussed by Fröhlich in 1954 and by Peierls in 1955; spin density wave states were postulated by Overhauser in 1962. It was recognized early that highly anisotropic band structures are important in leading to these ground states (why??).

Not surprisingly, experimental evidence for these ground states was found much later, when materials with a linear chain structure and metallic properties were discovered and investigated. Several groups of both organic and inorganic materials are now standard examples of density wave ground states; some members of these groups have been investigated in detail by a wide array of experimental techniques. (learn, which exactly?)

These notes give a fairly elementary, unsophisticated, and sometimes oversimplified discussion of the field. They reflect an experimentalist view; there is an emphasis on the close relation between theory and experiment - an important aspect of the field. The notes are based on lectures I gave at the Eidgenössische Technische Hochschule, Zurich in 1989 and subsequently at the University of California, Los Angeles in 1991; in both occasions to an audience including graduate and undergraduate students.

Because density waves arise in their simplest form in highly anisotropic (so-called quasi-one-dimensional materials) some fundamental aspects of the low dimensional electron gas will be discussed first. Chapter 2 focuses on the materials, on the various groups of so-called linear chain compounds. This is followed by a discussion of the mean field theory of CDW and SDW ground states and the basic experimental observations in Chapters 3 and 4. Because of the low dimensionality, fluctuation effects are important, and the phase transition is different from what is predicted by mean field theory. The nature of the phase transitions and fluctuations are discussed in Chapter 5; followed in Chapter 6 by a survey of the collective excitations called phasons, amplitudons, and magnons. Chapter 7 deals with the interaction between the ground states and the underlying lattice, and Chapter 8 with the interaction between density waves and impurities. This is followed by a discussion of electrodynamics and nonlinear transport phenomena in Chapters 9 and 10. One of the most spectacular observations in the field is the detection of current oscillations, and various interference phenomena which occur when both *dc* and ac driving fields are amplified. A recent review, adopted in part from Progress in Low Temperature Physics concludes these notes.

The phase transitions and essential features of the ground states are discussed by using second quantization formalism. While the various density wave states, together with the su-

perconducting ground state, can be discussed using a simple Hamiltonian with a q dependent interaction potential V(q) between the electrons, a traditional approach will be followed here: the charge density wave state is described starting from the Fröhlich Hamiltonian of electron-phonon interactions, while the spin density wave state will be discussed by treating the electron-electron interactions within the framework of the Hubbard model. Fluctuation effects and elementary excitations will be described within the framework of Ginzburg-Landau theory, and the interaction between density waves and the underlying lattice together with density wave-impurity interactions will also be discussed using this approach.

Several aspects of the ground states, phase transitions, and various excitations are similar to those of the superconducting state, and consequently extensive use will be made of expressions which have been worked out for BCS superconductors. These expressions will not be derived, but will merely be adopted from the literature. The same applies for the discussion of magnetic excitations which occur in the spin density wave state; which are similar to spin wave excitations well known for antiferromagnets.

Various topics, such as the microscopic description of the interaction of the collective modes with impurities, or some aspects of nonlinear transport, require a discussion which goes beyond the framework of these notes. In these cases only a short summary of the pertinent results will be given.

The field is relatively new, and is by no means a closed chapter of solid state physics. Consequently, many of the issues have not been completely resolved (this is particularly true for spin density waves) and parts of these notes reflect this "unfinished" aspect of the field. Several topics will not be covered by these notes. Density waves which arise in higher dimensions, such as the two-dimensional charge density waves observed in a certain group of materials, called dichalcogenides, and spin density waves in chromium and in its alloys, lie outside the scope of these notes. Also, the focus is on the simplest case of density waves: on the periodic modulations of the charge or spin density with a period which is incommensurate to the underlying lattice. Somewhat more complicated density waves, which arise in materials which have two conducting chains-with the material tetra-thiafulvalene-tetracyanoquinodimethane (TTF-TCNQ) the best known example-will not be discussed. The interplay between density waves and superconductivity, so-called field-induced spin density waves, and other topics, though very interesting in their own right, will also not be covered by these notes.

.1.2 Literature

A Bibliography

References from Density Waves in Solids by Gruiner

Chapter 1

Heeger, A.J., 1979, in Highly Conducting One-Dimensional Solids, edited by J. Devreese et al. (Plenum Press; New York, London).

Kittel, C., 1963, Quantum Theory of Solids (John Wiley and Sons, New York).

Schrieffer, J.R., 1964, Theory of Superconductivity (W.A. Benjamin, Inc., New York).

Solyom, J., 1979, Adv. Phys. 28, 201.

Emery, V., 1979, in Highly Conducting One-Dimensional Solids, edited by J. Devreese e $^{+}$al. (Plenum Press; New York, London).

Tinkham, M., 1975, Introduction to Superconductivity (McGraw Hill, New York).

Ziman, I.M., 1964. Principles of the Theory of Solids, (Cambridge University Press; Cambridge, London, New York and Melbourne).

Chapter 2

Bechgaard, K. et al., 1980, Solid State Comm. 33, 1119.

Bruesh, H. et al., 1975, Phys. Rev. B12, 219.

Carneiro, K., 1985, Electronic Properties of Inorganic Quasi-One-Dimensional Compounds, edited by P. Monceau (D. Reidel Publ. Co.; Dordrecht, Boston).

Geserich, H.P., 1985, Electronic Properties of Inorganic Quasi-One-Dimensional Compounds, edited by P. Monceau (D. Reidel Publ. Co.; Dordrecht, Boston).

Gressier, P. et al., 1984, Inorg. Chem. 23, 1221.

Jacobsen, C.S., D.B. Tanner and K. Bechgaard, 1983, I. Phys. Colloq. 46, 21.

Jerome, D. and H. Schultz, 1982, Adv. Phys. 32, 299.

Kikuchi, K. et al., 1987, Jap. J. Appl. Phys. 26, Suppl. 26-3, 1369.

Kanoda, K. et al., 1988, Phys. Rev. B38, 39.

Nakamura, T. et al., 1990, Solid State Comm. 75, 583.

Meerchant, A. and J. Rouxel, 1986, in Crystal Chemistry and Properties of Materials with Quasi-One-Dimensional Structures, edited by J. Rouxel (D. Reidel Publ. Co.; Dordrecht, Boston), p. 205.

Rouxel, J. and C. Schenker, 1989, in Charge Density Waves in Solids, edited by L.P. Gorkov and G. Grüner, "Modern Problems in Condensed Matter Sciences" (North Holland; Amsterdam, Oxford, New York, Tokyo).

Schlenker, C. and J. Dumas, 1986, in Crystal Chemistry and Properties of Materials with Quasi-One-Dimensional Structures, edited by J. Rouxel (D. Reidel Publ, Co.; Dordrecht, Boston).

Travaglini, G. et al., 1981, Solid State Comm. 37, 599.

Whangboo, M.H. and L. Schneemeyer, 1986, Inorg. Chem. 25, 2424.

Chapter 3

Allender, D., J.W. Bray and J. Bardeen, 1974, Phys. Rer. B9, 119.

Artemenko, S.N. and A.F. Volkov, 1983, Pisma Zh. Eksp. Tear Fiz. 17, 310.

Berthier, C. and P. Segranson, 1987, in Low Dimensional Conductors and Superconductors, edited by D. Jerome and L.G. Caron (Plenum Press, New York).

Berthier, C. et al., 1992, in Nuclear Spectroscopy on CDW Systems, edited by T. Butz and A. Lerf (Kluwer Academic Publ., Dordrecht, Boston, London).

Comes, R. et al., 1975, Phys. Stat. Sol. B71, 171.

Dai, Z., G. Slough and R.V. Coleman, Phys. Rev. Lett. 66, 1318 (1991) and references cited therein.
Eagen, C.F., S.A. Werner and R.B. Saillant, 1975, Phys. Rcv. B12, 2036.
Ekino, T. and J. Akimishu, 1987, Jap. J. Appl. Phys. 26, Suppl. 625.
Fournel, A. et al., 1986, Phys. Rev. Lett. 57, 2199.
Frölich, H., 1954, Proc. Roy. Soc. London Ser. A223, 296.
Grüner, G., 1988, Rev. Mod. Phys. 60, 1129.
Huang, X. and Maki, K. 1989, Phys. Rev. 340, 2575.
Jánossy, A., C. Berthier and P. Segransan, 1987, Phys. Scr. 19B, 578.
Johnston, D.C., M. Maki and G. Grüner, 1985, Solid State Comm. 53, 5.
Johnston, D.C., 1984, Phys. Rev. Lett. 52, 2049.
Kuper, C.G., 1955, Proc. R. Soc. A227, 214.
Kwok, R. et al., 1990, Phys. Rev. Lett. 65, 365.
Maki, K. and A. Virosztek., 1990, J. Magn. Magn. Mat. 90, 758.
Monceau, P., 1985, in Electronic Properties of Inorganic Quasi-One-Dimensional Compounds, edited by P. Monceau (D. Reidel Publ. Co.; Dordrecht, Boston).
Peierls, R.E., 1955, Quantum Theory of Solids (Oxford University Press, New York).
Pouget, J.P. and R. Comes, 1989, in Charge Density Waves in Solids, edited by L.P. Gor'kov and G. Grüner (North Holland; Amsterdam, Oxford, New York, Tokyo).
Pouget, J.P., 1987, in Low Dimensional Conductors and Superconductors, NATO ASI No. B155, edited by D. Jerome and L.G. Caron (Plenum Press, New York), 1987.
Rice, T.M., P.A. Lee and M.C. Cross, 1979, Phys. Rev. B20, 1345.
Ross, J.H., Z. Wang and C. Schlichter, 1986, Phys. Rev. Lett. 56, 663.
Schrieffer, J.R., 1964, Theory of Superconductivity (Benjamin, Inc.; New York, Amsterdam).
Slough, C.G. et al., 1989, Phys. Rev. B39, 5496.
Tinkham, M., 1975, Introduction to Superconductivity (R.E. Krieger, New York). Woll, E.J. and W. Kohn, 1962, Phys. Rev. 126, 1693.

Chapter 4

Anderson, P.W., 1990, in Current Trends in Condensed Matter, Particle Physics, and Cosmology, edited by J. Pati et al. (World Scientific; Singapore, New Jersey, London, Hong Kong).
Andrieux, A. et al., 1981, J. Phys. Lett. 42, L87.
Bechgaard, K. et al., 1980, Solid State Comm. 33, 1119.
Creuzet, F. et al., 1982, J. Phys. Lett. 43, L755.
Delrieux, J.M. et al., 1986, Physica 143D, 412.
Huang, X. and K. Maki, 1990, Phys. Rev. B42, 6498.
Kanoda, K. et al., 1988, Phys. Rev. B38, 39.
Ibid., 1990, B42, 8678.
Kikuchi, K. et al., 1987, lap. /. Appl. Phys. 26, Suppl. 26-3, 1369.
Le, L.P. et al., 1991, Europhys. Lett. 15, 547.
Mortensen, K. et al., 1981, Phys. Rev. Lett. 46, 1234; ibid., 1982, B25, 3319.
Nakamura, T. et al., 1990, Solid State Comm. 75, 583.
Overhauser, A.W., 1960, Phys. Rev. Lett. 4, 462.
Overhauser, A.W., 1962, Phys. Rev. 128, 1437.
Takahashi, T. et al., 1986, I. Phys. Soc. Japan 55, 1364.
Yamaji, J. 1982, J. Phys. Soc. Japan 5, 2787; ibid., 1983, 52, 1369.

Chapter 5

Aronowitz, J.A., P. Goldbart and G. Mozurkewich, 1990, Phys. Rev. Lett. 64, 2799.
Degiorgi, L. and G. Grüner 1992, de Physique 2, 253
Dietrich, W., 1976, Adv. Phys. 25, 615.
Ginzburg, V.L., 1960, S. Phys. Sol. State 2, 1824.
Girault, S. et al., 1988, Phys. Rev. B38, 7980.
Gorshunov, B.P. et al., (to be published).
Hauser, M.R. et al., 1991, Phys. Rev. B43, 8105.
Horowitz, B. et al., 1975, Phys. Rev. B12, 3174.
Johnston, D.C., M. Maki and G. Grüner, 1985, Solid State Comm. 53, 5.
Kwok, R. and S.E. Brown, 1989, Phys. Rev. Lett. 63, 895.
Kwok, R., S.E. Brown and G. Grüner, 1990, Phys. Rev. Lett. 65, 365.
Landau, L.D. and E.M. Lifschitz, 1959, Statistical Physics (Pergamon Press, London).
Lee, P.A., T.M. Rice and P.W. Anderson, 1973, Phys. Rev. Lett. 31, 462.
Pouget, J.P., 1989, in Low Dimcnsional Electronic Properties of Molybdenum Bronze's and Oxides, edited by C. Schlenker (Kluver Academic Publ.).
Pouget, J.P. and R. Comes, 1989, in Charge Density Waves in Solids, edited by L.P. Gor'kov and G. Grüner (North Holland; Amsterdam, Oxford, New York, Tokyo).
Scalapino, D.J., Y. Imry and P. Pincus, 1975, Phys. Rev. B11, 2042.
Schulz, H.J., 1987, in Low Dimensional Conductors and Superconductors, edited by E.D. Jerome and H.G. Caron (NATO ASI, Plenum Press, New York).
Soub, K. et al., 1976, Phys. Lett. A56, 302.

Chapter 6

Anderson, P.W., 1984, Basic Notions in Condensed Matter Physics (BenjaminCummings, Redwood City, CA).
Barisic, S., 1985, Electronic Properties of Materials with Quasi-One-Dir, ensional Structures, edited by P. Monceau (D. Reidel Publ. Co., Dordrecht, Boston).
Boriak, S. and A.W. Overhauser, 1977, Phys. Rew. B16, 5206.
Brazovskii, S. and I.E. Dzyaloshihskii, 1976, Sov. Phys. IETP 44, 1233.
Carlson, R.V. and A.M. Goldman, 1973, Phys. Rev. Lett. 32, 880; ibid., 1975, 34, 11.
Escribe-Filippini, C. et al., 1987, Synth. Met. 19, 931.
Fukuyama, H. and P.A. Lee, 1978, Phys. Rev. B17, 535.
Kittel, C., 1963, Quantum Theory of Solids (John Wiley and Sons, New York).
Kurihara, Y., 1980, J. Phus. Soc. Japan 49, 852.
Le, L.P. et al., 1993, Phys. Rev. B. (in press).
Lee, P.A. and H. Fukuyama, 1978, Phys. Rev. B17, 542.
Lee, P.A., T.M. Rice and P.W. Anderson, 1974, Solid State Comm. 14, 703.
Littlewood, P.B. and C.M. Varma, 1982, Phys. Rev. B26, 4883.
Maki, K. and G. Grüner, 1991, Phys. Rev. Lett. 66, 789.
Maki, K. and A. Virosztek, 1990, J. Magn. Magn. Mat. 90, 758.
Maki, K. and A. Virosztek, 1992, Phys. Rev. Lett. 69, 3265.
Nakane, Y. and S. Takada, 1985, J. Phys. Soc. Japan 54, 977.
Pouget, J.P. et al., 1992, Phys. Rev. Lett. 68, 2374.
Pouget, P. and R. Comes, 1989, in Charge Density Waves in Solids, edited by L.P. Gor'kov and G. Grüner, "Modern Problems in Condensed Matter Sciences" (North Holland; Amsterdam, Oxford, New York, Tokyo).
Psaltakis, G.C., 1987, Solid State Comm. 51, 535.

Schrieffer, J.R., X.G. Wen and S.C. Zhang, 1989, Phys. Rev. B39, 11663.
Schultz, H.J., 1977, Thesis, University of Hamburg (unpublished).
Torrance, J.B. et al., 1982, Phys. Rev. Lett. 49, 881.
Travaglini, G. et al., 1983, Solid State Comm. 45, 289.
Virosztek, A. and K. Maki, 1993, Phys. Rev. B (in press).

Chapter 7

Bak, Per and V.L. Pokrovsky, 1981, Phys. Rev. Lett. 47, 958.
Bishop, A.R., J.A. Krumansl and S.E. Trullinger, 1990, Physica ID.
Brazovskii, S., 1989, in Charge Density Waves in Solids, edited by L.P. Gorkov and G. Grüner "Modern Problems in Condensed Matter Sciences" (North Holland; Amsterdam, Oxford, New York, Tokyo).
Horowitz, B., 1986, in Solitons, eds: S. Trullinger et al., "Modern Problems in Condensed Matter Sciences" (North Holland; Amsterdam, Oxford, New York, Tokyo).
Lee, P.A., T.M. Rice and P.W. Anderson, 1979, Solid State Comm. 14, 703.
Maki, K. in Electronic Properties of Inorganic Quasi-One-Dimensional Compounds, edited by P. Monceau (D. Reidel Publ. Co., Dordrecht, Boston).
Pouget, I'. and R. Comes, 1989, in Charge Density Waaes in Solids, edited by L.l'. Gor'kov and G. Grüner (North Holland; Amsterdam, Oxford, New York, Tokyo).
Rice, M.J. et al., 1976, Phys. Rev. Lett. 36, 342.
Su, W.P. and J.R. Schrieffer, 1981, Phys. Rev. Lett. 46, 738.

Chapter 8

Biljakovich, K. et al., 1981, Phys. Rev. Lett. 57, 1907.
Biljakovich, K., J.C. Lasjammias and P. Monceau, 1989, Synth. Met. 29, F289.
Brown, S.E. et al., 1988, Phys. Rev. B37, 6551.
DeLand, S.M., G. Mozurkewich and L.D. Chapman, 1991, Phys. Rev. Lett. 66, 2026.
Efetov, K.B. and A.l. Larkin, 1977, Zh. Eksp. Tear. Fiz. 72, 7350.
Forro, L. et al., 1983, Phys. Rev. B27, 7600.
Fukuyama, H. and P.A. Lee, 1978, Phys. Rev. B17, 535.
Girault, S. et al., 1988, Phys. Rev. B38, 7980.
Imry, I. and S.K. Ma, 1975, Phys. Re'v. Lett. 35, 1399.
Lee, P.A. and T.M. Rice, 1979, Phys. Rev. B19, 3970.
Sham, L.J. and B.R. Patton, 1976, Phys. Rev. B13, 2151.
Sweetland, E. et al., 1990, Phys. Rev. Lett. 75, 3165.
Tamagai, T., K. Tsutsumi and S. Kagoshima, 1987, Synth. Met. 19, 923.
Tüttő, 1. and A. Zawadowski, 1985, Phys. Rev. Lett. B32, 2449.

Chapter 9

Degiorgi, L. et al., 1991, Phys. Rev. B44, 7808.
Donovan, S. et al. Phys. Rev. (to be published).
Frölich, H., 1954, Proc. R. Soc. London Ser. A223, 296.
Grüner, G., 1988, Mod. Phys. 60, 1129 (and references).
Lee, P.A., T.M. Rice and P.W. Anderson, 1974, Solid State Comm. 14
Kim, T.W. et al., 1991, Phys. Rev. B43, 6315.
Littlewood, P.B., 1987, Phys. Rev. B36, 3108.
Ngai, K.L., 1979, Comments Solid State Phys. 9, 127.

Pippard, A.B., 1953, Proc. R. Soc. London Ser. A216, 547.
Quinlivan, D. et al., 1990, Phys. Rev. Lett. 65, 1816.
Rice, M.J., 1976, Phys. Rev. Lett. 37, 36.
Tüttő, I. and A. Zawadowski, 1985, Phys. Rev. Lett. 32, 2449.
Wonneberger, W., 1991, Synth. Met. 41, 3793 (and references cited therein).
Wooten, F., 1972, Optical Properties of Solids (Academic Press).
Zawadowski, A., 1987, Synth. Met. 29, F469.

Chapter 10

Barone, A. and G. Paterno, 1982, Physics and Applications of the losephson Effect (John Wiley and Sons, New York).
Beyermann, W.P., L. Mihály and G. Grüner, 1986, Phys. Rei. Lett. 56, 1489.
Fleming, R.M. et al., 1978, Phys. Rev. B18, 5560.
Gor'kov, L.P., 1977, IETP Lett. 25, 358.
Grüner, G., 1988, Rer. Mod. Phys. 60, 1129.
Grüner, G., 1994, Rev. Mod. Phys. January issue.
Grüner, G., A. Zawadowski and P.M. Chaikin, 1981, Phys. Rea. Lett. 46, 511.
Grüner, G., W.G. Clark and A.M. Portis, 1981, Phys. Rev. B24, 3641.
Grüner, G. and A. Zettl, 1985, Physics Rep. 119, 117.
Littlewood, P.B., 1989, in Charge Density Waves in Solids, edited by L.P. Gor'kov and G. Grüner (North Holland; Amsterdam, Oxford, New York, Tokyo).
Mihály, G. et al., 1991, Phys. Rev. Lett. 66, 1806.
Mihály, G. et al., 1988, Phys. Rev. B37, 1097.
Monceau, P. et al., 1976, Phys. Rev. Lett. 37, 6902.
Myers, C.R. and J.P. Sethna, 1993, Phys. Rev. B47, 11171.
Narayan, O. and D.S. Fisher, 1992, Phys. Rev. B46, 11520.
Nomura, K., 1986, Physica, B143, 117.
Ross, J.H., Z. Wang and C. Slichter, 1986, Phys. Rev. Lett. 56, 663.
Segranson, P. et al., 1986, Phys. Rev. Lett. 56, 1854.
Tomic, S. et al., 1989, Phys. Rev. Lett. 62, 462.
Zettl, A. and G. Grüner, 1982, Phys. Rev. B26, 2298.

Chapter 11

Alstrom, P., M.H. Jensen and M.T. Levinsen, 1984, Phys. Rev. Lett. A103, 171.
Azbel, M.Ya. and Per Bak, 1984, Phys. Rev. B30, 3722.
Bak, Per, 1983, in Proc. Int. Symp. on Nonlinear Transport in Inorganic-Quast-One-Dimensional Conductors (Sapporo, Japan) (unpublished).
Bak, Per, T. Bohr, M.H. Jensen and R.V. Christianson, 1984, Solid State Comm 51, 231.
Bardeen, I., E. Ben-Jacob, A. Zettl and G. Grüner, 1982, Phys. Ror. Lett. 49, 493.
Beauchene, P., J. Dumas, A. Jánossy, J. Marcus and C. Schlenker, 1986, Physica B143, 126.
Bhattacharya, S., J.P. Stokes, M. Robbins and R.A. Klemm, 1985, Phys. Rer. Lett. 542453.
Bhattacharya, S., J.P. Stokes, M.J. Higgins and R.A. Klemm, 1987, Phys. Rev. Lett. 59, 1849.
Borodin, D.V., F.Ya. Nad', Ya.S. Savitskaya and S.V. Zaitsev-Zotov, 1986, Physica B143, 73.
Bourne, L.C., M.S. Sherwin and A. Zettl, 1986, Phys. Rev. Lett. 56, 1952.
Brown, S.E. and G. Grüner, 1985, Phys. Rea. B31, 8302.
Brown, S.E. and L. Mihály, 1985, Phys. Rew. Lett. 55, 742.
Brown, S.E., G. Mozurkewich and G. Grüner, 1984, Phys. Rev. Lett. 52, 2277.
Brown, S.E., G. Mozurkewich and G. Grüner, 1985a, Solid State Comm. 54, 23.

Brown, S.E., A. Jánossy and G. Grüner, 1985b, Phys. Rev. B31, 6869.
Brown, S.E., G. Grüner and L. Mihály, 1986a, Solid State Comm. 57, 165.
Brown, S.E., L. Mihály and G. Grüner, 1986b, Physica D23, 169.
Clark, T.D. and P.E. Lindelof, 1976, Phys. Rev. Lett. 37, 368.
Coppersmith, S.N. and P.B. Littlewood, 1985a, Phys. Rev. B31, 4049.
Coppersmith, S.N. and P.B. Littlewood, 1985b, in Proc. Int. Cont. on Charge Density Waves in Solids, Lecture Notes in Physics, Vol. 217, edited by J. Solyom and Gy. Hutiray, Springer Verlag, Berlin, p. 236.
Coppersmith, S.N. and P.B. Littlewood, 1986, Phys. Rev. Lett. 57, 1927.
Fack, H. and V. Kose, 1971, 1. Appl. Phys. 42, 320.
Fisher, D., 1985, Phys. Rev. B31, 1396.
Fleming, R.M., 1983, Solid State Comm. 43, 169.
Fleming, R.M. and Grimes, C.C., 1979, Phys. Rev. Lett. 42, 1423.
Fleming, R.M. and L.F. Schneemeyer, 1986, Phys. Rev. B33, 2930.
Fleming, R.M., L.F. Schneemeyer and R.J. Cava, 1985, Phys. Rev. B31, 1181.
Fukuyama, H. and P.A. Lee, 1978, Phys. Rev. B17, 535.
Gill, J.C., 1982, Solid State Comm. 44, 1041.
Grüner, G., 1988, Rev. Mod. Phys. 60, 1129.
Hall, R.P. and A. Zettl, 1984, Phys. Rev. B30, 2279.
Hall, R.P., M.F. Hundley and A. Zettl, 1986, Physica B143, 152.
Inoue, M. and S. Doniach, 1987, Phys. Rev. B33, 6244.
Jing, T.W. and N.P. Ong, 1986, Phys. Rev. B33, 5841.
Latyshev, Yu.I., V.E. Minakova, Ya.S. Santikaya and V.V. Frolov, 1986, Physica B143, 155.
Latyshev, Yu.I., V.E. Minakova and Ya.A. Zhanov, 1987, Pis'ma i' Zs. Eksp. and Teor. Fiz. 46, 31.
Lee, P.A. and T.M. Rice, 1979, Phys. Rev. B19, 3970.
Lindelof, P.E., 1981, Rep. Prog. Phys. 44, 949.
Link, G.L. and G. Mozurkewich, 1988, Solid State Comm. 65, 15.
Littlewood, P.B., 1986, Phys. Rev. B33, 6694.
Lyding, J.W., J.S. Hubacek, G. Gammic and R.E. Thorne, 1986, Phys. Rev. B33, 4341.
Maeda, A.N., Naito and S. Tanaka, 1983, Solid State Comm. 471001.
Maeda, A.N., Naito and S. Tanaka, 1985, J. Phys. Soc. Japan 54, 1912.
Matsukawa, H., 1987, J. Phys. Soc. Japan 56, 1522.
Monceau, P., J. Richard and M. Renard, 1980, Phys. Rer. Lett. 45, 43.
Monceau, P., M. Renard, J. Richard, M.C. Saint-Lager, H. Salva and Z.Z. Wang, 1983, Phys. Rev. B28, 1646.
Monceau, P., M. Renard, J. Richard and M.C. Saint-Lager, 1986, Physica B143, 64.
Mozurkewich, G. and G. Grüner, 1983, Phys. Rev. Lett. 51, 2206.
Mozurkewich, G., M. Maki and G. Grüner, 1983, Solid State Comm. 48, 453.
Ong, N.P. and K. Maki, 1985, Phys. Rev. B32, 6582.
Ong, N.P., G. Verma and K. Maki, 1984a, Phys. Rev. Lett. 52, 663.
Ong, N.P., C.B. Kalem and J.C. Eckert, 1984b, Phys. Rev. B30, 2902.
Parrilla, P. and A. Zettl, 1985, Phys. Rev. B32, 8427.
Renne, M.J. and D. Poulder, 1974, Rev. Phys. Appl. 9, 25.
Richard, J., P. Monceau, H. Papoulas and M. Renard, 1982, J. Phys. C15, 7157.
Segransan, P., A. Jánossy, C. Berthier, J. Marcus and P. Boutaud, 1986, Phys. Rev. Lett. 56, 1954.
Shapiro, S., 1963, Phys. Rev. Lett. 11, 80.
Sherwin, M.S., and A. Zettl, 1985, Phys. Rev. B32, 5536.
Sneddon, L., 1984, Phys. Rev. Lett. 52, 65.

Sneddon, L., M. Cross and D. Fisher, 1982, Phys. Rev. Lett. 49, 292.
Thorne, R.E., W.G. Lyons, J.M. Miller, J.W. Lyding and J.R. Tucker, 1986a, Phys. Rev. B34, 5988.
Thorne, R.E., J.R. Tucker, J. Bardeen, S.E. Brown and G. Grüner, 1986b, Phys. Rev. B33, 7342.
Thorne, R.E., W.G. Lyons, J.W. Lyding, J.R. Tucker and J. Bardeen, 1987a, Phys. Rev. B35, 6360.
Thorne, R.E., J.R. Tucker and J. Bardeen, 1987b, Phys. Rev. Lett. 58, 828.
Thorne, R.E., J.S. Hubacek, W.G. Lyons, J.W. Lyding and J.R. Tucker, 1988, Phys. Rev. B37, 10055.
Tua, P.F. and J. Ruvalds, 1985, Solid State Comm. 54, 471.
Tua, P.F. and Z. Zawadowski, 1984, Solid State Comm. 49, 19.
Verma, G. and N.P. Ong, 1984, Phys. Rev. B30, 2928.
Waldram, J.R. and R.H. Wu, 1982, J. Low Temp. Phys. 47, 363.
Weger, M., G. Grüner and W.G. Clark, 1980, Solid State Comm, 35, 243.
Weger, M., G. Grüner and W.G. Clark, 1982, Solid State Comm. 44, 1179.
Yeh, W.J., Da-Run He and Y.H. Kao, 1984, Phys. Rev. Lett. 52, 480.
Zettl, A. and G. Grüner, 1983, Solid State Comm. 46, 501.
Zettl, A. and G. Grüner, 1984, Phys. Rev. B29, 755.
Zettl, A. and G. Grüner, 1986, Comments Cond. Matter Phys. 12, 265.
Zettl, A., M.B. Kaiser and G. Grüner, 1985, Solid State Comm. 53, 649.

References from Electronic Properties of Inorganic Quasi-One-Dimensional Compounds by Monceau

1. R. L. Greene, G. B. Street, and L. J. Suter, Phys. Rev. Lett. 34, 577 (1975).

2. L. J. Azevedo, W. G. Clark, G. Deutscher, R. L. Greene, G. B. Street and L. J. Suter, Solid State Commun. 19, 197 (1976).

3. P. Monceau, J. Peyrard, J. Richard, and P. Molinié, Phys. Rev. Lett. 39, 161 (1977).

4. T. Sambongi, M. Yamamoto, K. Tsutsumi, Y. Shiozaki, K. Yamaya, and Y. Abe, J. Phys. Soc. Japan 42, 1421 (1977).

5. M. Yamamoto, J. Phys. Soc. Japan 45, 431 (1978).

6. R. H. Dee, D. H. Dollard, B. G. Turrell, and J. F. Carolan, Solid State Commun. 24, 469 (1977).

7. R. H. Dee, A. J. Berlinsky, J. F. Carolan, E. Klein, N. J. Stone, and B. G. Turrell, Solid State Commun. 22, 303 (1977).

8. R. H. Dee, J. F. Carolan, B. G. Turrell, and R. L. Greene, Phys. Rev. B22, 174 (1980).

9. R. A. Buhrman, C. M. Bastuscheck, J. C. Scott, and J. D. Kulick, in Inhomogeneous Superconductors - 1979, edited by D. V. Gubser, T. L. Francavilla, S. A. Wolf, and J. R. Leibowitz, (New York, American Institute of Physics, 1980), p. 207.

10. W. W. Fuller, P. M. Chaikin, and N. P. Ong, Solid State Commun. 30, 689 (1979).

11. P. Haen, G. Waysand, G. Boch, A. Waintal, P. Monceau, N. P. Ong, and A. M. Portis, J. de Phys. (Paris) 37, 179 (1976).

12. P. Haen, J. M. Mignot, P. Monceau, and M. Núñez Regueiro, J. de Phys. (Paris) 39, C6-703 (1978).

13. P. Haen, F. Lapierre, P. Monceau, M. Núñez Regueiro, and M. Richard, Solid State Commun. 26, 725 (1978).

14. J. F. Kwak, R. L. Greene, and W. W. Fuller, Phys. Rev. B20, 2658 (1979).

15. R. L. Civiak, C. Elbaum, L. F. Nichols, H. I. Kao, and M. M. Labes, Phys. Rev. B14, 5413 (1976).

16. R. L. Greene and G. B. Street, in Chemistry and Physics of One-Dimensional Metals, edited by H. J. Keller (Plenum, New York) (1977).

17. G. B. Street and R. L. Greene, IBM J. Res. Dev. 21, 99 (1977).

18. R. H. Dee, J. F. Carolan, B. G. Turrell, R. L. Greene, and G. B. Street, J. de Phys. (Paris) 39, C6-444 (1978).

19. M. Potel, R. Chevrel, M. Sergent, J. C. Armici, M. Decroux, and ∅. Fischer, J. Solid State Chem. 35, 286 (1980).

20. J. C. Armici, M. Decroux, Ø. Fischer, M. Potel, R. Chevrel, and M. Sergent, Solid State Commun. 33, 607 (1980).

21. Y. Tajima and K. Yamaya, J. Phys. Soc. Jpn. 53, 495 (1984).

22. K. Kawabata and M. Ido, Solid State Commun. 44, 1539 (1982).

23. A. A. Abrikosov, Sov. Phys. JETP 5, 1174 (1957); A. L. Fetter and P. C. Hohenberg, in Superconductivity, edited by R. D. Parks (Marcel Dekker, New York, 1969), p. 817.

24. D. Saint-James, G. Sarma, and E. J. Thomas, Type-II Superconductivity (Pergamon Press, New York, 1969); P. G. de Gennes, Superconductivity of Metals and Alloys (Benjamin, New York, 1966); A. A. Abrikosov, L. P. Gor'kov, and I. E. Dzyaloshinski, Methods of Quantum Field Theory in Statistical Physics (Prentice-Hall, Englewood Cliffs, New Jersey, 1963).

25. R. A. Klemm, A. Luther, and M. R. Beasley, Phys. Rev. B12, 877 (1975); L. N. Bulaevskii, Zh. Eksp. Teor. Fiz. 65, 1278 (1975).

26. D. E. Prober, R. E. Schwall, and M. R. Beasley, Phys. Rev. B21, 2717 (1980); R. C. Morris and R. V. Coleman, Phys. Rev. B7, 991 (1973).

27. S. T. Ruggiero, T. W. Barbee, Jr., and M. R. Beasley, Phys. Rev. Lett. 45, 1299 (1980).

28. This has been discussed by many authors. For a review, see V. J. Emery, in Highly Conducting One-Dimensional Solids, edited by J. Devreese, R. Evard, and V. van Doren (Plenum, New York, 1979).

29. J. Bardeen, Rev. Mod. Phys. 34, 667 (1962).

30. M. W. Denhoff and S. Gygax, Phys. Rev. B25, 4479 (1982).

31. E. Z. da Silva and B. L. Gyorffy, Phys. Rev. B20, 147 (1979).

32. R. A. Klemm and H. Gutfreund, Phys. Rev. B14, 1086 (1976).

33. H. Horowitz, H. Gutfreund, and M. Weger, Phys. Rev. B9, 1246 (1974); ibid, 12, 3174 (1975).

34. R. Sooryakumar and M. V. Klein, Phys. Rev. Lett. 45, 45 (1980).

35. P. B. Littlewood and C. M. Varma, Phys. Rev. Lett. 47, 811 (1981); Phys. Rev. B26, 4883 (1982).

36. D. E. Moncton, J. D. Axe, and F. J. DiSalvo, Phys. Rev. B16, 801 (1977); M. Barmatz, L. R. Testardi, and F. J. DiSalvo, Phys. Rev. B12, 4367 (1975).

37. P. Monceau, N. P. Ong, A. M. Portis, A. Meerschaut, and J. Rouxel, Phys. Rev. Lett. 37, 602 (1976).

38. J. Bardeen, L. N. Cooper, and J. R. Schrieffer, Phys. Rev. 108, 1175 (1957).

39. R. A. Klemm and J. R. Clem, Phys. Rev. B21, 1868 (1980).

40. D. R. Tilley, Proc. Phys. Soc. London 85, 1977 (1965).

41. B. S. Chandrasekhar, Appl. Phys. Lett. 1, 7 (1962); A. M. Clogston, Phys. Rev. Lett. 9, 266 (1962); T. P. Orlando and M. R. Beasley, Phys. Rev. Lett. 46, 1598 (1981).

42. A. A. Abrikosov and L. P. Gor'kov, Zh. Eks. i Teor. Fiz. 39, 1781 (1960). (Soviet Phys. JETP 12, 1243 (1961)).

43. C.-R. Hu, Phys. Rev. B6, 1756 (1972).

44. Note that there is an error in sign in Equation (58) of ref. 39. This implies that the dependence of H_{c1} upon the angle H makes with the normal to the $\hat{z}$ axis is as shown in Figure 11, not as in Figure 5 of ref. 39. This error also has implications for the dependence of the lower critical field upon the external field angle for a material of filamentary shape. The correct figure is shown in Figure 12. The author is grateful to H. Schwenk for pointing out this error.

45. J. A. Osborn, Phys, Rev. 67, 351 (1945); R. A. Klemm, J. Low Temp. Phys. 39, 589 (1980); see ref. 44.

46. H. Schwenk, K. Andres, and F. Wudl, (to be published).

47. V. G. Kogan, Phys. Rev. B24, 1572 (1981).

48. V. G. Kogan and J. R. Clem, Phys. Rev. B24, 2497 (1981).

49. W. Lawrence and S. Doniach, in Proceedings of the 12th International Conference on Low Temperature Physics, edited by Eizo Kanda (Academic, Kyoto, 1971) p. 361.

50. L. I. Turkevich and R. A. Klemm, Phys. Rev. B19, 2520 (1979).

51. Note that we have defined the azimuthal angle in the conventional fashion, consistent with Equation (2.2), but differing from ref. 50 by $\phi \to \pi/2 - \phi$.

52. E. T. Whittaker and G. H. Watson, A Course of Modern Analysis (Cambridge University, Cambridge, 1946) Sec. 19.12; W. Magnus and W. Winkler, Hill's Equation (Interscience, New York, 1966).

53. N. W. McLachlan, Theory and Application of Mathieu Functions (Dover, New York, 1964).

54. P. Manneville, J. de Phys. (Paris) 36, 701 (1975).

55. Note that the spin-orbit scattering rate differs by a factor of 2/3 from that in Klemm, Luther, and Beasley [25] This result is correct for two-dimensional scattering.

56. S. Alexander, Phys. Rev. B27, 1541 (1983).

57. M. Tinkham, Phys. Rev. 129, 2413 (1963).

58. P. G. de Gennes, C. R. Acad. Sci. B292, 279 (1981); ibid. B292, 9 (1981).

59. G. Deutscher, I. Grave, and S. Alexander, Phys. Rev. Lett. 48, 1497 (1982); G. Deutscher, O. Entin-Wohlman, S. Fishman, and Y. Shapira, Phys. Rev. B21, 5041 (1980); O. Entin-Wohlman, A. Kapitulnik, and Y. Shapira, Phys. Rev. B24, 6464 (1981).

60. B. B. Mandelbrot, The Fractal Geometry of Nature (Freeman, San Francisco, 1983), and Fractals: Form, Chance and Dimension (Freeman, San Francisco, 1977).

61. Y. Gefen, B. B. Mandelbrot, and A. Aharony, Phys. Rev. Lett. 45, 855 (1980); Y. Gefen, A. Aharony, B. B. Mandelbrot, and S. Kirkpatrick, Phys. Rev. Lett. 47, 1771 (1981).

62. A. S. Skal and B. I. Shklovskii, Fiz. Tekh. Poluprovodn. 8, 1586 (1974) (Sov. Phys. - Semicond 8, 1029 (1975)); P. G. de Gennes, J. de Phys. (Paris) Lett. 37, L1 (1976).